

SYSTEMATIC SYNTHESIS AND CHARACTERIZATION OF THE 2- λ^5 -
PHOSPHAQUINOLIN-2-ONE SCAFFOLD TOWARDS THEIR OPTIMIZATION
AND APPLICATION

by

JEREMY PATRICK BARD

A DISSERTATION

Presented to the Department of Chemistry and Biochemistry
and the Division of Graduate Studies at the University of Oregon
in partial fulfillment of the requirements
for the degree of
Doctor of Philosophy

September 2021

DISSERTATION APPROVAL PAGE

Student: Jeremy Patrick Bard

Title: Systematic Synthesis and Characterization of the 2- λ^5 -Phosphaquinolin-2-one Scaffold Towards Their Optimization and Application

This dissertation has been accepted and approved in partial fulfillment of the requirements for the Doctor of Philosophy degree in the Department of Chemistry and Biochemistry by:

Dr. Ramesh Jasti	Chairperson
Dr. Michael Haley	Co-Advisor
Dr. Darren Johnson	Co-Advisor
Dr. Michael Pluth	Core Member
Dr. John Halliwill	Institutional Representative

and

Andy Karduna	Interim Vice Provost for Graduate Studies
--------------	---

Original approval signatures are on file with the University of Oregon Division of Graduate Studies.

Degree awarded September 2021

© 2021 Jeremy Patrick Bard

DISSERTATION ABSTRACT

Jeremy Patrick Bard

Doctor of Philosophy

Department of Chemistry and Biochemistry

June 2021

Title: Systematic Synthesis and Characterization of the 2- λ^5 -Phosphaquinolin-2-one Scaffold Towards Their Optimization and Application

The recently discovered phosphaquinolinone scaffold combines photophysical activity and supramolecular functionality to serve as a promising new class of compounds for a variety of different applications. The first part of this dissertation focuses on our work in developing a deep, fundamental understanding of many different aspects of the structure, including the photophysical properties, the solution-state dimerization, and the solid-state crystal packing structures. This was performed through a series of systematic syntheses focuses on backbone composition, substituent group placement, and phosphorus center modification. Through a combination of experimental and computational approaches, a series of relationships and trends have been drawn to allow for prediction of both emission energy and dimerization strength of previously not prepared heterocycles based solely upon computed values. These trends open the door for guided design of future heterocycles.

The second part of this dissertation focuses on building off of the fundamental knowledge gained in the initial structure-property relationship studies and applying those findings to application-driven projects. The first of these involves preparing a series of conjugated host molecules that contain the phosphaquinolinone moiety. These hosts are capable of binding HSO_4^- both strongly and selectively and are able to extract it from

aqueous solutions. These hosts can potentially be utilized in high-level nuclear waste remediation processes, as the removal of HSO_4^- is crucial to improving the currently used vitrification methods. The second of these studies involves the development of the PN scaffold as a live cell imaging reagent. Initial results indicate that this scaffold indeed holds promise as a useful cell imaging reagent as it is non-cytotoxic, relatively pH-insensitive, and cell-permeable.

This dissertation contains both previously published and unpublished co-authored materials.

CURRICULUM VITAE

NAME OF AUTHOR: Jeremy Patrick Bard

GRADUATE AND UNDERGRADUATE SCHOOLS ATTENDED:

University of Oregon, Eugene
Eastern Oregon University, La Grande

DEGREES AWARDED:

Doctor of Philosophy, Chemistry, 2021, University of Oregon
Bachelor of Science, Chemistry, 2016, Eastern Oregon University

AREAS OF SPECIAL INTEREST:

Organic Chemistry
Physical Organic Chemistry

PROFESSIONAL EXPERIENCE:

Graduate Teaching Fellow, University of Oregon, 2016-2021
Instructor of Record, University of Oregon, 2020

GRANTS, AWARDS, AND HONORS:

Graduate Student Award for Excellence in the Teaching of Chemistry, University of Oregon, 2021
UO Doctoral Dissertation Research Fellowship, University of Oregon, 2020
Graduate Student Award for Excellence in the Teaching of Chemistry, University of Oregon, 2017
Dean's First Year Merit Award, University of Oregon, 2016
Student Leader of the Year, Eastern Oregon University, 2016
Outstanding Student of Chemistry, Eastern Oregon University, 2016
National SCI Scholar, Society of Chemical Industry, 2015

Sharing the Learning Funding Recipient, Eastern Oregon University, 2015

Outstanding Freshman Chemist, Eastern Oregon University, 2013

PUBLICATIONS:

Bard, J.P., McNeill, J.N., Zakharov, L.N., Johnson, D.W., Haley, M.M. *Isr. J. Chem.* **2021**, *61*, 217–221.

Bard, J.P., Johnson, D.W., Haley, M.M. *Synlett* **2020**, *31*, 1862–1877.

Bard, J.P., Mancuso, J.L., Deng, C.-L., Zakharov, L.N., Johnson, D.W., Haley, M.M. *Supramol. Chem.* **2020**, *32*, 49–55.

Bard, J.P., Bates, H.J., Deng, C.-L., Zakharov, L.N., Johnson, D.W., Haley, M.M. *J. Org. Chem.* **2020**, *85*, 85–91.

Deng, C.-L., Bard, J.P., Zakharov, L.N., Johnson, D.W., Haley, M.M. *Org. Lett.* **2019**, *21*, 6427–6431.

Nojo, W., Reingold, I.D., Bard, J.P., Chase, D.T., Deng, C.-L., Haley, M.M. *ChemPlusChem* **2019**, *84*, 1391–1395.

Deng, C.-L., Bard, J.P., Zakharov, L.N., Johnson, D.W., Haley, M.M. *J. Org. Chem.* **2019**, *84*, 8131–8139.

Bard, J.P., Deng, C.-L., Richardson, H.C., Odulio, J.M., Barker, J.E., Zakharov, L.N., Cheong, P.H.-Y., Johnson, D.W., Haley, M.M. *Org. Chem. Front.* **2019**, *6*, 1257–1265.

Deng, C.-L., Bard, J.P., Lohrman, J.A., Barker, J.E., Zakharov, L.N., Johnson, D.W., Haley, M.M. *Angew. Chem. Int. Ed.* **2019**, *58*, 3934–3938.

Frederickson, C.K., Barker, J.E., Dressler, J.J., Zhou, Z., Hanks, E.R., Bard, J.P., Zakharov, L.N., Petrukhnina, M.A., Haley, M.M. *Synlett* **2018**, *29*, 2562–2566 (highlighted by Swager, T.M. & Yoshinaga, K. *Synfacts* **2018**, *14*, 1243).

Bard, J.P., Deenik, P.R., Hamann, K.R., Morales, D.A., Cavinato, A.G (2016). In M.J. Mio & M.A. Benvenuto (eds.), *Building and Maintaining Award-Winning ACS Student Member Chapters, Volume 2: Specific Program Areas* (pp. 73–94). DOI: 10.1021/bk-2016-1230.ch008.

ACKNOWLEDGMENTS

There are countless people that I would like to thank, both personally and professionally. To my parents, Angie and Rob Bard, thank you for all of your love and support throughout my entire life. You have always been encouraging and supportive of my choices in schooling/jobs/life and without the two of you, I would certainly not have pushed myself to get a PhD. To the rest of my family in Eastern Oregon (La Grande) – the Irelands, the Bards, the Sams, the Vencills, Greg and Katie Mills – thank you all for making my visits back home overflow with love, family, and good times. To Ron Kelley, Anna Cavinato, Colby Heideman, and Colin Andrew at EOU, thank you for inspiring me to pursue chemistry, both in the lab and in the classroom. To my church family at the First Christian Church in La Grande, thank you all for the kind words, letters of encouragement, and constant support for me throughout my entire life.

In Eugene, I first want to thank everyone in my cohort, especially Hazel Fargher, Josh Barker, Jordan Levine, Tawney Knecht, Amber Rolland, and Ruth Maust, for going through this adventure of graduate school with me. Without the study sessions, coffee breaks, bar visits, daily banter, and inside jokes, grad school would have been much less entertaining, and the friendships formed will be something I will value forever, and I look forward to where the winds take us all. To my mentors and friends, Jeff Van Raden, Erik Leonhardt, Dr. Matt Cerda, Dan Seidenkranz, Brittany White-Mathieu, and Justin Dressler for always helping me with research, writing, and presentations. To past and present Haley lab members, Conerd, Justin, Josh, Gabby, Nolan, Bella, Efrain, and all of the undergraduates and rotation students that have come and gone from the lab, thank you all for making lab a very positive environment to work in. Even during tough times, I always

was able to look forward to fun conversations, random thoughts, endless jokes, and comradery. To Past and Present DWJ lab members, especially Ngoc-Minh, Jess, Toby, Jordan, Trevor, Hazel, Thais, Hannah, and Grace, thank you all for always being there to discuss topics of mental health, equity, and anything else I wandered over to your office to talk about. Both labs have really shaped how I think about both research and many other things outside of work. To the Students that I have mentored while here, Jenna Mancuso, Turner Newton, Jacob Odulio, Hannah Bates, Nolan McNeill, Isabel Lopez, Janiel Elizarraga-Oregel, Holden Howard, Arman Garcia, and Jacob Mayhugh, thank you all for working with me and helping me develop as a teacher and a mentor.

To my partner Hazel, thank you for being so loving and supportive throughout our time here. Without your love and support, I likely would not have made it through the challenges of grad school. Our many trips and movie nights are things I will always think about during hard times. To Chunlin, my main mentor and great friend, thank you for helping me settle in lab after a rough first year and teaching me all I know. Without you being there, I would not have been able to keep PN afloat like we did, and I will be forever grateful of the lessons you taught in tenacity, perseverance, confidence, and creativity.

To my thesis committee members, Dr. Ramesh Jasti, Dr. Michael Pluth, Dr. John Halliwill, thank you for your insight and guidance throughout grad school. To my advisors, Mike and Darren, words cannot express how grateful I am that you both were willing to have me join the lab despite my less than amazing performance during first year. You have both taught me how to wear the various hats needed in academia and you have both been supportive at every step. Lastly, I would like to thank the NSF (CHE-1607214) and the University of Oregon Graduate School (UO Doctoral Dissertation Fellowship) for funding.

This thesis is dedicated to David Lofdahl, who made undergraduate studies much more fun by being brilliant, creative, kind, ambitious, and an all-around amazing person and friend. While he wasn't able to go on to graduate school and further his studies, he's been with me in thoughts and memories of happy times throughout my PhD.

TABLE OF CONTENTS

Chapter	Page
I. BUMPY ROADS LEAD TO BEAUTIFUL PLACES: THE TWISTS AND TURNS IN DEVELOPING A NEW CLASS OF PN-HETEROCYCLES	1
1.1 Introduction.....	1
1.2 Initial Discovery.....	4
1.3 Setbacks Breathe New Life.....	8
1.4 A New Dynamic Duo Develops Dozens of Derivatives.....	10
1.5 Physicochemical Properties	14
1.5.1 Fluorescence	14
1.5.2 Molecular Structures	21
1.5.3 Solution Dimerization Studies	22
1.6 Applying What we have Learned	26
1.6.1 Development of Supramolecular Host.....	26
1.6.2 Use of PN Moiety as an Impressive Fluorophore.....	30
1.7 Conclusions and Outlook.....	31
II. SYNTHESIS, PHOTOPHYSICAL PROPERTIES, AND SELF-DIMERIZATION STUDIES OF 2-λ^5-PHOSPHAQUINOLIN-2-ONES	33
2.1 Introduction.....	33
2.2 Results and Discussion	36
2.2.1 Synthesis	36
2.2.2 Photophysical Properties.....	38
2.2.3 Dimer Formation in Solution.....	44

Chapter	Page
2.2.4 Dimer Formation in Solid State	49
2.3 Conclusions	51
2.4 Experimental Section	52
III. EXPLOITING THE HYDROGEN BOND DONOR/ACCEPTOR PROPERTIES OF PN-HETEROCYCLES: SELECTIVE ANION RECEPTORS FOR HYDROGEN SULFATE	68
3.1 Introduction	68
3.2 Results and Discussion	71
3.3 Conclusions	79
3.4 Experimental Section	80
IV. AMPLIFICATION OF THE QUANTUM YIELDS OF 2-λ^5-PHOSPHAQUINOLIN-2-ONES THROUGH PHOSPHORUS CENTER MODIFICATION.....	87
4.1 Introduction	87
4.2 Results and Discussion	89
4.3 Conclusions	95
4.4 Experimental Section	96
V. A HIGHLY FLUORESCENT PN-HETEROCYCLE-FUSED PYRENE DERIVATIVE WITH STRONG SELF-DIMERISATION THROUGH HYDROGEN BONDING.....	101
5.1 Introduction	101
5.2 Results and Discussion	103
5.3 Conclusions	107
5.4 Experimental Section	108

Chapter	Page
VI. THIONATION OF THE 2- λ^5 -PHOSPHAQUINOLIN-2-ONE SCAFFOLD WITH LAWESSON'S REAGENT	112
6.1 Introduction.....	112
6.2 Results and Discussion	113
6.3 Conclusions	120
6.4 Experimental Section	120
VII. UTILIZATION OF THE 2- λ^5 -PHOSPHAQUINOLIN-2-ONE SCAFFOLD AS A NON-CYTOTOXIC, pH-INSENSITIVE, AND LIVE CELL-PERMEABLE IMAGING REAGENT	126
7.1 Introduction.....	126
7.2 Results and Discussion	128
7.3 Conclusions and Future Works	136
7.4 Experimental Section	137
VIII. DEVELOPMENT OF A TRIPODAL SWITCHABLE, SELECTIVE, AND SENSITIVE HOST MOLECULE CAPABLE OF HSO ₄ ⁻ EXTRACTION TOWARDS NUCLEAR WASTE REMEDIATION.....	145
8.1 Introduction.....	145
8.2 Results and Discussion	149
8.3 Conclusions and Future Works.....	153
8.4 Experimental Section	155
IX. CONCLUDING REMARKS.....	160
APPENDICES	161
A. Supplementary Information for Chapter II	161
B. Supplementary Information for Chapter III	298

Chapter	Page
C. Supplementary Information for Chapter IV	359
D. Supplementary Information for Chapter V	404
E. Supplementary Information for Chapter VI	410
F. Supplementary Information for Chapter VII	431
G. Supplementary Information for Chapter VIII	448
H. Naphtho[2,1-e]-1,2-azaphosphorine 2-Oxide Derivatives: Synthesis, Optoelectronic Properties, and Self-Dimerization Phenomena (with Supplementary Information).....	454
I. PN-Containing Pyrene Derivatives: Synthesis, Structure, and Photophysical Properties (with Supplementary Information).....	554
REFERENCES CITED.....	622

LIST OF FIGURES

Figure	Page
1. Figure 1.1 Hydrogen- and halogen-bonding supramolecular hosts prepared and studied in the Haley/Johnson collaboration. Atoms involved in anion binding are bolded.....	3
2. Figure 1.2 Structure of the phosphaquinolone compared to analogous coumarin and carbostyryl moieties.	10
3. Figure 1.3 (a) HOMO (gray) and LUMO (purple) occupancy levels on the carbons in the 3 and 6 positions of the phosphaquinolone backbone as determined at the B3LYP/6-31g(d) level of theory. (b) Structure of disubstituted PN-naphthalene heterocycles 11 and (bottom) specific substituent groups and yields of each derivative for two-step cyclization/hydrolysis.	11
4. Figure 1.4 Relationship between the HOMO-LUMO gaps and the experimental emission energies of (blue) heterocycles 10b , 11a-11d and (red) heterocycles 10b , 11a-11d , and 11m	15
5. Figure 1.5 Representative phosphaquinolone scaffolds colored by their respective experimental emission colors	20
6. Figure 1.6 Comparison of all measured Stokes shifts and brightnesses	20
7. Figure 1.7 Single crystal structures of (a) 9j , (b) 10j monomer, and (c) 10j-10j dimer as representative structures for typical 9 and 10/11 structures. Ellipsoids drawn at 30% probability. Non-hydrogen bonding hydrogen atoms omitted for clarity	21
8. Figure 1.8 Representative LFER plots for dimerization strengths of heterocycles (a) 11d-11g and (b) 10b , 11b , 11d , and 11m	23
9. Figure 1.9 Comparison of all collected phosphaquinolone dimerization strengths	26
10. Figure 1.10 Partial ¹ H NMR spectra of a 1.13 mM solution of 28b in 10% DMSO- <i>d</i> ₆ in CDCl ₃ by itself and in the presence of 10 equiv. of each guest.....	28

Figure	Page
11. Figure 1.11 Coordination environment of HSO_4^- in the binding pocket of 28b in the solid state. Ellipsoids drawn at 30% probability. Non-hydrogen bonding hydrogens omitted for clarity.....	29
12. Figure 1.12 Emission color coordinates in the CIE 1931 chromaticity diagram of a 2:1:10 v:v:v mixture of 33a:33c:33d excited at 430 nm	30
13. Figure 2.1 Coumarin and two congeners, carbostyryl and phosphaquinolone, along with known phosphaquinolones A–F	34
14. Figure 2.2 Atomic contributions (calculated at B3LYP/6-31g(d) level of theory) to the HOMO (left) and LUMO (right) electron densities of the unsubstituted PN-heterocycle core and numbering order for core carbons (middle). Atomic contributions are shown only for the readily functionalizable positions	37
15. Figure 2.3 Emission spectra of (a) heterocycles 1b , 1d–1g and (b) heterocycles 1g–1l as well as (c) plot of trend between substituent electronic properties and emission energies of 1 . The σ value of 1k was approximated by addition of the σ_{meta} and σ_{para} values of the two nitrile groups. All experimental values collected in CHCl_3	40
16. Figure 2.4 (a) Calculated LUMO levels vs. Hammett parameter of R^1 substituents of $\text{R}^2 = t\text{-Bu}$ heterocycles 1 and (b) calculated HOMO levels vs. Hammett parameter of R^2 substituents of $\text{R}^1 = \text{CN}$ heterocycles 1 . Orbital energy levels calculated at the PBE0/6-311G(d,p) level of theory. The σ value of 1k was approximated by addition of the σ_{meta} and σ_{para} values of the two nitrile groups.....	42
17. Figure 2.5 Orientation of most dominant electronic transitions and the corresponding orbitals for heterocycles 1b , 1d–1g , and 1p ; orbital energies in eV	42
18. Figure 2.6 Correlation between calculated HOMO–LUMO energy gap levels <i>versus</i> experimental emission energies of (a) heterocycles 1b , 1d–1g , and (b) heterocycles 1b , 1d–1g , and 1p	44
19. Figure 2.7 Positive trends between EWG on (a) R^1 and (b) R^2 with dimerization constants of 1	46

Figure	Page
20. Figure 2.8 Schematic examples of (a) orbital overlap within monomer units in the R–S heterodimer structure and (b) poor alignment between orbitals within each monomer in the S–S homodimer structure, where the phenoxy oxygen lone pairs are represented in red and align with the P–O σ^* and P–N σ^* orbitals and the P–O σ^* and P–C σ^* orbitals, respectively	48
21. Figure 2.9 ΔG_{exp} values <i>versus</i> ΔG_{pred} . Blue data points were omitted from the initial model, and tested as a validation set of data, showing a good correlation to the model	49
22. Figure 2.10 Solid state structures of (a) the monomer and dimer of 1m and (b) the monomer and staggered hydrogen bonding network of 1e	50
23. Figure 2.11 Solid state N \cdots O distances plotted against solution state K_{dim} values measured in CDCl_3	51
24. Figure 3.1 a) Structure of the PN-heterocycle homodimer linked by self-complementary hydrogen bonds. b) Structure of receptors 1 studied in this work. The relevant protons are marked to assign NMR peaks	70
25. Figure 3.2 Partial ^1H NMR spectra of 1b (1.13 mm) in 10 vol% $[\text{D}_6]\text{DMSO}/\text{CDCl}_3$ in a) the absence and b) the presence of 10 equiv. hydrogen sulfate, c) nitrate, d) chloride, e) bromide, and f) iodide. All anions were used as their respective TBA salts. The two <i>meta</i> -protons with respect to H^b on the central nitrophenyl core are marked with (*)	73
26. Figure 3.3 a) X-ray structure of 1b · HSO_4^- complex; thermal ellipsoids are drawn at the 25% probability level. The TBA cation is omitted for clarity. b) The coordination environment of HSO_4^- showing seven hydrogen bonds (indicated by black dotted lines)	76
27. Figure 3.4 a) Snapshot showing the bond paths and BCPs for 1b · HSO_4^- complex based on AIM analysis. Red dots indicate BCPs, and blue dotted lines denote bond paths. Values of electron density $\rho(r)$ are given for the relevant BCPs (in a.u.). b) Snapshot showing the NCI plot for 1b · HSO_4^- complex. NCI regions are represented as solid surfaces and blue-green-red scaling from $-0.02 < \text{sign}(\lambda_2)\rho(r) < 0.02$ (in a.u.), where red surface indicates strong repulsion, blue surface strong attraction and green surface relatively weak interactions. Isosurface cutoff for NCI=0.5. The arrows in the Figure indicate the green isosurfaces existed between anion and alkyne moieties.	77

Figure	Page
28. Figure 4.1 Well-studied coumarin and carbostyryl scaffolds (top) compared to phosphaquinolone analogues (bottom).	88
29. Figure 4.2 Absorption (solid lines) and fluorescence (dotted lines) spectra of 2 in CHCl ₃ at 298 K.	91
30. Figure 4.3 Selected bond length and dihedral angle in the optimized S ₀ and S ₁ structures of 2f calculated by DFT and TD-DFT methods at the PCM(CHCl ₃)-PBE0/TZVP level of theory, respectively.	93
31. Figure 4.4 (a) Characteristic PN-heterocycle dimer for 2f with the O···N distance (Å) shown as well as (b) bond angles and (c) torsional angles formed within monomers upon dimerization. Ellipsoids drawn at 30% probability.	95
32. Figure 5.1 Previously reported phosphaquinolone scaffolds as well as new PN-fused pyrene 2	102
33. Figure 5.2 X-ray crystal structure of 2 showing both pyrene π–π stacking and phosphonamidate dimer distances; ellipsoids drawn at 30% probability.	104
34. Figure 5.3 ³¹ P NMR spectra of 2 from VC NMR experiment as well as generated fit and residuals (inset).	105
35. Figure 5.4 (a) Absorption and emission spectra of a 1 μM solution of 2 and (b) emission spectra of 2 at varying concentrations, showing excimer emission at higher concentrations in CHCl ₃ , where λ _{ex} = 365 nm.	106
36. Figure 6.1 Lawesson’s Reagent and a sampling of commonly prepared thiocarbonyl compounds.	112
37. Figure 6.2 ORTEP drawing of the thioheterocycle 2e <i>meso</i> -dimer; thermal ellipsoids drawn at 30 % probability level.	116
38. Figure 6.3 Stacked absorption and emission spectra of heterocycles 2	117
39. Figure 7.1 examples of core fluorophore scaffolds and the phosphaquinolone scaffold	127

Figure	Page
40. Figure 7.2 Initial images of HeLa cells upon treatment with a 25 μM solution of 1 and incubation for 30 minutes.	131
41. Figure 7.3 Initial images of HeLa cells upon treatment with a 25 μM solution of 3 and incubation for 30 minutes and b) cytotoxicity data.	133
42. Figure 7.4 Cytotoxicity studies on heterocycle 3 showing no significant cytotoxicity up to 150 μM	134
43. Figure 7.5 Colocalization with 8 and LysoTracker Deep Red.	136
44. Figure 8.1 Structures of the studied bisurea host 1 and hybrid PN-urea host 2 as well as the structure of proposed 3-armed host 3	147
45. Figure 8.2 The two conformations that 3 can take when in the presence of HSO_4^- (conformation A, left), or Cl^- (conformation B, right)	148
46. Figure 8.3 ^1H NMR titration experiment of 3 with additions of Cl^- . Free host is shown on top.	151
47. Figure 8.4 ^{31}P NMR titration experiment of 3 with additions of Cl^- . Free host is shown on top.	151
48. Figure 8.5 ^1H NMR titration experiment of 3 with additions of HSO_4^- . Free host is shown on top and the 1:1 3 : HSO_4^- point is shown in the dark blue spectrum.	152
49. Figure 8.6 ^{31}P NMR titration experiment of 3 with additions of HSO_4^- . Free host is shown on top and the 1:1 3 : HSO_4^- point is shown in the dark blue spectrum.	153

LIST OF TABLES

Table		Page
1.	Table 1.1 Photophysical properties for heterocycles 10	7
2.	Table 1.2 Synthetic yields for heterocycles 14 , 17 , 20 , and 27	12
3.	Table 1.3 Photophysical properties of disubstituted PN-naphthalenes 11	16
4.	Table 1.4 Photophysical properties of PN-anthracenes 14 , PN-phenanthrenes 17 and 20 , PN-pyrene 21 , and P-phenyl heterocycles 27	18
5.	Table 1.5 Dimerization strengths of select examples of heterocycles 10 , 11 , 17 , 20 , 21 , and 27	24
6.	Table 1.6 Photophysical properties of 3-ring PN pyrene derivatives 33	31
7.	Table 2.1 Photophysical properties for PN-heterocycles 1	39
8.	Table 2.2 Orbital energy levels for 1a–1p calculated at the PBE0/6-311G(d,p) level of theory.	41
9.	Table 2.3 Dimerization constants (M^{-1}) of heterocycles 1 in H ₂ O-saturated CDCl ₃	45
10.	Table 2.4 ΔG_{calc} and ΔG_{exp} values of heterocycles 1	47
11.	Table 2.5 Solid state N···O distances of selected heterocycles 1	51
12.	Table 3.1 Association constants (K_a , m^{-1}) of receptors 1 with various anions in 10 vol% [D ₆]DMSO/CDCl ₃ at 298 K.	72
13.	Table 4.1 Photophysical Properties and HOMO–LUMO Energy Gaps of Heterocycles 2a	91
14.	Table 4.2 Dimerization Constants and Energies for 2	94
15.	Table 6.1 Photophysical properties of heterocycles 2	118
16.	Table 7.1 Photophysical properties of new heterocycles in CHCl ₃ at 298 K.	129

17. Table 7.2 Photophysical properties of new heterocycles in ca. 5% DMSO in pH 7.4 PBS Buffer at 298 K.	130
---	-----

LIST OF SCHEMES

Scheme	Page
1. Scheme 1.1 Proposed synthesis of dithiol 5 and macrocyclic disulfide 6 redox pair along with the actual PN-heterocyclic product 7 formed from the reaction, which was confirmed by x-ray crystallography. ORTEP ellipsoids drawn at 50% probability. CCDC 1976534.	5
2. Scheme 1.2 Synthetic pathway for the various PN frameworks.	7
3. Scheme 1.3 Proposed mechanism of phosphonimidate 9 cyclization.	8
4. Scheme 1.4 Synthesis of PN-pyrene 21	13
5. Scheme 1.5 Synthesis of heterocycles 27	14
6. Scheme 1.6 Synthesis of hybrid hosts 28 . Relevant protons on 28 labeled for identification purposes for Figure 1.10.	28
7. Scheme 1.7 Synthesis of 3-ring PN pyrenes 33	31
8. Scheme 2.1 General synthetic pathway for disubstituted PN heterocycles.	37
9. Scheme 3.1 Synthesis of Iodoheterocycle Coupling Piece 5	81
10. Scheme 3.2 Synthesis of Ethynylaniline Coupling Piece 8 and Receptors 1a/1b	83
11. Scheme 4.1 Synthesis of Phosphaquinolinones 2	90
12. Scheme 5.1 Synthesis of PN-pyrene 2	103
13. Scheme 6.1 Conversion of oxo-heterocycles 1 to thio-heterocycles 2 with Lawesson's Reagent (LR).	114
14. Scheme 7.1 Synthesis of Heterocycle 1	129
15. Scheme 7.2 synthesis of methylated PN 3	131
16. Scheme 7.3 synthesis of heterocycle 8	134
17. Scheme 8.1 Synthesis of 3-armed hybrid host 3	150

CHAPTER I

BUMPY ROADS LEAD TO BEAUTIFUL PLACES: THE TWISTS AND TURNS IN DEVELOPING A NEW CLASS OF PN-HETEROCYCLES

This chapter includes previously published and co-authored material from Bard, J.P., Johnson, D.W., Haley, M.M. “Bumpy Roads Lead to Beautiful Places: The Twists and Turns in Developing a New Class of PN-Heterocycles.” *Synlett* **2020**, *31*, 1862–1877. This review article was written by Jeremy P Bard and editorial support was given by Michael. M. Haley and Darren W. Johnson. This accounts article overviews the story and science behind the initial discovery and fundamental studies on the phosphaquinolone scaffold. It summarizes and compares the findings from the first set of papers on the project and hints at where future studies on the project may be heading.

1.1 Introduction

The field of supramolecular chemistry continues to grow and diversify, especially as more creative, functional, and predictably dynamic systems are developed. From drug molecule encapsulation within supramolecular cavitands¹ to molecular machines,² supramolecular chemistry has applications in several different areas based on the variety of molecular interactions it entails. One application that has long been a hallmark of supramolecular chemistry is host–guest chemistry. Many disparate fields such as medical,^{1,3,4} agricultural,⁵ and environmental^{6–12} have benefited from host–guest chemistry

in recent years with the development of drug-containing capsules, nutrient sensors, and noncovalent waste remediation systems, respectively. Because of this broad yet varied applicability, host–guest ‘chemistry’ spans chemical biology, materials sciences, agricultural and food/fragrance research, biology, and biomedical engineering, among other fields.

Of the variety of potential guests, anionic species represent a specifically challenging target in this area due to their high solvation energies, diffuse charges, and lack of strong attractions between anions and most hosts.¹³ Anions are bound through hydrogen bonding or other similar reversible electrostatic interactions. Upon the binding of these guests, many hosts are monitored through chemical, photophysical, or physical methods, and the reversible response can then dynamically report anion concentration in the medium tested. In the lab, this typically is observed via NMR, UV/Vis, and/or fluorescence spectroscopies, while in real-world applications reporter devices such as electrochemical sensors, chemically sensitive field-effect transistors (ChemFETs), or fluorescence microscopy are preferred. There exist innumerable hosts capable of providing signal transduction or reporting guest binding, yet as more and more new and interesting analytes, cellular pathways, problematic contaminants, and chemical markers are discovered, the demand for new responsive hosts will continue to rise as well.

Towards this aim, our lab has developed several arylolethynyl frameworks (Figure 1.1) capable of binding a variety of anionic guest molecules, including halides,^{14–18} oxoanions,^{19–21} and hydrochalcogenides.^{22–24} These hosts take advantage of both their multidentate binding pockets formed from the *meta*-substitution of the phenyl or pyridyl

cores with two arylethynyl arms as well as the fluorescent nature of the π -conjugated backbone.

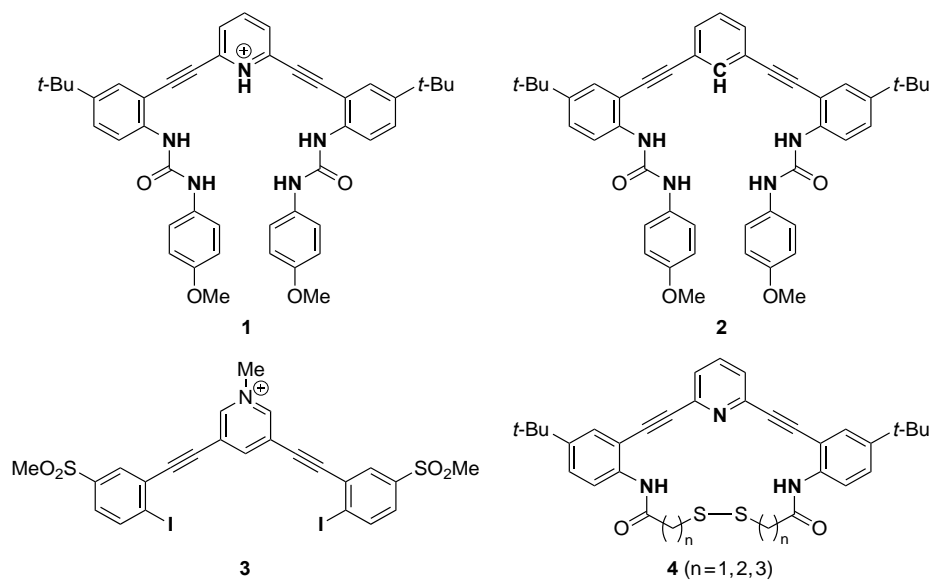


Figure 1.1 Hydrogen- and halogen-bonding supramolecular hosts prepared and studied in the Haley/Johnson collaboration. Atoms involved in anion binding are bolded.

The original hosts in this series were designed in 2006 by Orion Berryman in the Johnson lab and Charles Johnson in the Haley lab and were based on bis-sulfonamide binding units.²⁵ Our first graduate student to be formally co-advised on this project, Calden Carroll, quickly discovered that bisureas such as **1** were superior as these could offer four or five hydrogen bonds to the anionic guest in reproducible 1:1 host–guest binding stoichiometries, depending on the protonation state of the pyridine.¹⁴ This opened a floodgate of 13 eventual co-advised students and postdocs over the next 14 years who explored anion– π -interactions, the effect of increasing or reducing the number of urea binding units, the effects of different heterocyclic cores, and the physical organic chemistry of these receptors and their guests.^{16,19–24} Along the way, graduate student Blake Tresca further improved upon the early designs by replacing the pH-sensitive pyridine core with

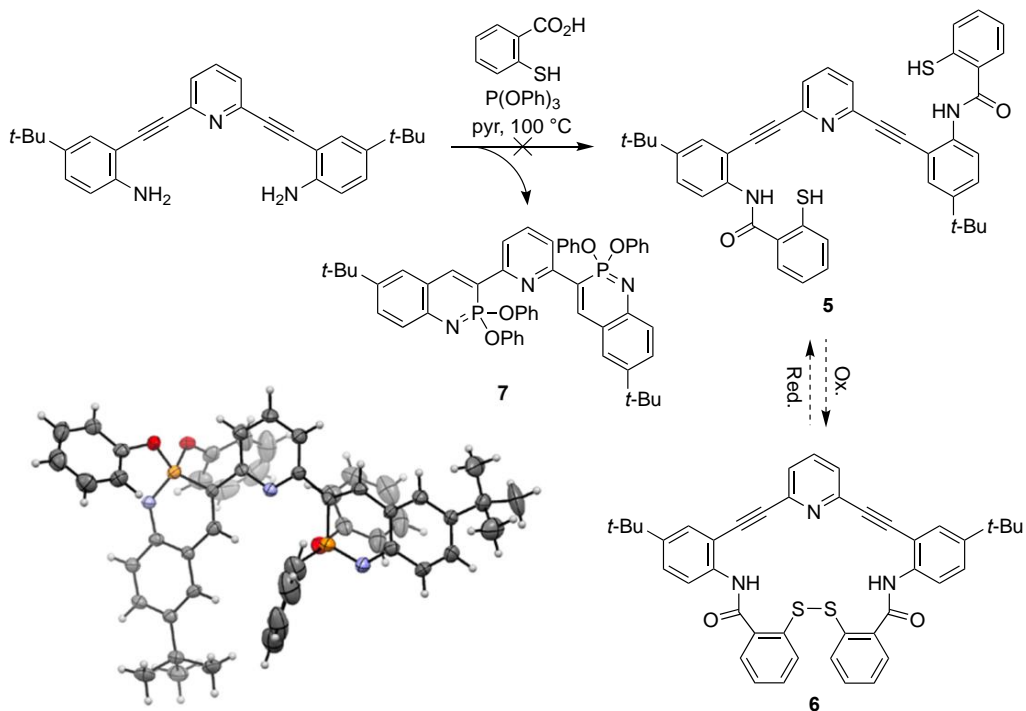
a benzene as in **2** and showed that the C–H···anion interaction could be tuned by installing electron-donating/electron-withdrawing groups *para* to the CH unit.²⁶ Very recently, postdoctoral researcher Jessica Lohrman extended this receptor class to include halogen-bonding recognition units by showing that we could switch out the urea groups with polarized iodine atoms (e.g., **3**).¹⁸

One less explored binding motif in our studies is that of bisamides, such as shown in **4**. One of our first examples of anion binding in the arylethynyl scaffolds was a derivative of **4** ($n = 1$) where Orion and Charles reduced the disulfide motif and protected it as the thioacetate; nonetheless, the receptor bound chloride weakly.²⁷ Several years later graduate student Chris Vonnegut and undergraduate Airlia Shonkwiler prepared a series of disulfide macrocycles based on **4** ($n = 1-3$).^{18,28} Of the molecules, thin films of **4** ($n = 3$) showed a turn-on fluorescence response in the presence of HCl, accompanied with a red shift in emission. X-ray crystallography revealed that the chloride anion sat nicely within the binding pocket of protonated **4** ($n = 3$). In contrast, when the film was treated with trifluoroacetic acid (TFA), it showed a different emission response than with HCl, suggesting a potential for discrimination between different anionic guests with host **4** ($n = 3$). We never guessed at the time that this simple modification would ultimately result in the surprising discovery of new PN-heterocycles.

1.2 Initial Discovery

The original purpose of the disulfide macrocycles was to function as cellular, redox-active probes between the fluorescent, reduced dithiol form and the nonfluorescent, oxidized disulfide state. Despite the best efforts of Calden and Chris,^{28,29} along with those of visiting Japanese graduate student Daisuke Inokuchi, we could never get this project

over the proverbial goal line: one methylene (**4**, $n = 1$) was incredibly reactive and oxidized to the 13-membered disulfide ring in a matter of minutes, whereas formation of the larger macrocycles (**4**, $n = 2-3$) required a strong chemical oxidant (iodine). As a final effort, Chris and Airlia decided to target dithiol **5**/disulfide **6** (Scheme 1.1) with the belief that it would be easier to reduce/oxidize. Attempts to condense the starting bisaniline with thiosalicylic acid using a variety of peptide-coupling conditions only gave polymeric products. In one last-ditch attempt they investigated a procedure for aromatic polypeptide synthesis that uses triphenylphosphite ($\text{P}(\text{OPh})_3$) in the presence of pyridine at high temperature;³⁰ however, as if Monty Python themselves dictated the formed product, it was now time for something completely different.



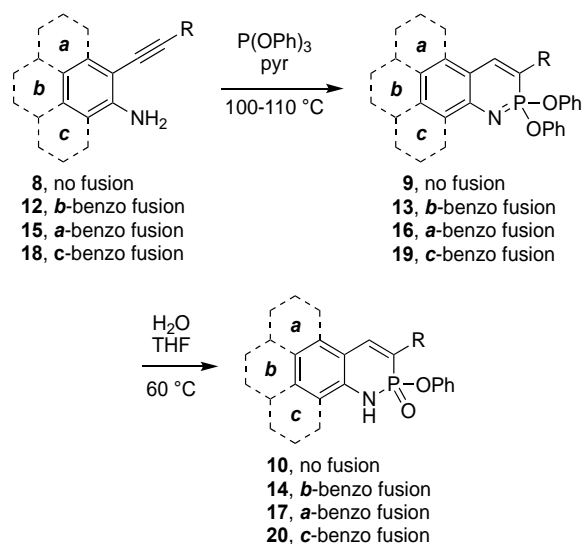
Scheme 1.1 Proposed synthesis of dithiol **5** and macrocyclic disulfide **6** redox pair along with the actual PN-heterocyclic product **7** formed from the reaction, which was confirmed by x-ray crystallography. ORTEP ellipsoids drawn at 50% probability. CCDC 1976534.

Analysis of the reaction mixture by TLC revealed the presence of a polar, highly fluorescent material as the main product. The ^1H NMR spectrum of the yellow solution showed that there were clearly too many aromatic signals, meaning the material almost certainly was not **5** or **6**. After sitting on the benchtop for a few days, yellow crystals suitable for X-ray diffraction had formed inside the NMR tube. Much to our surprise, the crystal structure revealed formation of the *meta*-terphenyl-like structure **7** where a 2,6-disubstituted pyridine ring linked two independent ‘phosphaquinoline’ moieties (Scheme 1.1).²⁸ This molecule had little to no precedent in the literature yet was clearly the main product of the reaction.

A quick literature search into similar systems dating back to the 1950s showed that while there are many known phosphorus heterocycles,^{31–39} along with reviews on similar conjugated organophosphorus materials,^{40,41} ‘PN-heterocycles’ (phosphorus- and nitrogen-containing) are rather rare as their synthesis and isolation are often plagued with difficulties.^{42–52}

Realizing we had potentially uncovered an efficient route to PN-heterocycles, we went back to the drawing board and simplified the synthetic sequence to start from *ortho*-ethynylanilines, which in turn are easily prepared from commercially available or previously published *ortho*-haloanilines. As shown in Scheme 1.2, treatment of ethynylaniline **8** with only $\text{P}(\text{OPh})_3$ at 100 °C (i.e., omitting the thiosalicylic acid) afforded phosphonimidate **9**, which we soon discovered could be hydrolyzed in wet THF to furnish phosphonamidate **10**. Both structures were confirmed by X-ray crystallography (vide infra). With this simplified synthesis, Vonnegut and Shonkwiler prepared a series of

congeners with aryl groups ranging from electron-rich to electron-poor (Scheme 1.2 and Table 1.1).



Scheme 1.2 Synthetic pathway for the various PN frameworks.

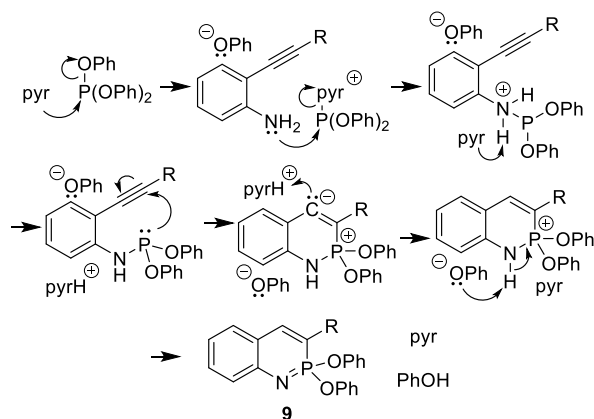
Table 1.1 Photophysical properties for heterocycles **10**

Entry	Yield (%) ^a	R	λ_{abs} (nm) ^b	λ_{em} (nm) ^b	Stokes shift (nm/cm ⁻¹) ^b
10a	39	3,5-(CF ₃) ₂ C ₆ H ₃	349	434	85/5600
10b	43	4-CNC ₆ H ₄	349	430	81/5400
10c	40	4-(CO ₂ Et)C ₆ H ₄	351	432	81/5300
10d	80	4-ClC ₆ H ₄	359	422	63/4200
10e	32	Ph	342	418	76/5300
10f	52	4-MeC ₆ H ₄	341	413	72/5100
10g	37	4-MeOC ₆ H ₄	339	410	71/5100
10h	— ^c	4-Me ₂ NC ₆ H ₄	— ^c	— ^c	— ^c
10i	73	<i>n</i> -pen	318	383	65/5300
10j	22	2-pyridyl	363	442	79/4900

^a Yields reported over two-step cyclization/hydrolysis. ^b Values collected in CHCl₃ at room temperature. ^c Not determined as the imidate did not hydrolyze to the amidate form.

Focusing on heterocycles **10**, nearly every derivative shared a common absorbance peak around 350 nm, yet emission wavelengths ranged from 383–442 nm and Stokes shifts ranged from 63–85 nm/4200–5600 cm^{-1} (Table 1.1). Our initial communication on this class of compounds also reported details of the emission spectra, showing a correlation between more withdrawing substituent groups and more redshifted emissions.⁵³

Chris then performed preliminary mechanistic studies to determine a rough reaction pathway for the cyclization (Scheme 1.3).²⁸ He found that the reaction does not proceed using a non-nucleophilic base such as diisopropylethylamine, suggesting that the relatively nucleophilic pyridine first adds to the $\text{P}(\text{OPh})_3$. The aniline nitrogen then can add to the activated phosphorus center to afford the respective phosphoramidite upon deprotonation. The alkyne is next likely attacked by the phosphorus center before a series of proton transfers to produce the heterocyclic imidate **9**.



Scheme 1.3 Proposed mechanism of phosphonimidate **9** cyclization.

1.3 Setbacks Breathe New Life

The initial excitement and momentum generated by our PN-heterocycle discovery was tempered by the fact both Vonnegut and Shonkwiler graduated in early 2016.

Nonetheless, the project would be given continuity and new life – or so that was the plan – by two new junior research team members and an undergraduate researcher in the group, Noah Takaesu, who Chris and Airlia had trained. Unfortunately, unforeseen personnel issues and re-evaluation of career goals by the junior members left only Noah to push the project forward by the end of winter 2017. At the same time, the project had been injected with its first generous funding through the US NSF ‘INFEWS’ program in the summer of 2016. As a result, a serious reassessment of the project direction, research personnel, and continuity was needed.

While ‘hope springs eternal’ serves as far more powerful guidance in the context of the current global pandemic, the metaphor fit the timing of Spring 2017 for this project – we were fortunate to breathe new life into the project by hiring postdoctoral researcher Chun-Lin Deng and (somehow, miraculously) convincing first-year graduate student Jeremy Bard to join the project. Though there was some overlap with Noah, he too soon graduated and left that summer for graduate school. Unfortunately, there was minimal knowledge transfer, something that everyone who has worked in a research lab knows is critical. Chun-Lin and Jeremy essentially had to start from scratch and figure out what to do with the project, and because of this, the rate of progress diminished greatly. Every research talk given on the project over the following year had a different introduction and scope, as we were trying to find the most compelling story we could tell and find how our work fit into the bigger picture of the grant and the over-arching project. Though a large amount of effort was being exerted, the barrier of no knowledge transfer with two new researchers to the project was almost too much to surmount. Some interesting results were generated over the next year, yet very few significant discoveries were made, resulting in

no papers for close to 18 months. After an arduous group meeting at the end of spring 2018, we elected to pull the plug on the PN-heterocycle studies and allow the project to sunset. This is probably one of the last things that a graduate student wants to hear right after they have advanced to candidacy (i.e., Bard), having just put so much thought and effort into the future of the project. Admittedly that meeting was a letdown, although we left with enough inspiration for the rest of the year to wrap things up and try to be creative, as sunsetting a project can provide a certain sense of freedom perhaps to try new ideas. And as many theologians, musicians, and even a butler once said, ‘the darkest hour is before the dawn’.

1.4 A New Dynamic Duo Develops Dozens of Derivatives

As Jeremy and Chun-Lin worked to tie up loose ends and finish their ongoing projects, Bard went back to the beginning to build off the initial results from Vonnegut on the PN-naphthalene system analogous to **10**. That initial report hinted that there was a lot that could be learned about this new moiety and begged the question as to whether phosphaquinolone optoelectronic properties could be modified in a similar fashion as coumarin and carbostyryl, two well-known, well-studied chromophores (Figure 1.2).⁵⁴⁻⁷² There is an obvious structural relationship between the latter two structures in Figure 1.2, where the carbonyl in carbostyryl is replaced with an isolobal P(OR)=O group to afford the phosphaquinolone scaffold.

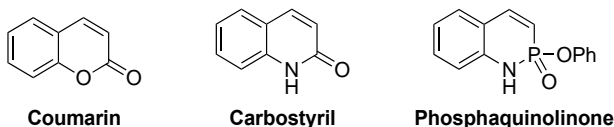


Figure 1.2 Structure of the phosphaquinolone compared to analogous coumarin and carbostyryl moieties.

Taking inspiration from the structure–property relationships drawn for the coumarin and carbostyryl family of fluorophores, Jeremy set out to perform structure–property relationship studies with substituent groups at two different sites upon the backbone. Frontier orbital occupancy calculations by Chun-Lin suggested that studying substituent effects of groups located at carbons 3 and 6 on the backbone (Figure 1.3, a) would be the most fruitful.^{73–77} Use of the same synthetic steps given in Scheme 1.2 furnished a large family of disubstituted heterocycles **11** (Figure 1.3, b), the properties of which are discussed in the next section.

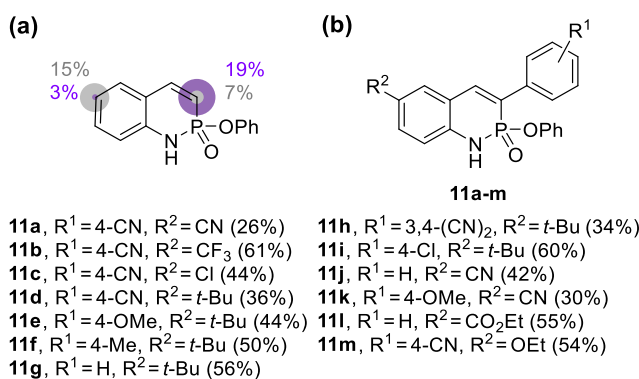


Figure 1.3 a) HOMO (gray) and LUMO (purple) occupancy levels on the carbons in the 3 and 6 positions of the phosphaquinoxaline backbone as determined at the B3LYP/6-31g(*d*) level of theory. b) Structure of disubstituted PN-naphthalene heterocycles **11** and (bottom) specific substituent groups and yields of each derivative for two-step cyclization/hydrolysis.

We were also curious about how extension of the arene π -electron backbone could affect the photophysical properties of the phosphaquinoxaline moiety. Noah had originally started examining this idea by using the synthetic steps outlined in Scheme 1.2, though starting on naphthalene derivative **12** rather than phenyl derivative **8**, to first give the PN-anthracene imidates **13** and subsequently amidates **14** in moderate to good yields (Table 1.2).⁷⁸

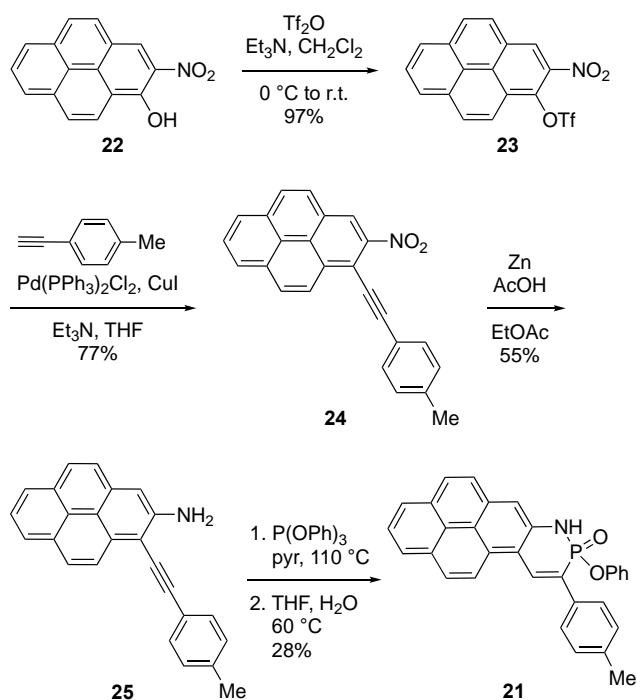
Building upon this linear extension of the aromatic backbone (*b* ring in Scheme 1.2), Chun-Lin's first study focused on the effect of its nonlinear extension (*a* and *c* rings).⁷⁹ Two families of PN-phenanthrene derivatives were prepared, where the first started with aminonaphthalenes **15** that were cyclized to 'bent-up' PN-phenanthrene imidates **16** and subsequently hydrolyzed to 'bent-up' amidates **17**. The second was made starting from cyclization of aminonaphthalenes **18** to 'bent-down' PN-phenanthrene imidates **19** and hydrolysis to amidates **20** (Scheme 1.2 and Table 1.2).

Table 1.2 Synthetic yields for heterocycles **14**, **17**, **20**, and **27**

Entry	R	Yield (%) ^a	Entry	R	Yield (%) ^a
14a	4-MeOC ₆ H ₄	47	20c	4-CNC ₆ H ₄	16
14b	4-MeC ₆ H ₄	70	20d	4-CH ₃ SO ₂ C ₆ H ₄	39
14c	4-CF ₃ C ₆ H ₄	33	20e	4-CF ₃ C ₆ H ₄	18
14d	4-CNC ₆ H ₄	51	20f	4-MeOC ₆ H ₄	16
17a	4-CNC ₆ H ₄	34	27a	CN	21
17b	4-CF ₃ C ₆ H ₄	31	27b	CF ₃	58
17c	4-MeOC ₆ H ₄	33	27c	Cl	31
17d	4-MeC ₆ H ₄	27	27d	H	61
20a	3,4-(CN) ₂ C ₆ H ₃	32	27e	<i>t</i> -Bu	65
20b	4-CF ₃ SO ₂ C ₆ H ₄	30	27f	OEt	31

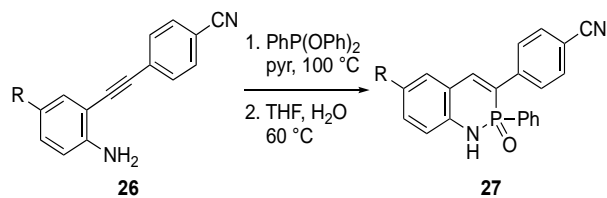
^aYields reported for two-step cyclization/hydrolysis.

To further expand the arene backbone, we next prepared PN-pyrene **21** following the steps outlined in Scheme 1.4. Reaction of known nitropyrenol **22** with triflic anhydride furnished nitrotriflate **23**. Sonogashira cross-coupling of **23** with 4-tolylacetylene furnished nitropyrene **24**, which was then reduced using Zn in AcOH to yield aminopyrene **25**. Lastly, cyclization of **25** with P(OPh)₃ and then hydrolysis gave PN-pyrene **21**.⁸⁰



Scheme 1.4 Synthesis of PN-pyrene **21**.

Having studied both substituent effects upon the backbone as well as effects of arene core modification, we then probed potential substituent effects directly upon the phosphorus center. For this, Jeremy, Chun-Lin, and rotation student Hannah Bates performed the cyclization reaction on a smaller set of substituted ethynylanilines **26**, except this time using $PhP(OPh)_2$ to afford the P-phenyl heterocycles **27** (Scheme 1.5).⁸¹ There were two reasons that we were interested in examining this P-substitution: (a) derivatives **27** have one less degree of freedom than their heterocycle **11** analogues, suggesting a potentially higher quantum yield, and (b) the change in both the steric and electronic nature of the phenyl group in **27** might have substantial effects upon the solid-state properties.



Scheme 1.5 Synthesis of heterocycles **27**.

1.5 Physicochemical Properties

1.5.1 Fluorescence

The photophysical properties of the original PN-heterocycles **10** (Table 1.1) achieved decent Stokes shifts and elucidated the relationship between emission energy and the electronic nature of the substituent groups. However, these initial results did not offer a thorough understanding as to why these properties were changing and/or why the general trends were present. In addition, neither complete characterization of the photophysical properties (i.e., absorption coefficients, quantum yields, fluorescence lifetimes) nor a comprehensive rationalization of the trends observed were performed at the time of the discovery.

Understanding these initial trends, building upon the initial family of molecules, and developing more complete sets of optoelectronic properties were the primary objectives Jeremy and his coworkers wanted to address with disubstituted heterocycles **11**. Upon successful synthesis, their photophysical properties were measured and are listed in Table 1.3. With this family, two trends for the effect of various substituent groups can be seen, where both more donating C6-substituent groups and more withdrawing C3-substituent groups led to redshifting in the emission. This correlates nicely with the frontier orbital occupancy calculations, which showed a predominance of the LUMO on C3 and a predominance of the HOMO on C6. These substituent effect trends support the hypothesis

that the emission is redshifting due to a lowering of the LUMO or a raising of the HOMO, respectively. To further support this idea, Chun-Lin calculated the geometries and energy levels of the HOMOs and LUMOs for each derivative, uncovering an interesting predictive tool. Not only did we see the expected trends within the HOMOs and LUMOs of analogous derivatives **11a–m**, but we also found a very nice correlation between the computationally predicted HOMO–LUMO energy gap and the experimental emission energies (Figure 1.4, blue). With this relationship, we realized that we potentially had an excellent way to predict the emission energies of future heterocycles based solely on their computationally derived HOMO–LUMO energy gaps.

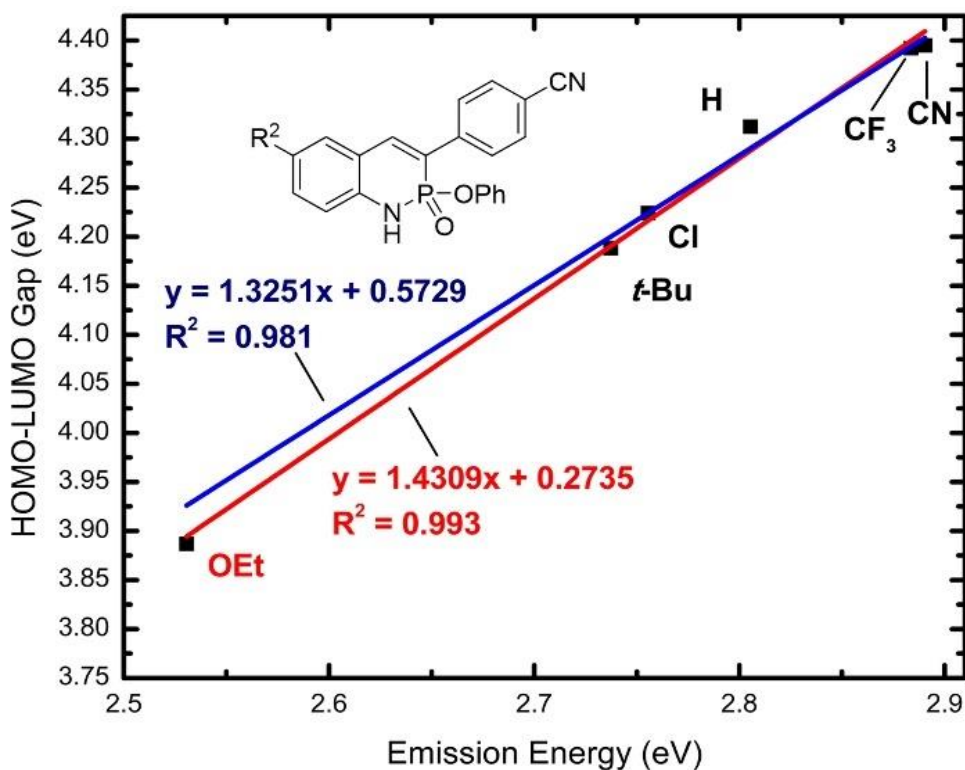


Figure 1.4 Relationship between the HOMO-LUMO gaps and the experimental emission energies of (blue) heterocycles **10b**, **11a-11d** and (red) heterocycles **10b**, **11a-11d**, and **11m**.

Table 1.3 Photophysical properties of disubstituted PN-naphthalenes **11**^a

compd	R ¹	R ²	λ_{abs} (nm), ϵ (M ⁻¹ cm ⁻¹)	λ_{em} (nm), ϕ (%) ^b	Stokes shift (nm/cm ⁻¹)	Brightness ($\epsilon \times \phi$)
11a	4-CN	CN	346, 12000	430, 18	84/5646	2160
11b	4-CN	CF ₃	341, 20000	429, 11	88/6015	2200
11c	4-CN	Cl	358, 23000	450, 11	92/5710	2530
11d	4-CN	<i>t</i> -Bu	358, 22000	453, 11	95/5858	2420
11e	4-OMe	<i>t</i> -Bu	344, 16000	421, 6	77/5316	960
11f	4-Me	<i>t</i> -Bu	343, 14000	424, 8	81/5569	1120
11g	H	<i>t</i> -Bu	343, 17000	430, 8	87/5899	1360
11h	3,4-(CN) ₂	<i>t</i> -Bu	371, 19000	477, 41	106/5989	7790
11i	4-Cl	<i>t</i> -Bu	345, 19000	431, 8	86/5784	1520
11j	H	CN	337, 12000	410, 13	73/5283	1560
11k	4-OMe	CN	345, 15000	471, 28	126/7754	4200
11l	H	CO ₂ Et	335, 12000	411, 10	76/5519	1200
11m	4-CN	OEt	379, 25000	490, 24	111/5977	6000

^a Values collected in CHCl₃ at room temperature. ^b Excited at 365 nm and collected using a quinine sulfate (in 0.1 M H₂SO₄) standard.

Based on this equation, we ‘screened’ many different theoretical congeners to see if we could achieve even more redshifted emission. Calculations suggested that an ethoxy group on the C6-position would have an immense effect on the emission energy, predicted to be 2.50 eV (496 nm). This was somewhat surprising, as the σ_{para} value of the –OEt substituent was not that much more donating than the previously most donating *tert*-butyl substituent of **11d**. Upon the synthesis of ethoxy-substituted **11m**, the emission was determined to be at 490 nm (2.53 eV), giving a nearly perfect match (Table 1.3). This demonstrated that we were able to reliably predict the emission energy of future congeners, as well as gave us a new predictive relationship between HOMO–LUMO energy gaps (Figure 1.4, red).

In addition to these two relationships, we also determined the complete set of photophysical properties (Table 1.3). These values were all suboptimal for their potential use as fluorescent dyes in most cases and begged the question of how could they be improved. This question served as a foundation for many aims of the project mentioned below.

As shown by the diversity of syntheses in Schemes 1.2, 1.4, and 1.5, we spent a large amount of time and effort examining the variety of effects that different backbone modifications have on the fluorescence of these heterocycles. From Noah's work with the PN-anthracenes, he found that **14** exhibited much more redshifted emissions and significantly larger Stokes shifts likely due to the increased conjugation of the backbone (Table 1.4). While **14** possessed significantly larger absorption coefficients, the molecules still retained low quantum yields, leading to low brightness values.

Following this study, Chun-Lin examined both 'bent-up' PN-phenanthrenes **17** and 'bent-down' PN-phenanthrenes **20**, the photophysical properties of which are also given in Table 1.4. With both families, we again noticed much more modest absorption coefficients and emission wavelengths yet found that quantum yields of up to 93% with heterocycles **20**; however, the absorption coefficients kept brightness values low.

To overcome this issue, Jeremy, with the help of rotation student Jenna Mancuso, prepared PN-pyrene **21**. Its emission maximum was 465 nm, affording a Stokes shift of 3800 cm^{-1} . Gratifyingly, we found that we not only achieved a quantum yield of 70% but also attained an absorption coefficient of $26000\text{ M}^{-1}\text{cm}^{-1}$, giving **21** a brightness value of $18000\text{ M}^{-1}\text{cm}^{-1}$ (Table 1.4). Further, fluorescence experiments at higher concentration suggested that above 2 mM in CHCl_3 , excimer formation could still be observed, illustrated

by the growth of a very redshifted peak in the emission spectrum at 582 nm.⁸²⁻⁸⁷ With some modification, this motif could have potential for integration into

Table 1.4 Photophysical properties of PN-anthracenes **14**, PN-phenanthrenes **17** and **20**, PN-pyrene **21**, and P-phenyl heterocycles **27**^a

Entry	λ_{abs} (nm), ϵ (M ⁻¹ cm ⁻¹)	λ_{em} (nm), ϕ (%) ^b	Stokes shift (nm / cm ⁻¹)	Brightness ($\epsilon \times \phi$)
14a	339, 27000	464, 7	125 / 7900	1900
14b	331, 27000	469, 9	138 / 8900	2400
14c	327, 21000	492, 2	165 / 10000	420
14d	336, 31000	506, 4	170 / 10000	1200
17a	384, 13000	461, 12	77 / 4300	1600
17b	375, 9800	450, 10	75 / 4400	980
17c	374, 25000	442, 16	68 / 4100	4000
17d	371, 15000	440, 9	69 / 4200	1400
20a	404, 12000	493, 93	89 / 4500	11000
20b	397, 5200	490, 80	93 / 4800	4100
20c	389, 10000	469, 36	80 / 4400	3600
20d	388, 7400	470, 66	82 / 4500	4900
20e	380, 6900	457, 29	77 / 4400	2000
20f	372, 6800	441, 19	69 / 4200	1300
21	395, 26000	465, 70	70 / 3800	18000
27a	348, 15000	447, 76	99 / 6400	11400
27b	343, 18000	449, 38	106 / 6900	6840
27c	360, 19000	474, 43	114 / 6700	8170
27d	352, 18000	467, 50	115 / 7000	9000
27e	360, 22000	475, 51	115 / 6700	11220
27f	381, 22000	515, 35	134 / 6800	7700

^a Values collected in CHCl₃ at room temperature. ^b Excited at 365 nm and collected using a quinine sulfate (in 0.1 M H₂SO₄) standard.

larger systems that could take advantage of both its photophysical and supramolecular properties.

Another factor that can be controlled with the PN-heterocycles that cannot be altered in either coumarin or carbostyryl is substitution at the phosphorus center. In the examples above, all contain a phenoxy group attached to the phosphorus center. To explore any potential substituent effects on this position as well, we prepared the P-phenyl family **27**. The photophysical properties of **27** were very exciting, as we saw an almost universal improvement compared to heterocycles **11** (Tables 1.3 and 1.4), specifically a dramatic increase in the quantum yields and a slight redshifting in the emissions as well as improvement of the Stokes shifts in most cases. We attributed this to both a slight rigidification of the scaffold as well as an increase in planarity between the aromatic core and the pendent aryl group in the excited state of **27** (based upon TD-DFT calculated geometries). This family is also favorable, as the synthesis, isolation, and solubility all allow for its easier production and use, suggesting that any future fluorophore applications should include this modification.

Several different families of phosphaquinolones have been built based off the simple cyclization found by Vonnegut and Shonkwiler, all of which having their own pros and cons. From these studies, we have accessed a wide range of emission wavelengths (383–515 nm), Stokes shifts (3800–10000 cm^{-1}), and brightness levels (420–18000 $\text{M}^{-1}\text{cm}^{-1}$, Figure 1.5 and Figure 1.6). In each family, we found that withdrawing substituents upon the pendent aryl groups lead to both redshifted emissions and subsequently larger Stokes shifts. We also determined that increasing the conjugation of the backbone leads to redshifting in the emission as well and can lead to increased brightness. Lastly, we found that the replacement of the P-phenoxy group with a P-phenyl group leads to even greater increases in brightness, redshifted emission colors, and larger Stokes shifts (Figure 1.6).

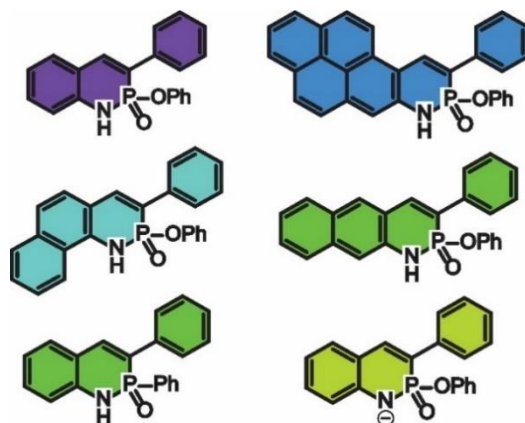


Figure 1.5 Representative phosphoquinolinone scaffolds colored by their respective experimental emission colors.

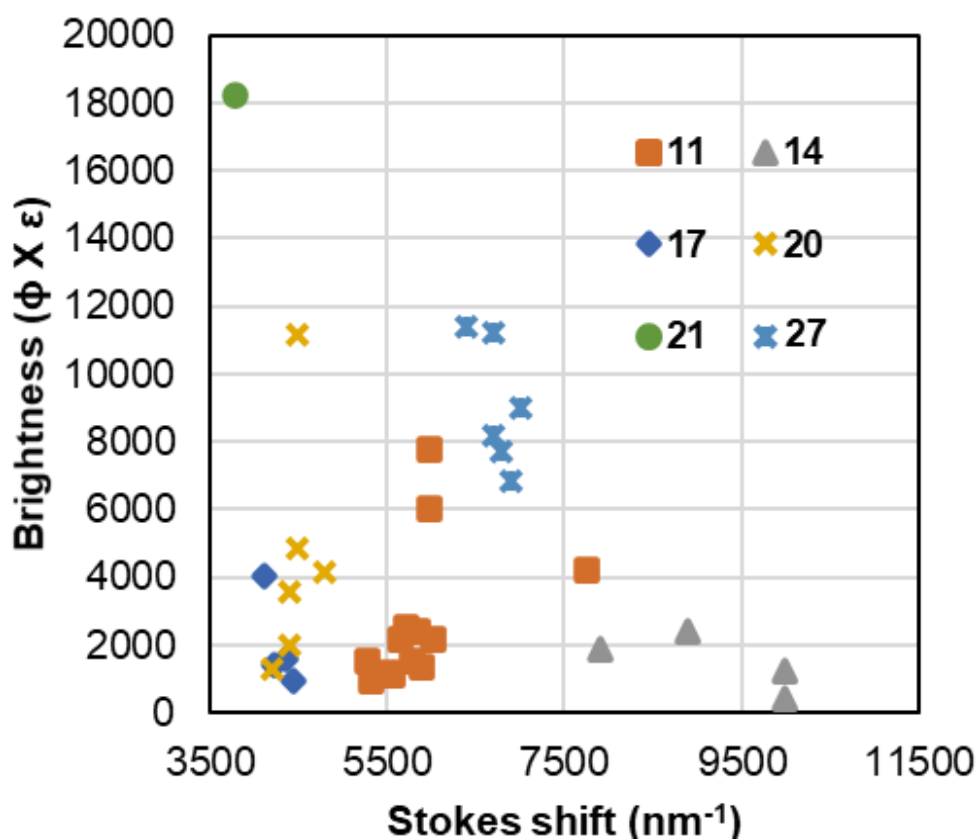


Figure 1.6 Comparison of all measured Stokes shifts and brightnesses.

1.5.2 Molecular Structures

An advantage of the PN-heterocycles is their high crystallinity, thus making it relatively easy to obtain molecular structures via single-crystal X-ray diffraction. Figure 1.7 shows archetypical structures for the imidate (e.g., **9**) and amidate (e.g., **10**) forms. Based on the bond lengths of the 17 structures obtained to date, the aromatic rings in the backbone as well as the pendent aryl rings on the heterocycles behave as true aromatics with bond lengths ranging from 1.38–1.40 Å. Within the PN-heterocyclic rings, the C=C double bonds are best described as isolated double bonds with bond lengths around 1.34–1.36 Å. The P–C and N–C bond lengths are also tightly clustered in the range of 1.76–1.79 Å and 1.38–1.40 Å, respectively. The greatest difference is the P–N bond length, which changes from 1.55–1.56 Å in **7** and **9j** (the only two imidate structures we have secured) to a range of 1.63–1.65 Å in the amidate form (where we have data for over a dozen structures). All of the structures show that the PN-heterocyclic rings have only small deviations from planarity. The dihedral angles between the heterocyclic cores and the pendent aryl rings varying from as little as 2° up to ca. 45°, which indicates very good to excellent communication between the two π -systems.

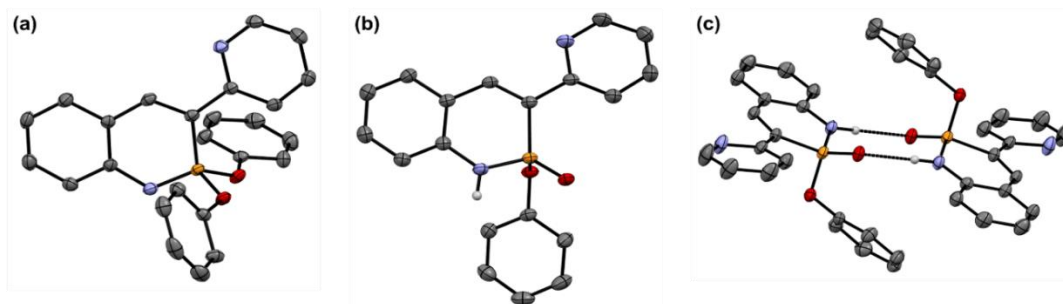


Figure 1.7 Single crystal structures of (a) **9j**, (b) **10j** monomer, and (c) **10j-10j** dimer as representative structures for typical **9** and **10/11** structures. Ellipsoids drawn at 30% probability. Non-hydrogen bonding hydrogen atoms omitted for clarity.

A hallmark characteristic of the amidate structures is dimerization in the solid state due to the adjacency of the P=O hydrogen-bond acceptor and the N–H hydrogen-bond donor. This permits nearly all of the amidates to form strong centrosymmetric, head-to-tail *meso*-dimers between one *R* and one *S* enantiomer with N–H···O bond lengths ranging from 2.77–2.82 Å (Figure 1.7, c). The tetrahedral phosphorus centers give the dimer a pseudo-eight membered chair arrangement connected by the two head to-tail N–H···(O)P hydrogen bonds. Interestingly, a decrease in the N–H···O bond lengths is observed when more withdrawing substituents are appended to the scaffold. These two factors hinted that there may be substituent effects in the solution-state dimer strengths as well (*vide infra*). The two exceptions to this common dimeric orientation involve sterically congested derivatives such as **11f**, where a staggered, ‘polymeric’ supramolecular system forms in which a single monomer hydrogen bonds to two separate monomers rather than forming the normal head-to-tail dimer.

1.5.3 Solution Dimerization Studies

Another series of studies performed on these scaffolds has been examination of substituent effects in the solution dimerization affinities of these compounds. To measure these dimerization strengths, we used variable-concentration (VC) ¹H NMR spectroscopy experiments followed by subsequent data fitting using nonlinear regression analysis to measure the dimerization strengths of each heterocycle.⁸⁸ Though more polar solvents, including DMSO and CH₃CN, destroy the dimer and/or permit limited solubility, H₂O-saturated CHCl₃ allowed us to collect consistent measurements across a range of similar compounds.

First, we performed these measurements upon heterocycles **11** as well as heterocycles **10b**, **10e**, and **10g** (Table 1.5). With these values, alongside the previously reported value of 130 M^{-1} for **10b**, we determined linear free energy relationships (LFERs) for substituent effects at both C3 and C6. In these, we found that withdrawing groups at either end of the backbone led to an increase in dimer strength, as shown by the two representative linear free energy relationship plots (Figure 1.8).

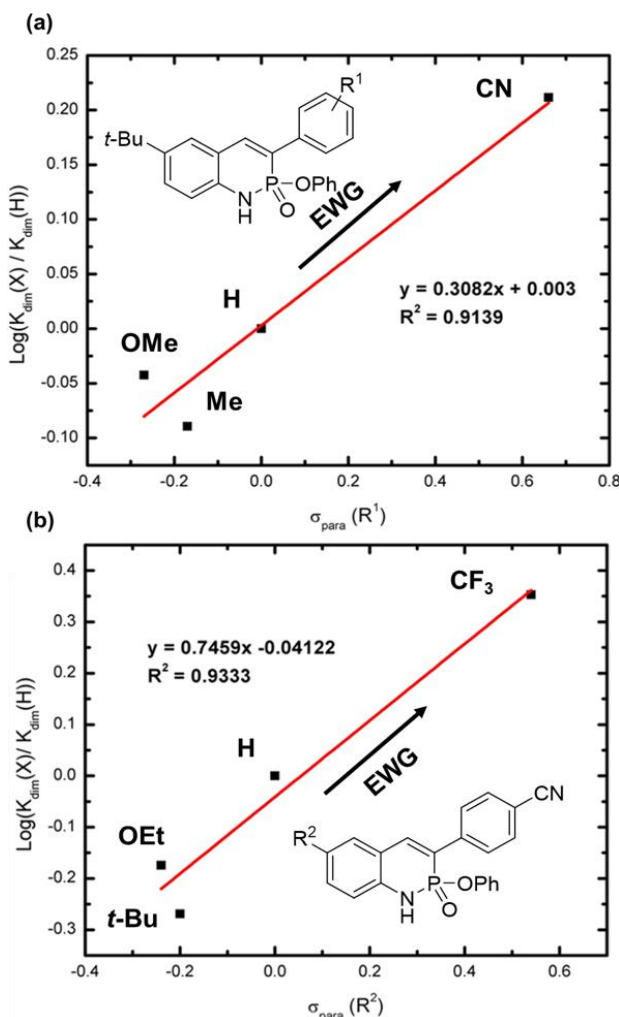


Figure 1.8 Representative LFER plots for dimerization strengths of heterocycles (a) **11d-11g** and (b) **10b, 11b, 11d, and 11m**.

Table 1.5 Dimerization strengths of select examples of heterocycles **10**, **11**, **17**, **20**, **21**, and **27**

Entry	$K_{\text{dim}} (\text{M}^{-1})^a$	Entry	$K_{\text{dim}} (\text{M}^{-1})^a$	Entry	$K_{\text{dim}} (\text{M}^{-1})^a$
10b	130	11l	200	20e	84
10e	62	11m	87	20f	77
10g	56	17a	206	21	179
11b	293	17b	150	27b	82
11d	70	17c	146	27c	54
11e	36	17d	121	27d	24
11f	38	20b	306	27e	22

^aValues collected in H₂O-saturated CDCl₃ at room temperature. Values reported with errors less than 15%.

Additionally, we determined that the R² substituents had a larger effect upon the dimer strength than analogous R¹ substituents, likely due to their proximity to the phosphaquinolone hydrogen. Within this series of derivatives, we determined a dimerization constant of 525 M⁻¹ for heterocycle **11j**, which is among the highest reported value for similar head-to-tail hydrogen-bonding dimers.⁸⁹

These findings prompted more questions. Why are these dimers so strong? Why do they prefer to dimerize as *meso*-dimers between *R* and *S* enantiomers? Are there any predictive trends similar to those observed for the emission energy? For answers, we turned to our collaborators 50 miles up the road from us at Oregon State University, the P. H.-Y. Cheong group. In Cheong's group, graduate student Camille Richardson performed an extensive amount of modeling of our systems and came to a few important conclusions. First, she found that there is likely a stereoelectronic effect aiding both the strength of our dimers as well as directing them to form dimers in the *meso*-dimer orientation. She also determined that there was indeed a linear relationship that could be used to predict the

strengths of each derivative based on the Hammett parameters of the two substituent groups.

Though solubility limited our ability to measure dimerization values for PN-anthracenes **14**, we determined dimerization strengths for nearly all other π -extended PN derivatives (Table 1.5), obtaining dimerization values from 121–206 M⁻¹ for **17**, 77–306 M⁻¹ for **20**, and 179 M⁻¹ for **21**. For PN-phenanthrenes **20**, Chun-Lin performed electrostatic potential (ESP) mapping, dipole calculations, and noncovalent interaction (NCI) plots to help explain the strengths and orientations of the dimers. The ESP maps showed that the N–H and P=O were the most electron-poor and electron-rich sites upon the scaffold, respectively. When dimerized, these two sites interact, which leads to a cancelling of the net dipole of the two monomers while in the *R-S meso*-dimer form. When looking at the analogous *S-S* dimer, less cancelling of the net dipole exists, and hugely repulsive domains are seen between the two adjacent –OPh groups of each monomer.

The dimerization constants of the P-phenyl heterocycles **27** (Table 1.5) range from 22–82 M⁻¹, which are roughly three times weaker than the analogous P-phenoxy heterocycles **10** or **11**. To explain this, we again turned to NCI analysis, as well as natural bonding orbital (NBO) analysis. When comparing the NCI plots of analogous **11** and **27** derivatives, a larger repulsive interaction between the phenyl ring of one monomer and the backbone of the other monomer is seen in **27** compared to the phenoxy in **11**. Additionally, a stronger interaction is observed within the NBO plot between the n_o of the P=O moiety of one monomer and the π^*_{N-H} of the other in **11** when compared to **27**.

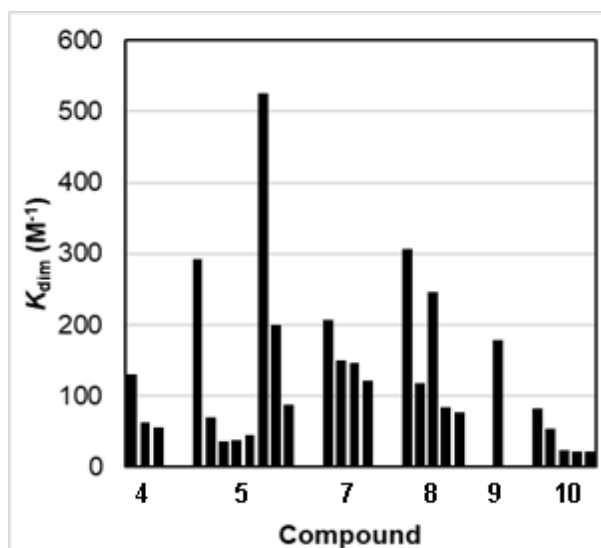


Figure 1.9 Comparison of all collected phosphaquinolone dimerization strengths.

With all these derivatives, we can achieve very strong and self-specific dimer formation with the phosphaquinolone moiety. A subtle interplay between sterics and electronics gives us many potential pathways to improve, modify, and tune the strengths of our dimers. The P-phenoxy families serve as more stable hydrogen bond dimers than the P-phenyl family, and we discovered that even the bulkier PN-phenanthrenes **17** and **20** can rival some of the strongest PN-naphthalene **11** dimer strengths (Figure 1.9).

1.6 Applying What We Have Learned

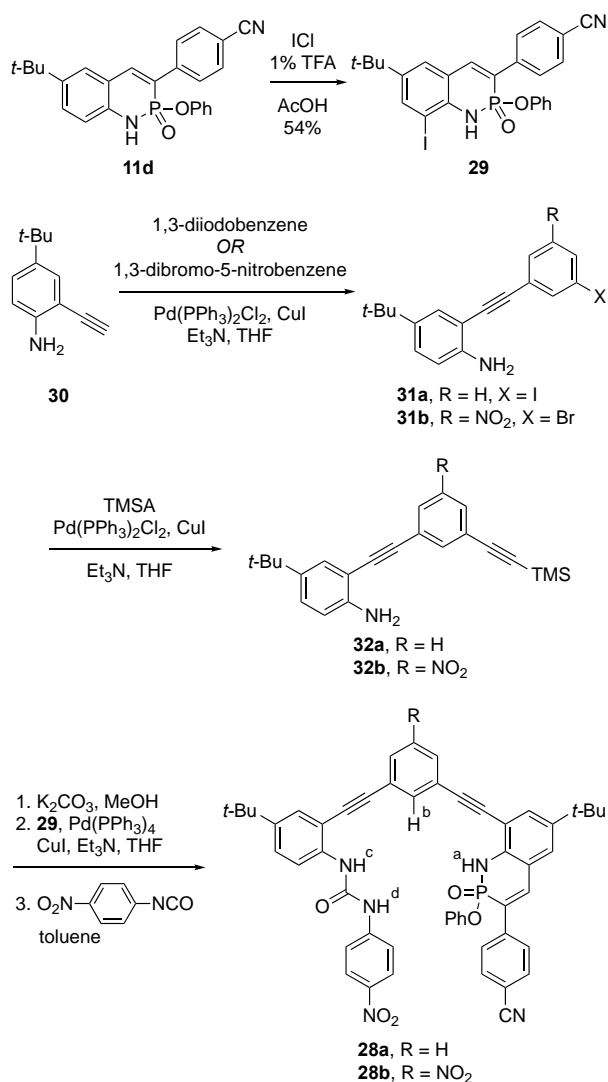
1.6.1 Development of Supramolecular Host

With the breadth of fundamental studies now in hand, we were finally ready to apply what we had learned. Through some careful design, thoughtful choice of substituent groups for the PN moiety guided by Jeremy's results, and many, many chromatography columns, Chun-Lin developed a two-armed host framework containing both PN-heterocycle and urea arms (**28** in Scheme 1.6).⁹⁰ The design of this unsymmetrical host featuring one urea 'arm' was critical: preliminary studies of bifunctional PN-compounds

showed that the molecules had too strong a tendency to form hydrogen-bonded polymers rather than serve as monomeric hosts for other molecular guests (a tendency that might be attractive in its own right to researchers in supramolecular polymers). The synthetic design for these ‘hybrid hosts’ started with iodination of **11d** with ICl to afford iodinated PN coupling partner **29** (Scheme 1.6). The other coupling partner was built via sequential Sonogashira cross-coupling reactions starting with terminal acetylene **30** and the respective dihalobenzene to give asymmetric intermediates **31**. Anilines **31** were then coupled with trimethylsilylacetylene (TMSA) to afford **32**. Finally, desilylation in basic MeOH, cross-coupling with **29**, and condensation with an isocyanate furnished hybrid hosts **28**.

Based on some simple geometric models, we believed that **28** would possess an excellent binding pocket for HSO_4^- due to the tetrahedral phosphorus center allowing for complementary numbers of hydrogen-bond donors and acceptors as well as a nonplanar binding pocket. Upon initial tests, we were excited to see significant peak shifts in the ^1H NMR and ^{31}P NMR spectra of the host upon treatment with TBAHSO₄ (Figure 1.10, bottom), from which we calculated a moderately strong association constant of 9600 M^{-1} in 10% DMSO-*d*₆ in CDCl₃. This result became even more exciting when we ran similar experiments with several other similar anionic guests, and none showed significant shifting of the phosphaquinolone N–H signal (H^a) (Figure 1.10).

Chun-Lin quickly assembled a manuscript with these results yet missing was one essential piece of data – an Xray structure of the host–guest complex. After hundreds of attempts and ‘one more try’ being said to the bosses countless times, Chun-Lin finally succeeded in growing single crystals suitable for X-ray crystallography, which clearly confirmed our design hypothesis.



Scheme 1.6 Synthesis of hybrid hosts **28**. Relevant protons on **28** labeled for identification purposes for Figure 1.10.

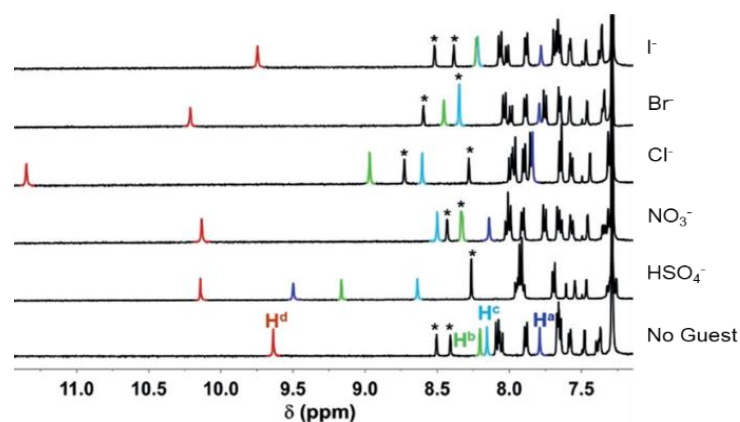


Figure 1.10 Partial ^1H NMR spectra of a 1.13 mM solution of **28b** in 10% $\text{DMSO-}d_6$ in CDCl_3 by itself and in the presence of 10 equiv. of each guest.

The structure showed seven hydrogen-bonding interactions between the host and the guest (Figure 1.11) and provided an ideal binding pocket for this highly acidic protic oxoanion.

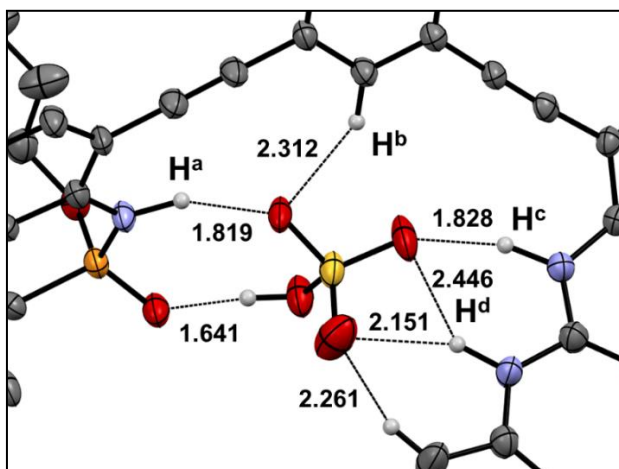


Figure 1.11 Coordination environment of HSO_4^- in the binding pocket of **28b** in the solid state. Ellipsoids drawn at 30% probability. Non-hydrogen bonding hydrogens omitted for clarity.

In addition to this nearly ideal geometric complementarity, the host exhibited reversible binding of HSO_4^- as well. Upon simple liquid–liquid extraction conditions with sulfuric acid solutions, we observed that our host both survived and bound a significant amount of HSO_4^- . After extraction, water washing of the organic layer of the host–guest complex showed a complete reversal of binding of the HSO_4^- guest and complete recovery of the host. This also highlights one unusual feature of this class of compounds for molecule and ion recognition: the PN unit, while slightly acidic itself, is quite robust in acid and can enable binding of highly acidic guests. The P=O hydrogen-bond acceptor motif is particularly privileged for this attribute, as it is an excellent hydrogen-bond acceptor while paradoxically being a poor base ($\text{p}K_{\text{aH}^+} \ll 0$).

1.6.2 Use of PN Moiety as an Impressive Fluorophore

Taking advantage of all we had learned about the fluorescence of these heterocycles, Chun-Lin developed the π -extended tricyclic PN-pyrenes **33** (Scheme 1.7).⁹¹ Starting from aminopyrenes **34**, cyclization with PhP(OPh)₂ and subsequent iodination furnished intermediates **35**. Lastly, Sonogashira cross-coupling accompanied by Pd-mediated indole formation gave **33a–d**. As this system includes the P-phenyl modification seen in **27**, the increased π -system of **21**, and the appropriate placement of substituent groups guided by our previous studies, we were able to access improved photophysical properties (large Stokes shifts, high brightness, and redshifted emission; Table 1.6) With these compounds we achieved both emission wavelengths up to 622 nm as well as the highest brightness values we have measured for the phosphaquinolone moiety (9700–22000 cm⁻¹M⁻¹). Through a series of computations that modeled the geometries and interactions in the excited state and spectroscopic experiments, we deduced that this was due to an increase in planarity upon excitation, as well as a suppression of any excimer formation. Additionally, we found that using a mixture of **33a**, **33c**, and **33d** we were able to produce nearly perfect white light emission in solution (Figure 1.12).

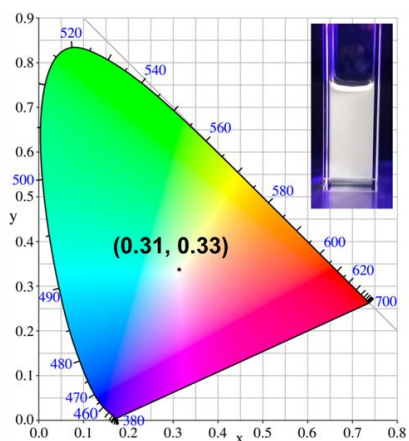
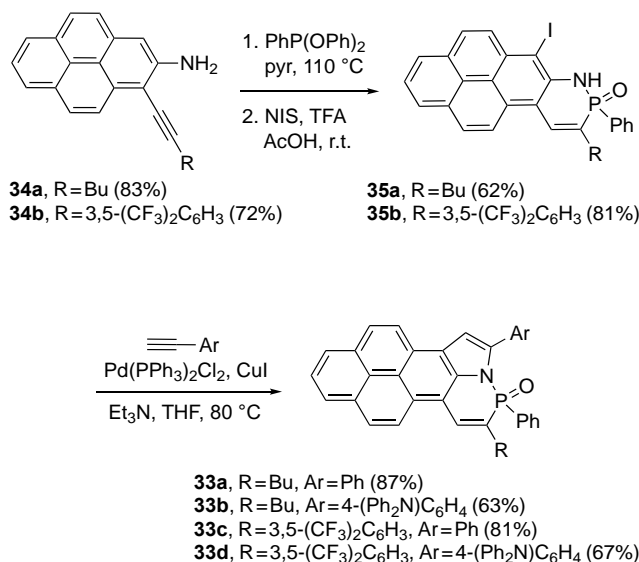


Figure 1.12 Emission color coordinates in the CIE 1931 chromaticity diagram of a 2:1:10 v:v:v mixture of **33a:33c:33d** excited at 430 nm.



Scheme 1.7 Synthesis of 3-ring PN pyrenes **33**.

Table 1.6 Photophysical properties of 3-ring PN pyrene derivatives **33**^a

Entry	λ_{abs} (nm), ϵ (M ⁻¹ cm ⁻¹)	λ_{em} (nm), ϕ (%) ^b	Stokes shift (nm/cm ⁻¹)	Brightness ($\epsilon \times \phi$)
33a	430, 38000	459, 57	29/1500	22000
33b	431, 32000	551, 62	120/5100	20000
33c	450, 32000	521, 61	71/3000	19000
33d	437, 42000	622, 23	185/6800	9700

^aValues collected in CHCl₃ at room temperature. ^bExcited at 365 nm and collected using a quinine sulfate (in 0.1 M H₂SO₄) standard.

7 Conclusions and Outlook

In the first three years of this new project, it went through quite a rollercoaster ride – as many projects do – that might have derailed it had it not been for the tenacity of Jeremy and Chun-Lin. The project went from an exciting accidental discovery, to something that had great potential during a period of research staff turnover, to a project which was slated for termination. However, over the last 18 months, a new light has shined on this

fluorophore class (or was it emitted?) through both fundamental studies and initial application-based projects. After a middle of the night stay of execution, what does this new metaphorical morning hold for this project?

With all we have learned from our original studies, and the variety of skills, instruments, and connections under the project's toolbelt, new directions are not lacking. We think some of the unusual properties of this receptor will enable new applications: the receptor is a fluorophore highly stable in acidic media, it has a strong hydrogen-bond donor adjacent to a powerful yet non basic hydrogen-bond acceptor, and the composition of matter is new while maintaining similarities to venerable compound classes of use in chemical biology, medicine, and supramolecular polymers among others. Work is currently underway looking for how this new recognition motif might target other oxoanionic guests, including phosphates due to their relevance in many areas. Additionally, perhaps following inspiration from D.W.J.'s academic family, work into utilization of this unusually strong dimer-forming moiety in a supramolecular capsule system is under consideration. Finally, with what we know about functionalizing this fluorophore, either through post synthetic modification or careful derivatization from the beginning, integration into both biological and other imaging applications might be around the corner.

CHAPTER II

SYNTHESIS, PHOTOPHYSICAL PROPERTIES, AND SELF-DIMERIZATION STUDIES OF 2- λ^5 -PHOSPHAQUINOLIN-2-ONES

This chapter includes previously published and co-authored material from Bard, J.P., Deng, C.-L., Richardson, H.C., Odulio, J.M., Barker, J.E., Zakharov, L.N., Cheong, P.H.-Y., Johnson, D.W., Haley, M.M. “Synthesis, Photophysical, and Dimerization Properties of 2- λ^5 -Phosphaquinolin-2-ones.” *Org. Chem. Front.* **2019**, *6*, 1257–1265. This a was written by Jeremy P Bard with editorial support was given by Michael. M. Haley and Darren W. Johnson. Experimental support was given by Chun-Lin Deng, Jacob M. Odulio, and Joshua E. Barker and computational support was supplied by H. Camille Richardson and Paul. H.-Y. Cheong. This chapter highlights one of the earliest structure-property relationship studies upon the phosphaquinolinone scaffold.

2.1 Introduction

The coumarin (2*H*-1-benzopyran-2-one) scaffold¹⁻⁷ along with its aza-analogue carbostyryl (2(1*H*)-quinolinone)⁸⁻¹³ comprise a fascinating class of compounds. In addition to marked physiological activity,^{14,15} the coumarin/carbostyryl framework has been widely established as one of the most useful small molecule fluorophores (Figure 2.1). With respectable Stokes shifts and quantum yields as well as good chemical stability, this scaffold and its derivatives have been the subject of a plethora of studies and applications.¹⁶⁻¹⁸ The variety of derivatization for both molecules is impressive, as a

multitude of substituents can be installed on the frameworks. Nonetheless, there are very few examples of modification of the base heterocyclic skeletons themselves, limiting the applications and functionalities to the lactone/lactam cores. Judicious modification of the backbone could afford a wealth of new derivatives whose improved and modified properties would allow for further applicability of these molecules.

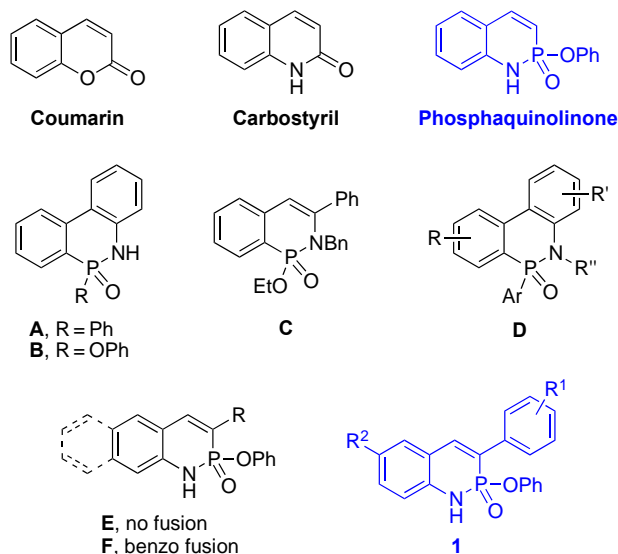


Figure 2.1 Coumarin and two congeners, carbostyryl and phosphaquinolinone, along with known phosphoramidates **A–F**.

One such modification could be replacement of the carbonyl moiety (C=O) with an isolobal P(OR)=O group to yield a “phosphaquinolinone”. While such six-membered heterocycles containing adjacent phosphorus and nitrogen (PN) atoms have been known since 1960 (phosphoramidate **A**, phosphonamidate **B**),^{19,20} their syntheses and isolation were often plagued by various challenges. More recent work has examined metal-mediated routes to phosphoramidates such as **C**.^{21–25} A family of structurally related phosphoramidates (*e.g.*, **D**) has also been investigated as a route to chiral phosphines.^{26–29} Further, a similar five-membered phosphoramidate system has recently been reported showing uniquely

flexible dimerization properties favourable for self-assembled soft materials.³⁰ Despite the recent revival in interest, structures that encompass such six-membered PN-heterocyclic motifs are rather uncommon.

To help address this issue, we recently reported a series of water- and air-stable phosphoramidates based on scaffold **E**.³¹ Along with the benzo-fused analogues **F**,³² this class of heterocycles is fluorescent, with electron withdrawing groups (EWG) at R leading to a red-shifted emission and electron donating groups (EDG) furnishing a blue-shifted emission. Additionally, the strong polarization of the oxygen in the hydrogen bond accepting P=O unit and the adjacent acidic N–H hydrogen bond donor lead to surprisingly strong dimerization between the *R* and *S* enantiomers (*meso*-dimer), potentially due to a minimization of repulsive secondary interactions. Though these properties are both intriguing and give promise for unique applications of this PN scaffold, a more detailed, systematic understanding of their fundamental structure-property relationships must be acquired first before any applications can be pursued. Herein we present the synthesis, optoelectronic properties, computational examination, and dimerization studies both in solution and in the solid state of a series of phosphoquinolinones based on phosphoramidate **1**.

We have dedicated this manuscript to Prof Julius Rebek, Jr. for his mentorship, friendship, and tremendous achievements in molecular recognition, self-replicating systems, tests for reactive intermediates, self-assembly, and hydrogen bonding, among many other areas. Therefore, we would be remiss not to point out that one of us (DWJ) learned of the strength of simple homo- and hetero-dimers of cyclic ureas, lactams, and cyclic sulfamides from, first, Rebek's report of a tetrameric hydrogen bonded capsule

assembled through strong, complementary hydrogen bonds between cyclic ureas and sulfamides;³³ and, second, from Prof. Rebek's class on molecular recognition at The Scripps Research Institute. In these studies, Rebek and coworkers discovered that heterodimers between simple model cyclic ureas and sulfamides were stronger than their homodimers.³³ Subsequent studies by Fraser Hof in the lab revealed the homodimer association constants ranged from 0.7 – 1.1 M⁻¹ and the heterodimer was almost two orders of magnitude more stable (K_a of 50 M⁻¹) in CD₂Cl₂.³⁴ Zimmerman and coworkers later performed an incredible service to this field by providing a survey of hundreds of such simple hydrogen bonded dimers.³⁵ These studies revealed a similar range for association constants in simple DA-AD hydrogen bonded systems in nonpolar solvents, underscoring the magnitude of association constants of upwards of 500 M⁻¹ in the compounds of class **1** (c.f. Table 2.3).

2.2 Results and Discussion

2.2.1 Synthesis

To modify the electron distribution on the six-membered PN heterocyclic core effectively, atomic coefficients analysis of the frontier molecular orbitals (FMOs) was performed on the unsubstituted PN-skeleton (Figure 2.2). The results show that carbon 3, on which the R¹-substituted aryl ring resides, has a higher contribution to the LUMO. In contrast, carbon 6 shows a higher contribution to the HOMO occupancy levels. These results suggest that an EDG on C6 would efficiently raise the energy level of the HOMO, while an EWG on C3 would readily lower the energy level of the LUMO.³⁶⁻³⁸ This should lead to a typical donor-acceptor (D-A) system and thus will likely push emission to longer wavelengths, in analogy to the well-established design principles for carbostyryl

fluorophore development to further red-shift emission and increase the quantum yield.^{10,13}

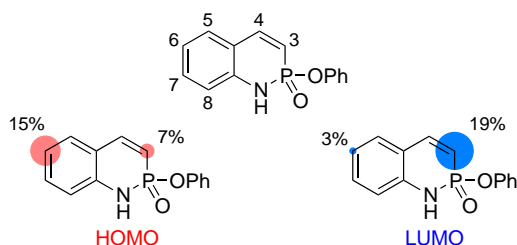
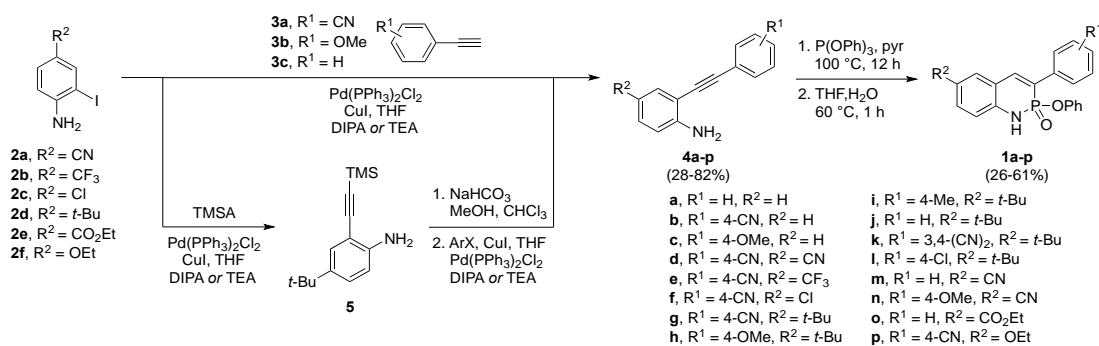


Figure 2.2 Atomic contributions (calculated at B3LYP/6-31g(d) level of theory) to the HOMO (left) and LUMO (right) electron densities of the unsubstituted PN-heterocycle core and numbering order for core carbons (middle). Atomic contributions are shown only for the readily functionalizable positions.



Scheme 2.1 General synthetic pathway for disubstituted PN heterocycles.

To test this hypothesis, a family of PN-heterocycles containing a variety of EWGs and EDGs on carbons 3 and 6 (**1a-1p**) were synthesized according to Scheme 2.1. Typically, readily accessible 2-iodoaniline derivatives **2**³⁹ were alkynylated with terminal arylacetylenes **3** via Sonogashira cross-coupling to form the requisite arylethynylaniline precursors **4**. Because of purification difficulties, compounds **4i-4l** were prepared by an alternate route. Starting from known aniline **5**,⁴⁰ desilylation and Sonogashira cross-coupling of the crude product with the respective aryl halide afforded the remaining arylethynylanilines **4i-4l**. Finally, precursors **4** were treated with P(OPh)₃ in pyridine for

12-48 h at 110 °C and subsequently hydrolyzed to furnish PN-heterocycles **1**. Yields of **1** range from 26-61%, and recrystallization from CHCl₃ and hexanes gave analytically pure product. Examination of the ¹H and ³¹P NMR spectra of **1** in CDCl₃ revealed a few interesting characteristics of this class of heterocycles. Specifically, the proton signal for the hydrogen attached to C4 shows up as a doublet with a relatively large coupling constant of *ca.* 40 Hz due to splitting by the phosphoramidate P. Additionally, the N–H proton shifts appear as a broad singlet within the 7-10 ppm range and the ³¹P shifts show up as a doublet (*J* = *ca.* 40 Hz) around 9-12 ppm; however, both signals shift somewhat as a function of concentration because of dimer formation in solution (*vide infra*; see Appendix A).

2.2.2 Photophysical Properties.

With compounds **1a-1o** in hand, their photophysical properties were measured and the results are summarized in Table 2.1. Based on the theoretical results above, one could expect that either withdrawing R¹ substituents or donating R² substituents would induce a red shift in the emission. In general, this hypothesis is corroborated by the absorption and emission properties of the designed families, where one group contains a withdrawing cyano group for R¹ and a variety of EDG and EWG for R² (Figures 2.3a and A.4, a), and the other contains a donating *tert*-butyl group for R² with a range of EDG and EWG for R¹ (Figures 2.3b and A.4, b). It is worth noting that the fluorescence behavior of the phosphaquinolines is similar to that of analogously substituted carbostyrils, though somewhat red-shifted. For example, 3-phenylcarbostyril absorbs at 345 nm, and emits at 410 nm, whereas **1a** absorbs at 354 nm and emits at 427 nm.¹³

Table 2.1 Photophysical properties for PN-heterocycles **1**^a

cmpd	R ¹	R ²	λ_{abs} (nm)	λ_{em} (nm)	Stokes	ϵ (cm ⁻¹ M ⁻¹)	ϕ (%) ^b	τ (ns) ^c
					Shift (nm/cm ⁻¹)			
1a	H	H	335	417	82/5869	13000	8	0.2
1b	4-CN	H	348	442	94/6112	22000	11	0.3
1c	4-OMe	H	340	411	71/5080	17000	7	0.2
1d	4-CN	CN	346	430	84/5646	12000	18	0.5
1e	4-CN	CF ₃	341	429	88/6015	20000	11	0.3
1f	4-CN	Cl	358	450	92/5710	23000	11	0.7
1g	4-CN	<i>t</i> -Bu	358	453	95/5858	22000	11	0.5
1h	4-OMe	<i>t</i> -Bu	344	421	77/5316	16000	6	0.3
1i	4-Me	<i>t</i> -Bu	343	424	81/5569	14000	8	0.3
1j	H	<i>t</i> -Bu	343	430	87/5899	17000	8	0.3
1k	3,4- (CN) ₂	<i>t</i> -Bu	371	477	106/5989	19000	41	1.9
1l	4-Cl	<i>t</i> -Bu	345	431	86/5784	19000	8	0.4
1m	H	CN	337	410	73/5283	12000	13	0.3
1n	4-OMe	CN	345	471	126/7754	15000	28	0.7
1o	H	CO ₂ Et	335	411	76/5519	12000	10	0.2
1p	4-CN	OEt	379	490	111/5977	25000	24	2.4

^a All measurements obtained at room temperature in CHCl₃. ^b Quantum yield measurements obtained with *ca.* 10⁻⁵ M solutions. ^c $\lambda_{\text{ex}} = 344$ nm; decay curves fitted to a monoexponential model.

In these two families, clear trends can be drawn between substituent group electronic character and the emission energy (Figure 2.3c), which are supported by further functional group orientations studied on both positions (Figure A.4).

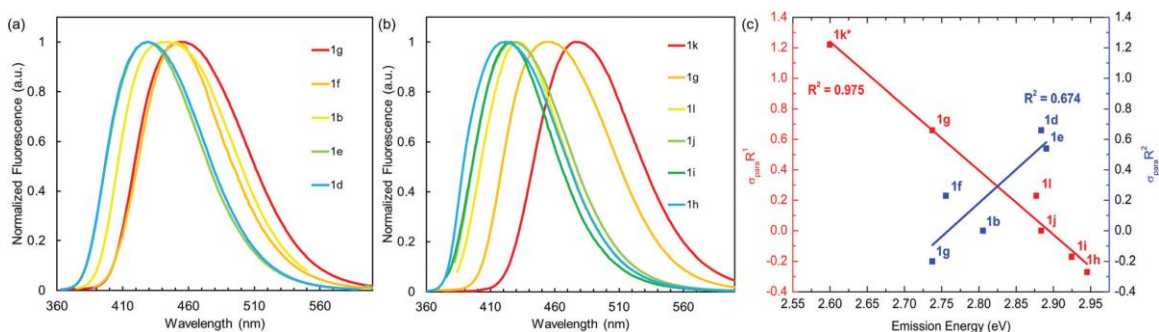


Figure 2.3 Emission spectra of a) heterocycles **1b**, **1d–1g** and b) heterocycles **1g–1l** as well as c) plot of trend between substituent electronic properties and emission energies of **1**. The σ value of **1k** was approximated by addition of the σ_{meta} and σ_{para} values of the two nitrile groups. All experimental values collected in CHCl_3 .

Though there is a linear trend between emission energies and the Hammett σ_{para} parameter⁴¹ on R^1 (red line in Figure 2.3c, $R^2 = 0.975$), the trend between emission energy and Hammett parameter on R^2 , though present, is not as clear (blue line in Figure 2.3c, $R^2 = 0.674$). These trends are exemplified when comparing emission wavelengths of **1k** (477 nm) and **1h** (421 nm) (Table 2.1), which contain a withdrawing 3,4-(CN)₂ moiety and a donating 4-OMe group, respectively.

To gain insight into these trends and correlate them to substituent effects on the electronic structures, density functional theory (DFT) calculations were performed on **1a–1p** (Table 2.2). Based on this data, there is indeed a substituent effect from groups on R^1 . The HOMO levels trend upwards with more donating groups, going from -6.89 (**1d**) to -6.43 eV (**1g**) (Table 2.2, Figure 2.4a), and the LUMO goes from -2.62 (**1k**) to -1.70 eV (**1h**) (Table 2.2, Figure 2.4b) with more withdrawing groups on R^1 . As shown in Figure 2.5, the FMOs of **1e–g** encompass the entire molecular systems, so the predominant transitions are $\pi \rightarrow \pi^*$ in nature.

Table 2.2 Orbital energy levels for **1a–1p** calculated at the PBE0/6-311G(d,p) level of theory

Cmpd	HOMO (eV)	LUMO (eV)	HOMO-LUMO Gap (eV)
1a	-6.40	-1.84	4.56
1b	-6.59	-2.28	4.31
1c	-6.08	-1.74	4.34
1d	-6.89	-2.50	4.39
1e	-6.83	-2.43	4.40
1f	-6.63	-2.41	4.22
1g	-6.43	-2.24	4.19
1h	-6.04	-1.70	4.34
1i	-6.22	-1.76	4.46
1j	-6.29	-1.81	4.48
1k	-6.58	-2.62	3.96
1l	-6.34	-1.91	4.43
1m	-6.69	-2.13	4.56
1n	-6.29	-2.03	4.26
1o	-6.55	-1.96	4.59
1p	-6.16	-2.27	3.89

TD-DFT was also performed to give a theoretical representation of the electronic transitions taking place (Figure 2.5). For each heterocycle, the $S_0 \rightarrow S_1$ transition is dominated by the HOMO \rightarrow LUMO transition, which is in good agreement with experimental absorption values (Table 2.1).

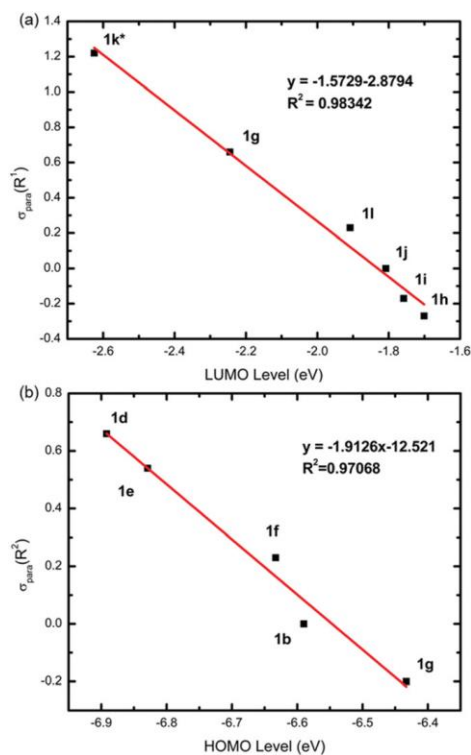


Figure 2.4 a) Calculated LUMO levels vs. Hammett parameter of R^1 substituents of $R^2 = t$ -Bu heterocycles **1** and b) calculated HOMO levels vs. Hammett parameter of R^2 substituents of $R^1 = \text{CN}$ heterocycles **1**. Orbital energy levels calculated at the PBE0/6-311G(d,p) level of theory. The σ value of **1k** was approximated by addition of the σ_{meta} and σ_{para} values of the two nitrile groups.

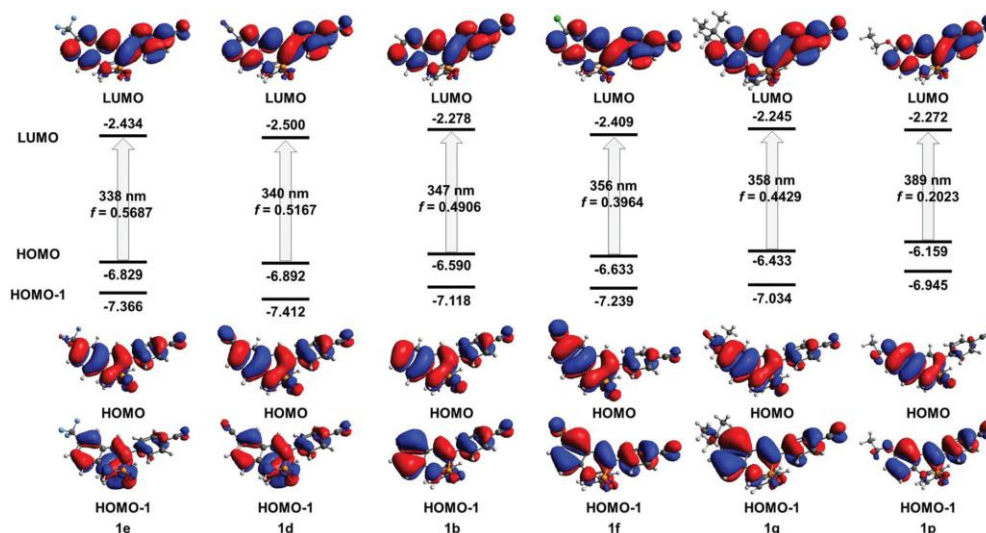


Figure 2.5 Orientation of most dominant electronic transitions and the corresponding orbitals for heterocycles **1b**, **1d–1g**, and **1p**; orbital energies in eV.

The second longest wavelength absorption (*ca.* 300 nm) is predominantly composed of the HOMO-1→LUMO transition and matches the experimental data for each heterocycle as well (Figure A.4). In an attempt to better understand the electrochemical nature of these orbitals cyclic voltammetry (CV) measurements were collected for a subset of heterocycles **1** (Figure A.22). While electrochemical gap values of *ca.* 4.0 eV could be determined, the poor behavior of the compounds upon measurement prevented accurate experimental determination of the HOMO and LUMO energy levels.

Comparison of the computed HOMO–LUMO energy gaps of **1** with the experimental emission energies (Figure 2.6a) showed that values are in very good agreement, such that the model should be able to predict emission energies accurately. To demonstrate this, we designed “optimized” heterocycle **1p** ($R^1 = 4\text{-CN}$ and $R^2 = \text{OEt}$), as the –OEt group can donate relatively strongly with a Hammett σ_{para} parameter of -0.24 and thus should afford a dramatically red-shifted emission. The HOMO (-6.16 eV) and LUMO (-2.27 eV) levels were calculated, yielding a HOMO–LUMO gap of 3.89 eV. Based on this value, and the trend given by the related heterocycles in Figure 2.6a, the predicted emission energy value for **1p** is 2.50 eV (496 nm). To validate this prediction, **1p** was prepared in a similar fashion shown in Scheme 2.1 starting from iodoaniline **2f**. Subsequent photophysical characterization showed $\lambda_{\text{em}} = 490$ nm ($\lambda_{\text{abs}} = 379$ nm, $\epsilon = 25000$ M $^{-1}$ cm $^{-1}$, $\phi = 24\%$, and $\tau = 2.4$ ns). This is in excellent agreement with the predicted value (Figure 2.6b), showing that the trend seen between emission and HOMO–LUMO energy gaps can be empirically used to predict the emission of this PN scaffold.

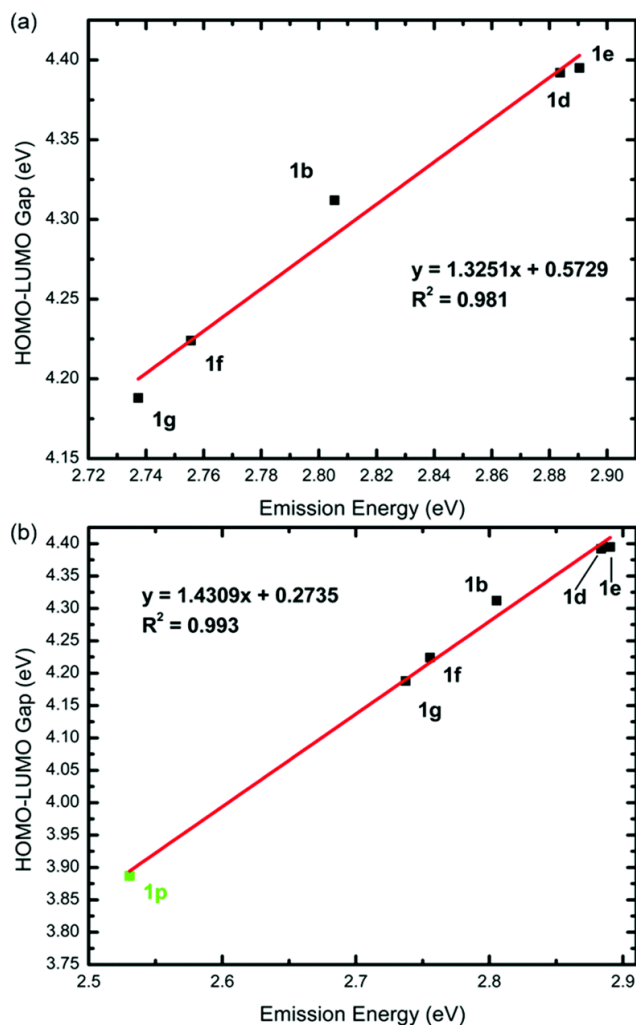


Figure 2.6 Correlation between calculated HOMO–LUMO energy gap levels *versus* experimental emission energies of (a) heterocycles **1b**, **1d–1g**, and (b) heterocycles **1b**, **1d–1g**, and **1p**.

2.2.3 Dimer Formation in Solution

In addition to studying the structure-property relationships between substituents and the photophysical aspects of heterocycles **1**, we have also investigated the effects that these substitutions have on the dimerization strengths. Based on the previously reported value of 130 M^{-1} for **1b**,³¹ and the role of the N-H hydrogen acting as the dominant hydrogen bonding unit, further polarization of the N-H bond should lead to even higher dimer strengths. Logic would follow that including various withdrawing groups upon the

scaffold should lead to this enhanced polarization. With these principles in mind, the dimer strengths of heterocycles **1** with a variety of EWG and EDG appended were studied using variable concentration (VC) NMR experiments in H₂O-saturated CDCl₃, with the results listed in Table 2.3 (see experimental section for measurement details).

Table 2.3 Dimerization constants (M⁻¹) of heterocycles **1** in H₂O-saturated CDCl₃^a

Entry	K_{dim}	Entry	K_{dim}
1a	62 ^b	1i	38 ^b
1b	130 ^c	1j	44
1c	56	1k	– ^d
1d	– ^d	1l	– ^d
1e	293	1m	525
1f	– ^d	1n	– ^d
1g	70	1o	200
1h	36	1p	87

^a All values $\pm 10\%$. ^b ³¹P NMR signal tracked concomitantly to give 65 M⁻¹ for **1a** and 41 M⁻¹ for **1i**, which agree well with the respective ¹H NMR values. ^c Previously reported in ref. 31. ^d Not measurable due to low solubility.

Once the data is organized into families sharing either a similar R¹ or R² group, the resultant two LFERs (Figures 2.7a and 2.7b) show that more withdrawing groups upon either R¹ or R² lead to stronger dimer formation. Notably, the strength changes over 2.5 times as much with varying σ_{para} of the substituents on R² than it does for R¹ based on the slope of the trends, showing the R² position is more sensitive to influencing dimerization strength. This is best illustrated when comparing heterocycles **1b** and **1m**, which have a nitrile group in place of R¹ and R², respectively. Installing the cyano unit on the *para* position with respect to the N–H in **1m** likely causes a much greater polarization, leading to a vastly increased dimer strength of 525 M⁻¹. To our knowledge, this value exceeds any previously reported for similar D–A dimer systems.³⁵

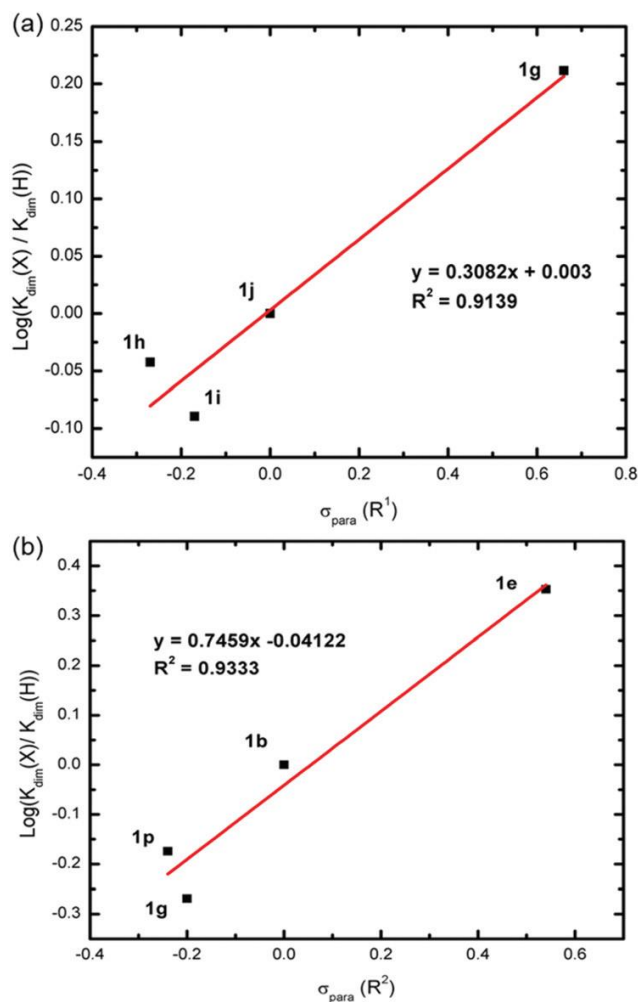


Figure 2.7 Positive trends between EWG on a) R¹ and b) R² with dimerization constants of **1**.

To better understand the nature of this dimerization, ΔG values (ΔG_{calc}) were calculated and compared to experimental values (ΔG_{exp}) (Table 2.4). While the computed ΔG_{calc} values are very similar to the ΔG_{exp} values, the trends do not track in all cases. The ΔG_{exp} values are incredibly close to each other, making it difficult to precisely match computationally. Interestingly, the gas phase free energies matched experimental trends more closely (Table A.17), with several additional computational methods explored (see Appendix A).

Table 2.4 ΔG_{calc} and ΔG_{exp} values of heterocycles **1**^a

Entry	ΔG_{calc}	ΔG_{exp}
1g	-3.1	-2.5
1b	-2.1	-2.9
1e	-2.4	-3.4
1p	-1.6	-2.6
1j	-2.2	-2.2
1m	-2.7	-3.7
1a	-3.3	-2.4
1o ^b	-2.6	-3.1
1h	-2.5	-2.1
1c	-2.5	-2.4

^a Optimization performed with PBE/6-31G(d); single points done at WB97X/6-311++G(2df,p). Solvation corrections done in CHCl₃ at PBE/6-31+G(d,p)/SMD. ^b CO₂Me ester substituent was used in place of the CO₂Et ester, which share very similar Hammett parameters, to lessen the computational load.

The models also show that the most stable dimer is always formed between one *R* and one *S* enantiomer because of stereoelectronic effects between phenoxy groups on each phosphorus center, corroborating the crystal packing structures reported in this paper (Figures 2.8, A.1-A.3 and A.6) as well as those of previous studies.^{31,32} In the heterodimer, the phenoxy oxygen lone pairs can donate into the P–O σ^* and P–N σ^* orbitals, which are stabilizing interactions (Figure 2.8a). In the homodimer only one phenoxy oxygen can be in the correct orientation to donate into the P–O σ^* and P–N σ^* orbitals; the other one is rotated to avoid steric collision between the phenoxy groups (Figure 2.8b). The rotated phenoxy group donates into the P–O σ^* and P–C σ^* orbitals, which are still stabilizing interactions, but less stabilizing than the lone pairs donating into the P–O σ^* and P–N σ^* orbitals. When the phenoxy groups are replaced with methoxy groups, there is no appreciable energy difference between the homodimer and heterodimer.

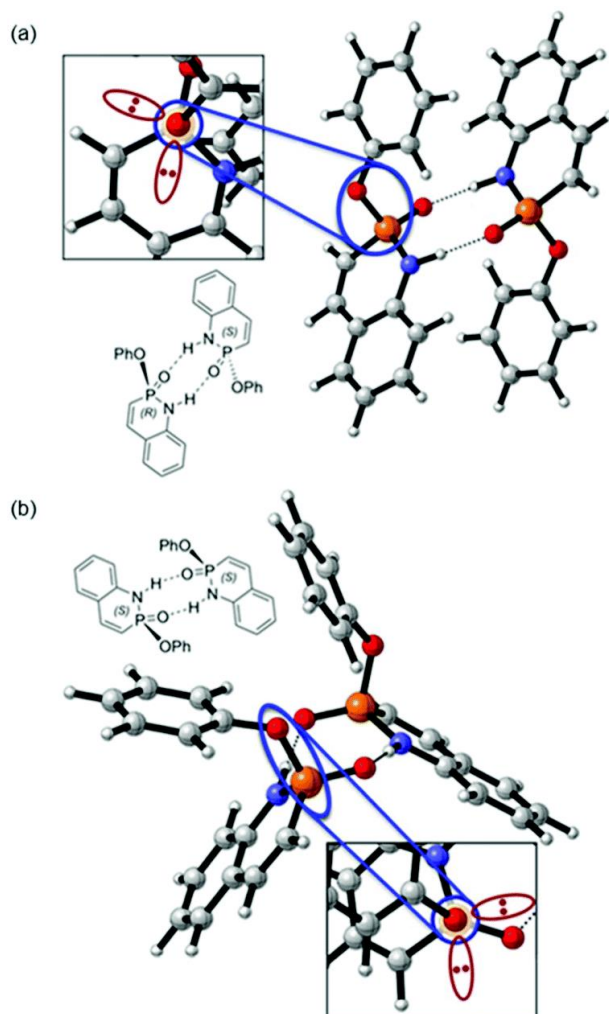


Figure 2.8 Schematic examples of (a) orbital overlap within monomer units in the R–S heterodimer structure and (b) poor alignment between orbitals within each monomer in the S–S homodimer structure, where the phenoxy oxygen lone pairs are represented in red and align with the P–O σ^* and P–N σ^* orbitals and the P–O σ^* and P–C σ^* orbitals, respectively.

Using a multiple linear regression model in R,^{42–44} the ΔG_{exp} values were plotted as a function of the σ_{para} values of both the R¹ and R² groups, giving a method for the prediction of the strength of a dimer with any combination of R¹ and R² substituent groups on any similar phosphorane molecule (Equation 2.1). Two values were excluded from the initial model and used as a validation set to verify the predictive ability of the model (Figure 2.9, Table A.18).

$$\Delta G_{\text{Pred}} = -2.53989 - 0.42865(\sigma_{\text{para}}R^1) - 1.42686(\sigma_{\text{para}}R^2)$$

Equation 2.1 Relationship between substituent group Hammett parameters and predicted strength of dimerization for heterocycles **1**.

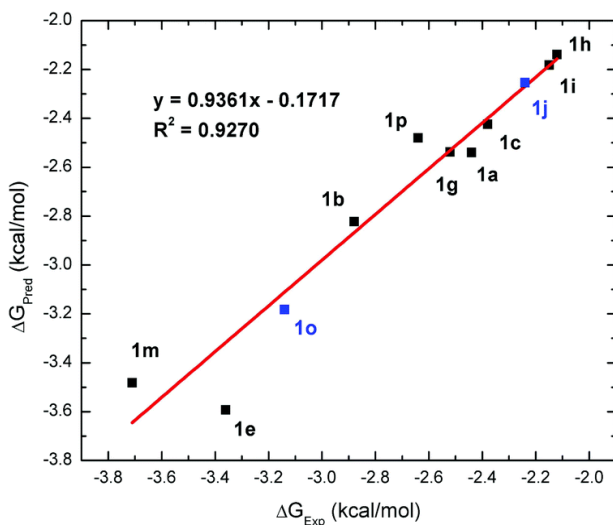


Figure 2.9 ΔG_{Exp} values versus ΔG_{Pred} . Blue data points were omitted from the initial model, and tested as a validation set of data, showing a good correlation to the model.

2.2.4 Dimer Formation in solid state

In an attempt to corroborate solution-state data for the strength of the hydrogen bonding interactions between **1** monomers with hydrogen bonding in the solid state, single crystals were grown by vapor diffusion of pentane into concentrated CHCl_3 solutions of **1b**, **1c**, **1e**, **1g**, and **1m** (Figures 2.10 and A.1-A.3). In the solid-state structures, heterocycles **1b**, **1c**, and **1m** crystalize as the previously observed^{31,32} *meso*-dimers discussed above (Figure 2.10a). Interestingly, both **1e** and **1g** instead form a staggered, repeating hydrogen bonding system, where the N–H and P=O moiety of each monomer coordinates with a different heterocycle, forming a continuous zigzag chain (Figure 2.10b). This alternative packing mode is likely due to steric interactions caused by the *t*-Bu and

the trifluoromethyl groups on **1e** and **1g**, respectively, thus likely inhibiting formation of the usual dimer structure in the solid state.

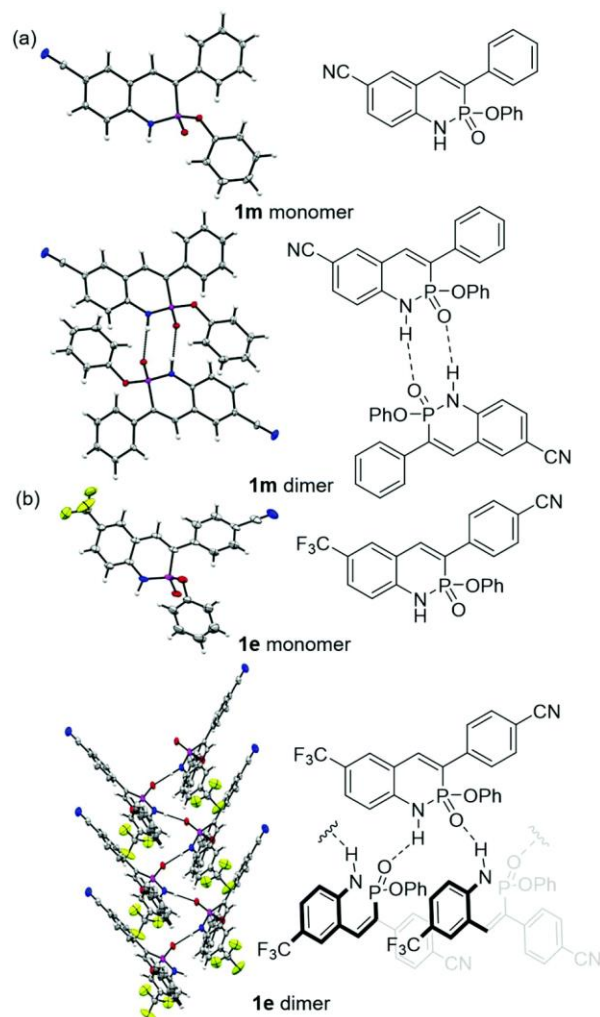


Figure 2.10 Solid-state structures of a) the monomer and dimer of **1m** and b) the monomer and staggered hydrogen bonding network of **1e**.

Regardless of the molecular packing, which can be influenced by various factors that do not affect the solution state, each structure shows the characteristic N–H•••O interactions of the phosphonamidate scaffold, distances that are summarized in Table 2.5. Compared to the respective solution state dimerization strength (Figure 2.11), the data is suggestive of a close relationship between the two, where the congeners with the higher

K_{dim} values indeed have shortened N–H•••O distances. Though there exist a multitude of factors that influence the solid state and the solution state separately, this relationship may hint toward potential guided design of these molecules as subunits in larger hydrogen-bonded systems.

Table 2.5 Solid state N•••O distances of selected heterocycles **1**

Entry	N•••O distance (Å)
1b	2.809(2)
1c	2.821(11)
1e	2.807(4)
1g	2.815(2)
1m	2.768(2)

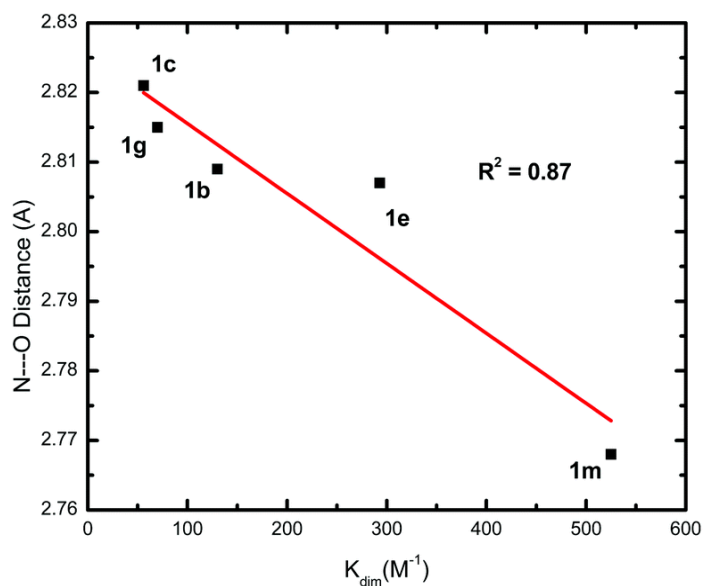


Figure 2.11 Solid-state N•••O distances plotted against solution state K_{dim} values measured in CDCl_3 .

2.3 Conclusions

In summary, we report an expedited synthesis of a unique PN heterocyclic scaffold, as well as studied the effects of substitution upon two sites. Specifically, the relationships between

calculated HOMO and LUMO levels of each derivative and the experimental emission characteristics were developed. The design principles learned from this correlation were then employed to synthesize another derivative with further red-shifted emission. In addition, we elucidated the nature of the very strong *meso*-dimers observed for these heterocycles by characterizing their solution state strengths as a function of substituent groups, comparing them with computed values, and correlating their solid-state N...O distances. The work described above addresses deficiencies in the knowledge about this new scaffold and provides both experimental and computational evidence towards current hypotheses surrounding them. This work will assist future guided design of this unique heterocycle for applications in chemosensing, anion sensing, and supramolecular materials, which we believe are worth additional exploration by us and hopefully others given the strong, complementary hydrogen bonding and emerging anion binding selectivity.⁴⁵

2.4 Experimental Section

General. All reactions requiring the lack of O₂ and H₂O were performed under an N₂ atmosphere using Schlenk technique. Column chromatography was performed using silica gel (240–300 mesh), with solvent systems being referenced to the most abundant solvent. NMR spectra were acquired at room temperature on a Varian Inova 500 (¹H: 500 MHz, ¹³C: 126 MHz, ¹⁹F: 471 MHz, ³¹P: 202 MHz) or a Bruker Avance III HD 500 equipped with a Prodigy multinuclear cryoprobe (¹H: 500 MHz, ¹³C: 126 MHz). ¹H and ¹³C chemical shifts (δ) are expressed in parts per million (ppm) relative to residual CHCl₃ shifts (¹H: 7.26 ppm, ¹³C: 77.16 ppm) or residual DMSO shifts (¹H: 2.50 ppm, ¹³C: 39.52 ppm). ³¹P NMR are referenced to 85% H₃PO₄ (δ 0 ppm) as an external reference, and ¹⁹F NMR are referenced to CFC₃ (δ 0 ppm) as an external standard. UV-vis spectra were recorded using

an Agilent Technologies Cary 60 UV-vis spectrophotometer in HPLC grade CHCl_3 . Fluorescence emission spectra were recorded using a Horiba Jobin Yvon FluoroMax-4 fluorimeter exciting at 365 nm. Quantum yields (ϕ) were determined through comparison of the emission and absorption intensities of the analyte to those of a 0.1M H_2SO_4 quinine sulfate.⁴⁶ Fluorescence lifetime measurements were recorded using a Horiba FluoroHub Single Photon Counting Controller with a TemPro Fluorescence Lifetime System attachment. High-resolution mass spectra (HRMS) were recorded on a Waters XEVO G2-XS mass spectrometer. CV measurements were collected using a Bio-Logic SP-50 potentiostat. Compounds **2a-2e**,³⁹ **4a-4c**,³¹ **1a-1c**,³¹ and **5**⁴⁰ were prepared as previously described.

General procedure for determination of solution-state dimerization strengths. CDCl_3 was mixed in a 1:1 ratio with H_2O , shaken vigorously, then allowed to separate. The organic phase was then separated and used to prepare *ca.* 20 μM solutions of heterocycle **1**. These solutions were then diluted through addition of known amounts of the CDCl_3 solvent, with NMR spectra being collected after each addition. The chemical shift of the N-H signal was tracked and fitted to generate the dimerization values.⁴⁷

General procedure for terminal acetylenes **3 or **5**'.** The TMS-protected variant of arylacetylene **3a-3b** (1.0 equiv.), or TMS-protected arylethynylaniline **5** (1.0 equiv.) when applicable, and NaCO_3 (3 equiv.) were dissolved in a 3:2 mixture of CHCl_3 :MeOH (0.06 M solution) and stirred for 3 hours. The solution was concentrated *in vacuo*, and the mixture was dissolved in CH_2Cl_2 before being added to a separatory funnel. The mixture was washed with deionized water (3x), dried (Na_2SO_4), filtered, and concentrated *in vacuo*

to yield the respective terminal acetylene **3** or **5'**. The crude material was immediately carried forward for the subsequent cross-coupling reaction.

General procedure for Sonogashira cross-coupling. Terminal arylacetylene **3** (1 equiv.), substituted iodoaniline **2** (1 equiv.), Pd(PPh₃)₂Cl₂ (0.1 equiv.), and CuI (0.1 equiv.) were added to THF (~0.14 M solution). For **4i-4l**, **3** and **2** were replaced by crude terminal arylethynylaniline **5'** (1 equiv.) and the appropriate haloarene (1 equiv.), respectively. The mixture was placed under an N₂ atmosphere and stirred for 10 min. DIPA or TEA was then added to achieve a 3:2 solvent to base ratio. The solution was stirred for 24-48 h before being filtered through silica gel and concentrated *in vacuo*. The crude material was then purified using column chromatography to give product **4**. Yields reported are the combined yields for respective deprotections of the arylacetylenes and the subsequent cross-coupling reactions.

General procedure for cyclizations. To a scintillation vial arylethynylaniline **4** (1 equiv.) and P(OPh)₃ (1.1–2.0 equiv.) were added and dissolved in pyridine (0.35 M). The vial was sealed and heated to 110 °C for 24-48 h. The mixture was then diluted with toluene, and the solvent was removed *in vacuo*. The crude material was redissolved in THF, and 5-10 drops of water were added. The solution was then heated at 60 °C for 1 h, before being dried (NaSO₄), filtered, and concentrated *in vacuo*. The crude mixture was then purified by column chromatography. Reported yields are listed for >95% pure product off the column, though all analyses were performed using solid that had been recrystallized from hexanes and CHCl₃ to a purity of at least 99% by NMR spectroscopy.

Iodoaniline 2f. In a round bottom flask, 4-amino-3-iodophenol⁴⁸ (782 mg, 3.3 mmol, 1.0 equiv.) and CsCO₃ (2.72 g, 8.3 mmol, 2.5 equiv.) were dissolved in DMF (18.5 mL) and

stirred at room temperature for 10 min. Using a syringe pump, EtI (468 mg, 3.0 mmol, 0.9 equiv.) in DMF (1.5 mL) was added to the solution over 6 h. After stirring an additional 48 h, the mixture was diluted with excess H₂O. The product was extracted using EtOAc and the organic layer was dried (Na₂SO₄), filtered, and concentrated *in vacuo* to obtain **2f** (443 mg, 51%) as a red-brown oil whose spectroscopic data matched those previously reported.⁴⁹

Arylethynylaniline 4d. Following the general Sonogashira procedure, iodoaniline **2a** (367 mg, 1.5 mmol, 1 equiv.), crude 4-ethynylbenzonitrile **3a** (191 mg, 1.5 mmol, 1 equiv.), Pd(PPh₃)₂Cl₂ (106 mg, 0.15 mmol, 0.1 equiv.), and CuI (29 mg, 0.15 mmol, 0.1 equiv.) were reacted for 48 h using DIPA as the base. Column chromatography (3:2 hexanes:EtOAc) afforded **4d** (201 mg, 55%) as a pale brown solid. ¹H NMR (500 MHz, CDCl₃) δ 7.70–7.59 (m, 5H), 7.41 (dd, *J* = 8.5, 2.0 Hz, 1H), 6.74 (d, *J* = 8.5 Hz, 1H), 4.79 (s, 2H). ¹³C NMR (126 MHz, CDCl₃) δ 151.22, 136.87, 134.09, 132.35, 132.16, 127.33, 119.16, 118.40, 114.45, 112.32, 107.16, 100.72, 94.46, 87.83. HRMS (ASAP) [M+H]⁺ calcd for C₁₆H₉N₃ 244.0875, found 244.0902.

Arylethynylaniline 4e. Following the general Sonogashira procedure, iodoaniline **2b** (1.01 g, 3.5 mmol, 1 equiv.), crude 4-ethynylbenzonitrile **3a** (445 mg, 3.5 mmol, 1 equiv.), Pd(PPh₃)₂Cl₂ (244 mg, 0.348 mmol, 0.1 equiv.), and CuI (66 mg, 0.348 mmol, 0.1 equiv.) were reacted for 48 h using DIPA as the base. Column chromatography (5:1 hexanes:EtOAc) afforded **4e** (282 mg, 28%) as a brick red solid. ¹H NMR (500 MHz, CDCl₃) δ 7.66 (d, *J* = 8.2 Hz, 2H), 7.63 (s, 1H), 7.61 (d, *J* = 8.3 Hz, 2H), 7.40 (dd, *J* = 8.5, 1.4 Hz, 1H), 6.77 (d, *J* = 8.6 Hz, 1H), 4.59 (s, 2H). ¹³C NMR (126 MHz, CDCl₃) δ 150.51, 132.32, 132.10, 130.02 (q, *J* = 4.0 Hz), 127.71, 127.57 (q, *J* = 3.6 Hz), 124.26 (q, *J* = 271

Hz), 120.25 (q, $J = 33.2$ Hz), 118.51, 114.15, 112.04, 106.43, 93.96, 88.98. ^{19}F NMR (471 MHz, CDCl_3) δ -61.60. HRMS (ASAP) $[\text{M}+\text{H}]^+$ calcd for $\text{C}_{16}\text{H}_9\text{F}_3\text{N}_2$ 287.0796, found 287.0829.

Arylethynylaniline 4f. Following the general Sonogashira procedure, iodoaniline **2c** (543 mg, 2.14 mmol, 1.0 equiv.), crude 4-ethynylbenzonitrile **3a** (272 mg, 2.14 mmol, 1 equiv.), $\text{Pd}(\text{PPh}_3)_2\text{Cl}_2$ (147 mg, 0.214 mmol, 0.10 equiv.), and CuI (40 mg, 0.214 mmol, 0.1 equiv.) were reacted for 24 h using TEA as the base. Column chromatography (5:1:1 hexanes:EtOAc: CH_2Cl_2) gave **4f** (329 mg, 61%) a dark orange solid. ^1H NMR (500 MHz, CDCl_3) δ 7.64 (dd, $J = 8.4, 2.1$ Hz, 2H), 7.59 (dd, $J = 8.4, 2.0$ Hz, 2H), 7.33 (s, 1H), 7.13 (d, $J = 8.7$ Hz, 1H), 6.67 (dd, $J = 8.8, 2.0$ Hz, 1H), 4.28 (s, 2H). ^{13}C NMR (126 MHz, CDCl_3) δ 146.79, 132.27, 132.05, 131.68, 130.76, 127.85, 122.57, 118.54, 115.83, 111.88, 108.16, 93.97, 89.28. HRMS (ASAP) $[\text{M}+\text{H}]^+$ calcd for $\text{C}_{15}\text{H}_9\text{ClN}_2$ 253.0533, found 253.0560.

Arylethynylaniline 4g. Following the general Sonogashira procedure, iodoaniline **2d** (414 mg, 1.5 mmol, 1 equiv.), crude 4-ethynylbenzonitrile **3a** (190 mg, 1.5 mmol, 1 equiv.), $\text{Pd}(\text{PPh}_3)_2\text{Cl}_2$ (105 mg, 0.15 mmol, 0.1 equiv.), and CuI (28.7 mg, 0.15 mmol, 0.1 equiv.) were reacted for 24 h using DIPA as the base. Column chromatography (4:1 hexanes:EtOAc) gave **4g** (201 mg, 49%) as a pale brown solid. ^1H NMR (500 MHz, CDCl_3) δ 7.62 (d, $J = 8.1$ Hz, 2H), 7.59 (d, $J = 8.1$ Hz, 2H), 7.37 (d, $J = 2.3$ Hz, 1H), 7.23 (dd, $J = 9.1, 2.7$ Hz, 1H), 6.70 (d, $J = 8.5$ Hz, 1H), 4.19 (s, 2H), 1.29 (s, 9H). ^{13}C NMR (126 MHz, CDCl_3) δ 145.87, 141.12, 132.14, 131.89, 128.93, 128.48, 128.22, 118.67, 114.64, 111.25, 106.34, 92.75, 91.40, 34.02, 31.45. HRMS (ASAP) $[\text{M}+\text{H}]^+$ calcd for $\text{C}_{19}\text{H}_{18}\text{N}_2$ 275.1548, found 275.1570.

Arylethynylaniline 4h. Following the general Sonogashira procedure, iodoaniline **2d** (410 mg, 1.5 mmol, 1 equiv.), crude 4-ethynylanisole **3b** (204 mg, 1.5 mmol, 1 equiv.), Pd(PPh₃)₂Cl₂ (103 mg, 0.15 mmol, 0.1 equiv.), and CuI (27 mg, 0.15 mmol, 0.1 equiv.) were reacted for 24 h using DIPA as the base. Column chromatography (15:1:1 hexanes:EtOAc:CH₂Cl₂) afforded **4h** (180 mg, 43%) as a red oil. ¹H NMR (500 MHz, CDCl₃) δ 7.48 (d, *J* = 8.8 Hz, 2H), 7.38 (d, *J* = 2.4 Hz, 1H), 7.17 (dd, *J* = 8.5, 2.4 Hz, 1H), 6.89 (d, *J* = 8.8 Hz, 2H), 6.69 (d, *J* = 8.4 Hz, 1H), 4.15 (s, 2H), 3.83 (s, 3H), 1.29 (s, 9H). ¹³C NMR (126 MHz, CDCl₃) δ 159.66, 145.37, 141.01, 133.05, 128.73, 126.88, 115.68, 114.39, 114.14, 108.03, 94.21, 85.14, 55.45, 34.05, 31.55. HRMS (ASAP) [M+H]⁺ calcd for C₁₉H₂₁NO 280.1701, found 280.1730.

Arylethynylaniline 4i. TMS-ethynylaniline **5** (599 mg, 2.44 mmol, 1 equiv.) was desilated using the general method, then the crude product was mixed with 4-iodotoluene (638 mg, 2.93 mmol, 1.2 equiv.), Pd(PPh₃)₂Cl₂ (171 mg, 0.244 mmol, 0.10 equiv.), and CuI (45 mg, 0.244 mmol, 0.1 equiv.) and reacted for 24 h using TEA as the base following the general Sonogashira procedure. Column chromatography (15:1:1 hexanes:EtOAc:CH₂Cl₂) afforded **4i** (508 mg, 79%) as an orange solid. ¹H NMR (500 MHz, CDCl₃) δ 7.43 (d, *J* = 8.1 Hz, 2H), 7.38 (d, *J* = 2.4 Hz, 1H), 7.21–7.12 (m, 3H), 6.69 (d, *J* = 8.3 Hz, 1H), 4.16 (s, 2H), 2.38 (s, 3H), 1.29 (s, 9H). ¹³C NMR (126 MHz, CDCl₃) δ 145.46, 141.01, 138.38, 131.50, 129.26, 128.79, 127.04, 120.48, 114.39, 107.88, 94.45, 85.86, 34.06, 31.56, 21.65. HRMS (ASAP) [M+H]⁺ calcd for C₁₉H₂₁N 264.1752, found 264.1754.

Arylethynylaniline 4j. TMS-ethynylaniline **5** (600 mg, 2.44 mmol, 1 equiv.) was desilated using the general method, then the crude product was mixed with iodobenzene (598 mg, 2.92 mmol, 1.2 equiv.), Pd(PPh₃)₂Cl₂ (172 mg, 0.244 mmol, 0.10 equiv.), and CuI (43 mg,

0.243 mmol, 0.1 equiv.) and reacted for 24 h using TEA as the base following the general Sonogashira procedure. Column chromatography (15:1:1 hexanes:EtOAc:CH₂Cl₂) gave **4j** (499 mg, 82%) as a brown oil. ¹H NMR (500 MHz, CDCl₃) δ 7.54 (d, *J* = 7.2 Hz, 2H), 7.46–7.31 (m, 4H), 7.19 (dd, *J* = 8.4, 2.5 Hz, 1H), 6.69 (d, *J* = 8.4 Hz, 1H), 4.16 (s, 2H), 1.29 (s, 9H). ¹³C NMR (126 MHz, CDCl₃) δ 145.54, 141.04, 131.62, 128.85, 128.50, 128.26, 127.24, 123.57, 114.44, 107.64, 94.30, 86.59, 34.07, 31.56. HRMS (ASAP) [M+H]⁺ calcd for C₁₈H₁₉N 250.1596, found 250.1606.

Arylethynylaniline 4k. TMS-ethynylaniline **5** (224 mg, 0.911 mmol, 1 equiv.) was desilated using the general method, then the crude product was mixed with 4-iodo-1,2-benzenedicarbonitrile (232 mg, 0.911 mmol, 1.0 equiv.), Pd(PPh₃)₂Cl₂ (64 mg, 0.091 mmol, 0.10 equiv.), and CuI (17 mg, 0.091 mmol, 0.1 equiv.) and reacted for 24 h using TEA as the base following the general Sonogashira procedure. Column chromatography (5:1:1 hexanes:EtOAc:CH₂Cl₂) afforded **4k** (199 mg, 73%) as a light orange solid. ¹H NMR (500 MHz, CDCl₃) δ 7.90 (s, 1H), 7.85–7.69 (m, 1H), 7.36 (s, 1H), 7.30–7.24 (m, 2H), 6.71 (dd, *J* = 8.7, 2.0 Hz, 1H), 4.18 (s, 2H), 1.29 (s, 9H). ¹³C NMR (126 MHz, CDCl₃) δ 146.26, 141.39, 135.79, 135.29, 133.62, 129.70, 129.18 (2C), 116.47, 115.39, 114.93, 114.89, 113.97, 105.37, 94.78, 91.00, 34.11, 31.46. HRMS (ASAP) [M+H]⁺ calcd for C₂₀H₁₇N₃ 300.1501, found 300.1511.

Arylethynylaniline 4l. TMS-ethynylaniline **5** (599 mg, 2.44 mmol, 1 equiv.) was desilated using the general method, then the crude product was mixed with 1-bromo-4-chlorobenzene (471 mg, 2.44 mmol, 1.0 equiv.), Pd(PPh₃)₂Cl₂ (172 mg, 0.244 mmol, 0.10 equiv.), and CuI (47 mg, 0.244 mmol, 0.1 equiv.) and reacted for 24 h using TEA as the base following the general Sonogashira procedure. Column chromatography (10:1:1

hexanes:EtOAc:CH₂Cl₂) gave **4l** (319 mg, 46%) as a brown oil. ¹H NMR (500 MHz, CDCl₃) δ 7.46 (d, *J* = 7.1 Hz, 2H), 7.37 (s, 1H), 7.33 (d, *J* = 7.4 Hz, 2H), 7.20 (d, *J* = 8.5 Hz, 1H), 6.69 (d, *J* = 8.5 Hz, 1H), 4.15 (s, 2H), 1.29 (s, 9H). ¹³C NMR (126 MHz, CDCl₃) δ 145.58, 141.12, 134.22, 132.78, 128.85, 128.84, 127.50, 122.09, 114.53, 107.27, 93.16, 87.64, 34.07, 31.53. HRMS (ASAP) [M+H]⁺ calcd for C₁₈H₁₈ClN 284.1206, found 284.1226.

Arylethynylaniline 4m. Following the general Sonogashira procedure, iodoaniline **2a** (1 g, 4.1 mmol, 1 equiv.), phenylacetylene (530 mg, 5.19 mmol, 1.25 equiv.), Pd(PPh₃)₂Cl₂ (287 mg, 0.41 mmol, 0.1 equiv.), and CuI (78 mg, 0.41 mmol, 0.1 equiv.) were reacted for 24 h using DIPA as the base. Column chromatography (8:1:1 then 6:1:1 hexanes:EtOAc:CH₂Cl₂) furnished **4m** (599 mg, 67%) as a dark brown oil. ¹H NMR (500 MHz, CDCl₃) δ 7.63 (d, *J* = 1.9 Hz, 1H), 7.58–7.46 (m, 2H), 7.44–7.28 (m, 4H), 6.71 (d, *J* = 8.5 Hz, 1H), 4.81 (s, 2H). ¹³C NMR (126 MHz, CDCl₃) δ 151.15, 136.44, 133.31, 131.68, 129.01, 128.63, 122.42, 119.50, 114.09, 108.28, 100.20, 96.32, 83.48. HRMS (ASAP) [M+H]⁺ calcd for C₁₅H₁₀N₂ 219.0922, found 219.0950.

Arylethynylaniline 4n. Following the general Sonogashira procedure, iodoaniline **2a** (358 mg, 1.5 mmol, 1 equiv.), crude 4-ethynylanisole **3b** (206 mg, 1.5 mmol, 1 equiv.), Pd(PPh₃)₂Cl₂ (103 mg, 0.15 mmol, 0.1 equiv.), and CuI (28 mg, 0.15 mmol, 0.1 equiv.) were reacted for 24 h using DIPA as the base. Column chromatography (8:1:1 then 2:1:1 hexanes:EtOAc:CH₂Cl₂) furnished **4n** (197 mg, 53%) as a yellow solid. ¹H NMR (500 MHz, CDCl₃) δ 7.62 (d, *J* = 1.9 Hz, 1H), 7.46 (d, *J* = 8.9 Hz, 2H), 7.35 (dd, *J* = 8.5, 2.0 Hz, 1H), 6.90 (d, *J* = 8.8 Hz, 2H), 6.70 (d, *J* = 8.5 Hz, 1H), 4.74 (s, 2H), 3.84 (s, 3H). ¹³C NMR (126 MHz, CDCl₃) δ 160.26, 150.98, 136.31, 133.25, 133.09, 119.56, 114.50,

114.32, 114.02, 108.81, 100.37, 96.47, 82.22, 55.51. HRMS (ASAP) $[M+H]^+$ calcd for $C_{16}H_{12}N_2O$ 249.1028, found 249.1028.

Arylethynylaniline 4o. Following the general Sonogashira procedure, iodoaniline **2e** (2.74 g, 9.4 mmol, 1 equiv.), phenylacetylene **3c** (1.09 g, 9.4 mmol, 1 equiv.), $Pd(PPh_3)_2Cl_2$ (200 mg, 0.285 mmol, 0.03 equiv.), and CuI (50 mg, 0.28 mmol, 0.03 equiv.) were reacted for 24 h using TEA as the base. Column chromatography (10:1:1 then 7:1:1 hexanes:EtOAc:CH₂Cl₂) gave **4o** (1.99 g, 80%) a light orange solid. ¹H NMR (500 MHz, CDCl₃) δ 8.10 (d, $J = 2.1$ Hz, 1H), 7.83 (dd, $J = 8.5, 2.0$ Hz, 1H), 7.56–7.50 (m, 2H), 7.42–7.30 (m, 3H), 6.70 (d, $J = 8.5$ Hz, 1H), 4.76 (s, 2H), 4.33 (q, $J = 7.2$ Hz, 2H), 1.37 (t, $J = 7.2$ Hz, 3H). ¹³C NMR (126 MHz, CDCl₃) δ 166.23, 151.55, 140.97, 134.38, 131.55, 131.17, 128.49, 122.93, 119.72, 113.34, 107.09, 95.12, 84.91, 60.58, 14.48. HRMS (ASAP) $[M+H]^+$ calcd for $C_{17}H_{15}NO_2$ 266.1181 found 266.1215.

Arylethynylaniline 4p. Following the general Sonogashira procedure, crude ethynylbenzotrile **3a** (477 mg, 3.75 mmol, 1.5 equiv.), 4-ethoxy-2-iodoaniline **2f** (655 mg, 2.49 mmol, 1.0 equiv.), $Pd(PPh_3)_2Cl_2$ (110 mg, 0.16 mmol, 0.063 equiv.), and CuI (29 mg, 0.15 mmol, 0.061 equiv.) were reacted for 24 h using TEA as the base. Column chromatography (5:1:1 hexanes:EtOAc:CH₂Cl₂) gave **4p** (551 mg, 56%) as a dark orange solid. ¹H NMR (500 MHz, CDCl₃) δ 7.72–7.51 (m, 4H), 6.90 (d, $J = 2.9$ Hz, 1H), 6.82 (dd, $J = 8.8, 2.9$ Hz, 1H), 6.69 (d, $J = 8.8$ Hz, 1H), 4.00 (s, 2H), 3.97 (q, $J = 7.0$ Hz, 2H), 1.38 (t, $J = 7.0$ Hz, 3H). ¹³C NMR (126 MHz, CDCl₃) δ 151.42, 142.48, 132.24, 132.00, 128.33, 119.42, 118.66, 116.98, 116.32, 111.54, 107.49, 93.09, 90.86, 64.38, 15.06. HRMS (ASAP) $[M+H]^+$ calcd for $C_{17}H_{14}N_2O$ 263.1184, found 263.1221

Phosphaquinolinone 1d. Following the general cyclization procedure, arylethynylaniline **4d** (200 mg, 0.82 mmol, 1 equiv.) and P(OPh)₃ (310 mg, 0.984 mmol, 1.2 equiv.) in pyridine were reacted for 24 h. Column chromatography (2:1:1 hexanes:EtOAc:CH₂Cl₂, R_f = 0.10) gave **1d** (109 mg, 26%) as a pale yellow solid; mp >250 °C. ¹H NMR (500 MHz, CDCl₃) δ 9.85 (s, 1H), 7.95 (d, *J* = 8.0 Hz, 2H), 7.80 (d, *J* = 7.9 Hz, 2H), 7.65 (s, 1H), 7.62 (d, *J* = 39.4 Hz, 1H), 7.53 (d, *J* = 8.4 Hz, 1H), 7.11 (d, *J* = 8.5 Hz, 1H), 7.07 (t, *J* = 7.7 Hz, 2H), 6.99 (t, *J* = 7.4 Hz, 1H), 6.83 (d, *J* = 7.9 Hz, 2H). ¹³C NMR (126 MHz, CDCl₃) δ 149.85 (d, *J* = 9.1 Hz), 143.52, 141.70 (d, *J* = 5.1 Hz), 139.29 (d, *J* = 8.8 Hz), 135.30, 134.05, 133.03, 129.80, 128.57 (d, *J* = 6.3 Hz), 125.78, 124.90 (d, *J* = 159 Hz), 121.03 (d, *J* = 4.1 Hz), 119.48 (d, *J* = 15.2 Hz), 118.56 (d, *J* = 10.0 Hz), 118.47, 118.41, 112.93, 104.99. ³¹P NMR (202 MHz, CDCl₃) δ 9.53 (d, *J* = 39.1 Hz). HRMS (ASAP) [M+H]⁺ calcd for C₂₂H₁₄N₃O₂P 384.0902, found 384.0903.

Phosphaquinolinone 1e. Following the general cyclization procedure, arylethynylaniline **4e** (260 mg, 0.917 mmol, 1 equiv.) and P(OPh)₃ (340 mg, 1.10 mmol, 1.2 equiv.) in pyridine were reacted for 48 h. Column chromatography (2:1:1 hexanes:EtOAc:CH₂Cl₂, R_f = 0.23) gave **1e** (286 mg, 61%) as a pale yellow solid; mp 227-229 °C. ¹H NMR (500 MHz, CDCl₃) δ 9.67 (s, 1H), 7.96 (d, *J* = 7.9 Hz, 2H), 7.78 (d, *J* = 8.0 Hz, 2H), 7.65 (d, *J* = 39.2 Hz, 1H), 7.59 (s, 1H), 7.50 (d, *J* = 7.5 Hz, 1H), 7.14 (d, *J* = 8.6 Hz, 1H), 7.07 (t, *J* = 7.7 Hz, 2H), 6.98 (t, *J* = 7.5 Hz, 1H), 6.86 (d, *J* = 7.8 Hz, 2H). ¹³C NMR (126 MHz, CDCl₃) δ 150.02 (d, *J* = 9.1 Hz), 142.71, 142.50 (d, *J* = 5.2 Hz), 139.70 (d, *J* = 9.0 Hz), 132.95, 129.73, 128.50 (d, *J* = 6.5 Hz), 127.22 125.58 (d, *J* = 1.7 Hz), 125.07, 124.25 (q, *J* = 160 Hz), 123.78 (q, *J* = 33.2 Hz), 122.91, 121.06 (d, *J* = 4.1 Hz), 118.88 (d, *J* = 15.0 Hz), 118.60, 118.10 (d, *J* = 9.8 Hz), 112.61. ³¹P NMR (202 MHz, CDCl₃) δ 10.09 (d, *J* = 39.2

Hz). ^{19}F NMR (471 MHz, CDCl_3) δ -61.91. HRMS (ASAP) $[\text{M}+\text{H}]^+$ calcd for $\text{C}_{22}\text{H}_{14}\text{F}_3\text{N}_2\text{O}_2\text{P}$ 427.0823, found 427.0808.

Phosphaquinolinone 1f. Following the general cyclization procedure, arylethynylaniline **4f** (285 mg, 1.13 mmol, 1 equiv.) and $\text{P}(\text{OPh})_3$ (699 mg, 2.25 mmol, 2 equiv.) in pyridine were reacted for 24 h. The crude mixture was recrystallized from hot CH_2Cl_2 and hexanes. The solid was isolated and washed with hexanes to afford **1f** (389 mg, 44%; $R_f = 0.22$ in 2:1:1 hexanes:EtOAc: CH_2Cl_2) as a yellow solid; mp >250 °C. ^1H NMR (500 MHz, $\text{DMSO}-d_6$) δ 10.30 (s, 1H), 8.07 (d, $J = 38.5$ Hz, 1H), 8.04 (d, $J = 7.6$ Hz, 2H), 7.96 (d, $J = 8.1$ Hz, 2H), 7.62 (s, 1H), 7.40 (d, $J = 8.8$ Hz, 1H), 7.23 (t, $J = 8.1$ Hz, 2H), 7.08 (d, $J = 7.4$ Hz, 2H), 6.87 (d, $J = 7.9$ Hz, 2H). ^{13}C NMR (126 MHz, $\text{DMSO}-d_6$) δ 149.97 (d, $J = 9.0$ Hz), 141.82 (d, $J = 4.0$ Hz), 139.83 (d, $J = 9.6$ Hz), 139.27, 132.78, 130.41 (d, $J = 107$ Hz), 129.65, 128.02 (d, $J = 6.5$ Hz), 125.01, 124.17, 124.11, 122.92, 120.80 (d, $J = 4.0$ Hz), 120.38 (d, $J = 15.1$ Hz), 118.64, 118.30 (d, $J = 9.8$ Hz), 110.77. ^{31}P NMR (202 MHz, $\text{DMSO}-d_6$) δ 8.36 (d, $J = 38.3$ Hz). HRMS (ASAP) $[\text{M}+\text{H}]^+$ calcd for $\text{C}_{21}\text{H}_{14}\text{ClN}_2\text{O}_2\text{P}$ 393.0560, found 393.0576.

Phosphaquinolinone 1g. Following the general cyclization procedure, arylethynylaniline **4g** (200 mg, 0.729 mmol, 1 equiv.) and $\text{P}(\text{OPh})_3$ (0.271 g, 0.874 mmol, 1.2 equiv.) in pyridine were reacted for 24 h. Column chromatography (2:1:1 hexanes:EtOAc: CH_2Cl_2 , $R_f = 0.30$) afforded **1g** (108 mg, 36%) as a pale yellow solid; mp >250 °C. ^1H NMR (500 MHz, CDCl_3) δ 8.39 (s, 1H), 7.95 (d, $J = 8.0$ Hz, 2H), 7.72 (d, $J = 7.5$ Hz, 2H), 7.68 (d, $J = 38.7$ Hz, 1H), 7.42–7.35 (m, 1H), 7.32 (s, 1H), 7.09 (t, $J = 7.7$ Hz, 2H), 6.98 (t, $J = 7.5$ Hz, 2H), 6.90 (d, $J = 8.0$ Hz, 2H), 1.31 (s, 9H). ^{13}C NMR (126 MHz, CDCl_3) δ 150.34 (d, $J = 9.0$ Hz), 144.49, 143.88 (d, $J = 5.1$ Hz), 140.64 (d, $J = 9.4$ Hz), 137.71 (d, $J = 2.0$ Hz),

132.73, 129.58, 129.26, 128.36 (d, $J = 6.4$ Hz), 127.46, 125.09, 122.76 (d, $J = 161$ Hz), 121.17 (d, $J = 4.1$ Hz), 119.21 (d, $J = 14.1$ Hz), 118.91, 117.34 (d, $J = 9.3$ Hz), 111.75, 34.34, 31.46. ^{31}P NMR (202 MHz, CDCl_3) δ 10.84 (d, $J = 39.6$ Hz). HRMS (ASAP) $[\text{M}+\text{H}]^+$ calcd for $\text{C}_{25}\text{H}_{23}\text{N}_2\text{O}_2\text{P}$ 415.1575, found 415.1588.

Phosphaquinolinone 1h. Following the general cyclization procedure, aryloethynylaniline **4h** (174 mg, 0.623 mmol, 1 equiv.) and $\text{P}(\text{OPh})_3$ (231 mg, 0.747 mmol, 1.2 equiv.) in pyridine were reacted for 24 h. Column chromatography (2:1:1 hexanes:EtOAc: CH_2Cl_2 , $R_f = 0.25$) afforded **1h** (115 mg, 44%) as a pale yellow solid; mp 98-101 °C. ^1H NMR (500 MHz, CDCl_3) δ 7.76 (d, $J = 8.3$ Hz, 2H), 7.53 (d, $J = 40.6$ Hz, 1H), 7.35–7.29 (m, 2H), 7.13 (t, $J = 7.7$ Hz, 2H), 7.05–6.91 (m, 6H), 6.88 (d, $J = 8.8$ Hz, 1H), 3.86 (s, 3H), 1.32 (s, 9H). ^{13}C NMR (126 MHz, CDCl_3) δ 159.99, 150.66 (d, $J = 8.9$ Hz), 144.28, 140.27 (d, $J = 6.3$ Hz), 136.76 (d, $J = 2.3$ Hz), 129.49, 129.18 (d, $J = 6.8$ Hz), 128.19 (d, $J = 9.4$ Hz), 127.74, 127.03, 124.88, 124.85 (d, $J = 159.4$ Hz), 121.34 (d, $J = 4.2$ Hz), 119.98 (d, $J = 14.2$ Hz), 116.77 (d, $J = 9.1$ Hz), 114.49, 55.53, 34.32, 31.52. ^{31}P NMR (202 MHz, CDCl_3) δ 10.99 (d, $J = 40.6$ Hz). HRMS (ASAP) $[\text{M} + \text{H}]^+$ calcd for $\text{C}_{25}\text{H}_{26}\text{NO}_3\text{P}$ 420.1729, found 420.1733.

Phosphaquinolinone 1i. Following the general cyclization procedure, aryloethynylaniline **4i** (251 mg, 1.93 mmol, 1 equiv.) and $\text{P}(\text{OPh})_3$ (718 mg, 2.314 mmol, 1.2 equiv.) in pyridine were reacted for 48 h. Column chromatography (2:1:1 hexanes:EtOAc: CH_2Cl_2 , $R_f = 0.50$) afforded **1i** (389 mg, 50%) as a yellow solid; mp 95-96 °C. ^1H NMR (500 MHz, CDCl_3) δ 7.78 (s, 1H), 7.73 (d, $J = 7.8$ Hz, 2H), 7.58 (d, $J = 40.4$ Hz, 1H), 7.30 (d, $J = 8.4$ Hz, 2H), 7.25 (d, $J = 6.4$ Hz, 2H), 7.09 (t, $J = 7.3$ Hz, 2H), 7.01–6.90 (m, 4H), 2.41 (s, 3H), 1.30 (s, 9H). ^{13}C NMR (126 MHz, CDCl_3) δ 150.73 (d, $J = 9.3$ Hz), 144.01, 141.22 (d, $J = 5.9$ Hz),

138.35, 137.20, 132.94 (d, $J = 9.1$ Hz), 129.74, 129.43, 127.92, 127.77 (d, $J = 6.7$ Hz), 126.96, 124.78 (d, $J = 159$ Hz), 124.73, 121.38 (d, $J = 4.1$ Hz), 119.72 (d, $J = 14.3$ Hz), 116.99 (d, $J = 9.2$ Hz), 34.28, 31.51, 21.43. ^{31}P NMR (202 MHz, CDCl_3) δ 11.79 (d, $J = 40.3$ Hz). HRMS (ASAP) $[\text{M} + \text{H}]^+$ calcd for $\text{C}_{25}\text{H}_{26}\text{NO}_2\text{P}$ 404.1779, found 404.1787.

Phosphaquinolinone 1j. Following the general cyclization procedure, arylethynylaniline **4j** (500 mg, 2.00 mmol, 1 equiv.) and $\text{P}(\text{OPh})_3$ (744 mg, 2.40 mmol, 1.2 equiv.) in pyridine were reacted for 24 h. Column chromatography (2:1:1 hexanes:EtOAc: CH_2Cl_2 , $R_f = 0.66$) gave **1j** (436 mg, 56%) as a yellow solid; mp 153-154 °C. ^1H NMR (500 MHz, CDCl_3) δ 7.78 (s, 1H), 7.73 (d, $J = 7.8$ Hz, 2H), 7.58 (d, $J = 40.4$ Hz, 1H), 7.32–7.23 (m, 4H), 7.09 (t, $J = 7.3$ Hz, 2H), 7.01–6.90 (m, 4H), 2.41 (s, 3H), 1.30 (s, 9H). ^{13}C NMR (126 MHz, CDCl_3) δ 150.68 (d, $J = 9.2$ Hz), 144.07, 142.03 (d, $J = 5.8$ Hz), 137.29 (d, $J = 2.0$ Hz), 135.88 (d, $J = 9.1$ Hz), 129.44, 129.01, 128.39, 128.15, 127.96 (d, $J = 6.6$ Hz), 127.06, 124.84 (d, $J = 160$ Hz), 124.77, 121.36 (d, $J = 4.2$ Hz), 119.61 (d, $J = 14.3$ Hz), 117.06 (d, $J = 9.2$ Hz), 34.29, 31.51. ^{31}P NMR (202 MHz, CDCl_3) δ 11.38 (d, $J = 40.1$ Hz). HRMS (ASAP) $[\text{M} + \text{H}]^+$ calcd for $\text{C}_{24}\text{H}_{24}\text{NO}_2\text{P}$ 390.1623, found 390.1621.

Phosphaquinolinone 1k. Following the general cyclization procedure, arylethynylaniline **4k** (218 mg, 0.729 mmol, 1 equiv.) and $\text{P}(\text{OPh})_3$ (452 mg, 1.46 mmol, 2 equiv.) in pyridine were reacted for 48 h. The crude mixture was triturated with hot EtOAc. The resulting yellow solid was isolated and washed with hexanes to afford **1k** (109 mg, 34%; $R_f = 0.24$ in 2:1:1 hexanes:EtOAc: CH_2Cl_2) as a light yellow solid; mp >250 °C. ^1H NMR (500 MHz, $\text{DMSO}-d_6$) δ 10.14 (s, 1H), 8.54 (s, 1H), 8.41 (d, $J = 8.4$ Hz, 1H), 8.32 (d, $J = 37.8$ Hz, 1H), 8.22 (d, $J = 8.3$ Hz, 1H), 7.55 (s, 1H), 7.48 (d, $J = 8.4$ Hz, 1H), 7.24 (t, $J = 7.7$ Hz, 2H), 7.09 (t, $J = 7.5$ Hz, 1H), 7.04 (d, $J = 8.5$ Hz, 1H), 6.90 (d, $J = 7.9$ Hz, 2H), 1.27 (s,

6H). ^{13}C NMR (126 MHz, $\text{DMSO-}d_6$) δ 150.06 (d, $J = 8.8$ Hz), 145.14, 145.12, 143.08, 141.17 (d, $J = 10.6$ Hz), 138.45 (d, $J = 2.3$ Hz), 134.43, 131.76 (d, $J = 5.5$ Hz), 131.52 (d, $J = 7.9$ Hz), 129.67, 129.61, 127.76, 124.94, 120.93 (d, $J = 4.1$ Hz), 119.72 (d, $J = 159$ Hz), 118.51 (d, $J = 14.8$ Hz), 116.46 (d, $J = 9.5$ Hz), 115.90 (d, $J = 17.6$ Hz), 115.30, 112.86, 33.89, 31.05. ^{31}P NMR (202 MHz, $\text{DMSO-}d_6$) δ 9.15 (d, $J = 37.7$ Hz). HRMS (ASAP) $[\text{M}+\text{H}]^+$ calcd for $\text{C}_{26}\text{H}_{22}\text{N}_3\text{O}_2\text{P}$ 440.1528, found 440.1542.

Phosphaquinolinone 1l. Following the general cyclization procedure, aryloethynylaniline **4l** (287 mg, 1.01 mmol, 1 equiv.) and $\text{P}(\text{OPh})_3$ (627 mg, 2.02 mmol, 2.0 equiv.) in pyridine were reacted for 24 h. Column chromatography (2:1:1 hexanes:EtOAc: CH_2Cl_2 ; $R_f = 0.36$) furnished **1l** (256 mg, 60%) as a yellow solid; mp 192-194 °C. ^1H NMR (500 MHz, CDCl_3) δ 7.85 (s, 1H), 7.76 (d, $J = 8.2$ Hz, 2H), 7.59 (d, $J = 39.8$ Hz, 1H), 7.41 (d, $J = 8.2$ Hz, 2H), 7.34 (d, $J = 8.5$ Hz, 1H), 7.31 (s, 1H), 7.10 (t, $J = 7.7$ Hz, 2H), 6.99 (t, $J = 7.4$ Hz, 1H), 6.96–6.86 (m, 3H), 1.31 (s, 9H). ^{13}C NMR (126 MHz, CDCl_3) δ 150.55 (d, $J = 9.2$ Hz), 144.29, 142.17 (d, $J = 5.8$ Hz), 137.28 (d, $J = 2.1$ Hz), 134.47, 134.38 (d, $J = 9.5$ Hz), 129.53, 129.21, 129.16, 128.44, 127.17 (d, $J = 1.8$ Hz), 124.92 (d, $J = 1.7$ Hz), 123.65 (d, $J = 160$ Hz), 121.27 (d, $J = 4.1$ Hz), 119.51 (d, $J = 14.2$ Hz), 117.11 (d, $J = 9.3$ Hz), 34.32, 31.49. ^{31}P NMR (202 MHz, CDCl_3) δ 11.02 (d, $J = 39.9$ Hz). HRMS (ASAP) $[\text{M}+\text{H}]^+$ calcd for $\text{C}_{24}\text{H}_{23}\text{ClINO}_2\text{P}$ 424.1233, found 424.1256.

Phosphaquinolinone 1m. Following the general cyclization procedure, aryloethynylaniline **4m** (587 mg, 2.69 mmol, 1 equiv.) and $\text{P}(\text{OPh})_3$ (1.084 g, 3.50 mmol, 1.3 equiv.) in pyridine were reacted for 24 h. Column chromatography (2:1:1 hexanes:EtOAc: CH_2Cl_2 ; $R_f = 0.20$) gave **1m** (405 mg, 42%) as a yellow solid; mp 249-251 °C. ^1H NMR (500 MHz, CDCl_3) δ 9.62 (s, 1H), 7.84 (d, $J = 7.5$ Hz, 2H), 7.61–7.39 (m, 6H), 7.13–7.03 (m, 3H), 6.96 (t, $J =$

7.4 Hz, 1H), 6.90–6.83 (m, 2H). ^{13}C NMR (126 MHz, CDCl_3) δ 150.21 (d, $J = 9.2$ Hz), 143.46 (d, $J = 1.8$ Hz), 139.91 (d, $J = 5.9$ Hz), 134.78, 133.20, 129.60 (d, $J = 1.6$ Hz), 129.36, 128.05 (d, $J = 6.5$ Hz), 126.69 (d, $J = 158$ Hz), 125.41 (d, $J = 1.8$ Hz), 121.27 (d, $J = 4.1$ Hz), 119.87 (d, $J = 15.3$ Hz), 118.82, 118.39 (d, $J = 9.6$ Hz), 104.34. ^{31}P NMR (202 MHz, CDCl_3) δ 10.31 (d, $J = 40.2$ Hz). HRMS (ASAP) $[\text{M}+\text{H}]^+$ calcd for $\text{C}_{21}\text{H}_{15}\text{N}_2\text{O}_2\text{P}$ 359.0949, found 359.0995.

Phosphaquinolinone 1n. Following the general cyclization procedure, aryloethynylaniline **4n** (190 mg, 0.76 mmol, 1 equiv.) and $\text{P}(\text{OPh})_3$ (285 mg, 0.92 mmol, 1.2 equiv.) in pyridine were reacted for 36 h. Column chromatography (2:1:1 hexanes:EtOAc: CH_2Cl_2 ($R_f = 0.10$) then 20:1 CH_2Cl_2 :MeOH) furnished **1n** (88 mg, 30%) as a yellow solid; mp 238-239 °C. ^1H NMR (500 MHz, CDCl_3) δ 9.75 (s, 1H), 7.80 (d, $J = 8.7$ Hz, 2H), 7.56 (s, 1H), 7.47 (d, $J = 40.4$ Hz, 1H), 7.42 (d, $J = 7.2$ Hz, 1H), 7.15–7.01 (m, 5H), 6.99–6.92 (m, 1H), 6.88 (d, $J = 8.4$ Hz, 2H), 3.90 (s, 3H). ^{13}C NMR (126 MHz, CDCl_3) δ 160.65, 150.25 (d, $J = 9.1$ Hz), 143.19 (d, $J = 1.8$ Hz), 138.16 (d, $J = 6.2$ Hz), 134.52, 132.84, 129.59, 129.31 (d, $J = 6.7$ Hz), 127.05 (d, $J = 8.8$ Hz), 126.23 (d, $J = 156$ Hz), 125.38 (d, $J = 1.8$ Hz), 121.29 (d, $J = 4.0$ Hz), 120.11 (d, $J = 15.3$ Hz), 118.90, 118.26 (d, $J = 9.7$ Hz), 114.82, 104.29, 55.60. ^{31}P NMR (202 MHz, CDCl_3) δ 10.64 (d, $J = 40.4$ Hz). HRMS (ASAP) $[\text{M}+\text{H}]^+$ calcd for $\text{C}_{22}\text{H}_{17}\text{N}_2\text{O}_3\text{P}$ 389.1055, found 389.1078.

Phosphaquinolinone 1o. Following the general cyclization procedure, aryloethynylaniline **4o** (1.69 g, 6.37 mmol, 1 equiv.) and $\text{P}(\text{OPh})_3$ (2.37 g, 7.65 mmol, 1.2 equiv.) in pyridine were reacted for 24 h. Column chromatography (2:1:1 hexanes:EtOAc: CH_2Cl_2 ; $R_f = 0.20$) afforded **1o** (1.42 g, 55%) as a yellow solid; mp 176-178 °C. ^1H NMR (500 MHz, CDCl_3) δ 9.60 (s, 1H), 8.02 (s, 1H), 7.90 (d, $J = 8.5$ Hz, 1H), 7.87 (d, $J = 7.7$ Hz, 2H), 7.65 (d, $J =$

40.6 Hz, 1H), 7.51 (t, $J = 7.5$ Hz, 2H), 7.45 (t, $J = 7.4$ Hz, 1H), 7.08 (d, $J = 8.5$ Hz, 1H), 7.03 (t, $J = 7.6$ Hz, 2H), 6.93 (d, $J = 7.4$ Hz, 1H), 6.90 (d, $J = 8.3$ Hz, 2H), 4.36 (q, $J = 6.9$ Hz, 3H), 1.39 (t, $J = 7.1$ Hz, 2H). ^{13}C NMR (126 MHz, CDCl_3) δ 166.10, 150.43 (d, $J = 9.1$ Hz), 143.76 (d, $J = 1.8$ Hz), 141.43 (d, $J = 6.0$ Hz), 135.31 (d, $J = 8.8$ Hz), 132.66, 131.52, 129.50 (d, $J = 1.6$ Hz), 129.22, 128.88, 128.02 (d, $J = 6.6$ Hz), 125.18 (d, $J = 15.8$ Hz), 125.14 (d, $J = 1.7$ Hz), 123.26, 121.34 (d, $J = 4.0$ Hz), 119.16 (d, $J = 15.0$ Hz), 117.41 (d, $J = 9.6$ Hz), 61.05, 14.52. ^{31}P NMR (202 MHz, CDCl_3) δ 11.25 (d, $J = 40.5$ Hz). HRMS (ASAP) $[\text{M}+\text{H}]^+$ calcd for $\text{C}_{23}\text{H}_{20}\text{NO}_4\text{P}$ 406.1208, found 406.1229.

Phosphaquinolinone 1p. Following the general cyclization procedure, arylethynylaniline **4p** (369 mg, 1.41 mmol, 1 equiv.) and $\text{P}(\text{OPh})_3$ (872 mg, 2.81 mmol, 2 equiv.) in pyridine were reacted for 48 h. Column chromatography (2:1:1 hexanes:EtOAc: CH_2Cl_2 ; $R_f = 0.12$) afforded **1p** (306 mg, 54%) as a yellow solid; mp 247-250 °C. ^1H NMR (500 MHz, CDCl_3) δ 7.92 (d, $J = 7.2$ Hz, 2H), 7.76–7.69 (m, 3H), 7.59 (d, $J = 38.8$ Hz, 1H), 7.11 (t, $J = 8.2$ Hz, 2H), 7.01 (t, $J = 7.6$ Hz, 1H), 6.98–6.87 (m, 4H), 6.85 (d, $J = 2.6$ Hz, 1H), 4.01 (q, $J = 7.0$ Hz, 2H), 1.41 (t, $J = 6.9$ Hz, 3H). ^{13}C NMR (126 MHz, CDCl_3) δ 153.71, 150.23 (d, $J = 9.0$ Hz), 143.00, 140.42 (d, $J = 9.2$ Hz), 133.75 (d, $J = 2.2$ Hz), 132.76, 129.63, 128.43 (d, $J = 6.6$ Hz), 125.23, 123.95 (d, $J = 16.1$ Hz), 121.17 (d, $J = 4.3$ Hz), 120.31 (d, $J = 14.1$ Hz), 119.87, 118.84, 118.57 (d, $J = 9.3$ Hz), 114.79, 111.95, 64.25, 14.99. ^{31}P NMR (202 MHz, CDCl_3) δ 10.29 (d, $J = 38.9$ Hz). HRMS (ASAP) $[\text{M}+\text{H}]^+$ calcd for $\text{C}_{23}\text{H}_{19}\text{N}_2\text{O}_3\text{P}$ 403.1212, found 403.1220.

CHAPTER III

EXPLOITING THE HYDROGEN BOND DONOR/ACCEPTOR PROPERTIES OF PN HETEROCYCLES: SELECTIVE ANION RECEPTORS FOR HYDROGEN SULFATE

This chapter includes previously published and co-authored material from Deng, C.-L., Bard, J.P., Lohrman, J.A., Barker, J.E., Zakharov, L.N., Johnson, D.W., Haley, M.M. “Exploiting the Hydrogen Bond Donor/Acceptor Properties of PN-Heterocycles: Selective Anion Receptors for Hydrogen Sulfate.” *Angew. Chem. Int. Ed.* **2019**, 58, 3934–3938. This story highlights our work on developing a hybrid urea- and phosphoquinoline-containing host for the binding of HSO_4^- in both aqueous and organic solutions.

3.1 Introduction

Selective detection and recognition of various anions have attracted substantial attention.¹ Hydrogen sulfate (bisulfate, HSO_4^-) is of considerable interest owing to its concern as a contaminant in agricultural and industrial fields.² This hydroxyanion is a moderate acid ($\text{pK}_a \approx 2.0$)³ and is abundant in aqueous sulfuric acid and salt solutions. Meanwhile, the important sulfate (SO_4^{2-}) anion will equilibrate with bisulfate ions in low pH environment. Hydrogen sulfate is the most prevalent inorganic component in lower and upper atmospheric aerosols and plays a role in aerosol homogeneous nucleation.⁴ Additionally, the HSO_4^- anion can also act as an important and effective catalyst for various chemical transformations.⁵ As a result, the design and development of various artificial

host molecules for HSO_4^- anion binding has become a highly desirable target in supramolecular chemistry.

Unfortunately, development of synthetic receptors that are capable of selective recognition and binding toward HSO_4^- has proven challenging because of its H-bonding donor/acceptor nature as well as its unique tetrahedral geometry.⁶ Over the past few decades, only a handful of selective receptors for HSO_4^- have been documented.^{7,8} These molecular systems are mainly composed of the well-known acidic (N–H, O–H) and/or neutral (C–H) hydrogen bond (HB) donors and basic nitrogen atoms (such as amine, imine, imidazole, or pyridine motifs)⁷ or carbonyl⁸ motifs as the perceived HB accepting sites. The resulting multidentate and/or macrocyclic architectures with convergent and complementary HB contacts typically give rise to strong anion binding affinities in solution phase, although selectivity is often far from optimum. Furthermore, stabilization of HSO_4^- by complexation with receptors bearing basic moieties in the solid state has always been challenging since the protic oxyanion is susceptible to proton transfer to the hostmolecules.^{7b,7d} Hydroxyanions including HSO_4^- are well-known to dimerize by forming anti-electrostatic, self-complementary $(\text{O–H})_{\text{anion}} \cdots \text{O}_{\text{anion}}$ hydrogen bonds in crystal structures,^{9,10} or are prone to undergo proton transfer to generate SO_4^{2-} ion,¹¹ both of which would facilitate the electrostatic contacts with the HB donors due to the pronounced and unitary negative charge density. As a consequence, these competitive processes make co-crystallization of host-guest complexes involving HSO_4^- a significant challenge. A search for structures involving monomeric, pristine HSO_4^- anion in the Cambridge Structural Database (CSD) reveals that numerous HSO_4^- co-crystals have been engineered/reported. Most of these examples are single component systems with undefined

or ill-defined binding cavities, in which HSO_4^- ions act as solvates to bridge the host molecules; thus, the limited coordinations to the anion found in these complexes likely result from crystal packing (Table B.1).

Our studies have demonstrated that arylethynyl-based bis-urea derivatives provide a preorganized, attractive binding pocket for spherical halide anions.¹² By modifying the number of urea donors and incorporating different aryl cores, the obtained tripodal¹³ and bipodal¹⁴ receptors effectively increase their selectivity for nitrate and dihydrogen phosphate binding, respectively. In our recent effort in developing novel fluorescent phosphorus- and nitrogen-containing (PN) heterocycles,¹⁵ we found that the cis-configured phosphoramidate motif exhibits extremely strong self-dimerization through self-complementary N–H and P=O HB donor/acceptor interactions (Figure 3.1a).¹⁶ Notably, the chiral phosphonyl group in this molecular system not only increases the HB acidity of the N@H but also functions as a strong hydrogen-bond-accepting^{17,18} subunit. This in turn confers higher affinities for anion recognition, especially for acidic anions like HSO_4^- , than the commonly-used amide functionality.

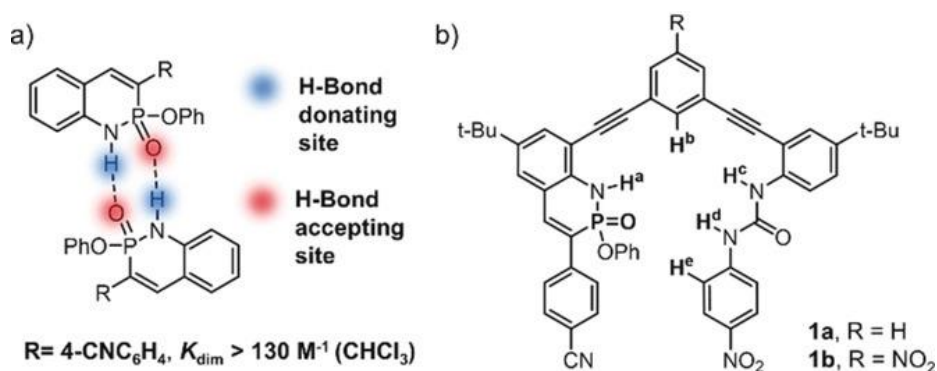


Figure 3.1 a) Structure of the PN-heterocycle homodimer linked by self-complementary hydrogen bonds. b) Structure of receptors **1** studied in this work. The relevant protons are marked to assign NMR peaks.

More importantly, the electrostatic and geometric complementarity between the non-planar alignment of the highly polarized P=O and acidic N–H moieties and HSO₄[−] anion suggest this unusual phosphonamidate could be a selective scaffold for HSO₄[−] anion-binding. Herein, we report the design and synthesis of two hybrid receptors **1** (Figure 3.1b) combining PN-heterocycle and urea units within an acyclic arylethynyl framework. Based on solution phase and solid-state analysis, in combination with DFT calculations, the precise spatial arrangement of HB binding sites (C–H, N–H, and P=O) in the structures are responsible for the observed high selectivity and affinity towards HSO₄[−] anion over halides and other oxyanions.

3.2 Results and Discussion

Receptors **1** were readily prepared based on the strategies utilized for related aryl-acetylene hosts in a stepwise manner (see Experimental Section) and their structures were confirmed by NMR and high-resolution mass spectra. The assignments for relevant protons (see Figure 3.1b) were inferred based on the corresponding ¹H-¹³C HSQC and ¹H-¹H NOESY experiments (Figures B.5–B.10). Single crystals of **1a** and **1b** were grown by slow evaporation of CH₂Cl₂/MeOH and CHCl₃/DMSO solutions, respectively, which unambiguously confirmed the structures of the anticipated host systems (Figures B.1 and B.2).¹⁹ The solid-state structures provide insight into the HB-accepting and -donating capabilities of the PN heterocycle and suggest the aromatic C–H bonds in the phenyl core could contribute HB interactions as well. To probe the anion-binding properties of the receptors, ¹H NMR spectroscopic studies were initially performed in 9:1 [D₆]DMSO/CDCl₃.²⁰ Upon addition of 10 equiv. of the tetrabutylammonium (TBA) salts of HSO₄[−], Cl[−], Br[−], I[−], NO₃[−], as well as ClO₄[−] anion (which are common interfering ions in

acidic media) to receptor **1a**, significant downfield shifts were observed for the proton signals of the urea N-H^d resonances in the cases of HSO₄⁻ and halides (Figure B.11). In contrast, subtle and negligible changes in the NMR spectra were found for I⁻ and ClO₄⁻, suggesting weak and no interactions, respectively. Quantitative NMR titration studies were then performed and the resulting binding isotherms were fit to a 1:1 binding model using a global fitting method to provide the binding constants (*K*_a) in Table 3.1. Comparison of the anion binding affinities in Table 3.1 revealed that both **1a** and **1b** show impressive HSO₄⁻ selectivity over halides and other oxoanions. The NO₂-substituted variant **1b**, compared to **1a**, exhibited nearly seven-fold higher binding strength with enhanced HSO₄⁻ selectivity. Binding of the halides to both receptors appears to be driven largely by the size/negative charge densities of the anions with *K*_a values decreasing in accord with the Hofmeister order of Cl⁻ > Br⁻ > I⁻. Notably, the trigonal-planar anion NO₃⁻ is bound weakly by both receptors.

Table 3.1 Association constants^a (*K*_a, M⁻¹) of receptors **1** with various anions in 10 vol% [D₆]DMSO/CDCl₃ at 298 K

	1a	RA ^b	1b	RA ^c
HSO ₄ ⁻	1420 (1480)	1	9600 (10 500)	1
NO ₃ ⁻	40 (30)	0.028	105 (100)	0.011
Cl ⁻	200	0.14	260	0.027
Br ⁻	30	0.021	75	0.008
I ⁻	– ^d	0	20	0.002
ClO ₄ ⁻	– ^d	0	– ^d	0

^a 1:1 binding fit. All reported association constants represent the average value from triplicate titrations. The values derived from ³¹P NMR titrations are given in parentheses. Uncertainties are less than 15 %. All anions were used as TBA salts. ^b RA=relative affinity. Relative to the ¹H NMR titration derived *K*_a for **1a**·HSO₄⁻. ^c Relative to the ¹H NMR titration derived *K*_a for **1b**·HSO₄⁻. ^d No binding or too weak to be quantified.

Inspection of the ^1H NMR spectra of the complexes provides useful information indicative of the coordination modes of **1b** with the different anions. As expected, all urea protons H^c and H^d showed anion-binding induced downfield shifts in varying degrees during titrations (Figure 3.2). The ^1H NMR spectrum of **1b** with HSO_4^- displayed a significant downfield shift of the phosphonamidate H^a resonance ($\Delta\delta = +1.72$ ppm). In addition, the signal attributed to the inner aromatic proton (H^b) moved considerably to the downfield region as well ($\Delta\delta = +0.96$ ppm), together with another C–H proton (H^c) of the nitrophenyl of the urea “arm” ($\Delta\delta = \text{ca.} +0.28$ ppm). It is worth noting that the other two magnetically non-equivalent proton signals belonging to the central nitrophenyl core were upfield shifted and eventually merged, which might be related to a dramatic conformational rearrangement to reorganize the two “arms” of **1b** upon the encapsulation of HSO_4^- . These observations suggested that HSO_4^- anion was directly included within the proposed cavity of hybrid receptor **1b** via the complementary HB interactions.

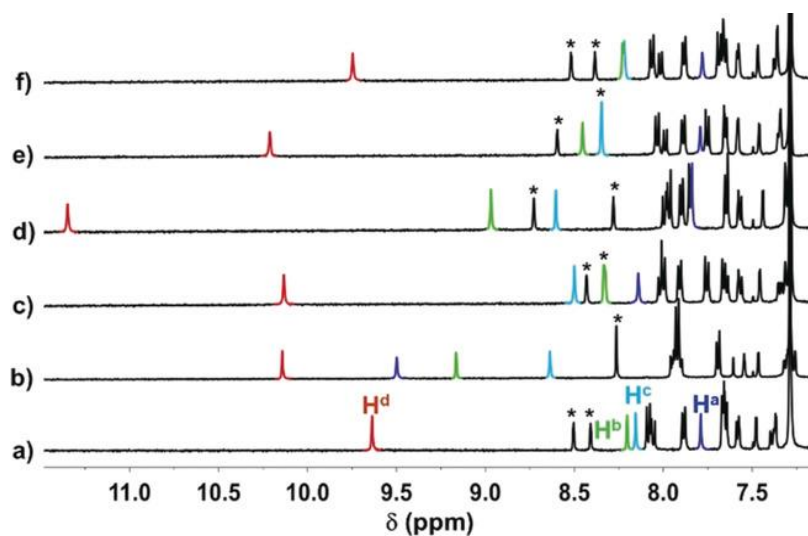


Figure 3.2 Partial ^1H NMR spectra of **1b** (1.13 mm) in 10 vol% $[\text{D}_6]\text{DMSO}/\text{CDCl}_3$ in a) the absence and b) the presence of 10 equiv. hydrogen sulfate, c) nitrate, d) chloride, e) bromide, and f) iodide. All anions were used as their respective TBA salts. The two *meta*-protons with respect to H^b on the central nitrophenyl core are marked with (*).

In contrast, a much smaller shift for H^a ($\Delta\delta = +0.35$ ppm) was detected in the case of NO₃⁻, indicating the phosphoramidate N–H proton also contributes to the guest complexation but to a lesser extent compared to HSO₄⁻. In addition, the small downfield shift for H^b suggested the aryl C–H hydrogen bond unit might not actively participate in complexation. Presumably, the trigonal-planar NO₃⁻ anion loosely bridges the two arms of the receptor via favorable HB interactions among the phosphoramidate and urea N–H subunits to form a two-site binding mode due to the constrained binding cavity, as indicated by the DFT modeling (see Appendix B). The Cl⁻/Br⁻ additions elicited little to no shifting of H^a, while considerable $\Delta\delta$ of 0.77 and 0.25 ppm occurred for the proton H^b, respectively. This implies that the smaller spherical halides are binding primarily in the vicinity of the urea cleft containing additional aromatic C–H hydrogen bond donor flanked by the central nitrophenyl core; thus, the low affinities observed for nitrate and the halides can be explained in terms of less hydrogen bonding complementarity and spatial fit toward the receptor, since all binding sites of **1b** are not fully utilized and the electronegative P=O binding unit may preclude the effective coordination for non-protic anions. Additionally, ¹H NMR competition experiments of receptor **1b** and HSO₄⁻ with NO₃⁻ or Cl⁻ anions were also performed (Figure B.43). The observed guest displacements between HSO₄⁻ and the competing anions demonstrate that receptor **1b** has a definitive binding preference for HSO₄⁻.

With regard to host **1a**, similar magnitudes of downfield shifts were also observed for the urea protons for nitrate and halide anions, whereas only very small downfield perturbations were observed for the protons H^b with the exception of HSO₄⁻ anion. Although the entropic contribution to binding cannot be neglected, the deletion or

deactivation of the C–H HB element seems to cause a large loss of all investigated anion affinities, and this effect is even more pronounced in the case of HSO_4^- , as shown by the association constants for **1** given in Table 3.1.

Gratifyingly, single crystals of the **1b**• HSO_4^- complex were obtained by diffusing n-pentane into a DMSO/ CHCl_3 solution of receptor **1b** containing an excess of TBAHSO₄.¹⁹ The resulting structure shows that the receptor adopts a twisted “U” shape conformation in which one HSO_4^- anion is nicely trapped inside the binding pocket of **1b** (Figure 3.3a). Within this solid-state structure, the distance between the oxygen atom in the P=O moiety and the oxygen atom in the HSO_4^- anion is 2.569 Å, and the N(H^a)•••O distance is 2.779 Å. These extremely short atomic distances engaged in HBs¹¹ indicate that the polarized P=O and acidic N–H^a units strongly attract the anion. Apparent triple N–H•••O hydrogen bonds between the urea motif and guest and two cooperative C(H^b)•••O and C(H^c)•••O interactions (3.177 and 3.096 Å, respectively) are also observed; thus, this overall structure is stabilized by seven intramolecular hydrogen bonds within the HSO_4^- anion (as well as the electrostatic interaction with a single TBA⁺ countercation), corroborating the results observed in solution and fulfilling our expectation that the phosphoramidate domain is involved in the binding via the formation of hetero-complementary hydrogen bonds. To the best of our knowledge, host **1b** is the only organic molecule reported to date that shows heptacoordination of a prototypic hydrogen sulfate ion by a single anion receptor, which can apparently be ascribed to the tight binding and ideal topological complementarity between the hybrid arylethynyl host and HSO_4^- . Additionally, the anion interacts with an adjacent receptor via two very weak intermolecular C–H•••O contacts to provide a weak

dimeric complex with pseudo-2:2 stoichiometry, which likely results from crystal packing effects (Figure B.4).

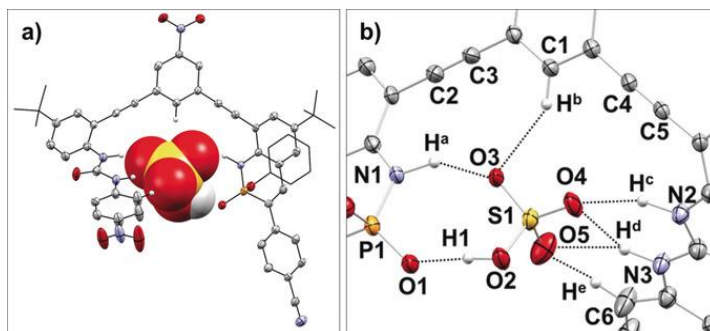


Figure 3.3 a) X-ray structure of **1b**·HSO₄⁻ complex; thermal ellipsoids are drawn at the 25% probability level. The TBA cation is omitted for clarity. b) The coordination environment of HSO₄⁻ showing seven hydrogen bonds (indicated by black dotted lines). Hydrogen-bond parameters (lengths [Å], angles [°]): O1-H1···O2: 1.63(6), 174(5), [O1···O2: 2.569(4)]; N1-H^a···O3: 1.82(4), 149(5), [N1···O3: 2.779(4)]; C1-H^b···O3: 2.312, 151.2, [C1···O3: 3.177]; N2-H^c···O4: 1.82(3), 159(4), [N2···O4: 2.834(5)]; N3-H^d···O4: 2.44(3), 139(3), [N3···O4: 3.307(6)]; N3-H^d···O5: 2.15(3), 155(3), [N3···O5: 3.130(6)]; C6-H^e···O5: 2.26, 146.3, [C6···O5: 3.096(7)]. S-O bond lengths [Å] within the HSO₄⁻ anion: S1···O2: 1.565(3), S1···O3: 1.425(3), S1···O4: 1.436(3), S1···O5: 1.429(4). Selected atomic distances [Å]: C2···O3: 3.494; C3···O3: 3.366; C4···O4: 3.501; C5···O4: 3.472.

To confirm that the P=O···(H-O)_{anion} hydrogen bonding observed in the solid state is retained in solution, ³¹P NMR measurements were performed under the same conditions on both receptors. Upon addition of TBAHSO₄ to receptor **1a**, the ³¹P signal underwent a significant downfield shift ($\Delta\delta \approx +3$ ppm) due to the deshielding effect exerted by HSO₄⁻ coordination to the electronegative oxygen atom of the P=O group. In contrast, small upfield signal perturbations ($\Delta\delta \approx -0.16$ ppm) were observed upon the addition of TBANO₃. This reverse signal shifting is most likely due to anion-induced polarization of the N-H^a bond involved in the binding, with a concomitant increase in the electron density of the N atom sensed by the neighboring P atom. In the case of the halides, no detectable or negligible chemical shift of the ³¹P nucleus signal was observed for either **1a** or **1b**. The phosphorus NMR experiments corroborated that the P=O domain of PN heterocycle served

as a HB acceptor for protic anion binding and demonstrated that the PN heterocyclic framework plays an important role in the superior affinity of **1** for the HSO_4^- ion over the other anions. Binding constants of the two receptors for HSO_4^- and NO_3^- based on ^{31}P NMR analysis are also given in Table 3.1 and are in good agreement with those obtained by ^1H NMR titration.

To further understand the interactions and structural aspects of the anionic complex, DFT calculations at the M06-2X/def2-TZVPP computational level were performed based on the geometry of the crystalline complex, where all H atoms were pre-optimized. The calculated electrostatic potential (V_s) of free host **1b** reveals that the preorganized cavity of the receptor possesses both electronegative and electropositive character (Figure B.50). On the basis of atoms in molecules (AIM) theory,²¹ the topological analysis of the electron density distinctly shows the bond critical points (BCPs) and the bond paths corresponding to those intermolecular interactions within the binary complex (Figure 3.4a).

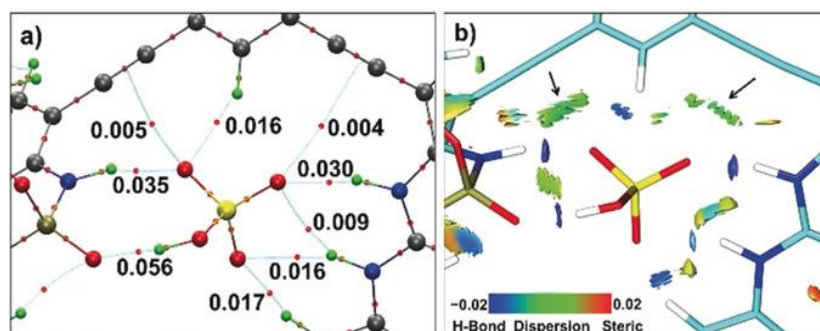


Figure 3.4 a) Snapshot showing the bond paths and BCPs for **1 b**· HSO_4^- complex based on AIM analysis. Red dots indicate BCPs, and blue dotted lines denote bond paths. Values of electron density $\rho(r)$ are given for the relevant BCPs (in a.u.). b) Snapshot showing the NCI plot for **1 b**· HSO_4^- complex. NCI regions are represented as solid surfaces and blue-green-red scaling from $-0.02 < \text{sign}(\lambda_2)\rho(r) < 0.02$ (in a.u.), where red surface indicates strong repulsion, blue surface strong attraction and green surface relatively weak interactions. Isosurface cutoff for $\text{NCI}=0.5$. The arrows in the Figure indicate the green isosurfaces existing between anion and alkyne moieties

The electron density $\rho(r)$ of $\text{P}=\text{O}\cdots(\text{H}-\text{O})$ anion as well as $\text{N}-\text{H}^{\text{a}}\cdots\text{O}$ interactions were calculated to be 0.056 and 0.035 a.u., respectively, which are beyond the proposed range of hydrogen bond criteria (>0.034 a.u.),²² suggesting unconventionally strong HB interactions. The degree of covalency of the intermolecular HB interactions within the complex were evaluated using Wiberg Bond Indices (WBI),²³ and the two higher values (0.07 and 0.05) were attributed to the $\text{P}=\text{O}\cdots(\text{H}-\text{O})$ anion and $\text{N}-\text{H}^{\text{a}}\cdots\text{O}$ interactions, respectively (Table B.3). These computational results suggest that the interactions between phosphoramidate and guest are the dominant element in the binding events, which may partly explain the significantly greater affinities of **1** observed for HSO_4^- anion. In addition, two BCPs with very small $\rho(r)$ were observed between the oxygen atoms in the HSO_4^- anion and alkyne units (i.e., $\text{C}2-\text{C}3\cdots\text{O}3$ and $\text{C}4-\text{C}5\cdots\text{O}4$ in Figure 3.3b), suggesting the existence of weak intermolecular interactions. Considering the appropriate atomic distances (3.366 to 3.501 Å) and the p-electron deficient character of acetylene units, these interactions could be suggestive of “anion- π ”-type interactions.¹³ Indeed, the shapes and sizes of the NCI (noncovalent interaction) isosurfaces clearly indicate there are at least dispersive forces (van der Waals interactions) between the anion and the acetylene inner edges (Figure 3.4b).

As receptors **1a/1b** are immiscible with water and have appreciable solubility in organic solvents, we next explored the extraction behavior of **1b** toward HSO_4^- via liquid–liquid extraction (LLE) experiments. A 2M NaHSO_4 or 2M H_2SO_4 aqueous solution (as the sources of HSO_4^-) containing TBANO_3 (10 mm, as a cation exchanger) was layered onto a solution of **1b** (10 mm) in CDCl_3 . The two non-miscible layers were thoroughly mixed for 30 min and allowed to settle, during which time the two layers separated and the CDCl_3

phase was analyzed by $^1\text{H}/^{31}\text{P}$ NMR spectroscopy. According to the comparison experiments, the obtained spectra from the extraction experiments indicate that nearly equimolar amounts (vs. **1b**) of TBAHSO₄ were transferred from aqueous solution into the organic phase (Figure B.45). The apparent extraction efficiencies for a single extraction were estimated to be ca. 100% and 92% in the cases of NaHSO₄ and H₂SO₄, respectively. In contrast, only trace amounts of HSO₄⁻ were extracted into the CDCl₃ phase in the absence of receptor (Figure B.47), primarily due to the high hydration energy of HSO₄⁻. The results demonstrated here are appealing since the hydrogen sulfate anion receptors could be potentially used to achieve direct extraction/removal of SO₄²⁻ anion from fairly acidic water without adjusting the pH. Notably, the hydrogen sulfate-bound receptor in CDCl₃ can be readily returned to its free form by simple water washing, suggesting that **1b** can be recycled when serving as an HSO₄⁻ anion extractant. Compared to the extensive and well-established sulfate LLE studies,²⁴ the release of the bound sulfate and recovery of the receptors are often not so feasible. In most cases, the sulfate-sequestering reagents were needed due to the prized strong binding affinities. Thus, the unique and efficient binding-release cycles presented here may be an added advantage for sulfate species biphasic extraction/transportation.

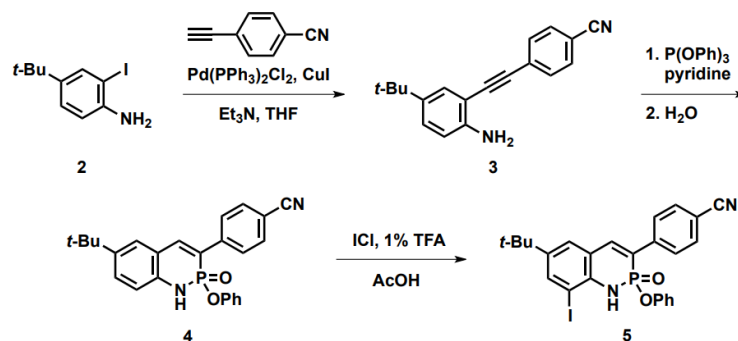
3.3 Conclusion

In summary, we have designed receptors containing phosphoramidate and urea motifs for selective recognition of HSO₄⁻ anion in organic solution. The geometrical complementarity in receptor-anion complexes has been unambiguously confirmed by NMR spectroscopy and single crystal X-ray analysis, as well as supported by DFT calculations. We have demonstrated that the phosphoramidate moiety of the PN-heterocycle is an HSO₄⁻ anion

selective recognition motif and the cooperation of other H-bond donors can significantly enhance anion binding affinity. Given that this unique scaffold can be readily tailored, these studies point the way to the rational design of promising synthetic receptors capable of transporting/removal of sulfuric acid, HSO_4^- salts, and even direct extraction of SO_4^{2-} anion in highly acidic aqueous environments.

3.4 Experimental Section

General Information. Tetrabutylammonium salts were dried under vacuum and stored in a desiccator over anhydrous CaSO_4 . All other materials were obtained from TCI-America, Sigma-Aldrich, or Acros and used as received. Reactions were performed under an inert N_2 atmosphere in dried glassware. NMR spectra were obtained on an Inova 500 MHz spectrometer (^1H : 500.11 MHz, ^{13}C 125.76 MHz, ^{31}P 202.46 MHz) or a Bruker Avance-III-HD 600 MHz (^1H : 599.98 MHz, ^{13}C : 150.87 MHz) spectrometer. Chemical shifts (δ) are expressed in ppm using residual non-deuterated solvent present in the bulk deuterated solvent (CDCl_3 : ^1H 7.26 ppm, ^{13}C 77.16 ppm; $\text{DMSO-}d_6$: ^1H 2.50 ppm, ^{13}C 39.52 ppm). ^{31}P chemical shifts are reported against 85% H_3PO_4 (δ 0 ppm) as external reference. Mass spectrometry (m/z) data were acquired using atmospheric solids analysis probe (ASAP). Mixed solvent systems were referenced to the most abundant solvent. All NMR spectra were processed using MestReNova NMR processing software. IR data were collected using the Thermo Fisher Nicolet 6700 FT-IR spectrometer, the vacuum-dried solid samples were prepared by KBr pellet technique. Analytical TLC was carried out on TLC plates (5 \times 10 cm with 0.25 mm thickness, silica gel 60 F254, Merck, Darmstadt, Germany) cut from the commercially available aluminum sheets. Aniline **2** and ethynylaniline **6** were synthesized following known procedures.¹²



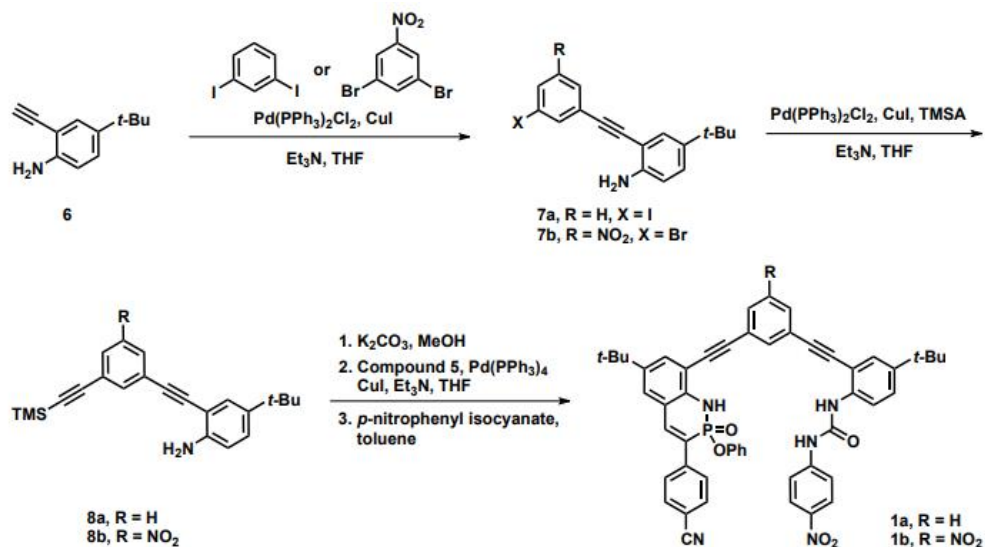
Scheme 3.1 Synthesis of Iodoheterocycle Coupling Piece **5**.

Ethynylaniline 3. To an N₂-degassed solution of 4-(*tert*-butyl)-2-iodoaniline¹² (**2**, 1.57 g, 5.70 mmol) and 4-ethynylbenzonitrile (0.86 g, 6.83 mmol) in 5:1 (v/v) THF/Et₃N (30 mL) were added CuI (53 mg, 0.28 mmol) and Pd(PPh₃)₂Cl₂ (196 mg, 0.28 mmol) at room temperature. The solution was stirred under N₂ for 12h, then the reaction mixture was diluted with CH₂Cl₂ and filtered through a 4 cm pad of silica. The filtrate was concentrated under reduced pressure. The crude product was purified by flash chromatography over silica gel to give **3** (1.29 g, 83%) as a brown solid; *R*_f = 0.17 (hexanes/EtOAc, 10:1). Mp 108–110 °C. ¹H NMR (500 MHz, CDCl₃) δ 7.61 (*ABm*, *J* = 8.1 Hz, 4H), 7.38 (d, *J* = 2.3 Hz, 1H), 7.24 (dd, *J* = 8.5, 2.3 Hz, 1H), 6.70 (d, *J* = 8.5 Hz, 1H), 4.19 (s, 2H), 1.29 (s, 9H). ¹³C NMR (126 MHz, CDCl₃) δ 145.9, 141.1, 132.1, 131.9, 128.9, 128.5, 128.2, 118.7, 114.6, 111.2, 106.3, 92.8, 91.4, 34.0, 31.4. HRMS (ASAP) *m/z* calcd for C₁₉H₁₉N₂ [M+H]⁺ 275.1548, found 275.1530.

Heterocycle 4. To a solution of aniline **3** (1.3 g, 4.74 mmol) in dry pyridine (5 mL) was added triphenylphosphite (1.9 mL, 7 mmol). The reaction flask was sealed and heated to 105 °C for 24 h. After cooling, the volatiles were removed *in vacuo*. Analytically pure material can be obtained from recrystallization using EtOAc to give **4** (1.20 g, 61%) as a yellow solid; *R*_f = 0.27 (CH₂Cl₂/EtOAc, 2:1). Mp > 200 °C. ¹H NMR (500 MHz, CDCl₃)

δ 8.39 (s, 1H), 7.95 (d, $J = 8.0$ Hz, 2H), 7.72 (d, $J = 8.0$ Hz, 2H), 7.68 (d, $J = 38.7$ Hz, 1H), 7.38 (dd, $J = 8.6, 2.0$ Hz, 1H), 7.32 (s, 1H), 7.09 (t, $J = 7.6$ Hz, 2H), 6.98 (t, $J = 7.5$ Hz, 2H), 6.90 (d, $J = 8.0$ Hz, 2H), 1.31 (s, 9H). ^{13}C NMR (126 MHz, CDCl_3) δ 150.3 (d, $J = 9.0$ Hz), 144.5, 143.9 (d, $J = 5.0$ Hz), 140.6 (d, $J = 9.3$ Hz), 137.7 (d, $J = 2.0$ Hz), 132.7, 129.6, 129.3, 128.4 (d, $J = 6.4$ Hz), 125.1, 121.2 (d, $J = 4.1$ Hz), 117.3 (d, $J = 9.3$ Hz), 111.8, 34.3, 31.5. ^{31}P NMR (202 MHz, CDCl_3) δ 10.84 (d, $J = 39.3$ Hz). HRMS (ASAP) m/z calcd for $\text{C}_{25}\text{H}_{24}\text{N}_2\text{O}_2\text{P}$ $[\text{M}+\text{H}]^+$ 415.1575, found 415.1588.

Iodoheterocycle 5. To a solution of **4** (106 mg, 0.256 mmol) in CH_2Cl_2 (2 mL) and AcOH (3 mL) was added TFA (0.05 mL). A 1.0 M solution of ICl in CH_2Cl_2 (0.32 mL) was added dropwise by syringe and the mixture stirred under N_2 overnight. The mixture was washed with saturated NaS_2O_3 (2×150 mL) and brine (150 mL), dried (MgSO_4) and evaporated. The crude product was purified by chromatography over silica gel (hexanes/ CH_2Cl_2 /EtOAc, 3:1:1) to give **5** (74 mg, 54%) as a light yellow solid; $R_f = 0.32$ (hexanes/ CH_2Cl_2 /EtOAc, 3:1:1). Mp > 200 °C. ^1H NMR (500 MHz, CDCl_3) δ 7.93 (d, $J = 8.0$ Hz, 2H), 7.83 (t, $J = 2.1$ Hz, 1H), 7.71 (d, $J = 8.1$ Hz, 2H), 7.58 (d, $J = 39.5$ Hz, 1H), 7.36 (d, $J = 2.1$ Hz, 1H), 7.21 (t, $J = 7.7$ Hz, 2H), 7.09 (t, $J = 7.4$ Hz, 1H), 6.92 (d, $J = 7.9$ Hz, 2H), 6.55 (s, 1H), 1.32 (s, 9H). ^{13}C NMR (126 MHz, CDCl_3) δ 149.8 (d, $J = 9.2$ Hz), 146.7, 142.9 (d, $J = 4.8$ Hz), 139.6 (d, $J = 9.7$ Hz), 138.4, 137.4, 132.7, 129.8, 128.7, 128.5 (d, $J = 6.7$ Hz), 125.8, 125.6, 124.5, 121.2 (d, $J = 4.1$ Hz), 120.3 (d, $J = 13.7$ Hz), 118.7, 112.2, 87.5 (d, $J = 8.9$ Hz), 34.4, 31.3. ^{31}P NMR (202 MHz, CDCl_3) δ 9.52 (d, $J = 39.5$ Hz). HRMS (ASAP) m/z calcd for $\text{C}_{25}\text{H}_{23}\text{IN}_2\text{O}_2\text{P}$ $[\text{M}+\text{H}]^+$ 541.0542, found 541.0542.



Scheme 3.2 Synthesis of Ethynylaniline Coupling Piece **8** and Receptors **1a/1b**.

Ethynylaniline 7a/7b. To an N₂-sparged solution of 1,3-diodobenzene (for **7a**) or 1,3-dibromo-5-nitrobenzene (for **7b**) (1.2 equiv.) and terminal acetylene **6**^{12a} (1.0 equiv.) in THF/Et₃N (0.05 M, v/v = 1:1) was added 5 mol% Pd(PPh₃)₂Cl₂ and 5 mol% CuI. The suspension was stirred at room temperature under an N₂ atmosphere for 12 h. The reaction mixture was concentrated *in vacuo* and purified *via* flash chromatography to give product **7** as a dark orange oil. **7a.** Yield: 52%; *R*_f = 0.47 (hexanes/EtOAc, 5:1). ¹H NMR (600 MHz, CDCl₃) δ 7.93 (t, *J* = 1.7 Hz, 1H), 7.67 (dt, *J* = 8.1, 1.3 Hz, 1H), 7.51 (dt, *J* = 7.8, 1.3 Hz, 1H), 7.41 (d, *J* = 2.3 Hz, 1H), 7.23 (dd, *J* = 8.5, 2.3 Hz, 1H), 7.09 (t, *J* = 7.8 Hz, 1H), 6.70 (d, *J* = 8.5 Hz, 1H), 4.19 (s, 2H), 1.32 (s, 9H). ¹³C NMR (151 MHz, CDCl₃) δ 145.6, 140.9, 140.0, 137.1, 130.5, 129.9, 128.8, 127.6, 125.5, 114.5, 106.9, 93.9, 92.5, 88.1, 34.0, 31.5. HRMS (ASAP) *m/z* calcd for C₁₈H₁₉IN [M+H]⁺ 376.0562, found 376.0555.

7b. Yield: 66%; *R*_f = 0.12 (hexanes/EtOAc, 10:1). ¹H NMR (500 MHz, CDCl₃) δ 8.33–8.31 (m, 2H), 7.99 (d, *J* = 2.1 Hz, 1H), 7.40 (t, *J* = 2.1 Hz, 1H), 7.29–7.27 (m, 1H), 6.73 (dd, *J* = 8.6, 1.7 Hz, 1H), 4.21 (s, 2H), 1.33 (s, 9H). ¹³C NMR (126 MHz, CDCl₃) δ 148.7,

146.1, 141.3, 139.6, 129.1, 128.6, 127.0, 125.9, 124.8, 122.8, 114.7, 105.8, 91.2, 90.7, 34.1, 31.5. HRMS (ASAP) m/z calcd for $C_{18}H_{18}BrN_2O_2$ $[M+H]^+$ 373.0552, found 373.0534.

Diethynylaniline 8a/8b. A ~0.1 M solution of the respective **7** (1.0 equiv.) in THF/Et₃N (0.05 M, v/v = 1:1) was purged for 15 min with N₂ and then TMSA (1.5 equiv.) was added *via* syringe. After an additional 5 min N₂ purging, CuI (0.1 equiv.) and Pd(PPh₃)₂Cl₂ (0.1 equiv.) were added to the reaction mixture. The flask was then purged for an additional 5 min, then sealed and stirred at room temperature under N₂ for 12 h. The mixture was concentrated and the residue chromatographed on silica gel (10:1 hexanes/EtOAc) to afford the desired TMS-protected ethynylsilane **8** as a colorless oil. **8a.** Yield: 90%; R_f = 0.32 (hexanes/EtOAc, 10:1). ¹H NMR (600 MHz, CDCl₃) δ 7.68 (t, J = 1.6 Hz, 1H), 7.49 (dt, J = 7.8, 1.4 Hz, 1H), 7.43 (dt, J = 7.8, 1.4 Hz, 1H), 7.39 (d, J = 2.4 Hz, 1H), 7.31–7.28 (m, 1H), 7.21 (dd, J = 8.5, 2.3 Hz, 1H), 6.69 (d, J = 8.5 Hz, 1H), 4.17 (s, 2H), 1.31 (s, 9H), 0.29 (s, 9H). ¹³C NMR (151 MHz, CDCl₃) δ 145.5, 140.9, 134.8, 131.4, 131.3, 128.8, 128.4, 127.4, 123.7, 123.5, 114.4, 107.2, 104.2, 95.0, 93.3, 87.2, 33.9, 31.4, 0.0. HRMS (ASAP) m/z calcd for $C_{23}H_{28}NSi$ $[M+H]^+$ 346.1991, found 346.1993.

8b. Yield: 80%; R_f = 0.24 (hexanes/EtOAc, 10:1). ¹H NMR (500 MHz, CDCl₃) δ 8.27–8.26 (m, 1H), 8.21–8.20 (m, 1H), 7.89–7.88 (m, 1H), 7.37 (d, J = 2.3 Hz, 1H), 7.24 (dd, J = 8.4, 2.3 Hz, 1H), 6.70 (d, J = 8.5 Hz, 1H), 4.18 (s, 2H), 1.30 (s, 9H), 0.28 (s, 9H). ¹³C NMR (126 MHz, CDCl₃) δ 148.2, 146.0, 141.2, 139.9, 129.1, 128.3, 125.7, 125.6, 125.6, 125.3, 114.7, 106.1, 101.7, 98.5, 91.3, 90.2, 34.1, 31.5, 0.2. HRMS (ASAP) m/z calcd for $C_{23}H_{27}N_2O_2Si$ $[M+H]^+$ 391.1842, found 391.1854.

Receptor 1a/1b. To a solution of **8** (1.0 equiv.) in MeOH (0.1 M) was added K₂CO₃ (3.0 equiv.). After stirring the suspension at room temperature for 3 h, the mixture was filtered

through a bed of Celite. After evaporation of the solvent, the crude residue was used directly in the next reaction.

To an N₂-sparged solution of **5** (1.2 equiv.) and the terminal acetylene in THF (0.05 M) was added 5 mol% Pd(PPh₃)₄ and 5 mol% CuI, followed by the addition of Et₃N (1.5 equiv.). The suspension was stirred at room temperature under an N₂ atmosphere for 1-2 h (monitored by TLC). The reaction mixture was concentrated *in vacuo* and purified *via* flash chromatography to give the desired crude diyne product as dark-orange oil.

To a solution of the crude product in dry toluene (0.1 M) was added 4-nitrophenyl isocyanate (1.2 equiv.), and the mixture was stirred at room temperature for 24 h. The reaction was diluted with hexanes and the light yellow precipitate was isolated. The material was redissolved in a minimal amount of DMSO (to remove the insoluble impurities when necessary), and the desired product precipitated as a fine light yellow powder upon the slow addition of EtOH.

1a. Yield: 44%; *R*_f = 0.34 (hexanes/CH₂Cl₂/EtOAc, 3:1:1). Mp > 150 °C (dec.). ¹H NMR (500 MHz, CDCl₃/DMSO-*d*₆, 4/1) δ 9.62 (s, 1H), 8.01 (s, 1H), 7.90–7.87 (m, 3H), 7.76 (t, *J* = 1.6 Hz, 1H), 7.40–7.37 (m, 2H), 7.66 (d, *J* = 2.8 Hz, 1H), 7.50 (d, *J* = 39.2 Hz, 1H), 7.49–7.44 (m, 6H), 7.38 (dt, *J* = 6.1, 1.7 Hz, 2H), 7.29 (d, *J* = 2.4 Hz, 1H), 7.19–7.16 (m, 3H), 6.93–6.90 (m, 2H), 6.81–6.78 (m, 1H), 6.72–6.70 (m, 2H), 1.12 (s, 9H), 1.11 (s, 9H). ¹³C NMR (126 MHz, CDCl₃/DMSO-*d*₆, 4/1) δ 151.9, 149.5 (d, *J* = 9.1 Hz), 145.9, 145.1, 143.7, 142.6, 141.2, 139.5 (d, *J* = 9.4 Hz), 137.5, 136.8, 134.4, 132.1, 131.6, 131.2 (d, *J* = 4.8 Hz), 129.1, 128.6, 128.3, 128.2, 127.8 (d, *J* = 6.5 Hz), 126.6, 124.8, 124.6, 124.1, 123.0, 122.8, 122.4, 120.6 (d, *J* = 4.1 Hz), 119.4, 118.9 (d, *J* = 13.9 Hz), 118.2, 117.3, 111.2 (d, *J* = 6.1 Hz), 110.0 (d, *J* = 8.8 Hz), 94.9, 93.6, 86.5, 84.4, 33.8, 33.8, 30.8, 30.8. ³¹P NMR

(202 MHz, CDCl₃/DMSO-*d*₆, 4/1) δ 9.13 (d, $J = 39.0$ Hz). IR (KBr) ν (cm⁻¹) 3432, 2960, 2227, 1719, 1597, 1504, 1331, 1203. HRMS (ASAP) m/z calcd for C₄₅H₄₁N₃O₂P [(M-C₇H₅N₂O₃)+H]⁺ 686.2936, found 686.2914.

1b. Yield: 41%; $R_f = 0.27$ (hexanes/CH₂Cl₂/EtOAc, 5:2:2). Mp > 150 °C (dec.). ¹H NMR (500 MHz, DMSO-*d*₆) δ 11.25 (s, 1H), 9.51 (s, 1H), 9.04 (s, 1H), 8.77 (d, $J = 2.2$ Hz, 1H), 8.65 (s, 1H), 8.61 (d, $J = 2.3$ Hz, 1H), 8.18 (d, $J = 38.9$ Hz), 8.17 (d, $J = 8.8$ Hz, 2H), 8.11 (d, $J = 8.1$ Hz, 2H), 8.01 (d, $J = 8.8$ Hz, 1H), 7.97 (d, $J = 8.0$ Hz, 2H), 7.80 (d, $J = 8.7$ Hz, 2H), 7.74 (s, 1H), 7.69 (d, $J = 2.3$ Hz, 1H), 7.61 (d, $J = 2.4$ Hz, 1H), 7.48 (dd, $J = 8.8, 2.4$ Hz, 1H), 7.20 (t, $J = 7.7$ Hz, 2H), 7.03 (t, $J = 7.4$ Hz, 1H), 6.95 (d, $J = 8.0$ Hz, 2H), 1.31 (s, 9H), 1.30 (s, 9H). ¹³C NMR (151 MHz, DMSO-*d*₆) δ 152.1, 150.2 (d, $J = 9.2$ Hz), 148.0, 146.6, 145.4, 143.3, 143.2 (d, $J = 3.6$ Hz), 141.0, 140.4, 140.0 (d, $J = 9.7$ Hz), 138.6, 137.6, 132.8, 132.4, 130.0, 129.7, 129.3, 128.1 (d, $J = 6.6$ Hz), 127.5, 126.1, 125.9, 125.1, 125.0, 124.5 (d, $J = 12.7$ Hz), 123.7, 122.6, 121.0 (d, $J = 3.9$ Hz), 120.5, 119.4 (d, $J = 14.8$ Hz), 118.8, 117.4, 111.2, 110.7, 109.2 (d, $J = 8.6$ Hz), 92.7, 92.1, 89.0, 87.8, 34.1, 34.0, 31.0, 30.9. ³¹P NMR (202 MHz, DMSO-*d*₆) δ 9.05 (d, $J = 38.7$ Hz). IR (KBr) ν (cm⁻¹) 3442, 2960, 2228, 1711, 1602, 1536, 1331, 1199. HRMS (ASAP) m/z calcd for C₄₅H₄₀N₄O₄P [(M-C₇H₅N₂O₃)+H]⁺ 731.2787, found 731.2765.

CHAPTER IV

AMPLIFICATION OF THE QUANTUM YIELDS OF 2- λ^5 -PHOSPHAQUINOLIN-2-ONES THROUGH PHOSPHORUS CENTER MODIFICATION

This chapter includes previously published and co-authored material from Bard, J.P., Bates, H.J., Deng, C.-L., Zakharov, L.N., Johnson, D.W., Haley, M.M. “Amplification of the Quantum Yields of 2- λ^5 -Phosphaquinolin-2-ones Through Phosphorus Center Modification.” *J. Org. Chem.* **2020**, *85*, 85–91. This work highlights our work on understanding the effects of placing a phenyl group in place of the traditional phenoxy group on the P center of the phosphaquinolinone scaffold. It draws structure-property relationships with both the supramolecular and photophysical properties.

4.1 Introduction

Small molecule fluorophores are used ubiquitously throughout many different fields, including chemical biology, molecular probe development, and materials for industrial and environmental sensing.¹⁻⁴ In many of these applications, a fluorophore must exhibit a few characteristics to be considered optimal: large Stokes shift, high brightness, and red-shifted emission. One such example of a molecule that meets these specifications is coumarin (Figure 4.1).⁵⁻¹⁴ An impressive number of coumarin-containing compounds have been reported throughout the literature that are collected either from in-lab syntheses or by isolation from natural sources.^{15,16} This scaffold has been the subject of a variety of

synthetic modifications, diversification by adding groups onto the backbone, or incorporation of the coumarin system into larger ring networks.¹⁷⁻¹⁹ Through these modifications, a tremendous breadth of understanding upon the structure–activity relations has been developed²⁰⁻²⁴ that have guided the design of many useful derivatives, which have emerged for applications in chemosensing and many other areas.²⁵⁻³¹

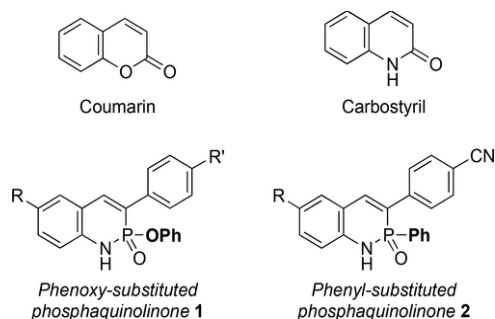


Figure 4.1 Well-studied coumarin and carbostyryl scaffolds (top) compared to phosphoquinolinone analogues (bottom).

Alongside the many derivatives of the parent coumarin scaffold, there is the nitrogen-containing structural analogue known as carbostyryl (Figure 4.1).³²⁻³⁷ Though not as widely utilized as coumarin, carbostyryl is the subject of many structure–property relationship studies, and it shows promise for use in both pharmaceutical discovery and fluorescence imaging applications.^{38,39} These carbostyryl analogues expand on the applications of the coumarin family through modifying the lactone core to a lactam. With further alteration of this core, new applications, functionality, and fluorescent properties are expected from this widely used fluorophore.

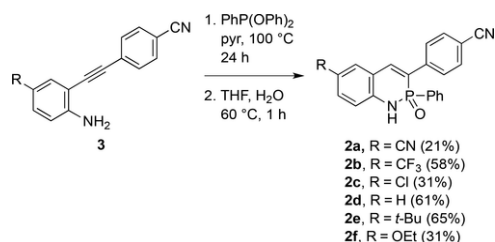
Recently, we reported a series of phosphorus- and nitrogen-containing (PN) phosphoquinolinone **1** derivatives (Figure 4.1).^{40,41} This scaffold, which is one of only a handful of similar heterocycles,⁴²⁻⁵² is also an isostere to carbostyryl and coumarin, with the only difference being the replacement of the lactam carbonyl with an isolobal, chiral

phosphorus center. We have performed a variety of structure–property studies that looked at the effects of both acene core modification and substitution at various points on the scaffold.^{40,41,53-56} In these studies, it was found that the emission wavelength can be moderately red-shifted through careful substitution of various groups on the backbone, affording significant Stokes shifts and modest quantum yields. On the basis of these design principles, this moiety has recently been implemented in a fluorescent receptor for HSO_4^- in acidic media, showing promise for future applications of this scaffold that take advantage of both its exceptional hydrogen bonding capabilities and its inherent fluorescence.⁵⁴ As clearly shown for the coumarin and carbostyryl motifs, systematic modification of various structural aspects can lead to very useful derivatives. In our continuing efforts to study the 2- λ^5 -phosphaquinolin-2-one skeleton, the next facet that we wanted to explore was the variation of the group attached to the phosphorus center. Disclosed herein is the substitution of a phenyl ring in place of the standard phenoxy upon the phosphorus center, generating a racemic mixture of heterocycle **2** (Figure 4.1). We also hypothesize that this would increase the quantum yield through rigidifying the scaffold. With these modifications, the reported compounds could have greater potential for applications in phosphorus-containing chemosensors and fluorophores, expanding on this pre-existing group of molecules.⁵⁷⁻⁶⁵

4.2 Results and Discussion

The synthesis of **2** starts from key arylethynylaniline intermediate **3**, prepared following previously reported methods.⁴⁰ Aniline **3** is then reacted with diphenyl phenylphosphonite ($\text{PhP}(\text{OPh})_2$) in pyridine at 100 °C. Subsequent hydrolysis in THF at 60 °C furnishes phenyl-appended heterocycles **2** in modest to good yields (Scheme 4.1).

^1H , ^{13}C , ^{31}P , and ^{19}F NMR spectra were collected for **2** (see Appendix C), which reveal that the direct attachment of the phenyl ring to the phosphorus center not only splits the signals of the phenyl ring ($J^{31\text{P},^1\text{H}}$ and $J^{31\text{P},^{13}\text{C}}$ values listed in the Experimental Section) but also affords coupling constants of *ca.* 30 Hz ($^3J^{31\text{P},^1\text{H}}$) for the alkene proton signal.



Scheme 4.1 Synthesis of Phosphaquinolinones **2**.

The photophysical properties of **2a–2f** in CHCl_3 are shown in Figure 4.2 and are compiled in Table 4.1. All derivatives share a common λ_{max} at *ca.* 300 nm, and the lowest energy absorption peaks range from 343 to 381 nm. The absorption coefficients for this scaffold stay within the range of 1.5×10^4 (for **2a**) to $2.2 \times 10^4 \text{ M}^{-1} \text{ cm}^{-1}$ (for **2e** and **2f**). The λ_{em} values range from 447 (for **2a**) to 515 nm (for **2f**) with Stokes shifts on the order of $6350\text{--}7000 \text{ cm}^{-1}$. Interestingly, the emission spectra of **2** show a *ca.* 20 nm bathochromic shift from those of the analogous congeners of **1**,⁴⁰ and the quantum yields of this scaffold show a dramatic improvement, on the order of a 4–5-fold increase in most cases. Brightness values range from 6.84×10^3 (for **2b**) to $1.14 \times 10^4 \text{ M}^{-1} \text{ cm}^{-1}$ (for **2a**), which are now on par with several optimized coumarin derivatives.⁶⁶

Fluorescence lifetime measurements were also performed (Figure C.6), and the radiative (k_r) and nonradiative (k_{nr}) decay rate constants were determined. The k_r values range from 0.06 to 0.19 ns^{-1} , and the k_{nr} values vary from 0.06 to 0.18 ns^{-1} , showing either equal rates or a slightly larger k_{nr} in most cases.

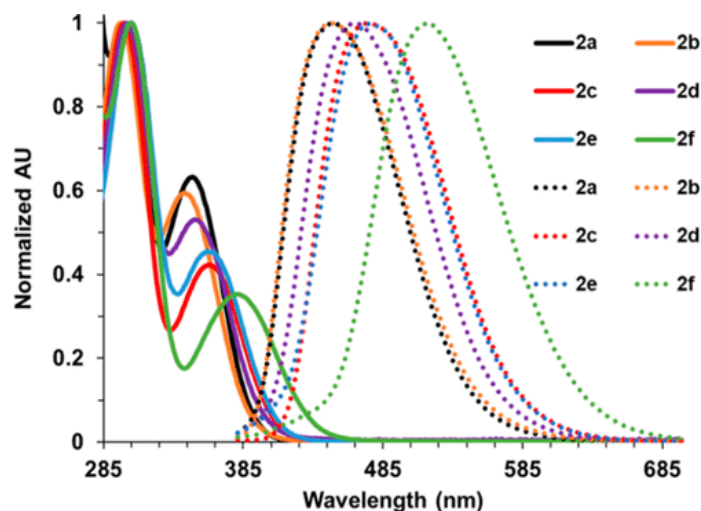


Figure 4.2 Absorption (solid lines) and fluorescence (dotted lines) spectra of **2** in CHCl_3 at 298 K.

Table 4.1. Photophysical Properties and HOMO–LUMO Energy Gaps of Heterocycles **2a**

cmpd	$\lambda_{\text{abs}}(\text{nm})/\epsilon$ ($\text{M}^{-1} \text{cm}^{-1}$)	$\lambda_{\text{em}}(\text{nm})/\phi$ (%)	Stokes shift (cm^{-1})	τ^b (ns)	k_r (ns^{-1})	k_n (ns^{-1})	ΔE_{opt} (eV)	ΔE_{DFT}^c (eV)
2a	348/15000	447/76	6360	4.1	0.19	0.06	3.19	4.40
2b	343/18000	449/38	6880	3.5	0.11	0.18	3.18	4.43
2c	360/19000	474/43	6680	4.8	0.09	0.12	3.05	4.23
2d	352/18000	467/50	7000	3.9	0.13	0.13	3.15	4.30
2e	360/22000	475/51	6730	4.2	0.12	0.12	3.04	4.21
2f	381/22000	515/35	6830	6.3	0.06	0.10	2.83	3.90

^a All values collected in CHCl_3 . ^b Decay curves fitted using a monoexponential fitting model. ^c Calculated at the PBE0/TZVP level of theory.

These values elucidate a potential explanation for the increased quantum yields when compared to similar values of phosphaquinolines **1**.⁴⁰ For **1**, the k_r values range from 0.10 to 0.30 ns^{-1} , which show similar values, whereas the k_{nr} values vary from 0.30 to 3.0 ns^{-1} , which are substantially faster in most cases. The diminished ratio of k_{nr} to k_r seen for **2** may suggest that the reduced degrees of freedom may indeed be the cause of the increased quantum yields.

To gain further understanding of these experimental results, the frontier orbitals for heterocycles **2** were calculated (Tables 4.1 and C.1–C.7). The narrowest HOMO–LUMO gap is seen for **2f** (3.90 eV), and the largest is for **2a** (4.40 eV). This trend arises because of a higher magnitude of HOMO destabilization than that of the stabilization of the LUMO with more donating substituents (Table C.1). These values also follow a similar trend to the optical gaps (Tables 4.1 or C.1). TD-DFT was then used to examine the S_0 to S_1 transition. It was found that the S_0 to S_1 transition is dominated by the HOMO–LUMO transition (Table C.1). Additionally, the distributions of the HOMOs and LUMOs show a slightly more pronounced separation due to a larger HOMO localization at the phosphorus center (Figure C.4). These observations suggest that π to π^* transitions are dominant, but there may be some intramolecular charge transfer (ICT) occurring in the excited state. The emission of **2** was then examined in solvents of varying polarities (Figures C.7–C.13 and Tables C.11–C.16). In these studies, bathochromatic shifting is observed in every case with more polar solvents. Compound **2f** showed the greatest shifting, ranging from emission wavelengths of 504 to 531 nm and Stokes shifts of 6070 and 7070 cm^{-1} in cyclohexane and acetonitrile, respectively.

The TD–DFT optimized S_1 state near the Franck–Condon geometry of **2f** shows that the dihedral angle between the parent core and appended 4-cyanophenyl substituent becomes smaller compared to the ground state (Figure 4.3). Additionally, the C–C bond connecting them is shortened by *ca.* 0.035 Å. The considerable geometric changes lead to a more conjugated system at the S_1 state, in which the HOMO–LUMO energy gap decreases by 0.9 eV (Figure C.5); thus, the computed emission wavelength of 541 nm is

within the observed emission maxima (Table 4.1). These computational results could further explain the large Stokes shift for this type of PN-heterocycle.

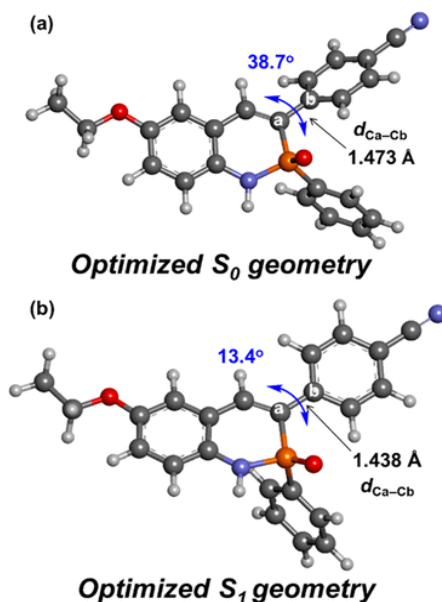


Figure 4.3 Selected bond length and dihedral angle in the optimized S₀ and S₁ structures of **2f** calculated by DFT and TD-DFT methods at the PCM(CHCl₃)-PBE0/TZVP level of theory, respectively.

In addition to improved fluorescence properties, we were curious to see how phenyl substitution would affect the strength of hydrogen bond dimerization we typically observe for phosphaquinolones. Variable concentration (VC) NMR experiments were performed in water-saturated CDCl₃ to assess the strength of dimerization (Tables 4.2 and C.17–C.21, Figures C.14–C.23). Heterocycles **2** exhibit dimerization strengths of 22 (for **2e** and **2f**) to 82 M⁻¹ (for **2b**). While these values are roughly 70–80% smaller than those measured for the analogous congeners of **1**, the strengths of dimerization for **2** again exceed those of many typical head-to-tail hydrogen bonded dimers.⁶⁷ This result suggests that this new entry into the phosphaquinolone family can still be implemented in supramolecular systems, as found in **1**.⁵⁴

Table 4.2. Dimerization Constants and Energies for 2

cmpd	$K_{\text{dim}} (\text{M}^{-1})$	$\Delta G_{\text{dim}} (\text{kcal mol}^{-1})$
2a ^a	-	-
2b	82	-2.6
2c	54	-2.3
2d	24	-1.8
2e	22	-1.8
2f	22	-1.8

^a Not determined because of minimal solubility in H₂O-saturated CDCl₃. Values reported with errors less than 15%.

Single crystals suitable for X-ray diffraction were grown by slowly diffusing pentane into a CHCl₃ solution of **2f**, and the resultant data are shown in Figures 4.4 and C.1–C.3. The structure of **2f** still features the typical *meso*-dimer between racemates (Figure 4.4a); however, the N···O distance in the dimer of **2f** (2.874 Å) is longer than those of heterocycles **1** (2.768–2.821 Å),⁴⁰ which supports the observation that the molecule should form a weaker dimer in the solution-state as well. This weakened hydrogen bonding interaction can potentially be explained by examining the pseudo six-membered ring formed between the monomers. The N···O–P (115.53°), O–P–N (116.66°), and P–N···O (104.57°) angles formed between the participating atoms in the dimer formation show significant deviation from the ideal 120° orientation (Figure 4.4b), likely caused by the large O–P–N–H torsional angle of 55.35° (Figure 4.4c). With an angle so much larger than the analogous angle found in the crystal structures of several derivatives of **1** (*ca.* 30–40°),⁴⁰ there is a less ideal orientation for the two monomers to associate, slightly weakening the interaction overall. By comparing optimized geometries of the *meso*-dimer of **2f** and its –OPh analogue, there are some additional steric clashes in **2f** among the C–H atoms in the phenyl ring and N–H moieties, according to the noncovalent interactions

(NCI) plot (Figure C.24). Moreover, the natural bond orbital (NBO) analyses predict a total contribution of the $n_{\text{O}} \rightarrow \sigma_{\text{NH}^*}$ interactions of $23.1 \text{ kcal mol}^{-1}$ for **2f** and $25.0 \text{ kcal mol}^{-1}$ for the respective $-\text{OPh}$ analogue (Figure C.25). Therefore, the strength of dimerization may decrease to some degree due to the weaker primary hydrogen bonding and extra steric hindrance, in agreement with the observed diminished K_{dim} for **2**.

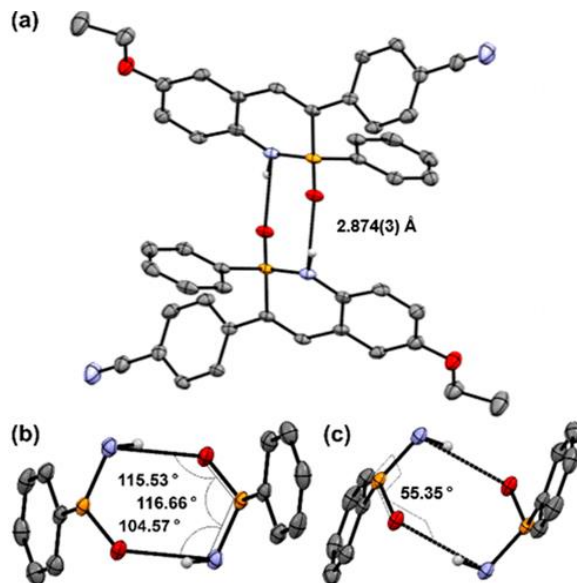


Figure 4.4 a) Characteristic PN-heterocycle dimer for **2f** with the $\text{O}\cdots\text{N}$ distance (\AA) shown as well as b) bond angles and c) torsional angles formed within monomers upon dimerization. Ellipsoids drawn at 30% probability.

4.3 Conclusion

In summary, we have shown the effects of the attachment of a phenyl group on the phosphorus center of the phosphaquinolone scaffold. This new class of PN-heterocycles not only has large Stokes shift values (up to 7000 cm^{-1}) but also shows a marked 4–5-fold increase in the quantum yield when compared to previously reported phenoxy-substituted compounds. Additionally, this modification retains the strong dimerization strengths of the scaffold in both the solid and solution states. This new modification deepens the fundamental understanding of the phosphaquinolone scaffold and allows for further

possibilities in the applications of this scaffold as a biologically or industrially relevant fluorophore, like the coumarin and carbostyryl scaffolds.

4.4 Experimental Section

General

All air- or water-free reactions were performed under a N₂ atmosphere using Schlenk techniques. Column chromatography was performed using silica gel (240–300 mesh), with solvent systems being referenced to the most abundant solvent. NMR spectra were acquired at room temperature on a Varian Inova 500 instrument (¹H: 500 MHz, ¹³C: 126 MHz, ¹⁹F: 471 MHz, ³¹P: 202 MHz) or a Bruker Avance III HD 500 apparatus equipped with a Prodigy multinuclear cryoprobe (¹H: 500 MHz, ¹³C: 126 MHz). ¹H and ¹³C chemical shifts (δ) are expressed in parts per million (ppm) relative to residual CHCl₃ shifts (¹H: 7.26 ppm, ¹³C: 77.16 ppm) or residual DMSO shifts (¹H: 2.50 ppm, ¹³C: 39.52 ppm). ³¹P and ¹⁹F NMR spectra are referenced to 85% H₃PO₄ (δ 0 ppm) and to CFCl₃ (δ 0 ppm), respectively, as the external standards. UV–vis spectra were recorded using an Agilent Technologies Cary 60 UV–vis spectrophotometer in HPLC-grade CHCl₃. Fluorescence emission spectra were recorded using a Horiba Jobin Yvon FluoroMax-4 fluorimeter exciting at 365 nm. Quantum yields (φ) were determined through a comparison of the emission and absorption intensities of the analyte to that of a 0.1 M H₂SO₄/quinine sulfate solution.⁶⁸ Fluorescence lifetime measurements were recorded using a Horiba FluoroHub Single Photon Counting Controller with a TemPro Fluorescence Lifetime System attachment. High-resolution mass spectra (HRMS) were recorded on a Waters XEVO G2-XS mass spectrometer. 2-Ethynylanilines **3a–3f**⁴⁰ and phenyl diphenylphosphonite (PhP(OPh)₂)⁶⁹ were prepared as previously described.

General Synthetic Procedure for Phosphaquinolinone 2

2-Ethynylaniline $\mathbf{3}$ (1.0 equiv.) and PhP(OPh) $_2$ (2.0 equiv.) were dissolved in pyridine (ca. 0.35 M). The vessel was sealed and heated to 100 °C for 24 h in an oil bath. The mixture was then diluted with toluene, and the solvent was removed *in vacuo*. This was repeated three times to remove all residual pyridine. The crude material was dissolved in THF, and ca. five drops of water were added. The solution was stirred at 60 °C for 1 h before being dried (Na $_2$ SO $_4$), filtered, and concentrated *in vacuo*. The crude mixture was then purified by column chromatography on silica gel. Reported yields are given for >95% pure material (by ^1H NMR spectroscopy), though subsequent recrystallization from hexanes and CH $_2$ Cl $_2$ was used to achieve analytically pure material.

Phosphaquinolinone 2a

Compound $\mathbf{2a}$ was synthesized from $\mathbf{3a}$ (462 mg, 1.9 mmol, 1 equiv.) and PhP(OPh) $_2$ (1.11 g, 3.8 mmol, 2 equiv.). Column chromatography (1:1 EtOAc:CH $_2$ Cl $_2$, R_f = 0.20) gave $\mathbf{2a}$ (149 mg, 21%) as a pale brown solid: mp > 250 °C; ^1H NMR (500 MHz, DMSO- d_6) δ 10.28 (d, J = 3.8 Hz, 1H), 8.14 (d, J = 2.0 Hz, 1H), 8.05 (d, J = 30.1 Hz, 1H), 7.82 (ABm, J = 8.4 Hz, 4H), 7.81–7.77 (m, 1H), 7.69–7.64 (m, 2H), 7.58–7.51 (m, 1H), 7.49–7.43 (m, 2H), 7.21 (d, J = 8.5 Hz, 1H); $^{13}\text{C}\{^1\text{H}\}$ NMR (126 MHz, DMSO- d_6) δ 143.1 (d, J = 3.8 Hz), 140.9 (d, J = 11.7 Hz), 139.3, 135.8, 133.8, 132.6, 132.5 (d, J = 2.7 Hz), 132.4 (d, J = 137.0 Hz), 132.2 (d, J = 10.8 Hz), 128.6 (d, J = 13.2 Hz), 128.1 (d, J = 6.1 Hz), 126.9 (d, J = 115.9 Hz), 119.2, 119.0 (d, J = 9.9 Hz), 118.5, 117.7 (d, J = 8.1 Hz), 110.6, 102.1; $^{31}\text{P}\{^1\text{H}\}$ NMR (202 MHz, DMSO- d_6) δ 7.77; HRMS (ASAP) $[\text{M} + \text{H}]^+$ calcd for C $_{22}$ H $_{15}$ N $_3$ OP 368.0953, found 368.0977.

Phosphaquinolinone 2b

Compound **2b** was synthesized from **3b** (700 mg, 2.4 mmol, 1 equiv.) and PhP(OPh)₂ (1.40 g, 4.8 mmol, 2 equiv.). Recrystallization from CH₂Cl₂ and hexanes gave **2b** (580 mg, 58%) as a yellow solid: mp > 250 °C; ¹H NMR (500 MHz, DMSO-*d*₆) δ 10.14 (d, *J* = 4.1 Hz, 1H), 8.16 (d, *J* = 30.1 Hz, 1H), 8.06 (d, *J* = 2.2 Hz, 1H), 7.85 (d, *J* = 8.3 Hz, 2H), 7.80 (d, *J* = 8.4 Hz, 2H), 7.73–7.63 (m, 3H), 7.53 (td, *J* = 7.4, 1.5 Hz, 1H), 7.49–7.43 (m, 2H), 7.25 (d, *J* = 8.5 Hz, 1H); ¹³C{¹H} NMR (126 MHz, DMSO-*d*₆) δ 142.5 (d, *J* = 3.7 Hz), 141.1 (d, *J* = 12.0 Hz), 139.9, 132.7 (d, *J* = 136.9 Hz), 132.6, 132.4 (d, *J* = 2.7 Hz), 132.2 (d, *J* = 10.7 Hz), 130.5, 128.5 (d, *J* = 13.2 Hz), 128.1 (d, *J* = 6.1 Hz), 127.4 (d, *J* = 3.7 Hz), 126.5 (d, *J* = 116.3 Hz), 124.5 (q, *J* = 271.2 Hz), 120.6 (q, *J* = 32.3 Hz), 118.6 (d, *J* = 13.0 Hz), 118.5, 117.4 (d, *J* = 7.9 Hz), 110.5; ³¹P{¹H} NMR (202 MHz, DMSO-*d*₆) δ 7.86; ¹⁹F NMR (471 MHz, DMSO-*d*₆) δ -59.92; HRMS (ASAP) [M + H]⁺ calcd for C₂₂H₁₅N₂O₃P 411.0874, found 411.0909.

Phosphaquinolinone **2c**

Compound **2c** was synthesized from **3c** (645 mg, 2.6 mmol, 1 equiv.) and PhP(OPh)₂ (1.5 g, 5.1 mmol, 2 equiv.). Column chromatography (1:1:1 hexanes:EtOAc:CH₂Cl₂, *R*_f = 0.10) followed by two rounds of recrystallization from CH₂Cl₂ and hexanes gave **2c** (300 mg, 31%) as a yellow solid: mp > 250 °C; ¹H NMR (500 MHz, DMSO-*d*₆) δ 9.80 (d, *J* = 4.2 Hz, 1H), 7.99 (d, *J* = 29.8 Hz, 1H), 7.83 (d, *J* = 8.4 Hz, 2H), 7.78 (d, *J* = 8.5 Hz, 2H), 7.73 (d, *J* = 2.5 Hz, 1H), 7.69–7.57 (m, 2H), 7.56–7.49 (m, 1H), 7.48–7.38 (m, 3H), 7.11 (d, *J* = 8.7 Hz, 1H); ¹³C{¹H} NMR (126 MHz, DMSO-*d*₆) δ 141.3 (d, *J* = 12.0 Hz), 139.4, 138.3 (d, *J* = 3.7 Hz), 132.8 (d, *J* = 136.6 Hz), 132.5, 132.3, 132.2, 130.7, 129.9, 128.5 (d, *J* = 13.1 Hz), 128.1 (d, *J* = 6.2 Hz), 126.5 (d, *J* = 116.8 Hz), 123.6, 120.2 (d, *J* = 12.6 Hz),

118.6, 118.4 (d, $J = 8.1$ Hz), 110.3; $^{31}\text{P}\{^1\text{H}\}$ NMR (202 MHz, DMSO- d_6) δ 7.69; HRMS (ASAP) $[\text{M} + \text{H}]^+$ calcd for $\text{C}_{21}\text{H}_{15}\text{N}_2\text{OPCl}$ 377.0611, found 377.0641.

Phosphaquinolinone 2d

Compound **2d** was synthesized from **3d** (151 mg, 0.69 mmol, 1 equiv.) and $\text{PhP}(\text{OPh})_2$ (463 mg, 1.4 mmol, 2 equiv.). Column chromatography (1:1:1 hexanes:EtOAc: CH_2Cl_2 , $R_f = 0.20$) gave **2d** (144 mg 61%) as a yellow solid: mp > 250 °C; ^1H NMR (500 MHz, CDCl_3) δ 7.73 (d, $J = 8.1$ Hz, 2H), 7.66 (d, $J = 30.4$ Hz, 1H), 7.71–7.66 (m, 2H), 7.54 (d, $J = 8.2$ Hz, 2H), 7.47–7.42 (m, 2H), 7.38–7.32 (m, 3H), 7.06 (t, $J = 7.5$ Hz, 1H), 6.97 (d, $J = 8.0$ Hz, 1H), 6.83 (br s, 1H); $^{13}\text{C}\{^1\text{H}\}$ NMR (126 MHz, CDCl_3) δ 141.5 (d, $J = 11.8$ Hz), 141.0 (d, $J = 3.0$ Hz), 138.8 (d, $J = 4.3$ Hz), 132.7 (d, $J = 10.8$ Hz), 132.6 (d, $J = 2.8$ Hz), 132.5, 132.2 (d, $J = 139.3$ Hz), 131.5, 131.2, 128.6 (d, $J = 13.8$ Hz), 128.4 (d, $J = 6.2$ Hz), 126.0 (d, $J = 119.5$ Hz), 121.4, 119.4 (d, $J = 12.1$ Hz), 118.8, 117.3 (d, $J = 7.7$ Hz), 111.6; $^{31}\text{P}\{^1\text{H}\}$ NMR (202 MHz, CDCl_3) δ 10.52; HRMS (ASAP) $[\text{M} + \text{H}]^+$ calcd for $\text{C}_{21}\text{H}_{16}\text{N}_2\text{OP}$ 343.1000, found 343.1030.

Phosphaquinolinone 2e

Compound **2e** was synthesized from **3e** (549 mg, 2.0 mmol, 1 equiv.) and $\text{PhP}(\text{OPh})_2$ (1.3 g, 4.0 mmol, 2 equiv.). Column chromatography (1:1:1 EtOAc: CH_2Cl_2 , $R_f = 0.25$) gave **2e** (520 mg, 65%) as a yellow solid: mp > 250 °C; ^1H NMR (500 MHz, CDCl_3) δ 7.73 (d, $J = 8.0$ Hz, 2H), 7.72–7.67 (m, 2H), 7.68 (d, $J = 30.3$ Hz, 1H), 7.53 (d, $J = 8.1$ Hz, 2H), 7.48–7.39 (m, 3H), 7.37–7.32 (m, 2H), 6.90 (d, $J = 8.4$ Hz, 1H), 6.48 (br s, 1H), 1.35 (s, 9H); $^{13}\text{C}\{^1\text{H}\}$ NMR (126 MHz, CDCl_3) δ 144.4, 141.7 (d, $J = 12.1$ Hz), 141.5, 136.4, 132.7 (d, $J = 10.8$ Hz), 132.5, 132.5, 132.4 (d, $J = 139.2$ Hz), 129.1, 128.5 (d, $J = 13.6$ Hz), 128.4 (d, $J = 6.4$ Hz), 127.6, 125.8 (d, $J = 119.9$ Hz), 119.0, 118.9 (d, $J = 8.4$ Hz), 116.9 (d, $J =$

7.3 Hz), 111.4, 34.4, 31.5; $^{31}\text{P}\{^1\text{H}\}$ NMR (202 MHz, CDCl_3) δ 10.44; HRMS (ASAP) $[\text{M} + \text{H}]^+$ calcd for $\text{C}_{25}\text{H}_{24}\text{N}_2\text{OP}$ 399.1628, found 399.1629.

Phosphaquinolinone **2f**

Compound **2f** was synthesized from **3f** (430 mg, 1.7 mmol, 1 equiv.) and $\text{PhP}(\text{OPh})_2$ (969 g, 3.3 mmol, 2 equiv.). Column chromatography (1:1:1 hexanes:EtOAc: CH_2Cl_2 , $R_f = 0.25$) gave **2f** (200 mg, 31%) as a pale yellow solid: mp > 250 °C; ^1H NMR (500 MHz, CDCl_3) δ 7.73–7.65 (m, 2H), 7.71 (d, $J = 8.6$ Hz, 2H), 7.59 (d, $J = 30.4$ Hz, 1H), 7.53 (d, $J = 8.2$ Hz, 2H), 7.47–7.42 (m, 1H), 7.37–7.31 (m, 2H), 6.98–6.93 (m, 2H), 6.88 (d, $J = 8.5$ Hz, 1H), 6.60 (br s, 1H), 4.04 (q, $J = 7.0$ Hz, 2H), 1.43 (t, $J = 7.0$ Hz, 3H); $^{13}\text{C}\{^1\text{H}\}$ NMR (126 MHz, CDCl_3) δ 153.5, 141.6 (d, $J = 12.0$ Hz), 140.7, 132.8 (d, $J = 10.7$ Hz), 132.7, 132.6 (d, $J = 3.0$ Hz), 132.5, 132.1 (d, $J = 140.4$ Hz), 128.5 (d, $J = 13.8$ Hz), 128.4 (d, $J = 6.4$ Hz), 126.7 (d, $J = 119.9$ Hz), 119.9, 119.8 (d, $J = 11.8$ Hz), 118.8, 118.2 (d, $J = 7.7$ Hz), 114.8, 111.5, 64.3, 15.0; $^{31}\text{P}\{^1\text{H}\}$ NMR (202 MHz, CDCl_3) δ 10.51; HRMS (ASAP) $[\text{M} + \text{H}]^+$ calcd for $\text{C}_{23}\text{H}_{20}\text{N}_2\text{O}_2\text{P}$ 387.1261, found 387.1283.

CHAPTER V

A HIGHLY FLUORESCENT PN-HETEROCYCLE-FUSED PYRENE DERIVATIVE WITH STRONG SELF-DIMERISATION THROUGH HYDROGEN BONDING

This chapter includes previously published and co-authored material from Bard, J.P., Mancuso, J.L., Deng, C.-L., Zakharov, L.N., Johnson, D.W., Haley, M.M. “A Highly Fluorescent PN-heterocycle-fused Pyrene Derivative with Strong Self-dimerization through Hydrogen Bonding.” *Supramol. Chem.* **2020**, *32*, 49–55. This story details our synthesis and analysis of a PN-fused pyrene derivative. Interesting photophysical and supramolecular characteristics based upon the unique scaffold are detailed.

5.1 Introduction

The pyrene moiety is a popular moiety in organic electronic devices because of its good hole transporting ability and excellent chemical stability.¹⁻³ Additionally, it is inherently fluorescent and, like many polycyclic arene systems, is subject to fluorescence quenching at higher concentrations due to the formation of π - π stacked excimers.⁴⁻⁹ This feature provides access to switchable fluorescent behavior in the presence of analytes such as metals and anions, given appropriate molecular design.¹⁰⁻¹² These hosts typically function through adjacent hydrogen bonding sites that coordinate with the guest and either promote or diminish intermolecular pyrene excimer formation. Similar structures featuring pyrene also exhibit switchable emission depending on environmental conditions, including

pressure,¹³ pH,¹⁴ and temperature.¹⁵ Further development of hydrogen bonding frameworks containing pyrene will enrich the library of high quantum yield hosts, while potentially providing additional fundamental insight into the complex excited state dynamics of this very interesting class of hosts.

Recently, there have been several reported phosphorus- and nitrogen-containing (PN) “phosphaquinolinone” scaffolds.^{16–19} These molecules are members of a small family of similar PN-heterocycles,^{20–31} and have shown promise as hydrogen bonding fluorophores.³² One tunable parameter of these fluorescent scaffolds is the effect of increasing conjugation length of the aromatic backbones, seen with naphthalene-,^{16,17} anthracene-,³³ and phenanthrene-like¹⁸ phosphaquinolinone structures (Figure 5.1).

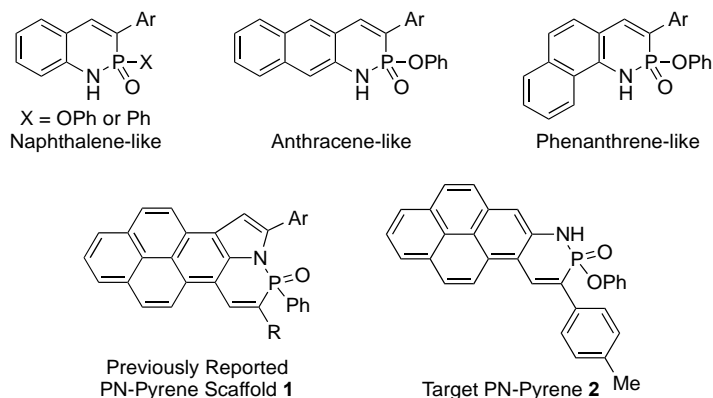


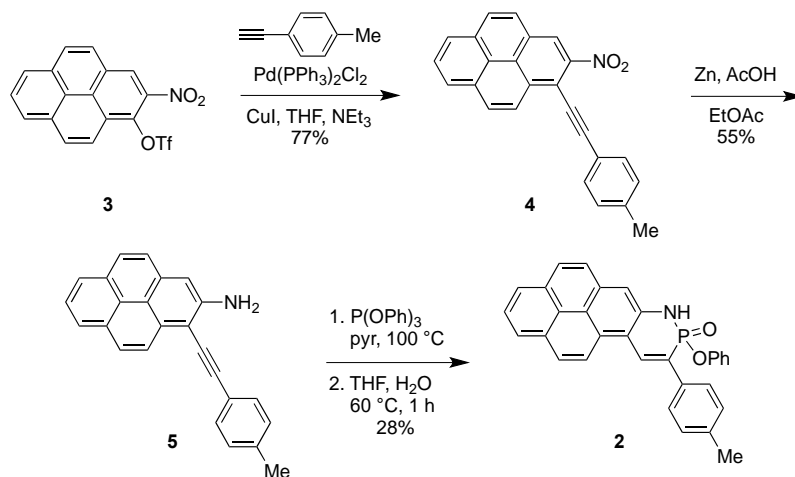
Figure 5.1 Previously reported phosphaquinolinone scaffolds as well as new PN-fused pyrene **2**.

One family of particular interest is the pyrene-containing derivatives **1**.¹⁹ These molecules showed a dramatic improvement in the photophysical properties compared to the parent pyrene scaffold. The increased conjugation of the arene backbone and functionalization of the phosphorus center with a phenyl group rather than the traditional phenoxy group led to not only increased quantum yields and red-shifted emissions, but also increased Stokes shifts. Though **1** holds promise for use in organic electronics, the

phosphaquinolinone hydrogen responsible for forming the characteristic, strong *meso*-dimers between enantiomers is absent due to the creation of a pyrrole motif subsequent to the formation of the phosphaquinolinone ring. Additionally, the typical pyrene excimer formation was suppressed in **1**, which leads to higher quantum efficiencies, yet depletes its capacity as a switchable host molecule. Here we report the new PN-heterocycle-fused pyrene derivative **2**, which retains the hydrogen bonding capabilities of the phosphaquinolinone moiety. Compound **2** couples superior fluorescent performance with the potential for supramolecular activity in a dynamic, responsive host.

5.2 Results and Discussion

Synthesis of **2** begins with Sonogashira cross-coupling of nitrotriflate **3**¹⁹ with 4-ethynyltoluene to afford nitropyrene **4**, which is then reduced to amine **5** with Zn in AcOH and EtOAc (Scheme 5.1). Finally, aminopyrene **5** is cyclized with P(OPh)₃ in pyridine and subsequently hydrolyzed in THF at 60 °C for 1 h to afford heterocycle **2** in modest yield. ¹H, ¹³C, and ³¹P NMR spectra were obtained, which showed the standard PN compound splitting of ~40 Hz for both the isolated alkene ¹H and ³¹P NMR signals (See Appendix D).



Scheme 5.1 Synthesis of PN-pyrene **2**.

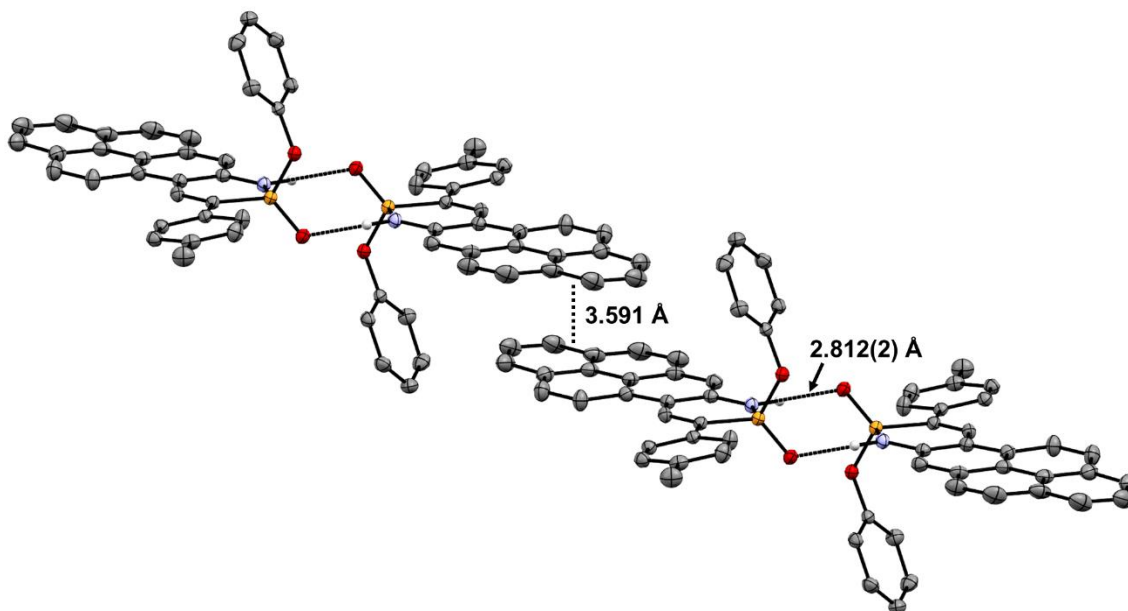


Figure 5.2 X-ray crystal structure of **2** showing both pyrene π - π stacking and phosphonamidate dimer distances; ellipsoids drawn at 30% probability.

Slow layering of pentane into a CHCl_3 solution of **2** was used to grow single crystals suitable for x-ray diffraction; the resultant crystal structure is shown in Figure 5.2. Arguably, the two most critical aspects of the structure are the familiar PN dimerization and pyrene π - π stacking. The PN dimer distance is 2.812(2) Å, as measured by the $\text{O}\cdots\text{N}$ distance between P(O) and NH hydrogen bonding pairs of adjacent molecules, and is within the range of dimer distances of previously reported phosphaquinolone structures (2.805–2.875 Å).^{16-18,33} Further, the pyrene moieties exhibit the typical slip-stacked face-to-face packing, with a distance of 3.591 Å between the two mean planes of each pyrene, which is similar to the packing of the previously reported anthracene-like phosphaquinolone.³³ One key difference is the near co-planarity between the pendant tolyl group and pyrene core with a dihedral angle of only 7.4°, which is smaller than the angle in previously reported phosphaquinolone heterocycles (dihedral angles 16-46°).¹⁶⁻

^{18,33} This may be the result of face-to-face packing between the tolyl group of one molecule with the pyrene of another (Figure D.2).

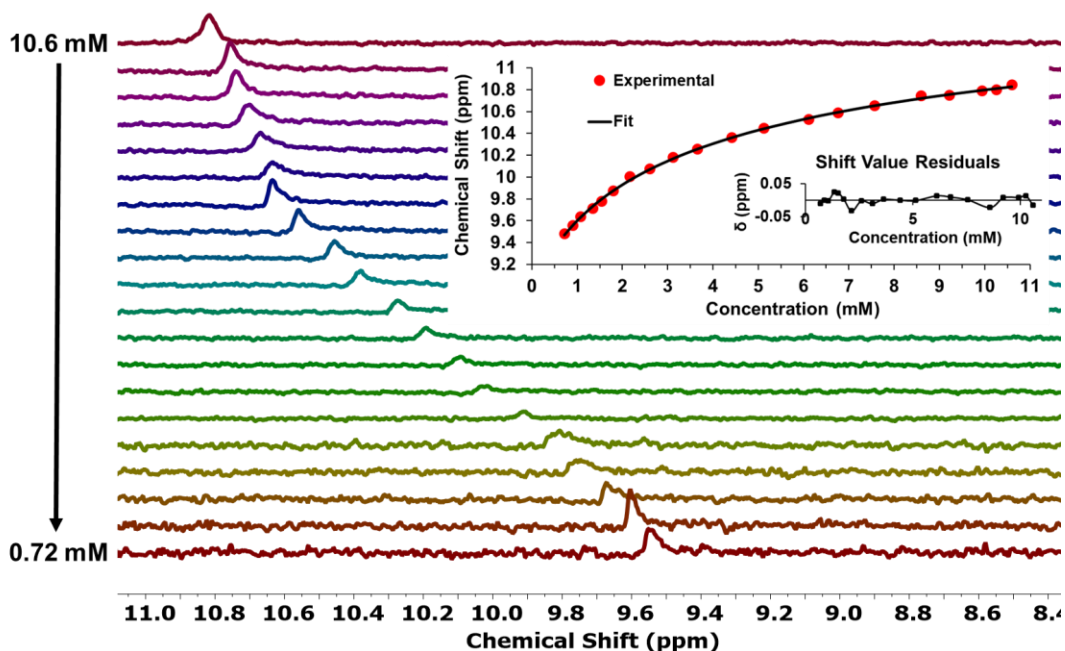


Figure 5.3 ³¹P NMR spectra of **2** from VC NMR experiment as well as generated fit and residuals (inset).

Variable concentration (VC) NMR studies were performed with a ~11 mM stock solution of **2** in H₂O-saturated CDCl₃ by diluting it with known amounts of solvent and tracking the ³¹P NMR signal after each addition (Figure 5.3).³⁴ Typical upfield shifting ($\Delta\delta \approx 1.2$ ppm) is observed as the concentration of the sample decreases. Non-linear regression analysis was then used to determine a solution-state dimerization strength (K_{dim}) value for **2** of 179 M^{-1} (Figure 5.3 inset). This value is both consistent with the dimerization strengths of structurally similar PN-phenanthrene analogues and among the strongest reported values for similar hydrogen bonding dimers.^{18,36}

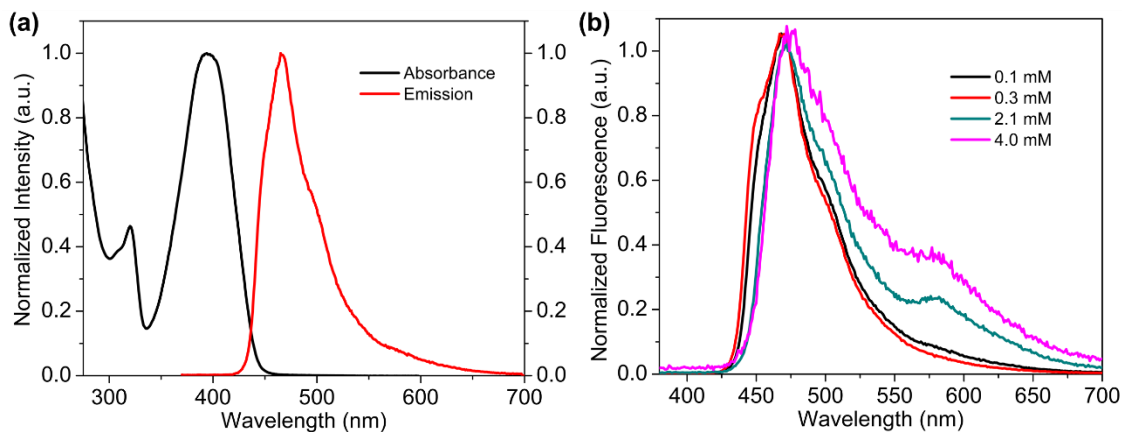


Figure 5.4 a) Absorption and emission spectra of a 1 μM solution of **2** and b) emission spectra of **2** at varying concentrations, showing excimer emission at higher concentrations in CHCl_3 , where $\lambda_{\text{ex}} = 365 \text{ nm}$.

The photophysical properties of **2** were studied with UV-vis and fluorescence spectroscopy. The absorbance and emission profiles of a $1 \times 10^{-6} \text{ M}$ solution of **2** (Figure 5.4a) demonstrate standard pyrene-like characteristics with an absorption maximum at 395 nm ($\epsilon = 2.6 \times 10^4 \text{ M}^{-1} \text{ cm}^{-1}$) and an emission maximum of 465 nm ($\phi = 70\%$, $\tau = 3 \text{ ns}$) upon excitation at 365 nm (Figure D.3, a).⁴ Though tolyl-appended **2** was chosen based on higher yields and better stability, it is expected that more withdrawing aryl groups on the pendent phenyl should lead to a redshifting in the emission, while more donating groups should lead to a blueshifting. This is based on the results for several previously studied classes of PN heterocycles, including the aforementioned naphthalene-,^{16,17} anthracene-,³³ and phenanthrene- like¹⁸ families.

To test for the formation of pyrene excimers, the fluorescence spectra were monitored as a function of concentration by diluting a sample from $4 \times 10^{-3} \text{ M}$ to $1 \times 10^{-4} \text{ M}$ (Figure 5.4b). Below $2 \times 10^{-3} \text{ M}$, only the emission profile of monomer is seen. Interestingly, at or above $2 \times 10^{-3} \text{ M}$ in concentration, the bands around 465 nm stay constant and a broad peak at 582 nm begins to grow in, which is coupled with a decrease

in the quantum efficiency of the solution and is consistent with known excimer behavior.⁴ A green-yellow emission is seen in the solid state, supporting the presence of a yellow fluorescing excimer mixed with the blue fluorescing monomer (Figure D.4, b). Additionally, this excimer formation is not seen when looking at 4×10^{-3} M samples in toluene, methanol, or 5% chloroform in methanol however, as shown by the emission spectra and the colors of the solutions upon excitation at 365 nm, where the chloroform solution has a more yellow emission than the others (Figures D.3, c and D.4). In an analogous 20% chloroform in methanol solution, a small shoulder begins to appear at 523 nm, potentially showing evidence for a minor formation of excimer in this solvent system as well (Figure D.4). As this excimer formation is observed only at higher concentrations in chloroform, compound **2** maintains a large quantum yield as the monomer in most concentrations yet retains promise for integration into systems that take advantage of the fluorescence quenching of the excimer.

5.3 Conclusions

A new PN-pyrene derivative has been prepared that retains the enhanced photophysical properties seen in pyrene-based systems and incorporates the structural motifs that enable supramolecular assembly, as **2** exhibits strong H-bonded phosphaquinolone dimer formation in solution and the solid state, an extended π - π stacking structure in the crystalline state, and monomer-excimer quenching dynamics. These structural features and concentration-dependent properties provide this highly fluorescent scaffold with the potential to be a useful supramolecular building block for

larger systems or networks and broaden the substrate scope and applicability of existing pyrene-containing supramolecular hosts and chemosensors.

5.4 Experimental Section

General. NMR spectra were acquired at room temperature on a Varian Inova 500 (^1H : 500 MHz, ^{13}C : 126 MHz, ^{31}P : 202 MHz) or a Bruker Avance III HD 500 equipped with a Prodigy multinuclear cryoprobe (^1H : 500 MHz, ^{13}C : 126 MHz). ^1H and ^{13}C chemical shifts (δ) are expressed in ppm relative to residual CHCl_3 shifts (^1H : 7.26 ppm, ^{13}C : 77.16 ppm). ^{31}P NMR are referenced to 85% H_3PO_4 (δ 0 ppm) as an external reference. UV-vis spectra were recorded using an Agilent Technologies Cary 60 UV-vis spectrophotometer in HPLC grade CHCl_3 . Fluorescence emission spectra were recorded using a Horiba Jobin Yvon FluoroMax-4 fluorimeter exciting at 365 nm. Fluorescence lifetime measurements were recorded using a Horiba FluoroHub Single Photon Counting Controller with a TemPro Fluorescence Lifetime System attachment. HRMS data were acquired on a Waters Synapt G2-Si ESI/LC-MS. All air-/water-free reactions were performed under an N_2 atmosphere using Schlenk techniques. Column chromatography was performed using silica gel (240–300 mesh), with solvent systems being referenced to the most abundant solvent. Compound **3** was prepared according to the literature;¹⁹ all other materials were used as received.

Dimerization and photophysical studies. Variable concentration (VC) NMR experiments were performed by sequentially diluting a 10 mM solution of **2** with known amounts of solvent, recording the ^{31}P NMR shift after each dilution, and fitting the peaks using non-linear regression analysis.³⁴ Quantum yield (ϕ) was determined through comparison of the

emission and absorption intensities of the analyte to that of a 0.1 M quinine sulfate in H₂SO₄ solution.³⁵

Synthesis of nitropyrene 4. Nitrotriflate **3**¹⁹ (185 mg, 0.47 mmol, 1 equiv.) was combined with 4-ethynyltoluene (0.052 mL, 0.70 mmol, 1.5 equiv.), Pd(PPh₃)₂Cl₂ (32 mg, 0.047 mmol, 0.1 equiv.), and CuI (9 mg, .047 mmol, 0.1 equiv.) in a round bottom flask. The vessel was then placed under N₂ through atmosphere exchange before dry THF (5 mL) and Et₃N (1 mL) were added. After reacting at room temperature for 24 h, the crude mixture was concentrated under reduced pressure using EtOAc to remove Et₃N, and the residue was purified using silica gel chromatography (20:1 hexanes:EtOAc) to give **4** (0.130 g, 77% yield) as an orange solid; mp 169.0–170.1 °C. ¹H NMR (500 MHz, CDCl₃) δ 8.75 (d, *J* = 9.2 Hz, 1H), 8.71 (s, 1H), 8.34–8.21 (m, 3H), 8.14 (t, *J* = 7.8 Hz, 1H), 8.11 (d, *J* = 7.7 Hz, 1H), 8.04 (d, *J* = 8.9 Hz, 1H), 7.68 (d, *J* = 7.6 Hz, 2H), 7.27 (d, *J* = 8.4 Hz, 2H), 2.44 (s, 3H). ¹³C NMR (126 MHz, CDCl₃) δ 147.7, 139.8, 133.2, 132.1, 132.0, 131.6, 130.3, 130.3, 130.1, 129.5, 128.0, 127.3, 126.9, 126.9, 126.1, 123.7, 119.9, 119.9, 112.2, 103.2, 83.4, 77.4, 21.9. HRMS [M+H]⁺ calcd for C₂₅H₁₆NO₂ 362.1181, found 362.1169.

Synthesis of aminopyrene 5. Nitropyrene **4** (175 mg, 0.48 mmol, 1 equiv.) was dissolved in 40 mL of EtOAc and 10 mL AcOH was added. Zn powder (317 mg, 4.8 mmol, 10 equiv.) was then added and the solution was stirred for one hour before being concentrated *in vacuo*. The crude mixture was purified through silica gel chromatography (15:1:1 hexanes:EtOAc:CH₂Cl₂), followed by recrystallization from CH₂Cl₂ and hexanes to afford **5** (88 mg, 0.26 mmol, 55%) as an orange solid; mp 127.4-128.1 °C. ¹H NMR (500 MHz, CDCl₃) δ 8.51 (d, *J* = 9.1 Hz, 1H), 8.18–8.05 (m, 3H), 7.98 (d, *J* = 9.1 Hz, 1H), 7.89 (d, *J* = 7.7 Hz, 1H), 7.83 (d, *J* = 8.8 Hz, 1H), 7.60 (d, *J* = 7.8 Hz, 2H), 7.49 (s, 1H), 7.24 (d, *J* =

8.4 Hz, 2H), 2.43 (s, 3H). ^{13}C NMR (126 MHz, CDCl_3) δ 146.4, 138.8, 133.0, 132.6, 131.6, 130.1, 129.9, 129.5, 129.4, 128.8, 128.7, 126.5, 125.9, 125.7, 125.2, 124.8, 124.8, 120.6, 118.9, 110.4, 101.0, 84.4, 21.7. HRMS $[\text{M}+\text{H}]^+$ calcd for $\text{C}_{25}\text{H}_{18}\text{N}$ 332.1439, found 332.1439.

Synthesis of PN-pyrene 2. Aminopyrene **5** (148 mg, 0.47 mmol, 1 equiv.) and $\text{P}(\text{OPh})_3$ (0.35 mL, 1.3 mmol, 3 equiv.) were dissolved in pyridine (1.5 mL). The reaction was put under a N_2 atmosphere using atmosphere exchange before the mixture was heated to 100 °C and left to stir for 24 hours. The crude mixture was then dissolved in toluene and the solvent was removed *in vacuo*. 10 mL of THF and several drops of H_2O were added to the mixture, which was then heated at 60 °C for one hour before being dried (Na_2SO_4), filtered, and concentrated *in vacuo*. This product mixture was then purified using silica gel chromatography (15:1:1→2:1:1 hexanes:EtOAc: CH_2Cl_2) and subsequent recrystallization from CH_2Cl_2 and hexanes to afford heterocycle **2** (62 mg, 0.13 mmol, 28%) as a yellow solid; mp >250 °C. ^1H NMR (500 MHz, CDCl_3) δ 8.74 (s, 1H), 8.72 (d, $J = 40.1$ Hz, 1H), 8.43 (d, $J = 9.3$ Hz, 1H), 8.14 (t, $J = 7.9$ Hz, 2H), 8.09 (d, $J = 9.2$ Hz, 1H), 8.00 (d, $J = 9.0$ Hz, 1H), 7.93 (t, $J = 7.2$ Hz, 3H), 7.83 (d, $J = 8.9$ Hz, 1H), 7.74 (s, 1H), 7.38 (d, $J = 7.7$ Hz, 2H), 7.04–6.94 (m, 4H), 6.87 (s, 1H), 2.49 (s, 3H). ^{13}C NMR (126 MHz, CDCl_3) δ 150.7 (d, $J = 9.2$ Hz), 138.7, 138.5 (d, $J = 2.6$ Hz), 136.1 (d, $J = 5.8$ Hz), 133.5 (d, $J = 9.3$ Hz), 133.3, 130.5, 130.0, 129.9, 129.7 (d, $J = 1.9$ Hz), 129.5, 129.4, 129.1, 128.0 (d, $J = 6.7$ Hz), 126.3, 126.2, 126.2 (d, $J = 164.4$ Hz), 125.4, 124.9 (d, $J = 1.7$ Hz), 124.8, 124.1, 121.4 (d, $J = 4.1$ Hz), 121.2, 120.6, 113.8 (d, $J = 13.2$ Hz), 113.7 (d, $J = 9.6$ Hz), 21.5. ^{31}P NMR (202 MHz, CDCl_3) δ 10.91 (d, $J = 40.2$ Hz). HRMS $[\text{M}+\text{H}]^+$ calcd for $\text{C}_{31}\text{H}_{23}\text{NO}_2\text{P}$ 472.1466, found 472.1463.

Crystal data for 2. Diffraction intensities for **2** were collected at 173 K on a Bruker Apex2 CCD diffractometer using CuK α radiation, $\lambda = 1.54178 \text{ \AA}$. Space group was determined based on systematic absences. Absorption correction was applied by SADABS.³⁷ Structure was solved by direct methods and Fourier techniques and refined on F^2 using full matrix least-squares procedures. All non-H atoms were refined with anisotropic thermal parameters. H atoms were refined in calculated positions in a rigid group model except the H atom at the N atom involved in H-bond that was refined with isotropic thermal parameter. All calculations were performed by the Bruker SHELXL-2014 package.³⁸ Compound **2**: C₃₁H₂₂NO₂P, M = 471.46, 0.12 x 0.09 x 0.03 mm, T = 173 K, Monoclinic, space group $P2_1/n$, $a = 14.0132(4) \text{ \AA}$, $b = 8.3450(2) \text{ \AA}$, $c = 20.0895(6) \text{ \AA}$, $\beta = 97.885(2)^\circ$, $V = 2327.06(11) \text{ \AA}^3$, $Z = 4$, $D_c = 1.346 \text{ Mg/m}^3$, $\mu(\text{Cu}) = 1.283 \text{ mm}^{-1}$, $F(000) = 984$, $2\theta_{\text{max}} = 133.21^\circ$, 16977 reflections, 4108 independent reflections [$R_{\text{int}} = 0.0444$], $R1 = 0.0502$, $wR2 = 0.1351$ and $\text{GOF} = 1.044$ for 4108 reflections (320 parameters) with $I > 2\sigma(I)$, $R1 = 0.0600$, $wR2 = 0.1448$ and $\text{GOF} = 1.045$ for all reflections, max/min residual electron density $+1.172/-0.260 \text{ e\AA}^{-3}$. CCDC 1952888 contains the supplementary crystallographic data for compound **2**. These data can be obtained free of charge from The Cambridge Crystallographic Data Centre at via www.ccdc.cam.ac.uk/data_request/cif.

CHAPTER VI

THIONATION OF THE 2- λ^5 -PHOSPHAQUINOLIN-2-ONE SCAFFOLD WITH LAWESSON'S REAGENT

This chapter includes previously published and co-authored material from Bard, J.P., McNeill, J.N., Zakharov, L.N., Johnson, D.W., Haley, M.M. "Thionation of the 2- λ^5 -Phosphaquinolin-2-one Scaffold with Lawesson's Reagent." *Isr. J. Chem.* **2021**, *61*, 217–221. This story focuses on our use of Lawesson's Reagent to thionate the phosphorus center of the phosphaquinolinone scaffold as well as the physicochemical changes observed after doing so.

6.1 Introduction

Lawesson's reagent (LR, Figure 6.1) is a widely-used thionating reagent that converts carbonyl groups into their respective thiocarbonyls, with several authoritative reviews highlighting its utility.^{1,2} This reagent reacts with a wide variety of carbonyl-containing scaffolds, including, but not limited to, ketones, amides, imides, and aldehydes. These transformations, beyond being structurally interesting, often lead to changes in the physicochemical properties of the scaffolds between the oxo and thio forms.

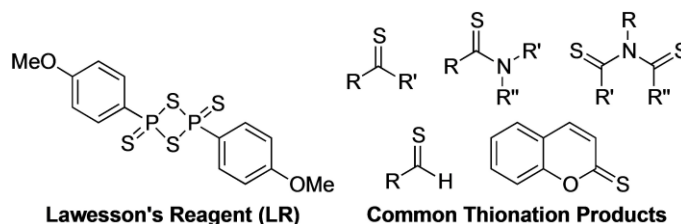


Figure 6.1 Lawesson's Reagent and a sampling of commonly prepared thiocarbonyl compounds.

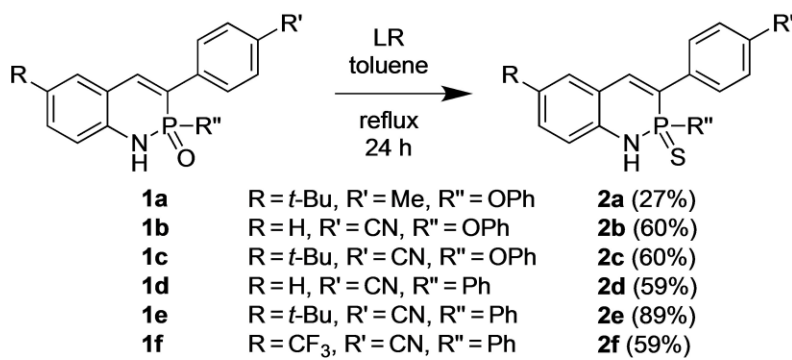
One framework of particular interest that has served as a substrate for LR is the well-studied fluorescent lactone coumarin.³⁻⁶ Coumarin, as well as other related fluorescent carbonyl-containing systems, exhibit red-shifted emissions and decreased quantum yields upon thionation with LR. Additionally, in many cases the thio form can be converted back to the respective oxo form through various means, a transformation which often shows a turn-on fluorescence response.^{5,7-9} Similarly, non-aromatic aminophosphonic esters have been converted to their respective thio forms as well.¹⁰⁻¹² The utility of LR and the physicochemical changes it imparts upon the substrates pose the question: what other carbonyl-like systems can be modified analogously?

In recent years, we have reported the synthesis and physicochemical studies of the coumarin-like 2- λ^5 -phosphaquinolin-2-one scaffold.¹³ In addition to their well-defined self-specific *meso*-dimerization, these phosphorus- and nitrogen-containing (PN) heterocycles have tunable emissive properties. Similar to the aforementioned analyses of coumarin derivatives, we have reported a series of studies to modify and improve the physicochemical properties of the 2- λ^5 -phosphaquinolin-2-ones through substituent group alteration, phosphorus center modification, and acene backbone elongation.¹³⁻¹⁵ To further explore the versatility and modularity of the phosphaquinolinone scaffold, we report herein the conversion of the phosphine oxide into the corresponding thionate form using Lawesson's reagent and discuss in detail the resultant structural and photophysical changes.

6.2 Results and Discussion

To accomplish this study, oxo-heterocycles **1a–1f** were prepared as previously reported.^{14,15} These were treated with LR in dry toluene under N₂ at reflux until only trace

starting material was observed via TLC (ca. 24 h), affording thioheterocycles **2a–2f** in modest to very good isolated yields (Scheme 6.1). The purification of heterocycles **2** nonetheless presented some challenges, as the reaction biproducts of LR are structurally similar to the attained products and/or may coordinate with the donor-acceptor face of the PN product. In the case of **2a**, this meant multiple rounds of silica gel chromatography and recrystallization, resulting in material likely being lost in purification and thus the diminished isolated yield.



Scheme 6.1 Conversion of oxo-heterocycles **1** to thio-heterocycles **2** with Lawesson's Reagent (LR).

Heterocycles **2** were examined by NMR spectroscopy (Figures E.7–E.25). First, the ³¹P NMR signals shift significantly downfield (~ 30–35 ppm) from their respective oxo analogs **1**, appearing around 40–50 ppm, which can be explained by the larger deshielding effect that the sulfur has upon the P center as seen for other examples in the literature.² Furthermore, the proton NMR spectra show the characteristic coupling between the P center and the carbon in the isolated C=C bond along the backbone. The coupling constants range from 30.5–37.7 Hz, and correlate to the standard splitting seen in these systems; however, the N–H proton signal appears solely as a doublet ($J = 6–7$ Hz), which before in heterocycles **1** has been observed only as a broad singlet. While slightly confusing, examination of the ³¹P NMR spectra indicates that the phosphorus center is likely coupling

to the adjacent N–H proton, as the phosphorus peaks appear as doublet of doublets for **2a–2c**, and doublet of triplets for **2d–2f**. It should be noted, however, that the coupling between the phosphorus center and the attached phenyl ring may mask this interaction. This coupling between the phosphorus center and the N–H proton could potentially be explained due to a more partially positively charged P atom resulting from the more polarized P–S bond. Furthermore, none of the characteristic shifting in any of the N–H signals was seen as a function of concentration, suggesting little to no *meso*-dimerization as is observed for heterocycles **1** in solution. This is likely due to the relatively large thiophosphonyl S acting as a “soft” Lewis base because of its more diffuse charge and the concurrent larger polarizability.¹⁶ This phenomenon is also observed for sulfur-containing H-bonds in proteins.^{17,18}

Slow diffusion of pentane into CH₂Cl₂ solutions of heterocycles **2d** and **2e** furnished single crystals suitable for X-ray diffraction. In the heterocyclic core of these structures, the P–N bond distances are 1.665(1) and 1.668(1) Å, the P–C bond distances are 1.794(2) and 1.802(1) Å, the N–C bond distances are 1.394(2) and 1.395(1) Å, and the isolated C=C double bond distances are both 1.355(2) Å, respectively. All of these bond lengths are within the ranges determined for previous PN-heterocycles,¹³ suggesting that thionation has no significant structural effect on the conjugated backbone. The only differences in bond lengths are observed for the P–N bond distances, which are about 0.02 Å longer than those in **1**,¹³ and, unsurprisingly, the P=S bond distances of **2d** and **2e** (1.959(1) and 1.958(1) Å) are ~ 0.5 Å longer than the respective P=O bonds in heterocycles **1** because of the larger sulfur atom.

The solid-state structures of the *meso*-dimers of **2d** and **2e** also provide some interesting observations (Figures 6.2 and E.1–E.4). The N···S intermolecular distance is 3.406(1) Å for **2d** and 3.404(1) Å for **2e**, which are significantly longer than any previously measured N···O bond distances (~ 2.77 – 2.82 Å).¹³ The P–N···S, N···S–P, and the S–P–N angles are 118.2°, 102.5°, and 115.7(1)° for **2d** and 114.6°, 107.4°, and 116.2(1)° for **2e**, respectively. These all deviate to varying degrees from the ideal 120° for the pseudo six-membered chair conformation, like their P=O analogues. Also, the S–P–N–H torsional angles for **2d** and **2e** are 56.5° and 60.7°, respectively. These characteristics further support the lack of solution-state dimerization since we have shown previously a correlation between solid-state distances/angles and solution-state dimerization strengths.¹⁵ Finally, the dihedral angle between the heterocyclic cores and the pendant 4-NCC₆H₄ groups is ca. 28–38°, illustrating good conjugation between the two π -units in the solid state.

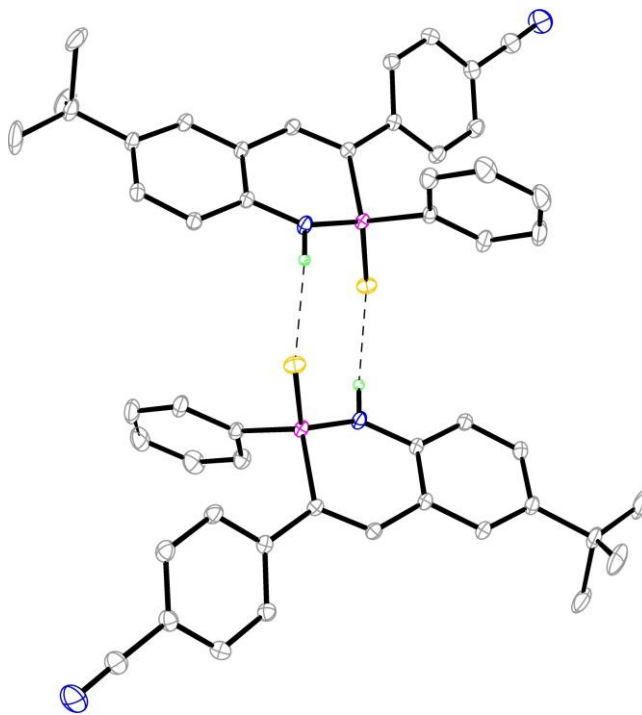


Figure 6.2 ORTEP drawing of the thioheterocycle **2e** *meso*-dimer; thermal ellipsoids drawn at 30 % probability level.

We next examined the effects of thionation upon the photophysical properties of **2** (Table 6.1, Figure 6.3). First, the lowest energy absorption peaks of thio-heterocycles **2** range from 348 to 372 nm. These fall in line with the typical PN heterocycle absorbance peaks, albeit they are slightly lower energy likely due to the lowered LUMO energies and subsequently lower π to π^* transitions upon introduction of the sulfur atoms in **2**.¹⁹ Furthermore, the absorption coefficients for **2** range from 12,700 to 20,800 $\text{M}^{-1} \text{cm}^{-1}$ for the $\lambda_{\text{abs,max}}$ peaks around 300 nm (see Appendix E) and from 6380 to 8600 $\text{M}^{-1} \text{cm}^{-1}$ for the lowest energy absorbances. These are within the range of those seen for oxo-heterocycles **1**, suggesting that there is no significant effect of the thionation upon the conjugation or absorptivity of the scaffold.

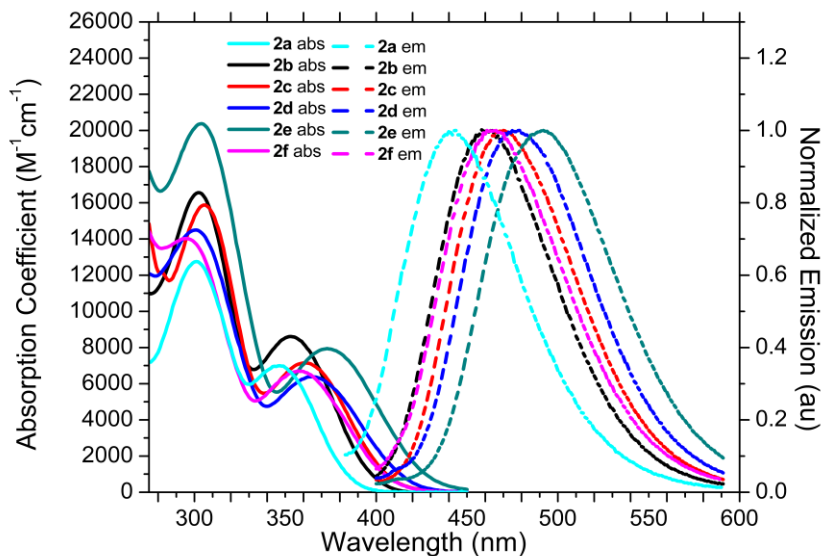


Figure 6.3 Stacked absorption and emission spectra of heterocycles **2**.

Table 6.1. Photophysical properties of heterocycles **2**^a

compd	λ_{abs} (nm)	λ_{em} (nm)	Stokes Shift (nm/cm ⁻¹)	ϵ (M ⁻¹ cm ⁻¹)	ϕ (%) ^b	τ (ns)
2a	348	444	96/6213	7180	2	0.10 ^c
2b	352	462	110/6764	8600	6	0.24 ^c
2c	350	470	120/7294	6520	3	0.19 ^c
2d	365	479	114/6520	6380	8	0.75 (76%), 4.6 (24%) ^d
2e	373	492	119/6484	7950	8	0.82 (85%), 4.8 (15%) ^d
2f	357	466	109/6552	6840	2	0.17 (84%), 3.0 (16%) ^d

^aAll values collected in CHCl₃ with ca. 10⁻⁵ M solutions. ^bCollected using a quinine sulfate in 0.1 M H₂SO₄ solution. ^cDecay curves fitted with a monoexponential model. ^dDecay curves fitted with a biexponential model.

When examining the emissive properties of **2**, however, a few interesting, yet predictable changes were observed. For P–OPh containing heterocycles **2a–2c**, ca. 20 nm redshifts in the emission are observed when compared to their respective oxo-heterocycle **1** derivatives. Similarly, the P–Ph containing heterocycles **2d–2f** exhibit 12, 27, and 17 nm redshifts compared to **1d–1f**, respectively. This is likely due to the weaker P–S bond in **2** compared to the P–O bond in **1** and the concurrent lower energy of the excited state (S1). With this lower energy S1 state, the S1 to S0 transition is lower in energy, as cited for thiocarbonyls vs. their parent carbonyls.²⁰ Furthermore, all derivatives of **2** exhibited decreased quantum yields (3–8%) compared to their **1** counterparts (11–52%). This is a common phenomenon as sulfur promotes the “heavy atom effect” which acts to quench fluorescence through several electronic transitions in the excited state.^{21,22} This effect is most pronounced in **2d–2f**, which show a dramatic reduction in quantum yield, though this

is likely just due to their respective **1** counterparts having higher quantum yields as previously described.¹⁴ An additional interesting difference between the P–OPh containing heterocycles **2a–2c** and the P–Ph containing congeners **2d–2f** is seen when determining the fluorescence lifetimes of the heterocycles. For the P–OPh heterocycles, the decays are monoexponential, and range from 0.10 to 0.24 ns, whereas the P–Ph heterocycles show biexponential lifetimes with a predominant shorter component (0.17 to 0.82 ns) as well as a longer-lived component (3.0 to 4.8 ns). This is likely due to the increased potential for charge transfer in the excited state of the P–Ph heterocycles as we have seen before.¹³ Examination of the absorption and emission of **2c** and **2e** in the more polar acetonitrile (Figure E.5 and Table E.1) indicate that this charge transfer is likely observed in this system as well, as **2e** shows a higher energy Stokes shift in the more polar solvent, yet **2c** shows a lower one. The frontier orbital geometries of the ground- and excited-state geometries were also examined by DFT and TDDFT calculations, respectively (Figure E.6 and Table E.2). A larger separation between frontier orbitals is observed in the HOMO and LUMO for the S₀ state of the P–Ph containing **2e** when compared to the respective P–OPh containing **2c**. When looking at the respective S₁ state geometries, a slightly larger orbital separation can be seen for **2e** as well, though it is not as dramatic as that of the ground state. This, paired with the increased Stokes shift of **2e** in a more polar solvent imply that a more prominent charge transfer event can be taking place for the P–Ph containing **2d–2f**, thus leading to the biexponential decay curves. This conjecture also is corroborated by the longer lifetime components observed with the P–Ph heterocycles since charge-transfer has longer lifetime than the dominant π^* to π transitions.

6.3 Conclusions

In summary, the utility and versatility of Lawesson's reagent has permitted the transformation of oxo-heterocycles **1a–1f** into their respective thiocarbonyl derivatives **2a–2f**, affording interesting changes in physicochemical properties as well as new functionality of the compounds. With LR working well to convert the phosphoquinolinone scaffolds in the same way, and the inherent diversity of performing the transformation upon this fluorescent phosphonyl center, it opens the door for the potential utilization of these P=O(S) heterocycles as turn-on fluorescent sensors, markers, or chemodosimeters for oxidizing/reducing species. These studies will be disclosed in due course.

6.4 Experimental Section

General. All oxygen- and water-free reactions were performed under an N₂ atmosphere using Schlenk technique. Column chromatography was performed using silica gel (240–300 mesh), with solvent systems being referenced to the most abundant solvent. NMR spectra were acquired at room temperature on a Bruker Avance III HD 600 equipped with a Prodigy multinuclear cryoprobe (¹H: 600 MHz, ¹³C: 151 MHz), a Varian Inova 500 (¹H: 500 MHz, ¹³C: 126 MHz, ³¹P: 202 MHz), or a Bruker Avance III HD 500 equipped with a Prodigy multinuclear cryoprobe (¹H: 500 MHz, ¹³C: 126 MHz, ³¹P: 202 MHz, ¹⁹F: 471 MHz). ¹H and ¹³C NMR chemical shifts (δ) are expressed in ppm relative to residual CHCl₃ (¹H: 7.26 ppm, ¹³C: 77.16 ppm) or DMSO (¹H: 2.50 ppm, ¹³C: 39.52 ppm) shifts. ³¹P NMR shifts are referenced to 85 % H₃PO₄ (δ 0 ppm) as an external reference. ¹⁹F NMR shifts are referenced to CFC₃ (δ 0 ppm) as an external reference. UVvis spectra were recorded using an Agilent Technologies Cary 60 UV-vis spectrophotometer in HPLC-grade CHCl₃. Fluorescence emission spectra were recorded using a Horiba Jobin Yvon FluoroMax-4

fluorimeter exciting at 365 nm. Quantum yields (ϕ) were determined through comparison of the emission and absorption intensities of the analyte to those of a 0.1 M H₂SO₄ quinine sulfate solution.^{23–25} Fluorescence lifetime measurements were recorded using a Horiba Fluoro-Hub Single Photon Counting Controller with a TemPro Fluorescence Lifetime System attachment. High-resolution mass spectra (HRMS) were recorded on a Waters XEVO G2-XS mass spectrometer. Oxo-heterocycles **1** were prepared as previously described.^{14,15}

General procedure for thionation. Oxo-heterocycles **1** (1 equiv.) were mixed with Lawesson's reagent (LR) (1.35–1.40 equiv.) in dry toluene (~ 0.005 M) under N₂. The mixture was heated to reflux for 24 h. After cooling to room temperature, the solvent was removed *in vacuo*. Silica gel chromatography of the residue and subsequent recrystallization afforded the pure thio-heterocycles **2** in modest to very good yield.

Heterocycle 2a: The general thionation procedure was performed on oxo-heterocycle **1a** (70 mg, 0.173 mmol, 1.00 equiv.) with LR (98 mg, 0.240 mmol, 1.40 equiv.) in toluene (60 mL). Two rounds of column chromatography (2:1:1 hexanes : EtOAc : CH₂Cl₂, R_f=0.90 then 20:1:1 hexanes : EtOAc : CH₂Cl₂, R_f=0.30) and subsequent recrystallization from pentane and CH₂Cl₂ afforded thio-heterocycle **2a** (20 mg, 27%) as a yellow solid. ¹H NMR (500 MHz, DMSO-*d*₆) δ 10.01 (d, J =6.0 Hz, 1H), 7.76 (d, J =37.7 Hz, 1H), 7.68 (d, J =7.8 Hz, 2H), 7.53 (s, 1H), 7.41 (d, J =8.6 Hz, 1H), 7.34 – 7.25 (m, 4H), 7.17 – 7.09 (m, 2H), 7.00 (d, J =7.9 Hz, 2H), 2.36 (s, 3H), 1.28 (s, 9H). ¹³C NMR (151 MHz, DMSO-*d*₆) δ 149.9 (d, J =10.9 Hz), 143.3, 138.7 (d, J =3.4 Hz), 137.5, 137.1 (d, J =6.7 Hz), 133.0 (d, J =12.4 Hz), 129.5, 129.0, 128.0 (d, J =7.0 Hz), 127.9, 127.1 (d, J =129.9 Hz), 127.1, 124.9, 121.9 (d, J =4.5 Hz), 119.9 (d, J =13.9 Hz), 116.3 (d, J =8.3 Hz), 33.9, 31.2, 20.8. ³¹P NMR

(202 MHz, DMSO-*d*₆) δ 56.3 (dd, $J=39.4, 2.9$ Hz). UV-vis (CHCl₃) λ_{\max} nm (ϵ ; M⁻¹cm⁻¹) 301 (12,700), 348 (7,180). HRMS (ASAP) [M+H]⁺ calcd for C₂₅H₂₇NOPS 420.1551, found 420.1523.

Heterocycle 2b: The general thionation procedure was performed on oxo-heterocycle **1b** (50 mg, 0.14 mmol, 1.00 equiv.) with LR (76 mg, 0.188 mmol, 1.35 equiv.) in toluene (25 mL). Column chromatography (2:1:1 hexanes:EtOAc: CH₂Cl₂, R_f=0.90) and subsequent recrystallization from hexanes and CH₂Cl₂ afforded thio-heterocycle **2b** (31 mg, 60%) as a pale yellow solid. ¹H NMR (500 MHz, CDCl₃) δ 7.87 (d, $J=7.9$ Hz, 2H), 7.74 (d, $J=8.0$ Hz, 2H), 7.54 (d, $J=36.5$ Hz, 1H), 7.42 (d, $J=7.8$ Hz, 1H), 7.39 (d, $J=8.0$ Hz, 1H), 7.25 (d, $J=8.1$ Hz, 2H), 7.14 (t, $J=7.7$ Hz, 1H), 7.11 (t, $J=7.7$ Hz, 1H), 6.98 (d, $J=7.9$ Hz, 2H), 6.95 (d, $J=8.1$ Hz, 1H), 6.37 (d, $J=6.2$ Hz, 1H). ¹³C NMR (126 MHz, CDCl₃) 149.5 (d, $J=11.3$ Hz), 140.6 (d, $J=12.9$ Hz), 140.4 (d, $J=2.8$ Hz), 138.9 (d, $J=6.9$ Hz), 132.4, 131.6, 131.4 (d, $J=2.0$ Hz), 129.6 (d, $J=2.0$ Hz), 129.3 (d, $J=6.9$ Hz), 128.0 (d, $J=133.5$ Hz), 125.7 (d, $J=2.3$ Hz), 122.5, 122.2 (d, $J=4.2$ Hz), 121.2 (d, $J=13.2$ Hz), 118.8, 116.9 (d, $J=7.8$ Hz), 112.1. ³¹P NMR (202 MHz, CDCl₃) 54.4 (dd, $J=37.1, 4.3$ Hz). UV-vis (CHCl₃) λ_{\max} nm (ϵ ; M⁻¹cm⁻¹) 302 (16,600), 352 (8,600). HRMS (ASAP) [M+H]⁺ calcd for C₂₁H₁₆N₂OPS 375.0719, found 375.0721.

Heterocycle 2c: The general thionation procedure was performed on oxo-heterocycle **1c** (155 mg, 0.373 mmol, 1.00 equiv.) with LR (210 mg, 0.519 mmol, 1.39 equiv.) in toluene (60 mL). Column chromatography (2:1:1 hexanes:EtOAc:CH₂Cl₂, R_f=0.90) and subsequent recrystallization from hexanes and CH₂Cl₂ afforded thio-heterocycle **2c** (31 mg, 60%) as a pale yellow solid. ¹H NMR (500 MHz, CDCl₃) δ 7.87 (d, $J=7.8$ Hz, 2H), 7.72 (d, $J=8.0$ Hz, 2H), 7.56 (d, $J=36.5$ Hz, 1H), 7.43 (dd, $J=8.4, 1.9$ Hz, 1H), 7.39 (s, 1H),

7.24 (d, $J=7.6$ Hz, 2H), 7.13 (t, $J=7.5$ Hz, 1H), 6.99 (d, $J=7.9$ Hz, 2H), 6.91 (d, $J=8.3$ Hz, 1H), 6.45 (d, $J=6.4$ Hz, 1H), 1.34 (s, 9H). ^{13}C NMR (126 MHz, CDCl_3) δ 149.6 (d, $J=11.2$ Hz), 145.5, 141.0 (d, $J=2.8$ Hz), 140.7 (d, $J=13.1$ Hz), 136.6 (d, $J=6.8$ Hz), 132.4, 129.6 (d, $J=2.0$ Hz), 129.3 (d, $J=7.0$ Hz), 129.2, 127.8 (d, $J=2.0$ Hz), 127.6 (d, $J=134.4$ Hz), 125.6 (d, $J=2.3$ Hz), 122.3 (d, $J=4.4$ Hz), 120.7 (d, $J=13.1$ Hz), 118.9, 116.7 (d, $J=7.7$ Hz), 111.9, 34.4, 31.4. ^{31}P NMR (202 MHz, CDCl_3) 54.9 (dd, $J=36.3, 5.1$ Hz). UV-vis (CHCl_3) λ_{max} nm (ϵ ; $\text{M}^{-1}\text{cm}^{-1}$) 306 (15,900), 350 (6,520). HRMS (ASAP) $[\text{M}+\text{H}]^+$ calcd for $\text{C}_{25}\text{H}_{24}\text{N}_2\text{OPS}$ 431.1334, found 431.1347.

Heterocycle 2d: The general thionation procedure was performed on oxo-heterocycle **1d** (85 mg, 0.248 mmol, 1.00 equiv.) with LR (134 mg, 0.347 mmol, 1.40 equiv.) in toluene (50 mL). Column chromatography (5:1:1 hexanes:EtOAc: CH_2Cl_2 , $R_f=0.50$) and subsequent recrystallization from CH_2Cl_2 and pentane afforded thio-heterocycle **2d** (65 mg, 59%) as a pale yellow solid. ^1H NMR (500 MHz, $\text{DMSO}-d_6$) δ 9.15 (d, $J=6.9$ Hz, 1H), 7.98 – 7.91 (m, 2H), 7.80 (d, $J=30.5$ Hz, 1H), 7.78 (d, $J=9.0$ Hz, 2H), 7.72 (d, $J=8.4$ Hz, 2H), 7.58 – 7.49 (m, 4H), 7.34 (t, $J=7.7$ Hz, 1H), 7.04 (d, $J=8.5$ Hz, 1H), 7.00 (td, $J=7.5, 1.1$ Hz, 1H). ^{13}C NMR (126 MHz, $\text{DMSO}-d_6$) δ 141.2 (d, $J=12.9$ Hz), 139.1, 138.9 (d, $J=5.2$ Hz), 134.3 (d, $J=106.1$ Hz), 132.2 (d, $J=2.8$ Hz), 132.1, 132.0 (d, $J=12.3$ Hz), 131.4, 131.1, 128.4 (d, $J=13.4$ Hz), 128.3 (d, $J=6.2$ Hz), 123.8 (d, $J=96.8$ Hz), 120.4, 119.4 (d, $J=13.0$ Hz), 118.6, 117.0 (d, $J=8.0$ Hz), 110.2. ^{31}P NMR (202 MHz, $\text{DMSO}-d_6$) δ 41.6 (dt, $J=34.4, 15.6$ Hz). UV-vis (CHCl_3) λ_{max} nm (ϵ ; $\text{M}^{-1}\text{cm}^{-1}$) 301 (14,500), 365 (6,380). HRMS (ASAP) $[\text{M}+\text{H}]^+$ calcd for $\text{C}_{21}\text{H}_{16}\text{N}_2\text{PS}$ 359.0762, found 359.0772.

Heterocycle 2e: The general thionation procedure was performed on oxo-heterocycle **1e** (199 mg, 0.500 mmol, 1.00 equiv.) with LR (283 mg, 0.700 mmol, 1.40 equiv.) in toluene

(100 mL). Column chromatography (2:1:1 hexanes:EtOAc:CH₂Cl₂, R_f=0.90) and subsequent recrystallization from hexanes and CH₂Cl₂ afforded thio-heterocycle **2e** (185 mg, 89%) as a dark yellow solid. ¹H NMR (500 MHz, DMSO-*d*₆) δ 9.02 (d, *J*=7.0 Hz, 1H), 7.97 – 7.90 (m, 2H), 7.83 (d, *J*=30.6 Hz, 1H), 7.79 (d, *J*=7.6 Hz, 2H), 7.71 (d, *J*=8.9 Hz, 2H), 7.57 – 7.47 (m, 4H), 7.41 (dd, *J*=8.3, 2.1 Hz, 1H), 6.97 (d, *J*=8.5 Hz, 1H), 1.30 (s, 9H). ¹³C NMR (126 MHz, DMSO-*d*₆) δ 142.7, 141.3 (d, *J*=12.9 Hz), 139.6, 136.5 (d, *J*=5.1 Hz), 134.7, 133.9, 132.2 (d, *J*=2.9 Hz), 132.0 (d, *J*=9.9 Hz), 128.8, 128.4 (d, *J*=13.4 Hz), 128.2 (d, *J*=6.3 Hz), 127.5, 123.5 (d, *J*=97.4 Hz), 118.9 (d, *J*= 12.8 Hz), 118.6, 116.7 (d, *J*=7.9 Hz), 110.1, 33.9, 31.2. ³¹P NMR (202 MHz, DMSO-*d*₆) δ 41.9 (dt, *J*=31.2, 15.6 Hz). UV-vis (CHCl₃) λ_{max} nm (ε; M⁻¹cm⁻¹) 303 (20,800), 373 (7,950). HRMS (ASAP) [M+H]⁺ calcd for C₂₅H₂₄N₂PS 415.1422, found 414.1398.

Heterocycle 2f: The general thionation procedure was performed on oxo-heterocycle **1f** (100 mg, 0.240 mmol, 1.00 equiv.) with LR (138 mg, 0.341 mmol, 1.40 equiv.) in toluene (75 mL). Column chromatography (2:1:1 hexanes:EtOAc:CH₂Cl₂, R_f=0.90) and subsequent recrystallization from hexanes and CH₂Cl₂ afforded thio-heterocycle **2 f** (61 mg, 59 %) as a yellow solid. ¹H NMR (600 MHz, DMSO-*d*₆) δ 9.71 (d, *J*=7.0 Hz, 1H), 8.00 – 7.91 (m, 3H), 7.96 (d, *J*=36.0 Hz, 1H), 7.80 – 7.74 (m, 4H), 7.67 (d, *J*=8.5 Hz, 1H), 7.58 (d, *J*=7.1 Hz, 1H), 7.57 – 7.51 (m, 2H), 7.19 (d, *J*=8.5 Hz, 1H). ¹³C NMR (126 MHz, DMSO-*d*₆) δ 141.9, 140.7 (d, *J*=12.7 Hz), 138.3, 133.7 (d, *J*=106.1 Hz), 132.5, 132.2, 132.1 (d, *J*=12.5 Hz), 128.6 (d, *J*=13.5 Hz), 128.4 (d, *J*=6.1 Hz), 127.7, 126.3, 125.4 (d, *J*=95.2 Hz), 124.4 (q, *J*= 543.8, 272.9 Hz), 120.7 (q, *J*=32.3 Hz), 119.1 (d, *J*= 13.2 Hz), 118.5, 117.7 (d, *J*=7.8 Hz), 110.6. ³¹P NMR (202 MHz, DMSO-*d*₆) δ 41.3 (dt, *J*=33.8, 15.9 Hz). ¹⁹F NMR (471 MHz, DMSO-*d*₆) δ -60.02. UV-vis (CHCl₃) λ_{max} nm (ε; M⁻¹cm⁻¹) 295

(14,000), 357 (6,840). HRMS (ASAP) $[M+H]^+$ calcd for $C_{22}H_{15}N_2F_3PS$ 427.0646, found 427.0639.

CHAPTER VII

UTILIZATION OF THE 2- λ^5 -PHOSPHAQUINOLIN-2-ONE SCAFFOLD AS A NON-CYTOTOXIC, pH-INSENSITIVE, AND CELL-PERMEABLE IMAGING REAGENT

This chapter includes unpublished work from an ongoing study that focuses on exploiting the phosphaquinolone as a cellular imaging reagent. This story was written by Jeremy P. Bard, synthesis and photophysical characterization were performed by Jeremy P. Bard with assistance from J. Nolan McNeill and Holden J. Howard. Cell assays were performed by Sarah G. Bolton. Editorial support was provided by Michael. D. Pluth, Michael M. Haley, and Darren W. Johnson.

7.1 Introduction

Advancements in cell/tissue imaging has benefited the understanding of biological systems and mechanisms enormously, thus the development of new imaging methods, higher power scopes, and more diverse chemical dyes remains an active area of chemical biology research. While there has been significant progress in all of these areas, the development of chemical chromophores and fluorophores stands out as one of the most well-studied and broadly understood.¹⁻¹⁰ A variety of fluorophores exist that span a series of brightnesses and emission colors, yet many are based on only a few “core” molecular scaffolds, including coumarins, xanthenes, cyanines, and BODIPY (Figure 7.1).

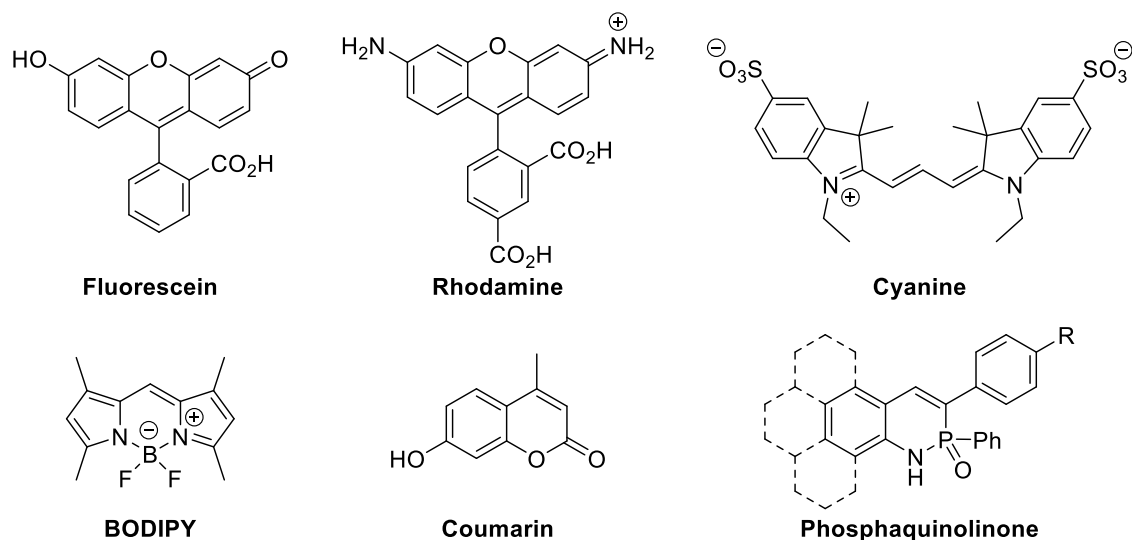


Figure 7.1 Examples of core fluorophore scaffolds and the phosphaquinolinone scaffold.

Many structure-property relationships focusing on substituent group placement, heteroatom insertion, and backbone modification have been built for these compounds, which have led to a thorough understanding of their capabilities and limitations.^{11–18} Examples of such limitations include pH-sensitivity, low brightnesses, chemical instability, cytotoxicity, and photobleaching. The development of unique chemical structures is paramount to further expanding the toolkit of cell imaging reagents available to chemical biologists.

Recently, a new phosphorus- and nitrogen-containing (PN) coumarin-like scaffold, the 2- λ^5 -phosphaquinolin-2-one framework, has been reported and has been shown to exhibit interesting photophysical properties (Figure 1).^{19,20} While a variety of P-containing heterocycles exist, relatively few contain the phosphoramidate moiety owing to difficulties in synthesis and purification, thus making this PN framework structurally unique and poised for potentially promising physicochemical properties. Primarily, this PN scaffold shows coumarin-like fluorescence, structural modularity, and very good Stokes shifts. In addition to a variety of studies examining the effect of arene core modification, several

structure-property relationships have been drawn for the substituent group placement along both the pendent aryl group, as well as the 6-position of the PN-naphthalene system. It was found that having electron-withdrawing groups (EWG) on the pendant aryl ring upon the carbon in the three position and/or electron-donating groups (EDG) upon the carbon in the 6-position both led to increased Stokes shifts and red shifted emissions.²¹ Additionally, placement of the more rigid phenyl group in place of the original phenoxy group on the phosphorus center leads to a 3- to 4-fold increase in the quantum yield of the scaffold.²²

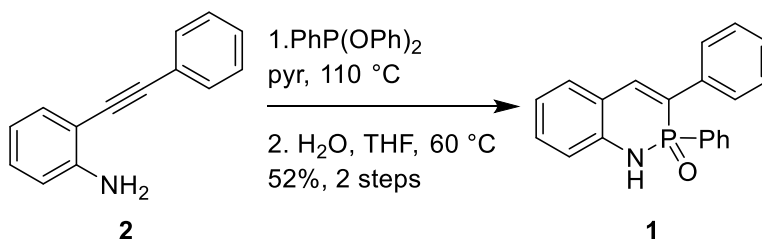
Furthermore, a vast majority of the prepared PN systems are compatible with Lipinski's Rule of Five (Ro5), as they have less than five hydrogen bond donors, less than ten hydrogen bond acceptors, weigh less than 500 amu, and have a low octanol-water partition coefficient,²³ suggesting that the scaffold should be able to permeate cell membranes. With these promising characteristics, the 2- λ^5 -phosphaquinolin-2-one scaffold warrants investigation as a cell imaging reagent.

7.2 Results and discussion

While this system holds promise for cell imaging, several proof-of-principle studies need to be performed first to ensure that the photophysical properties seen in organic solvents hold when in more cell-like solvents, that the phosphoramidate is non-cytotoxic, and that the dyes can enter cells as suggested by the Ro5 compatibility.

To first test the viability of this PN system in cell imaging applications, non-substituted PN derivative **1** was prepared through cyclization of 2-(2-phenylethynyl)-benzenamine **2** with PhP(OPh)₂ following the standard cyclization procedure (Scheme 7.1). This initial derivative was chosen due to its relatively low molecular weight, simple

molecular structure, and minimal number of H-bond donors and acceptors in accordance with Lipinski's Rule of 5.



Scheme 7.1 Synthesis of Heterocycle **1**.

Upon isolation, we first examined the photophysical properties of **1** in CHCl₃ (Figures F.1 and F.2, Table 7.1). The lowest energy absorption of **1** is 338 nm with an absorption maximum of 18000 M⁻¹cm⁻¹. The emission is at 441 nm with a 44% quantum yield. These values are in line with previously reported P-Ph heterocycles, showing a good quantum yield due to the structural rigidification caused by placing the phenyl group upon the phosphorus center instead of the traditional phenoxy.

Table 7.1 Photophysical properties of new heterocycles in CHCl₃ at 298 K

cmpd	$\lambda_{\text{abs,max}}$ (nm)	λ_{abs} (nm)	$\epsilon_{\text{abs,max}}$ (M ⁻¹ cm ⁻¹)	ϵ_{abs}^a (M ⁻¹ cm ⁻¹)	λ_{em} (nm)	Stokes shift (nm/cm ⁻¹)	Φ (%)	τ (ns)
1	293	338	17972	11000	441	103/6910	44	3.7
3	307	369	16201	7519	487	118/6567	24	6.1
7	306	357	24218	11886	471	114/6780	24	4.9
8	306	367	16700	7500	486	119/6671	63	5.9
9	305	368	14500	6654	487	119/6640	77	6.1

^a Lowest energy absorbance maximum.

To better represent the photophysical properties of **1** in an environment closer to that found in cellular assays, we next collected photophysical data in a DMSO/PBS buffer mixture (Figures F.1 and F.2, Table 7.2). Gratifyingly, relatively few changes are observed in these properties, as only a slight redshifting in the emission and moderate drop in quantum yield were observed.

Table 7.2 Photophysical properties of new heterocycles in ca. 5% DMSO in pH 7.4 PBS Buffer at 298 K

#	$\lambda_{\text{abs, max}}$ (nm)	λ_{abs} (nm)	$\epsilon_{\text{abs, max}}$ ($\text{M}^{-1}\text{cm}^{-1}$)	ϵ_{abs}^a ($\text{M}^{-1}\text{cm}^{-1}$)	$\epsilon_{\text{abs, 405}}$ ($\text{M}^{-1}\text{cm}^{-1}$)	λ_{em} (nm)	Stokes shift (nm/ cm^{-1})	Φ (%)	τ (ns)
1	290	336	17461	9140	183	452	116/7638	23	3.6
3	313	382	17506	10143	7192	499	117/6138	17	5.9
7	314	375	10711	7785	6037	485	110/6049	16	5.2
8	304	359	21000	9200	2300	500	141/7855	50	6.2
9	303	359	12980	5813	1117	493	134/7572	61	5.9

^a Lowest energy absorbance maximum.

With these properties, we wanted to see how **1** performed as a cell imaging reagent. For this, we first determined cell permeability of **1**, which was studied by treated HeLa cells with ca. 1×10^5 M solutions of our dye in 0.5% DMSO in PBS buffer for 30 minutes and imaging them on a confocal microscope. The PN dye was excited at 405 nm and imaged on the GFP channel (Figure 7.2). While the attained images were relatively dull based upon the minimal absorbance of **1** at 405 nm, they still showed evidence for cell permeation and integration of the dye into the cytosol of the cell.

We next wanted to measure the cytotoxicity of **1** and check what, if any, effect the phosphoquinolinone moiety has on cells. Live HeLa cells were treated with 1, 5, 10 and 20 μM solutions of **1** for 30 minutes. Cell death was measured using CCK-8 cell assay. Preliminary results suggest that no cytotoxicity is observed, though follow up studies need to be performed to confirm this. This proof-of-principle experiment indeed showed promise for the use of our PN derivatives for cell imaging, so our next step was to optimize the physicochemical properties of the dye. For this, we designed heterocycle **3** (Scheme 7.2).

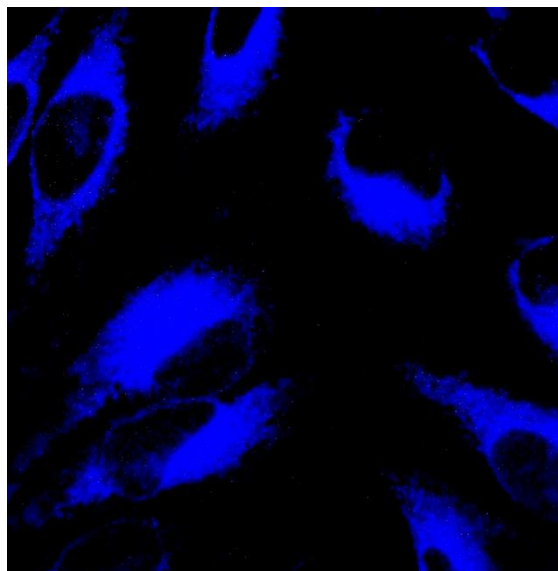
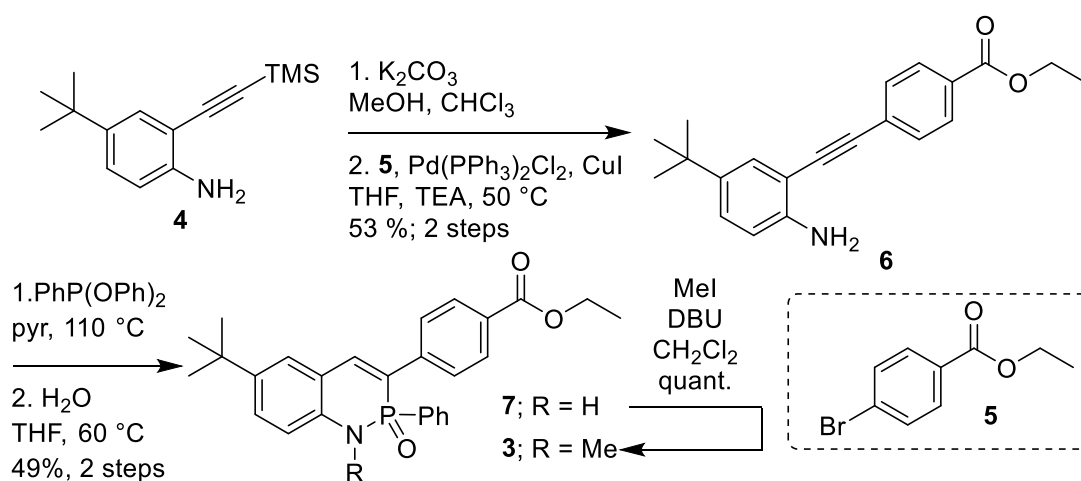


Figure 7.2 Initial images of HeLa cells upon treatment with a 25 μM solution of **1** and incubation for 30 minutes.

Not only does **3** retain the P-Ph substitution for improved quantum yield, but it also contains an EWG on the 3 position and an EDG on the 6 position, which leads to redshifted absorptions and emissions in these types of fluorophores. Additionally, **3** contains a methyl group upon the phosphonamide nitrogen, which removes the protic hydrogen and should impart base-insensitivity to the scaffold in addition to its inherent acid-stability.



Scheme 7.2 synthesis of methylated PN **3**.

For this synthesis of **3**, 4-tert-butyl-2-((trimethylsilyl)ethynyl)aniline **4** was first protodesilylated with K_2CO_3 before the resultant terminal acetylene was formed by Sonogashira cross-coupling with ethyl 4-bromobenzoate **5** to afford ethynyl aniline **6**. **6** was then cyclized following standard protocol with $PhP(OPh)_2$ to give heterocycle **7** in good yield. Next, **7** was treated with MeI and DBU to afford fluorophore **3** in quantitative yield after only minimal aqueous washing.

When examining the photophysical properties of heterocycle **3** in $CHCl_3$, large red shifts in both the absorption and emission spectra are observed, which aligns with our previous studies on the PN Scaffold (Figures F.1 and F.2, Table 7.1). In ca. 5% DMSO in pH 7.4 PBS buffer, nearly 50 nm red shifts are observed in both the lower energy absorption peak and the emission wavelengths (Figures F.1 and F.2, Table 7.2). This leads to a large increase in the absorbance at 405 nm, thus increasing the effective brightness of **3** in this imaging procedure.

Interestingly, methylation of the PN N–H in **3** leads to a 10 to 15 nm red shift in both the absorption and emission spectra in both solvent systems when compared to the unmethylated heterocycle **7**. Furthermore, the effects of methylation on acid- and base-sensitivity for the PN heterocycles reported herein were tested by preparing ca. 1×10^{-4} M solutions of each fluorophore were prepared in 5% DMSO in deionized H_2O or in $CHCl_3$. UV-vis and fluorescence spectra were collected in both of these solvent systems. Then, for the base-stability studies, either a concentrated solution of NaOH or DBU was added to bring the solution to ca. pH = 13 or 5% DBU in $CHCl_3$, respectively. The absorption and emission spectra were collected immediately after addition of the base. Then, the samples were left for 24 hours, before the absorption and emission spectra were collected again.

For the acid-stability studies, another set of ca. 1×10^4 M solutions of each fluorophore were prepared in 5% DMSO in deionized H₂O or CHCl₃, which again had their absorption and emission spectra collected. Then, either HCl or trifluoroacetic acid (TFA) was added to bring the solution to ca. pH = 2 or 5% TFA in CHCl₃, respectively. Spectra were collected immediately after addition of the acid, and again after 18 hours. Compared to unmethylated heterocycles **1** and **7**, which show a dramatic red shift and quench in the emission spectra after treatment with base, heterocycles, **3**, **9**, and **8** show relatively no change in their emission spectra upon treatment with base (Figures F.3 to F.7).

To test the imaging capabilities of **3**, HeLa cells were treated with the same procedure outlined for **1** (Figure 7.3). Gratifyingly images of **3** were much brighter than those of **1**, likely due to the increased absorbance at 405 nm. Cytotoxicity was measured using the same CCK-8 cell assay as mentioned above, which showed no cytotoxicity even up to 150 μ M dye concentration (Figure 7.4). These results present **3** as a more suitable cell imaging reagent, and further optimization and stability studies are underway to fully characterize it as such.

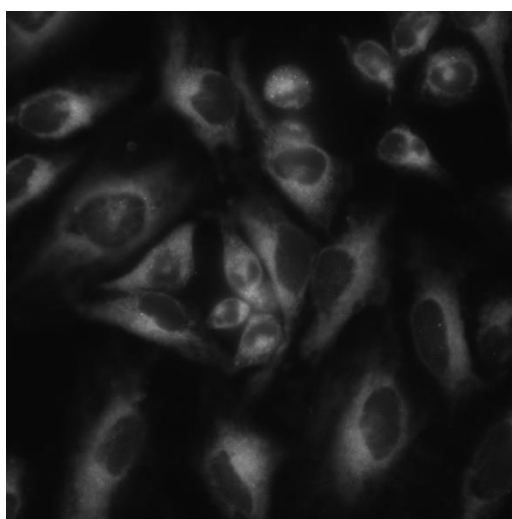


Figure 7.3 Initial images of HeLa cells upon treatment with a 25 μ M solution of **3** and incubation for 30 minutes.

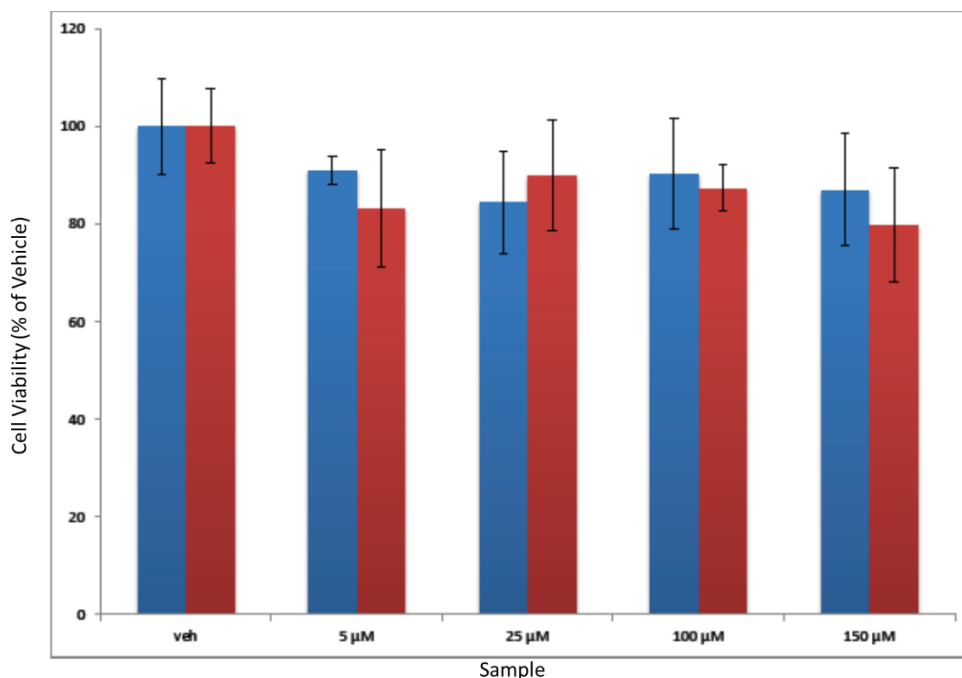
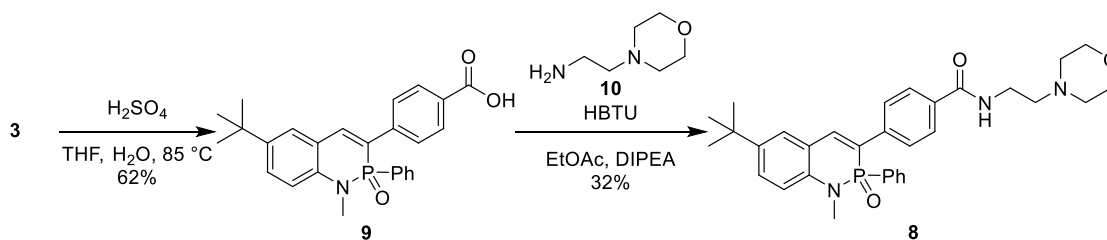


Figure 7.4 Cytotoxicity studies on heterocycle **3** showing no significant cytotoxicity up to 150 μM .

Next, we wanted to see if this new fluorophore scaffold could be further functionalized such that it could be appended to different subcellular location targeting groups. For this we designed heterocycle **8**, integrating the well-known lysosome-targeting morpholine unit.²⁴ To access **8**, we first hydrolyzed the ester group of **3** to give the respective carboxylic acid **9**. Peptide coupling with HBTU and 4-(2-aminoethyl)morpholine **10** is then used to afford **8** in moderate yields (Scheme 7.3). Crystals suitable for x-ray crystallography of **8** were grown, confirming the correct connectivity (Figures F.8 and F.9).



Scheme 7.3 synthesis of heterocycle **8**.

The photophysical properties of **8** are nearly identical to those of heterocycle **3** in CHCl₃ (Figures F.1 and F.2, Table 7.1). This makes sense because the only difference between the structures is the ethyl ester of **8** being replaced with the morpholine-containing amide arm, but of which are moderately EWG. Interestingly, the quantum yield of **8** is 63%, which is almost triple that of **3**, potentially due to solvent interaction with the hydrogen bond donating and accepting amide arm of **8** reducing thermal relaxations upon relaxation. This trend in the quantum yields is again seen in 5% DMSO in pH 7.4 PBS buffer. Additionally, **8** in this DMSO mixture shows a more blue-shifted absorption spectra, again suggesting that solvent coordination around the protic and polar amide arm may be influencing the photophysical properties of the scaffold (Figures F.1 and F.2, Table 7.2). While this blue-shifting in the absorbance leads to a decrease in the absorbance at 405 nm for imaging purposes, the increased quantum yield leaves the overall virtual brightness at 405 nm about the same as **3**.

The targeting capabilities of **8** are currently being studied through co-localization studies with lysotracker deep red (Figure 7.5). These tests were performed with three plates of HeLa cells where one is treated with 10 μM **8** (Figure 7.5, left), one is treated with 10 μM **8** and 75 nM LysoTracker Deep Red (Figure 7.5, right), and the third is treated with just DMSO and all cells are incubated for one hour. Then, cells were rinsed with FluoroBrite media and imaged on a Leica widefield scope. The probe was imaged with the DAPI long pass cube, and LysoTracker is imaged with Cy5. The images are all colored with a Red Hot filter. Similarities between the dye images and the lysotracker images can be observed, including small puncta throughout the cells indicating potential lysosome targeting. However, a large amount of both the dye as well as the lysotracker dyes are non-

localized throughout the cell, indicating a potential experimental, chemical, or instrumental issue during the experimental process. While this initial result is very exciting, higher resolution images must be collected to confirm the localization of **8** in the lysosome.

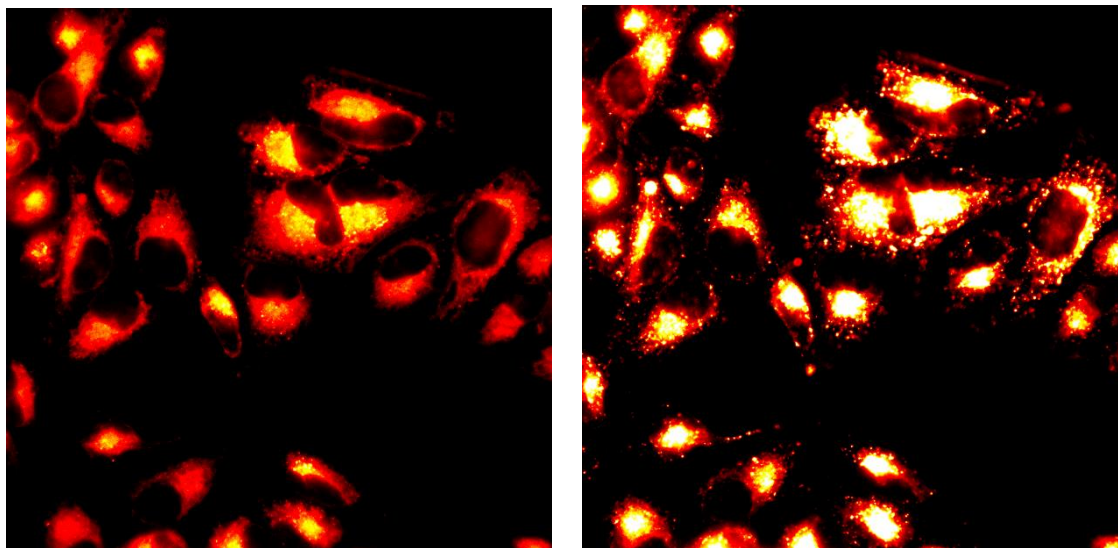


Figure 7.5 colocalization with **8** and Lysotracker Deep Red.

7.3 Conclusions and Future Works

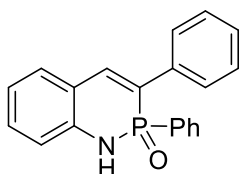
We have prepared a series of cell imaging reagents based upon the coumarin-like phosphoquinolinone scaffold. With good solubilities, excellent Stokes shift, and moderate brightnesses in DMSO/PBS mixtures, this PN framework is poised to expand the toolkit available to both chemists and chemical biologists for live cell imaging applications. These new dyes are non-cytotoxic, cell permeable, robust, and targetable. To gain a more comprehensive understanding of these dyes and their capabilities in a variety of imaging applications, a few studies must be performed. First and foremost, efforts are underway currently to attain higher resolution images that corroborate the localization of the dye into the lysosome of the cell. Once this is confirmed, other functional groups can be appended via similar peptide coupling conditions to broaden the scope of where these dyes can be targeted, including the mitochondria, the golgi apparatus, and the nucleus. Furthermore,

with the permeability presented by these simple naphthalene-like PN scaffolds, it could be beneficial to explore the larger acene backbone PN derivatives that have been developed in these imaging experiments as well. While the increased size of the scaffold may inhibit cell permeation, the inherently brighter fluorophores would give much brighter images of cells if they were able to enter cells. Lastly, while this study focuses on the methylated version of the scaffold, derivatives that retain the protic N-H may be an interesting class of dyes as well, since it has been shown that the phosphaquinolone scaffold increases in brightness and its emission red shifts dramatically upon deprotonation. While the scaffold decomposes upon deprotonation, the timescale of that decomposition has not been studied fully. If images using the deprotonated form of the dye are able to be collected before said decomposition occurs, then brighter images may be attainable. These studies, combined with the work herein, present the phosphaquinolone framework as a promising new class of cellular imaging agents.

7.4 Experimental Section

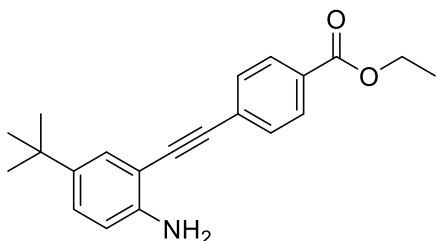
General. All oxygen- and water-free reactions were performed under an N₂ atmosphere using Schlenk technique. Column chromatography was performed using silica gel (240–300 mesh), with solvent systems being referenced to the most abundant solvent. NMR spectra were acquired at room temperature on a Varian Inova 500 (¹H: 500 MHz, ¹³C: 126 MHz, ³¹P: 202 MHz) or a Bruker Avance III HD 500 equipped with a Prodigy multinuclear cryoprobe (¹H: 500 MHz, ¹³C: 126 MHz, ³¹P: 202 MHz). ¹H and ¹³C NMR chemical shifts (δ) are expressed in ppm relative to residual CHCl₃ (¹H: 7.26 ppm, ¹³C: 77.16 ppm) or DMSO (¹H: 2.50 ppm, ¹³C: 39.52 ppm) shifts. ³¹P NMR shifts are referenced to 85% H₃PO₄ (δ 0 ppm) as an external reference. ¹⁹F NMR shifts are referenced to CFCl₃ (δ 0 ppm) as

an external reference. UV-vis spectra were recorded using an Agilent Technologies Cary 60 UV-vis spectrophotometer. Fluorescence emission spectra were recorded using a Horiba Jobin Yvon FluoroMax-4 fluorimeter exciting at 365 nm. Quantum yields (ϕ) were determined through comparison of the emission and absorption intensities of the analyte to those of a 0.1M H₂SO₄ quinine sulfate solution.²⁵ Fluorescence lifetime measurements were recorded using a Horiba FluoroHub Single Photon Counting Controller with a TemPro Fluorescence Lifetime System attachment. High-resolution mass spectra (HRMS) were recorded on a Waters XEVO G2-XS mass spectrometer.



H,H PhAZP **1** was prepared by treating 2-(2-phenylethynyl)-benzenamine **2** (665 mg, 3.4 mmol, 1 equiv.) with P(Ph)(OPh)₂ (2.0 g, 6.9 mmol, 2 equiv.) in pyridine (4 mL) and heating in a sand bath to 110 °C for 48 h. The reaction mixture was then cooled to room temperature before *ca.* 20 mL of toluene was added and the solvent was removed *in vacuo*. Two more analogous toluene washes were performed to fully remove pyridine from the mixture. The crude residue was then dissolved in minimal THF and 5 drops of water were added before the solution was heated to 60 °C for 1 h in a water bath. The mixture was then dried (Na₂SO₄), filtered, and concentrated *in vacuo*. Column chromatography (2:1:1 hexanes:EtOAc:CH₂Cl₂, *R_f* = 0.15) and subsequent recrystallization from CH₂Cl₂ and hexanes was used to give heterocycle **1** (565 mg, 52%) as a yellow solid: mp > 250 °C; ¹H NMR (500 MHz, Chloroform-*d*) δ 7.66 (d, *J* = 7.1 Hz, 1H), 7.65 – 7.61 (m, 1H), 7.62 (d, *J* = 32.7 Hz, 1H), 7.61 – 7.56 (m, 3H), 7.38 (t, *J* = 8.0 Hz, 2H), 7.33 – 7.17 (m, 6H), 7.01

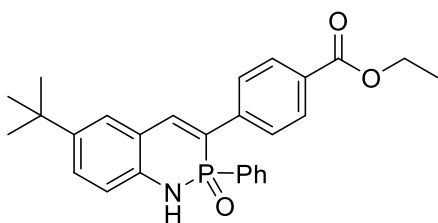
(d, $J = 8.1$ Hz, 1H), 6.99 (t, $J = 7.4$ Hz, 1H). ^{13}C NMR (126 MHz, Chloroform- d) δ 139.6 (d, $J = 3.6$ Hz), 139.0 (d, $J = 4.0$ Hz), 136.9 (d, $J = 11.5$ Hz), 133.2 (d, $J = 138.6$ Hz), 132.6 (d, $J = 10.6$ Hz), 132.0 (d, $J = 2.8$ Hz), 130.6, 130.5, 128.7, 128.3, 128.2, 127.9 (d, $J = 5.9$ Hz), 127.3 (d, $J = 117.7$ Hz), 120.8, 119.6 (d, $J = 12.3$ Hz), 117.2 (d, $J = 7.7$ Hz). ^{31}P NMR (202 MHz, Chloroform- d) δ 11.99; HRMS (ASAP) $[\text{M} + \text{H}]^+$ calcd for $\text{C}_{20}\text{H}_{17}\text{NOP}$ 318.1048, found 318.1032.



Aniline **6** was prepared by first dissolving 4-tert-Butyl-2-((trimethylsilyl)ethynyl)aniline **4** (2.18 g, 8.9 mmol, 1.0 equiv.) and K_2CO_3 (3.70 g, 26.7 mmol, 3.0 equiv.) in 70 mL of 1:1 MeOH: CHCl_3 and stirring at room temperature for 1.5 h. Once the protodesilylation reaction was complete by TLC, the reaction mixture was reduced *in vacuo*. The crude mixture was then suspended in ca. 20 mL CH_2Cl_2 and washed $3 \times$ with H_2O . The organic layer was collected, dried (Na_2SO_4), and concentrated *in vacuo*. The crude terminal acetylene was then carried forward to the next step.

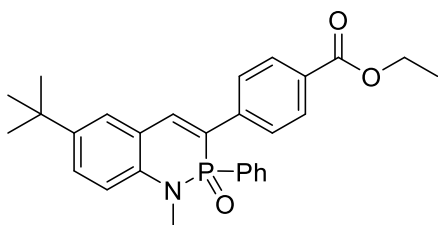
Sonogashira cross-coupling was then performed by adding Ethyl 4-bromobenzoate **5** (2.04 g, 8.9 mmol, 1.0 equiv.), CuI (119 mg, 0.623 mmol, 0.07 equiv.), and $\text{Pd}(\text{PPh}_3)_2\text{Cl}_2$ (437 mg, 0.623 mmol, 0.07 equiv.) to the crude terminal acetylene. This mixture was then dissolved in THF (30 mL) and the solution was made air-free using four rounds of atmosphere exchange with N_2 . TEA (30 mL) was then added via syringe before the reaction was heated to 50°C and stirred for 48 h. The reaction mixture was then cooled to room temperature and concentrated *in vacuo*. Three 20 mL portions of EtOAc were added to the

reaction mixture and subsequently removed *in vacuo* to remove the residual TEA. Column chromatography (16:1:1 hexanes:EtOAc:CH₂Cl₂, $R_f = 0.20$) was used to give aniline **6** (1.53 g, 53%) as an orange solid: mp > 97.5-98.8 °C; NMR ¹H NMR (500 MHz, Chloroform-*d*) δ 8.03 (d, $J = 8.4$ Hz, 2H), 7.58 (d, $J = 8.4$ Hz, 2H), 7.39 (d, $J = 2.4$ Hz, 1H), 7.21 (dd, $J = 8.5, 2.3$ Hz, 1H), 6.69 (d, $J = 8.5$ Hz, 1H), 4.39 (q, $J = 7.1$ Hz, 2H), 4.18 (s, 2H), 1.41 (t, $J = 7.2$ Hz, 3H), 1.29 (s, 9H). ¹³C NMR (126 MHz, Chloroform-*d*) δ 166.1, 145.6, 141.0, 131.3, 129.7, 129.5, 128.8, 128.1, 127.7, 114.4, 106.9, 93.6, 89.6, 61.1, 33.9, 31.4, 14.3; HRMS (ASAP) [M + H]⁺ calcd for C₂₁H₂₄NO₂ 322.1807, found 322.1816.



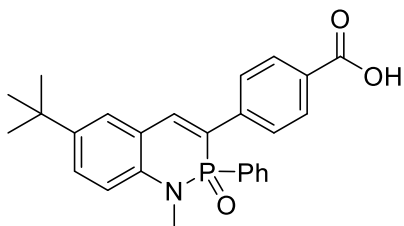
Heterocycle **7** was prepared by treating aniline **6** (960 mg, 2.98 mmol, 1.0 equiv.) with P(Ph)(OPh)₂ (1.76 g, 5.96 mmol, 2.0 equiv.) in pyridine (5 mL) and heating in a sand bath to 110 °C for 48 h. The reaction mixture was then cooled to room temperature before *ca.* 20 mL of toluene was added and the solvent was removed *in vacuo*. Two more analogous toluene washes were performed to fully remove pyridine from the mixture. The crude residue was then dissolved in minimal THF and 5 drops of water were added before the solution was heated to 60 °C for 1 h in a water bath. The mixture was then dried (Na₂SO₄), filtered, and concentrated *in vacuo*. Column chromatography (5:1:1 → 1:1:1 hexanes:EtOAc:CH₂Cl₂, $R_f = 0.15$ in 3:1:1) and subsequent recrystallization from CH₂Cl₂ and hexanes was used to give heterocycle X (652 mg, 49%) as a yellow solid: mp > 250 °C; NMR ¹H NMR (500 MHz, Chloroform-*d*) δ 7.90 (d, $J = 8.4$ Hz, 2H), 7.77 (d, $J = 3.0$ Hz, 1H), 7.68 (d, $J = 31.1$ Hz, 1H), 7.67 (d, $J = 8.1$ Hz, 2H), 7.63 (d, $J = 7.3$ Hz, 1H), 7.60

(d, $J = 7.3$ Hz, 1H), 7.40 (d, $J = 2.3$ Hz, 1H), 7.38 – 7.31 (m, 2H), 7.24 (dt, $J = 7.5, 3.9$ Hz, 2H), 6.99 (d, $J = 8.5$ Hz, 1H), 4.32 (q, $J = 7.1$ Hz, 2H), 1.36 (t, $J = 7.2$ Hz, 3H), 1.34 (s, 9H). ^{13}C NMR (126 MHz, Chloroform-*d*) δ 166.4, 143.6, 141.5 (d, $J = 11.6$ Hz), 140.9 (d, $J = 3.2$ Hz), 132.8 (d, $J = 139.4$ Hz), 132.5 (d, $J = 10.8$ Hz), 131.9 (d, $J = 2.7$ Hz), 129.7, 129.4, 128.5, 128.2, 128.1, 127.6 (d, $J = 6.2$ Hz), 127.1, 126.0 (d, $J = 119.1$ Hz), 118.7 (d, $J = 12.1$ Hz), 117.0 (d, $J = 7.6$ Hz), 61.0, 34.2, 31.4, 14.3. ^{31}P NMR (202 MHz, Chloroform-*d*) δ 11.79; HRMS (ASAP) $[\text{M} + \text{H}]^+$ calcd for $\text{C}_{27}\text{H}_{29}\text{NO}_3\text{P}$ 446.1888, found 446.1885.

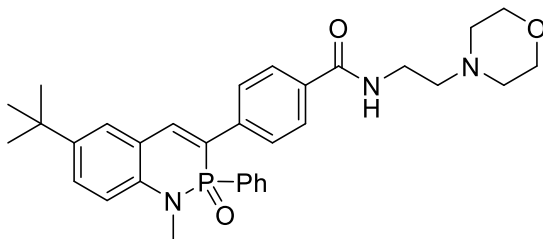


Methylated heterocycle **3** was prepared by dissolving tbu ester heterocycle **7** (78 mg, 0.175 mmol, 1.0 equiv.) in dry CH_2Cl_2 and the mixture was put under N_2 via atmosphere exchange. MeI (0.9 mL, 3.95 mmol, 22.5 equiv.) was then added before DBU (0.4 mL, 1.75 mmol, 10 equiv.) was added dropwise, which induced an immediate red-shift in both the color of solution and the emission color of the solution. The solution was let stir for 16 h, at which point the solution had returned to its original color and the reaction was complete via TLC. The reaction mixture was then reduced *in vacuo*, before being dissolved in CH_2Cl_2 , washed 3 \times with an aqueous NaHCO_3 solution to remove excess DBU. After drying (K_2CO_3), filtering, and concentration *in vacuo*, methylated PN heterocycle **3** was afforded as a yellow solid (79 mg, 98% yield) in an excellent yield: mp 125.4-126.8 $^\circ\text{C}$; NMR ^1H NMR (500 MHz, Chloroform-*d*) δ 7.91 (d, $J = 8.1$ Hz, 2H), 7.83 – 7.61 (m, 5H), 7.50 (d, $J = 8.7$ Hz, 1H), 7.46 (s, 1H), 7.39 (t, $J = 6.7$ Hz, 1H), 7.34 (td, $J = 7.5, 3.2$ Hz, 2H), 7.04 (d, $J = 8.7$ Hz, 1H), 4.33 (q, $J = 7.1$ Hz, 2H), 3.12 (d, $J = 7.7$ Hz, 3H), 1.37 (s,

9H), 1.35 (t, $J = 7.0$ Hz, 3H). ^{13}C NMR (126 MHz, Chloroform- d) δ 166.4, 143.3, 141.4 (d, $J = 11.7$ Hz), 141.0 (d, $J = 3.0$ Hz), 139.5, 132.4 (d, $J = 10.5$ Hz), 132.2 (d, $J = 138.1$ Hz), 132.0 (d, $J = 2.8$ Hz), 129.7, 129.5, 128.7, 128.5, 128.4, 127.7 (d, $J = 6.2$ Hz), 125.7 (d, $J = 117.8$ Hz), 120.0 (d, $J = 11.5$ Hz), 112.9 (d, $J = 5.0$ Hz), 61.0, 34.1, 31.5 (d, $J = 4.0$ Hz), 31.4, 14.3. ^{31}P NMR (202 MHz, Chloroform- d) δ 16.75; HRMS (ASAP) $[\text{M} + \text{H}]^+$ calcd for $\text{C}_{28}\text{H}_{31}\text{NO}_3\text{P}$ 460.2042, found 460.2068.



Heterocycle **9** was prepared by dissolving methylated heterocycle **3** (200 mg; 0.435 mmol, 1.0 equiv.) in 20 mL THF and 20 mL H_2SO_4 (30% v:v in H_2O) and heating to 85 °C under a reflux condenser for 24 hr. The reaction mixture was then cooled to room temperature before the organic layer was extracted with 5 \times rounds of ca. 40 mL EtOAc. The organic layer was the dried (K_2CO_3), filtered and concentrated *in vacuo*. Several round of recrystallization from CH_2Cl_2 and pentanes was used to remove residual EtOAc and afford carboxylic acid **9** (117 mg, 62%) as a yellow solid: mp > 250 °C; NMR ^1H NMR (500 MHz, $\text{DMSO-}d_6$) δ 8.06 (d, $J = 31.2$ Hz, 1H), 7.83 (d, $J = 8.2$ Hz, 2H), 7.79 (d, $J = 8.1$ Hz, 2H), 7.71 (s, 1H), 7.63 – 7.52 (m, 3H), 7.44 (dt, $J = 15.9, 7.5$ Hz, 3H), 7.14 (d, $J = 8.8$ Hz, 1H), 2.99 (d, $J = 7.6$ Hz, 3H), 1.33 (s, 9H). ^{13}C NMR (126 MHz, $\text{DMSO-}d_6$) δ 166.9, 142.6, 141.1, 141.0, 139.1, 132.3 (d, $J = 134.5$ Hz), 132.1, 131.8 (d, $J = 10.8$ Hz), 129.4, 129.3 (d, $J = 105.0$ Hz), 128.7, 128.6 (d, $J = 8.9$ Hz), 127.4 (d, $J = 6.1$ Hz), 124.9, 123.9, 119.5 (d, $J = 11.2$ Hz), 113.1, 33.8, 31.2, 31.1. ^{31}P NMR (202 MHz, $\text{DMSO-}d_6$) δ 15.7; HRMS (ASAP) $[\text{M} + \text{H}]^+$ calcd for $\text{C}_{26}\text{H}_{27}\text{NO}_3\text{P}$ 432.1729, found 432.1758.



Morpholine-containing PN heterocycle **8** was prepared via peptide coupling conditions. Carboxylic acid PN **9** (314 mg; 0.730 mmol, 1.0 equiv.) and HBTU (554 mg; 1.46 mmol, 2.0 equiv.) were added to a round-bottom flask, which was then put under an N₂ atmosphere via atmosphere exchange. This mixture was then dissolved in dry CH₂Cl₂ (18 mL) before 4-(2-aminoethyl)morpholine **10** (0.38 mL, 2.92 mmol, 4.0 equiv.) was added. Lastly, DIPEA (0.140 mL; 0.82 mmol, 1.0 equiv.) was added via Hamilton syringe. The reaction was stirred for 1 hour, at which point it showed complete conversion of starting material. The reaction mixture was then concentrated *in vacuo* before being suspended in MeCN and cooled in an ice bath for 1 h. Salt byproducts then crashed out and were filtered off. The organic solution was then reduced to dryness *in vacuo* and redissolved in minimal DCM. Pentanes was slow-layered and left overnight. This initial process led to a brown oil coating the bottom of the flask, which allowed for a cleaner product solution to be decanted, reconcentrated, and set up for another round of recrystallization following the same procedure. This led to a fluorescent, yellow oil suspending on the bottom of the flask with crystalline yellow solids dotted throughout. The organic layer was removed, and the oil/solid mixture was dried *in vacuo* to afford **8** (126 mg; 32% yield) as a yellow solid: mp > 234.5-235.9 °C. It is expected that the reaction yield is higher than this, however, due to structural similarities between the product and the coupling side-products, the isolation of more product presents a significant challenge. ¹H NMR (500 MHz, DMSO-*d*₆) δ 8.35 (t, *J* = 5.7 Hz, 1H), 8.04 (d, *J* = 31.4 Hz, 1H), 7.80 – 7.66 (m, 5H), 7.64 – 7.51 (m, 3H), 7.48

(td, $J = 7.3, 1.5$ Hz, 1H), 7.43 (td, $J = 7.1, 3.3$ Hz, 2H), 7.13 (d, $J = 8.7$ Hz, 1H), 3.55 (t, $J = 4.6$ Hz, 4H), 3.35 (d, $J = 6.7$ Hz, 2H), 2.99 (d, $J = 7.6$ Hz, 3H), 2.42 (t, $J = 7.0$ Hz, 2H), 2.39 (t, $J = 4.0$ Hz, 4H), 1.34 (s, 9H). ^{13}C NMR (126 MHz, DMSO- d_6) δ 165.6, 142.5, 140.6, 139.2 (d, $J = 12.0$ Hz), 139.0, 133.5, 132.4 (d, $J = 134.8$ Hz), 132.0, 132.0, 131.7 (d, $J = 10.3$ Hz), 128.6 (d, $J = 13.1$ Hz), 128.4, 127.3, 127.1 (d, $J = 6.2$ Hz), 124.5 (d, $J = 116.9$ Hz), 119.5 (d, $J = 11.3$ Hz), 113.0, 66.2, 57.3, 53.3, 36.5, 33.8, 31.2, 31.0 (d, $J = 3.7$ Hz). ^{31}P NMR (202 MHz, DMSO- d_6) δ 15.77; HRMS (ASAP) $[\text{M} + \text{H}]^+$ calcd for $\text{C}_{32}\text{H}_{39}\text{N}_3\text{O}_3\text{P}$ 544.2729, found 544.2737.

CHAPTER VIII

DEVELOPMENT OF A TRIPODAL SWITCHABLE, SELECTIVE, AND SENSITIVE HOST MOLECULE CAPABLE OF HSO_4^- EXTRACTION TOWARDS NUCLEAR WASTE REMEDIATION

This chapter includes unpublished work from an ongoing study that focuses on the development, synthesis, and utilization of a 3-armed, PN host molecule towards hydrogen sulfate extraction and remediation from aqueous solutions. This story was written by Jeremy P. Bard, synthesis was performed by Dr. Chun-Lin Deng and Jeremy P. Bard with assistance from J. Nolan McNeill. Titration data was collected by Jeremy P. Bard. Editorial support was provided by Michael M. Haley and Darren W. Johnson.

8.1 Introduction

Anions play an important role in several areas including biology, environmental sciences, and chemistry.¹⁻⁴ For this reason, a large library of compounds have been developed with the ability to detect many of these anions both selectively and sensitively.⁵ While halides and nitrate have a variety of hosts because of their simple shape and uniformity of charge, a majority of oxoanionic guests have relatively few hosts that are capable of binding them due to their combination of hydrogen bond donors and/or acceptors as well as their unique geometries. Of these oxoanions, the tetrahedral HSO_4^- stands out because of its roles as a chemical catalyst, environmental contaminate, and aerosol nucleation initiator. Furthermore, HSO_4^- acts as a major interferant in the treatment process of high-level nuclear waste by disrupting the efficient vitrification of the

radioactive TcO_4^- anion.⁶⁻⁹ Removal of the HSO_4^- contaminate from the aqueous nuclear waste solution prior to its treatment would allow for more efficient vitrification and subsequent storage of nuclear waste. Of the methods proposed to accomplish this task, liquid-liquid extraction (LLE) rises to the top as one of the more promising possibilities. LLE is performed by mixing an organic solution that is doped with an extractant with the aqueous nuclear waste solution. With judicious choice of extractant, the substrate of choice (HSO_4^-) is pulled into the organic solution, which upon separation of layers can be removed. Ideally, this organic layer can then be washed and recycled for future uses in LLE. These topics have built up quite an interest in HSO_4^- binding, sensing, and remediation, and several groups have developed hosts for HSO_4^- coordination.¹⁰⁻¹⁵ However, many of the examples shown do not exhibit excellent selectivity towards HSO_4^- . This prohibits their use as a potential extractant for nuclear waste remediation based upon the variety of different anions present in the aqueous slurry. Increased selectivity must be attained in a host before it can be explored as a potential extractant.

In line with our lab's interest in both anion binding with bisurea hosts (**1** in Figure 8.1) as well as exploration of the relatively new phosphorus- and nitrogen-containing (PN) phosphaquinolone scaffold,¹⁶⁻¹⁹ we recently reported two-armed scaffold **2**, which is capable of binding HSO_4^- both selectively (ca. 50:1 binding over similar competing ions) and strongly ($K_a = 9600 \text{ M}^{-1}$).^{ref} This selectivity was due in large part to both the tetrahedral geometry of the PN phosphoramidate arm as well as the complementary alignment of hydrogen bond donors and acceptors between the host and the guest.

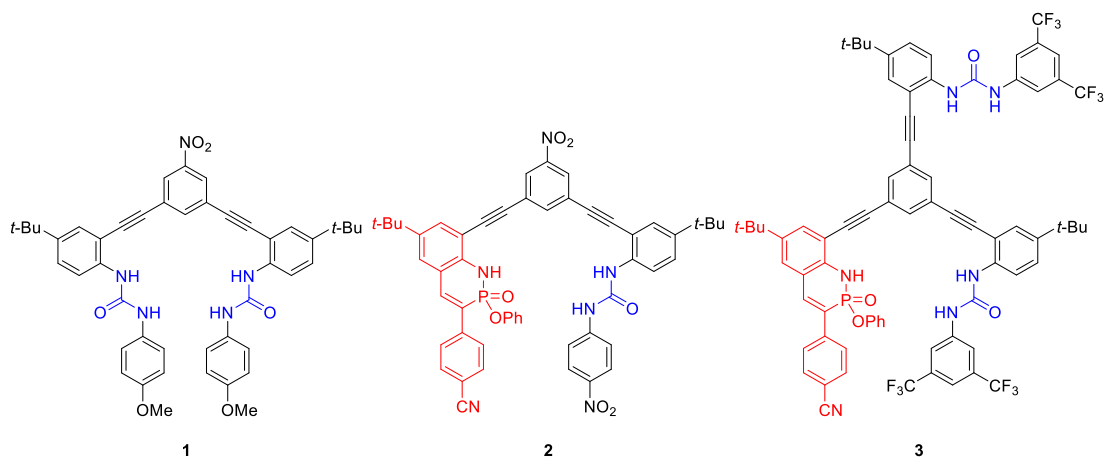


Figure 8.1 Structures of the studied bisurea host **1** and hybrid PN-urea host **2** as well as the structure of proposed 3-armed host **3**.

Gratifyingly, this host showed promise as a potential extract in LLE experiments as well, showing the ability to extract HSO_4^- even from sulfuric acid solutions. While this host performed very well as a proof of principle for the utilization of our PN scaffold as a host moiety for HSO_4^- , a great deal of clean water was used to subsequently release the bound HSO_4^- guest to allow for the reuse of the host. While this is not a problem on the lab-scale, the necessity to use large amounts of fresh water in the industrial scale of nuclear waste remediation diminishes some of the feasibility of this system. With this in mind, our lab has been developing a system that not only can use saline water as a way to release the bound HSO_4^- instead of fresh water, but also a system that actually benefits from the use of saline water; thus, we developed hybrid host **3** (Figure 8.2).

As shown in Figure 8.2, host **3** can exist in two different conformations: one where a binding pocket is composed of one urea arm and the PN arm (Conformation A) and the other where binding uses two urea arms (Conformation B). Conformation A replicates the binding pocket of the two-armed, PN-host **2**, whereas conformation B replicates the binding pocket of the more traditional bisurea binding scaffold **1** that has been studied extensively in our lab.¹⁷

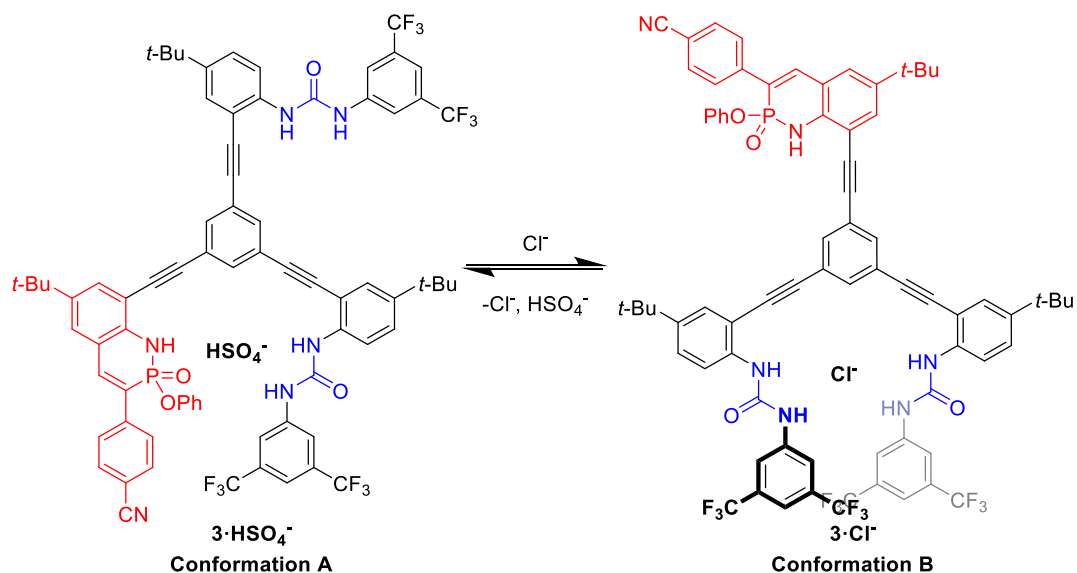


Figure 8.2 The two conformations that **3** can take when in the presence of HSO_4^- (conformation A, left), or Cl^- (conformation B, right).

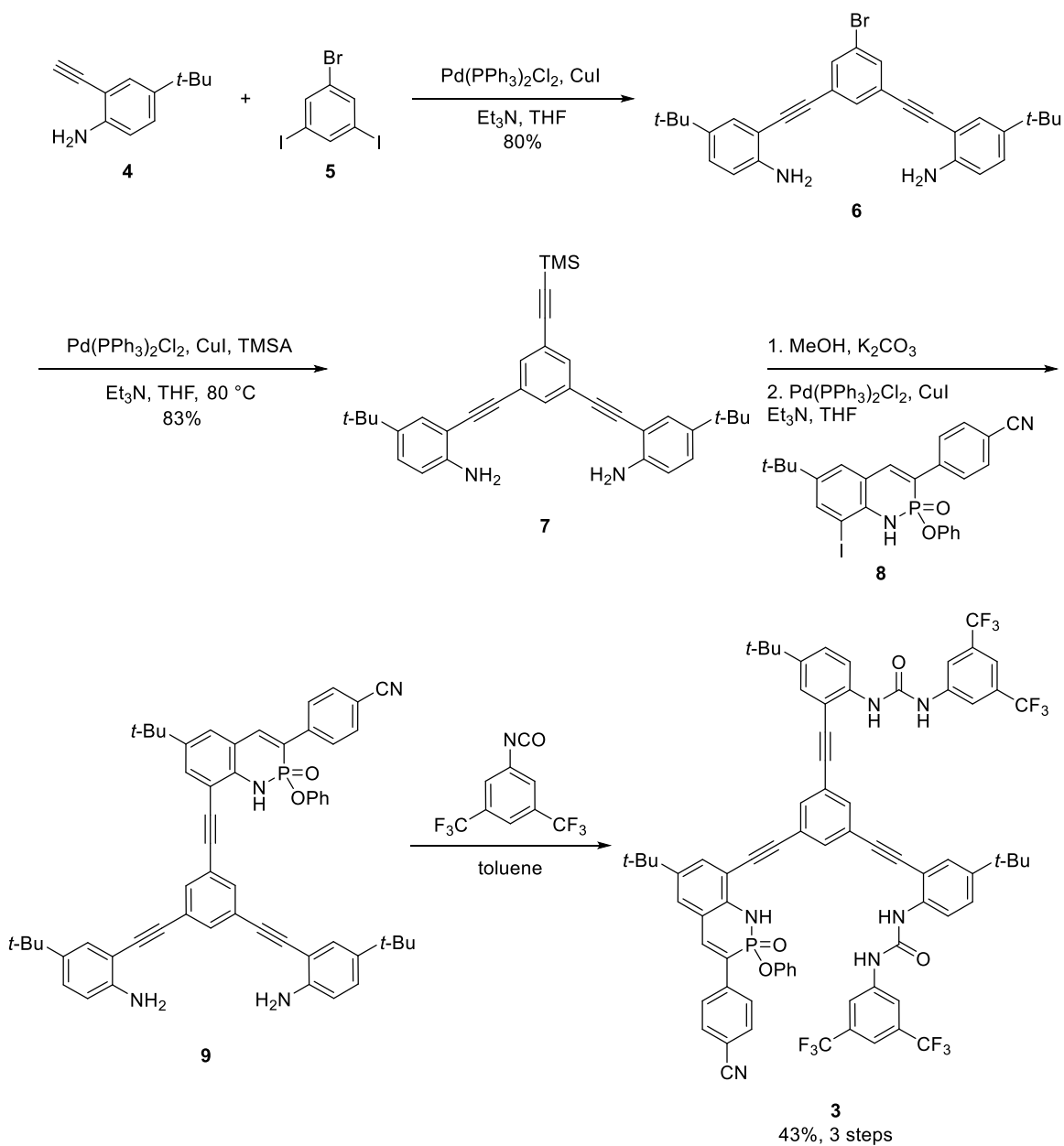
As mentioned previously, in Conformation A, **3** should exhibit strong and selective binding of HSO_4^- , yet conformation B loses the geometric complementarity of the PN center from its binding pocket and therefore should also lose the ability to bind HSO_4^- strongly. However, the bisurea pocket present in conformation B is identical to that of bisurea hosts **1**, which have been shown to bind Cl^- very strongly and selectively, indicating a potential for two separate binding modes for **3**. As shown for similar aryl ethynyl systems, the acetylene linkers can freely rotate in order to access different conformations depending on solvent, guest, and host morphology. By this logic, there should be a way to control this switching of conformations based solely on the environment the host is in. So, in the presence of HSO_4^- , **3** should reside in Conformation A by forming the $3 \cdot \text{HSO}_4^-$ complex. Conversely, in the presence of chloride, **3** should adopt conformation B, as it will then form the $3 \cdot \text{Cl}^-$ complex. Furthermore, if the $3 \cdot \text{HSO}_4^-$ complex is present, and the solution is mixed with Cl^- -containing water (e.g., sea water), then the host should both release HSO_4^- into the aqueous layer as well as favor a conformational switch to Conformation B, leading

to an additive effect of removing HSO_4^- from the host. This $\mathbf{3}\cdot\text{Cl}^-$ complex could then potentially be used directly in further LLE processes, or small amounts of fresh water could also be used to release the bound chloride, leading to less fresh water overall needed in the process.

8.2 Results and Discussion

To prepare host **3**, as outlined in Scheme 8.1, 4-*tert*-butyl-2-ethynylaniline **4** was Sonogashira cross-coupled with 1-bromo-3,5-diiodobenzene **5** to give dianiline **6**. Compound **6** was then Sonogashira cross-coupled with TMSA to afford TMS-protected acetylene **7**, which underwent protodesilylation and subsequent cross-coupling with iodinated PN heterocycle **8** to furnish the penultimate dianiline **9**. Lastly, compound **9** was treated with two equivalents of 3,5-bis(trifluoromethyl)phenyl isocyanate to afford final product **3** in good yield. While a majority of the characteristic ^{31}P splitting is not easily observed in either the ^1H or the ^{13}C NMR spectra due to the number and complexity of the signals, the characteristic PN ^{31}P signal is observed around 10 ppm.

Upon isolation, the anion binding abilities of **3** were tested using a variety of NMR titration experiments. First, sequential additions of a TBACl solution to a ca. 1 mM host solution in 10% d^6 -DMSO in CDCl_3 were performed and the ^1H and ^{31}P NMR signals were tracked after each addition (Figures 8.3 and 8.4, respectively). Gratifyingly, a simple pattern peak shifting can be observed, which is indicative of the typical bis-urea chloride binding that the traditional hosts in our lab have been shown to exhibit.



Scheme 8.1 Synthesis of 3-armed hybrid host **3**.

When analyzing the ^1H NMR spectra, the positions of the two urea signals were tracked and their change as a function of guest added was fit using non-linear regression analysis²⁰ to afford a binding constant of 5000 M^{-1} . Additionally, the ^{31}P NMR spectra show no significant shift upon treatment with TBACl, suggesting that **3** is indeed adopting

conformation B when in the presence of Cl^- . These shifting patterns reflect what have been seen for the analogous, previously reported bisurea systems.^{16–18}

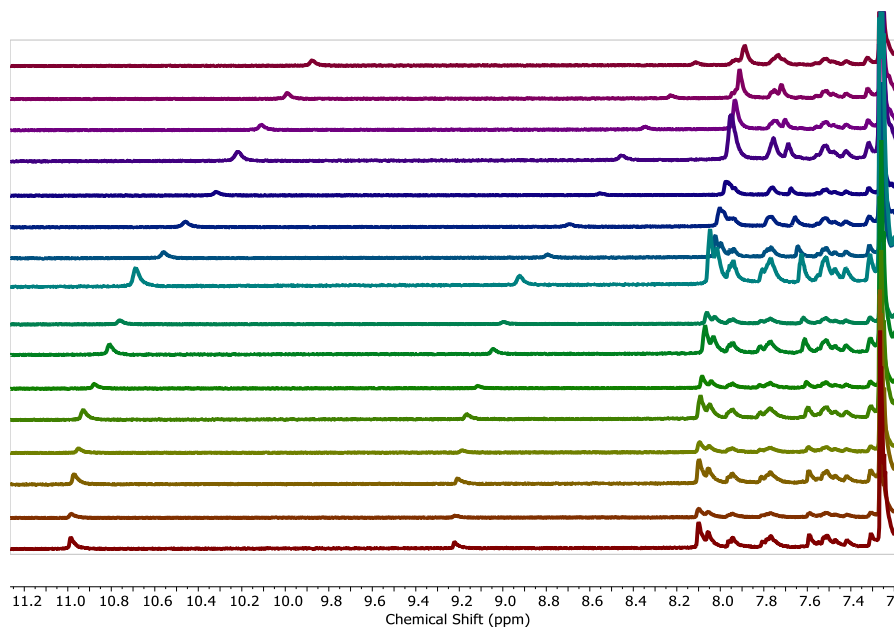


Figure 8.3 ^1H NMR titration experiment of **3** with additions of Cl^- . Free host is shown on top.

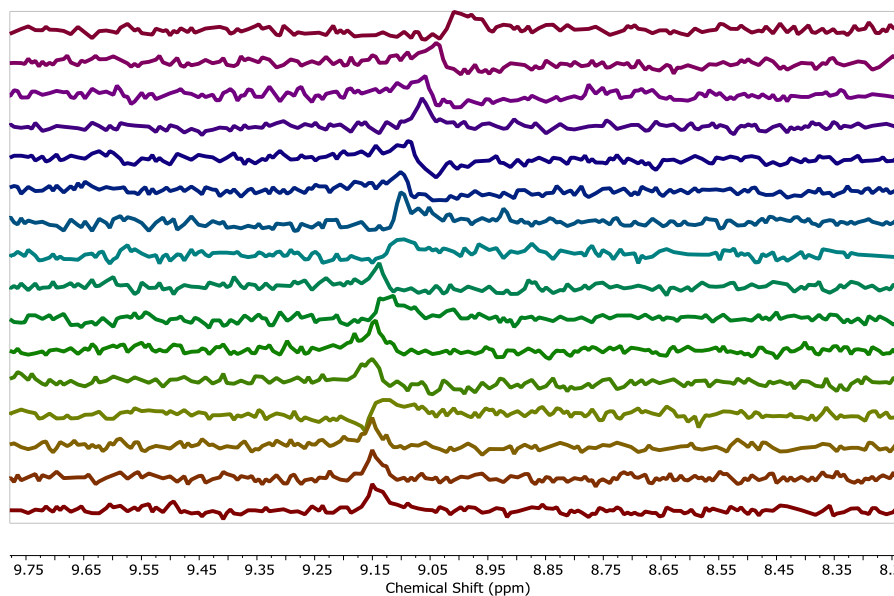


Figure 8.4 ^{31}P NMR titration experiment of **3** with additions of Cl^- . Free host is shown on top.

The same experiments were then performed using TBAHSO₄. When looking at the ¹H NMR spectra, however, an interesting trend is seen as the HSO₄⁻ guest concentration increases (Figure 8.5). Upon initial treatments with the guest, a consistent downfield trending shift is seen for the urea protons as well as the PN N-H, suggesting that the host is adopting conformation A. However, once a 1:1 host:guest ratio is reached, there is a change in the direction of shifting for some of the peaks. Once more guest is added after this equal ratio, the urea peak as well as the central aromatic proton begin shifting back upfield, while the PN N-H peak continues to shift consistently downfield.

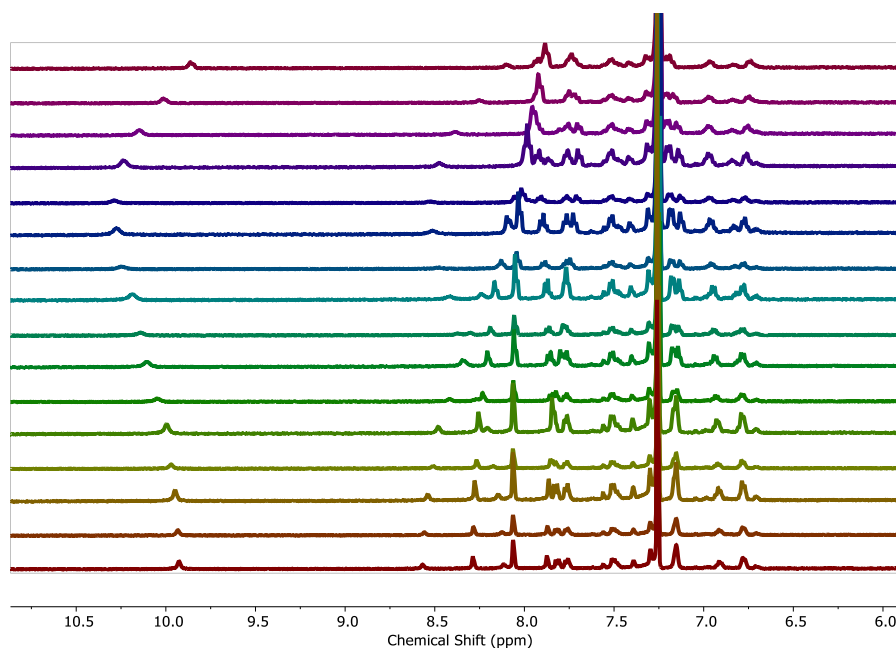


Figure 8.5 ¹H NMR titration experiment of **3** with additions of HSO₄⁻. Free host is shown on top and the 1:1 **3**:HSO₄⁻ point is shown in the dark blue spectrum.

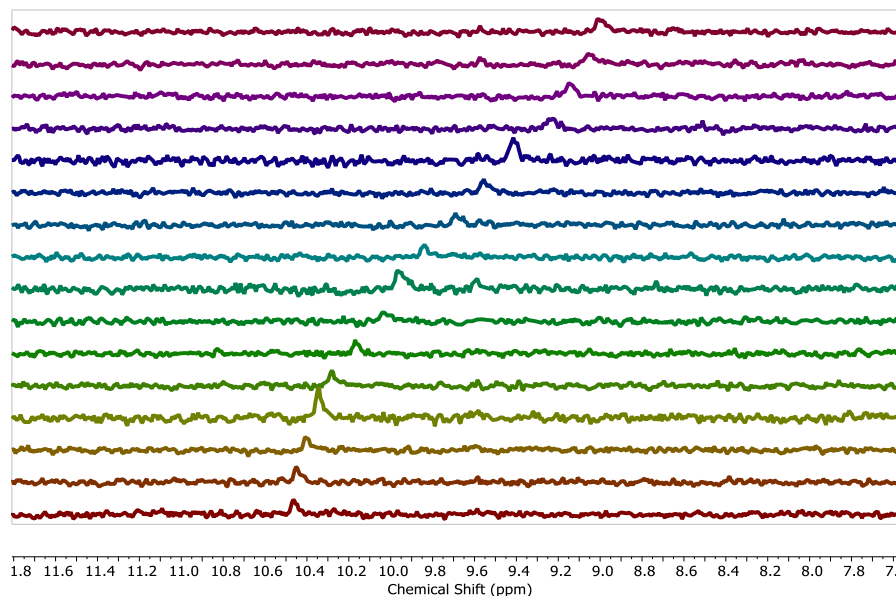


Figure 8.6 ^{31}P NMR titration experiment of **3** with additions of HSO_4^- . Free host is shown on top and the 1:1 **3**: HSO_4^- point is shown in the dark blue spectrum.

These results are very intriguing, as they suggest that there is indeed a conformation switch as well as potentially a binding mode transformation once there is excess guest present. When looking at the ^{31}P NMR spectra after each addition (Figure 8.6), there is the expected unidirectional shifting observed, suggesting that the PN center is taking place in the binding at every point of the experiment. When fitting the data from the ^{31}P NMR peak positions using non-linear regression analysis, a bimodal 2:1 host:guest model fit very well and gave a $K_{a,1} = 2000 \text{ M}^{-1}$ and a $K_{a,2} = 1000 \text{ M}^{-1}$. A qualitative competition experiment was then performed, which suggests that the host can indeed switch between conformations (See Appendix G).

8.3 Conclusions and Future Works

While this preliminary data suggests that our host has the potential to be used as a switchable, selective, and sensitive extractant in LLE experiments towards the remediation of high-level nuclear waste, further studies need to be performed to understand both the

mechanism(s) of binding for HSO_4^- and Cl^- , as well as the interplay between the two competing guests. First and foremost, a solid understanding of the mode of binding for HSO_4^- must be established, as this has an impact upon future studies upon the host's extraction and binding capabilities. This will be done using a multi-faceted approach. 2D-NMR experiments may help shed light on the conformation(s) that **3** is taking in solution in the presence of both one equivalent of HSO_4^- as well as an excess of HSO_4^- . This can be further supported by crystal growth attempts from mixed solutions containing these ratios of host and guest to try and capture the binding geometry at those points. Computational modelling of these binding events will also be paramount to understanding how our host is binding with HSO_4^- , which will help explain the complex shifting in the NMR spectra. More complex mathematical models may also be necessary to fit a more complex mode of binding than the currently hypothesized 2:1 host:guest binding ratio.

Once the mechanism of HSO_4^- binding is better understood, **3** will be screened against several other anions present in high-level nuclear waste. Two of the most abundant anions in high-level nuclear waste that will be tested with our host are fluoride and TcO_4^- , neither of which should be suitable guests owing to their extremely high electronegativity and the large size, respectively. For testing the binding affinity for TcO_4^- , ReO_4^- will be used as a non-radioactive analogue in its place as is common in these types of studies. With this library of binding data, both the selectivity and binding strength profiles will be built for host **3**, and binding of HSO_4^- will be attempted in mixed media with competing anions present as well, including Cl^- , F^- , and ReO_4^- . Speciation diagrams can be built to understand the nature of the host more fully when subjected to several guests at once.

LLE experiments with **3** can be performed and the results of which can be compared to those of hybrid host **2**. These will start with simple extraction experiments, taking HSO_4^- from aqueous solutions as well as sulfuric acid solutions to confirm similar extraction capabilities as **2**. In place of fresh water in the washing/recycling step after the initial HSO_4^- extraction, minimal amount of saline water will be used instead to test the design principles outlined above. It is expected that minimal saline water will be needed to fully remove HSO_4^- from the organic solution of **3**.

Then, further LLE experiments in the presence of competing anions will be performed. Initial tests will start with equimolar mixtures of Cl^- and HSO_4^- , then systematically approach mixtures that more closely represent the high-level nuclear waste we aim to remediate.

While these studies are still underway, we have made significant progress in the development of a potentially switchable, sensitive, and selective host for HSO_4^- extraction from aqueous solutions including high-level nuclear waste. Good binding strengths for HSO_4^- and Cl^- have been observed and potential conformational switching is corroborated by unique patterns in NMR titration experiments. Once a more complete understanding of the modes and mechanism of guest binding are achieved through a combination of experimental, computational, and mathematical methods, we will be more able to use host **3** as an extractant in LLE procedures for high-level nuclear waste remediation.

8.4 Experimental Section

General. NMR spectra were obtained on a Varian Inova 500 MHz (^1H : 500.11 MHz, ^{13}C 125.76 MHz, ^{19}F 470.53 MHz, ^{31}P 202.46 MHz) or a Bruker Avance-III-HD 600 MHz (^1H : 599.98 MHz, ^{13}C : 150.87 MHz) spectrometer. Chemical shifts (δ) are expressed in ppm

using residual non-deuterated solvent present in the bulk deuterated solvent (CDCl₃: ¹H 7.26 ppm, ¹³C 77.16 ppm; DMSO-*d*₆: ¹H 2.50 ppm, ¹³C 39.52 ppm). ¹⁹F chemical shifts are reported against CFCl₃ external standard (δ 0 ppm). ³¹P chemical shifts are reported against 85% H₃PO₄ (δ 0 ppm) as external reference. Mass spectra data were acquired on a Waters SYNAPT QToF in positive ion mode with a Shimadzu LC20AD HPLC front end. The solvents were MeCN:H₂O:0.1% HCO₂H at a flow rate of 0.05 mL min⁻¹ with a 5 μL injection on a loop injection. Preparative SEC was performed using a JAI Recycling Preparative HPLC (Model LC-9101) with a JAIGEL-1H preparative column with CHCl₃ as solvent. Analytical TLC was carried out on TLC plates (5 × 10 cm with 0.25 mm thickness, silica gel 60 F₂₅₄, Merck, Darmstadt, Germany) cut from the commercially available aluminium sheets. Solvents and reagents were used as purchased from suppliers, unless anhydrous conditions were employed, in which case, solvents were freshly distilled from sodium/benzophenone under N₂ atmosphere (THF) or as purchased. Ethynylaniline **4**, 3,5-diiodobromobenzene **5**, and iodoheterocycle **8** were synthesized by their reported procedures.¹⁹

Dianiline **6**. To an N₂-sparged solution of 3,5-diiodobromobenzene **5** (818 mg, 2 mmol) and terminal acetylene **4** (982 mg, 4 mmol) in THF/Et₃N (0.05 M, v/v = 1:1) was added 5 mol% Pd(PPh₃)₂Cl₂ and 5 mol% CuI. The suspension was stirred at room temperature under an N₂ atmosphere for 12 h. The reaction mixture was concentrated *in vacuo* and purified *via* flash chromatography to give product **6** (800 mg, 80%) as a dark orange oil. *R*_f = 0.27 (hexanes/EtOAc, 7:1). ¹H NMR (600 MHz, CD₂Cl₂) δ 7.65 (d, *J* = 1.7 Hz, 3H), 7.39 (d, *J* = 2.4 Hz, 2H), 7.23 (dd, *J* = 8.5, 2.4 Hz, 2H), 6.70 (d, *J* = 8.5 Hz, 2H), 4.23 (s,

4H), 1.30 (s, 18H). ^{13}C NMR (151 MHz, CD_2Cl_2) δ 146.4, 141.2, 133.7, 133.0, 129.2, 128.2, 126.0, 122.3, 114.7, 106.6, 92.2, 89.1, 34.2, 31.5.

Ethynylsilane **7**. A ~0.1 M solution of the **6** (500 mg, 1 mmol) in THF/ Et_3N (0.05 M, v/v = 1:1) was purged for 15 min with N_2 and then TMSA (0.2 mL, 1.5 mmol) was added *via* syringe. After an additional 5 min N_2 purging, CuI (19 mg, 0.1 mmol) and $\text{Pd}(\text{PPh}_3)_2\text{Cl}_2$ (70 mg, 0.1 mmol) were added to the reaction mixture. The flask was then purged for an additional 5 min, then sealed and stirred at 80 °C (oil bath) under N_2 for 12 h. The mixture was concentrated, and the residue chromatographed on silica gel (8:1 hexanes/ EtOAc) to afford the desired TMS-protected ethynylsilane **7** (428 mg, 83%) as a solid. R_f = 0.27 (hexanes/ EtOAc , 7:1). ^1H NMR (600 MHz, CDCl_3) δ 7.63 (t, J = 1.5 Hz, 1H), 7.57 (d, J = 1.6 Hz, 2H), 7.37 (d, J = 2.3 Hz, 2H), 7.21 (dd, J = 8.5, 2.3 Hz, 2H), 6.69 (d, J = 8.5 Hz, 2H), 4.19 (s, 4H), 1.29 (s, 18H), 0.26 (s, 9H). ^{13}C NMR (151 MHz, CDCl_3) δ 145.6, 141.1, 134.1, 133.9, 128.9, 127.7, 124.2, 124.0, 114.6, 107.1, 103.4, 95.9, 92.8, 87.9, 34.1, 31.5, 0.0.

Host **3**. To a solution of **7** (178 mg, 0.21 mmol, 1.0 equiv.) in 5 mL MeOH was added K_2CO_3 (86 mg, 0.62 mmol, 3.0 equiv.). After stirring the suspension at room temperature for 0.5 h, the mixture was filtered through a bed of Celite. After evaporation of the solvent, the crude residue was used directly in the next reaction. To an N_2 -sparged solution of **8** (135 mg, 0.25 mmol, 1.2 equiv.) and the resultant crude terminal acetylene (0.21 mmol, 1.0 equiv.) in 5 mL THF was added $\text{Pd}(\text{PPh}_3)_4$ (7 mg, 0.012 mmol, 0.05 equiv.) and 5 mol% CuI (2 mg, 0.012 mmol, 0.05 equiv.), followed by the addition of Et_3N (32 mg, 0.315 mmol, 1.5 equiv.). The suspension was stirred at room temperature under an N_2 atmosphere for 6 hours until completion by TLC. The reaction mixture was concentrated *in vacuo* and

purified *via* flash chromatography to give the desired crude diyne product **9** as dark-orange oil. To a solution **9** in 20 mL dry toluene was added 3,5-bis(trifluoromethyl)phenyl isocyanate (134 mg, 0.53 mmol, 2.5 equiv.), and the mixture was stirred at room temperature for 24 h. The reaction was diluted with hexanes and the light-yellow precipitate was isolated. The crude compounds were washed with toluene, then redissolved in CH₂Cl₂ (10 mL), the desired product **3** was precipitated as fine light-yellow powder upon the slow addition of hexanes. Yield: 123 mg, 43%. *R_f* = 0.33 (hexanes/EtOAc, 4:1). M.p. > 200 °C. ¹H NMR (600 MHz, DMSO-*d*₆) δ 10.13 (s, 2H), 9.42 (s, 1H), 8.39 (s, 2H), 8.20–8.06 (m, 12H), 7.95 (d, *J* = 7.9 Hz, 2H), 7.68–7.66 (m, 2H), 7.57–7.56 (m, 4H), 7.48 (dd, *J* = 8.9, 2.7 Hz, 2H) 7.18 (t, *J* = 7.6 Hz, 2H), 7.00 (t, *J* = 7.3 Hz, 1H), 6.93 (d, *J* = 7.9 Hz, 2H), 1.30 (s, 18H), 1.29 (s, 9H). ¹³C NMR (151 MHz, DMSO-*d*₆) δ 152.1, 150.2 (d, *J* = 8.9 Hz), 145.4, 143.2, 143.2, 141.5, 140.0 (d, *J* = 9.9 Hz), 138.4, 137.2, 134.5, 134.3, 132.7, 132.0, 130.7 (q, *J* = 32.7 Hz), 129.7, 129.5, 128.9, 128.0 (d, *J* = 6.5 Hz), 127.3, 125.9, 124.9, 124.1, 123.8, 123.6, 123.2, 122.6, 122.3, 120.9 (d, *J* = 4.0 Hz), 120.5, 120.2, 119.4 (d, *J* = 14.6 Hz), 118.7, 117.8 (d, *J* = 4.4 Hz), 114.5, 111.4, 110.6, 109.5 (d, *J* = 8.4 Hz), 93.6, 93.1, 87.3, 86.5, 34.0, 33.9, 30.9, 30.8. ³¹P{¹H} NMR (202 MHz, DMSO-*d*₆) δ 10.7. ¹⁹F{¹H} NMR (564 MHz, DMSO-*d*₆) δ –61.86.

NMR Titration Procedures. Roughly 1 mM solutions of **3** were prepared in 10% DMSO-*d*₆/CDCl₃. 600 μL of this stock was placed into an NMR tube to give the start point of each trial. Roughly 20 mM guest solutions were prepared using the host stock solution as the solvent. Throughout the experiment, aliquots of the guest solution were added to the NMR tube via Hamilton syringe and ³¹P and ¹H spectra were collected after each addition. *K_a* values were determined by tracking the respective ³¹P or ¹H NMR peaks and fitting them

using non-linear regression analysis. Each value reported is the average of at least 3 trials using the same conditions.

CHAPTER IX

CONCLUDING REMARKS

In this dissertation, I have discussed a variety of structure-property relationships performed upon the 2- λ^5 -phosphaquinolin-2-one scaffold. Chapter 1 highlights the context and discovery of the scaffold in our lab and overviews many of our initial studies upon the physicochemical properties of the scaffold. Chapters 2 and 4 discuss our studies specifically upon the PN-naphthalene system and our efforts towards understanding and improving both the photophysical properties and the supramolecular functionality of the framework. Chapter 3 highlights our initial work on developing a PN-containing host molecule that is capable of binding hydrogen sulfate and extracting it from aqueous solutions. Chapter 5 showcases our development of a PN-pyrene system as a part of our ongoing investigation into the effects of backbone modification. Chapter 6 covers our use of Lawesson's reagent to thionate the phosphorus center of the PN moiety. This thionated form has the potential to serve as a responsive host for reactive oxygen species. Chapter 7 is about our ongoing studies towards utilizing a variety of PN derivatives as live cell imaging reagents. Lastly, Chapter 8 overviews our development of a 3-armed host capable of binding both chloride and hydrogen sulfate. Due to the different binding modes required to bind these two guests, only one can likely be bound at a time, thus allowing for a controllable switchability between the two depending on conditions around the host. This may have implications in the use of this host in water and nuclear waste remediation activities.

APPENDIX A

SUPPLEMENTARY INFORMATION FOR CHAPTER 2

1. X-ray Structure Data

X-ray Crystallography. Diffraction intensities for **1c** and **1g** were collected at 173 K on a Bruker Apex2 DUO CCD diffractometer using CuK α and MoK α (**1b**) radiations, $\lambda = 1.54178 \text{ \AA}$ and 0.71073 \AA , respectively. Absorption corrections were applied by SADABS.¹ Space groups were determined based on systematic absences. Structures were solved by direct methods and Fourier techniques and refined on F^2 using full matrix least-squares procedures. All non-H atoms were refined with anisotropic thermal parameters. H atoms in **1b** and **1g** were found on the residual density maps and refined with isotropic thermal parameters. H atoms in **1c** were refined in calculated positions in a rigid group model. Crystals of **1c** were very thin plates with weak diffraction at high angles. Diffraction data for **1c** were collected only up to $2\theta_{\max} = 105.2^\circ$; nonetheless, the collected data provide an appropriate number of measured reflections per refined parameters: 4048 per 470. The structure of **1c** was determined in space groups $P2_12_12_1$ with the Flack parameter of 0.55(8). Three options to get the structure of **1c** in monoclinic space groups with beta angles close to 90° and refinements of them as possible twins have been checked, but the final data are given in orthorhombic space group $P2_12_12_1$ with a pseudo-center of symmetry. The structure of **1c** has been determined not precisely, but it clearly shows composition and the main features of the compound. All calculations were performed by the Bruker SHELXL-2014/7 package.²

Crystallographic Data for Ib: C₂₁H₁₅N₂O₂P, M = 358.32, 0.25 x 0.23 x 0.14 mm, T = 173(2) K, Monoclinic, space group C2/c, a = 24.331(4) Å, b = 10.2408(18) Å, c = 14.540(3) Å, β = 102.686(3)°, V = 3534.7(11) Å³, Z = 8, D_c = 1.347 Mg/m³, μ(Mo) = 0.173 mm⁻¹, F(000) = 1488, 2θ_{max} = 50.0°, 11395 reflections, 3113 independent reflections [R_{int} = 0.0369], R1 = 0.0369, wR2 = 0.0955 and GOF = 1.049 for 3113 reflections (295 parameters) with I > 2σ(I), R1 = 0.0568, wR2 = 0.1104 and GOF = 1.049 for all reflections, max/min residual electron density +0.246/-0.382 eÅ⁻³.

Crystallographic Data for Ic: C₂₁H₁₈NO₃P, M = 363.33, 0.08 x 0.06 x 0.02 mm, T = 173(2) K, Orthorhombic, space group P2₁2₁2₁, a = 8.4621(5) Å, b = 19.7458(10) Å, c = 21.2129(10) Å, V = 3544.5(3) Å³, Z = 8, Z' = 2, D_c = 1.362 Mg/m³, μ(Cu) = 1.549 mm⁻¹, F(000) = 1520, 2θ_{max} = 105.20°, 17029 reflections, 4048 independent reflections [R_{int} = 0.0716], R1 = 0.0738, wR2 = 0.1871 and GOF = 1.066 for 4048 reflections (470 parameters) with I > 2σ(I), R1 = 0.0849, wR2 = 0.1949 and GOF = 1.066 for all reflections, max/min residual electron density +0.979/-0.470 eÅ⁻³.

Crystallographic Data for Ig: C₂₅H₂₃N₂O₂P, M = 414.42, 0.25 x 0.23 x 0.14 mm, T = 173(2) K, Monoclinic, space group P2₁/n, a = 18.5757(4) Å, b = 6.1760(2) Å, c = 18.9148(5) Å, β = 98.809(2)°, V = 2144.38(10) Å³, Z = 4, D_c = 1.284 Mg/m³, μ(Cu) = 1.324 mm⁻¹, F(000) = 872, 2θ_{max} = 133.37°, 16784 reflections, 3790 independent reflections [R_{int} = 0.0630], R1 = 0.0408, wR2 = 0.0999 and GOF = 1.022 for 3790 reflections (363 parameters) with I > 2σ(I), R1 = 0.0564, wR2 = 0.1093 and GOF = 1.022 for all reflections, max/min residual electron density +0.352/-0.325 eÅ⁻³.

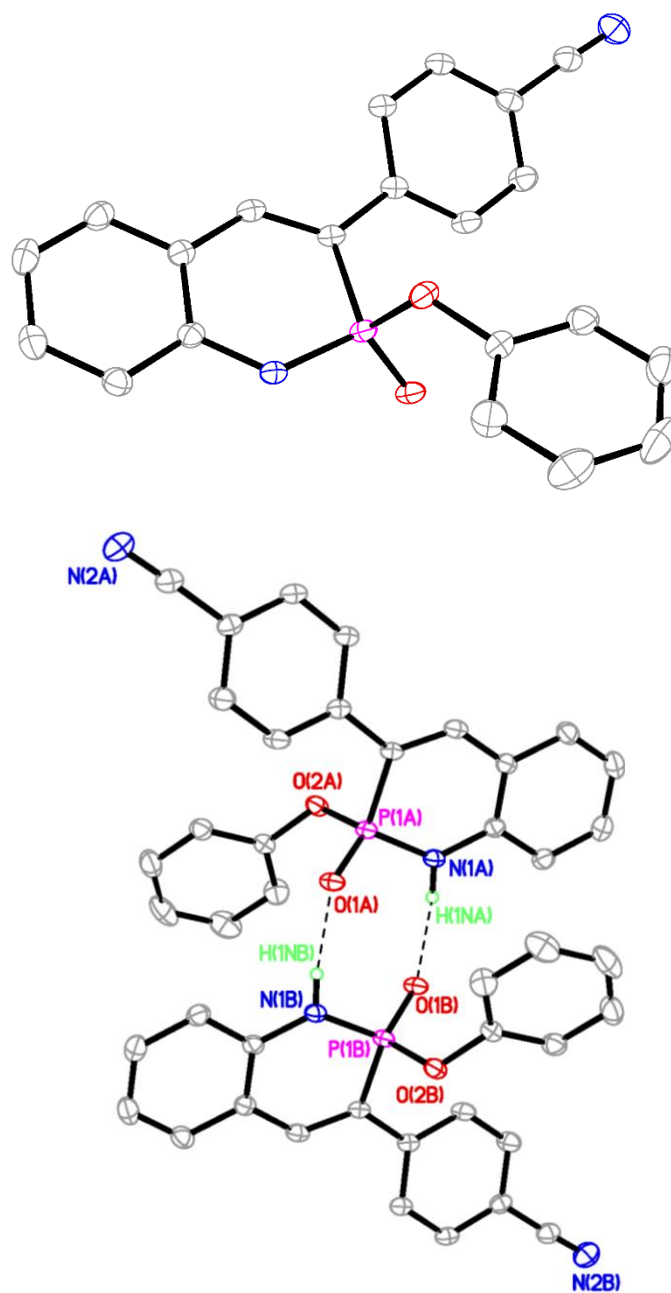


Figure A.1 ORTEP drawings of the (left) molecular structure of **1b** and (right) hydrogen-bonded dimeric pair of enantiomers; thermal ellipsoids drawn at 30% probability.

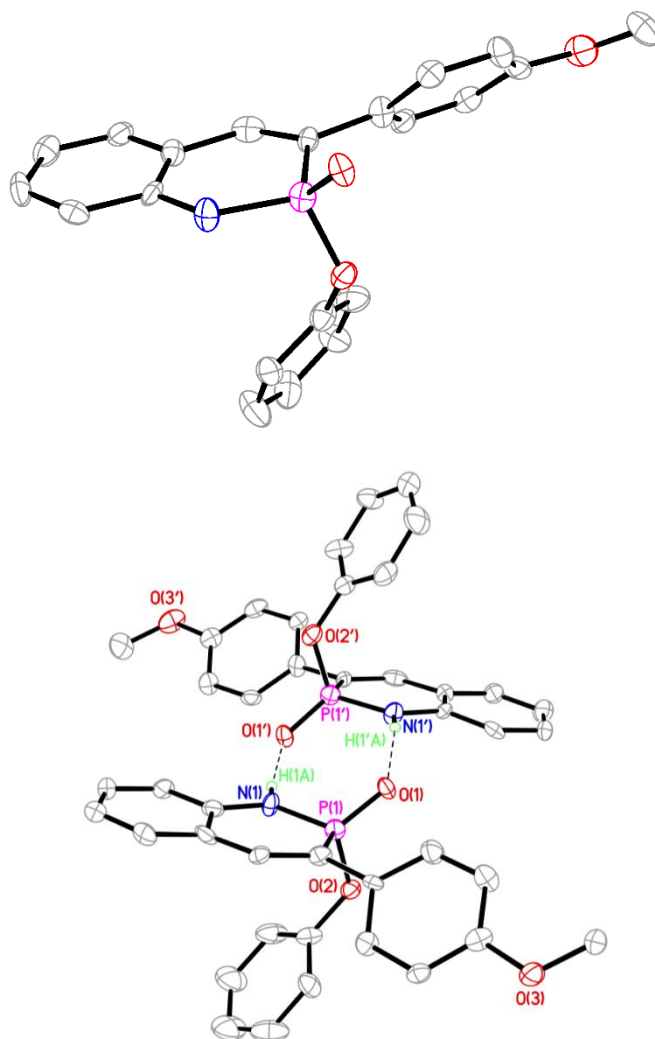


Figure A.2 ORTEP drawings of the (left) molecular structure of **1c** and (right) hydrogen-bonded dimeric pair of enantiomers; thermal ellipsoids drawn at 30% probability.

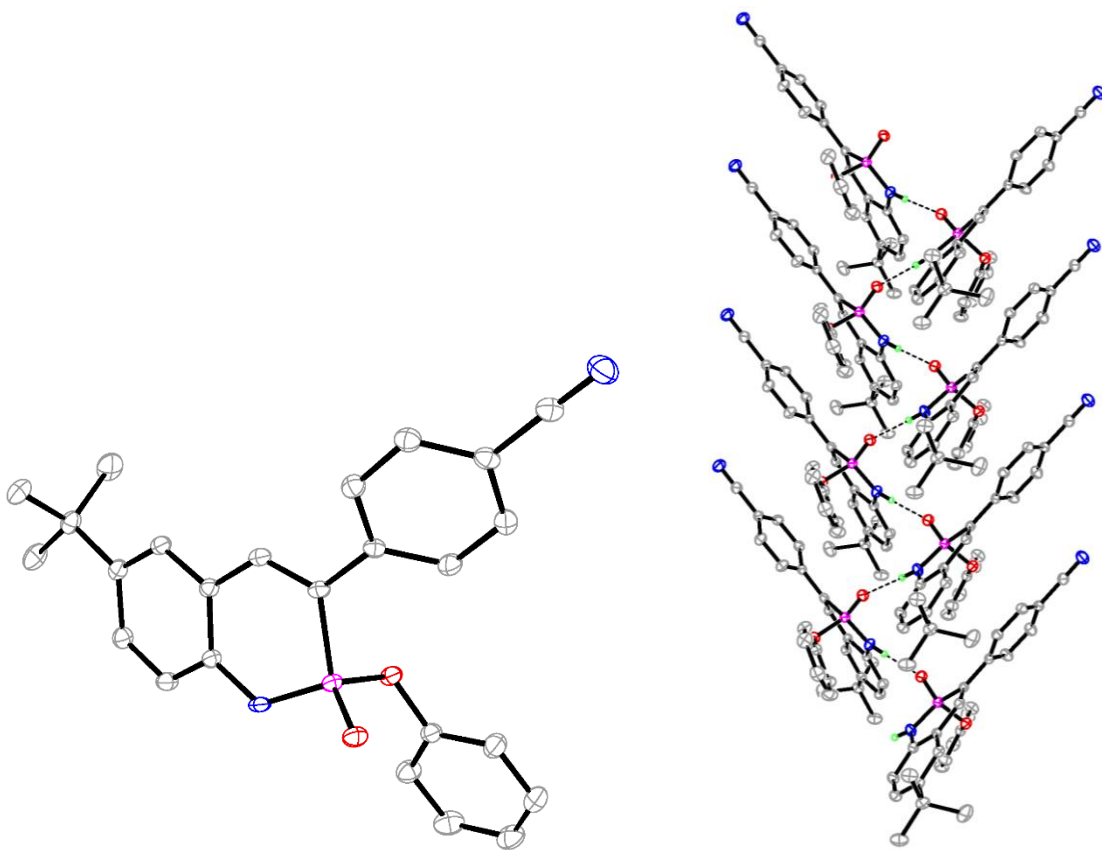


Figure A.3 ORTEP drawings of the (left) molecular structure of **1g** and (right) staggered crystal packing motif, likely due to steric repulsion of the bulky alkyl groups; thermal ellipsoids drawn at 30% probability.

2. Photophysical Properties of Selected Heterocycles **1**

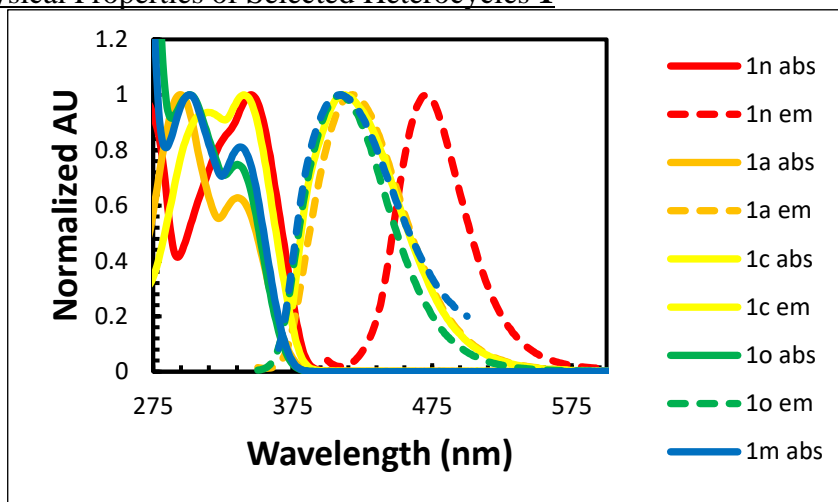


Figure A.4 Absorption and emission spectra of disparate heterocycles **1**.

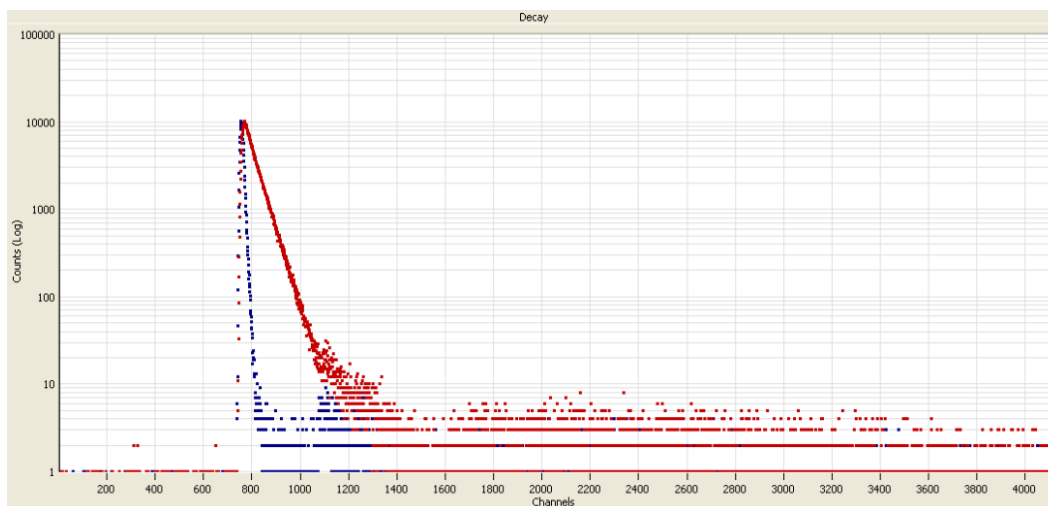


Figure A.5 Representative fluorescence decay curve for **1p** (red) plotted against Ludox background scattering curve (blue) used as a representative curve for all heterocycles **1**.

3. HOMO-LUMO Distributions of Related Subsets of Heterocycles **1**

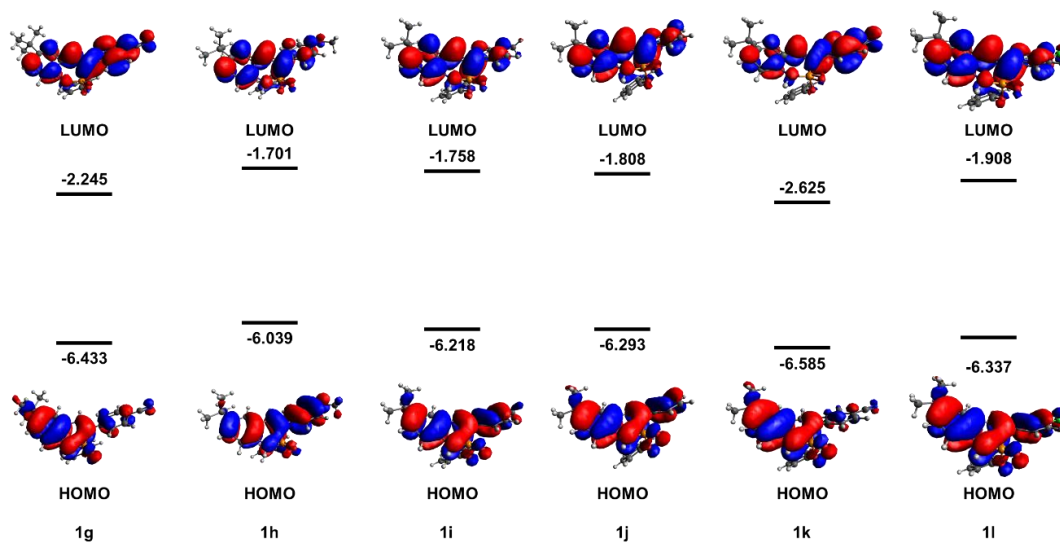


Figure A.6 HOMO and LUMO orbital distributions and energy levels for heterocycles **1g-1l**, where $R^2 = t\text{-Bu}$.

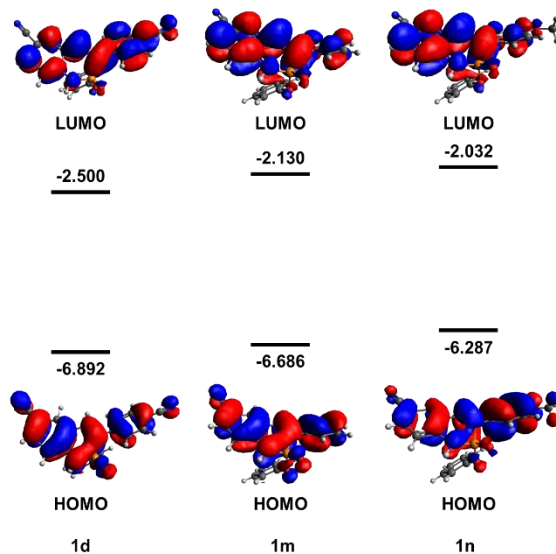


Figure A.7 HOMO and LUMO orbital distributions and energy levels for heterocycles **1d, 1m-1n**, where $R^2 = \text{CN}$.

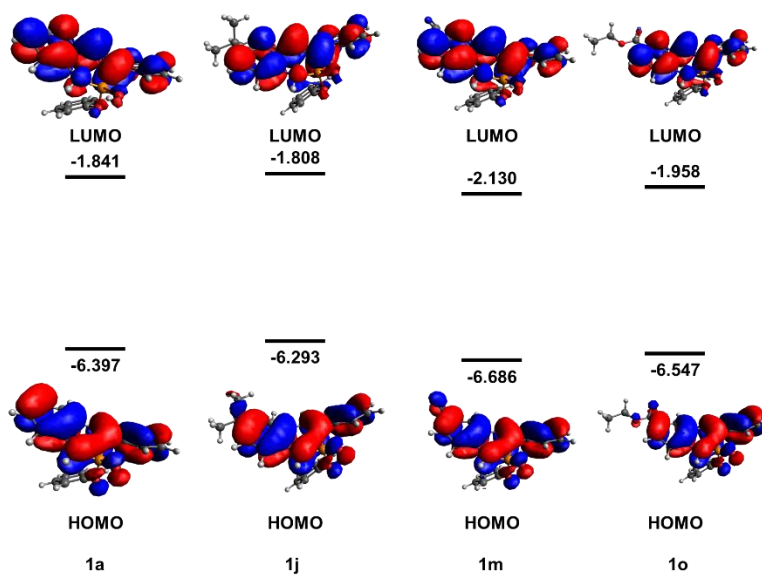


Figure A.8 HOMO and LUMO orbital distributions and energy levels for heterocycles **1a**, **1j**, **1m**, and **1o**, where $R^1 = H$.

4. Geometry Optimizations and Energies for Frontier Orbital Calculations

Table A.1 Theoretically optimized coordinates of **1a** (Cartesian Coordinate in Angstrom) at PBE0/6-311G(d,p) level of theory

Atom	x	y	z	
C	3.60625	-2.11651	-1.83390	
C	4.23195	-1.91891	-0.60148	
C	3.50464	-1.50718	0.50108	
C	2.12996	-1.28099	0.39242	
C	1.48134	-1.48318	-0.84139	Zero-point correction = 0.313690
C	2.24615	-1.90357	-1.94096	(Hartree/Particle)
N	1.40162	-0.88122	1.49956	Thermal correction to Energy =
P	-0.21277	-0.44565	1.58662	0.333021
C	-0.81586	-0.88831	-0.02998	Thermal correction to Enthalpy =
C	0.05941	-1.30782	-0.97654	0.333965
C	-2.25828	-0.73137	-0.31354	Thermal correction to Gibbs Free
C	-3.22915	-1.06329	0.63991	Energy = 0.263062
C	-4.57998	-0.93784	0.34167	
C	-4.98772	-0.47679	-0.90464	Sum of electronic and zero-point
C	-4.03164	-0.13315	-1.85496	Energies = -1317.051311
C	-2.68079	-0.25303	-1.56111	Sum of electronic and thermal
O	-0.89520	-0.95216	2.79785	Energies = -1317.031980
O	-0.25751	1.18596	1.66956	Sum of electronic and thermal
C	0.33803	2.01556	0.73539	Enthalpies = -1317.031036
C	-0.42540	2.51457	-0.31196	Sum of electronic and thermal
C	0.15688	3.39268	-1.21821	Free Energies = -1317.101939
C	1.48891	3.76724	-1.07750	
C	2.23924	3.26563	-0.01970	
C	1.66659	2.38842	0.89396	
H	5.29891	-2.08673	-0.50047	
H	3.99512	-1.35564	1.45752	
H	1.74097	-2.06197	-2.88884	
H	1.90514	-0.85119	2.37684	
H	-0.35011	-1.56730	-1.95127	
H	-2.91844	-1.42927	1.61198	
H	-5.31819	-1.20615	1.09015	
H	-4.33833	0.24212	-2.82578	
H	-1.94231	0.04664	-2.29770	
H	-1.46410	2.21703	-0.40101	
H	-0.43677	3.78745	-2.03593	
H	1.93929	4.45323	-1.78657	
H	3.27629	3.56006	0.10070	
H	2.23462	1.99903	1.73090	
H	4.18034	-2.43882	-2.69478	
H	-6.04376	-0.37857	-1.13265	

Table A.2 Theoretically optimized coordinates of **1b** (Cartesian Coordinate in Angstrom) at PBE0/6-311G(d,p) level of theory

Atom	x	y	z	
C	3.85295	-2.21588	-2.03236	
C	4.57497	-2.03426	-0.85062	
C	3.94727	-1.59519	0.30105	
C	2.57650	-1.32348	0.29420	
C	1.83126	-1.50973	-0.88689	Zero-point correction = 0.312508
C	2.49695	-1.95984	-2.03906	(Hartree/Particle)
N	1.94751	-0.89622	1.45038	Thermal correction to Energy =
P	0.36167	-0.40336	1.65599	0.333590
C	-0.37593	-0.84300	0.09378	Thermal correction to Enthalpy =
C	0.41086	-1.29287	-0.91608	0.334534
C	-1.83077	-0.66343	-0.07672	Thermal correction to Gibbs Free
C	-2.72371	-0.93434	0.96935	Energy = 0.260129
C	-4.08863	-0.79285	0.78812	
C	-4.59032	-0.37106	-0.44620	Sum of electronic and zero-point
C	-3.70976	-0.08307	-1.49416	Energies = -1409.214483
C	-2.34749	-0.22240	-1.30358	Sum of electronic and thermal
O	-0.24904	-0.87802	2.91689	Energies = -1409.193401
O	0.37093	1.22729	1.71804	Sum of electronic and thermal
C	0.91327	2.02931	0.72741	Enthalpies = -1409.192457
C	0.07552	2.56300	-0.24306	Sum of electronic and thermal
C	0.60724	3.41350	-1.20499	Free Energies = -1409.266862
C	1.96247	3.72582	-1.19493	
C	2.78763	3.19038	-0.21216	
C	2.26625	2.34082	0.75661	
H	5.64041	-2.23671	-0.82905	
H	4.51348	-1.45697	1.21666	
H	1.91693	-2.10587	-2.94502	
H	2.51354	-0.88817	2.28937	
H	-0.07819	-1.55184	-1.85348	
H	-2.33986	-1.26754	1.92662	
H	-4.77089	-1.01339	1.60066	
H	-4.09697	0.26049	-2.44628	
H	-1.67128	0.03495	-2.11119	
H	-0.98021	2.31671	-0.22893	
H	-0.04388	3.83643	-1.96259	
H	2.37309	4.39081	-1.94677	
H	3.84361	3.43750	-0.19292	
H	2.89376	1.92726	1.53743	
C	-5.99599	-0.22614	-0.63657	
N	-7.13434	-0.10941	-0.79343	
H	4.35089	-2.55970	-2.93134	

Table A.3 Theoretically optimized coordinates of **1c** (Cartesian Coordinate in Angstrom) at PBE0/6-311G(d,p) level of theory

Atom	x	y	z	
C	4.04791	-2.18084	-1.96899	
C	4.72895	-2.02832	-0.76014	
C	4.05953	-1.61508	0.37836	
C	2.69002	-1.34291	0.32940	
C	1.98521	-1.49946	-0.87996	Zero-point correction = 0. 346376
C	2.69193	-1.92225	-2.01675	(Hartree/Particle)
N	2.01859	-0.94233	1.47255	Thermal correction to Energy = 0.
P	0.42904	-0.44109	1.62653	368262
C	-0.25890	-0.84515	0.03356	Thermal correction to Enthalpy =
C	0.56439	-1.27857	-0.95331	0. 369206
C	-1.70243	-0.62778	-0.18138	Thermal correction to Gibbs Free
C	-2.64361	-0.89265	0.81702	Energy = 0. 293227
C	-4.00461	-0.71608	0.59626	
C	-4.45565	-0.26029	-0.64167	
C	-3.52463	0.02266	-1.64675	Sum of electronic and zero-point
C	-2.17533	-0.15387	-1.41605	Energies = -1431.448506
O	-0.22094	-0.92943	2.86347	Sum of electronic and thermal
O	0.45028	1.19120	1.72278	Energies = -1431.426620
C	1.02257	2.00511	0.76106	Sum of electronic and thermal
C	0.21704	2.55030	-0.23036	Enthalpies = -1431.425676
C	0.77901	3.41365	-1.16313	Sum of electronic and thermal
C	2.13274	3.72761	-1.10447	Free Energies = -1431.501655
C	2.92596	3.17936	-0.10262	
C	2.37397	2.31665	0.83723	
H	5.79301	-2.23219	-0.70568	
H	4.59270	-1.49870	1.31680	
H	2.14470	-2.04568	-2.94635	
H	2.55543	-0.94601	2.33019	
H	0.10892	-1.51053	-1.91450	
H	-2.30834	-1.25435	1.78270	
H	-4.69978	-0.94065	1.39547	
H	-3.88621	0.39590	-2.59853	
H	-1.46930	0.10148	-2.19957	
H	-0.83699	2.29774	-0.25662	
H	0.15275	3.84420	-1.93732	
H	2.56712	4.40238	-1.83400	
H	3.98085	3.42582	-0.04648	
H	2.97629	1.89089	1.63136	
O	-5.75131	-0.05413	-0.96019	
C	-6.72850	-0.31170	0.03072	
H	-6.58329	0.32573	0.90948	
H	-7.68825	-0.07943	-0.42784	
H	-6.71890	-1.36329	0.33694	
H	4.57585	-2.50403	-2.85868	

Table A.4 Theoretically optimized coordinates of **1d** (Cartesian Coordinate in Angstrom) at PBE0/6-311G(d,p) level of theory

Atom	x	y	z	
C	4.03554	-1.89142	-0.50339	
C	4.55251	-1.12826	0.55670	
C	3.70650	-0.40076	1.36273	
C	2.32468	-0.40682	1.13397	
C	1.79084	-1.17806	0.07920	Zero-point correction = 0.311380
C	2.66430	-1.91377	-0.72548	(Hartree/Particle)
N	1.48978	0.32135	1.94786	Thermal correction to Energy =
P	-0.17112	0.54823	1.81563	0.334281
C	-0.60360	-0.59713	0.51770	Thermal correction to Enthalpy =
C	0.37201	-1.25614	-0.15187	0.335225
C	-2.02963	-0.76501	0.17449	Thermal correction to Gibbs Free
C	-3.01796	-0.77985	1.16764	Energy = 0.256327
C	-4.34829	-0.97043	0.83563	
C	-4.71700	-1.14389	-0.50100	Sum of electronic and zero-point
C	-3.74176	-1.11664	-1.50317	Energies = -1501.376903
C	-2.41552	-0.92262	-1.16400	Sum of electronic and thermal
O	-0.87670	0.48608	3.11194	Energies = -1501.354002
O	-0.38741	2.04089	1.20819	Sum of electronic and thermal
C	0.15889	2.46865	0.00625	Enthalpies = -1501.353058
C	-0.62194	2.42363	-1.14066	Sum of electronic and thermal
C	-0.09804	2.90189	-2.33568	Free Energies = -1501.431956
C	1.19205	3.41950	-2.37957	
C	1.95817	3.46638	-1.22014	
C	1.44398	2.99334	-0.01830	
H	5.62055	-1.11226	0.73827	
H	4.10820	0.18595	2.18142	
H	2.25751	-2.51240	-1.53306	
H	1.92358	0.77715	2.74172	
H	0.06654	-1.94710	-0.93472	
H	-2.73622	-0.65168	2.20626	
H	-5.10494	-0.98955	1.61109	
H	-4.02968	-1.23502	-2.54112	
H	-1.67033	-0.87072	-1.95002	
H	-1.62958	2.02766	-1.08459	
H	-0.70488	2.87298	-3.23429	
H	1.59694	3.79258	-3.31382	
H	2.96117	3.87834	-1.24601	
H	2.02379	3.03721	0.89632	
C	-6.08682	-1.34051	-0.84608	
N	-7.19526	-1.50091	-1.12768	
C	4.91039	-2.64271	-1.33904	
N	5.62279	-3.25023	-2.01566	

Table A.5 Theoretically optimized coordinates of **1e** (Cartesian Coordinate in Angstrom) at PBE0/6-311G(d,p) level of theory

Atom	x	y	z	
C	-3.76888	-1.08396	-0.08227	
C	-4.09036	-0.10612	-1.02984	
C	-3.09254	0.59206	-1.67466	
C	-1.74716	0.33315	-1.38525	Zero-point correction = 0.313690
C	-1.41241	-0.65615	-0.43936	(Hartree/Particle)
C	-2.44579	-1.35365	0.20051	Thermal correction to Energy =
N	-0.75358	1.02705	-2.04102	0.333021
P	0.90340	0.98218	-1.77564	Thermal correction to Enthalpy =
C	1.06774	-0.40236	-0.66315	0.333965
C	-0.04244	-0.99219	-0.15666	Thermal correction to Gibbs Free
C	2.42404	-0.84145	-0.28050	Energy = 0.263062
C	3.47370	-0.84732	-1.20893	
C	4.73414	-1.28970	-0.84608	
C	4.97127	-1.73093	0.45846	Sum of electronic and zero-point
C	3.93587	-1.71666	1.39872	Energies = -1317.051311
C	2.68075	-1.26947	1.02964	Sum of electronic and thermal
O	1.69695	1.02466	-3.02169	Energies = -1317.031980
O	1.28116	2.30979	-0.91267	Sum of electronic and thermal
C	0.71209	2.61654	0.31442	Enthalpies = -1317.031036
C	1.41544	2.31622	1.47312	Sum of electronic and thermal
C	0.87861	2.67476	2.70380	Free Energies = -1317.101939
C	-0.34933	3.32459	2.77203	
C	-1.03868	3.62416	1.60234	
C	-0.50948	3.27449	0.36539	
H	-5.12820	0.10378	-1.26325	
H	-3.34524	1.34830	-2.40998	
H	-2.19027	-2.11959	0.92402	
H	-1.05270	1.64659	-2.78415	
H	0.10009	-1.83288	0.51937	
H	3.29312	-0.51052	-2.22305	
H	5.53772	-1.29844	-1.57304	
H	4.12361	-2.04313	2.41486	
H	1.89305	-1.23023	1.77369	
H	2.37557	1.81825	1.39877	
H	1.42642	2.44740	3.61201	
H	-0.76459	3.60330	3.73423	
H	-1.99204	4.13938	1.64841	
H	-1.02766	3.51616	-0.55519	
C	6.26883	-2.18748	0.83484	
N	7.31870	-2.55856	1.14127	
C	-4.87138	-1.80546	0.62193	
F	-4.42483	-2.83982	1.34753	
F	-5.78305	-2.28752	-0.24073	
F	-5.54155	-0.99651	1.46431	

Table A.6 Theoretically optimized coordinates of **1f** (Cartesian Coordinate in Angstrom) at PBE0/6-311G(d,p) level of theory

Atom	x	y	z	
C	3.96040	-1.76836	-0.39257	
C	4.45995	-0.98124	0.64353	
C	3.58879	-0.25194	1.42954	
C	2.21201	-0.29294	1.19424	
C	1.70778	-1.09640	0.15336	Zero-point correction = 0. 302705
C	2.60563	-1.83327	-0.63370	(Hartree/Particle)
N	1.34745	0.43180	1.99279	Thermal correction to Energy = 0.
P	-0.30414	0.64499	1.81453	325118
C	-0.70217	-0.54934	0.54999	Thermal correction to Enthalpy =
C	0.29430	-1.20945	-0.08955	0. 326063
C	-2.12010	-0.75342	0.19434	Thermal correction to Gibbs Free
C	-3.12245	-0.74745	1.17387	Energy = 0. 248120
C	-4.44478	-0.97264	0.83206	
C	-4.79275	-1.20283	-0.50166	
C	-3.80421	-1.19654	-1.49115	Sum of electronic and zero-point
C	-2.48622	-0.96718	-1.14216	Energies = -1868.684343
O	-1.04345	0.63228	3.09468	Sum of electronic and thermal
O	-0.52766	2.11282	1.14298	Energies = -1868.661930
C	0.05367	2.50551	-0.05268	Sum of electronic and thermal
C	-0.68503	2.40847	-1.22431	Enthalpies = -1868.660986
C	-0.12754	2.85510	-2.41639	Sum of electronic and thermal
C	1.15503	3.39259	-2.43385	Free Energies = -1868.738929
C	1.87968	3.49037	-1.25107	
C	1.33128	3.04948	-0.05227	
H	5.52632	-0.94006	0.82965	
H	3.97695	0.36104	2.23589	
H	2.22140	-2.45641	-1.43325	
H	1.75898	0.89863	2.79126	
H	0.01006	-1.92847	-0.85521	
H	-2.85678	-0.57454	2.21022	
H	-5.21162	-0.97487	1.59775	
H	-4.07586	-1.35836	-2.52767	
H	-1.73161	-0.93185	-1.91998	
H	-1.68778	1.99781	-1.18931	
H	-0.70218	2.78570	-3.33380	
H	1.58631	3.74099	-3.36584	
H	2.87691	3.91698	-1.25671	
H	1.87859	3.13149	0.87963	
C	-6.15420	-1.43525	-0.85681	
N	-7.25604	-1.62465	-1.14651	
Cl	5.06276	-2.68314	-1.38250	

Table A.7 Theoretically optimized coordinates of **1g** (Cartesian Coordinate in Angstrom) at PBE0/6-311G(d,p) level of theory

Atom	x	y	z	
C	-3.78872	-1.04922	-0.08147	
C	-4.06468	-0.04828	-1.02947	
C	-3.06412	0.65178	-1.67375	
C	-1.72247	0.38122	-1.39455	
C	-1.40791	-0.61829	-0.45895	Zero-point correction = 0.424771
C	-2.45478	-1.31179	0.17582	(Hartree/Particle)
N	-0.71497	1.06978	-2.04876	Thermal correction to Energy =
P	0.93380	1.00409	-1.77488	0.451389
C	1.07789	-0.39039	-0.67440	Thermal correction to Enthalpy =
C	-0.04411	-0.96993	-0.17601	0.452333
C	2.42576	-0.85102	-0.28950	Thermal correction to Gibbs Free
C	3.48384	-0.85226	-1.20908	Energy = 0.366540
C	4.73637	-1.31555	-0.84531	
C	4.95903	-1.78509	0.45208	
C	3.91616	-1.77560	1.38438	Sum of electronic and zero-point
C	2.66959	-1.30602	1.01454	Energies = -1566.201939
C	-4.93596	-1.79152	0.60118	Sum of electronic and thermal
O	1.74119	1.05731	-3.01360	Energies = -1566.175321
O	1.33224	2.32057	-0.89477	Sum of electronic and thermal
C	0.76692	2.61953	0.33364	Enthalpies = -1566.174377
C	1.47022	2.30635	1.48947	Sum of electronic and thermal
C	0.93881	2.65862	2.72427	Free Energies = -1566.260170
C	-0.28514	3.31513	2.80067	
C	-0.97582	3.62641	1.63475	
C	-0.45166	3.28302	0.39396	
C	-4.43260	-2.83417	1.59986	
C	-5.81522	-0.78371	1.35693	
C	-5.78146	-2.50820	-0.46227	
H	-5.09443	0.19404	-1.27209	
H	-3.31628	1.41873	-2.39935	
H	-2.17636	-2.07899	0.88977	
H	-1.00547	1.69226	-2.79218	
H	0.08802	-1.81745	0.49434	
H	3.31468	-0.49423	-2.21797	
H	5.54529	-1.31971	-1.56650	
H	4.09223	-2.12293	2.39576	
H	1.87732	-1.27002	1.75385	
H	2.42651	1.80196	1.40872	
H	1.48749	2.42083	3.62938	
H	-0.69629	3.58933	3.76602	
H	-1.92669	4.14577	1.68700	
H	-0.97205	3.53171	-0.52351	
H	-5.28625	-3.33584	2.06401	
H	-3.82272	-3.60203	1.11397	
H	-3.84176	-2.37827	2.40043	
H	-6.64676	-1.30125	1.84597	
H	-6.23994	-0.03156	0.68647	
H	-5.23783	-0.26237	2.12629	
H	-5.18041	-3.23981	-1.01041	
H	-6.61448	-3.03705	0.01193	
H	-6.20263	-1.80675	-1.18781	
C	6.24765	-2.26486	0.82904	
N	7.29052	-2.65519	1.13607	

Table A.8 Theoretically optimized coordinates of **1h** (Cartesian Coordinate in Angstrom) at PBE0/6-311G(d,p) level of theory

Atom	x	y	z	
C	-3.91744	-1.06325	-0.12959	
C	-4.18803	-0.08912	-1.09777	
C	-3.17538	0.60539	-1.74099	
C	-1.84007	0.35158	-1.43804	
C	-1.52900	-0.62602	-0.47453	Zero-point correction = 0.458391
C	-2.57918	-1.30851	0.15345	(Hartree/Particle)
N	-0.82320	1.03115	-2.09156	Thermal correction to Energy =
P	0.81835	0.99175	-1.77615	0.485905
C	0.96229	-0.37573	-0.64217	Thermal correction to Enthalpy =
C	-0.16329	-0.95850	-0.15975	0.486849
C	2.31140	-0.78408	-0.20585	Thermal correction to Gibbs Free
C	3.40082	-0.78058	-1.08095	Energy = 0.399136
C	4.66208	-1.19726	-0.67116	
C	4.86168	-1.62510	0.64060	
C	3.78419	-1.62025	1.53272	
C	2.53655	-1.20229	1.11587	
O	1.64863	1.03713	-3.00115	Sum of electronic and zero-point
O	1.18043	2.33650	-0.91732	Energies = -1588.435467
C	0.58693	2.65042	0.29242	Sum of electronic and thermal
C	1.26308	2.35584	1.46939	Energies = -1588.407953
C	0.70238	2.72516	2.68604	Sum of electronic and thermal
C	-0.52420	3.38021	2.72466	Enthalpies = -1588.407009
C	-1.18849	3.67174	1.53845	Sum of electronic and thermal
C	-0.63483	3.31091	0.31554	Free Energies = -1588.494722
H	-5.21199	0.14416	-1.36399	
H	-3.42205	1.35513	-2.48648	
H	-2.31087	-2.06019	0.89037	
H	-1.10444	1.63909	-2.85004	
H	-0.03525	-1.78700	0.53476	
H	3.25906	-0.45493	-2.10548	
H	5.47644	-1.18650	-1.38470	
H	3.95660	-1.93529	2.55590	
H	1.72294	-1.17645	1.83344	
H	2.21952	1.84796	1.41770	
H	1.22969	2.50045	3.60713	
H	-0.95846	3.66730	3.67609	
H	-2.14214	4.18830	1.56077	
H	-1.13533	3.54286	-0.61729	
O	6.04233	-2.04782	1.14122	
C	7.16517	-2.05530	0.27980	
H	7.39606	-1.04819	-0.08379	
H	7.99827	-2.42216	0.87708	
H	7.00916	-2.72448	-0.57314	
C	-5.01325	-1.84329	0.59810	
C	-4.83971	-3.34482	0.32448	
C	-4.90519	-1.58594	2.10853	
C	-6.41289	-1.43085	0.13940	
H	-4.91828	-3.55773	-0.74585	
H	-3.86887	-3.71093	0.66968	
H	-5.61623	-3.91551	0.84427	
H	-5.02861	-0.52220	2.33280	
H	-5.68319	-2.14069	2.64319	
H	-3.93649	-1.90269	2.50477	
H	-7.16102	-2.01397	0.68401	
H	-6.61006	-0.37269	0.33684	
H	-6.56211	-1.61664	-0.92862	

Table A.9 Theoretically optimized coordinates of **1i** (Cartesian Coordinate in Angstrom) at PBE0/6-311G(d,p) level of theory

Atom	x	y	z	
C	-3.74450	-0.84961	-0.11108	
C	-3.93587	0.12789	-1.09515	
C	-2.87145	0.73303	-1.74452	
C	-1.56021	0.38257	-1.43190	
C	-1.32891	-0.60260	-0.45379	Zero-point correction = 0.453011
C	-2.43002	-1.19309	0.18033	(Hartree/Particle)
N	-0.49368	0.97525	-2.08918	Thermal correction to Energy =
P	1.14187	0.79674	-1.78807	0.478948
C	1.17309	-0.55276	-0.62461	Thermal correction to Enthalpy =
C	0.00622	-1.03442	-0.12972	0.479892
C	2.48537	-1.06582	-0.18109	Thermal correction to Gibbs Free
C	3.55735	-1.20686	-1.07243	Energy = 0.395730
C	4.77146	-1.71899	-0.64121	
C	4.97098	-2.10354	0.68638	
C	3.90490	-1.95226	1.57317	
C	2.68655	-1.43763	1.15275	Sum of electronic and zero-point
O	1.96025	0.74149	-3.02016	Energies = -1513.289529
O	1.62851	2.12266	-0.96290	Sum of electronic and thermal
C	1.08291	2.51124	0.24789	Energies = -1513.263592
C	1.76364	2.20478	1.41916	Sum of electronic and thermal
C	1.25515	2.64446	2.63536	Enthalpies = -1513.262648
C	0.07594	3.38107	2.67916	Sum of electronic and thermal
C	-0.59284	3.68407	1.49838	Free Energies = -1513.346809
C	-0.09093	3.25345	0.27570	
H	-4.93789	0.43531	-1.36947	
H	-3.05752	1.48781	-2.50255	
H	-2.22120	-1.95187	0.92896	
H	-0.72818	1.59297	-2.85551	
H	0.07061	-1.85669	0.58105	
H	3.42852	-0.92112	-2.11050	
H	5.58326	-1.82582	-1.35519	
H	4.03357	-2.23032	2.61527	
H	1.88694	-1.30175	1.87396	
H	2.68173	1.63097	1.36306	
H	1.78598	2.41037	3.55208	
H	-0.31764	3.72269	3.63030	
H	-1.50906	4.26427	1.52458	
H	-0.59495	3.49260	-0.65336	
C	-4.89941	-1.53100	0.62397	
C	-4.84649	-3.04459	0.36792	
C	-4.77220	-1.26557	2.13154	
C	-6.26128	-1.01313	0.15831	
H	-4.93849	-3.26293	-0.70019	
H	-3.90922	-3.48307	0.72140	
H	-5.66766	-3.54534	0.89113	
H	-4.81027	-0.19277	2.34316	
H	-5.59273	-1.74983	2.67103	
H	-3.83261	-1.65437	2.53373	
H	-7.05386	-1.52654	0.71014	
H	-6.37309	0.06009	0.34073	
H	-6.42524	-1.20151	-0.90717	
C	6.29599	-2.64154	1.14124	
H	6.63136	-3.46096	0.49879	
H	7.06784	-1.86579	1.10314	
H	6.24468	-3.01242	2.16689	

Table A.10 Theoretically optimized coordinates of **1j** (Cartesian Coordinate in Angstrom) at PBE0/6-311G(d,p) level of theory

Atom	x	y	z	
C	-3.59840	-0.54999	-0.10998	
C	-3.63220	0.33034	-1.19841	
C	-2.47904	0.73109	-1.85409	
C	-1.23255	0.26530	-1.44200	
C	-1.15977	-0.62546	-0.35486	
C	-2.34752	-1.01061	0.28142	Zero-point correction = 0.425766
N	-0.07879	0.65325	-2.10406	(Hartree/Particle)
P	1.51034	0.28518	-1.73307	Thermal correction to Energy =
C	1.33350	-0.89156	-0.40653	0.450720
C	0.09975	-1.16792	0.08324	Thermal correction to Enthalpy =
C	2.55469	-1.50371	0.15870	0.451664
C	3.62735	-1.87996	-0.65954	Thermal correction to Gibbs Free
C	4.75352	-2.48084	-0.11155	Energy = 0.369322
C	4.83426	-2.71310	1.25652	
C	3.77982	-2.33167	2.08010	
C	2.65448	-1.72693	1.53854	Sum of electronic and zero-point
O	2.33097	-0.05220	-2.91796	Energies = -1474.038251
O	2.16938	1.62994	-1.07774	Sum of electronic and thermal
C	1.66167	2.26652	0.04101	Energies = -1474.013298
C	2.23284	2.00733	1.28016	Sum of electronic and thermal
C	1.77069	2.69183	2.39774	Enthalpies = -1474.012354
C	0.74624	3.62493	2.27658	Sum of electronic and thermal
C	0.18663	3.87754	1.02895	Free Energies = -1474.094695
C	0.64359	3.20144	-0.09634	
H	-4.57869	0.72132	-1.55217	
H	-2.54397	1.41364	-2.69601	
H	-2.26058	-1.70219	1.11451	
H	-0.20967	1.20638	-2.94130	
H	0.03782	-1.89821	0.88839	
H	3.56793	-1.70644	-1.72818	
H	5.57197	-2.77206	-0.76158	
H	3.83891	-2.49356	3.15142	
H	1.85195	-1.40161	2.19254	
H	3.03377	1.28038	1.35305	
H	2.21706	2.49505	3.36675	
H	0.38894	4.15777	3.15101	
H	-0.60784	4.60897	0.92604	
H	0.22608	3.39755	-1.07701	
H	5.71619	-3.18132	1.68060	
C	-4.85594	-1.01104	0.62824	
C	-4.98799	-2.53648	0.50586	
C	-4.74950	-0.62731	2.11165	
C	-6.12307	-0.37159	0.05802	
H	-5.07223	-2.83762	-0.54258	
H	-4.12589	-3.05367	0.93606	
H	-5.88301	-2.88138	1.03393	
H	-4.65854	0.45667	2.22904	
H	-5.64381	-0.95577	2.65109	
H	-3.88264	-1.09186	2.58930	
H	-6.99282	-0.72432	0.61966	
H	-6.09802	0.71961	0.13694	
H	-6.27749	-0.63869	-0.99190	

Table A.11 Theoretically optimized coordinates of **1k** (Cartesian Coordinate in Angstrom) at PBE0/6-311G(d,p) level of theory

Atom	x	y	z	
C	-3.96417	-1.13592	-0.29875	
C	-4.36704	0.05135	-0.92456	
C	-3.45540	0.97788	-1.40366	
C	-2.08688	0.75550	-1.27109	
C	-1.64436	-0.43099	-0.65490	
C	-2.59714	-1.34767	-0.18681	
N	-1.17191	1.67335	-1.76066	
P	0.49109	1.66841	-1.60064	
C	0.79729	0.04822	-0.92094	
C	-0.24523	-0.73338	-0.54050	
C	2.19475	-0.38921	-0.75155	
C	3.18150	-0.06372	-1.69205	
C	4.48535	-0.50412	-1.53800	
C	4.84568	-1.27910	-0.43695	
C	3.86693	-1.60086	0.52283	
C	2.56130	-1.15035	0.36357	
O	1.21505	2.09447	-2.81842	
O	0.87177	2.73249	-0.42499	
C	0.35879	2.66830	0.86111	
C	1.13436	2.10342	1.86484	
C	0.65029	2.08425	3.16746	
C	-0.59729	2.62468	3.46051	
C	-1.35894	3.19453	2.44637	
C	-0.88318	3.22281	1.14062	
H	-5.42133	0.26933	-1.04555	
H	-3.80656	1.88541	-1.88497	
H	-2.22474	-2.25542	0.27897	
H	-1.55477	2.44856	-2.28690	
H	-0.01472	-1.71505	-0.12993	
H	2.91585	0.53536	-2.55547	
H	5.23494	-0.25184	-2.27811	
H	1.83241	-1.38187	1.13080	
H	2.10977	1.69854	1.61936	
H	1.25464	1.64816	3.95563	
H	-0.97158	2.60858	4.47816	
H	-2.32860	3.62610	2.67009	
H	-1.46013	3.67651	0.34334	
C	-4.95155	-2.17297	0.23804	
C	-4.73133	-3.50826	-0.48851	
C	-4.71852	-2.36686	1.74370	
C	-6.40478	-1.74460	0.02752	
H	-4.89350	-3.39801	-1.56482	
H	-3.71770	-3.88949	-0.33746	
H	-5.43094	-4.26191	-0.11301	
H	-4.87141	-1.42944	2.28673	
H	-5.41766	-3.10986	2.14060	
H	-3.70452	-2.71704	1.95547	
H	-7.07124	-2.51236	0.43050	
H	-6.63141	-0.80630	0.54312	
H	-6.64459	-1.62339	-1.03329	
C	6.18919	-1.72817	-0.28903	
N	7.28080	-2.08721	-0.18019	
C	4.20279	-2.37389	1.67375	
N	4.46001	-2.99922	2.60879	
				Zero-point correction = 0.423005 (Hartree/Particle)
				Thermal correction to Energy = 0.451600
				Thermal correction to Enthalpy = 0.452544
				Thermal correction to Gibbs Free Energy = 0.361643
				Sum of electronic and zero-point Energies = -1658.357511
				Sum of electronic and thermal Energies = -1658.328916
				Sum of electronic and thermal Enthalpies = -1658.327972
				Sum of electronic and thermal Free Energies = -1658.418872

Table A.12 Theoretically optimized coordinates of **11** (Cartesian Coordinate in Angstrom) at PBE0/6-311G(d,p) level of theory

Atom	x	y	z	
C	-3.88485	-1.07681	-0.12885	
C	-4.18190	-0.06050	-1.04512	
C	-3.18905	0.67385	-1.67409	
C	-1.84565	0.42026	-1.40786	
C	-1.50866	-0.59919	-0.49762	
C	-2.53989	-1.32175	0.11741	Zero-point correction = 0.416338
N	-0.84882	1.14085	-2.04725	(Hartree/Particle)
P	0.79946	1.10001	-1.77113	Thermal correction to Energy =
C	0.97326	-0.31963	-0.70777	0.442430
C	-0.13533	-0.93424	-0.22645	Thermal correction to Enthalpy =
C	2.33386	-0.75448	-0.33183	0.443374
C	3.38724	-0.73505	-1.25424	Thermal correction to Gibbs Free
C	4.65390	-1.17643	-0.89936	Energy = 0.358508
C	4.87760	-1.63855	0.38929	
C	3.85678	-1.65720	1.33009	
C	2.59607	-1.20982	0.96639	Sum of electronic and zero-point
O	1.60730	1.20235	-3.00687	Energies = -1933.510024
O	1.17220	2.40240	-0.85693	Sum of electronic and thermal
C	0.59380	2.66456	0.37303	Energies = -1933.483931
C	1.28958	2.32983	1.52746	Sum of electronic and thermal
C	0.74391	2.64705	2.76556	Enthalpies = -1933.482987
C	-0.48673	3.29034	2.84695	Sum of electronic and thermal
C	-1.17014	3.62322	1.68268	Free Energies = -1933.567854
C	-0.63171	3.31488	0.43883	
H	-5.21298	0.17419	-1.28082	
H	-3.45710	1.45465	-2.37911	
H	-2.25055	-2.10458	0.81266	
H	-1.15111	1.77788	-2.77317	
H	0.01449	-1.79561	0.42238	
H	3.20974	-0.37806	-2.26231	
H	5.46104	-1.16495	-1.62196	
H	1.80845	-1.19514	1.71207	
H	2.25041	1.83489	1.44259	
H	1.28654	2.39184	3.66961	
H	-0.90901	3.53697	3.81495	
H	-2.12664	4.13179	1.73888	
H	-1.14652	3.58008	-0.47719	
C	-4.96005	-1.89725	0.58491	
C	-4.76299	-3.38739	0.26911	
C	-4.84134	-1.67816	2.10073	
C	-6.37079	-1.49790	0.14939	
H	-4.84558	-3.57249	-0.80603	
H	-3.78451	-3.74767	0.59838	
H	-5.52654	-3.98435	0.77823	
H	-4.98536	-0.62377	2.35502	
H	-5.60116	-2.26397	2.62833	
H	-3.86126	-1.98359	2.47766	
H	-7.10304	-2.11274	0.68041	
H	-6.58780	-0.45087	0.38190	
H	-6.52394	-1.65278	-0.92305	
H	4.04953	-2.00410	2.33823	
Cl	6.46619	-2.19351	0.83933	

Table A.13 Theoretically optimized coordinates of **1m** (Cartesian Coordinate in Angstrom) at PBE0/6-311G(d,p) level of theory

Atom	x	y	z	
C	3.83393	-1.45704	-0.39125	
C	4.15108	-0.75387	0.78211	
C	3.14769	-0.23260	1.56779	
C	1.80397	-0.39317	1.20655	
C	1.47040	-1.10507	0.03414	Zero-point correction = 0.312635
C	2.50145	-1.62968	-0.74792	(Hartree/Particle)
N	0.80858	0.12389	2.00223	Thermal correction to Energy =
P	-0.84556	0.18571	1.70406	0.333719
C	-1.01248	-0.86872	0.27562	Thermal correction to Enthalpy =
C	0.09810	-1.33539	-0.34253	0.334663
C	-2.37014	-1.15667	-0.23247	Thermal correction to Gibbs Free
C	-3.43922	-1.39456	0.64041	Energy = 0.260387
C	-4.69953	-1.69642	0.14076	
C	-4.91798	-1.76006	-1.23039	
C	-3.86554	-1.51300	-2.10596	Sum of electronic and zero-point
C	-2.60491	-1.20856	-1.61294	Energies = -1409.214524
O	-1.66100	-0.06751	2.90988	Sum of electronic and thermal
O	-1.16747	1.70228	1.20598	Energies = -1409.193440
C	-0.52398	2.31449	0.14123	Sum of electronic and thermal
C	-1.09461	2.25283	-1.12290	Enthalpies = -1409.192496
C	-0.47544	2.91249	-2.17793	Sum of electronic and thermal
C	0.70007	3.62557	-1.96833	Free Energies = -1409.266772
C	1.25470	3.68534	-0.69460	
C	0.64357	3.03108	0.36861	
H	5.18787	-0.61975	1.06676	
H	3.39571	0.31227	2.47224	
H	2.25128	-2.18178	-1.64717	
H	1.10125	0.53267	2.88127	
H	-0.04492	-1.97390	-1.21191	
H	-3.27454	-1.35293	1.71111	
H	-5.51511	-1.88566	0.83062	
H	-4.02908	-1.54523	-3.17800	
H	-1.79746	-0.98757	-2.30344	
H	-2.01621	1.69989	-1.26476	
H	-0.91830	2.87043	-3.16727	
H	1.17920	4.13947	-2.79440	
H	2.16600	4.24799	-0.52293	
H	1.05563	3.07999	1.36994	
H	-5.90462	-1.99357	-1.61615	
C	4.86995	-1.99484	-1.20676	
N	5.71256	-2.42948	-1.86698	

Table A.14 Theoretically optimized coordinates of **1n** (Cartesian Coordinate in Angstrom) at PBE0/6-311G(d,p) level of theory

Atom	x	y	z	
C	4.13012	-1.95175	-0.44566	
C	4.63210	-1.20587	0.63271	
C	3.77458	-0.47286	1.42249	
C	2.39942	-0.45827	1.15896	
C	1.87921	-1.21194	0.08489	Zero-point correction = 0.345214
C	2.76356	-1.95192	-0.70266	(Hartree/Particle)
N	1.55292	0.27431	1.95815	Thermal correction to Energy =
P	-0.09994	0.52869	1.77884	0.368901
C	-0.52186	-0.60024	0.46455	Thermal correction to Enthalpy =
C	0.46379	-1.26807	-0.18169	0.369845
C	-1.93974	-0.71569	0.07628	Thermal correction to Gibbs Free
C	-2.96649	-0.69317	1.02424	Energy = 0.289700
C	-4.29776	-0.83565	0.65261	
C	-4.63197	-0.99716	-0.69167	
C	-3.61558	-1.00730	-1.65354	Sum of electronic and zero-point
C	-2.29676	-0.86549	-1.27394	Energies = -1523.612105
O	-0.83794	0.48064	3.05870	Sum of electronic and thermal
O	-0.26802	2.03339	1.17759	Energies = -1523.588418
C	0.35604	2.47215	0.02016	Sum of electronic and thermal
C	-0.31805	2.38397	-1.19038	Enthalpies = -1523.587474
C	0.28737	2.87818	-2.33963	Sum of electronic and thermal
C	1.55182	3.45394	-2.27615	Free Energies = -1523.667620
C	2.21127	3.54159	-1.05498	
C	1.61515	3.05193	0.10131	
H	5.69527	-1.20665	0.84144	
H	4.16265	0.10137	2.25674	
H	2.37003	-2.53778	-1.52614	
H	1.97377	0.72577	2.76092	
H	0.16927	-1.94439	-0.98144	
H	-2.72175	-0.57536	2.07394	
H	-5.06167	-0.82235	1.41982	
H	-3.88994	-1.11393	-2.69709	
H	-1.52775	-0.84690	-2.03934	
H	-1.30665	1.93994	-1.21876	
H	-0.23577	2.81515	-3.28783	
H	2.01982	3.83910	-3.17541	
H	3.19385	3.99742	-0.99766	
H	2.10927	3.12448	1.06338	
O	-5.88861	-1.14093	-1.15902	
C	-6.95305	-1.12382	-0.22544	
H	-6.99538	-0.17118	0.31306	
H	-7.86379	-1.24899	-0.80852	
H	-6.86663	-1.94651	0.49220	
C	5.01399	-2.70868	-1.26621	
N	5.73396	-3.32112	-1.93066	

Table A.15 Theoretically optimized coordinates of **1o** (Cartesian Coordinate in Angstrom) at PBE0/6-311G(d,p) level of theory

Atom	x	y	z	
C	3.22779	-0.58397	0.10328	
C	3.29633	0.31198	1.17828	
C	2.14736	0.72269	1.82074	
C	0.89603	0.25246	1.40443	
C	0.80909	-0.65689	0.32888	Zero-point correction = 0.385127
C	1.98972	-1.05836	-0.30093	(Hartree/Particle)
N	-0.24681	0.66170	2.05465	Thermal correction to Energy =
P	-1.84740	0.28919	1.70401	0.410346
C	-1.68428	-0.90854	0.39467	Thermal correction to Enthalpy =
C	-0.45557	-1.19953	-0.09649	0.411290
C	-2.91289	-1.52223	-0.15234	Thermal correction to Gibbs Free
C	-3.98449	-1.87217	0.67864	Energy = 0.326868
C	-5.11829	-2.47392	0.14776	
C	-5.20703	-2.73238	-1.21501	
C	-4.15298	-2.37759	-2.05095	Sum of electronic and zero-point
C	-3.01973	-1.77256	-1.52689	Energies = -1583.957384
O	-2.64833	-0.03189	2.90506	Sum of electronic and thermal
O	-2.49599	1.62988	1.04140	Energies = -1583.932165
C	-1.99375	2.25162	-0.09036	Sum of electronic and thermal
C	-2.55755	1.96089	-1.32543	Enthalpies = -1583.931220
C	-2.09840	2.62879	-2.45428	Sum of electronic and thermal
C	-1.08593	3.57646	-2.34704	Free Energies = -1584.015643
C	-0.53524	3.86130	-1.10245	
C	-0.98849	3.20159	0.03406	
H	4.26000	0.68393	1.50380	
H	2.20536	1.41554	2.65398	
H	1.94443	-1.76051	-1.12691	
H	-0.11131	1.23871	2.87549	
H	-0.39829	-1.94210	-0.89011	
H	-3.91867	-1.67938	1.74356	
H	-5.93615	-2.74504	0.80704	
H	-4.21816	-2.56109	-3.11834	
H	-2.21697	-1.46904	-2.19094	
H	-3.35033	1.22412	-1.38745	
H	-2.53795	2.40758	-3.42104	
H	-0.73109	4.09594	-3.23040	
H	0.24904	4.60504	-1.01082	
H	-0.57904	3.42355	1.01269	
H	-6.09496	-3.20108	-1.62576	
C	4.42908	-1.05511	-0.62240	
O	4.40192	-1.82676	-1.55360	
O	5.55696	-0.53127	-0.13384	
C	6.77616	-0.93627	-0.78032	
C	7.91485	-0.24063	-0.08092	
H	6.71789	-0.66575	-1.83793	
H	6.86014	-2.02443	-0.71818	
H	8.86129	-0.52551	-0.54710	
H	7.81156	0.84483	-0.15049	
H	7.95462	-0.52057	0.97441	

Table A.16 Theoretically optimized coordinates of **1p** (Cartesian Coordinate in Angstrom) at PBE0/6-311G(d,p) level of theory

Atom	x	y	z	
C	3.85012	-1.24269	-0.01412	
C	4.19156	-0.29375	0.95549	
C	3.20100	0.40778	1.62691	
C	1.85437	0.18653	1.35452	
C	1.49835	-0.77311	0.38651	Zero-point correction = 0.373031
C	2.50871	-1.47316	-0.28156	(Hartree/Particle)
N	0.86742	0.87886	2.04650	Thermal correction to Energy =
P	-0.77666	0.89167	1.76484	0.398261
C	-0.97652	-0.46912	0.62704	Thermal correction to Enthalpy =
C	0.11923	-1.07342	0.10449	0.399205
C	-2.34250	-0.87124	0.23918	Thermal correction to Gibbs Free
C	-3.39214	-0.86489	1.16818	Energy = 0.315314
C	-4.66291	-1.27306	0.80174	
C	-4.91233	-1.69197	-0.50802	
C	-3.87748	-1.68933	-1.44915	Sum of electronic and zero-point
C	-2.61192	-1.27626	-1.07610	Energies = -1562.859584
O	-1.58878	0.94525	3.00064	Sum of electronic and thermal
O	-1.12635	2.24042	0.91204	Energies = -1562.834354
C	-0.53783	2.55267	-0.30183	Sum of electronic and thermal
C	-1.23852	2.29383	-1.47264	Enthalpies = -1562.833410
C	-0.68257	2.65981	-2.69252	Sum of electronic and thermal
C	0.56313	3.27678	-2.73976	Free Energies = -1562.917302
C	1.25092	3.53453	-1.55917	
C	0.70254	3.17674	-0.33301	
H	5.22747	-0.09021	1.19527	
H	3.48243	1.14137	2.37564	
H	2.24654	-2.21679	-1.02654	
H	1.17892	1.45484	2.81777	
H	-0.04479	-1.89698	-0.58779	
H	-3.20226	-0.54367	2.18566	
H	-5.46559	-1.27232	1.52985	
H	-4.07382	-1.99804	-2.46927	
H	-1.82462	-1.24626	-1.82100	
H	-2.21237	1.82077	-1.41490	
H	-1.22920	2.46396	-3.60884	
H	0.99362	3.56177	-3.69346	
H	2.21908	4.02287	-1.58823	
H	1.22158	3.38434	0.59534	
C	-6.22037	-2.11326	-0.88838	
N	-7.27904	-2.45596	-1.19806	
O	4.74111	-1.97459	-0.72460	
C	6.12758	-1.77942	-0.47542	
C	6.88889	-2.71136	-1.38432	
H	6.34848	-1.99432	0.57802	
H	6.39616	-0.73391	-0.67429	
H	7.96334	-2.59255	-1.22481	
H	6.62200	-3.75105	-1.18133	
H	6.66848	-2.49362	-2.43189	

5. Geometries and Methods Used for Modeling the Solution-State Dimerization of Heterocycles 1

Geometry optimizations of heterocycle 1 monomers with chloroform model:

Heterocycle **1g**

Supporting Information: polymerdetector-s-monomer-6-c-ch3-3-0006.log

Using Gaussian 09: AM64L-G09RevD.01 24-Apr-2013³
=====

=====
pbepbe/6-31G*/auto gfpri nt gfinpu t scf=(direct,tight,maxcycle=300,xqc)
opt=(maxcycle=250) freq=noraman iop(1/8=18) Temperature=298.15
#N Geom=AllCheck Guess=TCheck SCRF=Check Test GenChk RPBEPBE/6-
31G(d)/Auto
Freq

Pointgroup= C1 Stoichiometry= C25H23N2O2P C1[X(C25H23N2O2P)] #Atoms=
53
Charge = 0 Multiplicity = 1

SCF Energy= -1566.19434736 Predicted Change= -3.982743D-09
=====

=====
Optimization completed. {Found 2 times}
Item Max Val. Criteria Pass? RMS Val. Criteria Pass?
Force 0.00000 || 0.00045 [YES] 0.00000 || 0.00030 [YES]
Displ 0.00133 || 0.00180 [YES] 0.00133 || 0.00180 [YES]

Atomic Type	Coordinates (Angstroms)		
	X	Y	Z
C	1.674825	-0.719803	0.284938
C	2.860434	-1.379930	-0.128725
H	2.740609	-2.350346	-0.620399
C	4.136763	-0.846183	0.067569
C	5.426655	-1.551267	-0.392721
C	5.141342	-2.901908	-1.080078
H	4.631799	-3.608913	-0.401962
H	6.092492	-3.367588	-1.390476
H	4.520920	-2.779139	-1.985252
C	6.336966	-1.813598	0.833085
H	5.837844	-2.474733	1.562519
H	6.607019	-0.879182	1.354027
H	7.275452	-2.301014	0.513153
C	6.173642	-0.641704	-1.400567
H	6.437987	0.333253	-0.956348

H	5.554412	-0.449258	-2.293793
H	7.111150	-1.124949	-1.729444
C	4.208060	0.406732	0.727380
H	5.184553	0.868304	0.909135
C	3.069476	1.086315	1.154961
H	3.163091	2.054838	1.659384
C	1.788935	0.542765	0.932643
N	0.645676	1.194337	1.384711
H	0.778672	2.018474	1.974544
P	-0.969221	0.853700	0.959965
O	-1.916222	1.240999	2.060690
O	-1.252983	1.616171	-0.490703
C	-0.852545	-0.842224	0.367711
C	-2.097699	-1.604173	0.131812
C	0.393031	-1.357151	0.097711
H	0.438033	-2.391236	-0.272027
C	-2.165760	-2.572098	-0.900439
H	-1.310409	-2.711408	-1.568721
C	-3.317649	-3.327159	-1.109843
H	-3.356007	-4.066105	-1.915481
C	-4.454098	-3.125912	-0.293258
C	-4.407773	-2.148564	0.725371
H	-5.286517	-1.985649	1.356068
C	-3.249177	-1.399801	0.932086
H	-3.223366	-0.648080	1.726531
C	-1.379884	3.009954	-0.592490
C	-2.278035	3.738661	0.202818
H	-2.871966	3.221188	0.959943
C	-2.383311	5.123166	0.005438
H	-3.080949	5.698104	0.623542
C	-1.616299	5.769266	-0.974871
H	-1.711238	6.849438	-1.124714
C	-0.730295	5.023009	-1.766352
H	-0.129683	5.517107	-2.537240
C	-0.604939	3.640509	-1.576441
H	0.078562	3.038680	-2.182619
C	-5.640649	-3.898086	-0.505910
N	-6.614620	-4.535698	-0.680526

Statistical Thermodynamic Analysis

Temperature= 298.150 Kelvin Pressure= 1.00000 Atm

=====

SCF Energy= -1566.19434736 Predicted Change= -3.982743D-09

Zero-point correction (ZPE)= -1565.7813 0.41304

Internal Energy (U)= -1565.7536 0.44073

Enthalpy (H)= -1565.7526 0.44167
Gibbs Free Energy (G)= -1565.8413 0.35297

Frequencies -- 14.1273 23.3695 25.7166
Single points at WB97X/6-311++G2(df,p): -1567.94
Solvation Correction at PBE/6-31+G(d,p)/auto/Chloroform: -0.0351074

Heterocycle 1e

Supporting Information: polymerdetector-s-monomer-6-cf3-0006.log

Using Gaussian 09: AM64L-G09RevD.01 24-Apr-2013
=====

=====

```
# pbepbe/6-31G*/auto gfpri gfinpu scf=(direct,tight,maxcycle=300,xqc)
opt=(maxcycle=250) freq=norman iop(1/8=18) Temperature=298.15
#N Geom=AllCheck Guess=TCheck SCRF=Check Test GenChk RPBEPBE/6-
31G(d)/Auto
Freq
```

Pointgroup= C1 Stoichiometry= C22H14F3N2O2P C1[X(C22H14F3N2O2P)]
#Atoms= 44
Charge = 0 Multiplicity = 1

SCF Energy= -1745.88972035 Predicted Change= -2.495849D-07
=====

=====

```
Optimization completed. {Found 1 times}
Item Max Val. Criteria Pass? RMS Val. Criteria Pass?
Force 0.00006 || 0.00045 [ YES ] 0.00000 || 0.00030 [ YES ]
Displ 0.02645 || 0.00180 [ NO ] 0.02645 || 0.00180 [ NO ]
```

Atomic Coordinates (Angstroms)

Atomic Type	X	Y	Z
C	-1.620423	-0.820056	-0.230592
C	-2.771036	-1.510551	0.212978
H	-2.644606	-2.453240	0.754759
C	-4.053596	-1.027680	-0.042202
C	-5.267594	-1.748156	0.481889
F	-5.737243	-1.178783	1.629257
F	-5.003845	-3.053487	0.763030
F	-6.291036	-1.716626	-0.417712
C	-4.212443	0.171571	-0.767385
H	-5.217283	0.545798	-0.983697
C	-3.098774	0.877121	-1.213404
H	-3.226303	1.809289	-1.774395

C	-1.796388	0.404903	-0.942939
N	-0.685570	1.093747	-1.406810
H	-0.853786	1.877598	-2.041317
P	0.947877	0.857135	-0.959055
O	1.886596	1.241006	-2.062672
O	1.165778	1.696359	0.460508
C	0.906682	-0.821861	-0.305485
C	2.183497	-1.538029	-0.106099
C	-0.309357	-1.388420	-0.014105
H	-0.301777	-2.389290	0.439483
C	3.353353	-0.852333	0.297730
H	3.316314	0.226732	0.473731
C	4.550206	-1.536008	0.507919
H	5.445543	-0.995197	0.827131
C	4.611245	-2.934541	0.317301
C	3.452229	-3.630184	-0.095298
H	3.501046	-4.710112	-0.261605
C	2.262376	-2.936218	-0.308733
H	1.382930	-3.479080	-0.669218
C	1.148355	3.100730	0.517804
C	1.872055	3.900111	-0.380646
H	2.451320	3.430757	-1.179897
C	1.830537	5.293736	-0.224697
H	2.391484	5.924322	-0.922494
C	1.092753	5.878933	0.814226
H	1.073027	6.967158	0.929983
C	0.384270	5.061982	1.708214
H	-0.192102	5.508580	2.525053
C	0.405026	3.668951	1.561960
H	-0.140821	3.012869	2.246281
C	5.837389	-3.642026	0.532791
N	6.843399	-4.225734	0.712638

 Statistical Thermodynamic Analysis

Temperature= 298.150 Kelvin Pressure= 1.00000 Atm

=====
 SCF Energy= -1745.88972035 Predicted Change= -2.495849D-07
 Zero-point correction (ZPE)= -1745.5826 0.30708
 Internal Energy (U)= -1745.5568 0.33291
 Enthalpy (H)= -1745.5558 0.33385
 Gibbs Free Energy (G)= -1745.6435 0.24620

 Frequencies -- 6.3297 18.0278 19.5809
 Single points at WB97X/6-311++G2(df,p): -1747.7769
 Solvation Correction at PBE/6-31+G(d,p)/auto/Chloroform: -0.03398828

Heterocycle 1b

Supporting Information: 0006.log

Using Gaussian 09: AM64L-G09RevD.01 24-Apr-2013
=====

=====
pbepbe/6-31G*/auto gfprint gfinput scf=(direct,tight,maxcycle=300,xqc)
opt=(maxcycle=250) freq=noraman iop(1/8=18) Temperature=298.15
#N Geom=AllCheck Guess=TCheck SCRF=Check Test GenChk RPBEPBE/6-
31G(d)/Auto

Freq

Pointgroup= C1 Stoichiometry= C21H15N2O2P C1[X(C21H15N2O2P)] #Atoms=
41

Charge = 0 Multiplicity = 1

SCF Energy= -1409.16315011 Predicted Change= -4.056633D-09
=====

=====
Optimization completed. {Found 2 times}
Item Max Val. Criteria Pass? RMS Val. Criteria Pass?
Force 0.00000 || 0.00045 [YES] 0.00000 || 0.00030 [YES]
Displ 0.00122 || 0.00180 [YES] 0.00122 || 0.00180 [YES]

Atomic Type	Coordinates (Angstroms)		
	X	Y	Z
C	-1.161693	2.676854	-0.174198
C	-1.489591	3.935296	-0.736421
H	-0.700497	4.491200	-1.255651
C	-2.772521	4.467839	-0.638130
H	-3.003125	5.439836	-1.083419
C	-3.767282	3.745034	0.047921
H	-4.779155	4.153191	0.137253
C	-3.479278	2.503729	0.617245
H	-4.256844	1.943021	1.148177
C	-2.186165	1.953101	0.507049
N	-1.883963	0.733173	1.103069
H	-2.598056	0.319961	1.706799
P	-0.487790	-0.219804	0.877442
O	-0.164842	-1.011590	2.113049
O	-0.750347	-1.142306	-0.479635
C	0.672190	0.969966	0.186084
C	2.092629	0.581383	0.050274
C	0.192647	2.181837	-0.247773

H	0.922177	2.885962	-0.672016
C	2.869980	1.061414	-1.032048
H	2.398741	1.674124	-1.806837
C	4.219168	0.735592	-1.153610
H	4.804396	1.108572	-1.999144
C	4.834783	-0.099684	-0.193390
C	4.066020	-0.602048	0.879691
H	4.537387	-1.252481	1.622135
C	2.716769	-0.267871	0.997106
H	2.131152	-0.659561	1.834130
C	-1.600099	-2.260197	-0.477841
C	-1.443648	-3.311968	0.437930
H	-0.672914	-3.245787	1.209327
C	-2.295846	-4.421427	0.341993
H	-2.181113	-5.245289	1.054240
C	-3.279490	-4.486759	-0.655686
H	-3.935542	-5.360259	-0.725205
C	-3.415563	-3.429211	-1.567365
H	-4.177841	-3.472485	-2.352311
C	-2.578664	-2.308638	-1.480822
H	-2.664914	-1.473529	-2.182234
C	6.219977	-0.439889	-0.316694
N	7.359475	-0.716650	-0.419082

Statistical Thermodynamic Analysis

Temperature= 298.150 Kelvin Pressure= 1.00000 Atm

=====
SCF Energy= -1409.16315011 Predicted Change= -4.056633D-09
Zero-point correction (ZPE)= -1408.8602 0.30292
Internal Energy (U)= -1408.8382 0.32487
Enthalpy (H)= -1408.8373 0.32581
Gibbs Free Energy (G)= -1408.9142 0.24893

Frequencies -- 11.8031 19.0278 32.5940
Single points at WB97X/6-311++G2(df,p): -1410.6769
Solvation Correction at PBE/6-31+G(d,p)/auto/Chloroform: -0.03306504

Heterocycle **1p**

Supporting Information: 1-cn-2-eto-monomer-3.log

Using Gaussian 09: AM64L-G09RevD.01 24-Apr-2013

=====
#PBEPBE/6-31G(d)/auto gfpint gfinput scf=(direct,tight,maxcycle=300,xqc)
opt=(maxcycle=250) freq=noraman

#P Geom=AllCheck Guess=TCheck SCRF=Check Test GenChk RPBEPBE/6-31G(d)/Auto
Freq

Pointgroup= C1 Stoichiometry= C23H19N2O3P C1[X(C23H19N2O3P)] #Atoms=48

Charge = 0 Multiplicity = 1

SCF Energy= -1562.82081034 Predicted Change= -6.168975D-09

=====
Optimization completed. {Found 1 times}
Item Max Val. Criteria Pass? RMS Val. Criteria Pass?
Force 0.00000 || 0.00045 [YES] 0.00000 || 0.00030 [YES]
Displ 0.00235 || 0.00180 [NO] 0.00235 || 0.00180 [YES]

Atomic Coordinates (Angstroms)
Type X Y Z

C 1.902599 0.651089 0.358334
C 3.110139 1.290998 -0.030062
H 3.037643 2.268633 -0.514250
C 4.350779 0.691334 0.202012
C 4.397420 -0.567978 0.846452
H 5.374411 -1.025541 1.027057
C 3.226865 -1.209702 1.235014
H 3.278816 -2.186405 1.728752
C 1.967995 -0.621725 0.991479
N 0.795363 -1.245452 1.417050
H 0.892909 -2.069369 2.013513
P -0.794883 -0.865794 0.948811
O -1.785807 -1.252600 2.010684
O -1.052612 -1.588913 -0.527611
C -0.622284 0.839110 0.395679
C -1.841038 1.640571 0.154798
C 0.641638 1.326115 0.159817
H 0.719866 2.366141 -0.186665
C -1.865253 2.630754 -0.858286
H -0.995574 2.759555 -1.510046
C -2.992407 3.421401 -1.070950
H -2.997165 4.176986 -1.861932
C -4.147395 3.235745 -0.276995
C -4.144939 2.237137 0.721966
H -5.038220 2.086021 1.334944
C -3.011251 1.452040 0.931618
H -3.019461 0.683023 1.709688

C	-1.196428	-2.977454	-0.667205
C	-0.420027	-3.591311	-1.660610
H	0.276148	-2.981926	-2.244386
C	-0.559101	-4.966833	-1.887535
H	0.042984	-5.447605	-2.665680
C	-1.460097	-5.723390	-1.123136
H	-1.565465	-6.798228	-1.301653
C	-2.228377	-5.094182	-0.132950
H	-2.937721	-5.677023	0.464110
C	-2.109703	-3.716456	0.101119
H	-2.705315	-3.211725	0.865589
C	-5.308253	4.045195	-0.492494
N	-6.260860	4.713771	-0.669252
C	5.574509	2.501106	-0.789404
H	5.094613	3.255799	-0.133516
O	5.566860	1.221097	-0.140652
C	7.024047	2.864431	-1.070662
H	7.600953	2.921096	-0.133235
H	7.494530	2.112354	-1.724798
H	7.075804	3.845030	-1.572431
H	4.987814	2.447204	-1.729178

 Statistical Thermodynamic Analysis

Temperature= 298.150 Kelvin Pressure= 1.00000 Atm
 =====

=====

SCF Energy=	-1562.82081034	Predicted Change=	-6.168975D-09
Zero-point correction (ZPE)=	-1562.4585	0.36230	
Internal Energy (U)=	-1562.4323	0.38841	
Enthalpy (H)=	-1562.4314	0.38935	
Gibbs Free Energy (G)=	-1562.5177	0.30306	

 Frequencies -- 13.2719 21.5509 23.2439
 Single points at WB97X/6-311++G2(df,p): -1564.5292
 Solvation Correction at PBE/6-31+G(d,p)/auto/Chloroform: -0.03528503

Heterocycle **1j**

Supporting Information: 0002.log

Using Gaussian 09: AM64L-G09RevD.01 24-Apr-2013
 =====

=====

```
# pbepbe/6-31G*/auto gfpri gfinpu scf=(direct,tight,maxcycle=300,xqc)
opt=(maxcycle=250) freq=noraman iop(1/8=18) Temperature=298.15
```

#N Geom=AllCheck Guess=TCheck SCRF=Check Test GenChk RPBEPBE/6-31G(d)/Auto
Freq

Pointgroup= C1 Stoichiometry= C24H24NO2P C1[X(C24H24NO2P)] #Atoms= 52
Charge = 0 Multiplicity = 1

SCF Energy= -1474.04821420 Predicted Change= -3.066499D-09

Optimization completed on the basis of negligible forces. {Found 2 times}

Item	Max Val.	Criteria	Pass?	RMS Val.	Criteria	Pass?
Force	0.00000	0.00045	[YES]	0.00000	0.00030	[YES]
Displ	0.00269	0.00180	[NO]	0.00269	0.00180	[YES]

Atomic Coordinates (Angstroms)

Type	X	Y	Z
------	---	---	---

C	-1.876040	0.170058	0.262835
C	-3.145920	0.619356	-0.179591
H	-3.198459	1.639351	-0.573373
C	-4.295926	-0.173475	-0.128568
C	-5.675702	0.309803	-0.614395
C	-6.168478	-0.612171	-1.757854
H	-5.476691	-0.579631	-2.617391
H	-7.166197	-0.289994	-2.106818
H	-6.251101	-1.662837	-1.430949
C	-5.634394	1.757374	-1.144955
H	-4.953928	1.859391	-2.008711
H	-5.315521	2.471513	-0.365455
H	-6.642131	2.058658	-1.479345
C	-6.684046	0.252976	0.560360
H	-6.782147	-0.767118	0.969513
H	-7.685083	0.575429	0.221706
H	-6.368911	0.917047	1.383807
C	-4.145758	-1.477991	0.404214
H	-5.014250	-2.142445	0.468121
C	-2.916901	-1.956885	0.854251
H	-2.837738	-2.972389	1.259520
C	-1.766344	-1.146990	0.786933
N	-0.541683	-1.612361	1.259092
H	-0.540277	-2.536615	1.695654
P	0.981994	-0.874132	1.136205
O	1.837794	-1.033462	2.361737
O	1.574329	-1.686081	-0.195306

C	0.563671	0.774769	0.554142
C	1.651468	1.770865	0.401839
C	-0.735479	1.053222	0.205065
H	-0.949277	2.075242	-0.138402
C	2.725427	1.842944	1.320383
H	2.764510	1.134249	2.152841
C	3.719824	2.817647	1.174838
H	4.538996	2.860752	1.900462
C	3.670556	3.735038	0.115823
H	4.452157	4.494042	0.005369
C	2.618915	3.664338	-0.810375
H	2.580919	4.361378	-1.654407
C	1.625243	2.690156	-0.673608
H	0.831087	2.617111	-1.424373
C	2.907371	-1.627015	-0.622842
C	3.992964	-1.784206	0.252977
H	3.809794	-1.903336	1.323499
C	5.291991	-1.769592	-0.274599
H	6.143421	-1.887952	0.404205
C	5.508663	-1.614152	-1.651416
H	6.527508	-1.609246	-2.051796
C	4.411145	-1.467688	-2.512639
H	4.567372	-1.346258	-3.589746
C	3.106839	-1.470958	-2.002369
H	2.236303	-1.356037	-2.654794

Statistical Thermodynamic Analysis

Temperature= 298.150 Kelvin Pressure= 1.00000 Atm

=====
SCF Energy= -1474.04821420 Predicted Change= -3.066499D-09
Zero-point correction (ZPE)= -1473.6336 0.41456
Internal Energy (U)= -1473.6077 0.44041
Enthalpy (H)= -1473.6068 0.44136
Gibbs Free Energy (G)= -1473.6920 0.35612

Frequencies -- 6.5156 17.0003 21.9082
Single points at WB97X/6-311++G2(df,p): -1475.6946
Solvation Correction at PBE/6-31+G(d,p)/auto/Chloroform: -0.0323201

Heterocycle **1m**

Supporting Information: 0005.log

Using Gaussian 09: AM64L-G09RevD.01 24-Apr-2013
=====

pbepbe/6-31G*/auto gfpri nt gfi nput scf=(direct,tight,maxcycle=300,xqc)
 opt=(maxcycle=250) freq=norman iop(1/8=18) Temperature=298.15
 #N Geom=AllCheck Guess=TChe ck SCRF=Check Test GenChk RPBEPBE/6-
 31G(d)/Auto
 Freq

 Pointgroup= C1 Stoichiometry= C21H15N2O2P C1[X(C21H15N2O2P)] #Atoms=
 41
 Charge = 0 Multiplicity = 1

SCF Energy= -1409.16290164 Predicted Change= -6.773340D-09
 =====

Optimization completed. {Found 1 times}
 Item Max Val. Criteria Pass? RMS Val. Criteria Pass?
 Force 0.00000 || 0.00045 [YES] 0.00000 || 0.00030 [YES]
 Displ 0.00346 || 0.00180 [NO] 0.00346 || 0.00180 [YES]

Atomic Type	Coordinates (Angstroms)		
	X	Y	Z
C	2.187149	0.496204	-0.118091
C	3.508238	0.710855	0.323185
H	3.746167	1.640121	0.850814
C	4.523776	-0.233778	0.097155
C	4.214269	-1.425861	-0.605347
H	5.000127	-2.163697	-0.788807
C	2.918936	-1.657625	-1.053392
H	2.683430	-2.581772	-1.592310
C	1.892392	-0.718094	-0.811702
N	0.610362	-0.939709	-1.284476
H	0.469415	-1.753007	-1.888035
P	-0.815535	-0.074829	-0.888468
O	-1.780112	-0.086315	-2.038939
O	-1.392941	-0.751871	0.511646
C	-0.153358	1.458409	-0.215860
C	-1.086881	2.575712	0.055331
C	1.183243	1.519758	0.084402
H	1.558541	2.464144	0.502033
C	-2.192674	2.831351	-0.789969
H	-2.374506	2.178623	-1.648970
C	-3.041007	3.916110	-0.538706
H	-3.887106	4.101968	-1.208494
C	-2.812322	4.760936	0.556382
H	-3.480573	5.606217	0.750797
C	-1.728377	4.507706	1.411018

H	-1.553069	5.147691	2.282161
C	-0.878104	3.425032	1.167556
H	-0.060298	3.211252	1.863714
C	-1.956275	-2.037721	0.549550
C	-1.490571	-2.892944	1.558303
H	-0.703909	-2.542829	2.233076
C	-2.049678	-4.171299	1.684492
H	-1.691230	-4.839821	2.474155
C	-3.058665	-4.592989	0.805599
H	-3.492428	-5.592982	0.905594
C	-3.512428	-3.724688	-0.197825
H	-4.304057	-4.044532	-0.883591
C	-2.971733	-2.437478	-0.332924
H	-3.320263	-1.747429	-1.105147
C	5.854568	0.007499	0.563836
N	6.950241	0.202770	0.947392

 Statistical Thermodynamic Analysis

Temperature= 298.150 Kelvin Pressure= 1.00000 Atm
 =====

=====
 SCF Energy= -1409.16290164 Predicted Change= -6.773340D-09
 Zero-point correction (ZPE)= -1408.8599 0.30294
 Internal Energy (U)= -1408.8379 0.32491
 Enthalpy (H)= -1408.8370 0.32585
 Gibbs Free Energy (G)= -1408.9137 0.24919

Frequencies -- 14.9694 21.1450 29.8218
 Single points at WB97X/6-311++G2(df,p): -1410.677
 Solvation Correction at PBE/6-31+G(d,p)/auto/Chloroform: -0.0344051

Heterocycle **1a**

Supporting Information: 0005.log

Using Gaussian 09: AM64L-G09RevD.01 24-Apr-2013
 =====

=====
 # pbepbe/6-31G*/auto gfpri n gfinpu t scf=(direct,tight,maxcycle=300,xqc)
 opt=(maxcycle=250) freq=noraman iop(1/8=18) Temperature=298.15
 #N Geom=AllCheck Guess=TCheck SCRF=Check Test GenChk RPBEPBE/6-
 31G(d)/Auto
 Freq

Pointgroup= C1 Stoichiometry= C20H16NO2P C1[X(C20H16NO2P)] #Atoms= 40
 Charge = 0 Multiplicity = 1

SCF Energy= -1317.01704642 Predicted Change= -8.137098D-08

=====
=====
Optimization completed. {Found 1 times}
Item Max Val. Criteria Pass? RMS Val. Criteria Pass?
Force 0.00002 || 0.00045 [YES] 0.00000 || 0.00030 [YES]
Displ 0.00560 || 0.00180 [NO] 0.00560 || 0.00180 [NO]

Atomic Type	Coordinates (Angstroms)		
	X	Y	Z
C	-0.242448	2.635088	0.144449
C	-0.308901	3.933329	0.705682
H	-1.212457	4.210781	1.260748
C	0.733657	4.847035	0.563680
H	0.659859	5.842878	1.010281
C	1.878725	4.477381	-0.166316
H	2.704563	5.185460	-0.289655
C	1.977027	3.206546	-0.736237
H	2.871182	2.919422	-1.301216
C	0.931191	2.274593	-0.582149
N	1.006179	1.019756	-1.180170
H	1.796868	0.848532	-1.804660
P	0.010681	-0.331897	-0.881121
O	-0.079593	-1.219088	-2.091160
O	0.627790	-1.086162	0.471376
C	-1.446121	0.423959	-0.144087
C	-2.656720	-0.404313	0.061942
C	-1.364190	1.731008	0.267337
H	-2.264628	2.166075	0.723461
C	-3.482380	-0.192489	1.191396
H	-3.184618	0.543395	1.945781
C	-4.650510	-0.938106	1.376779
H	-5.270148	-0.761263	2.262452
C	-5.016001	-1.922105	0.445442
H	-5.927889	-2.509873	0.594015
C	-4.196476	-2.156321	-0.667649
H	-4.468652	-2.926248	-1.397386
C	-3.027286	-1.410948	-0.861198
H	-2.393382	-1.597166	-1.733364
C	1.879939	-1.711950	0.475661
C	2.690370	-1.471340	1.595363
H	2.327445	-0.799013	2.378291
C	3.939724	-2.097592	1.687404
H	4.571189	-1.912664	2.562817
C	4.381986	-2.950989	0.665135

H	5.360040	-3.437166	0.738340
C	3.560603	-3.181644	-0.447663
H	3.894783	-3.852653	-1.246257
C	2.301465	-2.571942	-0.551776
H	1.644874	-2.753528	-1.406549

 Statistical Thermodynamic Analysis

Temperature= 298.150 Kelvin Pressure= 1.00000 Atm
 =====

SCF Energy= -1317.01704642 Predicted Change= -8.137098D-08
 Zero-point correction (ZPE)= -1316.7125 0.30454
 Internal Energy (U)= -1316.6924 0.32457
 Enthalpy (H)= -1316.6915 0.32552
 Gibbs Free Energy (G)= -1316.7633 0.25371

Frequencies -- 15.8757 23.5736 41.1169
 Single points at WB97X/6-311++G2(df,p): -1318.4317
 Solvation Correction at PBE/6-31+G(d,p)/auto/Chloroform: -0.02998695

Heterocycle **1o***

Supporting Information: 1-h-2-co2me-monomer-5.log

Using Gaussian 09: AM64L-G09RevD.01 24-Apr-2013
 =====

#PBEPBE/6-31G(d)/auto gfpri nt gfinpu t scf=(direct,tight,maxcycle=300,xqc)
 opt=(maxcycle=250) freq=noraman
 #P Geom=AllCheck Guess=TChe ck SCRF=Check Test GenChk RPBE PBE/6-
 31G(d)/Auto
 Freq

Pointgroup= C1 Stoichiometry= C22H18NO4P C1[X(C22H18NO4P)] #Atoms= 46
 Charge = 0 Multiplicity = 1

SCF Energy= -1544.65655049 Predicted Change= -1.649204D-09
 =====

Optimization completed. {Found 2 times}
 Item Max Val. Criteria Pass? RMS Val. Criteria Pass?
 Force 0.00000 || 0.00045 [YES] 0.00000 || 0.00030 [YES]
 Displ 0.00127 || 0.00180 [YES] 0.00127 || 0.00180 [YES]

Atomic	Coordinates (Angstroms)		
Type	X	Y	Z

P	1.458613	0.104155	-0.898194
O	2.000550	0.776463	0.521835
C	2.566406	2.058230	0.584181
O	2.450087	0.149071	-2.025865
C	0.813023	-1.447903	-0.259001
C	1.765433	-2.543225	0.038187
N	0.028890	0.950759	-1.311906
H	0.170357	1.779461	-1.893950
C	-0.532156	-1.546801	-0.009055
H	-0.898027	-2.504712	0.385585
C	-1.555401	-0.549525	-0.237611
C	-1.265976	0.685346	-0.896122
C	2.083018	2.905139	1.592172
H	1.280207	2.550711	2.245338
C	2.644148	4.179653	1.744983
H	2.271013	4.840764	2.534199
C	3.673581	4.607287	0.893046
H	4.108959	5.604381	1.013576
C	4.145114	3.748127	-0.110070
H	4.952567	4.072363	-0.775141
C	3.602563	2.464831	-0.271319
H	3.964179	1.782293	-1.044122
C	-2.307380	1.601483	-1.161578
H	-2.074405	2.542551	-1.672425
C	-3.613526	1.321695	-0.770994
H	-4.411001	2.041331	-0.972854
C	-3.918487	0.110860	-0.107701
C	-2.888406	-0.804687	0.140750
H	-3.141254	-1.745467	0.641712
C	1.537806	-3.407723	1.134806
H	0.687734	-3.222627	1.799811
C	2.406837	-4.469781	1.402563
H	2.214648	-5.122135	2.261003
C	3.529916	-4.686457	0.589566
H	4.212965	-5.515150	0.803360
C	3.777297	-3.825980	-0.489163
H	4.653487	-3.982846	-1.127093
C	2.909356	-2.762888	-0.765397
H	3.106082	-2.098425	-1.612137
C	-5.290864	-0.250301	0.336934
O	-5.590491	-1.292960	0.909868
O	-6.201023	0.724505	0.032665
C	-7.548207	0.419389	0.443827
H	-7.909757	-0.494343	-0.055558
H	-7.597252	0.267853	1.534457
H	-8.149473	1.289122	0.144441

Statistical Thermodynamic Analysis

Temperature= 298.150 Kelvin Pressure= 1.00000 Atm
=====

=====

SCF Energy=	-1544.65655049	Predicted Change=	-1.649204D-09
Zero-point correction (ZPE)=	-1544.3103		0.34616
Internal Energy (U)=	-1544.2855		0.37098
Enthalpy (H)=	-1544.2846		0.37192
Gibbs Free Energy (G)=	-1544.3681		0.28837

Frequencies -- 14.5204 20.6541 27.0101
Single points at WB97X/6-311++G2(df,p): -1546.336
Solvation Correction at PBE/6-31+G(d,p)/auto/Chloroform: -0.0318351

Heterocycle **1h**

Supporting Information: polymerdetector-s-monomer-1-ome-2-c-ch3-3-0010.log

Using Gaussian 09: AM64L-G09RevD.01 24-Apr-2013
=====

=====

```
# pbepbe/6-31G*/auto gfprint gfinput scf=(direct,tight,maxcycle=300,xqc)
opt=(maxcycle=250) freq=noraman iop(1/8=18) Temperature=298.15
#N Geom=AllCheck Guess=TCheck SCRF=Check Test GenChk RPBEPBE/6-
31G(d)/Auto
Freq
```

Pointgroup= C1 Stoichiometry= C25H26NO3P C1[X(C25H26NO3P)] #Atoms= 56
Charge = 0 Multiplicity = 1

SCF Energy= -1588.44569629 Predicted Change= -2.458265D-09
=====

=====

```
Optimization completed.      {Found    1    times}
Item    Max Val.    Criteria    Pass?    RMS Val.    Criteria    Pass?
Force    0.00000 || 0.00045    [ YES ]    0.00000 || 0.00030    [ YES ]
Displ    0.00224 || 0.00180    [ NO ]    0.00224 || 0.00180    [ YES ]
```

Atomic Type	Coordinates (Angstroms)		
	X	Y	Z

C	-1.732515	-0.790906	-0.290861
C	-2.882769	-1.505540	0.128833
H	-2.713150	-2.457125	0.642247
C	-4.186513	-1.048685	-0.088497
C	-5.438345	-1.816682	0.377823

C	-6.254817	-0.925433	1.347088
H	-5.661581	-0.668463	2.241754
H	-7.166305	-1.454954	1.678424
H	-6.570280	0.018064	0.869707
C	-5.082586	-3.125987	1.111117
H	-4.525196	-3.822809	0.460746
H	-6.008086	-3.636427	1.429072
H	-4.478857	-2.938800	2.016634
C	-6.313023	-2.171034	-0.850855
H	-5.763259	-2.822172	-1.552344
H	-6.628891	-1.270098	-1.404294
H	-7.226264	-2.703890	-0.529865
C	-4.324812	0.182610	-0.775235
H	-5.324251	0.583950	-0.974389
C	-3.220716	0.915870	-1.207140
H	-3.362709	1.867596	-1.732261
C	-1.914690	0.448801	-0.964483
N	-0.803255	1.153256	-1.422201
H	-0.976960	1.965163	-2.017957
P	0.820599	0.916979	-0.965550
O	1.757961	1.357117	-2.056188
O	1.035660	1.723055	0.479767
C	0.802315	-0.771885	-0.345414
C	2.090280	-1.441381	-0.067060
C	-0.416030	-1.351013	-0.082029
H	-0.405446	-2.377446	0.310910
C	2.202945	-2.391453	0.979972
H	1.343713	-2.582932	1.631009
C	3.396571	-3.061213	1.228005
H	3.481481	-3.784017	2.045057
C	4.536218	-2.797057	0.438806
O	5.659599	-3.507270	0.766485
C	6.838726	-3.253369	0.005134
H	6.692779	-3.496382	-1.064766
H	7.612857	-3.911511	0.426048
H	7.163411	-2.199307	0.096579
C	4.454207	-1.844043	-0.592870
H	5.320922	-1.613368	-1.217158
C	3.246660	-1.177823	-0.835246
H	3.196064	-0.442827	-1.644379
C	1.045445	3.118204	0.579867
C	1.773483	3.937778	-0.298418
H	2.336103	3.483039	-1.117534
C	1.758579	5.325709	-0.096178
H	2.323815	5.969148	-0.779050
C	1.042514	5.890524	0.969082

H	1.043200	6.974706	1.120501
C	0.329212	5.056033	1.842907
H	-0.231177	5.485076	2.680358
C	0.323658	3.668843	1.649976
H	-0.227866	2.999898	2.317153

 Statistical Thermodynamic Analysis

Temperature= 298.150 Kelvin Pressure= 1.00000 Atm
 =====

SCF Energy= -1588.44569629 Predicted Change= -2.458265D-09
 Zero-point correction (ZPE)= -1587.9992 0.44641
 Internal Energy (U)= -1587.9708 0.47488
 Enthalpy (H)= -1587.9698 0.47582
 Gibbs Free Energy (G)= -1588.0606 0.38507

Frequencies -- 8.4463 20.2689 25.2397
 Single points at WB97X/6-311++G2(df,p): -1590.2295
 Solvation Correction at PBE/6-31+G(d,p)/auto/Chloroform: -0.03308909

Heterocycle **1c**

Supporting Information: 0006.log

Using Gaussian 09: AM64L-G09RevD.01 24-Apr-2013
 =====

pbepbe/6-31G*/auto gfpri nt gfinpu t scf=(direct,tight,maxcycle=300,xqc)
 opt=(maxcycle=250) freq=norm an iop(1/8=18) Temperature=298.15
 #N Geom=AllCheck Guess=TChe ck SCRF=Check Test GenChk RPBEPBE/6-
 31G(d)/Auto
 Freq

Pointgroup= C1 Stoichiometry= C21H18NO3P C1[X(C21H18NO3P)] #Atoms= 44
 Charge = 0 Multiplicity = 1

SCF Energy= -1431.41483237 Predicted Change= -5.835733D-09
 =====

Optimization completed. {Found 2 times}
 Item Max Val. Criteria Pass? RMS Val. Criteria Pass?
 Force 0.00002 || 0.00045 [YES] 0.00000 || 0.00030 [YES]
 Displ 0.00140 || 0.00180 [YES] 0.00140 || 0.00180 [YES]

Atomic	Coordinates (Angstroms)		
Type	X	Y	Z

C	1.433626	2.630608	0.146780
C	1.859537	3.860849	0.703689
H	1.122554	4.465520	1.244821
C	3.172869	4.309268	0.574235
H	3.476686	5.262390	1.016961
C	4.101174	3.527162	-0.137554
H	5.135531	3.867528	-0.250905
C	3.715702	2.309345	-0.702004
H	4.440498	1.699407	-1.253364
C	2.392275	1.846526	-0.561721
N	1.991530	0.652064	-1.155172
H	2.664314	0.187357	-1.768411
P	0.553572	-0.216132	-0.868561
O	0.155176	-1.010696	-2.081524
O	0.815094	-1.142027	0.493293
C	-0.518345	1.041423	-0.157168
C	-1.950466	0.727478	0.028780
C	0.050566	2.222662	0.253650
H	-0.620481	2.972298	0.695882
C	-2.680662	1.281282	1.111128
H	-2.163124	1.897198	1.853748
C	-4.037884	1.026150	1.277219
H	-4.594193	1.445006	2.121166
C	-4.720420	0.192144	0.365995
O	-6.051683	0.003270	0.621216
C	-6.771396	-0.856833	-0.260344
H	-6.359364	-1.883937	-0.252813
H	-6.768109	-0.471934	-1.297983
H	-7.803860	-0.875056	0.118103
C	-4.012609	-0.384068	-0.704717
H	-4.512158	-1.038502	-1.423231
C	-2.647260	-0.117781	-0.863903
H	-2.109617	-0.568053	-1.703996
C	1.615506	-2.290938	0.483052
C	1.429858	-3.326292	-0.447323
H	0.668321	-3.221351	-1.223673
C	2.239826	-4.467548	-0.358688
H	2.101147	-5.277262	-1.083105
C	3.211536	-4.583155	0.646061
H	3.834640	-5.481041	0.709328
C	3.377460	-3.542913	1.572752
H	4.130862	-3.623887	2.363464
C	2.583697	-2.391153	1.493370
H	2.695826	-1.567833	2.205020

Statistical Thermodynamic Analysis

Temperature= 298.150 Kelvin Pressure= 1.00000 Atm

```
=====
SCF Energy=   -1431.41483237   Predicted Change= -5.835733D-09
Zero-point correction (ZPE)=           -1431.0785  0.33628
Internal Energy (U)=           -1431.0558  0.35901
Enthalpy (H)=           -1431.0548  0.35995
Gibbs Free Energy (G)=           -1431.1330  0.28175
=====
```

```
-----
Frequencies --   13.3909           23.0996           31.2795
Single points at WB97X/6-311++G2(df,p): -1432.9668
Solvation Correction at PBE/6-31+G(d,p)/auto/Chloroform: -0.03086346
```

***Geometry optimizations of heterocycle 1 dimers with chloroform model:
R-S-Heterodimers***

Dimeric heterocycle **1g**

Supporting Information: polymerdetector-r-s-dimer-6-c-ch3-3-25-0004.log

```
-----
Using Gaussian 09: AM64L-G09RevD.01 24-Apr-2013
=====
```

```
=====
# pbepbe/6-31G*/auto gfprint ginput scf=(direct,tight,maxcycle=300,xqc)
opt=(maxcycle=250) freq=norman iop(1/8=18) Temperature=298.15
#N Geom=AllCheck Guess=TCheck SCRF=Check Test GenChk RPBEPBE/6-
31G(d)/Auto
Freq
=====
```

```
-----
Pointgroup= C1  Stoichiometry= C50H46N4O4P2  C1[X(C50H46N4O4P2)] #Atoms=
106
Charge = 0    Multiplicity = 1
=====
```

```
-----
SCF Energy= -3132.42114258    Predicted Change= -1.859898D-08
=====
```

```
=====
Optimization completed.    {Found    1    times}
Item    Max Val.    Criteria    Pass?    RMS Val.    Criteria    Pass?
Force    0.00000 || 0.00045 [ YES ]    0.00000 || 0.00030 [ YES ]
Displ    0.00444 || 0.00180 [ NO ]    0.00444 || 0.00180 [ YES ]
=====
```

```
-----
Atomic       Coordinates (Angstroms)
Type       X       Y       Z
=====
```

```
-----
C    -4.254132    -0.810428    0.290434
C    -5.356290    -1.705764    0.261682
H    -6.350106    -1.265182    0.131788
C    -5.211752    -3.088080    0.389654
=====
```

C	-6.399881	-4.068504	0.371835
C	-7.751792	-3.345605	0.205616
H	-7.945260	-2.640989	1.033475
H	-8.569764	-4.086522	0.202297
H	-7.805709	-2.787912	-0.745916
C	-6.432658	-4.857890	1.704510
H	-5.501700	-5.426969	1.868728
H	-7.269483	-5.579248	1.700792
H	-6.568402	-4.178155	2.563482
C	-6.231127	-5.059340	-0.807105
H	-6.227097	-4.526557	-1.773914
H	-7.063697	-5.785414	-0.818028
H	-5.290151	-5.630733	-0.732308
C	-3.887650	-3.580404	0.537562
H	-3.721238	-4.658720	0.637133
C	-2.778552	-2.740210	0.567545
H	-1.767980	-3.145534	0.682443
C	-2.943915	-1.342816	0.456847
N	-1.834349	-0.509132	0.463397
H	-0.896655	-0.971242	0.430023
P	-1.835262	1.174706	0.521459
O	-0.688159	1.756607	-0.285654
O	-1.765058	1.647653	2.112400
C	-3.529487	1.608759	0.131427
C	-3.882261	3.029732	-0.073891
C	-4.467310	0.600866	0.100348
H	-5.501659	0.891114	-0.132590
C	-5.149926	3.521541	0.323092
H	-5.848639	2.857535	0.841279
C	-5.512974	4.848729	0.103291
H	-6.493492	5.213988	0.422295
C	-4.604503	5.738591	-0.514090
C	-3.329217	5.266811	-0.896791
H	-2.622440	5.952882	-1.372675
C	-2.975957	3.935281	-0.678749
H	-1.989427	3.577840	-0.987871
C	-0.547911	1.595191	2.814414
C	-0.378980	0.590304	3.775927
H	-1.172818	-0.146915	3.926927
C	0.803405	0.559205	4.528474
H	0.940931	-0.222271	5.282893
C	1.804143	1.518852	4.316512
H	2.726636	1.488637	4.904994
C	1.619444	2.517776	3.348865
H	2.398571	3.267080	3.174408
C	0.439656	2.564903	2.593526

H	0.276325	3.335735	1.836398
C	-4.970002	7.104304	-0.738415
N	-5.270877	8.227091	-0.924292
P	1.835260	-1.174714	-0.521463
O	1.765070	-1.647669	-2.112401
C	0.547930	-1.595219	-2.814427
O	0.688154	-1.756616	0.285644
C	3.529485	-1.608754	-0.131417
C	3.882269	-3.029724	0.073907
N	1.834336	0.509124	-0.463408
H	0.896636	0.971225	-0.430032
C	4.467301	-0.600854	-0.100335
H	5.501651	-0.891095	0.132610
C	4.254115	0.810437	-0.290427
C	2.943895	1.342817	-0.456851
C	0.379011	-0.590350	-3.775961
H	1.172853	0.146864	-3.926967
C	-0.803365	-0.559262	-4.528521
H	-0.940881	0.222200	-5.282957
C	-1.804109	-1.518903	-4.316552
H	-2.726595	-1.488696	-4.905044
C	-1.619422	-2.517808	-3.348884
H	-2.398552	-3.267107	-3.174421
C	-0.439642	-2.564925	-2.593531
H	-0.276321	-3.335742	-1.836387
C	2.778524	2.740209	-0.567558
H	1.767950	3.145525	-0.682466
C	3.887616	3.580410	-0.537570
H	3.721198	4.658724	-0.637153
C	5.211720	3.088096	-0.389647
C	6.399843	4.068527	-0.371836
C	6.231100	5.059355	0.807113
H	6.227089	4.526566	1.773919
H	5.290119	5.630743	0.732333
H	7.063665	5.785435	0.818027
C	6.432596	4.857920	-1.704507
H	6.568332	4.178190	-2.563484
H	7.269417	5.579283	-1.700797
H	5.501632	5.426993	-1.868709
C	7.751760	3.345633	-0.205640
H	7.805704	2.787960	0.745903
H	8.569730	4.086552	-0.202358
H	7.945206	2.641001	-1.033489
C	5.356267	1.705781	-0.261673
H	6.350085	1.265206	-0.131776
C	2.975970	-3.935280	0.678761

H	1.989436	-3.577848	0.987876
C	3.329242	-5.266806	0.896807
H	2.622469	-5.952883	1.372689
C	4.604536	-5.738574	0.514118
C	5.513003	-4.848705	-0.103259
H	6.493527	-5.213954	-0.422254
C	5.149942	-3.521521	-0.323065
H	5.848654	-2.857508	-0.841247
C	4.970049	-7.104282	0.738451
N	5.270918	-8.227071	0.924328

 Statistical Thermodynamic Analysis

Temperature= 298.150 Kelvin Pressure= 1.00000 Atm
 =====

=====

SCF Energy=	-3132.42114258	Predicted Change=	-1.859898D-08
Zero-point correction (ZPE)=			-3131.5942 0.82689
Internal Energy (U)=			-3131.5370 0.88412
Enthalpy (H)=			-3131.5360 0.88507
Gibbs Free Energy (G)=			-3131.6958 0.72529

Frequencies -- 4.8989 8.6250 9.7633
 Single points at WB97X/6-311++G2(df,p): -3135.9149
 Solvation Correction at PBE/6-31+G(d,p)/auto/Chloroform: -0.05950948

Dimeric heterocycle **1e**

Supporting Information: polymerdetector-r-s-dimer-6-cf3-25-0014.log

 Using Gaussian 09: AM64L-G09RevD.01 24-Apr-2013
 =====

=====

```
# pbepbe/6-31G*/auto gfprint gfinput scf=(direct,tight,maxcycle=300,xqc)
opt=(maxcycle=250) freq=noraman iop(1/8=18) Temperature=298.15
#N Geom=AllCheck Guess=TCheck SCRF=Check Test GenChk RPBEPBE/6-
31G(d)/Auto
Freq
```

Pointgroup= C1 Stoichiometry= C44H28F6N4O4P2 C1[X(C44H28F6N4O4P2)]
 #Atoms= 88
 Charge = 0 Multiplicity = 1

SCF Energy=	-3491.81477091	Predicted Change=	-9.627271D-09
-------------	----------------	-------------------	---------------

=====

=====

Optimization completed.		{Found	1	times}		
Item	Max Val.	Criteria	Pass?	RMS Val.	Criteria	Pass?

Force 0.00001 || 0.00045 [YES] 0.00000 || 0.00030 [YES]
 Displ 0.00211 || 0.00180 [NO] 0.00211 || 0.00180 [YES]

Atomic Type	Coordinates (Angstroms)		
	X	Y	Z
C	-4.307926	-0.842193	0.340389
C	-5.428085	-1.706567	0.314631
H	-6.427782	-1.274365	0.205984
C	-5.280707	-3.085610	0.430042
C	-6.472034	-4.002569	0.358180
F	-6.416583	-4.968086	1.318584
F	-6.533134	-4.651375	-0.841453
F	-7.646439	-3.332560	0.512554
C	-3.987276	-3.638922	0.569555
H	-3.871129	-4.722197	0.672871
C	-2.865974	-2.818230	0.591924
H	-1.862460	-3.239869	0.706900
C	-3.007955	-1.414816	0.480508
N	-1.882030	-0.612298	0.482558
H	-0.955718	-1.098652	0.462976
P	-1.811876	1.075990	0.468163
O	-0.736466	1.589266	-0.471578
O	-1.546179	1.579533	2.022563
C	-3.519612	1.554820	0.217023
C	-3.838516	2.995340	0.103393
C	-4.489579	0.579870	0.200892
H	-5.525784	0.908398	0.039720
C	-2.953069	3.897883	-0.535310
H	-2.013329	3.523174	-0.951920
C	-3.271232	5.251158	-0.653914
H	-2.583033	5.936558	-1.157061
C	-4.488968	5.744909	-0.135863
C	-5.375908	4.856056	0.513138
H	-6.310589	5.237426	0.934248
C	-5.047301	3.506951	0.633869
H	-5.723400	2.840167	1.177879
C	-0.271205	1.984077	2.456843
C	0.692273	1.025954	2.798441
H	0.472966	-0.039330	2.677976
C	1.934202	1.459344	3.285174
H	2.694123	0.717424	3.551471
C	2.201294	2.828059	3.435177
H	3.171529	3.159367	3.818370
C	1.220988	3.772014	3.094040
H	1.422906	4.841675	3.211156

C	-0.022342	3.354329	2.599701
H	-0.801527	4.071553	2.325141
C	-4.817308	7.133352	-0.256767
N	-5.086302	8.274768	-0.356769
P	1.787213	-1.324966	-0.504910
O	1.697241	-1.910851	-2.055968
C	0.478699	-1.848633	-2.761932
O	0.651557	-1.840417	0.357670
C	3.479742	-1.725803	-0.072817
C	3.817556	-3.105809	0.339643
N	1.792045	0.362094	-0.586798
H	0.852449	0.824072	-0.586152
C	4.419640	-0.722134	-0.113672
H	5.458437	-1.004551	0.107605
C	4.207874	0.671756	-0.413730
C	2.895352	1.197327	-0.613085
C	-0.529046	-2.788729	-2.509881
H	-0.382992	-3.539735	-1.728994
C	-1.708072	-2.739710	-3.266699
H	-2.502476	-3.467493	-3.072253
C	-1.870941	-1.765558	-4.263083
H	-2.792388	-1.733794	-4.852883
C	-0.850018	-0.834408	-4.503791
H	-0.970907	-0.073632	-5.281620
C	0.332873	-0.868951	-3.751915
H	1.143345	-0.155749	-3.927389
C	2.714957	2.587525	-0.796567
H	1.698458	2.978251	-0.904291
C	3.814873	3.436658	-0.826359
H	3.668220	4.511546	-0.968383
C	5.123095	2.926281	-0.666725
C	6.301567	3.857003	-0.769018
F	6.594659	4.157890	-2.066869
F	7.426417	3.321656	-0.219055
F	6.057344	5.041664	-0.139712
C	5.306358	1.562439	-0.455766
H	6.315594	1.166066	-0.305495
C	3.210233	-4.230417	-0.267194
H	2.482030	-4.083113	-1.069843
C	3.555108	-5.526589	0.114422
H	3.085730	-6.387691	-0.369734
C	4.523362	-5.736701	1.121539
C	5.132314	-4.622229	1.741087
H	5.870315	-4.780700	2.532642
C	4.775133	-3.330533	1.356905
H	5.223148	-2.475100	1.872305

C	4.879676	-7.066179	1.516508
N	5.173433	-8.158696	1.840783

Statistical Thermodynamic Analysis

Temperature= 298.150 Kelvin Pressure= 1.00000 Atm
=====

=====

SCF Energy=	-3491.81477091	Predicted Change=	-9.627271D-09
Zero-point correction (ZPE)=	-3491.1993	0.61542	
Internal Energy (U)=	-3491.1460	0.66868	
Enthalpy (H)=	-3491.1451	0.66963	
Gibbs Free Energy (G)=	-3491.2990	0.51575	

Frequencies -- 5.2568 6.9680 11.8537
Single points at WB97X/6-311++G2(df,p): -3495.5933
Solvation Correction at PBE/6-31+G(d,p)/auto/Chloroform: -0.05570801

Dimeric heterocycle **1b**

Supporting Information: 0015.log

Using Gaussian 09: AM64L-G09RevD.01 24-Apr-2013
=====

=====

```
# pbepbe/6-31G*/auto gfpri n gfinpu t scf=(direct,tight,maxcycle=300,xqc)
opt=(maxcycle=250) freq=noraman iop(1/8=18) Temperature=298.15
#N Geom=AllCheck Guess=TCheck SCRF=Check Test GenChk RPBEPBE/6-
31G(d)/Auto
Freq
```

Pointgroup= C1 Stoichiometry= C42H30N4O4P2 C1[X(C42H30N4O4P2)] #Atoms= 82
Charge = 0 Multiplicity = 1

SCF Energy=	-2818.35838883	Predicted Change=	-2.252437D-07
-------------	----------------	-------------------	---------------

=====

=====

Optimization completed.	{Found 1 times}					
Item	Max Val.	Criteria	Pass?	RMS Val.	Criteria	Pass?
Force	0.00000	0.00045	[YES]	0.00000	0.00030	[YES]
Displ	0.02410	0.00180	[NO]	0.02410	0.00180	[NO]

Atomic Type	Coordinates (Angstroms)		
	X	Y	Z

C	-2.447119	-3.499944	0.909628
C	-2.633343	-4.894051	1.094337

H	-3.650528	-5.295644	1.018412
C	-1.563283	-5.740766	1.364866
H	-1.728574	-6.812434	1.508548
C	-0.262631	-5.201882	1.454394
H	0.586414	-5.857919	1.673054
C	-0.040592	-3.836935	1.276613
H	0.965964	-3.413078	1.353671
C	-1.124330	-2.972433	1.004713
N	-0.889167	-1.621399	0.796489
H	0.110230	-1.323712	0.721199
P	-2.027084	-0.393261	0.597346
O	-2.262172	0.338089	2.067287
C	-1.630647	1.535094	2.435182
O	-1.601391	0.608215	-0.460107
C	-3.568948	-1.288214	0.416081
C	-4.805625	-0.523998	0.142498
C	-3.568905	-2.652040	0.602119
H	-4.529742	-3.171691	0.480234
C	-6.049097	-0.957532	0.664068
H	-6.084676	-1.834317	1.318015
C	-7.228179	-0.265007	0.395959
H	-8.179109	-0.609980	0.812275
C	-7.197729	0.904264	-0.397901
C	-5.961924	1.359144	-0.908863
H	-5.933493	2.264576	-1.522073
C	-4.787430	0.655230	-0.642673
H	-3.837590	1.010590	-1.053242
C	-0.234282	1.630157	2.516873
H	0.398422	0.776891	2.251857
C	0.337380	2.837301	2.944110
H	1.427615	2.919648	3.004254
C	-0.472940	3.925740	3.297900
H	-0.018411	4.862663	3.635043
C	-1.868674	3.808043	3.220031
H	-2.509012	4.652274	3.496015
C	-2.454930	2.612452	2.783831
H	-3.540368	2.498968	2.709156
C	-8.404528	1.624479	-0.670566
N	-9.396812	2.216517	-0.895256
P	2.211381	0.207720	-0.607235
O	2.477935	-0.600641	-2.038228
C	1.486009	-1.447786	-2.567229
O	1.779767	-0.737147	0.499345
C	3.741428	1.126644	-0.443435
C	4.945197	0.449809	0.082898
N	1.061795	1.406922	-0.882817

H	0.063189	1.123406	-0.749763
C	3.741932	2.454503	-0.808943
H	4.704412	2.983127	-0.756699
C	2.625549	3.247903	-1.254705
C	1.297667	2.722716	-1.257977
C	0.744927	-0.997358	-3.667532
H	0.924523	0.007024	-4.061750
C	-0.206783	-1.851441	-4.242042
H	-0.788321	-1.507061	-5.103340
C	-0.416335	-3.135481	-3.717329
H	-1.163509	-3.796555	-4.167694
C	0.334068	-3.570690	-2.614934
H	0.171492	-4.568486	-2.194655
C	1.294695	-2.730031	-2.035803
H	1.887562	-3.051469	-1.175688
C	0.211411	3.556258	-1.601260
H	-0.801614	3.142734	-1.565929
C	0.438824	4.880799	-1.971674
H	-0.412626	5.514141	-2.241302
C	1.746338	5.409005	-2.004370
H	1.915156	6.448114	-2.301418
C	2.817631	4.598767	-1.642850
H	3.838480	4.998177	-1.644603
C	5.208418	-0.912597	-0.195763
H	4.516035	-1.477360	-0.826586
C	6.356631	-1.538027	0.288253
H	6.551423	-2.589196	0.057042
C	7.283766	-0.814398	1.071202
C	7.030407	0.544971	1.363276
H	7.736607	1.104469	1.983512
C	5.875009	1.158029	0.881306
H	5.669702	2.198874	1.150792
C	8.463972	-1.452896	1.570296
N	9.434862	-1.977555	1.979602

Statistical Thermodynamic Analysis

Temperature= 298.150 Kelvin Pressure= 1.00000 Atm
=====

=====

SCF Energy=	-2818.35838883	Predicted Change=	-2.252437D-07
Zero-point correction (ZPE)=			-2817.7513 0.60700
Internal Energy (U)=			-2817.7057 0.65262
Enthalpy (H)=			-2817.7048 0.65356
Gibbs Free Energy (G)=			-2817.8396 0.51873

Frequencies --	4.2468	8.3317	13.2541
----------------	--------	--------	---------

Single points at WB97X/6-311++G2(df,p): -2821.3888
Solvation Correction at PBE/6-31+G(d,p)/auto/Chloroform: -0.05543327

Dimeric heterocycle **1p**

Supporting Information: 1-cn-2-eto-5.log

Using Gaussian 09: AM64L-G09RevD.01 24-Apr-2013
=====

=====

```
#PBEPBE/6-31G(d)/auto gfpri gfinpu scf=(direct,tight,maxcycle=300,xqc)
opt=(maxcycle=250) freq=noraman
#P Geom=AllCheck Guess=TCheck SCRF=Check Test GenChk RPBEPBE/6-
31G(d)/Auto
Freq
```

```
Pointgroup= C1  Stoichiometry= C46H38N4O6P2  C1[X(C46H38N4O6P2)] #Atoms=
96
Charge = 0  Multiplicity = 1
```

```
SCF Energy= -3125.67367442      Predicted Change= -1.462814D-07
```

=====

```
Optimization completed.      {Found 1 times}
Item  Max Val.  Criteria  Pass?  RMS Val.  Criteria  Pass?
Force  0.00017 || 0.00045 [ YES ]  0.00003 || 0.00030 [ YES ]
Displ  0.00200 || 0.00180 [ NO ]   0.00200 || 0.00180 [ YES ]
```

Atomic Type	Coordinates (Angstroms)		
	X	Y	Z
C	-4.139498	-1.885553	0.263789
C	-4.950636	-3.044729	0.408778
H	-6.031258	-2.933358	0.285107
C	-4.381540	-4.286589	0.696620
C	-2.974453	-4.387785	0.831333
H	-2.543433	-5.368967	1.051489
C	-2.163325	-3.268582	0.692751
H	-1.076873	-3.351076	0.799722
C	-2.729302	-2.002778	0.420673
N	-1.903580	-0.894893	0.252523
H	-0.874950	-1.070571	0.197562
P	-2.395901	0.712210	0.195430
O	-1.447843	1.547001	-0.646408
O	-2.523045	1.286491	1.750447
C	-4.133963	0.597161	-0.230026

C	-4.871458	1.816815	-0.621314
C	-4.746041	-0.629980	-0.101083
H	-5.817328	-0.679267	-0.341813
C	-4.245332	2.850874	-1.360618
H	-3.189994	2.751429	-1.630414
C	-4.957902	3.982248	-1.757535
H	-4.464082	4.767857	-2.336890
C	-6.323480	4.119600	-1.423167
C	-6.955736	3.102774	-0.671556
H	-8.006843	3.214366	-0.389867
C	-6.235962	1.977499	-0.275535
H	-6.729729	1.220335	0.341379
C	-1.365858	1.611793	2.478982
C	-0.733906	2.845983	2.276169
H	-1.124037	3.530533	1.518566
C	0.388047	3.171457	3.050665
H	0.892984	4.129377	2.889223
C	0.865159	2.275420	4.019072
H	1.740812	2.535159	4.622482
C	0.217215	1.046694	4.214139
H	0.584214	0.344720	4.970036
C	-0.902672	0.705729	3.442354
H	-1.424190	-0.246042	3.579367
C	-7.057235	5.279400	-1.830095
N	-7.661326	6.232447	-2.165617
C	-6.498953	-5.413693	0.728141
H	-6.767422	-5.047382	-0.283791
O	-5.071371	-5.458997	0.863669
C	-7.025943	-6.821659	0.957063
H	-6.757995	-7.178980	1.964762
H	-8.124605	-6.833321	0.862903
H	-6.604555	-7.520668	0.216302
H	-6.922367	-4.704194	1.468219
P	1.852321	-0.408350	-0.555758
O	1.997016	-0.690075	-2.187917
C	2.349160	-1.933559	-2.734722
O	0.879319	-1.370117	0.103803
C	3.526878	-0.327962	0.089012
C	4.258393	-1.574240	0.404650
N	1.345399	1.185353	-0.534544
H	0.315244	1.345916	-0.617723
C	4.117168	0.912181	0.199770
H	5.147296	0.939390	0.582288
C	3.526242	2.197134	-0.072418
C	2.151684	2.314624	-0.419866
C	3.382402	-1.929663	-3.682435

H	3.885987	-0.987106	-3.916225
C	3.739903	-3.128968	-4.311997
H	4.545470	-3.128533	-5.053632
C	3.074105	-4.321989	-3.993798
H	3.357177	-5.258083	-4.485356
C	2.041102	-4.308170	-3.045392
H	1.512560	-5.234605	-2.797016
C	1.665261	-3.115074	-2.412141
H	0.858210	-3.087272	-1.676509
C	1.589355	3.597295	-0.605389
H	0.528899	3.677601	-0.864237
C	2.372499	4.736750	-0.468689
H	1.945318	5.732276	-0.622125
C	3.746866	4.637991	-0.136944
C	4.309916	3.376523	0.062752
H	5.364087	3.263757	0.330004
C	3.601002	-2.701133	0.956974
H	2.523871	-2.653957	1.138753
C	4.309639	-3.857207	1.283052
H	3.790061	-4.716531	1.716944
C	5.703343	-3.926854	1.063375
C	6.369262	-2.814957	0.498983
H	7.444528	-2.870669	0.305806
C	5.653198	-1.665546	0.171768
H	6.176279	-0.830022	-0.303830
C	6.432425	-5.112104	1.398791
N	7.032598	-6.086006	1.676568
C	5.806764	5.787455	0.298631
H	5.940145	5.284043	1.278088
O	4.412939	5.832143	-0.036985
C	6.313290	7.220498	0.347938
H	7.385713	7.232880	0.604525
H	6.182251	7.714190	-0.628817
H	5.765818	7.801725	1.107802
H	6.356166	5.196533	-0.462568

Statistical Thermodynamic Analysis

Temperature= 298.150 Kelvin Pressure= 1.00000 Atm

=====

=====

SCF Energy= -3125.67367442 Predicted Change= -1.462814D-07
Zero-point correction (ZPE)= -3124.9479 0.72574
Internal Energy (U)= -3124.8940 0.77966
Enthalpy (H)= -3124.8930 0.78061
Gibbs Free Energy (G)= -3125.0475 0.62611

Frequencies -- 3.6817 6.6552 11.4552
Single points at WB97X/6-311++G2(df,p): -3129.0918
Solvation Correction at PBE/6-31+G(d,p)/auto/Chloroform: -0.05959069

Dimeric heterocycle **1j**

Supporting Information: 0018.log

Using Gaussian 09: AM64L-G09RevD.01 24-Apr-2013
=====

=====
pbepbe/6-31G*/auto gfprint ginput scf=(direct,tight,maxcycle=300,xqc)
opt=(maxcycle=250) freq=noraman iop(1/8=18) Temperature=298.15
#N Geom=AllCheck Guess=TCheck SCRF=Check Test GenChk RPBEPBE/6-
31G(d)/Auto
Freq

Pointgroup= C1 Stoichiometry= C48H48N2O4P2 C1[X(C48H48N2O4P2)] #Atoms=
104
Charge = 0 Multiplicity = 1

SCF Energy= -2948.13012412 Predicted Change= -1.531703D-08
=====

=====
Optimization completed. {Found 2 times}
Item Max Val. Criteria Pass? RMS Val. Criteria Pass?
Force 0.00001 || 0.00045 [YES] 0.00000 || 0.00030 [YES]
Displ 0.00168 || 0.00180 [YES] 0.00168 || 0.00180 [YES]

Atomic Type	Coordinates (Angstroms)		
	X	Y	Z
C	4.253562	-0.886991	0.254948
C	5.609251	-0.463912	0.267596
H	6.364477	-1.213928	0.010874
C	5.991513	0.841169	0.582211
C	7.457515	1.313851	0.590671
C	7.822566	1.837490	2.002218
H	7.173028	2.674339	2.311058
H	8.866506	2.199662	2.019006
H	7.723634	1.038208	2.756985
C	7.632659	2.457599	-0.440139
H	6.978855	3.317147	-0.214023
H	7.391047	2.109446	-1.459669
H	8.676631	2.819968	-0.438377
C	8.439608	0.182318	0.226601

H	9.474212	0.566252	0.248783
H	8.253212	-0.212347	-0.787768
H	8.380304	-0.657182	0.941438
C	4.949657	1.754760	0.893132
H	5.195980	2.794003	1.136849
C	3.609684	1.382838	0.896924
H	2.824695	2.112360	1.120822
C	3.240765	0.057181	0.583225
N	1.900904	-0.302085	0.571784
H	1.206882	0.468218	0.706588
P	1.236189	-1.801600	0.185312
O	0.097414	-1.690992	-0.816531
O	0.709236	-2.472699	1.609911
C	2.666590	-2.801449	-0.204897
C	2.456569	-4.225465	-0.559282
C	3.919154	-2.237228	-0.116825
H	4.770807	-2.879675	-0.382942
C	1.327396	-4.643761	-1.303405
H	0.592148	-3.899484	-1.625482
C	1.156354	-5.991647	-1.642953
H	0.278369	-6.291764	-2.225127
C	2.103128	-6.950269	-1.254993
H	1.966659	-8.003039	-1.523551
C	3.222937	-6.550083	-0.510252
H	3.960369	-7.291541	-0.184370
C	3.393614	-5.206801	-0.159403
H	4.247590	-4.912532	0.459898
C	-0.648842	-2.583136	1.936359
C	-1.335026	-1.481638	2.465756
H	-0.824762	-0.518136	2.560848
C	-2.674587	-1.636766	2.849895
H	-3.220083	-0.777373	3.253079
C	-3.313477	-2.878365	2.715975
H	-4.360191	-2.992088	3.016060
C	-2.608935	-3.972039	2.190704
H	-3.101771	-4.944383	2.084921
C	-1.271612	-3.830110	1.794971
H	-0.703025	-4.667155	1.378415
P	-1.236214	1.801395	-0.185467
O	-0.709106	2.472295	-1.610094
C	0.649050	2.582681	-1.936418
O	-0.097518	1.690706	0.816458
C	-2.666505	2.801501	0.204525
C	-2.456257	4.225556	0.558644
N	-1.901156	0.301942	-0.571890
H	-1.207309	-0.468559	-0.706400

C	-3.919152	2.237467	0.116540
H	-4.770708	2.880127	0.382453
C	-4.253739	0.887185	-0.254908
C	-3.241068	-0.057170	-0.583018
C	1.335188	1.481153	-2.465784
H	0.824831	0.517711	-2.560993
C	2.674814	1.636219	-2.849740
H	3.220333	0.776809	-3.252854
C	3.313763	2.877772	-2.715676
H	4.360525	2.991440	-3.015618
C	2.609229	3.971481	-2.190461
H	3.102121	4.943785	-2.084587
C	1.271848	3.829620	-1.794898
H	0.703257	4.666669	-1.378362
C	-3.610168	-1.382868	-0.896366
H	-2.825282	-2.112522	-1.120208
C	-4.950176	-1.754645	-0.892375
H	-5.196640	-2.793917	-1.135823
C	-5.991915	-0.840856	-0.581613
C	-7.457976	-1.313362	-0.589939
C	-7.633270	-2.456914	0.441051
H	-8.677300	-2.819117	0.439362
H	-7.391592	-2.108642	1.460524
H	-6.979616	-3.316612	0.215067
C	-7.823110	-1.837183	-2.001405
H	-7.724040	-1.038041	-2.756300
H	-8.867109	-2.199189	-2.018136
H	-7.173696	-2.674185	-2.310090
C	-8.439917	-0.181644	-0.226036
H	-8.380526	0.657731	-0.941013
H	-8.253443	0.213162	0.788263
H	-9.474572	-0.565446	-0.248135
C	-5.609479	0.464258	-0.267364
H	-6.364592	1.214437	-0.010784
C	-3.393000	5.207000	0.158346
H	-4.246910	4.912770	-0.461065
C	-3.222107	6.550325	0.508934
H	-3.959305	7.291872	0.182727
C	-2.102381	6.950429	1.253842
H	-1.965744	8.003228	1.522199
C	-1.155909	5.991686	1.642242
H	-0.277999	6.291741	2.224561
C	-1.327168	4.643762	1.302950
H	-0.592155	3.899395	1.625355

Statistical Thermodynamic Analysis

Temperature= 298.150 Kelvin Pressure= 1.00000 Atm

```
=====
SCF Energy= -2948.13012412    Predicted Change= -1.531703D-08
Zero-point correction (ZPE)= -2947.3000 0.83009
Internal Energy (U)= -2947.2465 0.88353
Enthalpy (H)= -2947.2456 0.88447
Gibbs Free Energy (G)= -2947.3943 0.73574
-----
```

Frequencies -- 4.3339 12.4357 15.4786

Single points at WB97X/6-311++G2(df,p):

Solvation Correction at PBE/6-31+G(d,p)/auto/Chloroform:

Dimeric heterocycle **1m**

Supporting Information: 0005.log

Using Gaussian 09: AM64L-G09RevD.01 24-Apr-2013
=====

```
=====
# pbepbe/6-31G*/auto gfpint gfinput scf=(direct,tight,maxcycle=300,xqc)
opt=(maxcycle=250) freq=noraman iop(1/8=18) Temperature=298.15
#N Geom=AllCheck Guess=TCheck SCRF=Check Test GenChk RPBEPBE/6-
31G(d)/Auto
Freq
-----
```

Pointgroup= C1 Stoichiometry= C42H30N4O4P2 C1[X(C42H30N4O4P2)] #Atoms= 82

Charge = 0 Multiplicity = 1

SCF Energy= -2818.36002288 Predicted Change= -1.463986D-09
=====

```
=====
Optimization completed.            {Found    1    times}
Item    Max Val.    Criteria    Pass?    RMS Val.    Criteria    Pass?
Force    0.00000 || 0.00045    [ YES ]    0.00000 || 0.00030    [ YES ]
Displ    0.00255 || 0.00180    [ NO ]    0.00255 || 0.00180    [ YES ]
-----
```

Atomic Coordinates (Angstroms)

Atomic Type	X	Y	Z
C	-4.163177	-1.208498	0.535223
C	-5.185352	-2.173970	0.646497
H	-6.223624	-1.870526	0.476891
C	-4.899309	-3.510646	0.965807
C	-3.548741	-3.898689	1.176011
H	-3.322160	-4.938504	1.428414

C	-2.524596	-2.967470	1.068657
H	-1.482411	-3.259835	1.231411
C	-2.811581	-1.617739	0.752794
N	-1.777025	-0.712324	0.629527
H	-0.805202	-1.098932	0.667313
P	-1.884049	0.956234	0.365021
O	-1.705668	1.699771	1.832935
C	-0.490145	2.282075	2.230176
O	-0.843864	1.431397	-0.631766
C	-3.626475	1.211663	0.037844
C	-4.089460	2.579553	-0.296316
C	-4.488408	0.151313	0.174281
H	-5.550226	0.343704	-0.033130
C	-3.315465	3.441407	-1.108685
H	-2.352126	3.094145	-1.494353
C	-3.783167	4.720104	-1.435004
H	-3.173301	5.369688	-2.071746
C	-5.024628	5.166568	-0.960392
H	-5.386519	6.167578	-1.216926
C	-5.796203	4.325054	-0.144674
H	-6.758513	4.670199	0.247828
C	-5.332040	3.048799	0.189659
H	-5.921117	2.415441	0.861302
C	0.590907	1.479171	2.618242
H	0.514680	0.388686	2.564103
C	1.766618	2.098763	3.066665
H	2.617439	1.478680	3.367517
C	1.853455	3.496987	3.135375
H	2.773182	3.973159	3.489395
C	0.757534	4.283386	2.749443
H	0.818217	5.375344	2.802248
C	-0.421108	3.679170	2.290750
H	-1.287802	4.270383	1.980660
C	-5.953829	-4.471337	1.072926
N	-6.818801	-5.265432	1.158726
P	1.915469	-1.215377	-0.352615
O	1.771292	-1.979332	-1.820955
C	0.503866	-2.066513	-2.430607
O	0.867259	-1.692731	0.634773
C	3.653547	-1.444082	0.017355
C	4.120869	-2.754313	0.528823
N	1.782307	0.447375	-0.639511
H	0.805404	0.824785	-0.669091
C	4.500453	-0.373581	-0.139440
H	5.565128	-0.552739	0.064926
C	4.162349	0.973596	-0.536239

C	2.805866	1.367647	-0.751744
C	-0.386304	-3.079612	-2.051090
H	-0.106293	-3.772882	-1.253374
C	-1.624257	-3.175312	-2.701815
H	-2.328609	-3.959335	-2.405666
C	-1.961131	-2.271665	-3.720637
H	-2.928530	-2.351985	-4.226301
C	-1.055286	-1.267214	-4.092204
H	-1.312271	-0.560889	-4.888069
C	0.184592	-1.156867	-3.446882
H	0.906132	-0.382610	-3.722628
C	2.500475	2.716893	-1.049267
H	1.451882	3.004123	-1.174876
C	3.514947	3.656769	-1.168209
H	3.274532	4.697480	-1.403009
C	4.872633	3.279044	-0.987148
C	5.175454	1.946160	-0.668010
H	6.218239	1.652984	-0.508324
C	3.611047	-3.971702	0.022916
H	2.859597	-3.952499	-0.772177
C	4.088014	-5.197362	0.500956
H	3.686725	-6.129332	0.089310
C	5.079252	-5.235892	1.492162
H	5.448925	-6.196427	1.865458
C	5.588455	-4.035048	2.008336
H	6.351400	-4.053123	2.793637
C	5.110335	-2.807689	1.537350
H	5.483845	-1.874828	1.973236
C	5.916871	4.248634	-1.113349
N	6.773332	5.049958	-1.215766

Statistical Thermodynamic Analysis

Temperature= 298.150 Kelvin Pressure= 1.00000 Atm

=====

SCF Energy= -2818.36002288 Predicted Change= -1.463986D-09
Zero-point correction (ZPE)= -2817.7528 0.60718
Internal Energy (U)= -2817.7072 0.65277
Enthalpy (H)= -2817.7063 0.65371
Gibbs Free Energy (G)= -2817.8401 0.51983

Frequencies -- 6.6629 8.2195 11.1622

Single points at WB97X/6-311++G2(df,p): -2821.3924

Solvation Correction at PBE/6-31+G(d,p)/auto/Chloroform: -0.05603817

Dimeric heterocycle **1a**

Supporting Information: 0003.log

 Using Gaussian 09: AM64L-G09RevD.01 24-Apr-2013
 =====

=====

```
# pbepbe/6-31G*/auto gfpinput scf=(direct,tight,maxcycle=300,xqc)
opt=(maxcycle=250) freq=noraman iop(1/8=18) Temperature=298.15
#N Geom=AllCheck Guess=TCheck SCRF=Check Test GenChk RPBEPBE/6-
31G(d)/Auto
Freq
```

```
Pointgroup= C1  Stoichiometry= C40H32N2O4P2  C1[X(C40H32N2O4P2)] #Atoms=
80
Charge = 0  Multiplicity = 1
```

```
SCF Energy= -2634.06625433      Predicted Change= -3.719026D-08
```

=====

```
Optimization completed.      {Found      1      times}
Item  Max Val.  Criteria  Pass?  RMS Val.  Criteria  Pass?
Force  0.00001 || 0.00045 [ YES ]   0.00000 || 0.00030 [ YES ]
Displ  0.00447 || 0.00180 [ NO ]    0.00447 || 0.00180 [ YES ]
```

Atomic Type	Coordinates (Angstroms)		
	X	Y	Z
C	-3.334148	2.486946	-1.202693
C	-3.836091	3.720881	-1.687434
H	-4.910672	3.916458	-1.592765
C	-2.997633	4.671938	-2.261933
H	-3.406029	5.617326	-2.631264
C	-1.615220	4.409787	-2.350797
H	-0.944137	5.156483	-2.788027
C	-1.085494	3.205294	-1.889094
H	-0.011999	2.998177	-1.946092
C	-1.936411	2.227169	-1.330508
N	-1.399758	1.032442	-0.866584
H	-0.356291	0.966668	-0.821943
P	-2.254391	-0.324444	-0.351229
O	-1.518729	-1.058965	0.754758
O	-2.510459	-1.306139	-1.675872
C	-3.908254	0.300423	-0.062506
C	-4.882552	-0.526781	0.685069
C	-4.213374	1.552865	-0.542304
H	-5.249094	1.894946	-0.405494
C	-5.808962	0.081753	1.562894

H	-5.762065	1.163945	1.725591
C	-6.756683	-0.683584	2.250856
H	-7.461003	-0.190581	2.929429
C	-6.790973	-2.076707	2.089934
H	-7.527503	-2.676713	2.634375
C	-5.868343	-2.695535	1.234014
H	-5.887256	-3.782283	1.099907
C	-4.923959	-1.932320	0.538547
H	-4.227902	-2.423014	-0.148879
C	-1.417876	-1.948298	-2.283774
C	-0.919159	-1.424361	-3.484046
H	-1.364441	-0.515212	-3.898429
C	0.138772	-2.081691	-4.127212
H	0.532922	-1.677175	-5.065224
C	0.693538	-3.244436	-3.572304
H	1.523674	-3.750435	-4.075413
C	0.183357	-3.756243	-2.369995
H	0.616419	-4.657984	-1.925030
C	-0.879486	-3.113300	-1.720596
H	-1.287793	-3.495479	-0.781540
P	2.111310	0.077483	0.439919
O	2.249749	0.957885	1.842556
C	1.423687	2.048649	2.140721
O	1.405744	0.874771	-0.641123
C	3.799602	-0.469033	0.200476
C	4.820879	0.529145	-0.196486
N	1.291183	-1.348998	0.810491
H	0.248619	-1.275292	0.820246
C	4.112871	-1.782292	0.461272
H	5.157803	-2.083650	0.300640
C	3.229131	-2.831517	0.903727
C	1.832262	-2.598235	1.075749
C	0.044725	1.885924	2.335783
H	-0.419548	0.902113	2.212209
C	-0.725954	3.003503	2.686588
H	-1.804936	2.883875	2.830515
C	-0.126123	4.259768	2.856945
H	-0.734699	5.126222	3.134978
C	1.257066	4.401190	2.669778
H	1.733507	5.378400	2.801671
C	2.038656	3.296561	2.306164
H	3.117288	3.383070	2.145613
C	0.987956	-3.653265	1.488490
H	-0.079622	-3.450859	1.623954
C	1.517697	-4.920851	1.728115
H	0.851658	-5.726396	2.054975

C	2.895792	-5.169790	1.562857
H	3.304823	-6.166098	1.755077
C	3.730730	-4.133292	1.155078
H	4.804435	-4.309418	1.020286
C	4.514611	1.588845	-1.082972
H	3.498544	1.678012	-1.479543
C	5.500513	2.507893	-1.462228
H	5.242764	3.317174	-2.153825
C	6.808646	2.393979	-0.970779
H	7.576663	3.115103	-1.269533
C	7.122813	1.354192	-0.082536
H	8.135704	1.265723	0.324885
C	6.140160	0.438022	0.306161
H	6.385352	-0.342367	1.034301

 Statistical Thermodynamic Analysis

Temperature= 298.150 Kelvin Pressure= 1.00000 Atm
 =====

=====

SCF Energy=	-2634.06625433	Predicted Change=	-3.719026D-08
Zero-point correction (ZPE)=		-2633.4560	0.61017
Internal Energy (U)=		-2633.4142	0.65198
Enthalpy (H)=		-2633.4133	0.65292
Gibbs Free Energy (G)=		-2633.5386	0.52763

Frequencies --	4.8961	8.0606	12.5771
----------------	--------	--------	---------

Single points at WB97X/6-311++G2(df,p): -2636.899
 Solvation Correction at PBE/6-31+G(d,p)/auto/Chloroform: -0.04980344

Heterocycle 1o*

Supporting Information: 1-h-2-co2me-dimer-8.log

 Using Gaussian 09: AM64L-G09RevD.01 24-Apr-2013
 =====

=====

```
#PBEPBE/6-31G(d)/auto gfpint gfinput scf=(direct,tight,maxcycle=300,xqc)
opt=(maxcycle=250) freq=noraman
#P Geom=AllCheck Guess=TCheck SCRF=Check Test GenChk RPBEPBE/6-
31G(d)/Auto
Freq
```

Pointgroup= C1 Stoichiometry= C44H36N2O8P2 C1[X(C44H36N2O8P2)] #Atoms=
 92
 Charge = 0 Multiplicity = 1

SCF Energy=	-3089.34722096	Predicted Change=	-5.808904D-08
-------------	----------------	-------------------	---------------

```

=====
=====
Optimization completed.      {Found 1 times}
Item  Max Val.  Criteria  Pass?  RMS Val.  Criteria  Pass?
Force 0.00001 || 0.00045 [ YES ]  0.00000 || 0.00030 [ YES ]
Displ 0.00619 || 0.00180 [ NO ]   0.00619 || 0.00180 [ YES ]
=====

```

Atomic Type	Coordinates (Angstroms)		
	X	Y	Z
C	4.232766	0.927589	-0.118239
C	5.591898	0.544079	-0.114126
H	6.347117	1.277097	0.186344
C	5.989513	-0.747026	-0.478860
C	5.001343	-1.689340	-0.853941
H	5.324982	-2.697190	-1.130311
C	3.656298	-1.344510	-0.870450
H	2.890679	-2.075345	-1.148899
C	3.253876	-0.036579	-0.510203
N	1.908992	0.288913	-0.515747
H	1.233748	-0.480203	-0.734732
P	1.196445	1.771005	-0.138743
O	0.015782	1.661674	0.807245
O	0.736878	2.316530	-1.635714
C	2.585849	2.782810	0.368178
C	2.331384	4.185500	0.777197
C	3.852754	2.255920	0.297937
H	4.679707	2.904612	0.619715
C	1.199136	4.536979	1.549543
H	0.491176	3.757755	1.847093
C	0.990285	5.864875	1.940967
H	0.110952	6.115008	2.543864
C	1.897554	6.868046	1.571888
H	1.729371	7.905496	1.879133
C	3.018444	6.534530	0.796328
H	3.724920	7.312066	0.486727
C	3.230577	5.210068	0.397836
H	4.087286	4.964225	-0.238781
C	-0.412522	3.098468	-1.835890
C	-0.285321	4.491627	-1.909335
H	0.692902	4.953895	-1.748277
C	-1.422407	5.263483	-2.185581
H	-1.330751	6.353017	-2.244446
C	-2.667542	4.648427	-2.384176
H	-3.552146	5.256582	-2.598759
C	-2.776009	3.251769	-2.309571

H	-3.744426	2.764273	-2.461265
C	-1.646002	2.467317	-2.038951
H	-1.707412	1.376442	-1.989230
P	-1.214962	-1.854269	0.080288
O	-0.757324	-2.420805	1.570093
C	0.380080	-3.224121	1.756195
O	-0.033580	-1.734109	-0.863328
C	-2.609442	-2.853975	-0.438215
C	-2.359149	-4.246195	-0.884045
N	-1.920382	-0.373166	0.473810
H	-1.242623	0.394748	0.687419
C	-3.875782	-2.331079	-0.336136
H	-4.707551	-2.972292	-0.659827
C	-4.250305	-1.012914	0.117140
C	-3.266152	-0.052308	0.505207
C	1.620404	-2.614081	1.980999
H	1.695946	-1.523108	1.959021
C	2.739489	-3.419252	2.235985
H	3.713553	-2.948307	2.402834
C	2.613545	-4.815878	2.273541
H	3.489996	-5.440301	2.474077
C	1.361635	-5.409752	2.054426
H	1.256276	-6.499199	2.084211
C	0.235198	-4.616983	1.794023
H	-0.747777	-5.063531	1.618044
C	-3.664362	1.247325	0.896555
H	-2.893772	1.975392	1.168782
C	-5.011379	1.590468	0.922304
H	-5.311869	2.595802	1.228496
C	-6.003575	0.648675	0.555156
C	-5.607630	-0.632121	0.154764
H	-6.383222	-1.348529	-0.137606
C	-3.254690	-5.279911	-0.521001
H	-4.105295	-5.050388	0.129679
C	-3.046807	-6.593964	-0.954484
H	-3.750490	-7.378828	-0.657343
C	-1.934050	-6.907988	-1.749656
H	-1.769257	-7.937427	-2.084410
C	-1.030437	-5.895929	-2.103048
H	-0.157285	-6.130866	-2.720820
C	-1.234861	-4.578258	-1.676300
H	-0.529508	-3.792173	-1.961556
O	8.262028	-0.184437	-0.108200
C	7.408952	-1.187562	-0.482360
O	7.791489	-2.314604	-0.780801
C	9.650282	-0.569408	-0.094095

H	10.199338	0.327243	0.225882
H	9.817384	-1.400414	0.610628
H	9.976661	-0.888137	-1.097584
C	-7.458282	0.954460	0.565030
O	-8.344808	0.165073	0.253736
O	-7.709432	2.238782	0.966083
C	-9.108231	2.582030	0.994613
H	-9.555026	2.480830	-0.008049
H	-9.656039	1.926841	1.691519
H	-9.146278	3.626934	1.332988

 Statistical Thermodynamic Analysis

Temperature= 298.150 Kelvin Pressure= 1.00000 Atm
 =====

=====

SCF Energy=	-3089.34722096	Predicted Change=	-5.808904D-08
Zero-point correction (ZPE)=			-3088.6536 0.69353
Internal Energy (U)=			-3088.6023 0.74491
Enthalpy (H)=			-3088.6013 0.74585
Gibbs Free Energy (G)=			-3088.7485 0.59870

Frequencies -- 4.7697 11.2384 12.1183
 Single points at WB97X/6-311++G2(df,p): -3092.7102
 Solvation Correction at PBE/6-31+G(d,p)/auto/Chloroform: -0.05165733

Dimeric heterocycle **1h**

Supporting Information: 1-ome-2-c-ch3-3-0016.log

 Using Gaussian 09: AM64L-G09RevD.01 24-Apr-2013
 =====

=====

```
# pbepbe/6-31G*/auto gfprint gfinput scf=(direct,tight,maxcycle=300,xqc)
opt=(maxcycle=250) freq=noraman iop(1/8=18) Temperature=298.15
#N Geom=AllCheck Guess=TCheck SCRF=Check Test GenChk RPBEPBE/6-
31G(d)/Auto
Freq
```

Pointgroup= C1 Stoichiometry= C50H52N2O6P2 C1[X(C50H52N2O6P2)] #Atoms=
 112
 Charge = 0 Multiplicity = 1

SCF Energy=	-3176.92196624	Predicted Change=	-1.433711D-07
-------------	----------------	-------------------	---------------

=====

Optimization completed. {Found 1 times}
 Item Max Val. Criteria Pass? RMS Val. Criteria Pass?

Force 0.00002 || 0.00045 [YES] 0.00000 || 0.00030 [YES]
 Displ 0.13324 || 0.00180 [NO] 0.13324 || 0.00180 [NO]

Atomic Type	Coordinates (Angstroms)		
	X	Y	Z
C	4.134783	-1.300405	-0.473561
C	5.097701	-2.338685	-0.569618
H	6.147294	-2.054579	-0.442619
C	4.753407	-3.672230	-0.802438
C	3.369995	-3.962797	-0.928702
H	3.047243	-4.996144	-1.096282
C	2.392209	-2.975067	-0.848520
H	1.329906	-3.224204	-0.939167
C	2.760265	-1.629488	-0.640399
N	1.780584	-0.646267	-0.552406
H	0.788447	-0.974215	-0.501625
P	2.033297	1.016312	-0.498035
O	0.974064	1.717485	0.335029
O	2.052775	1.590947	-2.066095
C	3.764157	1.171243	-0.062285
C	4.284532	2.477205	0.392300
C	4.548543	0.043079	-0.149306
H	5.619845	0.169254	0.062740
C	3.802980	3.695489	-0.131901
H	3.032040	3.680556	-0.908549
C	4.311931	4.929802	0.289179
H	3.914415	5.847640	-0.150971
C	5.330008	4.972219	1.260199
O	5.901001	6.116584	1.749508
C	5.409979	7.357896	1.248127
H	4.332238	7.486607	1.464844
H	5.574108	7.451093	0.157415
H	5.982836	8.138186	1.770223
C	5.820514	3.765695	1.801697
H	6.596933	3.814530	2.571112
C	5.300082	2.546174	1.378285
H	5.664502	1.622052	1.839514
C	0.879571	1.596484	-2.836812
C	-0.144147	2.518882	-2.577943
H	-0.048147	3.206945	-1.734601
C	-1.279064	2.526256	-3.400594
H	-2.087213	3.234642	-3.190646
C	-1.382517	1.631631	-4.476000
H	-2.270589	1.642710	-5.116010
C	-0.345916	0.720392	-4.727195

H	-0.420885	0.018623	-5.564403
C	0.789664	0.694822	-3.906081
H	1.607958	-0.009661	-4.081196
C	5.793117	-4.804098	-0.909532
C	5.672262	-5.484706	-2.296108
H	6.397659	-6.314253	-2.380760
H	5.875883	-4.765447	-3.108271
H	4.664741	-5.903231	-2.461442
C	7.237791	-4.288499	-0.750336
H	7.400449	-3.820114	0.236384
H	7.498181	-3.551803	-1.530599
H	7.944941	-5.131392	-0.838609
C	5.527900	-5.853994	0.198762
H	5.622240	-5.401800	1.201226
H	6.255673	-6.682257	0.123934
H	4.516627	-6.287958	0.119231
P	-1.925348	-0.823822	0.519363
O	-1.878379	-1.288826	2.116376
C	-0.713894	-1.752416	2.738663
O	-0.878537	-1.560943	-0.295859
C	-3.669805	-1.036073	0.166993
C	-4.210520	-2.409053	0.059626
N	-1.709767	0.845112	0.438901
H	-0.716259	1.167995	0.400550
C	-4.461844	0.084913	0.080380
H	-5.527428	-0.077504	-0.136255
C	-4.061687	1.465232	0.211436
C	-2.693499	1.824050	0.386405
C	-0.767164	-3.020954	3.331644
H	-1.683559	-3.611142	3.239401
C	0.352533	-3.501595	4.023247
H	0.313816	-4.492060	4.488983
C	1.517584	-2.725050	4.112470
H	2.392832	-3.106167	4.648314
C	1.555718	-1.458380	3.511856
H	2.460602	-0.844914	3.575351
C	0.438846	-0.958072	2.827494
H	0.466733	0.035584	2.369153
C	-2.344267	3.186156	0.465461
H	-1.292288	3.454281	0.609291
C	-3.327156	4.174344	0.376922
H	-3.011721	5.218787	0.450154
C	-4.695860	3.859281	0.207338
C	-5.023776	2.499193	0.127068
H	-6.069568	2.197320	-0.009638
C	-3.458929	-3.465967	-0.514803

H	-2.445958	-3.267236	-0.877896
C	-3.992920	-4.746744	-0.635159
H	-3.413693	-5.558238	-1.086047
C	-5.299679	-5.022525	-0.184647
O	-5.727515	-6.313038	-0.352778
C	-7.046764	-6.627548	0.085971
H	-7.808309	-6.026564	-0.447307
H	-7.162320	-6.473613	1.176167
H	-7.193592	-7.692123	-0.148148
C	-6.058868	-3.991957	0.402062
H	-7.064999	-4.180023	0.785200
C	-5.509320	-2.710137	0.522695
H	-6.097328	-1.930851	1.019117
C	-5.798403	4.933640	0.113089
C	-6.820370	4.726999	1.258887
H	-6.333007	4.820335	2.244776
H	-7.293104	3.731202	1.210116
H	-7.623364	5.483883	1.198138
C	-5.231411	6.363796	0.226035
H	-6.054996	7.095573	0.158629
H	-4.519086	6.589151	-0.587147
H	-4.718853	6.527489	1.190254
C	-6.526693	4.808699	-1.248517
H	-6.984162	3.812955	-1.378304
H	-5.826776	4.969289	-2.086985
H	-7.332767	5.561080	-1.324581

Statistical Thermodynamic Analysis

Temperature= 298.150 Kelvin Pressure= 1.00000 Atm

=====
SCF Energy= -3176.92196624 Predicted Change= -1.433711D-07
Zero-point correction (ZPE)= -3176.0280 0.89387
Internal Energy (U)= -3175.9693 0.95262
Enthalpy (H)= -3175.9684 0.95356
Gibbs Free Energy (G)= -3176.1320 0.78995

Frequencies -- 1.7009 5.6735 8.6199
Single points at WB97X/6-311++G2(df,p): -3180.4925
Solvation Correction at PBE/6-31+G(d,p)/auto/Chloroform: -0.05649918

Dimeric heterocycle **1c**

Supporting Information: 0006.log

Using Gaussian 09: AM64L-G09RevD.01 24-Apr-2013

```

=====
# pbepbe/6-31G*/auto gfprint gfinput scf=(direct,tight,maxcycle=300,xqc)
opt=(maxcycle=250) freq=noraman iop(1/8=18) Temperature=298.15
#N Geom=AllCheck Guess=TCheck SCRF=Check Test GenChk RPBEPBE/6-
31G(d)/Auto
Freq

```

```

-----
Pointgroup= C1  Stoichiometry= C42H36N2O6P2  C1[X(C42H36N2O6P2)] #Atoms=
88
Charge = 0  Multiplicity = 1

```

```

-----
SCF Energy= -2862.86173312  Predicted Change= -1.891495D-09
=====

```

```

=====
Optimization completed.      {Found 1 times}
Item  Max Val.  Criteria  Pass?  RMS Val.  Criteria  Pass?
Force  0.00000 || 0.00045 [ YES ]  0.00000 || 0.00030 [ YES ]
Displ  0.00449 || 0.00180 [ NO ]   0.00449 || 0.00180 [ YES ]

```

```

-----
Atomic      Coordinates (Angstroms)
Type        X          Y          Z
-----
C   -2.552034   3.522551  -0.887574
C   -2.634502   4.907993  -1.174413
H   -3.616487   5.391881  -1.114498
C   -1.507392   5.649463  -1.520029
H   -1.596060   6.717347  -1.741154
C   -0.251245   5.012714  -1.572973
H    0.643642   5.586989  -1.834677
C   -0.130029   3.650544  -1.295906
H    0.843613   3.150555  -1.322065
C   -1.273870   2.892538  -0.964174
N   -1.139184   1.542274  -0.658199
H   -0.166257   1.155887  -0.651008
P   -2.383058   0.426609  -0.425195
O   -1.998610  -0.612405   0.613424
O   -2.737918  -0.275645  -1.891624
C   -3.833734   1.450920  -0.190767
C   -5.105786   0.812331   0.210250
C   -3.726673   2.792704  -0.473356
H   -4.633011   3.400364  -0.339549
C   -5.140391  -0.275950   1.109723
H   -4.200700  -0.670916   1.507667
C   -6.350865  -0.850864   1.517119
H   -6.331250  -1.685398   2.222556

```

C	-7.568463	-0.346595	1.024231
O	-8.808354	-0.827483	1.350486
C	-8.865066	-1.929904	2.253178
H	-8.430829	-1.673022	3.238386
H	-8.342056	-2.816641	1.846694
H	-9.933396	-2.160937	2.375265
C	-7.552742	0.730305	0.112980
H	-8.505347	1.095434	-0.282565
C	-6.343873	1.291902	-0.286432
H	-6.351598	2.100884	-1.024311
C	-1.876958	-1.248361	-2.424646
C	-0.951171	-0.865330	-3.404771
H	-0.890964	0.184287	-3.706537
C	-0.124948	-1.840980	-3.979904
H	0.601210	-1.548259	-4.745292
C	-0.221959	-3.180495	-3.575378
H	0.429495	-3.937526	-4.023564
C	-1.153745	-3.547658	-2.592919
H	-1.226973	-4.589747	-2.265390
C	-1.989813	-2.583298	-2.013603
H	-2.722400	-2.846568	-1.246200
P	1.829632	-0.546270	0.486157
O	2.014090	0.150715	1.987566
C	2.362805	1.497835	2.153568
O	1.479494	0.499673	-0.556843
C	3.290744	-1.548016	0.222449
C	4.576535	-0.867843	-0.052366
N	0.619174	-1.678041	0.757955
H	-0.352529	-1.294027	0.789930
C	3.191744	-2.912320	0.366796
H	4.107456	-3.496194	0.195170
C	2.017158	-3.682146	0.692254
C	0.749439	-3.055516	0.877605
C	1.380142	2.492361	2.055897
H	0.353354	2.215318	1.800926
C	1.734491	3.827571	2.293738
H	0.970921	4.607748	2.208724
C	3.053303	4.161959	2.635779
H	3.324120	5.205969	2.823907
C	4.023598	3.153856	2.737568
H	5.054875	3.407503	3.004741
C	3.684383	1.815593	2.495230
H	4.428270	1.016308	2.562317
C	-0.389449	-3.839471	1.164435
H	-1.353352	-3.337327	1.295933
C	-0.276056	-5.225174	1.274524

H	-1.167223	-5.819321	1.503172
C	0.969630	-5.861911	1.100198
H	1.052762	-6.949165	1.190316
C	2.093235	-5.092518	0.810764
H	3.068727	-5.571905	0.666688
C	4.655697	0.287817	-0.871196
H	3.740727	0.696206	-1.310476
C	5.878492	0.900314	-1.134104
H	5.938190	1.787553	-1.771598
C	7.070774	0.382969	-0.587918
O	8.216223	1.060280	-0.911235
C	9.444172	0.556808	-0.390477
H	10.228360	1.223673	-0.777679
H	9.639114	-0.477066	-0.734444
H	9.458916	0.579489	0.716260
C	7.014723	-0.755972	0.238377
H	7.918120	-1.167127	0.695829
C	5.778880	-1.360011	0.500357
H	5.745523	-2.222331	1.174956

 Statistical Thermodynamic Analysis

Temperature= 298.150 Kelvin Pressure= 1.00000 Atm
 =====

=====
 SCF Energy= -2862.86173312 Predicted Change= -1.891495D-09
 Zero-point correction (ZPE)= -2862.1879 0.67382
 Internal Energy (U)= -2862.1408 0.72089
 Enthalpy (H)= -2862.1398 0.72184
 Gibbs Free Energy (G)= -2862.2767 0.58501

Frequencies -- 5.2586 8.0191 15.3657
 Single points at WB97X/6-311++G2(df,p): -2865.9697
 Solvation Correction at PBE/6-31+G(d,p)/auto/Chloroform: -0.05096194

Homodimeric S-S heterocycle 1g:

Supporting Information: polymerdetector-s-s-dimer-6-c-ch3-3-0008.log

Using Gaussian 09: AM64L-G09RevD.01 24-Apr-2013
 =====

=====
 # pbepbe/6-31G*/auto gfpri n gfinpu t scf=(direct,tight,maxcycle=300,xqc)
 opt=(maxcycle=250) freq=noraman iop(1/8=18) Temperature=298.15
 #N Geom=AllCheck Guess=TCheck SCRF=Check Test GenChk RPBEPBE/6-
 31G(d)/Auto
 Freq

Pointgroup= C1 Stoichiometry= C50H46N4O4P2 C1[X(C50H46N4O4P2)] #Atoms= 106

Charge = 0 Multiplicity = 1

SCF Energy= -3132.42079857 Predicted Change= -1.709265D-08

Optimization completed. {Found 1 times}
Item Max Val. Criteria Pass? RMS Val. Criteria Pass?
Force 0.00000 || 0.00045 [YES] 0.00000 || 0.00030 [YES]
Displ 0.01361 || 0.00180 [NO] 0.01361 || 0.00180 [NO]

Atomic Type	Coordinates (Angstroms)		
	X	Y	Z
C	-2.360729	3.056319	-0.915451
C	-2.487288	4.330514	-1.520618
H	-3.408915	4.526672	-2.081811
C	-1.500531	5.319511	-1.432022
C	-1.705908	6.690247	-2.108202
C	-2.955005	7.378333	-1.502956
H	-3.865663	6.771313	-1.644040
H	-3.125946	8.357118	-1.986447
H	-2.827239	7.547903	-0.419792
C	-1.918519	6.490470	-3.629662
H	-2.080747	7.465269	-4.123860
H	-2.797015	5.857345	-3.842024
H	-1.038547	6.012084	-4.093411
C	-0.495919	7.626087	-1.908697
H	-0.687430	8.589687	-2.411382
H	0.427763	7.203666	-2.341831
H	-0.312686	7.839806	-0.840965
C	-0.333364	4.987137	-0.703702
H	0.474631	5.717181	-0.606241
C	-0.166649	3.743751	-0.092074
H	0.750101	3.512025	0.459673
C	-1.175209	2.765976	-0.179814
N	-0.995474	1.526096	0.423554
H	-0.054033	1.340633	0.837755
P	-2.065347	0.234944	0.453016
O	-1.433645	-1.103555	0.109337
O	-2.589655	0.270520	2.025927
C	-3.434913	0.794143	-0.564743
C	-4.589127	-0.106876	-0.780611
C	-3.399581	2.072287	-1.075599
H	-4.243502	2.379287	-1.709527

C	-4.430651	-1.512123	-0.866385
H	-3.431657	-1.945691	-0.763499
C	-5.526562	-2.345928	-1.088116
H	-5.388363	-3.428917	-1.154976
C	-6.821097	-1.800058	-1.233947
C	-6.995229	-0.400426	-1.139182
H	-7.998427	0.026138	-1.230157
C	-5.896507	0.424649	-0.908028
H	-6.054663	1.501595	-0.793611
C	-3.236803	-0.822570	2.628980
C	-4.575844	-0.654364	3.007112
H	-5.082888	0.287222	2.777034
C	-5.234424	-1.697398	3.671972
H	-6.281142	-1.572108	3.967615
C	-4.558605	-2.893717	3.954994
H	-5.076285	-3.706970	4.473701
C	-3.216295	-3.041198	3.575652
H	-2.677179	-3.966815	3.802911
C	-2.542132	-2.006081	2.912770
H	-1.494675	-2.107381	2.620681
C	-7.947219	-2.653605	-1.463438
N	-8.873741	-3.354418	-1.653425
P	2.324795	-0.343488	0.872231
O	2.767623	-1.328251	2.131634
C	1.889286	-1.706723	3.158971
O	1.602301	0.902698	1.355859
C	3.904022	-0.217059	0.029997
C	4.961265	0.649413	0.594441
N	1.371443	-1.220880	-0.202031
H	0.339241	-1.206042	-0.034417
C	4.105536	-0.996287	-1.086479
H	5.083370	-0.914205	-1.581841
C	3.167108	-1.883211	-1.726131
C	1.814096	-1.973569	-1.284900
C	1.701224	-3.081441	3.359721
H	2.191501	-3.791033	2.686902
C	0.902837	-3.513631	4.428002
H	0.760878	-4.586768	4.593843
C	0.292995	-2.579867	5.279344
H	-0.332573	-2.919393	6.110753
C	0.486243	-1.207846	5.059382
H	0.010346	-0.474495	5.718369
C	1.289845	-0.758681	4.001929
H	1.453394	0.305602	3.818341
C	0.914184	-2.791526	-1.993542
H	-0.129704	-2.836659	-1.666877

C	1.349911	-3.528578	-3.095983
H	0.619461	-4.157684	-3.611819
C	2.688817	-3.483206	-3.553130
C	3.191580	-4.297146	-4.762959
C	4.327660	-5.245881	-4.305195
H	4.707199	-5.831337	-5.161895
H	3.968558	-5.953481	-3.537935
H	5.178419	-4.688146	-3.877461
C	3.735068	-3.332544	-5.845999
H	4.114500	-3.905213	-6.711340
H	4.564605	-2.712105	-5.465792
H	2.942191	-2.653448	-6.204229
C	2.074343	-5.151462	-5.396566
H	1.662159	-5.886945	-4.683452
H	2.480968	-5.713684	-6.254744
H	1.243057	-4.529415	-5.772534
C	3.563875	-2.645074	-2.851883
H	4.609050	-2.556770	-3.172368
C	6.326408	0.291936	0.470232
H	6.594964	-0.663908	0.010119
C	7.338680	1.115530	0.958244
H	8.387407	0.820826	0.858862
C	7.013705	2.328928	1.606613
C	5.655903	2.687057	1.758655
H	5.399392	3.622106	2.265100
C	4.649091	1.859748	1.261449
H	3.601729	2.151543	1.380614
C	8.049355	3.178139	2.112014
N	8.901504	3.877471	2.524831

Statistical Thermodynamic Analysis

Temperature= 298.150 Kelvin Pressure= 1.00000 Atm

SCF Energy= -3132.42079857 Predicted Change= -1.709265D-08
Zero-point correction (ZPE)= -3131.5936 0.82715
Internal Energy (U)= -3131.5364 0.88432
Enthalpy (H)= -3131.5355 0.88527
Gibbs Free Energy (G)= -3131.6949 0.72587

Frequencies -- 4.0915 7.9697 10.1404

Geometries for the Testing of Stereoelectronic Effect:

R-S-dimer, no phenyl group, phenoxy replaced with methoxy, R2 = H

Supporting Information: r-s-paired-down-9-1.log

Using Gaussian 09: AM64L-G09RevD.01 24-Apr-2013

```
=====
=====
#PBEPBE/6-31G(d)/auto gfpint ginput scf=(direct,tight,maxcycle=300,xqc)
opt=(maxcycle=250) freq=norman
#P Geom=AllCheck Guess=TCheck SCRF=Check Test GenChk RPBEPBE/6-
31G(d)/Auto
Freq
```

```
-----
Pointgroup= C1  Stoichiometry= C18H20N2O4P2  C1[X(C18H20N2O4P2)] #Atoms=
46
```

```
Charge = 0  Multiplicity = 1
```

```
-----
SCF Energy= -1789.52557403      Predicted Change= -1.144653D-06
=====
=====
```

```
Optimization completed.      {Found 1 times}
Item  Max Val.  Criteria  Pass?  RMS Val.  Criteria  Pass?
Force  0.00002 || 0.00045 [ YES ]   0.00000 || 0.00030 [ YES ]
Displ  0.02018 || 0.00180 [ NO ]    0.02018 || 0.00180 [ NO ]
```

```
-----
Atomic      Coordinates (Angstroms)
Type        X          Y          Z
-----
C          -4.321048   0.508797  -0.275566
C          -5.637427  -0.012893 -0.299174
H          -6.438325   0.620962 -0.697961
C          -5.922805  -1.293788  0.165463
H          -6.947438  -1.676170  0.141231
C          -4.874138  -2.093701  0.663758
H          -5.084343  -3.104051  1.030332
C          -3.565504  -1.614981  0.702113
H          -2.748680  -2.231629  1.092589
C          -3.271316  -0.309938  0.243036
N          -1.960414   0.142351  0.274023
H          -1.230589  -0.546398  0.571687
P          -1.388452   1.685379  -0.132567
O          -1.151755   2.524313  1.259666
C          0.066305   2.280198  2.000608
H          0.952502   2.537341  1.396119
H          0.130531   1.223655  2.317881
H          0.017225   2.927866  2.888251
O          -0.115626   1.614291  -0.961915
C          -2.831995   2.454364  -0.808695
H          -2.718711   3.453846  -1.239175
C          -4.045177   1.828550  -0.796883
```

H	-4.903951	2.360573	-1.229543
P	1.388473	-1.685416	0.132494
O	1.151824	-2.524367	-1.259737
C	-0.066243	-2.280317	-2.000687
H	-0.952434	-2.537425	-1.396174
H	-0.017165	-2.928048	-2.888285
H	-0.130480	-1.223796	-2.318033
O	0.115626	-1.614349	0.961811
C	2.832014	-2.454367	0.808665
H	2.718740	-3.453859	1.239124
N	1.960414	-0.142382	-0.274095
H	1.230585	0.546344	-0.571804
C	4.045176	-1.828513	0.796926
H	4.903947	-2.360514	1.229620
C	4.321030	-0.508746	0.275636
C	3.271299	0.309954	-0.243024
C	3.565467	1.615007	-0.702084
H	2.748644	2.231627	-1.092606
C	4.874082	2.093773	-0.663652
H	5.084273	3.104133	-1.030211
C	5.922748	1.293899	-0.165294
H	6.947366	1.676316	-0.140999
C	5.637388	0.012991	0.299320
H	6.438287	-0.620837	0.698151

 Statistical Thermodynamic Analysis

Temperature= 298.150 Kelvin Pressure= 1.00000 Atm

=====
 SCF Energy= -1789.52557403 Predicted Change= -1.144653D-06
 Zero-point correction (ZPE)= -1789.1749 0.35058
 Internal Energy (U)= -1789.1493 0.37622
 Enthalpy (H)= -1789.1484 0.37716
 Gibbs Free Energy (G)= -1789.2337 0.29187

 Frequencies -- 11.7392 22.4312 25.2322
 Single Points at WB97X/6-311++G2(df,p)= -1791.3035

S-S-dimer, no phenyl group, phenoxy replaced with methoxy, R2 = H
 Supporting Information: s-s-paired-down-2.log

 Using Gaussian 09: AM64L-G09RevD.01 24-Apr-2013

=====
 #PBEPBE/6-31G(d)/auto gfpint gfinput scf=(direct,tight,maxcycle=300,xqc)
 opt=(maxcycle=250) freq=noraman

#P Geom=AllCheck Guess=TCheck SCRF=Check Test GenChk RPBEPBE/6-31G(d)/Auto
Freq

Pointgroup= C1 Stoichiometry= C18H20N2O4P2 C1[X(C18H20N2O4P2)] #Atoms=46

Charge = 0 Multiplicity = 1

SCF Energy= -1789.52544372 Predicted Change= -7.797984D-08

=====
Optimization completed. {Found 1 times}
Item Max Val. Criteria Pass? RMS Val. Criteria Pass?
Force 0.00001 || 0.00045 [YES] 0.00000 || 0.00030 [YES]
Displ 0.01478 || 0.00180 [NO] 0.01478 || 0.00180 [NO]

Atomic Coordinates (Angstroms)
Type X Y Z

C 3.980661 0.983034 0.321143
C 4.994916 1.868411 -0.118888
H 5.794373 2.129743 0.584596
C 4.989231 2.401754 -1.404364
H 5.783174 3.082475 -1.725363
C 3.944087 2.057412 -2.286387
H 3.924984 2.473255 -3.299358
C 2.928518 1.190057 -1.888981
H 2.113485 0.923428 -2.570073
C 2.934747 0.635885 -0.587885
N 1.909048 -0.217213 -0.207946
H 1.143738 -0.366852 -0.904190
P 1.736228 -1.040694 1.263012
O 0.321743 -0.943548 1.815187
O 2.155933 -2.610238 1.025309
C 3.090425 -0.405856 2.207591
H 3.177666 -0.735510 3.247260
C 3.993744 0.465335 1.669761
H 4.810771 0.823176 2.311799
C 1.142856 -3.522823 0.540604
H 0.865450 -3.283972 -0.501260
H 0.244319 -3.480587 1.178010
H 1.592551 -4.525977 0.583392
P -1.644201 -0.792562 -1.382676
O -1.969534 -2.403717 -1.283365
C -3.181879 -2.829586 -0.630300
H -4.073221 -2.374449 -1.099271

H	-3.163016	-2.570843	0.442917
H	-3.225625	-3.922719	-0.748284
O	-0.253420	-0.684986	-1.969732
C	-2.979779	0.008854	-2.231223
H	-3.101009	-0.213289	-3.296427
N	-1.810576	-0.178386	0.186926
H	-1.045369	-0.451936	0.851944
C	-3.801293	0.904720	-1.606639
H	-4.592829	1.383911	-2.199938
C	-3.720006	1.308582	-0.221842
C	-2.712199	0.776498	0.639140
C	-2.629245	1.223975	1.977993
H	-1.839376	0.818047	2.618846
C	-3.536716	2.165685	2.459409
H	-3.458479	2.499810	3.499358
C	-4.546804	2.689738	1.626338
H	-5.255603	3.427873	2.012972
C	-4.625740	2.262501	0.304235
H	-5.396599	2.667303	-0.362266

 Statistical Thermodynamic Analysis

Temperature= 298.150 Kelvin Pressure= 1.00000 Atm
 =====

=====
 SCF Energy= -1789.52544372 Predicted Change= -7.797984D-08
 Zero-point correction (ZPE)= -1789.1749 0.35053
 Internal Energy (U)= -1789.1492 0.37624
 Enthalpy (H)= -1789.1482 0.37718
 Gibbs Free Energy (G)= -1789.2343 0.29112

 Frequencies -- 8.2965 21.6464 23.4530
 Single Points at WB97X/6-311++G2(df,p)= -1791.3029

Monomer, no phenyl group, phenoxy replaced with methoxy, R2 = H

Supporting Information: monomer-paired-down-4-1.log

 Using Gaussian 09: AM64L-G09RevD.01 24-Apr-2013
 =====

=====
 #PBEPBE/6-31G(d)/auto gffprint gffinput scf=(direct,tight,maxcycle=300,xqc)
 opt=(maxcycle=250) freq=noraman
 #P Geom=AllCheck Guess=TCHECK SCRF=Check Test GenChk RPBEPBE/6-
 31G(d)/Auto
 Freq

 Pointgroup= C1 Stoichiometry= C9H10NO2P C1[X(C9H10NO2P)] #Atoms= 23

Charge = 0 Multiplicity = 1

SCF Energy= -894.744992190 Predicted Change= -1.581251D-09
=====

=====
Optimization completed. {Found 2 times}
Item Max Val. Criteria Pass? RMS Val. Criteria Pass?
Force 0.00000 || 0.00045 [YES] 0.00000 || 0.00030 [YES]
Displ 0.00059 || 0.00180 [YES] 0.00059 || 0.00180 [YES]

Atomic Coordinates (Angstroms)
Type X Y Z

P 1.587328 0.016446 0.360501
O 2.443100 -0.431675 -0.977249
C 3.885448 -0.388680 -0.919804
H 4.253046 -1.160602 -1.613758
H 4.244836 -0.593222 0.101687
H 4.249267 0.600331 -1.252074
O 2.369488 -0.177215 1.629911
C 0.885330 1.622055 0.062804
H 1.578047 2.470214 0.064811
N 0.208414 -0.967557 0.135945
H 0.374798 -1.973499 0.212026
C -0.455388 1.827697 -0.071551
H -0.816803 2.858343 -0.191975
C -1.473129 0.799229 -0.071501
C -1.124030 -0.580207 0.038346
C -2.142602 -1.557835 0.028424
H -1.868676 -2.615831 0.113972
C -3.481802 -1.184711 -0.084855
H -4.254870 -1.960049 -0.087655
C -3.841643 0.172117 -0.192582
H -4.892912 0.461357 -0.279932
C -2.841245 1.141534 -0.185700
H -3.101887 2.203102 -0.269015

Statistical Thermodynamic Analysis

Temperature= 298.150 Kelvin Pressure= 1.00000 Atm
=====

=====
SCF Energy= -894.744992190 Predicted Change= -1.581251D-09
Zero-point correction (ZPE)= -894.5705 0.17440
Internal Energy (U)= -894.5583 0.18662
Enthalpy (H)= -894.5574 0.18757
Gibbs Free Energy (G)= -894.6097 0.13519
=====

Frequencies -- 31.6694 56.6009 90.8014
Single Points at WB97X/6-311++G2(df,p)= -895.63309

R-S-dimer, no phenyl group, with phenoxy, R2 = H
Supporting Information: r-s-no-ph-oph-8.log

Using Gaussian 09: AM64L-G09RevD.01 24-Apr-2013
=====

=====
#PBEPBE/6-31G(d)/auto gfpri nt gfinpu t scf=(direct,tight,maxcycle=300,xqc)
opt=(maxcycle=250) freq=noraman
#P Geom=AllCheck Guess=TChe ck SCRF=Check Test GenChk RPBE PBE/6-
31G(d)/Auto
Freq

Pointgroup= C1 Stoichiometry= C28H24N2O4P2 C1[X(C28H24N2O4P2)] #Atoms=
60
Charge = 0 Multiplicity = 1

SCF Energy= -2172.53686587 Predicted Change= -8.193969D-08
=====

=====
Optimization completed. {Found 1 times}
Item Max Val. Criteria Pass? RMS Val. Criteria Pass?
Force 0.00002 || 0.00045 [YES] 0.00000 || 0.00030 [YES]
Displ 0.00560 || 0.00180 [NO] 0.00560 || 0.00180 [NO]

Atomic Coordinates (Angstroms)
Type X Y Z

C -3.959543 -1.820499 0.212476
C -5.340573 -1.828097 -0.103624
H -6.006684 -2.456746 0.499096
C -5.852031 -1.059536 -1.144728
H -6.921247 -1.081024 -1.375249
C -4.977194 -0.245045 -1.893266
H -5.369221 0.373214 -2.707635
C -3.612715 -0.213760 -1.613082
H -2.931576 0.425132 -2.184628
C -3.084734 -1.008348 -0.570401
N -1.721781 -0.961184 -0.305480
H -1.173051 -0.237694 -0.823914
P -0.861304 -1.846354 0.847501
O -0.112978 -3.120856 0.085904

C	1.205472	-3.060101	-0.381525
O	0.150234	-0.996835	1.596197
C	-2.153783	-2.673617	1.725540
H	-1.867796	-3.272425	2.595580
C	-3.457923	-2.586684	1.329111
H	-4.211061	-3.136443	1.910688
C	2.120681	-3.981366	0.145274
H	1.790827	-4.672129	0.926726
C	3.434430	-3.998989	-0.341678
H	4.151098	-4.718803	0.067661
C	3.831994	-3.097836	-1.340448
H	4.861148	-3.108470	-1.713117
C	2.904247	-2.182867	-1.858652
H	3.204800	-1.474173	-2.637401
C	1.582321	-2.162624	-1.391160
H	0.858630	-1.451605	-1.801550
P	0.861730	1.846950	-0.847132
O	0.111969	3.119424	-0.083481
C	-1.206890	3.057290	0.382645
O	-0.148785	0.997179	-1.596914
C	2.153111	2.677306	-1.723901
H	1.866311	3.277314	-2.592846
N	1.723423	0.961090	0.304360
H	1.175519	0.236276	0.821822
C	3.457350	2.591580	-1.327520
H	4.209725	3.143436	-1.908097
C	3.959995	1.824275	-0.212111
C	3.086268	1.009713	0.569461
C	-1.583356	2.159899	1.392492
H	-0.859058	1.449928	1.803632
C	-2.905668	2.178730	1.858949
H	-3.205947	1.470088	2.637858
C	-3.834184	3.092230	1.339506
H	-4.863638	3.101754	1.711376
C	-3.437018	3.993296	0.340504
H	-4.154284	4.711954	-0.069826
C	-2.122851	3.977089	-0.145395
H	-1.793283	4.667873	-0.926952
C	3.615270	0.214248	1.610965
H	2.934931	-0.426342	2.181567
C	4.979692	0.246940	1.891250
H	5.372527	-0.372017	2.704698
C	5.853456	1.063753	1.143983
H	6.922634	1.086324	1.374575
C	5.341008	1.833236	0.104048
H	6.006299	2.463706	-0.497673

Statistical Thermodynamic Analysis

Temperature= 298.150 Kelvin Pressure= 1.00000 Atm
=====

=====

SCF Energy=	-2172.53686587	Predicted Change=	-8.193969D-08
Zero-point correction (ZPE)=	-2172.0843	0.45248	
Internal Energy (U)=	-2172.0526	0.48425	
Enthalpy (H)=	-2172.0516	0.48520	
Gibbs Free Energy (G)=	-2172.1519	0.38491	

Frequencies -- 11.5080 17.8701 18.7386
Single Points at WB97X/6-311++G2(df,p)= -2174.7879

S-S-dimer, no phenyl group, with phenoxy, R2 = H

Supporting Information: s-s-no-ph-oph-14.log

Using Gaussian 09: AM64L-G09RevD.01 24-Apr-2013
=====

=====

```
#PBEPBE/6-31G(d)/auto gfpri nt gfi nput scf=(direct,tight,maxcycle=300,xqc)
opt=(maxcycle=250) freq=norman
#P Geom=AllCheck Guess=TCheck SCRF=Check Test GenChk RPBEPBE/6-
31G(d)/Auto
Freq
```

```
Pointgroup= C1    Stoichiometry= C28H24N2O4P2    C1[X(C28H24N2O4P2)] #Atoms=
60
Charge = 0    Multiplicity = 1
```

```
SCF Energy= -2172.53781442            Predicted Change= -7.759443D-08
```

=====

```
Optimization completed.            {Found    1    times}
Item    Max Val.    Criteria    Pass?    RMS Val.    Criteria    Pass?
Force    0.00002 || 0.00045    [ YES ]    0.00000 || 0.00030    [ YES ]
Displ    0.00836 || 0.00180    [ NO ]    0.00836 || 0.00180    [ NO ]
```

Atomic Type	Coordinates (Angstroms)		
	X	Y	Z
C	-2.514247	-3.153270	-0.020475
C	-3.159726	-4.213336	-0.703166
H	-3.781325	-4.902670	-0.119677
C	-3.015331	-4.389245	-2.076117
H	-3.522836	-5.213892	-2.585102

C	-2.204246	-3.493812	-2.802945
H	-2.080233	-3.622767	-3.883316
C	-1.554117	-2.438796	-2.165158
H	-0.923336	-1.741208	-2.726118
C	-1.703238	-2.251180	-0.772701
N	-1.042352	-1.195095	-0.156282
H	-0.422300	-0.607841	-0.763156
P	-1.082094	-0.755012	1.471110
O	0.273203	-0.481705	2.091330
O	-1.897329	0.690932	1.579560
C	-2.095672	-2.023214	2.174833
H	-2.247232	-1.999391	3.258664
C	-2.659399	-3.003939	1.408595
H	-3.274803	-3.763355	1.910719
C	-3.058307	0.947186	0.838246
C	-4.309354	0.772471	1.445462
H	-4.360392	0.393763	2.470506
C	-5.468808	1.098410	0.727941
H	-6.449235	0.966193	1.197492
C	-5.374530	1.592742	-0.581258
H	-6.282245	1.846769	-1.138176
C	-4.114308	1.764906	-1.173743
H	-4.035018	2.155385	-2.193567
C	-2.946116	1.445729	-0.468264
H	-1.954203	1.582326	-0.909933
P	2.088183	0.714035	-1.101476
O	2.367525	2.320113	-0.788110
C	1.379094	3.215648	-0.362624
O	0.666405	0.502114	-1.592479
C	3.463019	0.327210	-2.145272
H	3.444045	0.720400	-3.166288
N	2.433721	-0.182910	0.288077
H	1.664217	-0.262716	0.992235
C	4.517058	-0.415950	-1.697396
H	5.345730	-0.608740	-2.392884
C	4.649363	-0.997651	-0.381816
C	3.600263	-0.881853	0.579052
C	1.284514	4.430774	-1.054888
H	1.941255	4.608200	-1.911520
C	0.353214	5.389069	-0.633529
H	0.278814	6.339995	-1.171678
C	-0.483876	5.130575	0.462348
H	-1.217339	5.877378	0.782650
C	-0.376471	3.910203	1.144387
H	-1.026356	3.691179	1.997458
C	0.563048	2.948744	0.745519

H	0.653781	2.008575	1.297745
C	3.728960	-1.514388	1.836283
H	2.905857	-1.431686	2.553679
C	4.885148	-2.229066	2.144378
H	4.970961	-2.708538	3.125167
C	5.938626	-2.338050	1.213495
H	6.843895	-2.898282	1.465220
C	5.809812	-1.730826	-0.032115
H	6.612719	-1.814562	-0.774032

 Statistical Thermodynamic Analysis

Temperature= 298.150 Kelvin Pressure= 1.00000 Atm
 =====

=====
 SCF Energy= -2172.53781442 Predicted Change= -7.759443D-08
 Zero-point correction (ZPE)= -2172.0850 0.45274
 Internal Energy (U)= -2172.0534 0.48439
 Enthalpy (H)= -2172.0524 0.48533
 Gibbs Free Energy (G)= -2172.1521 0.38564

Frequencies -- 11.2709 14.3932 21.3146
 Single Points at WB97X/6-311++G2(df,p)= -2174.7875

Monomer, no phenyl group, with phenoxy, R2 = H

Supporting Information: monomer-no-ph-oph-1.log

Using Gaussian 09: AM64L-G09RevD.01 24-Apr-2013
 =====

=====
 #PBEPBE/6-31G(d)/auto gfpri n gfinpu t scf=(direct,tight,maxcycle=300,xqc)
 opt=(maxcycle=250) freq=noraman
 #P Geom=AllCheck Guess=TChe ck SCRF=Check Test GenChk RPBEPBE/6-
 31G(d)/Auto
 Freq

Pointgroup= C1 Stoichiometry= C14H12NO2P C1[X(C14H12NO2P)] #Atoms= 30
 Charge = 0 Multiplicity = 1

SCF Energy= -1086.25102464 Predicted Change= -6.309716D-09
 =====

=====
 Optimization completed. {Found 1 times}
 Item Max Val. Criteria Pass? RMS Val. Criteria Pass?
 Force 0.00000 || 0.00045 [YES] 0.00000 || 0.00030 [YES]
 Displ 0.00242 || 0.00180 [NO] 0.00242 || 0.00180 [YES]

Atomic Type	Coordinates (Angstroms)		
	X	Y	Z
P	-0.141238	1.383577	-0.293497
O	-1.159878	0.706874	0.837693
C	-2.317458	-0.004087	0.496968
O	-0.849078	2.191585	-1.341450
C	1.071704	2.114360	0.779002
H	0.810450	3.068487	1.246884
N	0.753592	0.087098	-0.961338
H	0.319092	-0.379185	-1.760637
C	2.278266	1.526623	1.012518
H	2.979079	2.033814	1.689970
C	2.750373	0.284359	0.436630
C	1.984697	-0.411773	-0.546921
C	-3.267564	0.491166	-0.411002
H	-3.088613	1.446520	-0.910017
C	-4.422034	-0.265237	-0.659477
H	-5.165416	0.114938	-1.368337
C	-4.635084	-1.488511	-0.007354
H	-5.542636	-2.067836	-0.205205
C	-3.679985	-1.963378	0.903962
H	-3.837258	-2.915686	1.421424
C	-2.516187	-1.225899	1.157647
H	-1.757986	-1.577294	1.863741
C	2.503033	-1.589767	-1.126369
H	1.912635	-2.116763	-1.884692
C	3.747319	-2.083291	-0.732986
H	4.127363	-3.002079	-1.191437
C	4.508738	-1.414575	0.244123
H	5.483129	-1.805690	0.550564
C	4.008099	-0.244380	0.810707
H	4.591729	0.296110	1.564937

Statistical Thermodynamic Analysis

Temperature= 298.150 Kelvin Pressure= 1.00000 Atm

SCF Energy= -1086.25102464 Predicted Change= -6.309716D-09
Zero-point correction (ZPE)= -1086.0255 0.22546
Internal Energy (U)= -1086.0103 0.24062
Enthalpy (H)= -1086.0094 0.24157
Gibbs Free Energy (G)= -1086.0701 0.18086

Frequencies -- 17.1823 18.8685 36.2698
Single Points at WB97X/6-311++G2(df,p)= -1087.3754

Computational Methods Attempted for Solution-state Dimer Strength Predictions:

- Optimizations at PBE/6-31G(d)/Auto using Gaussian 09
 - Single points in gas phase at PBE/6-311++G(2df,p)/auto using Gaussian 09
 - Solvation Correction in chloroform and gas at PBE/6-31+G(d,p) with D3 and D3BJ corrections using Gaussian 09
 - Single points at M062X/ 6-311++G(2df,p)/CPCM/H2O using Gaussian 09
 - Single points at M062X/ 6-311++G(2df,p)/CPCM/Choroform using Gaussian 09
 - Single points at M062X/ 6-311++G(2df,p)/SMD/H2O using Gaussian 09
 - Single points at M062X/ 6-311++G(2df,p)/SMD/Chloroform using Gaussian 09
 - Single points at M062X/ 6-311++G(2df,p)/CPCM/H2O using Gaussian 16
 - Single points at M062X/ 6-311++G(2df,p)/CPCM/Choroform using Gaussian 16
 - Single points at M062X/ 6-311++G(2df,p)/SMD/H2O using Gaussian 16
 - Single points at M062X/ 6-311++G(2df,p)/SMD/Chloroform using Gaussian 16
 - Single points in gas phase at PBE/6-311++G(2df,p)/auto in Gaussian 16
 - Single points in gas phase at PBE/def2TZVPP/auto using Gaussian 09
 - Single points in gas phase at PBE/ def2-QZVPP/RIJCOSX/auto using ORCA
 - Single points in gas phase at PBE/ def2-TZVPP/RIJCOSX/auto using ORCA
 - Single points in gas phase at WB97X/6-311++G(2df,p) using Gaussian 09
 - Solvation Correction in chloroform and gas at PBE/6-31+G(d,p) using Gaussian 09
- Optimizations at PBE/6-31G(d) using Gaussian 09
 - No single points or solvation correction
- Optimizations at B3LYP/6-31G(d) using Gaussian 09
 - No single points or solvation correction

Representative Drawings of R-S and S-S Dimer Orientations:

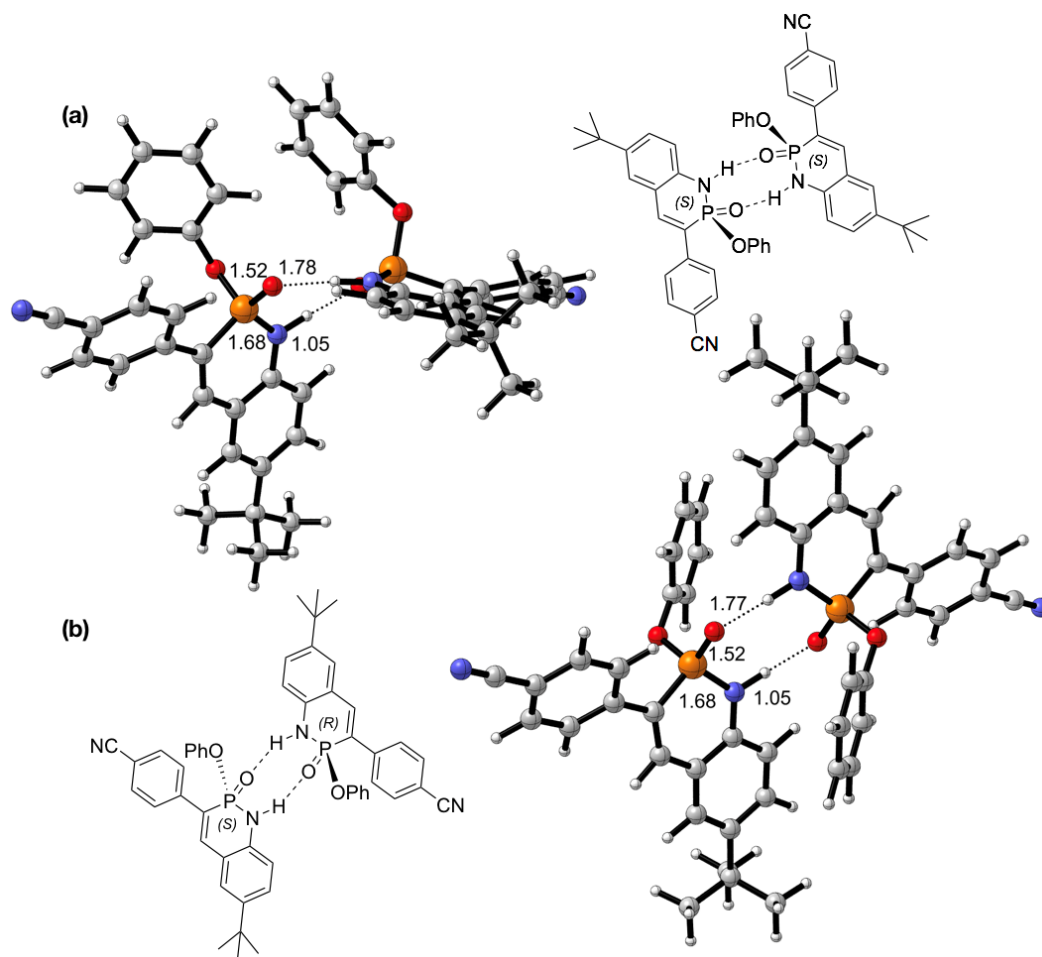


Figure A.9 Chemical structures and predicted geometries of the a) S-S homodimer and b) R-S heterodimer of **1g**.

Gas-Phase Free Energy Values Compared to Experimental Values:

Table A.17 Comparison between gas phase free energy predictions and experimental free energy values collected in H₂O-saturated CHCl₃

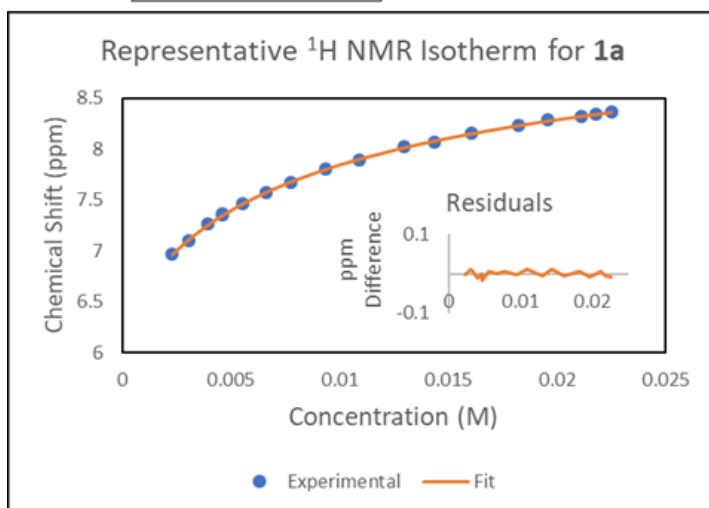
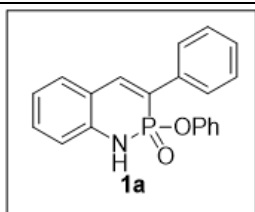
Entry	(R1,R2)	Computed ΔG (gas phase) (kcal/mol)	Exp. ΔG (kcal/mol)
1b	(4-CN,H)	-8.8	-2.9
1e	(4-CN,CF ₃)	-10.1	-3.4
1p	(4-CN,EtO)	-8.5	-2.6
1m	(H,CN)	-10.7	-3.7
1a	(H,H)	-9.7	-2.4
1o	(H,CO ₂ Et)	-10.2	-3.1
1h	(4-OMe, <i>t</i> -Bu)	-8.5	-2.1
1c	(4-OMe,H)	-9.2	-2.4

Data for Figure 2.9:

Table A.18 Data for the construction and validation of Hammett parameter-based prediction of K_{eq}

Entry	(R ¹ ,R ²)	σ_{R1}	σ_{R2}	K_{eq}	Predicted	Dataset
1h	(4-OMe, <i>t</i> -Bu)	-0.27	-0.2	-2.12	-2.138783	Training
1i	(4-Me, <i>t</i> -Bu)	-0.17	-0.2	-2.15	-2.181648	Training
1c	(4-OMe,H)	-0.27	0	-2.38	-2.424156	Training
1a	(H,H)	0	0	-2.44	-2.539892	Training
1g	(4-CN, <i>t</i> -Bu)	0.66	-0.2	-2.52	-2.537431	Training
1p	(4-CN,EtO)	0.66	-0.24	-2.64	-2.480356	Training
1b	(4-CN,H)	0.66	0	-2.88	-2.822803	Training
1e	(4-CN,CF ₃)	0.66	0.54	-3.36	-3.59331	Training
1m	(H,CN)	0	0.66	-3.71	-3.481622	Training
1j	(H, <i>t</i> -Bu)	0	-0.2	-2.24	-2.254519	Validation
1o	(H,CO ₂ Et)	0	0.45	-3.14	-3.181981	Validation

6. Data for Dimerization Constant (K_{dim}) Values for **1a-p**



Concentration (M)	Chemical Shift (ppm)
0.02333	8.4318
0.022577419	8.4099
0.021871875	8.3918
0.020286957	8.3456
0.018916216	8.2854
0.016664286	8.2215
0.014891489	8.1333
0.013459615	8.0656
0.01128871	7.9515
0.009720833	7.8526
0.008044828	7.7263
0.006861765	7.6216
0.005736885	7.5012
0.004761224	7.4309
0.004761224	7.3995
0.00408105	7.3095
0.00317415	7.1509
0.002380612	6.9814

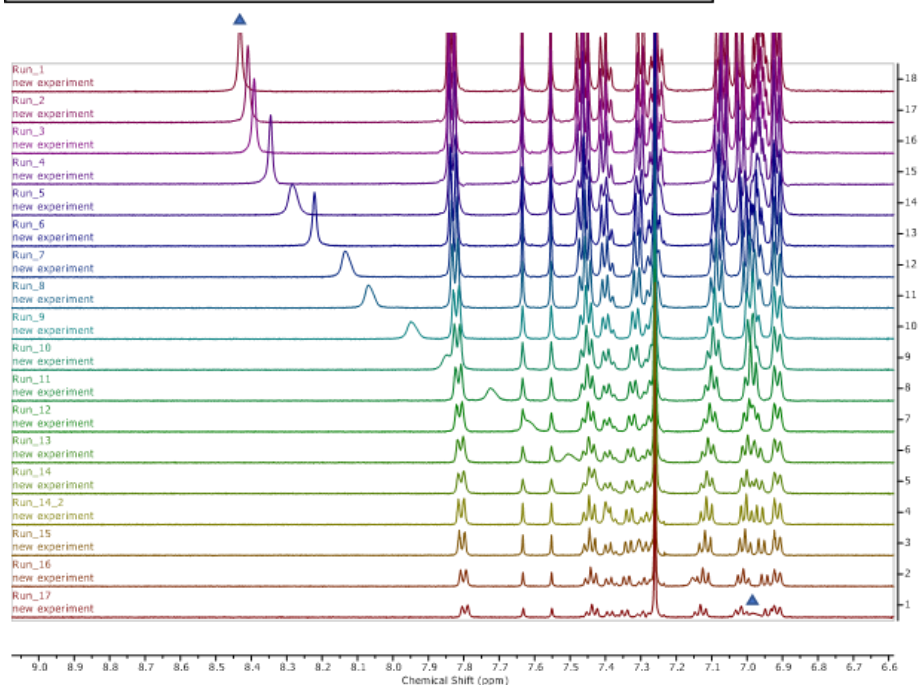
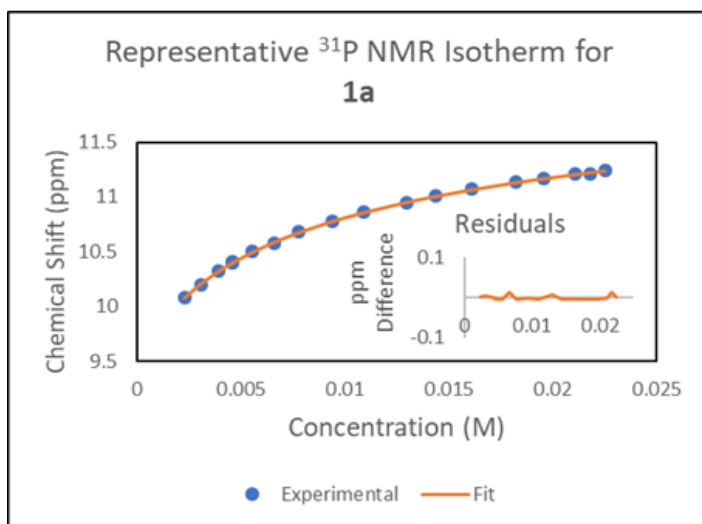


Figure A.10 Representative ^1H NMR binding isotherm with residuals inset (top left), dilution data (top right), and ^1H NMR spectra (bottom) for solution-state dimerization strength studies of **1a** stacked top to bottom with initial and final peak positions marked.



Concentration (M)	Chemical Shift (ppm)
0.0225	11.23715111
0.021774194	11.22065211
0.02109375	11.20459081
0.019565217	11.16621178
0.018243243	11.1301332
0.016071429	11.0639155
0.014361702	11.0043667
0.012980769	10.95033586
0.010887097	10.85553704
0.009375	10.77456868
0.007758621	10.67231395
0.006617647	10.58717881
0.005532787	10.49298134
0.004591837	10.39757619
0.004591837	10.39757619
0.00393586	10.32134385
0.003061224	10.20344861
0.002295918	10.08001827

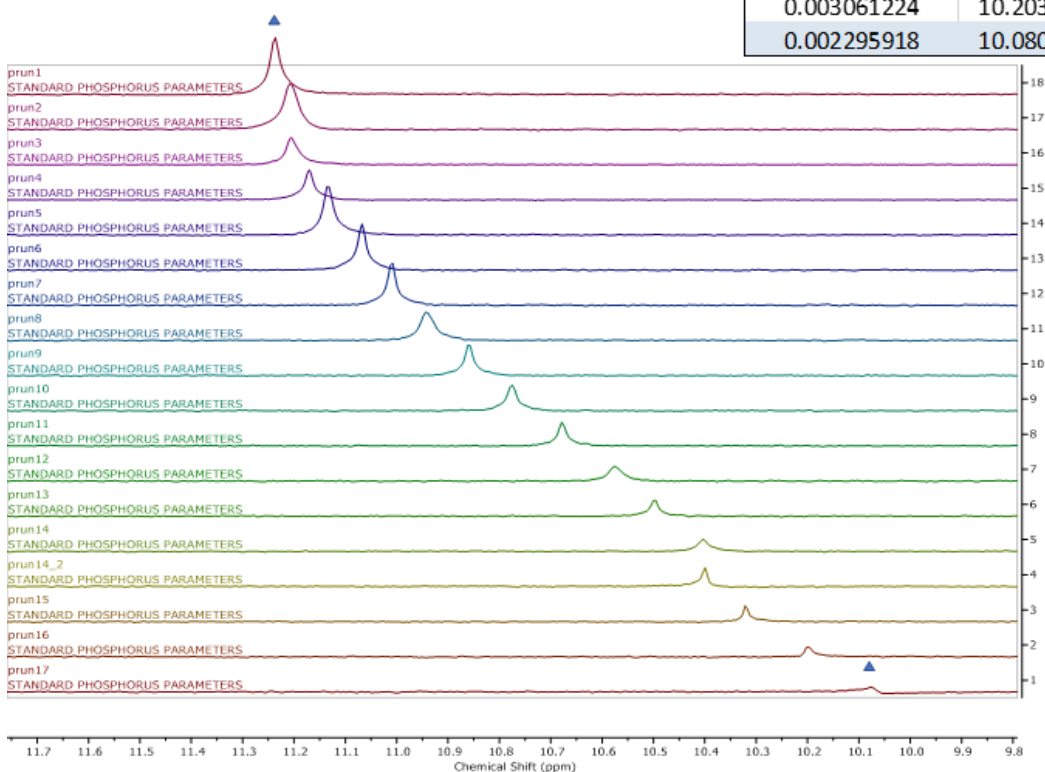
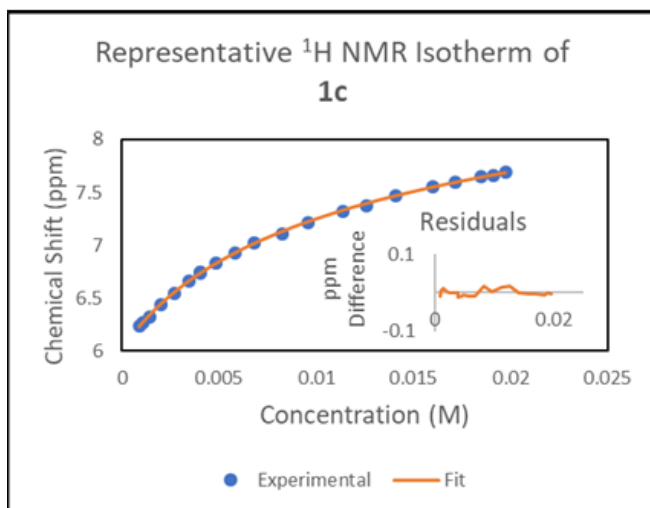
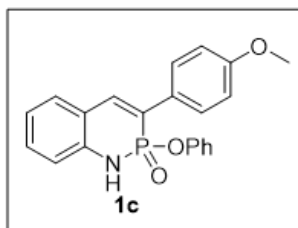


Figure A.11 Representative ^{31}P NMR binding isotherm with residuals inset (top left), dilution data (top right), and stacked ^{31}P NMR spectra (bottom) for solution-state dimerization strength studies of **1a** stacked top to bottom with initial and final peak positions marked.



Concentration (M)	Chemical Shift (ppm)
0.01975	7.688
0.019112903	7.6627
0.018515625	7.6496
0.017173913	7.5973
0.016013514	7.55
0.014107143	7.4672
0.012606383	7.3775
0.011394231	7.316
0.009556452	7.2151
0.008229167	7.1102
0.006810345	7.0236
0.005808824	6.9308
0.004856557	6.8327
0.004030612	6.744
0.004030612	6.7327
0.00345481	6.657
0.002687075	6.5484
0.002015306	6.4392
0.001422569	6.3223
0.001099258	6.2638
0.000895692	6.2369

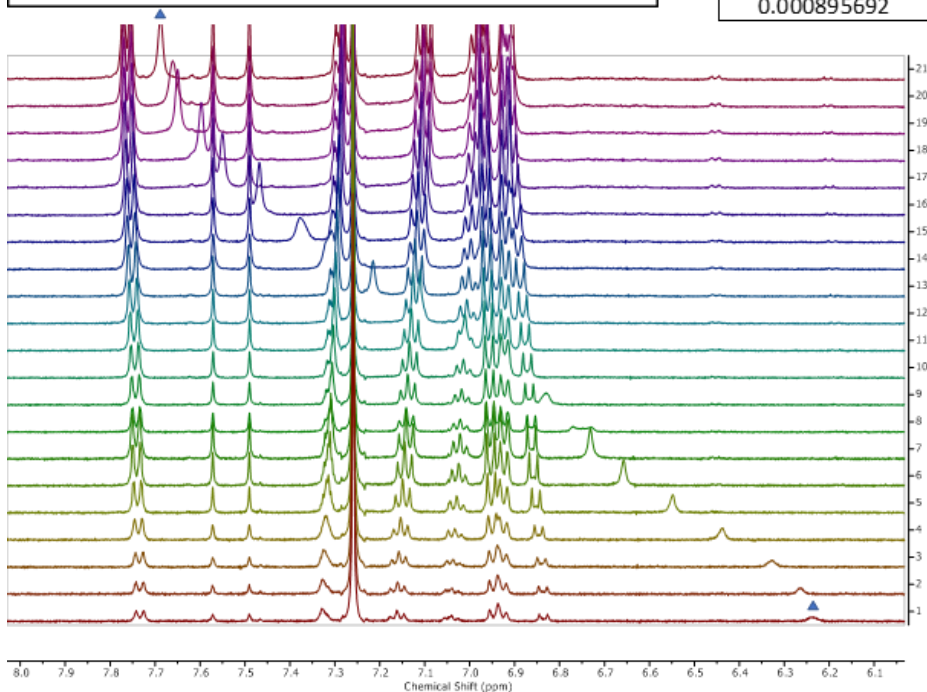
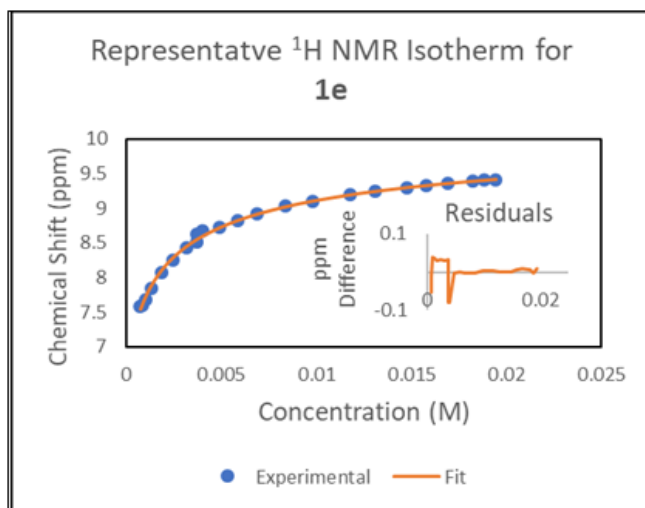
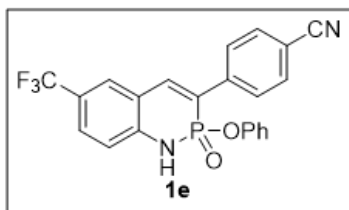


Figure A.12 Representative ^1H NMR binding isotherm with residuals inset (top left), dilution data (top right), and stacked ^1H NMR spectra (bottom) for solution-state dimerization strength studies of **1c** stacked top to bottom with initial and final peak positions marked.



Concentration (M)	Chemical Shift (ppm)
0.019435	9.4085
0.018808065	9.4076
0.018220313	9.3837
0.0169	9.3513
0.015758108	9.3215
0.014760759	9.2995
0.013102247	9.2433
0.011778788	9.1916
0.00979916	9.101
0.008389209	9.026
0.0069	8.9196
0.005859799	8.824
0.004879079	8.7199
0.004034948	8.6799
0.003713694	8.6295
0.003713694	8.5148
0.003183167	8.4219
0.002475796	8.2586
0.001856847	8.0742
0.001310716	7.845
0.001012826	7.68
0.000825265	7.605
0.000742739	7.59

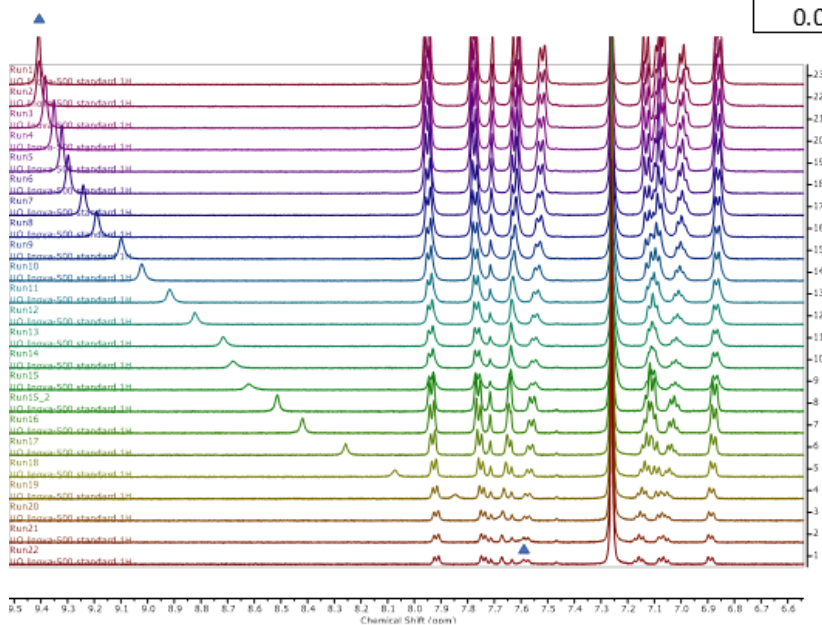
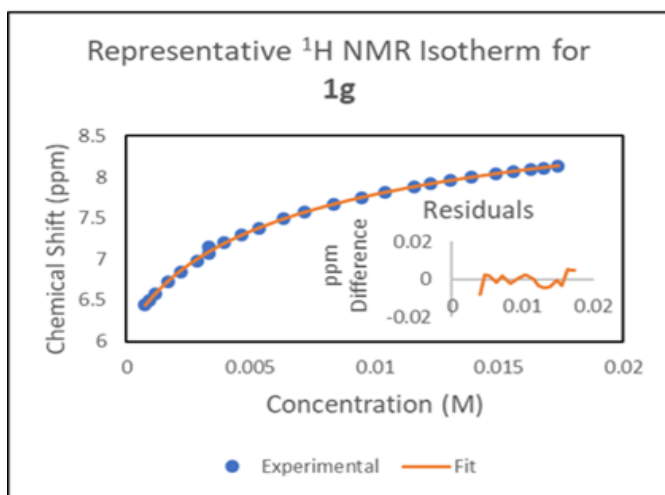
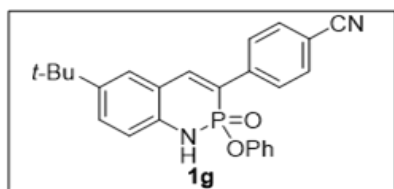


Figure A.13 Representative ^1H NMR binding isotherm with residuals inset (top left), dilution data (top right), and stacked ^1H NMR spectra (bottom) for solution-state dimerization strength studies of **1e** stacked top to bottom with initial and final peak positions marked.



Concentration (M)	Chemical Shift (ppm)
0.01737	8.13
0.016809677	8.11
0.016284375	8.09
0.015555224	8.07
0.014888571	8.04
0.013896	8
0.0130275	7.96
0.012261176	7.92
0.01158	7.88
0.010422	7.81
0.009474545	7.75
0.0083376	7.67
0.007187586	7.57
0.006316364	7.49
0.005344615	7.38
0.004632	7.29
0.00393283	7.2
0.003308571	7.15
0.003308571	7.07
0.002835918	6.98
0.002205714	6.85
0.001654286	6.72
0.001167731	6.58
0.000902338	6.5
0.000735238	6.45

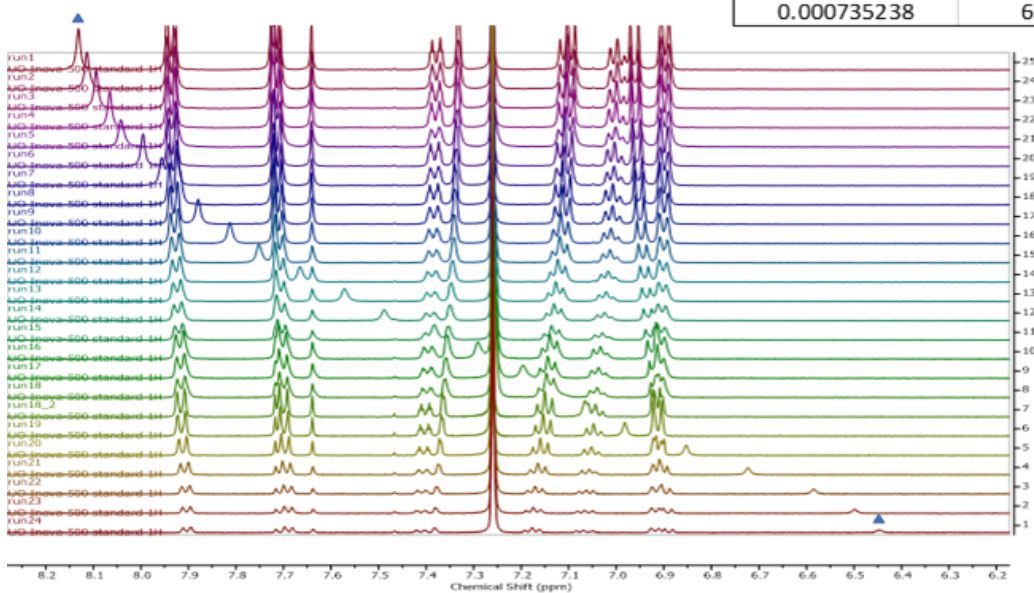
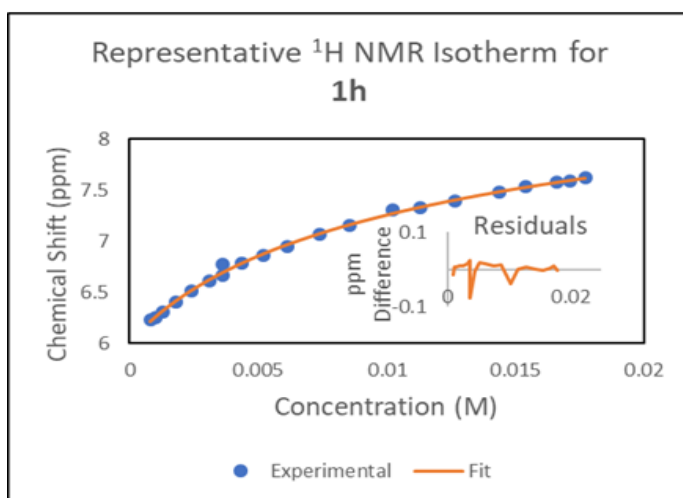
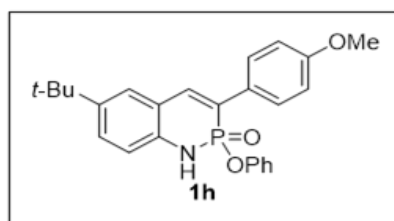


Figure A.14 Representative ^1H NMR binding isotherm with residuals inset (top left), dilution data (top right), and stacked ^1H NMR spectra (bottom) for solution-state dimerization strength studies of **1g** stacked top to bottom with initial and final peak positions marked.



Concentration (M)	Chemical Shift (ppm)
0.01771	7.619
0.01713871	7.5881
0.016603125	7.5739
0.0154	7.5321
0.014359459	7.4836
0.01265	7.3975
0.011304255	7.3319
0.010217308	7.3104
0.008569355	7.1501
0.007379167	7.0637
0.006106897	6.9509
0.005208824	6.8607
0.004354918	6.79
0.003614286	6.77
0.003614286	6.67
0.003097959	6.61
0.002409524	6.51
0.001807143	6.41
0.00127563	6.31
0.000985714	6.25
0.000803175	6.23

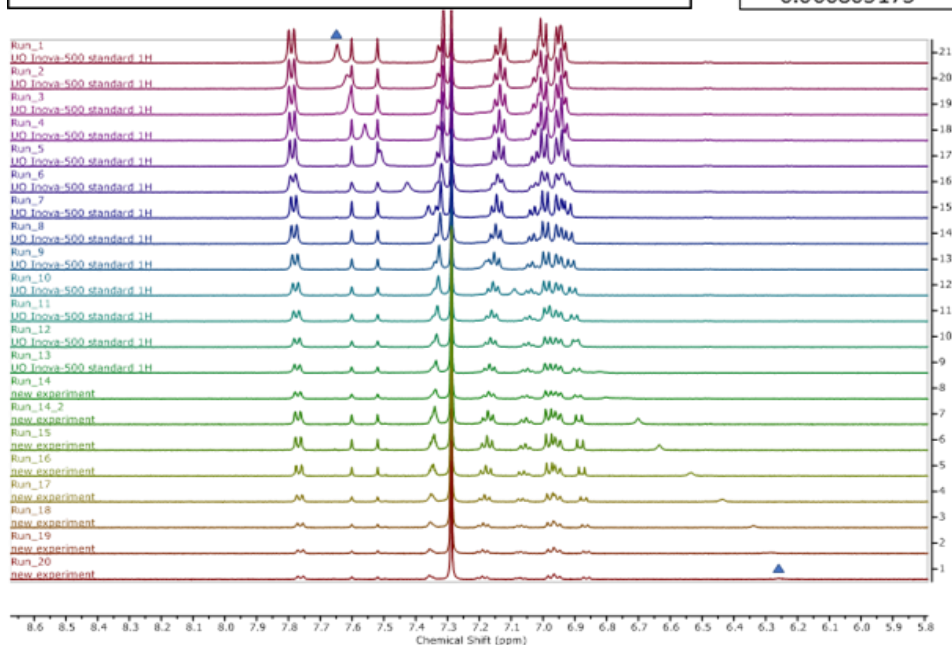


Figure A.15 Representative ^1H NMR binding isotherm with residuals inset (top left), dilution data (top right), and stacked ^1H NMR spectra (bottom) for solution-state dimerization strength studies of **1h** stacked top to bottom with initial and final peak positions marked.

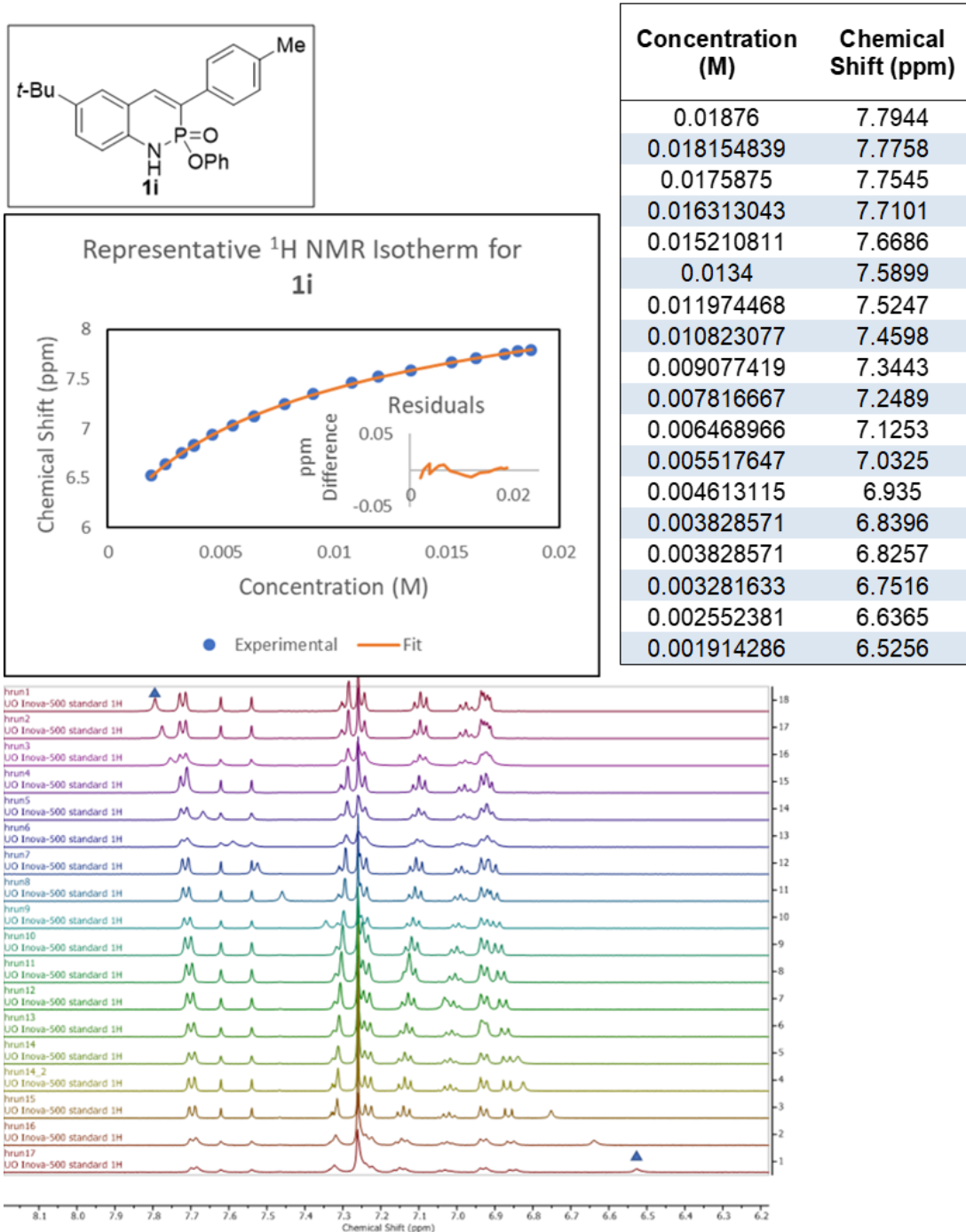
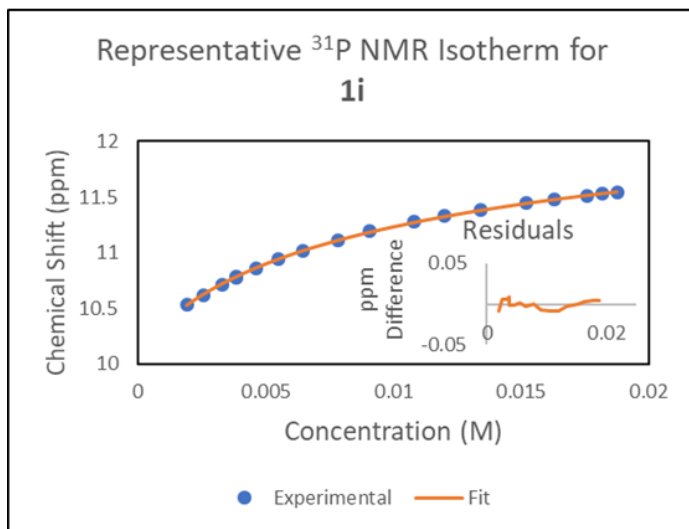


Figure A.16 Representative ¹H NMR binding isotherm with residuals inset (top left), dilution data (top right), and stacked ¹H NMR spectra (bottom) for solution-state dimerization strength studies of **1i** stacked top to bottom with initial and final peak positions marked.



Concentration (M)	Chemical Shift (ppm)
0.01876	11.5429
0.018154839	11.5269
0.0175875	11.5107
0.016313043	11.4745
0.015210811	11.4425
0.0134	11.3816
0.011974468	11.3313
0.010823077	11.2792
0.009077419	11.1906
0.007816667	11.1089
0.006468966	11.0197
0.005517647	10.9395
0.004613115	10.8612
0.003828571	10.781
0.003828571	10.7703
0.003281633	10.7103
0.002552381	10.6147
0.001914286	10.534

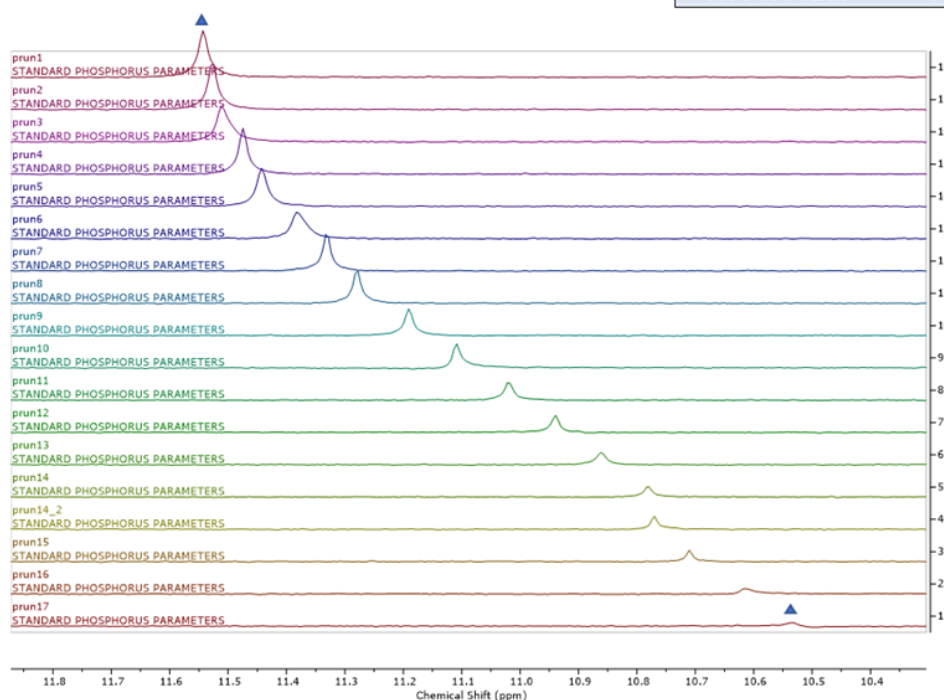
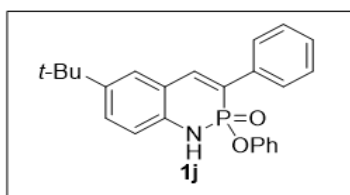


Figure A.17 Representative ^{31}P NMR binding isotherm with residuals inset (top left), dilution data (top right), and stacked ^{31}P NMR spectra (bottom) for solution-state dimerization strength studies of **1i** stacked top to bottom with initial and final peak positions marked.



Concentration (M)	Chemical Shift (ppm)
0.02118	7.9745
0.020496774	7.9501
0.01985625	7.9312
0.018417391	7.8803
0.017172973	7.83
0.016086076	7.79
0.014278652	7.7096
0.012836364	7.6395
0.010678992	7.5142
0.009142446	7.4104
0.007519527	7.2867
0.00638593	7.187
0.005317155	7.076
0.004397232	7.0185
0.004397232	6.9522
0.003769056	6.8695
0.002931488	6.7443
0.002198616	6.606
0.001551964	6.486
0.001199245	6.4037
0.000977163	6.3645

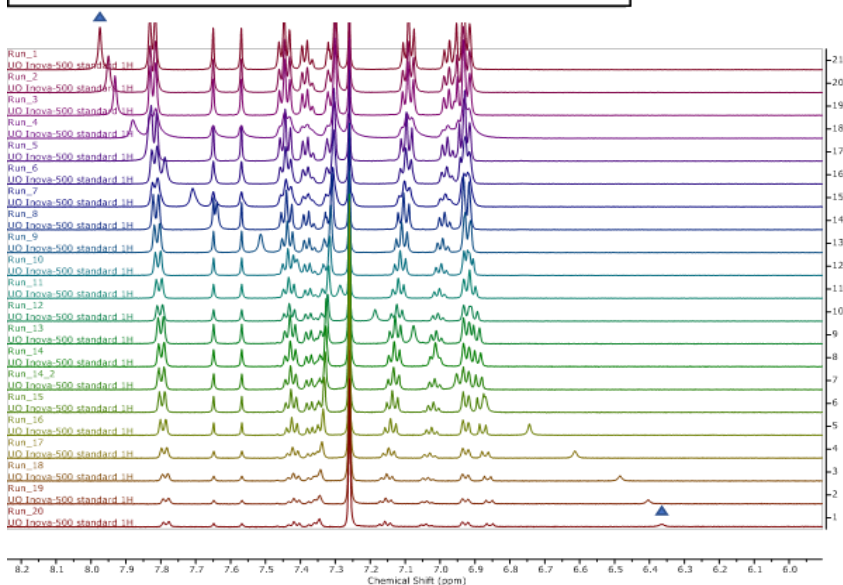
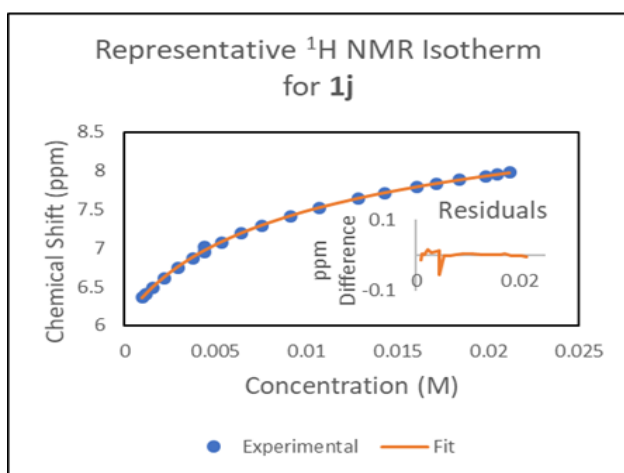
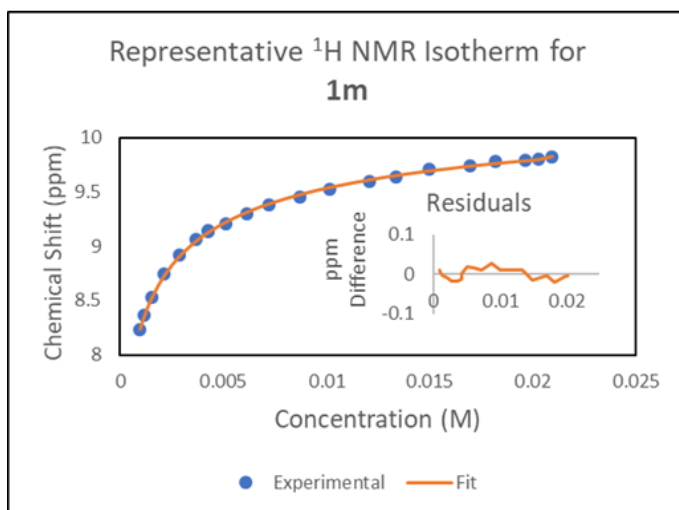
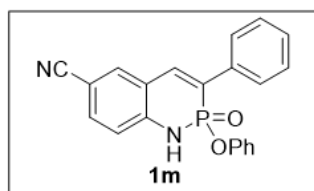


Figure A.18 Representative ^1H NMR binding isotherm with residuals inset (top left), dilution data (top right), and stacked ^1H NMR spectra (bottom) for solution-state dimerization strength studies of **1j** stacked top to bottom with initial and final peak positions marked.



Concentration (M)	Chemical Shift (ppm)
0.02093	9.8246
0.020254839	9.8
0.019621875	9.79
0.0182	9.7794
0.01697027	9.74
0.01495	9.7061
0.013359574	9.64
0.012075	9.6
0.010127419	9.53
0.008720833	9.45
0.007217241	9.38
0.006155882	9.3
0.005146721	9.21
0.004271429	9.13
0.004271429	9.1438
0.003661224	9.0663
0.002847619	8.9243
0.002135714	8.7485
0.001507563	8.5291
0.001164935	8.3653
0.000949206	8.2316

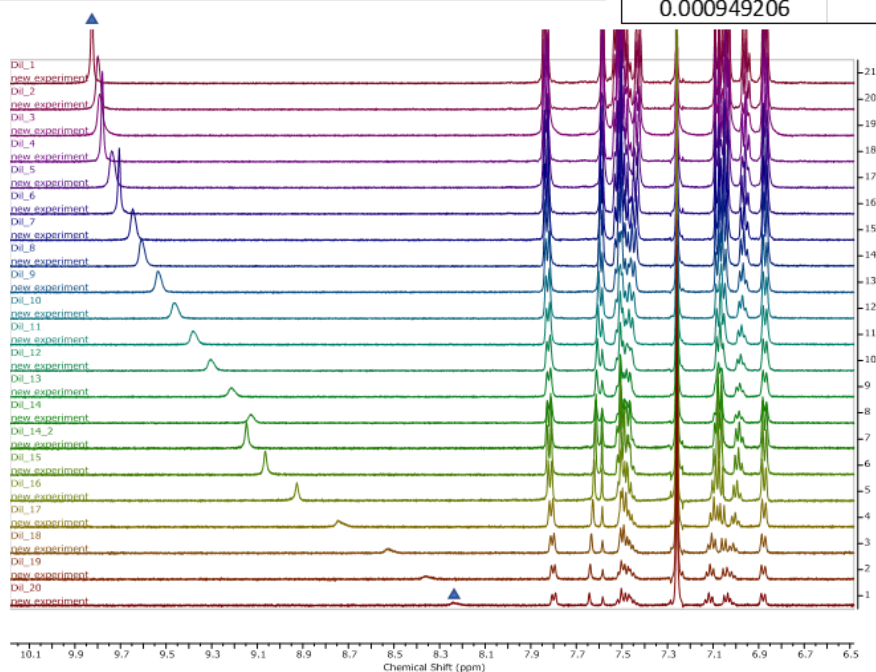
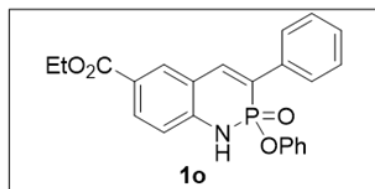


Figure A.19 Representative ^1H NMR binding isotherm with residuals inset (top left), dilution data (top right), and stacked ^1H NMR spectra (bottom) for solution-state dimerization strength studies of **1m** stacked top to bottom with initial and final peak positions marked.



Concentration (M)	Chemical Shift (ppm)
0.017245161	9.2
0.01670625	9.1915
0.015495652	9.154
0.014448649	9.1099
0.012728571	9.0538
0.011374468	8.9816
0.010280769	8.9246
0.008622581	8.825
0.007425	8.7351
0.006144828	8.6192
0.005241176	8.5212
0.004381967	8.4057
0.003636735	8.3111
0.003636735	8.2793
0.003117201	8.1793
0.00242449	8.0127
0.001818367	7.816

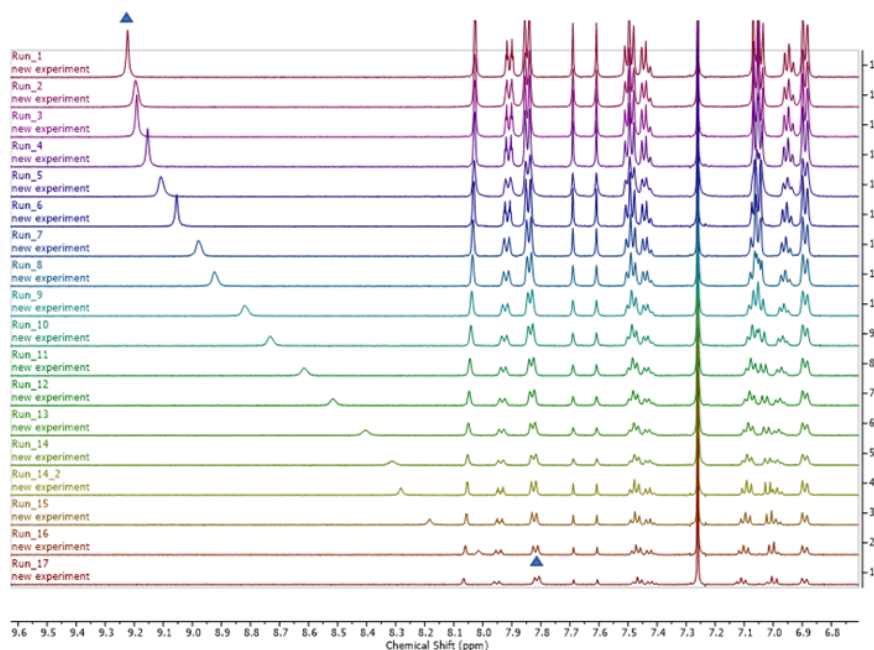
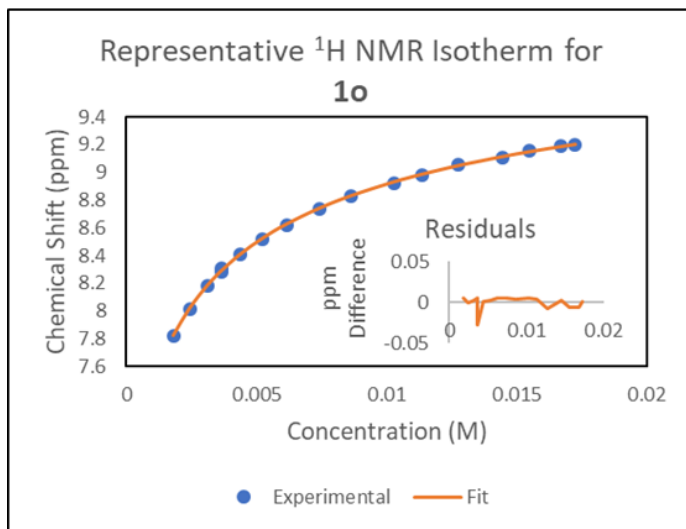
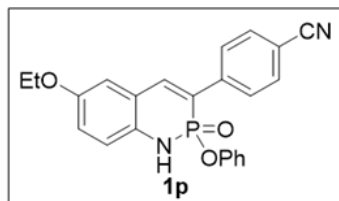


Figure A.20 Representative ^1H NMR binding isotherm with residuals inset (top left), dilution data (top right), and stacked ^1H NMR spectra (bottom) for solution-state dimerization strength studies of **1o** stacked top to bottom with initial and final peak positions marked.



Concentration (M)	Chemical Shift (ppm)
0.02024	8.2294
0.019587097	8.216
0.018975	8.1935
0.0176	8.152
0.016410811	8.1095
0.014457143	8.0286
0.012919149	7.9525
0.011676923	7.8866
0.009793548	7.7745
0.008433333	7.681
0.00697931	7.5541
0.005952941	7.4537
0.004977049	7.3653
0.004130612	7.25
0.004130612	7.2247
0.003540525	7.13
0.002753741	6.98
0.002065306	6.85

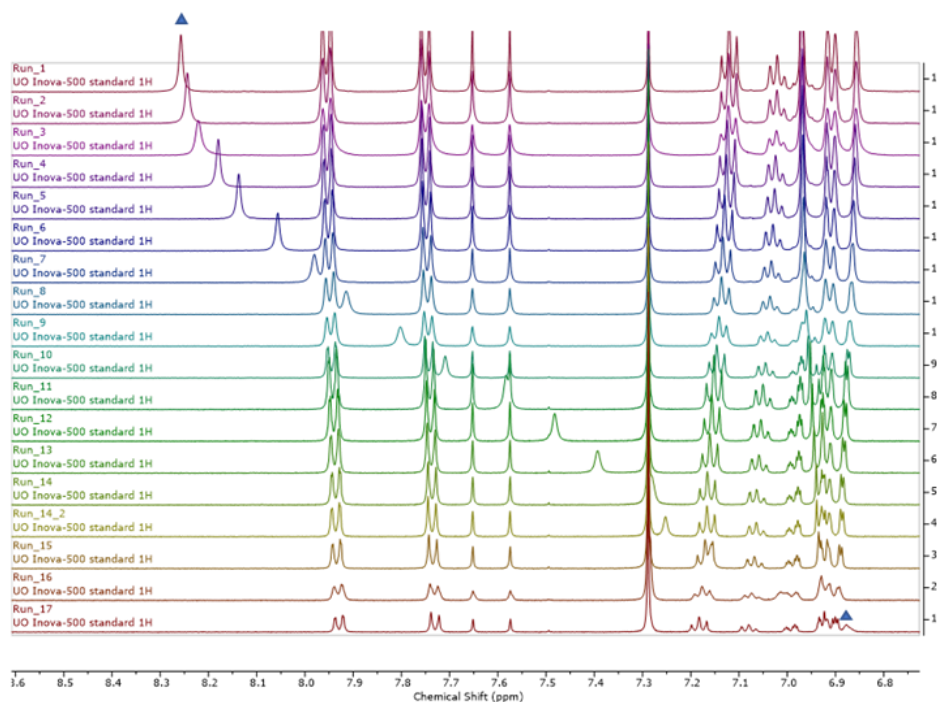
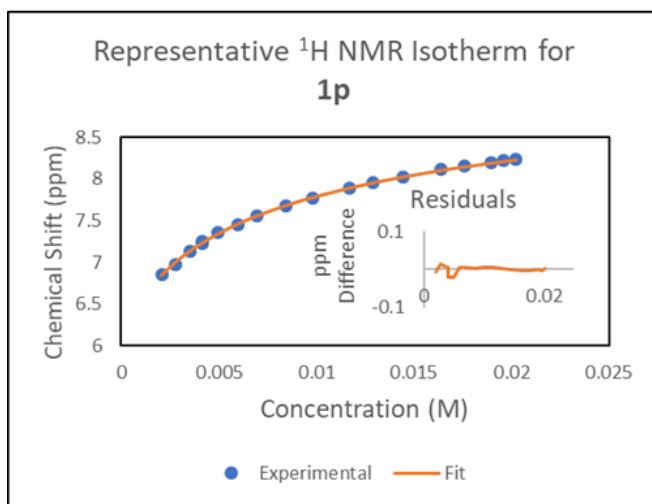


Figure A.21 Representative ^1H NMR binding isotherm with residuals inset (top left), dilution data (top right), and stacked ^1H NMR spectra (bottom) for solution-state dimerization strength studies of **1p** stacked top to bottom with initial and final peak positions marked.

7. Cyclic Voltammetry Studies

Cyclic voltammetry (CV) measurements taken with a Bio-Logic SP-50 potentiostat. Samples were prepared as *ca.* 1 mM solutions in air- and water-free dichloromethane with 0.1 M TBA-PF₆ electrolyte solution. Samples were referenced using Fc/Fc⁺ as an external reference. Figure A.22 shows the voltammogram of **1j** as a representative voltammogram for heterocycles **1** and shows several oxidation and reduction peaks. Of interest, the difference of 4.003 eV between the lowest energy oxidation event (1.682 eV vs Fc/Fc⁺) and the lowest energy reduction event (-2.319 eV vs Fc/Fc⁺) corresponds nicely with the energy gaps determined by theoretical and spectroscopic methods.

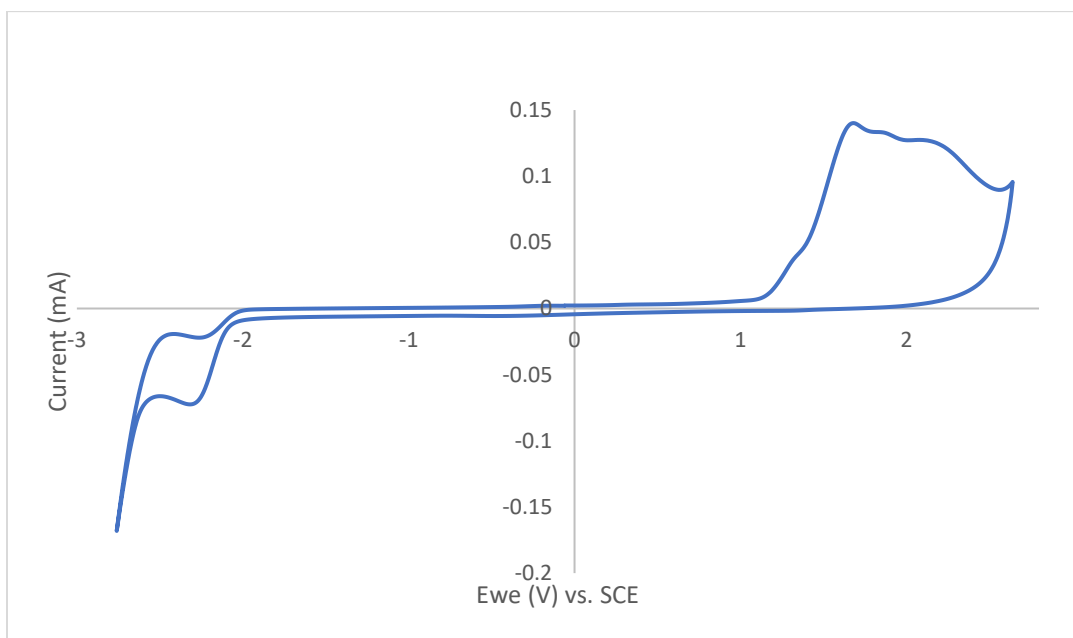
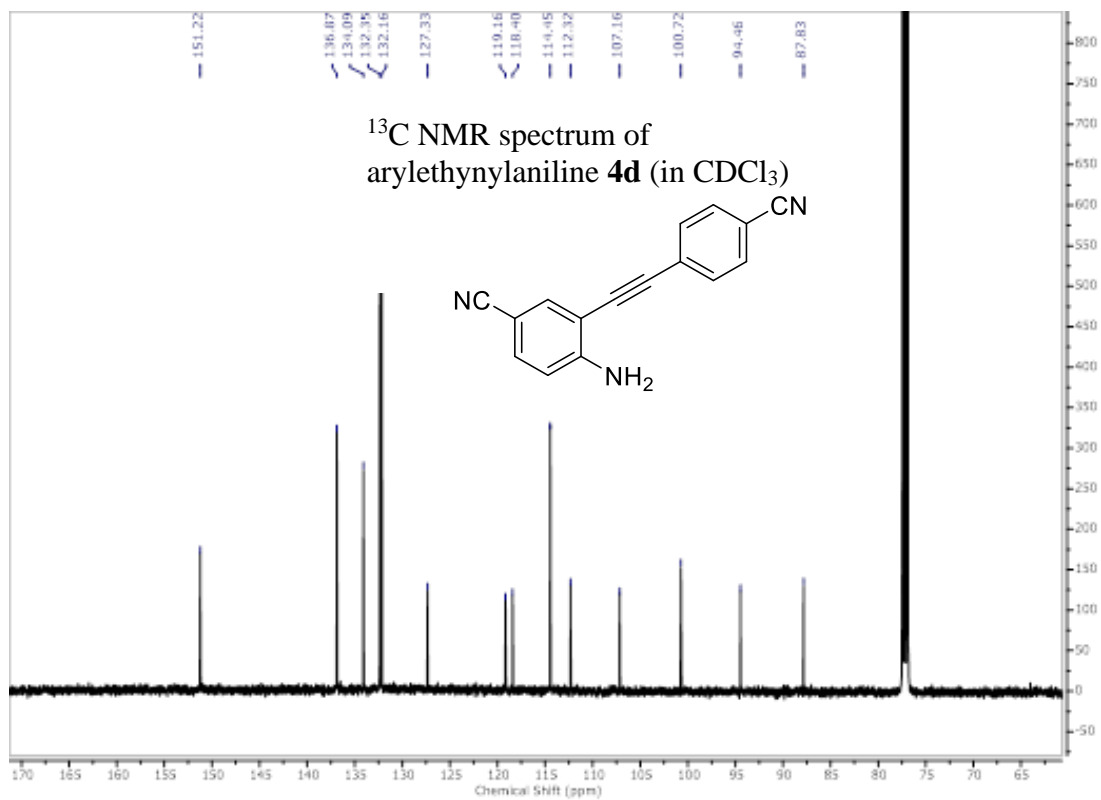
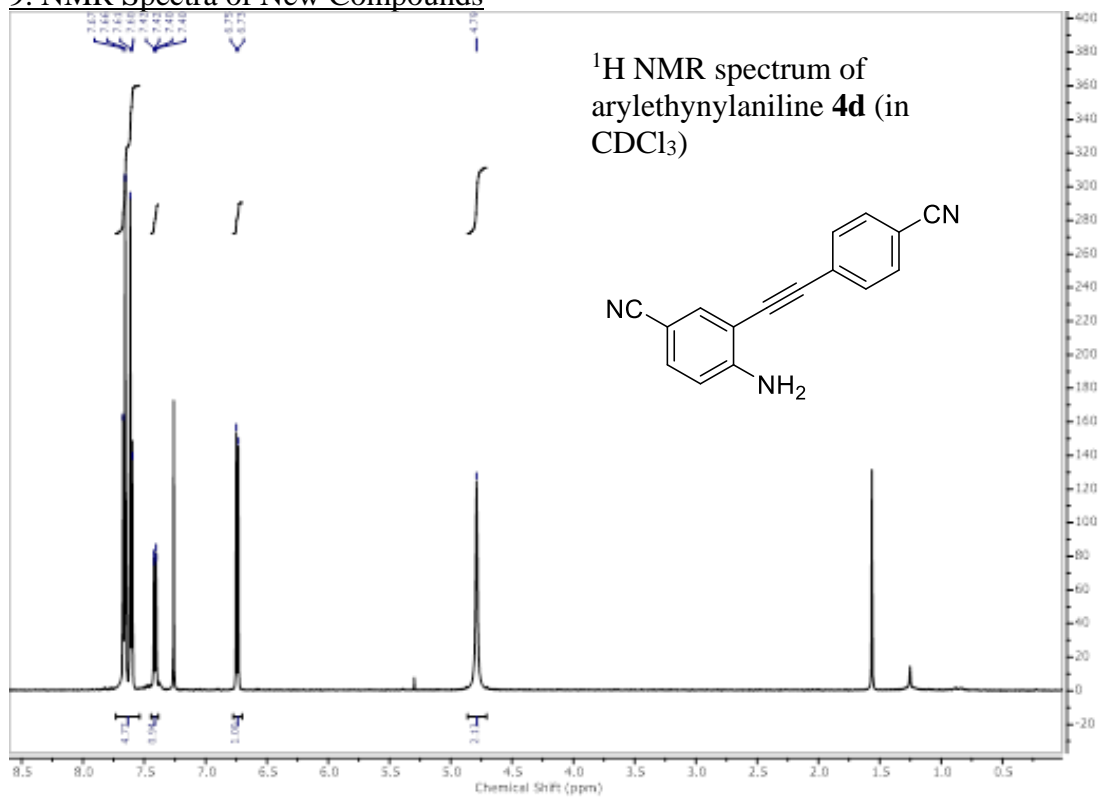
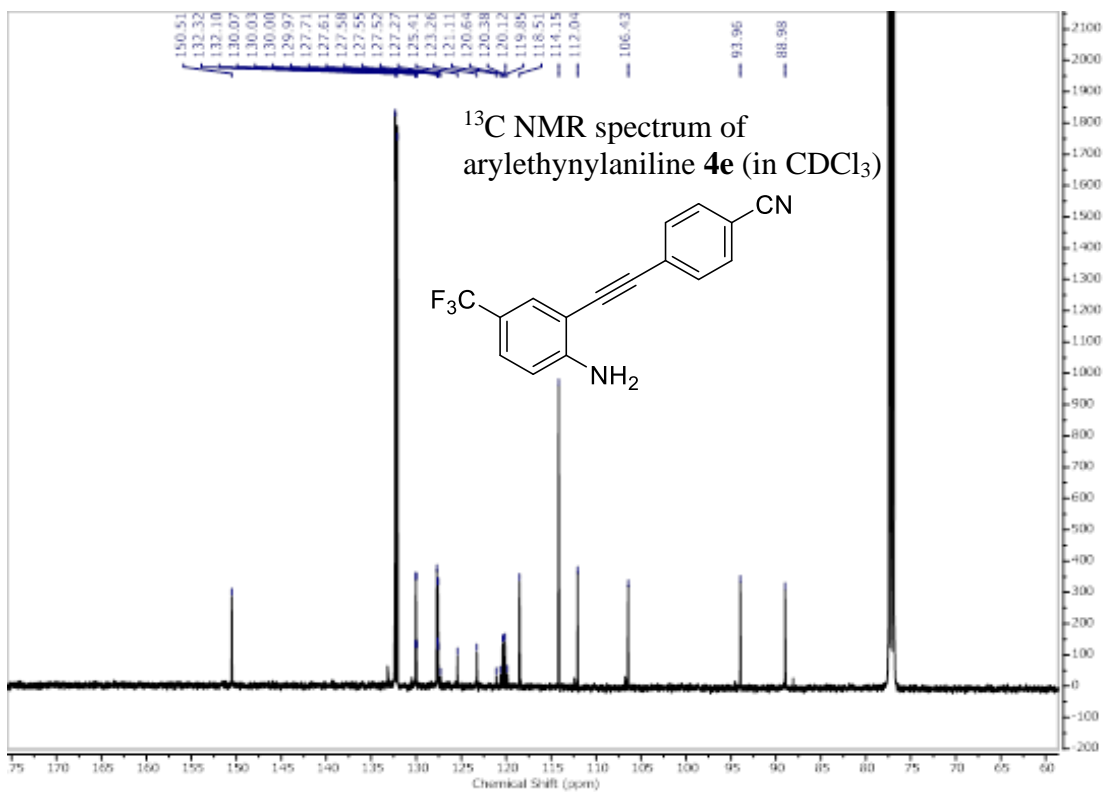
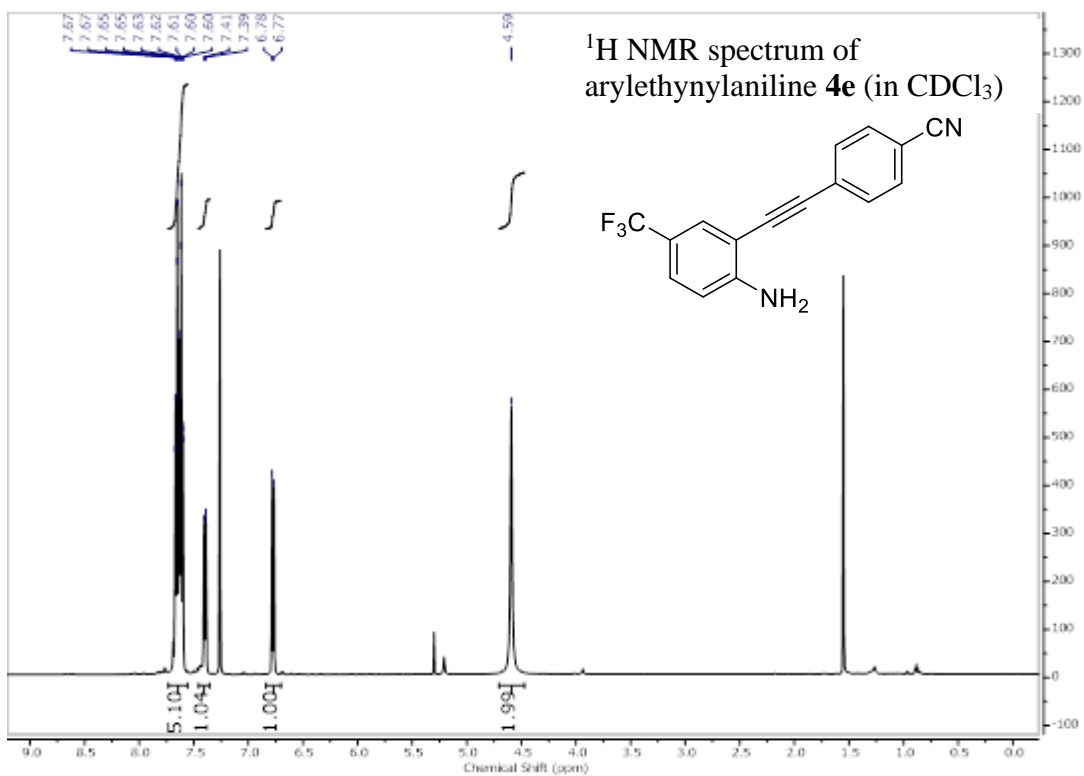
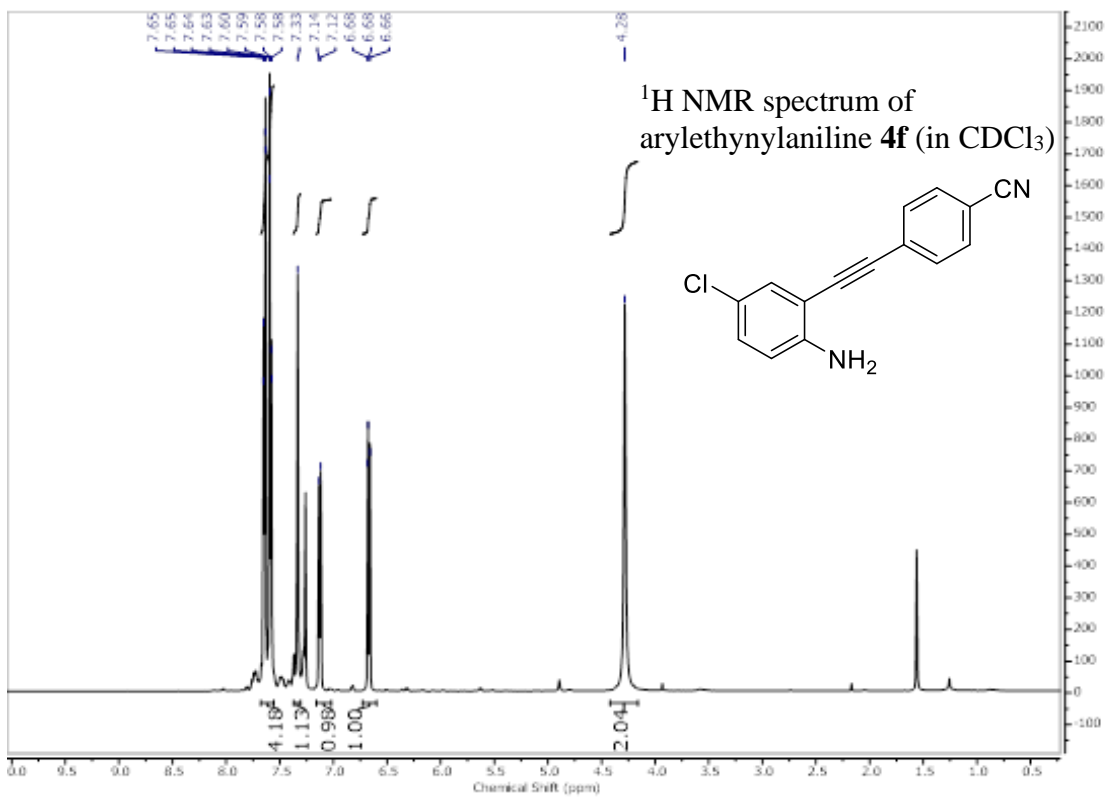
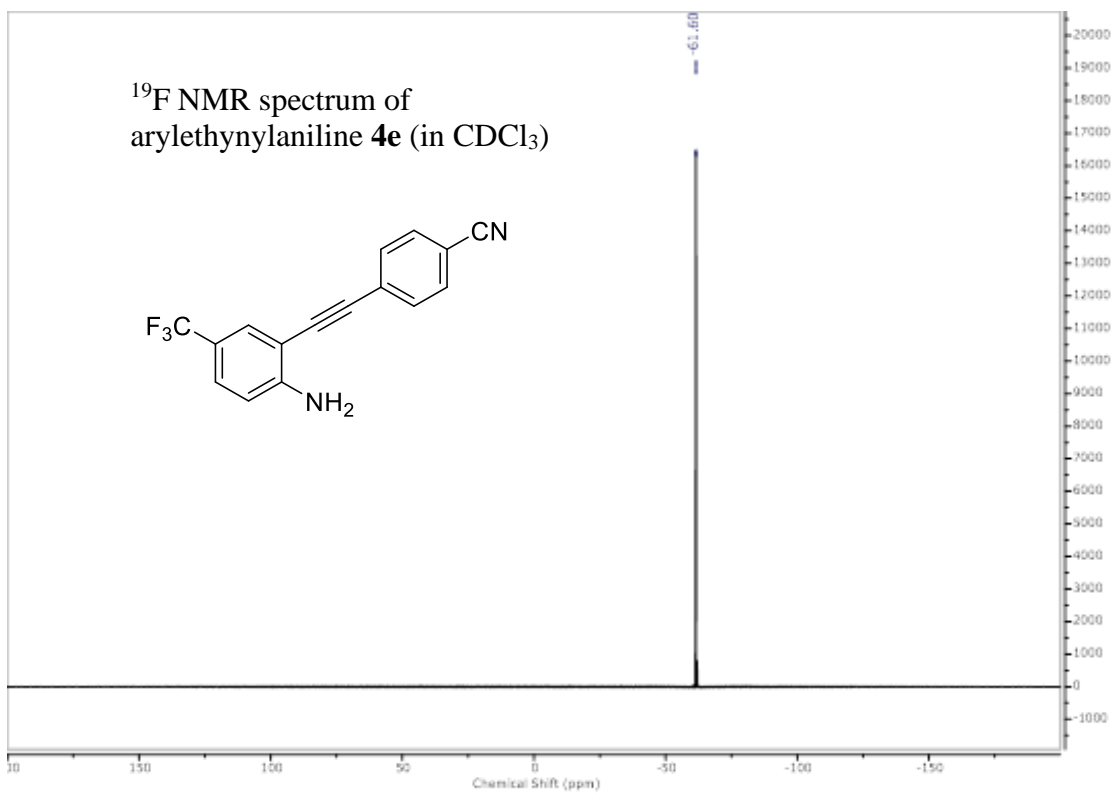


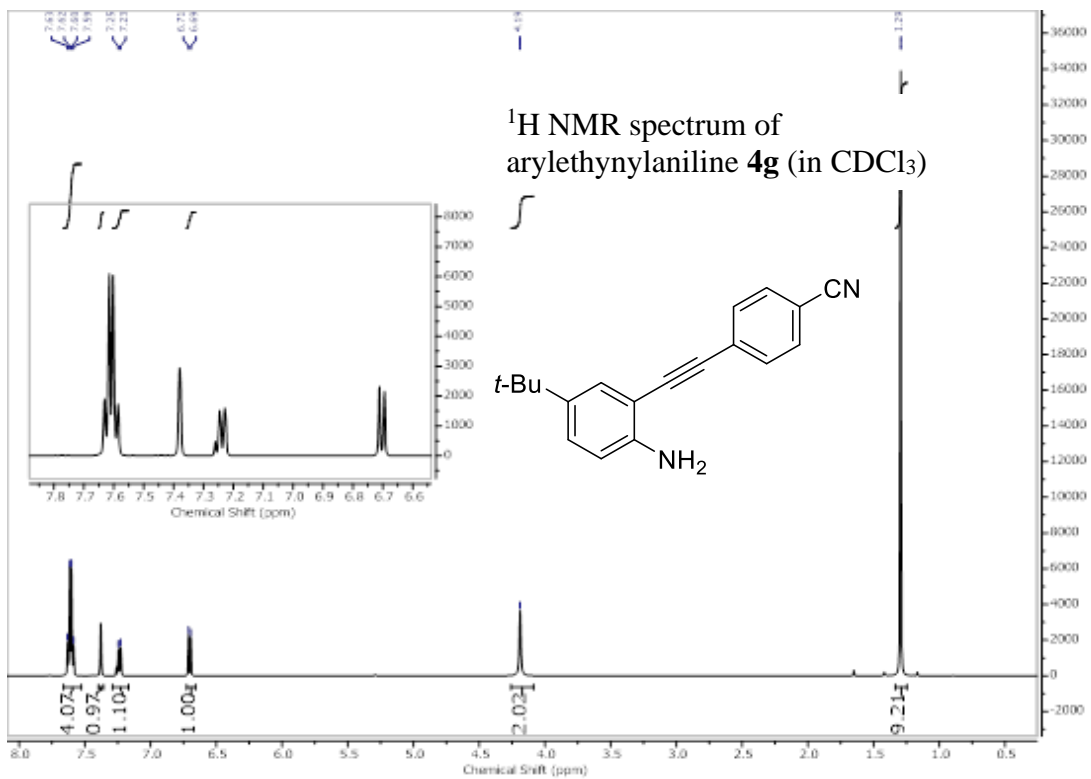
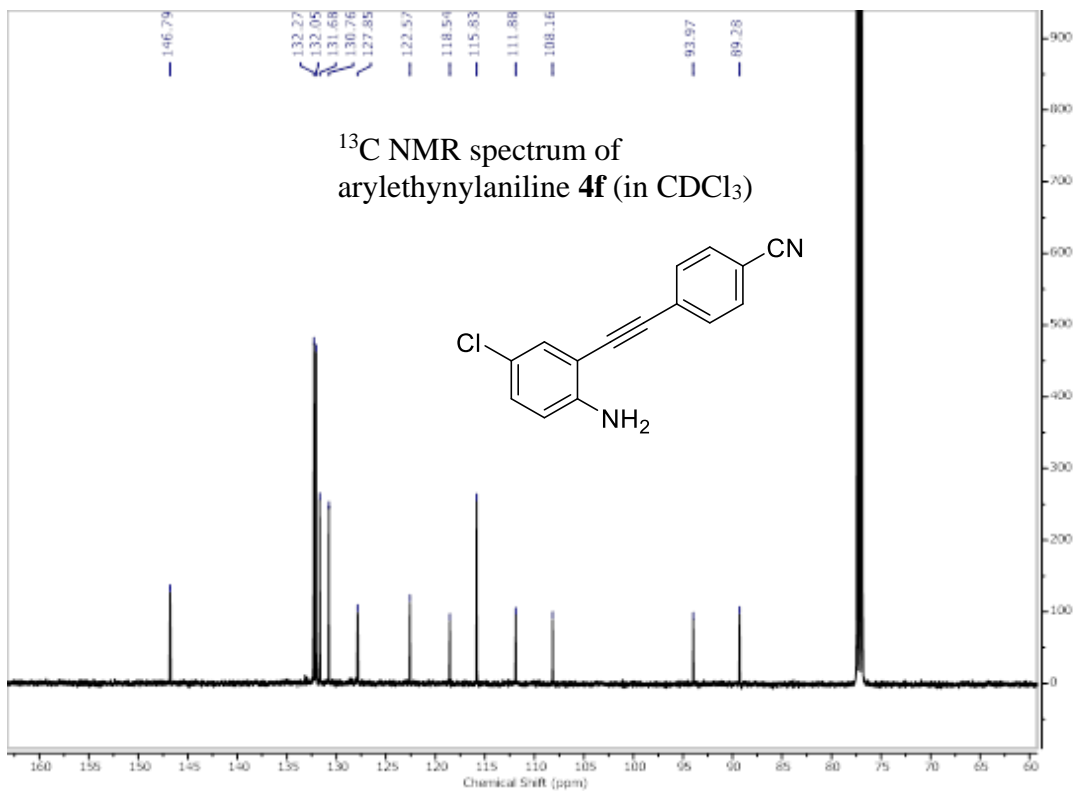
Figure A.22 Cyclic voltammogram showing oxidation and reduction potentials for **1j** as a representative curve for heterocycles **1**.

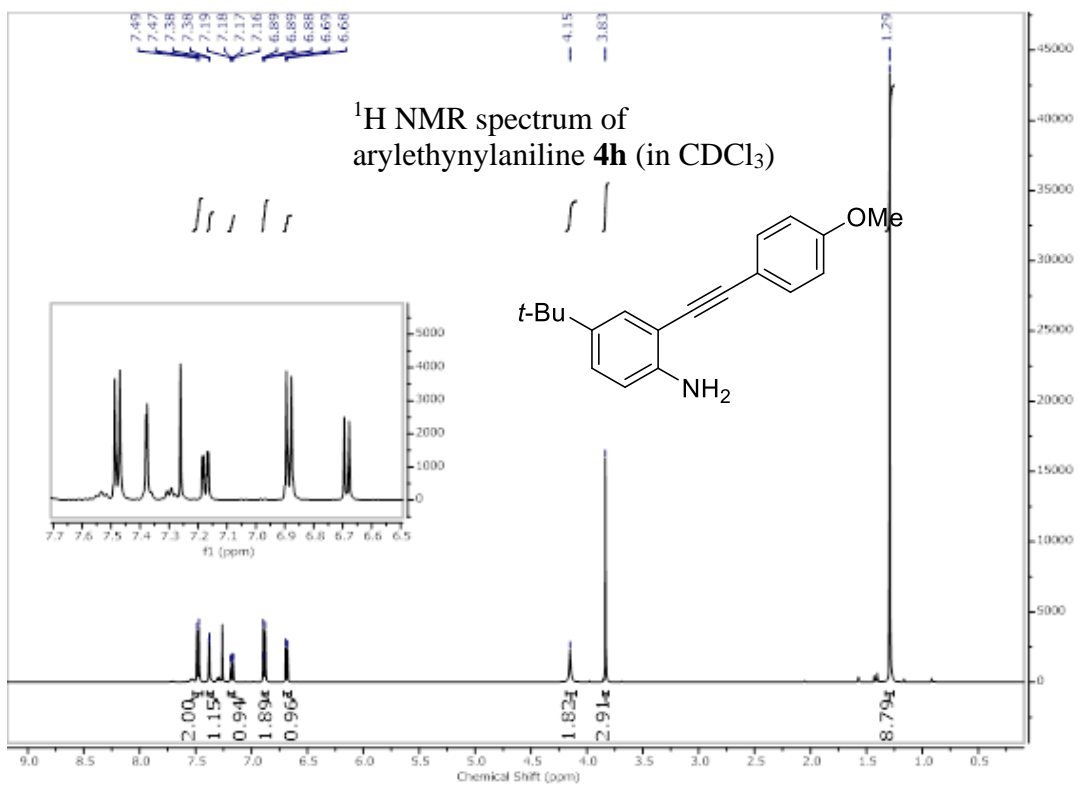
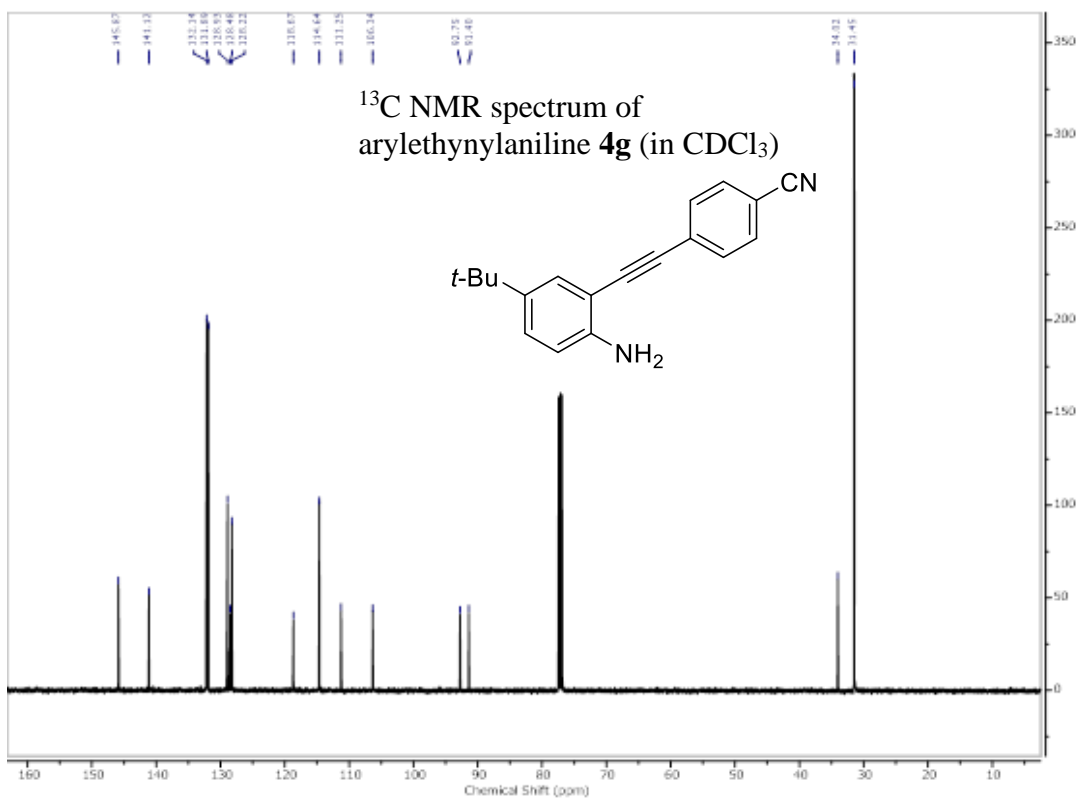
9. NMR Spectra of New Compounds

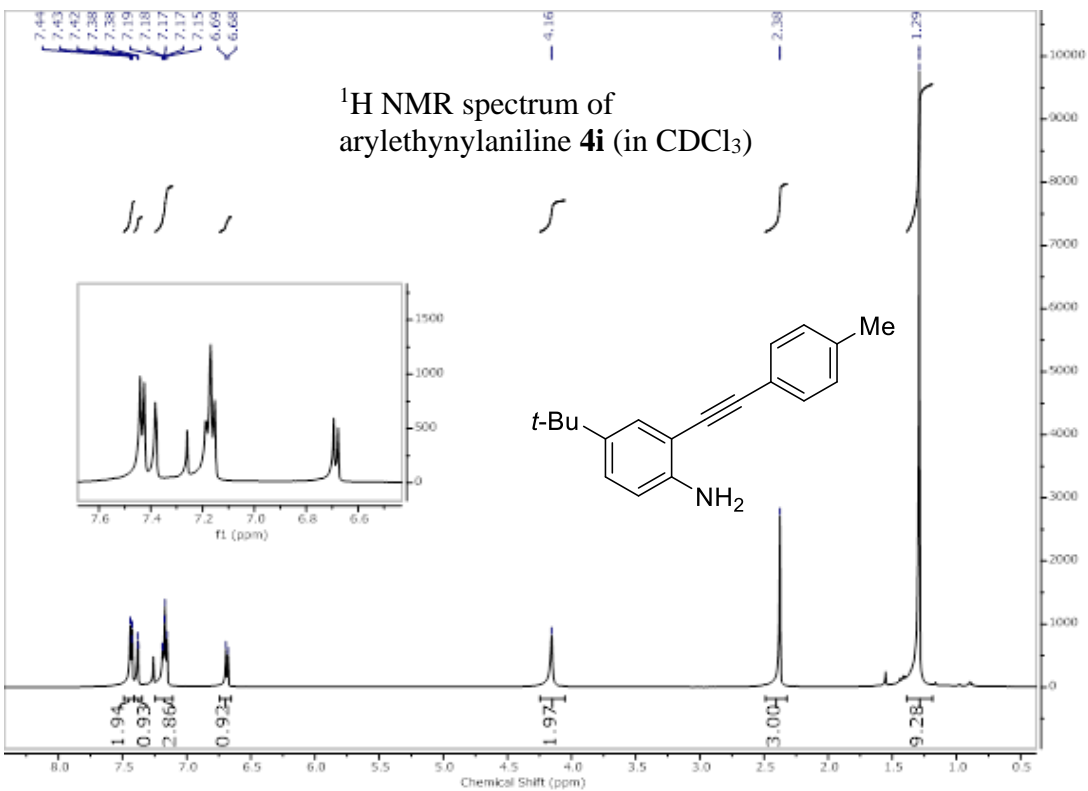
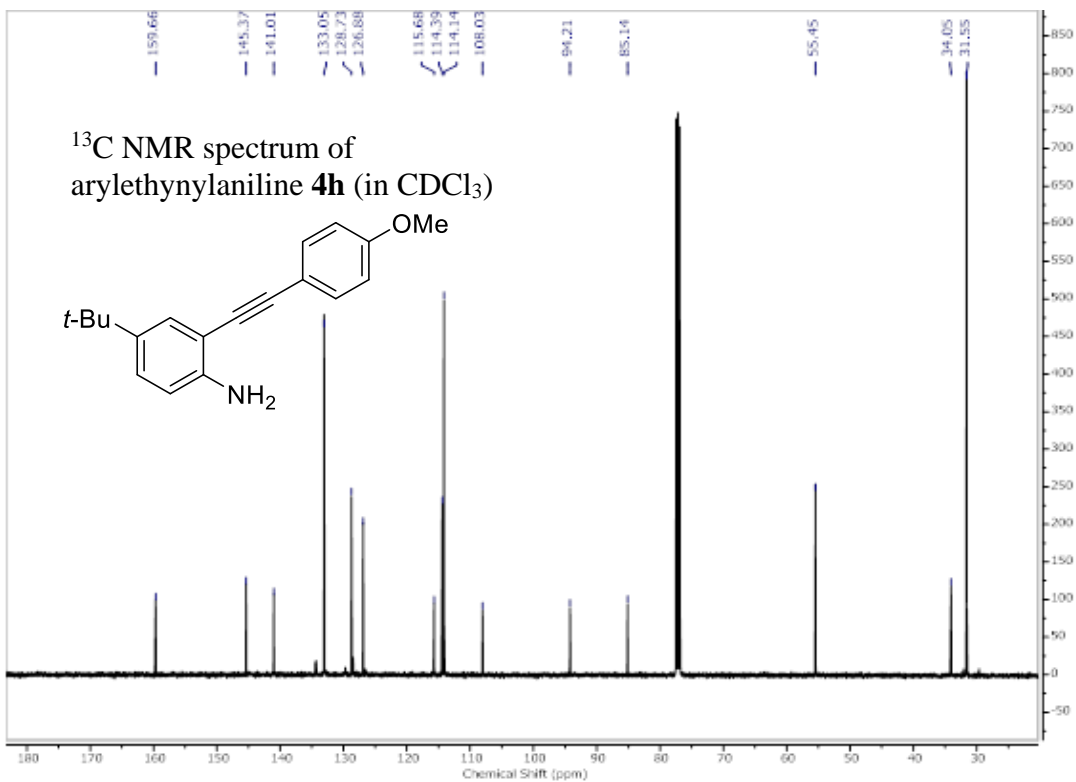


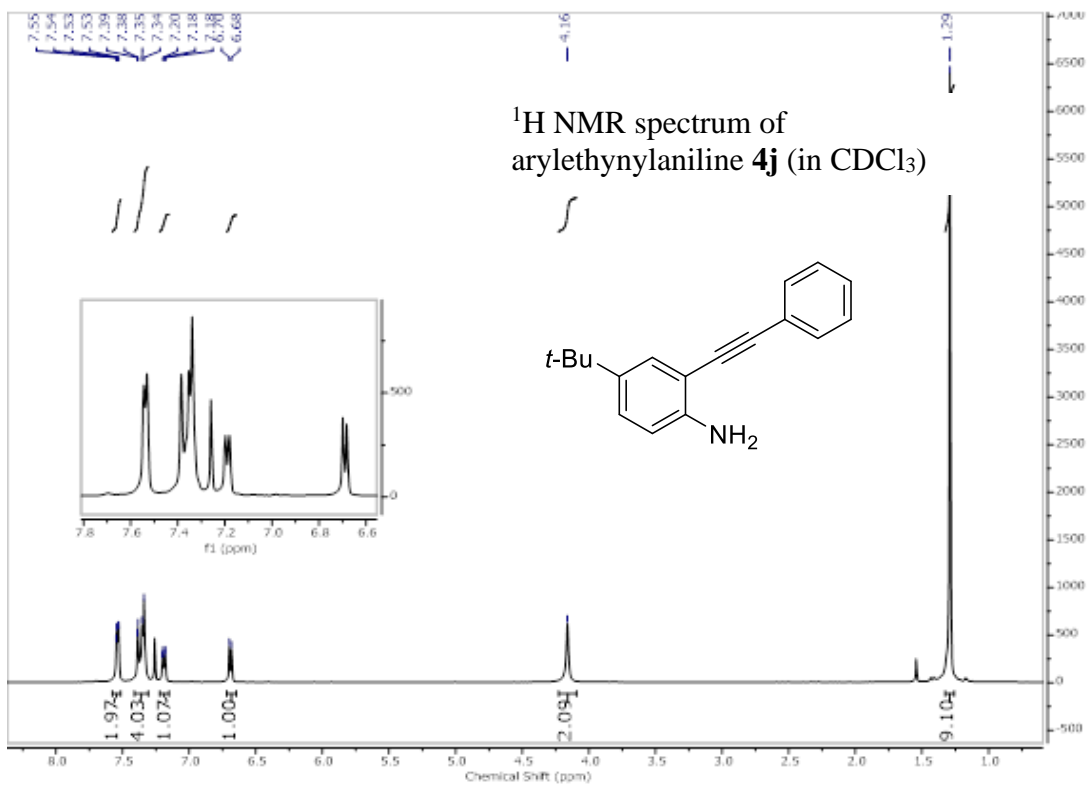
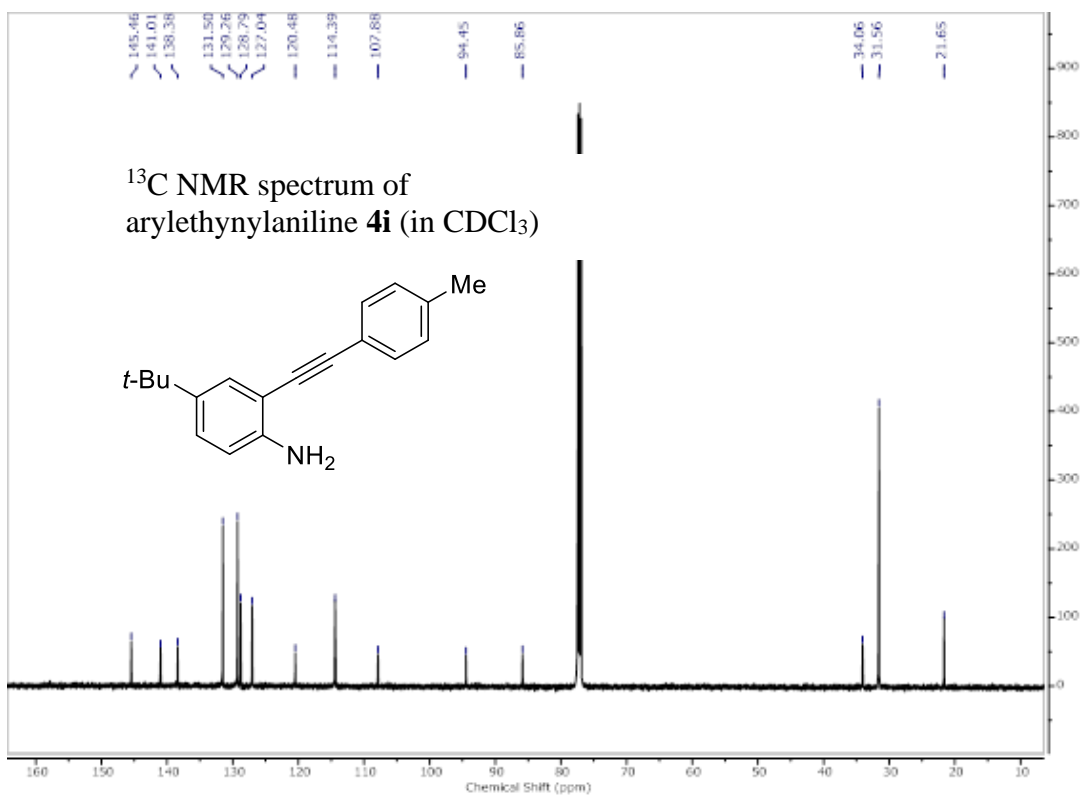


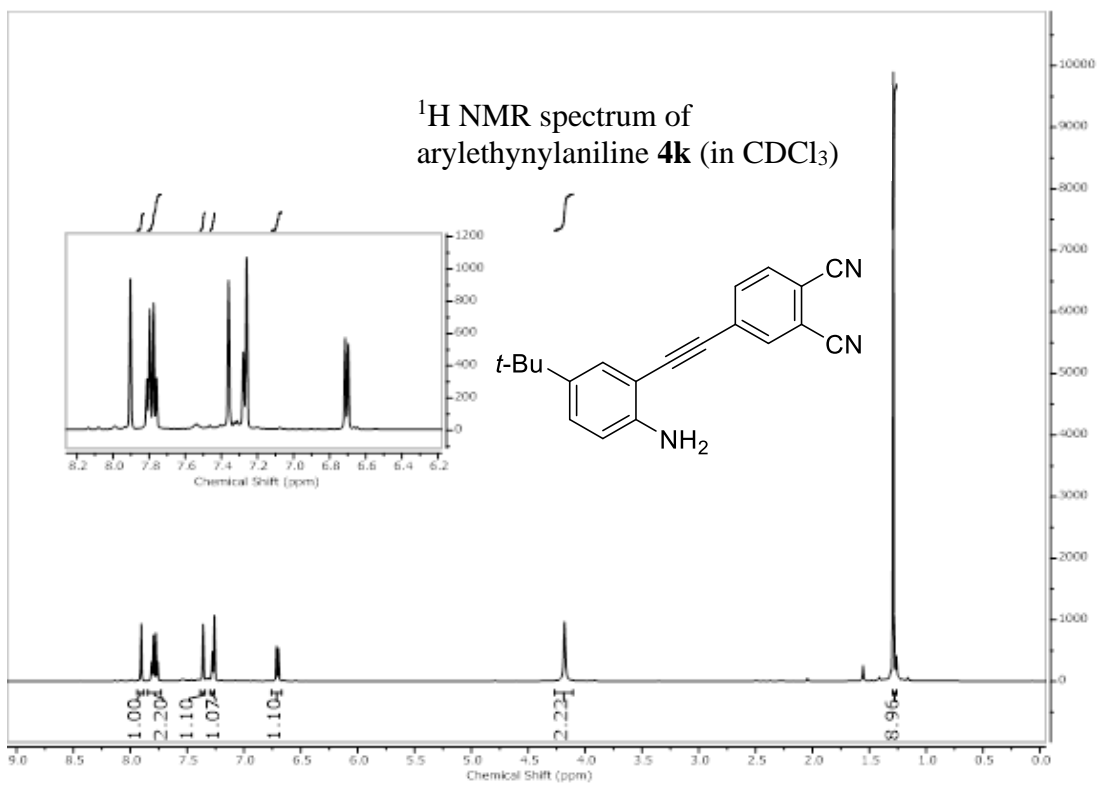
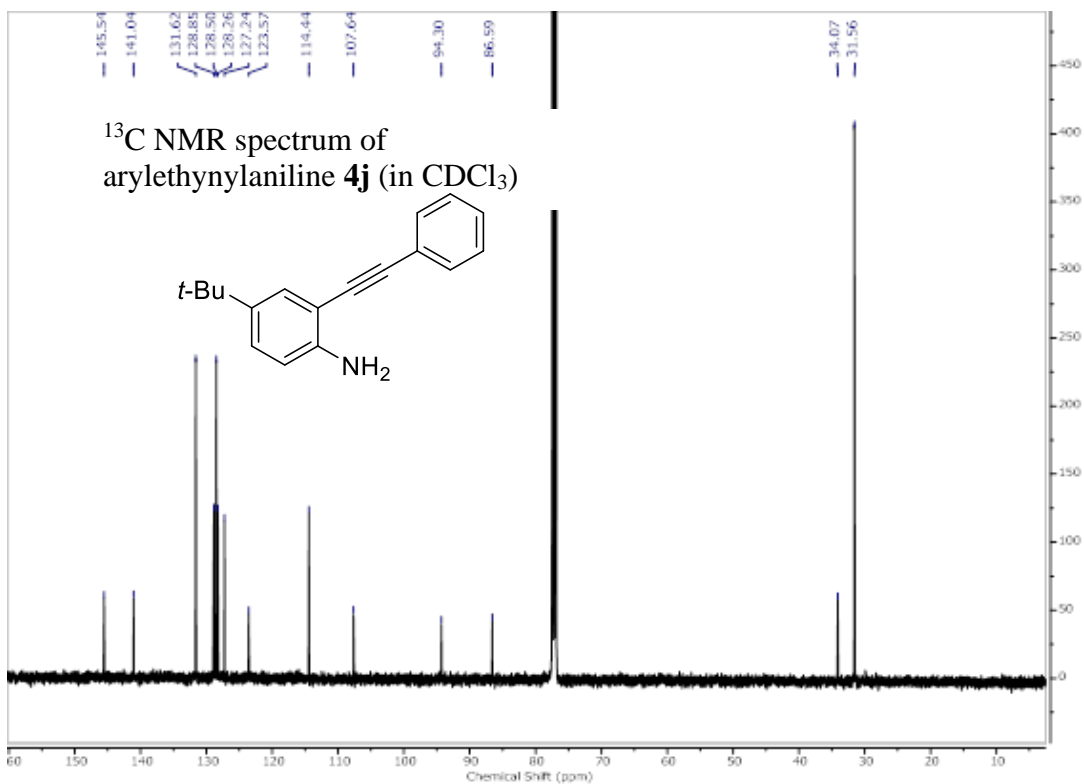


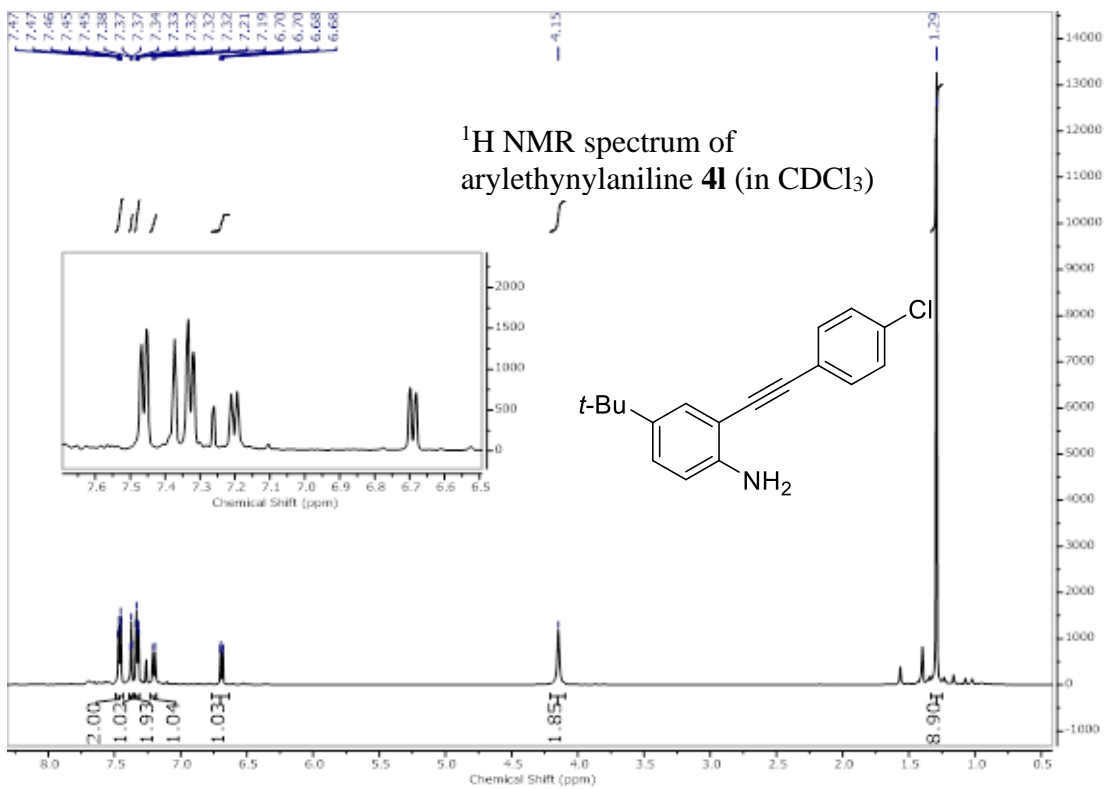
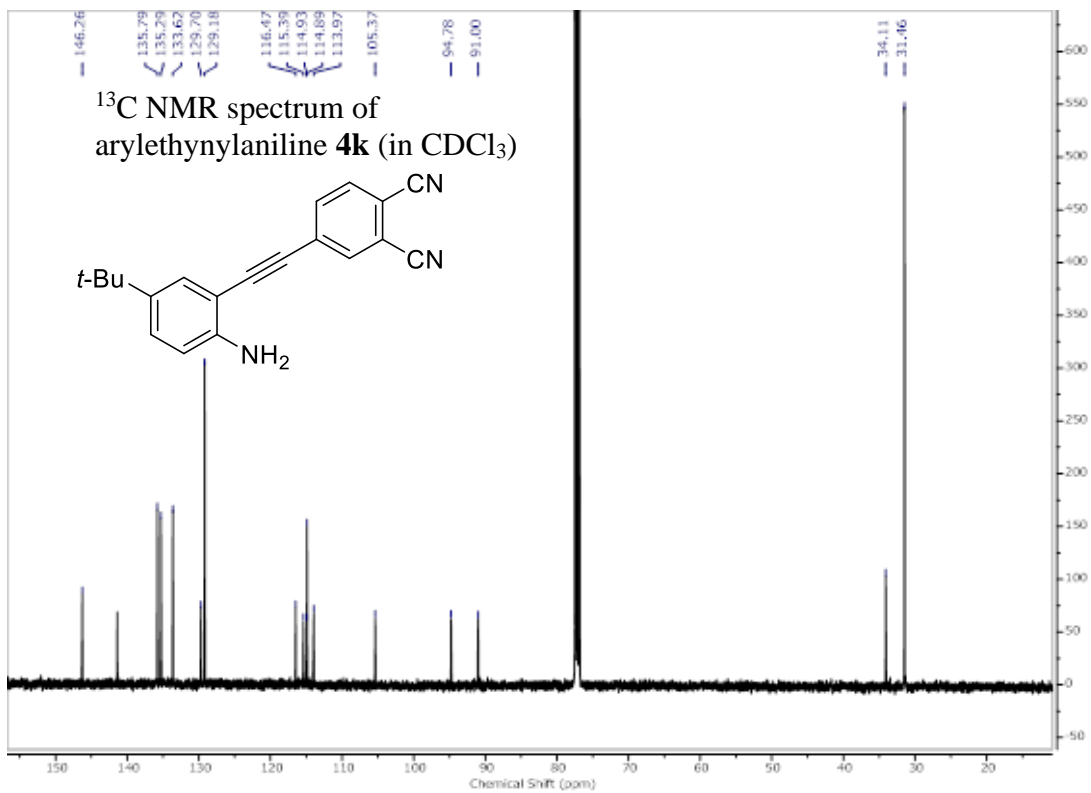


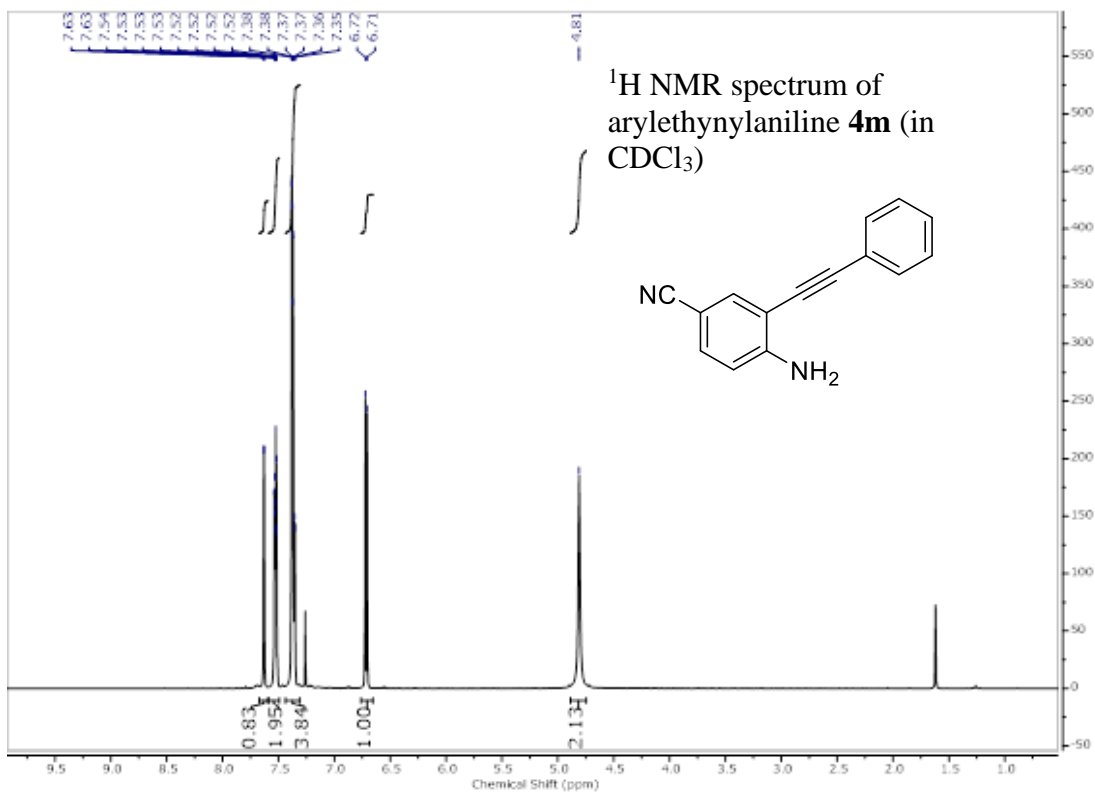
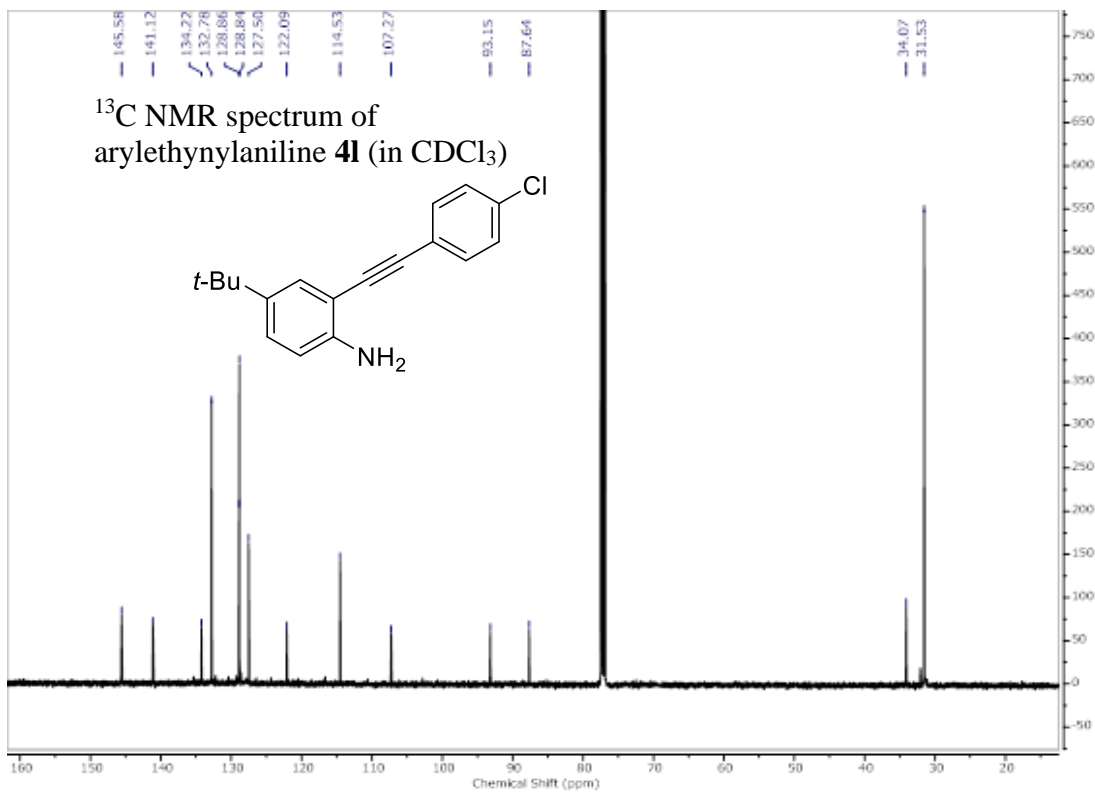


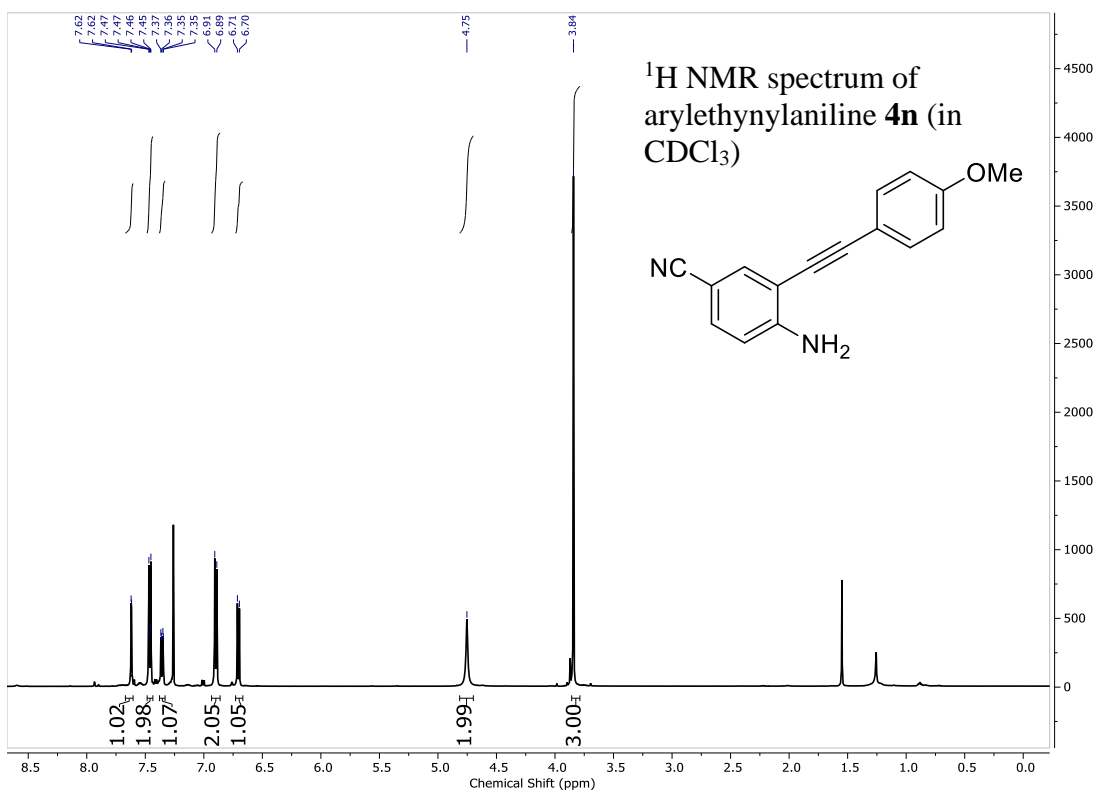
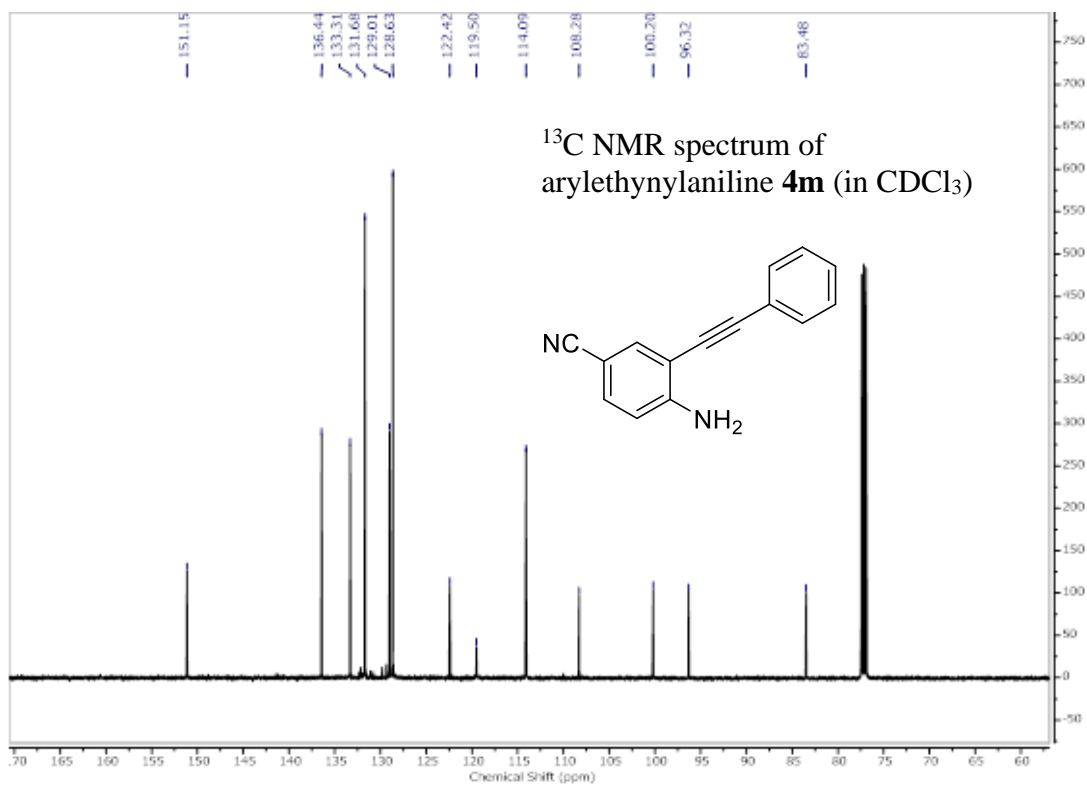


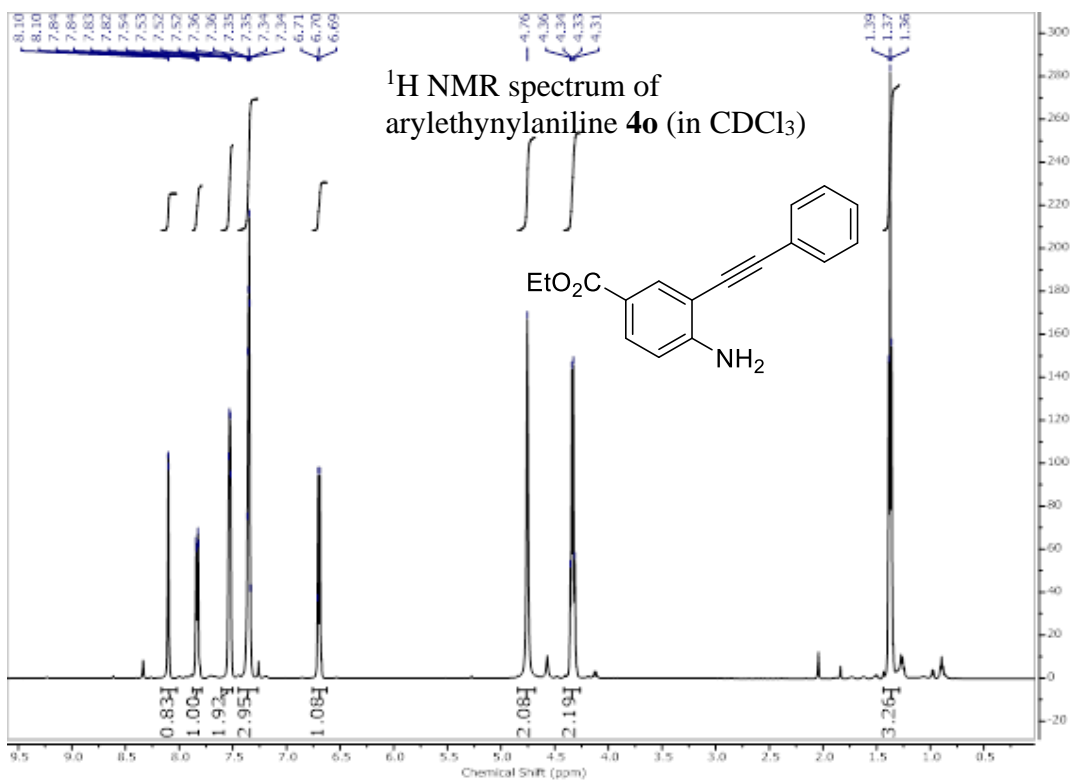
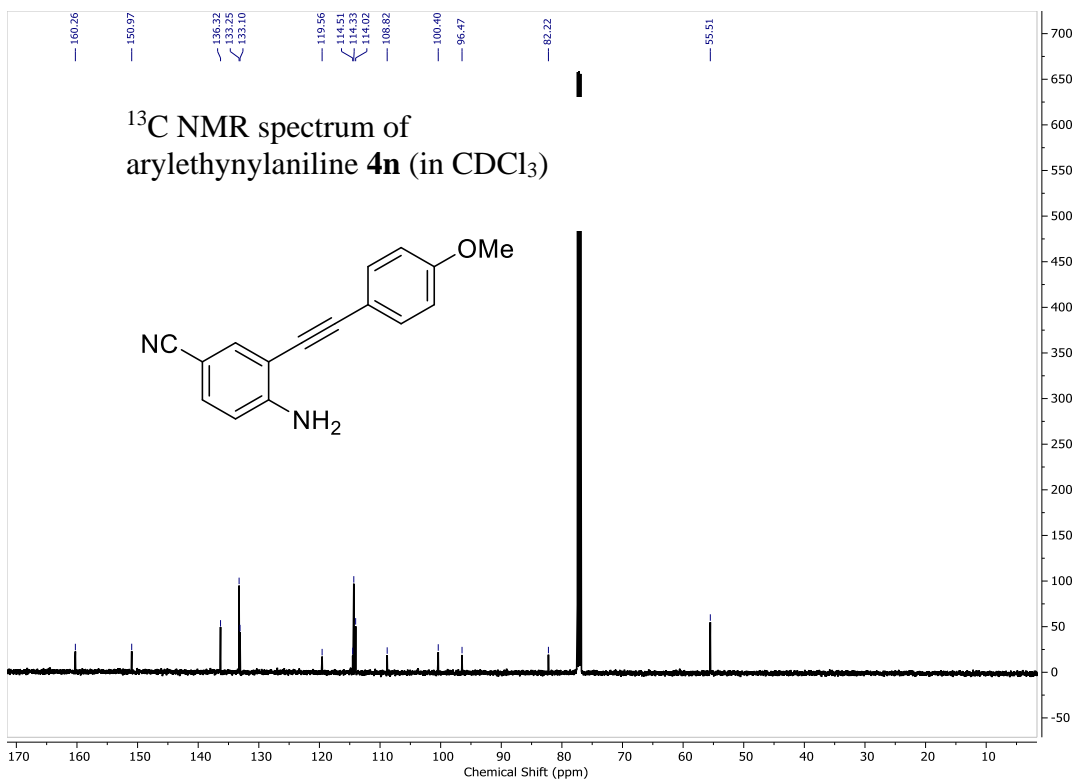


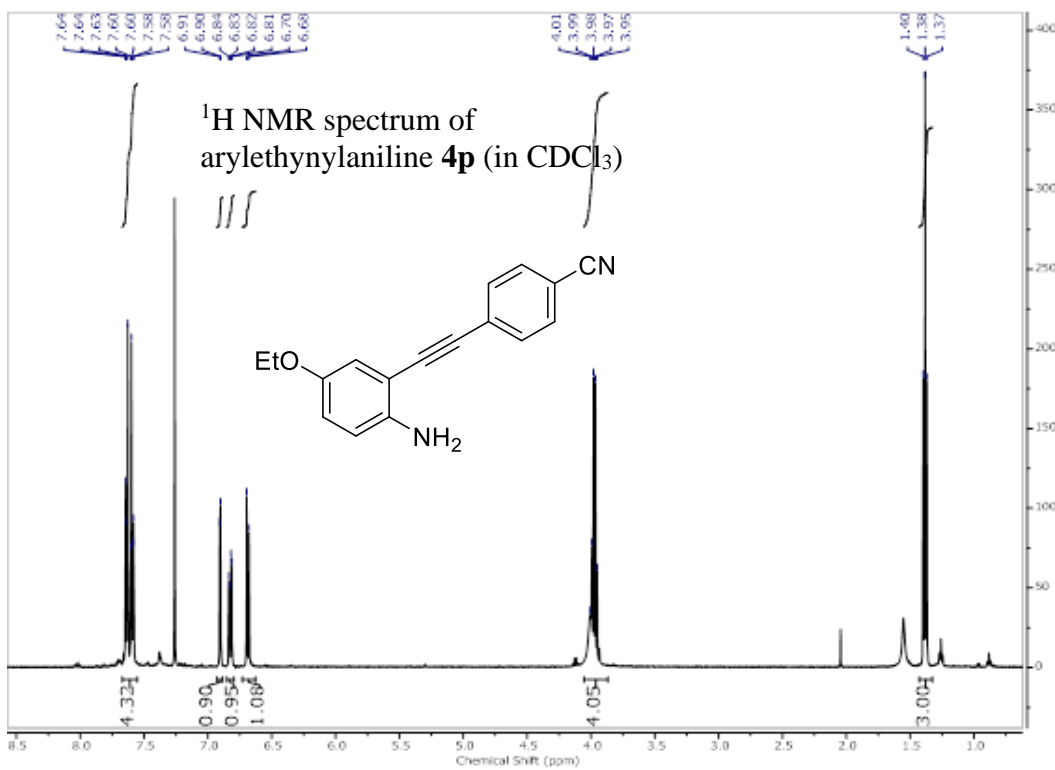
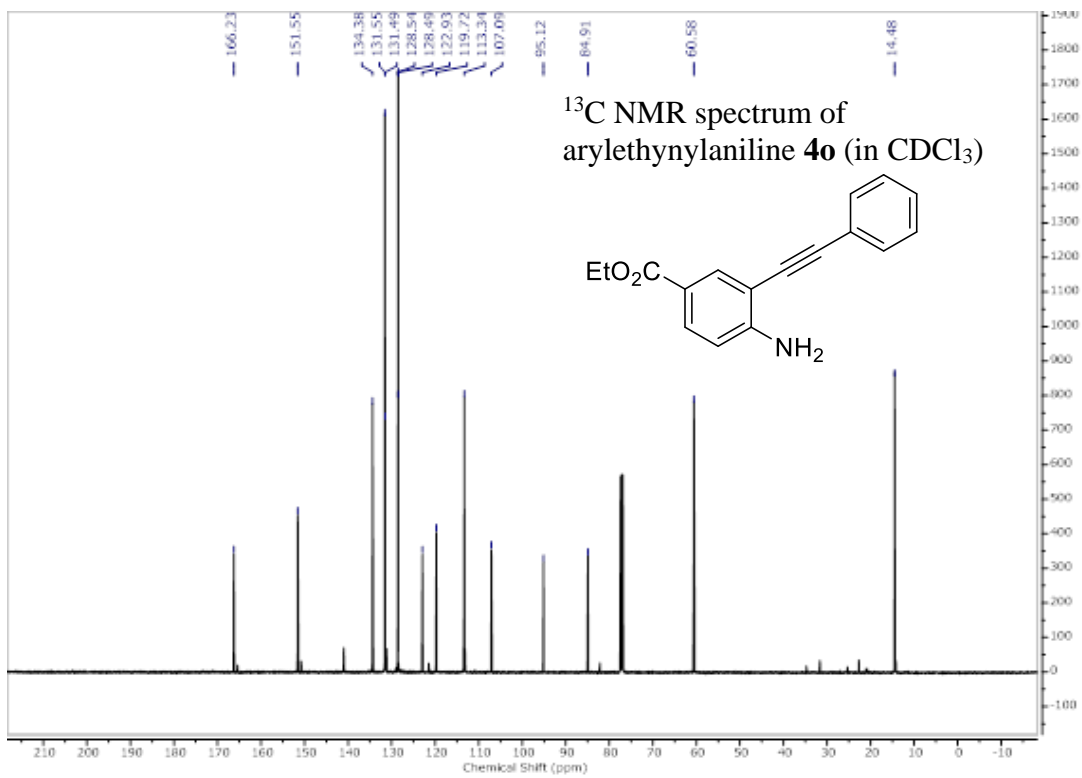


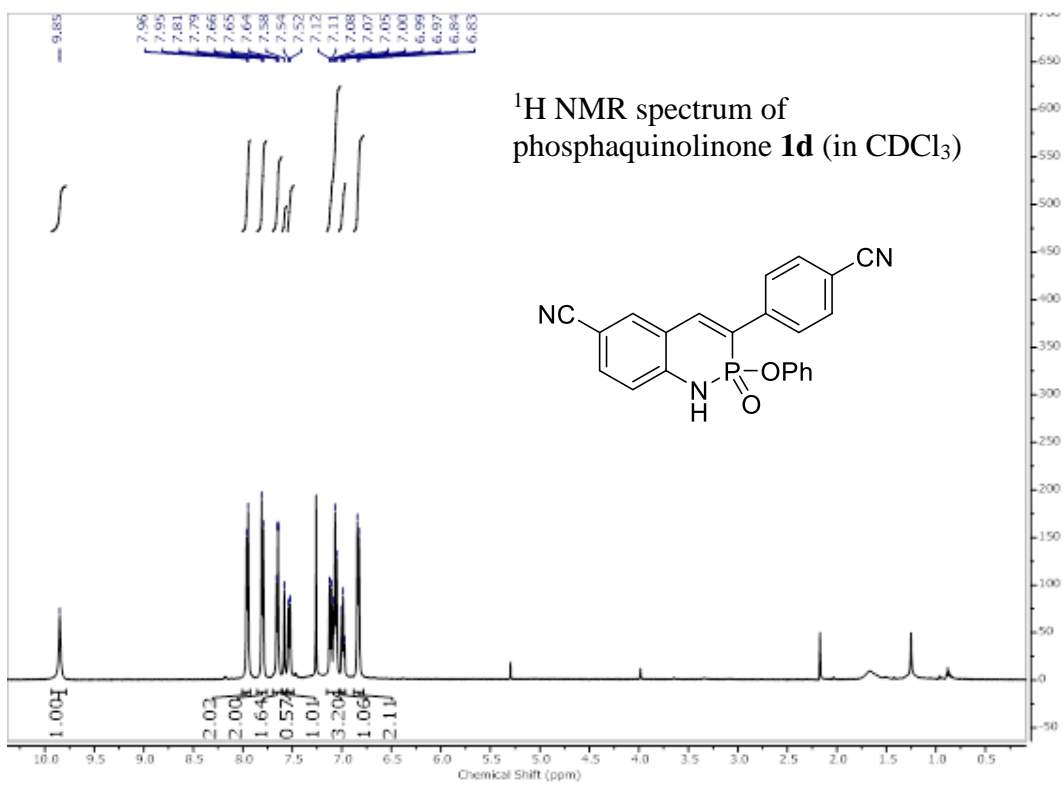
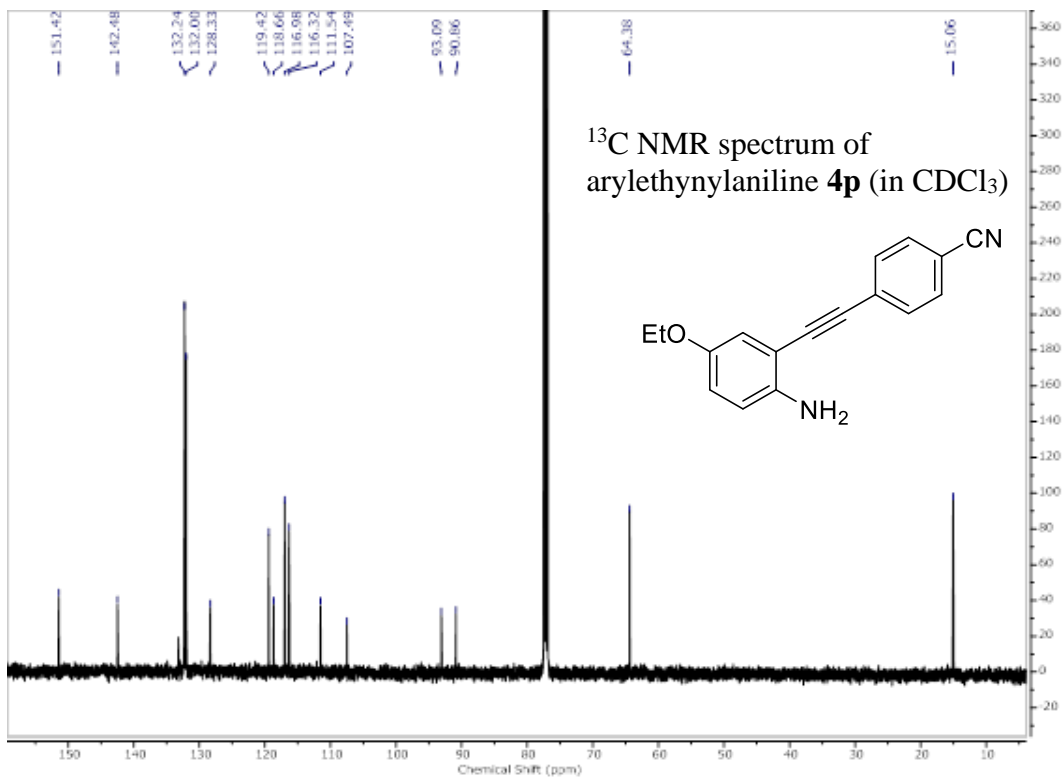


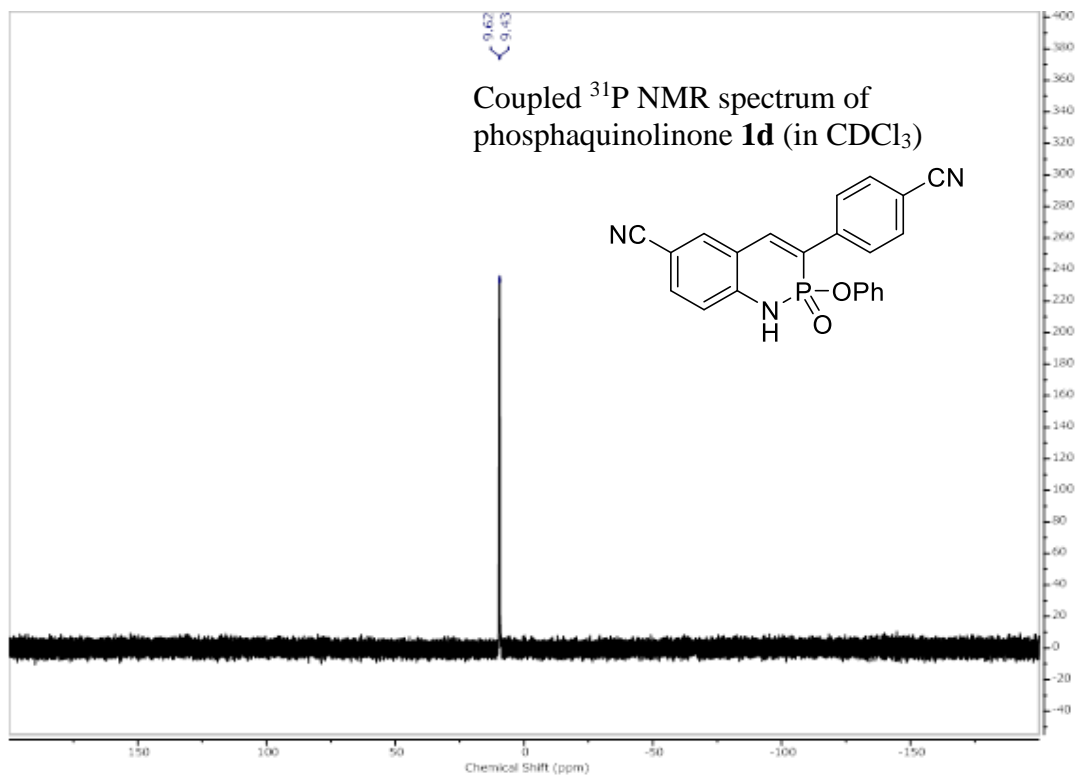
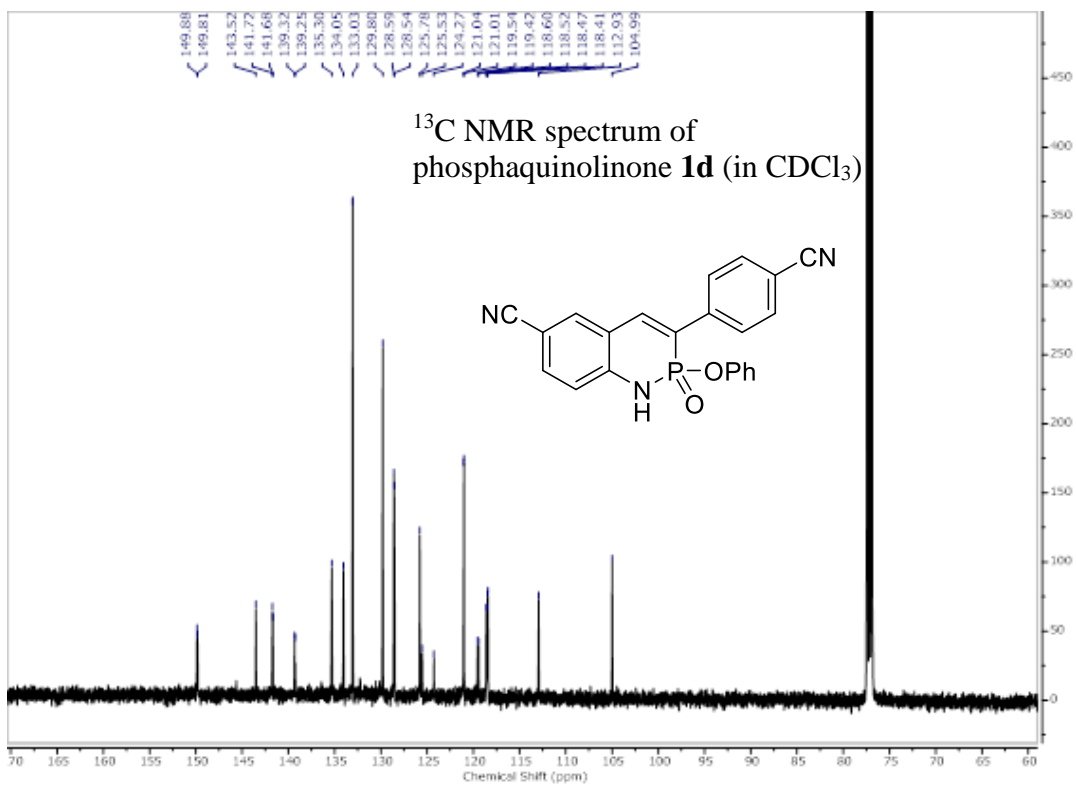


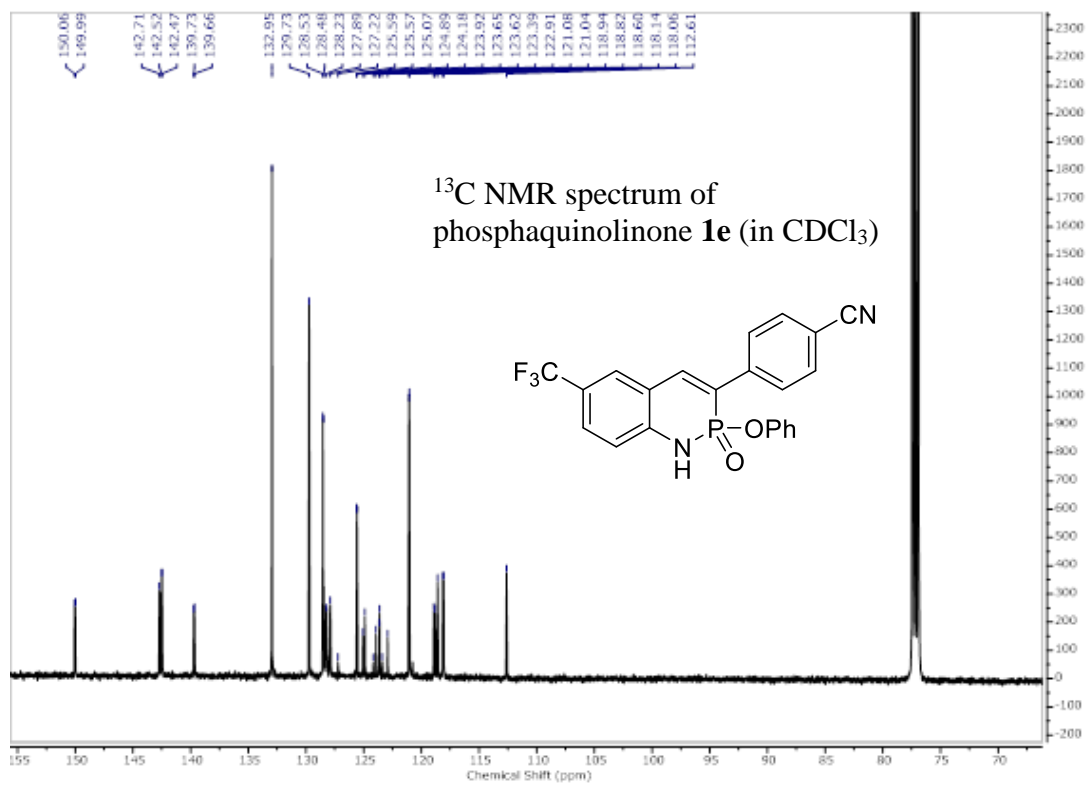
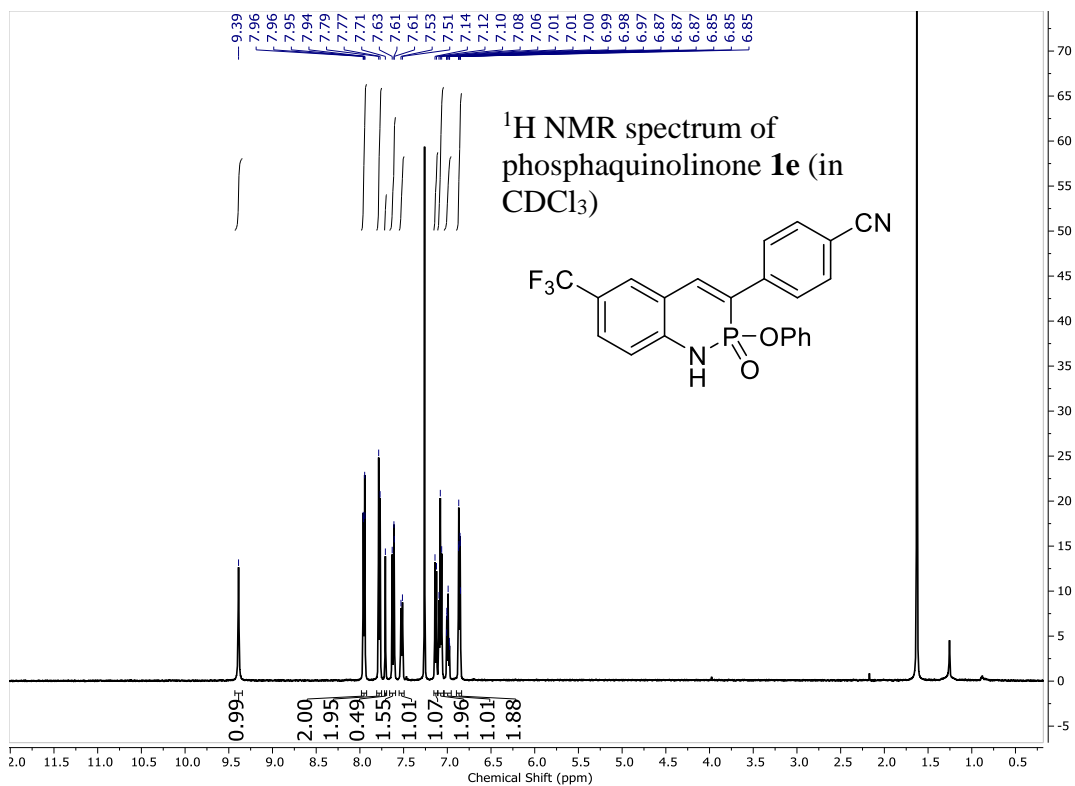


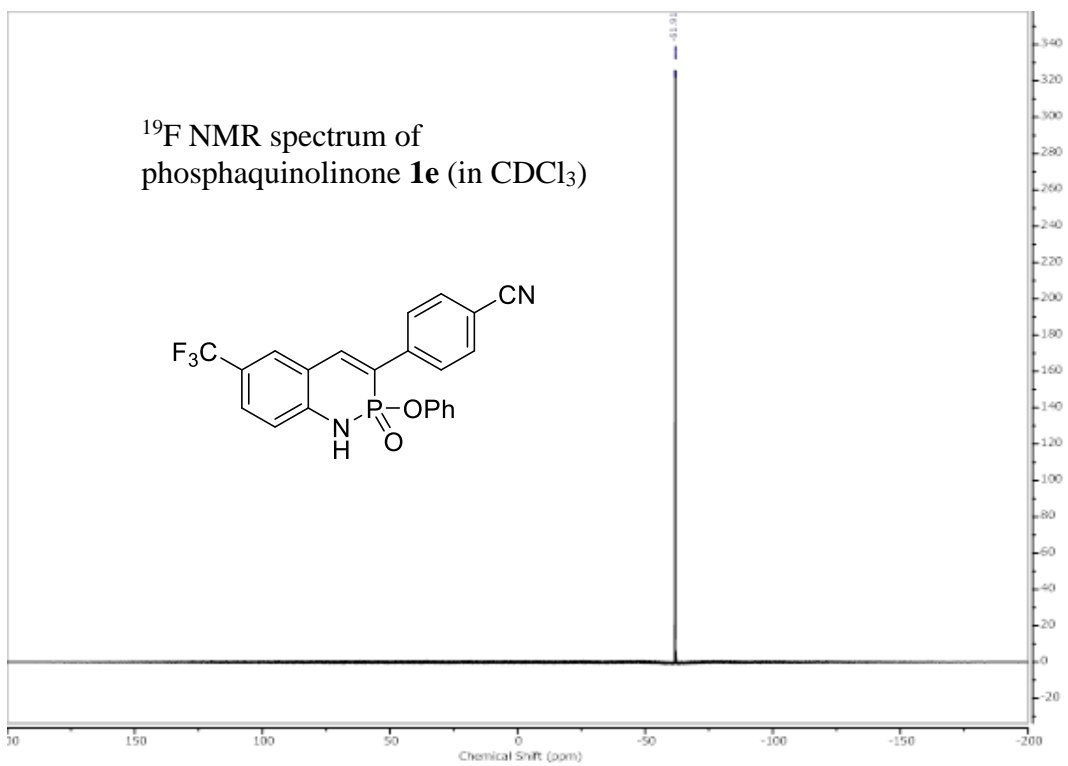
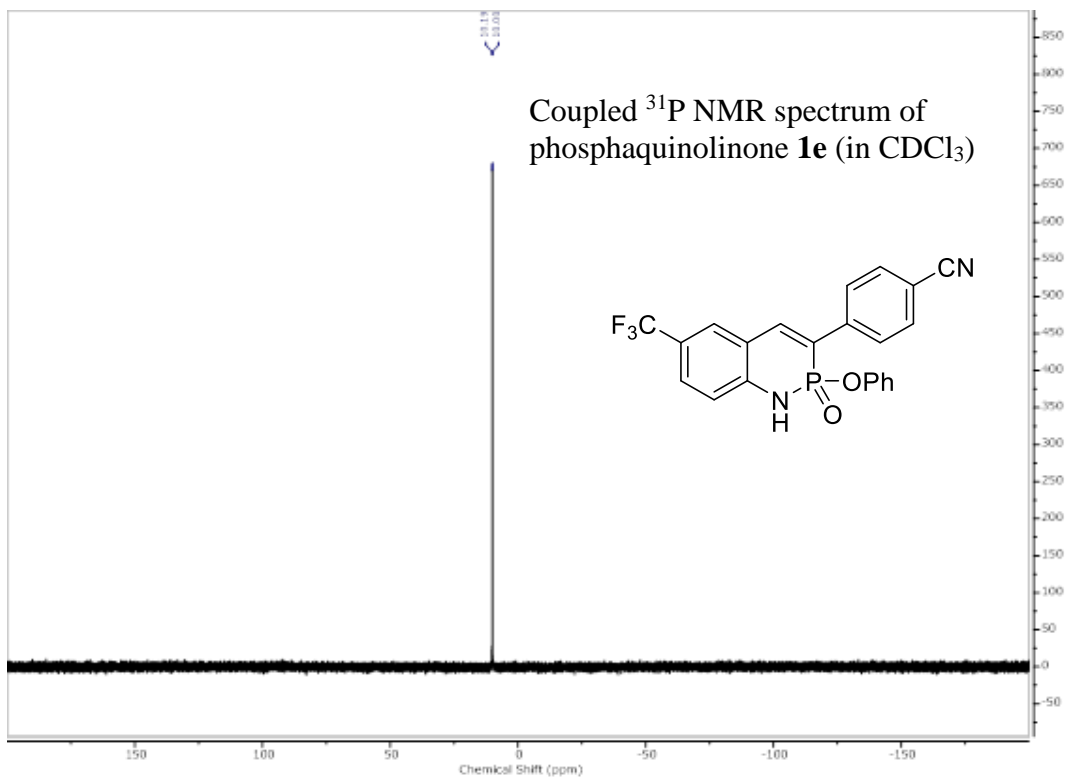


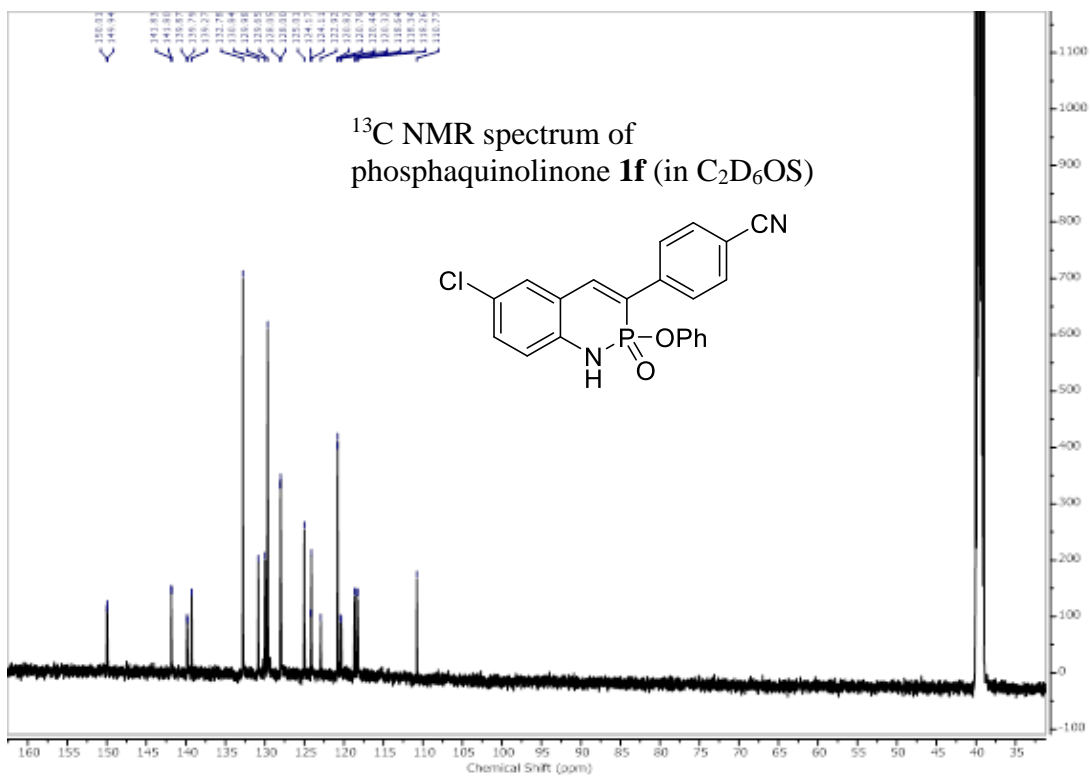
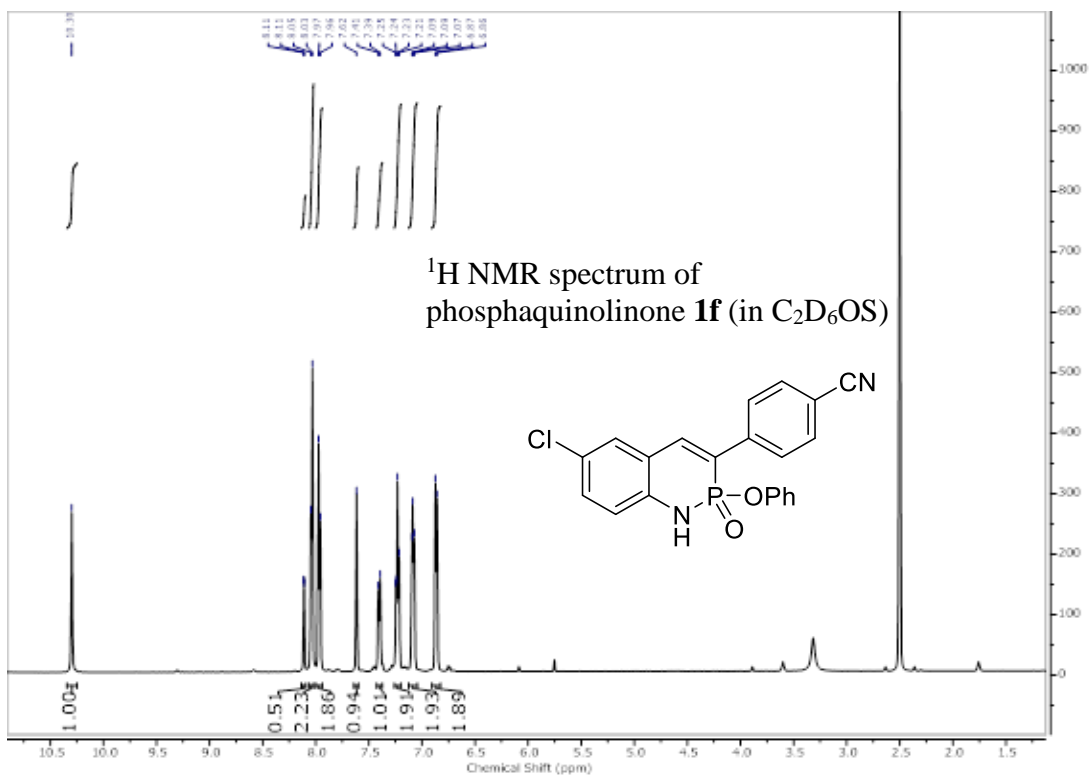


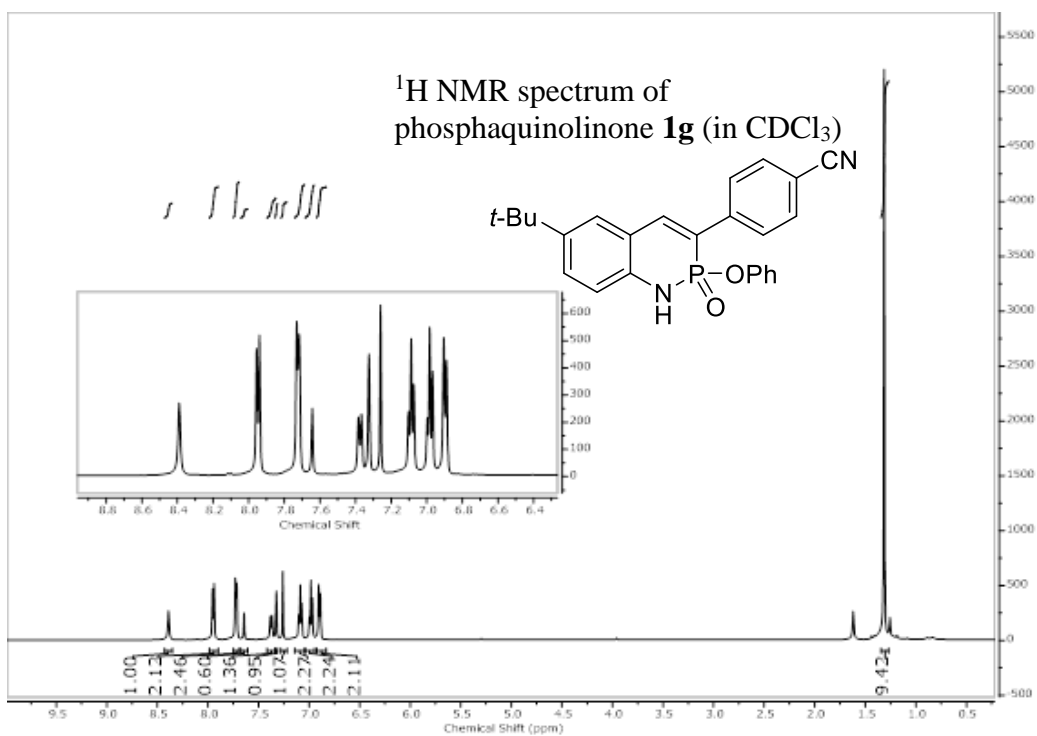
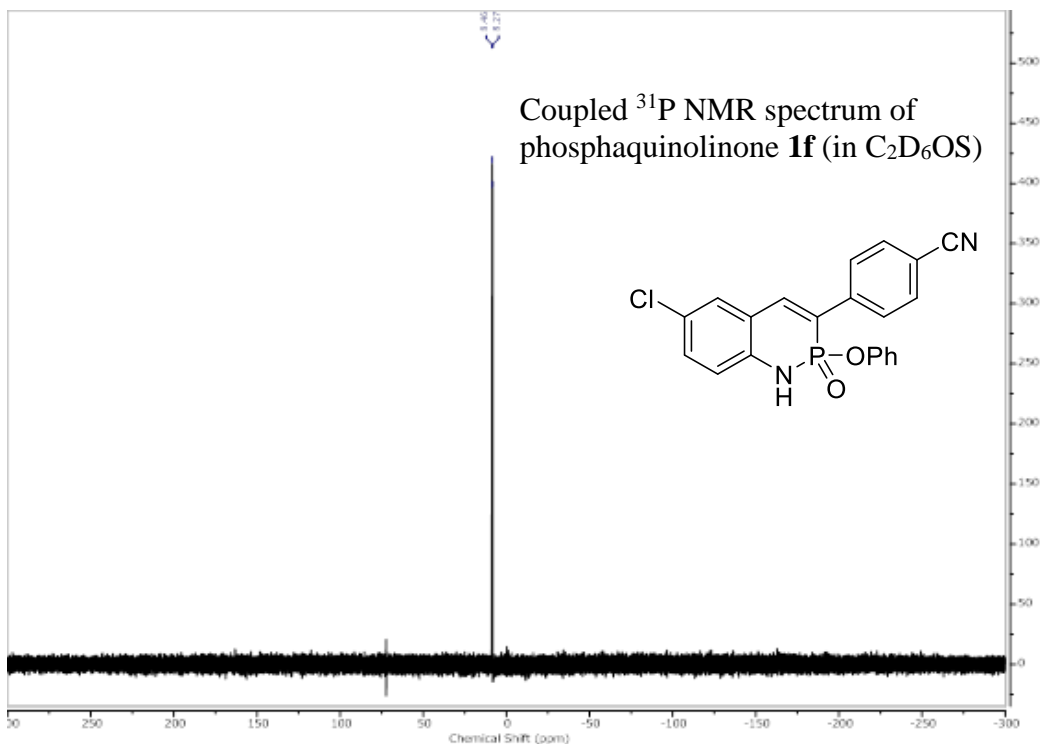


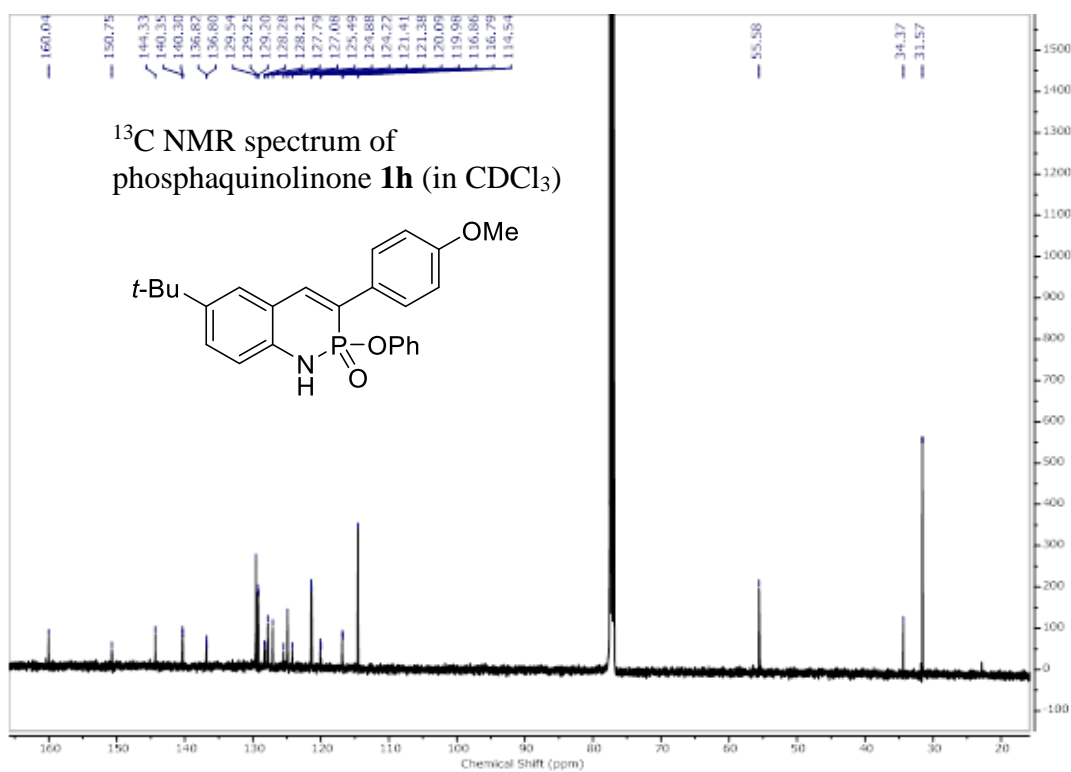
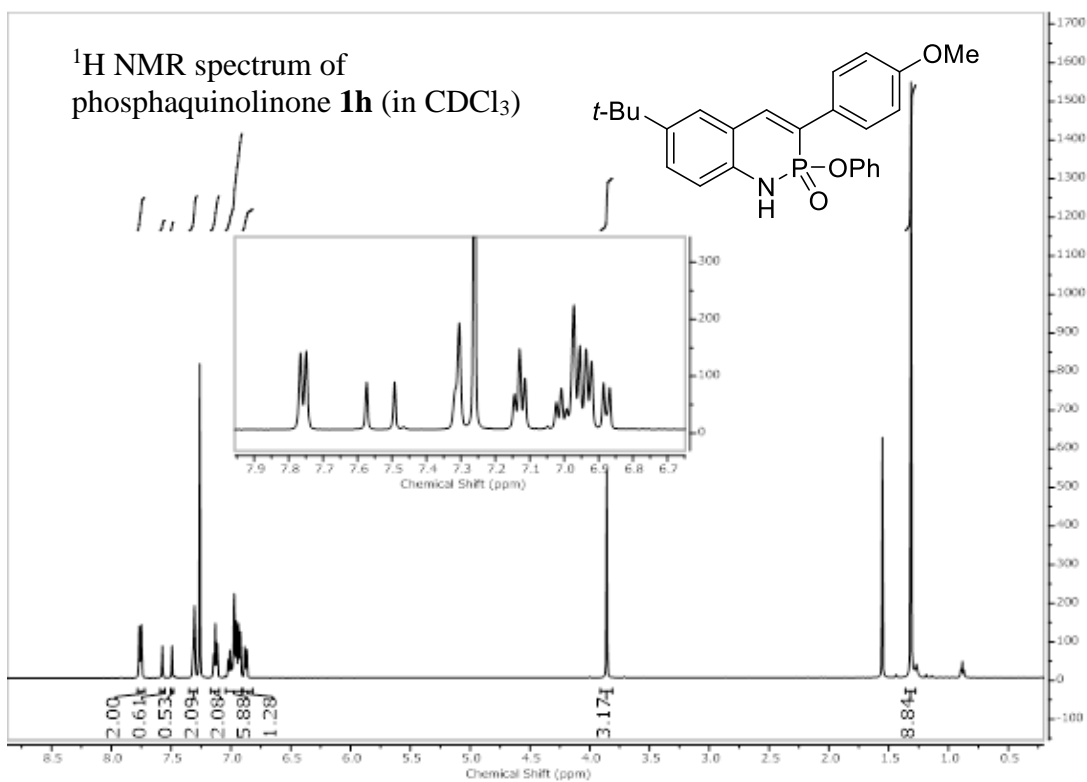


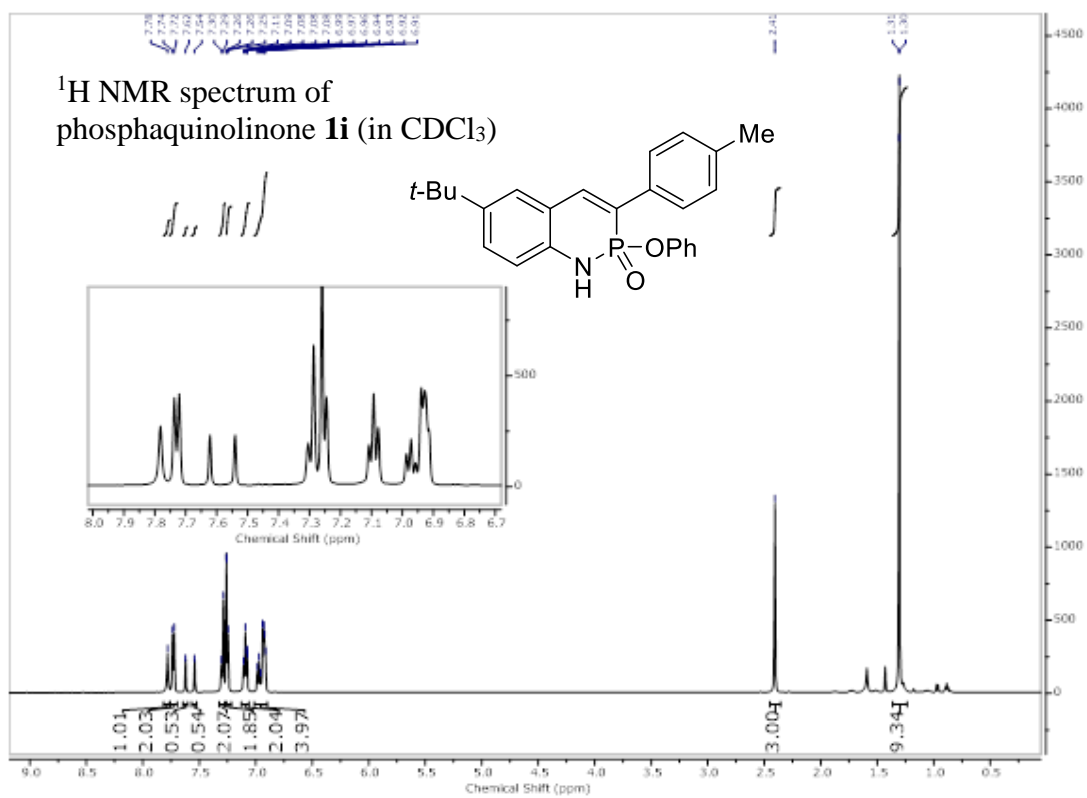
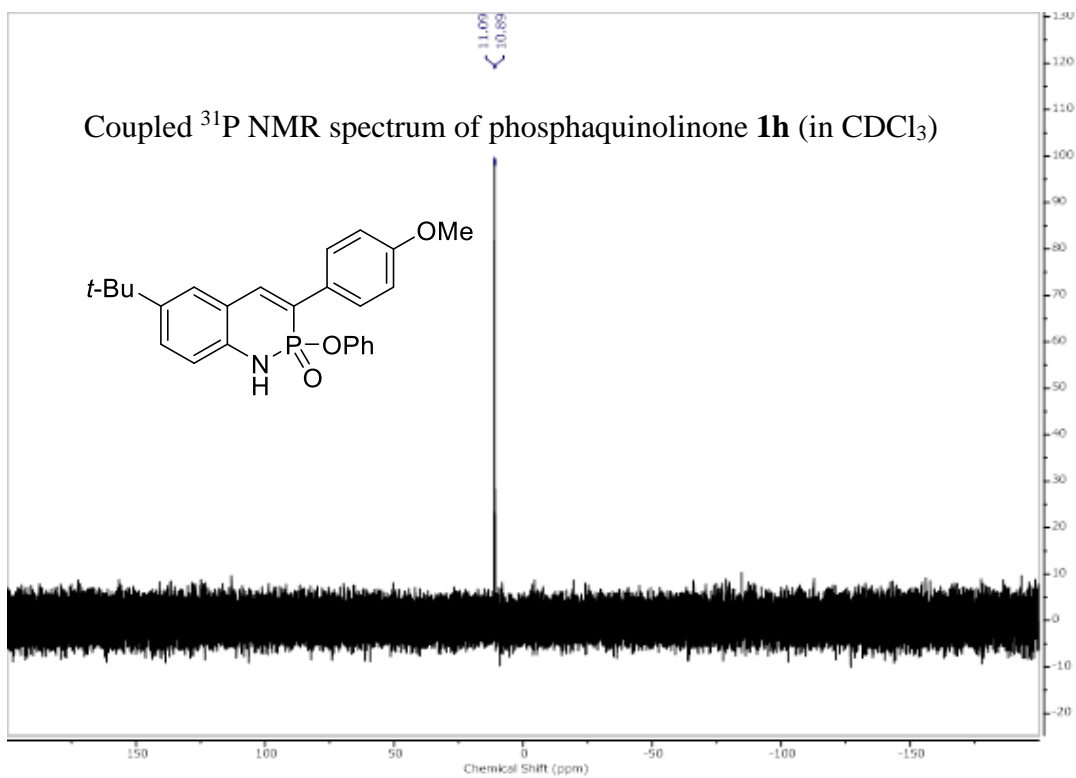


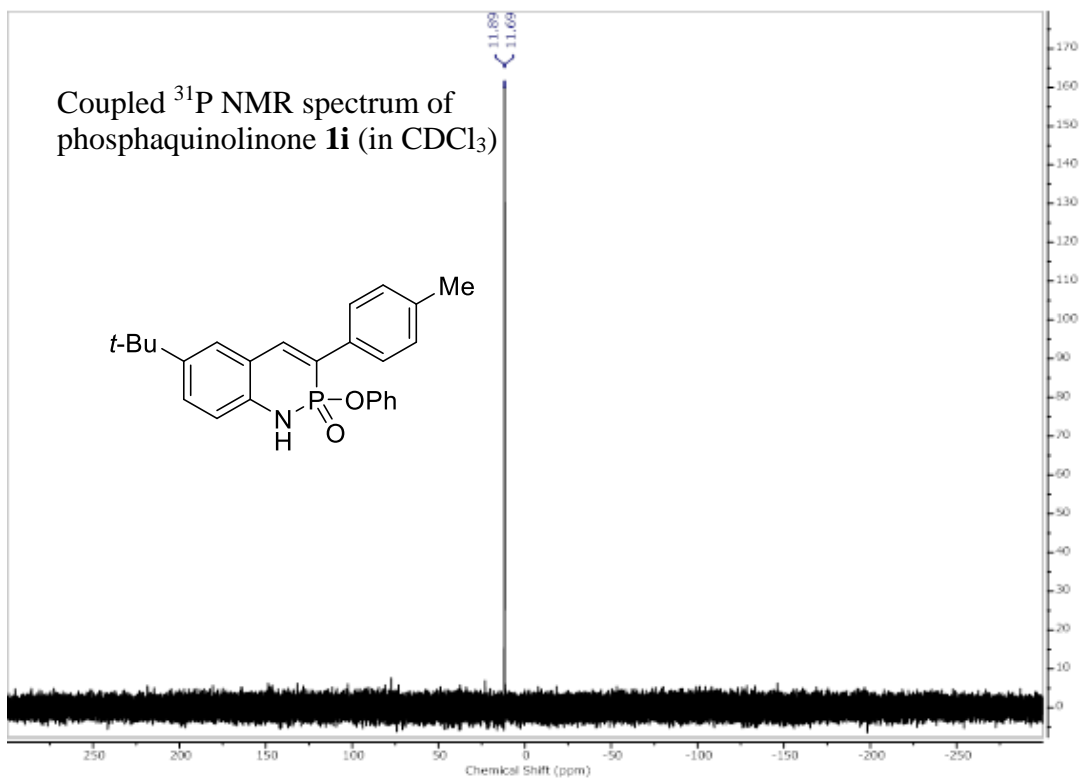
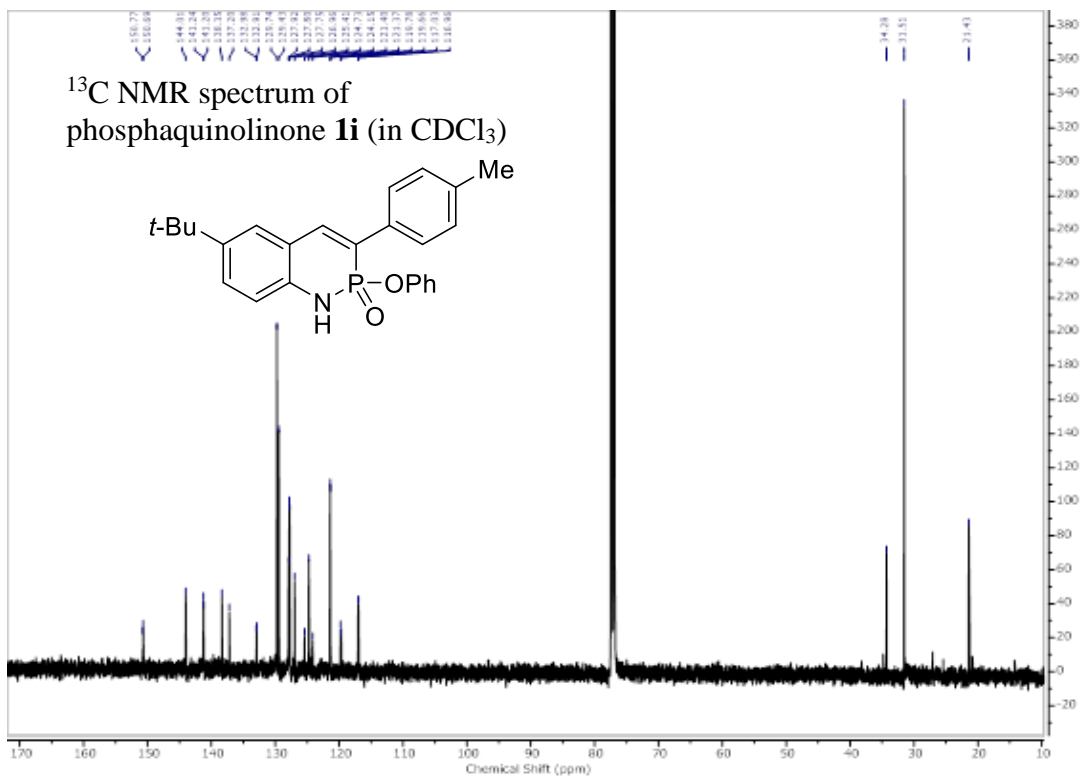


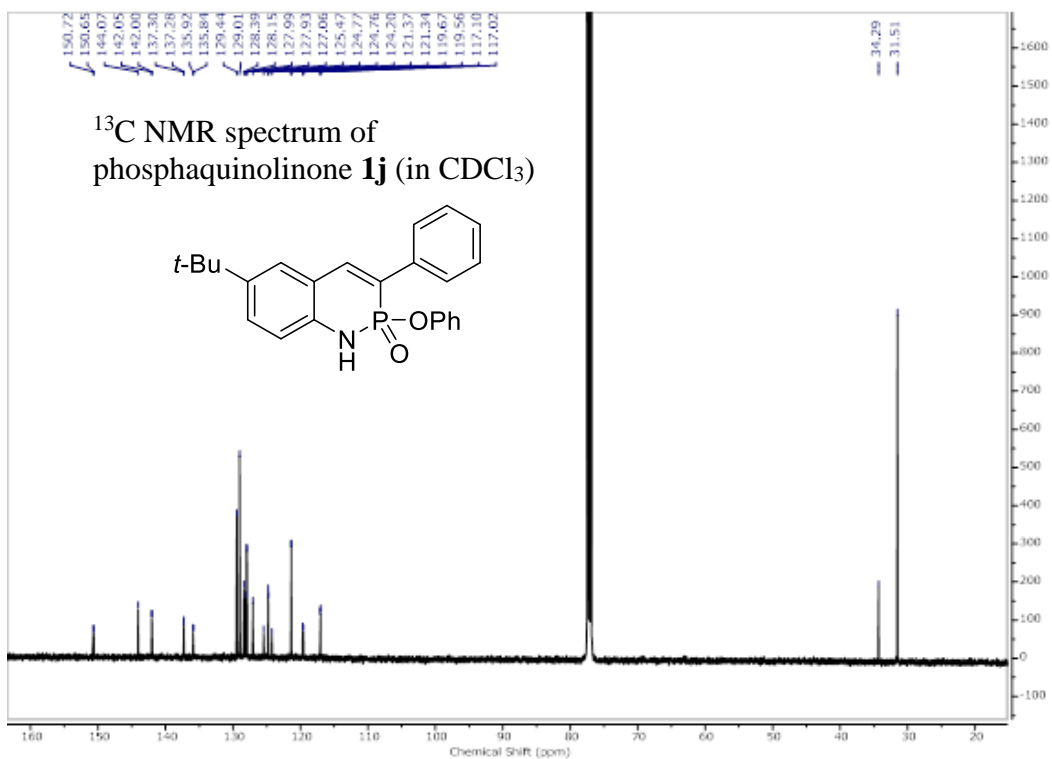
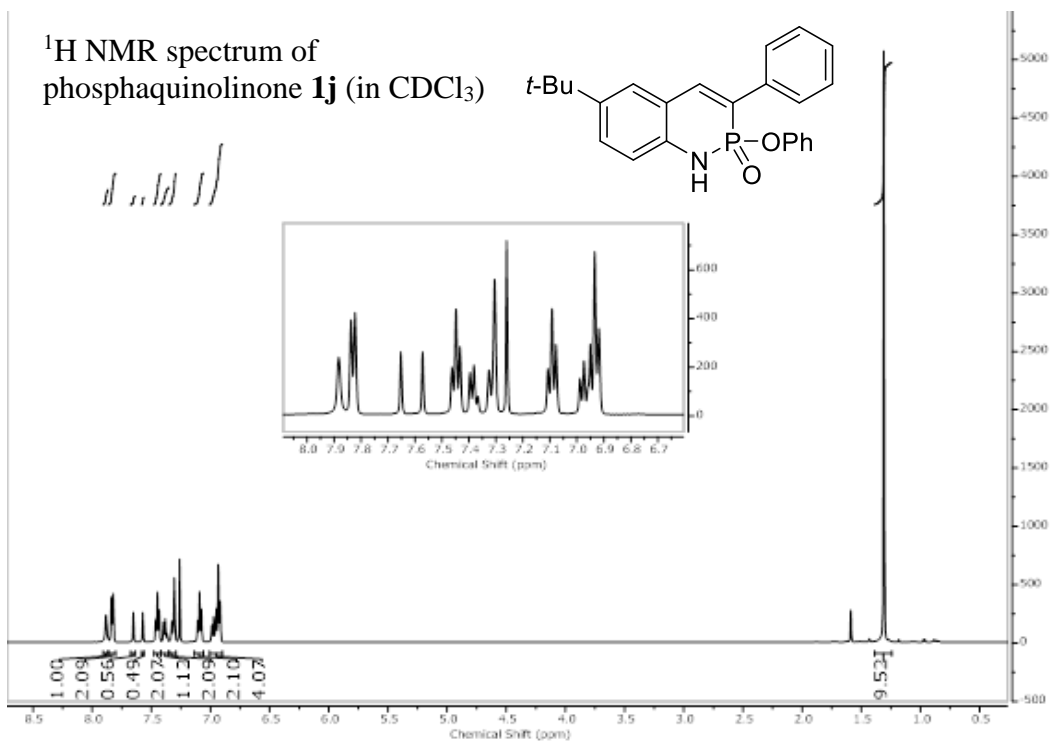


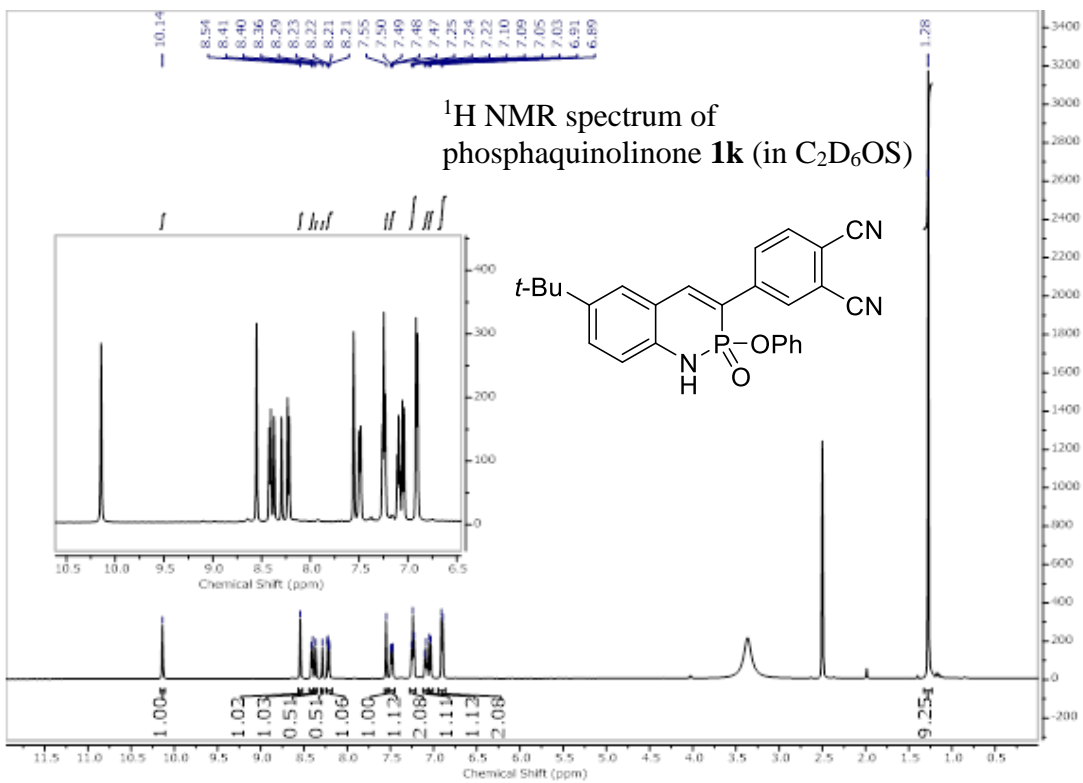
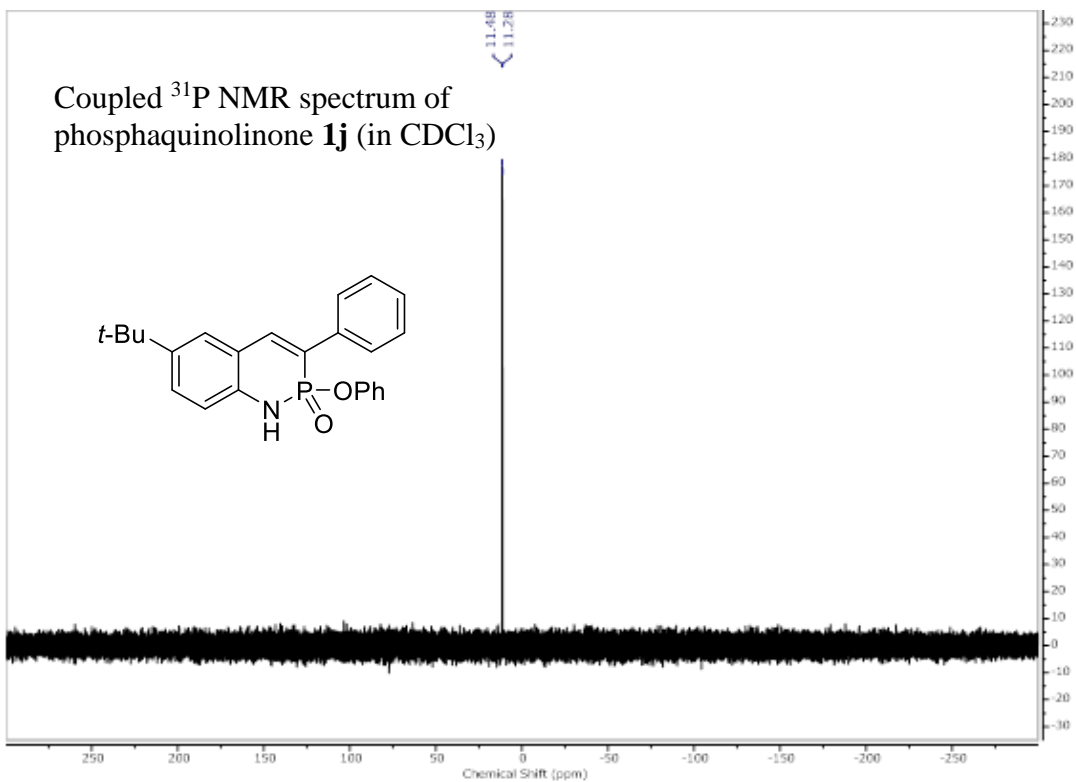


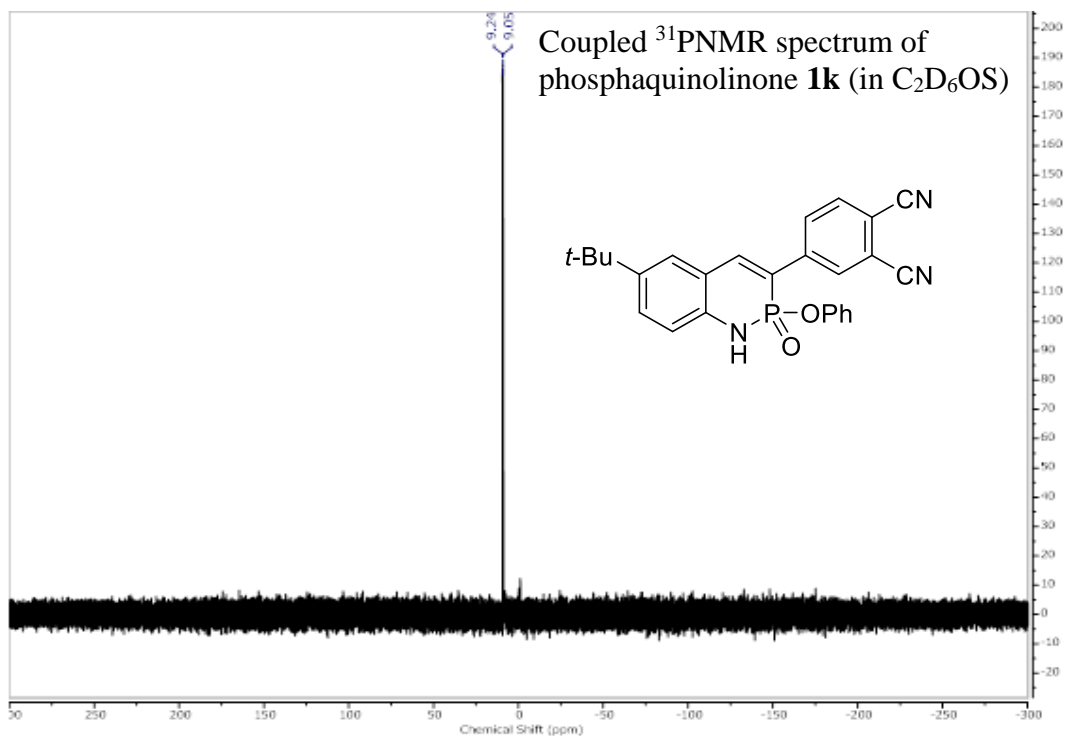
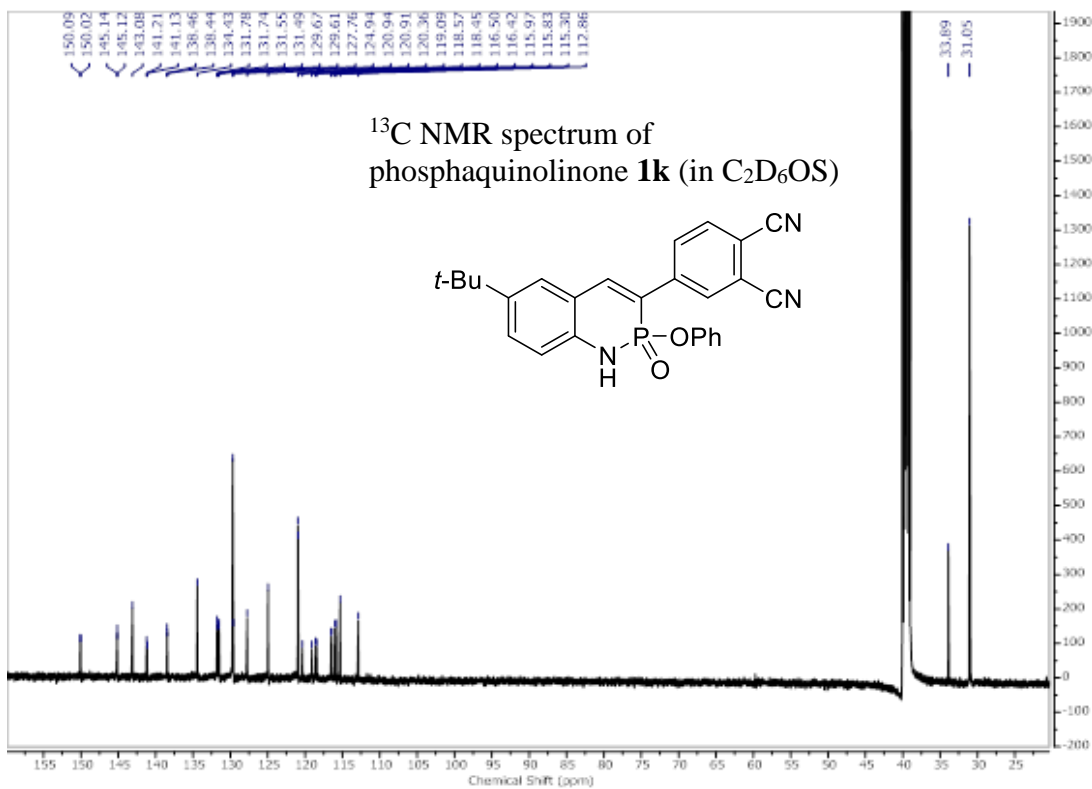


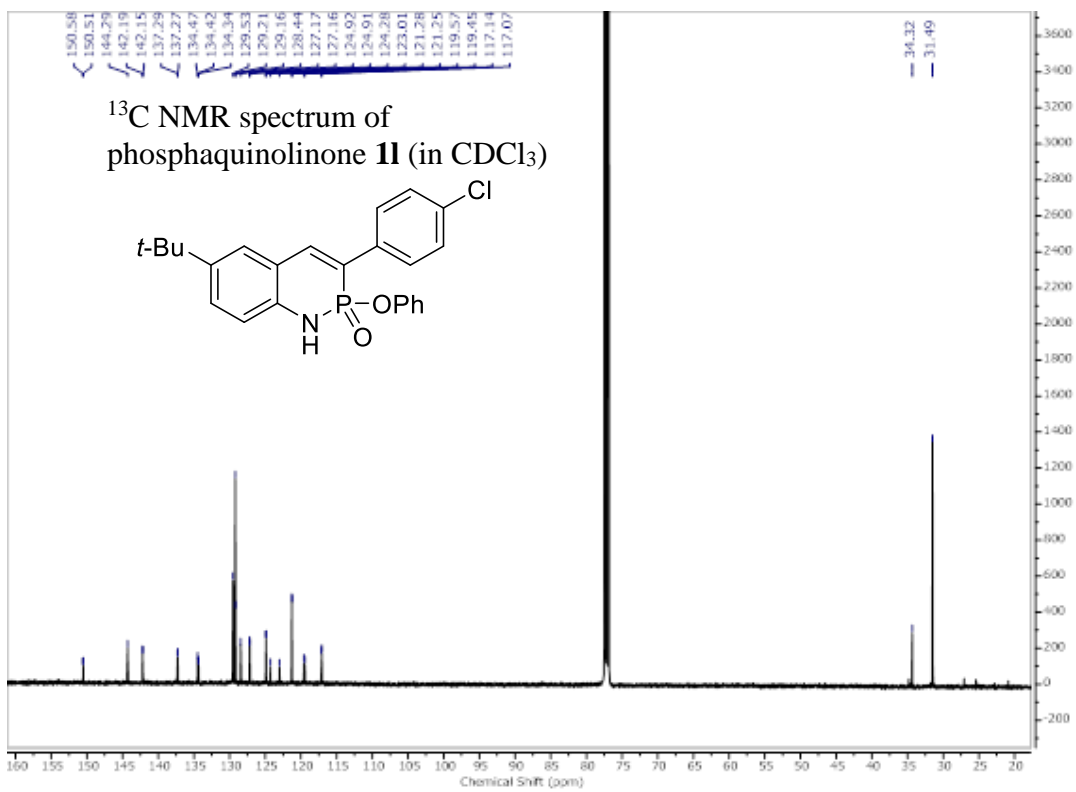
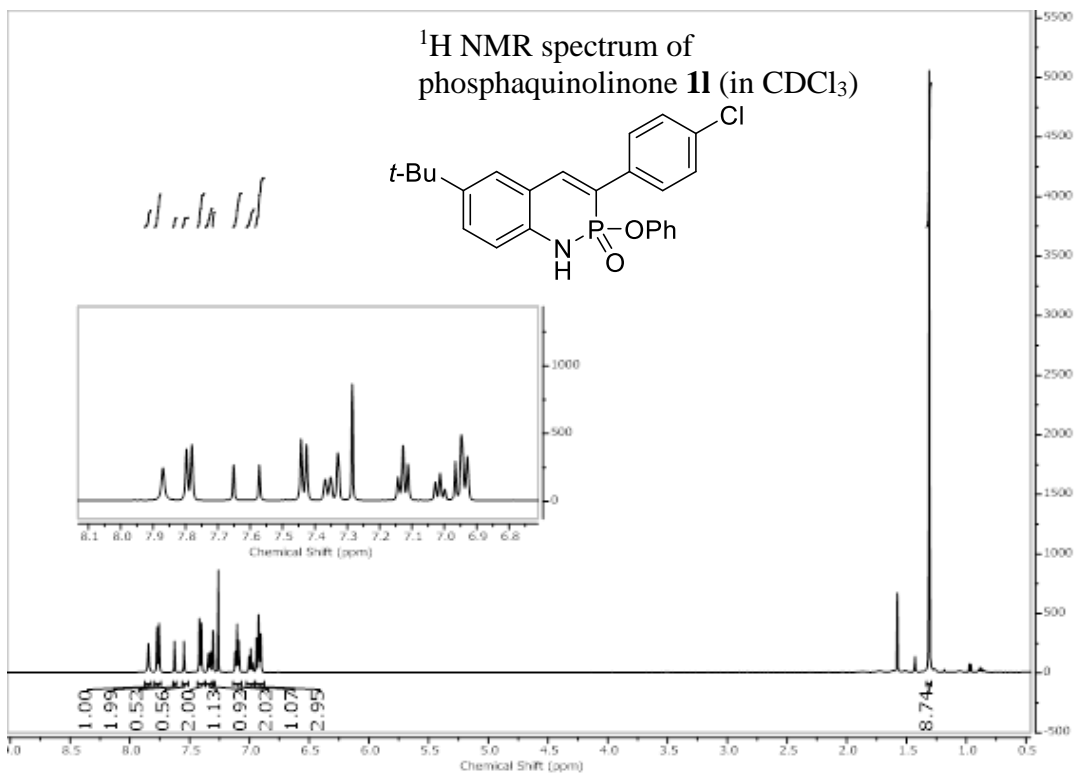


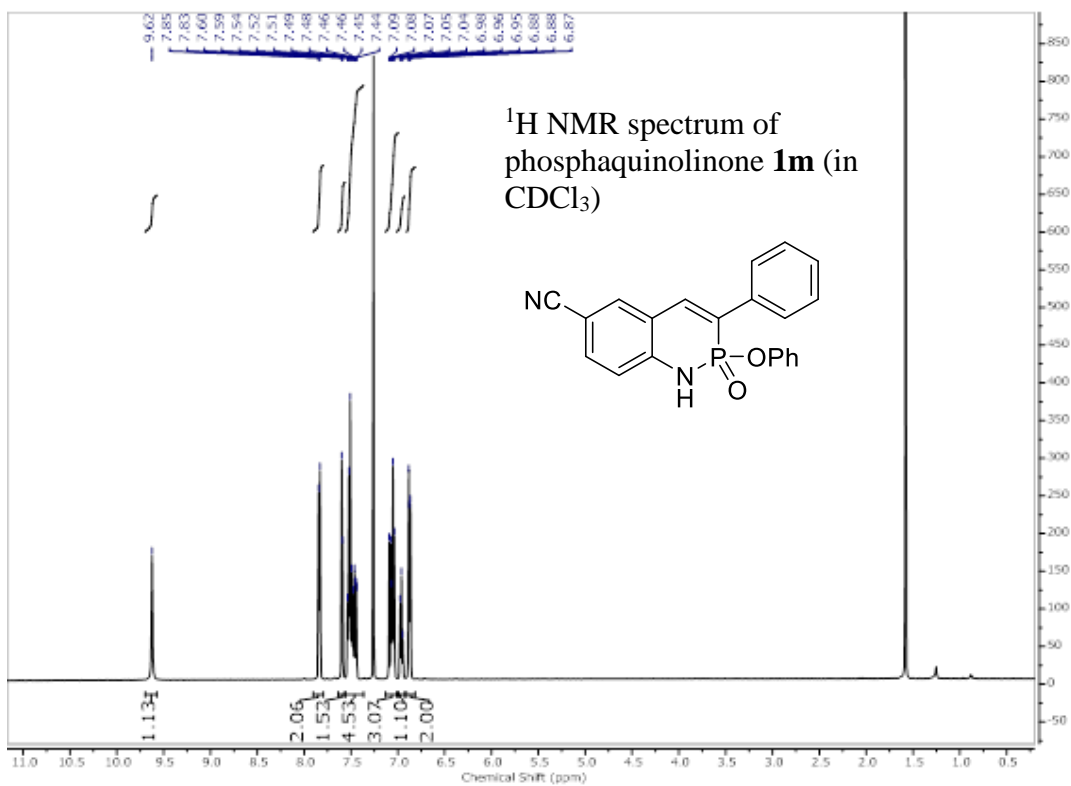
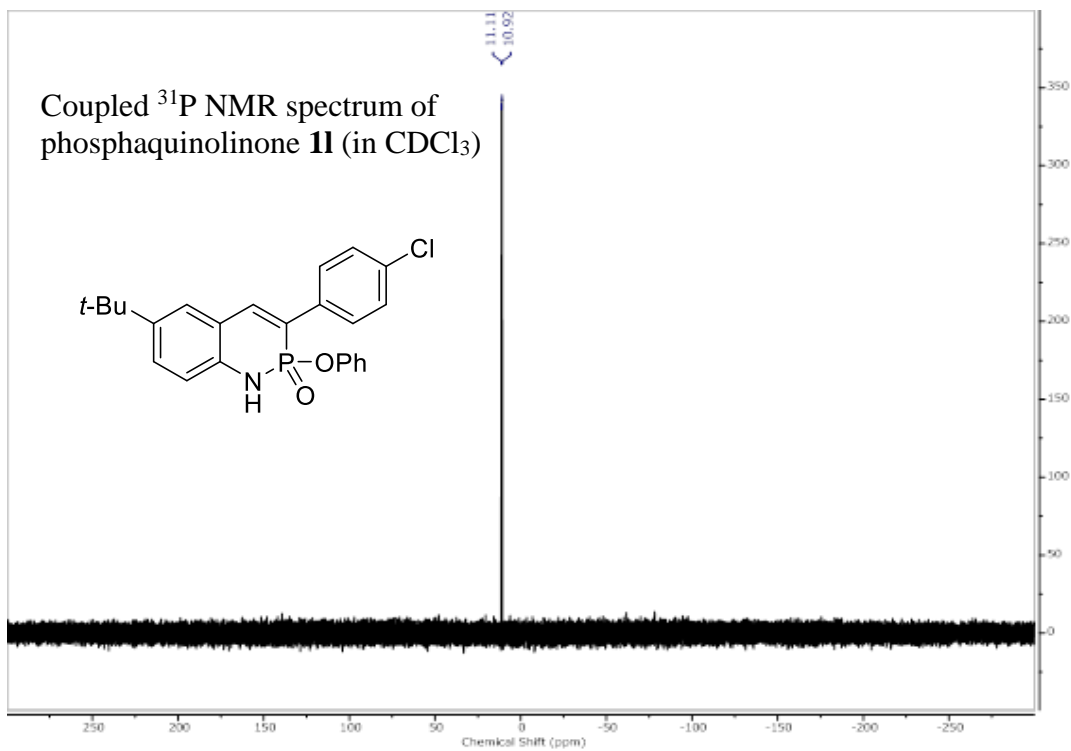


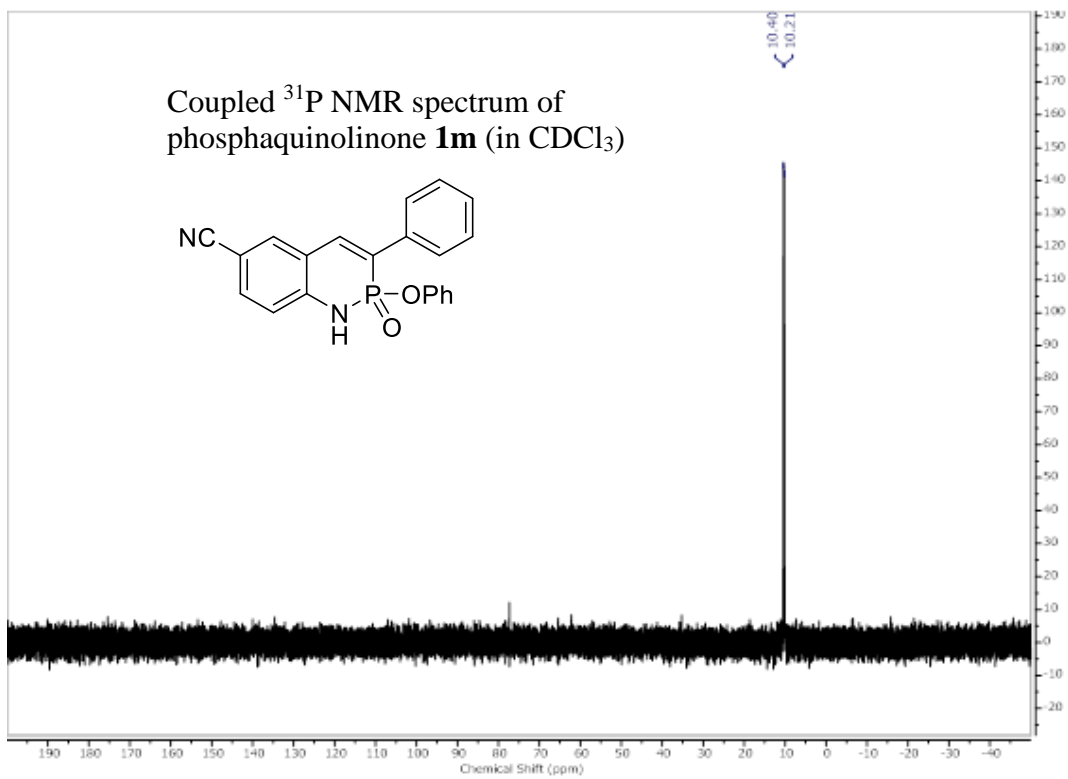
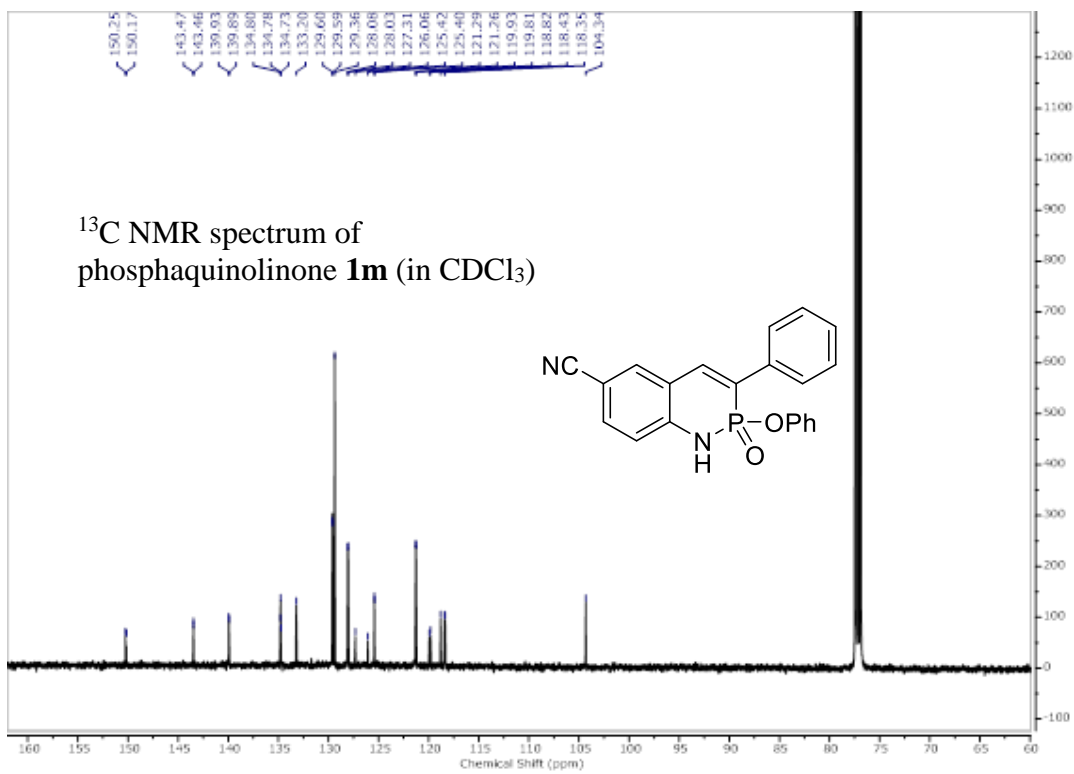


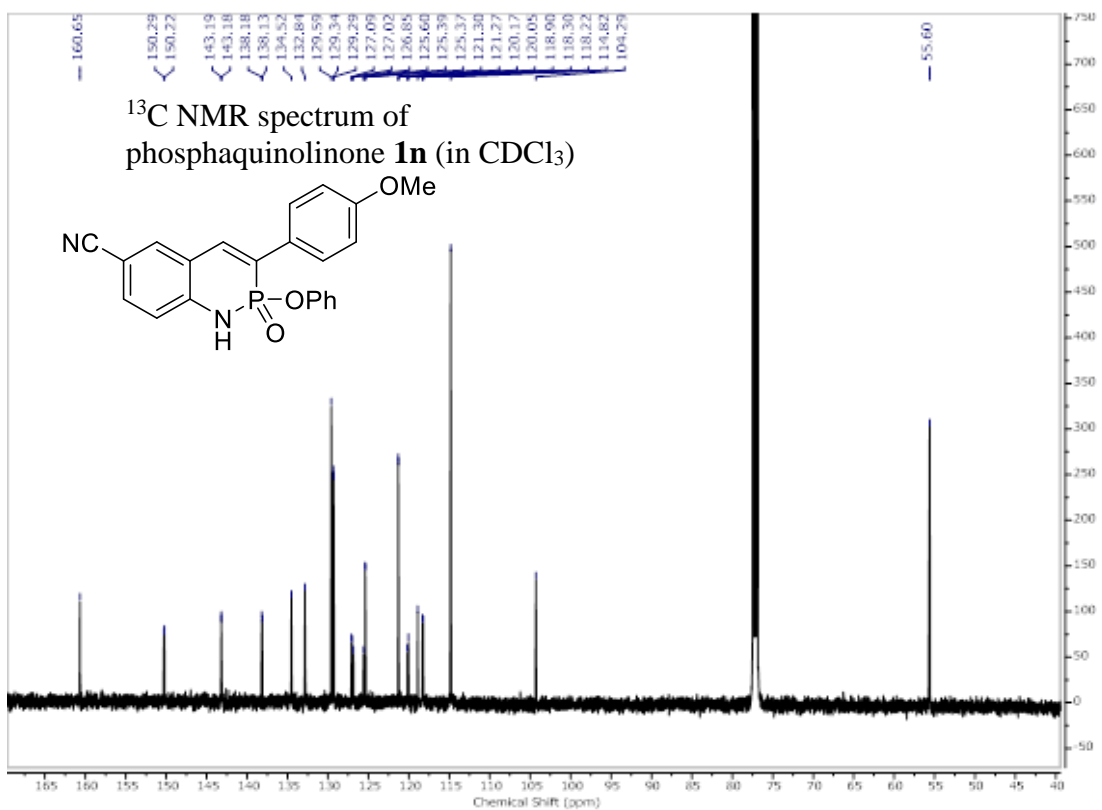
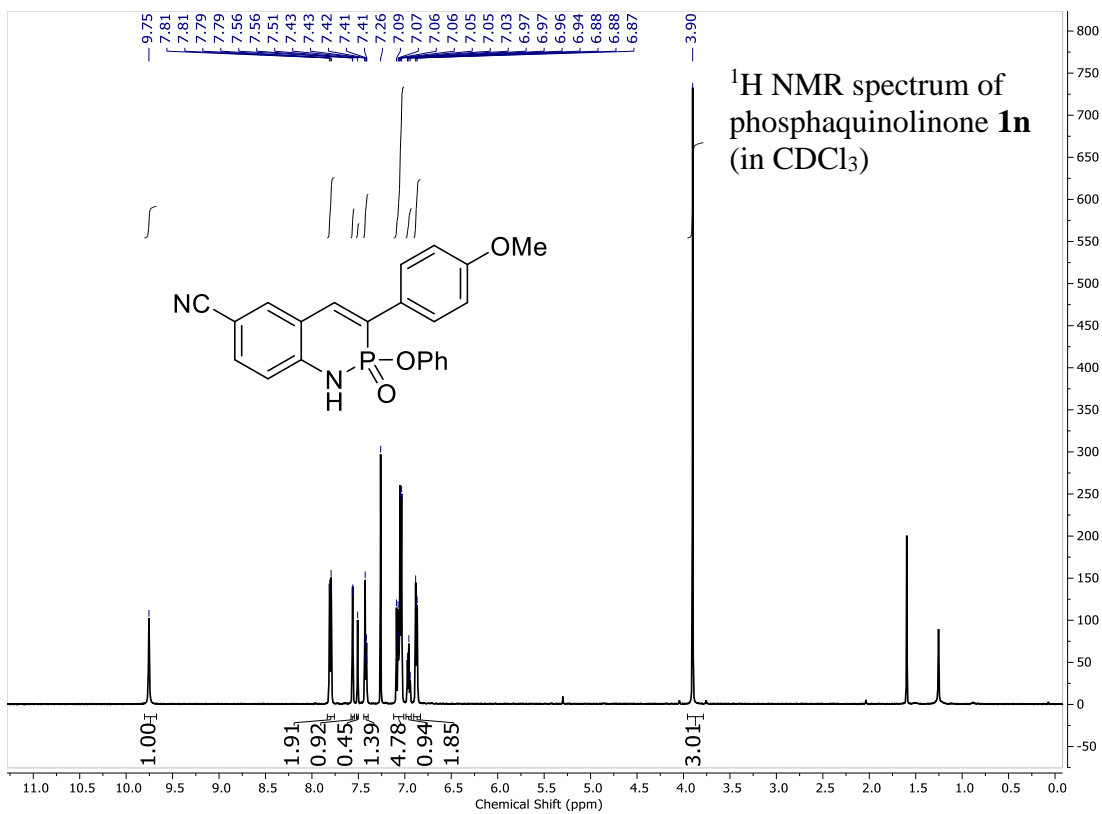


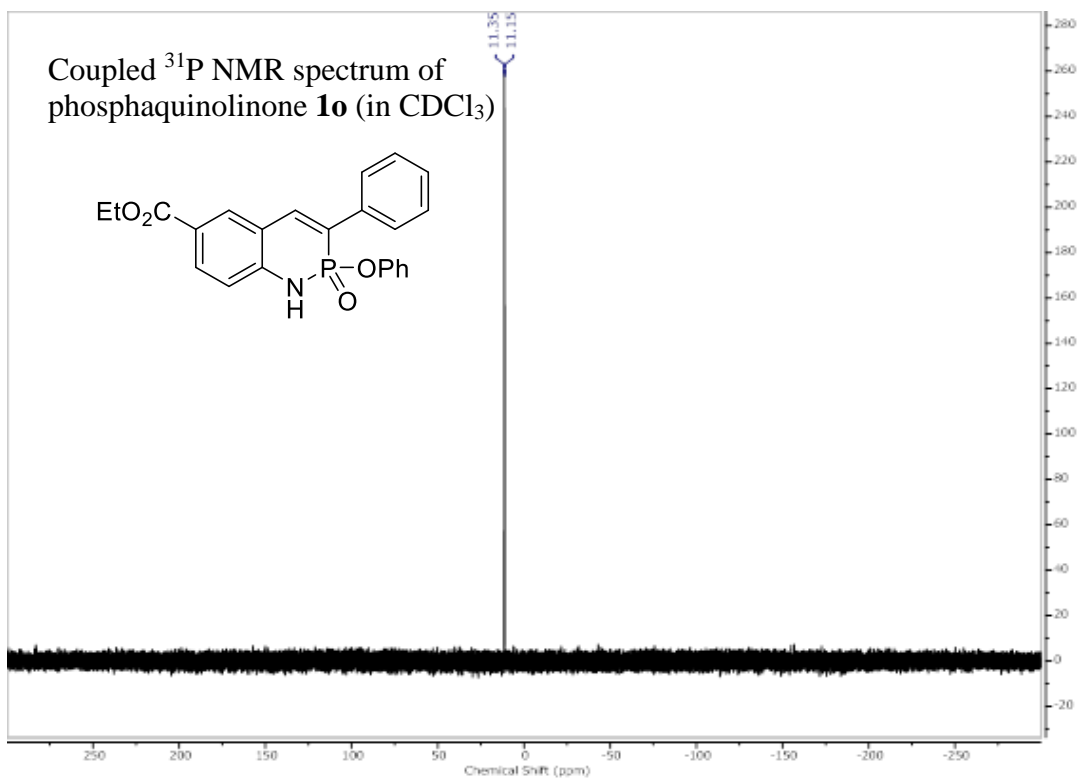
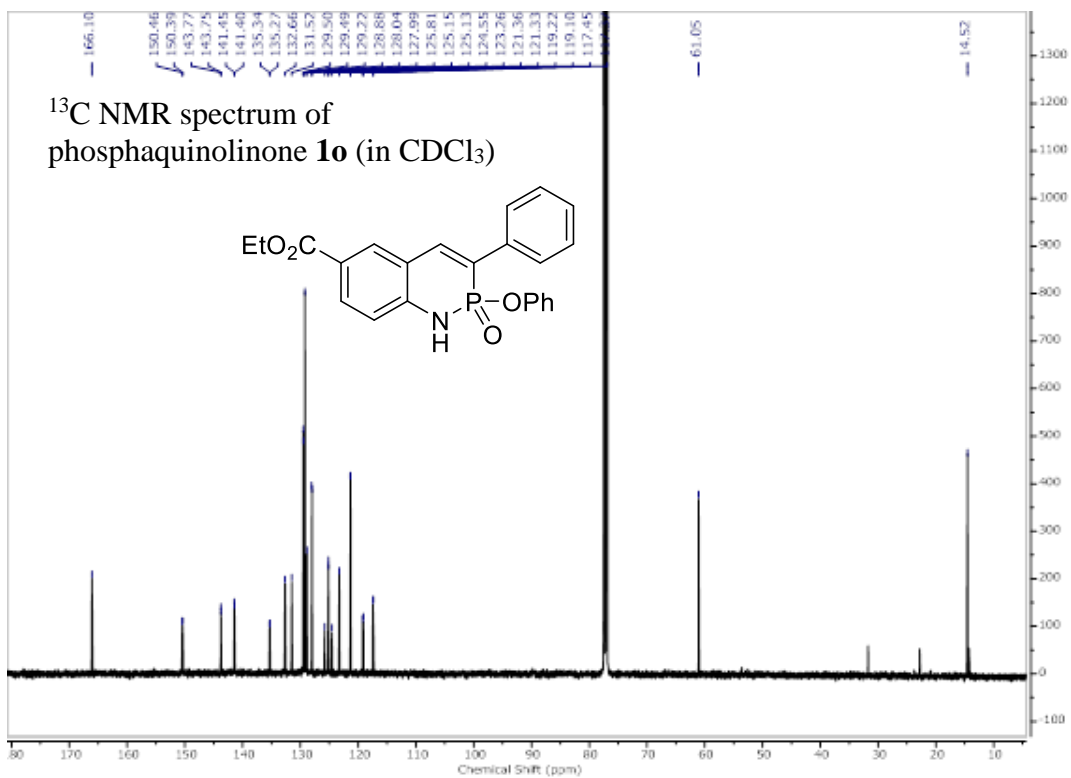


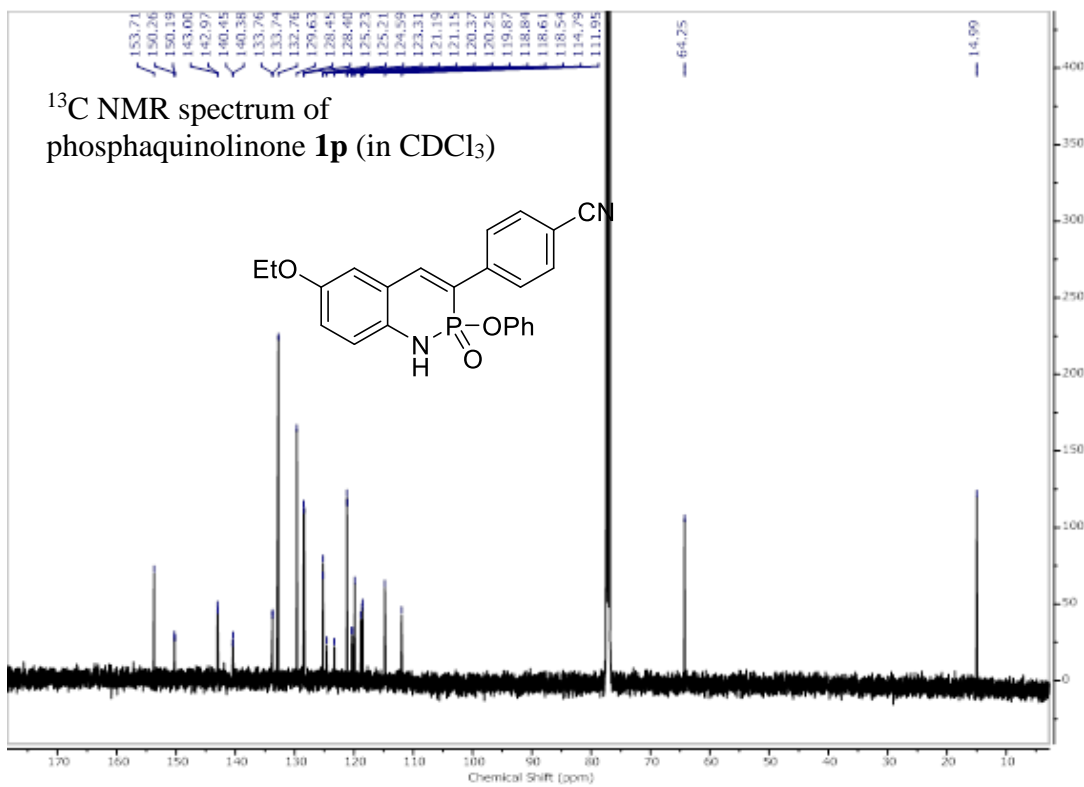
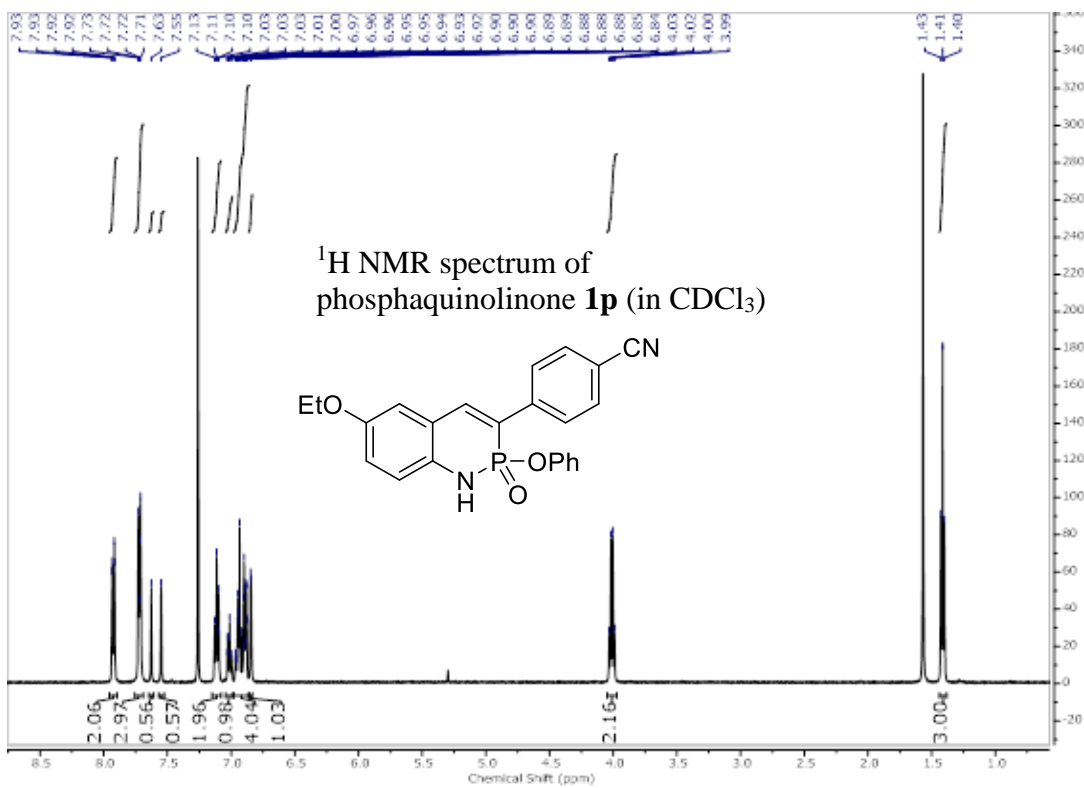


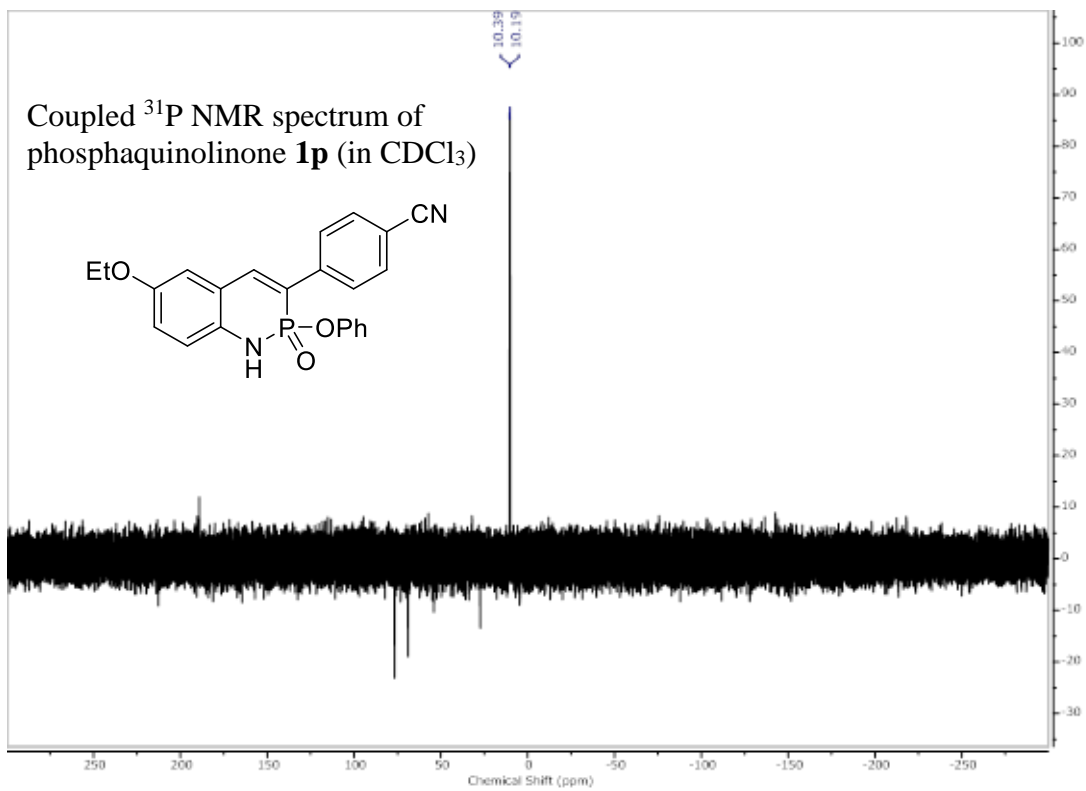












APPENDIX B

SUPPLEMENTARY INFORMATION FOR CHAPTER 3

1. CCDC Search Results

Search criteria for monomeric HSO_4^- solid-state complexes were made by drawing the chemical structure of HSO_4^- and using the “exact” designation. 450 results were found showing chains, metal-containing species, water/solvent-bridged, homodimers and oligomers; only monomer species with synthetic receptors were selected. For numerous HSO_4^- homodimers, see: E. M. Fatila, E. B. Twum, A. Sengupta, M. Pink, J. A. Karty, K. Raghava-chari, A. H. Flood, *Angew. Chem. Int. Ed.* **2016**, *55*, 14057–14062.¹

Table B.1 CCDC results of selected monomeric HSO_4^- solid-state complexes

Database Identifier	Reference
BURKAB	<i>CrystEngComm</i> 2010 , <i>12</i> , 413
ISOWAP	<i>Org. Biomol. Chem.</i> 2011 , <i>9</i> , 4444
MIJTAB	<i>J. Am. Chem. Soc.</i> 2007 , <i>129</i> , 8692
NELWAE	<i>Inorg. Chem.</i> 2012 , <i>51</i> , 4833
XIBCOB	<i>Polyhedron</i> 2013 , <i>50</i> , 622
FAZCEP	<i>Inorg. Chem.</i> 2007 , <i>46</i> , 2846
UMOHIN	<i>New J. Chem.</i> 2004 , <i>28</i> , 1301
DALRIT	<i>J. Med. Chem.</i> 2003 , <i>46</i> , 3865
ASOXEN	<i>Cryst. Growth Des.</i> 2011 , <i>11</i> , 4463
	<i>Chem. Commun.</i> 2016 , <i>52</i> , 11139

3. X-ray Crystallographic Data

X-ray Crystallography. Diffraction intensities for **1a**, **1b** and **1b**• HSO_4^- were collected at 173 K on a Bruker Apex2 CCD diffractometer using $\text{CuK}\alpha$ radiation, $\lambda = 1.54178 \text{ \AA}$. Space groups were determined based on systematic absences (**1a**) and intensity statistics (**1b** and **1b**• HSO_4^-). Absorption corrections were applied by SADABS.² Structures were solved by

direct methods and Fourier techniques and refined on F^2 using full matrix least-squares procedures. All non-H atoms were refined with anisotropic thermal parameters. H atoms in all structures were refined in calculated positions in a rigid group model, except the H atoms at the N atoms and the H atoms in MeOH and HSO₄ groups (in **1a** and **1b**•HSO₄⁻, respectively) involved in H-bonds. Positions of these H atoms were found on the residual density map and refined with isotropic thermal parameters with restrictions on its bond distance; the standard N–H and O–H bond lengths were used in the refinements as the targets for corresponding bonds. Terminal *t*-Bu groups in all structures and a counterion NBu₄⁺ in **1b**•HSO₄⁻ are disordered. Thermal ellipsoids for these groups and some other terminal groups and solvent molecules as well in the structures are significantly elongated. Some solvent molecules (expecting a mixture of CHCl₃/(CH₃)₂SO/pentane) in **1b**•HSO₄⁻ are highly disordered around an inversion center and was treated by SQUEEZE;³ the correction of the X-ray data by SQUEEZE is 127 electron/cell. These not resolved solvent molecules have not been included in the total formula of the compound. Due to a lot of disordered groups in the structures, X-ray diffraction from crystals of **1b** and **1b**•HSO₄⁻ at high angles is very weak and reflection statistics at high angles are poor. Even using a strong *Incoatec* I μ S Cu source, it was possible to collect data only up to $2\theta_{\max} = 100.75^\circ$ (**1b**) and 104.42° (**1b**•HSO₄⁻); thus, the resolution for these X-ray structures is not very high. Nonetheless, diffraction data collected for these structures provide appropriate numbers of measured reflections per refined parameters (5160/631 in **1b** and 8208/818 in **1b**•HSO₄⁻) and the X-ray structures clearly show the chemical results. All calculations were performed by the Bruker SHELXL-2014 package.⁴

Crystallographic Data for 1a: C₅₄H₅₀Cl₂N₅O₅P, M = 966.86, 0.07 x 0.04 x 0.04 mm, T = 173(2) K, Monoclinic, space group *P2₁/n*, *a* = 12.8174(11) Å, *b* = 29.801(3) Å, *c* = 13.9869(11) Å, β = 114.808(3)°, *V* = 4849.6(8) Å³, *Z* = 4, *D_c* = 1.324 Mg/m³, μ(Cu) = 1.974 mm⁻³, *F*(000) = 2024, 2θ_{max} = 135.50°, 31807 reflections, 8432 independent reflections [*R*_{int} = 0.0702], *R*1 = 0.1002, *wR*2 = 0.2512 and GOF = 1.086 for 8432 reflections (627 parameters) with *I* > 2σ(*I*), *R*1 = 0.1414, *wR*2 = 0.2902 and GOF = 1.086 for all reflections, max/min residual electron density +0.853/−1.205 eÅ⁻³. CCDC 1884079.

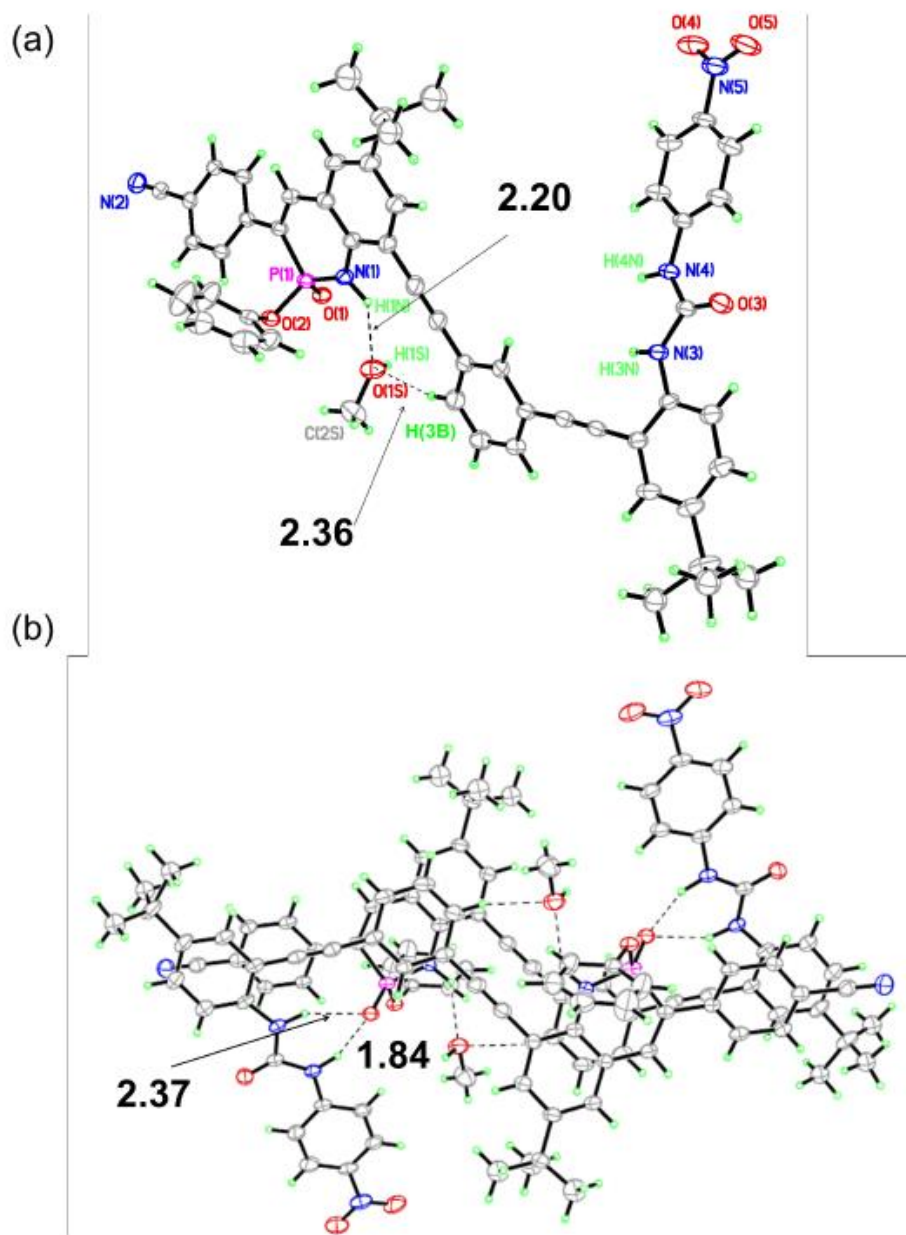


Figure B.1 X-ray structure of **1a** a) and the dimer of **1a** b), showing the coordination of MeOH solvent molecules; thermal ellipsoids drawn at the 30% probability level. The dotted lines denote hydrogen-bonding interactions with distances shown in Å. The *t*-Bu groups are disordered. In the solid-state structure, the oxygen atom of the MeOH solvent guest accepts a hydrogen bond from both a phosphonamidate N–H moiety and an aromatic hydrogen atom in the phenyl backbone, while the P=O motif accepts H-bonds from the two urea N–H units of an adjacent molecule. As a result, two molecules are stacked in a head-to-tail fashion through these hydrogen bond interactions to form a dimeric structure and the monomer exhibits an open ‘S’ conformation.

Crystallographic Data for 1b: C₅₄H₄₉N₆O₈PS, M = 973.02, 0.11 x 0.02 x 0.01 mm, T = 173(2) K, Triclinic, space group *P*-1, *a* = 13.4164(10) Å, *b* = 13.7420(12) Å, *c* = 14.3491(11) Å, α = 107.705(6)°, β = 98.455(6)°, γ = 93.057(6)°, *V* = 2479.3(4) Å³, *Z* = 2, *D*_c = 1.303 Mg/m³, μ (Cu) = 1.388 mm⁻¹, *F*(000) = 1020, $2\theta_{\max}$ = 100.75°, 15858 reflections, 5160 independent reflections [*R*_{int} = 0.0833], *R*1 = 0.0749, *wR*2 = 0.1904 and *GOF* = 1.012 for 5160 reflections (631 parameters) with *I* > 2σ(*I*), *R*1 = 0.1303, *wR*2 = 0.2326 and *GOF* = 1.012 for all reflections, max/min residual electron density +0.530/−0.523 eÅ⁻³. CCDC 1884080.

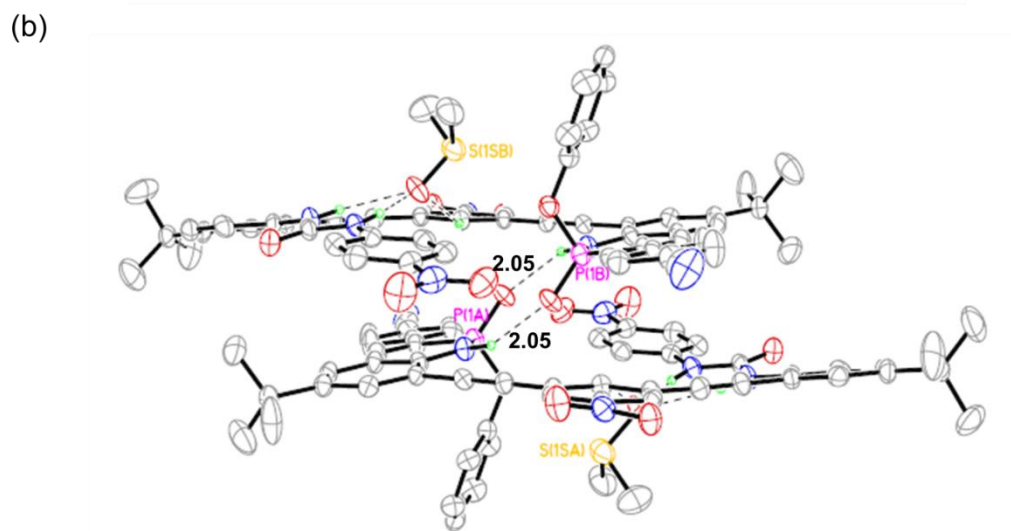
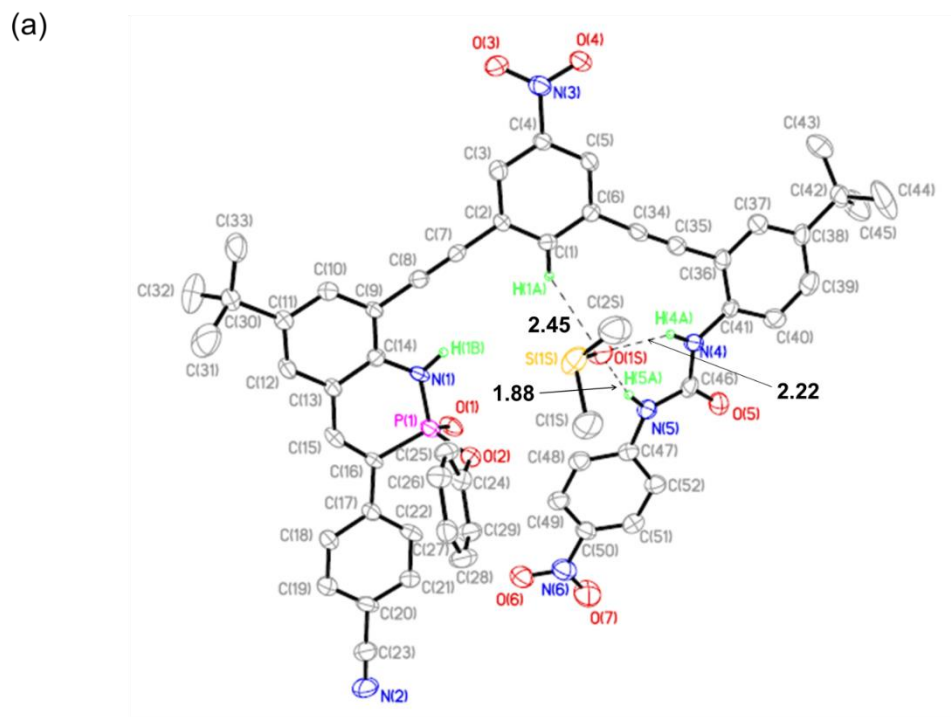


Figure B.2 X-ray structure of **1b** a) and the dimer of **1b** b), showing the coordination of DMSO solvent molecules; thermal ellipsoids drawn at the 30% probability level. The dotted lines denote hydrogen-bonding interactions with distances shown in Å. Receptor **1b** adopts a slightly twisted ‘*U*’ conformation and donates two hydrogen bonds through the urea moiety and another weak C–H hydrogen bond through the nitrophenyl core to provide an electropositive pocket, which accommodates the electronegative oxygen atom of DMSO solvent. The PN-heterocycle unit interacts with another host molecule through N–H and P=O hydrogen bonding interactions to form a centrosymmetrical dimer.

Crystallographic Data for 1b•HSO₄⁻ [TBA]⁺ complex: C₆₈H₈₀N₇O₁₁PS, M = 1234.42, 0.17 x 0.05 x 0.01 mm, T = 173(2) K, Triclinic, space group *P*-1, *a* = 11.3009(5) Å, *b* = 18.4309(8) Å, *c* = 19.7252(10) Å, α = 108.978(3)°, β = 102.353(3)°, γ = 97.591(3)°, *V* = 3703.7(3) Å³, *Z* = 2, *D_c* = 1.107 Mg/m³, μ (Cu) = 1.057 mm⁻¹, *F*(000) = 1312, $2\theta_{\max}$ = 104.42°, 28307 reflections, 8208 independent reflections [*R*_{int} = 0.0652], *R*₁ = 0.0688, *wR*₂ = 0.1822 and *GOF* = 1.001 for 8208 reflections (818 parameters) with *I* > 2σ(*I*), *R*₁ = 0.1059, *wR*₂ = 0.2024 and *GOF* = 1.005 for all reflections, max/min residual electron density +0.462/−0.292 eÅ⁻³. CCDC 1884081.

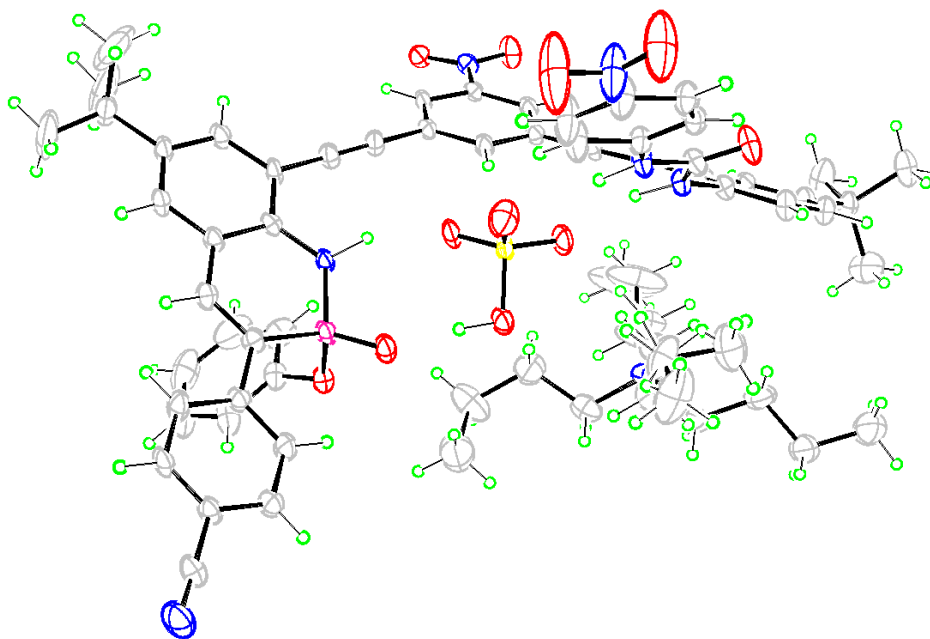


Figure B.3 X-ray structure of **1b**•HSO₄⁻ [TBA]⁺ complex; thermal ellipsoids drawn at the 30% probability level. The dotted lines denote hydrogen-bonding interactions.

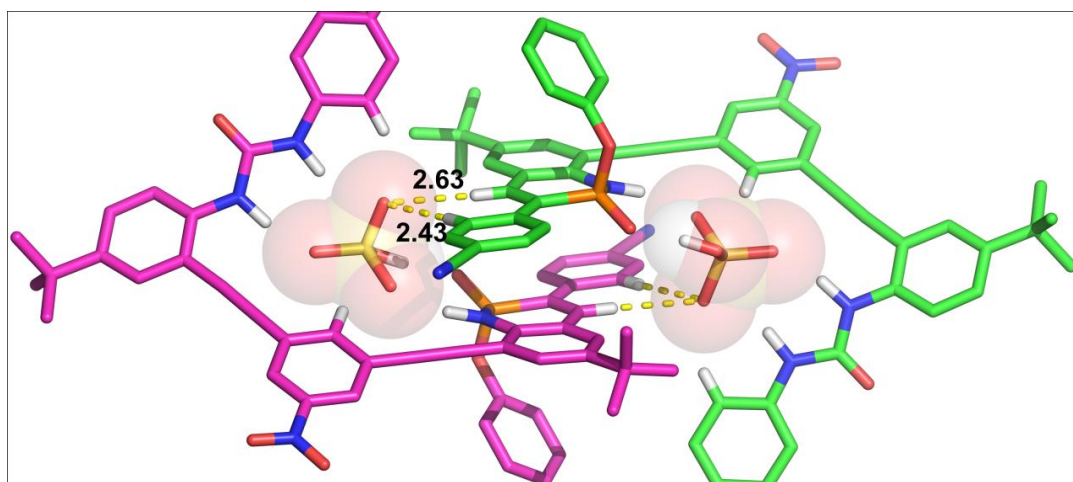


Figure B.4 Snapshot showing 2:2 dimeric complex provided by additional C–H···O contacts. The dotted lines denote hydrogen-bonding interactions with distances shown in Å.

4. 2D NMR Spectroscopic Data for 1

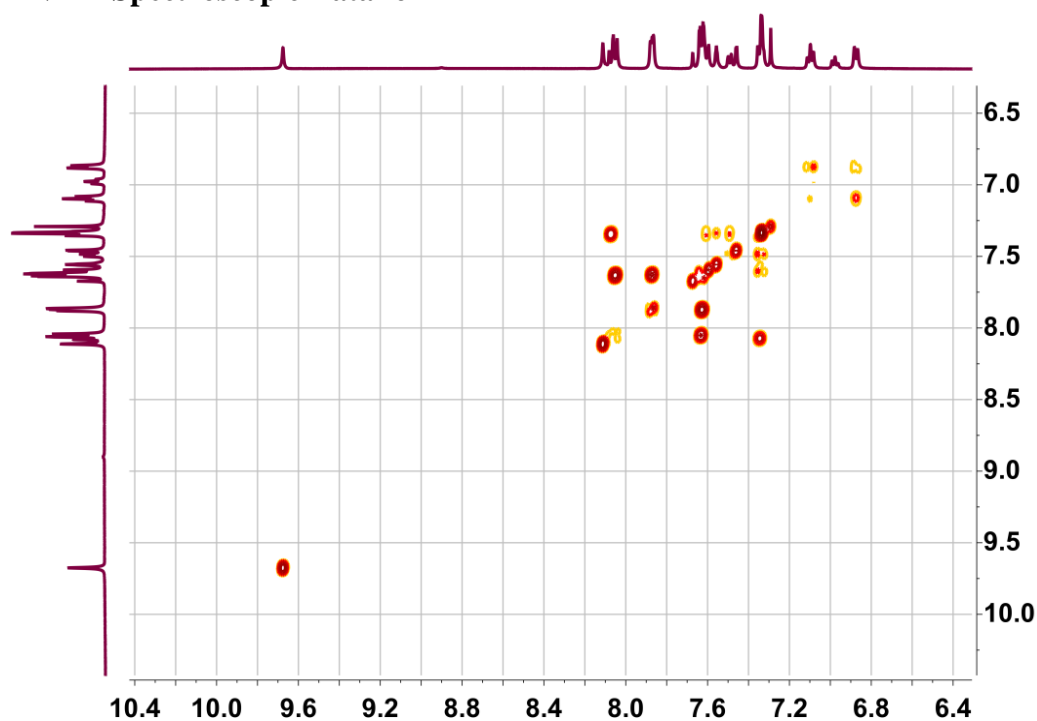


Figure B.5 ^1H - ^1H gradient COSY spectrum of **1a** in 10% DMSO- d_6 /CDCl $_3$.

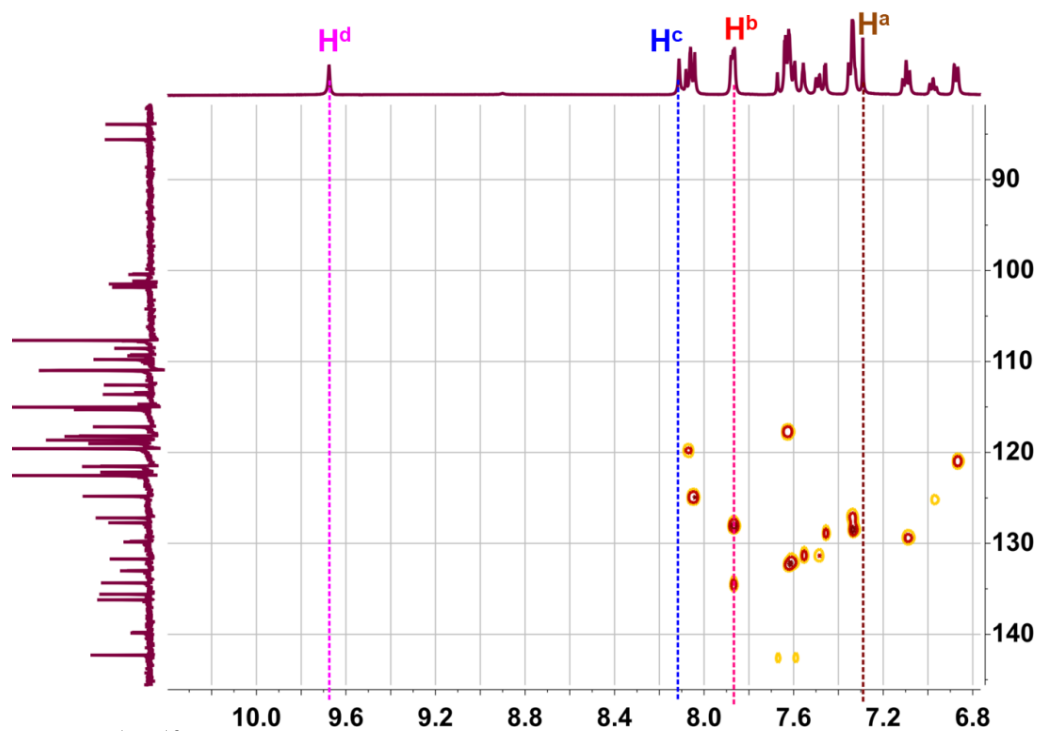


Figure B.6 ^1H - ^{13}C HSQC NMR spectrum of **1a** in 10% DMSO- d_6 /CDCl $_3$. This result supports that H^a, H^c and H^d are N-H protons.

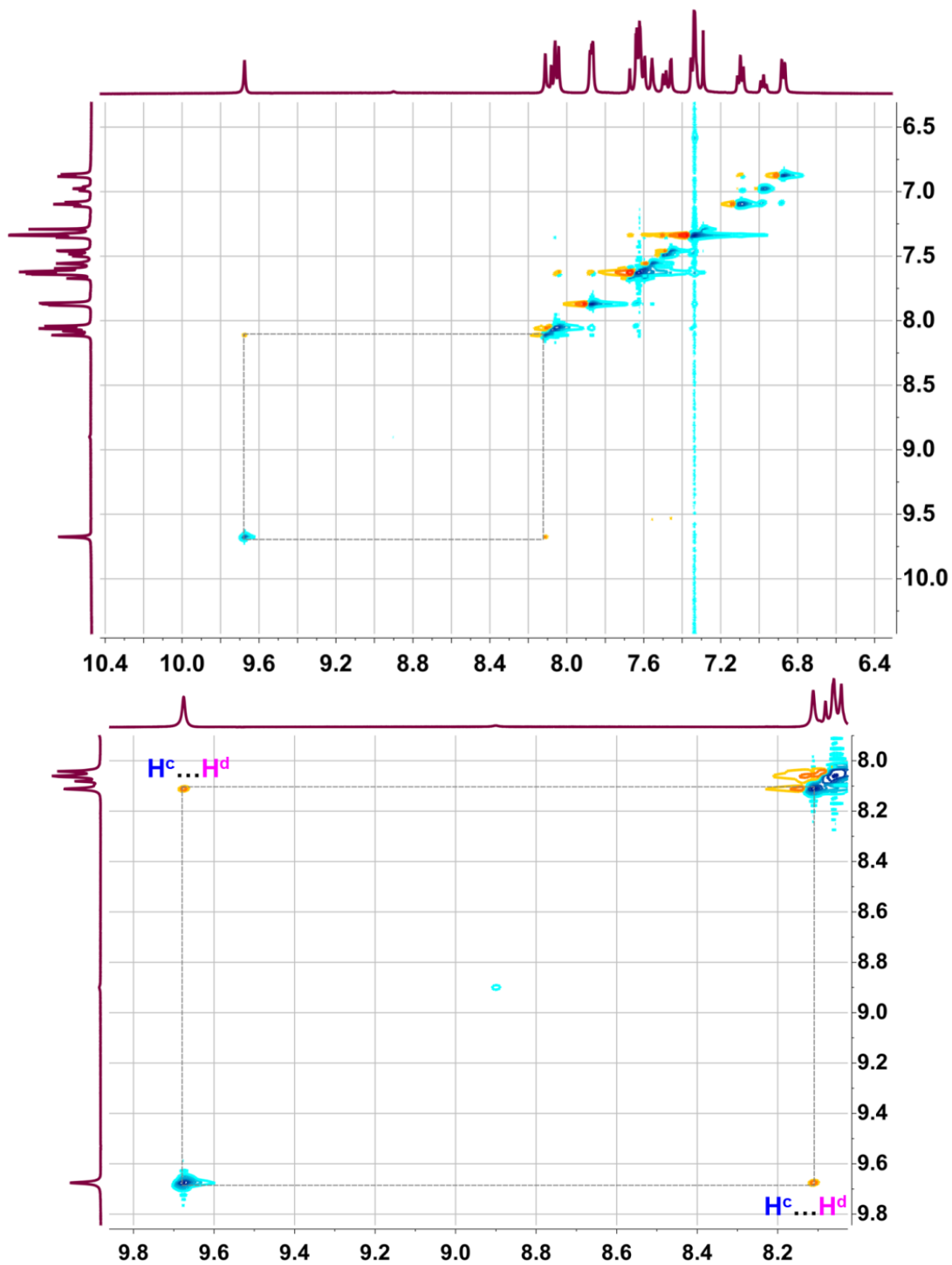


Figure B.7 ^1H - ^1H NOESY (top: whole spectrum; bottom: partial spectrum showing the cross peak/correlation of H^c and H^d) of **1a** in 10% $\text{DMSO-}d_6/\text{CDCl}_3$.

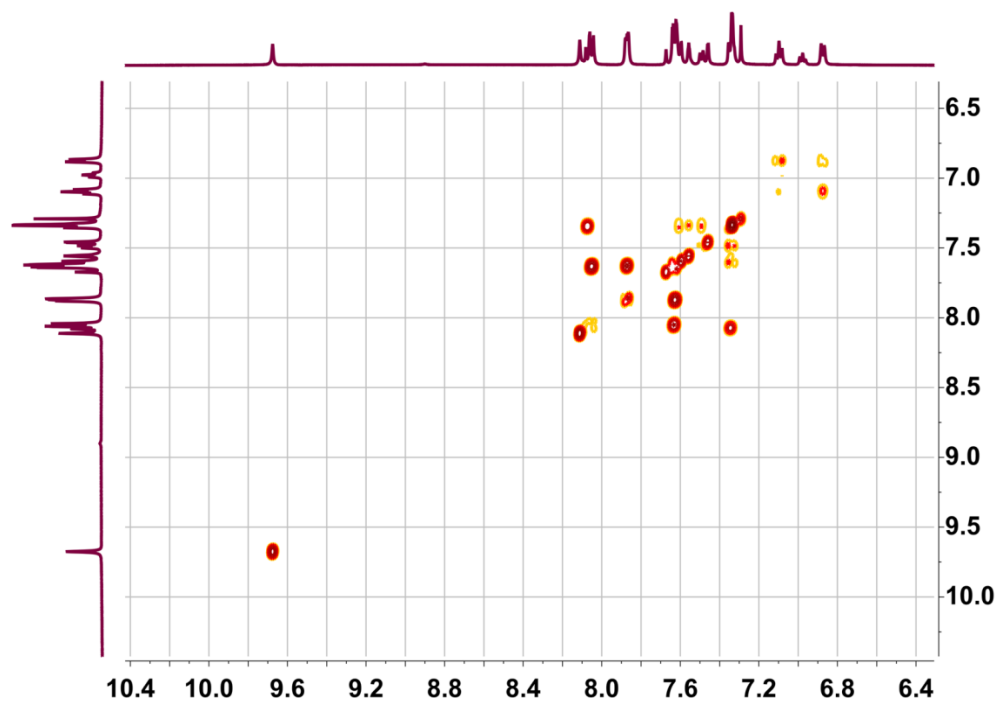


Figure B.8 ^1H - ^1H gradient COSY spectrum of **1b** in 10% $\text{DMSO-}d_6/\text{CDCl}_3$.

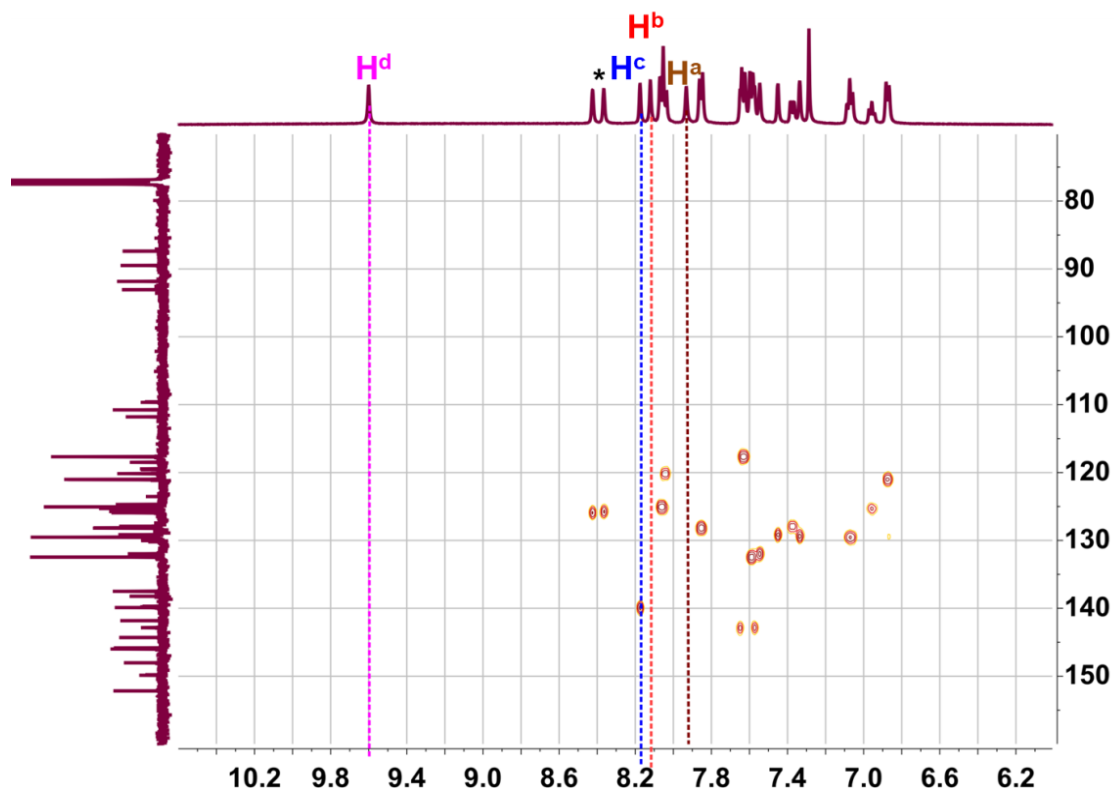


Figure B.9 ^1H - ^{13}C HSQC spectrum of **1b** in 10% $\text{DMSO-}d_6/\text{CDCl}_3$. This result supports that H^a , H^c and H^d are N-H protons.

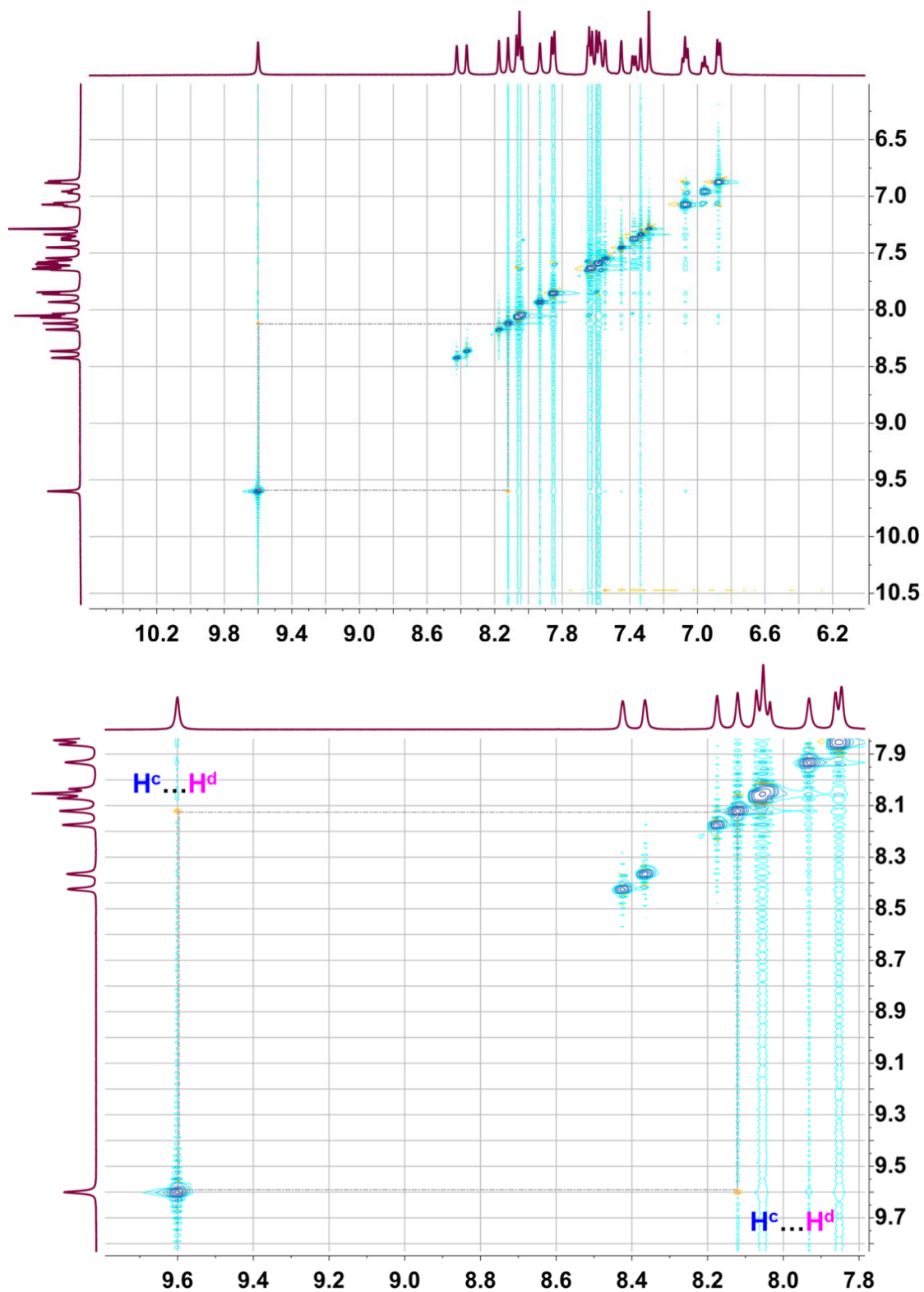


Figure B.10 ^1H - ^1H NOESY (top: whole spectrum; bottom: partial spectrum showing the cross peak/correlation of H^{c} and H^{d}) of **1b** in 10% $\text{DMSO-}d_6/\text{CDCl}_3$.

5. Interaction of 1a with Various Anions

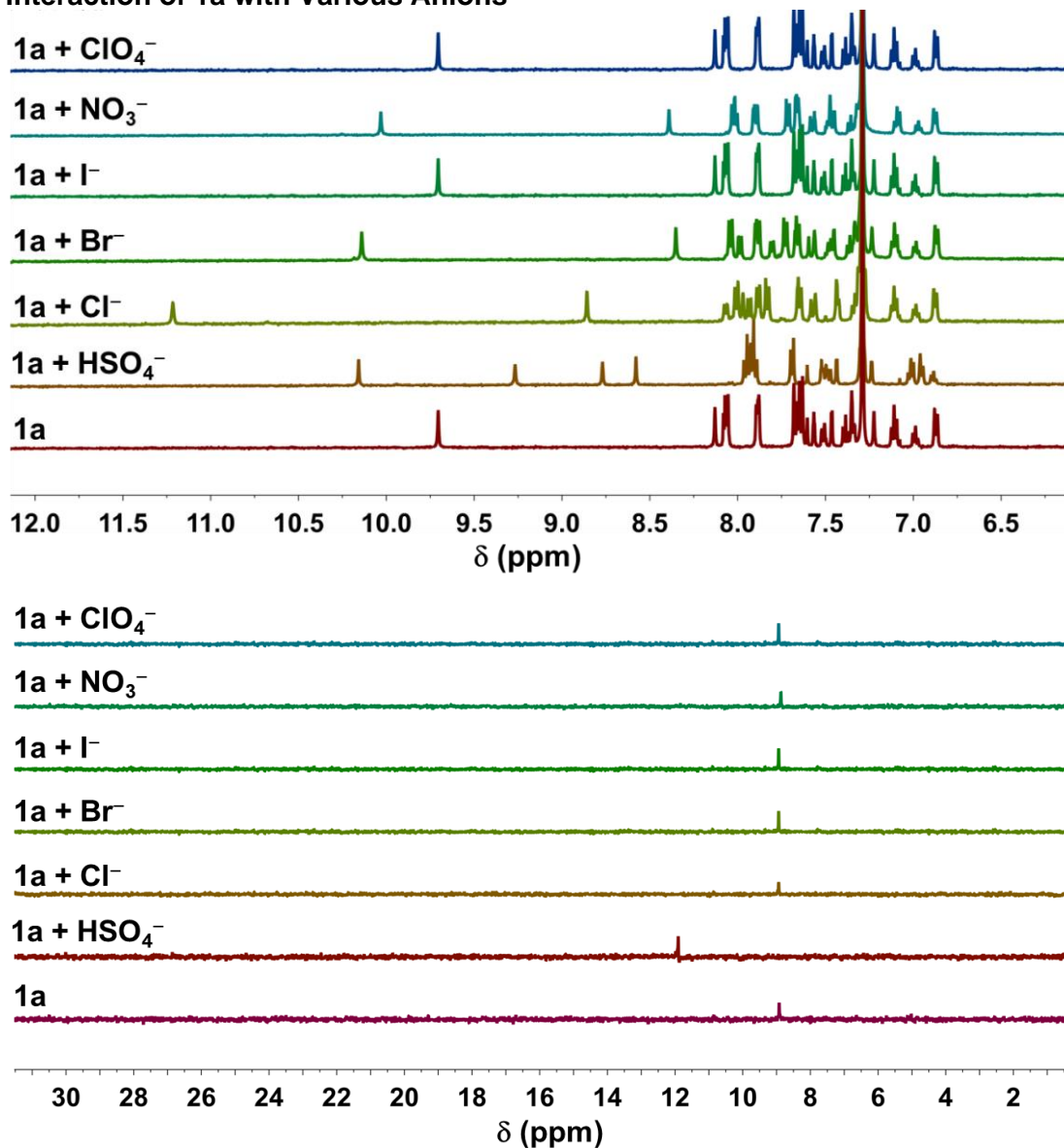


Figure B.11 Partial ¹H NMR (top) and ³¹P NMR (bottom) spectra of **1a** (1.0 mM) in 10 vol% DMSO-*d*₆/CDCl₃ in the absence and the presence of 10 equiv. of various anions. All anions were used as their respective TBA salts.

6. Representative NMR Titration Data

Solutions of host (10 ~ 20 mg) were prepared using 10% DMSO-*d*₆/CDCl₃ in a volumetric flask to a final concentration of approximately 0.0005-0.0015 M. In each case, 600 μL of this solution was transferred to an NMR tube, and the remainder of the solution was used to generate the guest stock solution to a concentration of 0.005–0.060 M to maintain a constant host concentration throughout the titration. Aliquots of the guest solution were added *via* Hamilton gas tight syringes to the host solution in the NMR tube, and a spectrum was obtained *via* a Varian Inova 500 at 298 K after thorough mixing. Association constants (*K*_a) were calculated by nonlinear curve fitting of the obtained titration isotherms ($\Delta\delta > \pm 0.2$ ppm) using the reported 1:1 binding model.⁵ The reported association constants were the average of triplicate titrations, which were calculated from the simultaneous fitting of downfield shifting proton resonances (H^b, H^c and H^d for hydrogen sulfate, H^a, H^c and H^d for nitrate, H^c and H^d for halides. The H^a, H^e resonances may not be explicitly determined due to the slow exchange regime problems with disappearing or overlapping peaks during ¹H NMR studies in the case of hydrogen sulfate). Similarly, the chemical shifts change ($\Delta\delta > \pm 0.1$ ppm) of the P atom resonances during titrations were also recorded and fitted.

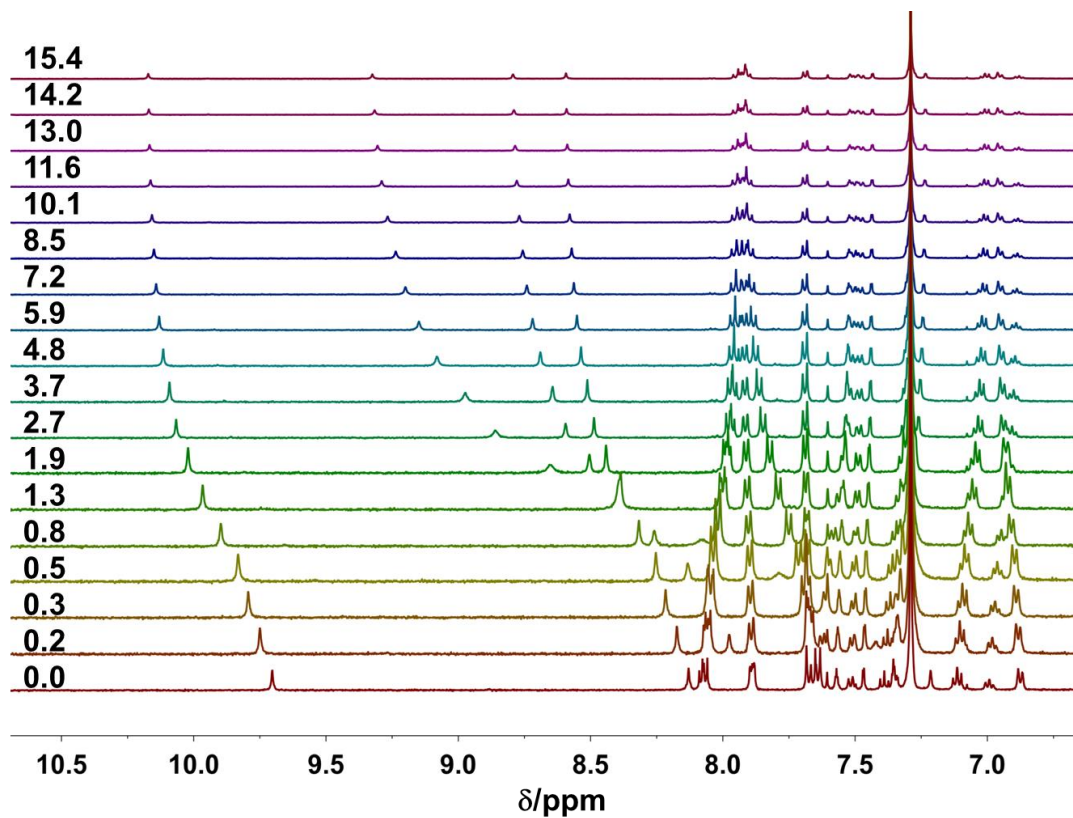


Figure B.12 Representative ¹H NMR titration of **1a** (1.0 mM in 10% DMSO-*d*₆/CDCl₃) with tetrabutylammonium hydrogen sulfate as stacked spectra with hydrogen sulfate equivalents increasing bottom to top.

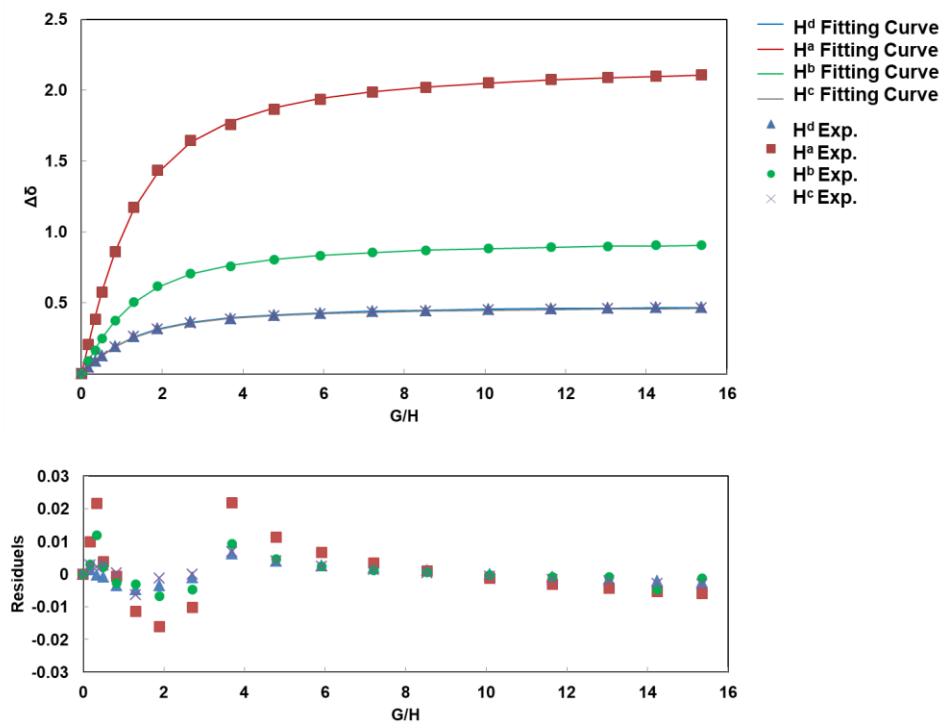


Figure B.13 Representative binding isotherm and fit curves for HSO_4^- titration of **1a** in 10% $\text{DMSO-}d_6/\text{CDCl}_3$ by ^1H NMR.

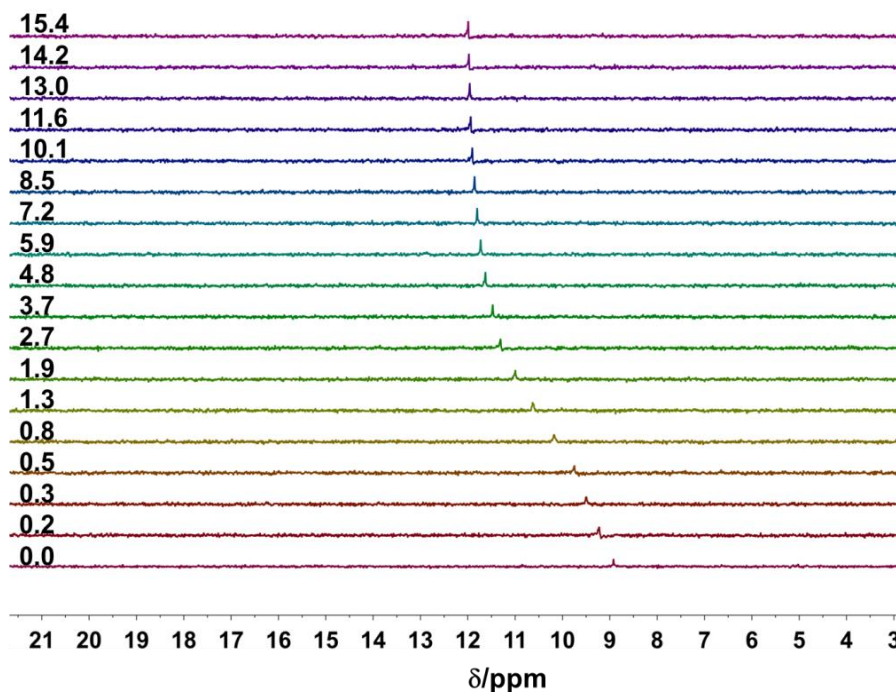


Figure B.14 Representative ^{31}P NMR titration of **1a** (1.0 mM) with tetrabutylammonium hydrogen sulfate as stacked spectra with hydrogen sulfate equivalents increasing bottom to top in 10% $\text{DMSO-}d_6/\text{CDCl}_3$.

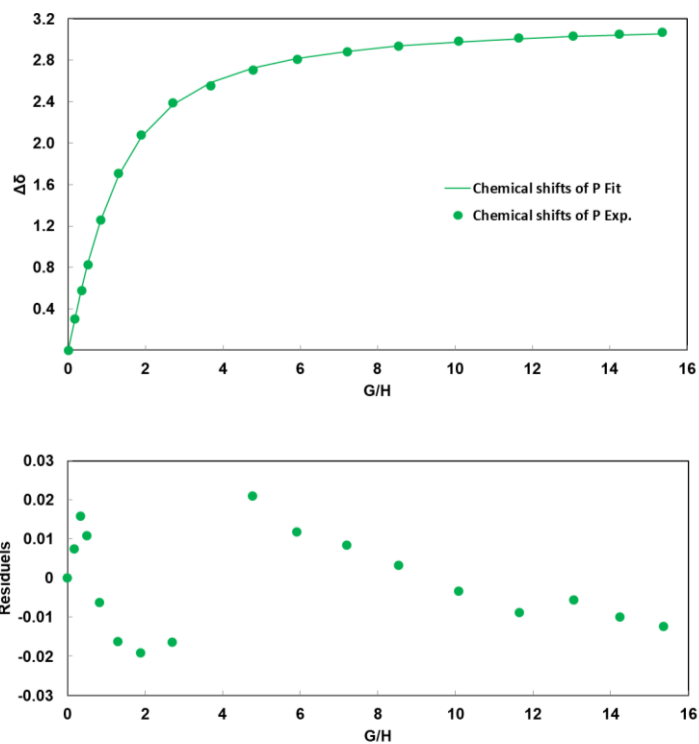


Figure B.15 Representative binding isotherm and fit curves for HSO_4^- titration of $\mathbf{1a}$ in 10% $\text{DMSO-}d_6/\text{CDCl}_3$ by ^{31}P NMR.

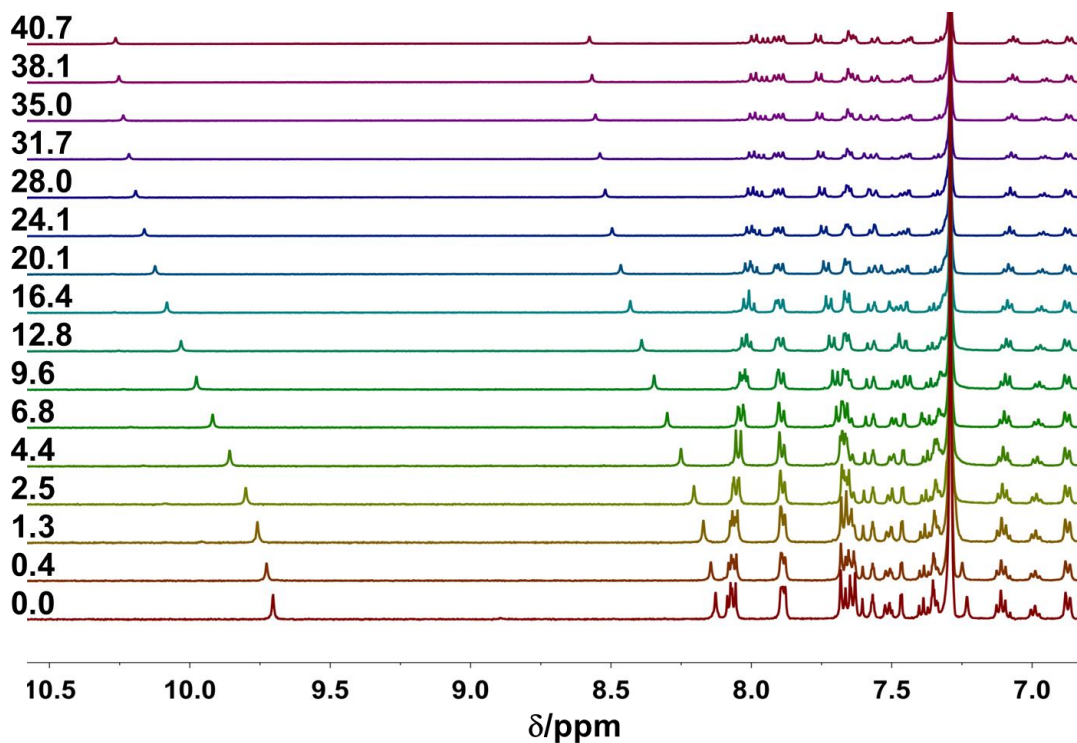


Figure B.16 Representative ^1H NMR titration of $\mathbf{1a}$ (1.38 mM) with tetrabutylammonium nitrate as stacked spectra with nitrate equivalents increasing bottom to top in 10% $\text{DMSO-}d_6/\text{CDCl}_3$.

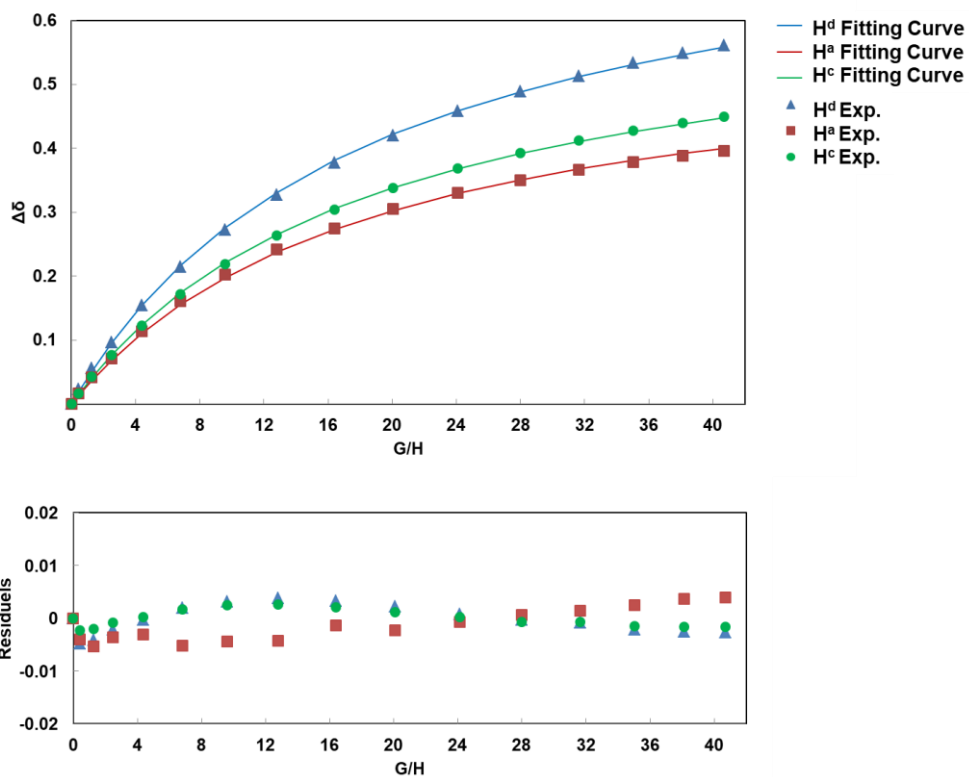


Figure B.17 Representative binding isotherm and fit curves for NO_3^- titration of **1a** in 10% $\text{DMSO-}d_6/\text{CDCl}_3$ by ^1H NMR.

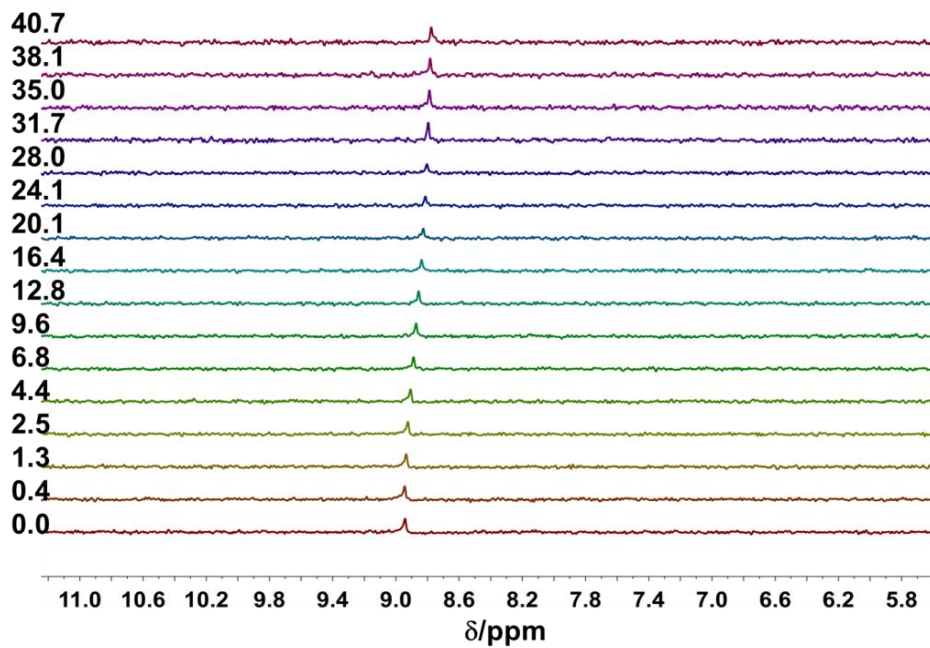


Figure B.18 Representative ^{31}P NMR titration of **1a** (1.38 mM) with tetrabutylammonium nitrate as stacked spectra with nitrate equivalents increasing bottom to top in 10% $\text{DMSO-}d_6/\text{CDCl}_3$.

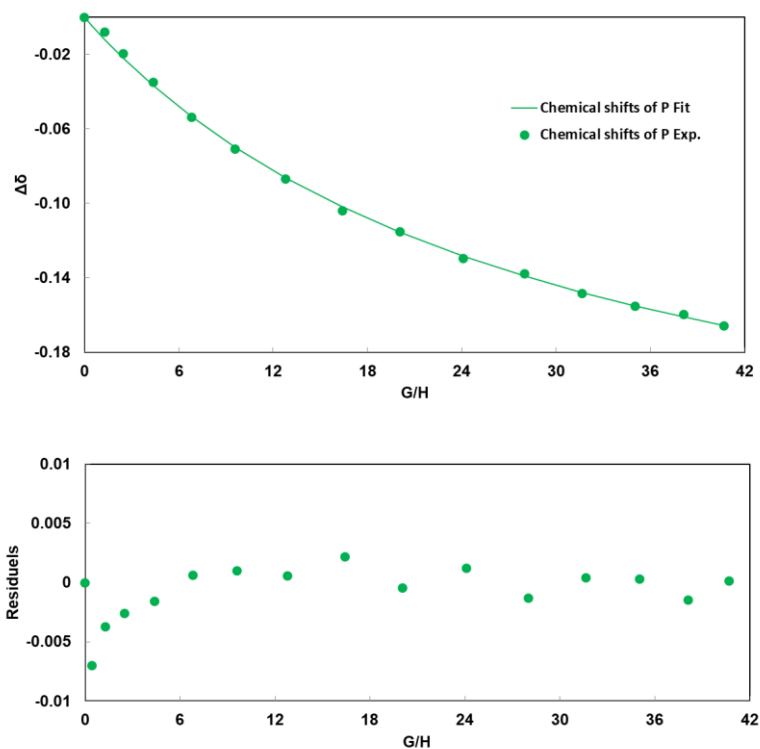


Figure B.19 Representative binding isotherm and fit curves for NO_3^- titration of **1a** in 10% $\text{DMSO-}d_6/\text{CDCl}_3$ by ^{31}P NMR.

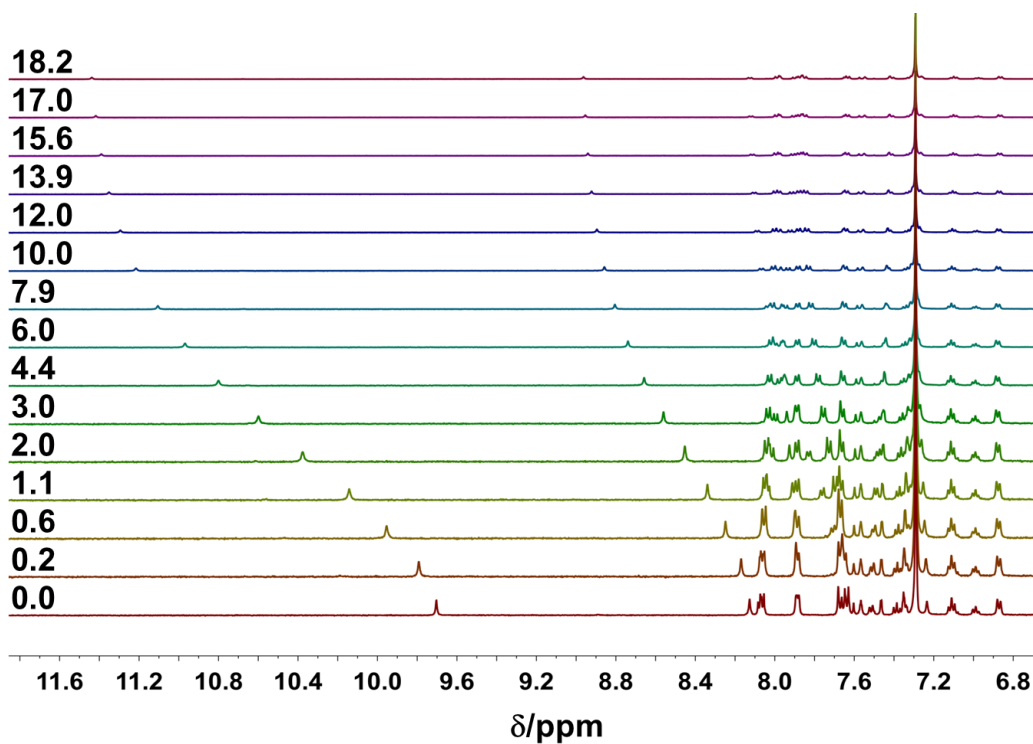


Figure B.20 Representative ¹H NMR titration of **1a** (1.37 mM) with tetrabutylammonium chloride as stacked spectra with chloride equivalents increasing bottom to top in 10% DMSO-*d*₆/CDCl₃.

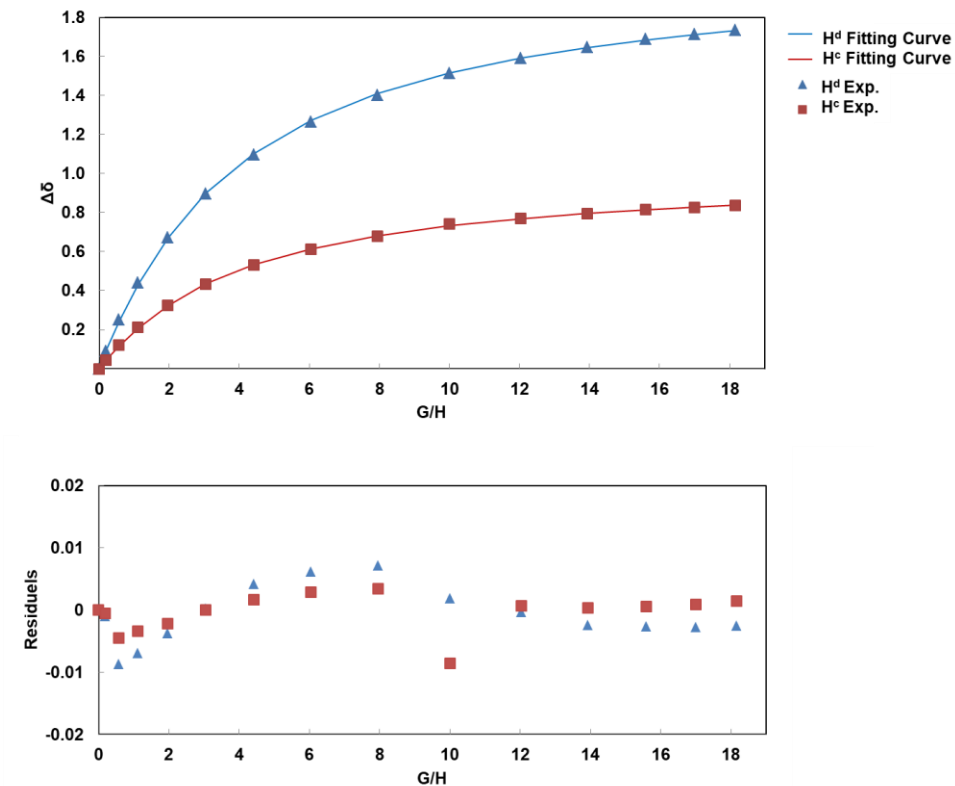


Figure B.21 Representative binding isotherm and fit curves for Cl^- titration of **1a** in 10% $\text{DMSO-}d_6/\text{CDCl}_3$ by ^1H NMR.

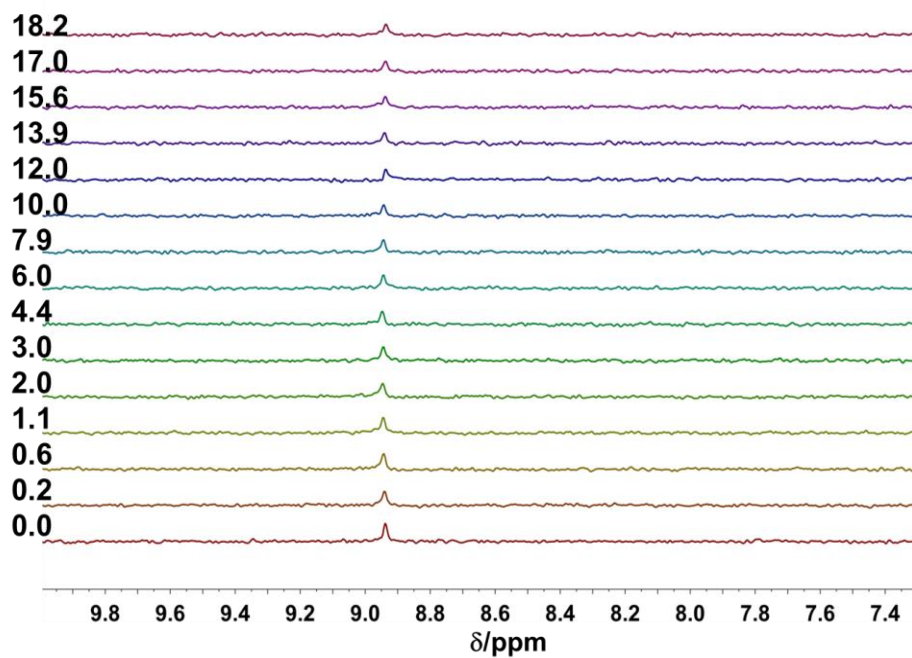


Figure B.22 Representative ^{31}P NMR titration of **1a** (1.37 mM) with tetrabutylammonium chloride as stacked spectra with chloride equivalents increasing bottom to top in 10% $\text{DMSO-}d_6/\text{CDCl}_3$.

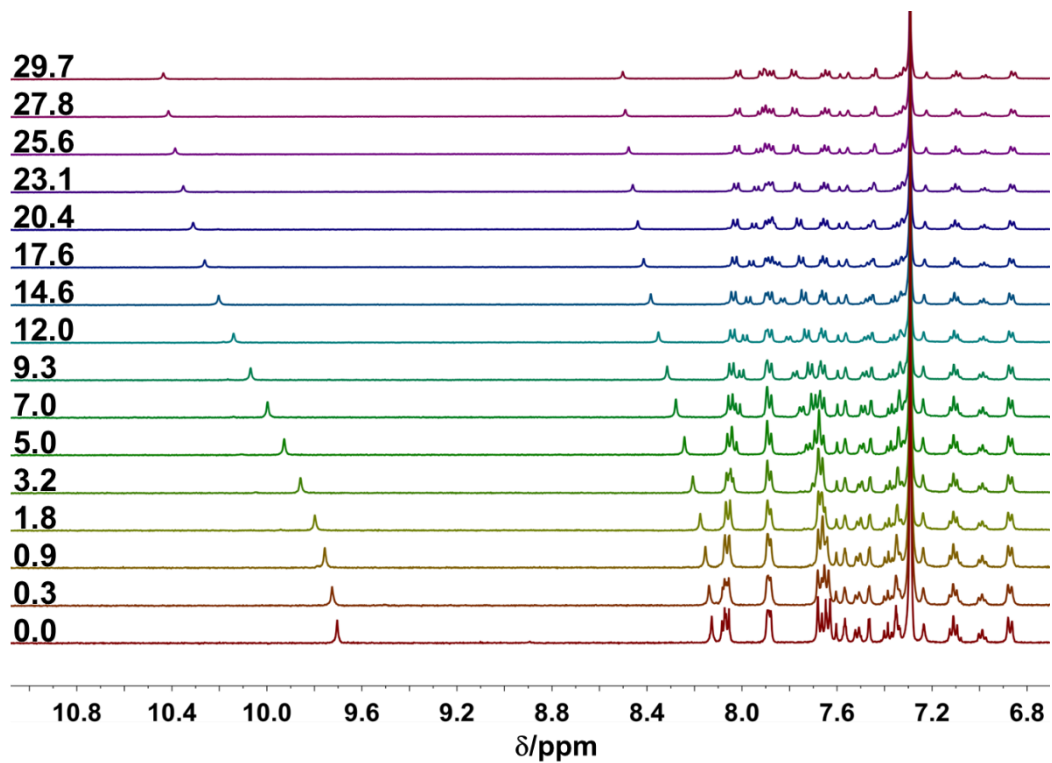


Figure B.23 Representative ^1H NMR titration of **1a** (1.37 mM) with tetrabutylammonium bromide as stacked spectra with bromide equivalents increasing bottom to top in 10% $\text{DMSO-}d_6/\text{CDCl}_3$.

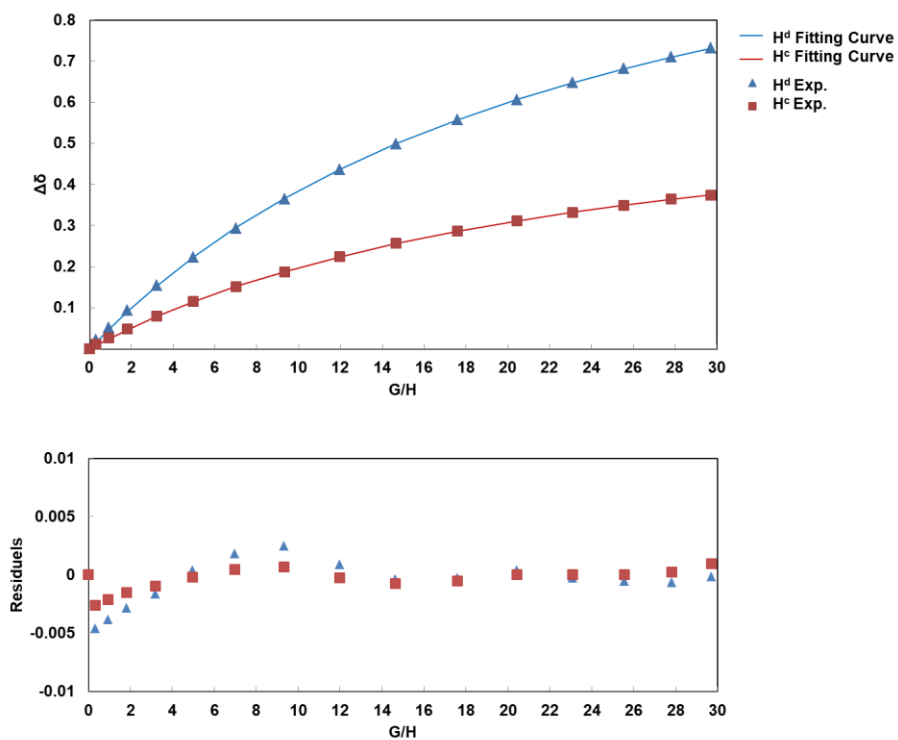


Figure B.24 Representative binding isotherm and fit curves for Br⁻ titration of **1a** in 10% DMSO-*d*₆/CDCl₃ by ¹H NMR.

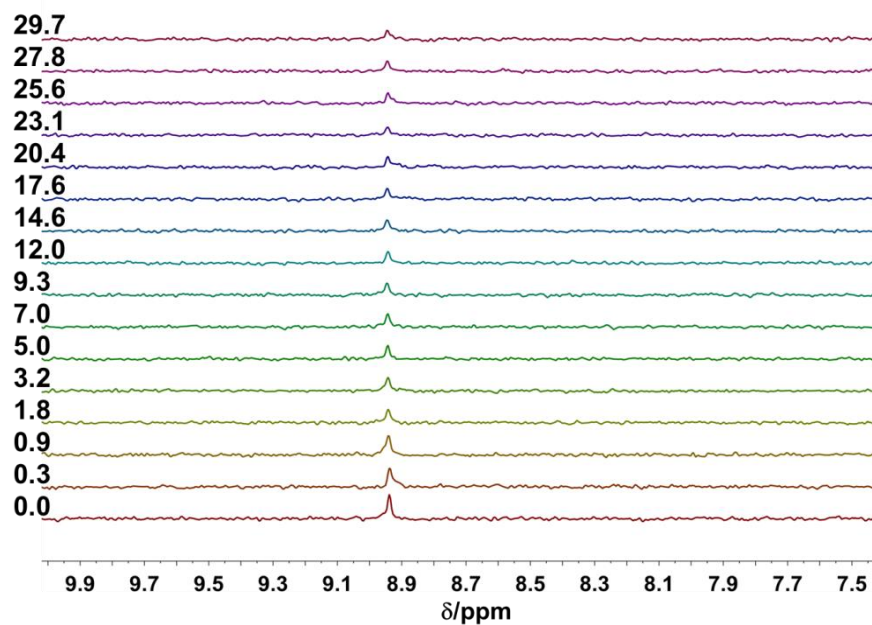


Figure B.25 Representative ³¹P NMR titration of **1a** (1.37 mM) with tetrabutylammonium bromide as stacked spectra with bromide equivalents increasing bottom to top in 10% DMSO-*d*₆/CDCl₃.

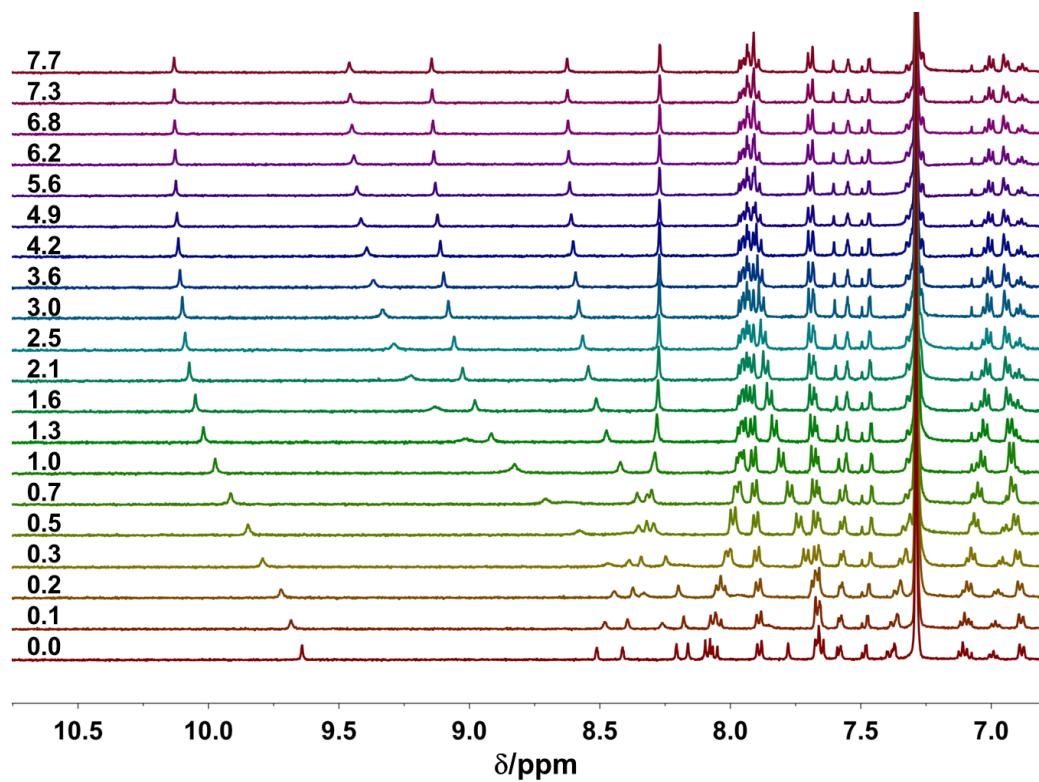


Figure B.26 Representative ^1H NMR titration of **1b** (0.56 mM) with tetrabutylammonium hydrogen sulfate as stacked spectra with hydrogen sulfate equivalents increasing bottom to top in 10% $\text{DMSO-}d_6/\text{CDCl}_3$.

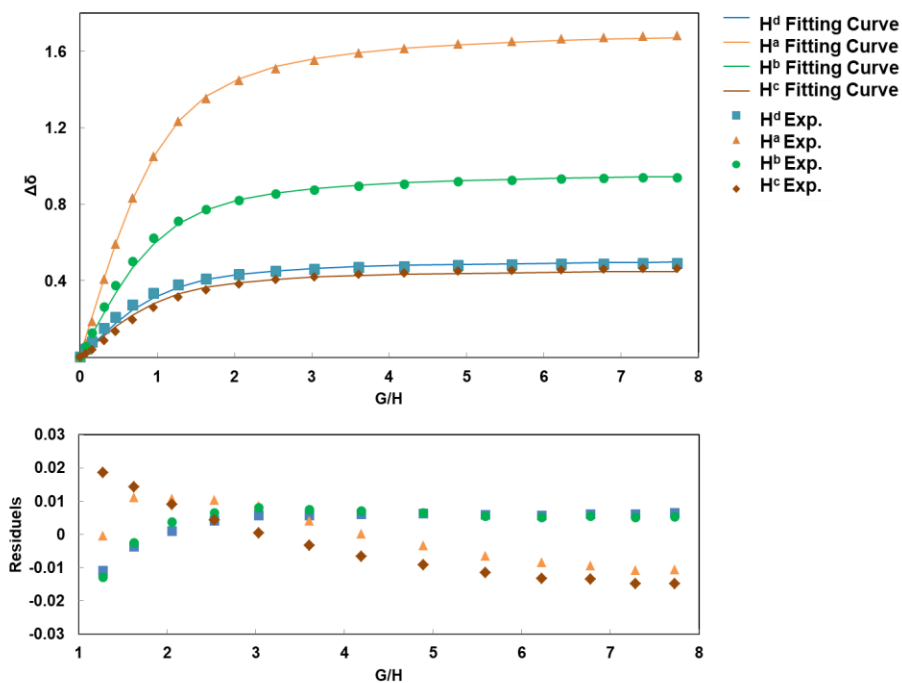


Figure B.27 Representative binding isotherm and fit curves for HSO_4^- titration of **1b** in 10% $\text{DMSO-}d_6/\text{CDCl}_3$ by ^1H NMR.

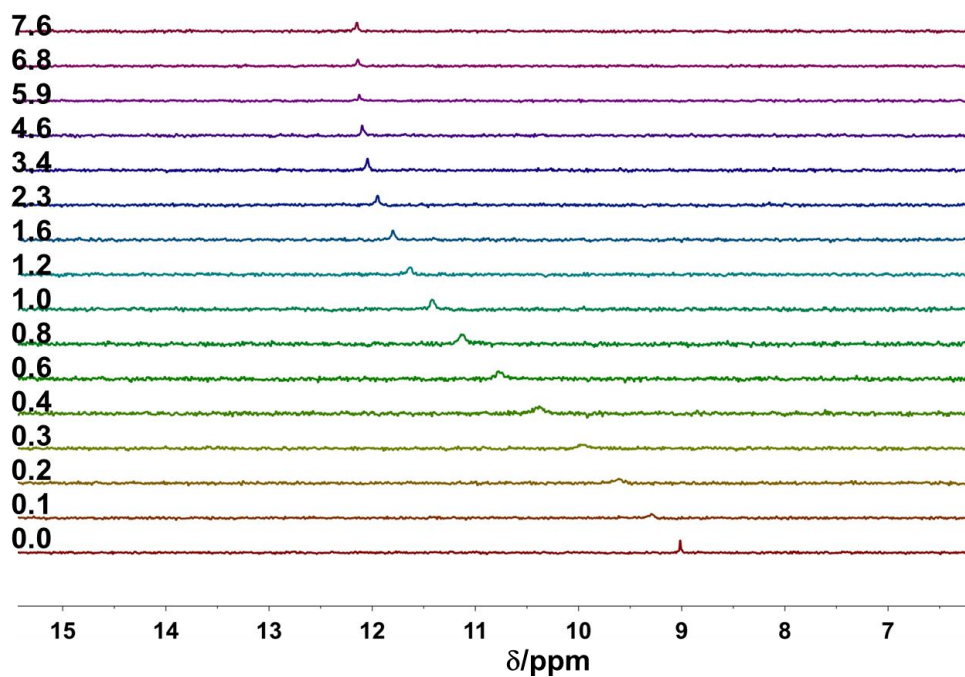


Figure B.28 Representative ^{31}P NMR titration of **1b** (1.66 mM) with tetrabutylammonium hydrogen sulfate as stacked spectra with hydrogen sulfate equivalents increasing bottom to top in 10% $\text{DMSO-}d_6/\text{CDCl}_3$ (discernible ^{31}P NMR resonance signals cannot be detected when $[\mathbf{1b}] \leq 1$ mM).

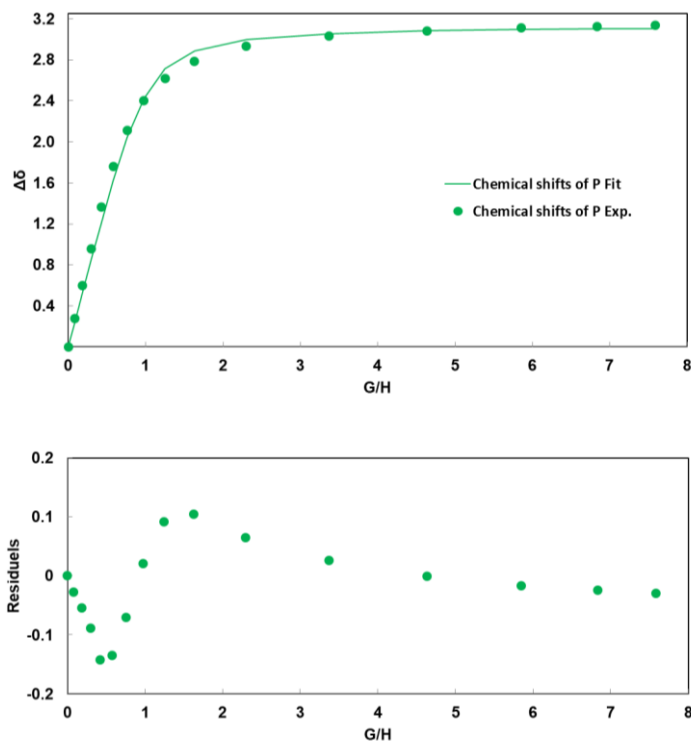


Figure B.29 Representative binding isotherm and fit curves for HSO_4^- titration of **1b** in 10% $\text{DMSO-}d_6/\text{CDCl}_3$ by ^{31}P NMR.

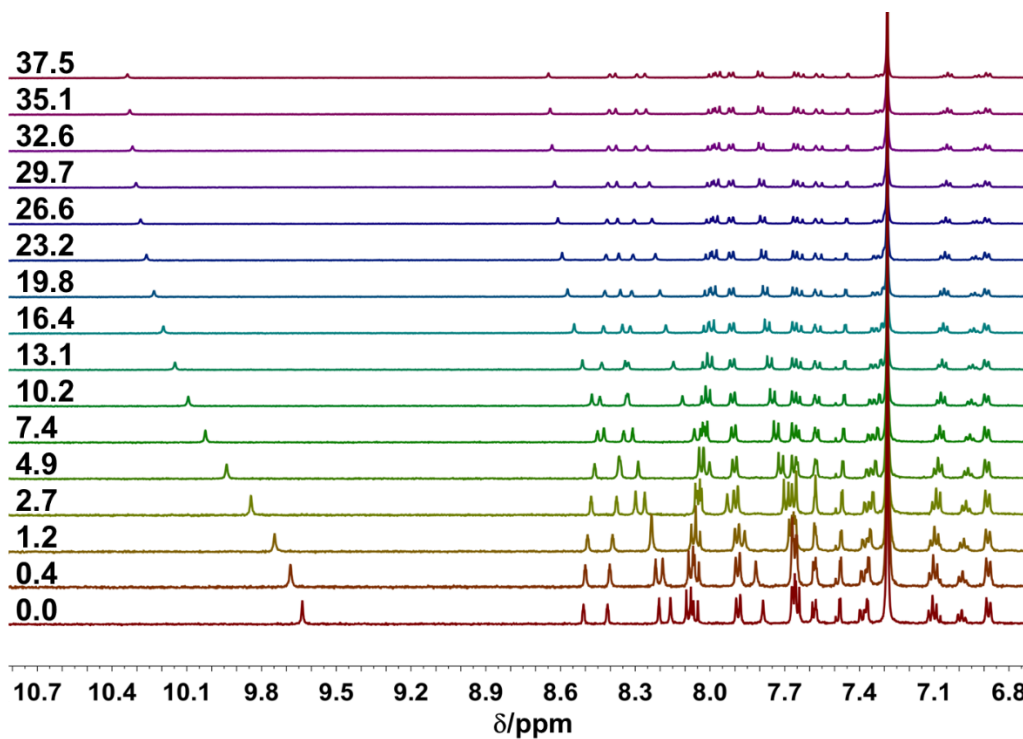


Figure B.30 Representative ^1H NMR titration of **1b** (1.08 mM) with tetrabutylammonium nitrate as stacked spectra with nitrate equivalents increasing bottom to top in 10% $\text{DMSO-}d_6/\text{CDCl}_3$.

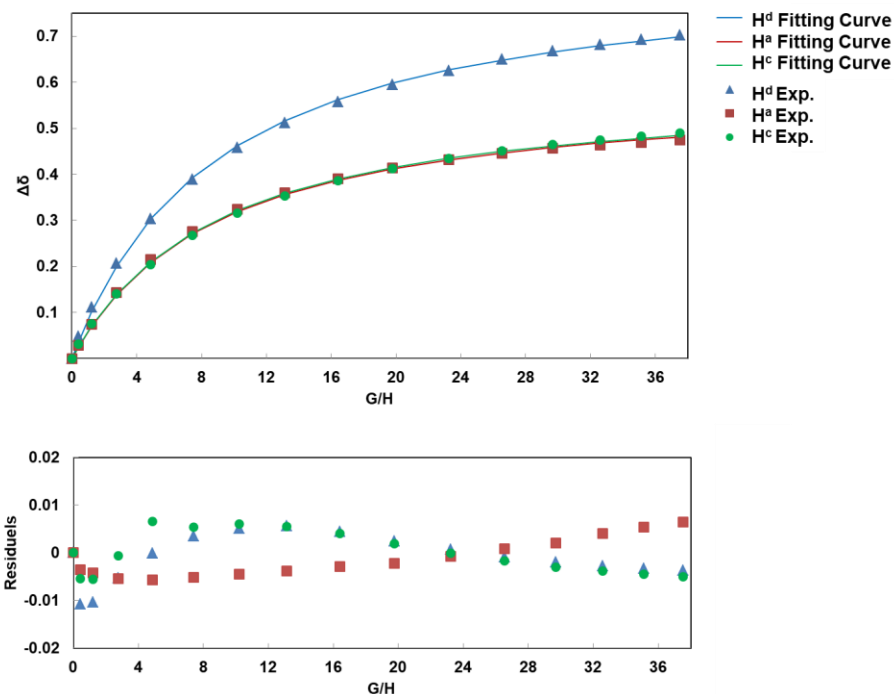


Figure B.31 Representative binding isotherm and fit curves for NO_3^- titration of **1b** in 10% $\text{DMSO-}d_6/\text{CDCl}_3$ by ^1H NMR.

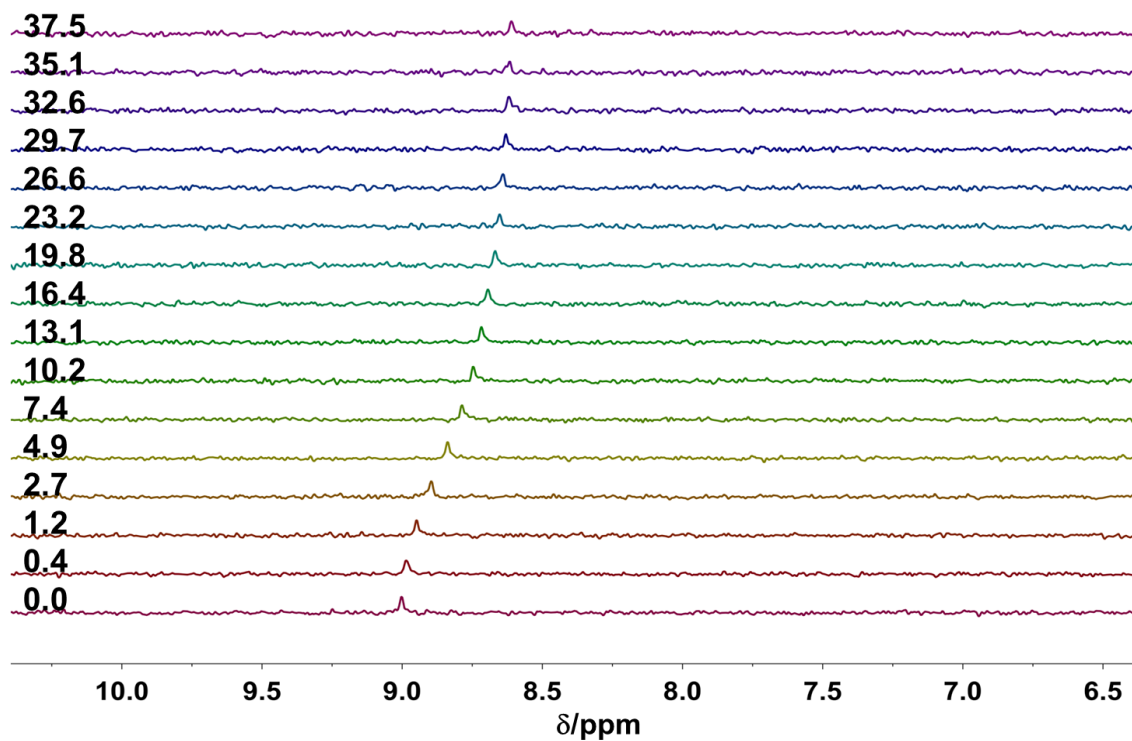


Figure B.32 Representative ^{31}P NMR titration of **1b** (1.08 mM) with tetrabutylammonium nitrate as stacked spectra with nitrate equivalents increasing bottom to top in 10% $\text{DMSO-}d_6/\text{CDCl}_3$.

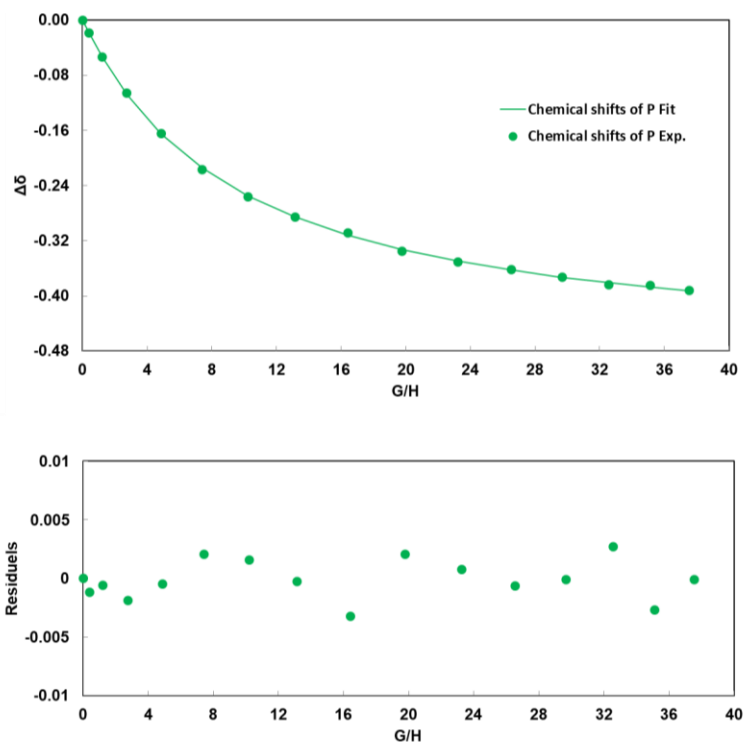


Figure B.33 Representative binding isotherm and fit curves for NO_3^- titration of **1b** in 10% $\text{DMSO-}d_6/\text{CDCl}_3$ by ^{31}P NMR.

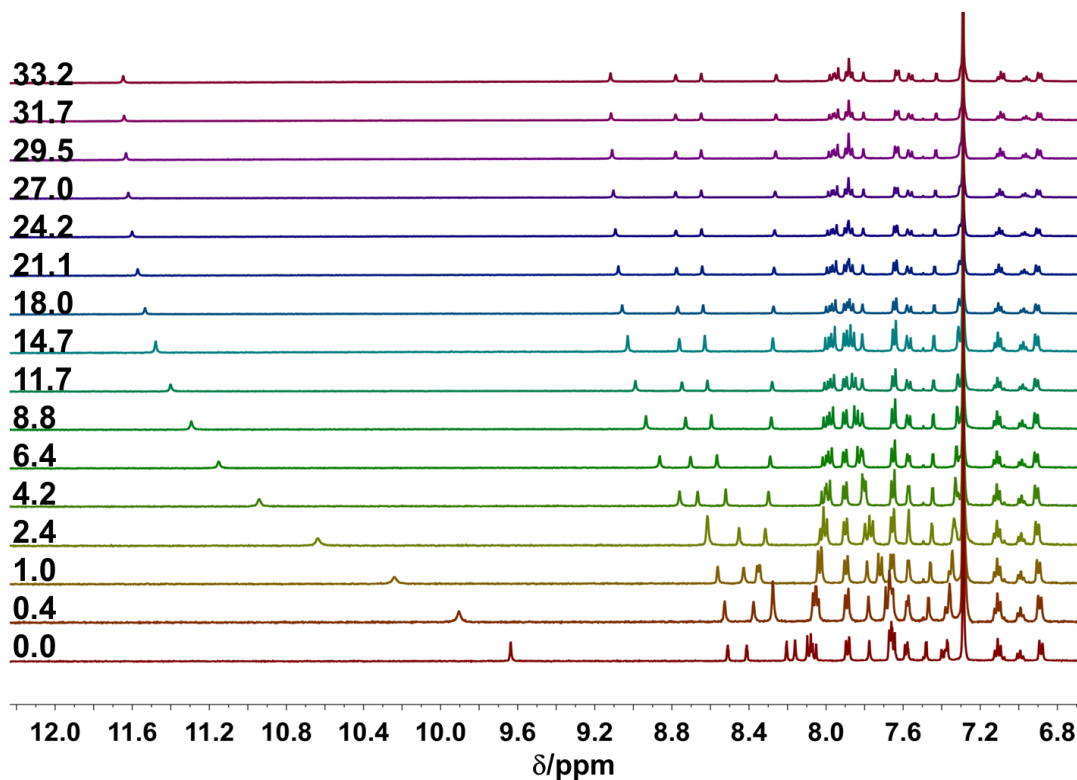


Figure B.34 Representative ^1H NMR titration of **1b** (1.24 mM) with tetrabutylammonium chloride as stacked spectra with chloride equivalents increasing bottom to top in 10% $\text{DMSO-}d_6/\text{CDCl}_3$.

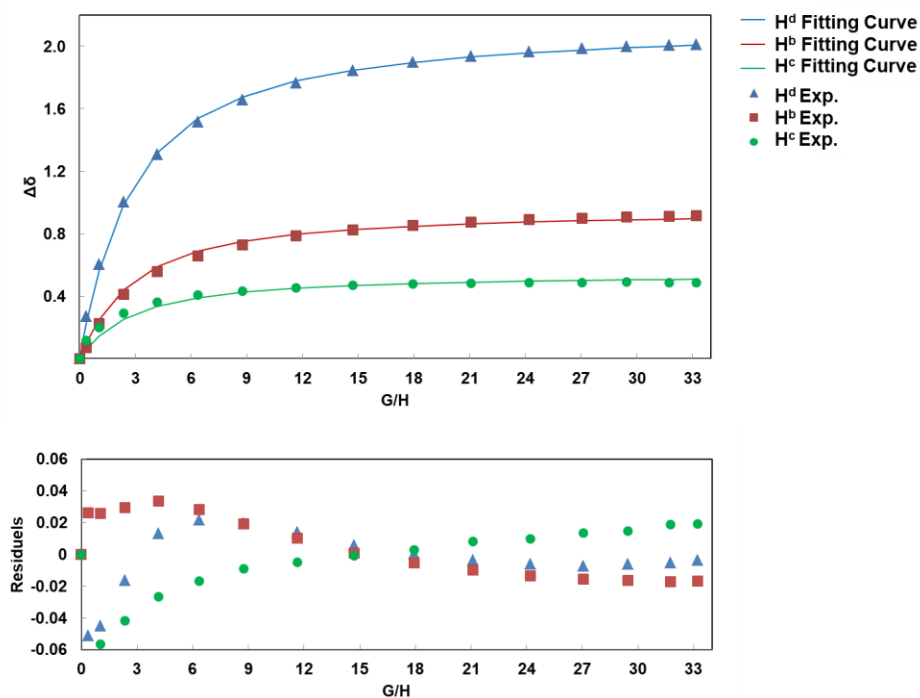


Figure B.35 Representative binding isotherm and fit curves for Cl^- titration of **1b** in 10% $\text{DMSO-}d_6/\text{CDCl}_3$ by ^1H NMR.

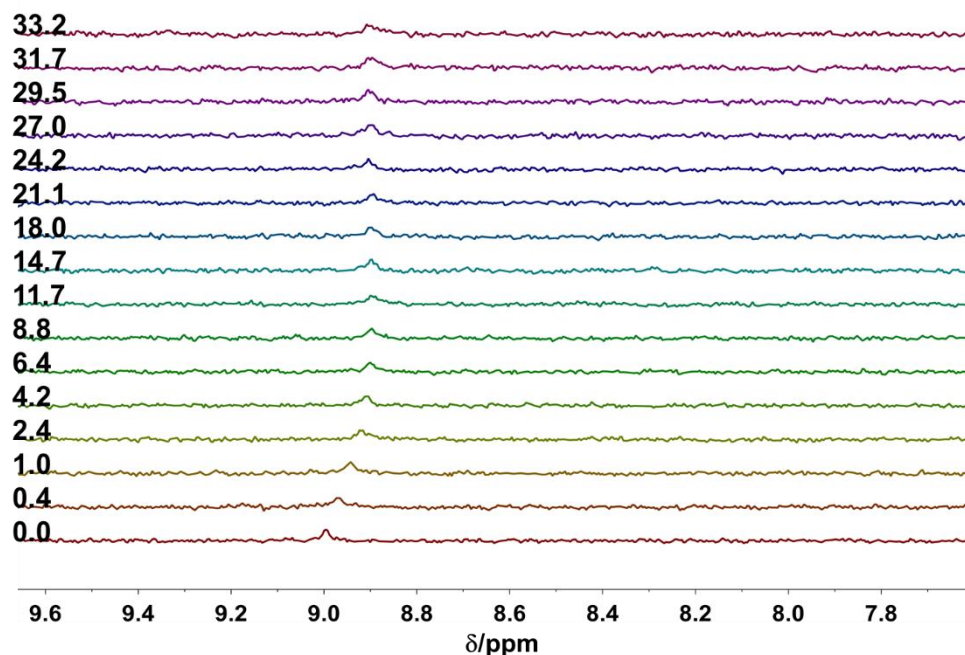


Figure B.36. Representative ^{31}P NMR titration of **1b** (1.24 mM) with tetrabutylammonium chloride as stacked spectra with chloride equivalents increasing bottom to top in 10% $\text{DMSO}-d_6/\text{CDCl}_3$.

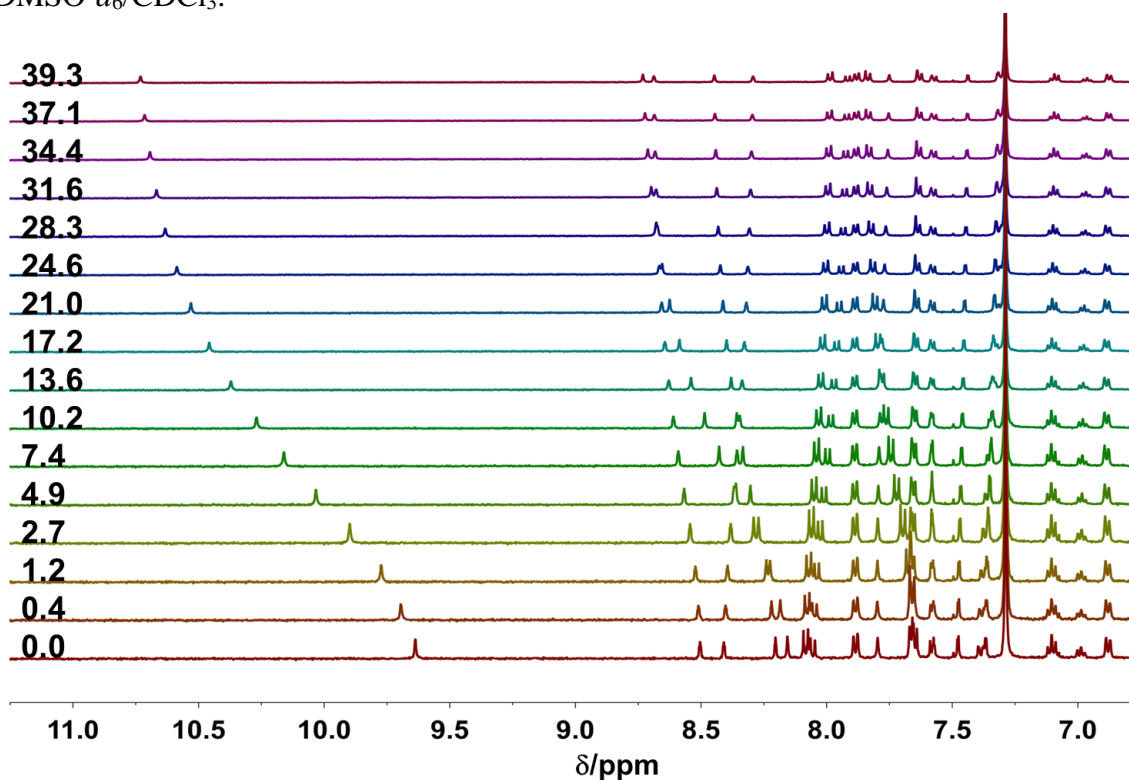


Figure B.37 Representative ^1H NMR titration of **1b** (1.09 mM) with tetrabutylammonium bromide as stacked spectra with bromide equivalents increasing bottom to top in 10% $\text{DMSO}-d_6/\text{CDCl}_3$.

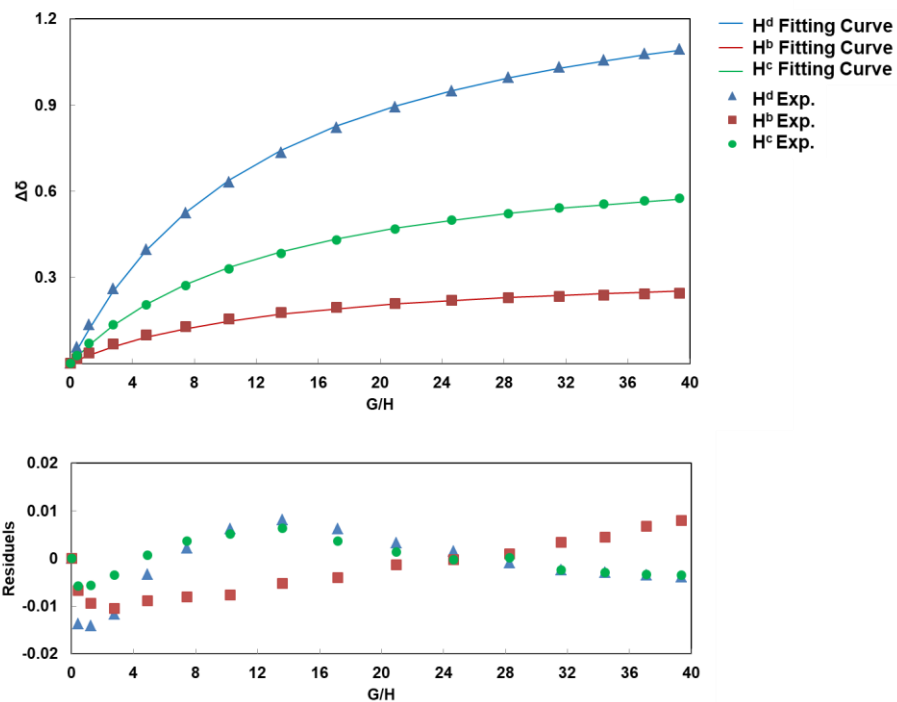


Figure B.38 Representative binding isotherm and fit curves for Br^- titration of **1b** in 10% $\text{DMSO-}d_6/\text{CDCl}_3$ by ^1H NMR.

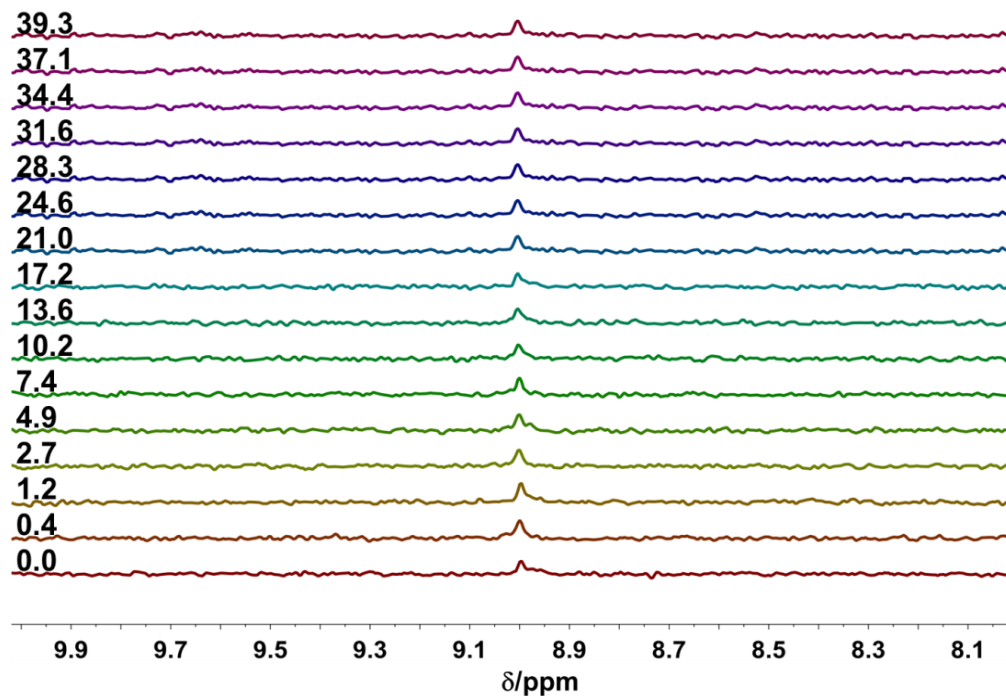


Figure B.39 Representative ^{31}P NMR titration of **1b** (1.09 mM) with tetrabutylammonium bromide as stacked spectra with bromide equivalents increasing bottom to top in 10% $\text{DMSO-}d_6/\text{CDCl}_3$.

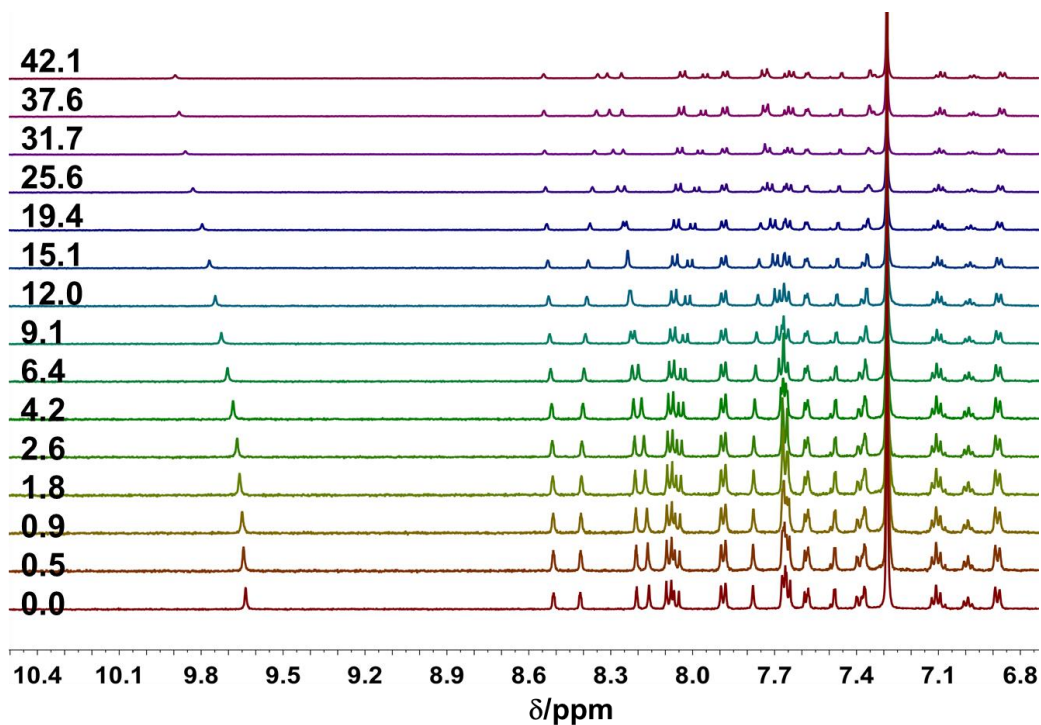


Figure B.40 Representative ^1H NMR titration of **1b** (1.12 mM) with tetrabutylammonium iodide as stacked spectra with bromide equivalents increasing bottom to top in 10% $\text{DMSO-}d_6/\text{CDCl}_3$.

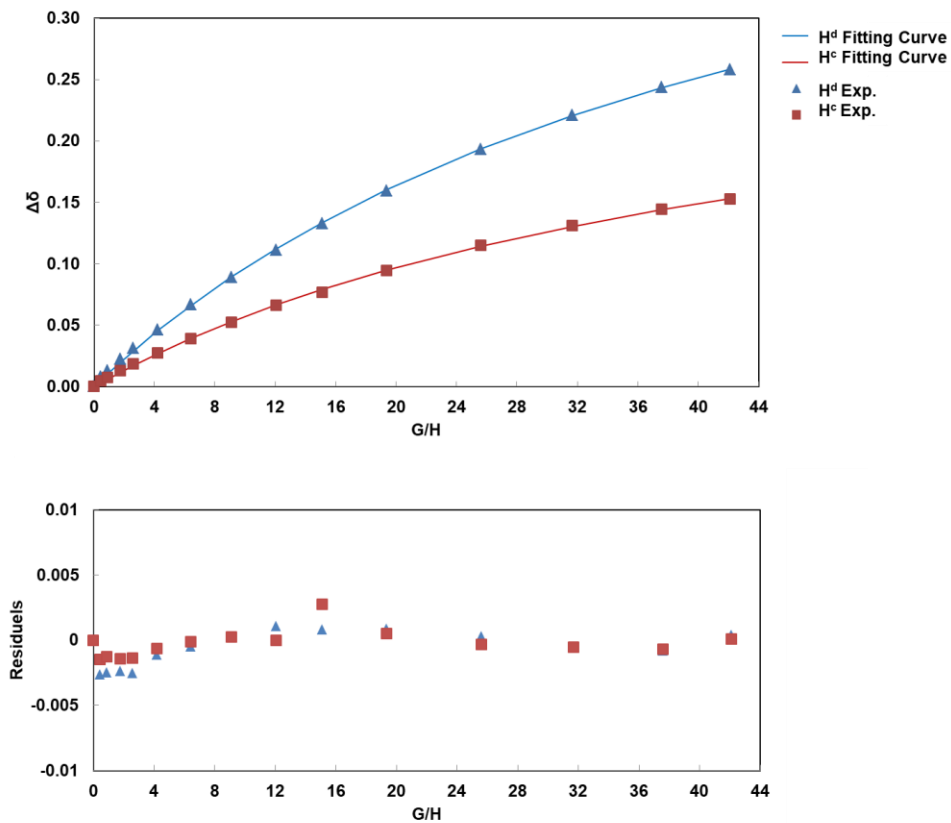


Figure B.41 Representative binding isotherm and fit curves for Γ^- titration of **1b** in 10% DMSO- d_6 /CDCl $_3$ by ^1H NMR.

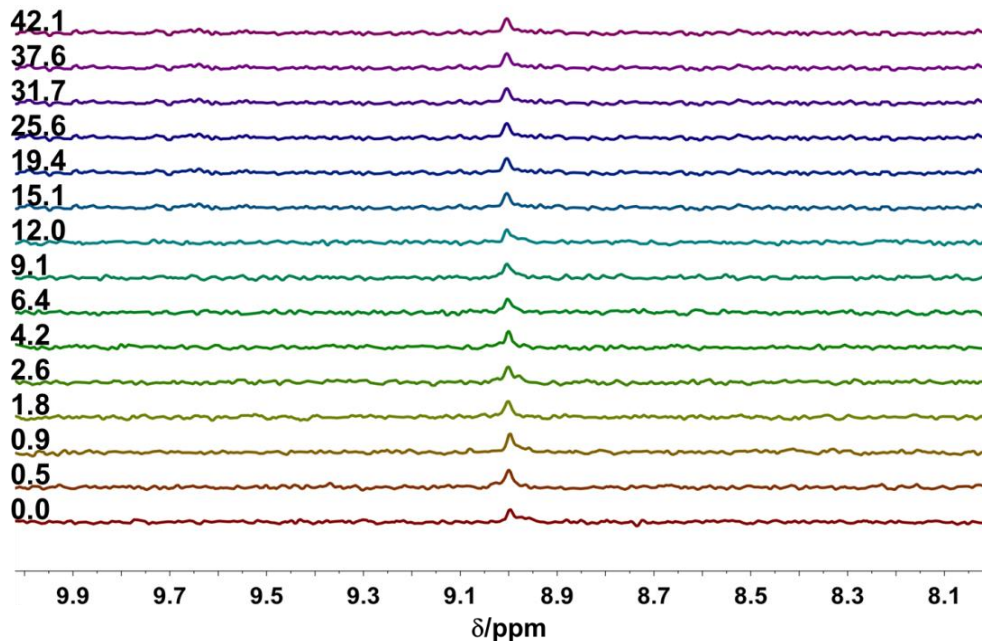


Figure B.42 Representative ^{31}P NMR titration of **1b** (1.12 mM) with tetrabutylammonium iodide as stacked spectra with bromide equivalents increasing bottom to top in 10% DMSO- d_6 /CDCl $_3$.

7. Competition Experiments of **1b** with Anions

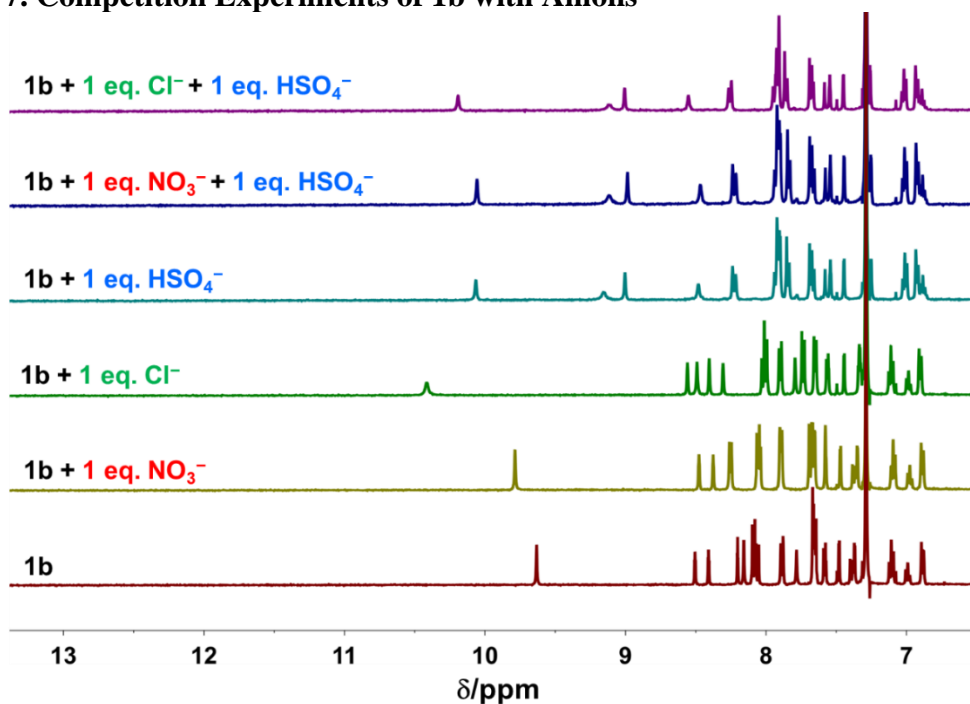
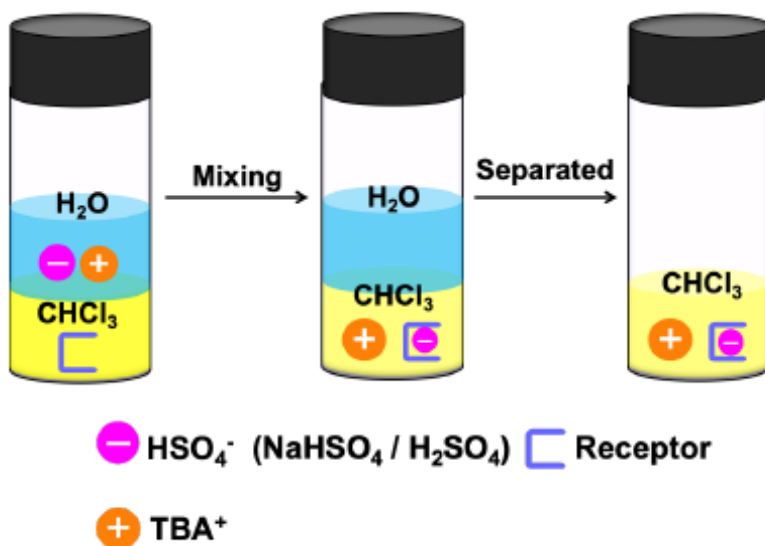


Figure B.43 Partial ^1H NMR spectra of receptor **1b** (1.5 mM) in the presence of one equivalent of Cl^- and NO_3^- anions (added as TBA salts) in 10% DMSO- d_6 /CDCl $_3$.

8. Hydrogen Sulfate Extraction Experiments

For this initial study, the hydrogen sulfate extraction behavior of **1b** was examined with ^1H NMR and ^{31}P NMR spectroscopy.

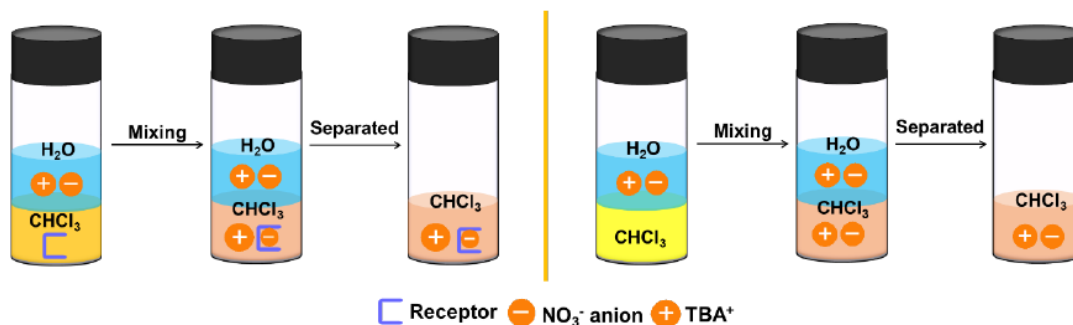
8.1 Extraction experiments



Liquid-liquid extractions using **1b** as the extractant were undertaken as follows: **1b** (10 mM) in 0.8 mL CDCl_3 and 0.8 mL NaHSO_4 (2 M) (HSO_4^- is characterized as a weak acid and will dissociate in either non-pH buffered or dilute aqueous solution, thus higher concentration of HSO_4^- sources were employed in this study, $[\text{HSO}_4^-]/[\mathbf{1b}] \approx 184$ in theory) or H_2SO_4 (2 M, $[\text{HSO}_4^-]/[\mathbf{1b}] \approx 200$ in theory) in deionized H_2O solution (containing 10 mM TBANO_3) were placed in a vial. The two phases were mixed thoroughly by stirring at rt. After 30 min, the stirring was stopped and the vial was allowed to stand for 1 h to fully separate the two phases. The CDCl_3 phase (0.7 mL) were carefully separated and dried (Na_2SO_4). After filtration, the spectra of the resulting CDCl_3 phase (0.6 mL) were then recorded. The purity and nature of the extracted product were determined by ^1H NMR and ^{31}P NMR spectroscopy (Figure B.45).

To estimate the apparent extraction efficiency (i.e., the molar percent of extractant containing TBAHSO₄ after contact with a corresponding concentrated aqueous solution), 1,3,5-trimethoxybenzene (TMB) was used as an internal standard (10 mM, pre-dissolved in CDCl₃) and TBAHSO₄ as the cation exchanger, the results were obtained *via* calculation of the integration ratio of the peaks from ¹H NMR spectroscopy (Figure B.46).

8.2 Blank experiment



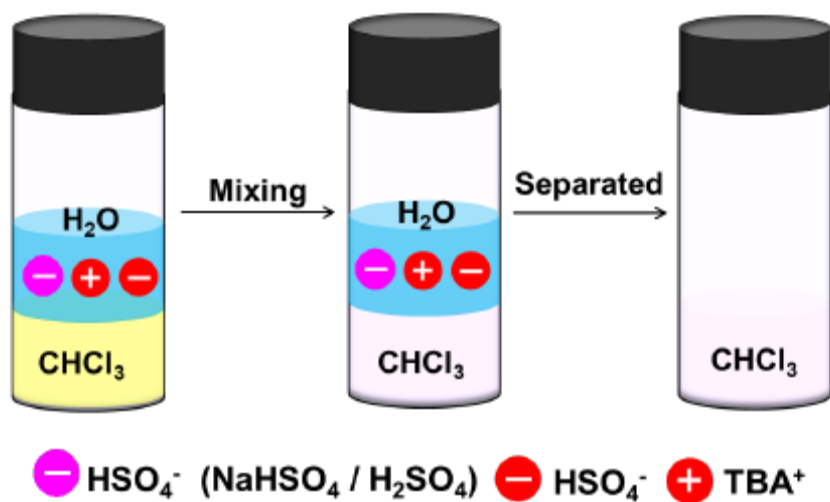
1b (10 mM) in 0.8 mL CDCl₃ and 0.8 mL deionized H₂O solution (containing 10 mM TBANO₃) were placed in a vial. The two phases were mixed thoroughly by stirring at rt. After 30 min, the stirring was stopped and the vial was allowed to stand for 1 h to fully separate the two phases. The CDCl₃ phase (0.7 mL) was carefully separated and dried (Na₂SO₄). After filtration, the spectra were recorded (Figure B.45). The extraction efficiency was *ca.* 67%, determined by using TMB as an internal standard *via* ¹H NMR.

Unfortunately, our attempt to extract TBAHSO₄ from water using **1b** in the presence of equal molar amounts of TBANO₃ was unsuccessful. This result is not surprising. We found that even pure CDCl₃ (without receptor) is capable of capturing considerable amount of TBANO₃ (*ca.* 43% extraction) from water solution, probably due to the small hydration energy of TBANO₃. Since all the studied interfering anion TBA salts are somewhat hydrophobic compared to bisulfate anion based on the Hofmeister sequence, which preclude the potential selective extraction in the presence of competitive anions at this stage.

8.3 Comparison experiments

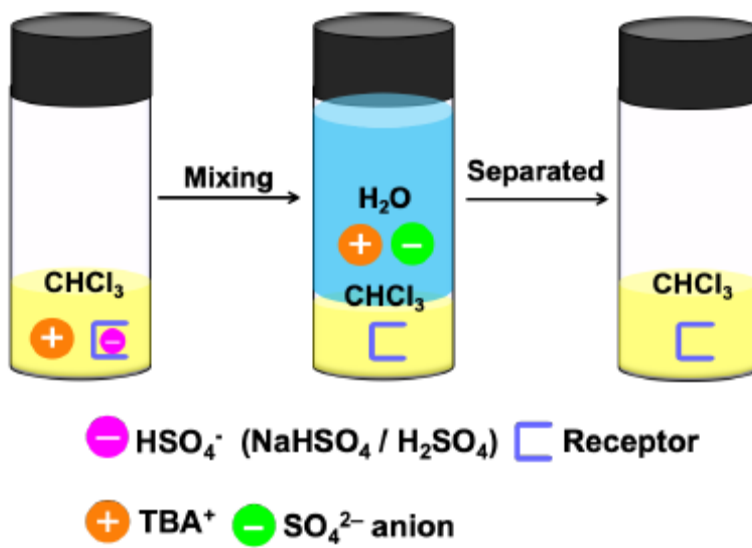
Comparison experiments were conducted by directly adding aliquots of TBAHSO₄ to the CDCl₃ solution of **1b** (10 mM). The spectra of **1b** in the presence of 0.7, 0.8, 0.9, 0.95, 1.0, 1.2 and 2.0 equivalents of TBAHSO₄ were recorded (Figure B.44).

8.4 Control experiments



0.8 mL neat CDCl₃ (i.e. without host **1b**) and 0.8 mL NaHSO₄ (2 M) or H₂SO₄ (2 M) in deionized H₂O solution (containing 10 mM TBAHSO₄) were placed in a vial. The two phases were mixed thoroughly by stirring at rt. After 1 h, the stirring was stopped and the vial was allowed to stand for 1 h to fully separate the two phases. The CDCl₃ phase (0.7 mL) was carefully separated and dried (Na₂SO₄). After filtration, the spectra of the resulting CDCl₃ phase (0.6 mL) was then recorded (Figure B.47).

8.5 Recycling experiments



The resulting CDCl₃ phases in NMR tubes from extraction experiments were evaporated, and redissolved in 1 mL CDCl₃, and 20 mL deionized H₂O was also added to the same vial. After thoroughly mixing the two phases for 1 h by stirring at rt. The guest was released in the form of sulfate anion from the receptor and transferred to the H₂O phase due to the chemical dissociation of bisulfate in dilute aqueous solution. The recycled receptors were ascertained by ¹H NMR spectra (Figure B.48).

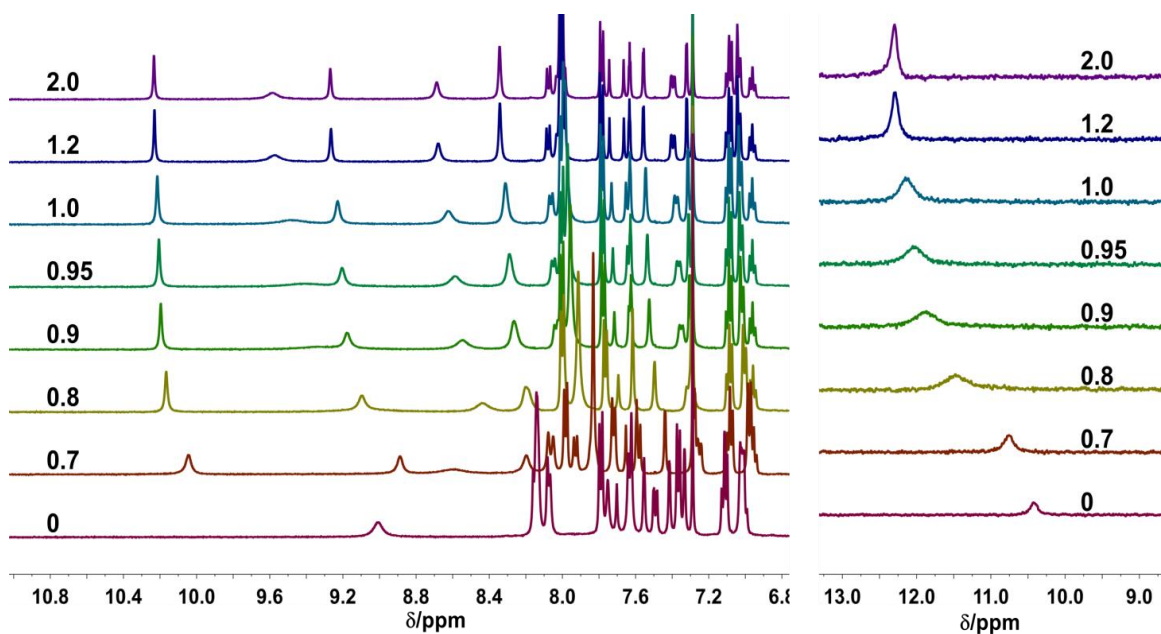


Figure B.44 Partial ^1H NMR (500 MHz) (left) and ^{31}P NMR (202 MHz) (right) spectra (in CDCl_3 , 298 K) of **1b** with TBAHSO₄ as stacked spectra with TBAHSO₄ equivalents increasing bottom to top.

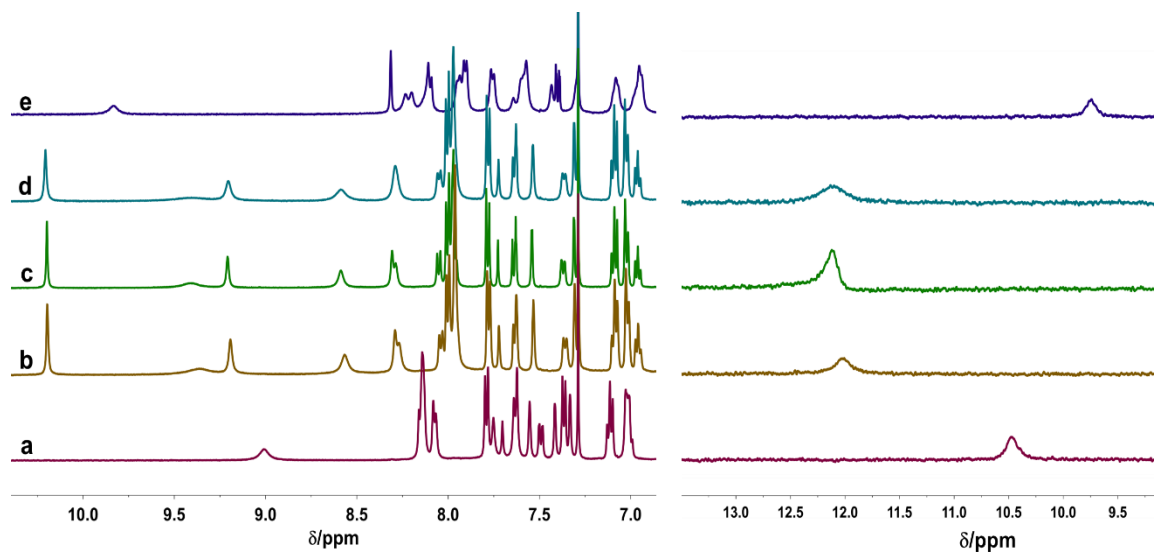


Figure B.45 Partial ^1H NMR (500 MHz) (left) and ^{31}P NMR (202 MHz) (right) spectra (in CDCl_3 , 298 K) of a) receptor **1b** (10 mM); b) the CDCl_3 phase after extraction from 2 M H_2SO_4 ; c) the CDCl_3 phase after extraction from 2 M NaHSO_4 ; d) **1b** in the comparison experiment by direct adding 1.0 eq. of TBAHSO₄; e) blank experiment.

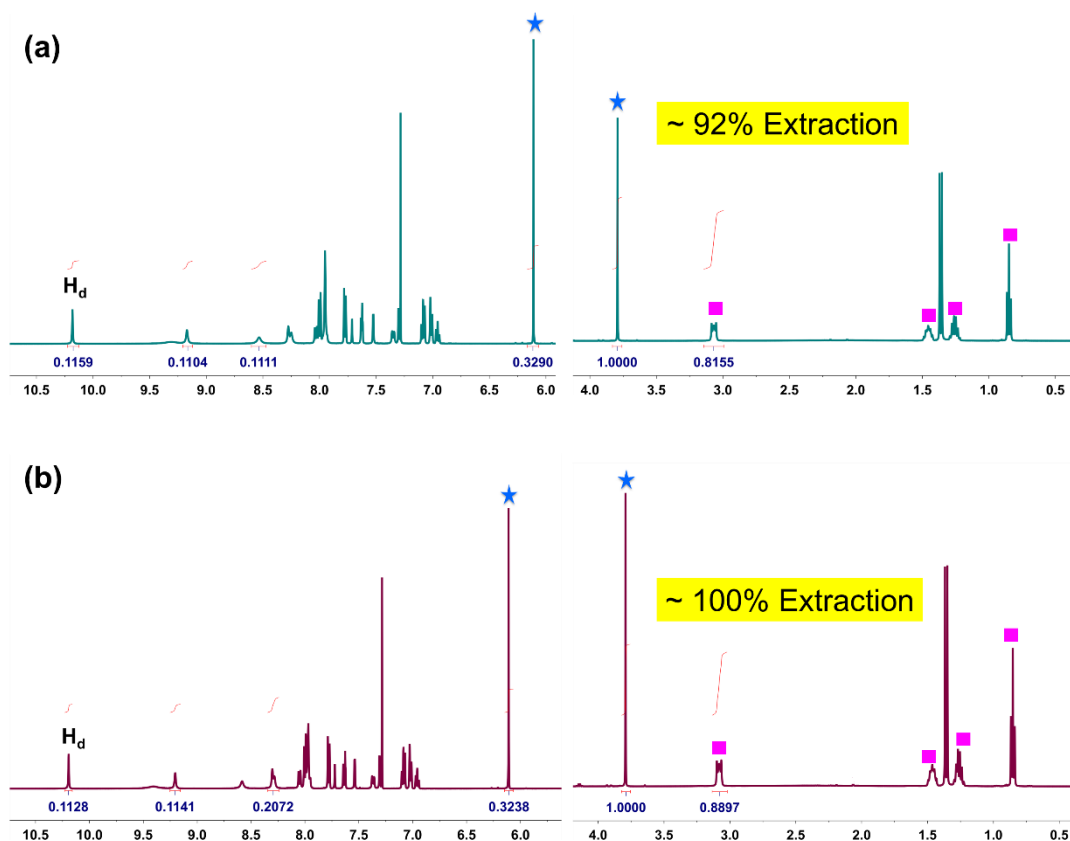


Figure B.46 Partial ^1H NMR spectra (500 MHz) of a) the CDCl_3 phase (containing TMB internal standard) after extraction from $2\text{ M H}_2\text{SO}_4$ in the extraction experiment, showing *ca.* 92% uptake of TBAHSO_4 ; b) the CDCl_3 phase (containing TMB internal standard) after extraction from 2 M NaHSO_4 in the extraction experiment, showing *ca.* 100% uptake of TBAHSO_4 . All the relevant peaks for each spectrum are integrated at the same scale. The TBA^+ counterion is marked with pink squares. The TMB standard is marked with blue stars.

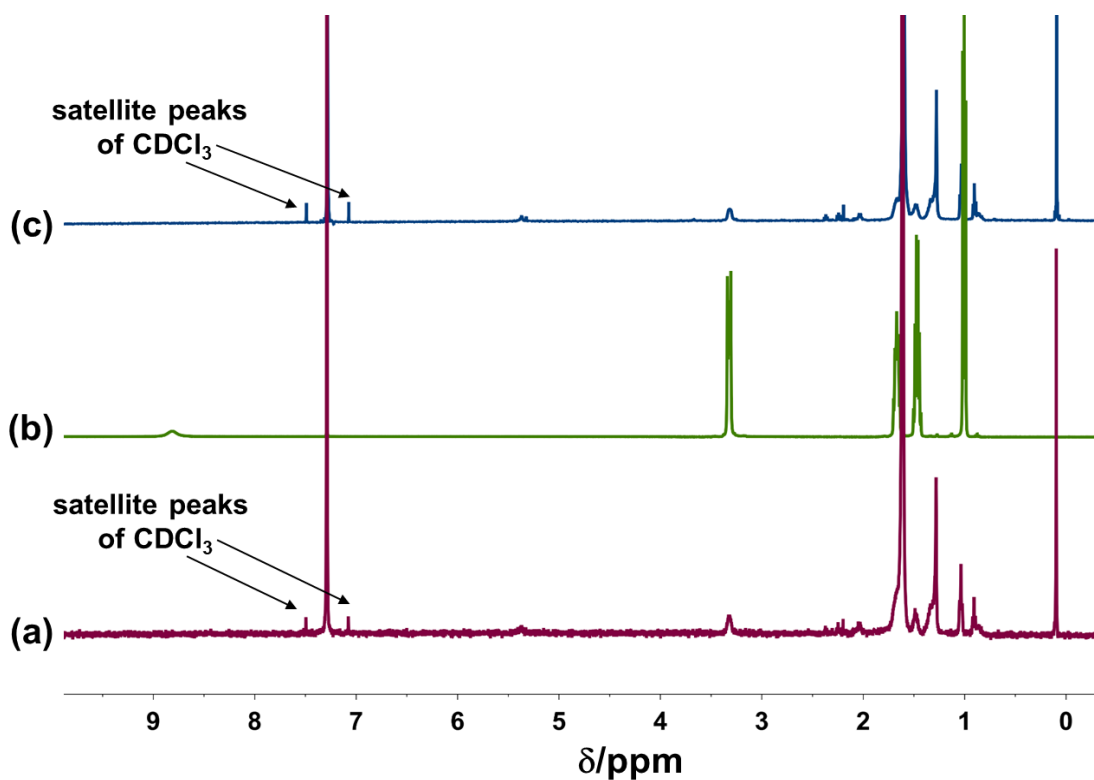


Figure B.47 Partial ^1H NMR spectra (500 MHz, CDCl_3) of a) the CDCl_3 phase after extraction from 2 M H_2SO_4 in the control experiment; b) TBAHSO_4 ; c) the CDCl_3 phase after extraction from 2 M NaHSO_4 in the control experiment. The spectral intensities of a) and c) were zoomed-in by 10 times, showing only trace amounts of bisulfate anion were extracted into CDCl_3 phase.

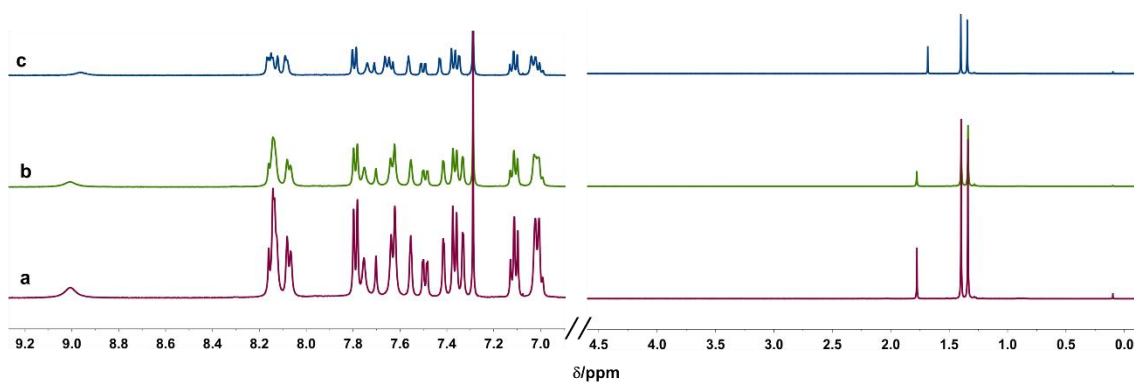


Figure B.48 Partial ^1H NMR spectra (500 MHz, CDCl_3) of a) receptor **1b** and the recycled **1b** from the extraction experiments of b) NaHSO_4 aqueous solution and c) H_2SO_4 aqueous solution.

9. Computational Details

For **1b**•Cl⁻ and **1b**•NO₃⁻ complexes (The *t*-Bu groups in receptors were omitted to reduce computational costs) were built manually by placing corresponding anions in the tentatively proposed conformations of receptors and optimized by the PM6-D3H4⁶ *semi*-empirical method. Afterwards, all the obtained structures were further optimized by carrying out the DFT calculations using the M06-2X functional⁷ along with the 6-31G(d,p) basis set. The solvent effects are included using the polarizable continuum model (PCM)⁸ (solvent: CHCl₃). The frequency calculations were also performed on the structures to ensure no imaginary frequency.

A constrained optimization in gas phase was performed to the single crystal structure of **1b**•HSO₄⁻, where non-H atoms were frozen and only H atoms were fully optimized at M06-2X/Def2-TZVPP⁹ level of theory. The distribution of electrostatic potential, $V(r)$, on the molecular surfaces of **1b** were computed at the M06-2X/6-31G(d,p) level in gas phase from previously optimized structures of their complexes with HSO₄⁻ anion, after removal of HSO₄⁻ anion of the corresponding complex. The $V(r)$ was evaluated on the 0.001 e/Bohr³ contour of $\rho(r)$ to generate the $V_S(r)$. The most negative and most positive $V_S(r)$ values (i.e. $V_{S,\min}$ and $V_{S,\max}$, respectively) for electrostatic potential surface energies were calculated (Figure B.50).

The QTAIM¹⁰ analyses were conducted based on the optimized geometries of **1b**•HSO₄⁻. QTAIM topological parameter $G(r)$ is the Lagrangian kinetic energy and $V(r)$ is the local potential electron energy density. A negative Laplacian of electron density [$\nabla^2\rho(r)$] shows the excess potential energy at the BCP which means that the electronic charge is contracted between two nuclei (covalent interaction), while a positive $\nabla^2\rho(r)$ reveals that the kinetic energy contribution is greater than the potential energy (closed-shell electrostatic

interaction). The sign of electronic energy $H(r)$ on the Hamiltonian at BCP determines whether the accumulation of charge at a given point is stabilizing [$H(r) < 0$] or destabilizing [$H(r) > 0$]. The nature of hydrogen bond can be evaluated by means of the $-[G(r)/V(r)]$. If $-[G(r)/V(r)] > 1$, then the hydrogen bond has non-covalent character while for the $0.5 < -[G(r)/V(r)] < 1$, the hydrogen bond has partly covalent character (Table B.2).¹¹ To visualize the position and different types of non-covalent interactions in 3D space, the gradient isosurfaces (cutoff = 0.5 a.u.) of the reduced density gradient (RDG)¹² at low densities, colored on a blue–green–red scale according to values of $\text{sign}(\lambda_2)\rho(r)$ (ranging from -0.02 to 0.02 a.u.) were obtained.

The PM6-D3H4 optimizations were performed with MOPAC2016¹³ and all the DFT calculations were carried out by Gaussian 09 software package.¹⁴ The Wiberg bond indices¹⁵ (WBI) were calculated based on the DFT optimized structures of the complexes of $\mathbf{1} \cdot \text{HSO}_4^-$, which were performed using the Natural Bond Orbital (NBO) program, within the Gaussian 09 suite. The Multiwfn package program¹⁶ was employed for obtaining electrostatic potential surface energy extremes ($V_{S,\text{min}}$ and $V_{S,\text{max}}$) and visualizing the bond paths and to calculate the bond critical points (BCPs). Also, this program has been used to obtain the RDG function.

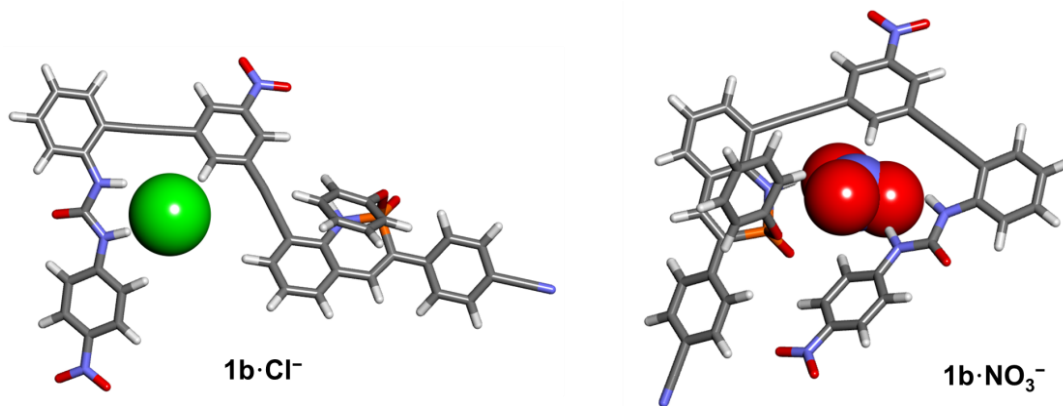


Figure B.49 DFT-optimized complexes (at M06-2X/6-31G(d,p) level of theory) of **1b**•Cl⁻ (left) and **1b**•NO₃⁻ (right). In the structures, the anions are shown in CPK model, and host molecules are depicted in stick representation. The *t*-Bu groups were omitted to reduce computational costs.

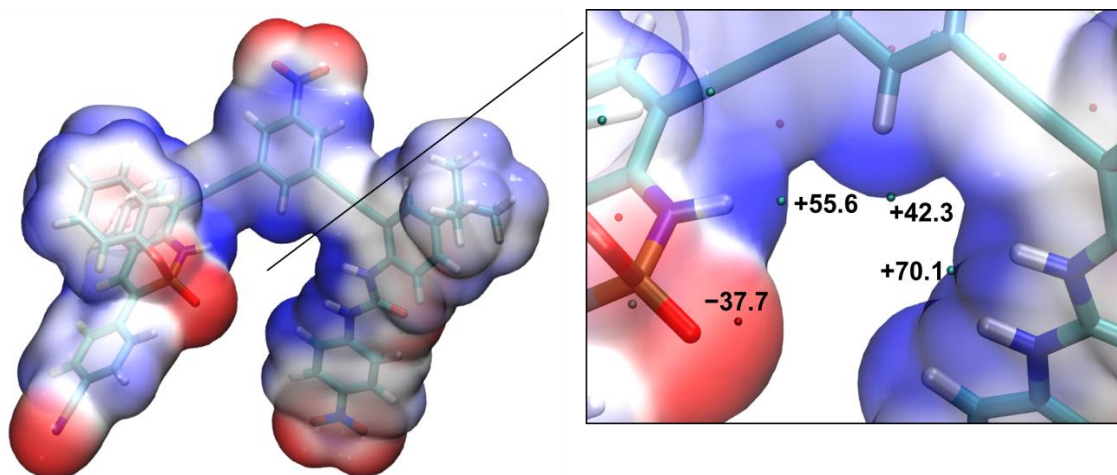


Figure B.50 The electrostatic potential (ESP) surfaces (isosurface = 0.001 a.u.) of free **1b** calculated at M06-2X/6-31G(d,p) level of theory in gas phase. Red indicates negative charge density, and blue positive charge density. Surface minima ($V_{S,\min}$) and maxima ($V_{S,\max}$) of ESP energies (in kcal mol⁻¹) are represented as orange and cyan dots, respectively.

Table B.2 Values of the density of all electrons $\rho(r)$, Laplacian of electron density $\nabla^2\rho(r)$, local potential electron energy density $V(r)$, energy density $H(r)$, Lagrangian kinetic energy $G(r)$ (in a.u.) at the bond critical points (BCPs) for selected significant H-bond interactions in the crystal structure of **1b**•HSO₄⁻ complex, calculated at M06-2X/Def2-TZVPP level of theory

	1b •HSO ₄ ⁻					
	$\rho(r)$	$\nabla^2\rho(r)$	$V(r)$	$H(r)$	$G(r)$	$-[G(r)/V(r)]$
N–H ^a •••O _{anion}	0.03501	0.10936	-0.03403	0.00335	0.03068	0.90169
C–H ^b •••O _{anion}	0.01603	0.06265	-0.01151	0.00208	0.01359	1.18049
N–H ^c •••O _{anion}	0.03007	0.10555	-0.02845	0.00103	0.02742	0.96372
N–H ^d •••O _{anion}	0.00945; 0.01559	0.03881; 0.05915	-0.00612; -0.01131	0.00179; 0.01739	0.00791; 0.01305	1.29290; 1.15372
N–H ^e •••O _{anion}	0.01662	0.06994	-0.01260	0.00244	0.01504	1.19378
P=O•••(H– O) _{anion}	0.05616	0.12312	-0.06416	0.01669	0.04747	0.73986

Table B.3 Wiberg Bond Indices (WBIs) for the relevant HB interactions in the crystal structure of **1b**•HSO₄⁻ complex, calculated at M06-2X/Def2-TZVPP level of theory

HB interactions	WBI
N–H ^a •••O _{anion}	0.0493
C–H ^b •••O _{anion}	0.0094
N–H ^c •••O _{anion}	0.0356
N–H ^d •••O _{anion}	0.0049; 0.0155
N–H ^e •••O _{anion}	0.0069
P=O•••(H–O) _{anion}	0.0717

Table B.4 Cartesian coordinates for **1b**•HSO₄⁻

	X	Y	Z
S	0.85947400	0.90394500	-0.60559800
O	0.00452700	-0.19498400	-0.30070800
O	2.20135700	0.49929400	-0.91811500
O	0.77574900	1.98521500	0.32367400
O	0.34269600	1.50294000	-1.95708400
H	-0.63960100	1.57543300	-1.92876500
P	-3.23196300	0.52596500	-1.41259100
O	-2.22039500	1.50747400	-1.81300400
O	-3.43699600	-0.40343500	-2.70314300
O	1.49820000	-7.46860000	1.99392300
O	3.57329500	-7.14365000	1.57628100
O	6.02092000	2.92488300	0.65292200
O	1.33746900	7.39577500	4.35208800
O	3.30954800	7.95098800	4.42820300
N	-2.76190900	-0.42069900	-0.16124500
N	-8.08589700	5.97457500	-4.51060900
N	2.43192200	-6.74786100	1.66466900
N	4.87006900	1.16458500	-0.23243100
N	3.74667100	2.78974100	0.89940100
N	2.48406300	7.23955600	4.01215100
C	1.62195500	-2.73276000	0.71780800
H	1.39059100	-1.70975400	0.44718500
C	0.59852800	-3.53975500	1.23632600
C	0.88331200	-4.86349400	1.56658400
H	0.12522300	-5.52129100	1.96258700
C	2.16025900	-5.33599500	1.34849100
C	3.17391000	-4.56264000	0.82988300
H	4.15652300	-4.98447100	0.68348700
C	2.90639600	-3.22266400	0.51509200
C	-0.71537400	-3.02110500	1.38080200
C	-1.82856700	-2.56847200	1.49282200

C	-3.15587300	-2.04450400	1.62167500
C	-4.03544100	-2.57944900	2.58125500
H	-3.64320800	-3.37182200	3.20299600
C	-5.34338400	-2.12957400	2.73898400
C	-5.76270300	-1.13115000	1.88609700
H	-6.77637200	-0.75664900	1.94377500
C	-4.93332100	-0.56891900	0.92495100
C	-3.60724900	-1.01659700	0.78682900
C	-5.46837900	0.49477200	0.08091600
H	-6.47374000	0.79709000	0.33634400
C	-4.81680000	1.09274500	-0.96009400
C	-5.51580600	2.17917700	-1.75225400
C	-6.78229100	2.61076400	-1.38704600
H	-7.29911400	2.20040900	-0.53521300
C	-7.42262700	3.58070400	-2.11750500
H	-8.41210900	3.90523100	-1.82429000
C	-6.81902800	4.14842800	-3.18838800
C	-5.56344800	3.74450500	-3.56300100
H	-5.07863000	4.20118800	-4.41452600
C	-4.90444100	2.77638800	-2.83145200
H	-3.90104400	2.49164000	-3.11753900
C	-7.51007000	5.16224600	-3.93579800
C	-4.30295300	-1.49661400	-2.65953200
C	-5.53974100	-1.34617200	-3.20996400
H	-5.80453600	-0.38538400	-3.63358000
C	-6.42186100	-2.40399100	-3.21584300
H	-7.40873000	-2.29886700	-3.64399200
C	-6.01842300	-3.60031700	-2.64893000
H	-6.70455400	-4.43820900	-2.64116700
C	-4.74736200	-3.77359500	-2.11942300
H	-4.44328900	-4.72266900	-1.70190100
C	-3.85925100	-2.68146700	-2.11945800
H	-2.85840300	-2.75528400	-1.71671000
C	-6.27721900	-2.71916300	3.77209200
C	-5.79594500	-2.28691000	5.12234400
H	-4.75517600	-2.56294900	5.29304200
H	-6.39536700	-2.74454600	5.91179400
H	-5.86008000	-1.20207700	5.25248100
C	-7.64781800	-2.31609200	3.68114000
H	-7.76937100	-1.23653500	3.79297200
H	-8.23469800	-2.78016400	4.47571400
H	-8.11872300	-2.59783300	2.73342700
C	-6.09906800	-4.18935600	3.90494100
H	-5.08423000	-4.46099600	4.18317500
H	-6.33560900	-4.72997100	2.98216600
H	-6.76002000	-4.57893900	4.68078600

C	3.94826900	-2.38349000	0.02980900
C	4.84077800	-1.68264000	-0.34392800
C	5.93600400	-0.90553700	-0.87631900
C	7.01760000	-1.59020400	-1.47132200
H	6.95737000	-2.66945900	-1.47816600
C	8.09232000	-0.94308600	-2.02091900
C	8.07830800	0.43964100	-1.96796000
H	8.89096400	1.00988700	-2.39998500
C	7.03934600	1.14511000	-1.38425700
H	7.06571700	2.22273000	-1.35030600
C	5.96442100	0.48828700	-0.81038800
C	9.27930000	-1.67112700	-2.65318000
C	9.25169300	-3.16049900	-2.37970300
H	9.22653600	-3.36167800	-1.30816300
H	10.14619800	-3.62936300	-2.79314900
H	8.38720700	-3.64545400	-2.83743400
C	9.33008600	-1.36054400	-4.12483500
H	9.40712700	-0.28675200	-4.29678200
H	8.43230400	-1.71301000	-4.63767200
H	10.19486300	-1.83872400	-4.59176700
C	10.61157000	-1.13575600	-2.04769300
H	10.63739700	-1.29018200	-0.96824600
H	10.74409900	-0.07268300	-2.24188200
H	11.45235600	-1.66781000	-2.49638600
C	4.95779000	2.33683400	0.44968800
C	3.50939800	3.92136800	1.65560700
C	2.19158000	4.09878600	2.08947600
H	1.43657000	3.38231300	1.79782800
C	1.84665000	5.21676700	2.84077000
H	0.82993800	5.37528700	3.16584800
C	2.82581200	6.09200700	3.19307200
C	4.11411300	5.93920000	2.78813500
H	4.85674500	6.66712900	3.08083600
C	4.46445300	4.85427100	2.02653900
H	5.48350600	4.72397100	1.70526200
H	3.94528400	0.75206100	-0.37220300
H	2.90999200	2.27895100	0.62346500
H	-1.73388100	-0.51903900	-0.06839700

Table B.5 Cartesian coordinates for **1b•Cl⁻**

	X	Y	Z
N	-3.81011800	-0.34394800	-0.73864900
N	-12.95812800	1.59925300	-1.11656200

N	6.46259900	-0.78094900	0.59344100
N	6.02799900	1.41598200	0.15237800
N	6.38616900	6.81935000	-1.29820000
N	0.39687400	-6.01243900	-2.09282100
C	1.80634800	-2.42848300	-0.36116000
C	0.46429200	-2.53525800	-0.74884600
C	-0.01005500	-3.71823000	-1.32498100
C	0.88595300	-4.76411700	-1.48906000
C	2.21856900	-4.69425800	-1.11356500
C	2.68375300	-3.50383300	-0.54073300
C	-0.39735000	-1.41406500	-0.52717500
C	-1.03897300	-0.41445100	-0.28582600
C	-1.79269200	0.75742400	0.02449000
C	-1.16856000	1.87729800	0.58101600
C	-1.90995700	3.00435400	0.92670700
C	-3.27960700	3.01203400	0.71474700
C	-3.93961400	1.90532500	0.16038500
C	-3.18725100	0.76731700	-0.18670800
C	-5.37444600	1.94397800	-0.04653500
C	-6.16047200	0.90519800	-0.41355500
C	-7.62177400	1.04181400	-0.58945000
C	-8.16769700	2.22371300	-1.10978000
C	-9.53918700	2.37376900	-1.24284800
C	-10.38826500	1.32715700	-0.86637800
C	-9.85891700	0.13485300	-0.36196900
C	-8.48570800	-0.00268500	-0.22675000
C	-11.81210500	1.47649800	-1.00647500
C	-5.09162200	-0.83552200	1.99072300
C	-5.90065400	-0.01345500	2.76714500
C	-5.35356900	0.60598700	3.88781500
C	-4.01474700	0.40595600	4.21805900
C	-3.22117300	-0.43095900	3.43564200
C	-3.75867800	-1.06209000	2.31764300
C	4.04898400	-3.38064300	-0.12975600
C	5.20302000	-3.27885000	0.22552200
C	6.56882400	-3.19761100	0.63899000
C	7.28353400	-4.38132800	0.87566000
C	8.61593800	-4.34275100	1.25403100
C	9.24217700	-3.10618800	1.40725300
C	8.55148800	-1.92104900	1.18999100
C	7.20726100	-1.94692400	0.79757000
C	6.99454600	0.43490900	0.20925200
C	6.19440900	2.73772300	-0.21927300
C	7.39959700	3.28599900	-0.69731200
C	7.45261400	4.62479100	-1.04890700
C	6.31618000	5.41643000	-0.92803900

C	5.11131300	4.89531300	-0.45965300
C	5.05481000	3.56207100	-0.10855200
O	-5.94691300	-1.62281900	-1.64926500
O	-5.63152900	-1.44174700	0.85695400
O	8.17653000	0.61227300	-0.04929500
O	5.37594500	7.49837700	-1.18252600
O	7.45155700	7.25708700	-1.70840900
O	-0.77066100	-6.05772000	-2.43685100
O	1.18644100	-6.93183000	-2.21497700
P	-5.43408700	-0.71998300	-0.59906500
H	-3.19239400	-1.08933400	-1.05073700
H	5.44696600	-0.84706900	0.67484000
H	5.08202000	1.15349500	0.47138100
H	2.17267600	-1.50811100	0.09071600
H	-1.04130700	-3.82750100	-1.63512200
H	2.87414000	-5.54220900	-1.26466000
H	-0.09704400	1.84073900	0.74790800
H	-1.41713700	3.86552100	1.36207000
H	-3.86886700	3.88476800	0.98075900
H	-5.85111700	2.90535200	0.14316000
H	-7.50878500	3.02216000	-1.43467700
H	-9.95578100	3.28901700	-1.64828800
H	-10.52206300	-0.67363400	-0.07566900
H	-8.08408000	-0.92806700	0.17502700
H	-6.93721300	0.13804900	2.48151500
H	-5.97562500	1.25090500	4.49966900
H	-3.59016300	0.89775000	5.08669200
H	-2.17867300	-0.59202700	3.68911000
H	-3.15417800	-1.70913900	1.68954100
H	6.76919300	-5.32809900	0.74936100
H	9.15986800	-5.26406100	1.43035000
H	10.28305900	-3.05927400	1.71134300
H	9.04289300	-0.96734600	1.31666800
H	8.27491200	2.66095000	-0.78277400
H	8.37127400	5.06293100	-1.41886200
H	4.24248600	5.53645200	-0.37857800
H	4.13046700	3.12753200	0.26150600
Cl	3.28140300	0.35454800	1.18561400

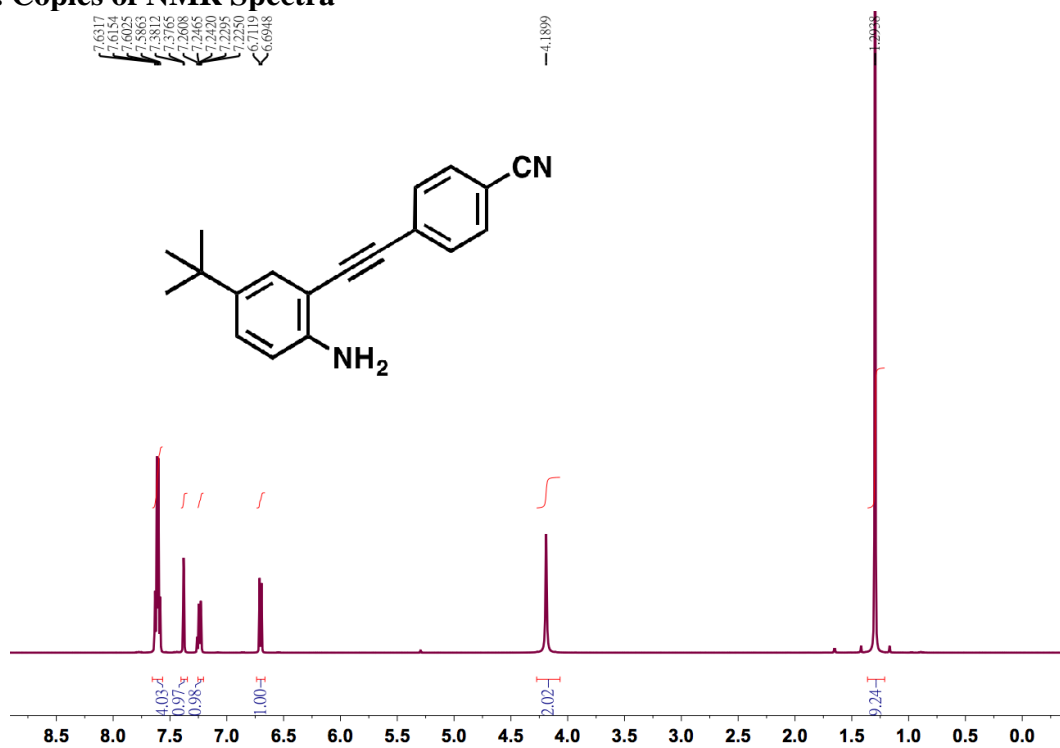
Table B.6 Cartesian coordinates for **1b•NO₃⁻**

	X	Y	Z
P	2.24133900	-0.89001400	-0.63371700
N	1.17179900	-2.16783200	-0.51063900

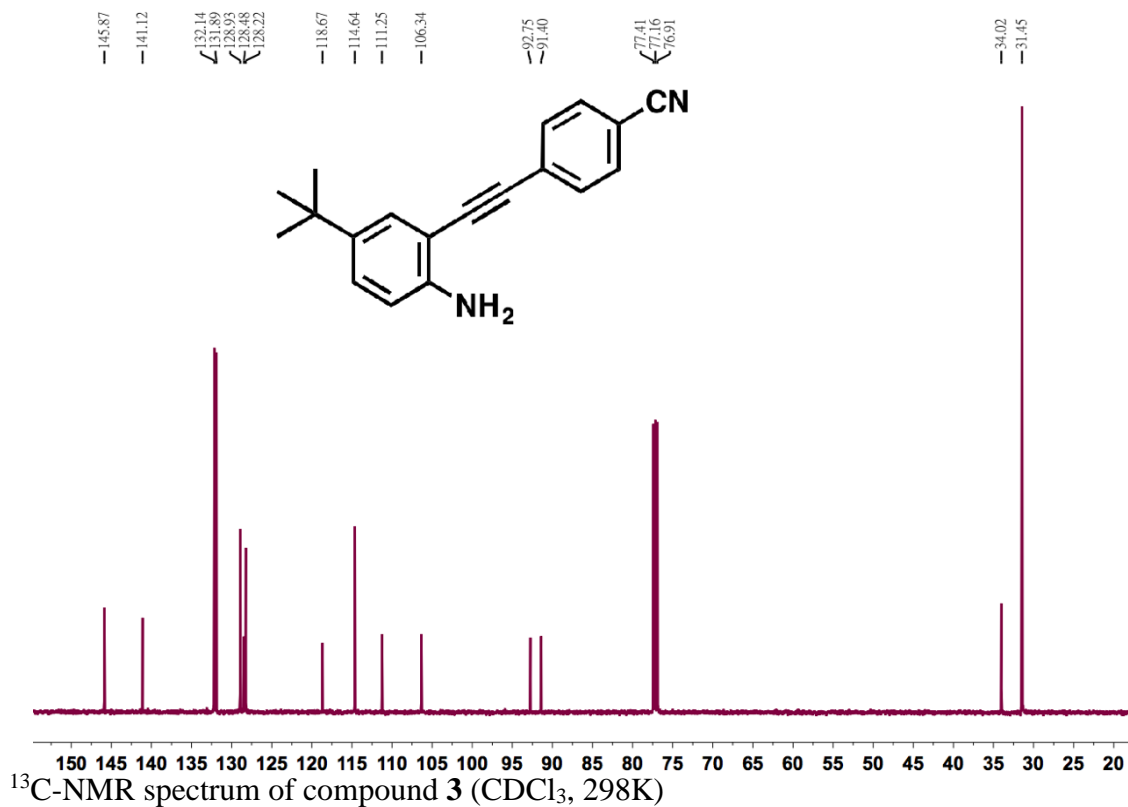
C	1.42637800	-3.37301500	0.11996800
C	2.75021600	-3.79844400	0.35868600
C	3.87944200	-2.98920300	-0.05309800
C	3.82313200	-1.72844400	-0.53664300
C	0.35761700	-4.21032800	0.51714600
C	0.62242800	-5.43640100	1.13206900
C	1.92908200	-5.85350400	1.36743500
C	2.97703500	-5.03479000	0.97934300
C	-0.98706600	-3.78258400	0.30367800
C	-2.11628000	-3.39306900	0.10540000
C	5.04507400	-1.00580000	-0.95346100
C	6.05462700	-1.68846400	-1.64737700
C	7.22559100	-1.04403100	-2.01420000
C	7.39454700	0.30841700	-1.69836200
C	6.39180100	1.00953400	-1.02027600
C	5.22582100	0.35221500	-0.65289000
O	2.02760800	0.02213600	-1.77943500
N	-3.61326100	3.25344100	-0.04975300
C	-2.44703900	3.94934100	0.20872300
N	-1.33570700	3.19291600	-0.08373200
O	-2.41094200	5.09193900	0.64136700
C	-0.00625600	3.57492900	0.03001000
C	0.43020900	4.74526700	0.67837800
C	1.78686000	5.01646300	0.75868000
C	2.70017700	4.13082600	0.19536600
C	2.28637700	2.97550500	-0.46277100
C	0.93728300	2.70246000	-0.54094500
C	-5.69749000	-3.40425100	-0.84213900
C	-4.42015000	-3.87378700	-0.58003400
C	-3.45303400	-2.95621500	-0.15425600
C	-5.08712700	-1.16047300	-0.29042600
C	-6.05933600	-2.07253200	-0.71818900
C	-4.91371100	3.73436900	0.11263800
C	-5.96980500	2.79215900	0.08657500
C	-5.22942800	5.09067900	0.26745500
C	-6.55533700	5.48812800	0.39381600
C	-7.59821000	4.56384700	0.36179000
C	-7.29853100	3.21972600	0.20528000
C	-5.40578800	0.22613400	-0.15953400
C	-5.68056400	1.40101400	-0.04935000
C	-3.79357100	-1.60806600	0.00101900
N	4.11914500	4.40643300	0.31406400
C	8.60781000	0.98107200	-2.07949800
N	9.58834000	1.51532100	-2.38582900
O	4.47016500	5.46247800	0.81736200
O	4.90582800	3.55952200	-0.09271900

N	-6.71912700	-4.36714000	-1.27973100
O	-7.83687700	-3.94303400	-1.51263200
O	-6.39141700	-5.53574500	-1.38141000
H	0.19901800	-1.94275100	-0.76334700
H	4.85918800	-3.45255900	0.06193600
H	-0.21775800	-6.05470800	1.42954900
H	2.12071700	-6.80580500	1.84774800
H	4.00455800	-5.34319400	1.15066800
H	5.90550100	-2.72821800	-1.91961800
H	8.00241300	-1.57518900	-2.55294800
H	6.52394000	2.05750800	-0.77797000
H	4.46172900	0.90151300	-0.10964500
H	-3.51901600	2.28554700	-0.35217300
H	-1.49740100	2.26621200	-0.48181900
H	-0.29009300	5.42078700	1.11373200
H	2.14542900	5.90476100	1.26408600
H	2.99912100	2.29846500	-0.91643100
H	0.61739800	1.78909100	-1.03000000
H	-4.18440800	-4.92214500	-0.70829900
H	-7.06737400	-1.75424600	-0.94982900
H	-4.43312600	5.81881700	0.28986700
H	-6.77259000	6.54502100	0.51259400
H	-8.62848700	4.88772800	0.45718200
H	-8.08507500	2.47296400	0.17687200
H	-3.05257400	-0.90475800	0.36549600
O	2.15504700	-0.02784100	0.75125000
C	2.11166800	-0.69620600	1.96941000
C	0.89410500	-1.18426500	2.43560700
C	3.28677900	-0.85202900	2.69603700
C	0.86542100	-1.85560400	3.65437700
H	0.00481900	-1.03891500	1.82909200
C	3.24107300	-1.51997800	3.91728900
H	4.21560400	-0.45504900	2.29806400
C	2.03427700	-2.02648000	4.39483600
H	-0.07635400	-2.24681900	4.02578200
H	4.15254500	-1.64629600	4.49258000
H	2.00403400	-2.55158000	5.34386100
O	-0.83603400	0.09744800	-0.05808800
O	-2.26919500	0.80511600	-1.51457900
O	-1.27832400	-1.09551200	-1.80517200
N	-1.45338100	-0.06925100	-1.13355300

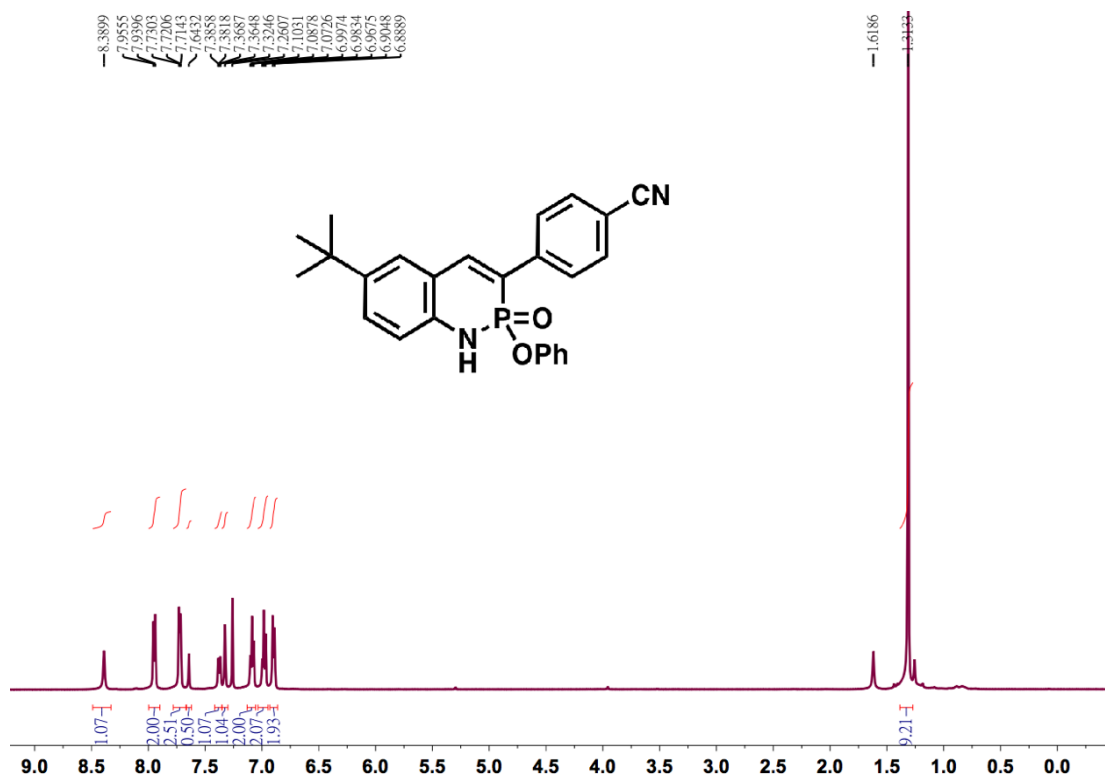
11. Copies of NMR Spectra



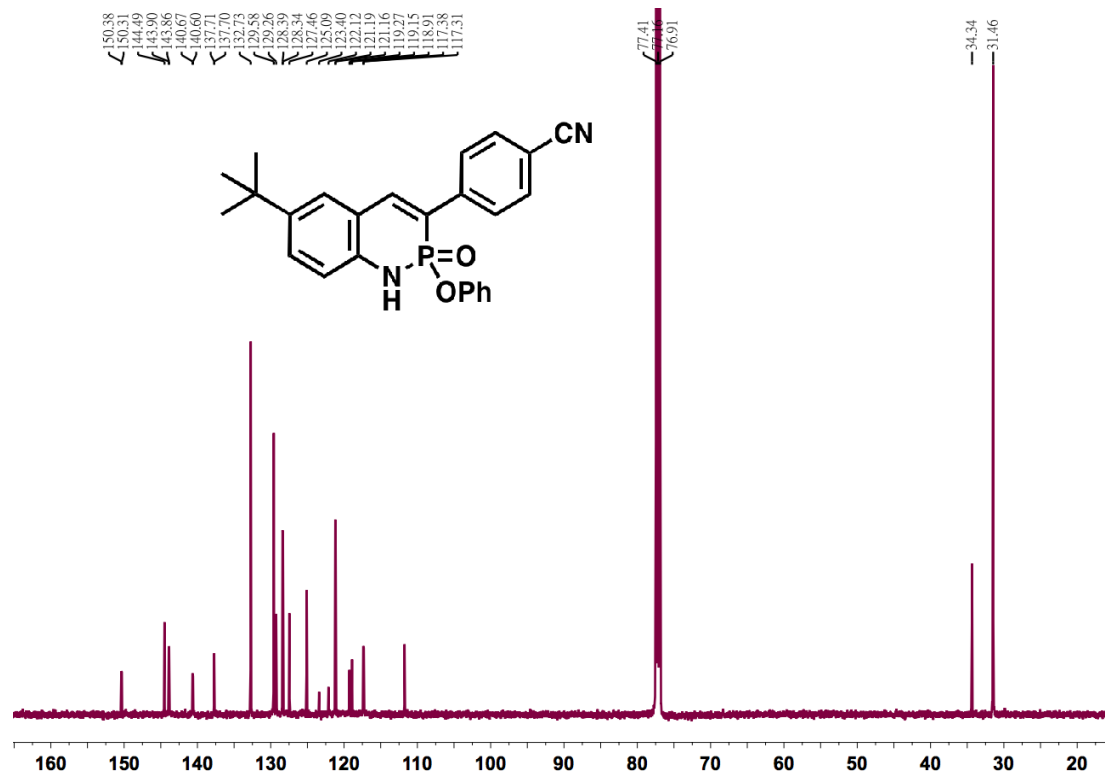
$^1\text{H-NMR}$ spectrum of compound **3** (CDCl_3 , 298K)



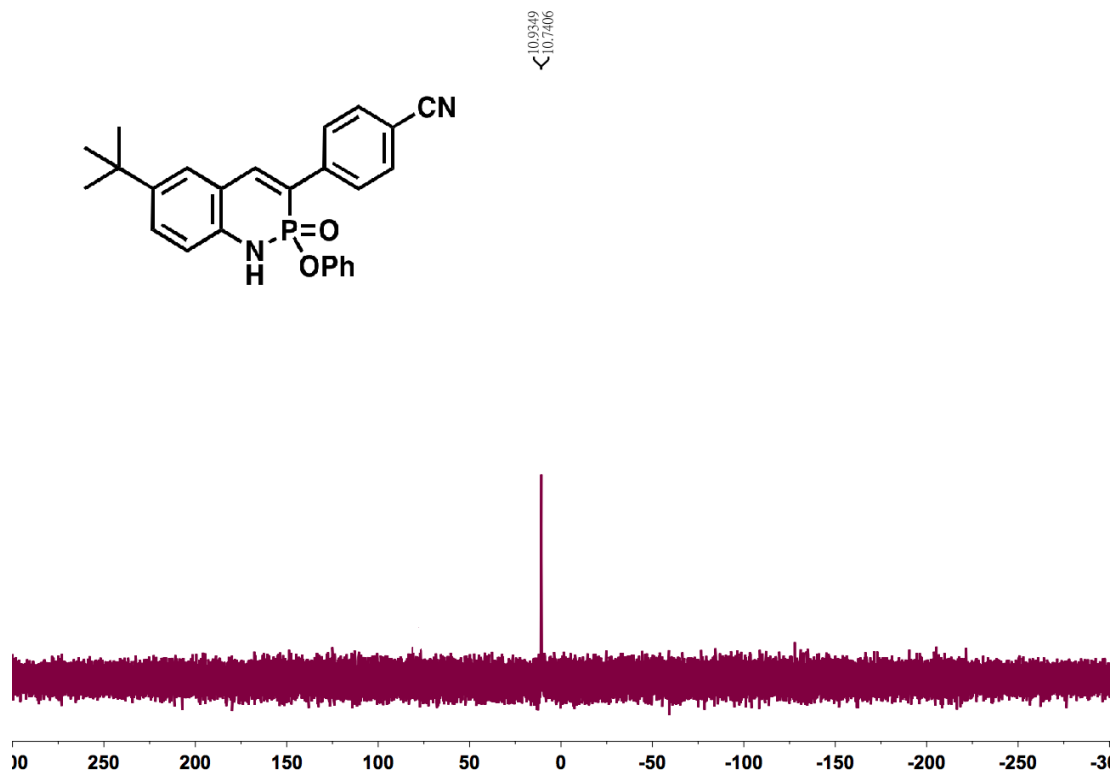
$^{13}\text{C-NMR}$ spectrum of compound **3** (CDCl_3 , 298K)



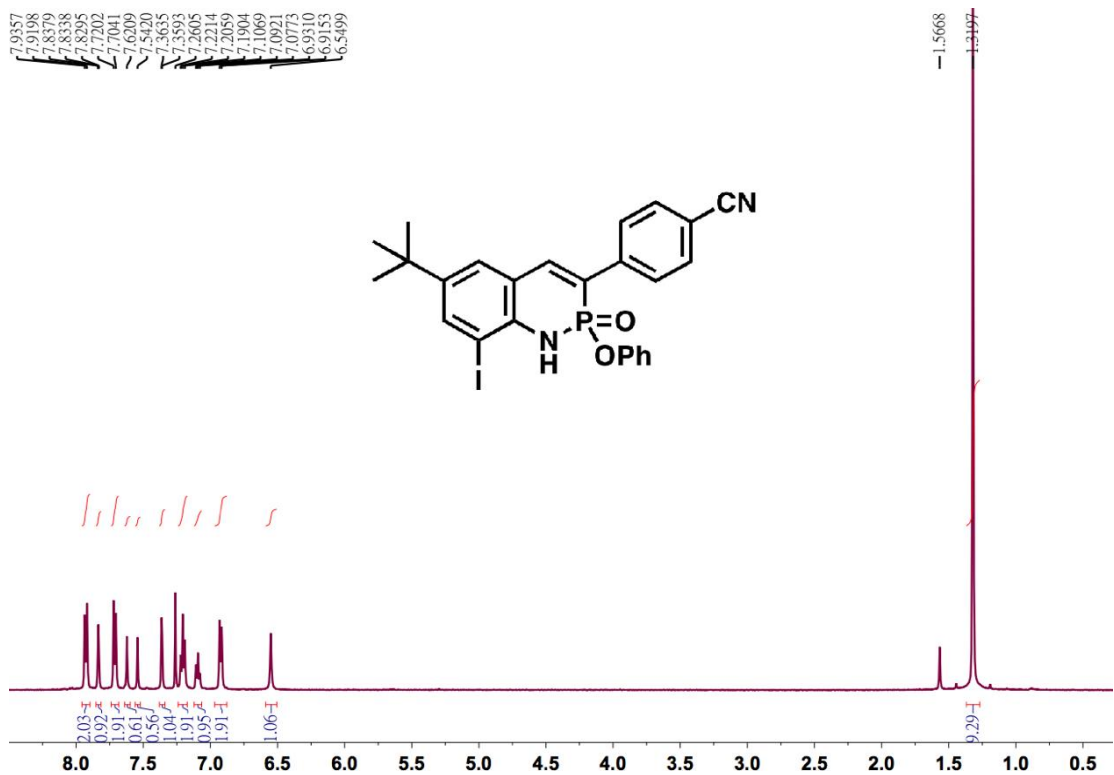
¹H-NMR spectrum of compound 4 (CDCl₃, 298K)



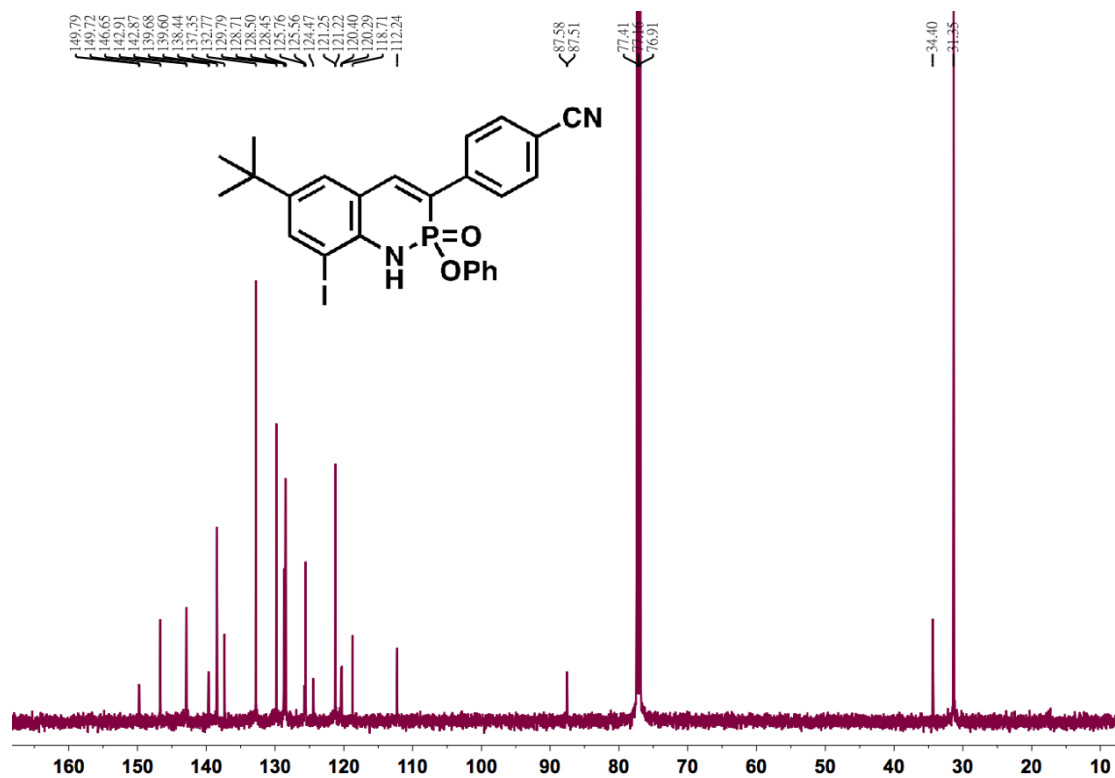
¹³C-NMR spectrum of compound 4 (CDCl₃, 298K)



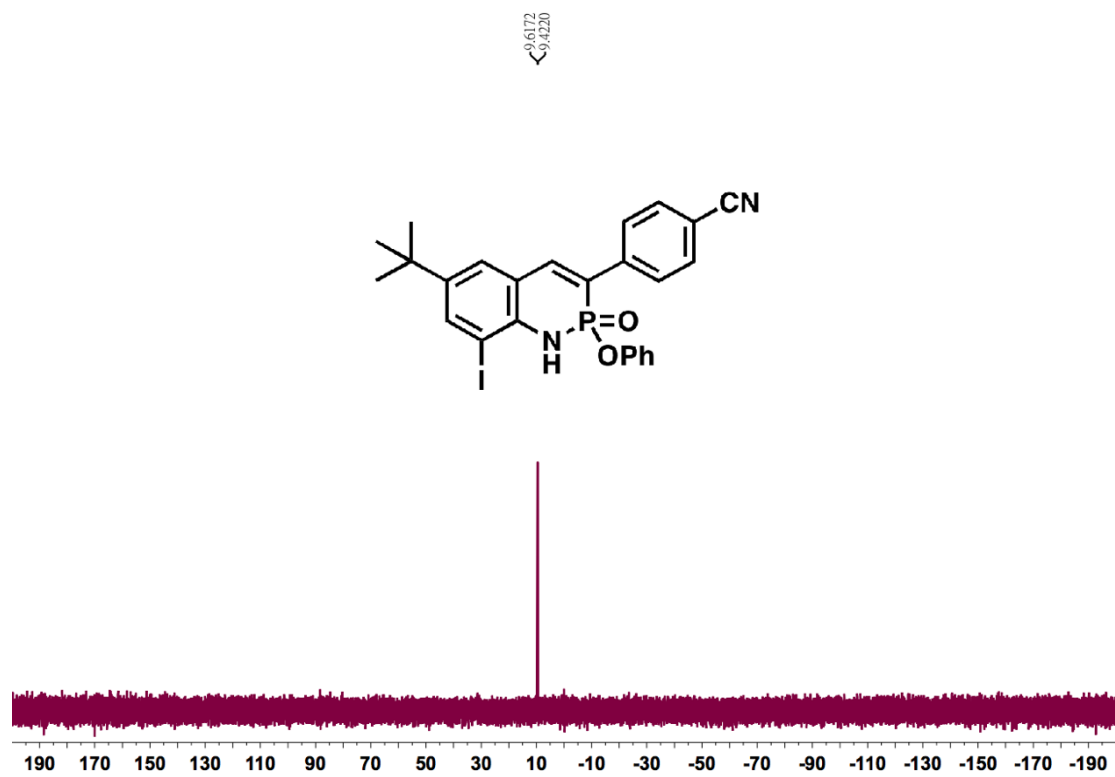
^{31}P -NMR spectrum of compound 4 (CDCl_3 , 298K)



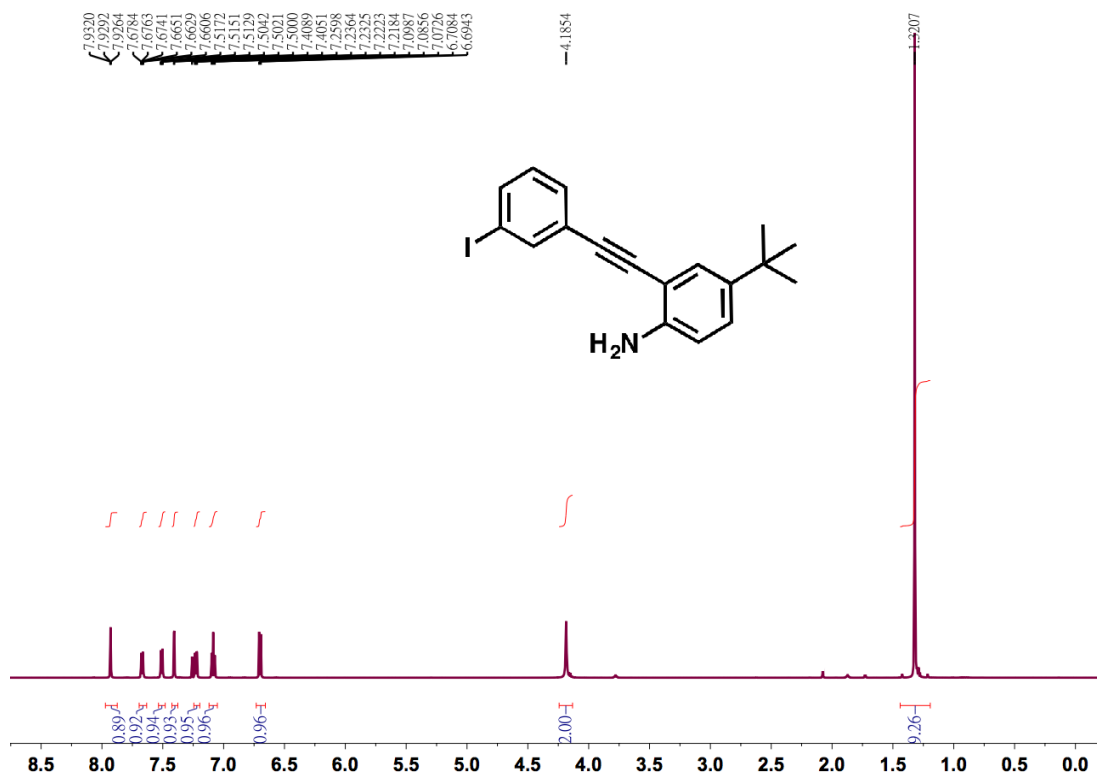
^1H -NMR spectrum of compound 5 (CDCl_3 , 298K)



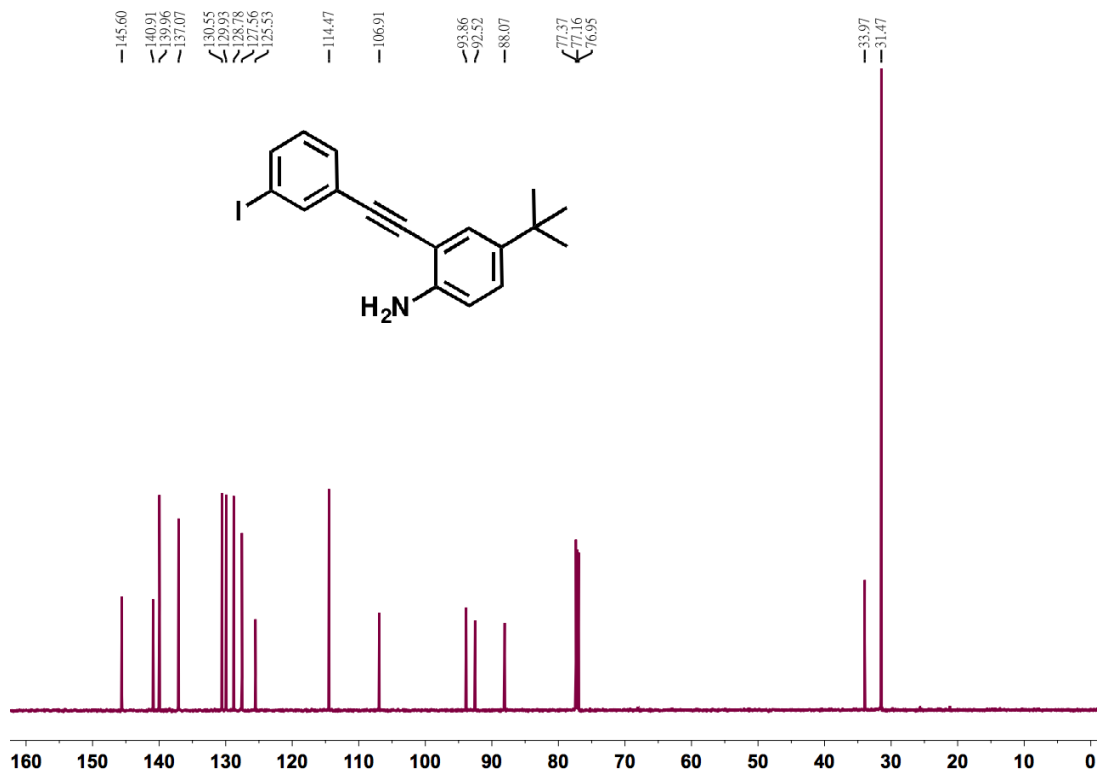
¹³C-NMR spectrum of compound 5 (CDCl₃, 298K)



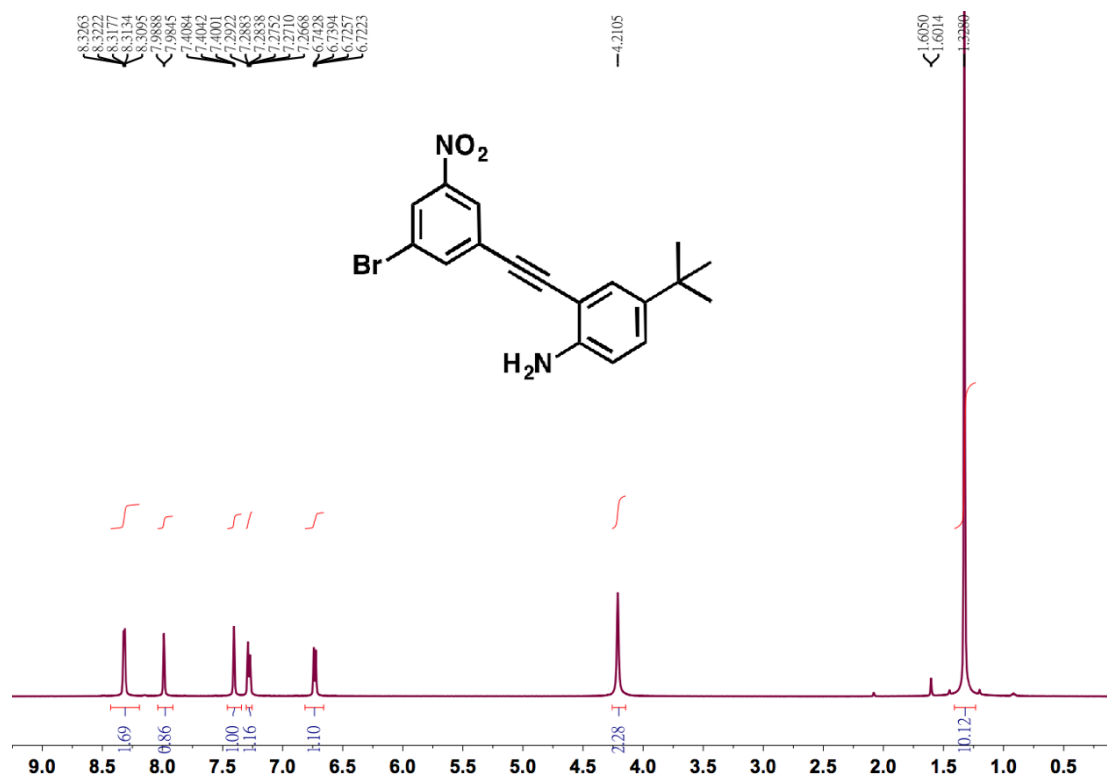
³¹P-NMR spectrum of compound 5 (CDCl₃, 298K)



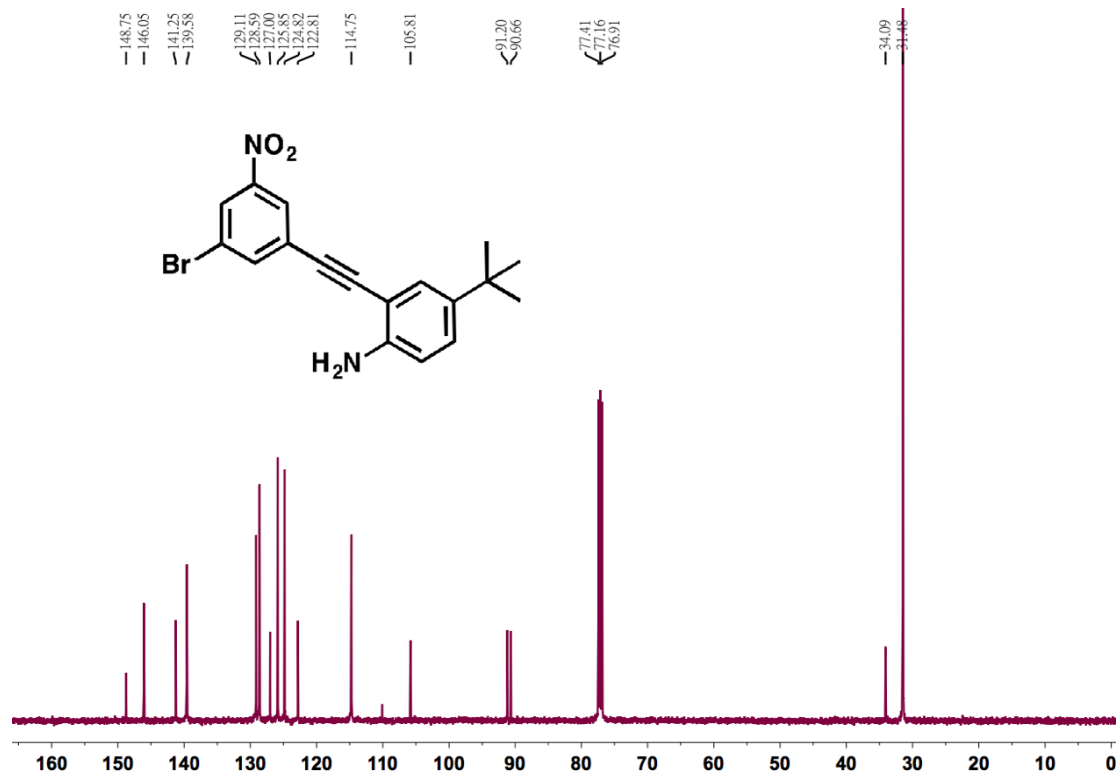
¹H-NMR spectrum of compound 7a (CDCl₃, 298K)



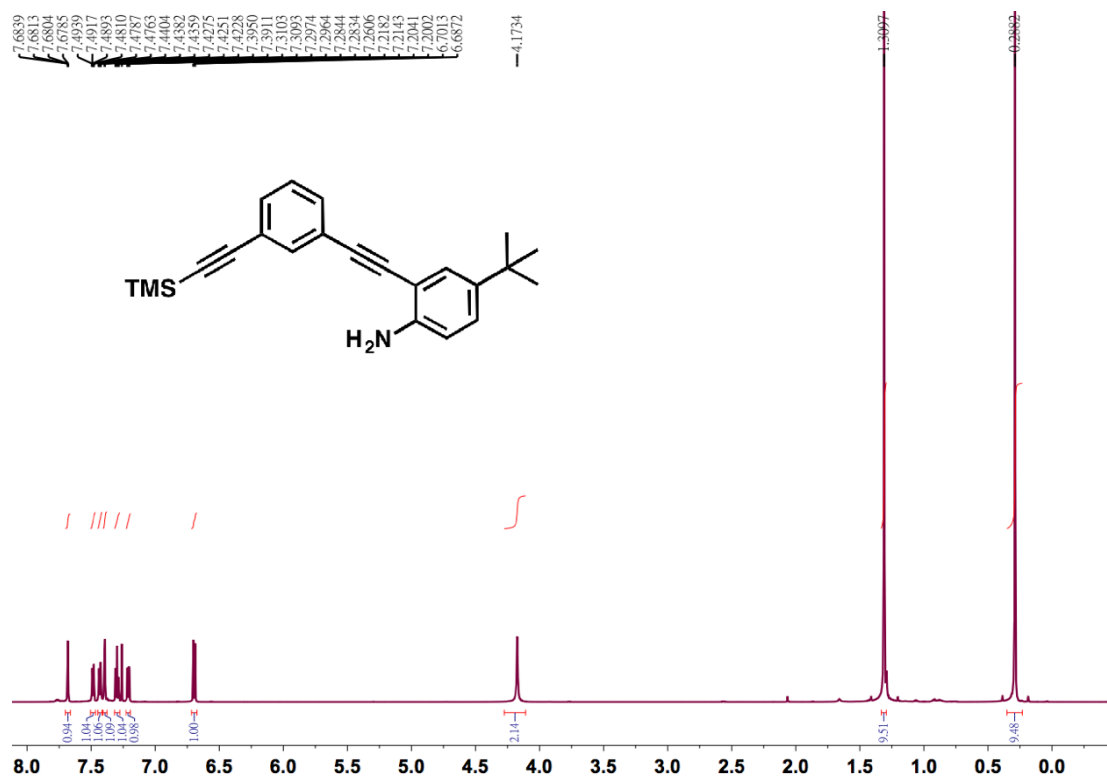
¹³C-NMR spectrum of compound 7a (CDCl₃, 298K)



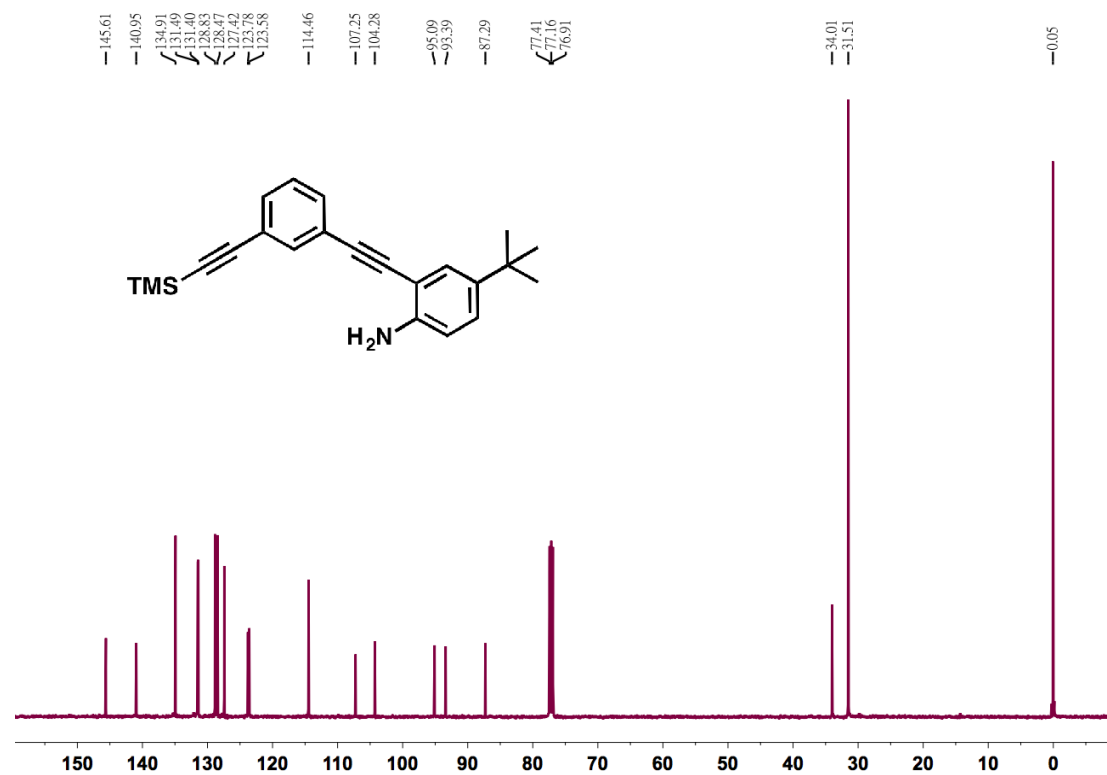
¹H-NMR spectrum of compound **7b** (CDCl₃, 298K)



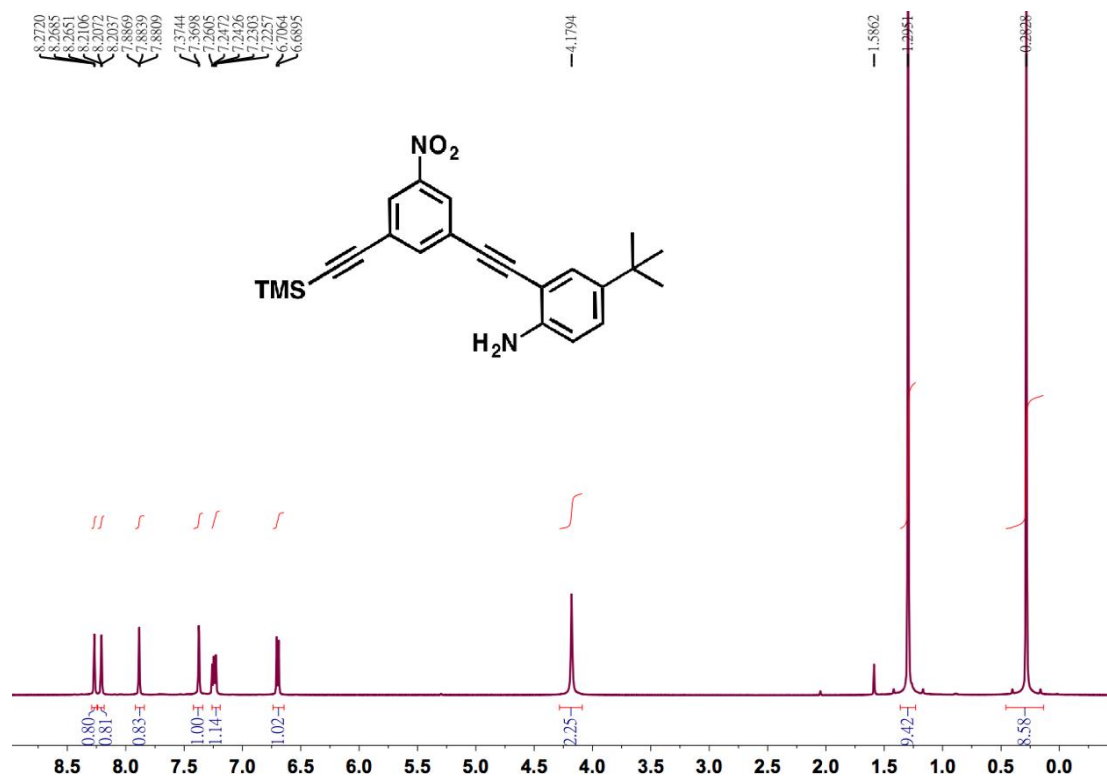
¹³C-NMR spectrum of compound **7b** (CDCl₃, 298K)



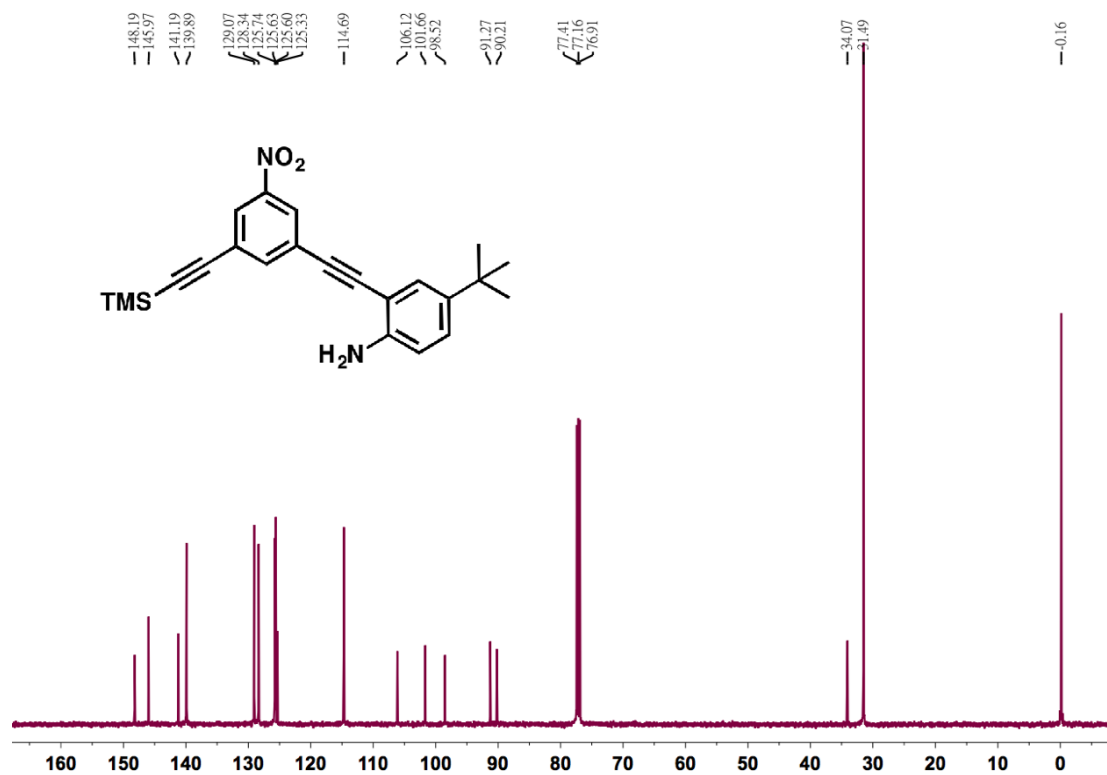
¹H-NMR spectrum of compound **8a** (CDCl₃, 298K)



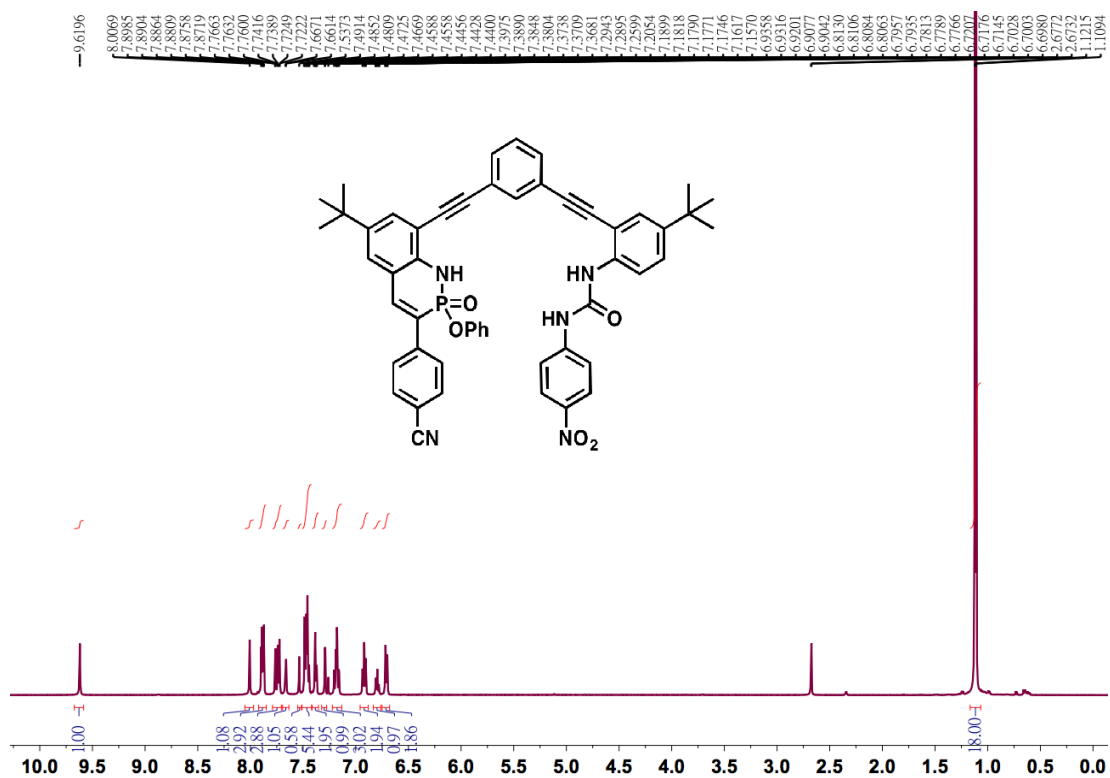
¹³C-NMR spectrum of compound **8a** (CDCl₃, 298K)



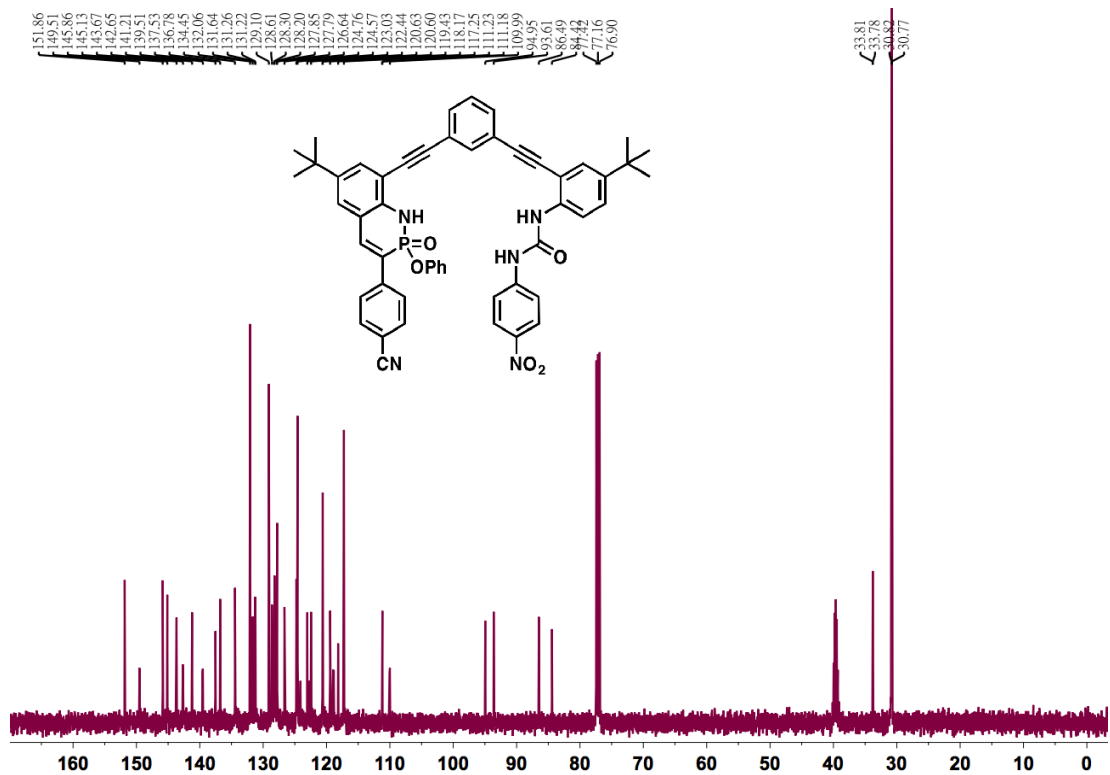
¹H-NMR spectrum of compound **8b** (CDCl₃, 298K)



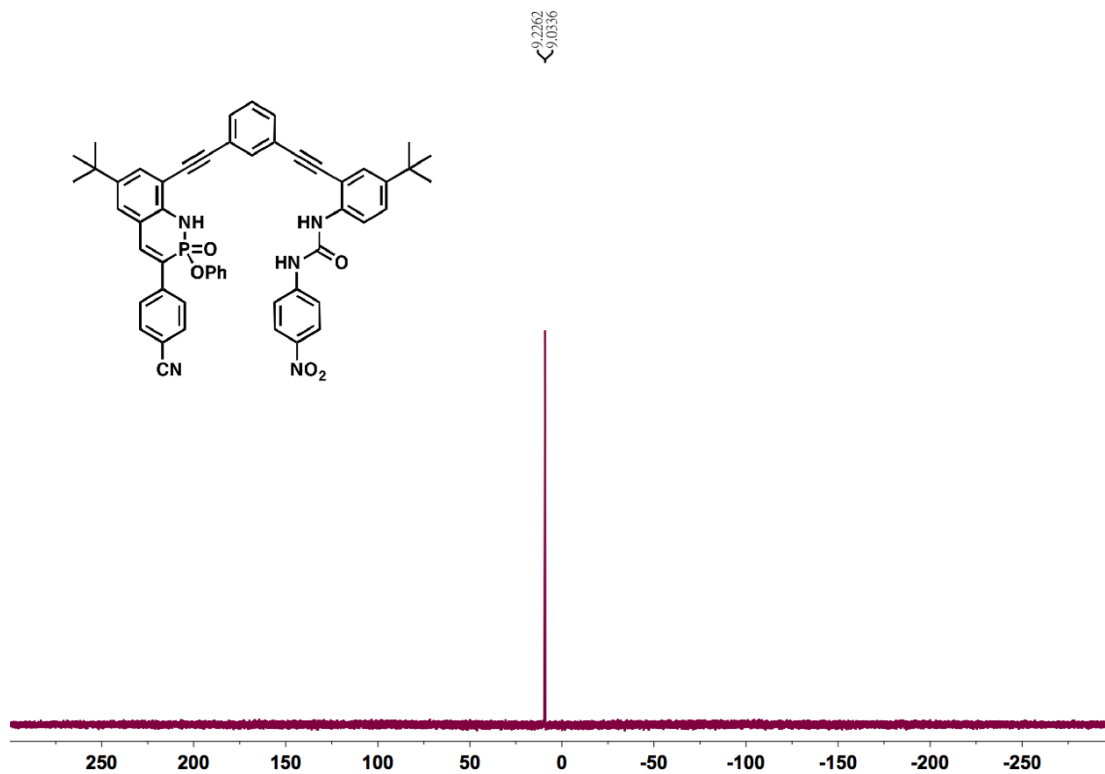
¹³C-NMR spectrum of compound **8b** (CDCl₃, 298K)



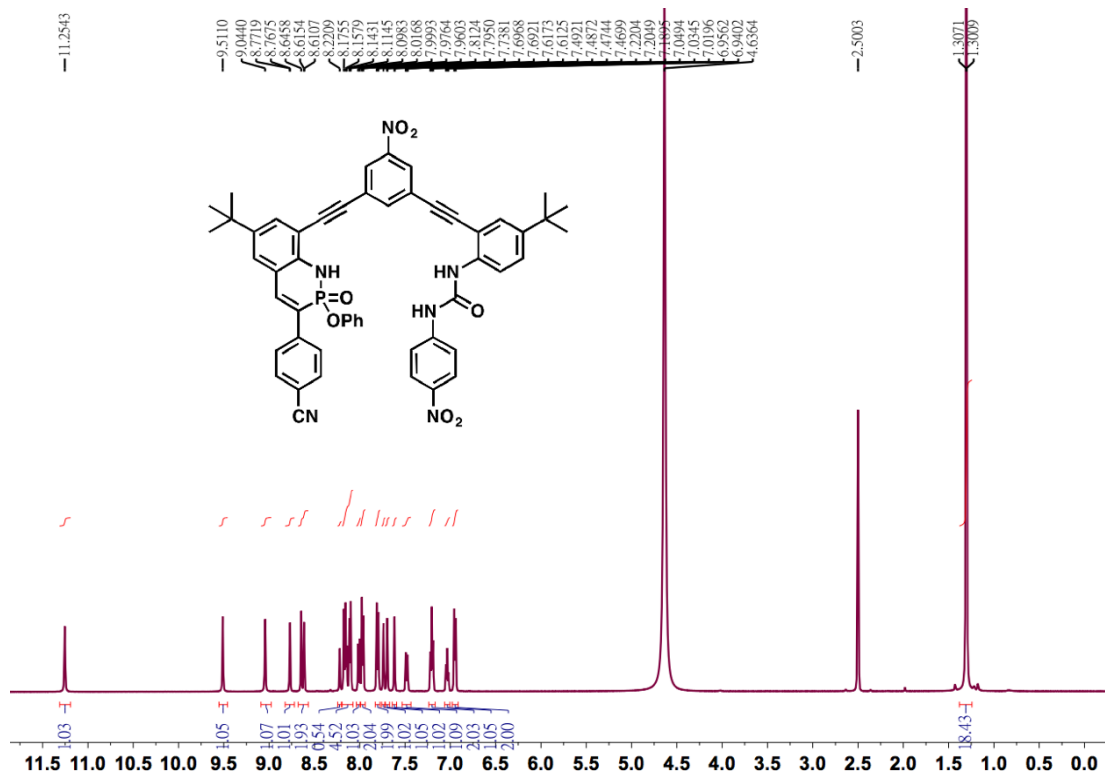
¹H-NMR spectrum of compound **1a** (CDCl₃/DMSO-*d*₆ = 4/1, 298K)



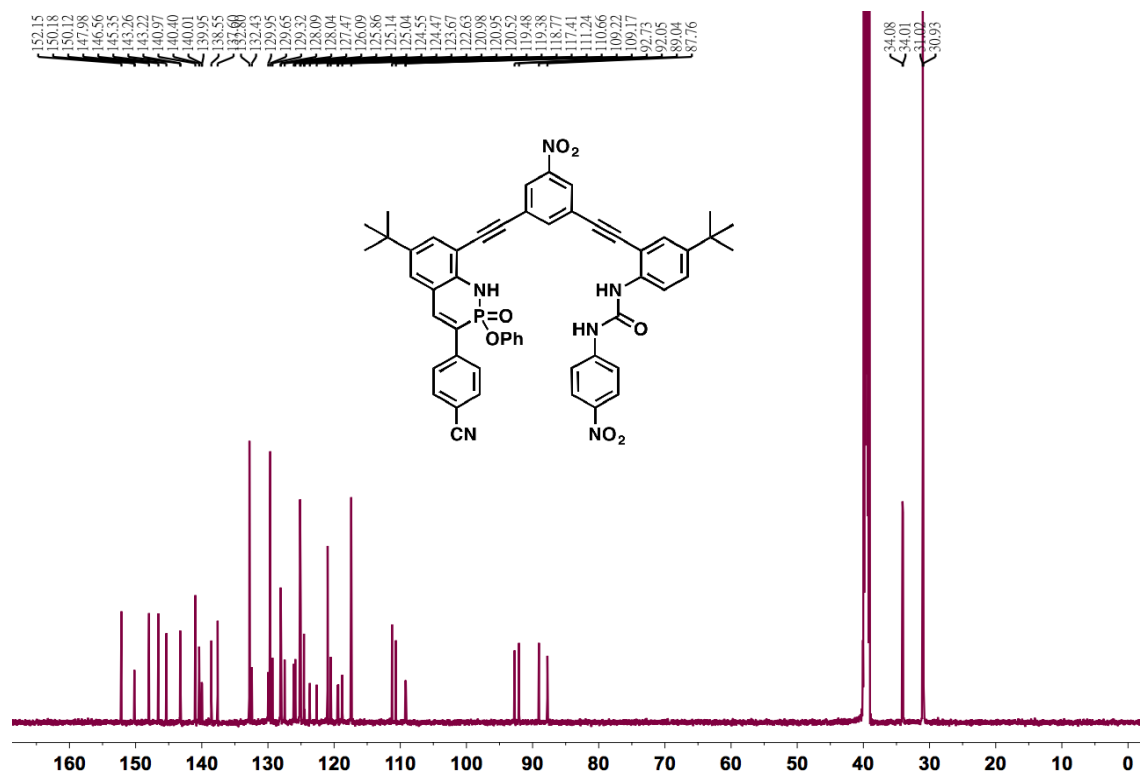
¹³C-NMR spectrum of compound **1a** (CDCl₃/DMSO-*d*₆ = 4/1, 298K)



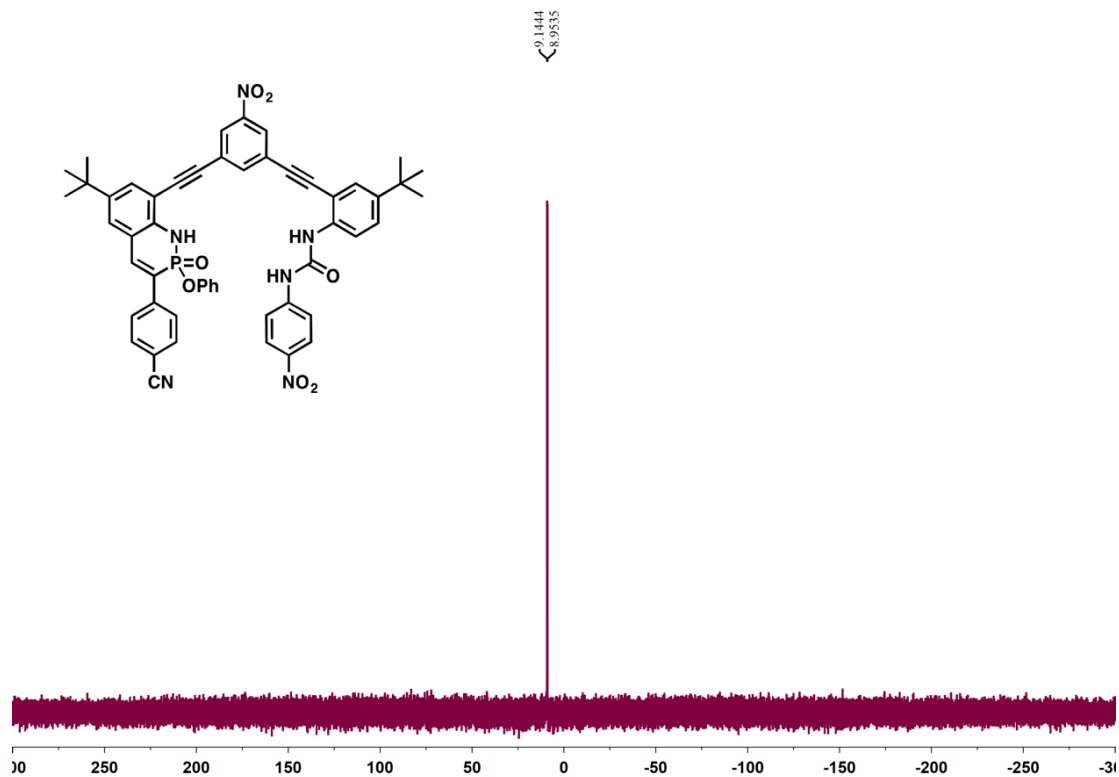
³¹P-NMR spectrum of compound **1a** (CDCl₃/DMSO-*d*₆ = 4/1, 298K)



¹H-NMR spectrum of compound **1b** (DMSO-*d*₆, 298K)



¹³C-NMR spectrum of compound **1b** (DMSO-*d*₆, 298K)



³¹P-NMR spectrum of compound **1b** (DMSO-*d*₆, 298K)

APPENDIX C

SUPPLEMENTARY INFORMATION FOR CHAPTER 4

1. Crystallographic Data for 2f

General. Diffraction intensities for **2f** were collected at 173 K on a Bruker Apex2 CCD diffractometer using CuK α radiation, $\lambda = 1.54178$ Å. Space group was determined based on systematic absences. Absorption correction was applied by SADABS.¹ Structure was solved by direct methods and Fourier techniques and refined on F^2 using full matrix least-squares procedures. All non-H atoms were refined with anisotropic thermal parameters. H atoms were refined in calculated positions in a rigid group model except the H atom at the N atom involved in H-bond which was found on the residual density map and refined with isotropic thermal parameter. In the crystal structure the main molecules form a dimer unit via N-H...O H-bonds which are packed in columns. Solvent molecules CHCl₃ fill out empty space between such the columns and are highly disordered. These disordered solvent molecules were treated by SQUEEZE.² The corrections of the X-ray data by SQUEEZE are 220 electron/cell; the required values are 232 electron/cell for four CHCl₃ molecules in the full unit cell. All calculations were performed by the Bruker SHELXL-2014 package.³

Crystallographic Data for 2f: C₂₄H₂₀Cl₃O₂P, M = 505.74, 0.15 x 0.08 x 0.06 mm, T = 173(2) K, Monoclinic, space group $P2_1/c$, $a = 17.7865(8)$ Å, $b = 8.1543(4)$ Å, $c = 18.4012(8)$ Å, $\beta = 117.199(3)^\circ$, $V = 2373.7(2)$ Å³, $Z = 4$, $D_c = 1.415$ Mg/m³, $\mu(\text{Cu}) = 4.335$ mm⁻¹, $F(000) = 1040$, $2\theta_{\text{max}} = 133.15^\circ$, 13893 reflections, 4116 independent reflections [$R_{\text{int}} = 0.0465$], $R1 = 0.0570$, $wR2 = 0.1562$ and $\text{GOF} = 1.021$ for 4116 reflections (257

parameters) with $I > 2\sigma(I)$, $R1 = 0.0699$, $wR2 = 0.1630$ and $GOF = 1.021$ for all reflections, max/min residual electron density $+0.588/-0.275 \text{ e}\text{\AA}^{-3}$. CCDC 1944053.

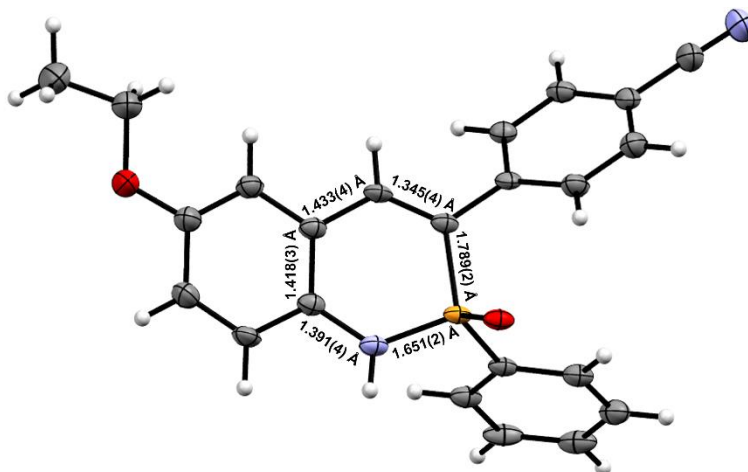


Figure C.1 ORTEP drawing of **2f** with selected bond lengths listed; thermal ellipsoids drawn at 30% probability. Crystals grown with slow diffusion of pentane into a solution of **2** in CHCl_3 .

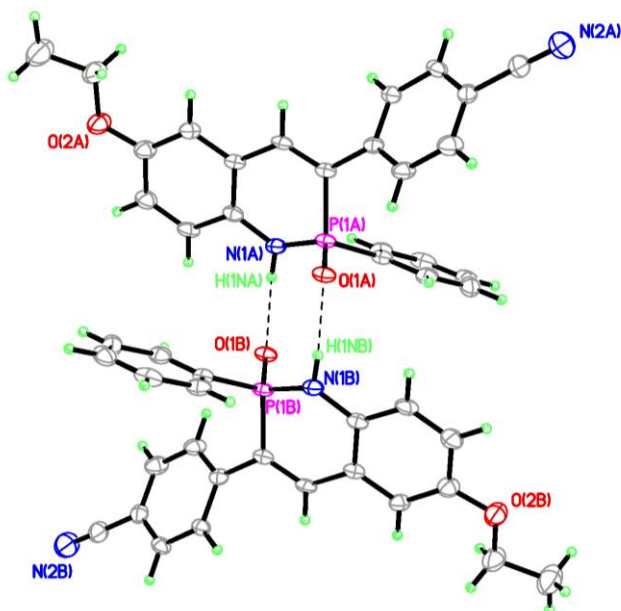


Figure C.2 ORTEP drawing of the racemic dimer of **2f**; thermal ellipsoids drawn at 30% probability.

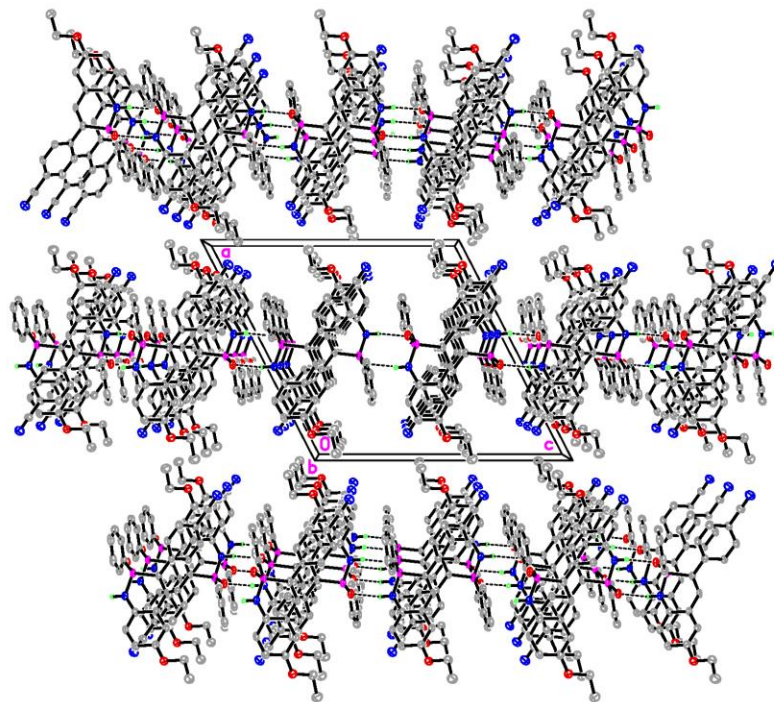


Figure C.3 ORTEP drawing of the crystal packing of **2f** looking down the b-axis.

2. Frontier Orbital Values and TD-DFT Excitations

Ground state calculations

Table C.1 Calculated Frontier Orbitals and First Excitation Values for **2**^a

compd	E_{HOMO}	E_{LUMO}	ΔE_{DFT}	$S_0 \rightarrow S_1$ computed (nm), osc. Strength
2a	-6.800	-2.405	4.395	341, 0.505
2b	-6.750	-2.319	4.431	337, 0.535
2c	-6.531	-2.296	4.235	354, 0.392
2d	-6.510	-2.294	4.303	348, 0.486
2e	-6.481	-2.178	4.207	358, 0.361
2f	-6.353	-2.146	3.896	389, 0.195

^a Calculated at the PBE0/TZVP level of theory; values reported in eV.

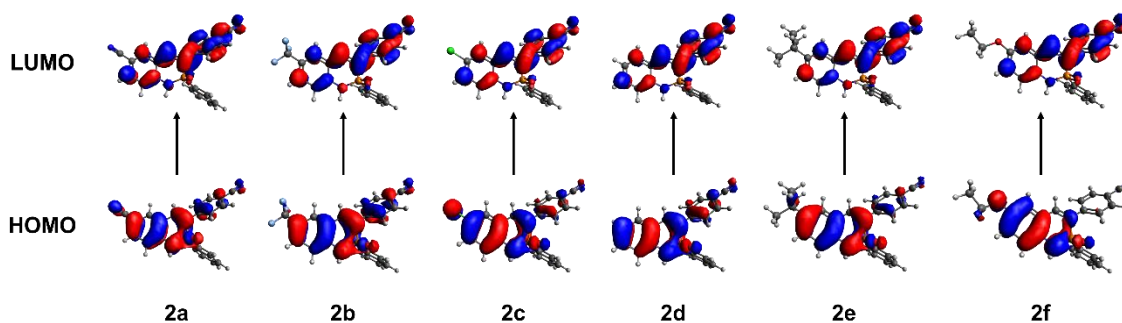


Figure C.4 Frontier orbital shapes (isovalue = 0.3) of heterocycles **2**; calculated at the PBE0/TZVP level of theory.

Excited state calculations

These initial structures were optimized using the functional PBE0^{4,5} (25% full-range HF exchange) and TZVP basis set⁶ as implemented in Gaussian 09.⁷ In addition, all the optimized structures were confirmed by frequency analysis and the number of imaginary frequencies was zero. TD-DFT vertical excitation calculations and geometry optimization of the first excited state (S_1) were performed at the same level of theory. The PCM solvation model^{8,9} was used to account for the solvent effects of the chloroform.

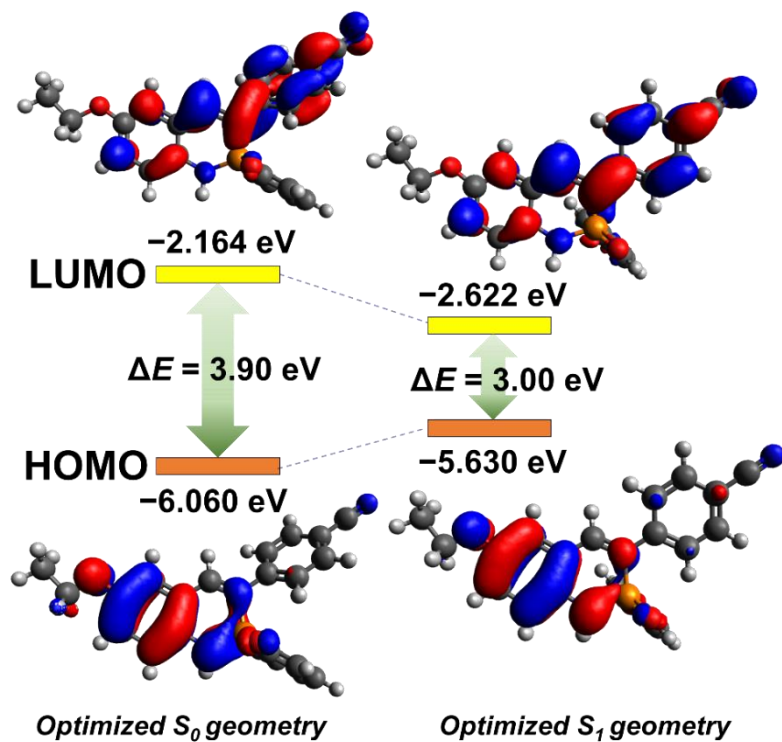


Figure C.5 HOMO-LUMO pictorial representations (isovalue = 0.3), energies and their differences (ΔE) in the optimized S_0 and S_1 structures of **2f** calculated by the DFT and TD-DFT methods at the PCM(CHCl_3)-PBE0/TZVP level of theory, respectively.

3. Geometry Optimizations and Coordinates

Ground state geometries

Table C.2 Cartesian coordinates of the optimized geometry of **2a** determined at the PBE0/TZVP level of theory

Atom	x	y	z
C	-4.85224	-0.99453	0.24314
C	-5.06467	0.36876	-0.01362
C	-3.99796	1.19772	-0.26557
C	-2.68944	0.69768	-0.26948
C	-2.46321	-0.67090	-0.00881
C	-3.55816	-1.49676	0.24538
N	-1.62915	1.54068	-0.48129
P	-0.05268	1.09981	-0.96544
C	0.01373	-0.57214	-0.28708
C	-1.13106	-1.21587	0.02816
C	1.32888	-1.22391	-0.17733
C	2.32937	-1.00360	-1.13093
C	3.55719	-1.62907	-1.02594
C	3.81064	-2.48996	0.04330
C	2.82419	-2.71342	1.00652
C	1.60209	-2.08011	0.89538
O	0.24116	1.20873	-2.43673
H	-6.07224	0.76605	-0.01630
H	-4.16680	2.24964	-0.46799
H	-3.38832	-2.54835	0.44662
H	-1.86453	2.51486	-0.62006
H	-1.06114	-2.25919	0.32868
H	2.13135	-0.35505	-1.97675
H	4.32091	-1.45850	-1.77493
H	3.02505	-3.37115	1.84342
H	0.85418	-2.23445	1.66438
C	5.07615	-3.13557	0.15614
N	6.10029	-3.65817	0.24771
C	1.00594	2.19506	0.01314
C	1.97814	2.94304	-0.64517
C	0.86604	2.29013	1.39720
C	2.80595	3.78889	0.08033
H	2.07444	2.85806	-1.72158
C	1.69724	3.13388	2.11728
H	0.10786	1.70840	1.91080
C	2.66562	3.88319	1.45833
H	3.56138	4.37440	-0.43113
H	1.59006	3.20904	3.19339
H	3.31411	4.54305	2.02388
C	-5.95519	-1.85468	0.50419
N	-6.85123	-2.54976	0.71725

Zero-point correction = 0.306046 (Hartree/Particle); Thermal correction to energy = 0.328311; Thermal correction to enthalpy = 0.329256; Thermal correction to Gibbs free energy = 0.252414; Sum of electronic and zero-point energies = -1426.281789; Sum of electronic and thermal energies = -1426.259523; Sum of electronic and thermal enthalpies = -1426.258579; Sum of electronic and thermal free energies = -1426.335421.

Table C.3 Cartesian coordinates of the optimized geometry of **2b** determined at the PBE0/TZVP level of theory

Atom	x	y	z
C	4.33256	0.25239	0.07266
C	4.36740	-1.12574	-0.14433
C	3.19680	-1.82533	-0.36097
C	1.96424	-1.16425	-0.36534
C	1.91814	0.22872	-0.13593
C	3.11747	0.91433	0.07864
N	0.79435	-1.87023	-0.54497
P	-0.71412	-1.24659	-1.00223
C	-0.55995	0.42532	-0.35685
C	0.66485	0.93655	-0.08900
C	-1.78476	1.23382	-0.22255
C	-2.83620	1.11740	-1.14210
C	-3.97972	1.88534	-1.01112
C	-4.09599	2.78768	0.05013
C	-3.05815	2.90828	0.97984
C	-1.92102	2.13323	0.84339
O	-1.06879	-1.33987	-2.44972
H	5.31560	-1.64935	-0.14765
H	3.22816	-2.89645	-0.53066
H	3.08031	1.98498	0.25349
H	0.90195	-2.87056	-0.65853
H	0.72898	1.98857	0.18318
H	-2.74143	0.43697	-1.98120
H	-4.78302	1.79523	-1.73288
H	-3.15443	3.59763	1.81044
H	-1.13530	2.20738	1.58703
C	-5.27351	3.57973	0.18954
N	-6.22685	4.22181	0.30316
C	-1.87332	-2.16682	0.02964
C	-2.99233	-2.74612	-0.56830
C	-1.67521	-2.28375	1.40740
C	-3.90785	-3.44425	0.21021
H	-3.13095	-2.64787	-1.63956
C	-2.59376	-2.97976	2.18044
H	-0.80363	-1.83295	1.87151
C	-3.70888	-3.55955	1.58133

H	-4.77702	-3.89756	-0.25393
H	-2.44117	-3.07162	3.25034
H	-4.42561	-4.10321	2.18781
C	5.58540	1.02927	0.31687
F	5.71872	2.05264	-0.54614
F	6.68573	0.27257	0.20460
F	5.60776	1.57440	1.54852

Zero-point correction = 0.312616 (Hartree/Particle); Thermal correction to energy = 0.335712; Thermal correction to enthalpy = 0.336656; Thermal correction to Gibbs free energy = 0.257793; Sum of electronic and zero-point energies = -1670.857410; Sum of electronic and thermal energies = -1670.834315; Sum of electronic and thermal enthalpies = -1670.833370; Sum of electronic and thermal free energies = -1670.912234.

Table C.4 Cartesian coordinates of the optimized geometry of **2c** determined at the PBE0/TZVP level of theory

Atom	x	y	z
C	4.76530	-0.84753	-0.21352
C	4.95235	0.51406	0.01777
C	3.85707	1.32309	0.25213
C	2.56393	0.79136	0.25768
C	2.37737	-0.58478	0.01677
C	3.49994	-1.39313	-0.21621
N	1.46788	1.61180	0.44837
P	-0.06873	1.13040	0.96633
C	-0.10263	-0.53610	0.28870
C	1.05876	-1.16265	-0.01869
C	-1.40505	-1.21599	0.17783
C	-2.41834	-1.00066	1.12223
C	-3.63596	-1.64912	1.01591
C	-3.86748	-2.52873	-0.04558
C	-2.86886	-2.74659	-1.00019
C	-1.65681	-2.09032	-0.88811
O	-0.35888	1.22487	2.42868
H	5.95108	0.93373	0.01736
H	4.00140	2.38257	0.43708
H	3.36185	-2.45261	-0.39989
H	1.67299	2.59782	0.54848
H	1.01106	-2.21043	-0.31023
H	-2.23659	-0.33867	1.96189
H	-4.40883	-1.48285	1.75717
H	-3.05318	-3.41765	-1.83095
H	-0.90062	-2.23953	-1.65088
C	-5.12144	-3.19771	-0.15958
N	-6.13694	-3.74019	-0.25236
C	-1.17198	2.18283	0.00032
C	-2.19830	2.86079	0.65770

C	-1.02047	2.31216	-1.38225
C	-3.06654	3.67011	-0.06545
H	-2.30167	2.75103	1.73180
C	-1.89224	3.11874	-2.10022
H	-0.22075	1.78506	-1.89284
C	-2.91380	3.79763	-1.44141
H	-3.86269	4.20063	0.44554
H	-1.77547	3.22002	-3.17380
H	-3.59348	4.42828	-2.00484
Cl	6.14889	-1.86580	-0.50514

Zero-point correction = 0.298482 (Hartree/Particle); Thermal correction to energy = 0.320018; Thermal correction to enthalpy = 0.320963; Thermal correction to Gibbs free energy = 0.245463; Sum of electronic and zero-point energies = -1793.507492; Sum of electronic and thermal energies = -1793.485956; Sum of electronic and thermal enthalpies = -1793.485012; Sum of electronic and thermal free energies = -1793.560511.

Table C.5 Cartesian coordinates of the optimized geometry of **2d** determined at the PBE0/TZVP level of theory

Atom	x	y	z
C	4.87957	-2.33820	-0.55510
C	5.40340	-1.07460	-0.27234
C	4.56839	-0.01982	0.04974
C	3.18339	-0.20570	0.09586
C	2.63866	-1.47362	-0.19415
C	3.51235	-2.52485	-0.51570
N	2.34180	0.85710	0.37539
P	0.75066	0.75975	0.93800
C	0.26395	-0.80418	0.19669
C	1.21640	-1.68909	-0.18898
C	-1.17160	-1.12470	0.11863
C	-2.06875	-0.69107	1.10523
C	-3.41442	-1.00319	1.02777
C	-3.89511	-1.75842	-0.04594
C	-3.01376	-2.19077	-1.04236
C	-1.67175	-1.86848	-0.95930
O	0.53974	0.85819	2.41437
H	6.47569	-0.91258	-0.30076
H	4.98133	0.95935	0.27178
H	3.08676	-3.49915	-0.73586
H	2.80016	1.74837	0.51685
H	0.89018	-2.67426	-0.51917
H	-1.69940	-0.12656	1.95449
H	-4.09666	-0.67053	1.80128
H	-3.38796	-2.76407	-1.88250
H	-1.00217	-2.17782	-1.75409

C	-5.28099	-2.08196	-0.12992
N	-6.40367	-2.34505	-0.19896
C	-0.07738	2.10620	0.06374
C	-0.88916	2.97892	0.78798
C	0.06664	2.26802	-1.31618
C	-1.55170	4.01136	0.13447
H	-0.98883	2.84211	1.85939
C	-0.59871	3.29914	-1.96466
H	0.70009	1.58949	-1.87873
C	-1.40739	4.16985	-1.23917
H	-2.18113	4.69171	0.69792
H	-0.48711	3.42552	-3.03617
H	-1.92673	4.97494	-1.74843
H	5.53887	-3.16167	-0.80375

Zero-point correction = 0.308146 (Hartree/Particle); Thermal correction to energy = 0.328403; Thermal correction to enthalpy = 0.329347; Thermal correction to Gibbs free energy = 0.257198; Sum of electronic and zero-point energies = -1334.037270; Sum of electronic and thermal energies = -1334.017013; Sum of electronic and thermal enthalpies = -1334.016068; Sum of electronic and thermal free energies = -1334.088218.

Table C.6 Cartesian coordinates of the optimized geometry of **2e** determined at the PBE0/TZVP level of theory

Atom	x	y	z
C	4.35248	0.21049	0.07235
C	4.33995	-1.17064	-0.16139
C	3.16166	-1.86961	-0.36931
C	1.93366	-1.21055	-0.35366
C	1.90847	0.17770	-0.11411
C	3.12016	0.85067	0.09372
N	0.74735	-1.90753	-0.51892
P	-0.74060	-1.26142	-0.99010
C	-0.56897	0.40515	-0.33619
C	0.66375	0.89745	-0.06005
C	-1.78056	1.23340	-0.20894
C	-2.83472	1.12515	-1.12718
C	-3.96518	1.91354	-1.00623
C	-4.06710	2.83118	0.04353
C	-3.02744	2.94420	0.97248
C	-1.90413	2.14776	0.84649
O	-1.09672	-1.34365	-2.43972
H	5.27024	-1.72536	-0.18728
H	3.19132	-2.94032	-0.54750
H	3.06805	1.91990	0.27852
H	0.84423	-2.90826	-0.63491
H	0.73924	1.94775	0.21772

H	-2.75058	0.43374	-1.95842
H	-4.76930	1.82839	-1.72779
H	-3.11227	3.64495	1.79488
H	-1.11817	2.21716	1.59035
C	-5.22999	3.64586	0.17141
N	-6.17152	4.30702	0.27540
C	-1.92693	-2.16603	0.02901
C	-3.05613	-2.71550	-0.57772
C	-1.73891	-2.29931	1.40660
C	-3.99141	-3.39891	0.19059
H	-3.18671	-2.60599	-1.64895
C	-2.67669	-2.98045	2.17009
H	-0.85902	-1.87219	1.87731
C	-3.80214	-3.52974	1.56168
H	-4.86839	-3.82863	-0.28143
H	-2.53109	-3.08441	3.23994
H	-4.53410	-4.06162	2.16049
C	5.63766	1.00664	0.30357
C	5.74841	2.11833	-0.75049
H	5.77949	1.69730	-1.75979
H	4.90443	2.81180	-0.70109
H	6.66472	2.69643	-0.59303
C	6.88485	0.12698	0.20409
H	6.88632	-0.66501	0.95924
H	6.97790	-0.33603	-0.78307
H	7.77572	0.74011	0.36767
C	5.60079	1.63565	1.70446
H	5.53400	0.86334	2.47670
H	6.51095	2.21793	1.88161
H	4.74564	2.30666	1.82388

Zero-point correction = 0.420029 (Hartree/Particle); Thermal correction to energy = 0.445957; Thermal correction to enthalpy = 0.446901; Thermal correction to Gibbs free energy = 0.362564; Sum of electronic and zero-point energies = -1491.024374; Sum of electronic and thermal energies = -1490.998446; Sum of electronic and thermal enthalpies = -1490.997502; Sum of electronic and thermal free energies = -1491.081839.

Table C.7 Cartesian coordinates of the optimized geometry of **2f** determined at the PBE0/TZVP level of theory

Atom	x	y	z
C	4.47588	-0.49543	-0.11516
C	4.55087	0.88383	0.10641
C	3.39489	1.62204	0.31345
C	2.14145	1.01628	0.30167
C	2.05466	-0.37183	0.06988
C	3.22937	-1.10406	-0.13277

N	0.98169	1.76709	0.45969
P	-0.51584	1.18392	0.96994
C	-0.42817	-0.48686	0.30598
C	0.77737	-1.03553	0.01956
C	-1.67841	-1.25610	0.18321
C	-2.71804	-1.10476	1.11169
C	-3.88606	-1.83701	0.99485
C	-4.04100	-2.73965	-0.06140
C	-3.01604	-2.89482	-1.00048
C	-1.85444	-2.15464	-0.87810
O	-0.83990	1.26621	2.42738
H	5.50541	1.39434	0.12376
H	3.46976	2.69084	0.48664
H	3.17401	-2.17336	-0.30815
H	1.11904	2.76509	0.55595
H	0.80395	-2.08652	-0.26323
H	-2.59360	-0.42479	1.94740
H	-4.67904	-1.71914	1.72410
H	-3.14145	-3.58368	-1.82771
H	-1.07896	-2.25603	-1.62926
C	-5.24310	-3.49585	-0.18623
N	-6.21661	-4.10928	-0.28810
C	-1.68565	2.14206	-0.01896
C	-2.78685	2.71979	0.61264
C	-1.51424	2.28933	-1.39736
C	-3.71017	3.44529	-0.13109
H	-2.90542	2.59902	1.68402
C	-2.44008	3.01266	-2.13633
H	-0.65624	1.84030	-1.88745
C	-3.53719	3.59020	-1.50293
H	-4.56501	3.89692	0.36070
H	-2.30706	3.12759	-3.20671
H	-4.25970	4.15509	-2.08268
O	5.54569	-1.30193	-0.32098
C	6.84268	-0.72057	-0.29182
C	7.84268	-1.82535	-0.52364
H	7.01082	-0.23888	0.68006
H	6.92205	0.04825	-1.07137
H	8.85712	-1.41944	-0.50995
H	7.76385	-2.58608	0.25638
H	7.67376	-2.30144	-1.49231

Zero-point correction = 0.368617 (Hartree/Particle); Thermal correction to energy = 0.393025; Thermal correction to enthalpy = 0.393970; Thermal correction to Gibbs free energy = 0.312175; Sum of electronic and zero-point energies = -1487.682390; Sum of electronic and thermal energies = -1487.657981; Sum of electronic and thermal enthalpies = -1487.657037; Sum of electronic and thermal free energies = -1487.738831.

Representative excited state geometry

Table C.8 Cartesian coordinates for compound **2f** (S_1)

Atom	x	y	z
C	4.19754	0.83011	0.04258
C	4.43859	-0.30536	-0.75296
C	3.34960	-0.99099	-1.24675
C	2.02893	-0.57501	-0.98158
C	1.76910	0.59205	-0.18219
C	2.87518	1.25433	0.31293
N	0.98402	-1.27177	-1.48236
P	-0.70551	-1.07234	-1.17069
C	-0.75456	0.54008	-0.40889
C	0.43970	1.06313	0.08325
C	-2.03546	1.16742	-0.22284
C	-3.26152	0.49519	-0.47023
C	-4.47749	1.09997	-0.26071
C	-4.54758	2.42475	0.21555
C	-3.34562	3.11750	0.45118
C	-2.13156	2.50968	0.23727
O	-1.47016	-1.33310	-2.42262
H	5.44102	-0.64467	-0.97311
H	3.50091	-1.87627	-1.85654
H	2.75354	2.14216	0.92323
H	1.20261	-2.08660	-2.04452
H	0.38969	1.94048	0.71954
H	-3.25594	-0.52378	-0.83955
H	-5.39269	0.55342	-0.45885
H	-3.38120	4.14509	0.79654
H	-1.23161	3.09014	0.40068
C	-5.79638	3.04886	0.44241
N	-6.82004	3.56105	0.62818
C	-1.02320	-2.31567	0.10097
C	-1.88954	-3.36767	-0.20702
C	-0.43713	-2.24196	1.36922
C	-2.16463	-4.33891	0.74848
H	-2.34218	-3.41212	-1.19192
C	-0.71523	-3.21626	2.31544
H	0.22229	-1.41627	1.61968
C	-1.57745	-4.26674	2.00635
H	-2.84004	-5.15319	0.50835
H	-0.26328	-3.15571	3.29972
H	-1.79397	-5.02592	2.75041
O	5.14428	1.57982	0.58991
C	6.52855	1.25640	0.38195
C	7.34720	2.28195	1.12018

H	6.73510	1.27453	-0.69282
H	6.71378	0.24638	0.76081
H	8.40933	2.06646	0.98366
H	7.14692	3.28556	0.73949
H	7.12518	2.25966	2.18909

Geometries of 2 *meso*-dimer and analogous 1 *meso*-dimer

Table C.9 Cartesian coordinates for compound **2f·2f** (*meso*-dimer)

Atom	x	y	z
P	-1.95724	0.60235	-0.15810
O	-1.13426	0.91794	1.07453
O	-4.86819	-5.45211	-0.32378
N	-1.72792	-0.90711	-0.85743
N	-6.92721	6.54145	1.19270
C	-3.73766	0.57706	0.11224
C	-4.39950	-0.59867	0.11116
H	-5.45545	-0.58653	0.37173
C	-3.84837	-1.89655	-0.20763
C	-2.54204	-2.01925	-0.69556
C	-2.07237	-3.28570	-1.07125
H	-1.07359	-3.37896	-1.48229
C	-2.86947	-4.39809	-0.93597
H	-2.50799	-5.37646	-1.22553
C	-4.17029	-4.28817	-0.42388
C	-4.65455	-3.04354	-0.07520
H	-5.65812	-2.91755	0.30781
C	-4.41821	1.86371	0.36187
C	-5.70140	2.08442	-0.14977
H	-6.17936	1.31735	-0.74569
C	-6.35626	3.28249	0.06722
H	-7.34684	3.44695	-0.33573
C	-5.72281	4.29106	0.79408
C	-4.43772	4.09287	1.29858
H	-3.95194	4.87940	1.86064
C	-3.79259	2.88822	1.08154
H	-2.80197	2.72981	1.49055
C	-6.39194	5.54025	1.01540
C	-1.60300	1.78258	-1.48582
C	-0.61820	2.74784	-1.31084
H	-0.06610	2.78759	-0.38140
C	-0.34559	3.65095	-2.33102
H	0.42602	4.39841	-2.19596
C	-1.06490	3.59304	-3.51740
H	-0.85633	4.29959	-4.31093
C	-2.05424	2.62939	-3.69172

H	-2.61274	2.58634	-4.61790
C	-2.32146	1.72118	-2.67885
H	-3.08473	0.96234	-2.81326
C	-6.18694	-5.38880	0.20600
H	-6.80431	-4.74129	-0.42516
H	-6.15489	-4.95833	1.21243
C	-6.73651	-6.79556	0.23574
H	-7.74918	-6.78877	0.63901
H	-6.76584	-7.21498	-0.76966
H	-6.11603	-7.43412	0.86410
H	-0.75384	-1.07946	-1.13391
P	1.95156	-0.64866	0.19274
O	1.08688	-0.96110	-1.01172
O	4.69506	5.48289	0.53051
N	1.68726	0.83535	0.93440
N	7.06869	-6.35013	-1.57736
C	3.71838	-0.55160	-0.13926
C	4.34473	0.64290	-0.10761
H	5.39135	0.67402	-0.40224
C	3.76786	1.90828	0.28504
C	2.47046	1.97330	0.80554
C	1.97625	3.20980	1.24574
H	0.98434	3.25755	1.68084
C	2.74001	4.34850	1.13996
H	2.35923	5.30349	1.47902
C	4.03159	4.29657	0.59628
C	4.54060	3.08158	0.18481
H	5.53862	2.99783	-0.22352
C	4.43069	-1.80350	-0.46702
C	5.73087	-2.00838	0.00685
H	6.19822	-1.25657	0.63004
C	6.41634	-3.17373	-0.28147
H	7.41988	-3.32672	0.09277
C	5.79805	-4.16492	-1.04428
C	4.49709	-3.98263	-1.51265
H	4.02348	-4.75542	-2.10340
C	3.82065	-2.81055	-1.22348
H	2.81680	-2.66345	-1.60302
C	6.50213	-5.37893	-1.34047
C	1.69613	-1.88524	1.49285
C	0.64469	-2.78840	1.38896
H	-0.01285	-2.74941	0.53080
C	0.44143	-3.73291	2.38765
H	-0.38232	-4.43095	2.30814
C	1.29730	-3.78013	3.48005
H	1.14343	-4.52010	4.25539

C	2.35300	-2.87906	3.58311
H	3.01798	-2.91732	4.43630
C	2.55094	-1.92835	2.59314
H	3.36803	-1.21946	2.67405
C	6.00897	5.47632	-0.01461
H	6.65036	4.82286	0.58592
H	5.97823	5.08342	-1.03618
C	6.51872	6.89823	0.00350
H	7.52896	6.93518	-0.40423
H	6.54128	7.28223	1.02310
H	5.87721	7.54089	-0.59909
H	0.70937	0.98002	1.21499

Table C.10 Cartesian coordinates for compound $2\mathbf{f}^{\bullet}\cdot 2\mathbf{f}^{\bullet}$ (*meso*-dimer for -OPh analogue)

Atom	x	y	z
P	1.92141	0.79131	-0.26147
O	0.78543	1.51236	-0.92423
O	6.53956	-3.99151	-1.19988
N	2.02262	-0.82536	-0.62475
N	4.97709	8.03803	0.16496
C	3.59102	1.36451	-0.52551
C	4.57382	0.46252	-0.73510
H	5.58336	0.84492	-0.86408
C	4.43734	-0.97249	-0.81836
C	3.18131	-1.58317	-0.74275
C	3.09026	-2.97766	-0.82535
H	2.11643	-3.44875	-0.76712
C	4.22370	-3.74153	-0.97276
H	4.15972	-4.82045	-1.03252
C	5.48901	-3.14105	-1.05234
C	5.58959	-1.76691	-0.97746
H	6.54735	-1.26819	-1.03595
C	3.87197	2.80945	-0.37778
C	5.03179	3.22763	0.28458
H	5.69956	2.49146	0.71451
C	5.32555	4.57143	0.42127
H	6.22247	4.88754	0.93716
C	4.44618	5.52323	-0.09631
C	3.27888	5.12301	-0.74537
H	2.60112	5.86640	-1.14344
C	2.99450	3.77540	-0.88166
H	2.09196	3.46511	-1.39128
C	4.74073	6.91971	0.04861
C	7.83932	-3.42380	-1.31227
H	8.06387	-2.84264	-0.41180
H	7.86840	-2.74857	-2.17381

C	8.82206	-4.55834	-1.48203
H	9.83191	-4.16050	-1.58264
H	8.79387	-5.22113	-0.61745
H	8.58521	-5.13637	-2.37497
H	1.13240	-1.32490	-0.52414
P	-1.83870	-0.83501	-0.24159
O	-0.58006	-1.54000	0.16537
O	-6.03526	4.24836	0.94534
N	-1.79480	0.81008	-0.03092
N	-4.96926	-7.90305	1.34215
C	-3.39028	-1.28890	0.51650
C	-4.28646	-0.31809	0.79650
H	-5.24232	-0.62508	1.21435
C	-4.11342	1.10510	0.61877
C	-2.88448	1.63685	0.21450
C	-2.74464	3.02402	0.08792
H	-1.78912	3.43301	-0.21776
C	-3.81060	3.85580	0.33656
H	-3.71118	4.92879	0.23273
C	-5.05144	3.33451	0.73214
C	-5.19474	1.96973	0.87834
H	-6.13228	1.53222	1.19349
C	-3.71128	-2.72292	0.68277
C	-4.99895	-3.18586	0.38912
H	-5.74136	-2.49828	0.00330
C	-5.33121	-4.51660	0.56144
H	-6.32798	-4.86844	0.33091
C	-4.36480	-5.41187	1.02114
C	-3.07251	-4.96965	1.30158
H	-2.32861	-5.67016	1.65720
C	-2.74907	-3.63508	1.12870
H	-1.74774	-3.29074	1.35074
C	-4.70057	-6.79521	1.19888
C	-7.30470	3.76745	1.37118
H	-7.69766	3.06517	0.62875
H	-7.19240	3.23607	2.32210
C	-8.21923	4.96014	1.52189
H	-9.20286	4.63183	1.85789
H	-8.33183	5.47687	0.56903
H	-7.81697	5.65942	2.25452
H	-0.90390	1.25228	-0.29356
O	1.65012	0.93158	1.34869
O	-2.03326	-1.14197	-1.84182
C	2.42198	0.19621	2.24001
C	3.51657	0.80032	2.83895
C	2.06499	-1.11320	2.52760

C	4.27398	0.07137	3.74738
H	3.75515	1.82865	2.59475
C	2.83279	-1.83172	3.43459
H	1.19713	-1.54270	2.04046
C	3.93610	-1.24381	4.04341
H	5.12751	0.53465	4.22565
H	2.56580	-2.85461	3.66811
H	4.52892	-1.80929	4.75059
C	-3.06789	-0.51671	-2.52823
C	-4.25761	-1.20300	-2.71875
C	-2.88728	0.76802	-3.01906
C	-5.29228	-0.58260	-3.40703
H	-4.35624	-2.20940	-2.33039
C	-3.93080	1.38009	-3.70142
H	-1.94065	1.27030	-2.86233
C	-5.13323	0.70995	-3.89317
H	-6.22390	-1.11125	-3.56359
H	-3.80062	2.38351	-4.08590
H	-5.94271	1.19250	-4.42543

4. Photophysical Properties in Different Solvents

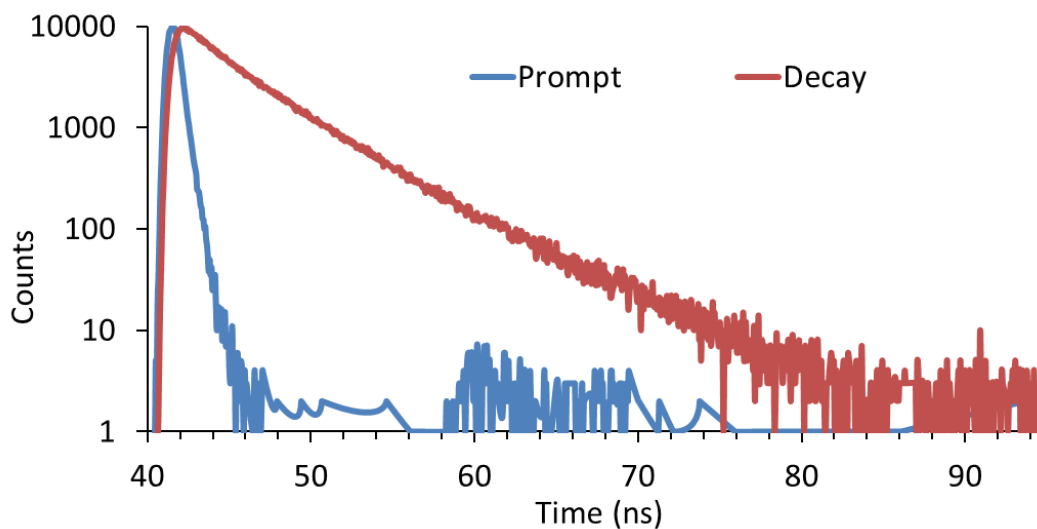


Figure C.6 Fluorescence decay curve of **2d** vs Ludox Prompt sample.

Solvent effects on fluorescence

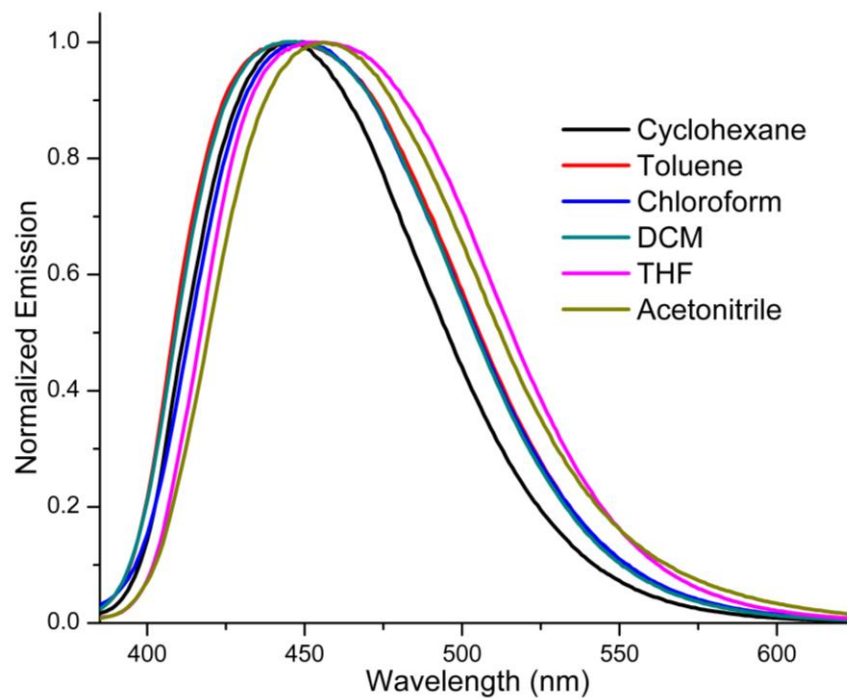
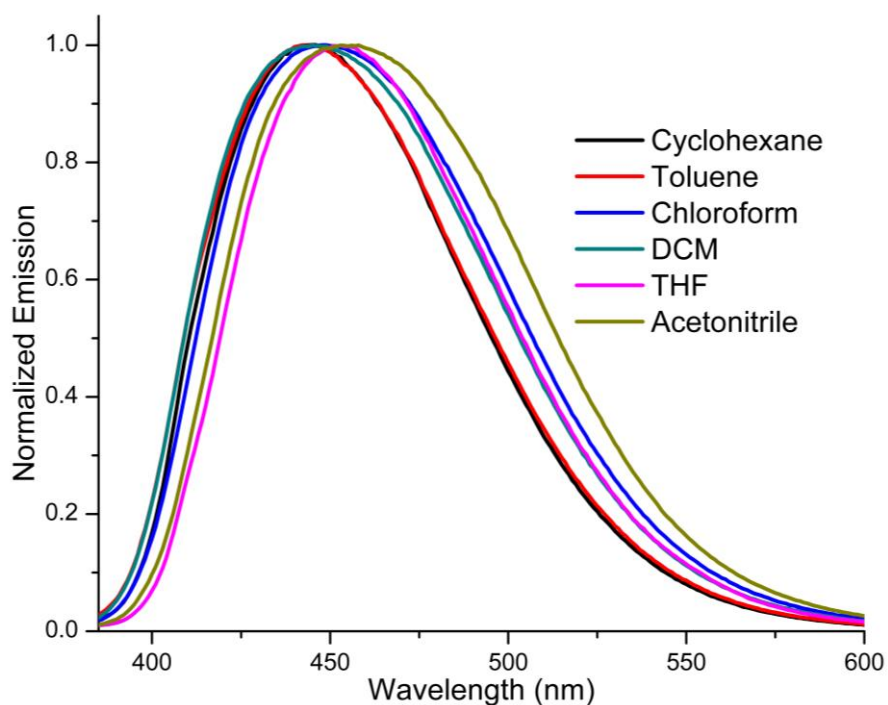


Figure C.7 Emission spectra of **2a** in various solvents.

Table C.11 Photophysical properties of **2a** in various solvents

	Cyclohexane	Toluene	Chloroform	DCM	THF	Acetonitrile
λ_{abs}	353	351	348	349	358	350
λ_{em}	445	446	452	448	456	456
Stokes Shift (nm)	92	95	104	99	98	106

**Figure C.8** Emission spectra of **2b** in various solvents.**Table C.12** Photophysical properties of **2b** in various solvents

	Cyclohexane	Toluene	Chloroform	DCM	THF	Acetonitrile
λ_{abs}	346	346	343	344	358	345
λ_{em}	442	442	447	445	453	458
Stokes Shift (nm)	96	96	104	101	95	113

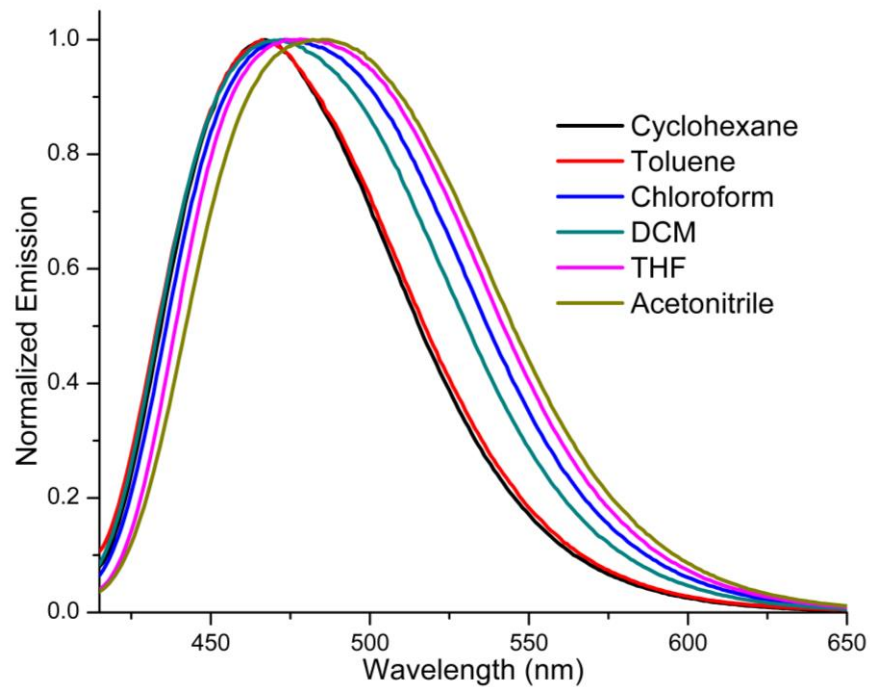


Figure C.9 Emission spectra of **2c** in various solvents.

Table C.13 Photophysical properties of **2c** in various solvents

	Cyclohexane	Toluene	Chloroform	DCM	THF	Acetonitrile
λ_{abs}	366	365	360	365	367	363
λ_{em}	467	466	474	472	480	486
Stokes Shift (nm)	101	101	114	107	113	123

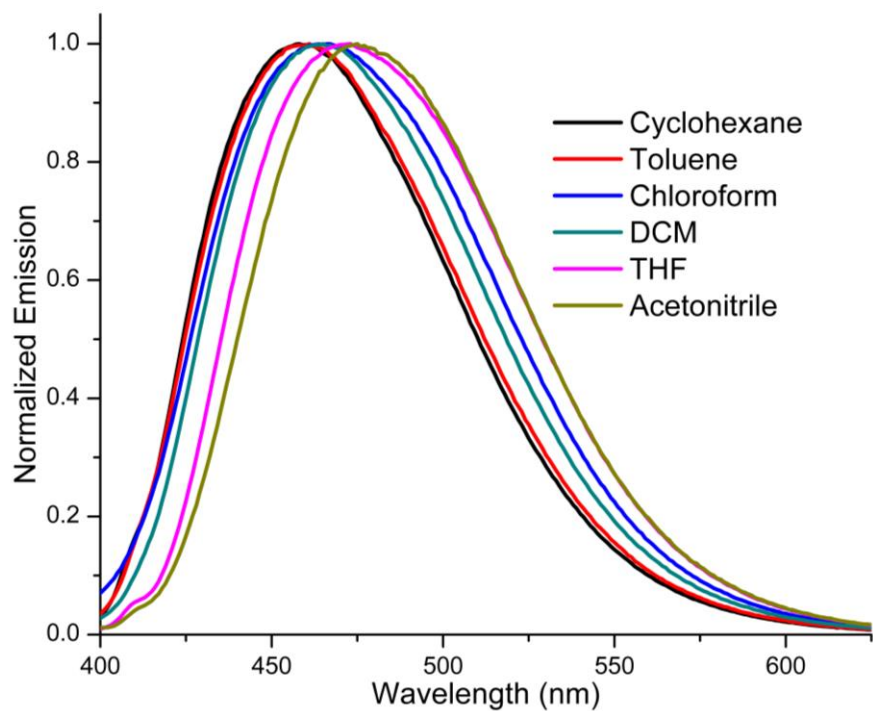


Figure C.10 Emission spectra of **2d** in various solvents.

Table C.14 Photophysical properties of **2d** in various solvents

	Cyclohexane	Toluene	Chloroform	DCM	THF	Acetonitrile
λ_{abs}	355	353	352	365	361	357
λ_{em}	458	461	467	465	473	475
Stokes Shift (nm)	103	108	115	100	112	118

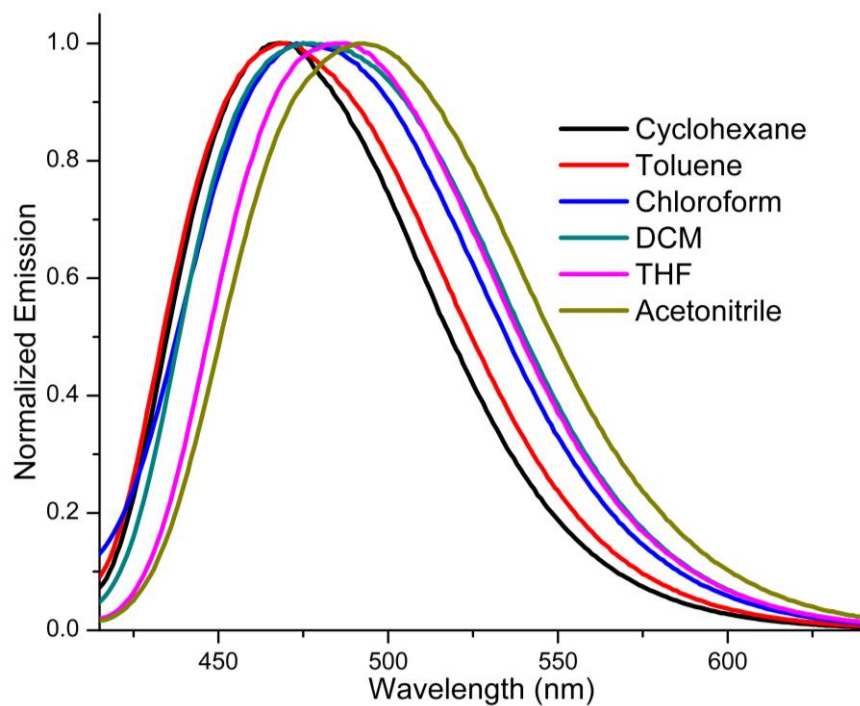


Figure C.11 Emission spectra of **2e** in various solvents.

Table C.15 Photophysical properties of **2e** in various solvents

	Cyclohexane	Toluene	Chloroform	DCM	THF	Acetonitrile
λ_{abs}	365	361	360	362	368	365
λ_{em}	467	469	473	478	488	493
Stokes Shift (nm)	102	108	113	116	120	128

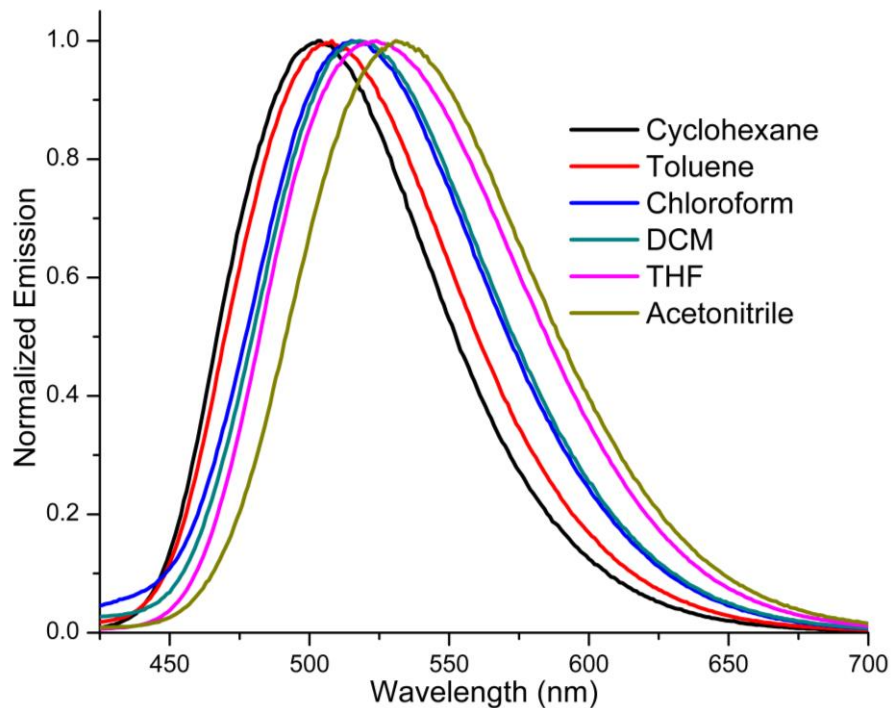


Figure C.12 Emission spectra of **2f** in various solvents.

Table C.16 Photophysical properties of **2f** in various solvents

	Cyclohexane	Toluene	Chloroform	DCM	THF	Acetonitrile
λ_{abs}	386	384	381	386	387	386
λ_{em}	504	508	515	518	524	531
Stokes Shift (nm)	118	124	134	132	137	145

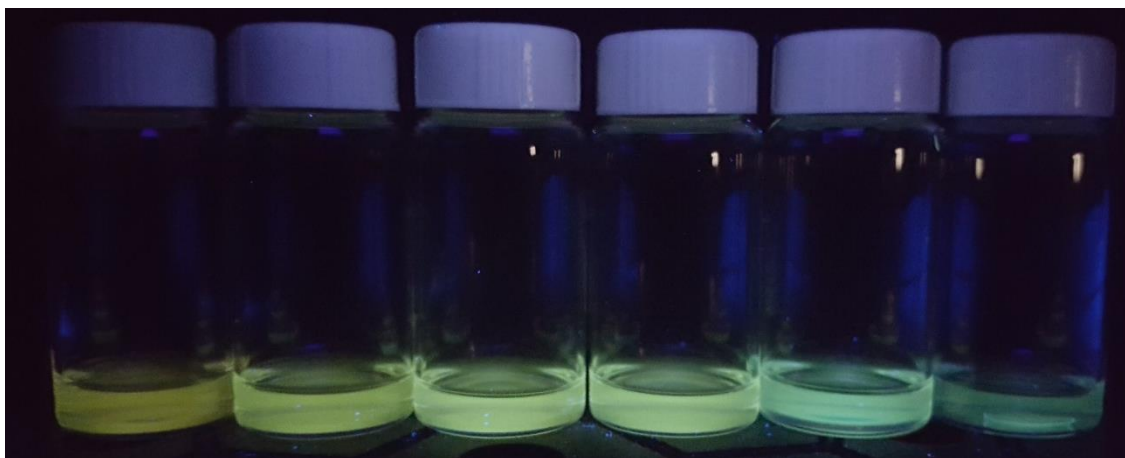


Figure C.13 Fluorescent image of **2f** in Acetonitrile, THF, DCM, Chloroform, Toluene, Cyclohexane (left to right).

5. Experimental and Computational Examination of the Dimer **Solution-state studies of dimer strength**

General procedure for variable concentration (VC) NMR experiments. CDCl_3 was added in a 1:1 ratio to H_2O , shaken vigorously, then allowed to separate. The organic phase was then separated and used to prepare *ca.* 10 mM solutions of heterocycle **2**. These solutions were then diluted through addition of known amounts of the H_2O -saturated CDCl_3 solvent, with ^{31}P NMR spectra being collected after each addition. The ^{31}P NMR spectra were chosen over those of ^1H NMR for these experiments since they give comparable results to ^1H NMR signals and the ^1H NMR signals become impossible to track at lower concentrations due to complex splitting of multiple signals by the phosphorus center. The chemical shift of the phosphorus signal was tracked and fitted to generate the dimerization values.¹⁰

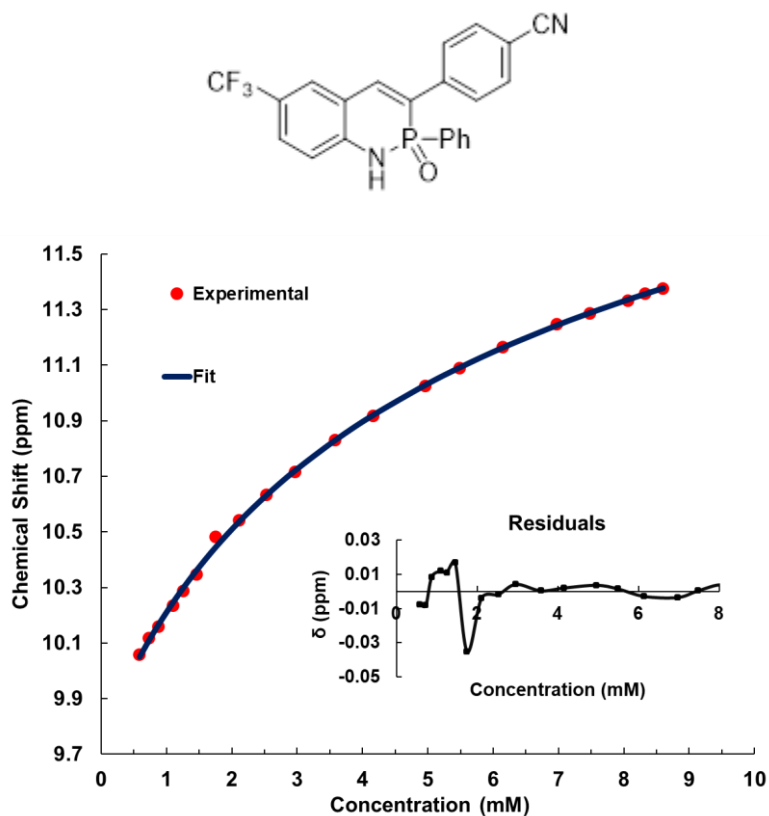


Figure C.14 Binding isotherm (red), fit (blue), and residuals (inset) of VC NMR of **2b**.

Table C.17 Experimental and fitting data for VC NMR experiment of **2b**

Concentration (mM)	Experimental δ (ppm)	Fit δ (ppm)
8.60	11.3755	11.37636588
8.32	11.3583	11.35553759
8.06	11.3315	11.33535491
7.48	11.2871	11.28750165
6.97	11.2465	11.24300097
6.14	11.1654	11.16255996
5.49	11.09	11.09160143
4.96	11.0247	11.02836421
4.16	10.918	10.92008376
3.58	10.8299	10.83033275
2.96	10.7164	10.72063772
2.53	10.6342	10.6324564
2.11	10.5421	10.53825939
1.76	10.4816	10.44649514
1.46	10.3465	10.36343269
1.25	10.2875	10.29857999
1.10	10.2345	10.24644727
0.877	10.1592	10.16767483
0.731	10.1191	10.11087501
0.585	10.0577	10.05013847

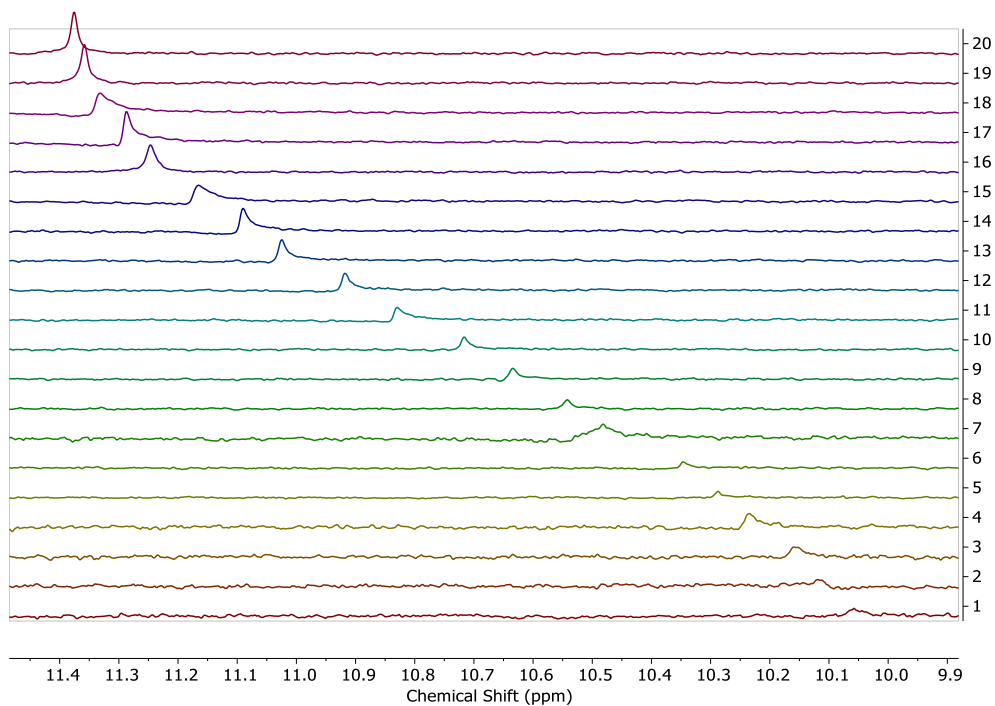


Figure C.15 Representative ^{31}P NMR spectra for VC NMR of **2b**.

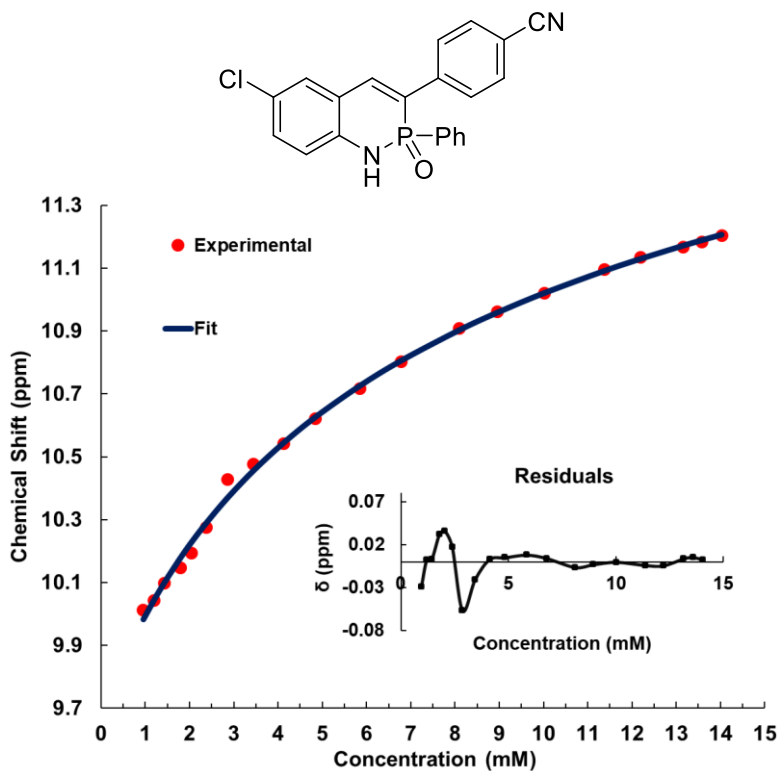


Figure C.16 Binding isotherm (red), fit (blue), and residuals (inset) of VC NMR of **2c**.

Table C.18 Experimental and fitting data for VC NMR experiment of **2c**

Concentration (mM)	Experimental δ (ppm)	Fit δ (ppm)
14.0	11.2039	11.2064793
13.6	11.1831	11.1885475
13.2	11.1672	11.1711442
12.2	11.1341	11.1297717
11.4	11.0951	11.0911563
10.0	11.0212	11.0209934
8.96	10.9617	10.9586984
8.09	10.9091	10.9028468
6.79	10.8023	10.8064342
5.84	10.7176	10.7257245
4.84	10.6209	10.6260187
4.12	10.5419	10.5449533
3.45	10.4777	10.4573812
2.86	10.4277	10.3710209
2.39	10.2748	10.2918817
2.04	10.1932	10.2294034
1.79	10.1464	10.1787126
1.43	10.0982	10.1012771
1.19	10.0425	10.0447712
0.954	10.0123	9.98368372

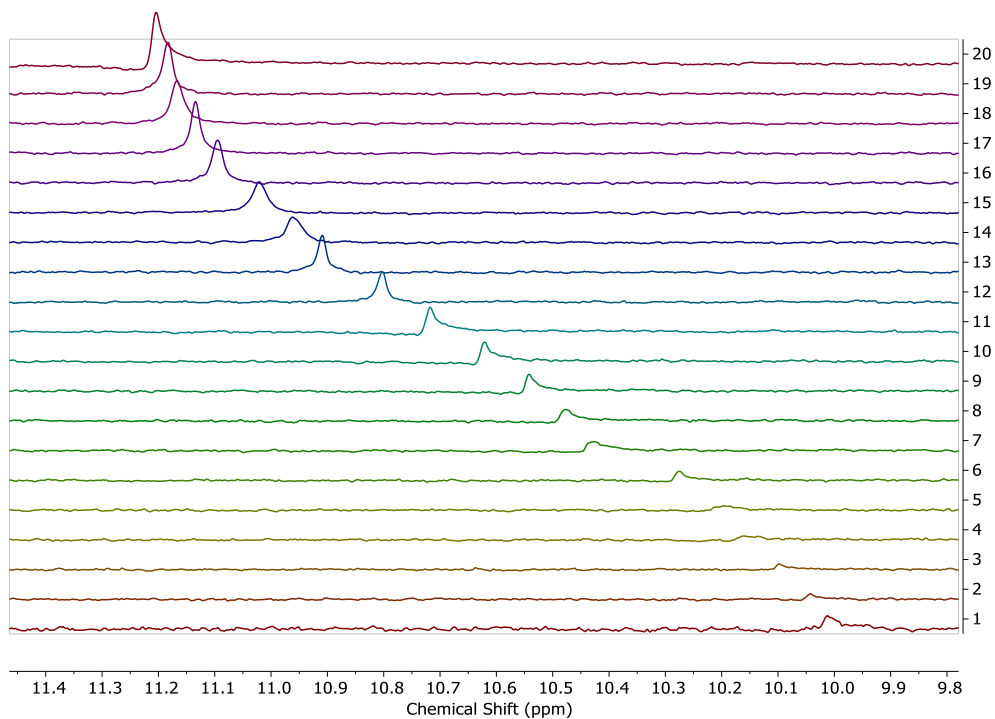


Figure C.17 Representative ^{31}P NMR spectra for VC NMR of **2c**.

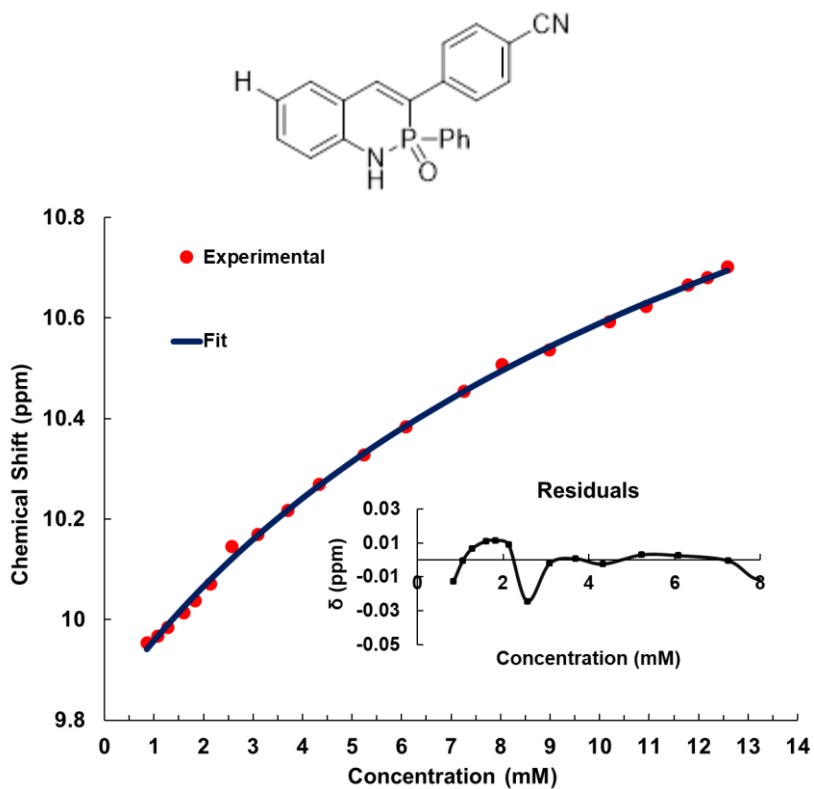


Figure C.18 Binding isotherm (red), fit (blue), and residuals (inset) of VC NMR of **2d**.

Table C.19 Experimental and fitting data for VC NMR of **2d**

Concentration (mM)	Experimental δ (ppm)	Fit δ (ppm)
12.6	10.7014	10.694546
12.2	10.6799	10.679281
11.8	10.6658	10.664594
10.9	10.6234	10.630185
10.2	10.5926	10.598709
9.00	10.5362	10.543093
8.03	10.5069	10.495405
7.25	10.4546	10.453992
6.09	10.3830	10.385454
5.24	10.3280	10.330913
4.34	10.2696	10.267033
3.70	10.2173	10.217883
3.09	10.1697	10.167531
2.57	10.1452	10.120592
2.14	10.0711	10.079881
1.83	10.0379	10.049254
1.60	10.0143	10.025362
1.28	9.9839	9.9904767
1.07	9.9667	9.9662182
0.856	9.9540	9.9410965

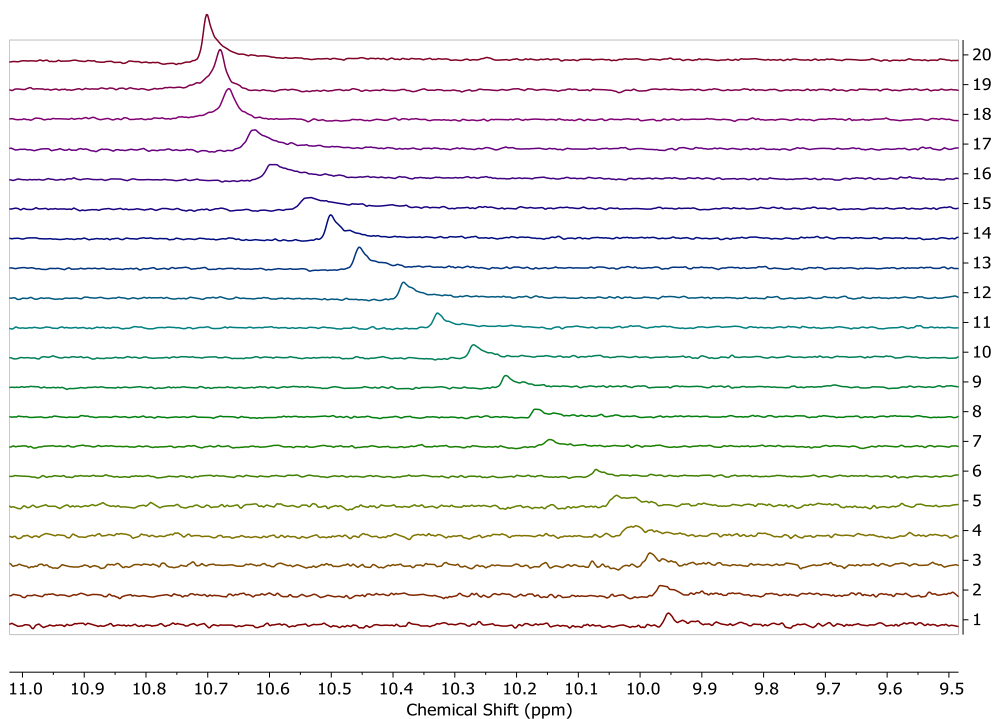


Figure C.19 Representative ^{31}P NMR spectra for VC NMR of **2d**.

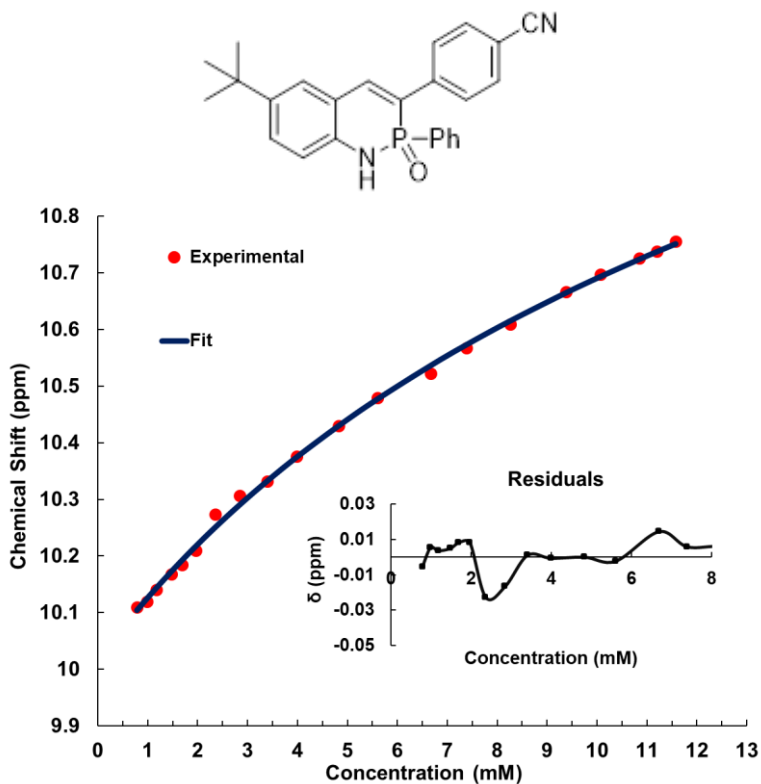


Figure C.20 Binding isotherm (red), fit (blue), and residuals (inset) of VC NMR of **2e**.

Table C.20 Experimental and fitting data for VC NMR of **2e**

Concentration (mM)	Experimental δ (ppm)	Fit δ (ppm)
11.6	10.7552	10.75070613
11.2	10.7379	10.73691784
10.9	10.7255	10.72367435
10.1	10.6966	10.69273486
9.39	10.6656	10.66454316
8.27	10.609	10.61499453
7.39	10.5668	10.57278564
6.68	10.5217	10.53634355
5.60	10.4786	10.47648406
4.83	10.4291	10.42926445
3.99	10.3749	10.37444554
3.41	10.3314	10.33263873
2.85	10.3066	10.29015441
2.36	10.2735	10.25087549
1.97	10.2087	10.21706939
1.69	10.1835	10.19180097
1.48	10.1671	10.17218912
1.18	10.1399	10.14371351
0.985	10.1185	10.12402601
0.788	10.109	10.1037383

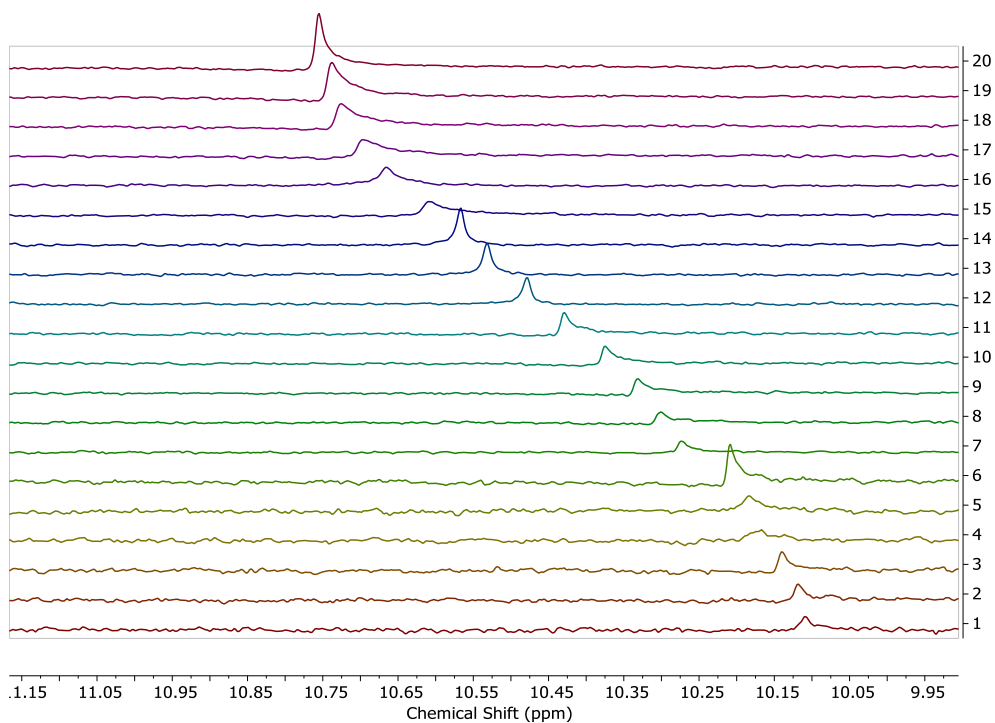


Figure C.21 Representative ^{31}P NMR spectra for VC NMR of **2e**.

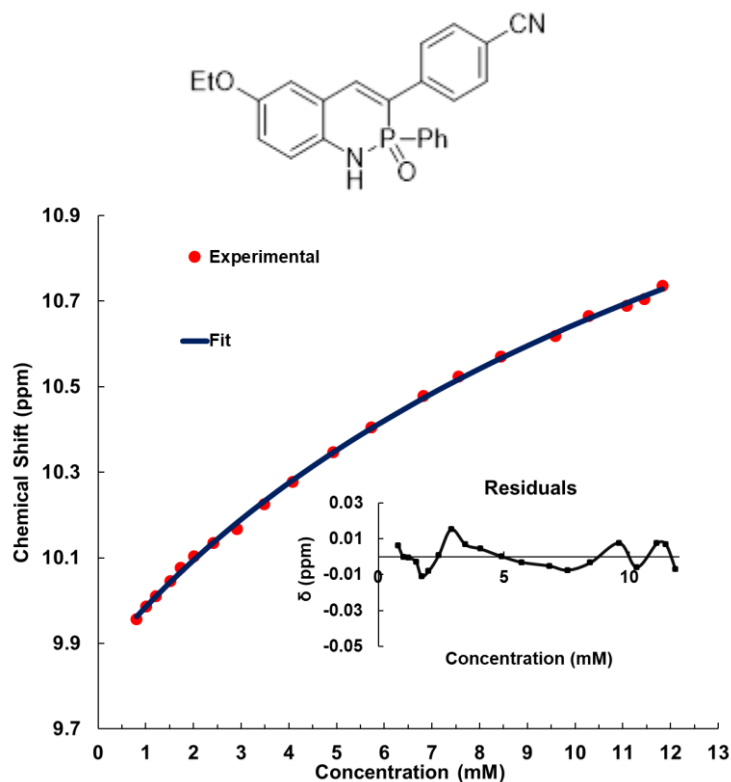


Figure C.22 Binding isotherm (red), fit (blue), and residuals (inset) of VC NMR of **2f**.

Table C.21 Experimental and fitting data for VC NMR of **2f**

Concentration (mM)	Experimental δ (ppm)	Fit δ (ppm)
11.8	10.7356	10.7285531
11.4	10.7052	10.712116
11.0	10.689	10.6963319
10.3	10.6654	10.6594712
9.59	10.6183	10.6259015
8.45	10.5703	10.5669423
7.55	10.5243	10.51676
6.83	10.4787	10.4734671
5.72	10.4056	10.4024241
4.93	10.3464	10.3464462
4.08	10.2772	10.2815335
3.48	10.2254	10.2320847
2.91	10.1666	10.1818864
2.41	10.1348	10.1355237
2.01	10.1038	10.0956594
1.72	10.0768	10.0658868
1.51	10.0456	10.0427937
1.21	10.01	10.0092865
1.01	9.9864	9.98613666
0.805	9.9561	9.96229545

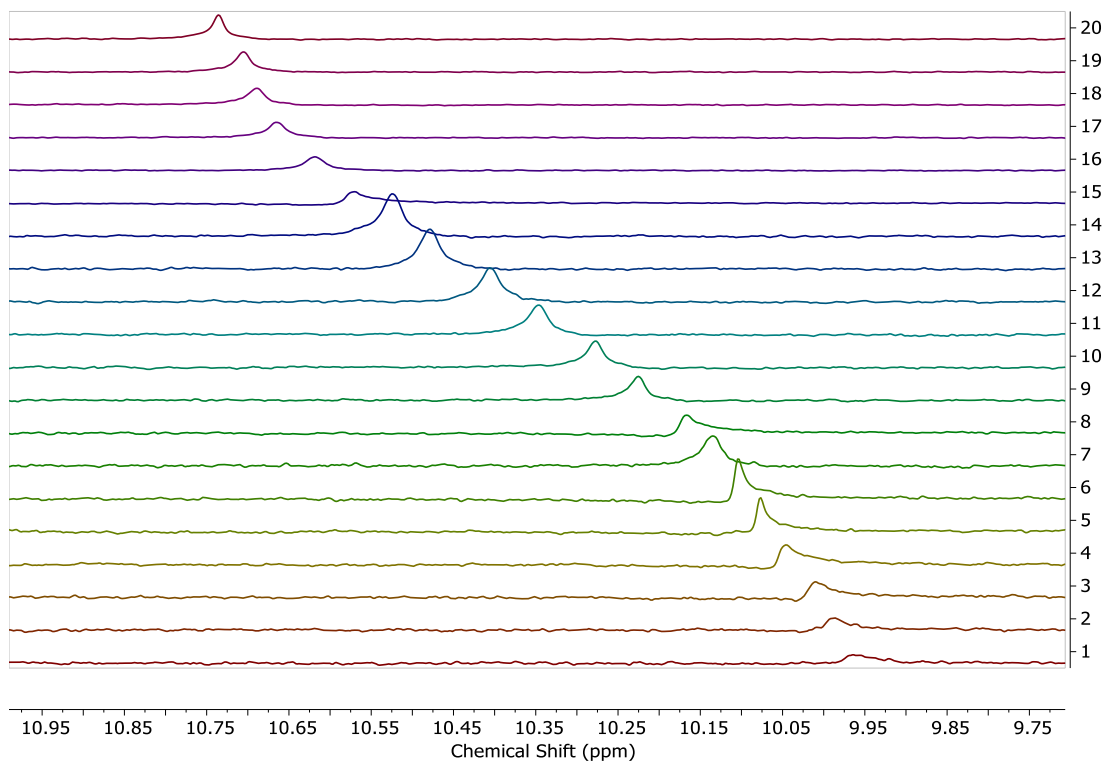


Figure C.23 Representative ^{31}P NMR spectra for VC NMR experiment of **2f**.

Computational studies on dimer interactions

The geometries for dimeric complexes of **2f** and its -OPh counterpart were fully optimized without symmetry constraint by using the functional M06-2X¹¹ (accounting for the contributions of H-bond/dispersion forces) and TZVP basis set as implemented in Gaussian 09. The PCM solvation model was used to account for the effects of the chloroform environment. All of the optimized structures were confirmed by frequency calculations to be minima using the same level of theory. The solution-phase optimized geometries were used in the following calculations. The natural bond order (NBO) analyses were carried out using NBO 3.1 embedded in Gaussian 09 package. The NCI plot were performed by using the Multiwfn program.¹²

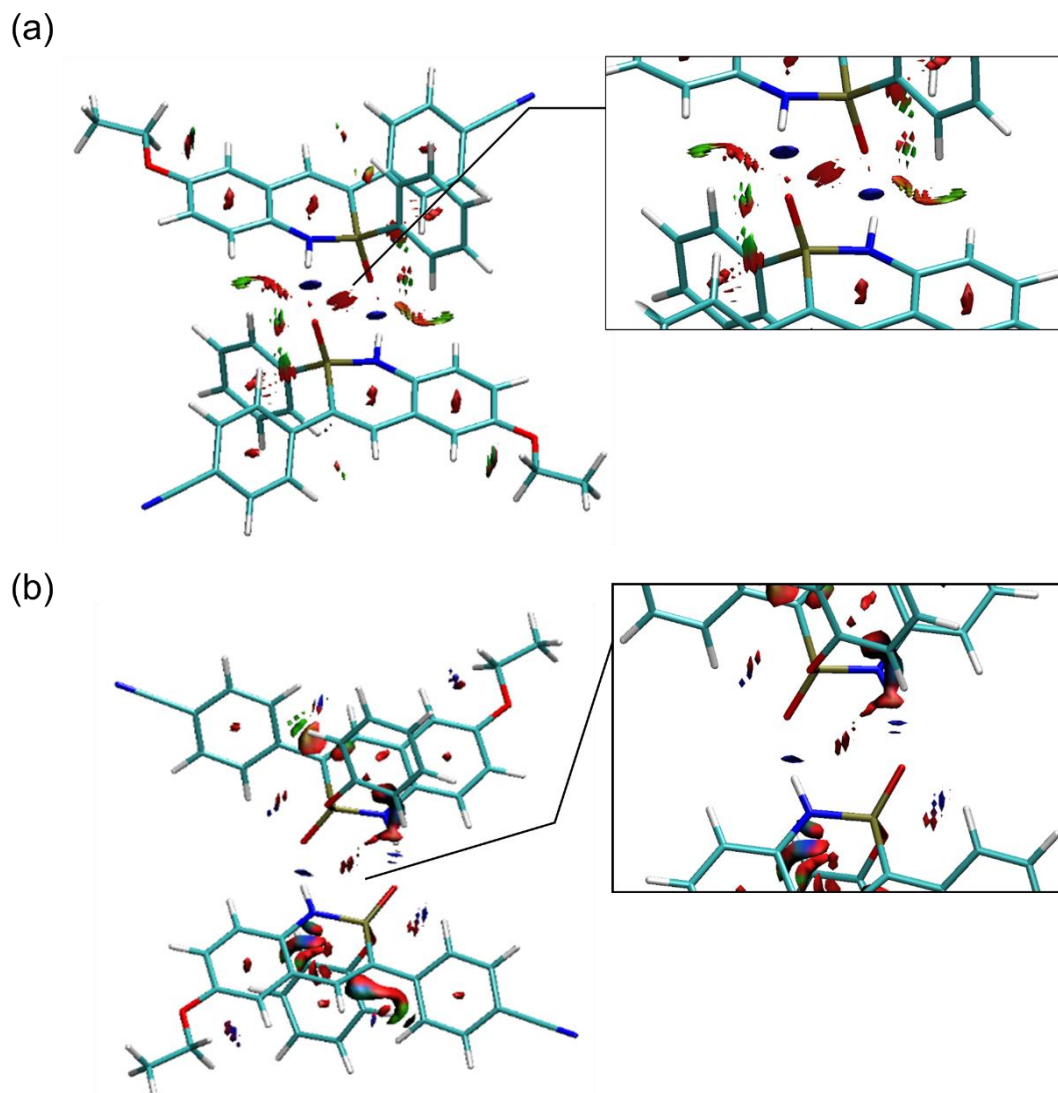


Figure C.24 The NCI plots for a) **2f** and b) its -OPh analogue *meso*-dimeric motifs at the PCM(CHCl₃)-M06-2X/TZVP equilibrium geometries. NCI regions are represented as solid surfaces and blue–green–red scaling from $-0.02 < \text{sign}(\lambda_2)\rho(r) < 0$ (in a.u.), where red surface indicates strong repulsion, blue surface strong attraction and green surface relatively weak interactions. Isosurface cutoff for NCI = 0.5.

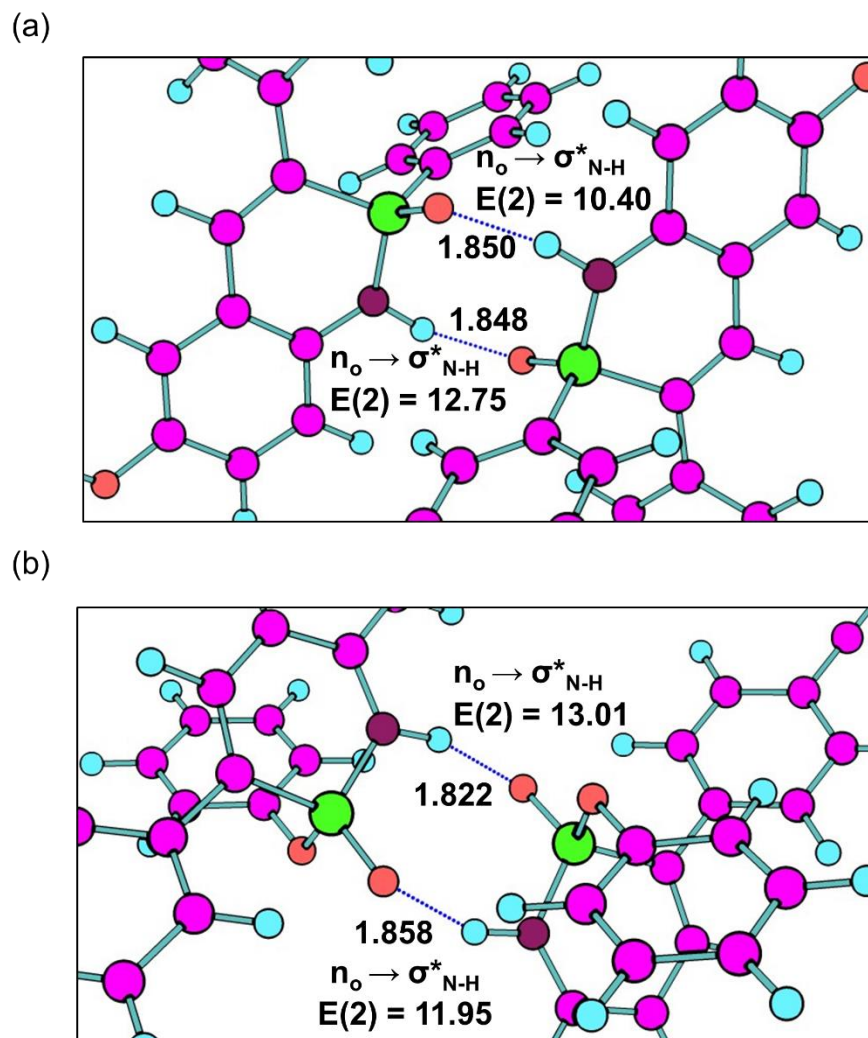


Figure C.25 The NBO charge transfer stabilization energy [second-order perturbation energies $E(2)$, in kcal/mol] for the indicated H-bond interactions in a) **2f** and b) its -OPh analogue at PCM(CHCl_3)-M06-2X/TZVP equilibrium geometries of the *meso*-dimeric motifs. The indicated H-bond interactions shown by the broken line, and H-bond distances in Å.

7. Copies of NMR Spectra

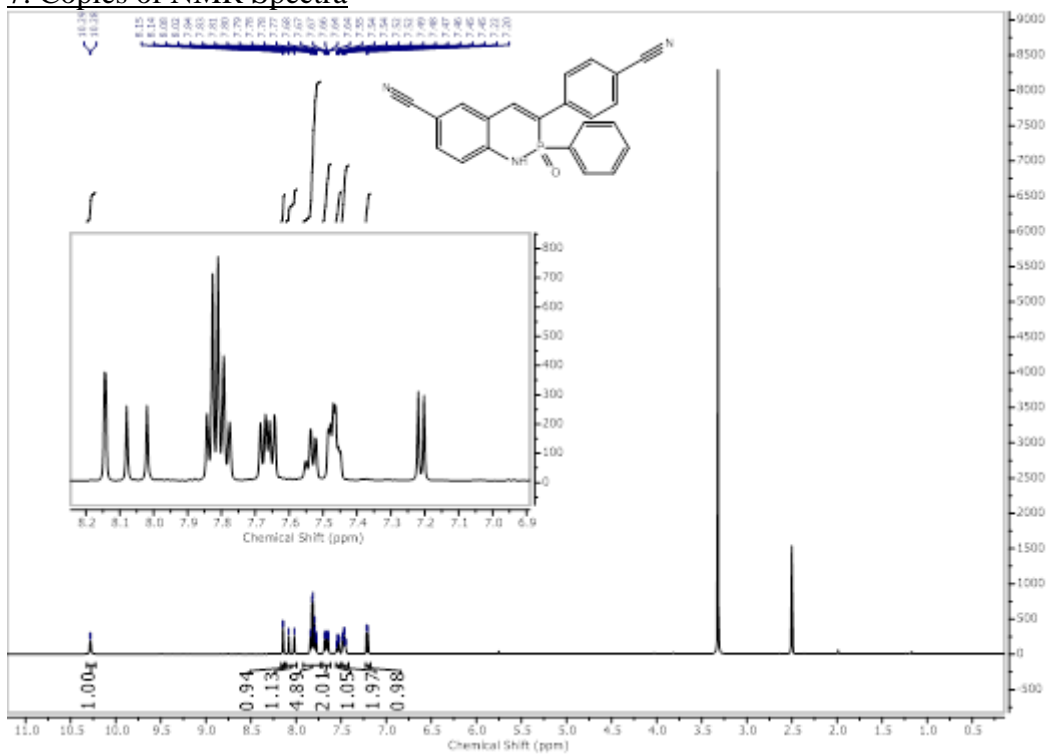


Figure C.26 ¹H NMR spectrum of **2a** in DMSO-d₆.

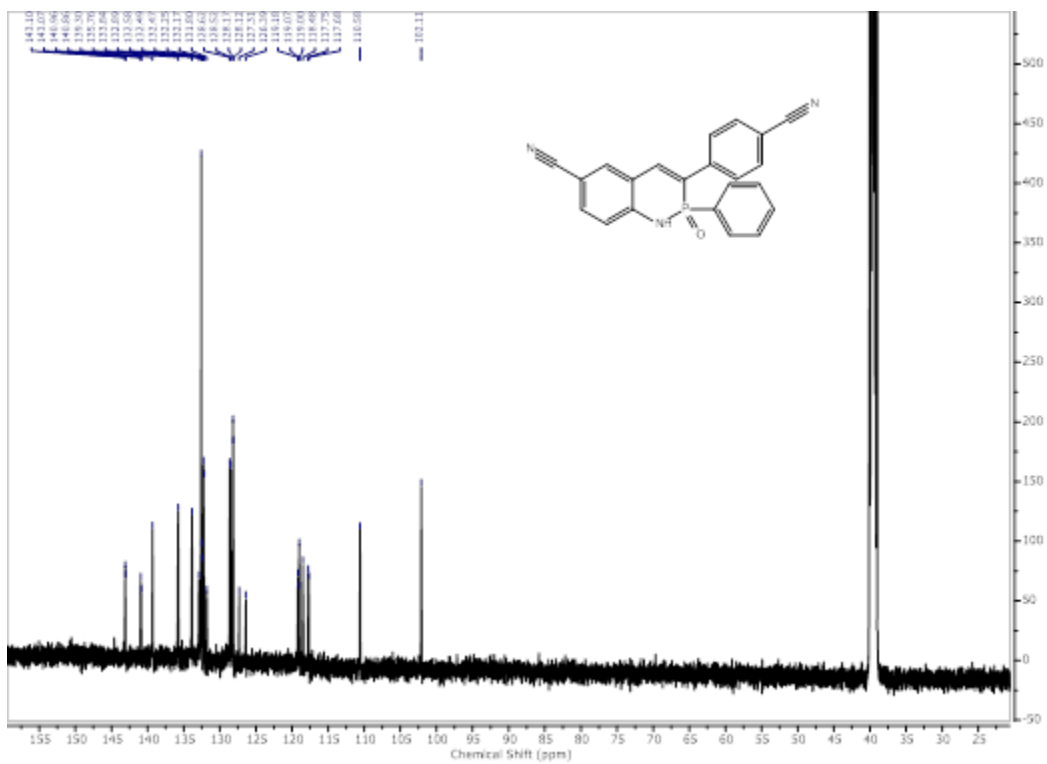


Figure C.27 ¹³C NMR spectrum of **2a** in DMSO-d₆.

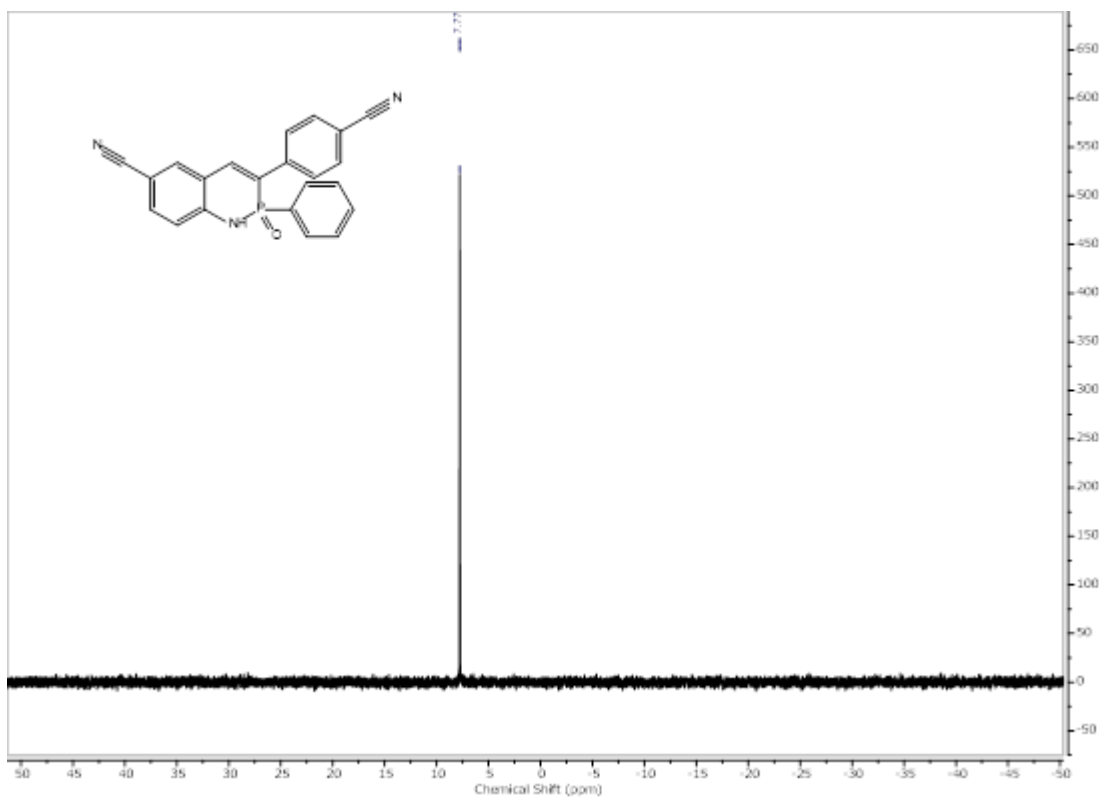


Figure C.28 ^{31}P NMR spectrum of **2a** in DMSO-d_6 .

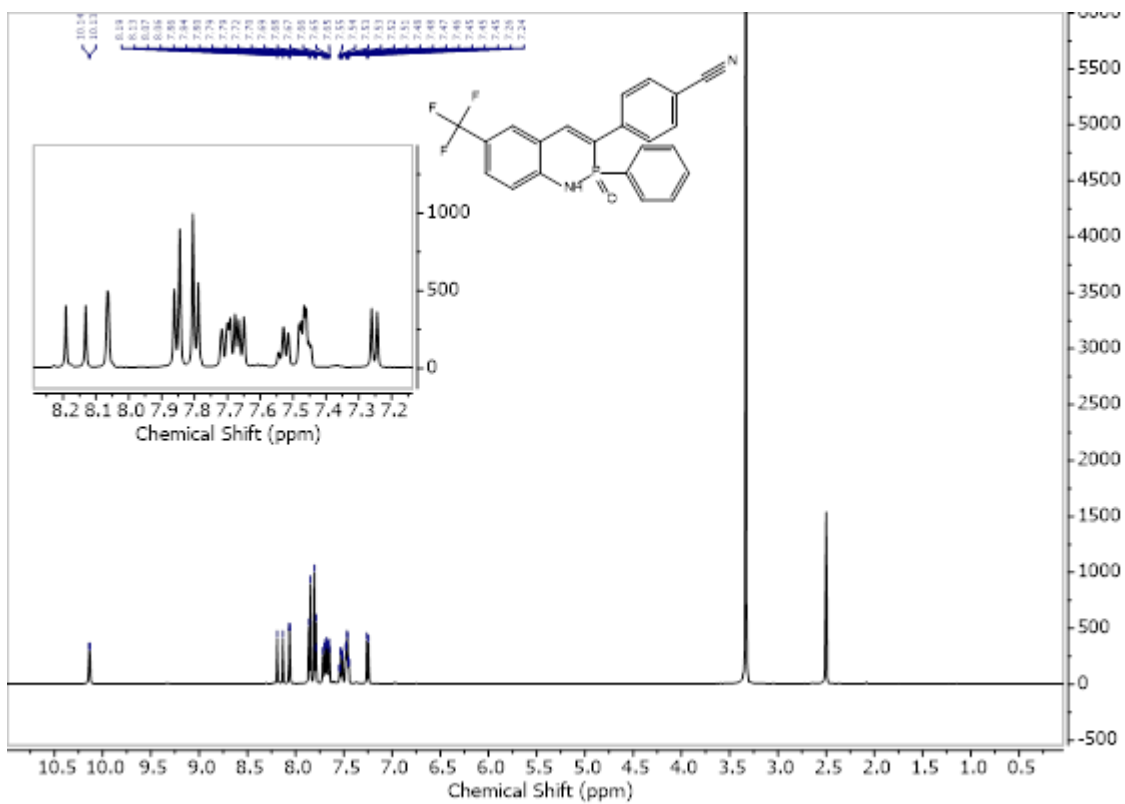


Figure C.29 ^1H NMR spectrum of **2b** in DMSO-d_6 .

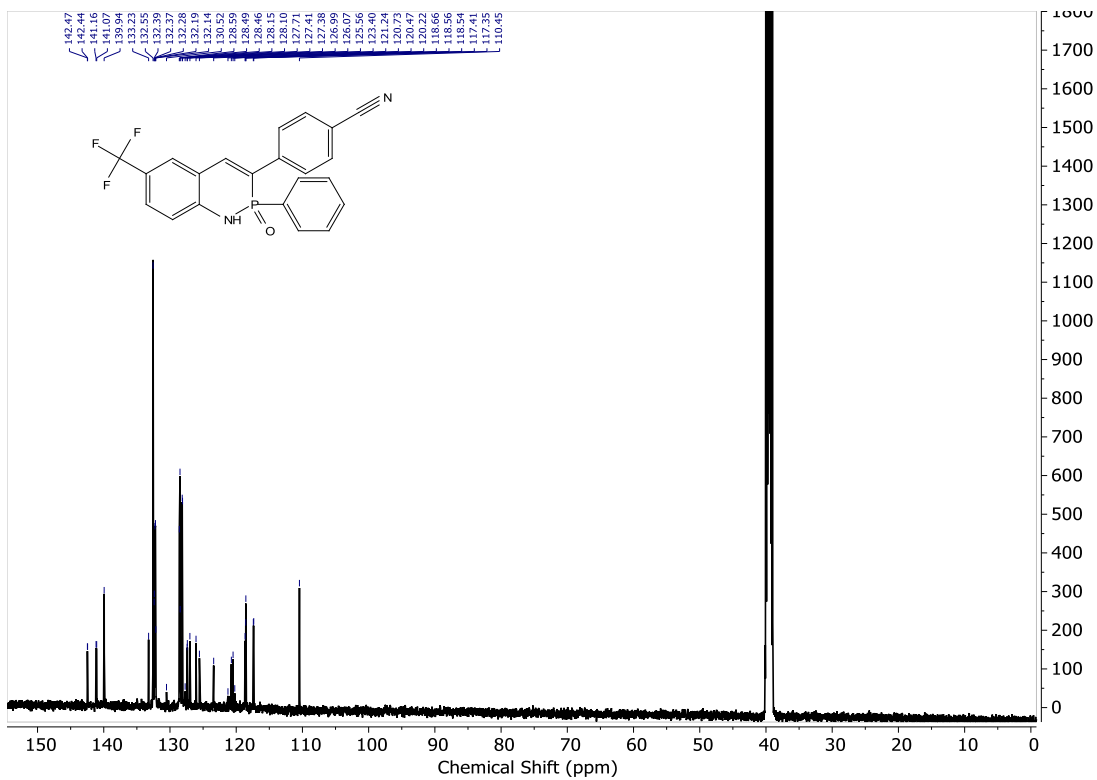


Figure C.30 ^{13}C NMR spectrum of **2b** in DMSO-d_6 .

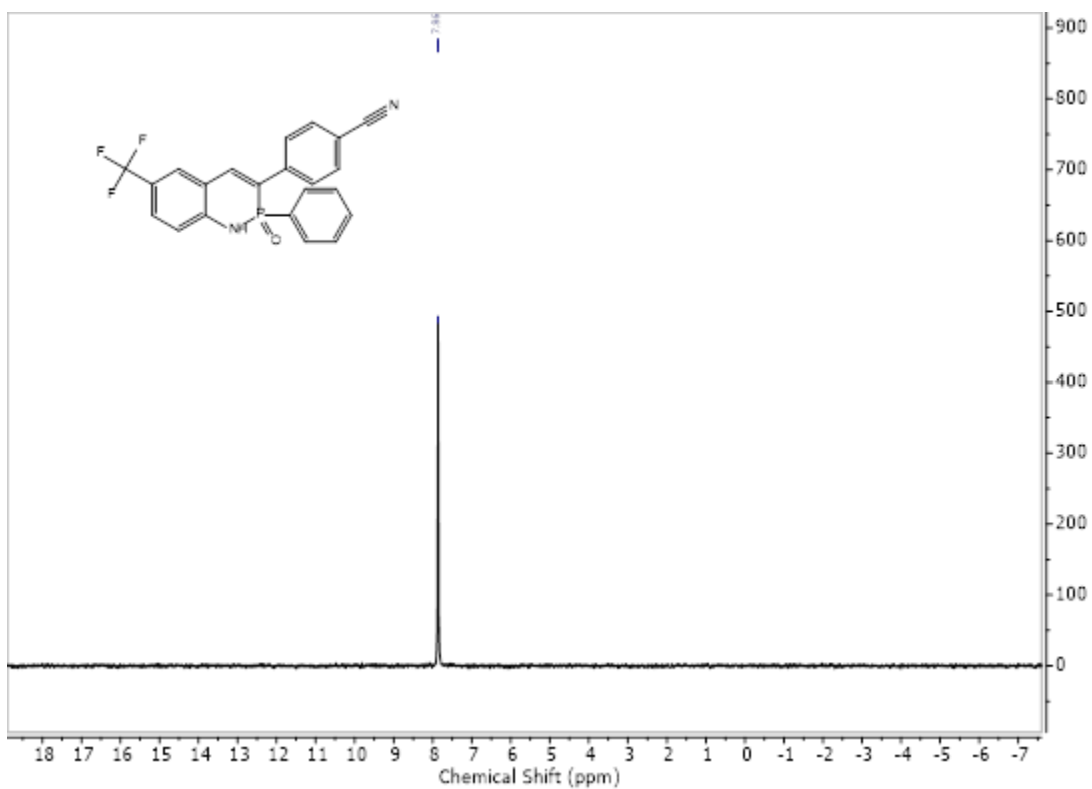


Figure C.31 ^{31}P NMR spectrum of **2b** in DMSO-d_6 .

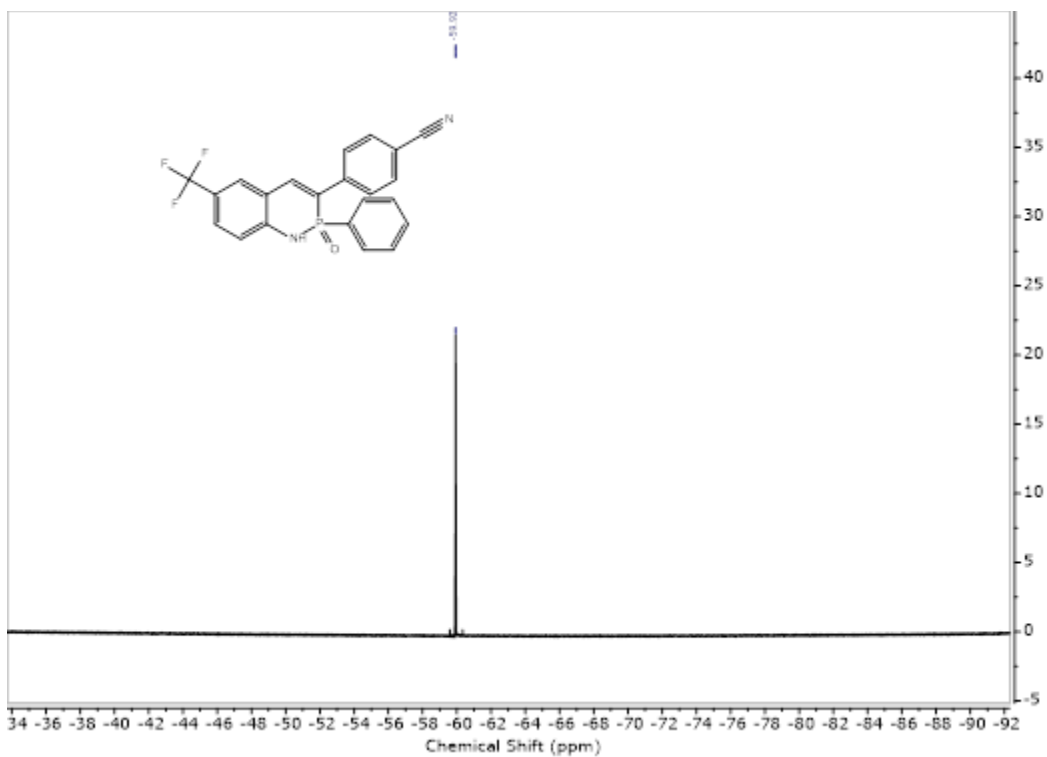


Figure C.32 ^{19}F NMR spectrum of **2b** in DMSO-d_6 .

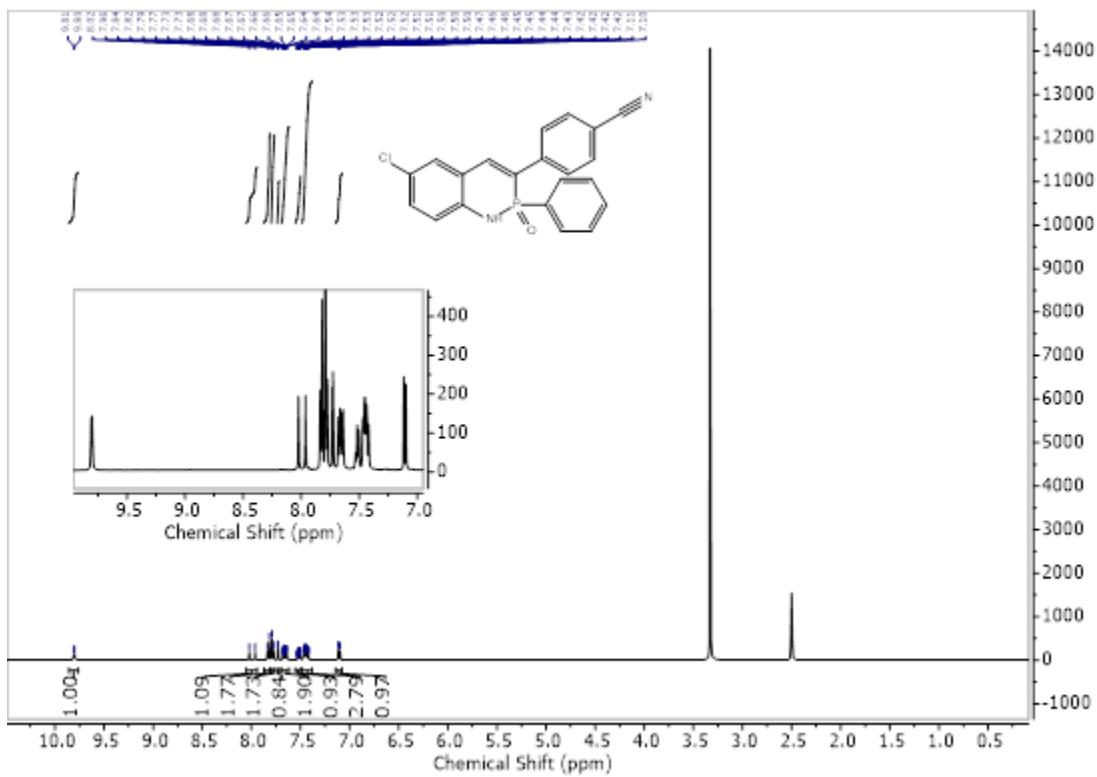


Figure C.33 ^1H NMR spectrum of **2c** in DMSO-d_6 .

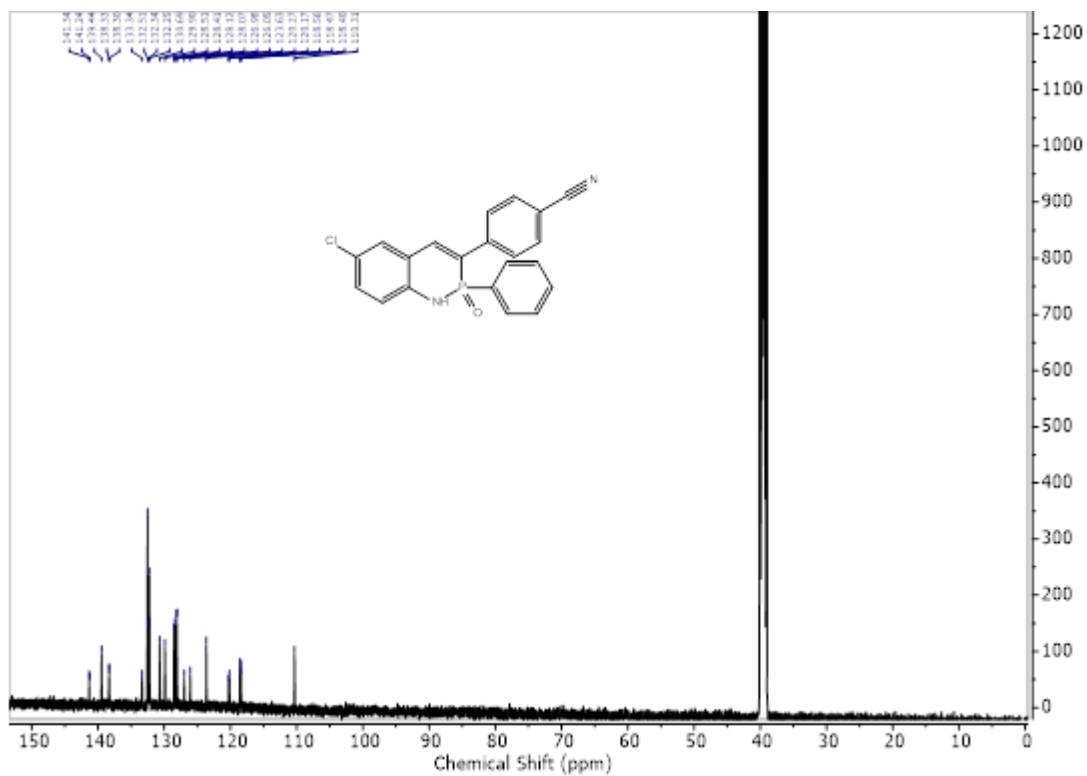


Figure C.34 ^{13}C NMR spectrum of **2c** in DMSO-d_6 .

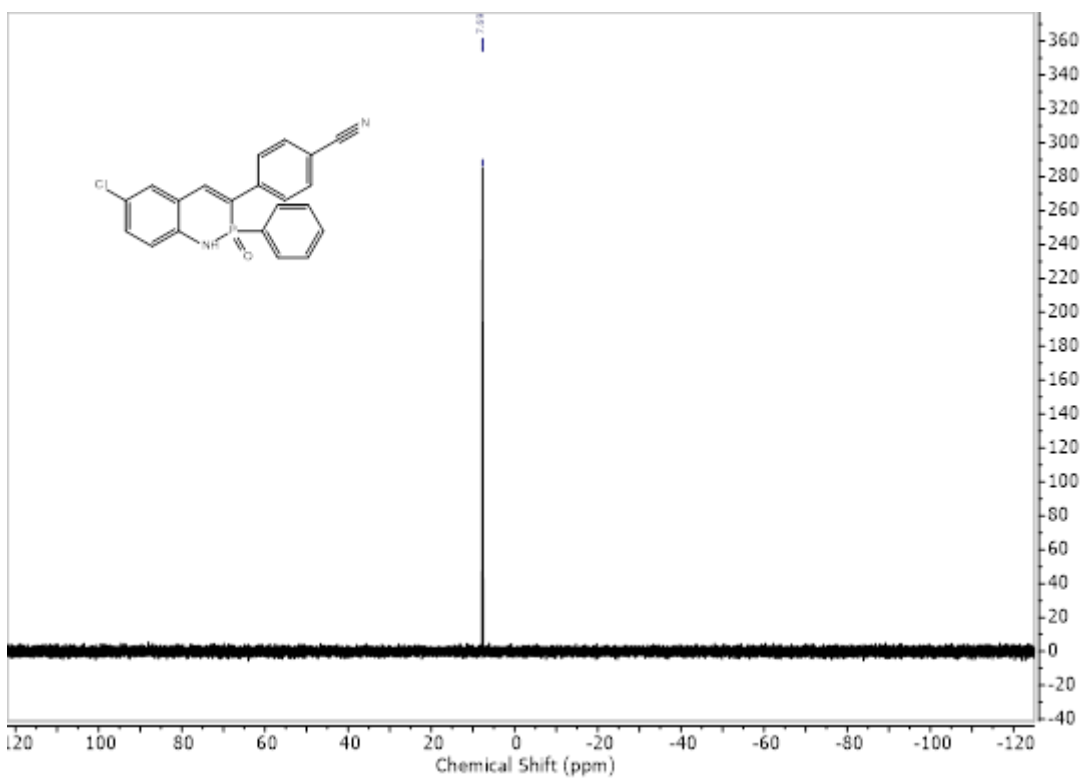


Figure C.35 ^{31}P NMR spectrum of **2c** in DMSO-d_6 .

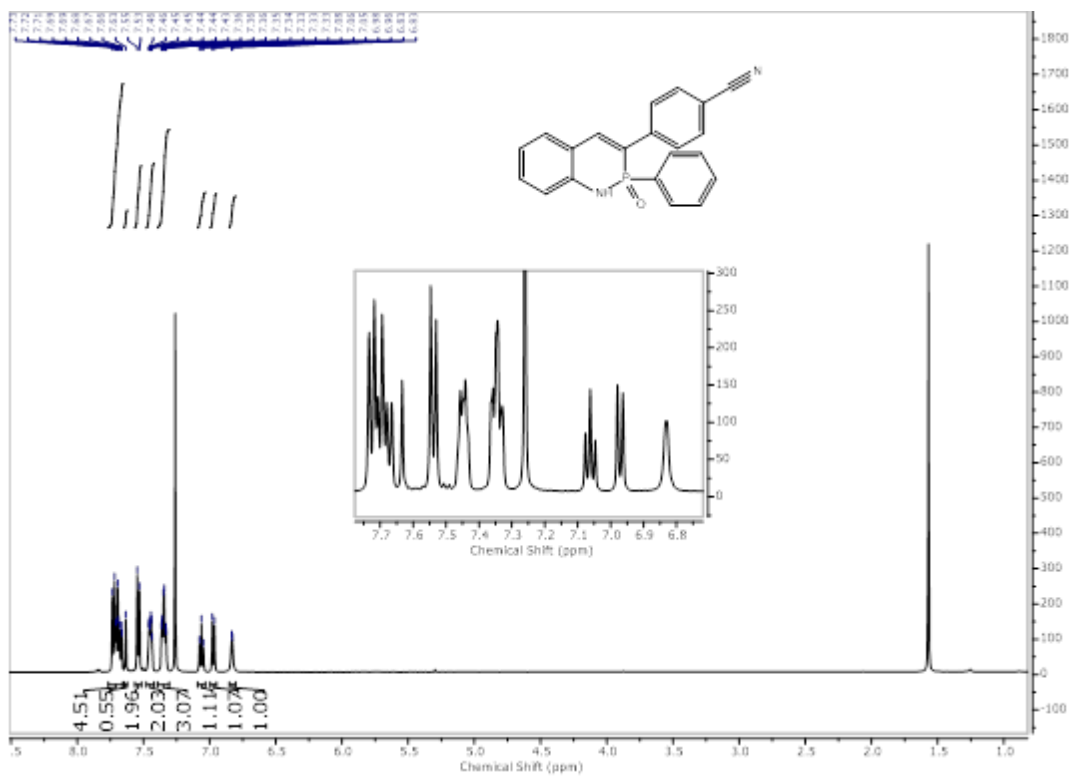


Figure C.36 ^1H NMR spectrum of **2d** in CDCl_3 .

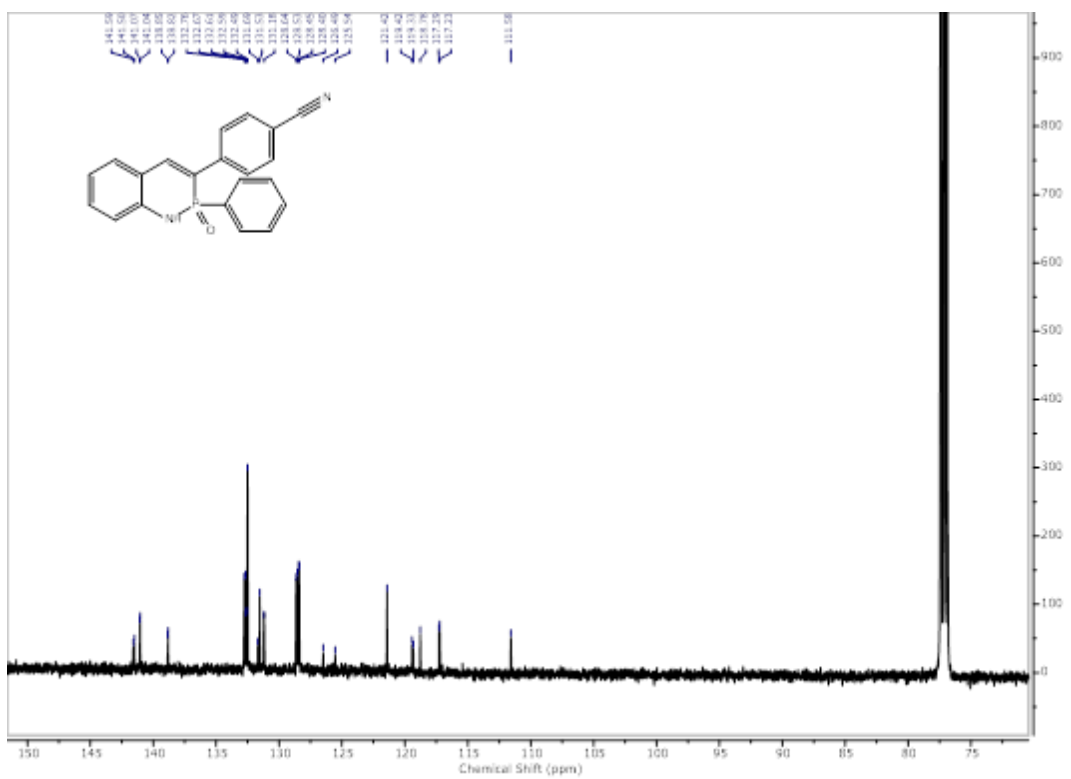


Figure C.37 ^{13}C NMR spectrum of **2d** in CDCl_3 .

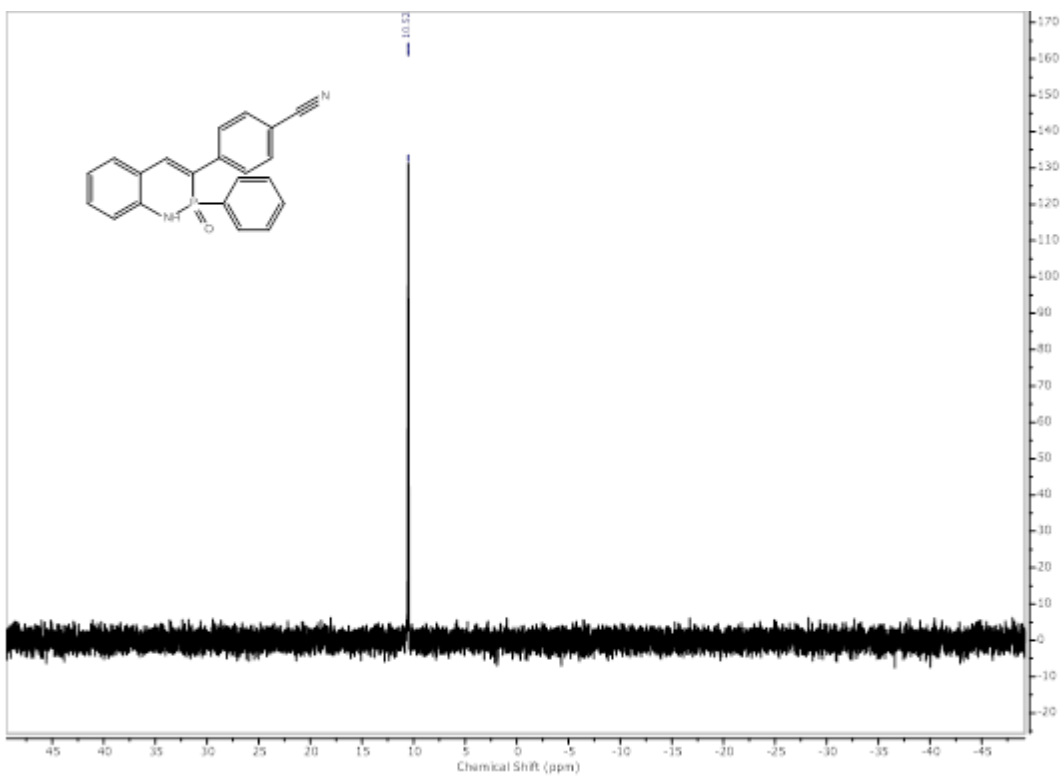


Figure C.38 ^{31}P NMR spectrum of **2d** in CDCl_3 .

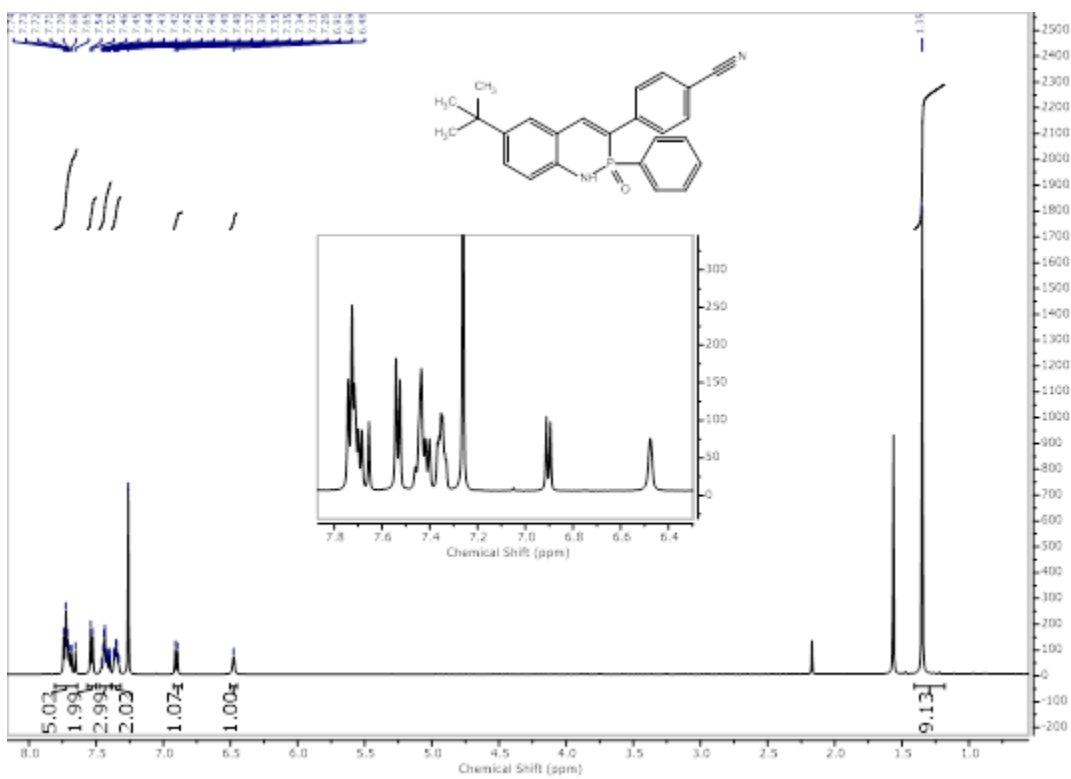


Figure C.39 ^1H NMR spectrum of **2e** in CDCl_3 .

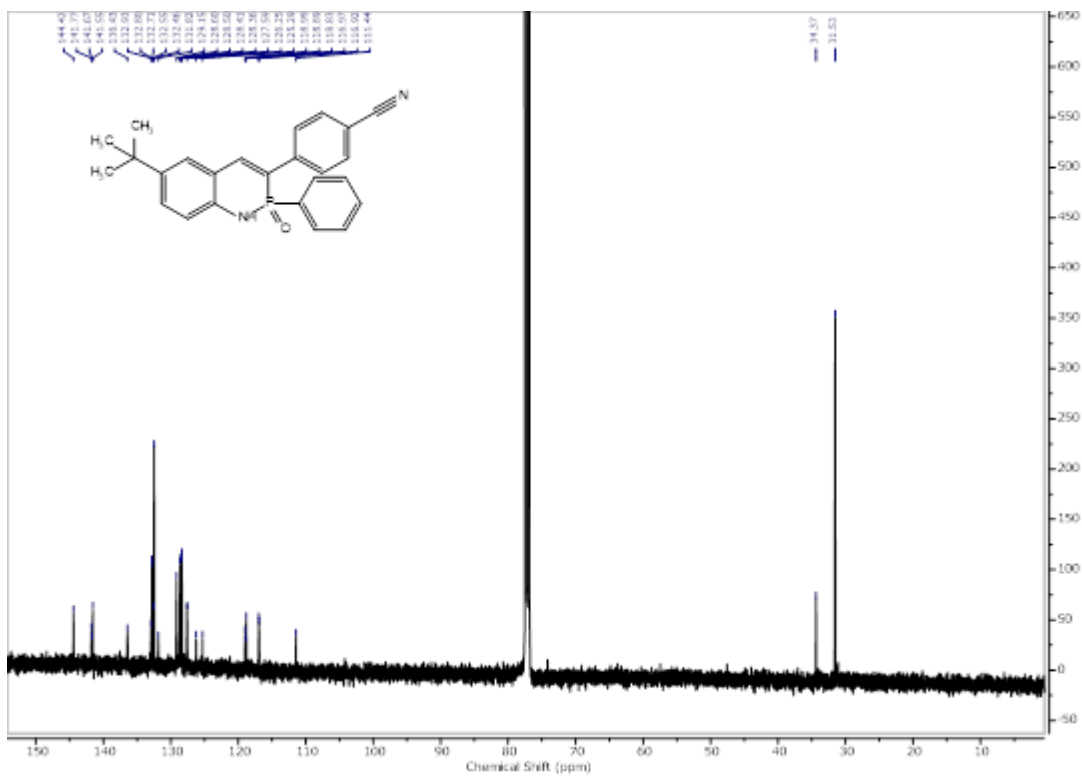


Figure C.40 ^{13}C NMR spectrum of **2e** in CDCl_3 .

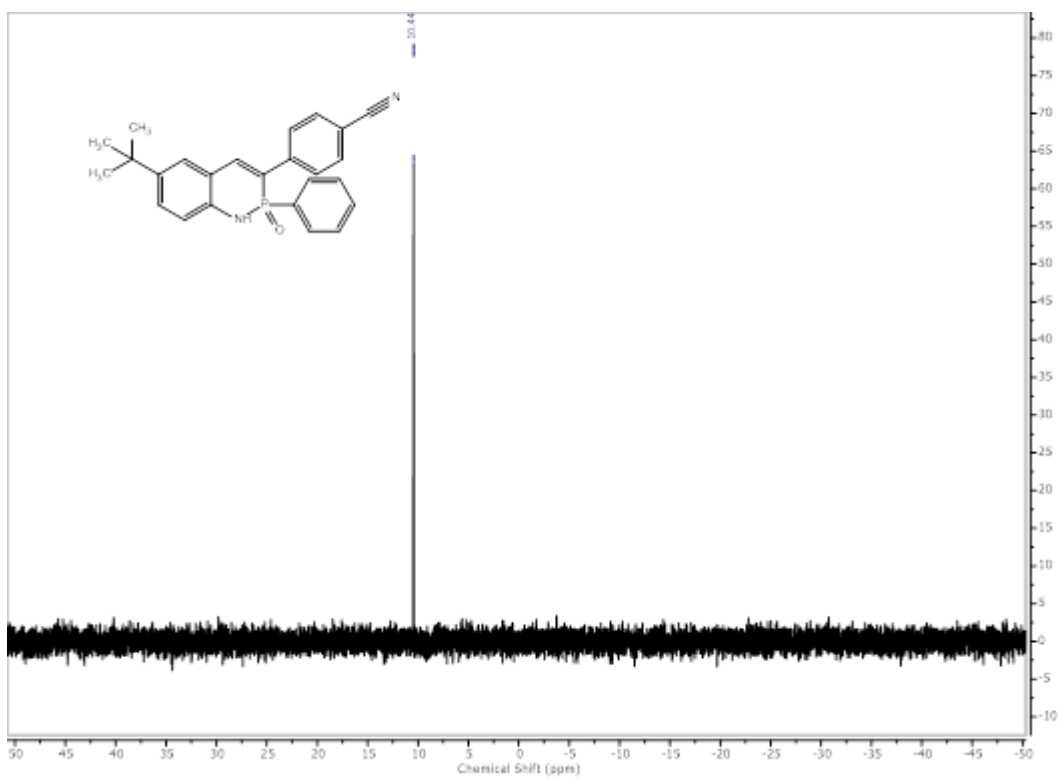
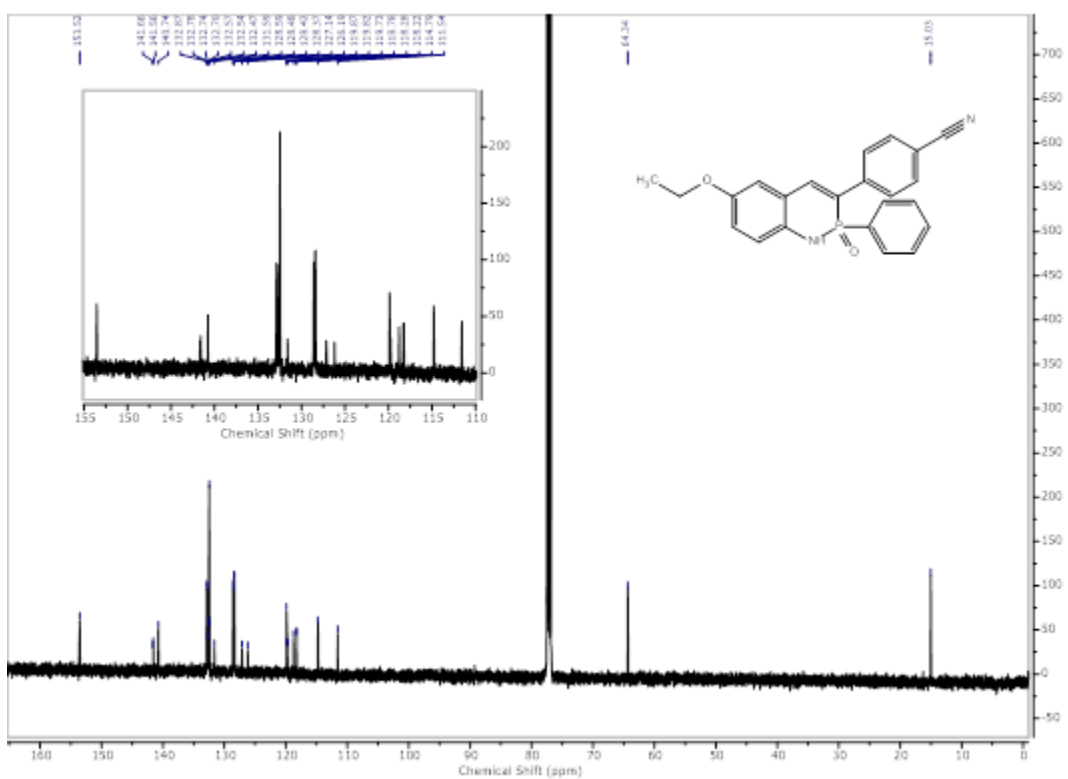
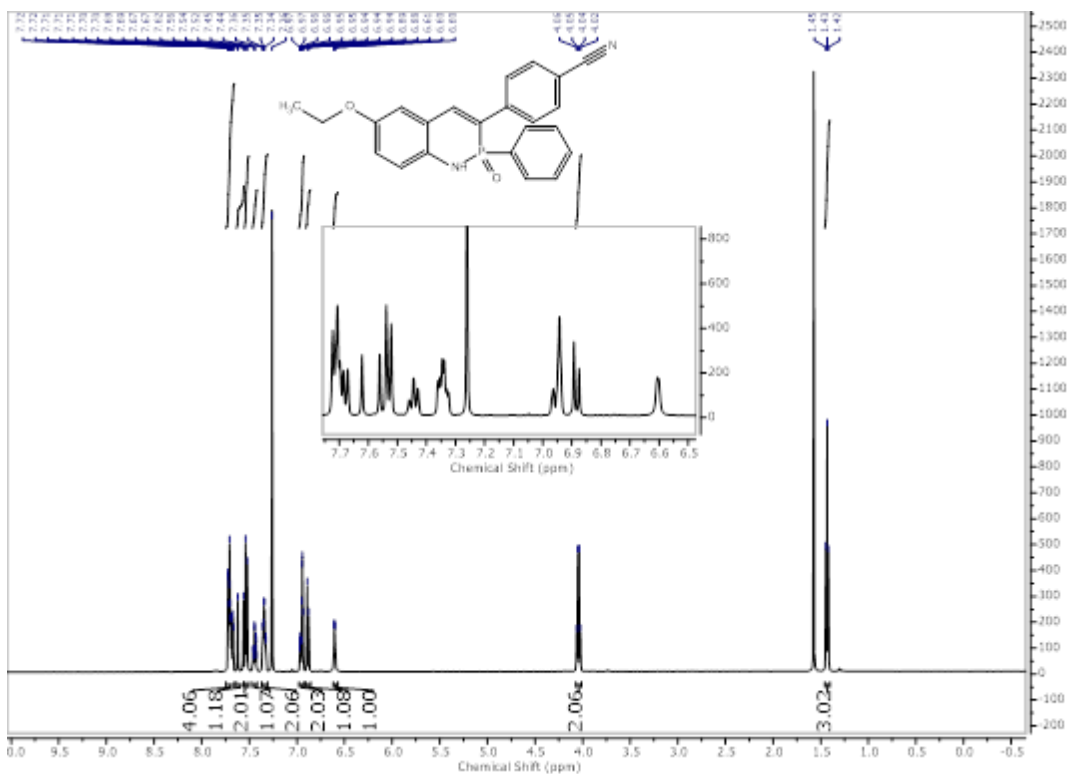


Figure C.41 ^{31}P NMR spectrum of **2e** in CDCl_3 .



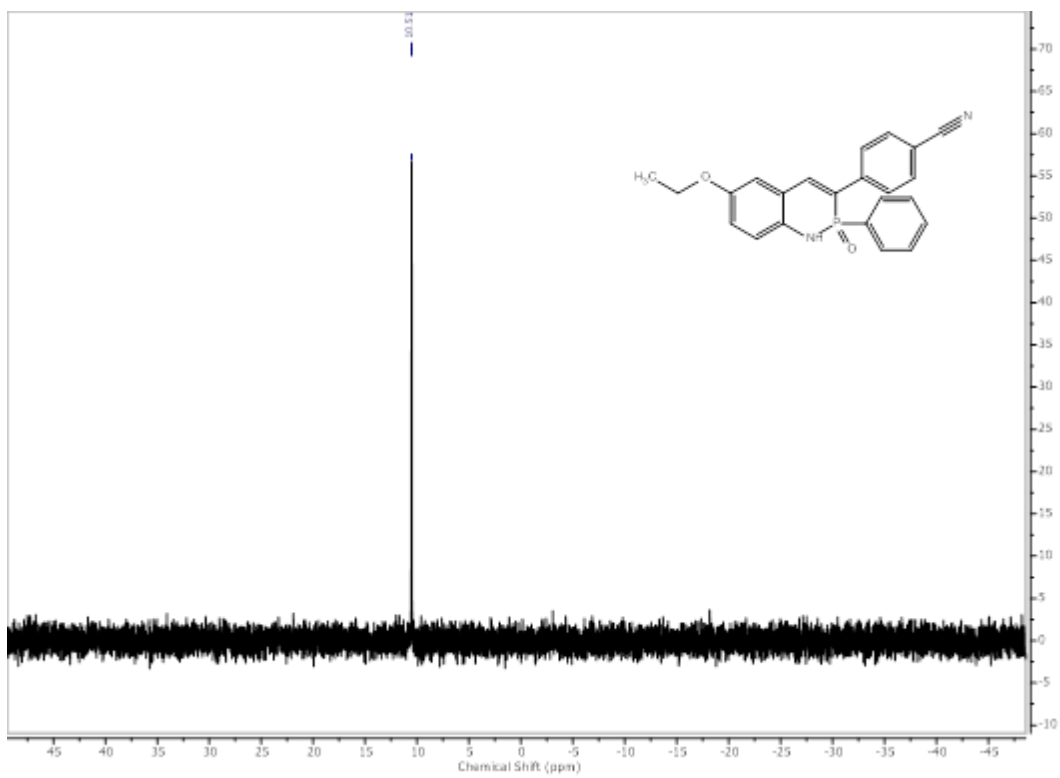


Figure C.44 ^{31}P NMR spectrum of **2f** in CDCl_3 .

APPENDIX D

SUPPLEMENTARY INFORMATION FOR CHAPTER 5

Additional Crystallographic Figures

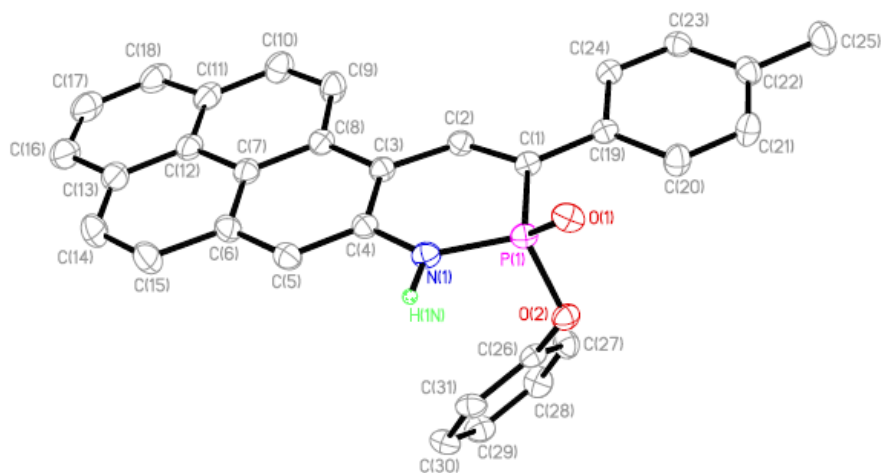


Figure D.1 ORTEP drawing of PN-fused pyrene **2**; thermal ellipsoids drawn at 30% probability. Crystals grown from slow layering of pentane into a concentrated solution of **2** in chloroform.

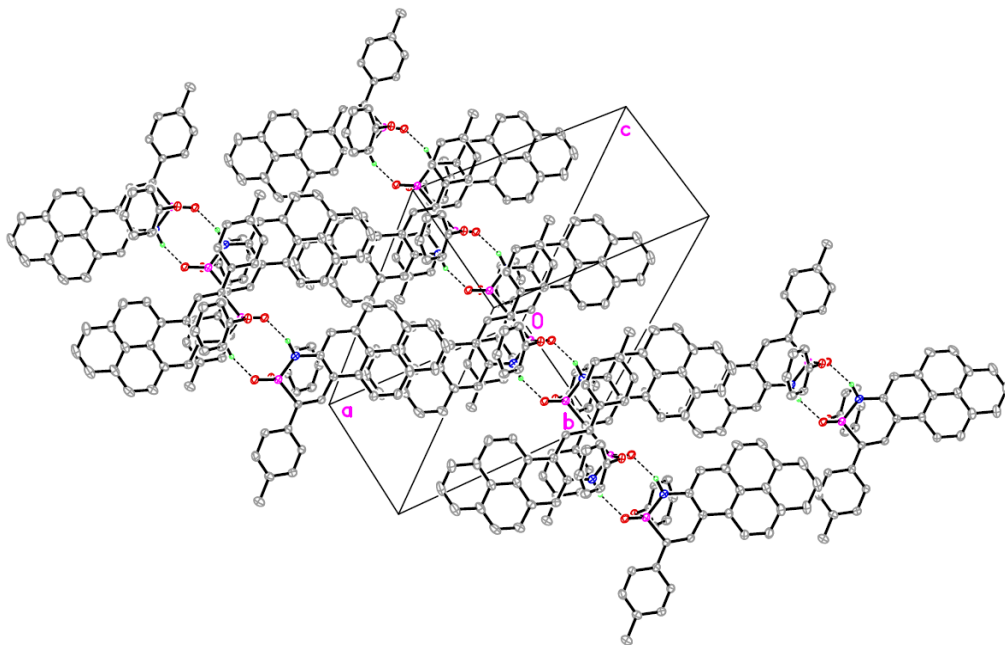


Figure D.2 ORTEP drawing of the crystal packing of **2**. Crystals grown from slow layering of pentane into a concentrated solution of **2** in chloroform.

Photophysical Studies in Different Solvents and the Solid state

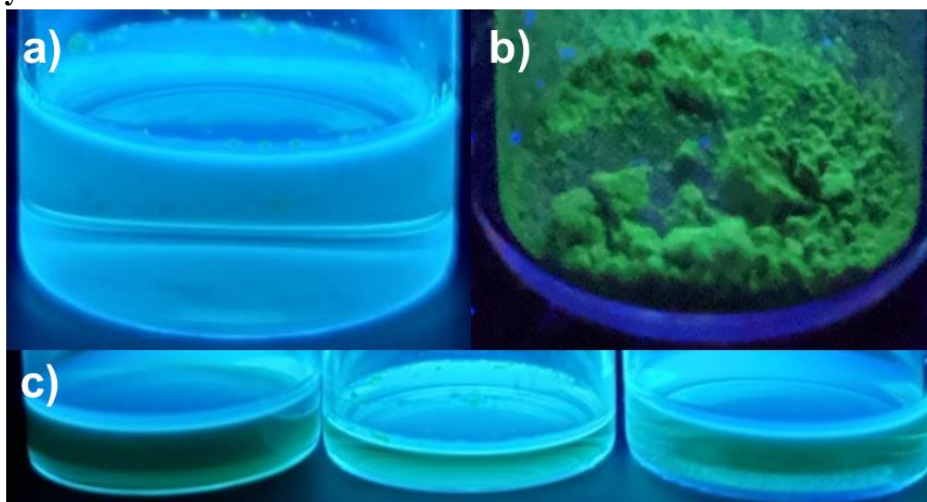


Figure D.3 Fluorescence images of **2** in a) chloroform (*ca.* 1 μM), b) the solid state, and c) (left to right) toluene, chloroform, and methanol at *ca.* 4 mM in concentration. All samples were excited at 365 nm.

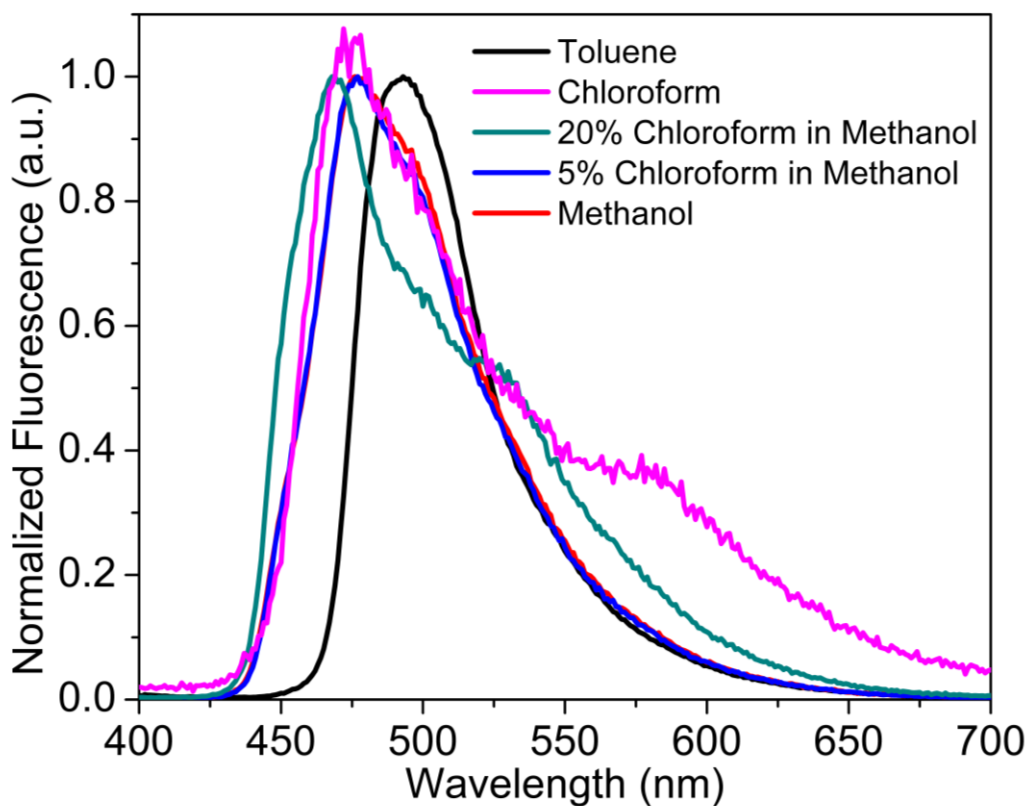


Figure D.4 Fluorescence spectra of 4 mM solutions of **2** in a variety of solvents. Samples excited at 365 nm.

Copies of NMR Spectra for New Compounds

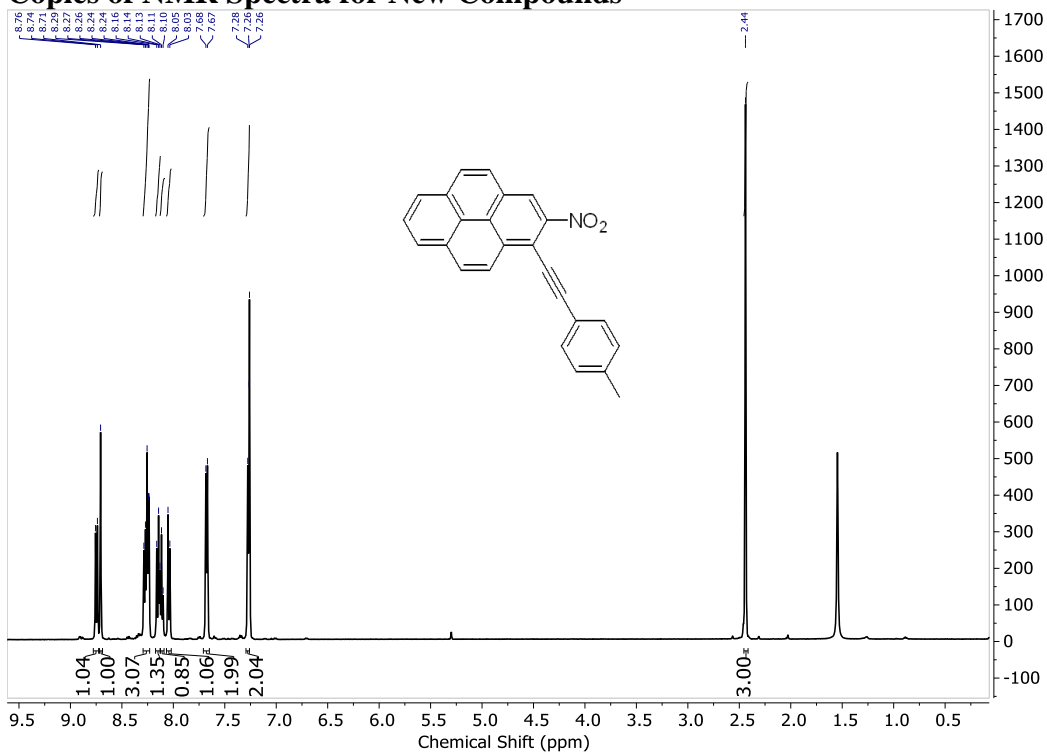


Figure D.5 ¹H NMR spectrum of **4** in CDCl₃.

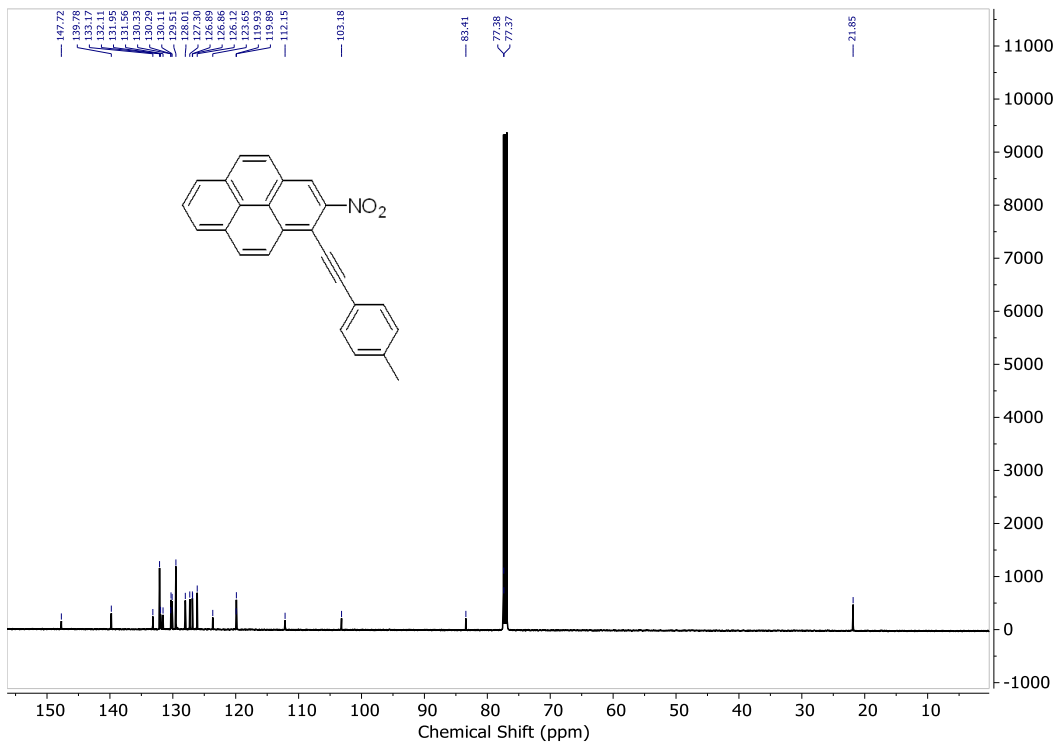


Figure D.6 ¹³C NMR spectrum of **4** in CDCl₃.

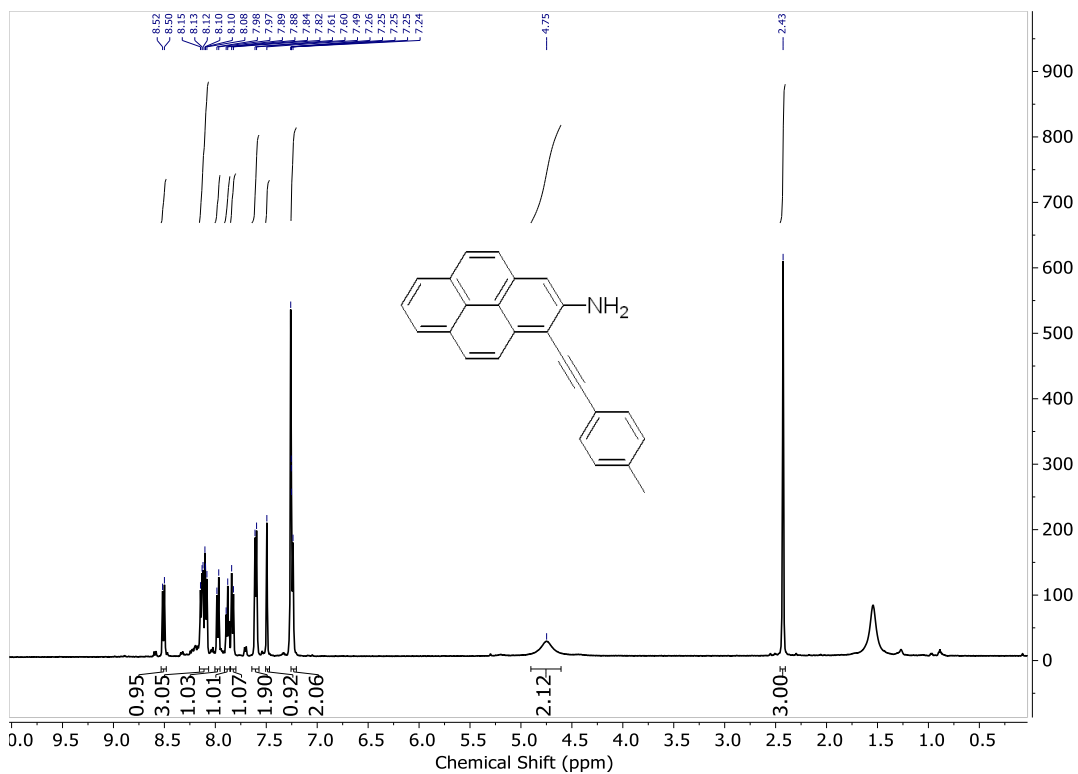


Figure D.7 ^1H NMR spectrum of **5** in CDCl_3 .

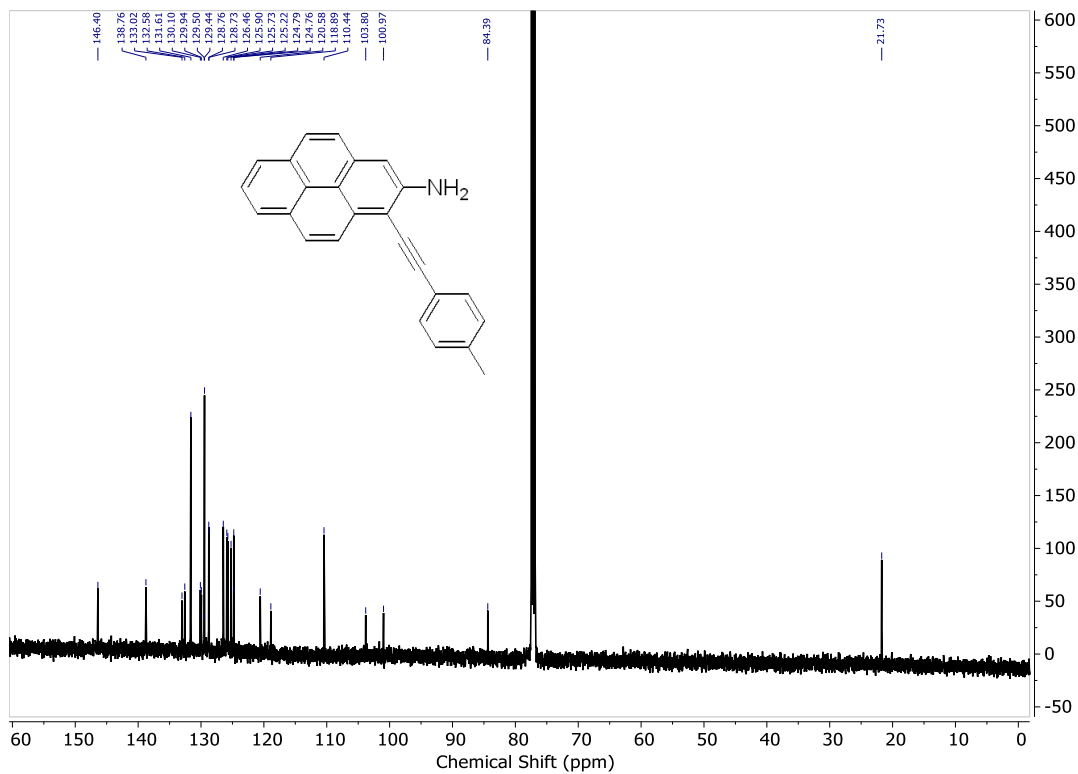


Figure D.8 ^{13}C NMR spectrum of **5** in CDCl_3 .

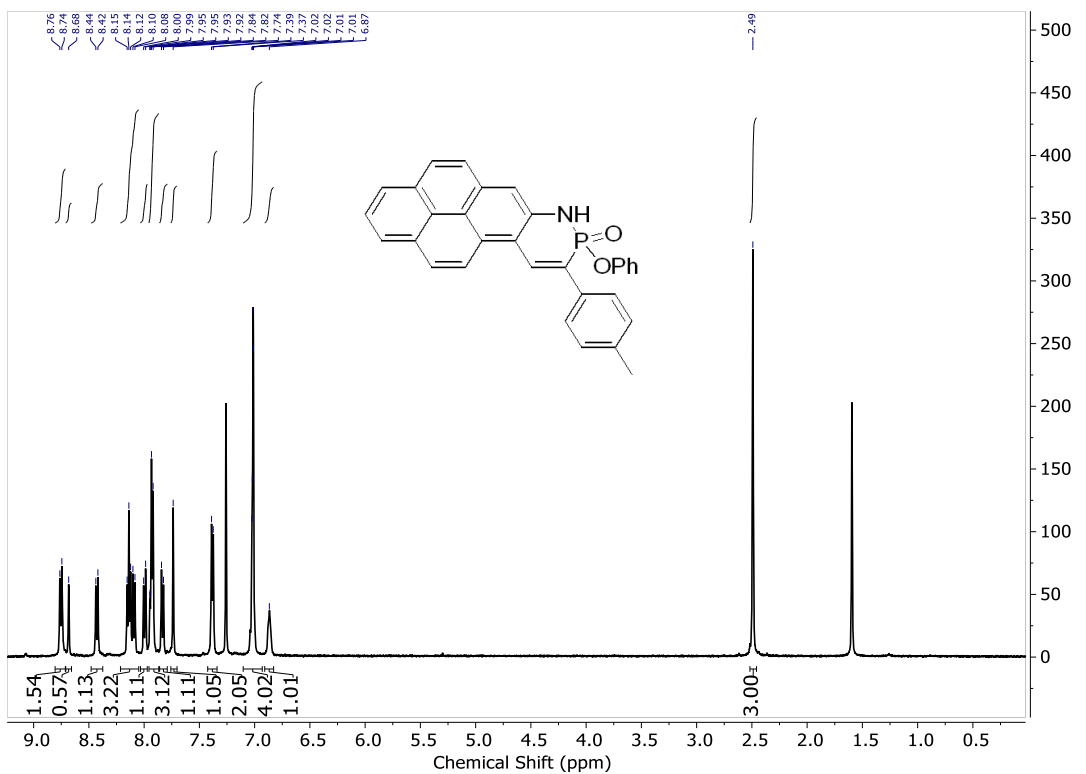


Figure D.9 ^1H NMR spectrum of **2** in CDCl_3 .

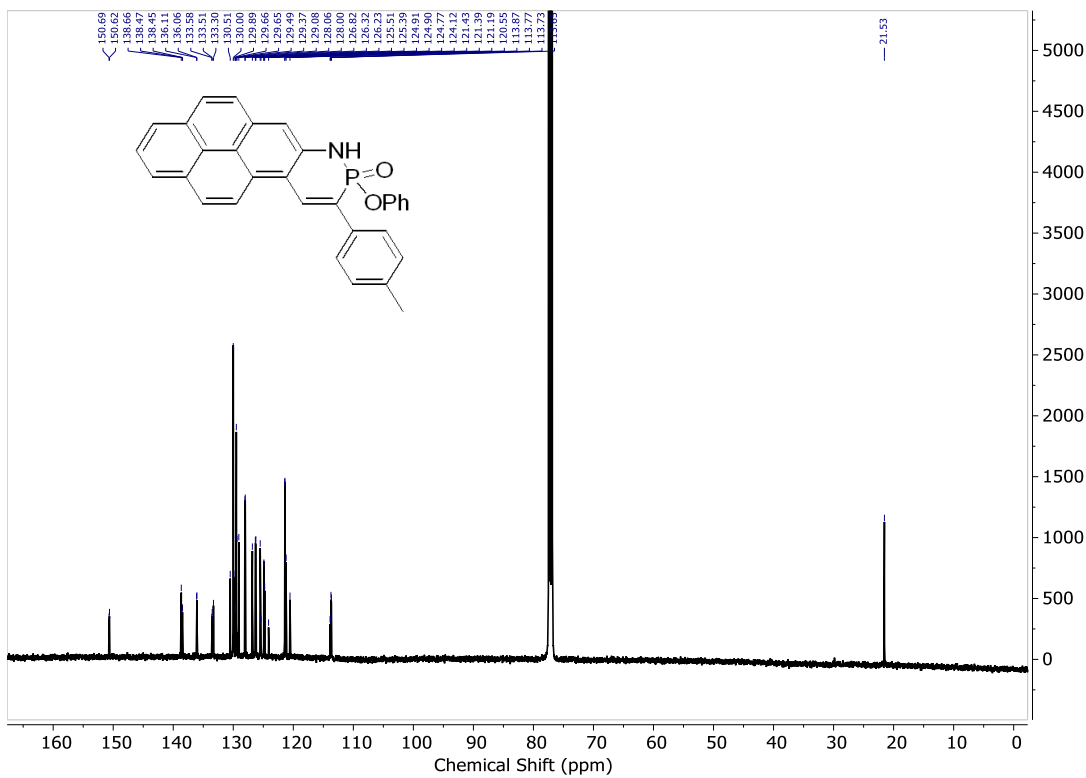


Figure D.10 ^{13}C NMR spectrum of **2** in CDCl_3 .

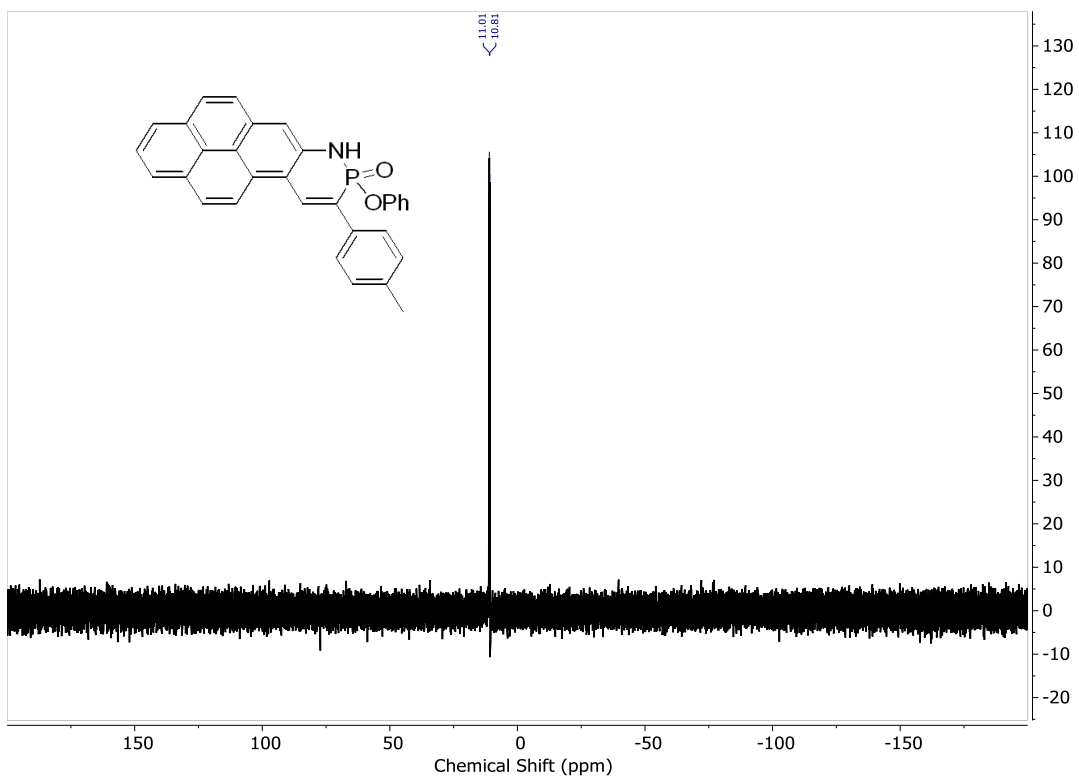


Figure D.11 ^{31}P NMR spectrum of **2** in CDCl_3 .

APPENDIX E

SUPPLEMENTARY INFORMATION FOR CHAPTER 6

1. X-ray Crystallographic Details

General. Diffraction intensities for **2d** and **2e** were collected at 173 K on a Bruker Apex2 CCD diffractometer using MoK α radiation, $\lambda = 0.71073$ Å. Space groups were determined based on intensity statistics (**2d**) and systematic absences (**2e**). Absorption corrections were applied by SADABS.^[1] Structures were solved by direct methods and Fourier techniques and refined on F^2 using full matrix least-squares procedures. All non-H atoms were refined with anisotropic thermal parameters. H atoms in both structures were refined in calculated positions in a rigid group model except the H atoms at the N atoms involved in forming H-bonds. These H atoms were found from the diffraction data and refined with isotropic thermal parameters. The standard N–H bond distance was used in the refinement as the target for corresponding bond length. In both structures the main molecules form dimer units via N–H \cdots S H-bonds. Crystal structure of **2d** includes also solvent molecule CH₂Cl₂. Terminal Me-groups in **2e** are disordered over two positions in ratio 1:1. All calculations were performed by the Bruker SHELXL-2014 package.^[2]

Crystallographic Data for 2d: C₂₂H₁₇Cl₂N₂PS, M = 443.30, 0.24 x 0.18 x 0.12 mm, T = 173(2) K, Triclinic, space group $P-1$, $a = 8.8716(14)$ Å, $b = 10.6480(16)$ Å, $c = 11.6935(18)$ Å, $\alpha = 83.063(2)^\circ$, $\beta = 80.956(2)^\circ$, $\gamma = 86.672(2)^\circ$, $V = 1082.0(3)$ Å³, $Z = 2$, $D_c = 1.361$ Mg m⁻³, $\mu(\text{Mo}) = 0.481$ mm⁻¹, $F(000) = 456$, $2\theta_{\text{max}} = 60.18^\circ$, 17797 reflections, 6236 independent reflections [$R_{\text{int}} = 0.0291$], $R1 = 0.0454$, $wR2 = 0.1283$ and GOF = 1.058 for 6236 reflections (257 parameters) with $I > 2\sigma(I)$, $R1 = 0.0537$, $wR2 = 0.1354$ and GOF = 1.060 for all reflections, max/min residual electron density +1.155/–0.652 eÅ⁻³. CCDC 2034968.

Crystallographic Data for 2e: C₂₅H₂₃N₂PS, M = 414.48, 0.23 x 0.23 x 0.11 mm, T = 173(2) K, Monoclinic, space group $C2/c$, $a = 19.716(4)$ Å, $b = 12.307(2)$ Å, $c = 18.192(3)$ Å, $\beta = 99.272(3)^\circ$, $V = 4356.5(14)$ Å³, $Z = 8$, $D_c = 1.264$ Mg m⁻³, $\mu(\text{Mo}) = 0.236$ mm⁻¹, $F(000) = 1744$, $2\theta_{\text{max}} = 60.042^\circ$, 24992 reflections, 6375 independent reflections [$R_{\text{int}} = 0.0366$], $R1 = 0.0378$, $wR2 = 0.1027$ and GOF = 1.020 for 6375 reflections (293

parameters) with $I > 2\sigma(I)$, $R1 = 0.0450$, $wR2 = 0.1078$ and $GOF = 1.026$ for all reflections, max/min residual electron density $+0.458/-0.256 \text{ e}\text{\AA}^{-3}$. CCDC 2034967.

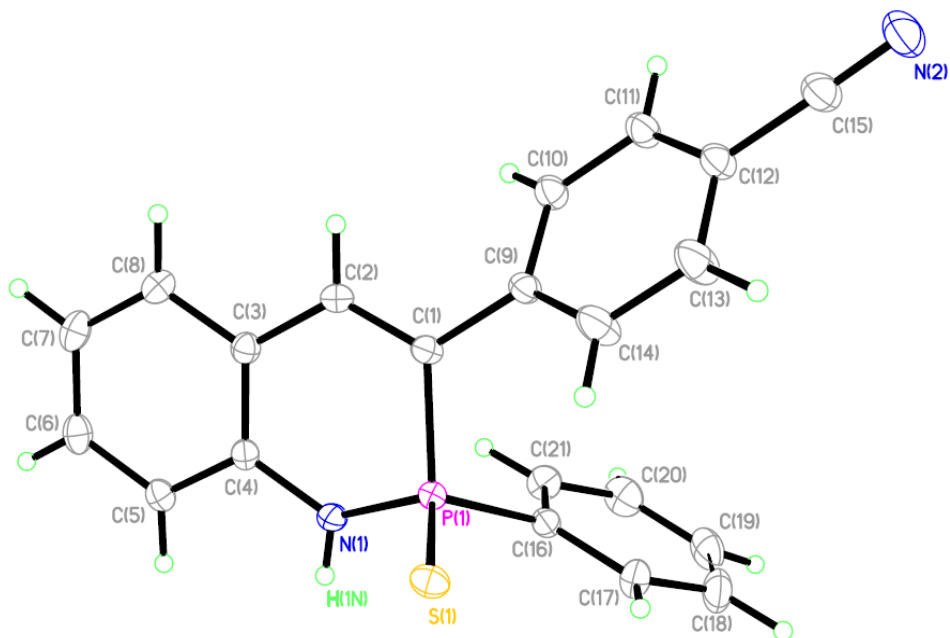


Figure E.1 ORTEP drawing of thio-heterocycle **2d**; thermal ellipsoids drawn at 30% probability.

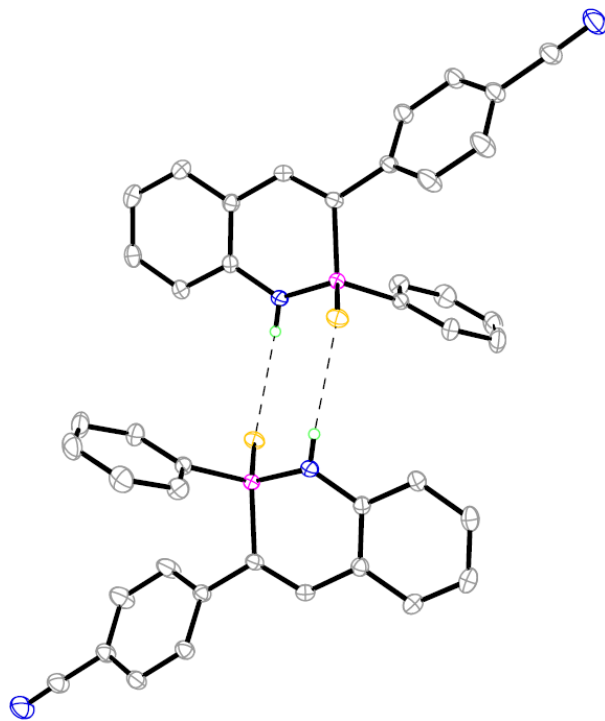


Figure E.2 ORTEP drawing of the racemic dimer of thio-heterocycle **2d**; thermal ellipsoids drawn at 30% probability.

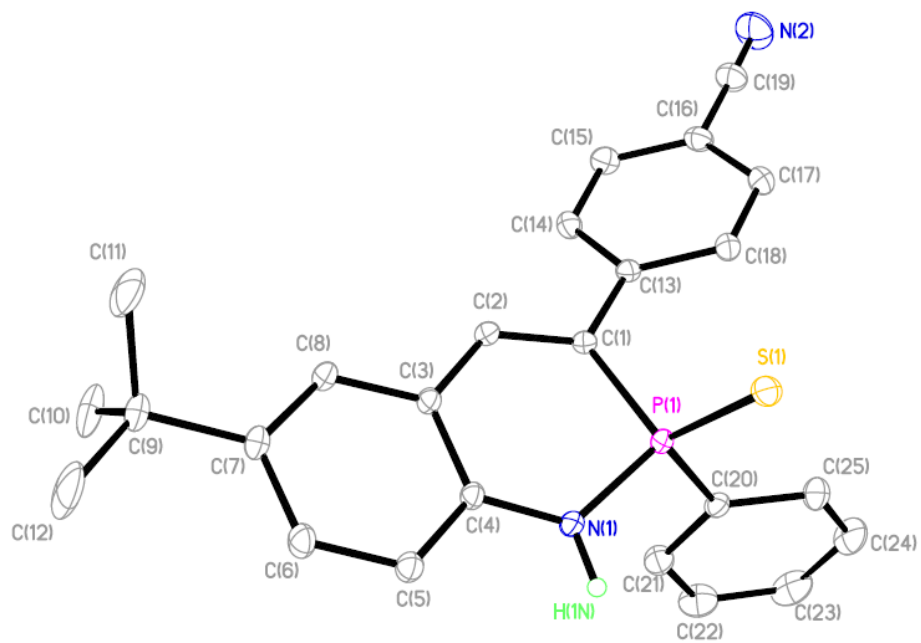


Figure E.3 ORTEP drawing of thio-heterocycle **2e**; thermal ellipsoids drawn at 30% probability.

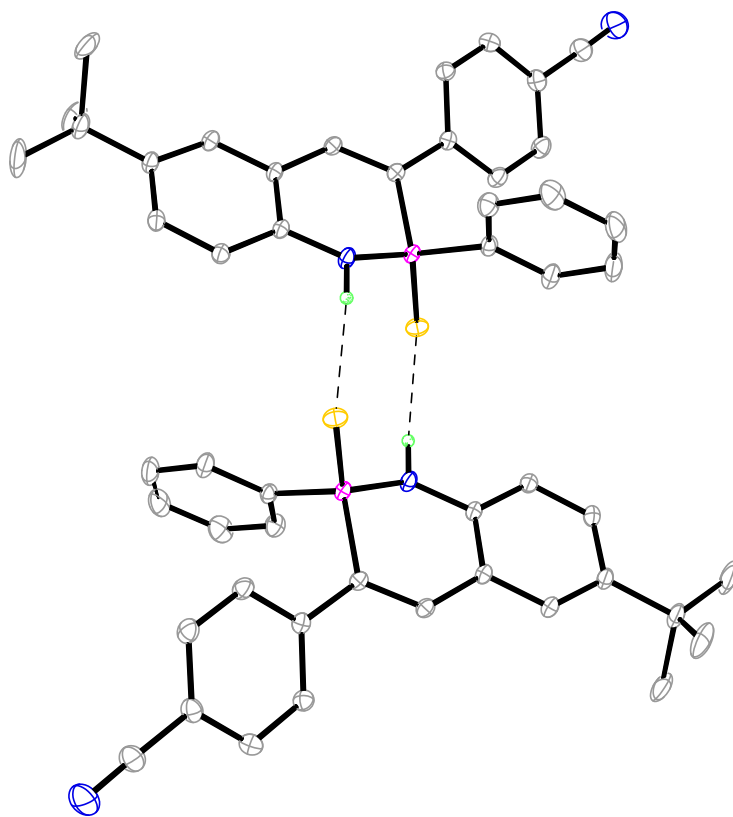


Figure E.4 ORTEP drawing of the racemic dimer of thio-heterocycle **2e**; thermal ellipsoids drawn at 30% probability.

2. Comparison of the Photophysical Properties of **2c** and **2e** in CHCl₃ vs. MeCN

Table E.1 Photophysical properties of heterocycles **2c** and **2e** in CHCl₃ and MeCN^a

cmpd	solvent	λ_{abs} (nm)	λ_{em} (nm)	Stokes shift (nm)	Stokes shift (cm ⁻¹)
2c	MeCN	371	497	26	6834
	CHCl ₃	373	492	19	6484
2e	MeCN	360	484	24	7116
	CHCl ₃	350	470	20	7304

^aAll values collected using ca. 10⁻⁵ M solutions.

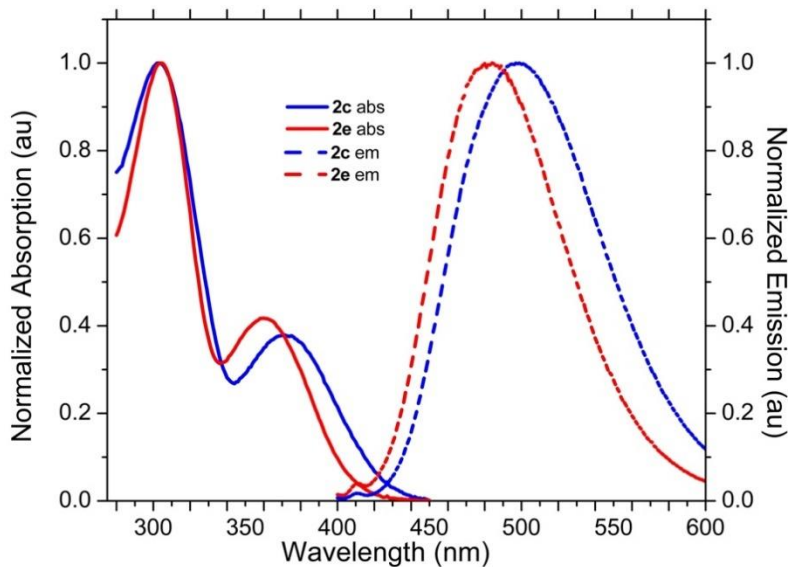


Figure E.5 Stacked absorption and emission spectra of **2c** and **2e** in MeCN.

3. TD-DFT studies and coordinates for selected heterocycles 2

Ground state calculations:

The initial structures were optimized at the ground state using the functional PBE0^{3,4} (25% full-range HF exchange) and TZVP basis set⁵ as implemented in Gaussian 09.⁶ In addition, all the ground state optimized structures were confirmed by frequency analysis and the number of imaginary frequencies was zero. TD-DFT vertical excitation calculations and geometry optimization of the first excited state (S₁) were performed at the same level of theory and the PCM solvation model^{7,8} was used to account for the solvent effects of chloroform.

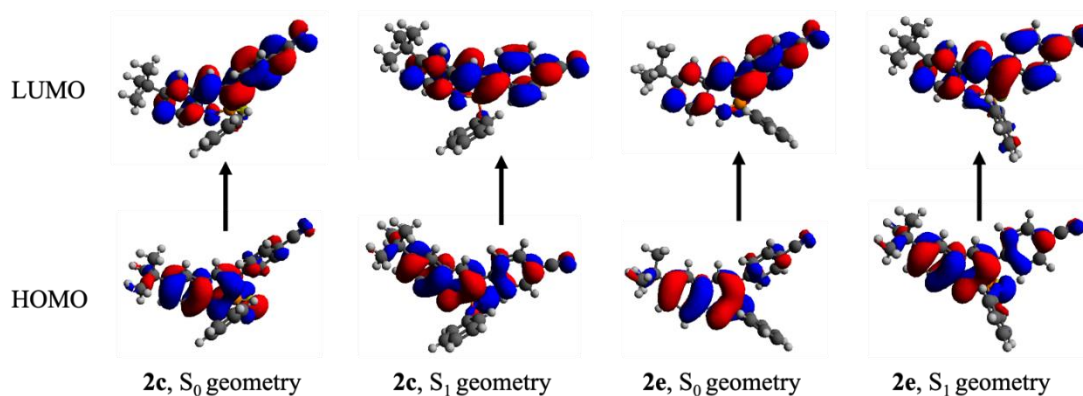


Figure E.6 Frontier orbital plots (isovalue = 0.2) of heterocycles **2c** and **2e** in the optimized S₀ and S₁ structures calculated by DFT and TD-DFT methods at the PCM(CHCl₃)-PBE0/TZVP level of theory, respectively.

Table E.2 Calculated frontier orbitals and first excitation values for compounds **2c** and **2e**^a

Compound	E_{HOMO}	E_{LUMO}	ΔE_{DFT}	S ₀ to S ₁ computed (nm), osc. strength
2c	-6.385	-2.995	3.390	366, 0.3008
2e	-6.266	-2.996	3.270	379, 0.2913

^aCalculated at the PCM(CHCl₃)-PBE0/TZVP level of theory, energy values reported in eV.

Ground state geometries:

Cartesian coordinates for compound **2c**:

Zero-point correction = 0.421712 (Hartree/Particle)

Thermal correction to Energy = 0.449176

Thermal correction to Enthalpy = 0.450120

Thermal correction to Gibbs Free Energy = 0.361543
 Sum of electronic and zero-point Energies = -1889.158422
 Sum of electronic and thermal Energies = -1889.130957
 Sum of electronic and thermal Enthalpies = -1889.130013
 Sum of electronic and thermal Free Energies = -1889.218591

C	5.9109860000	-1.0127790000	1.1533730000
C	5.0355570000	-1.8264830000	0.1914770000
C	5.8782310000	-2.2674180000	-1.0123200000
C	4.5534540000	-3.0772420000	0.9234020000
C	3.8750230000	-0.9607620000	-0.2912030000
C	4.1298800000	0.2285300000	-0.9900630000
C	3.1157770000	1.0456670000	-1.4423340000
C	1.7816580000	0.7081810000	-1.2116480000
N	0.7623840000	1.5129150000	-1.6795590000
P	-0.9026400000	1.3908620000	-1.4009190000
C	-1.0061200000	-0.2540390000	-0.6674560000
C	-2.3262920000	-0.8359160000	-0.3580790000
C	-3.3835040000	-0.8088680000	-1.2726080000
C	-4.5954720000	-1.4010130000	-0.9689250000
C	-4.7803940000	-2.0320500000	0.2615900000
C	-6.0290760000	-2.6445490000	0.5766760000
N	-7.0368070000	-3.1420540000	0.8343530000
C	-3.7362490000	-2.0562460000	1.1881880000
C	-2.5300550000	-1.4590360000	0.8792290000
C	0.1312770000	-0.9026690000	-0.3258710000
O	-1.2645780000	2.4235910000	-0.1630650000
C	-0.7323110000	2.3172380000	1.1083410000
C	0.5478280000	2.7796580000	1.3788630000
C	1.0316030000	2.7193560000	2.6783080000
C	0.2401010000	2.2157260000	3.7010410000
C	-1.0455880000	1.7721210000	3.4204710000
C	-1.5373290000	1.8222950000	2.1245000000
S	-1.9364900000	1.9272820000	-2.9483300000
C	1.4890200000	-0.4795060000	-0.5275740000
C	2.5481010000	-1.2863390000	-0.0827700000
H	6.7510340000	-1.6187540000	1.5047120000
H	5.3363510000	-0.6881710000	2.0245830000
H	6.3226080000	-0.1225060000	0.6724890000
H	6.7174460000	-2.8853170000	-0.6803300000
H	6.2898970000	-1.4132420000	-1.5546170000
H	5.2798940000	-2.8533350000	-1.7145290000
H	5.4155870000	-3.6633620000	1.2506640000
H	3.9468950000	-3.7180320000	0.2778810000
H	3.9686850000	-2.8280810000	1.8129310000
H	5.1535950000	0.5278980000	-1.1865150000

H	3.3519020000	1.9591990000	-1.9789680000
H	1.0148430000	2.2389420000	-2.3353090000
H	-3.2475000000	-0.3279230000	-2.2329560000
H	-5.4050740000	-1.3814320000	-1.6884960000
H	-3.8824770000	-2.5329880000	2.1500590000
H	-1.7361450000	-1.4493370000	1.6170950000
H	0.0155770000	-1.8839840000	0.1309170000
H	1.1504390000	3.1905500000	0.5785580000
H	2.0315340000	3.0802630000	2.8916370000
H	0.6203960000	2.1775430000	4.7153260000
H	-1.6762230000	1.3921060000	4.2166050000
H	-2.5419540000	1.4919570000	1.8890350000
H	2.2871050000	-2.1993170000	0.4395920000

Cartesian coordinates for compound **2e**:

Zero-point correction = 0.417734 (Hartree/Particle)

Thermal correction to Energy = 0.444242

Thermal correction to Enthalpy = 0.445186

Thermal correction to Gibbs Free Energy = 0.359416

Sum of electronic and zero-point Energies = -1813.978974

Sum of electronic and thermal Energies = -1813.952466

Sum of electronic and thermal Enthalpies = -1813.951522

Sum of electronic and thermal Free Energies = -1814.037292

C	-5.5134060000	-2.5541420000	-0.3364810000
C	-5.7067050000	-1.0403170000	-0.2763330000
C	-6.4388910000	-0.5979280000	-1.5498110000
C	-6.5737670000	-0.7140440000	0.9466330000
C	-4.3789170000	-0.2953860000	-0.1682330000
C	-4.3630320000	1.1053570000	-0.1094380000
C	-3.1889360000	1.8214890000	-0.0055380000
C	-1.9601230000	1.1636360000	0.0437700000
N	-0.7727910000	1.8749150000	0.0828850000
P	0.6771600000	1.2807940000	0.7773640000
C	0.5353370000	-0.4516120000	0.2524370000
C	1.7461860000	-1.2836930000	0.1754320000
C	2.7880400000	-1.1676940000	1.1022840000
C	3.9099890000	-1.9690870000	1.0104470000
C	4.0192120000	-2.9096580000	-0.0150450000
C	5.1762550000	-3.7369800000	-0.1124530000
N	6.1114950000	-4.4067090000	-0.1932350000
C	2.9901670000	-3.0313820000	-0.9504710000
C	1.8753710000	-2.2217880000	-0.8555390000
C	-0.6930050000	-0.9575440000	0.0037130000
C	1.9441970000	2.0719940000	-0.2697400000
C	3.0220780000	2.7235510000	0.3176920000

C	3.9902660000	3.3150210000	-0.4819300000
C	3.8826180000	3.2541400000	-1.8639200000
C	2.8048500000	2.6030560000	-2.4522650000
C	1.8349930000	2.0117300000	-1.6584450000
S	0.9329160000	1.5958390000	2.6935360000
C	-1.9389530000	-0.2382240000	-0.0130420000
C	-3.1527770000	-0.9332340000	-0.1209270000
H	-6.4873560000	-3.0434320000	-0.4146000000
H	-5.0240540000	-2.9378290000	0.5626400000
H	-4.9238130000	-2.8545050000	-1.2068760000
H	-7.3959390000	-1.1204100000	-1.6368640000
H	-5.8453570000	-0.8225280000	-2.4397250000
H	-6.6457810000	0.4746140000	-1.5471510000
H	-7.5317180000	-1.2381960000	0.8821530000
H	-6.7845460000	0.3552260000	1.0203620000
H	-6.0773920000	-1.0217260000	1.8703510000
H	-5.2969050000	1.6559260000	-0.1408660000
H	-3.2171070000	2.9057080000	0.0404230000
H	-0.8792140000	2.8773600000	0.1634100000
H	2.7009890000	-0.4586020000	1.9178120000
H	4.7060270000	-1.8767210000	1.7395250000
H	3.0790830000	-3.7505850000	-1.7558930000
H	1.0983310000	-2.2967700000	-1.6076070000
H	-0.7640590000	-2.0266980000	-0.1886550000
H	3.0856060000	2.7640590000	1.4001820000
H	4.8301430000	3.8244290000	-0.0231240000
H	4.6408550000	3.7153430000	-2.4871630000
H	2.7207010000	2.5567080000	-3.5322540000
H	0.9900340000	1.5072400000	-2.1143230000
H	-3.0997850000	-2.0149650000	-0.1631400000

Excited state geometries:

Cartesian coordinates for compound **2c**:

C	-6.0817380000	-0.6876210000	-1.3217830000
C	-5.1841790000	-1.7042300000	-0.5995640000
C	-5.9842810000	-2.3765590000	0.5264430000
C	-4.7676490000	-2.7777690000	-1.6023920000
C	-3.9939660000	-0.9738650000	0.0026500000
C	-4.2163960000	0.0404470000	0.9624980000
C	-3.1623760000	0.7246390000	1.5238190000
C	-1.8476450000	0.4407970000	1.1410920000
N	-0.8143850000	1.1775720000	1.6479910000
P	0.8565340000	0.8901360000	1.4861420000
C	0.9519070000	-0.4693090000	0.3531570000
C	2.2395580000	-1.0185130000	0.0618810000
C	3.4524530000	-0.3454340000	0.3753850000

C	4.6791450000	-0.8912070000	0.0895890000
C	4.7744910000	-2.1428310000	-0.5450510000
C	6.0350380000	-2.7020610000	-0.8532660000
N	7.0678480000	-3.1614550000	-1.1049920000
C	3.5879890000	-2.8264390000	-0.8714610000
C	2.3639850000	-2.2827880000	-0.5802090000
C	-0.2558430000	-0.9713650000	-0.1610030000
O	1.4310340000	2.2723410000	0.8177200000
C	1.0092160000	2.7149340000	-0.4369120000
C	0.0040700000	3.6666870000	-0.5014020000
C	-0.3790000000	4.1591260000	-1.7414810000
C	0.2402670000	3.7022200000	-2.8976240000
C	1.2494360000	2.7520500000	-2.8130240000
C	1.6435280000	2.2527040000	-1.5788190000
S	1.6567120000	0.7221410000	3.2698870000
C	-1.5725120000	-0.6010580000	0.2002740000
C	-2.6833290000	-1.2646170000	-0.3491330000
H	-6.9462250000	-1.2003300000	-1.7527470000
H	-5.5388830000	-0.1936700000	-2.1314950000
H	-6.4536410000	0.0825540000	-0.6431070000
H	-6.8462720000	-2.8999350000	0.1036170000
H	-6.3574170000	-1.6515220000	1.2525220000
H	-5.3698920000	-3.1059700000	1.0600470000
H	-5.6608620000	-3.2655470000	-1.9994860000
H	-4.1486190000	-3.5499100000	-1.1384630000
H	-4.2194490000	-2.3546800000	-2.4480110000
H	-5.2247590000	0.2909860000	1.2674530000
H	-3.3427670000	1.5071100000	2.2539420000
H	-1.0504800000	1.8715370000	2.3484210000
H	3.4318520000	0.6350500000	0.8359850000
H	5.5819520000	-0.3479400000	0.3424570000
H	3.6464840000	-3.7978100000	-1.3489130000
H	1.4780250000	-2.8569780000	-0.8183230000
H	-0.1855550000	-1.7558450000	-0.9055440000
H	-0.4596600000	4.0215190000	0.4112480000
H	-1.1611610000	4.9073520000	-1.8007000000
H	-0.0604840000	4.0900740000	-3.8640070000
H	1.7411830000	2.3977600000	-3.7117600000
H	2.4356880000	1.5179920000	-1.4992750000
H	-2.4799650000	-2.0472510000	-1.0689210000

Cartesian coordinates for compound **2e**:

C	-5.2454010000	-2.5083080000	-1.2165510000
C	-5.5172560000	-1.2050930000	-0.4686420000
C	-6.3164670000	-0.2728020000	-1.3922770000
C	-6.3575390000	-1.5261800000	0.7770540000

C	-4.2408030000	-0.5011010000	-0.0376460000
C	-4.3272730000	0.7241320000	0.6625370000
C	-3.1919690000	1.3923610000	1.0550970000
C	-1.9217980000	0.8739350000	0.7653650000
N	-0.8084620000	1.5748220000	1.1024290000
P	0.8466420000	1.1241470000	0.9314330000
C	0.7323760000	-0.5223570000	0.2341720000
C	1.9362480000	-1.2799130000	0.0910280000
C	3.2283240000	-0.6954830000	0.1699200000
C	4.3716320000	-1.4425130000	0.0338080000
C	4.2961200000	-2.8266270000	-0.2073050000
C	5.4701920000	-3.5968550000	-0.3648760000
N	6.4323650000	-4.2288720000	-0.4921100000
C	3.0269420000	-3.4290720000	-0.2941030000
C	1.8868680000	-2.6811520000	-0.1515210000
C	-0.5269840000	-0.9798410000	-0.1660090000
C	1.4745330000	2.2877820000	-0.3153180000
C	2.3029150000	3.3387390000	0.0697510000
C	2.7833580000	4.2216160000	-0.8875860000
C	2.4348640000	4.0599080000	-2.2214390000
C	1.6097020000	3.0069500000	-2.6054300000
C	1.1308250000	2.1177040000	-1.6585070000
S	1.6803210000	1.3182690000	2.7125620000
C	-1.7893170000	-0.3845480000	0.0941930000
C	-2.9764120000	-1.0163050000	-0.3019070000
H	-6.1960000000	-2.9642360000	-1.5026280000
H	-4.7076540000	-3.2295580000	-0.5959740000
H	-4.6712120000	-2.3407450000	-2.1313620000
H	-7.2406580000	-0.7674230000	-1.7035190000
H	-5.7428770000	-0.0256730000	-2.2890830000
H	-6.5881590000	0.6603930000	-0.8948850000
H	-7.2814370000	-2.0284710000	0.4773370000
H	-6.6311290000	-0.6248960000	1.3291730000
H	-5.8133400000	-2.1880330000	1.4552500000
H	-5.2941490000	1.1526000000	0.8948110000
H	-3.2655560000	2.3384680000	1.5809250000
H	-0.9461540000	2.4579950000	1.5809120000
H	3.3358220000	0.3725710000	0.3171240000
H	5.3406600000	-0.9617140000	0.0972110000
H	2.9540470000	-4.4971370000	-0.4642090000
H	0.9304800000	-3.1872320000	-0.1872400000
H	-0.5639620000	-1.9149580000	-0.7140930000
H	2.5735100000	3.4529730000	1.1141680000
H	3.4314280000	5.0375120000	-0.5884830000
H	2.8119400000	4.7503830000	-2.9673750000
H	1.3464420000	2.8745870000	-3.6486270000

H	0.5035180000	1.2861080000	-1.9622240000
H	-2.8797190000	-1.9595250000	-0.8247590000

5. Copies of NMR Spectra

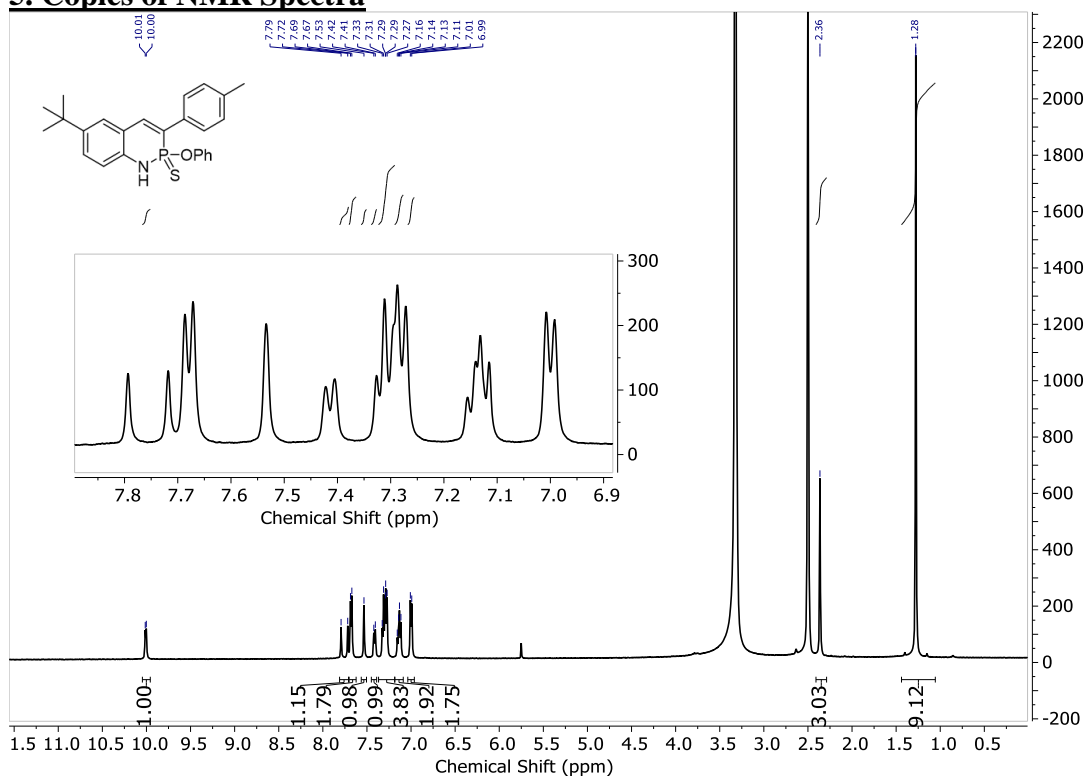


Figure E.7 ^1H NMR spectrum of **2a** in $\text{DMSO-}d_6$.

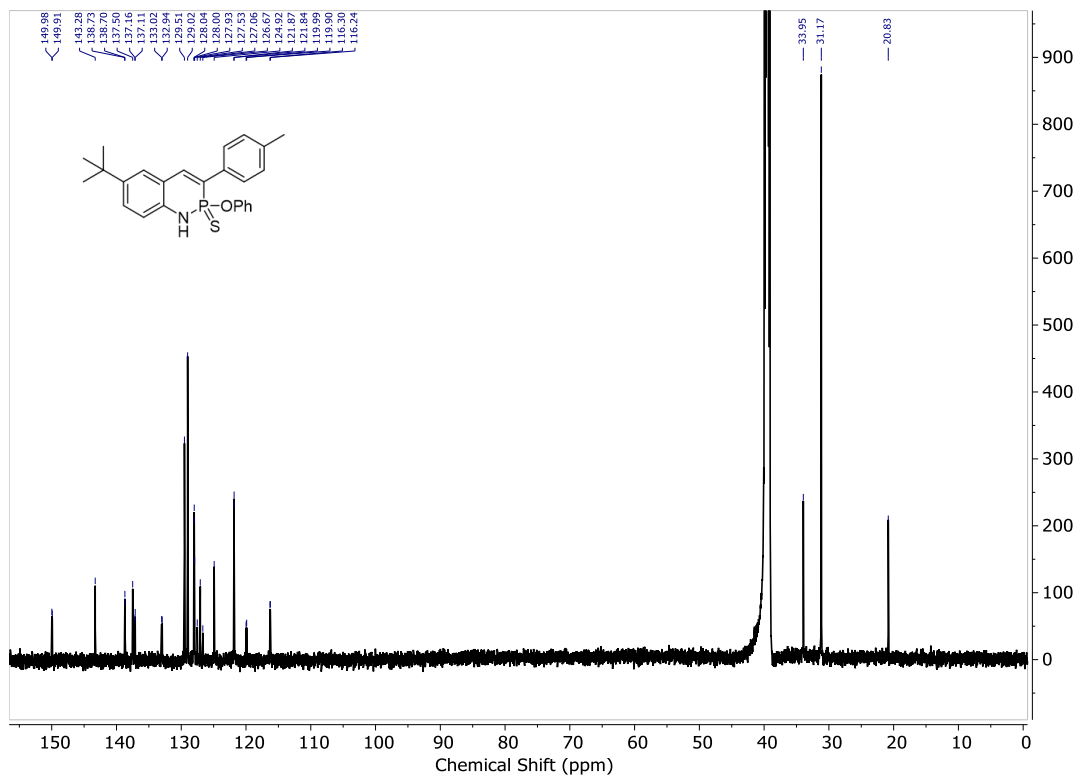


Figure E.8 ^{13}C NMR spectrum of **2a** in $\text{DMSO-}d_6$.

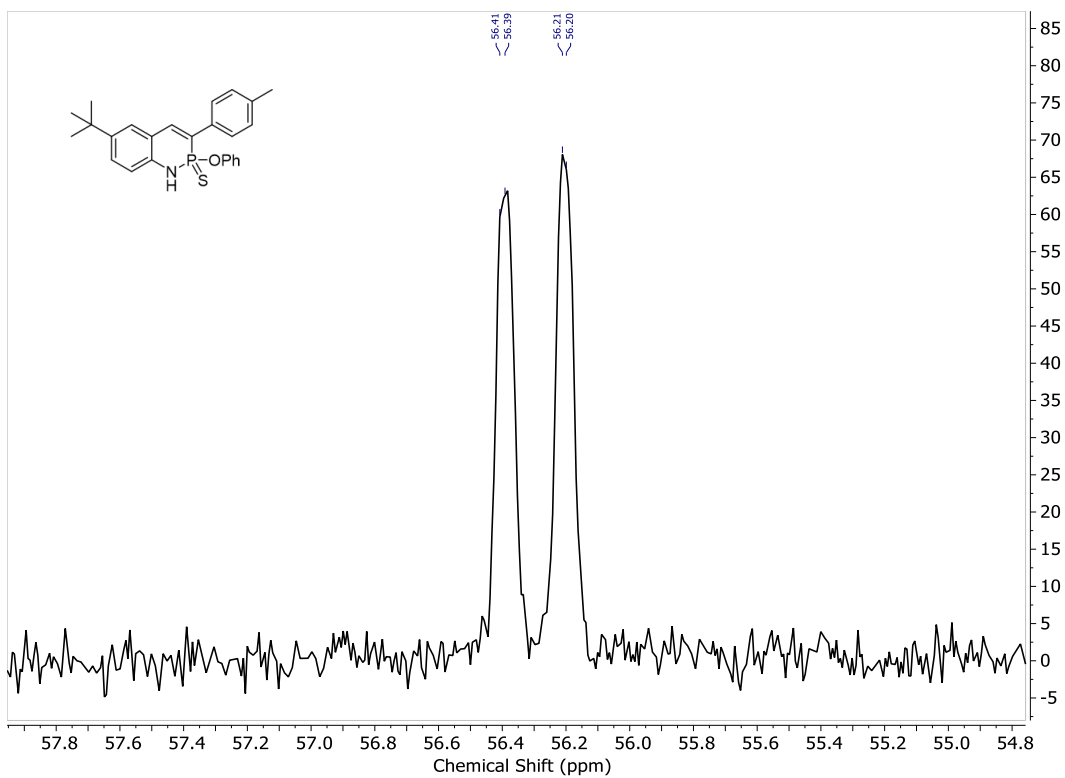


Figure E.9 ³¹P NMR spectrum of **2a** in DMSO-*d*₆.

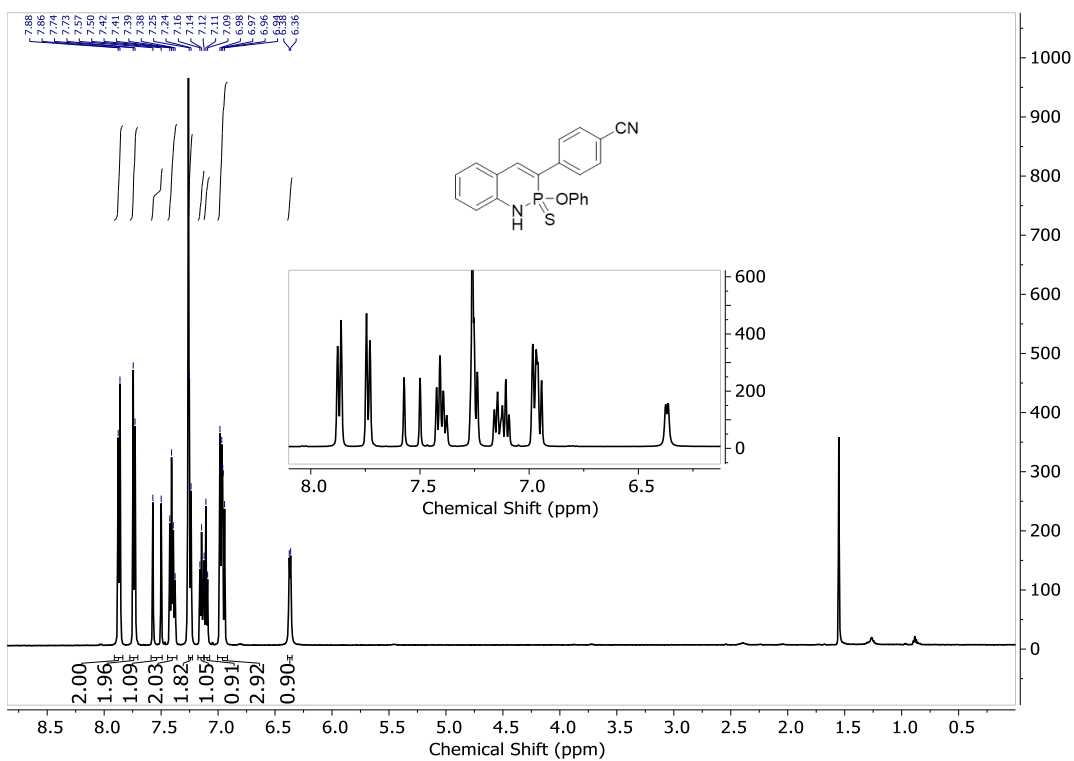


Figure E.10 ¹H NMR spectrum of **2b** in CDCl₃.

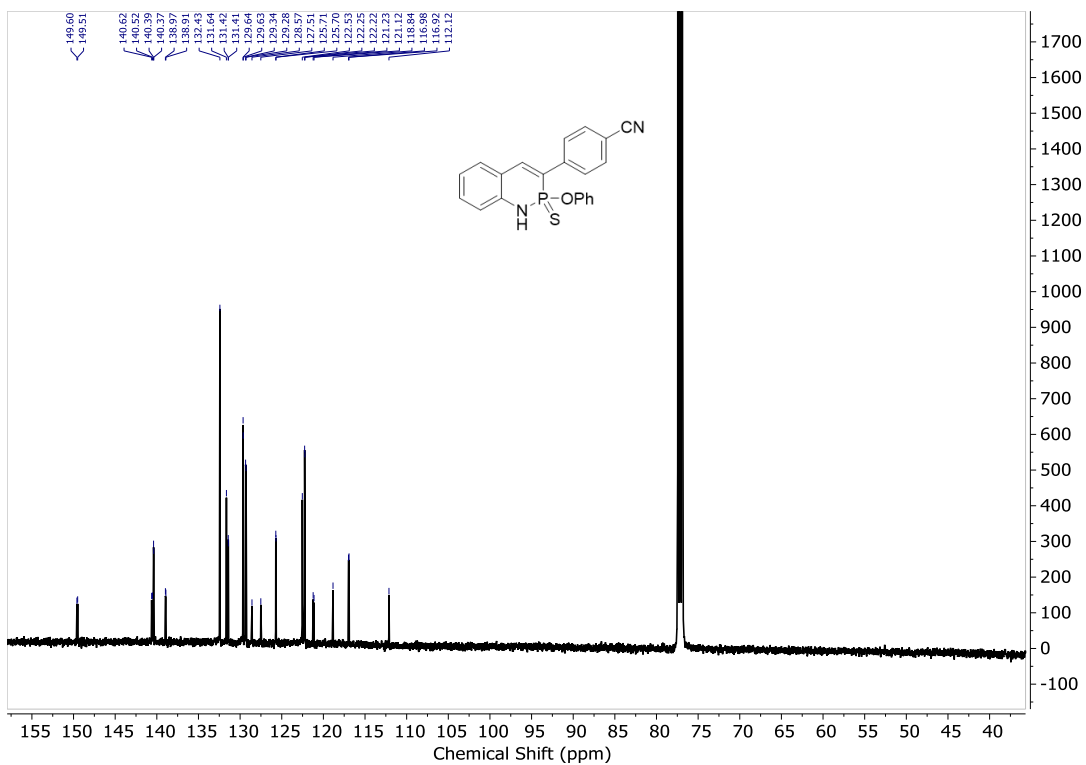


Figure E.11 ^{13}C NMR spectrum of **2b** in CDCl_3 .

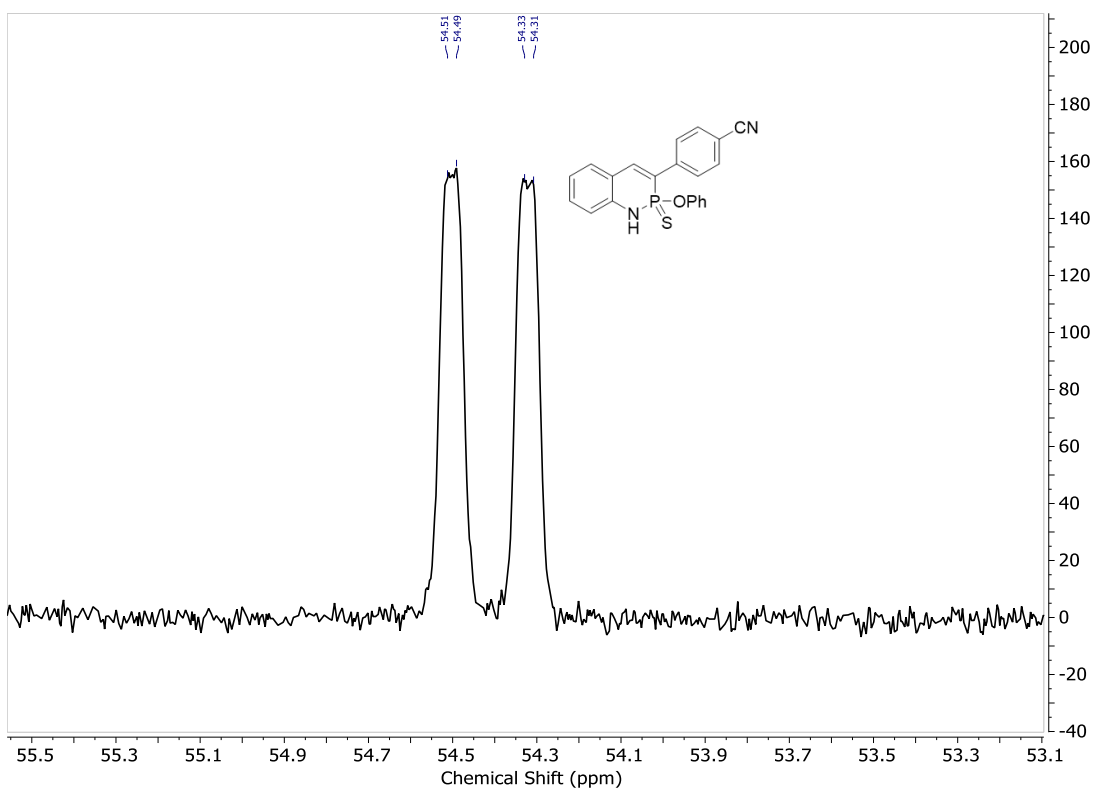


Figure E.12 ^{31}P NMR spectrum of **2b** in CDCl_3 .

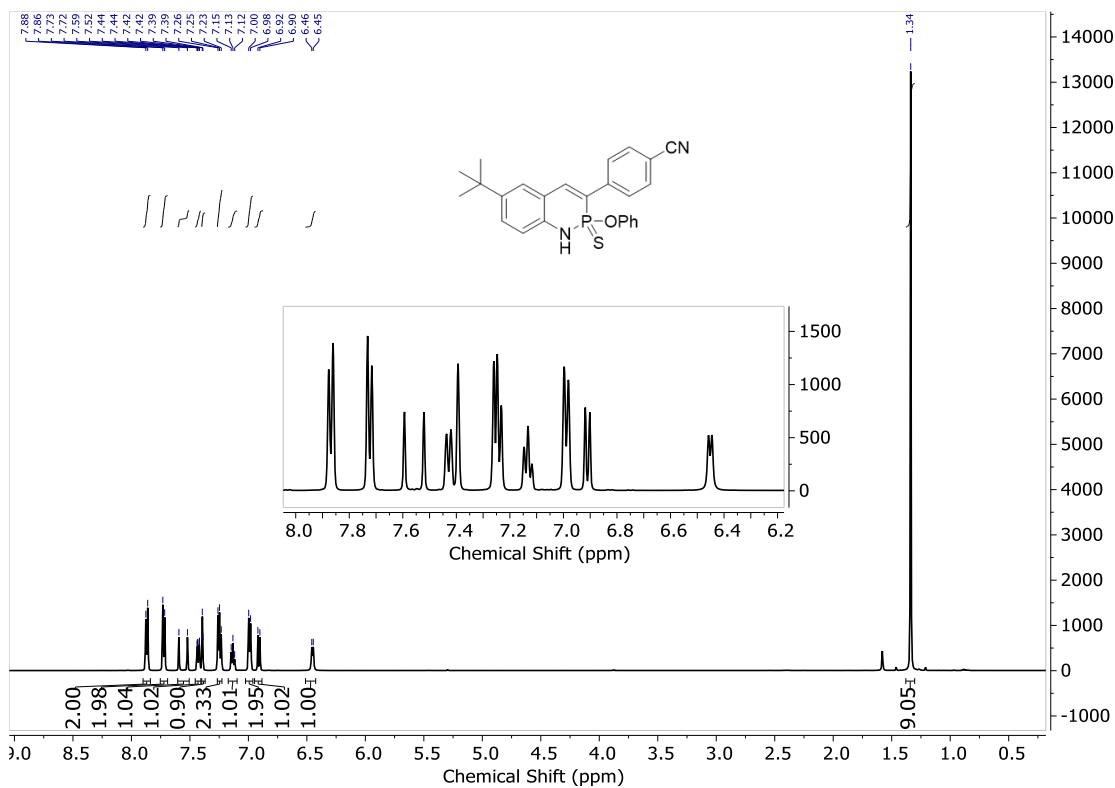


Figure E.13 ¹H NMR spectrum of **2c** in CDCl₃.

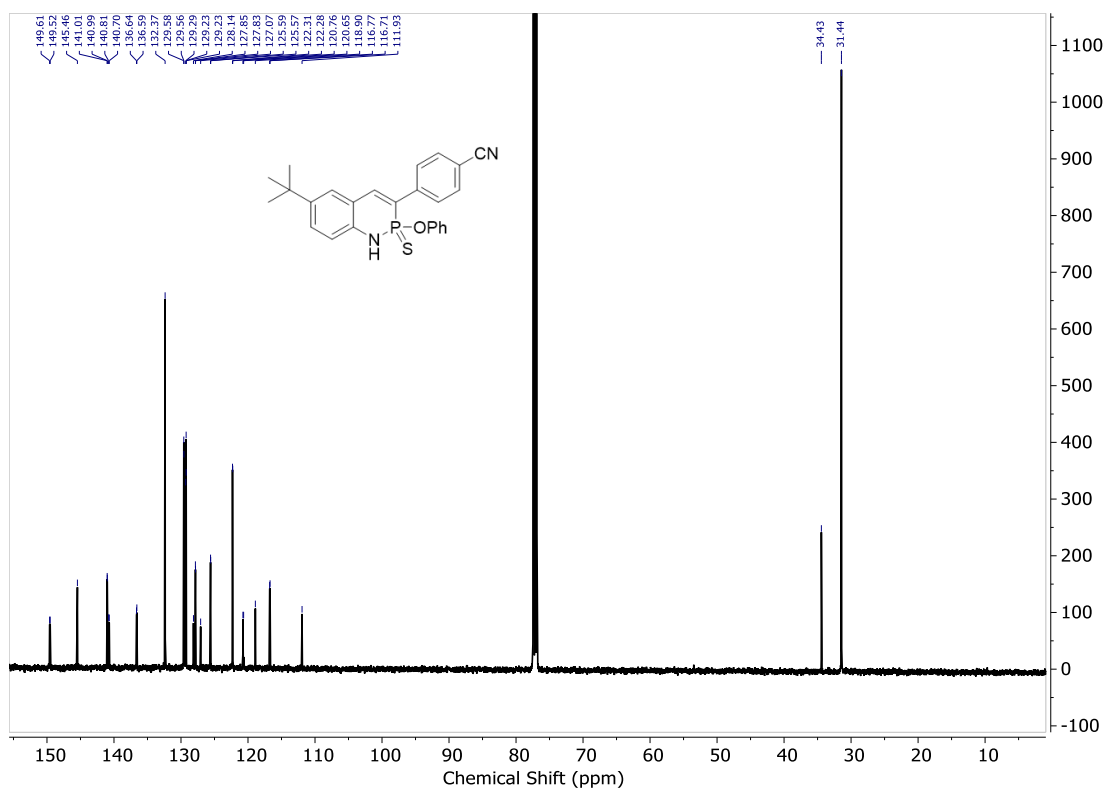


Figure E.14 ¹³C NMR spectrum of **2c** in CDCl₃.

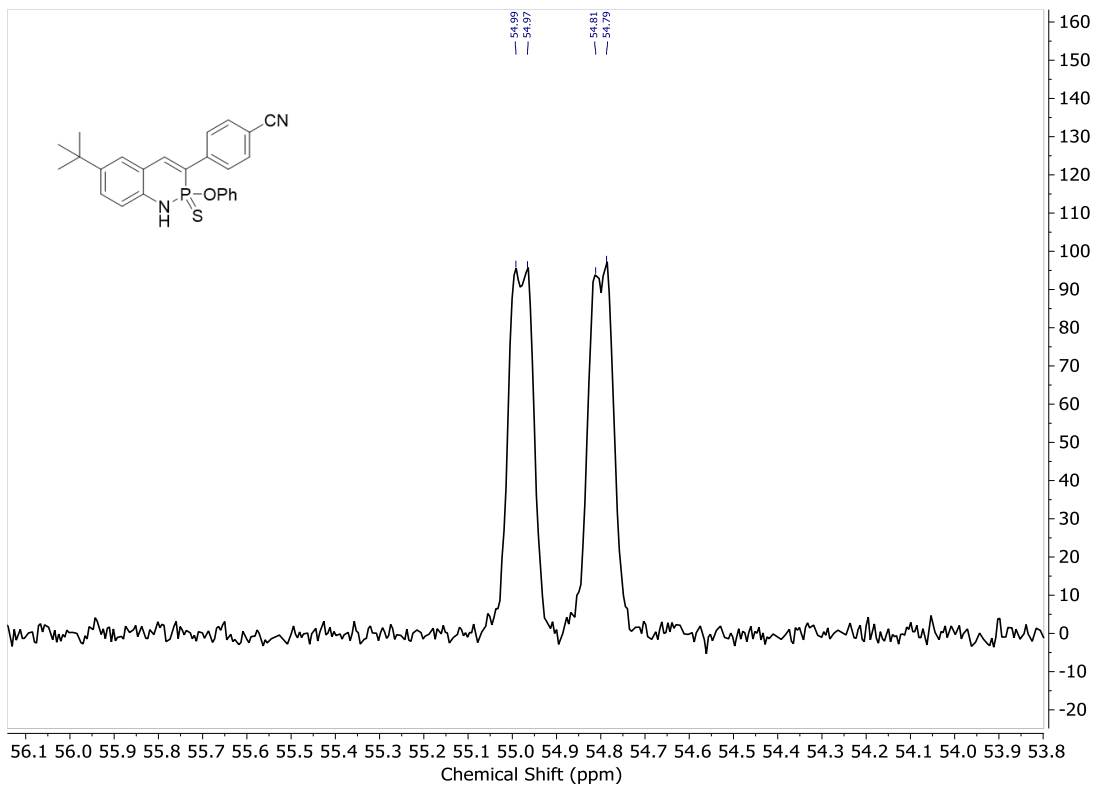


Figure E.15 ^{31}P NMR spectrum of **2c** in CDCl_3 .

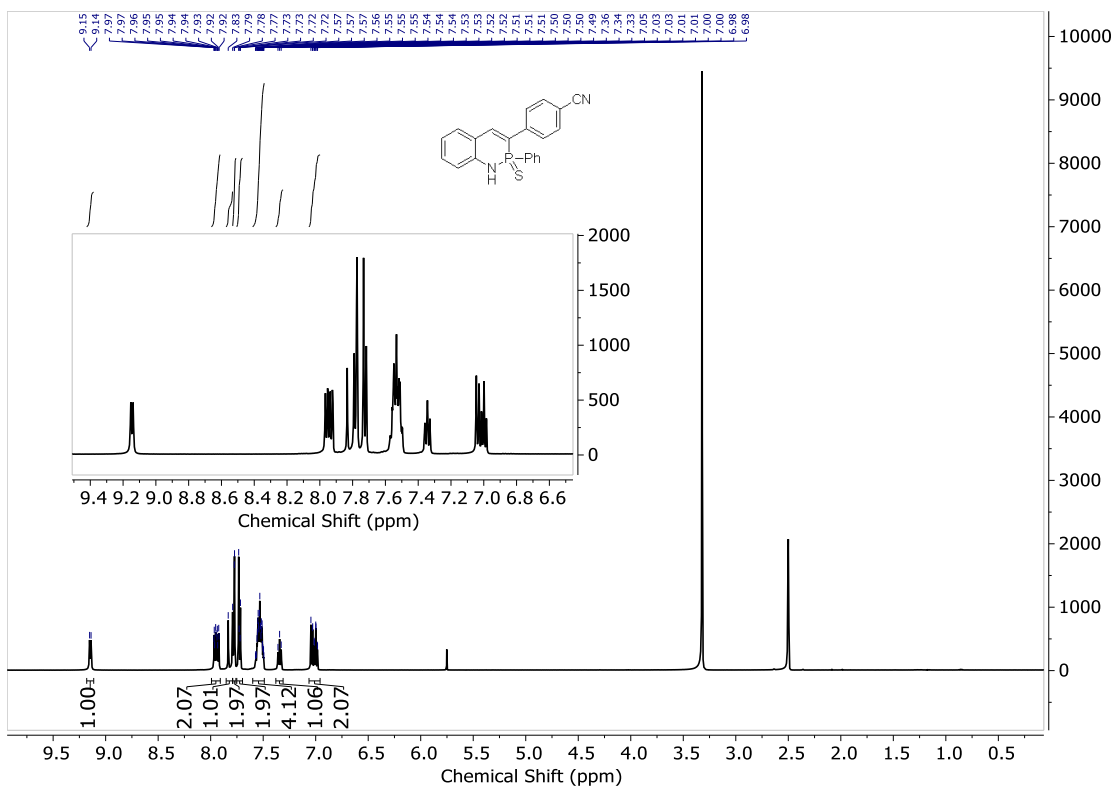


Figure E.16 ^1H NMR spectrum of **2d** in $\text{DMSO}-d_6$.

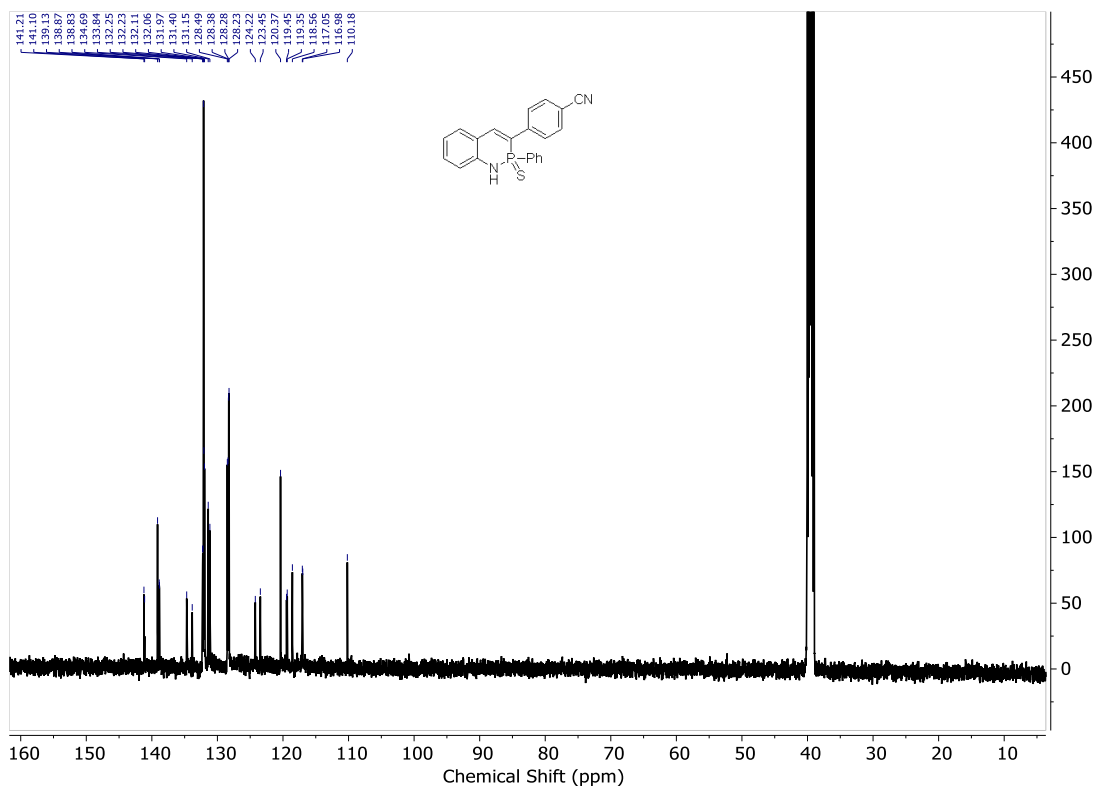


Figure E.17 ^{13}C NMR spectrum of **2d** in $\text{DMSO-}d_6$.

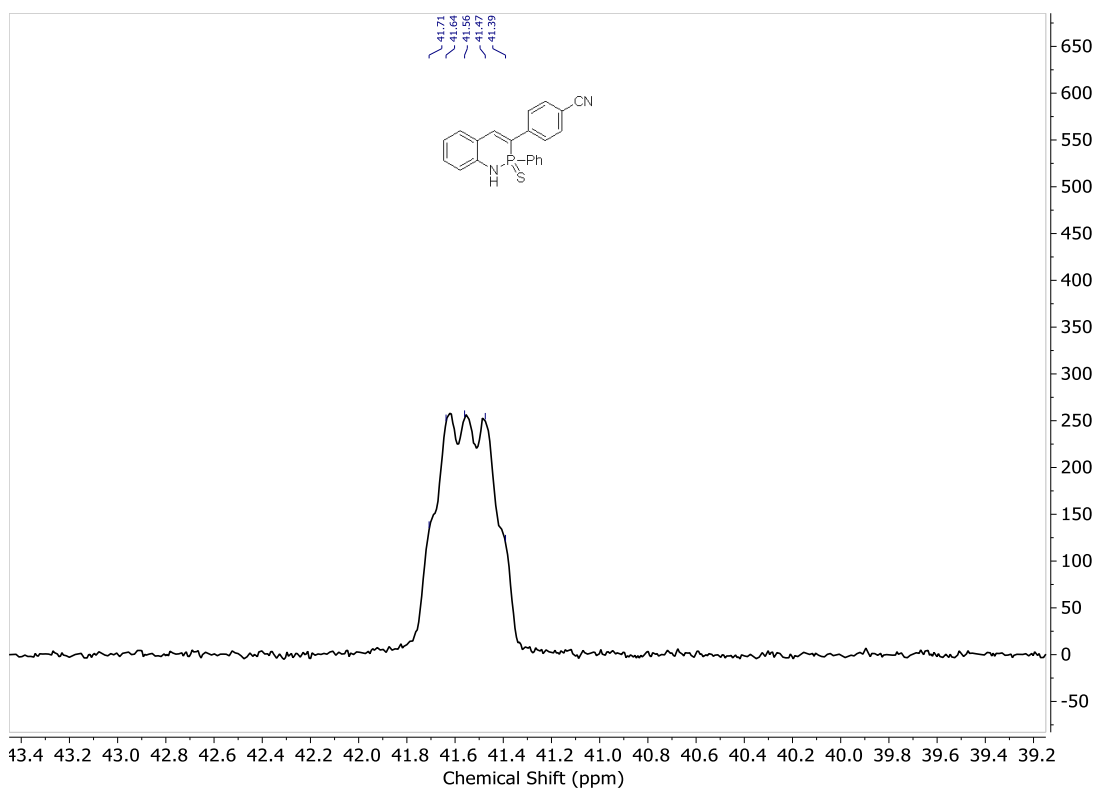


Figure E.18 ^{31}P NMR spectrum of **2d** in $\text{DMSO-}d_6$.

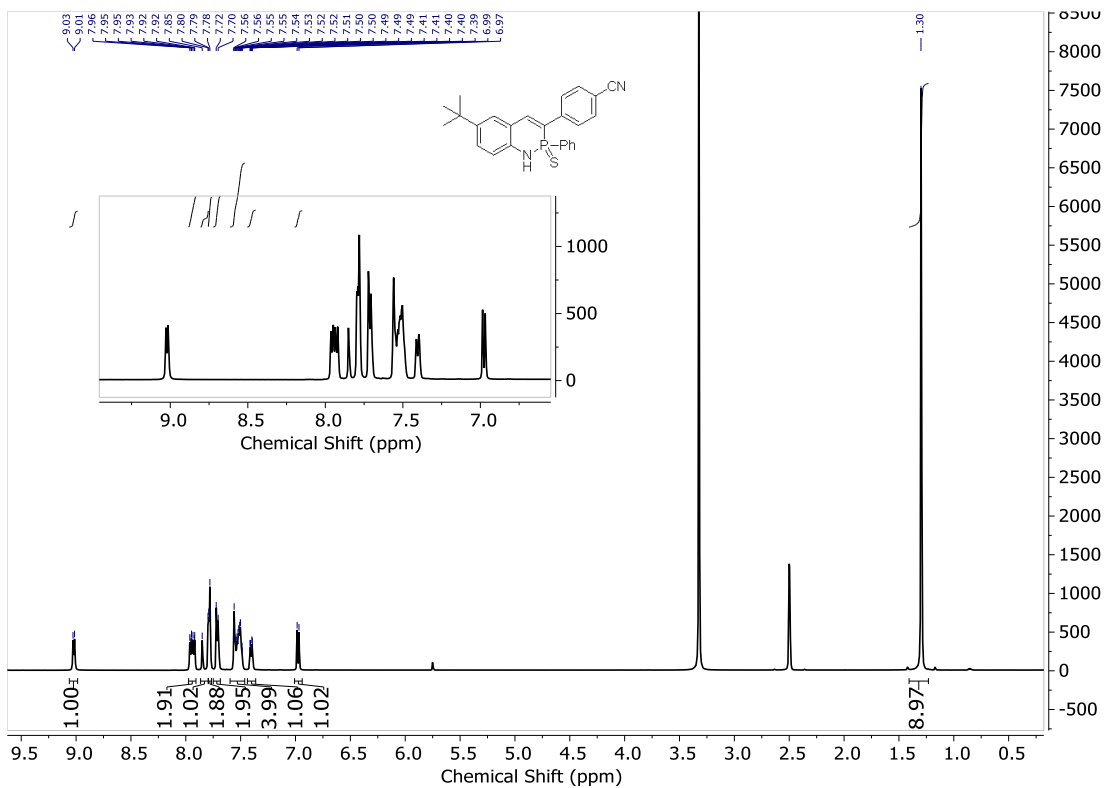


Figure E.19 ¹H NMR spectrum of **2e** in DMSO-*d*₆.

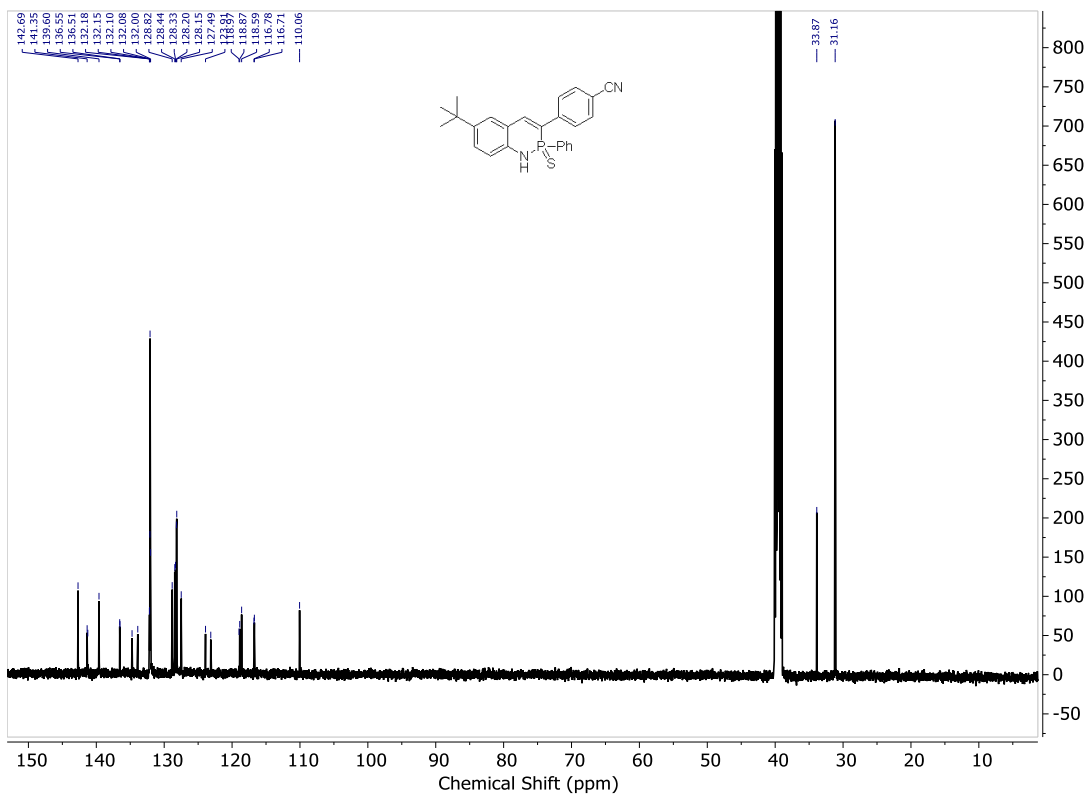


Figure E.20 ¹³C NMR spectrum of **2e** in DMSO-*d*₆.

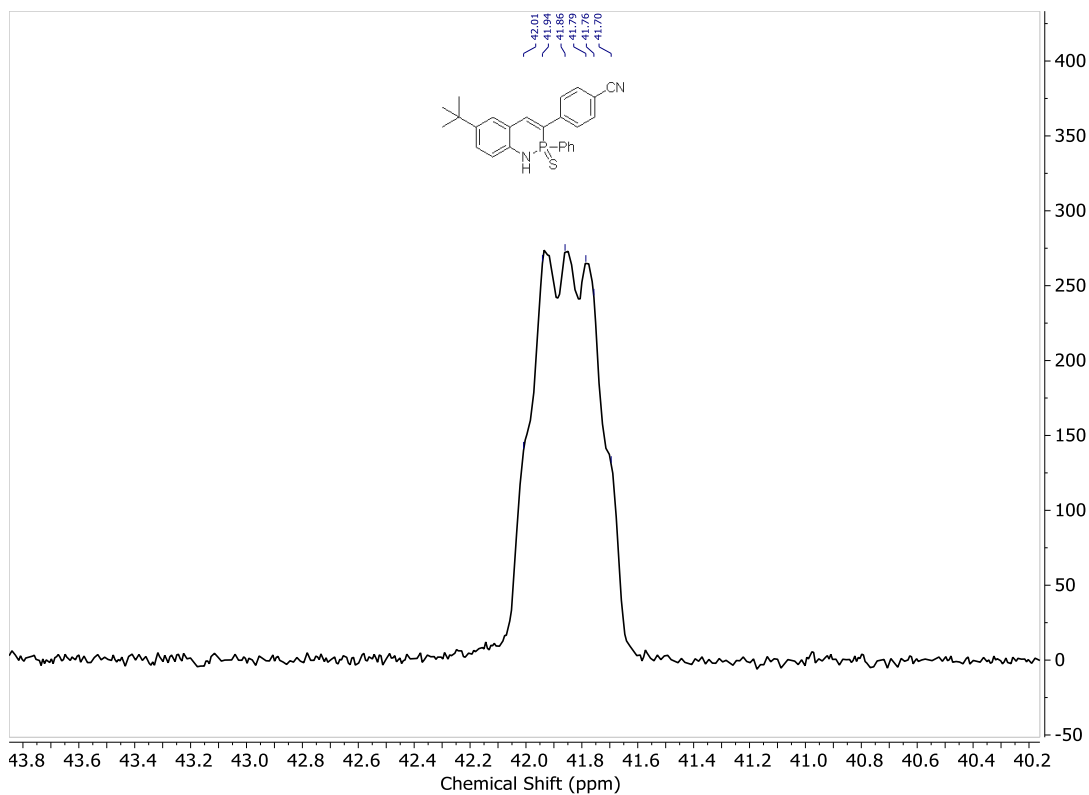


Figure E.21 ^{31}P NMR spectrum of **2e** in $\text{DMSO-}d_6$.

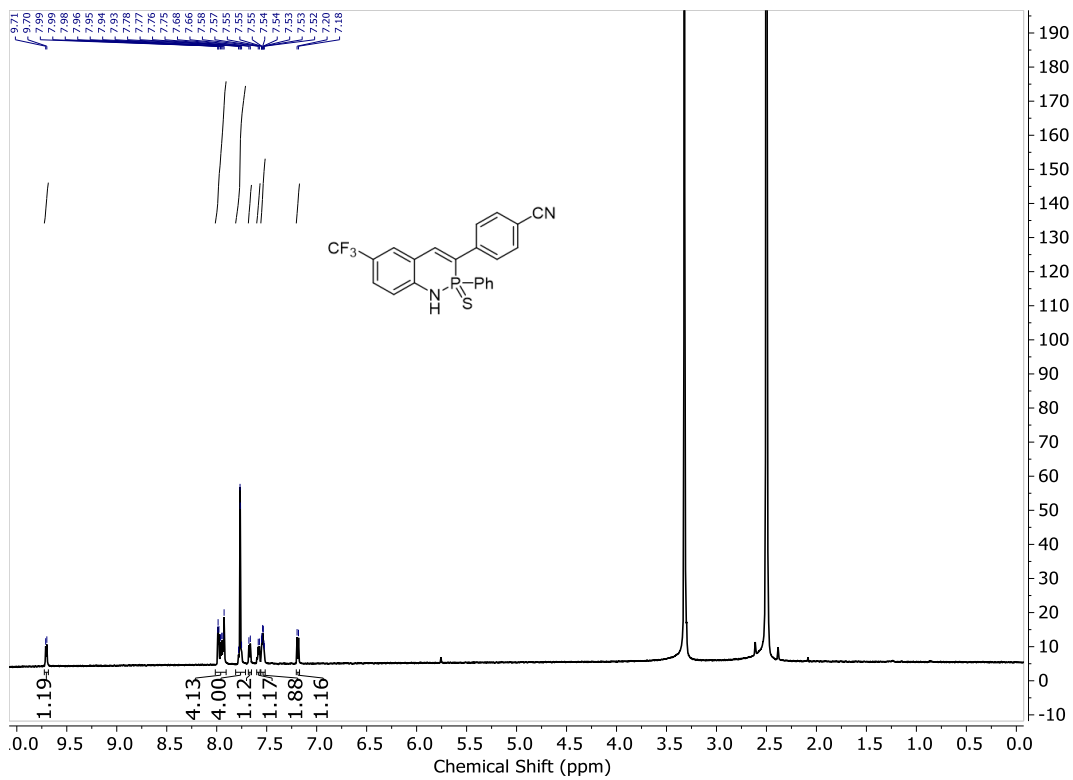


Figure E.22 ^1H NMR spectrum of **2f** in $\text{DMSO-}d_6$.

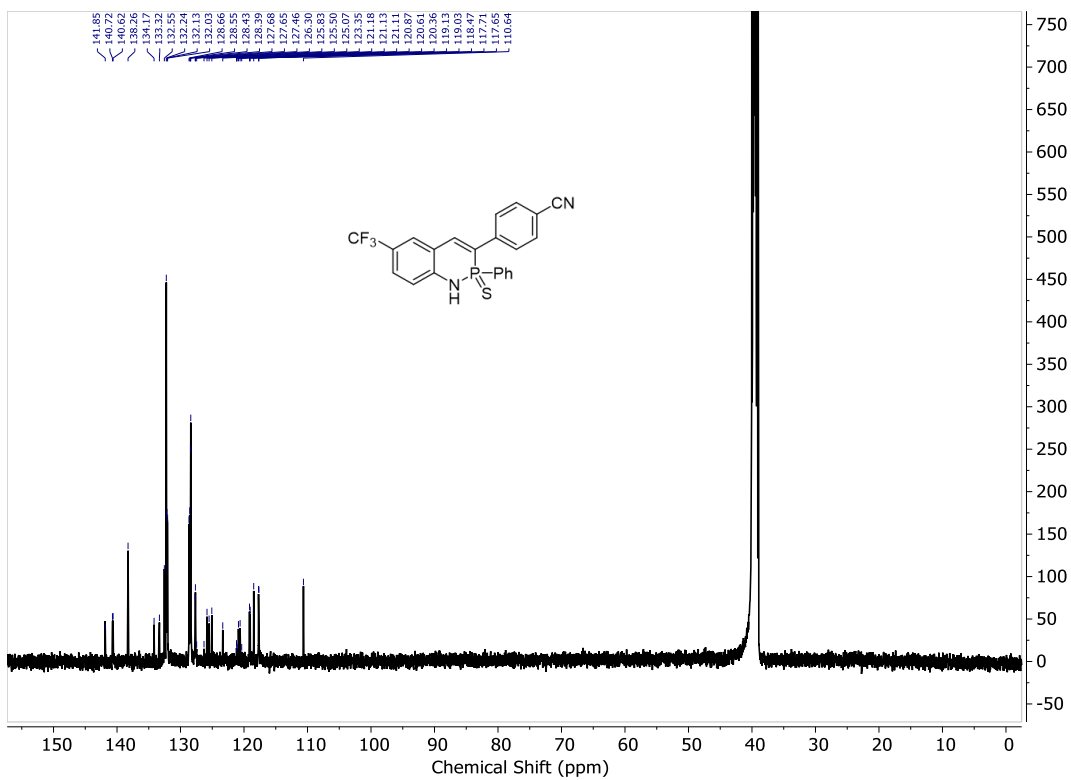


Figure E.23 ^{13}C NMR spectrum of **2f** in $\text{DMSO-}d_6$.

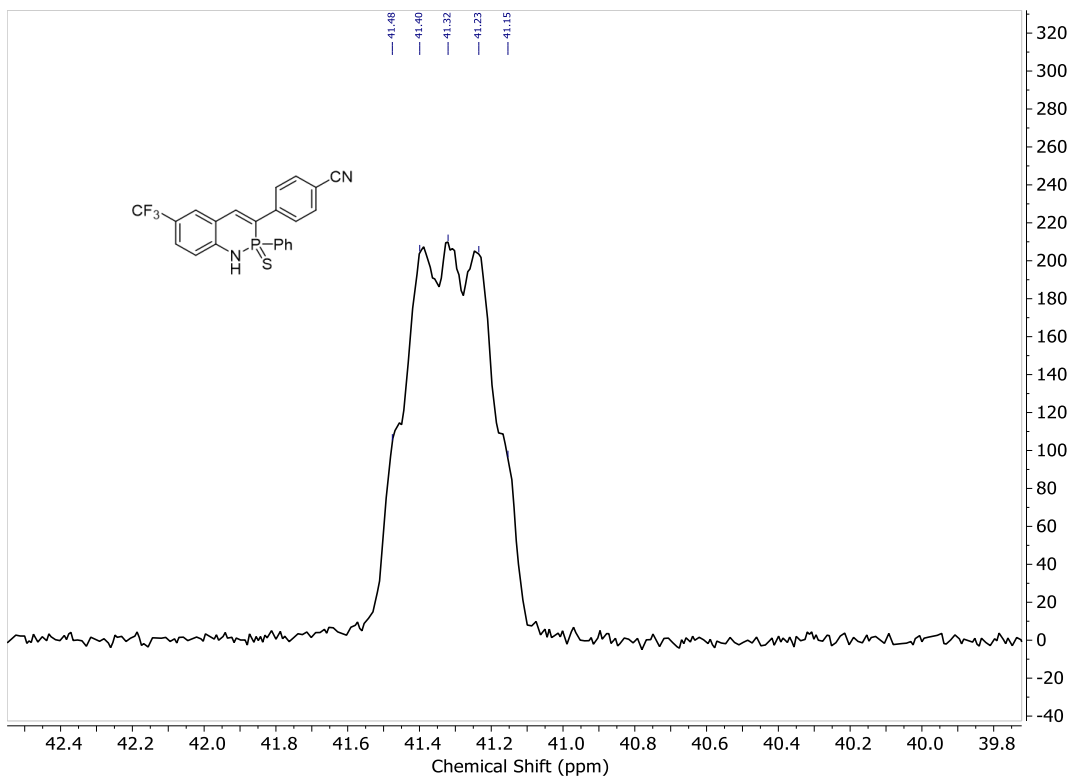


Figure E.24 ^{31}P NMR spectrum of **2f** in $\text{DMSO-}d_6$.

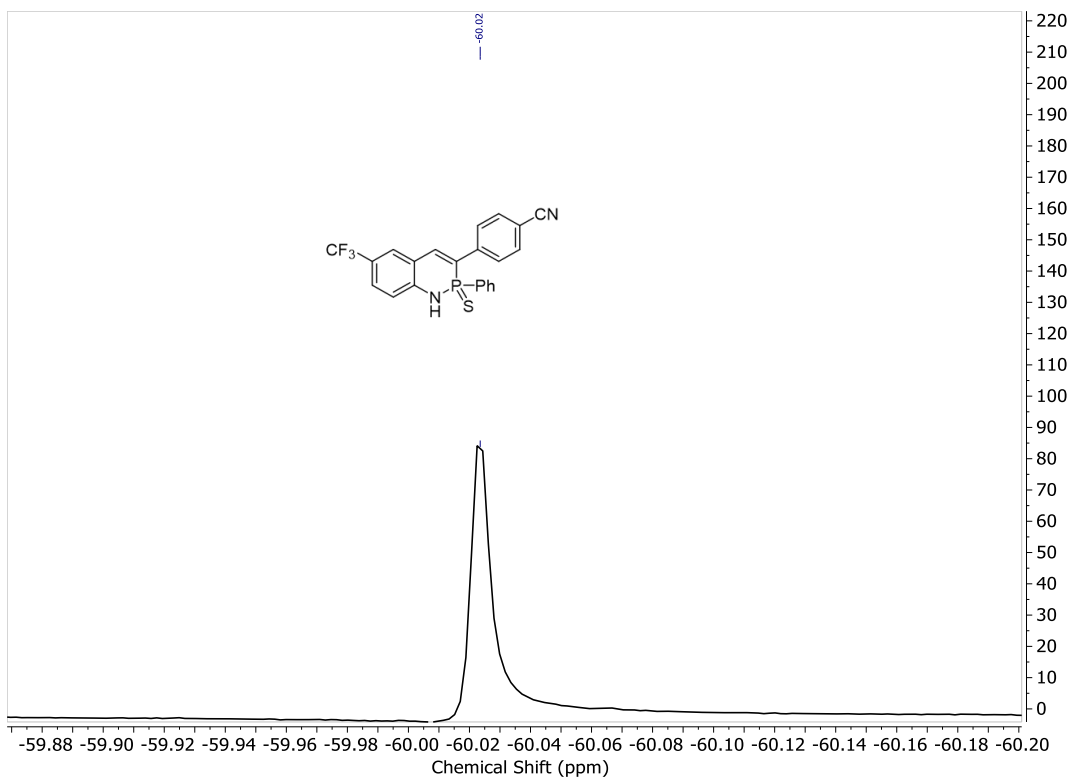


Figure E.25 ¹⁹F NMR spectrum of **2f** in DMSO-*d*₆.

APPENDIX F

SUPPLEMENTARY INFORMATION FOR CHAPTER 7

Photophysical Properties

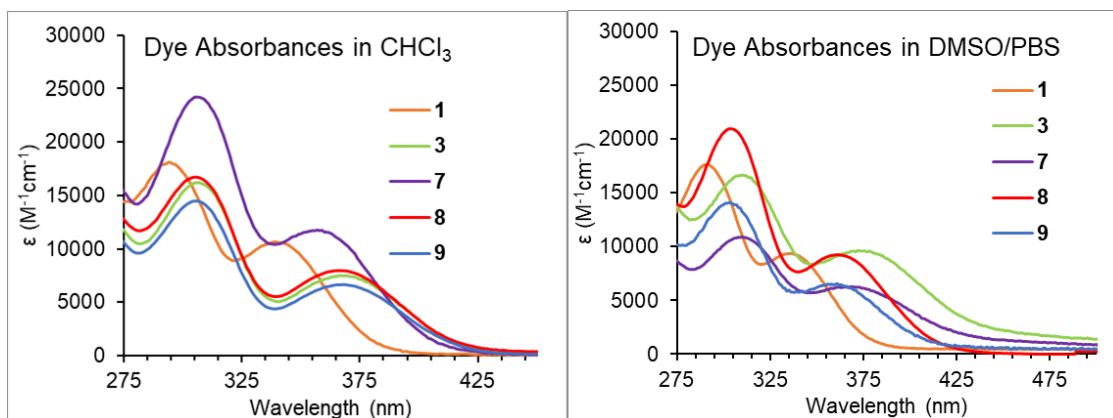


Figure F.1 UV-vis absorption spectra of new heterocycles in (left) CHCl₃ and (right) ~5% DMSO in pH 7.4 PBS buffer.

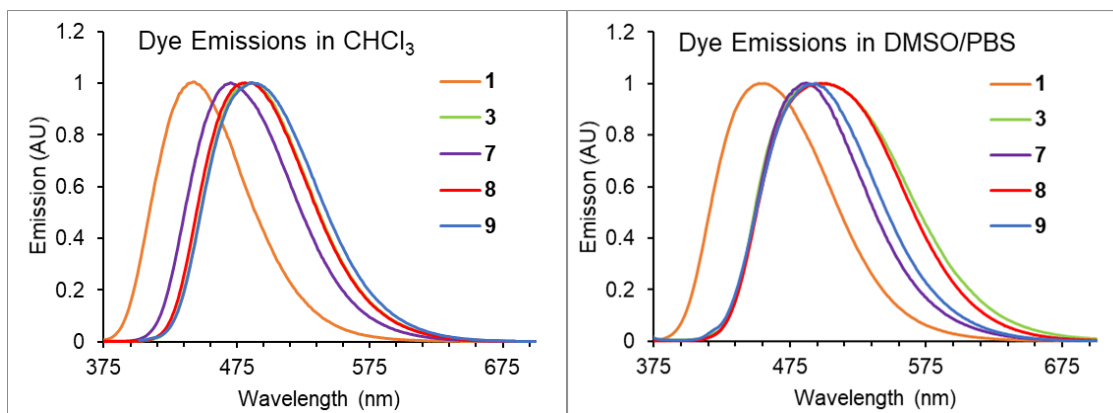


Figure F.2 Emission spectra of new heterocycles in (left) CHCl₃ and (right) ~5% DMSO in pH 7.4 PBS buffer.

Acid base stabilities studies

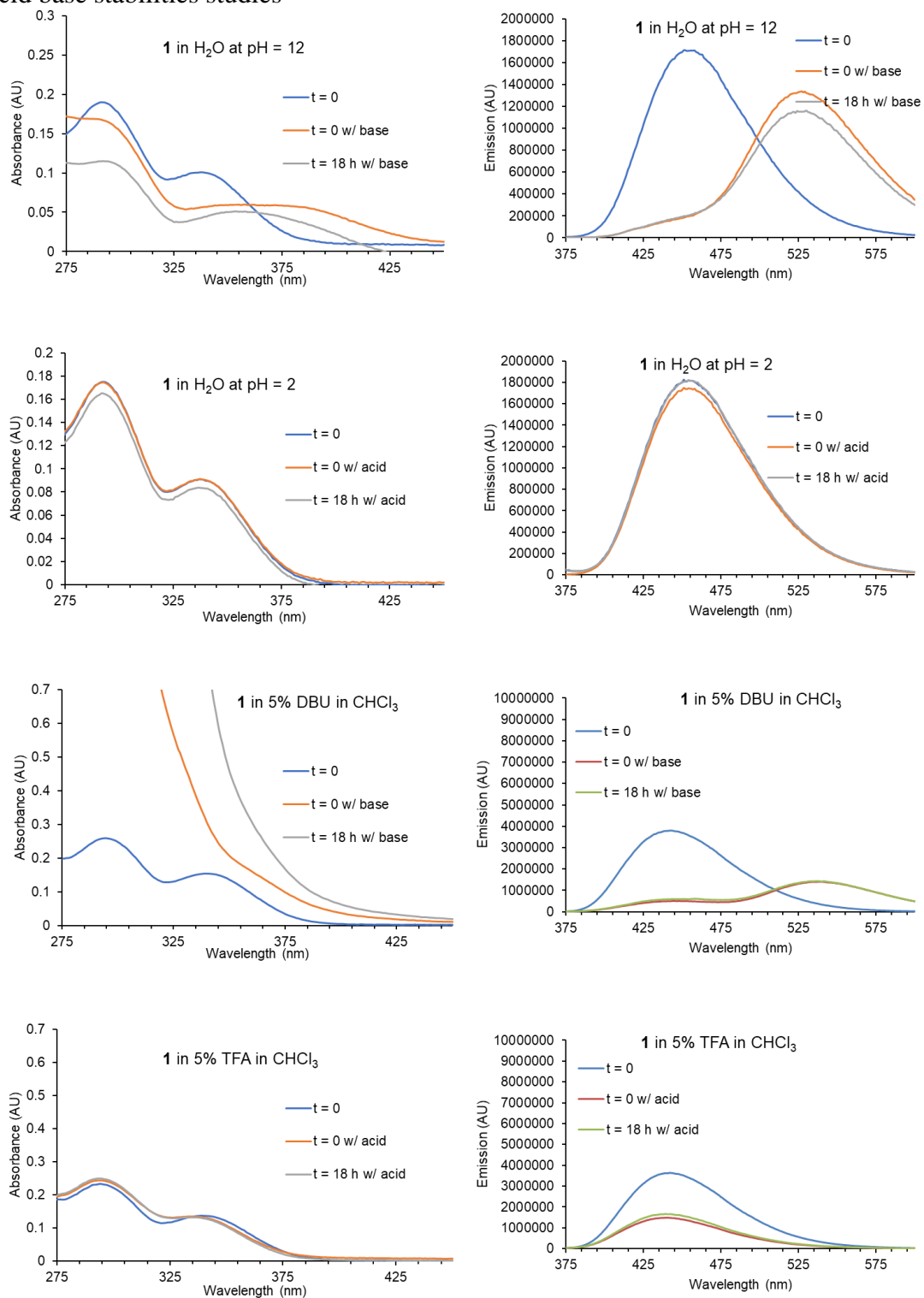


Figure F.3 (left) absorption spectra of **1** before and after addition of acid or base.

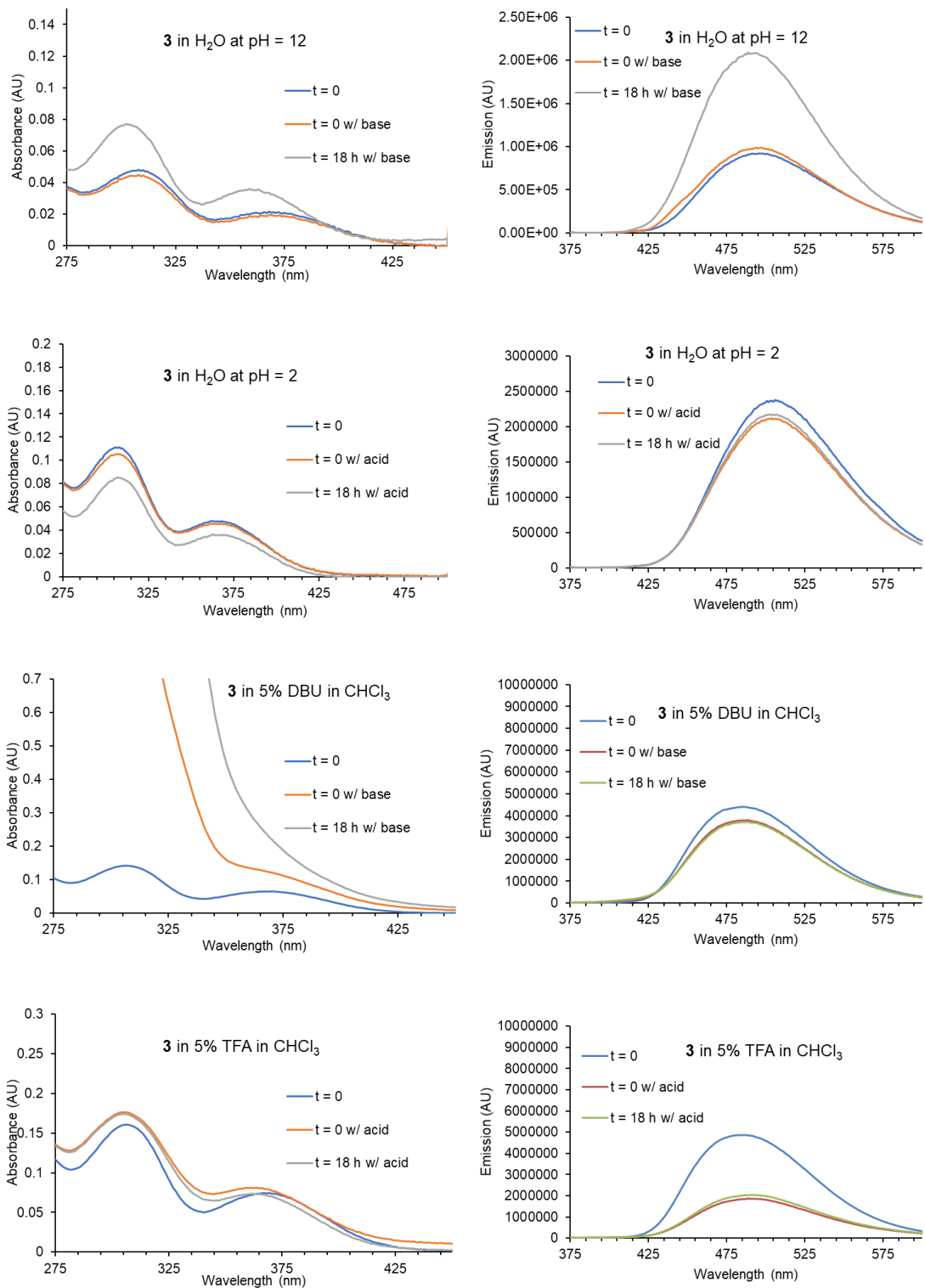


Figure F.4 (left) absorption spectra of **3** before and after addition of acid or base.

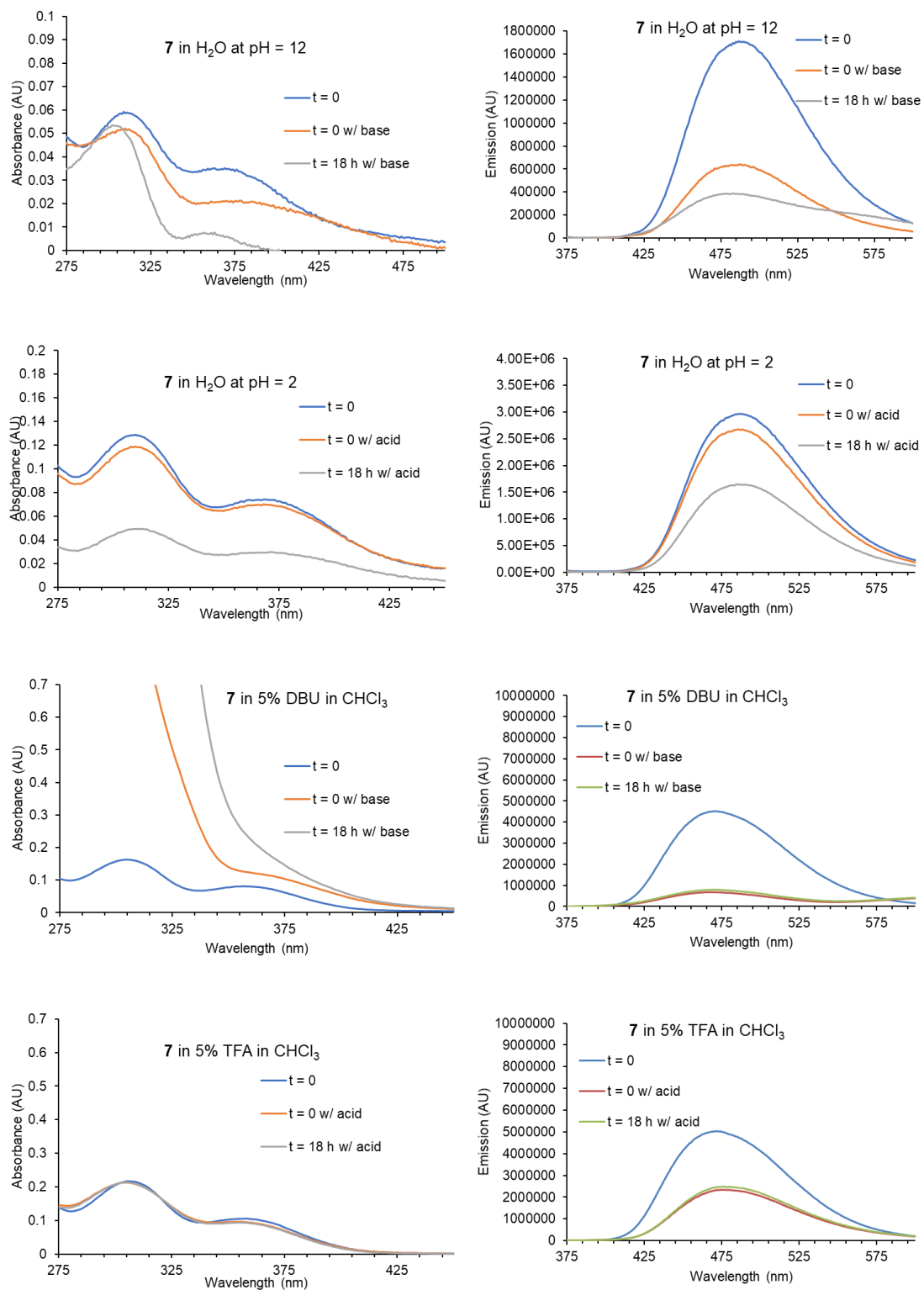


Figure F.5 (left) absorption spectra of **7** before and after addition of acid or base.

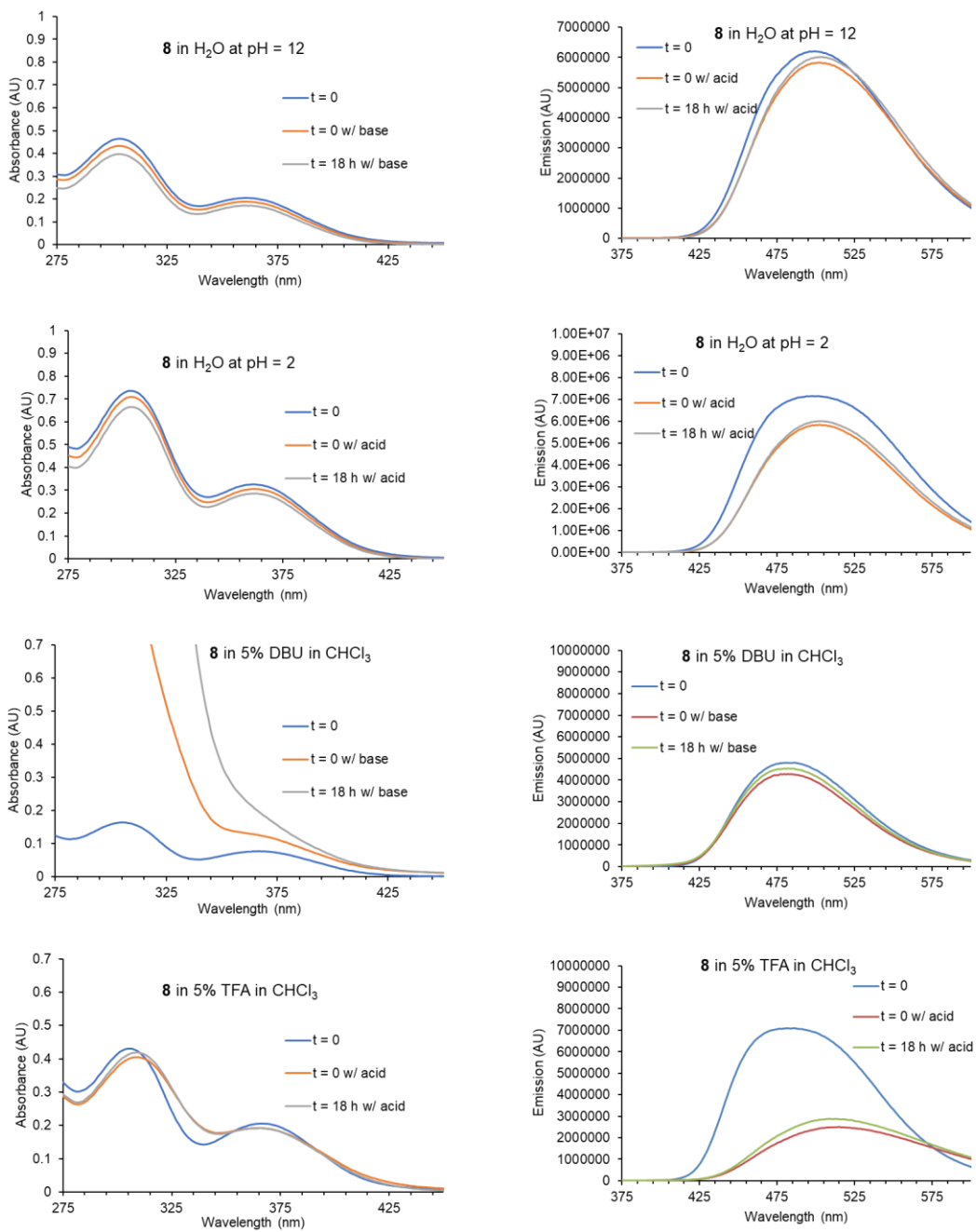


Figure F.6 (left) absorption spectra of **8** before and after addition of acid or base.

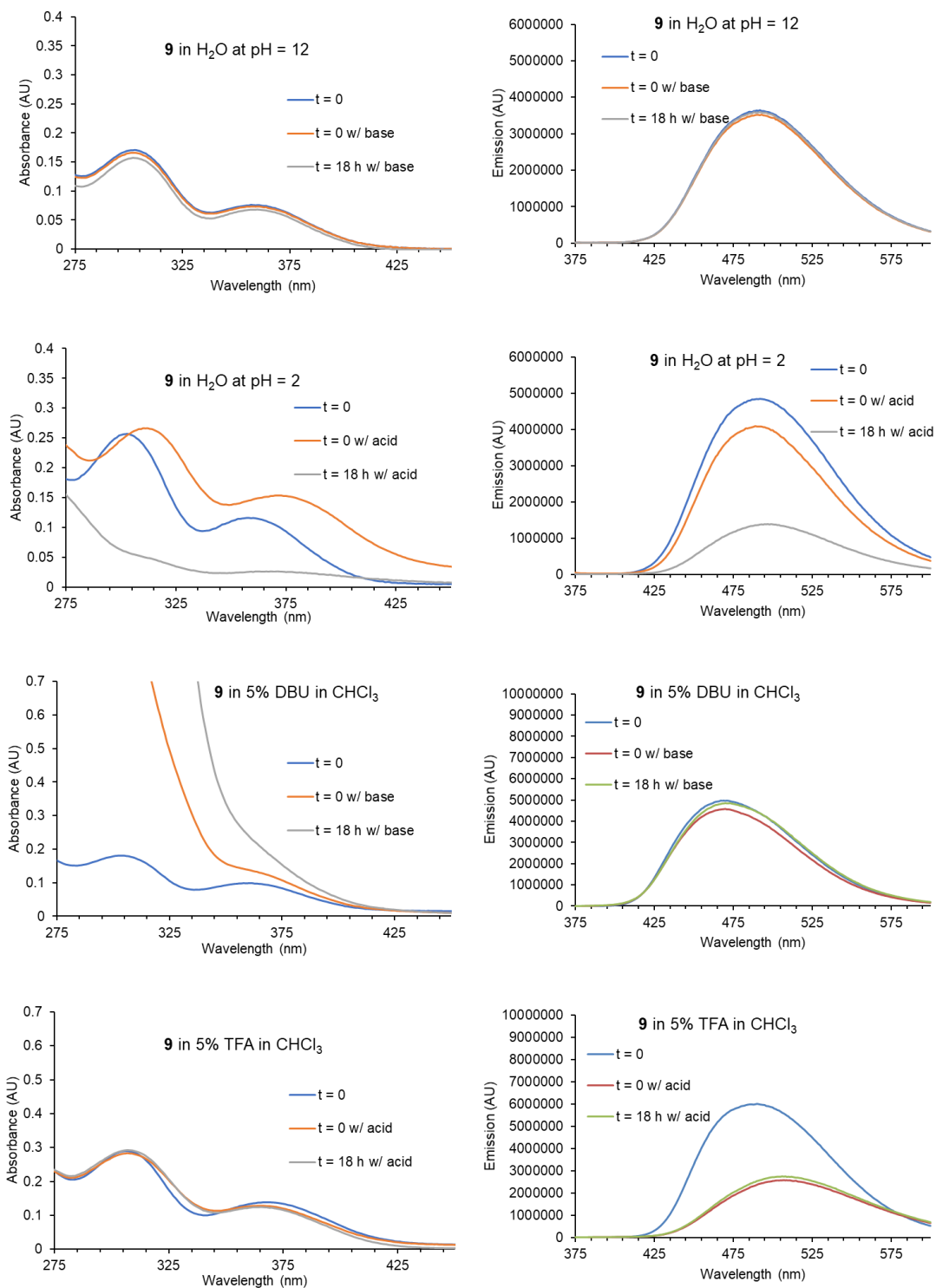


Figure F.7 (left) absorption spectra of **9** before and after addition of acid or base.

Crystallographic Structures of **8**

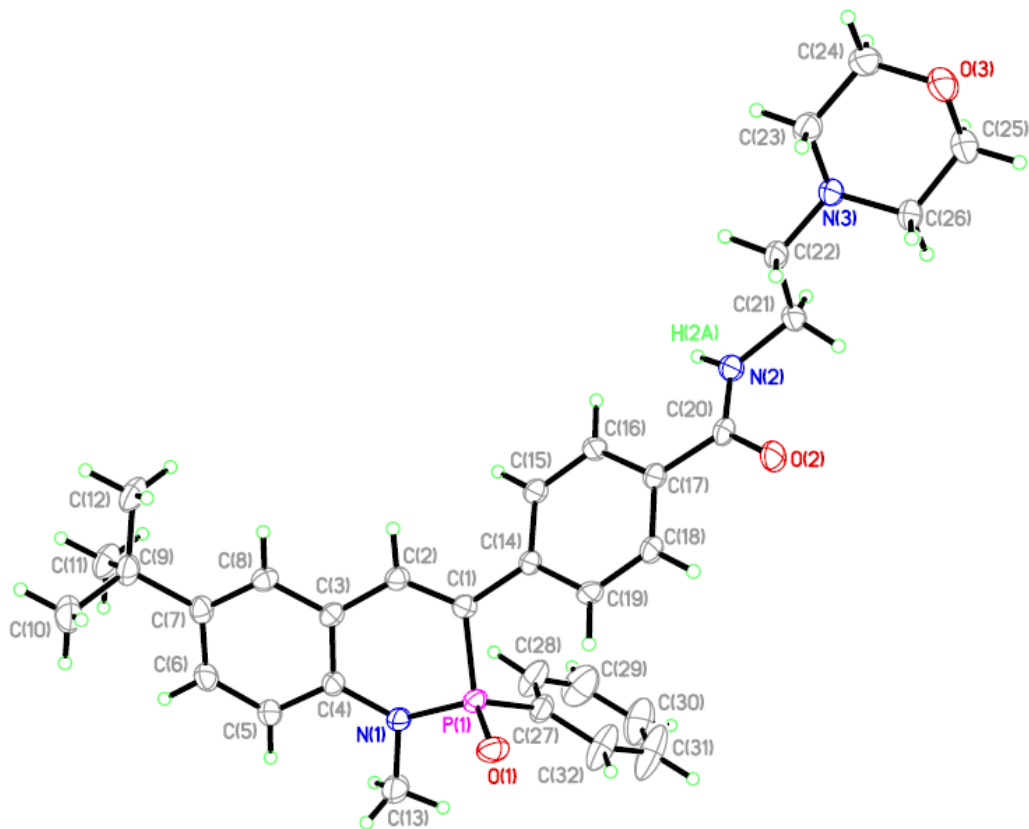


Figure F.8 ORTEP drawing of heterocycle **8**; thermal ellipsoids drawn at 30% probability.

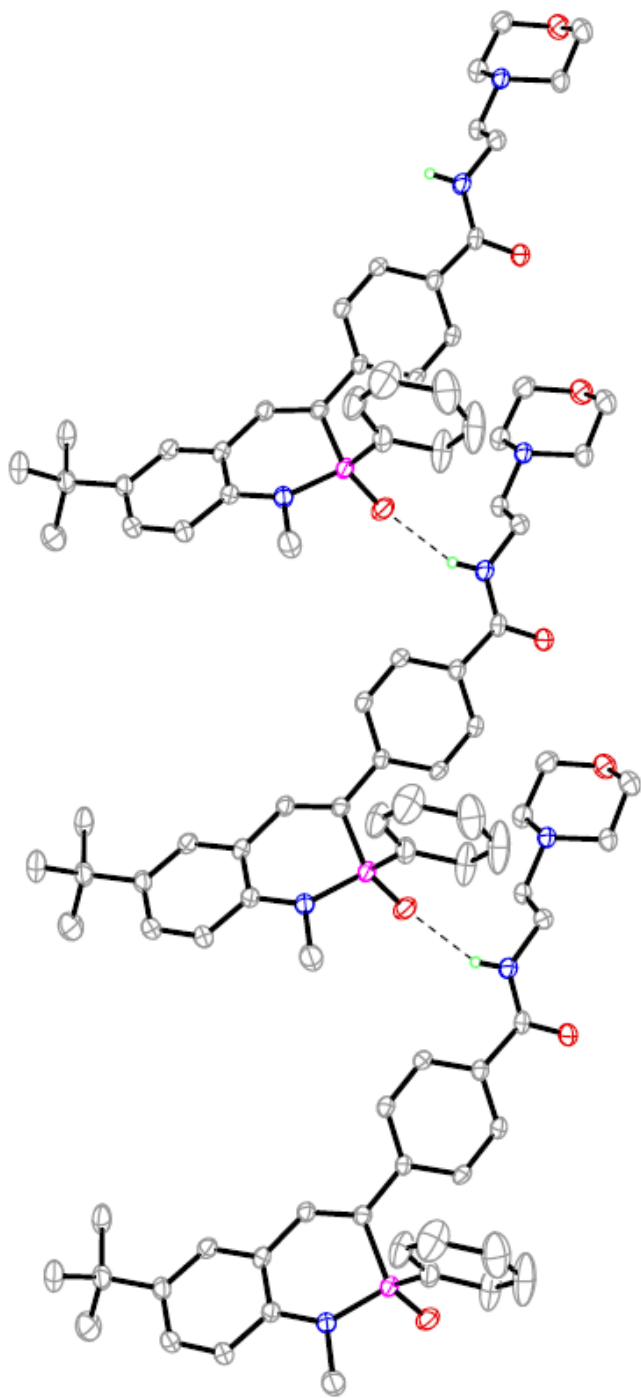
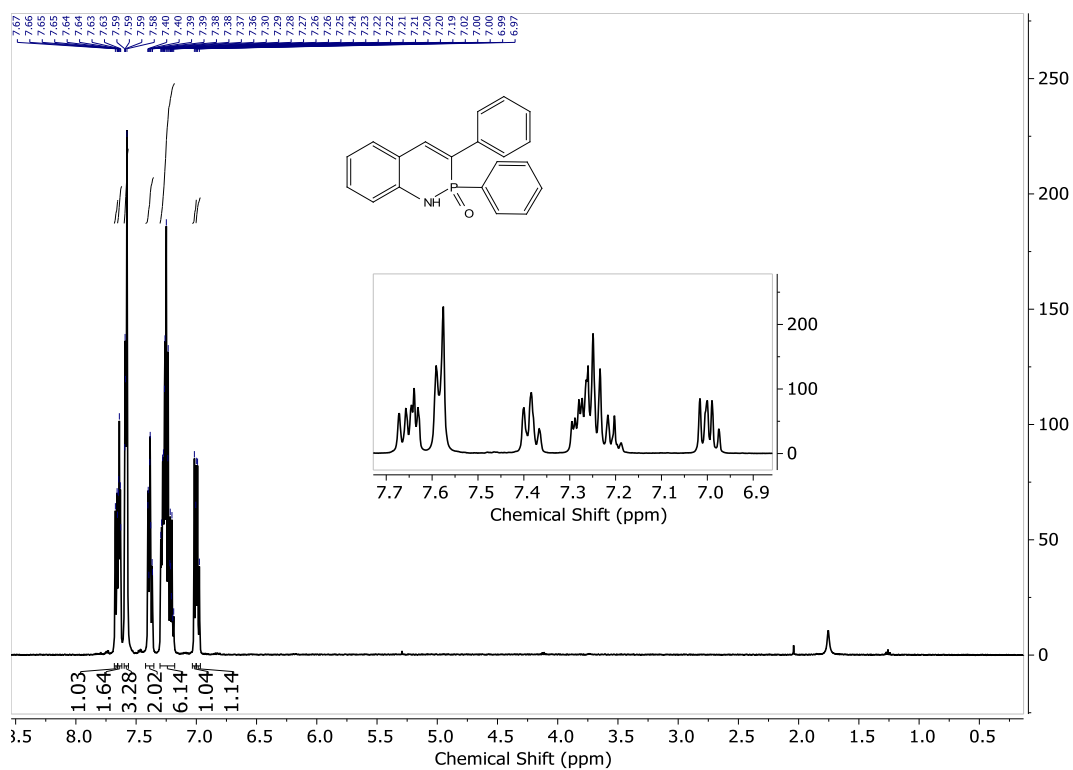
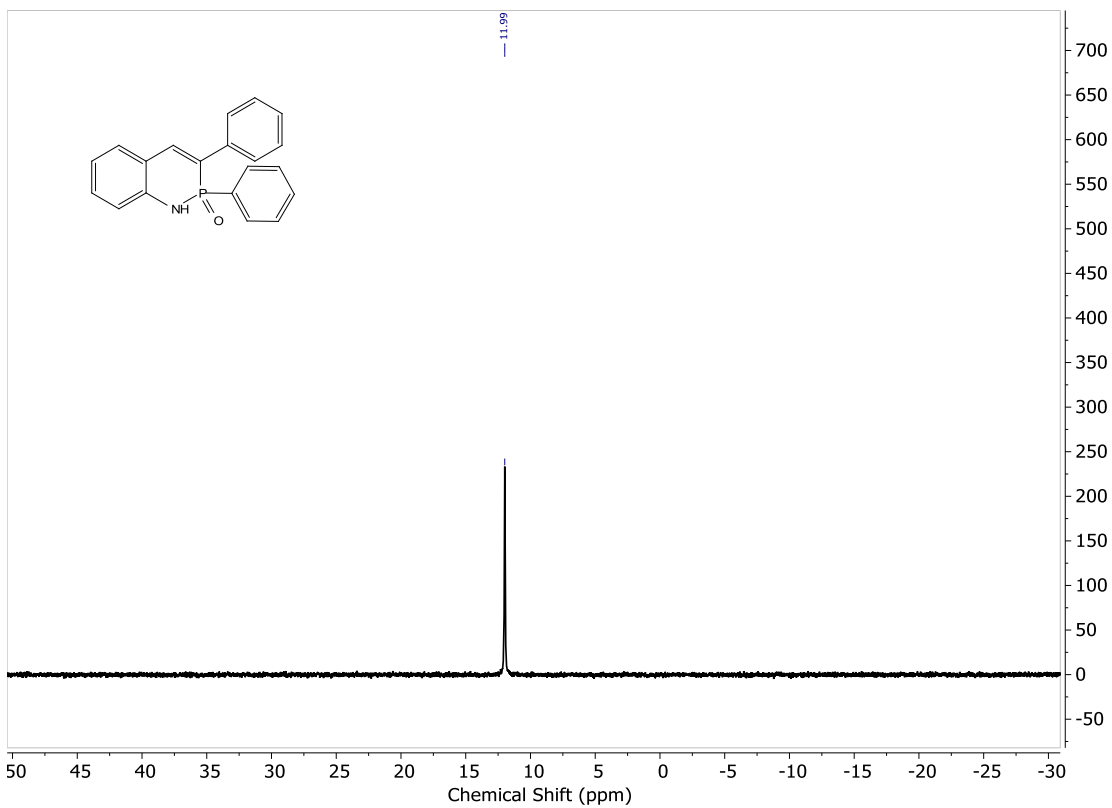
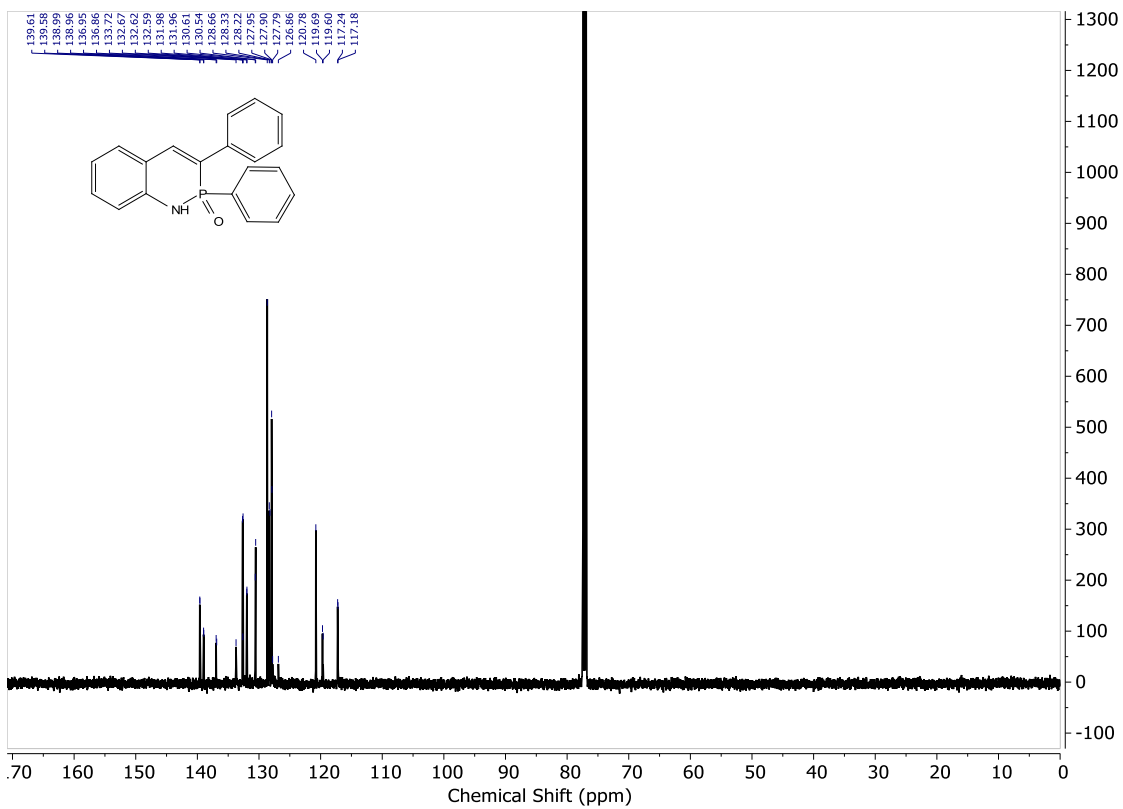
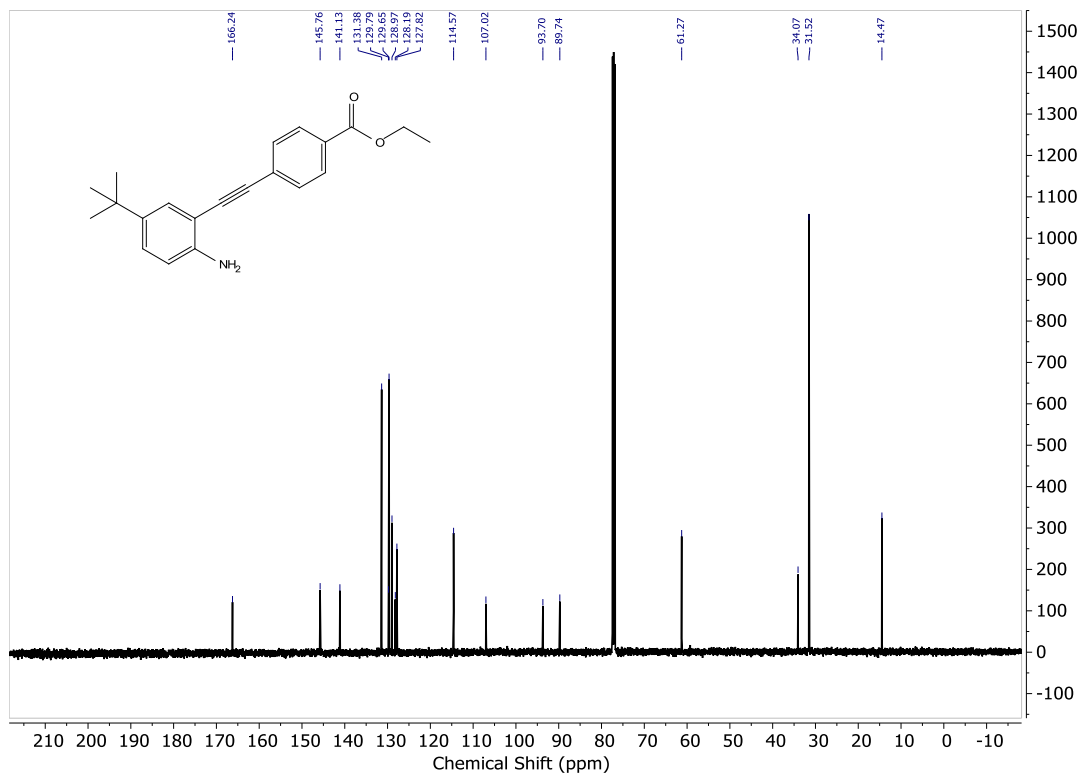
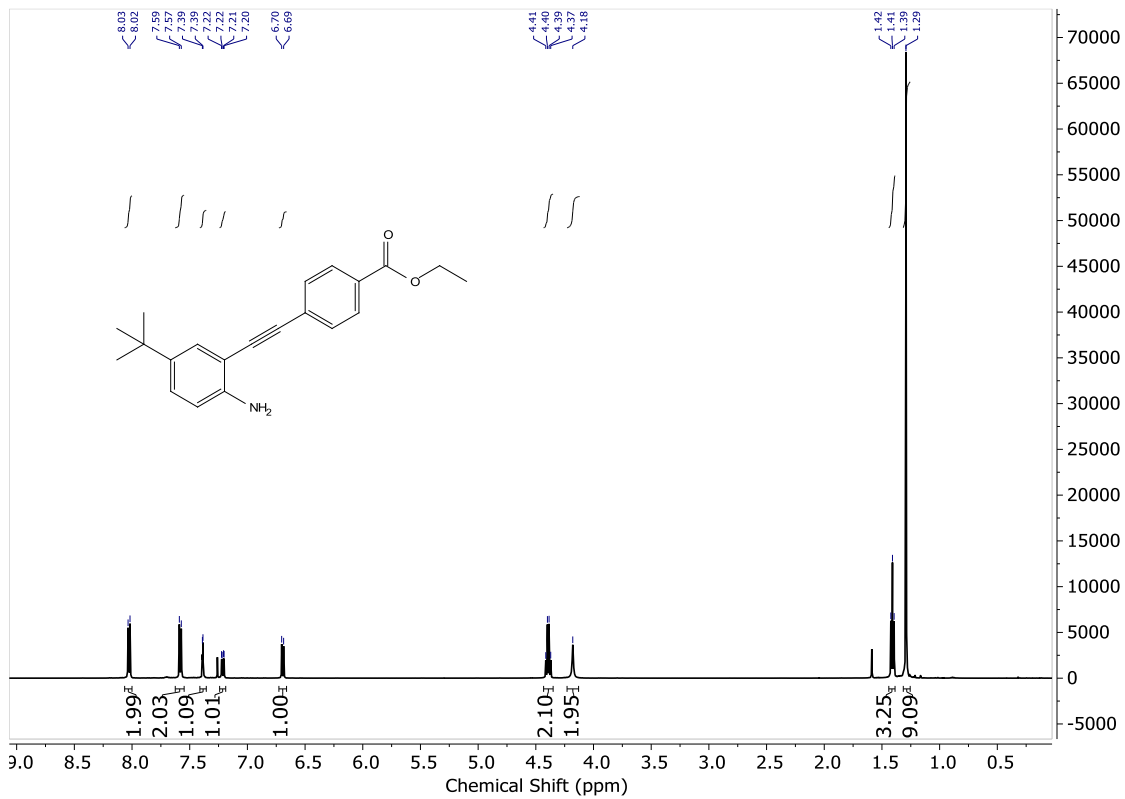


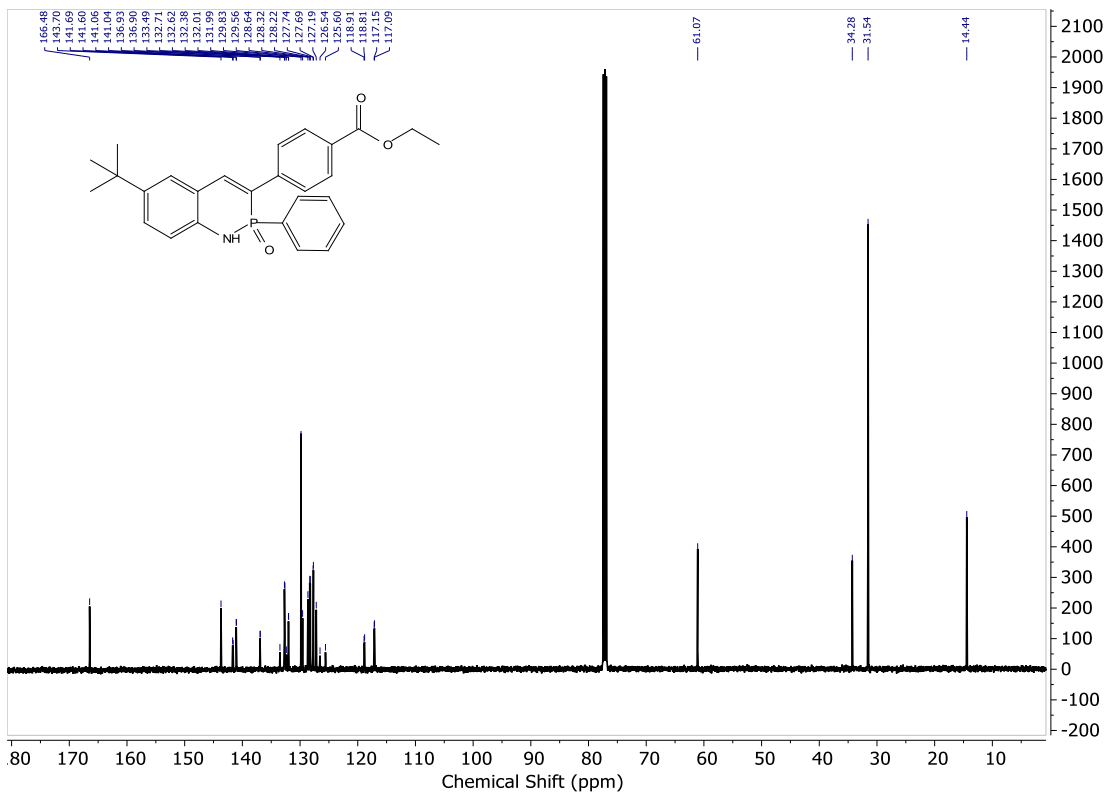
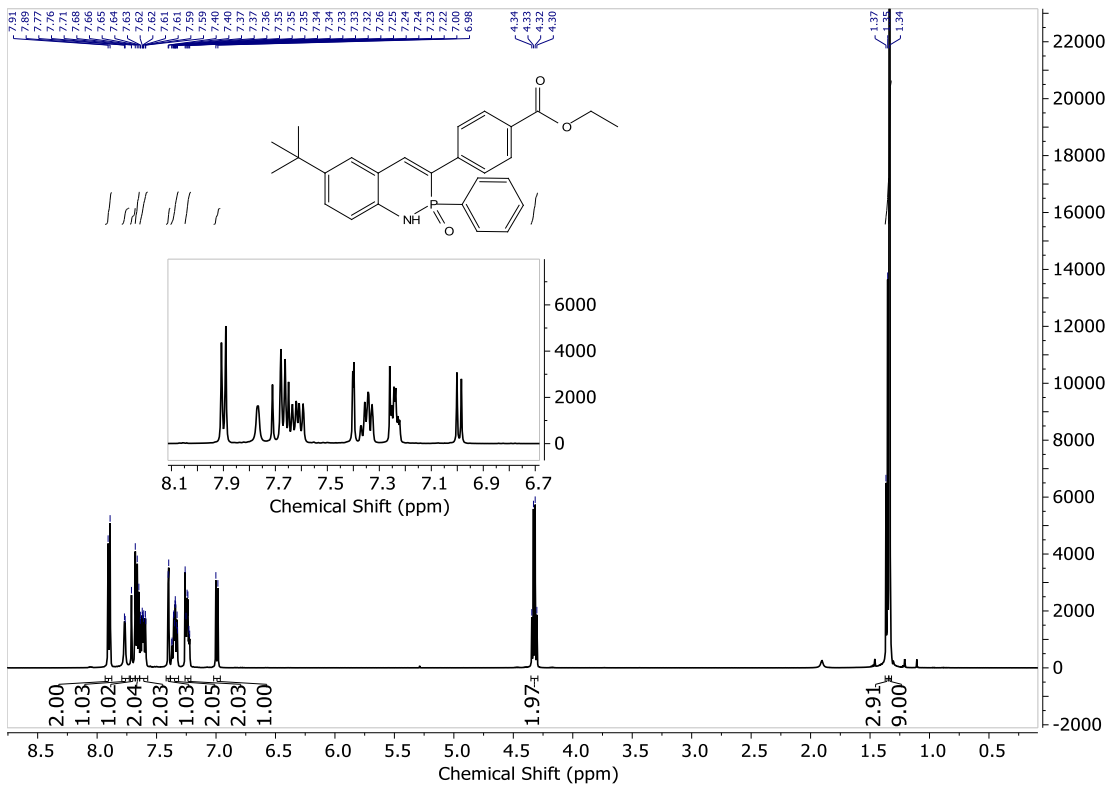
Figure F.9 ORTEP drawing of amide-directed hydrogen bonding seen in the solid state for heterocycle **8**; thermal ellipsoids drawn at 30% probability.

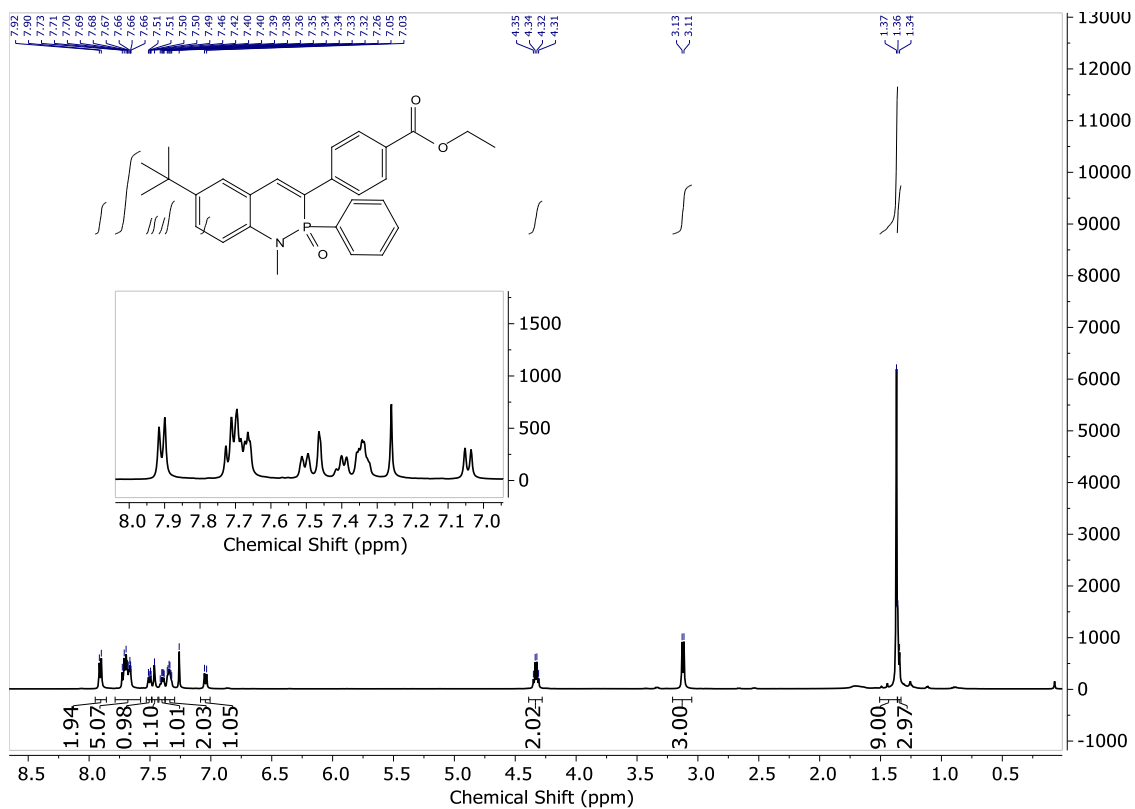
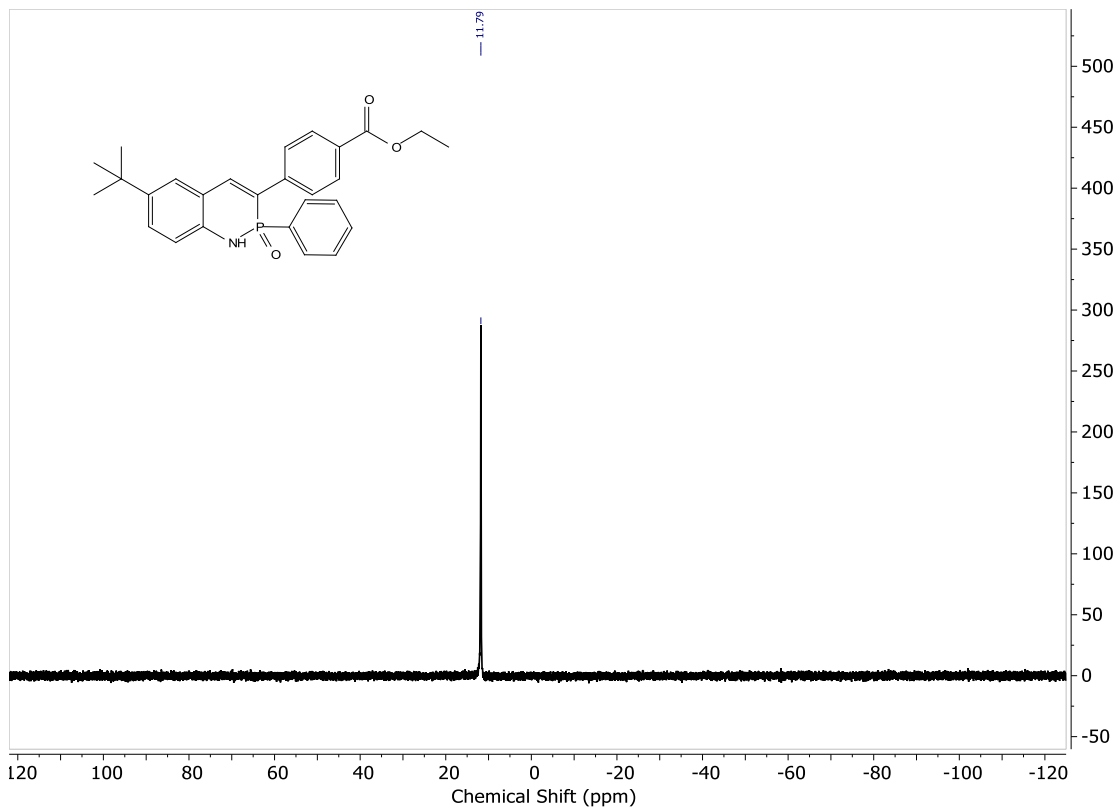
Copies of NMR Spectra

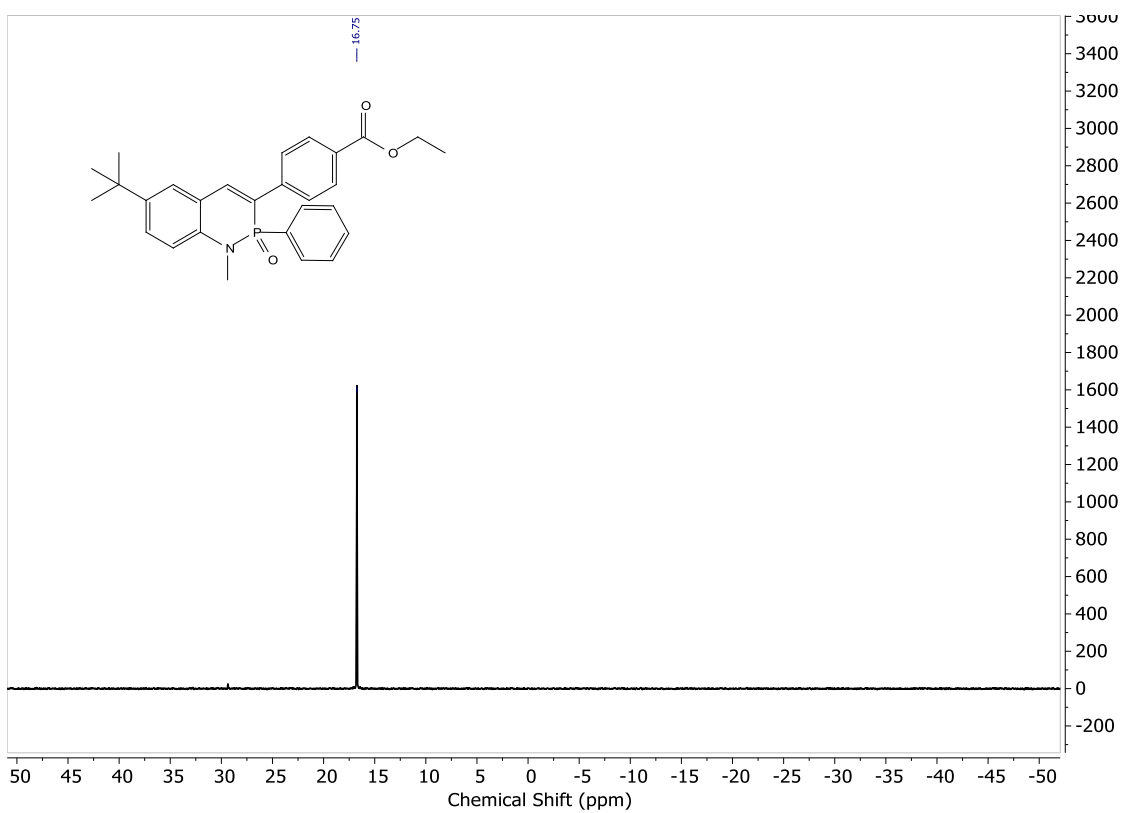
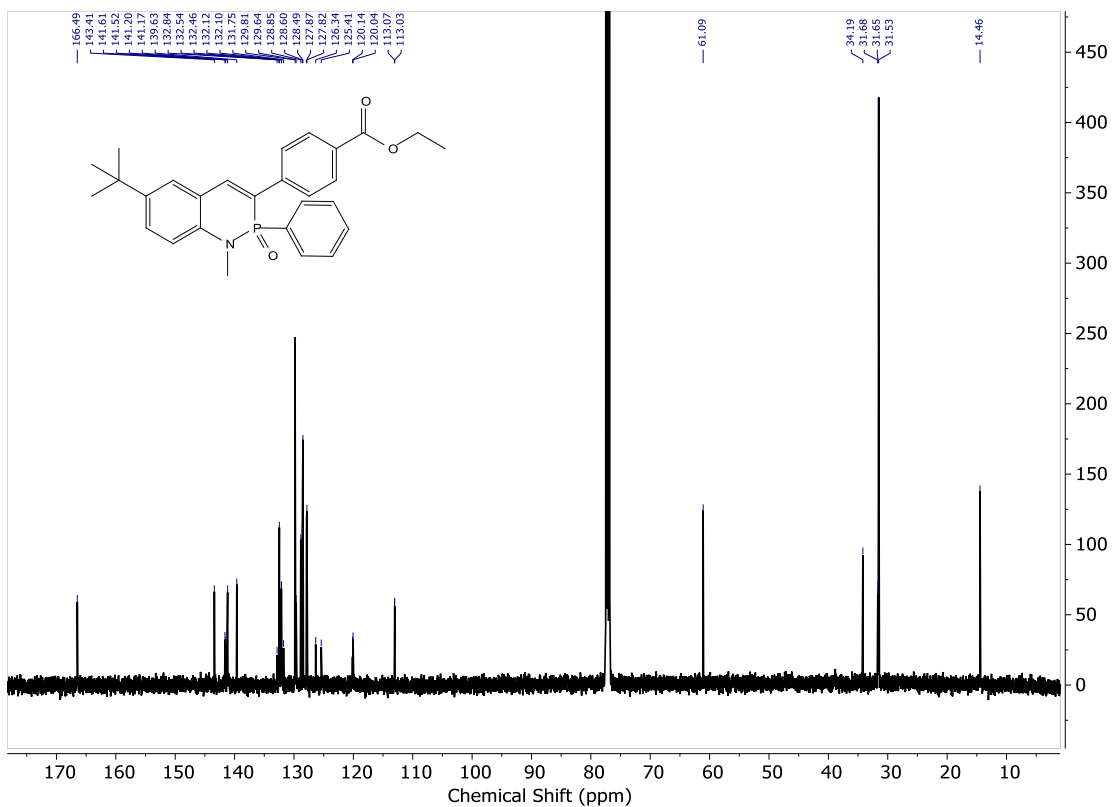


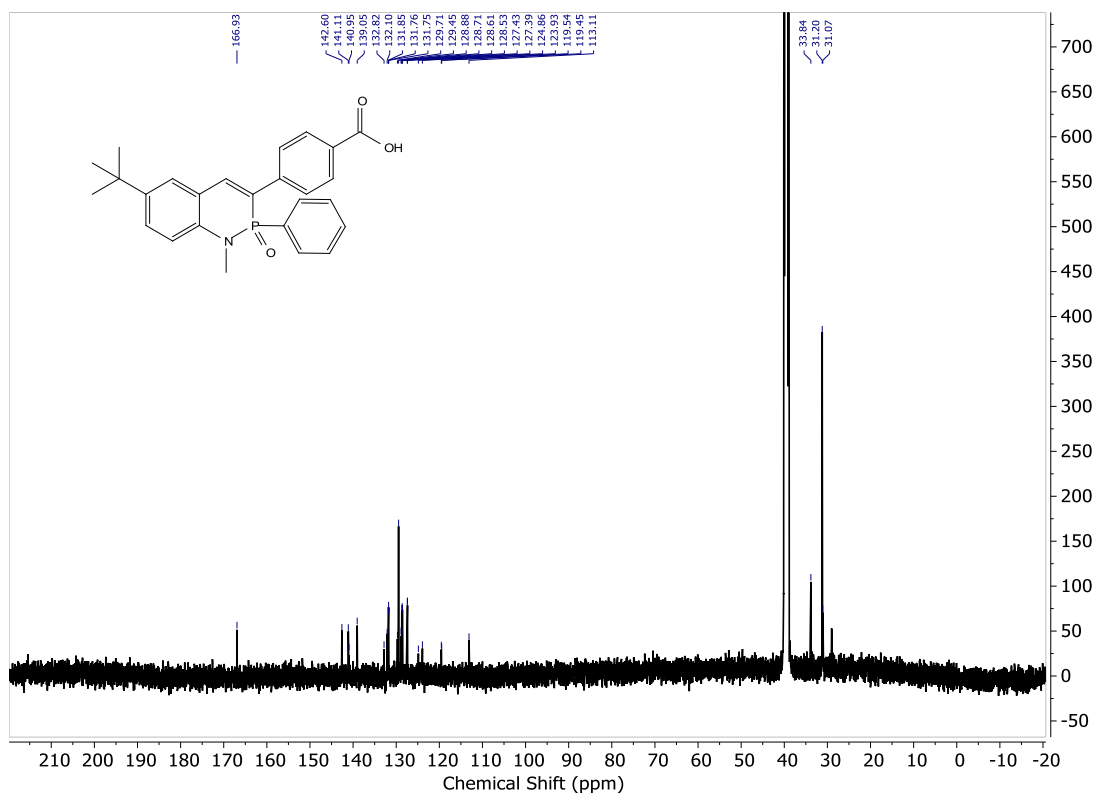
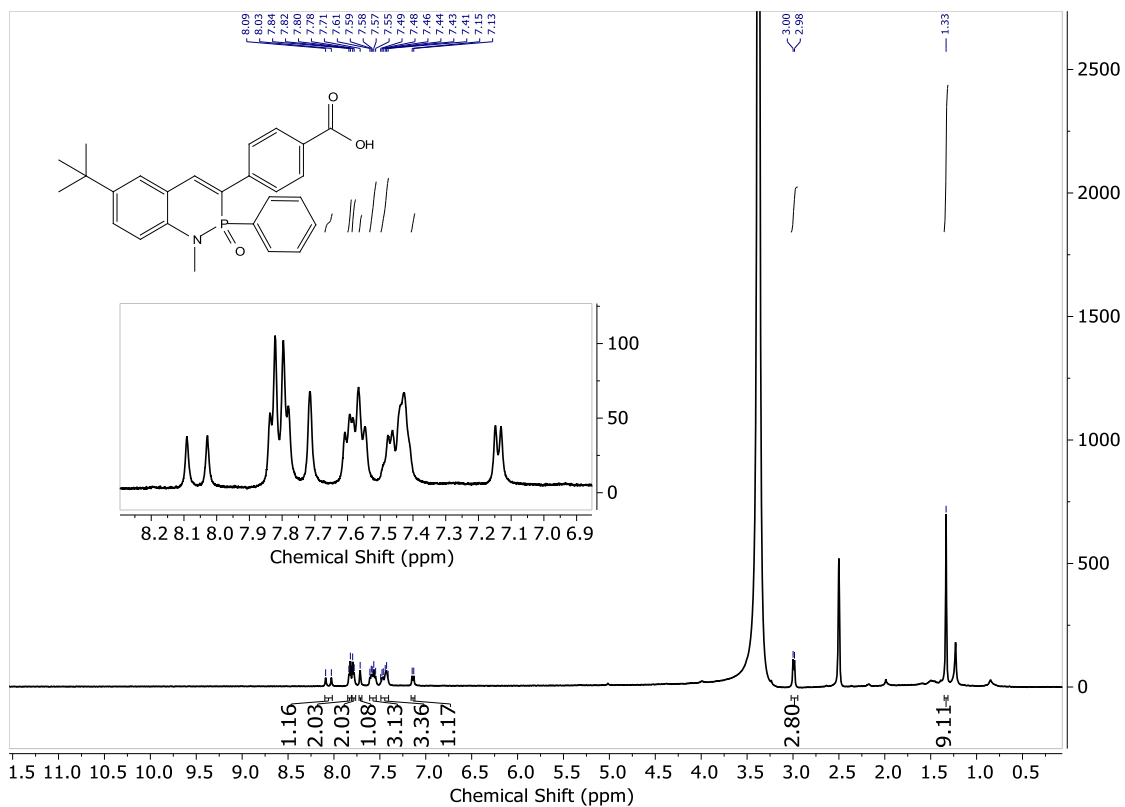


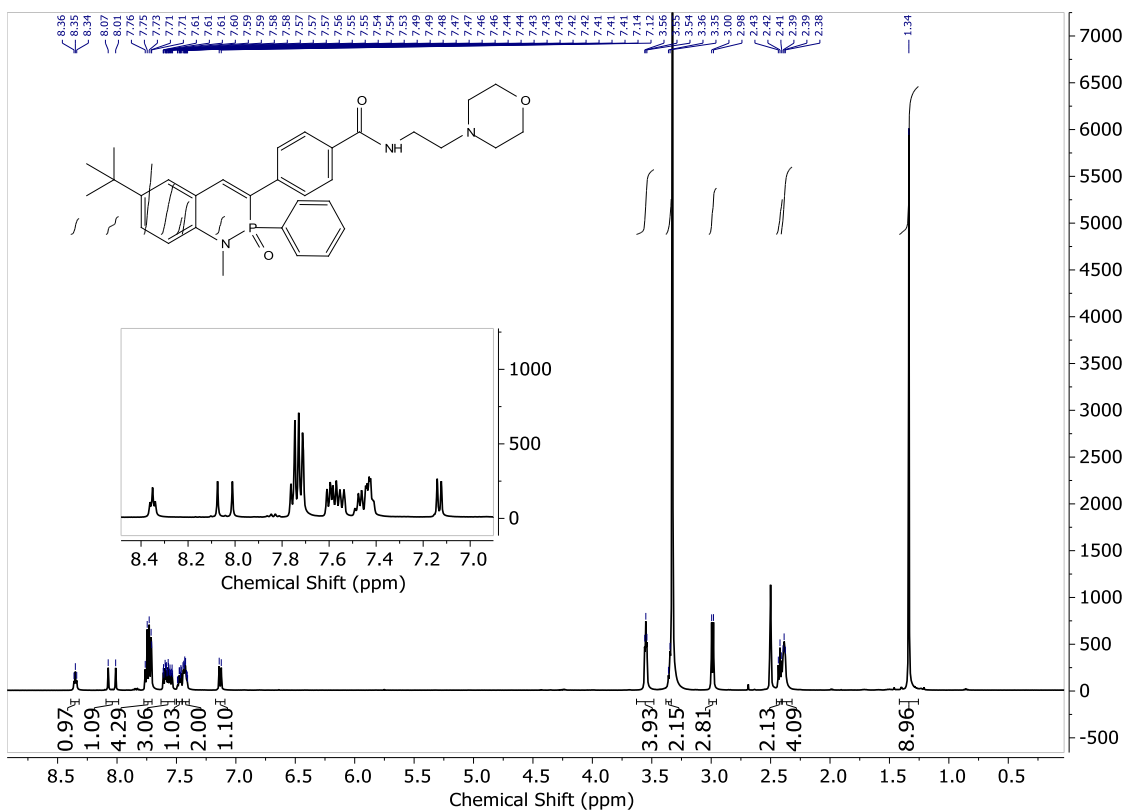
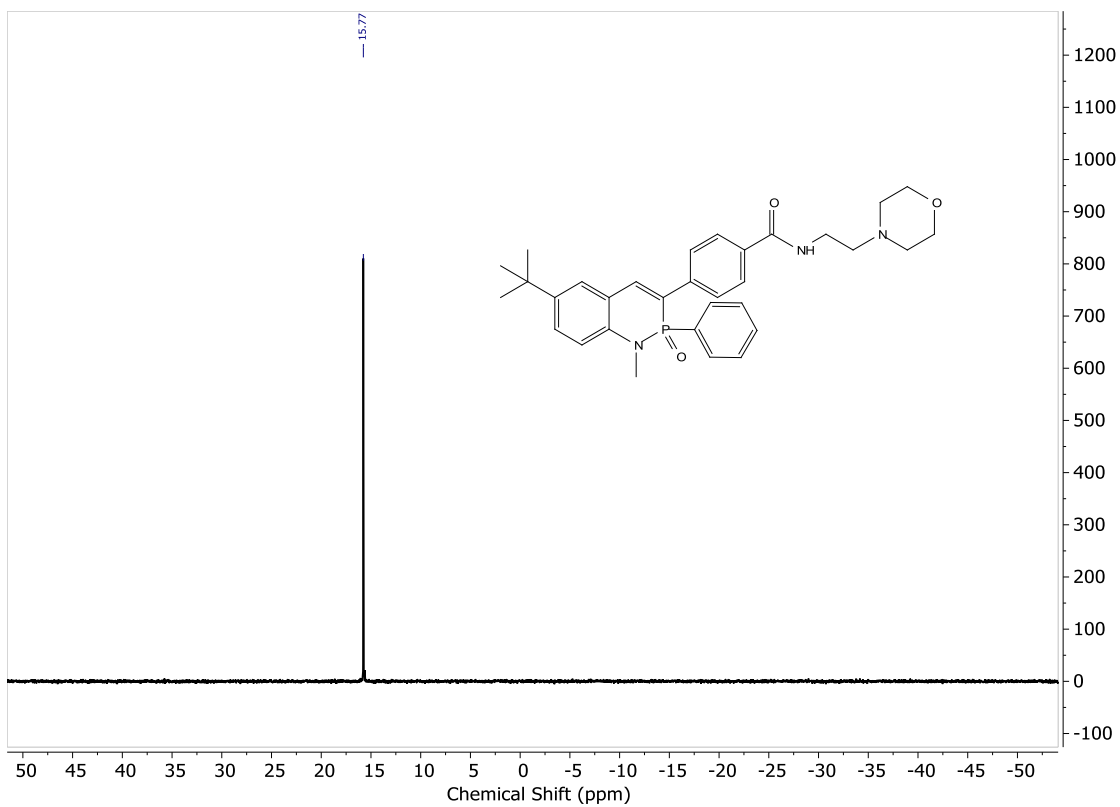


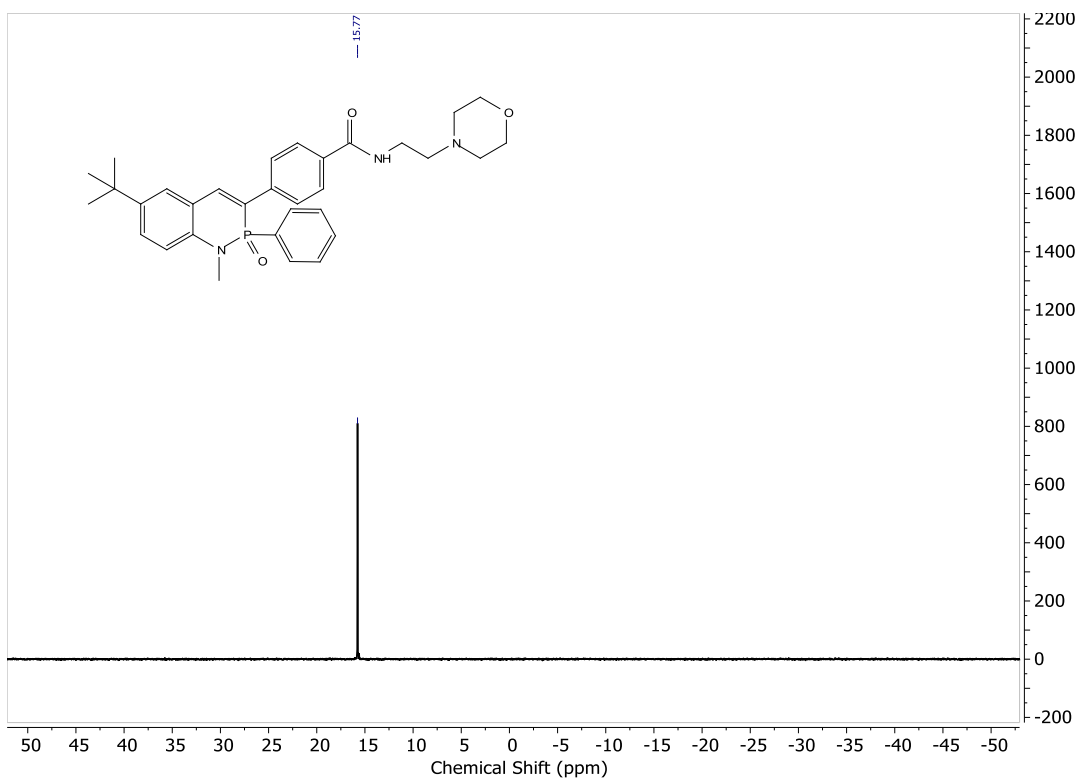
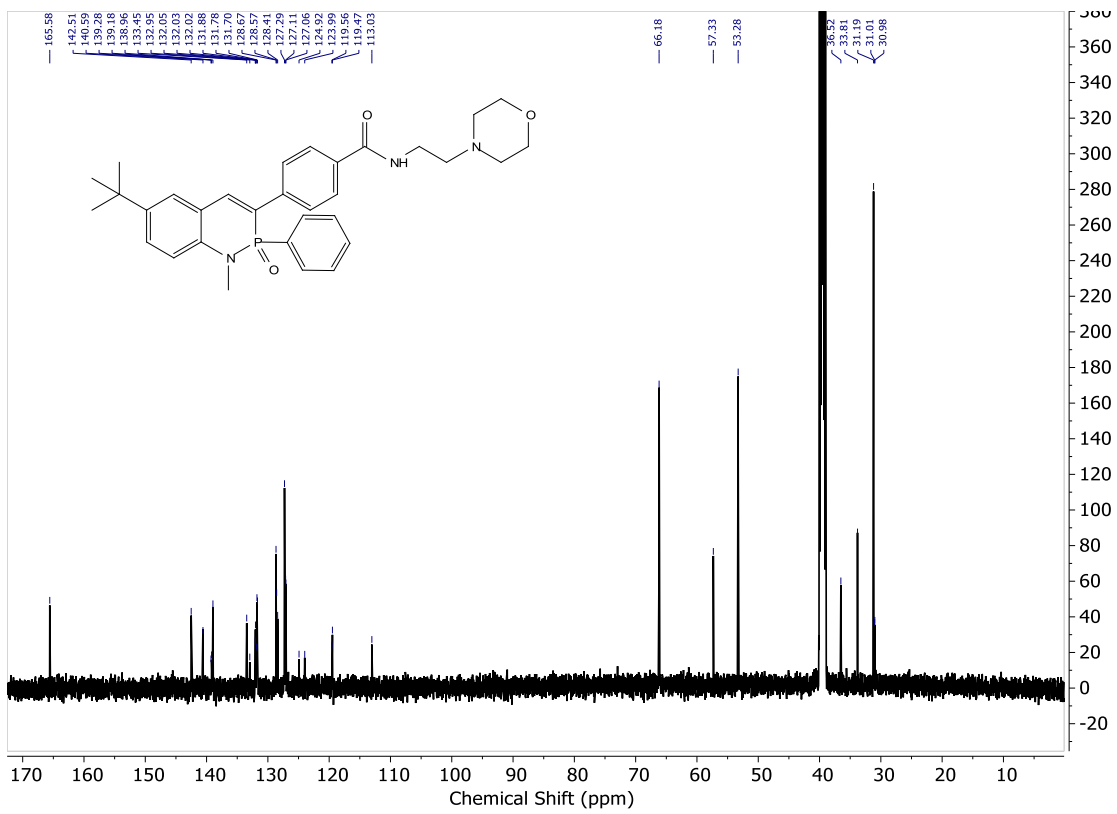








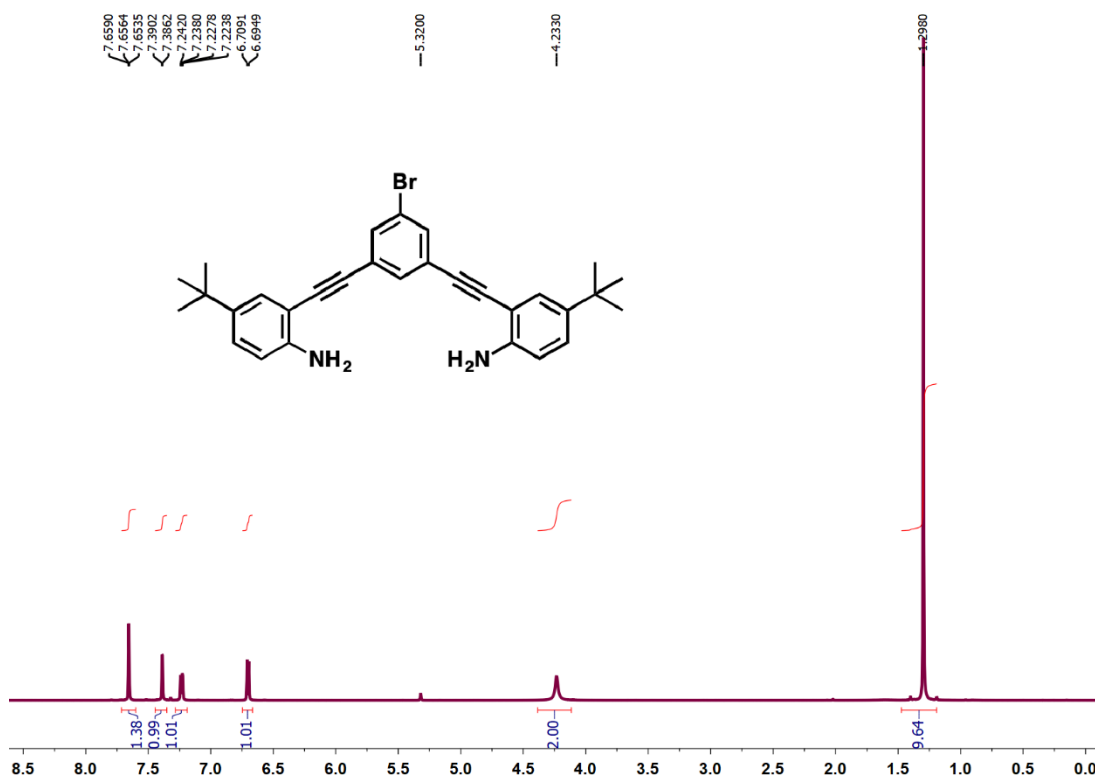




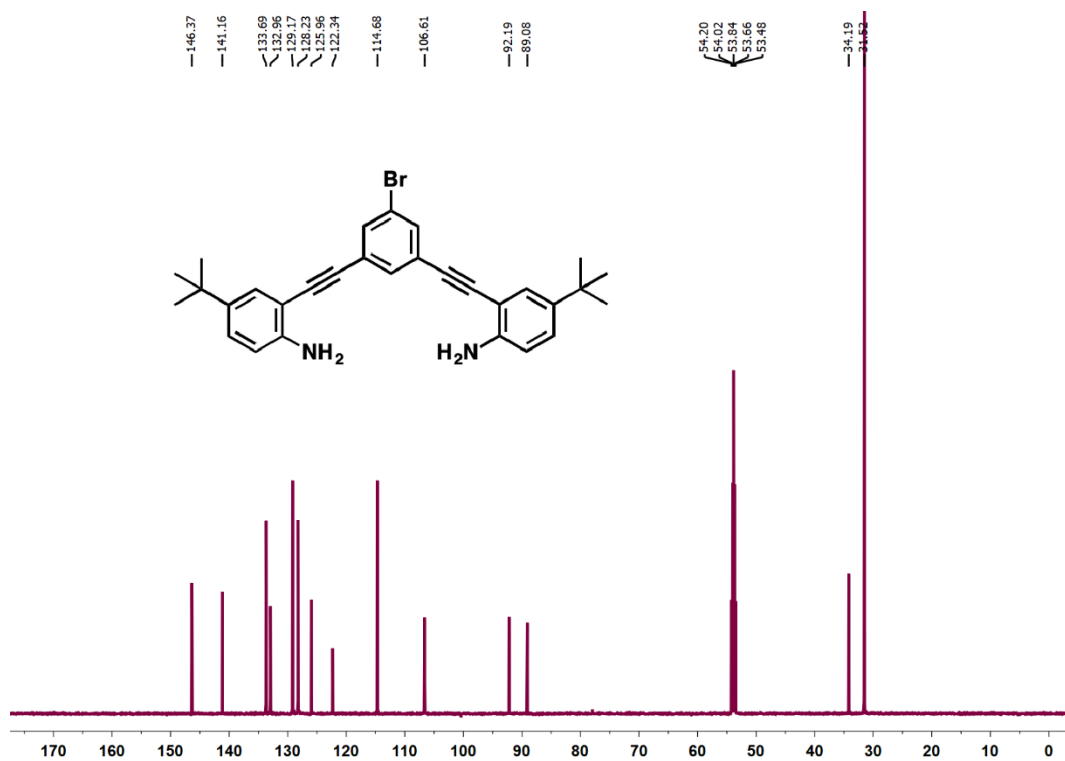
APPENDIX G

SUPPLEMENTARY INFORMATION FOR CHAPTER 8

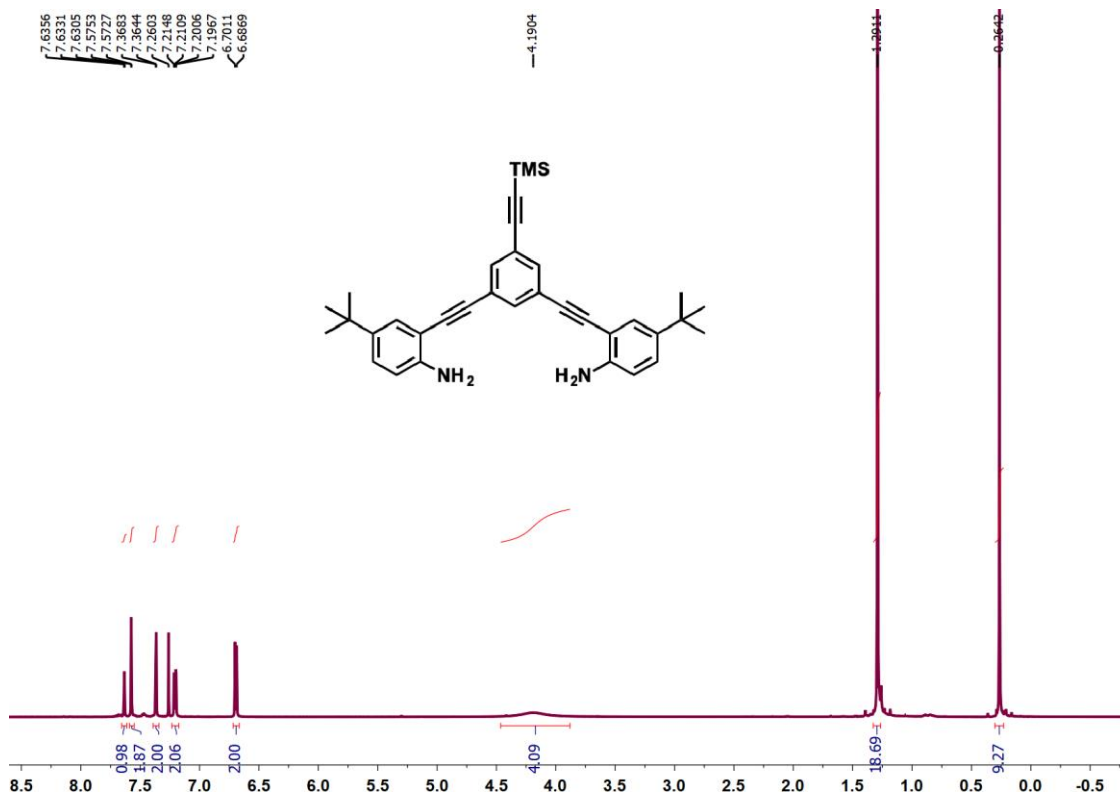
Copies of NMR spectra:



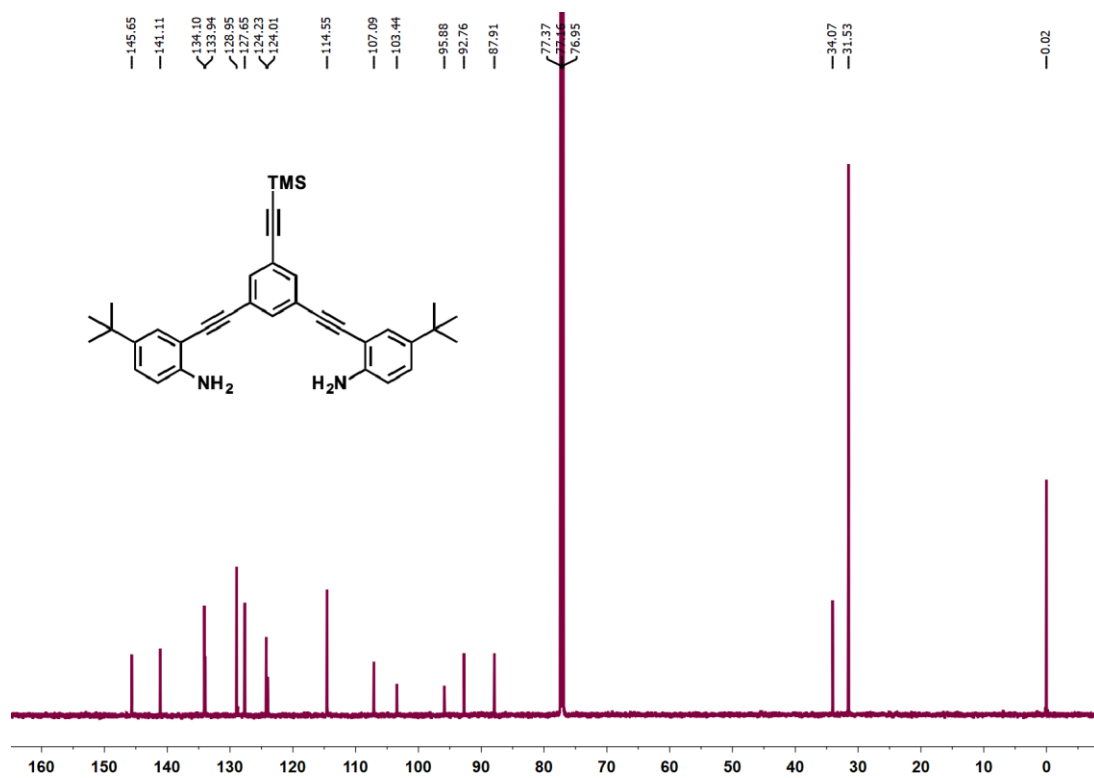
¹H NMR spectrum of **6** in CD₂Cl₂.



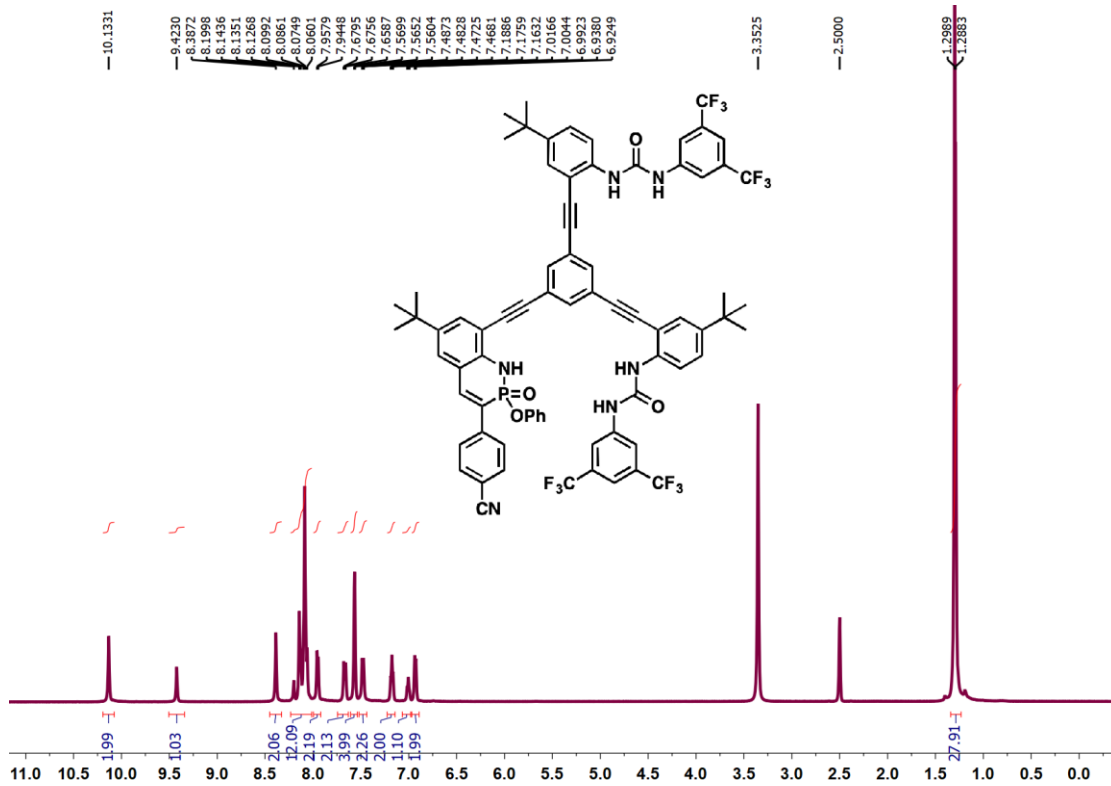
^{13}C NMR spectrum of **6** in CD_2Cl_2 .



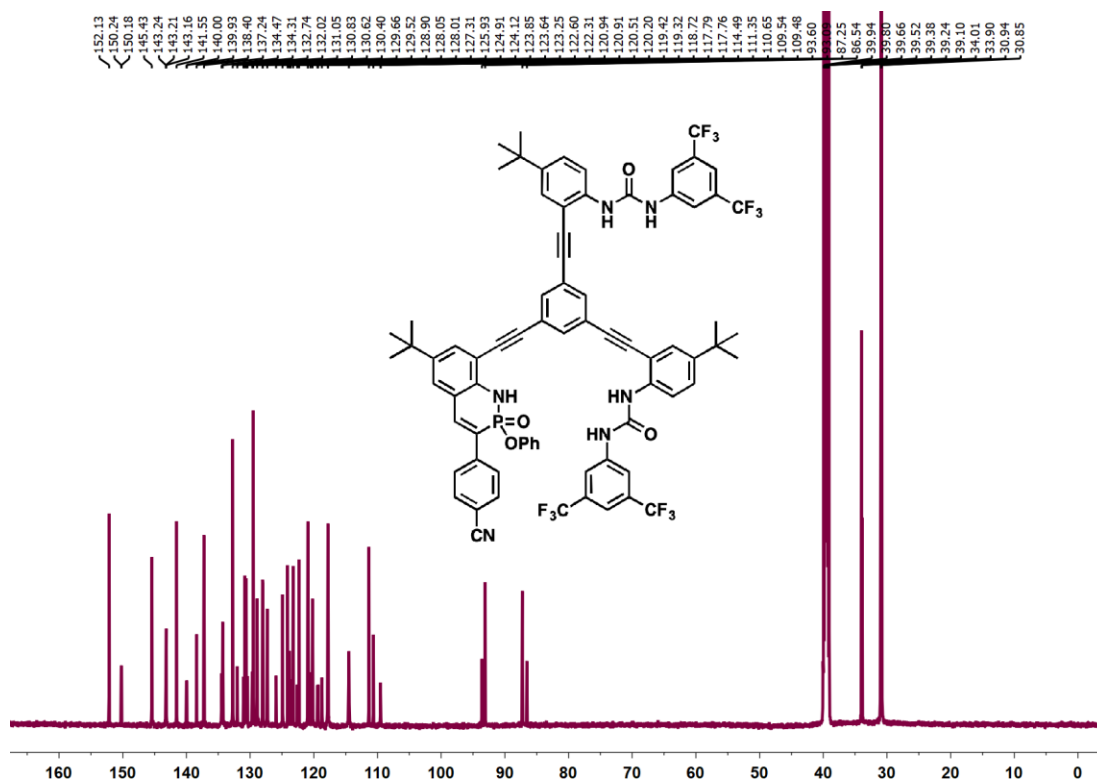
^1H NMR spectrum of **7** in CDCl_3 .



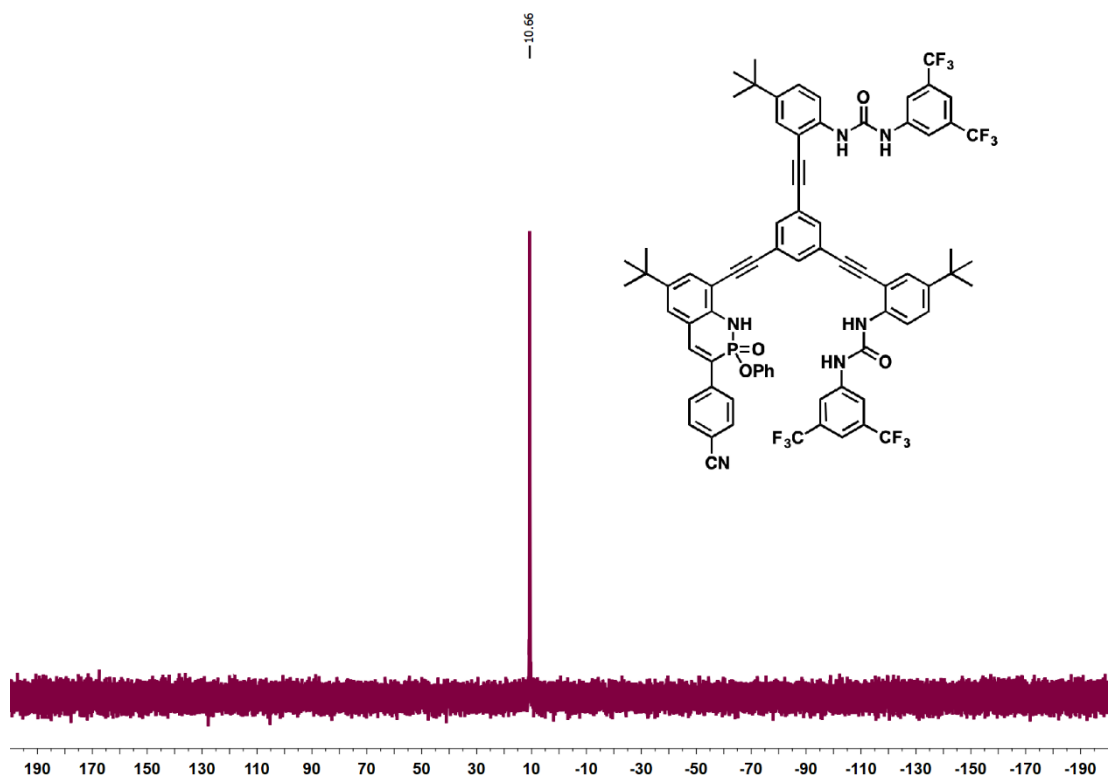
^{13}C NMR spectrum of **7** in CDCl_3 .



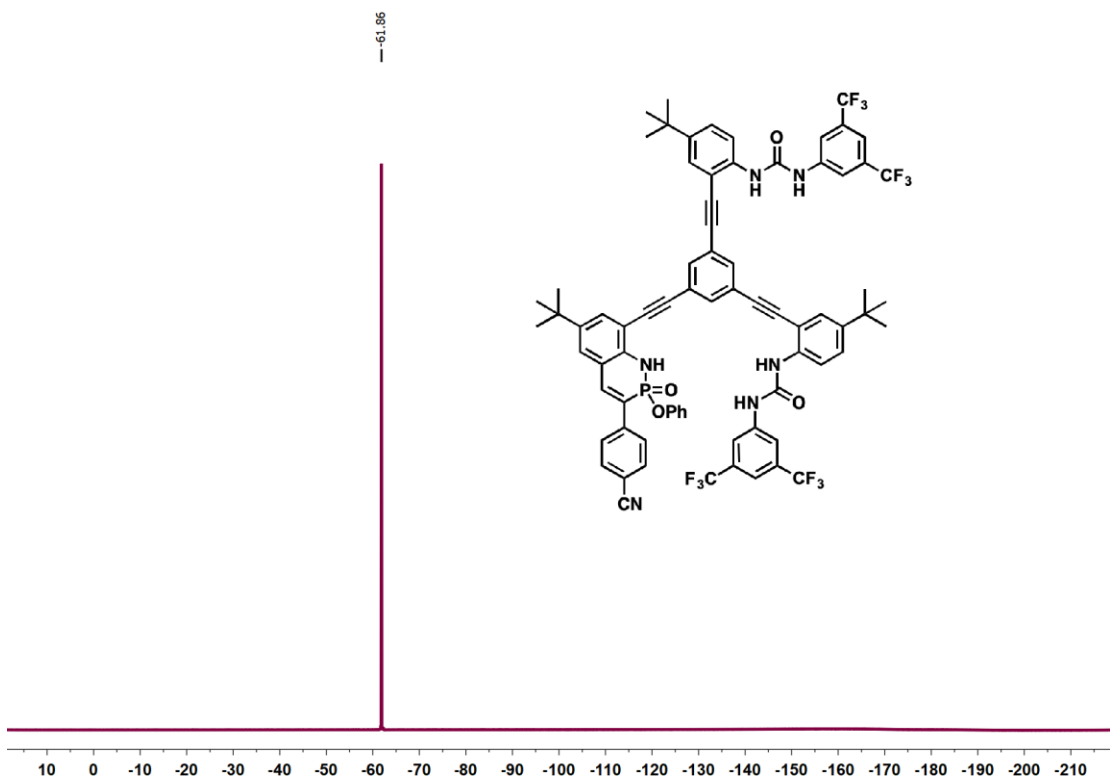
^1H NMR spectrum of **3** in $\text{DMSO}-d_6$.



^{13}C NMR spectrum of **3** in $\text{DMSO-}d_6$.



³¹P {¹H} NMR spectrum of **3** in DMSO-*d*₆.



¹⁹F {¹H} NMR spectrum of **3** in DMSO-*d*₆.

APPENDIX H

NAPHTHO[2,1-*e*]-1,2-AZAPHOSPHORINE 2-OXIDE DERIVATIVES: SYNTHESIS, OPTOELECTRONIC PROPERTIES, AND SELF-DIMERIZATION PHENOMENA (WITH SUPPLEMENTARY INFORMATION)

This Appendix includes previously published and co-authored material from Deng, C.-L., Bard, J.P., Zakharov, L.N., Johnson, D.W., Haley, M.M. “Naphtho[2,1-*e*]-1,2-azaphosphorine-2-oxides Derivatives: Synthesis, Optoelectronic Properties, and Self-Dimerization Phenomena.” *J. Org. Chem.* **2019**, *84*, 8131–8139 and the associated Supplementary Information document. The bulk of the writing and synthesis for this study was performed by Dr. Chun-Lin Deng, with assistance from Jeremy P. Bard. Editorial support was provided by Michael M. Haley and Darren W. Johnson.

Introduction

Six-membered phosphorus- and nitrogen-containing (PN-) heterocycles based on the azaphosphinine/azaphosphorine scaffold have been studied for over half a century. Phosphinamidate **1** and phosphonamidate **2** (Figure H.1) represent two of the earliest known examples, disclosed in 1960 by the groups of Dewar¹ and Campbell,² respectively. Nonetheless, such molecules were scarcely explored in the following 45+ years, mainly because of the lack of viable and reliable synthetic methods to prepare them. This has changed in the past decade, however, as significant efforts have been devoted to metal-mediated C–H functionalization routes to relevant analogues such as **3**³ and **4**,⁴ molecules

that have emerged as versatile building blocks for the modular syntheses of organocatalysts and chiral ligands.

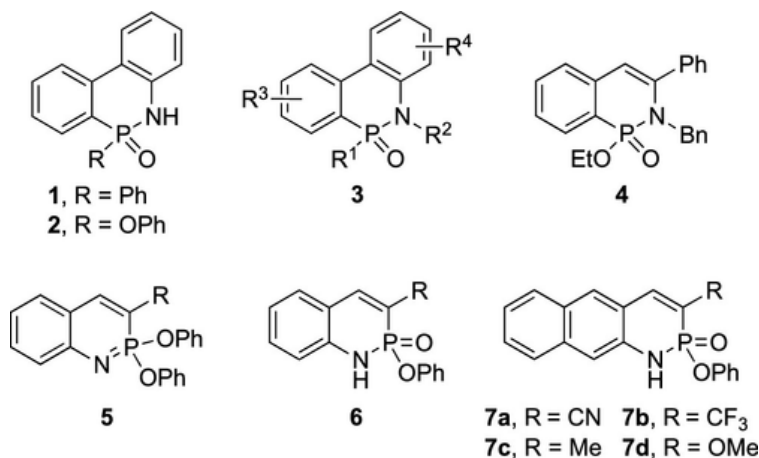


Figure H.1 Chemical structures of selected, known six-membered PN-heterocycles **1–7**.

Despite these efforts, feasible construction of N-unsubstituted phosphonamidates remains underexplored. Such systems are appealing as the phosphonamide motif features a hydrogen-bond-donating N–H moiety and one strong hydrogen-bond-accepting phosphoryl group.^{5,6} The latter not only provides a source of chirality but also functions as an electron-withdrawing group to increase the acidity of the N–H motif. The hydrogen bond donor/acceptor results in intermolecular self-association events, which could trigger the formation of various well-ordered supramolecular complexes, leading to novel supramolecular polymers⁷ and programmable molecular architectures.⁸ In addition, scant attention has been paid to the electronic properties of these heterocycles, as the unique nature of the phosphorus-containing frameworks would make them particularly attractive skeletons for new classes of phosphorus-containing electronic materials, fluorophores, and chemosensors.^{9,10}

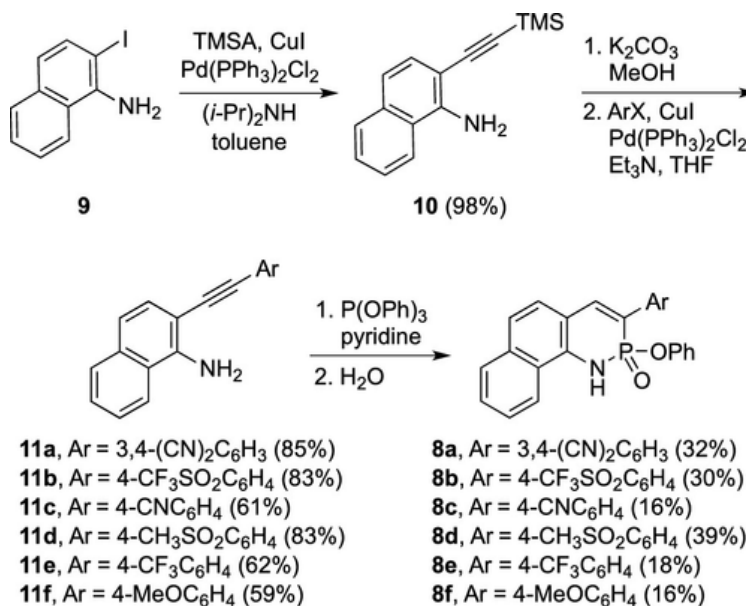
We reported a metal-free, one-pot tandem synthetic method that provides 2- λ^5 -phosphaquinolines **5** and 2- λ^5 -phosphaquinolin-2-ones **6** in good yields, thus allowing for

the facile preparation of diversiform PN-heterocycles with tunable emission properties.¹¹ More recently, we described the preparation of a series of linearly fused naphtho[2,3-*e*]-1,2-azaphosphorine-2-oxides **7** exhibiting considerably large Stokes shifts;¹² however, their low quantum efficiencies could limit optoelectronic applications to some extent. Also, it is of fundamental importance to unravel the factors that influence H-bonding within these systems, not only to predict their self-association behavior but also to provide insights into elaborating these compounds as molecular recognition motifs.¹³ Herein, we report the synthesis, electronic characterization, and self-dimerization behavior of a series of angular naphtho-fused PN-heterocyclic systems that exhibit enhanced quantum yields over their linearly fused congeners.

Results and Discussion

As shown in Scheme H.1, the synthesis of the requisite alkyne precursors **11** for our study started by cross-coupling (trimethylsilyl)acetylene (TMSA) with iodonaphthalenamine **9**. Protodesilylation of **10** and a second cross-coupling utilizing the appropriate *para*-substituted haloarene afforded a series of tolane derivatives **11** containing various aryl substituents in moderate to good yield (see the Supplementary Information section below). In all cases, the P(OPh)₃-mediated cyclization of **11** proceeded smoothly to give the corresponding phosphinimidates, which were subsequently hydrolyzed with minimal amounts of water to provide the desired phosphonamidates **8**. The crude materials were purified by silica gel column chromatography followed by preparative size-exclusion chromatography (SEC) and then recrystallization to furnish the analytically pure products in modest overall yields. Compounds **8a–f** are air- and thermally-stable solids and were

fully characterized by conventional techniques (^1H , ^{13}C , and ^{31}P NMR spectroscopy as well as HRMS).



Scheme H.1 Synthesis of PN-Heterocycles **8**.

Characteristic to these molecules in their proton NMR spectra in CDCl $_3$ are the N–H singlet and the ^{31}P -coupled doublet ($J \sim 40$ Hz) in the 9.3–9.7 and 7.7–7.9 ppm range, respectively. These peaks shift downfield progressively as the pendant aryl group becomes more electron deficient. Alternatively, this same effect results in the ^{31}P peaks shifting upfield, though there is a definite concentration dependence on their chemical shift (due to dimerization, *vide infra*).

Single crystals of **8c** and **8d** suitable for X-ray diffraction were obtained by slow evaporation of their CHCl $_3$ or CH $_2$ Cl $_2$ solutions, respectively. Various depictions of the structures are shown in Figure H.2 and Figure H.7 (for **8d**), as well as Figure H.8 (for **8c**), and select bond lengths and angles are compiled in Table H.4. As expected, both the N–H donor and P=O acceptor groups in **8c** and **8d** are involved in hydrogen bond formation to crystallize *meso*-dimeric complexes in the solid state. Both **8c** (H \cdots O 1.90(3) Å/160(5)°,

1.86(3) Å/154(4)°, respectively) and **8d** (H···O 2.06(3) Å/166(2)°) display short H-bond interactions. Notably, a pair of weak intermolecular C–H H-bonds (H···O 2.45 Å/165°, 2.43 Å/165° for **8c**, H···O 2.41 Å/163° for **8d**, respectively) were observed in the crystalline lattice, which are supported by the observed light red circles in the Hirshfeld surface analysis of **8d** (Figure H.2b). Examination of the packing diagram of **8c** reveals that two antiparallel naphthalene moieties are stacked to form a face-to-face π -interaction at a distance of 3.38 Å. For **8d**, effective π – π interactions occur between the *p*-cyanophenyl units and naphthalene cores (see the Supplementary Information section below).

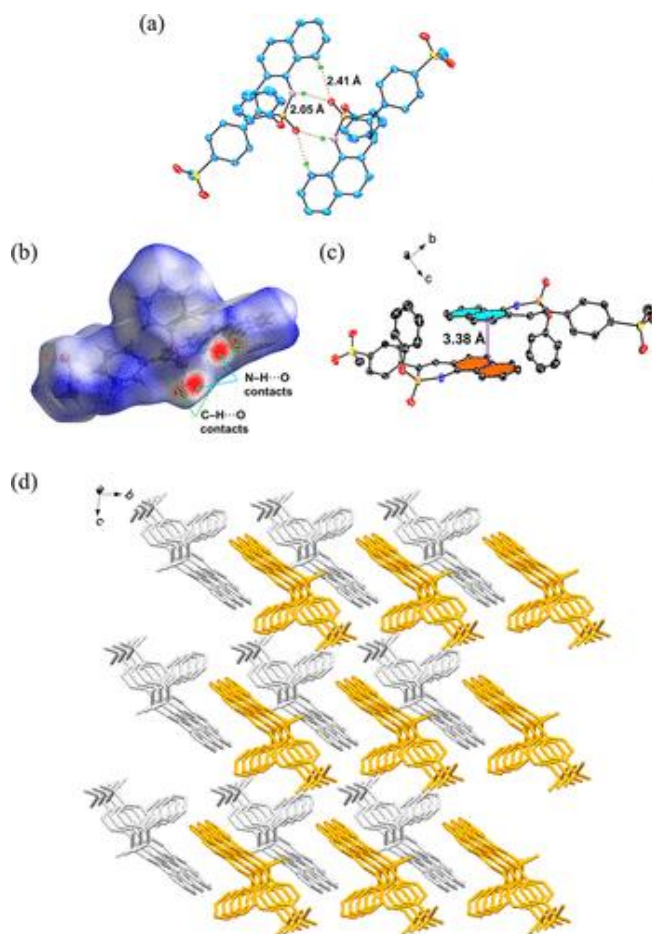


Figure H.2 (a) ORTEP drawing of the dimer structure of **8d** via hydrogen bonds; thermal ellipsoids drawn at 50% probability. (b) d_{norm} (red: -0.502 to blue: 1.427 Å) mapped on the Hirshfeld surface of **8d**. The surface regions with intermolecular H-bond interactions

are drawn in red. (c) Intermolecular π contacts. (d) Molecular packing diagram viewed along the a -axis. All hydrogen atoms not involved in the interactions are omitted for clarity. Optoelectronic Properties

As shown in Figure H.3, the UV/vis absorption spectra of **8a–f** exhibit two weaker bands at ca. 320–450 nm with the strongest bands in the 275–310 nm range. The lowest energy absorption bands in **8a–e** are red-shifted with increasing electron-withdrawing ability of the terminal *para*-substituents with regard to **8f**.

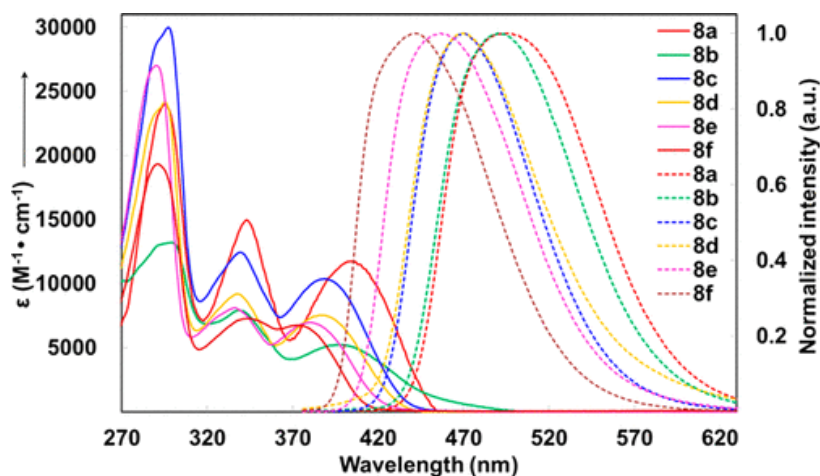


Figure H.3 Electronic absorption (solid line) and emission spectra (dotted line) of **8** in CHCl_3 at 298 K.

To elucidate the origin of the low energy absorption bands and electronic structures of the new PN-heterocycles, TD-DFT calculations at the PBE0/6-311G(d) level of theory were performed on the previously optimized geometries of **8**. As shown in Figure H.4, the calculated excitation energies for all compounds were found to be in good agreement with the experimentally obtained lowest energy absorption bands (Table H.1). The lowest energy absorption bands correspond to the $S_0 \rightarrow S_1$ electronic transitions, which are dominated by the transitions from HOMO \rightarrow LUMO. Figure H.4 shows that the LUMO and HOMO of **8f** encompass the entire molecular system; therefore, its absorption bands appear to be $\pi \rightarrow \pi^*$ transitions. With respect to **8a**, the HOMO coefficients reside mainly

on the naphthalene and PN heterocyclic moiety, whereas the terminal phthalonitrile substituent dominates the LUMO; thus, the $S_0 \rightarrow S_1$ transition of **8a** appears to have some charge-transfer (CT) character. As with the other four compounds, from **8e** to **8b**, the orbital coefficients in the LUMO gradually shift to the pendant phenyl units, whereas the contributions of the naphthalene-fused PN-heterocyclic rings to the HOMOs remain almost unchanged. This suggests that the effect of CT in the $S_0 \rightarrow S_1$ transition becomes more prominent with stronger EWG. These calculations suggest that the attachment of the pendant phenyl units to the parent core can significantly change the electronic structure of these molecules.

Table H.1 Photophysical Data of PN-Heterocycles **8** in CHCl_3 at 298 K

compd	λ_{max} (nm) ^a	λ_{em} (nm)	Φ_{F} ^c	τ^d (ns)
8a	404 (4.07)	493	0.93	1.0/4.4 (3/97)
8b	397 (3.72)	490	0.80	1.0/4.0 (4/96)
8c	389 (4.01)	469	0.36	1.8/3.9 (28/72)
8d	388 (3.87)	470	0.66	2.6
8e	380 (3.84)	457	0.29	1.7
8f	372 ^b (3.83)	441	0.19	0.8

^a The longest absorption maximum wavelengths; molar absorption coefficients as $\log \epsilon$ ($\text{M}^{-1} \text{cm}^{-1}$) given in parentheses. ^b A broad absorption band. ^c The relative fluorescence quantum yield determined with quinine sulfate in 0.1 M H_2SO_4 as a standard ($\lambda_{\text{ex}} = 360 \text{ nm}$, $\Phi_{\text{F}} = 0.54$). ^d For **8a–c**, fitted with biexponential model and the amplitudes of two lifetimes given in parentheses; for **8d–f**, fitted with monoexponential model.

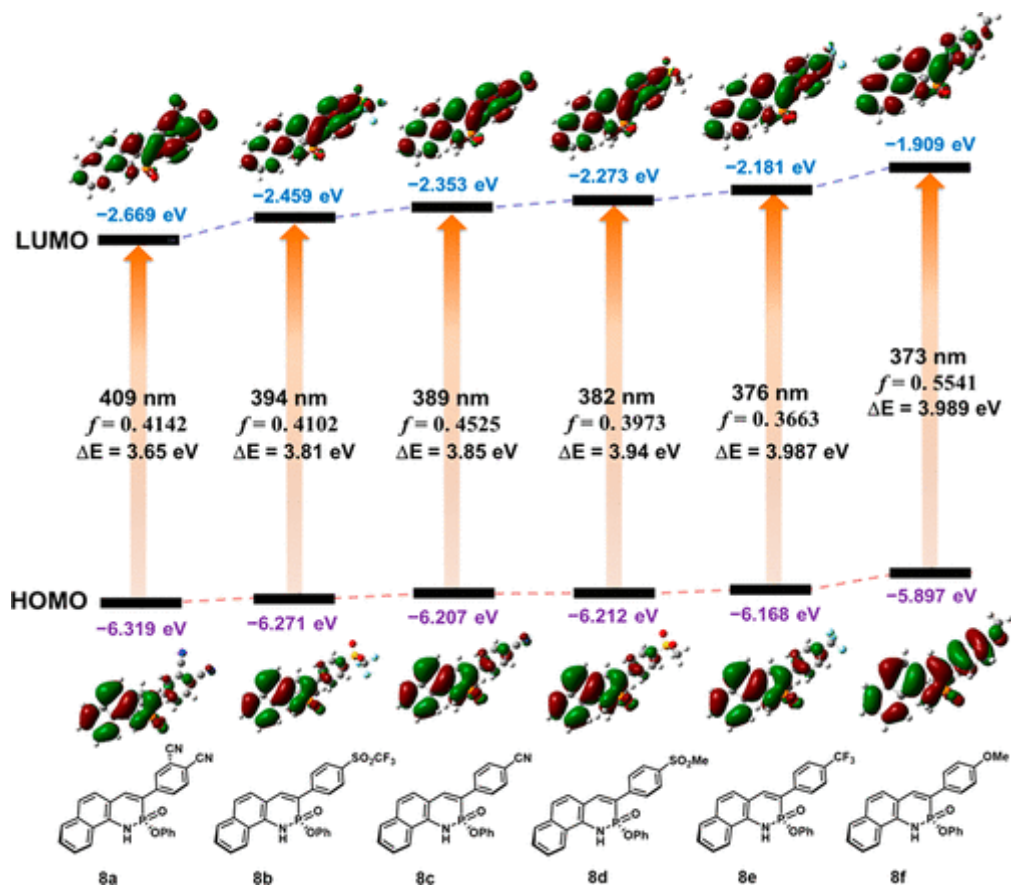


Figure H.4 Kohn–Sham molecular orbitals, excitation energies, and oscillator strengths for **8**, calculated at the TD-PBE0/6-311G(d) level of theory.

In contrast, the fluorescence maxima (λ_{em}) are red-shifted significantly following the same trend as the absorption spectra (Figure H.3). As shown in Table H.1, the compounds appended with the electron-withdrawing substituents possess moderate to excellent emission quantum efficiencies (0.29–0.93), compared to those small values ($\Phi_F < 0.1$) observed among the relevant PN-heterocycles.^{10,11} The TD-DFT calculations show that the $S_0 \rightarrow S_1$ excitations in linear analogues **7**¹¹ have very small oscillator strengths (Figure H.15), which may partly account for the lower quantum yields of **7** relative to **8**. The emission peak for **8f** is unaffected by solvents of varying polarity; however, the emission peaks for **8a–d** were bathochromically shifted and broadened in varying degrees with the increasing solvent polarity (see Supplementary information section below), which is

consistent with the involvement of CT transitions.¹⁴ The fluorescence decay histograms of **8d–f** were fitted with a single exponential function with the fluorescence lifetimes ranging from 0.8 to 2.6 ns (Table H.1). By contrast, only the biexponential model can be reasonably applied to **8a–c**, indicating that different emissive species exist in the excited state. There is a trend in the amplitudes of the two components; as the *para*-substituent becomes more electron-withdrawing, the longer-lived excited state becomes dominant. Considering the different electronic structures of **8**, the excitations for **8d–f** seem to take place locally within the phenanthrene-like heterocyclic fragment, whereas some added intramolecular charge transfer (ICT) occurred between the central core and 3-aryl moieties in **8a–c**, which correspond to the mixed $\pi \rightarrow \pi^*/\text{ICT}$ states. Additionally, the TD-DFT-optimized geometry of the S₁ state of **8a–f** show that the whole molecular system becomes more conjugated compared to the ground state, as a result of decreasing the dihedral angle and shortening the length of the connecting C–C bond between the plane of the 3-phenyl group and the plane of the tricyclic core (Table H.5). These geometric relaxations favor the electron delocalization and eventually lower the HOMO–LUMO energy gaps, thereby contributing to their Stokes shifts; thus, the TD-DFT predicted emission wavelength with increased oscillator strength is within the observed emission maxima (Tables H.1 and H.6).

Self-Dimerization

Unlike the linear-fused regioisomers **7**, compounds **8** (aside from **8a**) exhibit appreciable solubility in CHCl₃, which allows for the investigation of their dimerization behavior in solution by variable concentration (VC) NMR spectroscopy experiments. When a water-saturated CDCl₃ solution of **8b** was diluted from 17 mM, the resonances of the P atom showed upfield shifts of ca. 1 ppm, indicating disassociation of dimer **8b·8b** (Figure H.5a).

Meanwhile, the proton of the phosphonamide NH also gradually shifted upfield with decreasing concentration. Nonlinear regression analysis of the chemical shift data of the NH proton and P atom yielded the dimerization constant (K_{dim}) values of 308 and 289 M^{-1} , respectively. The results are consistent with the expected strong N–H/P=O head-to-tail hydrogen bond pairs. Additional K_{dim} data for the dimerization of the other phosphonamidates are summarized in Table H.2. The dimerization constants for **8b** and **8d**, with their electron-withdrawing substituent in the 3-aryl position were measured to be over 200 M^{-1} . In contrast, both compound **8e**, with a less electron-poor group, and **8f**, bearing an electron-donating group, show K_{dim} values less than 100 M^{-1} . It is noteworthy that the obtained self-association constants are significantly larger than those of structurally related C=O/N–H motifs.¹⁵

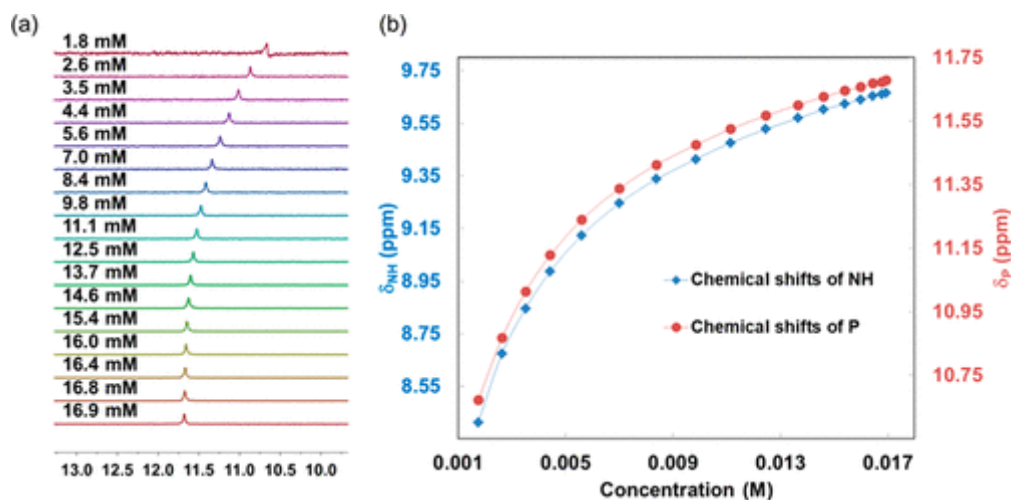


Figure H.5 (a) Stacked partial ^{31}P NMR spectra of **8b** at various concentrations. (b) Chemical shifts of phosphonamidate NH proton and P atom resonances in **8b** during the dilution NMR experiments.

Table H.2 Dimerization Constants (K_{dim}) of **8** in H_2O -Saturated CDCl_3 at 298 K^a

cmpd	K_{dim} (M^{-1})	cmpd	K_{dim} (M^{-1})
8a	^b	8d	246
8b	306 (290)	8e	84
8c	117	8f	77

^a All of the reported dimerization constants represent the average value from triplicate titrations. Uncertainties are less than 10%. The values derived from ³¹P NMR titrations are given in parentheses.^b Not determined due to the insolubility in H₂O-saturated CDCl₃.

To gain insight into the self-association properties, the calculated electrostatic potential (ESP) showed that the domain with the largest global positive ESP ($V_{s,max}$) is located on the N–H moiety of **8b**, accompanied by the most negative ESP ($V_{s,min}$) on the P=O local surface (Figure H.6a). Similar distribution patterns of ESP are found within all other molecular systems. According to the “best donor-best acceptor” empirical rule proposed by Etter,¹⁶ we posit that the assembly via the N–H/P=O hydrogen bonds would cancel out their surface global extremes to form stable self-complementary dimers. As suggested in the solid structure, another important aspect of self-association is that a monomer always adopts an “edge to edge” antiparallel orientation with respect to its enantiomer, while the dimer consisting of two homochiral monomers was never observed. We note that the distribution of positive and negative charge across the PN-heterocycle core is uneven and would give rise to a permanent dipole moment (μ_g), which was calculated to be 6.5 D (Figure H.6b). On the other hand, the dipole moment for the anticipated (*R,S*)-*meso*-dimer is negligible ($\mu_g \approx 0$ D). The result is not surprising since the dipole moment vectors in the two monomers are also in an antiparallel arrangement because of the centrosymmetric structure of *meso*-dimer. In contrast, the suggested (*S,S*)-dimer would still possess a small dipole moment (0.4 D) relative to the monomer. It seems that this unique antiparallel alignment feature for self-association is directly related to the most favorable orientation for dipolar anisotropy, in which the dipole moments for two monomers are effectively canceled. Furthermore, the noncovalent interactions (NCI) plot reveals that additional long-range repulsive domains appear between the –OPh moieties in the (*S,S*)-dimer (Figure

6d), which could act as some kind of destabilizing steric clash. Meanwhile, the predicted interaction energy (ΔE_{int}) in the gas phase for the resulting (*R,S*)-*meso*-dimer is 3 kJ mol⁻¹ more negative than that of the proposed (*S,S*)-dimer counterpart, although their H-bond parameters are comparable (Figure H.6c). Therefore, these findings indicate PN-heterocycles **8** have greater propensity for formation of the *meso*-dimer compared to the (*S,S*)- or (*R,R*)-dimer.

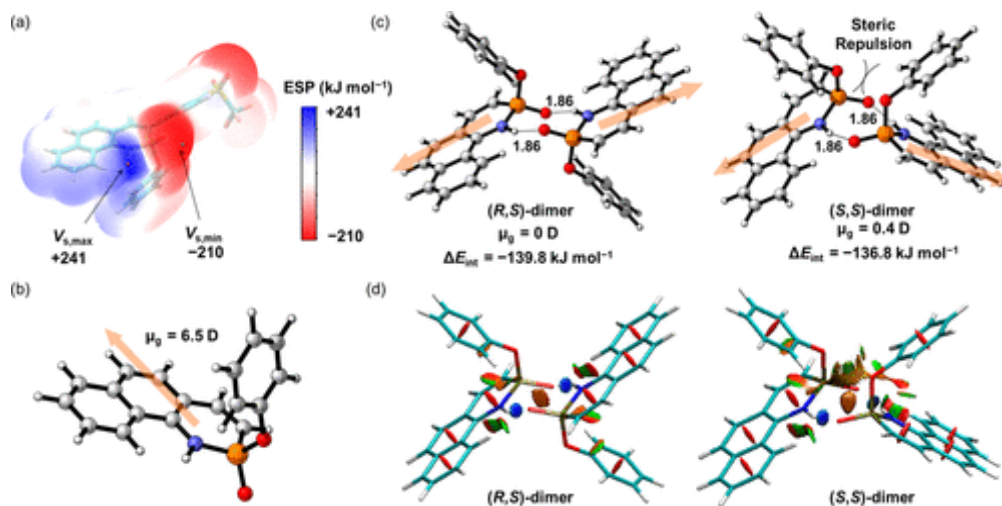


Figure H.6 (a) Electrostatic potential surface (isovalue = 0.001 au) of **8b**. Surface global minima ($V_{s,\text{min}}$) and maxima ($V_{s,\text{max}}$) are represented as cyan and orange dots, respectively. (b) Molecular dipole moment (in debye) for the PN-heterocycle core is denoted by the light orange arrow pointing from the negative pole to the positive pole. (c) Optimized structures with hydrogen bond distances (in Å), molecular dipole moments, and the interaction energies (ΔE_{int} , kJ mol⁻¹) for the (*R,S*)-dimer and (*S,S*)-dimer. The electrostatic potential surface was obtained at the M06-2X/TZVP level of theory. All the dipole moments were calculated at the M06-2X/ma-def2-TZVP level. The interaction energy (ΔE_{int}) is defined as the gas-phase electronic energy difference between dimer and its isolated monomers and calculated at the M06-2X/ma-def2-TZVP//M06-2X/TZVP level of theory, which was corrected for the basis set superposition error (BSSE) in both complexes. (d) NCI plots for two dimeric motifs at the M06-2X/TZVP equilibrium geometries. NCI regions are represented as solid surfaces and blue–green–red scaling from $-0.03 < \text{sign}(\lambda_2)\rho(r) < 0.01$ (in au), where red surface indicates strong repulsion, blue surface strong attraction and green surface relatively weak interactions. Isosurface cutoff for NCI = 0.5.

To understand the energetic differences on dimerization, we analyzed the geometric aspects of the hydrogen bonds of each dimer. The DFT optimizations on these *meso*-

dimeric complexes at the PCM(CHCl₃) M06-2X/TZVP level of theory revealed that the two H-bond distances near N–H/P=O moieties are nearly identical to each other. The values of electron density $\rho(r)$ at the hydrogen bond critical points (BCPs) derived from the atoms in molecules (AIM) topological analysis fall within a narrow window (0.029–0.031 au). Meanwhile, the total hydrogen-bonding energies for the N–H \cdots O=P H-bonds are estimated to be ca. $-74.5 \text{ kJ mol}^{-1}$ for each dimer complex, suggesting they have similar primary H-bond strengths regardless of the appended *p*-substituents (Table H.23). By comparing computationally derived $V_{s,\text{max}}$ (related to H-bond acidity of N–H) and $V_{s,\text{min}}$ (related to H-bond basicity of P=O) values¹⁷ across this series of compounds, there is a general increase in $V_{s,\text{max}}$ absolute values and a concurrent decrease in $V_{s,\text{min}}$ absolute values with the increasing electron-withdrawing abilities of the 3-aryl substituents (as judged by the increasing Hammett substituent parameters,¹⁸ $\sigma_p = \sim 1.22$ for **8a**, 0.96 for **8b**, 0.66 for **8c**, 0.72 for **8d**, 0.54 for **8e**, and -0.27 for **8f**) (Figure H.17). Presumably, the comparable hydrogen bond lengths could be interpreted by the balance between the increased H-bond donor ability of N–H and the reduced H-bond acceptor ability of P=O from **8f** to **8a**; however, the total interaction energy (ΔE_{int}) for the dimerization in the gas phase computed at the M06-2X/ma-def2-TZVP//PCM(CHCl₃)-M06-2X/TZVP level of theory shows the order of **8a** > **8b** > **8d** > **8c** > **8e** > **8f** and agrees qualitatively well with the respective experimentally determined Gibbs free association energies (Table H.3).

Table H.3 Theoretical Interaction Energies in the Gas Phase (ΔE_{int}), Experimental Binding Gibbs Free Energy Change (ΔG_{exp}) of the Self-Dimerization of **8**, Total SAPT0 Energy (E_{SAPT}), Electrostatic Term (E_{ele}), Non-electrostatic Components (ΔE_{nonele}) (the Sum of Contributions from the Dispersion, Exchange and Induction Terms, E_{nonele}) in the SAPT0 Energy Partitions, and the Calculated Molecular Dipole Moments of Monomer ($\mu_{\text{g,mono}}$) and Their Respective Dimer ($\mu_{\text{g,di}}$) of **8**^a

cmpd	ΔE_{int} ^b	ΔG_{exp} ^c	E_{SAPT} ^d	E_{ele}	E_{nonele}	$\mu_{\text{g,mono}}$	$\mu_{\text{g,di}}$
8a	-124.3		-170.2	-176.4	6.2	13.5	0

8b	-123.1	-14.3	-156.3	-166.4	10.2	11.2	0.8
8c	-122.4	-11.9	-154.8	-165.3	10.5	10.1	0
8d	-122.7	-13.7	-154.8	-164.5	9.7	10.4	0
8e	-121.1	-11.1	-152.8	-163.3	10.5	8.4	0
8f	-119.6	-10.8	-152.3	-162.7	10.4	4.2	0.2

^a Energies in kJ mol⁻¹, molecular dipole moments in debye. ^b With BSSE corrections.

^c $\Delta G_{\text{exp}} = -RT \ln K_{\text{dim}}$. ^d SAPT0 calculations with jun-cc-pVDZ basis set.

To determine the fundamental factors of energy differences, symmetry-adapted perturbation theory (SAPT) was utilized to decompose the binding energies into different energy terms. The total SAPT0/jun-cc-pVDZ energies (E_{SAPT}) demonstrate the same trend found in gas-phase interaction energies. According to the SAPT0 energy decomposition, the electrostatic interactions are the leading contributors to stabilization, followed by induction and dispersion, whereas the exchange energies appear repulsive (Table H.25). We further note that the sum of contributions from nonelectrostatic components (E_{nonele}) are similar for all of the considered systems except **8a** and vary within the narrow range of +9.7 to +10.5 kJ mol⁻¹ (Table H.3), acting as the destabilizing term for overall interacting energies. Hence, the induction and dispersion energies are heavily outweighed by the large positive exchange energies. Consequently, the electrostatics alone are comparable to the total interaction energies of these dimeric complexes ($E_{\text{ele}} \approx E_{\text{SAPT}}$). Notably, the electrostatic components also display a distinct trend with the order of **8a** > **8b** > **8c** > **8d** > **8e** > **8f**. This analysis supports the conclusion that the higher interaction energies for these types of molecular systems are mainly due to the pronounced electrostatic interactions.

In the context of structural similarities among the monomers and their dimers as well as the dipolar properties for this type of compound, we assumed that the dimers were stabilized by some additional intermolecular stabilizations such as possible permanent

dipole–dipole/atomic charge–dipole interactions (accounted in E_{ele} term). To further gauge the effect of dipolar interactions, we performed calculations for the dipole moments of **8** and their corresponding *meso*-dimers at the M06-2X/ma-def2-TZVP level of theory, and the results are shown in Table H.3 and Figure H.18. The magnitude of dipole moment for the monomeric compound ($\mu_{\text{g,mono}}$) increases with the order of **8f** < **8e** < **8c** < **8d** < **8b** < **8a** (ranging from 4.2 to 13.5 D), which is in line with the trend for the calculated ΔE_{int} . As expected, the nearly quenched molecular dipole moments were found among all of the examined dimer systems. The larger $\mu_{\text{g,mono}}$ would result in more pronounced electrostatic interactions. These results suggest that the monomeric polarity difference model suitably describes the experimental tendencies for all the addressed dimeric adducts and the enhanced dipolar/charge-dipole interactions between the (*R*)- and (*S*)-monomers could be one of the influential factors for the increased overall dimeric stabilization, though it should be noted that many other considerations, including solvation and dispersive elements such as π – π interactions could also play a role during the actual dimerization events, at least in chloroform solution.

Conclusions

In summary, we have prepared a new type of fluorescent naphtho-fused PN-heterocycle via the P(OPh)₃-mediated cyclization protocol. Both the experimental results and the DFT calculations have revealed that the pendant phenyl rings have a significant impact on their optical properties, electronic structure, and self-association behaviors. The incorporation of a strong electron-withdrawing group leads to a redshift in the spectrum with good photoluminescence quantum yields, as well as strong dimerization in solution state. The monomeric polarity model can successfully explain the overall dimerization stabilities, and

it suggests that appreciable tuning of the self-association ability would be possible by modifying the dipole moment of the monomer, i.e., by further tuning the 3-aryl substituents among these PN-heterocycles. These results provide not only an understanding of the nature of the π -extended PN-heterocyclic skeletons but also a basis for designing intriguing motifs for constructing fluorescent probes and sensors. Furthermore, the strong self-dimerization patterns suggest that this class of molecules could be useful as novel monomeric components for supramolecular assemblies.

Experimental Section

General Methods

NMR spectra were obtained on a Varian Inova 500 MHz spectrometer (^1H : 500.11 MHz, ^{13}C 125.76 MHz, ^{19}F 470.53 MHz, ^{31}P 202.46 MHz) or a Bruker Avance-III-HD 600 MHz (^1H : 599.98 MHz, ^{13}C : 150.87 MHz) spectrometer. Chemical shifts (δ) are expressed in ppm using residual nondeuterated solvent present in the bulk deuterated solvent (CDCl_3 : ^1H 7.26 ppm, ^{13}C 77.16 ppm; $\text{DMSO}-d_6$: ^1H 2.50 ppm, ^{13}C 39.52 ppm). ^{19}F chemical shifts are reported against CFCl_3 external standard (δ 0 ppm). ^{31}P chemical shifts are reported against 85% H_3PO_4 (δ 0 ppm) as external reference. Mass spectra data were acquired on a Waters SYNAPT QToF in positive ion mode with a Shimadzu LC20AD HPLC front end. The solvents were $\text{MeCN}/\text{H}_2\text{O}/0.1\% \text{HCO}_2\text{H}$ at a flow rate of 0.05 mL min^{-1} with a $5 \mu\text{L}$ injection on a loop injection. Preparative SEC was performed using a JAI Recycling Preparative HPLC (Model LC-9101) with a JAIGEL-1H preparative column with CHCl_3 as solvent. Analytical TLC was carried out on TLC plates ($5 \times 10 \text{ cm}$ with 0.25 mm thickness, silica gel 60 F₂₅₄, Merck, Darmstadt, Germany) cut from commercially available aluminum sheets. Solvents and reagents were used as purchased from suppliers, unless

anhydrous conditions were employed, in which case solvents were freshly distilled from sodium/benzophenone under N₂ atmosphere (THF) or as purchased. 2-Iodonaphthalenamine **9**¹⁹ was synthesized according to the literature method.

2-(Trimethylsilylethynyl)naphthalenamine **10**: A ~0.1 M solution of iodonaphthalenamine **9** (150 mg, 0.6 mmol) in toluene (4 mL) and (*i*-Pr)₂NH (4 mL) was purged for 15 min with N₂. TMSA (88 mg, 0.125 mL, 0.9 mmol) was added via syringe. After an additional 5 min of N₂ purging, CuI (11.4 mg, 0.06 mmol) and [Pd(PPh₃)₂Cl₂] (42 mg, 0.06 mmol) were added to the reaction mixture. The flask was then purged for an additional 5 min, sealed, and stirred at room temperature under N₂ for 12 h. The mixture was then concentrated and the residue chromatographed on silica gel to afford the desired ethynylsilane **10** (131 mg, 98%) as a colorless oil: *R*_f = 0.4 (hexanes/EtOAc, 8:1); ¹H NMR (500 MHz, CDCl₃) δ 7.79–7.73 (m, 2H), 7.47–7.45 (m, 2H), 7.35 (d, *J* = 8.4 Hz, 1H), 7.18 (d, *J* = 8.5 Hz, 1H), 4.87 (s, 2H), 0.31 (s, 9H); ¹³C{¹H} NMR (126 MHz, CDCl₃) δ 145.6, 134.3, 128.7, 128.5, 126.8, 125.5, 122.5, 121.1, 118.0, 103.0, 102.0, 100.6, 0.39; HRMS (ESI) *m/z* calcd for C₁₅H₁₈NSi [M + H⁺] 240.1209, found 240.1206.

General Procedure for Synthesis of 2-(Phenylethynyl)naphthalenamines **11**: To a solution of alkyne **10** (1.0 equiv.) in MeOH/CH₂Cl₂ (1:1, ~0.01 M) was added K₂CO₃ (3.0 equiv.). The suspension was stirred at room temperature for 2–3 h and then filtered through a bed of Celite. After evaporation of the solvent, the crude residue was used directly in the next reaction. To an N₂-sparged solution of bromoarene (for **11a–e**) or iodoarene (for **11f**) (1.2 equiv.) and terminal acetylene (1.0 equiv.) in 1:1 THF/DIPA was added 5 mol % of [Pd(PPh₃)₂Cl₂] and 5 mol % of CuI. The suspension was stirred at room temperature under an N₂ atmosphere for 24 h. In the case of the 4-bromobenzonitrile starting material, the

solution was heated to 60 °C (oil bath) for 12 h. The reaction mixture was cooled, concentrated in vacuo, and purified via flash chromatography to give the desired product **11** as a dark-orange oil.

4-((1-Aminonaphthalen-2-yl)ethynyl)phthalonitrile **11a**: The general procedure was followed using 4-iodophthalonitrile (254 mg, 1.0 mmol). Purification by column chromatography (silica gel, hexanes/EtOAc 3:1) gave **11a** (249 mg, 85%) as a waxy solid: $R_f = 0.28$ (hexanes/EtOAc, 3:1); $^1\text{H NMR}$ (600 MHz, $\text{DMSO-}d_6$) δ 8.49 (s, 1H), 8.27 (d, $J = 8.4$ Hz, 1H), 8.14–8.09 (m, 2H), 7.76 (d, $J = 8.1$ Hz, 1H), 7.52 (t, $J = 7.4$ Hz, 1H), 7.47 (t, $J = 7.6$ Hz, 1H), 7.32 (d, $J = 8.4$ Hz, 1H), 7.09 (d, $J = 8.5$ Hz, 1H), 6.54 (s, 2H); $^{13}\text{C}\{^1\text{H}\}$ NMR (151 MHz, $\text{DMSO-}d_6$) δ 148.4, 135.7, 135.3, 134.6, 134.0, 129.2, 128.6, 128.1, 127.6, 125.0, 123.0, 121.8, 116.0, 115.7, 115.6, 115.0, 112.1, 96.6, 95.8, 92.5; HRMS (ESI) m/z calcd for $\text{C}_{20}\text{H}_{12}\text{N}_3$ [$\text{M} + \text{H}^+$] 294.1031, found 294.1052.

2-((4-((Trifluoromethyl)sulfonyl)phenyl)ethynyl)naphthalen-1-amine **11b**: The general procedure was followed using 1-bromo-4-[(trifluoromethyl)sulfonyl]-benzene (722 mg, 2.5 mmol). Purification by column chromatography (silica gel, hexanes/EtOAc, 5:1) gave **11b** (779 mg, 83%) as a dark-orange oil: $R_f = 0.29$ (hexanes/EtOAc, 4:1); $^1\text{H NMR}$ (500 MHz, CDCl_3) δ 8.02 (d, $J = 8.1$ Hz, 2H), 7.83–7.77 (m, 4H), 7.54–7.49 (m, 2H), 7.42 (d, $J = 8.5$ Hz, 1H), 7.25 (d, $J = 8.7$ Hz, 1H), 4.99 (s, 2H); $^{13}\text{C}\{^1\text{H}\}$ NMR (126 MHz, CDCl_3) δ 146.0, 134.8, 132.7, 132.3, 130.9, 129.6, 128.9, 128.3, 127.6, 125.9, 121.2, 119.9 (q, $J = 327.0$ Hz), 118.5, 100.2, 94.1, 93.8; $^{19}\text{F NMR}$ (471 MHz, CDCl_3) δ –78.24; HRMS (ESI) m/z calcd for $\text{C}_{19}\text{H}_{13}\text{F}_3\text{NO}_2\text{S}$ [$\text{M} + \text{H}^+$] 376.0619, found 376.0626.

2-(2-(4-Cyanophenyl)ethynyl)naphthalen-1-amine **11c**: The general procedure was followed using 4-bromobenzonitrile (154 mg, 0.8 mmol). Purification by column

chromatography (silica gel, hexanes/EtOAc, 5:1) gave **11c** (130 mg, 61%) as a tan oil: $R_f = 0.18$ (hexanes/EtOAc, 5:1); $^1\text{H NMR}$ (500 MHz, CDCl_3) δ 7.84 (d, $J = 7.9$ Hz, 1H), 7.80 (d, $J = 7.1$ Hz, 1H), 7.68–7.64 (m, 4H), 7.55–7.50 (m, 2H), 7.43 (d, $J = 8.5$ Hz, 1H), 7.27 (m, 1H), 4.97 (s, 2H); $^{13}\text{C}\{^1\text{H}\}$ NMR (126 MHz, CDCl_3) δ 145.5, 134.6, 132.2, 131.8, 128.9, 128.6, 128.3, 127.3, 125.8, 122.5, 121.1, 118.7, 118.4, 111.3, 100.8, 94.2, 91.9; HRMS (ESI) m/z calcd for $\text{C}_{19}\text{H}_{13}\text{N}_2$ [$\text{M} + \text{H}^+$] 269.1079, found 269.1076.

2-((4-(Methylsulfonyl)phenyl)ethynyl)naphthalen-1-amine **11d**: The general procedure was followed using 1-bromo-4-(methylsulfonyl)benzene (235 mg, 1.0 mmol). Purification by column chromatography (hexanes/ CH_2Cl_2 /EtOAc, 3:1:1) gave **11d** (266 mg, 83%) as a waxy solid: $R_f = 0.12$ (hexanes/EtOAc, 2:1); $^1\text{H NMR}$ (500 MHz, $\text{DMSO}-d_6$) δ 8.26 (d, $J = 8.2$ Hz, 1H), 7.96–7.90 (m, 4H), 7.76 (d, $J = 7.9$ Hz, 1H), 7.51–7.44 (m, 2H), 7.34 (d, $J = 8.4$ Hz, 1H), 7.10 (d, $J = 8.4$ Hz, 1H), 6.37 (s, 2H), 3.24 (s, 3H); $^{13}\text{C}\{^1\text{H}\}$ NMR (126 MHz, $\text{DMSO}-d_6$) δ 147.6, 139.4, 134.4, 131.8, 128.8, 128.2, 127.4, 127.3, 125.1, 123.0, 122.0, 116.0, 97.8, 93.7, 92.2, 43.6; HRMS (ESI) m/z calcd for $\text{C}_{19}\text{H}_{16}\text{NO}_2\text{S}$ [$\text{M} + \text{H}^+$] 322.0902, found 322.0916.

2-(2-(4-(Trifluoromethyl)phenyl)ethynyl)naphthalen-1-amine **11e**: The general procedure was followed using 1-bromo-4-(trifluoromethyl)benzene (450 mg, 2.0 mmol). Purification by column chromatography (hexanes/EtOAc, 10:1) gave **11e** (386 mg, 62%) as a tan oil: $R_f = 0.42$ (hexanes/EtOAc, 10:1); $^1\text{H NMR}$ (500 MHz, CDCl_3) δ 7.83–7.81 (m, 1H), 7.79–7.77 (m, 1H), 7.67–7.62 (m, 4H), 7.52–7.48 (m, 2H), 7.43 (d, $J = 8.5$ Hz, 1H), 7.25 (d, $J = 8.5$ Hz, 1H), 4.93 (s, 2H); $^{13}\text{C}\{^1\text{H}\}$ NMR (126 MHz, CDCl_3) δ 145.2, 134.5, 131.6, 129.8 (q, $J = 32.8$ Hz), 128.8, 128.4, 127.4 (q, $J = 1.3$ Hz), 127.2, 125.7, 125.5 (q, $J = 3.8$ Hz),

124.1 (q, $J = 272$ Hz), 122.5, 121.1, 118.4, 101.2, 94.3, 89.7; ^{19}F NMR (471 MHz, CDCl_3) $\delta -62.68$; HRMS (ESI) m/z calcd for $\text{C}_{19}\text{H}_{13}\text{F}_3\text{N}$ [$\text{M} + \text{H}^+$] 312.1000, found 312.1008.

2-(2-(4-Methoxyphenyl)ethynyl)naphthalen-1-amine **11f**: The general procedure was followed using 4-iodoanisole (357 mg, 1.5 mmol). Purification by column chromatography (hexanes/EtOAc, 10:1) gave **11f** (241 mg, 59%) as a tan oil: $R_f = 0.39$ (hexanes/EtOAc, 5:1); ^1H NMR (500 MHz, CDCl_3) δ 7.84–7.79 (m, 2H), 7.54 (d, $J = 8.5$ Hz, 2H), 7.50–7.45 (m, 3H), 7.27 (m, 1H), 6.93 (d, $J = 8.2$ Hz, 2H), 4.91 (s, 2H), 3.87 (s, 3H); $^{13}\text{C}\{^1\text{H}\}$ NMR (126 MHz, CDCl_3) δ 159.7, 144.5, 134.1, 133.0, 128.8, 128.6, 126.6, 125.5, 122.7, 121.1, 118.2, 115.7, 114.2, 102.6, 95.5, 85.6, 55.5; HRMS (ESI) m/z calcd for $\text{C}_{19}\text{H}_{16}\text{ON}$ [$\text{M} + \text{H}^+$] 274.1232, found 274.1245.

General Procedure for Synthesis of PN-Heterocycles **8**

To a solution of amine **11** (0.5 mmol) in dry pyridine (1 mL) was added triphenyl phosphite (171 mg, 0.55 mmol). The reaction vessel was sealed and heated to 100 °C (oil bath) for 18–24 h. After cooling, the volatiles were removed in vacuo. The residue was purified through flash chromatography on silica gel (eluting with $\text{CH}_2\text{Cl}_2/\text{EtOAc}$, 15/1–3/1 (v/v) containing 0.05% MeOH) to give the crude product, which then was further purified via preparative SEC (if necessary). In most cases, the desired fractions were accompanied by a small amount of unknown persistent aromatic impurities. Analytically pure product can be obtained from recrystallization by slow evaporation of its CHCl_3 solution at room temperature. The reported yields are overall yields. (Note: The chemical shifts of ^{31}P resonances can vary with concentration; thus, we reported the H coupled ^{31}P NMR spectra).

2-Phenoxy-3-(3,4-dicyanophenyl)-1*H*-naphtho[2,1-*e*][1,2]azaphosphinine 2-oxide **8a**: yellow solid (69 mg, 32%); $R_f = 0.57$ (hexanes/ $\text{CH}_2\text{Cl}_2/\text{EtOAc}$, 1:2:2); mp > 200 °C; ^1H

NMR (600 MHz, DMSO-*d*₆) δ 10.33 (s, 1H), 8.66 (m, 1H), 8.61 (m, 1H), 8.47 (m, 1H), 8.43 (d, *J* = 37.9 Hz, 1H), 8.25 (d, *J* = 8.2 Hz, 1H), 7.92 (d, *J* = 7.3 Hz, 1H), 7.66–7.61 (m, 2H), 7.57–7.52 (m, 2H), 7.16 (t, *J* = 7.7 Hz, 2H), 7.18–7.14 (m, 2H), 7.03 (m, 1H), 6.92–6.90 (m, 2H); ¹³C{¹H} NMR (151 MHz, DMSO-*d*₆) δ 149.9 (d, *J* = 9.0 Hz), 145.1 (d, *J* = 3.7 Hz), 141.0 (d, *J* = 10.5 Hz), 138.0, 134.5, 131.8 (d, *J* = 5.9 Hz), 131.5 (d, *J* = 8.1 Hz), 129.6, 128.4 (d, *J* = 16.5 Hz), 128.0, 126.5, 125.1, 123.1 (d, *J* = 8.2 Hz), 122.7, 121.1, 120.93 (d, *J* = 3.9 Hz), 119.7 (d, *J* = 12.9 Hz), 118.6, 115.98 (d, *J* = 19.6 Hz), 115.4, 114.90 (d, *J* = 15.2 Hz), 112.8; ³¹P NMR (202 MHz, DMSO-*d*₆) δ 10.43 (d, *J* = 37.7 Hz); UV/vis (CHCl₃) λ_{max} (log ϵ) 404 (4.07), 343 (4.17) nm; HRMS (ESI) *m/z* calcd for C₂₆H₁₇N₃O₂P [M + H⁺] 434.1058, found 434.1047.

2-Phenoxy-3-(4-((trifluoromethyl)sulfonyl)phenyl)-1*H*-naphtho[2,1-

e][1,2]azaphosphinine 2-oxide **8b**: yellow solid (77 mg, 30%); *R_f* = 0.43 (hexanes/CH₂Cl₂/EtOAc, 1:2:2); mp > 200 °C; ¹H NMR (500 MHz, CDCl₃) δ 9.71 (s, 1H), 8.52 (d, *J* = 8.5 Hz, 1H), 8.23–8.21 (m, 2H), 8.14 (d, *J* = 8.2 Hz, 2H), 7.91 (d, *J* = 38.7 Hz, 1H), 7.84 (d, *J* = 8.1 Hz, 1H), 7.64–7.61 (m, 1H), 7.51–7.47 (m, 2H), 7.39 (d, *J* = 8.5 Hz, 1H), 7.00–6.97 (m, 2H), 6.93–6.89 (m, 3H); ¹³C{¹H} NMR (151 MHz, CDCl₃) δ 149.9 (d, *J* = 8.9 Hz), 144.9 (d, *J* = 4.8 Hz), 144.6 (d, *J* = 9.8 Hz), 138.1 (d, *J* = 2.8 Hz), 135.0, 131.4, 130.1, 129.6, 128.8 (d, *J* = 6.7 Hz), 128.6 (d, *J* = 19.0 Hz), 127.5, 126.7, 125.3, 123.9 (d, *J* = 8.1 Hz), 122.7, 122.0, 121.4, 121.2 (d, *J* = 4.1 Hz), 121.1, 120.4, 120.0 (q, *J* = 325.9 Hz), 115.4 (d, *J* = 14.9 Hz); ³¹P NMR (202 MHz, CDCl₃) δ 11.72 (d, *J* = 38.9 Hz); ¹⁹F NMR (471 MHz, CDCl₃) δ -78.22; UV/vis (CHCl₃): λ_{max} (log ϵ) 375 (3.72), 338 (3.90) nm; HRMS (ESI) *m/z* calcd for C₂₅H₁₈NO₄F₃PS [M + H⁺] 516.0646, found 516.0648.

2-Phenoxy-3-(4-cyanophenyl)-1*H*-naphtho[2,1-*e*][1,2]azaphosphinine 2-oxide **8c**: yellow solid (33 mg, 16%); $R_f = 0.58$ (hexanes/CH₂Cl₂/EtOAc, 1:2:2); mp > 200 °C; ¹H NMR (500 MHz, CDCl₃) δ 9.76 (s, 1H), 8.56 (d, $J = 8.5$ Hz, 1H), 8.09 (d, $J = 8.0$ Hz, 2H), 7.85 (d, $J = 39.3$ Hz, 1H), 7.86 (d, $J = 8.1$ Hz, 1H), 7.81 (d, $J = 8.3$ Hz, 2H), 7.65 (m, 1H), 7.54 (m, 1H), 7.49 (d, $J = 8.5$ Hz, 1H), 7.39 (d, $J = 8.5$ Hz, 1H), 7.02–6.99 (m, 2H), 6.95–6.90 (m, 3H); ¹³C{¹H} NMR (151 MHz, CDCl₃) δ 150.1 (d, $J = 8.9$ Hz), 143.7, 140.5, 137.6, 134.8, 132.7, 129.5, 128.7, 128.2, 128.2, 127.5, 126.6, 125.2, 123.8, 122.6, 121.8, 121.2 (d, $J = 4.2$ Hz), 119.0, 115.5 (d, $J = 16.7$ Hz), 111.7; ³¹P NMR (202 MHz, CDCl₃) δ 12.09 (d, $J = 39.3$ Hz); UV/vis (CHCl₃) λ_{max} (log ε) 389 (4.01), 340 (4.09) nm; HRMS (ESI) m/z calcd for C₂₅H₁₈N₂O₂P [M + H⁺] 409.1106, found 409.1106.

2-Phenoxy-3-(4-(methylsulfonyl)phenyl)-1*H*-naphtho[2,1-*e*][1,2]azaphosphinine 2-oxide **8d**: yellow solid (90 mg, 39%); $R_f = 0.27$ (hexanes/CH₂Cl₂/EtOAc, 1:2:2); mp > 200 °C; ¹H NMR (500 MHz, CDCl₃) δ 9.40 (s, 1H), 8.48 (d, $J = 8.4$ Hz, 1H), 8.14 (d, $J = 8.1$ Hz, 2H), 8.08–8.06 (m, 2H), 7.85 (d, $J = 39.2$ Hz, 1H), 7.84 (d, $J = 8.1$ Hz, 1H), 7.61 (t, $J = 7.5$ Hz, 1H), 7.55 (t, $J = 7.6$ Hz, 1H), 7.47 (d, $J = 8.6$ Hz, 1H), 7.38 (d, $J = 8.5$ Hz, 1H), 7.01–6.97 (m, 2H), 6.93–6.89 (m, 2H), 3.14 (s, 3H); ¹³C{¹H} NMR (151 MHz, CDCl₃) δ 150.0 (d, $J = 9.1$ Hz), 144.0 (d, $J = 5.1$ Hz), 141.6 (d, $J = 9.7$ Hz), 139.8, 137.5 (d, $J = 2.8$ Hz), 134.8, 129.5, 128.7, 128.5 (d, $J = 6.7$ Hz), 128.3, 128.1, 127.5, 126.7, 125.21, 123.8 (d, $J = 8.0$ Hz), 122.4, 122.3, 121.9, 121.24 (d, $J = 4.2$ Hz), 121.2, 115.5 (d, $J = 14.9$ Hz), 44.8; ³¹P NMR (202 MHz, CDCl₃) δ 11.92 (d, $J = 38.9$ Hz); UV/vis (CHCl₃) λ_{max} (log ε) 388 (3.87), 337 (3.96) nm; HRMS (ESI) m/z calcd for C₂₅H₂₁NO₄PS [M + H⁺] 462.0929, found 462.0933.

2-Phenoxy-3-(4-(trifluoromethyl)phenyl)-1*H*-naphtho[2,1-*e*][1,2]azaphosphinine 2-oxide **8e**: yellow solid (40 mg, 18%); $R_f = 0.74$ (hexanes/CH₂Cl₂/EtOAc, 1:2:2); mp > 200 °C; ¹H NMR (500 MHz, CDCl₃) δ 9.38 (s, 1H), 8.47 (d, $J = 8.5$ Hz, 1H), 8.05 (d, $J = 8.0$ Hz, 2H), 7.82 (d, $J = 8.1$ Hz, 1H), 7.80 (d, $J = 39.4$ Hz, 1H), 7.76 (d, $J = 8.0$ Hz, 2H), 7.59 (dd, $J = 8.2, 6.7$ Hz, 1H), 7.50 (ddd, $J = 8.4, 6.9, 1.3$ Hz, 1H), 7.45 (d, $J = 8.5$ Hz, 1H), 7.37 (d, $J = 8.5$ Hz, 1H), 7.00–6.97 (m, 2H), 6.94–6.88 (m, 3H); ¹³C{¹H} NMR (126 MHz, CDCl₃) δ 150.2 (d, $J = 9.1$ Hz), 143.3 (d, $J = 5.2$ Hz), 139.5 (d, $J = 9.6$ Hz), 137.3, 134.7, 130.2 (q, $J = 32.8$ Hz), 129.5, 128.6, 128.1, 128.1, 128.0, 127.5, 126.6, 126.0 (q, $J = 3.8$ Hz), 125.1, 124.3 (q, $J = 273$ Hz), 123.8 (d, $J = 8.0$ Hz), 123.1, 122.3, 121.8, 121.7, 121.3 (d, $J = 4.2$ Hz), 115.6 (d, $J = 14.9$ Hz); ³¹P NMR (202 MHz, CDCl₃) δ 12.14 (d, $J = 39.4$ Hz); ¹⁹F NMR (471 MHz, CDCl₃) δ -62.51; UV/vis (CHCl₃) λ_{max} (log ε) 380 (3.84), 337 (3.91) nm; HRMS (ESI) m/z calcd for C₂₅H₁₈NO₂F₃P [M + H⁺] 452.1027, found 452.1030.

2-Phenoxy-3-(4-methoxyphenyl)-1*H*-naphtho[2,1-*e*][1,2]azaphosphinine 2-oxide **8f**: colorless waxy solid (33 mg, 16%); $R_f = 0.53$ (hexanes/CH₂Cl₂/EtOAc, 1:2:2); mp > 200 °C; ¹H NMR (500 MHz, CDCl₃) δ 9.29 (s, 1H), 8.51 (d, $J = 8.1$ Hz, 1H), 7.94–7.92 (m, 2H), 7.82 (m, 1H), 7.69 (d, $J = 40.6$ Hz, 1H), 7.58–7.52 (m, 2H), 7.44 (d, $J = 8.5$ Hz, 1H), 7.36 (d, $J = 8.5$ Hz, 1H), 7.08 (d, $J = 8.5$ Hz, 2H), 7.01–6.96 (m, 4H), 6.90 (m, 1H), 3.94 (s, 3H); ¹³C{¹H} NMR (151 MHz, CDCl₃) δ 160.0, 150.5 (d, $J = 9.2$ Hz), 140.4 (d, $J = 6.3$ Hz), 136.4, 134.2, 129.3, 129.1 (d, $J = 6.9$ Hz), 128.4, 128.3 (d, $J = 9.3$ Hz), 127.5, 127.4, 126.4, 124.8, 124.0, 123.9 (d, $J = 8.0$ Hz), 122.9, 122.3, 121.4 (d, $J = 4.2$ Hz), 121.3, 115.9 (d, $J = 15.1$ Hz), 114.5, 55.6; ³¹P NMR (202 MHz, CDCl₃) δ 13.07 (d, $J = 40.7$ Hz); UV/vis (CHCl₃) λ_{max} (log ε) 372 (3.86), 356 (3.87) nm; HRMS (ESI) m/z calcd for C₂₅H₂₁NO₃P [M + H⁺] 414.1259, found 414.1261.

Supplementary Information

1. X-ray Structure Data and Molecular Packing

Diffraction intensities for **8c** and **8d** were collected at 173 K on a Bruker Apex2 CCD diffractometer using CuK α radiation, $\lambda = 1.54178$ Å. Space groups were determined based on intensity statistics. Absorption corrections were applied by SADABS.²⁰ Structures were solved by direct methods and Fourier techniques and refined on F^2 using full matrix least-squares procedures. All non-H atoms were refined with anisotropic thermal parameters. All H atoms in **8d** and H atoms at the N atoms in **8c** involved in H-bonds were found on the residual density maps and refined with isotropic thermal parameters. Other H atoms in **8c** were refined in calculated positions in a rigid group model. Solvent molecules CHCl₃ in **8c** fill out in the packing a space between main molecules and its positions appear to be partially occupied or highly disordered. As a result, diffraction intensities at high angles are very weak. These solvents molecules on **8c** were treated by SQUEEZE.²¹ The correction of the X-ray data by SQUEEZE is 228 electron/cell; the required value is 232 electron/cell for four CHCl₃ molecules in the full unit cell. All calculations were performed by the Bruker SHELXL-2014 package²² The ORTEP drawings were made with the Diamond²³ and Ortep-3²⁴ programs. The visualization and exploration of the intermolecular close contacts of the structure was achieved by the Hirshfeld surface analysis with the Crystal Explorer software.²⁵ CCDC 1900247 and 1900248 contain the supplementary crystallographic data for this paper. These data can be obtained free of charge from The Cambridge Crystallographic Data Centre at www.ccdc.cam.ac.uk/data_request/cif.

Crystallographic data for 8c: C₂₅H₁₇N₂O₂P•CHCl₃, M = 527.74, 0.11 × 0.03 × 0.02 mm, T = 173(2) K, Triclinic, space group *P*-1, *a* = 12.7196(6) Å, *b* = 14.8501(7) Å, *c* = 15.4304(7) Å, α = 117.135(3)°, β = 106.977(3)°, γ = 94.402(3)°, *V* = 2404.1(2) Å³, *Z* = 4, *D*_c = 1.458 Mg m⁻³, μ (Cu) = 4.310 mm⁻¹, *F*(000) = 1080, 2 θ _{max} = 133.44°, 30824 reflections, 8446 independent reflections [*R*_{int} = 0.0546], *R*1 = 0.1027, *wR*2 = 0.2856 and *GOF* = 1.115 for 8446 reflections (549 parameters) with *I* > 2 σ (*I*), *R*1 = 0.1241, *wR*2 = 0.3052 and *GOF* = 1.119 for all reflections, max/min residual electron density +1.335/−0.332 eÅ⁻³. CCDC 1900247.

Crystallographic data for 8d: C₂₅H₂₀NO₄PS, M = 461.45, 0.12 × 0.09 × 0.07 mm, T = 173(2) K, Triclinic, space group *P*-1, *a* = 8.3012(3) Å, *b* = 11.3430(4) Å, *c* = 13.0055(5) Å, α = 93.515(2)°, β = 103.769(2)°, γ = 110.518(2)°, *V* = 1099.77(7) Å³, *Z* = 2, *D*_c = 1.393 Mg m⁻³, μ (Cu) = 2.273 mm⁻¹, *F*(000) = 480, 2 θ _{max} = 133.10°, 12225 reflections, 3871 independent reflections [*R*_{int} = 0.0453], *R*1 = 0.0370, *wR*2 = 0.0993 and *GOF* = 1.029 for 3871 reflections (369 parameters) with *I* > 2 σ (*I*), *R*1 = 0.0424, *wR*2 = 0.1039 and *GOF* = 1.029 for all reflections, max/min residual electron density +0.399/−0.342 eÅ⁻³. CCDC 1900248.

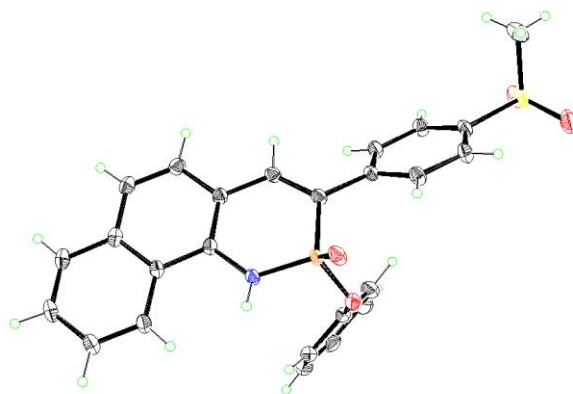


Figure H.7. ORTEP drawing of the structure of **8d** (thermal ellipsoids drawn at 30% probability). Single crystals suitable for X-ray diffraction were obtained by slow evaporation of CH_2Cl_2 solution at room temperature.

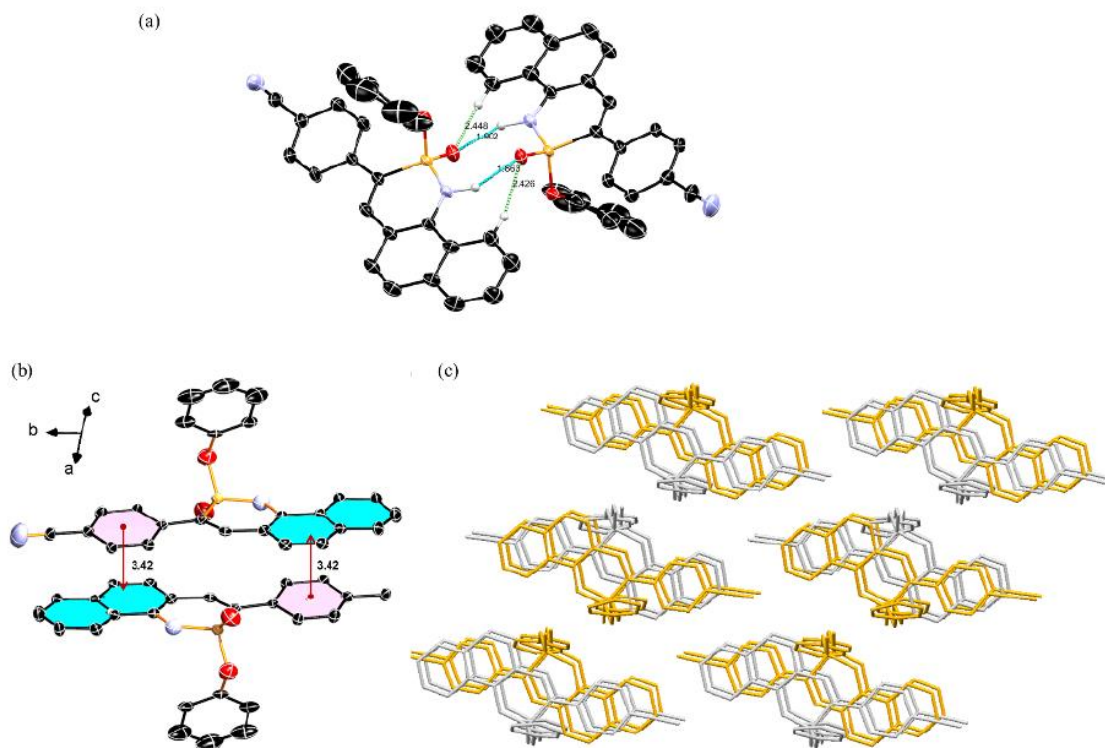
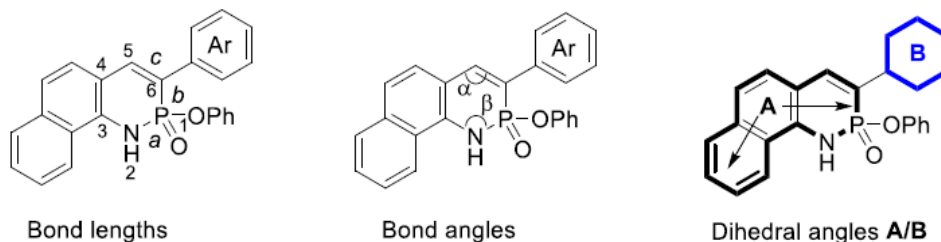


Figure H.8 (a) ORTEP drawing of the dimer structure of **8c** *via* hydrogen-bonding (thermal ellipsoids drawn at 30% probability). Single crystals suitable for X-ray diffraction were obtained by slow evaporation of CHCl_3 solution at room temperature; (b) Intermolecular π contacts; (c) The molecular packing diagram viewed along the a -axis. All hydrogen atoms not involved in H-bonding interactions are omitted for clarity; the distances of contacts are in Å.

Table H.4. Selected bond lengths, bond angles, and dihedral angles of PN-heterocycles **8c** and **8d**. There are no significant differences of the selected bond angles and lengths among the two structures. The dihedral angle between the tricyclic cores and their intersections with the pendant phenyl plane exhibit the value of 7° for **8c** and 40° in **8d**, respectively, which is likely attributable to the packing effects in the solid state.



cmpd	8c	8d
Bond Length (Å)		
<i>a</i>	1.632/1.635	1.648
<i>b</i>	1.771/1.760	1.762
<i>c</i>	1.353/1.351	1.347
Bond angle (°)		
α	128.2/128.9	127.4
β	128.1/128.2	127.8
Deviation of P atom (Å)^a	0.05/0.11	0.25
Dihedral angle A/B θ (°)^b	7.1/7.6	40.2

^a The average distance of the P atom from the mean plane **A** defined by the other 13 non-H atoms in the tricyclic core. ^b Dihedral angles between the mean plane **A** defined by the other 13 non-H atoms and the pendant phenyl plane **B**.

2. Photophysical Properties

UV/Vis data were obtained on an HP 8453 UV/Vis spectrometer. Fluorescence data were acquired with a Horiba Jobin-Yvon FluoroMax-4 fluorescence spectrophotometer. Dilute solutions in degassed spectral grade CHCl_3 in a 1 cm quartz cell were used for measurements. Quantum yields were calculated by comparison with freshly prepared quinine sulfate in 0.1M H_2SO_4 with excitation at 360 nm using an excitation slit width of 2.5 nm for all samples, and emission integrated across the range 380–650 nm. To minimize the re-absorption effects, the absorbance in the 10 mm fluorescence cuvette was about 0.05–0.07 at 360 nm. Fluorescence lifetimes were measured using time correlated single photon counting (TCSPC). Dilute solutions were prepared and placed in a 1 cm optical path quartz cuvette. A pulsed nanoLED was used to excite the samples at 344 nm at a 1 MHz repetition rate. The emission was detected *via* a longpass filter. The decay profiles of were fitted reasonably well using the bi-exponential (for **8a-c**) and mono-exponential functions (for **8d-f**).

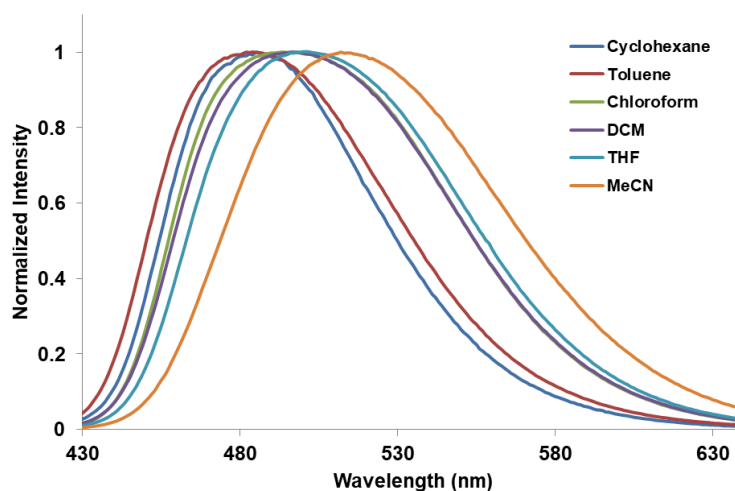


Figure H.9 Fluorescence spectra of **8a** in various solvents.

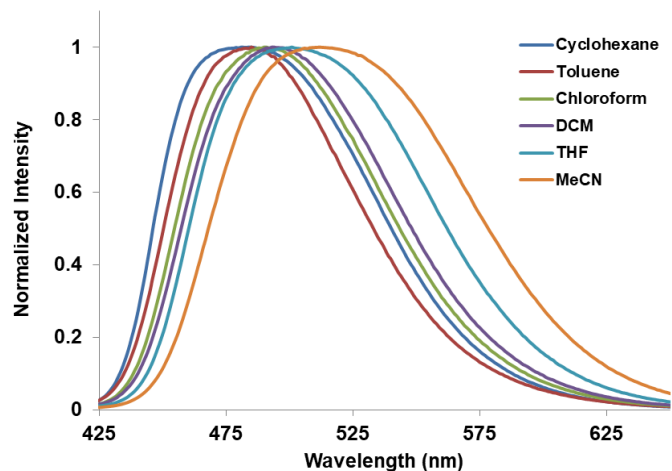


Figure H.10 Fluorescence spectra of **8b** in various solvents.

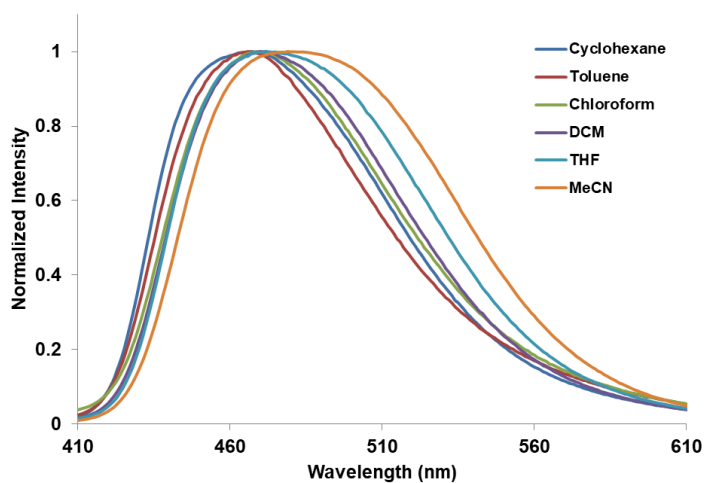


Figure H.11 Fluorescence spectra of **8c** in various solvents.

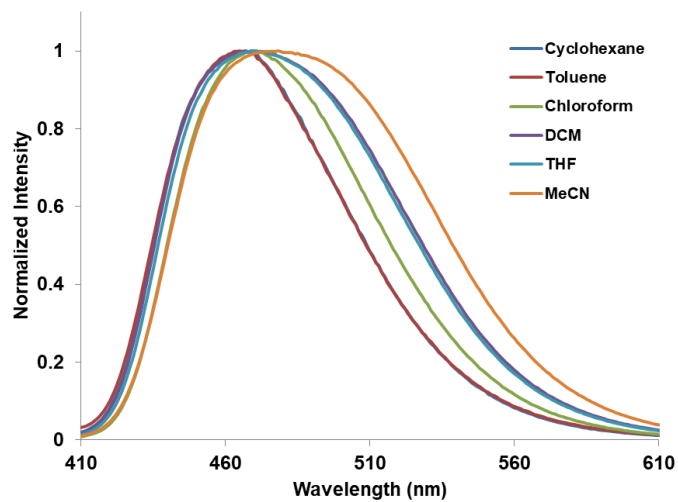


Figure H.12 Fluorescence spectra of **8d** in various solvents.

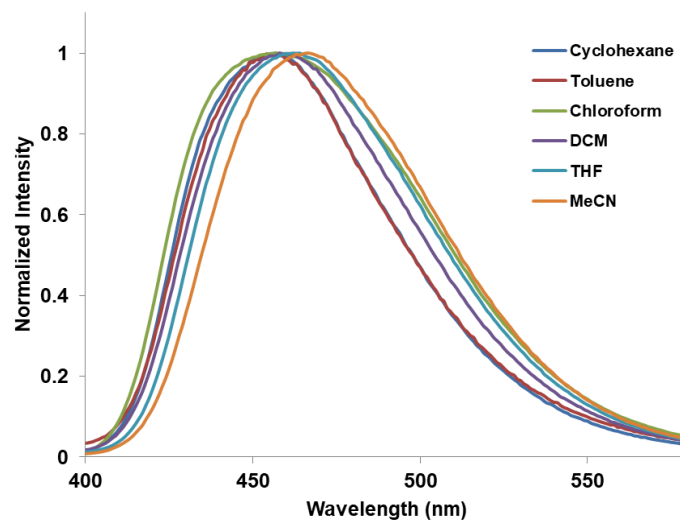


Figure H.13 Fluorescence spectra of **8e** in various solvents.

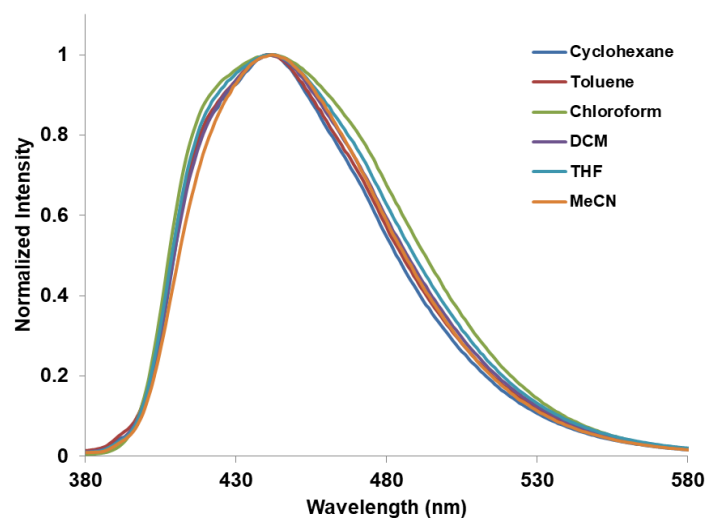


Figure H.14 Fluorescence spectra of **8f** in various solvents.

3. Theoretical calculations

This work benefited from access to the University of Oregon high performance computer, Talapas. The initial structures of **7**, **8c** and **8d** were generated from the above X-ray crystallography data. Other similar structures are adjusted according to the structures in the single crystal.

3.1 TD-DFT calculations

These initial structures were optimized using the functional PBE07 and 6-311G(d) basis set as implemented in Gaussian 09.²⁷ In addition, all the optimized structures were confirmed by frequency analysis and the number of imaginary frequencies was zero. TD-DFT vertical excitation calculations and geometry optimization of the first excited state (S_1) were performed at the same level of theory. The PCM solvation model²⁸ was used to account for the solvent effects of the chloroform.

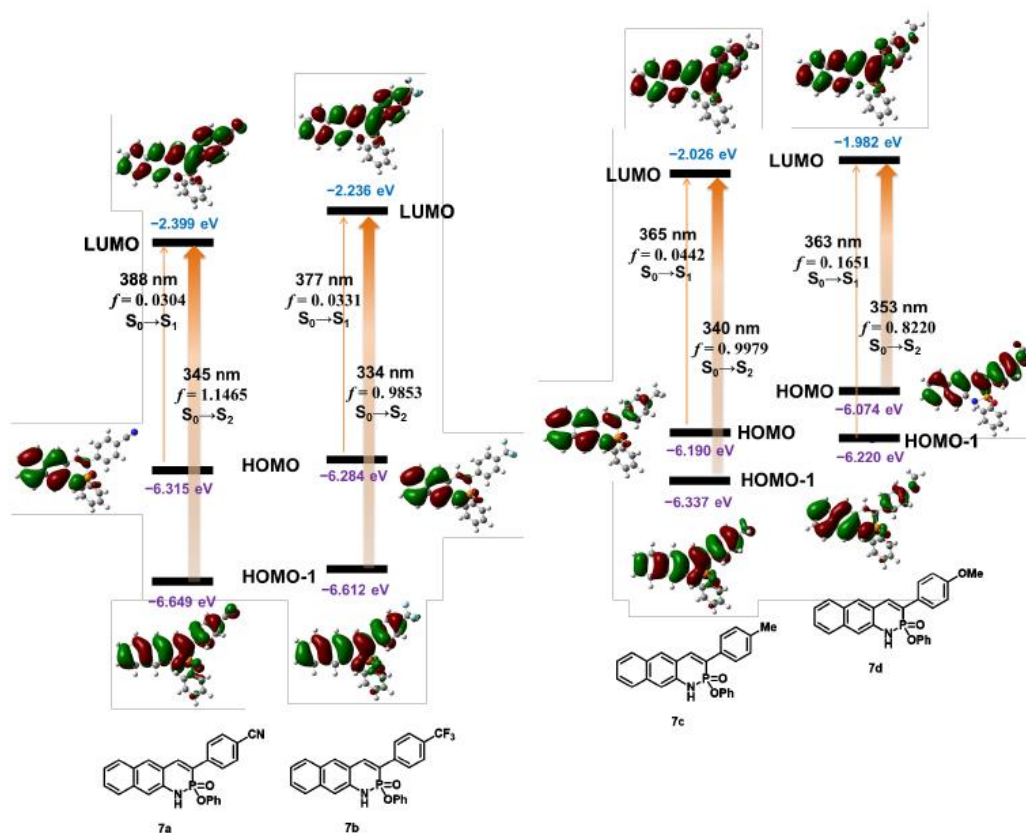
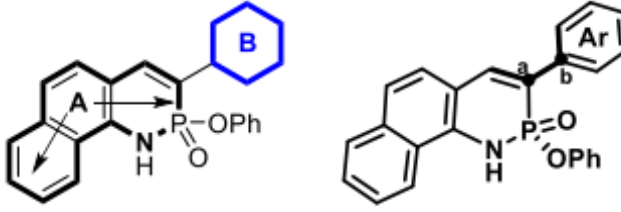


Figure H.15 Kohn-Sham molecular orbitals, excitation energies, and oscillator strengths for PN-heterocycles **7a-d**, calculated at the TD-PBE0/6-311G(d) level of theory. For **7a-c**, the $S_0 \rightarrow S_1$ electronic transitions are dominated by the transitions from HOMO \rightarrow LUMO with very small oscillator strengths ($f < 0.1$), while the transitions from HOMO-1 \rightarrow LUMO contribute the $S_0 \rightarrow S_2$ electronic transitions with large oscillator strengths ($f \approx 1$). For **7d**, the $S_0 \rightarrow S_1$ electronic transitions mainly correspond to the transitions from HOMO-1 \rightarrow LUMO, while the $S_0 \rightarrow S_2$ electronic transition is predominated by the transitions from HOMO \rightarrow LUMO.

Table H.5 The S₀/S₁ geometries of **8**


	Dihedral angles (θ) A/B		Bond length (d) Ca-Cb	
	S ₀		S ₁	
	θ ($^\circ$) ^a	d (Å)	θ ($^\circ$) ^a	d (Å)
8a	32.93	1.473	12.70	1.440
8b	34.23	1.474	8.90	1.438
8c	32.77	1.474	7.17	1.436
8d	34.82	1.476	7.91	1.437
8e	33.77	1.476	11.04	1.439
8f	33.82	1.475	14.26	1.434

^a Dihedral angles between the mean plane **A** defined by the other 13 non-H atoms and the pendant phenyl plane **B**.

Table H.6 The frontier molecular orbital energies in the S₁ states and TD-DFT predicted emission wavelengths of **8**.

	HOMO (eV)	LUMO (eV)	ΔE_{H-L} (eV)	$\lambda_{em,cal}$ (nm) ^a	$\lambda_{em,exp}$ (nm)
8a	-6.144	-2.948	3.196	485 (0.6025)	493
8b	-6.124	-2.86	3.264	477 (0.6002)	490
8c	-6.023	-2.721	3.302	468 (0.7179)	469
8d	-6.042	-2.68	3.362	461 (0.6329)	470
8e	-5.98	-2.569	3.411	452 (0.5917)	457
8f	-5.592	-2.305	3.287	461 (0.9252)	441

^a The calculated oscillator strength (f) given in parentheses.

Table H.7 Cartesian coordinates for compound **8a** (S₀)

	X	Y	Z
C	-3.35271900	-1.20420200	2.53300500
C	-2.00606500	-1.14125900	2.35750400
C	-4.22602400	-1.08607300	1.41893800
C	-3.69077000	-0.89475000	0.11278200
C	-2.26894600	-0.84593400	-0.04256000
C	-1.43143400	-0.96170300	1.06865300
N	-1.71933000	-0.70538700	-1.29922200
P	-0.11889700	-0.43998600	-1.72505300
C	0.72457600	-0.77490500	-0.19769700
C	-0.00503900	-0.95929700	0.93481100
O	0.28286000	-1.14480500	-2.96141600
C	2.19697100	-0.80638500	-0.18933100
C	2.90576700	-0.30244100	0.90712000
C	4.29465400	-0.35462200	0.94599400
C	5.01025000	-0.90607100	-0.13436900
C	4.30590600	-1.38831500	-1.23642400
C	2.92235600	-1.33665000	-1.26534100
C	-5.62753400	-1.14792400	1.58124800
C	-6.47254400	-1.02166000	0.50731500
C	-5.94612600	-0.81825400	-0.78126800
C	-4.58803400	-0.75466000	-0.97185700
O	0.03899600	1.15615200	-2.00919200
C	-0.27586800	2.13487200	-1.07858700
C	-1.58530700	2.58133300	-0.95811100
C	-1.87333300	3.60036900	-0.05744800
C	-0.86157200	4.16953800	0.70809200
C	0.44713200	3.71957800	0.56861400
C	0.74589600	2.69858200	-0.32581700
C	6.43288500	-0.96755300	-0.11363100
N	7.58579900	-1.02406300	-0.10777500
H	-3.77670500	-1.34565800	3.52182700
H	-1.33787800	-1.23336800	3.20848900
H	-2.34428500	-0.80180400	-2.08693400
H	0.54400900	-1.16380900	1.85277400
H	2.37779700	0.15847600	1.73386400
H	4.85006700	-1.81113200	-2.07275300
H	2.39189700	-1.72135800	-2.12874700
H	-6.02784800	-1.29689400	2.57972800
H	-7.54716800	-1.07167100	0.64978200
H	-6.61475800	-0.70588500	-1.62817700
H	-4.22565600	-0.57795000	-1.97980500
H	-2.36366000	2.14011600	-1.57070400
H	-2.89513200	3.95265200	0.04006500
H	-1.09117700	4.96744100	1.40660700
H	1.24364100	4.16664600	1.15473700

H	1.76299800	2.34545800	-0.45811700
C	4.98087700	0.17131800	2.08058100
N	5.52306600	0.59947600	3.00481400

Table H.8 Cartesian coordinates for compound **8a** (S_1)

	X	Y	Z
C	-3.39447600	-2.12734200	1.75355100
C	-2.02528300	-2.03930100	1.59915400
C	-4.27675300	-1.51497200	0.83190700
C	-3.73039200	-0.79758600	-0.27517300
C	-2.31187500	-0.74729100	-0.42997500
C	-1.43492500	-1.35307100	0.52811900
N	-1.75001000	-0.15357300	-1.51464900
P	-0.12124800	0.26906500	-1.77801700
C	0.75173900	-0.66481500	-0.54281800
C	-0.01344400	-1.32565400	0.41045600
O	0.20981400	0.15284300	-3.21226200
C	2.19062500	-0.60187600	-0.52644900
C	2.91774600	-0.99630100	0.62227200
C	4.29830700	-0.94713600	0.66366100
C	5.04517300	-0.49710900	-0.45929100
C	4.32601600	-0.09651400	-1.60345100
C	2.95469800	-0.14534700	-1.64003100
C	-5.66833100	-1.59125500	0.99522700
C	-6.52744800	-0.97478600	0.09997700
C	-5.99720500	-0.25894400	-0.97570300
C	-4.62653900	-0.16853900	-1.16052300
O	-0.02208100	1.83396500	-1.35360300
C	-0.26250000	2.31781200	-0.07481200
C	-1.54839700	2.70981100	0.27179300
C	-1.77463400	3.24417400	1.53535100
C	-0.72427600	3.38403800	2.43550200
C	0.55979100	2.99253700	2.06913100
C	0.79810700	2.45550600	0.81004000
C	6.45416900	-0.44525000	-0.43628400
N	7.61298300	-0.39646400	-0.42898000
H	-3.80704800	-2.67336800	2.59554300
H	-1.37681100	-2.52309600	2.32220300
H	-2.36032300	0.12362600	-2.27251800
H	0.50901900	-1.90364800	1.16590000
H	2.39902300	-1.31616100	1.51747200
H	4.87369400	0.24689100	-2.47399100
H	2.45137700	0.14512500	-2.55516000
H	-6.06478900	-2.14278700	1.84209900
H	-7.60086100	-1.04170800	0.23633500
H	-6.66013400	0.23804400	-1.67568500
H	-4.26880200	0.41942600	-1.99977100
H	-2.35364100	2.60705000	-0.44772700

H	-2.77643000	3.55649000	1.81190700
H	-0.90412400	3.80414100	3.41959300
H	1.38476600	3.10765800	2.76456100
H	1.79360800	2.15239500	0.50501000
C	4.95960000	-1.34377300	1.86206800
N	5.48579500	-1.66890600	2.83780300

Table H.9 Cartesian coordinates for compound **8b** (S₀)

	X	Y	Z
C	4.73875000	-1.43517200	-2.28175300
C	3.38197200	-1.38595600	-2.20740100
C	5.52825800	-1.16648200	-1.13207700
C	4.89818700	-0.84098300	0.10352900
C	3.46806700	-0.81021400	0.15356700
C	2.71431400	-1.07249600	-0.99159800
N	2.82636300	-0.53873000	1.34344500
P	1.19429900	-0.26707600	1.62376900
C	0.46802500	-0.78507500	0.08743500
C	1.28127800	-1.08275700	-0.96023500
O	0.72306200	-0.83867900	2.90352000
C	-1.00025200	-0.83686400	-0.02966900
C	-1.62391200	-0.44697000	-1.22465400
C	-2.99823200	-0.51720400	-1.36605500
C	-3.75856500	-0.97670300	-0.29450200
C	-3.17249900	-1.35437600	0.90940100
C	-1.79530200	-1.28061700	1.03743300
C	6.93874800	-1.20886600	-1.19054100
C	7.70360500	-0.93801400	-0.08387800
C	7.08360100	-0.60394000	1.13390600
C	5.71441900	-0.55539600	1.22335200
O	0.99085600	1.34769100	1.71720600
C	1.31463000	2.22192600	0.69138100
C	2.61937600	2.67679300	0.55161500
C	2.91370800	3.59419300	-0.45074100
C	1.91267800	4.05532500	-1.29860400
C	0.60843900	3.59844800	-1.14026800
C	0.30371900	2.67802300	-0.14450700
H	5.23436700	-1.68014500	-3.21556100
H	2.77696700	-1.59276600	-3.08513700
H	3.39266400	-0.53046800	2.17965800
H	0.80212900	-1.39806300	-1.88588600
H	-1.02764600	-0.06191800	-2.04459000
H	-3.78334000	-1.72121100	1.72629800
H	-1.32611200	-1.58310200	1.96642000
H	7.41089600	-1.46035000	-2.13569300
H	8.78636300	-0.97521000	-0.14619100
H	7.68849900	-0.37899400	2.00599700
H	5.27910500	-0.27678600	2.17798600
H	3.38946500	2.32001400	1.22640100

H	3.93202400	3.95204200	-0.56362900
H	2.14713300	4.77447100	-2.07657400
H	-0.17993300	3.96130500	-1.79202800
H	-0.70952700	2.31856400	-0.00040700
H	-3.47689300	-0.22392500	-2.29326100
S	-5.51126100	-1.06128500	-0.46401300
O	-5.86831300	-1.08042600	-1.87223300
O	-6.05471700	-2.02290700	0.47894400
C	-6.06094100	0.61549800	0.16137000
F	-7.37311100	0.70025800	0.03456800
F	-5.72797100	0.75218700	1.43431100
F	-5.48497600	1.57157500	-0.55096500

Table H.10 Cartesian coordinates for compound **8b** (S₁)

	X	Y	Z
C	4.73844200	-1.02285500	-2.42829800
C	3.36401800	-1.07703900	-2.32342900
C	5.55623200	-0.85437600	-1.28427200
C	4.93497000	-0.73861300	-0.00284400
C	3.51337700	-0.81943100	0.08209700
C	2.70057100	-0.97416000	-1.09064600
N	2.88168400	-0.79074000	1.28519200
P	1.22420400	-0.57674800	1.61253900
C	0.44510400	-0.94839600	0.06136900
C	1.28084400	-1.06846400	-1.04902200
O	0.86234700	-1.27827200	2.86095900
C	-0.99090700	-0.97457500	-0.00597500
C	-1.66767200	-0.93470200	-1.25989600
C	-3.03818400	-0.95575900	-1.34042300
C	-3.80309900	-1.03354400	-0.16594400
C	-3.17273700	-1.06855900	1.09006400
C	-1.80064600	-1.04532000	1.16207100
C	6.95313700	-0.79117600	-1.39063100
C	7.74877000	-0.61487100	-0.26928100
C	7.14582500	-0.48997200	0.98447200
C	5.76768700	-0.54772800	1.11788800
O	1.05366300	1.02316900	1.86056100
C	1.27965200	1.99634700	0.89921400
C	2.54384500	2.55972700	0.78638300
C	2.75235800	3.57396400	-0.14166600
C	1.70608900	4.01656200	-0.94313500
C	0.44366600	3.44538400	-0.81305000
C	0.22315600	2.43053900	0.10969400
H	5.20777300	-1.11149700	-3.40266800
H	2.76684200	-1.21221700	-3.21937200
H	3.44798900	-0.84182200	2.12163100
H	0.81803400	-1.26903500	-2.00923700
H	-1.10625700	-0.85762400	-2.18307000

H	-3.76669200	-1.14335600	1.99392100
H	-1.33318700	-1.11599600	2.13776300
H	7.40623300	-0.88194900	-2.37314600
H	8.82777500	-0.56966100	-0.36457400
H	7.75756600	-0.34227200	1.86803400
H	5.35329200	-0.42599000	2.11353400
H	3.34567000	2.21275300	1.42934500
H	3.73698600	4.02111300	-0.23238700
H	1.87184300	4.81037600	-1.66409600
H	-0.37844700	3.79278700	-1.43034400
H	-0.75552600	1.97868000	0.22866200
H	-3.53153900	-0.92296700	-2.30552600
S	-5.53234600	-1.01773500	-0.26719100
O	-5.96871900	-1.41425300	-1.59939100
O	-6.12238900	-1.59609300	0.93211900
C	-5.97291700	0.79790800	-0.16381300
F	-7.28769900	0.93689900	-0.24853400
F	-5.55528300	1.30239700	0.98932300
F	-5.40083500	1.46149300	-1.16050000

Table H.11 Cartesian coordinates for compound **8c** (S_0)

	X	Y	Z
C	3.22839300	-1.50801600	-2.28489100
C	1.87212300	-1.43161200	-2.21931200
C	4.01564400	-1.24997300	-1.13149200
C	3.38348800	-0.90794400	0.09862200
C	1.95411300	-0.85146700	0.13955400
C	1.20256600	-1.10164900	-1.00917800
N	1.30932400	-0.56705300	1.32512600
P	-0.31854500	-0.26317700	1.59329700
C	-1.04683900	-0.75996300	0.05073500
C	-0.23139700	-1.08069800	-0.98809400
O	-0.81281300	-0.82908300	2.86726800
C	-2.51545000	-0.76693000	-0.07818800
C	-3.12096600	-0.38675600	-1.28509900
C	-4.49518200	-0.41644300	-1.43429500
C	-5.30257300	-0.81644700	-0.36410400
C	-4.71442200	-1.17920900	0.85094000
C	-3.33758300	-1.15164300	0.99047900
C	5.42560300	-1.31836000	-1.18042500
C	6.18816600	-1.05634600	-0.07010000
C	5.56629300	-0.70529500	1.14204800
C	4.19766200	-0.63184700	1.22228700
O	-0.48469800	1.35611800	1.69366700
C	-0.06631200	2.23123500	0.70419500
C	1.24445400	2.69069100	0.70081000
C	1.63880500	3.61019600	-0.26413000
C	0.72976400	4.06810200	-1.21178300

C	-0.58189100	3.60574900	-1.19102500
C	-0.98621700	2.68360100	-0.23280400
C	-6.72022900	-0.84429600	-0.51153200
N	-7.86860300	-0.86715600	-0.63361700
H	3.72490000	-1.76603000	-3.21475000
H	1.26888100	-1.62891300	-3.10050600
H	1.86963600	-0.57065000	2.16525700
H	-0.70988700	-1.38585300	-1.91744200
H	-2.50876400	-0.03941300	-2.11055200
H	-4.94896400	-0.11741800	-2.37255800
H	-5.33807600	-1.48671100	1.68281800
H	-2.88932500	-1.44147500	1.93381800
H	5.89919500	-1.58243100	-2.12145400
H	7.27048200	-1.11329100	-0.12516100
H	6.16951300	-0.48675500	2.01697700
H	3.76093900	-0.34071200	2.17251400
H	1.94009300	2.33562800	1.45322000
H	2.66201600	3.97183200	-0.27012500
H	1.04124400	4.78851600	-1.96107300
H	-1.29895100	3.96575700	-1.92198100
H	-2.00778100	2.32065400	-0.19580800

Table H.12 Cartesian coordinates for compound **8c** (S_1)

	X	Y	Z
C	3.33514800	-1.34259400	-2.26457200
C	1.96243200	-1.34810100	-2.20948500
C	4.11917700	-1.06775800	-1.11245100
C	3.45601000	-0.79605500	0.12390200
C	2.03374400	-0.83738200	0.16446100
C	1.25496000	-1.09225200	-1.01787800
N	1.36298400	-0.67871900	1.33844800
P	-0.29629300	-0.40177400	1.58589900
C	-1.03348600	-0.87292700	0.04278800
C	-0.16058400	-1.13381000	-1.02219700
O	-0.72198400	-0.99490700	2.87094000
C	-2.46289900	-0.84506900	-0.07987300
C	-3.10060000	-0.95791400	-1.34909300
C	-4.46806600	-0.92614100	-1.47563600
C	-5.29202100	-0.77946200	-0.34351700
C	-4.68470900	-0.66514500	0.92333900
C	-3.31676300	-0.69929200	1.04927800
C	5.51799200	-1.05039100	-1.17064700
C	6.27926300	-0.76831300	-0.04549000
C	5.63679000	-0.48720000	1.16289100
C	4.25508900	-0.49706100	1.24910900
O	-0.43499600	1.21680700	1.70987700
C	-0.15417400	2.11091600	0.68875500
C	1.13068300	2.62345400	0.56627700
C	1.39369400	3.56219900	-0.42520500

C	0.38059700	3.98129400	-1.28014700
C	-0.90293300	3.46200600	-1.14054500
C	-1.17756000	2.52227100	-0.15478000
C	-6.69980900	-0.74478700	-0.47827100
N	-7.85329100	-0.71482200	-0.59039400
H	3.83852200	-1.54950900	-3.20360300
H	1.39193700	-1.56406100	-3.10717300
H	1.89879700	-0.68444900	2.19610700
H	-0.59848600	-1.40390300	-1.97686400
H	-2.51012000	-1.04835600	-2.25277700
H	-4.91994600	-1.00686500	-2.45879700
H	-5.30397800	-0.55875200	1.80747000
H	-2.88940000	-0.64070000	2.04409700
H	6.00368400	-1.26144300	-2.11879000
H	7.36189800	-0.76011800	-0.10467300
H	6.22154900	-0.25299200	2.04623400
H	3.80700400	-0.24777800	2.20595900
H	1.90736200	2.29521200	1.24868400
H	2.39511300	3.96854800	-0.52405100
H	0.58894400	4.71626600	-2.05075800
H	-1.69920200	3.79098100	-1.80040200
H	-2.17316000	2.11123300	-0.02813700

Table H.13 Cartesian coordinates for compound **8d** (S_0)

	X	Y	Z
C	3.96658600	-1.62228000	-2.28954600
C	2.61589300	-1.49139300	-2.19730000
C	4.78780800	-1.37535800	-1.15774900
C	4.19583200	-0.98672300	0.07848900
C	2.77082100	-0.87660800	0.14881700
C	1.98567900	-1.11621400	-0.97938800
N	2.16315600	-0.54964500	1.34365200
P	0.55589300	-0.17100600	1.63707100
C	-0.22434900	-0.67273000	0.12268600
C	0.55367200	-1.04105500	-0.92816500
O	0.06314400	-0.68190900	2.93448100
C	-1.69610300	-0.62978100	0.02847100
C	-2.31365600	-0.21371200	-1.15967200
C	-3.69401300	-0.19730300	-1.27697400
C	-4.46842100	-0.59100700	-0.19189300
C	-3.88386700	-0.99695100	1.00158700
C	-2.50181700	-1.01157200	1.11042500
C	6.19280100	-1.49973300	-1.23451700
C	6.98857100	-1.24625500	-0.14575000
C	6.40698700	-0.84655100	1.07137900
C	5.04422900	-0.71877100	1.17863800
O	0.46024400	1.45722300	1.69813000
C	0.91630100	2.28566500	0.68577000
C	2.24681000	2.68416100	0.66989800

C	2.68261600	3.55665600	-0.32038400
C	1.79498500	4.02875600	-1.28129000
C	0.46349100	3.62804200	-1.24829400
C	0.01770000	2.75316200	-0.26443600
H	4.43258700	-1.91538000	-3.22477200
H	1.98678800	-1.67957900	-3.06221500
H	2.74033300	-0.56487100	2.17220200
H	0.04252500	-1.34438700	-1.84067400
H	-1.70705900	0.11885100	-1.99548900
H	-4.50381500	-1.32062800	1.83043400
H	-2.03891300	-1.33692000	2.03490500
H	6.63552900	-1.80026600	-2.17963700
H	8.06645200	-1.34661600	-0.22195500
H	7.03708900	-0.63298600	1.92842700
H	4.63952900	-0.38917000	2.13049200
H	2.92574600	2.31728300	1.43179900
H	3.72150800	3.87004000	-0.33630400
H	2.13891500	4.71194800	-2.05096800
H	-0.23621600	3.99911000	-1.99047800
H	-1.01902700	2.43708400	-0.21872100
H	-4.16844000	0.11128900	-2.20190900
S	-6.24336400	-0.55716900	-0.33035900
O	-6.58686700	-0.61833800	-1.74964100
O	-6.79035100	-1.55176400	0.58960200
C	-6.69337200	1.05737900	0.27475200
H	-6.37399500	1.15321000	1.31148500
H	-6.22679700	1.81685100	-0.35099200
H	-7.77987100	1.12182200	0.20457700

Table H.14 Cartesian coordinates for compound **8d** (S_1)

	X	Y	Z
C	4.07929300	-1.39921200	-2.30775000
C	2.70727300	-1.37003800	-2.21310600
C	4.90283500	-1.14432900	-1.17971300
C	4.28109000	-0.85592900	0.07474400
C	2.86031400	-0.85963100	0.15554600
C	2.04059100	-1.09501500	-1.00392900
N	2.22702600	-0.68363100	1.34765700
P	0.58374000	-0.35339700	1.63765300
C	-0.20967700	-0.81846200	0.12381300
C	0.62458800	-1.10059100	-0.96690900
O	0.17718800	-0.91542000	2.94284300
C	-1.64340600	-0.75679900	0.04033600
C	-2.31346900	-0.83946200	-1.21332700
C	-3.68582600	-0.77385600	-1.30330900
C	-4.45541100	-0.62786700	-0.14561700
C	-3.83378200	-0.54771400	1.10643400
C	-2.46116900	-0.61517400	1.19552500

C	6.29934100	-1.16340600	-1.27716500
C	7.09951900	-0.90249600	-0.17335400
C	6.49806500	-0.60712800	1.05217200
C	5.11875500	-0.58068400	1.17700100
O	0.50417300	1.27234800	1.74835600
C	0.79511300	2.14744800	0.71493900
C	2.08531000	2.64647000	0.59003500
C	2.36157800	3.56693500	-0.41490000
C	1.35664100	3.98148000	-1.28161100
C	0.06768400	3.47641100	-1.13979100
C	-0.22029500	2.55552000	-0.14023200
H	4.54900600	-1.61993400	-3.26102800
H	2.10719400	-1.57338300	-3.09431100
H	2.78594900	-0.70073700	2.19020600
H	0.15240900	-1.36476700	-1.90676300
H	-1.74839800	-0.93719900	-2.13227200
H	-4.43478500	-0.46327300	2.00544100
H	-2.00458900	-0.59261600	2.17881400
H	6.75253900	-1.38622800	-2.23855100
H	8.17987800	-0.92258000	-0.26270300
H	7.11271300	-0.39041600	1.91959300
H	4.70434400	-0.32303200	2.14672400
H	2.85611000	2.32210600	1.28116000
H	3.36721600	3.96224900	-0.51559100
H	1.57561300	4.70147700	-2.06332900
H	-0.72197900	3.80185900	-1.80936100
H	-1.22011100	2.15536000	-0.01213700
H	-4.17446400	-0.84659600	-2.26915700
S	-6.20778700	-0.50332800	-0.27156500
O	-6.62821900	-1.13303300	-1.52489200
O	-6.79911100	-0.94812900	0.99138100
C	-6.53289400	1.24566500	-0.42239900
H	-6.16093100	1.75662400	0.46467500
H	-6.04775600	1.62258700	-1.32177100
H	-7.61525400	1.35916700	-0.49908300

Table H.15 Cartesian coordinates for compound **8e** (S_0)

	X	Y	Z
C	3.75052200	-1.60949100	-2.29428600
C	2.39947300	-1.48491300	-2.19599600
C	4.57549900	-1.35611000	-1.16680700
C	3.98694600	-0.96720100	0.07107400
C	2.56169200	-0.86199200	0.14698000
C	1.77282100	-1.10909200	-0.97666400
N	1.95759000	-0.53095900	1.34225000
P	0.34631700	-0.17499200	1.64759200
C	-0.43632300	-0.66757800	0.13119300
C	0.34053800	-1.03676200	-0.92003600
O	-0.12714900	-0.70992600	2.94290400

C	-1.90834000	-0.61878900	0.03654800
C	-2.52564500	-0.21707800	-1.15613800
C	-3.90524700	-0.19561400	-1.27153800
C	-4.69823500	-0.55947400	-0.18668400
C	-4.10257900	-0.94118500	1.01001400
C	-2.72049800	-0.96792100	1.12283500
C	5.98076000	-1.47463200	-1.24921400
C	6.78013400	-1.21603100	-0.16433500
C	6.20184500	-0.81728600	1.05469700
C	4.83900600	-0.69490400	1.16734900
O	0.23011000	1.45034900	1.73373800
C	0.60607300	2.29914500	0.70532500
C	1.93248700	2.69236600	0.58176300
C	2.28444100	3.58678000	-0.42257300
C	1.31865800	4.08652100	-1.28937500
C	-0.00738900	3.69086100	-1.14812600
C	-0.36970200	2.79346600	-0.15051600
H	4.21369900	-1.90245500	-3.23099700
H	1.76742300	-1.67805200	-3.05772600
H	2.53925900	-0.53615100	2.16778600
H	-0.17255900	-1.33914300	-1.83176900
H	-1.91905200	0.10851400	-1.99465500
H	-4.36506100	0.12562800	-2.19974600
H	-4.71639600	-1.21639500	1.86038600
H	-2.26436900	-1.27040100	2.05847100
H	6.42072500	-1.77498900	-2.19571000
H	7.85811300	-1.31196100	-0.24493000
H	6.83447600	-0.60043600	1.90906800
H	4.43705000	-0.36671200	2.12084000
H	2.67436500	2.30549600	1.27151800
H	3.31986800	3.89623700	-0.52249600
H	1.59775600	4.78753200	-2.06922600
H	-0.76806100	4.08335500	-1.81552200
H	-1.40005400	2.48007300	-0.02114300
C	-6.18732900	-0.57974600	-0.32989000
F	-6.62433800	-1.74833300	-0.83771700
F	-6.81444800	-0.41329200	0.84359400
F	-6.62748100	0.38252100	-1.15704700

Table H.16 Cartesian coordinates for compound **8e** (S₁)

	X	Y	Z
C	3.84892700	-1.43999300	-2.28621400
C	2.47822400	-1.40540800	-2.20172500
C	4.66799700	-1.16792000	-1.15648200
C	4.03778800	-0.85870100	0.08947500
C	2.61870400	-0.86700700	0.16356700
C	1.80258100	-1.10977400	-0.99998600
N	1.97945400	-0.69564400	1.35513800
P	0.33859800	-0.34656100	1.63333400

C	-0.44741900	-0.79836500	0.11551600
C	0.38981700	-1.10357200	-0.97043100
O	-0.08233100	-0.90319200	2.93730200
C	-1.87939200	-0.69964100	0.01292300
C	-2.53223800	-0.71345900	-1.24901300
C	-3.90474600	-0.62566400	-1.35178400
C	-4.69824100	-0.51260300	-0.20871000
C	-4.08197200	-0.48948600	1.04745600
C	-2.71147200	-0.58152700	1.15792700
C	6.06373600	-1.18964700	-1.24429000
C	6.85835000	-0.90981400	-0.13937200
C	6.24943300	-0.58992500	1.07615100
C	4.86954400	-0.56039600	1.19215900
O	0.27638800	1.28166400	1.74785800
C	0.55752200	2.15209400	0.70856800
C	1.85743900	2.61006300	0.53510600
C	2.12480400	3.52494500	-0.47734400
C	1.10128300	3.97577900	-1.30315700
C	-0.19714600	3.51247200	-1.11260100
C	-0.47601200	2.59658300	-0.10594200
H	4.32477500	-1.67632600	-3.23283900
H	1.88288700	-1.61912000	-3.08386800
H	2.53141000	-0.73643300	2.20144600
H	-0.08386300	-1.37753400	-1.90720800
H	-1.95315200	-0.76088400	-2.16344700
H	-4.36807300	-0.62773600	-2.33269900
H	-4.68432600	-0.40185700	1.94568900
H	-2.26837200	-0.59043000	2.14767000
H	6.52313200	-1.42926300	-2.19881000
H	7.93925000	-0.93239400	-0.22188100
H	6.85901600	-0.35442800	1.94241900
H	4.44698000	-0.27590400	2.15090700
H	2.64361700	2.25751900	1.19420800
H	3.13832000	3.88742500	-0.61587500
H	1.31326100	4.69162300	-2.09065400
H	-1.00149600	3.86642000	-1.74943300
H	-1.48264500	2.22853600	0.05931100
C	-6.18173000	-0.47704400	-0.31424500
F	-6.74052100	-1.69688300	-0.14852000
F	-6.74149800	0.31466100	0.61898000
F	-6.60054000	-0.03344600	-1.51240400

Table H.17 Cartesian coordinates for compound **8f** (S_0)

	X	Y	Z
C	3.28337400	-1.48620000	-2.34080100
C	1.92832000	-1.42638200	-2.22726100
C	4.10662100	-1.22178300	-1.21539400
C	3.51142800	-0.88939300	0.03599700
C	2.08404600	-0.84966700	0.12528100

C	1.29585800	-1.10720400	-0.99556300
N	1.47473900	-0.57186000	1.33286100
P	-0.14654200	-0.27803800	1.64979600
C	-0.92500200	-0.78517600	0.13633300
C	-0.13996700	-1.10323600	-0.92501000
O	-0.58870100	-0.83728700	2.94650200
C	-2.39779300	-0.78109800	0.05973500
C	-3.04840000	-0.37688500	-1.10923400
C	-4.43313100	-0.39593400	-1.21977800
C	-5.20771600	-0.81677100	-0.13791700
C	-4.57247200	-1.20612000	1.04469100
C	-3.19468500	-1.18580500	1.14311600
C	5.51529400	-1.27454100	-1.31125500
C	6.31203900	-1.00686200	-0.22679900
C	5.72660700	-0.66569100	1.00646900
C	4.36068800	-0.60765300	1.13239500
O	-0.31874400	1.34398900	1.75327200
C	0.05390900	2.21696800	0.74610400
C	1.35536100	2.70081100	0.70105700
C	1.70486500	3.62095000	-0.28050300
C	0.76085700	4.05547000	-1.20471700
C	-0.54042600	3.56778800	-1.14378400
C	-0.89989600	2.64506300	-0.16843000
H	3.74994100	-1.73623900	-3.28837900
H	1.29798300	-1.62952900	-3.08812500
H	2.06304300	-0.56034800	2.15325800
H	-0.64771400	-1.41186500	-1.83782400
H	-2.46543400	-0.01357300	-1.95016800
H	-4.89275100	-0.06723400	-2.14429600
H	-5.18491500	-1.52778800	1.88057800
H	-2.72205800	-1.49831800	2.06771900
H	5.95984000	-1.53195100	-2.26831400
H	7.39254300	-1.05211500	-0.31800900
H	6.35615700	-0.44312000	1.86176200
H	3.95253200	-0.32525100	2.09788200
H	2.07891100	2.36256700	1.43470800
H	2.72080500	4.00093800	-0.31844600
H	1.03739400	4.77629200	-1.96730600
H	-1.28430400	3.90779900	-1.85745600
H	-1.91131000	2.25874600	-0.10202900
O	-6.55678200	-0.87206200	-0.13558600
C	-7.24012800	-0.49104600	-1.31218900
H	-7.04690600	0.55656400	-1.56517800
H	-6.96364300	-1.12804500	-2.15869700
H	-8.29926000	-0.61869400	-1.09740400

Table H.18 Cartesian coordinates for compound **8f** (S_1)

	X	Y	Z
C	3.35589900	-1.75743400	-2.12240200

C	2.00324700	-1.78527700	-2.00823000
C	4.17978800	-1.23398500	-1.07463100
C	3.55341300	-0.74128900	0.11500200
C	2.14714300	-0.82146600	0.23543600
C	1.32697600	-1.31131400	-0.84286200
N	1.53299200	-0.49011300	1.42111700
P	-0.10696100	-0.21810600	1.70507600
C	-0.89472400	-0.89305000	0.27886600
C	-0.06603200	-1.35840400	-0.77455400
O	-0.48381900	-0.63019200	3.07786600
C	-2.32251300	-0.82192200	0.16662200
C	-2.98782800	-1.01810400	-1.07454800
C	-4.36220200	-0.95568000	-1.19045200
C	-5.15045100	-0.68290800	-0.06457600
C	-4.52036900	-0.47670800	1.17686900
C	-3.15588900	-0.54825200	1.29058100
C	5.57030900	-1.19156100	-1.19013700
C	6.36508800	-0.67431400	-0.17378600
C	5.76010000	-0.17255200	0.98372500
C	4.38801400	-0.19901400	1.12912300
O	-0.30251000	1.40837500	1.63725700
C	-0.05533800	2.17215100	0.51225400
C	1.22527100	2.65813100	0.27882500
C	1.45376700	3.47070500	-0.82570600
C	0.41038400	3.79641800	-1.68530000
C	-0.86861100	3.30884000	-1.43568000
C	-1.10764700	2.49329700	-0.33641200
H	3.83604200	-2.13005200	-3.02247400
H	1.39699200	-2.17875400	-2.81905600
H	2.10565100	-0.46700900	2.25390300
H	-0.55643600	-1.81983700	-1.62614500
H	-2.41198500	-1.19445900	-1.97525200
H	-4.81562600	-1.11095700	-2.16246100
H	-5.14150400	-0.27485300	2.04322100
H	-2.70610700	-0.41951800	2.26936100
H	6.02984400	-1.57209300	-2.09827400
H	7.44434200	-0.65083500	-0.28157300
H	6.37158300	0.25212000	1.77387600
H	3.95815400	0.23661300	2.02587100
H	2.02749800	2.40180700	0.96234300
H	2.45321600	3.85095400	-1.01131500
H	0.59207900	4.43292900	-2.54528500
H	-1.68862300	3.56476400	-2.09927300
H	-2.09894200	2.10774700	-0.12399900
O	-6.48860700	-0.59929300	-0.06657500
C	-7.18044300	-0.79497400	-1.28655000
H	-6.88962200	-0.04598800	-2.02935200
H	-7.00170800	-1.79829100	-1.68475700
H	-8.23599400	-0.68104400	-1.05054600

Table H.19 Cartesian coordinates for compound **7a**

	X	Y	Z
C	3.76708	-2.08152	-0.32091
C	2.38146	-2.27970	-0.44485
C	4.22851	-0.92525	0.37739
C	3.28718	-0.01785	0.90539
C	1.93519	-0.22670	0.75903
C	1.45915	-1.38660	0.07198
N	1.00850	0.64170	1.32283
P	-0.60656	0.76571	0.91944
C	-0.98370	-0.86503	0.29728
C	0.04869	-1.66772	-0.05219
O	-1.40118	1.36471	2.01670
C	-2.39045	-1.25766	0.10315
C	-2.76358	-2.02205	-1.01119
C	-4.07240	-2.43063	-1.18899
C	-5.04634	-2.07011	-0.25193
C	-4.69219	-1.29262	0.85450
C	-3.37959	-0.88841	1.02540
C	4.71205	-2.99201	-0.85736
C	6.05536	-2.76960	-0.71177
C	6.51284	-1.62425	-0.02092
C	5.62459	-0.72537	0.51045
O	-0.70506	1.60141	-0.47797
C	-0.44234	2.96145	-0.55929
C	0.64750	3.36593	-1.31860
C	0.90540	4.72378	-1.46661
C	0.08310	5.66448	-0.85534
C	-1.00345	5.24233	-0.09644
C	-1.27608	3.88742	0.05502
C	-6.39808	-2.48644	-0.43090
N	-7.49269	-2.82553	-0.57569
H	2.02133	-3.16555	-0.96156
H	3.64149	0.86279	1.43459
H	1.36509	1.34812	1.95108
H	-0.19162	-2.65080	-0.45386
H	-2.02405	-2.27787	-1.76223
H	-4.34829	-3.01725	-2.05808
H	-5.44661	-1.00922	1.57977
H	-3.11291	-0.28667	1.88638
H	4.35190	-3.86990	-1.38633
H	6.77353	-3.47049	-1.12479
H	7.57998	-1.45807	0.08918
H	5.98246	0.15241	1.04080
H	1.27362	2.61602	-1.79030
H	1.75342	5.04506	-2.06308
H	0.28657	6.72392	-0.97273

H	-1.65045	5.97152	0.38086
H	-2.11705	3.54289	0.64500

Table H.20 Cartesian coordinates for compound **7b**

	X	Y	Z
C	4.00277	-2.51575	-0.32109
C	2.60051	-2.50152	-0.41789
C	4.64924	-1.43132	0.34491
C	3.86766	-0.38169	0.86954
C	2.49695	-0.38484	0.75167
C	1.83549	-1.46951	0.09610
N	1.72651	0.62452	1.31544
P	0.14035	0.98634	0.94161
C	-0.49386	-0.57584	0.35470
C	0.39545	-1.53278	0.00219
O	-0.52803	1.71594	2.04406
C	-1.94942	-0.74774	0.19154
C	-2.46037	-1.44582	-0.90980
C	-3.82308	-1.64863	-1.05296
C	-4.70261	-1.14753	-0.09821
C	-4.21280	-0.43616	0.99201
C	-2.84884	-0.23441	1.13484
C	4.78731	-3.56960	-0.85342
C	6.15154	-3.55294	-0.73424
C	6.79211	-2.47877	-0.07546
C	6.06184	-1.44487	0.45078
O	0.14263	1.81223	-0.46606
C	0.62974	3.10750	-0.56554
C	1.76644	3.31554	-1.33541
C	2.24982	4.60870	-1.49742
C	1.60374	5.68008	-0.88966
C	0.46744	5.45428	-0.11975
C	-0.02930	4.16639	0.04630
H	2.09902	-3.33091	-0.90988
H	4.36110	0.44475	1.37405
H	2.20080	1.27642	1.92446
H	-0.00171	-2.47252	-0.37840
H	-1.78593	-1.81402	-1.67558
H	-4.20174	-2.19240	-1.91127
H	-4.89543	-0.04648	1.73908
H	-2.47404	0.31683	1.98942
H	4.28760	-4.39176	-1.35800
H	6.74586	-4.36317	-1.14405
H	7.87404	-2.47610	0.01383
H	6.55972	-0.62247	0.95647
H	2.25334	2.46638	-1.80319
H	3.13554	4.77663	-2.10196
H	1.98306	6.68871	-1.01775
H	-0.04254	6.28630	0.35549
H	-0.91088	3.97354	0.64594
C	-6.17834	-1.31857	-0.27662
F	-6.82390	-1.39472	0.89756
F	-6.47910	-2.42850	-0.96893

F -6.72501 -0.28757 -0.94839

Table H.21 Cartesian coordinates for compound **7c**

	X	Y	Z
C	3.81772	-1.79224	-0.30419
C	2.45737	-2.12615	-0.42859
C	4.16236	-0.58660	0.37747
C	3.13438	0.22982	0.89212
C	1.80998	-0.11451	0.74867
C	1.45014	-1.32258	0.07431
N	0.80201	0.66385	1.30351
P	-0.81985	0.62193	0.90548
C	-1.03638	-1.03688	0.28284
C	0.07152	-1.73847	-0.05108
O	-1.66064	1.14696	2.00708
C	-2.40194	-1.54937	0.06701
C	-2.69627	-2.34243	-1.04917
C	-3.96677	-2.86323	-1.23732
C	-4.99727	-2.60630	-0.33037
C	-4.70487	-1.80447	0.77291
C	-3.43608	-1.27821	0.97096
C	4.84923	-2.61285	-0.82514
C	6.16439	-2.25825	-0.68066
C	6.50603	-1.06350	-0.00707
C	5.53178	-0.24846	0.50877
O	-1.00480	1.45451	-0.48862
C	-0.87685	2.83293	-0.55497
C	0.16528	3.35138	-1.31262
C	0.29001	4.72944	-1.44525
C	-0.61676	5.57917	-0.82043
C	-1.65379	5.04437	-0.06306
C	-1.79306	3.66777	0.07314
H	2.18748	-3.04939	-0.93490
H	3.39782	1.14783	1.41086
H	1.08887	1.41041	1.92086
H	-0.07319	-2.74107	-0.45057
H	-1.92724	-2.53446	-1.79122
H	-4.16577	-3.47263	-2.11512
H	-5.48517	-1.58695	1.49749
H	-3.23925	-0.66144	1.84085
H	4.57860	-3.52934	-1.34204
H	6.94857	-2.89198	-1.08220
H	7.55147	-0.79176	0.10194
H	5.80012	0.66831	1.02614
H	0.85953	2.67133	-1.79482
H	1.10071	5.13807	-2.04026
H	-0.51728	6.65470	-0.92546
H	-2.36615	5.70165	0.42563
H	-2.59264	3.23602	0.66324
C	-6.37940	-3.14334	-0.55765
H	-6.95968	-2.47080	-1.19899

H	-6.35595	-4.11834	-1.05047
H	-6.92820	-3.25000	0.38074

Table H.22 Cartesian coordinates for compound **7d**

	X	Y	Z
C	3.74075	-2.24608	-0.31603
C	2.34191	-2.36980	-0.39278
C	4.28755	-1.09827	0.33198
C	3.41297	-0.12544	0.85843
C	2.04778	-0.26436	0.75998
C	1.48544	-1.41439	0.12380
N	1.18862	0.67028	1.32466
P	-0.42983	0.87188	0.96326
C	-0.92114	-0.75039	0.40282
C	0.05617	-1.61982	0.05481
O	-1.14768	1.55591	2.06462
C	-2.35434	-1.04978	0.24341
C	-2.80655	-1.81359	-0.83563
C	-4.14691	-2.14433	-0.98598
C	-5.07837	-1.70099	-0.04599
C	-4.64412	-0.92038	1.02931
C	-3.30870	-0.59674	1.16902
C	4.61775	-3.22241	-0.85133
C	5.97573	-3.07185	-0.75207
C	6.51749	-1.93496	-0.11061
C	5.69596	-0.97295	0.41796
O	-0.51958	1.67848	-0.45546
C	-0.18180	3.01659	-0.57963
C	0.90223	3.33846	-1.38606
C	1.23401	4.67446	-1.57870
C	0.49094	5.67716	-0.96459
C	-0.59022	5.33846	-0.15754
C	-0.93613	4.00626	0.03899
H	1.91831	-3.24918	-0.87117
H	3.82897	0.75041	1.34915
H	1.60526	1.37775	1.91366
H	-0.25137	-2.59875	-0.31007
H	-2.10257	-2.13879	-1.59532
H	-4.45181	-2.73081	-1.84434
H	-5.37833	-0.57778	1.75097
H	-2.99303	0.00758	2.01209
H	4.19418	-4.09410	-1.34251
H	6.64048	-3.82417	-1.16436
H	7.59510	-1.82555	-0.03665
H	6.11724	-0.10101	0.91027
H	1.46643	2.54120	-1.85833
H	2.07770	4.92997	-2.21211
H	0.75171	6.71956	-1.11666
H	-1.17570	6.11614	0.32281
H	-1.77314	3.72656	0.66753
O	-6.40189	-1.96224	-0.09479
C	-6.88669	-2.75287	-1.16104

H	-7.95950	-2.84285	-1.00229
H	-6.70424	-2.27474	-2.12890
H	-6.43581	-3.75061	-1.15556

3.2 Dimerization

The geometries for **8a-f** and their dimeric complexes were fully optimized without symmetry constraint by using the functional M06-2X²⁹ (accounting for the contributions of H-bond/ dispersion forces) and TZVP basis set³⁰ as implemented in Gaussian 09. The PCM solvation model was used to account for the effects of the chloroform environment. All of the optimized structures were confirmed by frequency calculations to be minima using the same level of theory. The solution-phase optimized geometries were used in all the energy calculations. Single point calculations were computed at a higher level using the minimally diffuse-augmented ma-def2-TZVP (ma-TZVP) basis set³¹ (obtained from <https://comp.chem.umn.edu/basissets/basis.cgi>). The interaction energy (ΔE_{int}) is defined as the gas-phase electronic energy difference between dimer and its isolated monomers (The enantiomers have exactly the same electronic energies), and the basis set superposition error (BSSE) were corrected by the counterpoise correction (CP) method,³² as implemented in Gaussian 09. All the reported dipole moments were obtained at the M06-2X/ma-def2-TZVP level in gas phase. The distribution of electrostatic potential, $V(r)$, on the molecular surfaces of **8** were computed at the M06-2X/TZVP level in gas phase. The $V(r)$ was evaluated on the 0.001 e/Bohr³ contour of $\rho(r)$ to generate the $V_S(r)$. The most negative and most positive $V_S(r)$ values (i.e., $V_{S,\text{min}}$ and $V_{S,\text{max}}$, respectively) for electrostatic potential surface energies were calculated. The QTAIM analyses³³ were based on the optimized geometries of dimers in CHCl₃. The estimated energies (E_{HB}) of hydrogen bonding interactions (for X-H...O type in neutral system, X = C, N, O) were calculated using the empirical formula [$E_{\text{HB}}=1/2V(r)$] reported by Espinosa *et al.*,³⁴ where $V(r)$ denotes the local potential electron energy density at the (3, -1) bond critical points (BCPs). Of

note, while it is clear that the estimated E_{HB} have important role in energetic aspect of the dimer complex, they are not the total interaction energy (Table H.23). The quantitative molecular surface analysis, NCI plot and QTAIM analysis were performed by using the Multiwfn program.³⁵

Energy decomposition calculations were undertaken on these optimized dimeric complexes using SAPT0.³⁶ Based on a rigorous perturbation expansion of the intermolecular interactions, SAPT0 energies can be decomposed into a sum of four physically meaningful contributions; i.e., electrostatic (E_{ele}), dispersion (E_{dis}), induction (E_{ind}), and exchange repulsion (E_{exc}). The first three components are attractive whereas the last is repulsive (Table H.25). All of the SAPT0 calculations have been performed using the Psi4 open-source quantum chemistry package,³⁷ employing the density fitting procedure. Considering the molecular system size, the jun-cc-pVDZ basis-set (truncated Dunning-style basis set) was adopted for all the calculations since it provides the best trade-off between computational cost and accuracy.³⁸

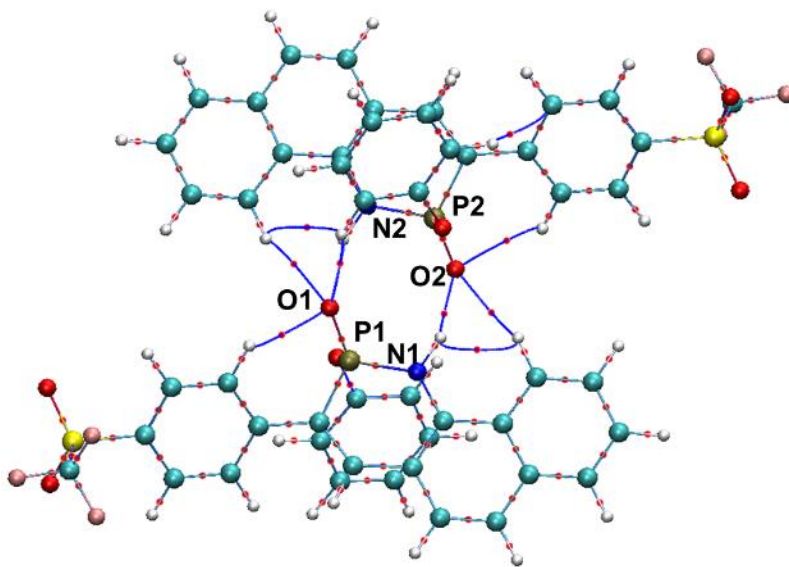


Figure H.16 The representative QTAIM analysis graphs for **8b•8b** complex showing the (3, -1) bond critical points (BCPs) (red dots) and bond paths (blue dotted lines).

Table H.23 Double hydrogen bond lengths d (in Å), topological analysis values (in a.u.) of the density of all electrons $\rho(r)$, Laplacian of electron density $\nabla^2\rho(r)$ and local potential electron energy density $V(r)$ at the (3, -1) bond critical points (BCPs) as well as the estimated energies E_{HB} (in kcal mol⁻¹) of these bonds among the optimized dimeric complexes, calculated at PCM(CHCl₃)-M06-2X/TZVP level of theory.

	d	$\rho(r)$	$\nabla^2\rho(r)$	$V(r)$	E_{HB}
8a	1.86; 1.86	0.0302; 0.0302	0.1157; 0.1156	-0.0281; -0.0280	-8.9; -8.8
8b	1.85; 1.86	0.0305; 0.0302	0.1144; 0.1170	-0.0285; -0.0279	-8.9; -8.8
8c	1.86; 1.86	0.0305; 0.0305	0.1156; 0.1156	-0.0283; -0.0283	-8.9; -8.9
8d	1.86; 1.85	0.0305; 0.0308	0.1145; 0.1159	-0.0285; -0.0286	-8.9; -9.1
8e	1.86; 1.85	0.0301; 0.0306	0.1137; 0.1171	-0.0277; -0.0286	-8.7; -9.0
8f	1.84; 1.86	0.0314; 0.0290	0.1187; 0.1133	-0.0299; -0.0271	-9.4; -8.5

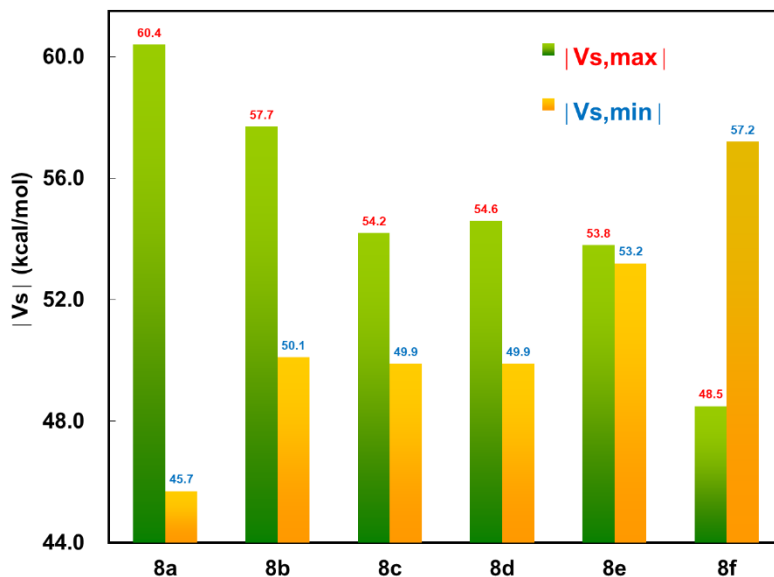


Figure H.17 The calculated electrostatic potential surface minima absolute value ($|V_{s,\text{min}}|$) and maxima absolute value ($|V_{s,\text{max}}|$) of **8**.

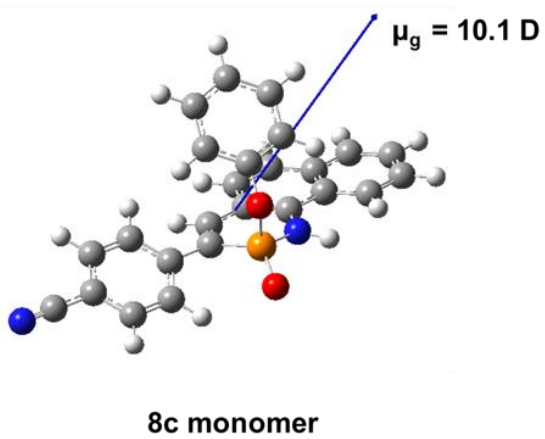
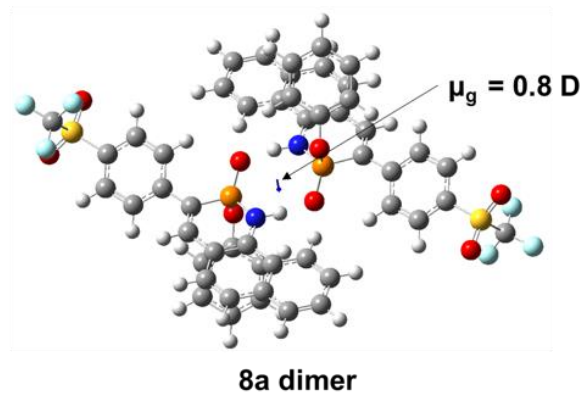
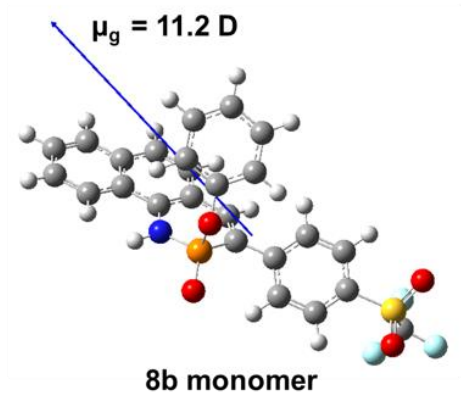
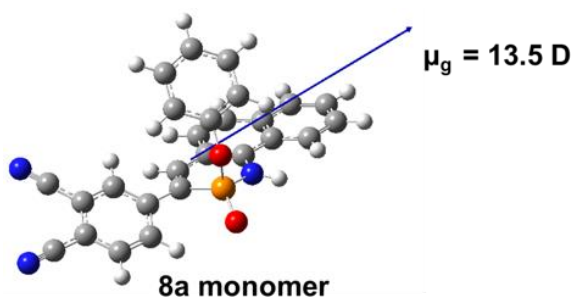
Table H.24 The interaction energies ΔE_{int}^a (in gas phase, all in a.u.), electronic energies for **8** and their dimeric complexes and BSSE energies (E_{BSSE}) for the intermolecular interactions calculated at M06-2X/ma-def2-TZVP//PCM(CHCl₃)-M06-2X/TZVP level of theory

	E_{monomer}	E_{dimer}	E_{BSSE}	ΔE_{int}
8a	-1656.496751	-3313.041598	0.001113037	-0.046982963
8b	-2357.697214	-4715.442129	0.001108823	-0.046592177
8c	-1564.253165	-3128.553662	0.001090228	-0.046241772
8d	-2059.937954	-4119.923383	0.00110601	-0.04636899
8e	-1809.097417	-3618.241641	0.001043752	-0.045763248
8f	-1586.530518	-3173.107187	0.00096453	-0.04518647

^a $\Delta E_{\text{int}} = E_{\text{dimer}} - 2 E_{\text{monomer}} + E_{\text{BSSE}}$.

Table H.25 E_{ele} , E_{exc} , E_{ind} and E_{dis} , in the SAPT0 approach correspond to electrostatic exchange, induction and dispersion energy terms and total SAPT0 energy (E_{SAPT}), respectively. All values are in kJ mol⁻¹

	E_{ele}	E_{exc}	E_{ind}	E_{dis}	E_{SAPT}
8a	-176.4	143.8	-64.0	-73.6	-170.2
8b	-166.4	138.5	-61.6	-66.7	-156.3
8c	-165.3	141.6	-63.1	-68.0	-154.8
8d	-164.5	137.4	-60.8	-66.9	-154.8
8e	-163.3	139.5	-62.4	-66.6	-152.8
8f	-162.7	144.8	-65.1	-69.3	-152.3



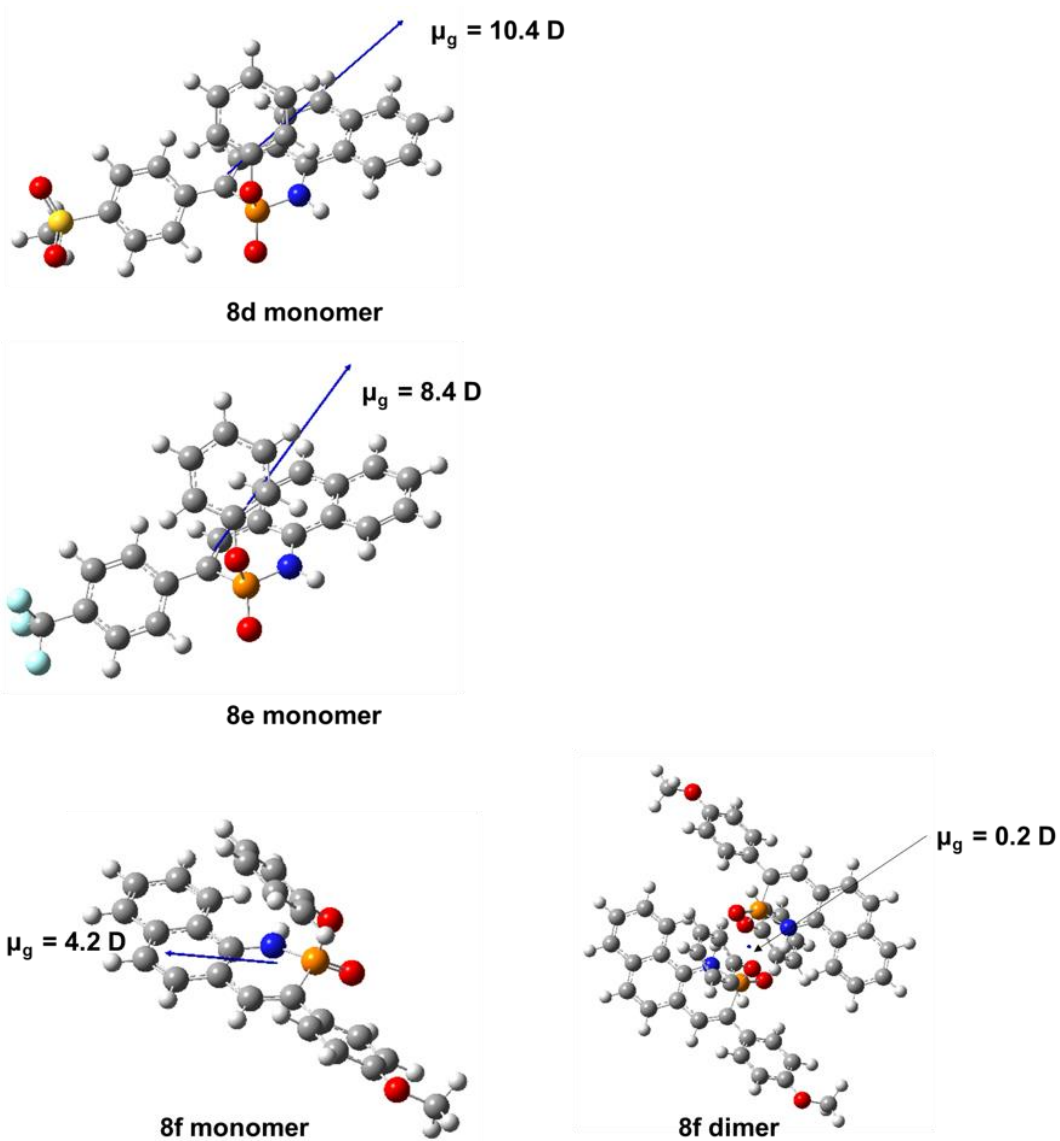


Figure H.18 The plots of molecular dipole moments (in Debye) for **8** and their respective dimer with the vectors originating from the center of mass.

Table H.26. Cartesian coordinates for compound **8a**

	X	Y	Z
P	-0.06729	-1.26801	-1.30942
O	0.04071	0.03486	-2.29522
O	0.37326	-2.45608	-2.08912
N	-1.66192	-1.35598	-0.79442
C	0.77801	-0.80799	0.19344
C	0.04930	-0.39275	1.25290
C	-1.38734	-0.32079	1.35347
C	-2.21483	-0.79972	0.34467
C	-3.64042	-0.74494	0.48793
C	-4.17980	-0.21533	1.68895
C	-3.31175	0.26289	2.70998
C	-1.96664	0.21059	2.54032
C	-4.53031	-1.17965	-0.52432
C	-5.88668	-1.11523	-0.34258
C	-6.42121	-0.60803	0.85802
C	-5.58423	-0.16573	1.84686
C	2.25553	-0.79859	0.20146
C	2.93731	0.23159	0.85557
C	4.32397	0.24367	0.89335
C	5.05671	-0.77144	0.25873
C	4.38040	-1.78528	-0.41033
C	2.99552	-1.79588	-0.44118
C	-0.37704	1.28734	-1.86104
C	0.56146	2.16183	-1.33363
C	0.15114	3.42275	-0.92032
C	-1.18285	3.79729	-1.03433
C	-2.10896	2.91121	-1.57179
C	-1.70950	1.64847	-1.99181
H	-2.27877	-1.85343	-1.42505
H	0.58851	-0.09133	2.14827
H	-3.74394	0.66599	3.61748
H	-1.29831	0.57316	3.31264
H	-4.15874	-1.56039	-1.46767
H	-6.55160	-1.45112	-1.12824
H	-7.49485	-0.56442	0.99241
H	-5.98462	0.23525	2.77088
H	2.39128	1.04045	1.32403
H	2.48153	-2.59432	-0.96068
H	1.59617	1.84834	-1.26035
H	0.87741	4.11474	-0.51197
H	-1.49917	4.78066	-0.71027
H	-3.14757	3.20181	-1.66914

H	-2.41563	0.94803	-2.42041
C	6.48854	-0.76555	0.29339
N	7.63615	-0.76751	0.31957
C	4.99950	1.31182	1.57128
N	5.53116	2.17046	2.11665
H	4.94310	-2.56740	-0.90252

Table H.27. Cartesian coordinates for compound **8a•8a**

	X	Y	Z
P	1.90604	-0.50927	0.28823
O	2.14538	-0.36271	-1.31994
O	1.30666	0.78854	0.74063
N	0.94770	-1.85024	0.53426
C	3.46091	-1.01286	0.99139
C	3.62819	-2.31092	1.33514
C	2.66970	-3.37543	1.22620
C	1.36740	-3.13848	0.79829
C	0.44462	-4.22575	0.64934
C	0.87736	-5.53104	0.99535
C	2.20303	-5.74108	1.47065
C	3.06377	-4.69977	1.57139
C	-0.86300	-4.05174	0.13408
C	-1.70455	-5.12350	-0.01092
C	-1.28226	-6.41539	0.35530
C	-0.02017	-6.61137	0.84717
C	4.55690	-0.02761	1.06906
C	5.87216	-0.40844	0.78195
C	6.91386	0.49795	0.85931
C	6.66430	1.82290	1.20587
C	5.34774	2.22166	1.47458
C	4.30638	1.30429	1.40853
C	2.44242	-1.49474	-2.07112
C	3.76675	-1.78475	-2.35747
C	4.05908	-2.91637	-3.10845
C	3.03573	-3.74204	-3.55574
C	1.71267	-3.43015	-3.26449
C	1.40597	-2.29791	-2.52262
H	4.59337	-2.59754	1.74740
H	2.50958	-6.74483	1.73637
H	4.07824	-4.85586	1.91908
H	-1.21614	-3.07252	-0.16600
H	-2.69609	-4.98348	-0.42171

H	-1.95937	-7.25171	0.23761
H	0.31660	-7.60376	1.12252
H	6.07613	-1.42542	0.47066
H	3.29619	1.62611	1.62741
H	4.54292	-1.11949	-1.99903
H	5.08928	-3.15140	-3.34445
H	3.26873	-4.62563	-4.13553
H	0.91283	-4.06982	-3.61484
H	0.38407	-2.02557	-2.28402
C	-7.75450	-2.76046	-1.28954
N	-8.63693	-3.49291	-1.34061
C	7.74730	2.75882	1.27266
N	8.62960	3.49152	1.32249
C	-5.05963	-3.58857	-1.82108
N	-4.79681	-4.67632	-2.07713
H	-7.93492	-0.19380	-0.65486
H	-0.02237	-1.68990	0.24884
H	7.92716	0.19297	0.63471
C	5.05341	3.58538	1.81147
N	4.79082	4.67277	2.06928
P	-1.91382	0.50661	-0.29632
O	-2.15559	0.36226	1.31163
O	-1.31448	-0.79207	-0.74630
N	-0.95444	1.84676	-0.54289
C	-3.46739	1.01004	-1.00249
C	-3.63370	2.30792	-1.34743
C	-2.67506	3.37220	-1.23769
C	-1.37334	3.13503	-0.80814
C	-0.45032	4.22204	-0.65881
C	-0.88226	5.52731	-1.00588
C	-2.20734	5.73758	-1.48273
C	-3.06830	4.69650	-1.58397
C	0.85670	4.04784	-0.14208
C	1.69846	5.11940	0.00326
C	1.27698	6.41126	-0.36400
C	0.01547	6.60743	-0.85727
C	-4.56355	0.02507	-1.08151
C	-5.87934	0.40667	-0.79788
C	-6.92120	-0.49941	-0.87673
C	-6.67133	-1.82484	-1.22125
C	-5.35428	-2.22438	-1.48637
C	-4.31274	-1.30731	-1.41890
C	-2.45305	1.49537	2.06101
C	-3.77759	1.78614	2.34559
C	-4.07038	2.91879	3.09483
C	-3.04725	3.74471	3.54219

C	-1.72398	3.43204	3.25274
C	-1.41684	2.29879	2.51263
H	0.01533	1.68625	-0.25668
H	-4.59810	2.59456	-1.76148
H	-2.51327	6.74131	-1.74924
H	-4.08233	4.85275	-1.93289
H	1.20924	3.06866	0.15881
H	2.68953	4.97924	0.41511
H	1.95424	7.24741	-0.24600
H	-0.32069	7.59979	-1.13345
H	-6.08375	1.42406	-0.48823
H	-3.30217	-1.62976	-1.63504
H	-4.55359	1.12066	1.98718
H	-5.10076	3.15440	3.32947
H	-3.28058	4.62906	4.12066
H	-0.92432	4.07190	3.60317
H	-0.39475	2.02586	2.27549

Table H.28. Cartesian coordinates for compound **8b**

	X	Y	Z
S	5.61567	0.37629	0.07635
P	-1.24911	0.13035	1.77483
O	-1.39075	1.75998	1.68533
O	-0.74411	-0.20093	3.13403
O	6.18686	0.45726	1.41966
O	5.97790	1.32825	-0.97330
N	-2.77131	-0.50598	1.45944
C	-0.34080	-0.35107	0.31669
C	-1.02404	-0.81521	-0.75230
C	-2.44367	-1.04598	-0.85464
C	-3.28853	-0.90261	0.23984
C	-4.68917	-1.18673	0.11631
C	-5.18381	-1.61649	-1.14283
C	-4.29852	-1.75536	-2.24760
C	-2.97824	-1.47938	-2.10059
C	-5.60127	-1.03897	1.18946
C	-6.93231	-1.31962	1.02565
C	-7.41984	-1.75753	-0.22129
C	-6.56258	-1.89960	-1.27894
C	1.12215	-0.14404	0.28104
C	1.72638	0.33877	-0.88721
C	3.09726	0.50483	-0.95742

C	3.85790	0.19577	0.16403
C	3.28933	-0.26129	1.34509
C	1.91526	-0.42322	1.40014
C	6.15973	-1.29851	-0.57959
C	-1.85599	2.36194	0.52246
C	-0.93322	2.86766	-0.38160
C	-1.38994	3.48541	-1.53828
C	-2.75440	3.59116	-1.78390
C	-3.66555	3.08830	-0.86284
C	-3.22060	2.47268	0.30065
H	-3.36924	-0.57216	2.27423
H	-0.45032	-1.07410	-1.63912
H	-4.69722	-2.08624	-3.19873
H	-2.29524	-1.58619	-2.93529
H	-5.26870	-0.69503	2.16026
H	-7.61452	-1.20012	1.85776
H	-8.47369	-1.97706	-0.33953
H	-6.92700	-2.23139	-2.24426
H	1.11475	0.60551	-1.74015
H	3.56650	0.88428	-1.85657
H	3.90766	-0.48525	2.20535
H	1.45502	-0.78110	2.31207
H	0.12491	2.77365	-0.16795
H	-0.67636	3.88652	-2.24753
H	-3.10709	4.07119	-2.68802
H	-4.72928	3.17587	-1.04604
H	-3.91793	2.08424	1.03258
F	5.74680	-2.25718	0.23376
F	7.47841	-1.31545	-0.64851
F	5.65151	-1.49944	-1.78513

Table H.29. Cartesian coordinates for compound **8b•8b**

	X	Y	Z
S	-8.59680	-0.69151	0.23307
P	-1.72217	1.01303	0.12729
O	-1.61704	1.03417	1.75720
O	-1.60070	-0.42578	-0.27372
O	-8.45504	-2.14314	0.26821
O	-9.41169	0.05003	1.18960
N	-0.51945	2.00375	-0.46573
C	-3.20019	1.90610	-0.29803
C	-3.08118	3.20063	-0.67082

C	-1.86830	3.95303	-0.85052
C	-0.61881	3.35155	-0.74464
C	0.57497	4.11644	-0.96265
C	0.44736	5.49160	-1.28378
C	-0.84322	6.08298	-1.38953
C	-1.95416	5.33510	-1.18107
C	1.87048	3.55612	-0.85117
C	2.98326	4.32463	-1.07153
C	2.85730	5.68686	-1.40280
C	1.61603	6.25449	-1.50246
C	-4.51259	1.24861	-0.13579
C	-5.58857	1.95953	0.40853
C	-6.83777	1.37571	0.52427
C	-6.99562	0.06268	0.10368
C	-5.94329	-0.67849	-0.41525
C	-4.69906	-0.08212	-0.52889
C	-9.33062	-0.30223	-1.45320
C	-1.43163	2.24383	2.41681
C	-2.53410	2.90736	2.93084
C	-2.34355	4.11450	3.59077
C	-1.06638	4.64416	3.72480
C	0.02772	3.96008	3.20808
C	-0.14706	2.74933	2.55251
H	0.40849	1.58299	-0.36697
H	-3.99970	3.74114	-0.88939
H	-0.91759	7.13352	-1.64035
H	-2.93924	5.77908	-1.26487
H	2.00689	2.51454	-0.58715
H	3.96751	3.88086	-0.99181
H	3.74482	6.28155	-1.57791
H	1.50850	7.30308	-1.75339
H	-5.43582	2.97173	0.76194
H	-7.67544	1.91192	0.95209
H	-6.10267	-1.70506	-0.72053
H	-3.86466	-0.63930	-0.93435
H	-3.51768	2.46794	2.81601
H	-3.19570	4.64010	4.00256
H	-0.92292	5.58767	4.23503
H	1.02411	4.36949	3.31484
H	0.68630	2.18935	2.14293
S	8.53361	0.57630	-0.79184
P	1.71743	-0.99221	0.08287
O	1.56776	-1.02097	-1.54304
O	1.61996	0.45015	0.47884
O	8.38563	2.02242	-0.91458
O	9.21707	-0.24100	-1.78870

N	0.52225	-1.96772	0.71584
C	3.19837	-1.89792	0.46867
C	3.08145	-3.17277	0.90492
C	1.87031	-3.90394	1.16299
C	0.62174	-3.30182	1.05147
C	-0.57182	-4.05213	1.31635
C	-0.44445	-5.41260	1.69486
C	0.84565	-6.00315	1.81171
C	1.95609	-5.27013	1.55438
C	-1.86700	-3.49344	1.19263
C	-2.97981	-4.24930	1.45272
C	-2.85380	-5.59647	1.84089
C	-1.61303	-6.16229	1.95583
C	4.50613	-1.27959	0.17065
C	5.52107	-2.04781	-0.41293
C	6.75509	-1.49262	-0.69960
C	6.96107	-0.15167	-0.40620
C	5.97220	0.64170	0.15760
C	4.74208	0.07365	0.44269
C	9.49028	0.30633	0.80318
C	1.37390	-2.23607	-2.19003
C	2.46752	-2.89319	-2.73074
C	2.26918	-4.10617	-3.37774
C	0.99363	-4.64811	-3.47154
C	-0.09160	-3.97009	-2.92885
C	0.09054	-2.75325	-2.28652
H	-0.40619	-1.55032	0.61238
H	4.00307	-3.71700	1.10005
H	0.91974	-7.04186	2.10776
H	2.94062	-5.71460	1.64215
H	-2.00367	-2.46357	0.88605
H	-3.96363	-3.80723	1.35958
H	-3.74110	-6.18137	2.04736
H	-1.50596	-7.19941	2.25072
H	5.32628	-3.08162	-0.67015
H	7.54095	-2.07196	-1.16759
H	6.16812	1.68722	0.35993
H	3.95604	0.67344	0.88291
H	3.45000	-2.44450	-2.64534
H	3.11386	-4.62665	-3.81092
H	0.84426	-5.59614	-3.97166
H	-1.08698	-4.38851	-3.00624
H	-0.73528	-2.19621	-1.85834
F	8.90195	0.95444	1.79704
F	10.71961	0.75600	0.64739
F	9.52395	-0.98701	1.09040

F	-8.58444	-0.84828	-2.40183
F	-9.36713	1.00995	-1.63403
F	-10.55340	-0.79136	-1.51500

Table H.30. Cartesian coordinates for compound **8c**

	X	Y	Z
P	-0.35441	-0.70530	1.51094
O	-0.45461	0.85524	2.00311
O	-0.88820	-1.55386	2.61019
N	1.26338	-1.00200	1.17314
C	-1.08460	-0.74019	-0.11643
C	-0.27001	-0.71580	-1.19348
C	1.17304	-0.72041	-1.20652
C	1.91358	-0.86830	-0.04058
C	3.34625	-0.90524	-0.09016
C	3.98219	-0.79551	-1.35449
C	3.20171	-0.64813	-2.53457
C	1.84744	-0.61264	-2.45492
C	4.15310	-1.02093	1.06821
C	5.51952	-1.05051	0.97376
C	6.14907	-0.95979	-0.28320
C	5.39446	-0.83247	-1.41803
C	-2.55682	-0.68313	-0.24047
C	-3.13999	0.08460	-1.25598
C	-4.51265	0.13274	-1.40832
C	-5.32718	-0.57949	-0.52655
C	-4.76318	-1.33177	0.50295
C	-3.38715	-1.37872	0.64484
C	0.01690	1.87891	1.19068
C	-0.88371	2.56294	0.38782
C	-0.42187	3.59740	-0.41533
C	0.92626	3.93773	-0.41310
C	1.81391	3.24882	0.40442
C	1.36261	2.21506	1.21594
H	1.81133	-1.28826	1.97537
H	-0.73802	-0.70659	-2.17526
H	3.70720	-0.56501	-3.48876
H	1.24517	-0.50417	-3.34955
H	3.70858	-1.07965	2.05386
H	6.11882	-1.13698	1.87137
H	7.22983	-0.98544	-0.34621
H	5.86799	-0.75234	-2.38975

H	-2.51090	0.66523	-1.91956
H	-2.95137	-1.96916	1.44051
H	-1.92926	2.27887	0.40256
H	-1.11875	4.13919	-1.04287
H	1.28273	4.74299	-1.04294
H	2.86371	3.51484	0.41467
H	2.03956	1.67112	1.86331
C	-6.75216	-0.52862	-0.67676
N	-7.89370	-0.48711	-0.79954
H	-5.40153	-1.87895	1.18451
H	-4.95869	0.72727	-2.19521

Table H.31. Cartesian coordinates for compound **8c•8c**

	X	Y	Z
P	-1.91537	-0.50274	0.20770
O	-2.01241	-0.37529	-1.41794
O	-1.37332	0.81255	0.68264
N	-0.94498	-1.81607	0.54520
C	-3.51149	-1.03924	0.77523
C	-3.67059	-2.33184	1.13880
C	-2.66849	-3.36367	1.17882
C	-1.33855	-3.09537	0.87383
C	-0.35581	-4.13949	0.93268
C	-0.77340	-5.44099	1.30909
C	-2.13999	-5.68879	1.62110
C	-3.04656	-4.68311	1.55630
C	1.00740	-3.92170	0.61799
C	1.91139	-4.94888	0.68886
C	1.49964	-6.23939	1.07108
C	0.18580	-6.47633	1.37233
C	-4.63815	-0.08468	0.71951
C	-5.89213	-0.50773	0.26597
C	-6.96372	0.36501	0.22287
C	-6.79184	1.68946	0.62435
C	-5.54380	2.12831	1.06501
C	-4.47584	1.24954	1.10783
C	-2.25561	-1.50744	-2.18523
C	-3.55717	-1.79969	-2.56061
C	-3.79551	-2.92653	-3.33641
C	-2.74160	-3.74481	-3.72301
C	-1.44236	-3.43114	-3.34162
C	-1.18844	-2.30555	-2.56991

H	0.03318	-1.64608	0.29434
H	-4.66481	-2.63748	1.45741
H	-2.43756	-6.68911	1.90897
H	-4.08795	-4.86658	1.79389
H	1.36130	-2.94441	0.31301
H	2.95151	-4.76438	0.45213
H	2.22451	-7.04159	1.12694
H	-0.14225	-7.46629	1.66632
H	-6.01879	-1.52749	-0.07657
H	-3.50896	1.58919	1.45629
H	-4.35815	-1.14009	-2.24913
H	-4.80708	-3.16329	-3.64102
H	-2.93255	-4.62366	-4.32509
H	-0.61908	-4.06419	-3.64700
H	-0.18639	-2.02951	-2.26140
P	1.91529	0.50277	-0.20779
O	2.01246	0.37526	1.41785
O	1.37321	-0.81251	-0.68274
N	0.94490	1.81611	-0.54525
C	3.51140	1.03927	-0.77532
C	3.67051	2.33188	-1.13883
C	2.66841	3.36372	-1.17882
C	1.33847	3.09542	-0.87386
C	0.35574	4.13954	-0.93267
C	0.77333	5.44105	-1.30903
C	2.13993	5.68886	-1.62102
C	3.04649	4.68317	-1.55626
C	-1.00747	3.92174	-0.61799
C	-1.91146	4.94892	-0.68882
C	-1.49971	6.23945	-1.07099
C	-0.18587	6.47639	-1.37223
C	4.63807	0.08472	-0.71959
C	5.89199	0.50774	-0.26586
C	6.96359	-0.36500	-0.22272
C	6.79176	-1.68942	-0.62434
C	5.54378	-2.12824	-1.06518
C	4.47581	-1.24947	-1.10803
C	2.25575	1.50734	2.18519
C	3.55742	1.79978	2.56000
C	3.79592	2.92654	3.33588
C	2.74204	3.74455	3.72312
C	1.44267	3.43069	3.34230
C	1.18860	2.30519	2.57051
H	-0.03326	1.64613	-0.29440
H	4.66473	2.63753	-1.45743
H	2.43750	6.68919	-1.90885

H	4.08789	4.86665	-1.79384
H	-1.36138	2.94444	-0.31305
H	-2.95158	4.76441	-0.45210
H	-2.22457	7.04165	-1.12682
H	0.14219	7.46636	-1.66618
H	6.01860	1.52746	0.07680
H	5.41908	-3.15644	-1.37858
H	3.50899	-1.58911	-1.45663
H	4.35839	1.14040	2.24801
H	4.80759	3.16344	3.64005
H	2.93310	4.62333	4.32526
H	0.61942	4.06352	3.64820
H	0.18645	2.02899	2.26248
C	-7.89825	2.60185	0.57519
N	-8.78405	3.33183	0.53442
C	7.89819	-2.60179	-0.57514
N	8.78398	-3.33177	-0.53433
H	-5.41905	3.15654	1.37830
H	7.93036	-0.03292	0.13201
H	-7.93054	0.03290	-0.13171

Table H.32. Cartesian coordinates for compound **8d**

	X	Y	Z
S	-6.24291	-0.22705	-0.31014
P	0.56680	-0.49522	1.64602
O	0.52828	1.10620	1.99079
O	0.06016	-1.22155	2.84164
O	-6.80348	-0.24546	1.05286
O	-6.56150	0.90289	-1.20241
N	2.15960	-0.87364	1.27340
C	-0.23427	-0.66612	0.05980
C	0.53138	-0.79272	-1.04587
C	1.97163	-0.85375	-1.11752
C	2.75861	-0.89180	0.02681
C	4.18642	-0.97012	-0.07513
C	4.77002	-1.03818	-1.36698
C	3.94264	-1.00995	-2.52382
C	2.59460	-0.91705	-2.39551
C	5.03815	-0.96026	1.05651
C	6.39813	-1.04101	0.91331
C	6.97556	-1.13065	-0.36883
C	6.17702	-1.12523	-1.48062

C	-1.70805	-0.55699	-0.00999
C	-2.30196	0.12978	-1.07579
C	-3.67910	0.23125	-1.17327
C	-4.46333	-0.34393	-0.18376
C	-3.90381	-1.00813	0.89698
C	-2.52394	-1.11183	0.98221
C	-6.73128	-1.73582	-1.13070
C	0.96248	2.03510	1.05308
C	0.01930	2.67220	0.26066
C	0.44265	3.61583	-0.66593
C	1.79491	3.91190	-0.79626
C	2.72610	3.26980	0.01098
C	2.31397	2.32790	0.94558
H	2.73543	-1.09264	2.07747
H	0.02067	-0.87139	-2.00292
H	4.40767	-1.06372	-3.50048
H	1.95837	-0.89432	-3.27271
H	4.63249	-0.87431	2.05695
H	7.03315	-1.02993	1.79021
H	8.05178	-1.19657	-0.47039
H	6.61029	-1.18509	-2.47240
H	-1.67806	0.60994	-1.81956
H	-4.14077	0.77248	-1.98984
H	-4.53605	-1.42943	1.66907
H	-2.07596	-1.62912	1.82092
H	-6.43483	-2.57860	-0.50883
H	-6.24736	-1.76865	-2.10523
H	-7.81543	-1.68983	-1.23470
H	-1.02862	2.42453	0.38111
H	-0.28812	4.12129	-1.28512
H	2.12270	4.64670	-1.52078
H	3.77976	3.50212	-0.08189
H	3.02580	1.82534	1.58875

Table H.33. Cartesian coordinates for compound **8d•8d**

	X	Y	Z
S	-8.59831	0.75220	0.22915
P	-1.71727	-0.98096	0.04956
O	-1.71438	-1.01757	-1.58386
O	-1.56196	0.46058	0.42849
O	-8.40339	2.20174	0.10272
O	-9.40770	0.00819	-0.74384
N	-0.48167	-1.97023	0.57474

C	-3.16878	-1.86503	0.57155
C	-3.02943	-3.15364	0.95578
C	-1.80859	-3.90608	1.08123
C	-0.56653	-3.30972	0.89282
C	0.63787	-4.07014	1.06634
C	0.52742	-5.43866	1.42022
C	-0.75582	-6.02713	1.60296
C	-1.87643	-5.28152	1.44087
C	1.92622	-3.51097	0.88439
C	3.04962	-4.27457	1.06517
C	2.94075	-5.63105	1.42530
C	1.70646	-6.19708	1.59564
C	-4.48797	-1.20806	0.45935
C	-5.58792	-1.92279	-0.02706
C	-6.83944	-1.33360	-0.10288
C	-6.98155	-0.01427	0.29924
C	-5.90365	0.72743	0.75763
C	-4.65572	0.12997	0.83329
C	-9.28415	0.43842	1.85657
C	-1.62296	-2.23984	-2.23777
C	-2.78408	-2.85924	-2.67198
C	-2.69036	-4.08047	-3.32637
C	-1.44914	-4.66890	-3.53434
C	-0.29523	-4.02881	-3.09792
C	-0.37354	-2.80400	-2.44979
H	0.43913	-1.55856	0.39856
H	-3.93544	-3.69056	1.22869
H	-0.81669	-7.07319	1.87555
H	-2.85582	-5.72332	1.58353
H	2.04924	-2.47354	0.59841
H	4.02827	-3.83068	0.93283
H	3.83660	-6.22211	1.56728
H	1.61265	-7.24080	1.87150
H	-5.45195	-2.94071	-0.37180
H	-7.69270	-1.87046	-0.49891
H	-6.04375	1.76508	1.03471
H	-3.80304	0.69463	1.18772
H	-8.63737	0.90180	2.59792
H	-9.35439	-0.63749	1.99847
H	-10.27129	0.89782	1.85709
H	-3.73795	-2.37519	-2.50020
H	-3.58996	-4.57129	-3.67548
H	-1.38012	-5.62310	-4.04035
H	0.67361	-4.48297	-3.26265
H	0.50861	-2.27637	-2.10525
S	8.59956	-0.78680	-0.15702

P	1.73333	0.99377	-0.11678
O	1.69036	0.99521	1.51674
O	1.58386	-0.43844	-0.53123
O	8.38882	-2.23482	-0.03758
O	9.39939	-0.05283	0.83138
N	0.51524	1.99930	-0.65172
C	3.20131	1.88190	-0.58413
C	3.07731	3.17933	-0.94221
C	1.86260	3.94117	-1.07529
C	0.61389	3.34771	-0.92690
C	-0.58255	4.12088	-1.09678
C	-0.45825	5.49728	-1.41361
C	0.83139	6.08134	-1.56123
C	1.94463	5.32478	-1.39838
C	-1.87689	3.56690	-0.94435
C	-2.99254	4.34281	-1.12026
C	-2.86990	5.70690	-1.44575
C	-1.62966	6.26824	-1.58546
C	4.51299	1.21325	-0.45449
C	5.60462	1.90771	0.07726
C	6.84922	1.30660	0.17364
C	6.99183	-0.00477	-0.25328
C	5.92115	-0.72681	-0.75794
C	4.68079	-0.11714	-0.85525
C	9.31563	-0.47605	-1.77180
C	1.54017	2.19777	2.19645
C	2.66643	2.84753	2.67547
C	2.51030	4.04848	3.35542
C	1.24332	4.58596	3.54432
C	0.12527	3.91551	3.06212
C	0.26547	2.71075	2.38752
H	-0.41061	1.58962	-0.50263
H	3.99179	3.71747	-1.18264
H	0.90348	7.13340	-1.80649
H	2.92884	5.76397	-1.51322
H	-2.01110	2.52412	-0.68368
H	-3.97573	3.90326	-1.00943
H	-3.75972	6.30788	-1.58402
H	-1.52489	7.31805	-1.83276
H	5.46726	2.91868	0.44135
H	7.69555	1.82722	0.60450
H	6.05976	-1.75938	-1.05436
H	3.83403	-0.66599	-1.24676
H	8.67865	-0.93397	-2.52492
H	9.39599	0.59951	-1.91102
H	10.29933	-0.94250	-1.75571

H	3.64162	2.40231	2.51874
H	3.38177	4.56335	3.73943
H	1.12675	5.52501	4.06952
H	-0.86323	4.33142	3.21016
H	-0.58639	2.15975	2.00469

Table H.34. Cartesian coordinates for compound **8e**

	X	Y	Z
P	-0.29534	-0.66583	-1.57442
O	-0.25070	0.90238	-2.05197
O	0.22224	-1.48955	-2.70023
N	-1.89283	-1.00974	-1.18922
C	0.48779	-0.69901	0.02827
C	-0.71690	1.90413	-1.20968
C	-2.50843	-0.89189	0.04442
H	-2.45763	-1.30839	-1.97511
C	-0.29256	-0.70527	1.12998
C	1.96272	-0.60576	0.10461
C	0.19545	2.60093	-0.43146
C	-2.07062	2.20572	-1.18053
C	-1.73508	-0.73948	1.18802
C	-3.93796	-0.94613	0.13540
H	0.20620	-0.69380	2.09646
C	2.56011	0.16629	1.10942
C	2.78072	-1.26707	-0.81385
C	-0.26225	3.61294	0.40208
H	1.24655	2.34385	-0.48798
C	-2.51759	3.21705	-0.33903
H	-2.75676	1.65176	-1.80941
C	-2.37429	-0.65193	2.45643
C	-4.53864	-0.85589	1.41827
C	-4.77598	-1.05637	-1.00106
C	3.93601	0.24944	1.21121
H	1.93908	0.72098	1.80212
C	4.16266	-1.18110	-0.71782
H	2.33556	-1.86099	-1.60169
C	-1.61775	3.91809	0.45463
H	0.44367	4.16421	1.01099
H	-3.57338	3.45611	-0.30743
C	-3.72527	-0.70852	2.57569
H	-1.74795	-0.54092	3.33396
C	-5.94813	-0.90968	1.52164

C	-6.13869	-1.10173	-0.86842
H	-4.35803	-1.09549	-1.99912
C	4.73516	-0.42643	0.29416
H	4.38893	0.84979	1.99160
H	4.78511	-1.70350	-1.43242
H	-1.97115	4.70560	1.10819
H	-4.20309	-0.64035	3.54523
C	-6.73319	-1.03300	0.40711
H	-6.39430	-0.84514	2.50738
H	-6.76274	-1.18269	-1.74954
H	-7.81141	-1.07127	0.50056
C	6.22515	-0.32703	0.43441
F	6.88031	-0.89248	-0.58589
F	6.66625	-0.92462	1.55737
F	6.64057	0.94969	0.50642

Table H.35. Cartesian coordinates for compound **8e•8e**

	X	Y	Z
P	-1.78816	-0.87952	-0.00718
O	-1.92584	-0.95876	-1.63350
O	-1.54531	0.56338	0.31758
N	-0.55054	-1.90801	0.43154
C	-3.22182	-1.68192	0.67048
C	-1.90096	-2.20091	-2.25429
C	-0.65838	-3.21856	0.84820
H	0.36993	-1.54183	0.17123
C	-3.09361	-2.94157	1.14274
C	-4.52796	-0.99219	0.59844
C	-3.09799	-2.84120	-2.53274
C	-0.67799	-2.76539	-2.58546
C	-1.89537	-3.73658	1.21413
C	0.52138	-4.03089	0.93178
H	-3.99143	-3.41848	1.52985
C	-5.67741	-1.70863	0.24627
C	-4.64412	0.37190	0.87645
C	-3.06686	-4.08390	-3.15206
H	-4.03020	-2.35623	-2.26920
C	-0.66155	-4.01052	-3.19809
H	0.23230	-2.22377	-2.35399
C	-1.97988	-5.07445	1.69141
C	0.39432	-5.36120	1.40567
C	1.79905	-3.56121	0.54233

C	-6.91279	-1.08858	0.20257
H	-5.59397	-2.75689	-0.01372
C	-5.88189	0.99592	0.83043
H	-3.76113	0.93888	1.14175
C	-1.85166	-4.67164	-3.47886
H	-3.99498	-4.59276	-3.37923
H	0.28626	-4.46548	-3.45580
C	-0.88126	-5.86297	1.78819
H	-2.95401	-5.45157	1.98010
C	1.54929	-6.17101	1.49001
C	2.89818	-4.37375	0.63629
H	1.93245	-2.55549	0.16281
C	-7.01253	0.26649	0.49552
H	-7.79674	-1.64913	-0.07556
H	-5.96565	2.05079	1.05594
H	-1.83110	-5.64238	-3.95691
H	-0.95578	-6.87981	2.15226
C	2.77519	-5.69138	1.11582
H	1.44285	-7.18471	1.85782
H	3.86907	-3.99813	0.33964
H	3.65194	-6.32285	1.18496
O	1.54529	-0.47282	-0.79240
P	1.77738	0.91986	-0.28916
O	1.75263	0.81025	1.34202
N	0.60281	2.01661	-0.73475
C	3.28128	1.76563	-0.71596
C	1.70292	1.96721	2.10846
C	0.76475	3.36729	-0.96135
H	-0.33948	1.64672	-0.58303
C	3.21609	3.07884	-1.02771
C	4.56258	1.03970	-0.58425
C	2.88193	2.48937	2.61663
C	0.47488	2.56148	2.35876
C	2.03806	3.90266	-1.12037
C	-0.39375	4.20717	-1.06327
H	4.15481	3.58297	-1.24742
C	5.66545	1.66995	0.00350
C	4.69644	-0.27697	-1.02971
C	2.82813	3.64235	3.38904
H	3.81713	1.98375	2.40841
C	0.43706	3.71722	3.12689
H	-0.42191	2.10853	1.95120
C	2.18182	5.29105	-1.39703
C	-0.20827	5.58614	-1.33553
C	-1.70947	3.71457	-0.88719
C	6.87539	1.01167	0.12167

H	5.56031	2.67636	0.39014
C	5.90970	-0.93949	-0.91054
H	3.84765	-0.77521	-1.48034
C	1.60937	4.25995	3.64011
H	3.74161	4.05669	3.79663
H	-0.51454	4.19413	3.32422
C	1.10503	6.10851	-1.50184
H	3.18369	5.68487	-1.52249
C	-1.34271	6.42239	-1.43779
C	-2.78764	4.55322	-0.99405
H	-1.89020	2.67100	-0.65985
C	6.99494	-0.29551	-0.33733
H	7.72348	1.50323	0.58274
H	6.01052	-1.95515	-1.26886
H	1.57303	5.16038	4.23948
H	1.22588	7.16382	-1.71119
C	-2.60546	5.92080	-1.27359
H	-1.19044	7.47420	-1.64945
H	-3.78745	4.15900	-0.86388
H	-3.46575	6.57296	-1.35560
C	8.32131	-0.98629	-0.19395
C	-8.36764	0.91420	0.47175
F	8.28253	-2.25576	-0.61293
F	8.73544	-1.00216	1.08231
F	9.28242	-0.36648	-0.89674
F	-8.29235	2.24990	0.47904
F	-9.10730	0.55732	1.53402
F	-9.06852	0.56009	-0.61551

Table H.36. Cartesian coordinates for compound **8f**

	X	Y	Z
P	-0.26940	-0.71877	1.45205
O	-0.35916	0.83047	1.98780
O	-0.83098	-1.58669	2.52326
N	1.35212	-1.03143	1.14550
C	-0.96705	-0.69813	-0.18939
C	0.13426	1.87046	1.21184
C	2.03323	-0.88020	-0.05032
H	1.87742	-1.33997	1.95388
C	-0.12539	-0.66316	-1.24429
C	-2.43475	-0.59317	-0.33383
C	-0.74792	2.59204	0.42100

C	1.48415	2.18752	1.26177
C	1.31999	-0.69098	-1.22606
C	3.46570	-0.93993	-0.06934
H	-0.56977	-0.61503	-2.23563
C	-2.98760	0.20656	-1.34512
C	-3.30757	-1.26834	0.51787
C	-0.26308	3.64537	-0.34304
H	-1.79679	2.32005	0.41335
C	1.95855	3.24066	0.48947
H	2.14608	1.61317	1.89830
C	2.02325	-0.56136	-2.45520
C	4.13123	-0.80942	-1.31674
C	4.24644	-1.10233	1.10186
C	-4.35310	0.30025	-1.51322
H	-2.33421	0.77793	-1.99435
C	-4.68640	-1.17871	0.36077
H	-2.91008	-1.88855	1.31172
C	1.08919	3.96786	-0.31463
H	-0.94513	4.21574	-0.96159
H	3.01171	3.49146	0.51912
C	3.37897	-0.61753	-2.50771
H	1.44297	-0.41719	-3.35941
C	5.54419	-0.86909	-1.35156
C	5.61395	-1.15314	1.03495
H	3.78129	-1.18115	2.07669
C	-5.21480	-0.39403	-0.65983
H	-4.77998	0.92272	-2.28978
H	-5.32911	-1.72479	1.03706
H	1.46321	4.78800	-0.91451
H	3.90562	-0.51823	-3.44891
C	6.27246	-1.03930	-0.20542
H	6.03917	-0.77170	-2.31106
H	6.19180	-1.27626	1.94234
O	-6.53917	-0.23603	-0.89646
H	7.35378	-1.08197	-0.24625
C	-7.44871	-0.91044	-0.04154
H	-7.33093	-0.58348	0.99476
H	-8.44329	-0.64600	-0.39254
H	-7.31805	-1.99394	-0.10309

Table H.37. Cartesian coordinates for compound **8f•8f**

X	Y	Z
---	---	---

P	-1.87727	-0.68069	0.17148
O	-1.98103	-0.61162	-1.45804
O	-1.50782	0.70686	0.60703
N	-0.74026	-1.84587	0.53838
C	-3.39095	-1.40305	0.75905
C	-2.08540	-1.78249	-2.19450
C	-0.95502	-3.13845	0.96551
H	0.20124	-1.56967	0.24522
C	-3.36759	-2.67436	1.21609
C	-4.64297	-0.63213	0.60775
C	-3.34204	-2.24345	-2.55451
C	-0.92840	-2.44885	-2.57087
C	-2.23241	-3.55678	1.31713
C	0.15798	-4.03886	1.06878
H	-4.31300	-3.09374	1.55328
C	-5.81639	-1.27348	0.18693
C	-4.69986	0.73630	0.86191
C	-3.44048	-3.40737	-3.30573
H	-4.21791	-1.68415	-2.24801
C	-1.04282	-3.61309	-3.31801
H	0.03185	-2.04233	-2.27379
C	-2.42634	-4.88572	1.78604
C	-0.07876	-5.35824	1.53134
C	1.47704	-3.66466	0.71447
C	-7.00063	-0.58091	0.05234
H	-5.78720	-2.32873	-0.05897
C	-5.88817	1.44598	0.72771
H	-3.80488	1.25493	1.18317
C	-2.29413	-4.09425	-3.68511
H	-4.41596	-3.77540	-3.59750
H	-0.14829	-4.14564	-3.61504
C	-1.39483	-5.76010	1.89195
H	-3.43110	-5.18702	2.05896
C	1.00896	-6.25507	1.63042
C	2.50896	-4.55941	0.82342
H	1.69660	-2.66784	0.35142
C	-7.04515	0.78778	0.32361
H	-7.90704	-1.07073	-0.27872
H	-5.89466	2.50472	0.94482
H	-2.37469	-5.00255	-4.26829
H	-1.55440	-6.76994	2.24839
C	2.27553	-5.86856	1.28525
H	0.81762	-7.26021	1.98771
H	3.51192	-4.25261	0.55502
O	-8.25176	1.38434	0.15791
H	3.09912	-6.56655	1.36828

C	-8.33895	2.77199	0.40320
H	-7.67903	3.33435	-0.26349
H	-9.37122	3.04863	0.20621
H	-8.09188	3.00704	1.44226
O	1.41633	-0.62147	-0.76687
P	1.83250	0.72616	-0.25684
O	1.92694	0.56219	1.36857
N	0.73934	1.94851	-0.56176
C	3.37461	1.41953	-0.80087
C	2.06131	1.69004	2.16545
C	1.01695	3.27206	-0.83554
H	-0.21903	1.67879	-0.32081
C	3.41037	2.72834	-1.13109
C	4.58217	0.56891	-0.75052
C	3.32940	2.09980	2.54636
C	0.92208	2.36797	2.57418
C	2.31559	3.66719	-1.13384
C	-0.05108	4.23031	-0.83733
H	4.37195	3.13392	-1.43835
C	5.79213	1.08740	-0.26875
C	4.55868	-0.75917	-1.17042
C	3.45816	3.22070	3.35585
H	4.19021	1.53339	2.21153
C	1.06647	3.48818	3.38088
H	-0.04872	2.00549	2.25485
C	2.57281	5.02733	-1.46077
C	0.24793	5.57818	-1.16178
C	-1.38498	3.88475	-0.51009
C	6.93494	0.31648	-0.23204
H	5.82528	2.10639	0.09937
C	5.70451	-1.54638	-1.13737
H	3.63414	-1.18235	-1.54318
C	2.32997	3.91692	3.77086
H	4.44268	3.54834	3.66473
H	0.18603	4.02831	3.70516
C	1.58253	5.95435	-1.47826
H	3.59232	5.30883	-1.69797
C	-0.79648	6.53029	-1.16379
C	-2.37270	4.83427	-0.51933
H	-1.64863	2.86871	-0.24170
C	6.89906	-1.00890	-0.66847
H	7.86985	0.70973	0.14553
H	5.64916	-2.56850	-1.48411
H	2.43399	4.79136	4.40023
H	1.79051	6.98741	-1.72745
C	-2.07910	6.17066	-0.85116

H	-0.55796	7.55674	-1.41735
H	-3.38784	4.55224	-0.26999
O	8.06972	-1.68941	-0.59121
H	-2.86938	6.91083	-0.85696
C	8.07363	-3.03908	-1.00557
H	9.08951	-3.39683	-0.86157
H	7.38820	-3.64032	-0.40134
H	7.80253	-3.13028	-2.06112

4. Measurements of Dimerization Constants K_{dim}

Self-dimerization equilibria were studied by virtue of ^1H NMR spectroscopic (additional ^{31}P NMR analysis for **8b**) dilution experiments in water-saturated CDCl_3 (ca. 0.8% water in CHCl_3). Nonlinear regression analysis has been performed to fit the following equation³⁹ by using the curve-fitting technique with OriginPro 8.0 program. The error of K_{dim} is the standard deviation of three measurements.

$$\delta_{\text{obs}} = \delta_{\text{m}} + (\delta_{\text{d}} - \delta_{\text{m}}) \frac{1 + 4K_{\text{dim}}[\text{H}] - \sqrt{1 + 8K_{\text{dim}}[\text{H}]}}{4K_{\text{dim}}[\text{H}]}$$

where

$[\text{H}]$ is the total concentration

K_{dim} is the dimerization constant

δ_{m} is the free chemical shift of the monomer

δ_{d} is the limiting bound chemical shift of the dimer

δ_{obs} is the observable chemical shift;

The chemical shifts at each concentration were recorded and fitted into the dimerization equation to determine the optimum solutions for the dimerization constant (K_{dim}), and the bound (δ_{d}) and free chemical shifts (δ_{m}).

Self-dimerization of **8b**

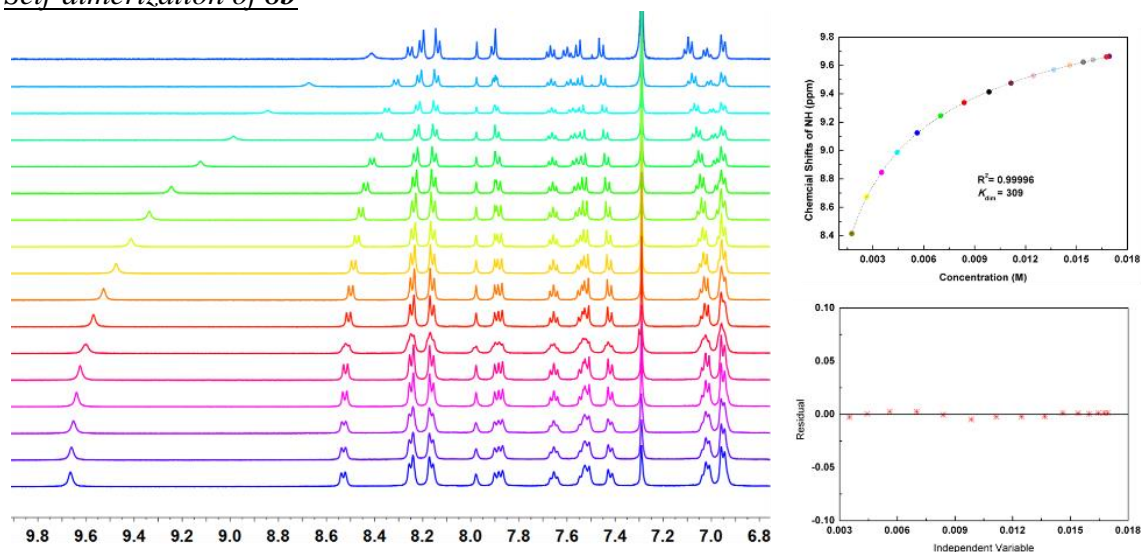


Figure H.19. Stacked partial ^1H NMR spectra of compound **8b** at different concentrations in water-saturated CDCl_3 (298 K). Determination of the dimerization constant of **8b**·**8b**, fitting result based on chemical shifts of phosphoramidate NH.

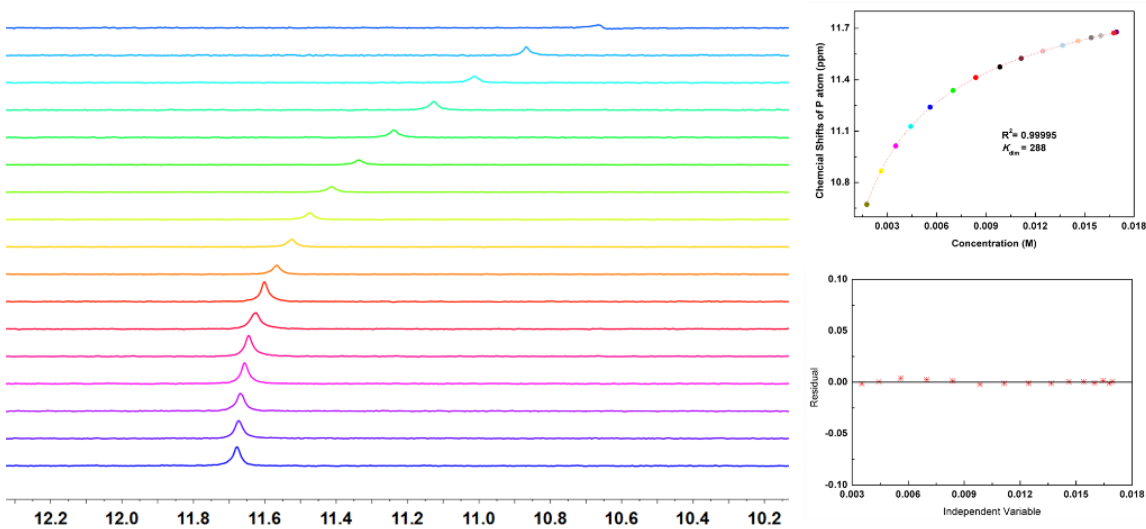


Figure H.20. Stacked partial ^{31}P NMR spectra of compound **8b** at different concentrations in water-saturated CDCl_3 (298 K). Determination of the dimerization constant of **8b**·**8b**, fitting result based on chemical shifts of P atom.

Self-dimerization of 8c

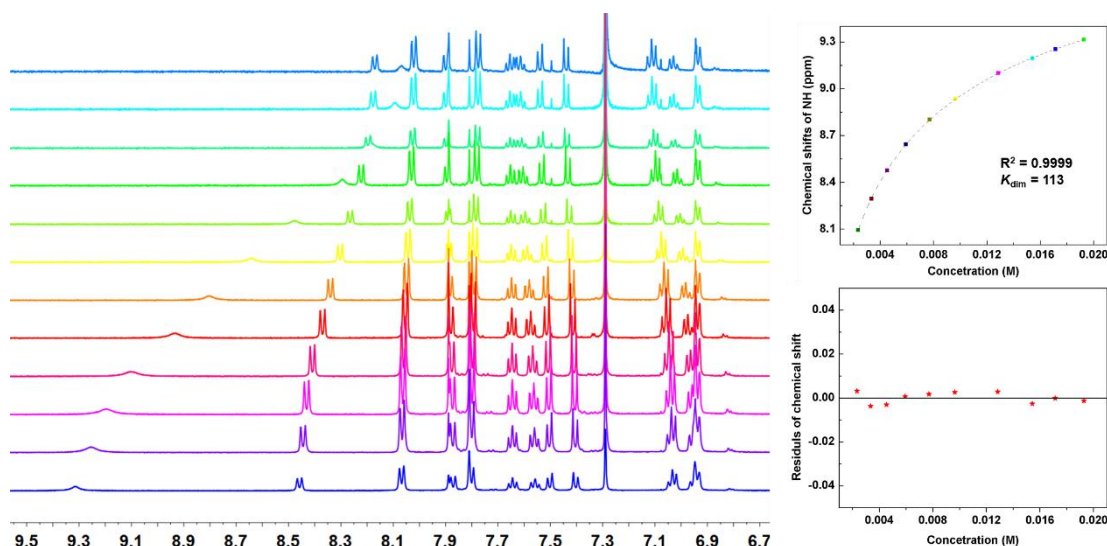


Figure H.21. Stacked partial ^{31}P NMR spectra of compound **8c** at different concentrations in water-saturated CDCl_3 (298 K). Determination of the dimerization constant of **8c**·**8c**, fitting result based on chemical shifts of phosphoramidate NH.

Self-dimerization of 8d

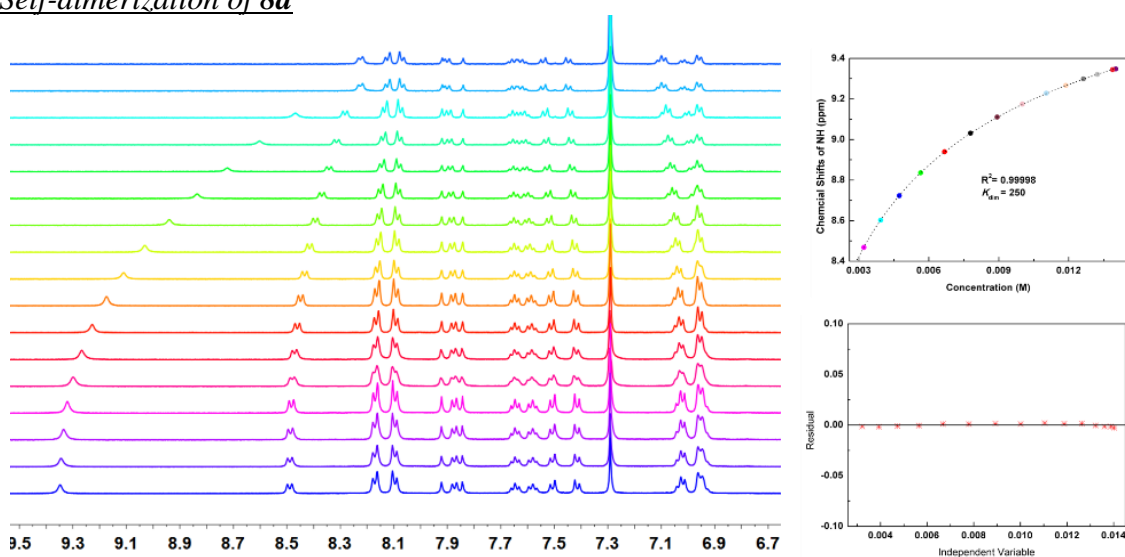


Figure H.22. Stacked partial ^1H NMR spectra of compound **8d** at different concentrations in water-saturated CDCl_3 (298 K). Determination of the dimerization constant of **8d**·**8d**, fitting result based on chemical shifts of phosphoramidate NH.

Self-dimerization of 8e

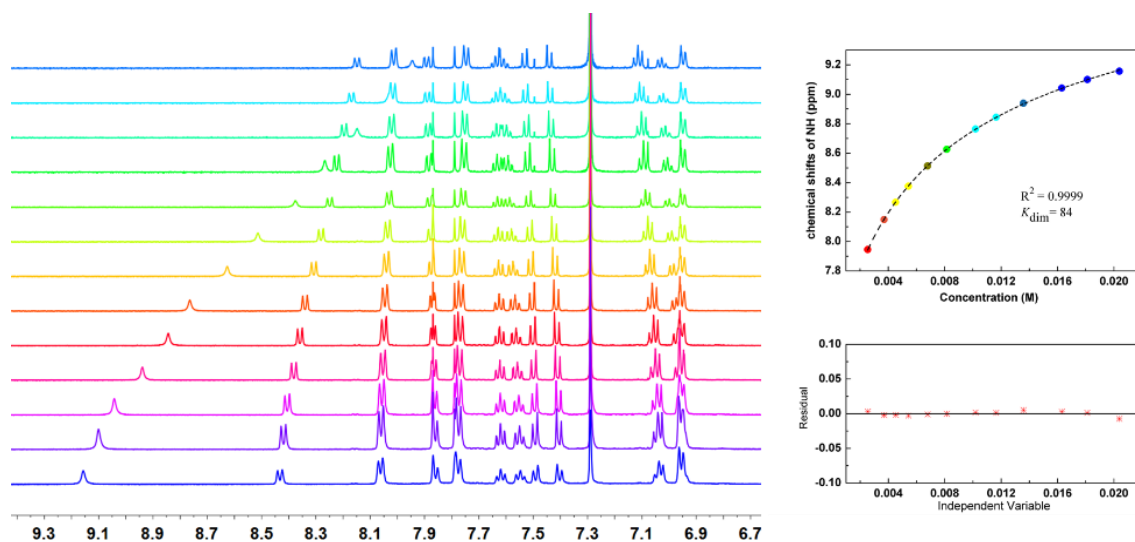


Figure H.23. Stacked partial ¹H NMR spectra of compound **8e** at different concentrations in water-saturated CDCl₃ (298 K). Determination of the dimerization constant of **8e**·**8e**, fitting result based on chemical shifts of phosphoramidate NH.

Self-dimerization of 8f

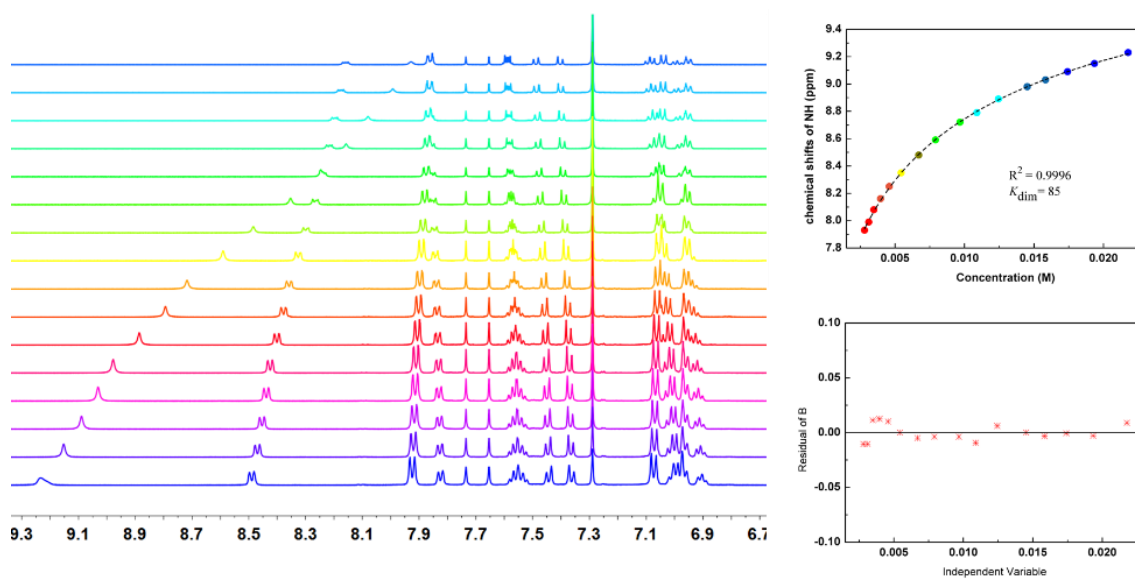
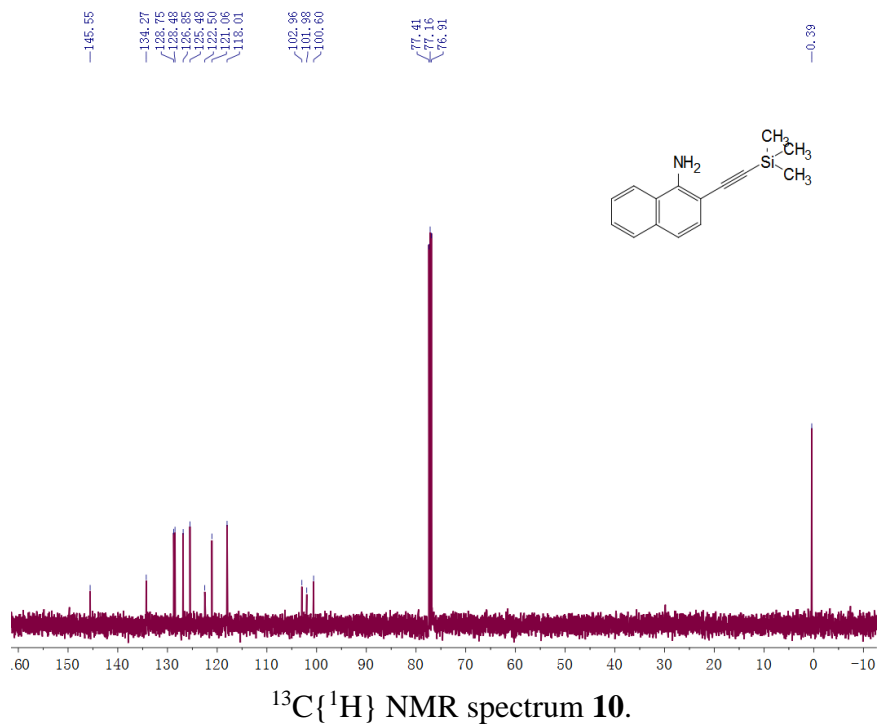
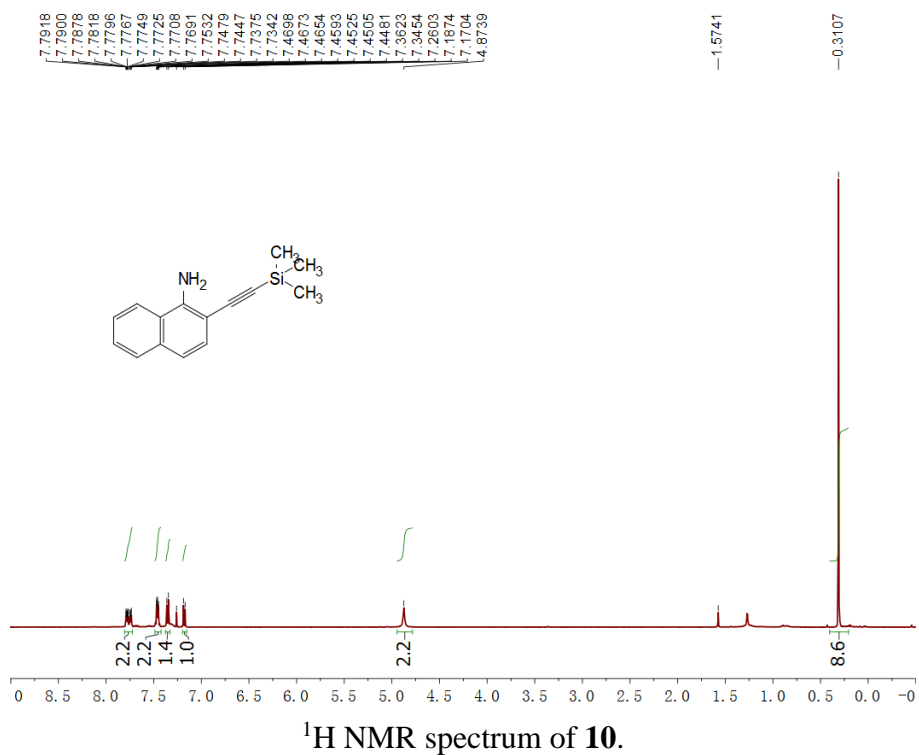
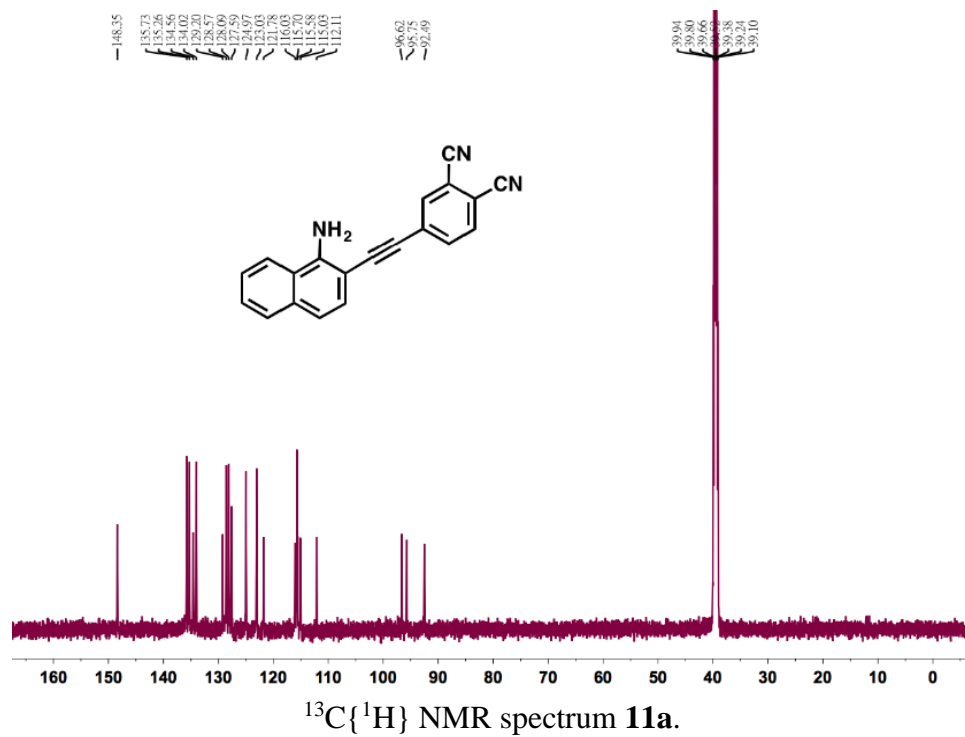
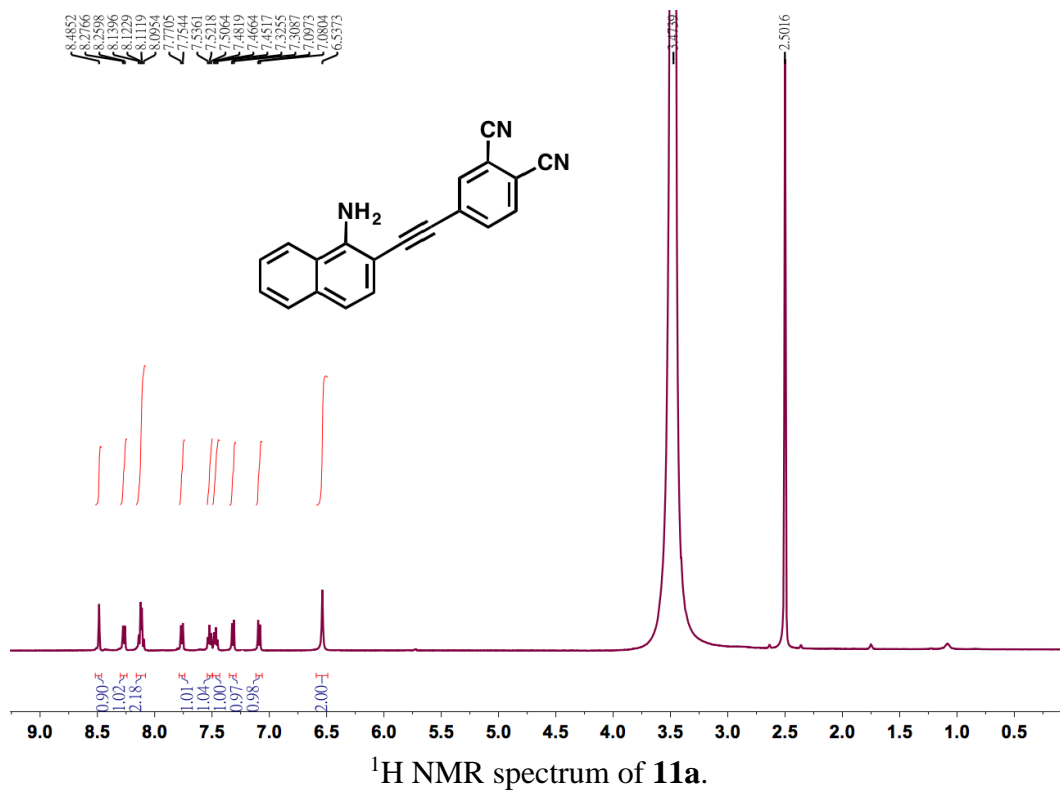
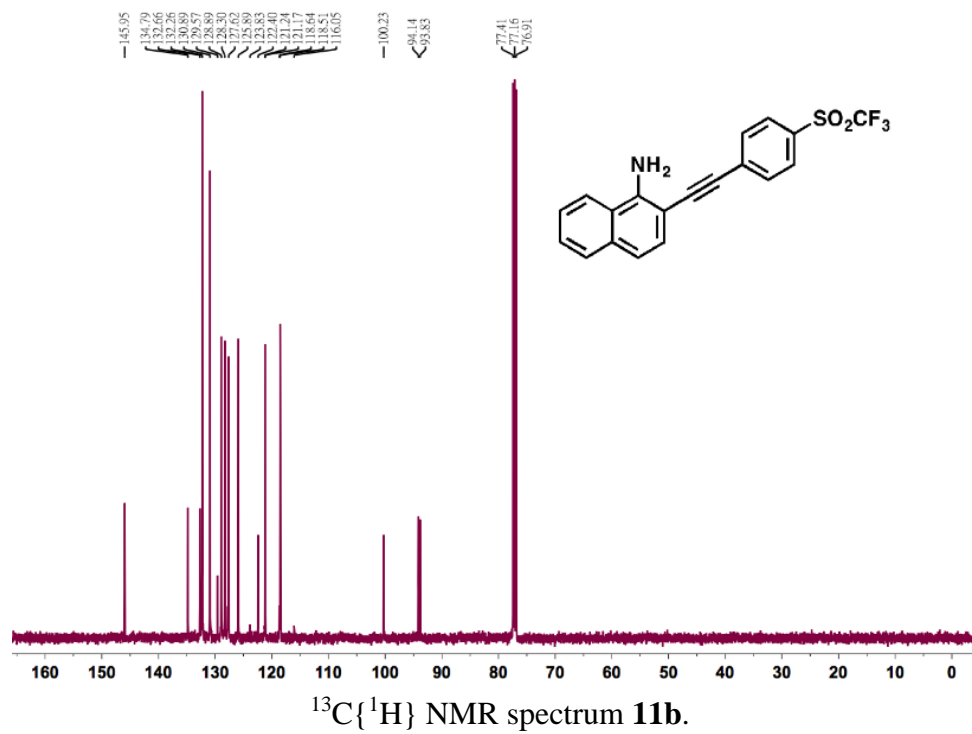
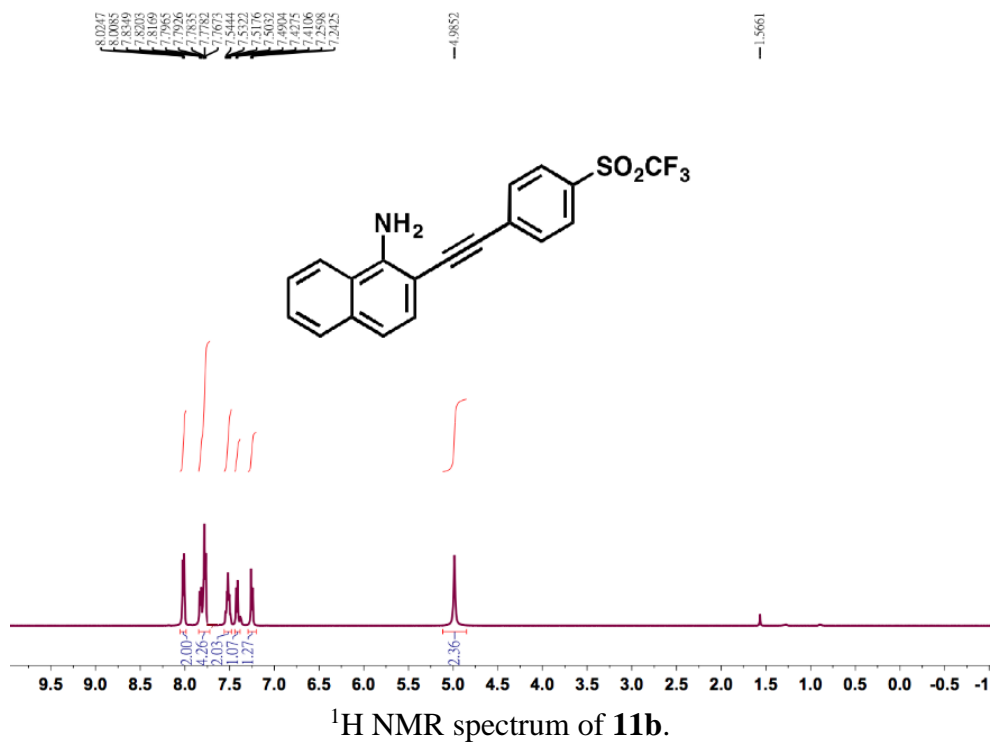


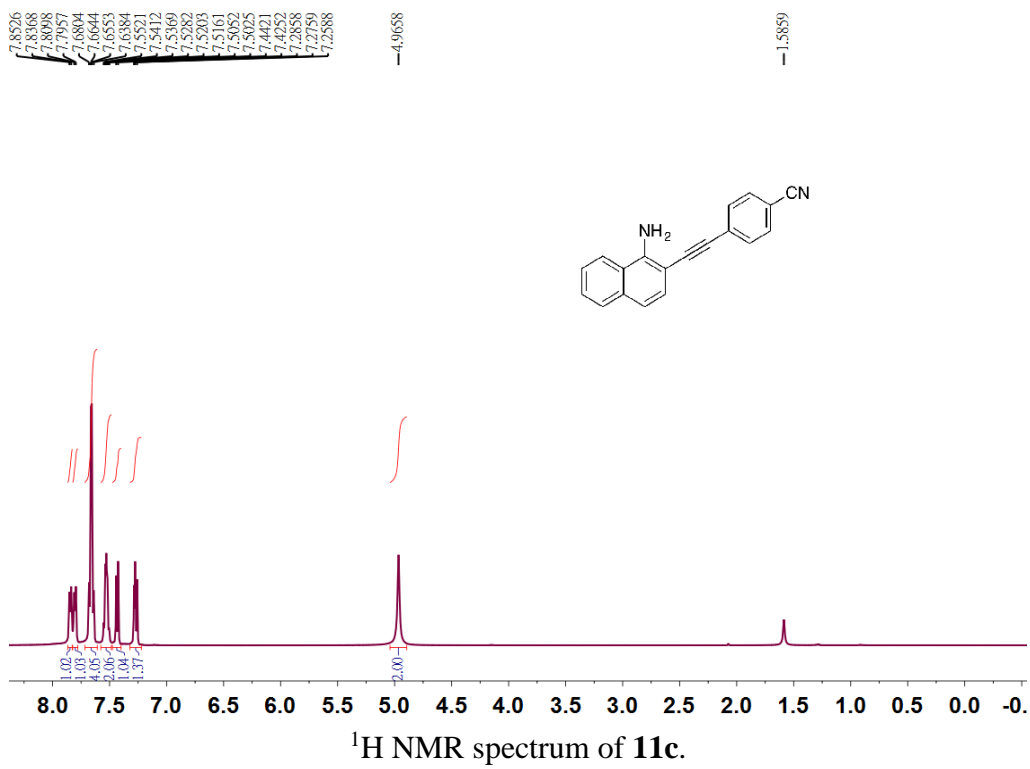
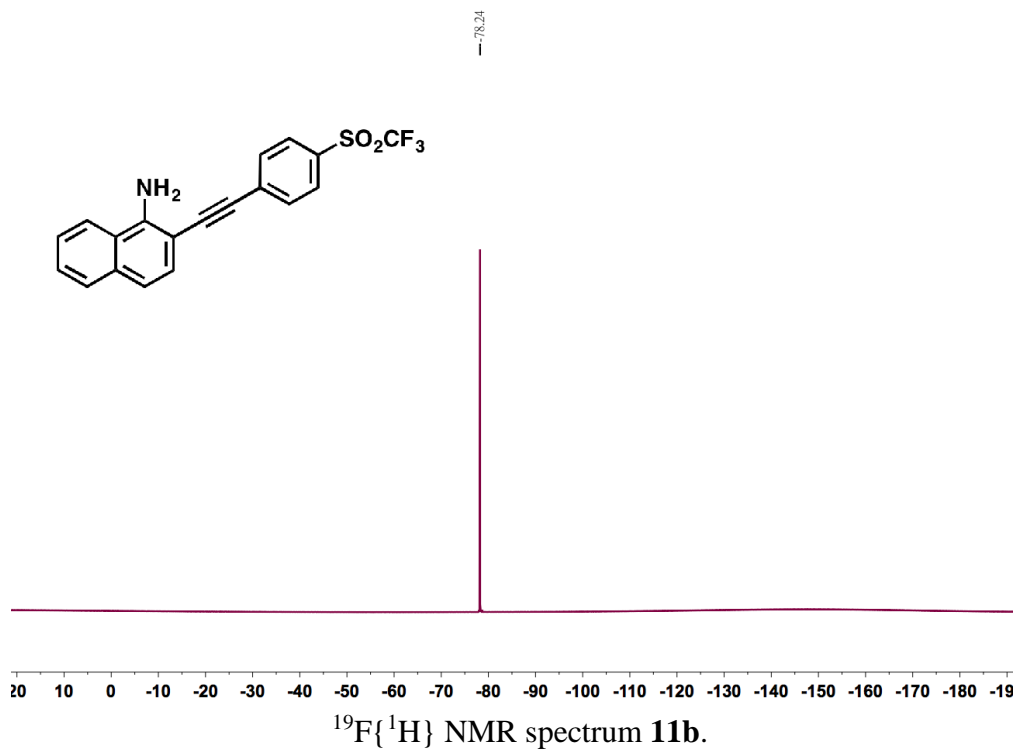
Figure H.24. Stacked partial ¹H NMR spectra of compound **8f** at different concentrations in water-saturated CDCl₃ (298 K). Determination of the dimerization constant of **8f**·**8f**, fitting result based on chemical shifts of phosphoramidate NH.

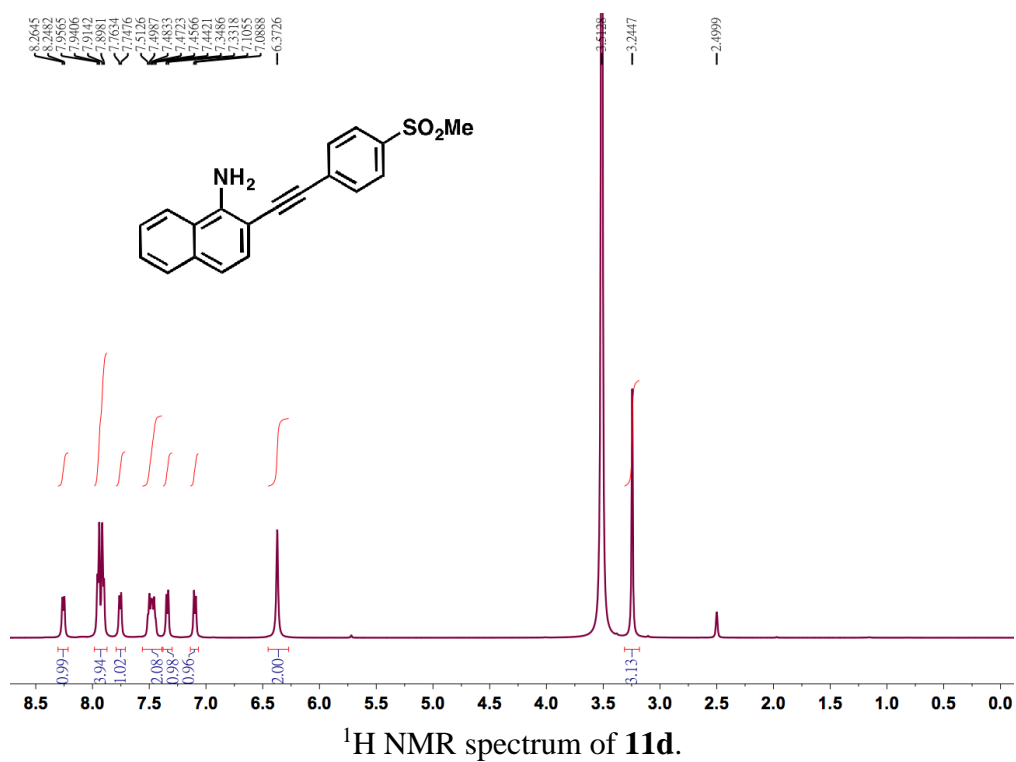
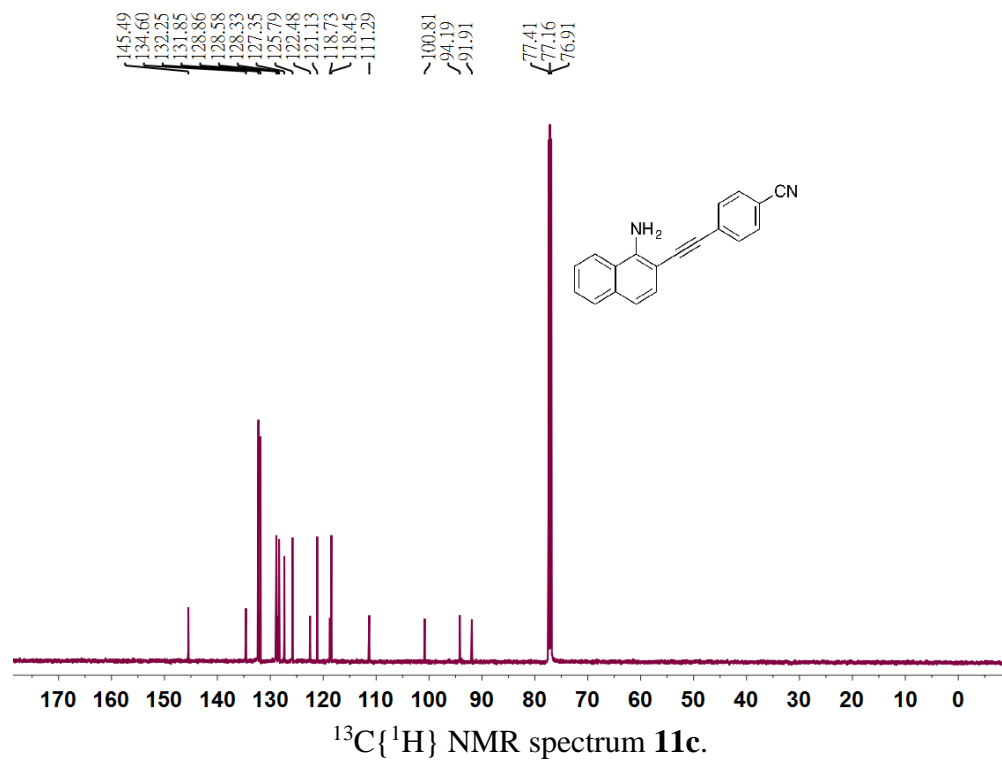
6. Copies of NMR Spectra for New Compounds

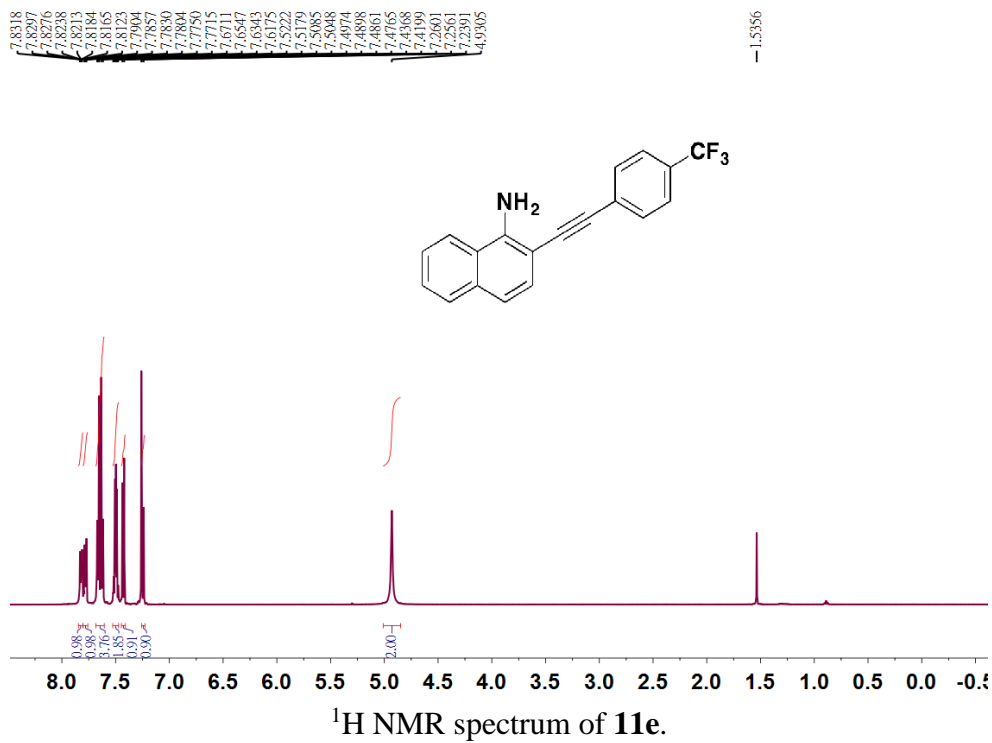
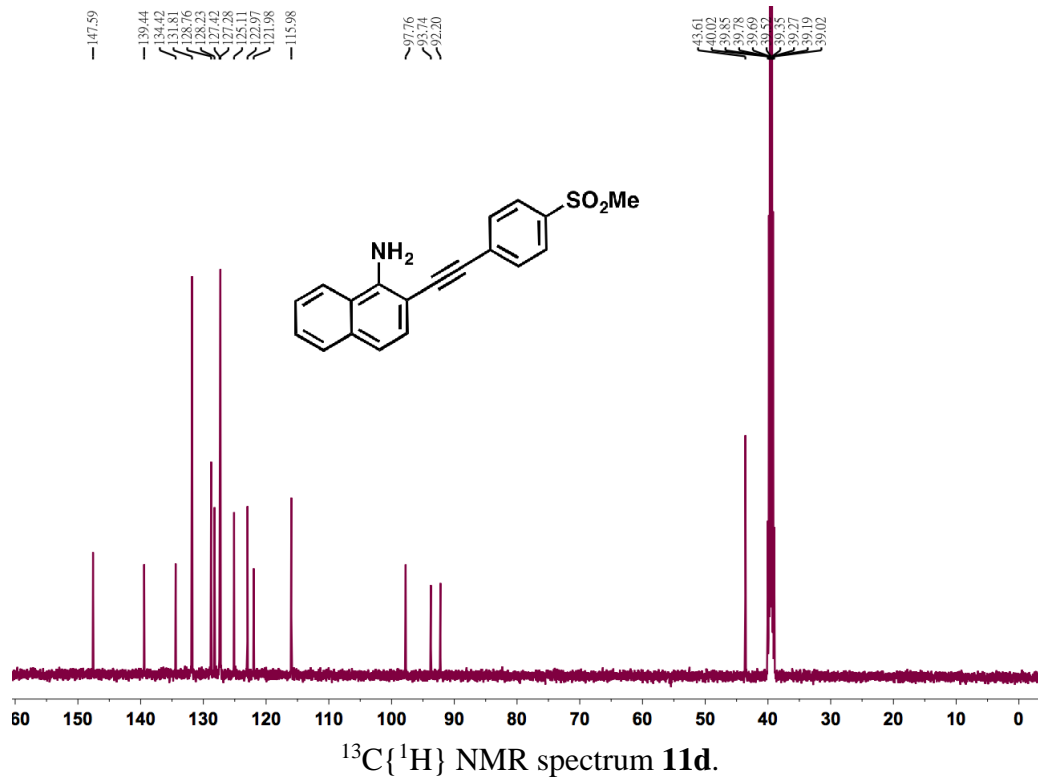


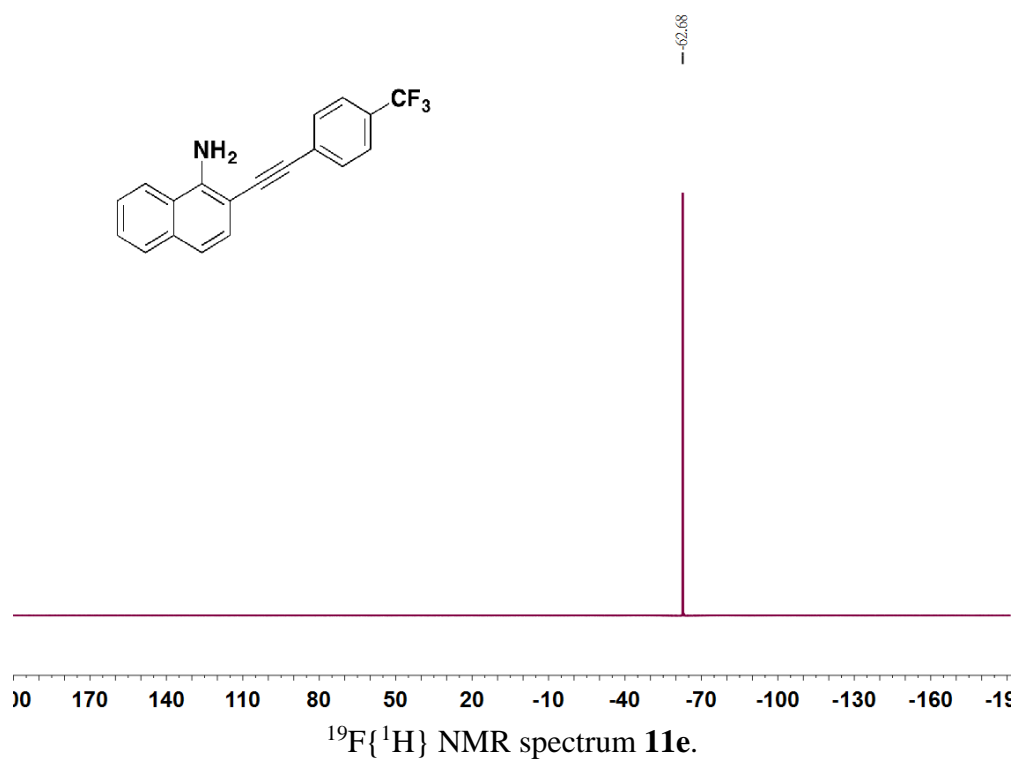
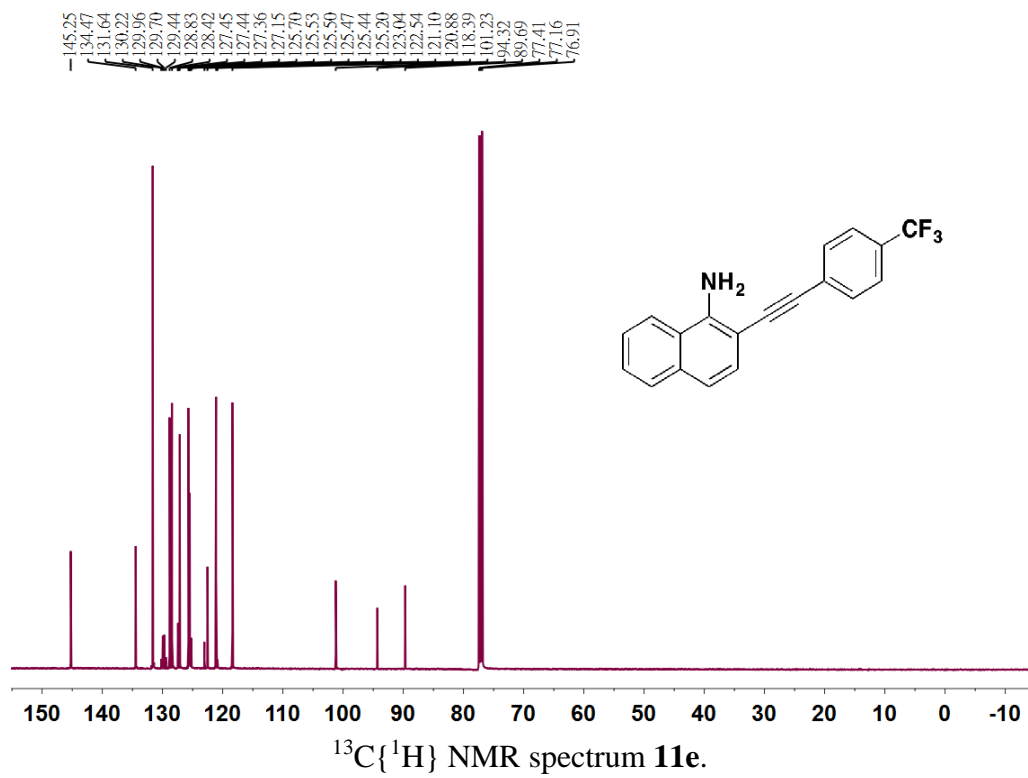


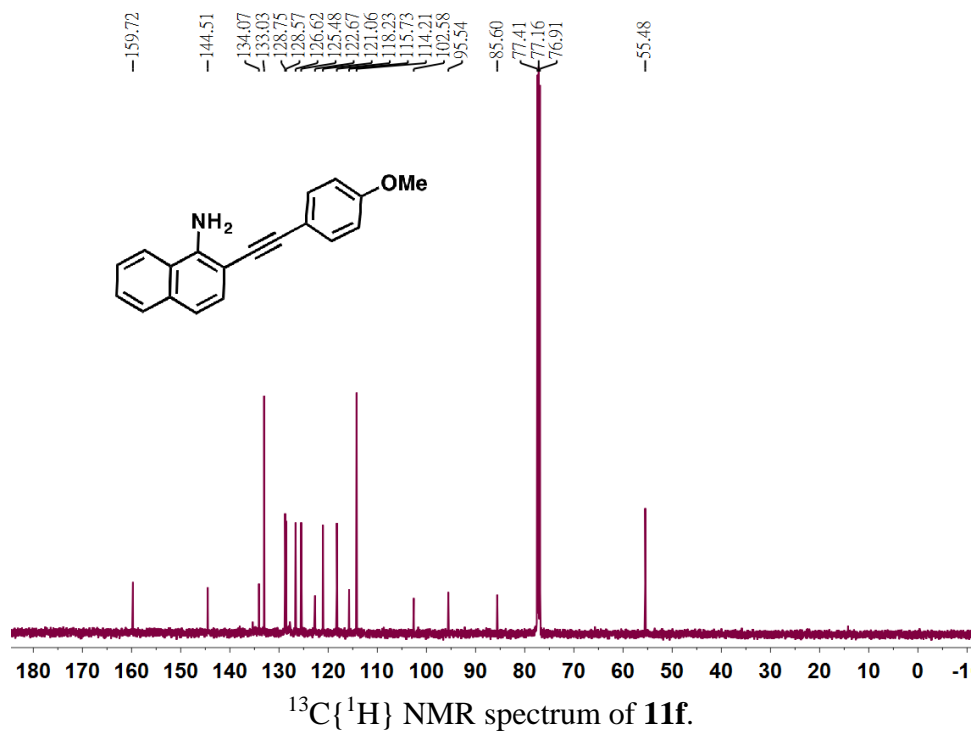
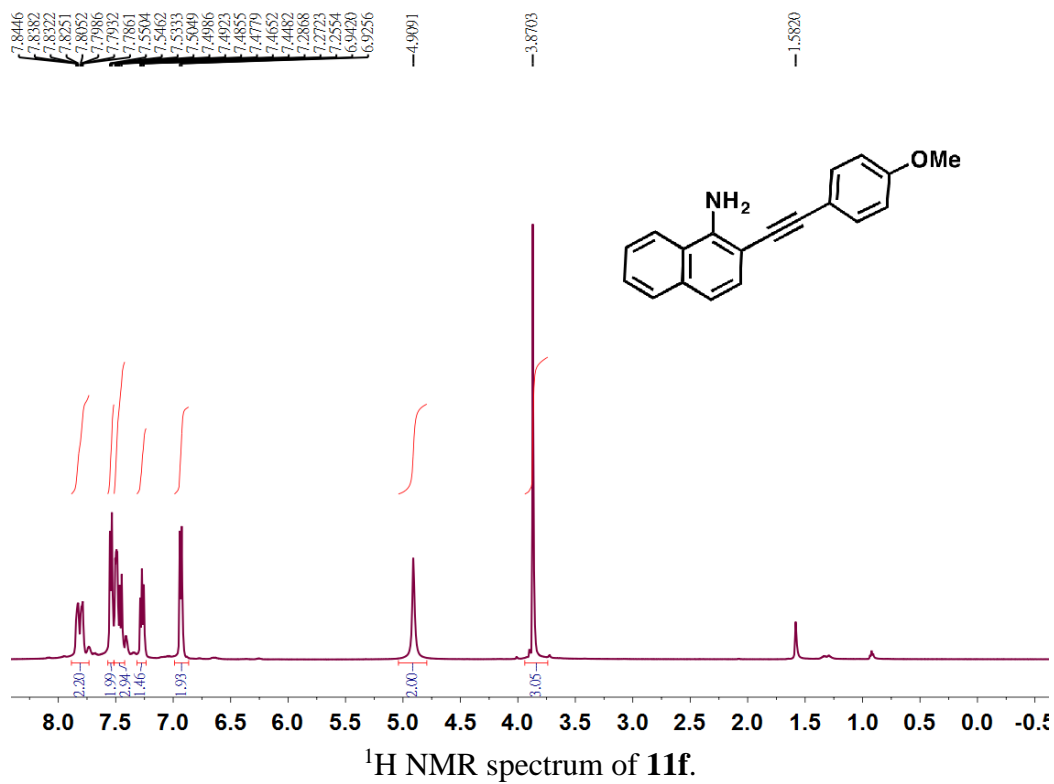


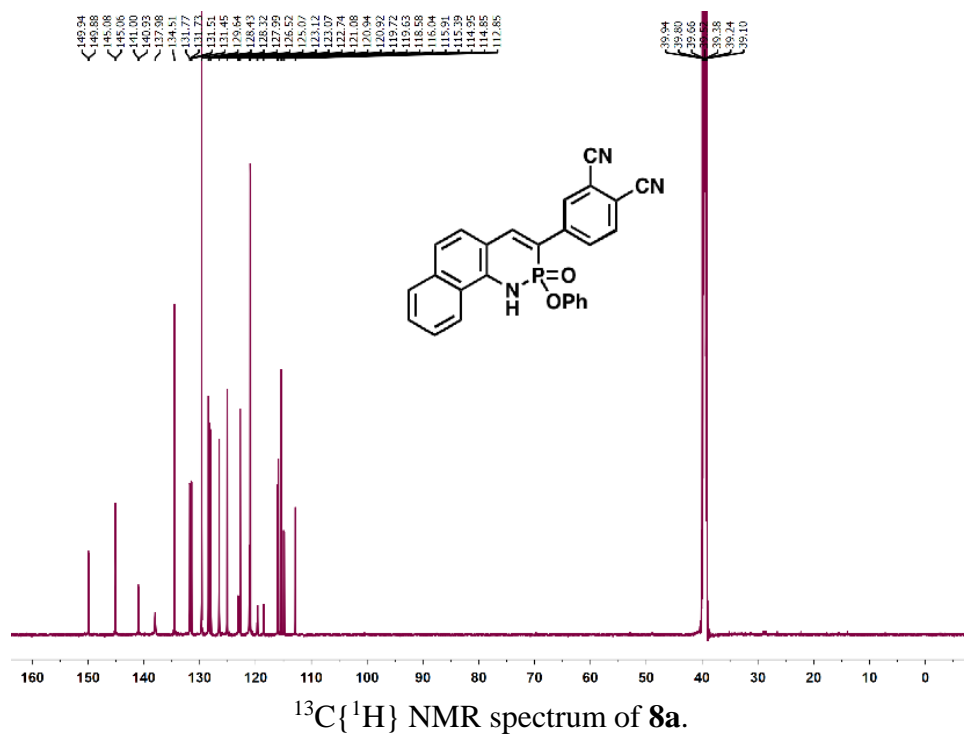
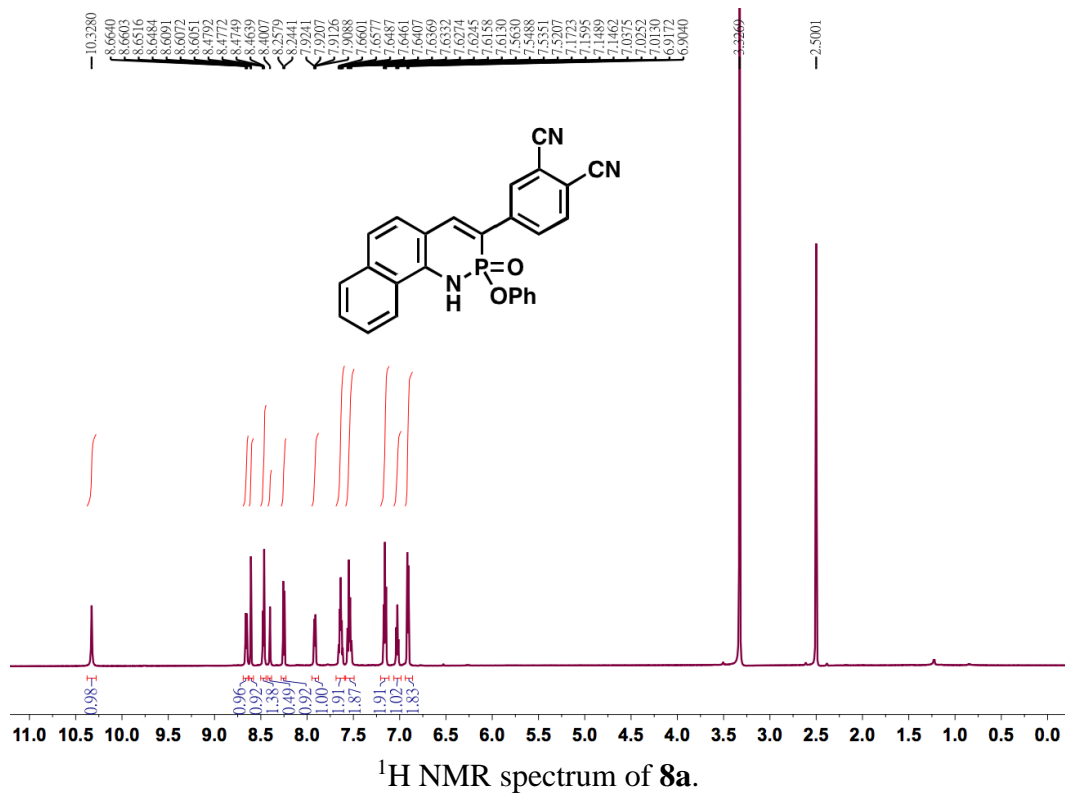


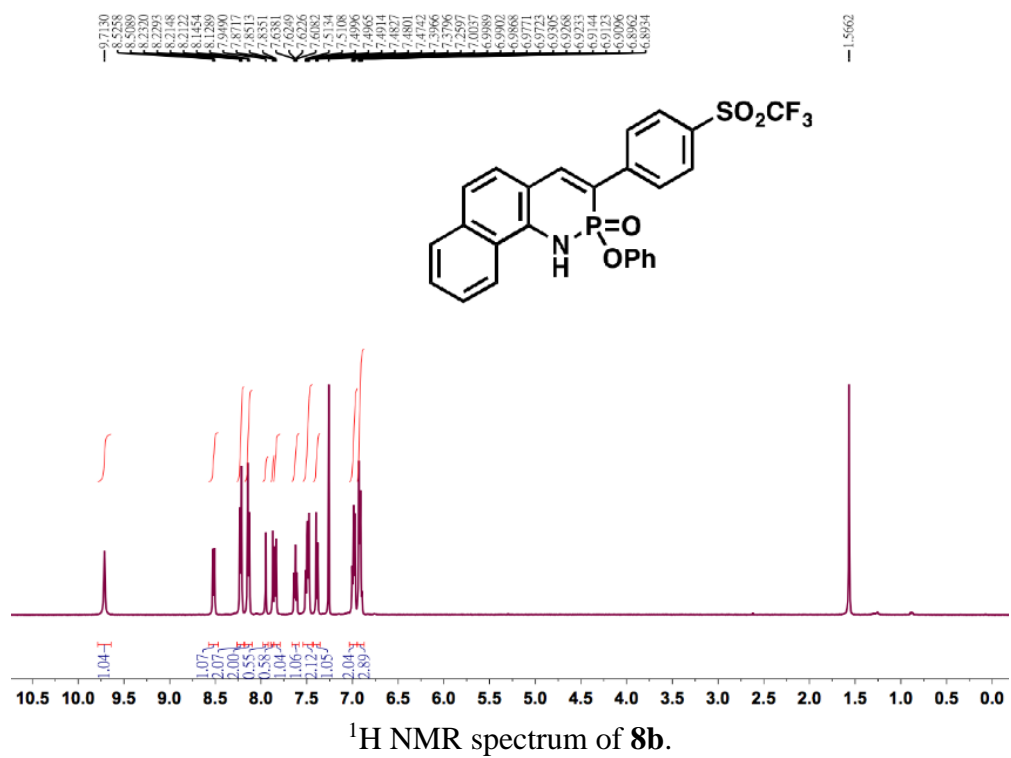
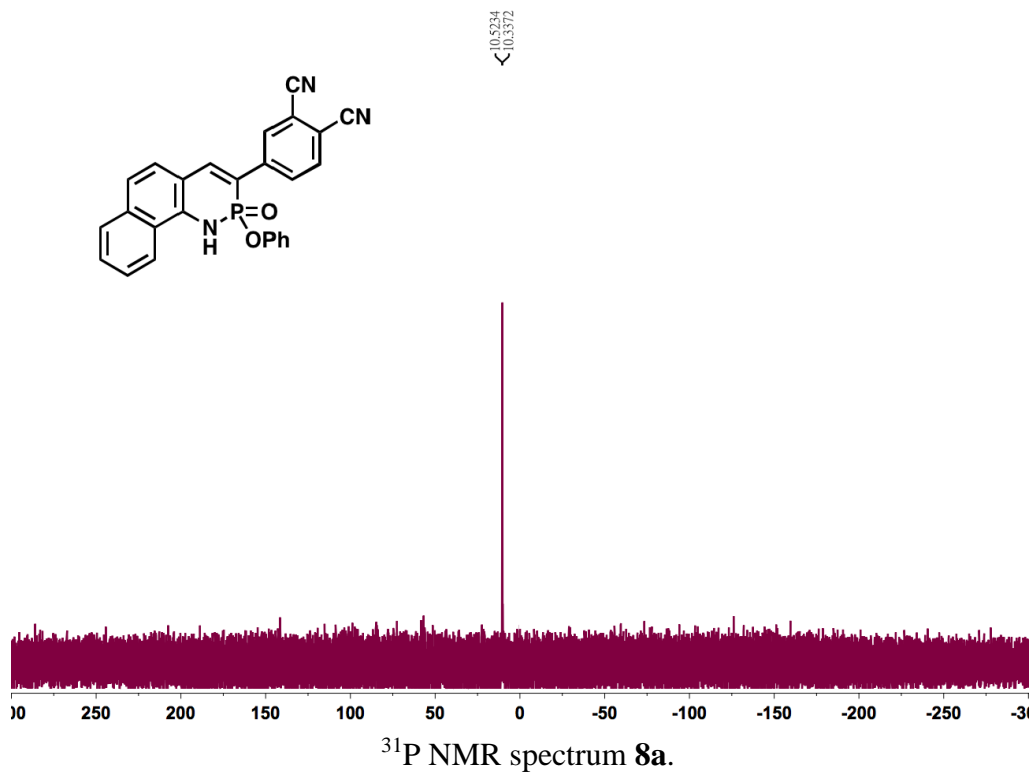


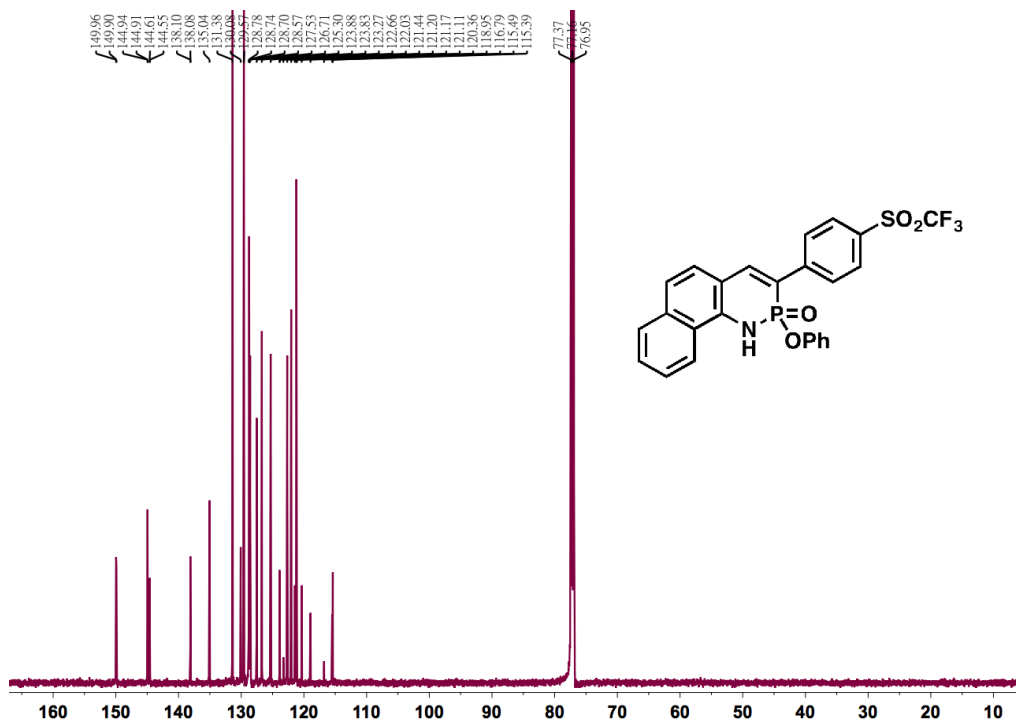




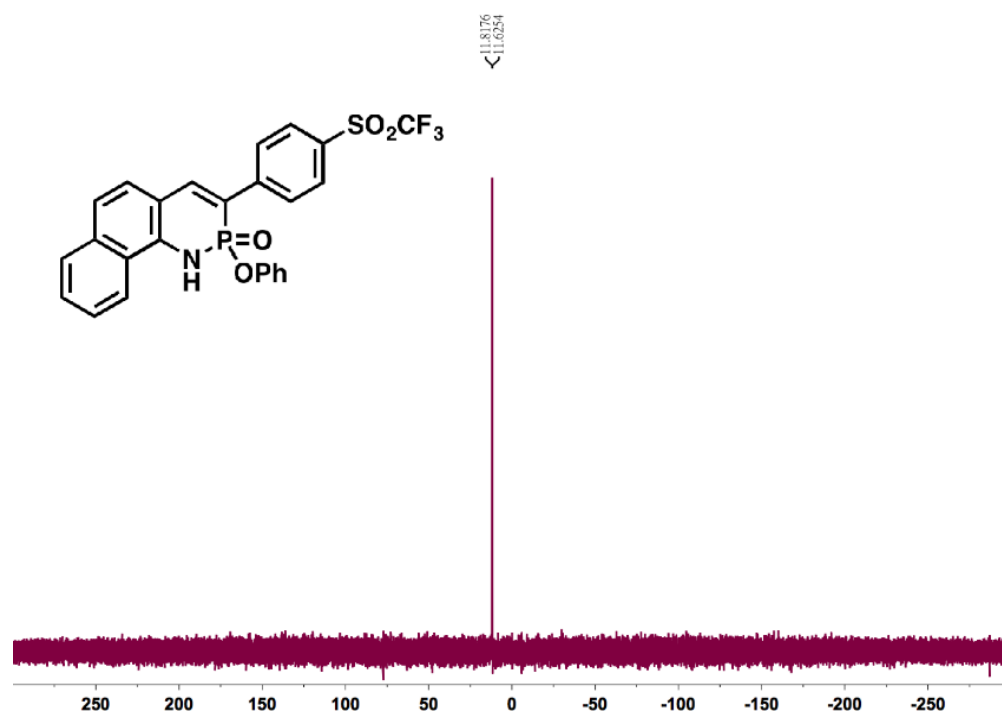




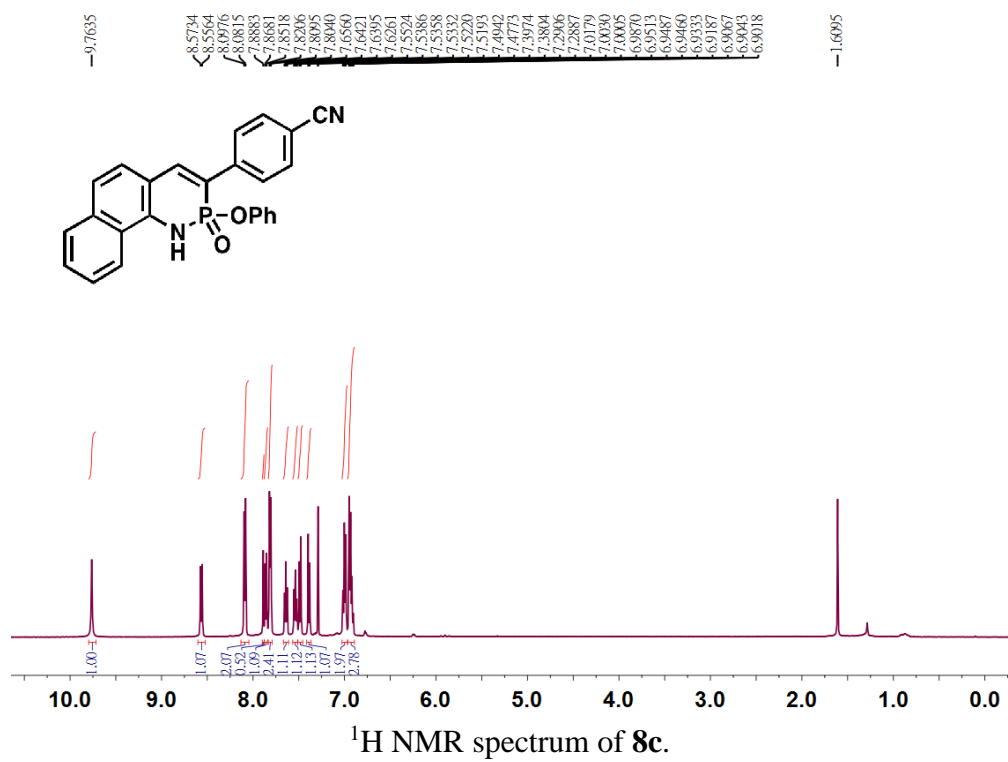
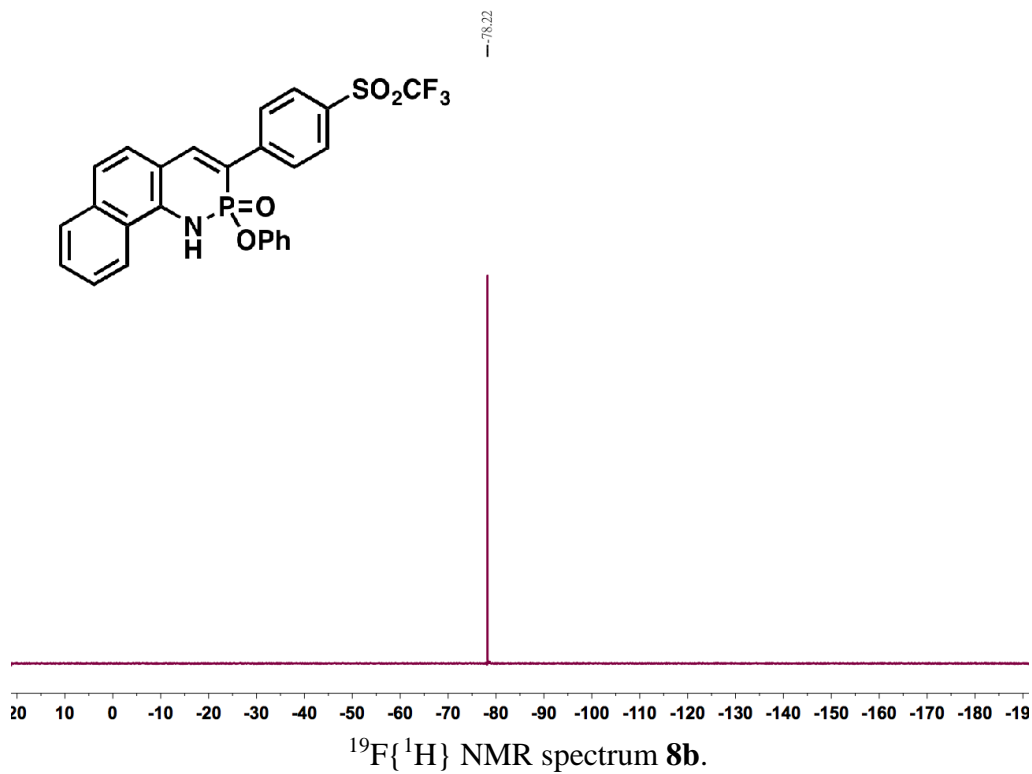


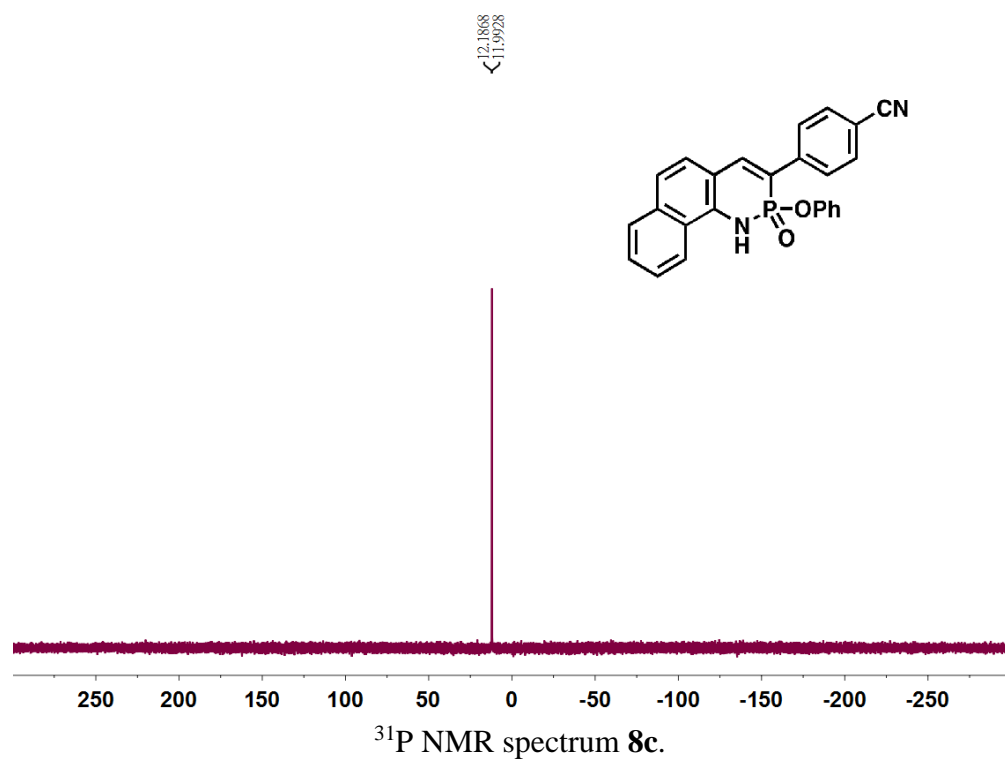
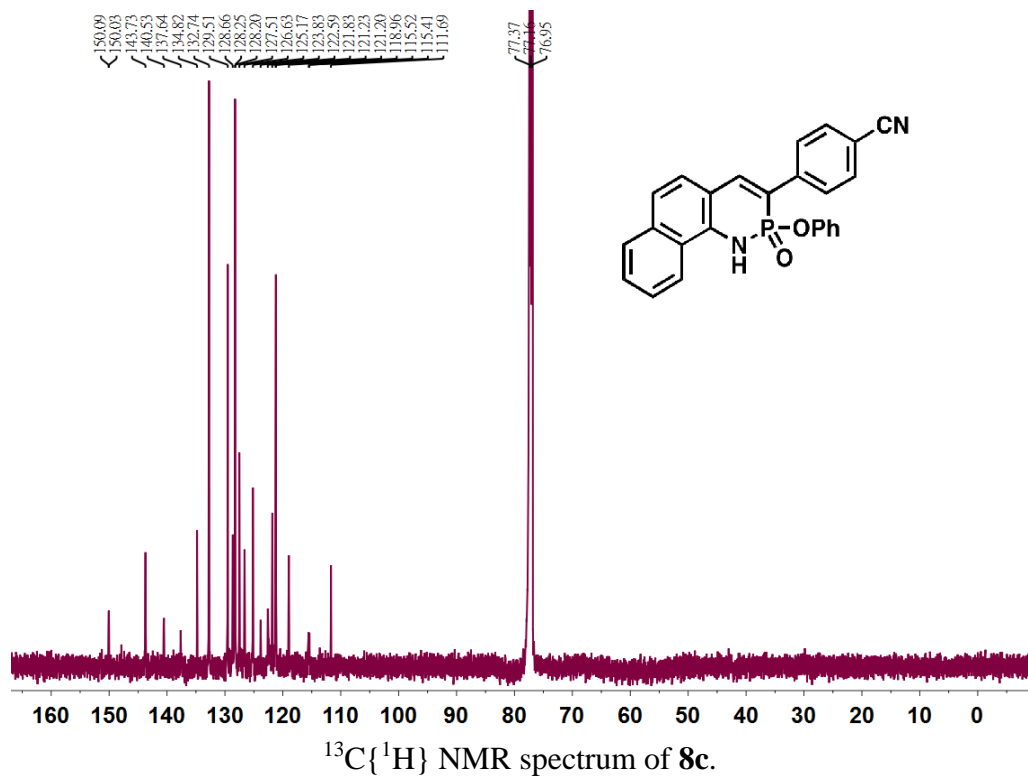


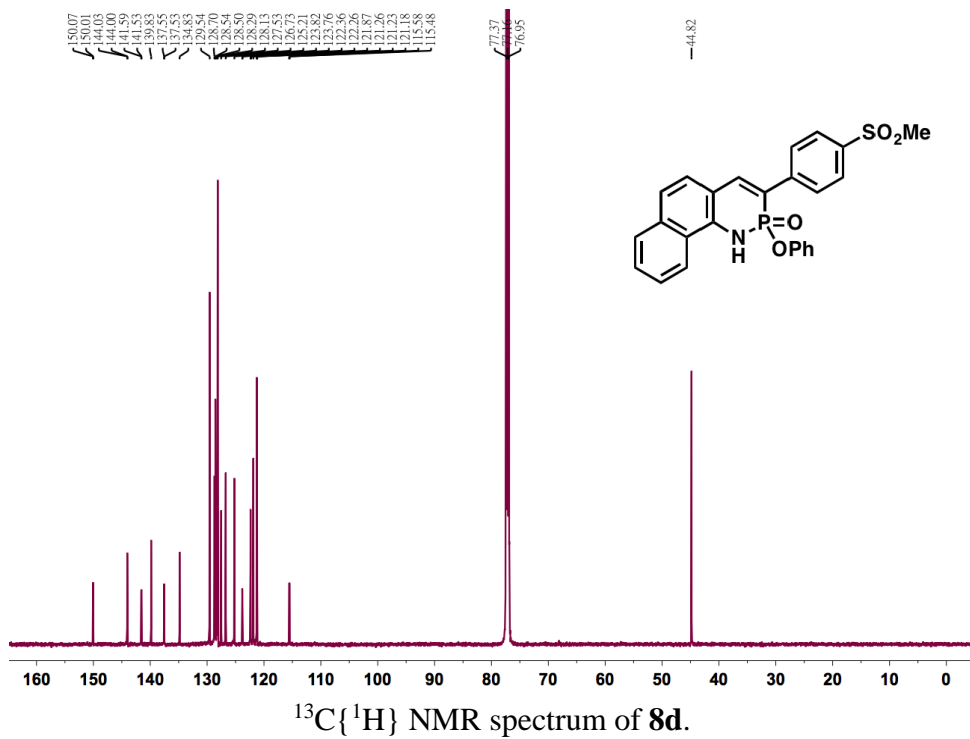
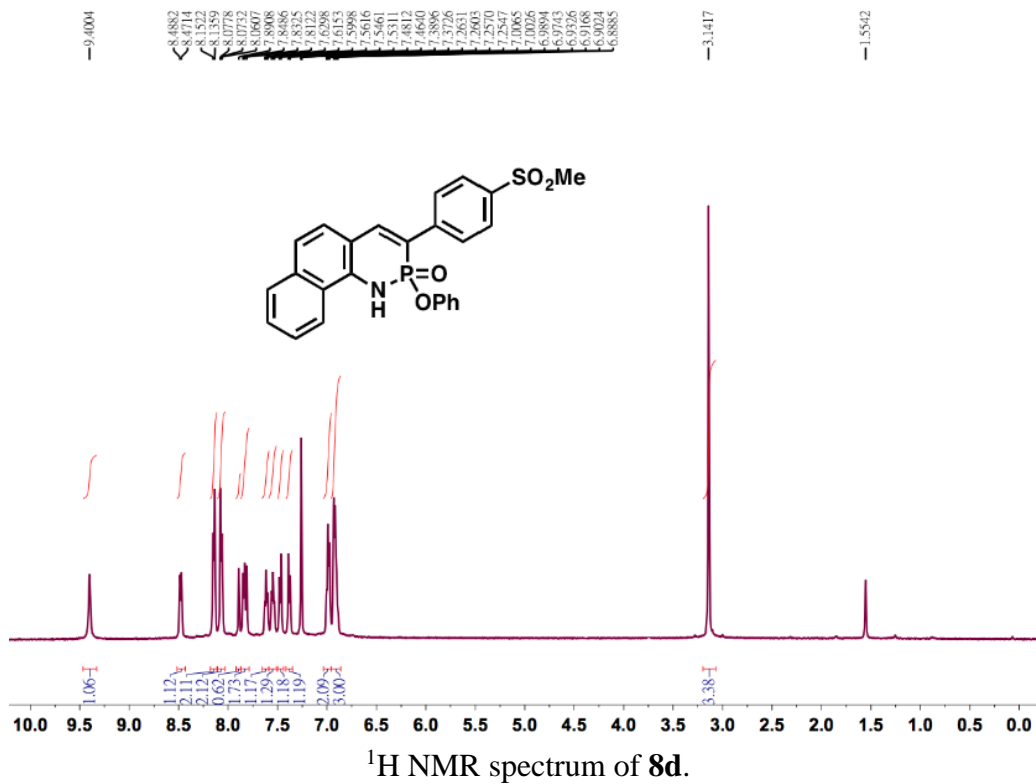
$^{13}\text{C}\{^1\text{H}\}$ NMR spectrum of **8b**.

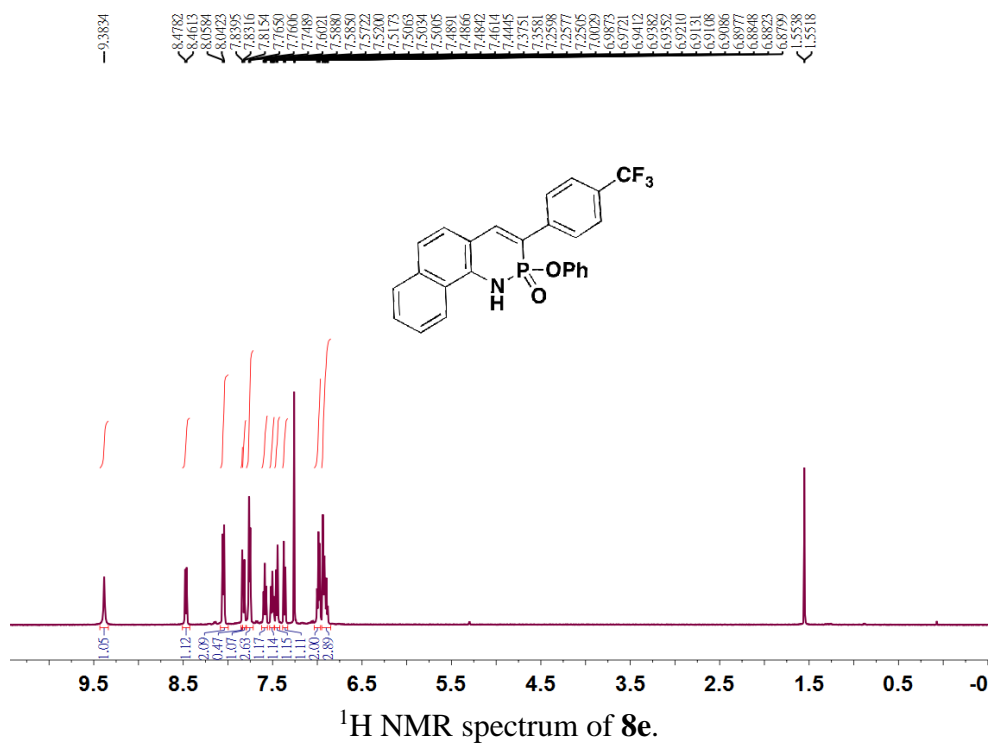
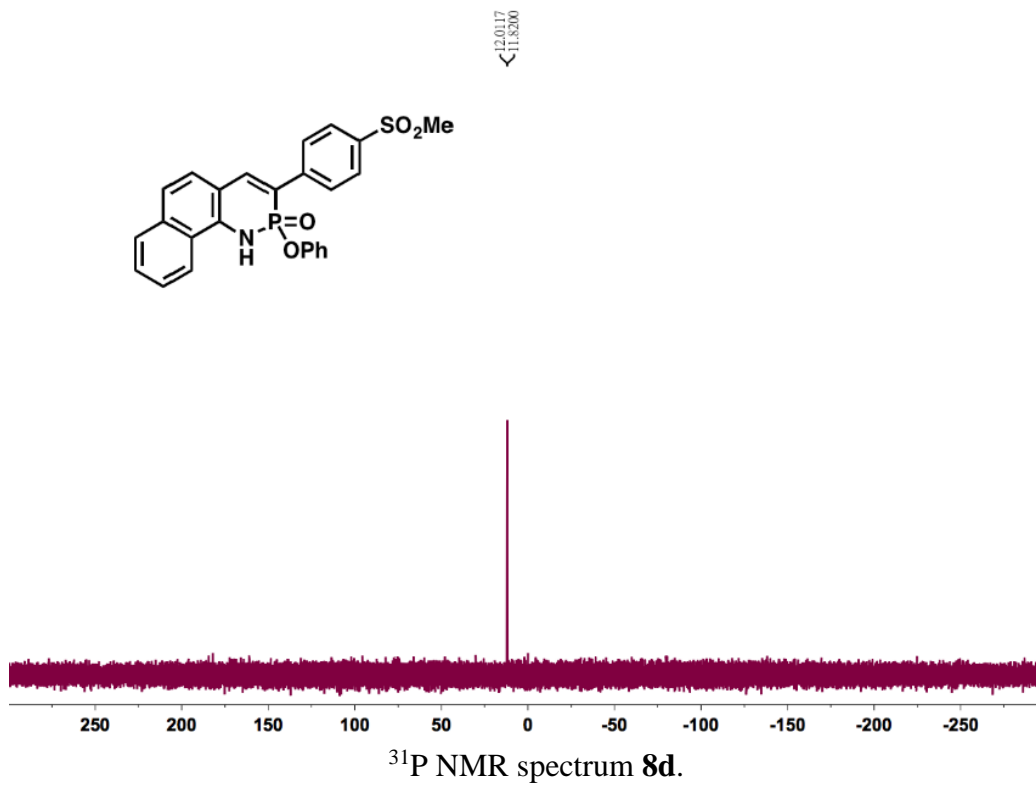


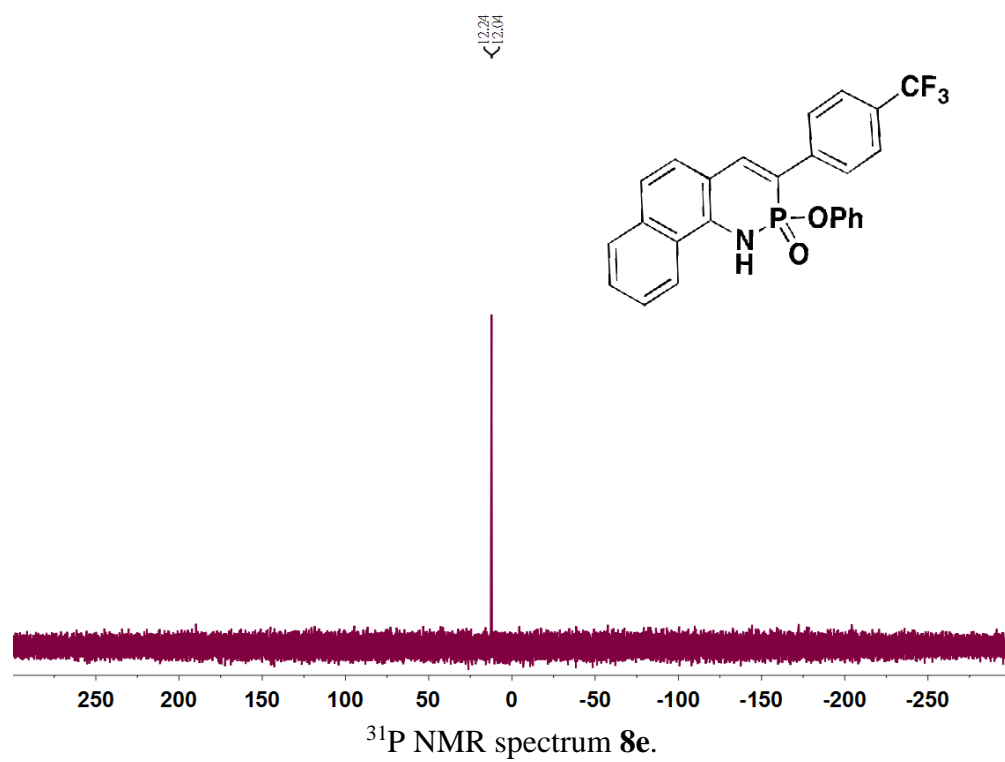
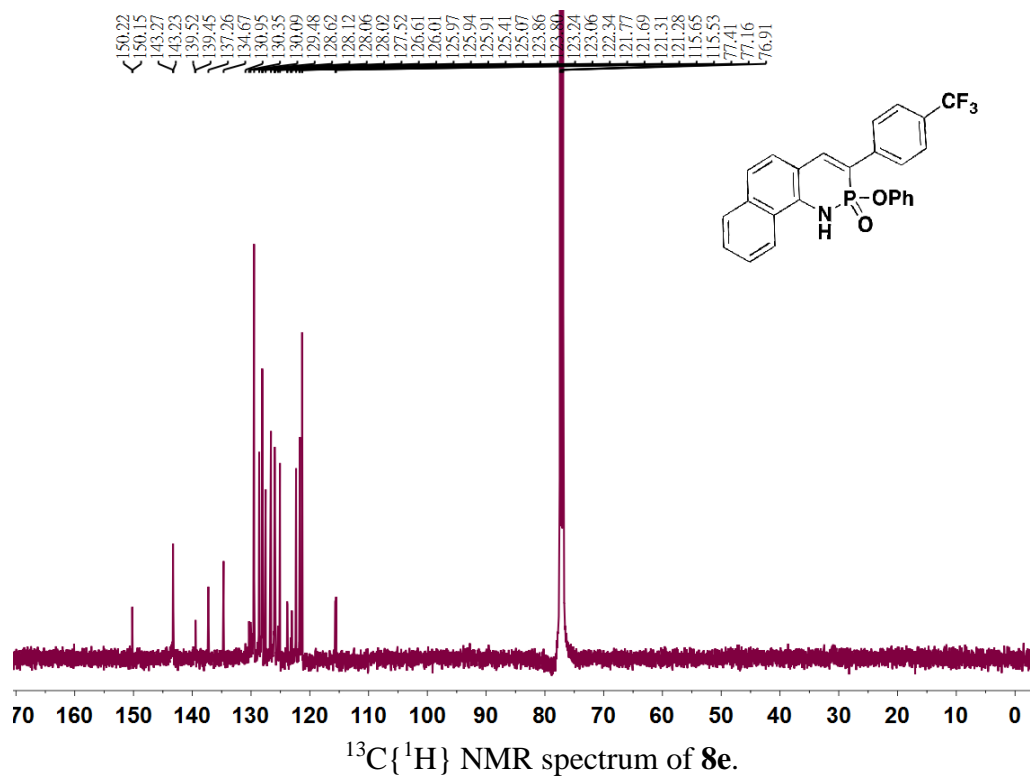
^{31}P NMR spectrum **8b**.

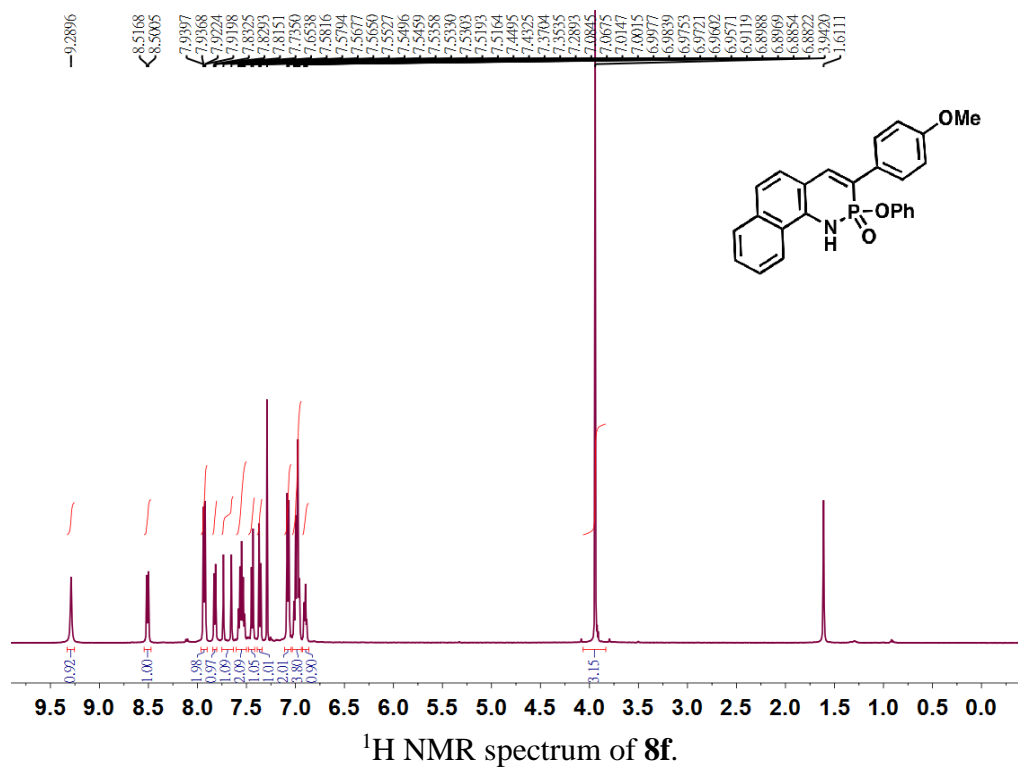
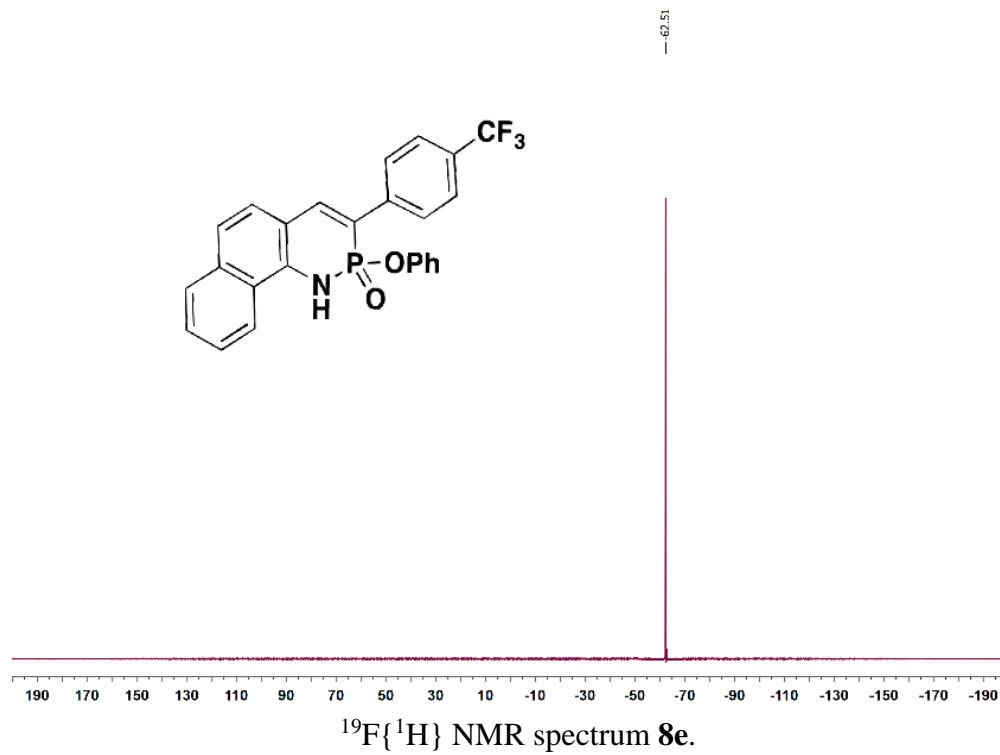


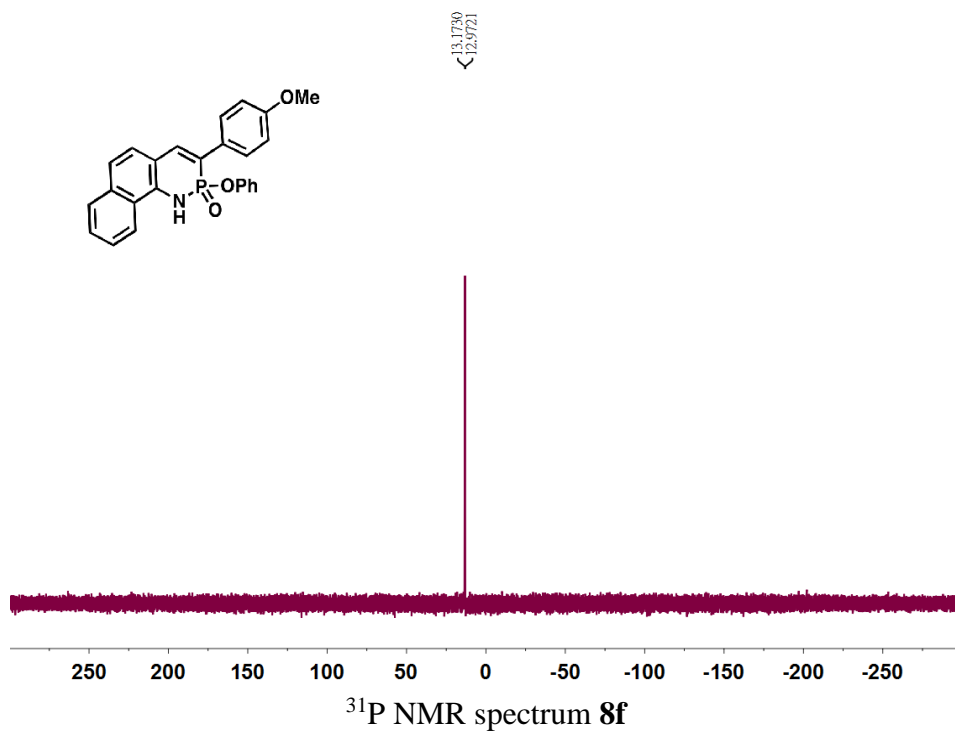
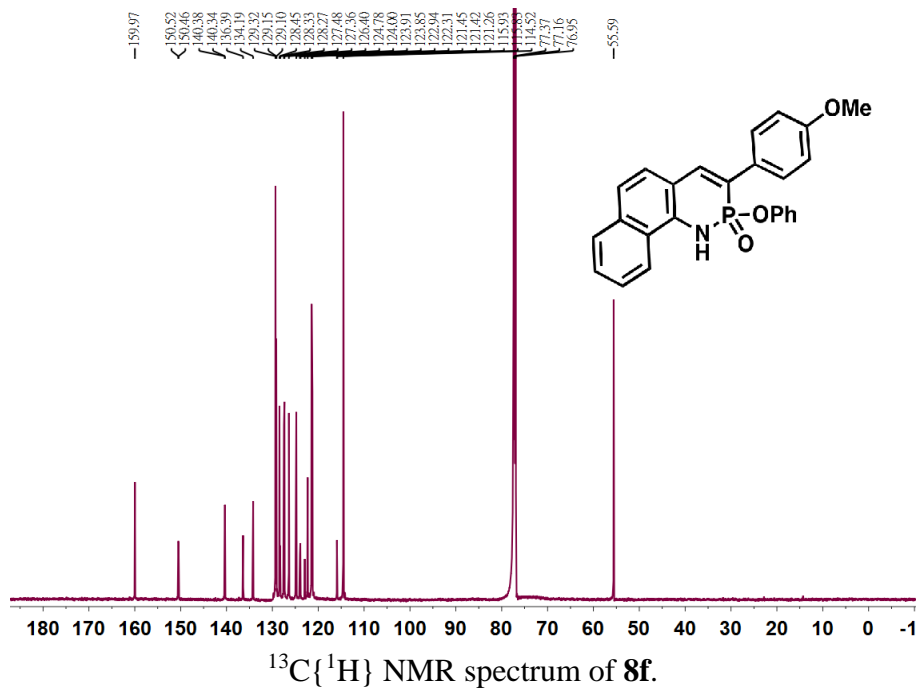












APPENDIX I

PN-CONTAINING PYRENE DERIVATIVES: SYNTHESIS, STRUCTURE, AND PHOTOPHYSICAL PROPERTIES (WITH SUPPLEMENTARY INFORMATION)

This Appendix includes previously published and co-authored material from Deng, C.-L., Bard, J.P., Zakharov, L.N., Johnson, D.W., Haley, M.M. “PN-Containing Pyrene Derivatives: Synthesis, Structure and Photophysical Properties.” *Org. Lett.* **2019**, *21*, 6427–6431 and the associated Supplementary Information document. The bulk of the writing and synthesis for this study was performed by Dr. Chun-Lin Deng, with assistance from Jeremy P. Bard. Editorial support was provided by Michael M. Haley and Darren W. Johnson.

Introduction:

Among various polycyclic aromatic hydrocarbons (PAHs), pyrene and its derivatives are of great interest because of their unique optical properties, outstanding chemical stability, good hole transporting ability, and their applications in organic electronic devices¹ and chemosensors.² When used as light-emitting materials, however, there are some drawbacks for the parent pyrene such as deep blue emission with a small Stokes shift and the formation of fluorescence quenching π -aggregates/excimers in condensed media.³ As a result, numerous efforts have been devoted for improving/altering the photophysical properties. The most common synthetic strategy for developing novel pyrene derivatives is to introduce various substituents at the 1/3/6/8-positions, 4/5/9/10-positions (the K-region),

and 2- or 2/7-positions on the pyrene core (Figure I.1a).⁴ Despite these efforts, the preparation of multisubstituted pyrenes at the non-K-region (1/2/3- and/or 6/7/8-positions) is still rather challenging.

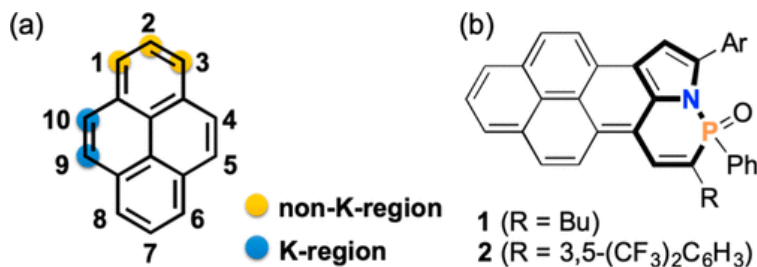


Figure I.1 (a) Numbering system for pyrene and its K-region and non-K-region. (b) Chemical structures of **1** and **2** in this work.

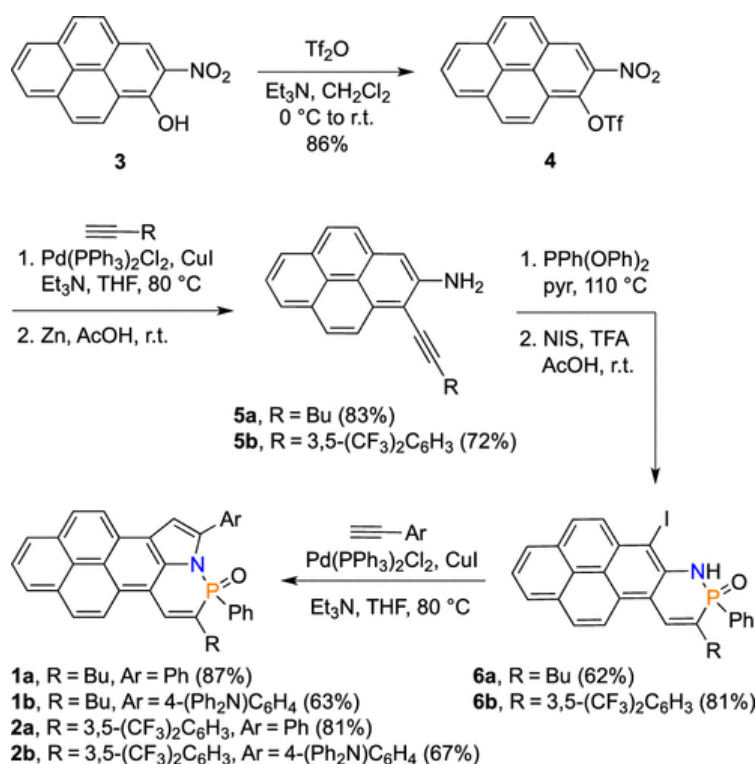
The main group element-containing PAHs are strongly attractive since the incorporation of electron-donating/electron-accepting heteroatoms could readily tailor the electronic structures and also affect the intermolecular interactions due to their unique molecular geometries, which can be used to modulate the molecular solubility/morphology.⁵ These appealing characteristics make heteroatom-containing PAHs promising candidates for better-performing luminescent materials and organic electronics.⁶ Although there have been extensive studies on heterocycle-fused pyrenes on the K-region⁷ or heteroatom-functionalized pyrene derivatives at the “conventional” sites,^{4a,8} only a handful of non-K-region fused heterocycles such as sulfur-bridged pyrene-thienoacene,⁹ pyrene-benzo[*b*]phosphole and -benzo[*b*]silole,¹⁰ B,O-annelated pyrene derivative,¹¹ and BN Lewis pair chelated pyrenes¹² have been developed thus far. Nonetheless, their electronic structures and emission properties were altered only to a limited extent, suggesting that additional synthetic efforts remain to achieve a dramatic change in pyrene optoelectronic/redox properties within a general molecular framework.

In parallel with our efforts to devise novel fluorescent PN-heterocycles,¹³ we describe herein the preparation and photophysical properties of two types of non-K region fused PN-heterocyclic pyrene derivatives **1** and **2** (Figure I.1b) by a straightforward synthetic strategy. An important feature of this class of pyrene derivatives is that the optoelectronic/redox properties can be remarkably and rationally tuned by simple switching of the pendant substituents. Density functional theory (DFT) calculations¹⁴ revealed that the carbon atomic coefficients of the highest occupied molecular orbital (HOMO) for the PN-embedded core is dominant at the carbon atom connecting the -Ar group (C_{Ar}), while the carbon atom connecting the -R group (C_R) has a larger contribution to the lowest unoccupied molecular orbital (LUMO) (see Supplementary Information section below). It is expected that introduction of an electron-donating group (EDG) at C_{Ar} and an electron-withdrawing group (EWG) at C_R would readily destabilize and stabilize the HOMO and LUMO levels, respectively. The electronic perturbations and substituent effects on the parent core might trigger a bathochromic shift of λ_{em} as well as provide modifiable energy levels.

Results and discussion

The modular syntheses of pyrene derivatives **1** and **2** are shown in Scheme I.1. The key steps involve a PPh(OPh)₂-mediated cyclization and a one-pot sequential Sonogashira cross-coupling/heteroannulation. The synthesis of PN-fused pyrene **1** commenced with the conversion of the hydroxyl group of 1-hydroxy-2-nitropyrene **3** to triflate **4** by treatment with trifluoromethanesulfonic anhydride. Sonogashira cross-coupling of **4** with 1-hexyne followed by subsequent reduction of the nitro group using zinc powder furnished amine **5a**. Treatment of **5a** with PPh(OPh)₂ in boiling pyridine followed by *in situ* hydrolysis as

described previously^{13a} gave the crude phosphinamidate after minimal purification. We found that the resultant PN-heterocycle can be exclusively monoiodinated at the 3-position of the pyrene using NIS to afford **6a**. Finally, the Sonogashira cross-coupling/*5-endo-dig* cyclization sequences using the appropriate arylacetylene provided PN-heterocycles **1a** and **1b** in 87% and 63% yield over the two steps, respectively. Compounds **2a/2b** with 3,5-bis(trifluoromethyl)phenyl were prepared in a similar manner. All the compounds are air- and thermally stable. In particular, **1b** and **2a/2b** have good solubilities in a wide variety of polar and nonpolar organic solvents. All the target structures were fully characterized by conventional techniques (¹H, ¹³C, ¹⁹F, and ³¹P NMR and HRMS spectroscopy).



Scheme I.1 Synthesis of Pyrene Derivatives **1** and **2**.

Single crystals of **1a** suitable for X-ray diffraction were obtained by slow evaporation of hexanes into a CHCl₃ solution. The phosphoryl group is a stereocenter and thus the

molecule crystallizes as a racemic mixture. The ORTEP diagram of one enantiomer with atom numbering and selected bond lengths is shown in Figure I.2a (CCDC 1936450). The newly formed pyrrole ring is nearly coplanar with the pyrene core whereas the six-membered PN-heterocycle is nonplanar, as the tetrahedral P atom is distorted ~ 0.2 Å out of the mean plane along with a slightly twisted torsion angle (C1–C2–C3–C4 = $2.7(2)^\circ$). In the crystal lattice of **1a**, the highly polarized P=O moiety forms two C–H hydrogen bonds with adjacent molecules. No distinct intermolecular π – π stacking interaction was observed, which can be attributed to the shielding effect of the bulky phenyl substituent on the phosphorus center and the propeller-like arrangement of the peripheral benzene ring on the pyrrole ring (where $\varphi = 51.4^\circ$). Instead, multiple C–H $\cdots\pi$ interactions between the neighboring molecules arranged in an edge-to-face and face-to-face fashion with the distances from ~ 2.81 to 2.87 Å can be identified (see Supplementary Information section below). The unique packing mode would efficiently prevent excimer formation to avoid fluorescence quenching and red-shifting. Based on the crystal structure, we also performed nucleus-independent chemical shift (NICS) calculations to investigate the influence of PN-heterocycle fusion on the aromaticity of the molecular system. The pyrrole ring on the periphery of **1a** has relatively negative NICS(1) values of -8.01 and -8.92 and can be classified as aromatic (Figure I.2b). The PN heterocyclic ring shows small positive values (0.86 and 0.28), indicating that it is nonaromatic. The phenyl rings along the short and long-axis of the molecule exhibit qualitatively similar NICS values that are typical for pyrene. The results obtained from the NICS computations are in agreement with the structural parameters of the crystal structure.

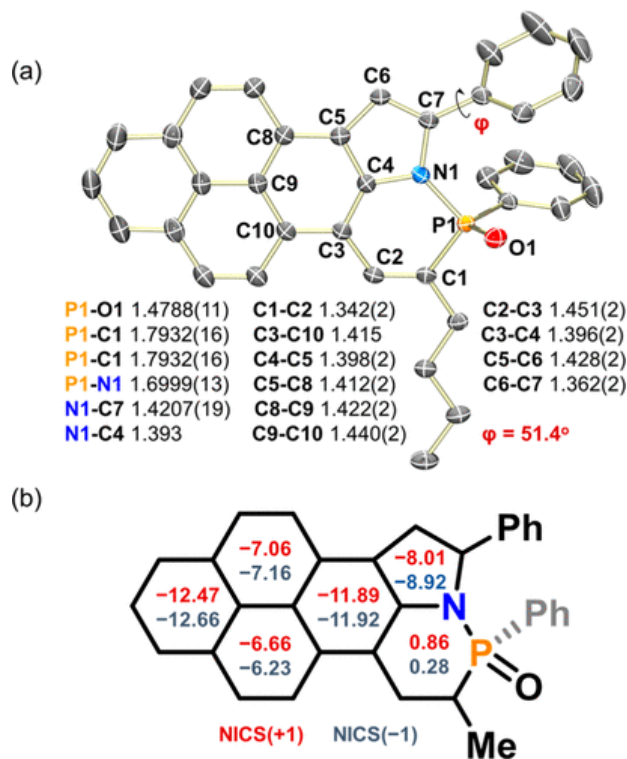


Figure I.2 (a) X-ray crystallographic structure of **1a** with the thermal ellipsoids drawn at 50% probability; all hydrogen atoms are omitted for clarity. Bond lengths in Å, and ϕ denotes the dihedral angle between the pyrrolyl and the appended phenyl substituent. (b) NICS(± 1) indices (in ppm) of **1a'** (where the *n*-butyl group in **1a** is replaced by a methyl group) determined at the GAIO-B3LYP/pcSseg-2 level of theory. The symbols +1/−1 denote the 1 Å points above/below the defined mean planes.

The absorption spectra of **1** and **2** in CH₂Cl₂ solution are similar, as shown in Figure I.3. Compounds **1a/1b** feature two strong absorption shoulders centered at ca. 430 and 410 nm, while broad and slightly red-shifted absorption bands with low-energy absorption (440–450 nm) are observed for **2a/2b**. Wide-range tunable emission color from blue to red (Figure I.3) with high quantum yields (Table I.1) was observed among these types of pyrene derivatives. The emission spectrum of **1a** shows the presence of vibronic structure and the Stokes shift is small. These characteristics suggest that the structural displacement between the ground state (*S*₀) and excited state is small due to the structural rigidity of **1a**.

By contrast, the emission bands of **1b** and **2** become structureless and increasingly red-shifted in the order of **2a** → **1b** → **2b**. Notably, red-emissive **2b** exhibits a large apparent Stokes shift (6806 cm^{-1}) while maintaining a relatively good quantum yield. In all cases, no excimer-like or dual emission peaks were detected at higher concentration (up to 10^{-4} M^{-1}). Also noteworthy is that the shape of the emission spectra for the colloidal suspensions of **1b** and **2b** (in THF/water mixtures) exhibits no change compared to their respective solution counterparts (Figures I.8 and I.10). Impressively, white-light emission could be achieved if appropriate ratios of **1a**, **2a**, and **2b** were mixed in CH_2Cl_2 solution under a single excitation (Figure I.12). This observation demonstrates that there is no significant energy transfer among the three pyrene derivatives, which suggests the potential for preparation of multicolor emissive materials.¹⁵

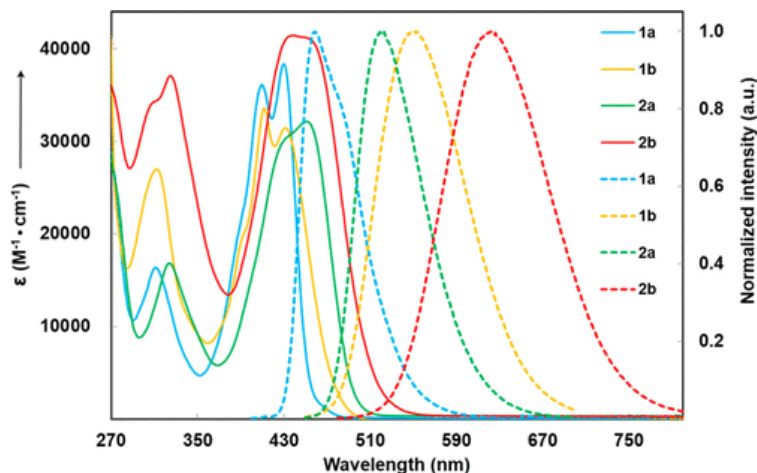


Figure I.3 Electronic absorption (solid line) and emission spectra (dotted line) of **1** and **2** in CH₂Cl₂ at 298 K.

Table I.1 Photophysical Data of **1** and **2** in CH₂Cl₂ at 298 K

compd	λ_{max} (nm) ^a	λ_{em} (nm)	Φ_{F} ^c	Stokes Shift (cm ⁻¹)
1a	430 (4.58)	459	0.57	1469
1b	431 (4.50)	551	0.62	5053
2a	450 (4.51)	521	0.61	3028
2b	437 ^b (4.62)	622	0.23	6806

^a The longest absorption maximum wavelengths, molar absorption coefficients as log ϵ (M⁻¹ cm⁻¹) given in parentheses. ^b A broad absorption band. ^c The relative fluorescence quantum yield.

With increasing solvent polarity from cyclohexane to MeCN, the fluorescence spectra of triphenylamine-substituted **1b** and **2b** displayed a bathochromic shift of 61 and 87 nm, respectively (see Figures I.14, I.16 and Table I.2). Their positive solvatochromism is attributed to the distinctly separated HOMO–LUMO distributions in their electronic structures, as revealed by the DFT calculations. Lippert–Mataga plots of **2b** show good linear correlation with the solvent polarity (Figure I.17). The dipole moment change ($\Delta\mu$) between the S₀ and the excited state is estimated to be 15.0 D. The time-dependent (TD-)

DFT calculated dipole moment of the first excited state (S_1) near the Franck–Condon (FC) geometry of **2b** is up to 23.7 D, which is significantly large compared to its S_0 state (7.0 D). Both the DFT calculations and experimental results indicate that **2b** is a typical push–pull type system with remarkable intramolecular charge transfer (ICT) character. In contrast, the photophysical parameters of **1a** and **2a** exhibit limited solvent effect, which are mainly from locally excited $\pi \rightarrow \pi^*$ states of the parent core. As shown in Figure I.25, in the S_1 state of **2b**, the phenyl groups at the C_{Ar} - and C_R -positions in the S_0 state are oriented in a twisted fashion relative to the molecular plane (dihedral angles: $45.5^\circ/44.2^\circ$), whereas their orientation becomes more coplanar in S_1 ($30.1^\circ/25.6^\circ$). The C–C bond lengths connecting the central core and the phenyl groups at the C_{Ar} - and C_R -positions are shortened by 0.02 and 0.03 Å, respectively. Meanwhile, the bond order indices for the relevant bonds within the peripheral and heterocyclic rings alternate in various degrees upon switching from S_0 to S_1 (Figure I.26), suggesting effective electron delocalization occurs among the pendant substituents and PN-heterocycle fused pyrene in the S_1 . Consequently, destabilized HOMO and lower LUMO energies were realized at the lowest excited state relative to S_0 and lead to a smaller energy gap by ~ 0.5 eV. Thus, the geometric relaxations caused by facile EWG/EDG rotations with respect to the central core are responsible for the observed large Stokes shift for **2b**.

The fluorescence quantum yields of **1b** and **2b** decrease with the increasing solvent polarity (Table I.3). Additionally, the calculated nonradiative decay rate constant (k_{nr}) for both compounds increases faster than the radiative term (k_r) with increasing solvent polarity (Figures I.19 and I.21). In considering their small energy gaps¹⁶ and imperceptible increase of emission intensity under oxygen-free conditions (negligible intersystem crossing), the

diminished fluorescence could be ascribed to the free intramolecular rotation of the EWG/EDG that dissipates the excited state energy via nonradiative pathway. Nevertheless, the unrestrained intramolecular rotation could be suppressed effectively when the fluorophore is dispersed in an aggregated state, as compound **2b** shows aggregation-induced emission (AIE) behavior (Figure I.11) with an increased fluorescence quantum yield (0.44) for its colloidal suspension. Thus, this type of pyrene derivatives with the facile ability to modify the Ar- and R-substituents could be a promising platform for expanding the scope of pyrene-based AIE luminogens.¹⁷

The electrochemical properties of **1** and **2** were investigated using cyclic voltammetry (Figure I.22 and Table I.4). Within the potential window of CH₂Cl₂, **1** exhibited two oxidation and one reduction waves, whereas **2** showed two oxidation and two reduction waves. The two fully reversible oxidation potentials for **1b** and **2b** are comparable and appear at less positive potential regions owing to the presence of the stronger electron-donating ability of the triphenylamine substituent. The introduction of the 3,5-bis(trifluoromethyl)phenyl group in **2** results in not only increased reversibility for the first reduction process but also a significantly positive shift of the reductive potentials. The calculated HOMO and LUMO energy levels from these potentials are mainly dependent on the appended C_R/C_{Ar} substituents. Overall, the energy gaps between electrochemical oxidation and reduction are consistent with the HOMO–LUMO gaps obtained by the DFT calculations and the UV/vis results (Table I.4).

Conclusions

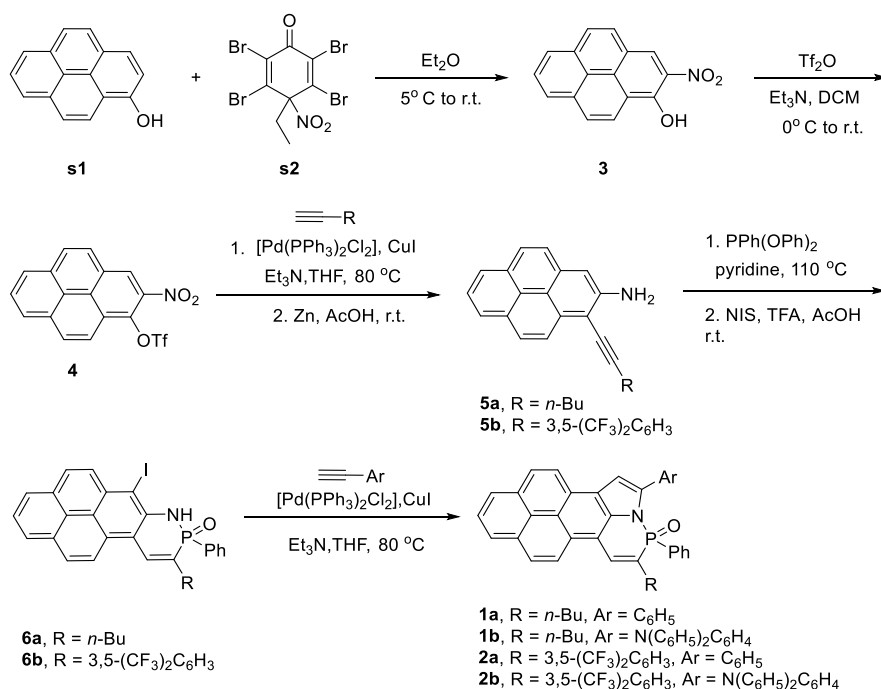
In conclusion, we have prepared a novel type of fluorescent PN-embedded pyrene derivatives via a PPh(OPh)₂-mediated cyclization and sequential Sonogashira cross-coupling/heteroannulation protocol. Both the experimental results and the DFT calculations have revealed that the electronic structures and electrochemical properties could be significantly tailored by appending the EDG/EWG at appropriate positions in the core structures. These appealing characteristics should make pyrene-based PN-heterocycles promising candidates for solution-processable organic electronics and intriguing fluorescent probes and sensors.

Supplementary Information

1. Synthesis

General. NMR spectra were obtained on a Varian Inova 500 MHz (¹H: 500.11 MHz, ¹³C 125.76 MHz, ¹⁹F 470.53 MHz, ³¹P 202.46 MHz) or a Bruker Avance-III-HD 600 MHz (¹H: 599.98 MHz, ¹³C: 150.87 MHz) spectrometer. Chemical shifts (δ) are expressed in ppm using residual non-deuterated solvent present in the bulk deuterated solvent (CDCl₃: ¹H 7.26 ppm, ¹³C 77.16 ppm; DMSO-*d*₆: ¹H 2.50 ppm, ¹³C 39.52 ppm). ¹⁹F chemical shifts are reported against CFC₃ external standard (δ 0 ppm). ³¹P chemical shifts are reported against 85% H₃PO₄ (δ 0 ppm) as external reference. Mass spectra data were acquired on a Waters SYNAPT QToF in positive ion mode with a Shimadzu LC20AD HPLC front end. The solvents were MeCN:H₂O:0.1% HCO₂H at a flow rate of 0.05 mL min⁻¹ with a 5 μL injection on a loop injection. Preparative SEC was performed using a JAI Recycling Preparative HPLC (Model LC-9101) with a JAIGEL-1H preparative column with CHCl₃ as solvent. Analytical TLC was carried out on TLC plates (5 × 10 cm with 0.25 mm

thickness, silica gel 60 F₂₅₄, Merck, Darmstadt, Germany) cut from the commercially available aluminium sheets. Solvents and reagents were used as purchased from suppliers, unless anhydrous conditions were employed, in which case, solvents were freshly distilled from sodium/benzophenone under N₂ atmosphere (THF) or as purchased. 1-Hydroxypyrene (**s1**),¹⁸ 2,3,5,6-tetrabromo-4-ethyl-4-nitro-2,5-cyclohexadien-1-one (**s2**),¹⁹ 3,5-bis(trifluoromethyl)phenylethyne²⁰ and phenyldiphenoxyphosphine [PPh(OPh)₂]²¹ were synthesized by their reported procedures.



Scheme I.2 Synthesis of **1** and **2**.

1-Hydroxy-2-nitropyrene (**3**). To a solution of 1-hydroxypyrene (**s1**, 123 mg, 0.5 mmol) in Et₂O (50 mL) cooled to 5 °C was added reagent **s2** (123 mg, 0.5 mmol) in small portions

over 5 min. The reaction mixture was stirred for 1 h at room temperature while following the reaction by TLC. The mixture was filtered, and the collected solid was dried under the vacuum to provide **3** (140 mg, 81%) as a brown-orange solid. $R_f = 0.67$ (hexane). $^1\text{H NMR}$ (500 MHz, CDCl_3) δ 8.78 (s, 1H), 8.38–8.33 (m, 4H), 8.25 (d, $J = 8.9$ Hz, 1H), 8.21 (t, $J = 7.7$ Hz, 1H), 8.11 (d, $J = 8.9$ Hz, 1H). The obtained $^1\text{H NMR}$ spectral data were in good agreement with those previously reported.²²

2-Nitropyren-1-yl trifluoromethanesulfonate (**4**). To a solution of **3** (123 mg, 0.5 mmol) in CH_2Cl_2 (20 mL) was added Et_3N (0.2 mL, 1.5 mmol) at room temperature. The mixture was cooled to 0 °C and then trifluoromethanesulfonic anhydride (92 μL , 0.55 mmol) was added dropwise over 2 min. After stirring for 12 h at rt, the reaction mixture was quenched with H_2O (10 mL), then the layers were separated. The aqueous layer was extracted with CH_2Cl_2 (20 mL \times 3) and the combined organic layer was washed with 3 N HCl and then dried over Na_2SO_4 and then filtered. The solvent was evaporated under reduced pressure and the crude material purified by flash column chromatography (4:1 hexane/ CH_2Cl_2) to afford **4** (140 mg, 81%) as an amorphous yellow solid. $R_f = 0.37$ (4:1 hexane/ CH_2Cl_2). $^1\text{H NMR}$ (500 MHz, CDCl_3) δ 8.78 (s, 1H), 8.38–8.33 (m, 4H), 8.25 (d, $J = 8.9$ Hz, 1H), 8.21 (t, $J = 7.7$ Hz, 1H), 8.11 (d, $J = 8.9$ Hz, 1H). $^{13}\text{C}\{^1\text{H}\}$ NMR (126 MHz, CDCl_3) δ 139.6, 133.1, 131.7, 131.6, 131.1, 130.8, 130.4, 128.8, 127.9, 127.5, 127.3, 126.7, 125.7, 123.3, 120.6, 120.2, 118.8 (q, $J = 320.8$ Hz). $^{19}\text{F}\{^1\text{H}\}$ NMR (471 MHz, CDCl_3) δ -72.5. HRMS (ESI) m/z calcd for $\text{C}_{17}\text{H}_9\text{F}_3\text{NO}_5\text{S}$ $[\text{M}+\text{H}]^+$ 396.0154, found 396.0145.

1-(Hex-1-ynyl)pyren-2-amine (**5a**). To an N_2 -degassed solution of **4** (116 mg, 0.34 mmol) and 1-hexyne (0.12 mL, 1 mmol) in 5:1 (v/v) THF/ Et_3N (30 mL) was added CuI (2 mg, 0.002 mmol) and $\text{Pd}(\text{PPh}_3)_2\text{Cl}_2$ (21 mg, 0.03 mmol). The solution was stirred at 80 °C (oil

bath) under N₂ for 12 h, then the reaction mixture was diluted with CH₂Cl₂ and filtered through a 4 cm pad of silica. The filtrate was concentrated under reduced pressure and the crude product purified by flash chromatography (hexanes/EtOAc/CH₂Cl₂, 20:1:1) over silica to give a brown oil. *R*_f = 0.47 (4:1 hexane/CH₂Cl₂). This oil was then dissolved in AcOH (10 mL), activated Zn powder (221 mg, 3.4 mmol) was added and the mixture stirred at r.t. for 1 h. H₂O (20 mL) was added and the aqueous layer extracted with CH₂Cl₂ (20 mL × 2). The combined organic layer was washed with saturated NaHCO₃ solution and dried over Na₂SO₄. Following evaporation of the solvent under reduced pressure, the crude residue was purified by flash column chromatography (hexane/EtOAc/CH₂Cl₂, 16:1:1) to afford **5a** (84 mg, 83%) as a yellow solid. *R*_f = 0.24 (8:1 hexane/EtOAc). Mp 153–156 °C. ¹H NMR (500 MHz, CDCl₃) δ 8.41 (d, *J* = 9.1 Hz, 1H), 8.11 (d, *J* = 7.6 Hz, 1H), 8.08–8.07 (m, 2H), 7.95 (d, *J* = 8.9 Hz, 1H), 7.86 (t, *J* = 7.6 Hz, 1H), 7.81 (d, *J* = 8.9 Hz, 1H), 7.47 (s, 1H), 4.65 (s, 2H), 2.72 (t, *J* = 7.1 Hz, 2H), 1.81–1.76 (m, 2H), 1.66–1.61 (m, 2H), 1.04 (t, *J* = 7.3 Hz, 3H). ¹³C{¹H} NMR (126 MHz, CDCl₃) δ 146.3, 132.9, 131.9, 130.1, 129.9, 128.5, 128.3, 126.4, 125.6, 125.5, 125.2, 124.7, 124.6, 110.4, 110.3, 102.0, 76.0, 31.4, 22.4, 20.0, 13.9. HRMS (ESI) *m/z* calcd for C₂₀H₂₂N [M+H]⁺ 298.1596, found 298.1640.

1-((3,5-bis(trifluoromethyl)phenyl)ethynyl)pyren-2-amine (**5b**). To an N₂-degassed solution of **4** (240 mg, 0.69 mmol) and 3,5-bis(trifluoromethyl)phenylethyne¹⁹ (310 mg, 1.04 mmol) in 5:1 (v/v) THF/Et₃N (30 mL) was added CuI (13 mg, 0.07 mmol) and Pd(PPh₃)₂Cl₂ (50 mg, 0.07 mmol). The solution was stirred at 80 °C (oil bath) under N₂ for 12 h, then the reaction mixture was diluted with CH₂Cl₂ and filtered through a 4 cm pad of silica. The filtrate was concentrated under reduced pressure and the crude product purified by flash chromatography (hexanes/EtOAc, 30:1) over silica to give a brown oil. *R*_f = 0.31

(20:1 hexane/CH₂Cl₂). This oil was then dissolved in AcOH (10 mL), activated Zn powder (455 mg, 7 mmol) was added, and the mixture stirred at r.t. for 1 h. H₂O (20 mL) was added and the aqueous layer extracted with CH₂Cl₂ (30 mL × 2). The combined organic layer was washed with saturated NaHCO₃ solution and dried over Na₂SO₄. Following evaporation of the solvent under reduced pressure, the crude residue was purified by flash column chromatography (hexanes/EtOAc, 8:1) to afford **5b** (227 mg, 72%) as a yellow solid. *R*_f = 0.24 (8:1 hexane/EtOAc). Mp 113–115 °C. ¹H NMR (500 MHz, CDCl₃) δ 8.41 (d, *J* = 9.0 Hz, 1H), 8.15 (t, *J* = 8.0 Hz, 2H), 8.11–8.08 (m, 3H), 7.99 (d, *J* = 8.9 Hz, 1H), 7.91–7.87 (m, 2H), 7.81 (d, *J* = 8.9 Hz, 1H), 7.45 (s, 1H), 4.71 (s, 2H). ¹³C{¹H} NMR (126 MHz, CDCl₃) δ 146.9, 133.5, 133.4, 132.3 (q, *J* = 33.7 Hz), 131.3 (q, *J* = 3.7 Hz), 130.0, 129.8, 129.5, 129.4, 126.4, 126.2, 126.0, 125.0, 124.6, 123.2 (q, *J* = 273.0 Hz), 121.6 (q, *J* = 3.8 Hz), 121.6, 118.8, 110.5, 101.6, 97.5, 89.0. ¹⁹F{¹H} NMR (471 MHz, CDCl₃) δ –63.0. HRMS (ESI) *m/z* calcd for C₂₆H₁₄F₆N [M+H]⁺ 454.1030, found 454.1023.

Iodoheterocycle 6a. To a solution of aniline **5a** (58 mg, 0.19 mmol) in dry pyridine (1 mL) was added PPh(OPh)₂ (115 mg, 0.39 mmol). The reaction flask was sealed and heated to 110 °C for 24 h. After cooling, toluene (20 mL) was added and the volatiles were removed *in vacuo*. The residue was dissolved in THF/H₂O mixture (10 mL, v/v, 20:1). After heating at 60 °C (water bath) for 1 h, the THF layer was dried (Na₂SO₄), filtered and the solvent removed under reduced pressure. The crude residue was purified by flash chromatography (CH₂Cl₂/EtOAc, 2:1) over silica to give a brown oil. *R*_f = 0.21 (2:1 CH₂Cl₂/EtOAc). This oil was dissolved in AcOH (5 mL) and TFA (0.05 mL) added. NIS (47 mg, 0.2 mmol) was added and the mixture stirred for 1 h at r.t. The mixture was washed with saturated Na₂S₂O₃ (2 × 15 mL) and brine (15 mL) solutions, dried (MgSO₄) and evaporated. The crude product

was purified by chromatography over silica (CH₂Cl₂/EtOAc, 5:1) to give **6a** (65 mg, 62%) as a yellow solid. $R_f = 0.72$ (2:1 CH₂Cl₂/EtOAc). Mp > 200 °C. ¹H NMR (500 MHz, CDCl₃) δ 8.52 (d, $J = 9.4$ Hz, 1H), 8.37 (d, $J = 34.3$ Hz, 1H), 8.28 (d, $J = 9.2$ Hz, 1H), 8.23–8.20 (m, 3H), 8.10 (d, $J = 9.3$ Hz, 1H), 7.99 (t, $J = 7.6$ Hz, 1H), 7.92–7.87 (m, 2H), 7.61–7.58 (m, 1H), 7.50–7.54 (m, 2H), 7.18 (s, 1H), 2.64–2.50 (m, 2H), 1.76–1.67 (m, 1H), 1.66–1.56 (m, 1H), 1.44–1.33 (m, 2H), 0.90 (t, $J = 7.4$ Hz, 3H). ¹³C{¹H} NMR (151 MHz, CDCl₃) δ 137.4 (d, $J = 2.8$ Hz), 134.2, 133.3 (d, $J = 4.1$ Hz), 132.8, 132.8, 132.7 (d, $J = 2.8$ Hz), 132.4, 131.8, 131.0, 130.2, 130.0, 129.9, 129.6, 129.5, 129.1, 128.8, 128.7, 126.8, 126.8, 125.9, 124.0, 121.3, 121.1, 113.8 (d, $J = 11.8$ Hz), 92.4 (d, $J = 7.3$ Hz), 32.0 (d, $J = 4.5$ Hz), 31.9 (d, $J = 12.0$ Hz), 22.6, 14.0. ³¹P{¹H} NMR (201MHz, CDCl₃) δ 13.5. HRMS (ESI) m/z calcd for C₂₈H₂₄INOP [M+H]⁺ 548.0640, found 548.0629.

Iodoheterocycle 6b. To a solution of aniline **5b** (164 mg, 0.36 mmol) in dry pyridine (1 mL) was added PPh(OPh)₂ (213 mg, 0.72 mmol). The reaction flask was sealed and heated to 110 °C for 24 h. After cooling, toluene (20 mL) was added and the volatiles were removed *in vacuo*. The residue was dissolved in THF/H₂O mixture (15 mL, v/v, 20:1). After heating at 60 °C (water bath) for 1 h, the THF layer was dried (Na₂SO₄), filtered, and the solvent was concentrated under reduced pressure. The resulting crude product was purified by flash chromatography (CH₂Cl₂/EtOAc, 15:1) over silica to give a brown oil. $R_f = 0.51$ (10:1 CH₂Cl₂/EtOAc). This oil was dissolved in AcOH (5 mL) and TFA (0.05 mL) added. NIS (96 mg, 0.43 mmol) was added and the mixture stirred for 1 h at r.t. The mixture was washed with saturated NaS₂O₃ (2 × 15 mL) and brine (15 mL) solutions, dried (MgSO₄) and evaporated. The crude product was purified by chromatography over silica (CH₂Cl₂/EtOAc, 40:1) to give **6b** (205 mg, 81%) as a yellow solid. $R_f = 0.83$ (2:1

CH₂Cl₂/EtOAc). Mp > 200 °C. ¹H NMR (600 MHz, THF-*d*₈) δ 8.99 (d, *J* = 30.0 Hz, 1H), 8.78 (d, *J* = 9.4 Hz, 1H), 8.54 (s, 2H), 8.29–8.23 (m, 4H), 8.15–8.11 (m, 2H), 7.98 (t, *J* = 7.6 Hz, 1H), 7.90 (s, 1H), 7.85–7.81 (m, 2H), 7.45–7.37 (m, 3H). ¹³C{¹H} NMR (151 MHz, THF-*d*₈) δ 140.0 (d, *J* = 12.7 Hz), 138.8 (d, *J* = 2.9 Hz), 135.5 (d, *J* = 2.1 Hz), 135.4, 134.1, 133.2, 132.7, 132.6, 131.9 (d, *J* = 2.7 Hz), 131.7, 131.3 (q, *J* = 33.2 Hz), 131.3, 130.3, 130.1, 129.9, 129.6, 128.3 (br q), 128.0, 128.0, 127.2, 127.0, 126.8, 126.4, 125.8, 123.6, 123.5 (q, *J* = 273.3 Hz), 121.4, 120.9 (br q), 120.7, 113.4 (d, *J* = 10.7 Hz), 91.1 (d, *J* = 7.6 Hz). ¹⁹F{¹H} NMR (471 MHz, THF-*d*₈) δ –63.6. ³¹P{¹H} NMR (243 MHz, THF-*d*₈) δ 7.8. HRMS (ESI) *m/z* calcd for C₃₂H₁₈F₆INOP [M+H]⁺ 704.0075, found 704.0060.

PN-Heterocycle 1a. To an N₂-degassed solution of **6a** (41 mg, 0.07 mmol) and phenylacetylene (90 mg, 0.08 mmol) in 5:1 (v/v) THF/Et₃N (6 mL) was added CuI (1.5 mg, 0.007 mmol) and Pd(PPh₃)₂Cl₂ (14 mg, 0.007 mmol). The solution was stirred at r.t. for 6 h and monitored by TLC [new spot: *R*_f = 0.80 (2:1 CH₂Cl₂/EtOAc)]. After that, the mixture was heated at 80 °C (oil bath) under N₂ for 2 h, then the reaction mixture was diluted with CH₂Cl₂ and filtered through a 4 cm pad of silica. The filtrate was concentrated under reduced pressure and the residue purified by flash column chromatography (hexanes/EtOAc, 6:1) to provide **1a** (32 mg, 87%) as a yellow solid. *R*_f = 0.25 (hexanes/EtOAc, 4:1). Mp > 200 °C. ¹H NMR (600 MHz, CDCl₃) δ 8.66 (d, *J* = 9.2 Hz, 1H), 8.50 (d, *J* = 8.5 Hz, 1H), 8.48 (d, *J* = 35.5 Hz, 1H), 8.27–8.23 (m, 3H), 8.18 (d, *J* = 9.2 Hz, 1H), 8.01 (t, *J* = 7.6 Hz, 1H), 7.61 (dt, *J* = 6.9, 1.4 Hz, 2H), 7.44 (d, *J* = 2.6 Hz, 1H), 7.33–7.24 (m, 6H), 7.18–7.14 (m, 2H), 2.63–2.51 (m, 2H), 1.83–1.76 (m, 1H), 1.69–1.62 (m, 1H), 1.45–1.35 (m, 2H), 0.90 (t, *J* = 7.4 Hz, 4H). ¹³C{¹H} NMR (151 MHz, CDCl₃) δ 144.9 (d, *J* = 1.8 Hz), 133.2, 132.8 (d, *J* = 3.7 Hz), 132.4, 132.1, 132.1, 132.0,

131.8, 131.7, 131.5, 131.3, 131.1, 130.6, 130.5, 129.7, 128.9, 128.6, 128.2, 128.0, 127.8, 127.7, 126.2, 125.9, 125.7, 125.6, 125.5, 125.5, 124.2 (d, $J = 5.1$ Hz), 123.7, 121.8, 121.7, 111.9 (d, $J = 10.2$ Hz), 107.8 (d, $J = 5.8$ Hz), 32.5 (d, $J = 3.9$ Hz), 32.1 (d, $J = 12.6$ Hz), 22.6, 14.0. $^{31}\text{P}\{^1\text{H}\}$ NMR (243 MHz, CDCl_3) δ 14.8. HRMS (ESI) m/z calcd for $\text{C}_{36}\text{H}_{29}\text{NOP}$ $[\text{M}+\text{H}]^+$ 522.1987, found 522.1979.

PN-Heterocycle 1b. A similar procedure was followed using *N, N*-diphenyl-4-ethynylaniline⁴ (22 mg, 0.08 mmol). Purification by column chromatography (silica gel, hexanes/EtOAc, 5:1) gave the crude product, which then further purified by preparative SEC to provide **1b** (30 mg, 63%) as an amorphous orange powder. $R_f = 0.34$ (hexanes/EtOAc, 4:1). ^1H NMR (500 MHz, CD_2Cl_2) δ 8.70 (d, $J = 9.3$ Hz, 1H), 8.55 (d, $J = 8.9$ Hz, 1H), 8.49 (d, $J = 34.6$ Hz, 1H), 8.29–8.25 (m, 3H), 8.20 (d, $J = 9.3$ Hz, 1H), 8.03 (t, $J = 7.6$ Hz, 1H), 7.56–7.53 (m, 2H), 7.49 (d, $J = 2.6$ Hz, 1H), 7.45–7.37 (m, 3H), 7.32–7.28 (m, 6H), 7.09–7.06 (m, 6H), 6.92–6.90 (m, 2H), 2.63–2.49 (m, 2H), 1.76–1.70 (m, 1H), 1.65–1.57 (m, 1H), 1.42–1.34 (m, 2H), 0.89 (t, $J = 7.4$ Hz, 3H). $^{13}\text{C}\{^1\text{H}\}$ NMR (151 MHz, CDCl_3) δ 148.1, 147.6, 144.9 (d, $J = 2.0$ Hz), 133.2, 132.7 (d, $J = 3.6$ Hz), 132.5, 132.2, 132.1, 132.0, 131.6, 131.1, 130.6, 130.4, 129.6, 129.4, 128.8, 128.2, 128.1, 127.7, 126.1, 125.9 (d, $J = 9.0$ Hz), 125.6, 125.5, 125.4, 125.4, 124.6, 124.3 (d, $J = 5.2$ Hz), 123.6, 123.2, 122.7, 121.8, 121.7, 111.8 (d, $J = 10.1$ Hz), 107.4 (d, $J = 5.7$ Hz), 32.5 (d, $J = 4.2$ Hz), 32.0 (d, $J = 12.7$ Hz), 22.6, 14.0. $^{31}\text{P}\{^1\text{H}\}$ NMR (202 MHz, CDCl_3) δ 14.0. HRMS (ESI) m/z calcd for $\text{C}_{48}\text{H}_{38}\text{N}_2\text{OP}$ $[\text{M}+\text{H}]^+$ 689.2722, found 689.2739.

PN-Heterocycle 2a. To an N_2 -degassed solution of **6b** (43 mg, 0.06 mmol) and phenylacetyl-ene (61 mg, 0.6 mmol) in 5:1 (v/v) THF/ Et_3N (6 mL) was added CuI (2 mg, 0.006 mmol) and $\text{Pd}(\text{PPh}_3)_2\text{Cl}_2$ (10 mg, 0.006 mmol). The solution was stirred at room

temperature for 8 h and monitored by TLC [new spot: $R_f = 0.85$ ($\text{CH}_2\text{Cl}_2/\text{EtOAc}$, 2:1)]. After that, the solution was stirred at 65 °C (oil bath) under N_2 for 2 h, then the reaction mixture was diluted with CH_2Cl_2 and filtered through a 4 cm pad of silica. The filtrate was concentrated under reduced pressure and the residue purified by flash column chromatography (hexanes/EtOAc, 6:1) to provide **2a** (33 mg, 81%) as an orange-yellow oil. $R_f = 0.34$ (hexanes/EtOAc, 5:1). ^1H NMR (600 MHz, CDCl_3) δ 8.79 (d, $J = 30.8$ Hz, 1H), 8.69 (d, $J = 9.2$ Hz, 1H), 8.52 (d, $J = 8.8$ Hz, 1H), 8.33–8.30 (m, 3H), 8.25 (d, $J = 9.2$ Hz, 1H), 8.22 (s, 2H), 8.06 (t, $J = 7.6$ Hz, 1H), 7.78 (s, 1H), 7.58–7.57 (m, 2H), 7.50 (d, $J = 2.8$ Hz, 1H), 7.30–7.22 (m, 6H), 7.11–7.08 (m, 2H). $^{13}\text{C}\{^1\text{H}\}$ NMR (151 MHz, CDCl_3) δ 144.8 (d, $J = 2.8$ Hz), 139.7 (d, $J = 13.3$ Hz), 135.8 (d, $J = 2.3$ Hz), 133.2, 132.5 (d, $J = 2.8$ Hz), 132.0 (q, $J = 33.2$ Hz), 131.9, 131.8, 131.7, 131.6, 131.3, 131.0, 130.7, 130.5, 130.1, 128.9 (d, $J = 4.4$ Hz), 128.8, 128.2 (d, $J = 14.3$ Hz), 127.8, 127.2, 127.2, 127.0, 127.0, 126.6, 126.2, 125.8, 125.6, 124.1 (d, $J = 5.5$ Hz), 123.6, 123.3 (q, $J = 273.3$ Hz), 122.4, 121.8 (brq), 121.4, 111.0 (d, $J = 8.9$ Hz), 108.4 (d, $J = 6.0$ Hz). $^{19}\text{F}\{^1\text{H}\}$ NMR (471 MHz, CDCl_3) δ -62.8. $^{31}\text{P}\{^1\text{H}\}$ NMR (243 MHz, CDCl_3) δ 11.8. HRMS (ESI) m/z calcd for $\text{C}_{40}\text{H}_{23}\text{F}_6\text{NOP}$ $[\text{M}+\text{H}]^+$ 678.1421, found 678.1426.

PN-Heterocycle 2b. A similar procedure was followed using *N,N*-diphenyl-4-ethynylaniline (20 mg, 0.07 mmol). Purification by column chromatography (hexanes/EtOAc, 12:1) on silica gave the crude product, which then further purified by preparative SEC to provide **2b** (34 mg, 67%) as an orange-red oil. $R_f = 0.40$ (hexanes/EtOAc, 5:1). ^1H NMR (500 MHz, CDCl_3) δ 8.74 (d, $J = 30.8$ Hz, 1H), 8.63 (d, $J = 9.3$ Hz, 1H), 8.48 (d, $J = 8.9$ Hz, 1H), 8.31–8.27 (m, 3H), 8.22–8.20 (m, 3H), 8.05 (t, $J = 7.6$ Hz, 1H), 7.80 (s, 1H), 7.50–7.48 (m, 3H), 7.41–7.33 (m, 3H), 7.32–7.28 (m, 4H),

7.23–7.20 (m, 2H), 7.09–7.06 (m, 6H), 6.93–6.90 (m, 2H). $^{13}\text{C}\{^1\text{H}\}$ NMR (151 MHz, CDCl_3) δ 148.4, 147.5, 144.9 (d, $J = 2.5$ Hz), 139.7 (d, $J = 13.3$ Hz), 135.7 (d, $J = 2.1$ Hz), 133.2, 132.5 (d, $J = 2.8$ Hz), 132.3, 132.2, 132.1, 132.0 (q, $J = 33.2$ Hz), 131.8, 130.9, 130.9, 130.4, 130.0, 129.4, 128.8, 128.7, 128.3, 128.2, 127.0, 127.0, 126.8, 126.5, 126.2, 125.8, 125.6, 125.2, 124.7, 124.2 (d, $J = 5.5$ Hz), 123.6, 123.4, 123.3 (q, $J = 273.3$ Hz), 122.5, 121.8 (brq), 121.7, 121.4, 110.9 (d, $J = 9.0$ Hz), 108.0 (d, $J = 6.0$ Hz). $^{19}\text{F}\{^1\text{H}\}$ NMR (471 MHz, CDCl_3) δ -62.8. $^{31}\text{P}\{^1\text{H}\}$ NMR (202 MHz, CDCl_3) δ 11.4. HRMS (ESI) m/z calcd for $\text{C}_{52}\text{H}_{32}\text{F}_6\text{N}_2\text{OP}$ $[\text{M}+\text{H}]^+$ 845.2156, found 845.2175.

2. X-ray Structure Data and Molecular Packing

Diffraction intensities for **1a** were collected at 173 K on a Bruker Apex2 CCD diffractometer using CuK α radiation, $\lambda = 1.54178 \text{ \AA}$. Space group was determined based on systematic absences. Absorption corrections were applied by SADABS.²³ Structure was solved by direct methods and Fourier techniques and refined on F^2 using full matrix least-squares procedures. All non-H atoms were refined with anisotropic thermal parameters. All H atoms in the structure were found from the residual density map and refined without any restrictions with isotropic thermal parameters. All calculations were performed by the Bruker SHELXL-2014 package.²⁴ CCDC 1936450 contains the supplementary crystallographic data for this paper. These data can be obtained free of charge from The Cambridge Crystallographic Data Centre at www.ccdc.cam.ac.uk/data_request/cif.

Crystallographic data for 1a: C₃₆H₂₈NOP, M = 521.56, 0.09 x 0.08 x 0.06 mm, T = 173(2) K, Monoclinic, space group $P2_1/c$, $a = 8.6693(4) \text{ \AA}$, $b = 19.7886(8) \text{ \AA}$, $c = 15.5913(7) \text{ \AA}$, $\beta = 98.068(2)^\circ$, $V = 2648.3(2) \text{ \AA}^3$, $Z = 4$, $D_c = 1.308 \text{ Mg/m}^3$, $\mu(\text{Cu}) = 1.150 \text{ mm}^{-1}$, $F(000) = 1096$, $2\theta_{\text{max}} = 133.11^\circ$, 24252 reflections, 4670 independent reflections [$R_{\text{int}} = 0.0572$], $R1 = 0.03681$, $wR2 = 0.0987$ and $\text{GOF} = 1.029$ for 4670 reflections (464 parameters) with $I > 2\sigma(I)$, $R1 = 0.0438$, $wR2 = 0.1045$ and $\text{GOF} = 1.029$ for all reflections, max/min residual electron density $+0.286/-0.381 \text{ e\AA}^{-3}$. CCDC 1936450.

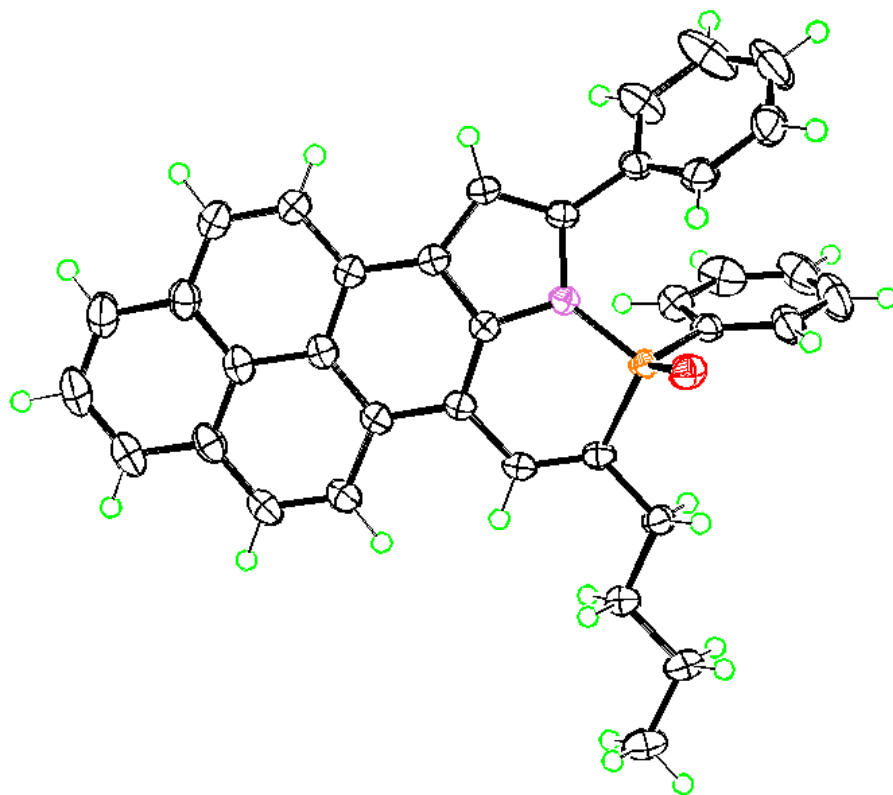


Figure I.4 ORTEP drawing of the structure of **1a** (thermal ellipsoids drawn at 50% probability). Single crystal suitable for X-ray diffraction were obtained by diffusing *n*-hexanes into CHCl_3 solution at room temperature.

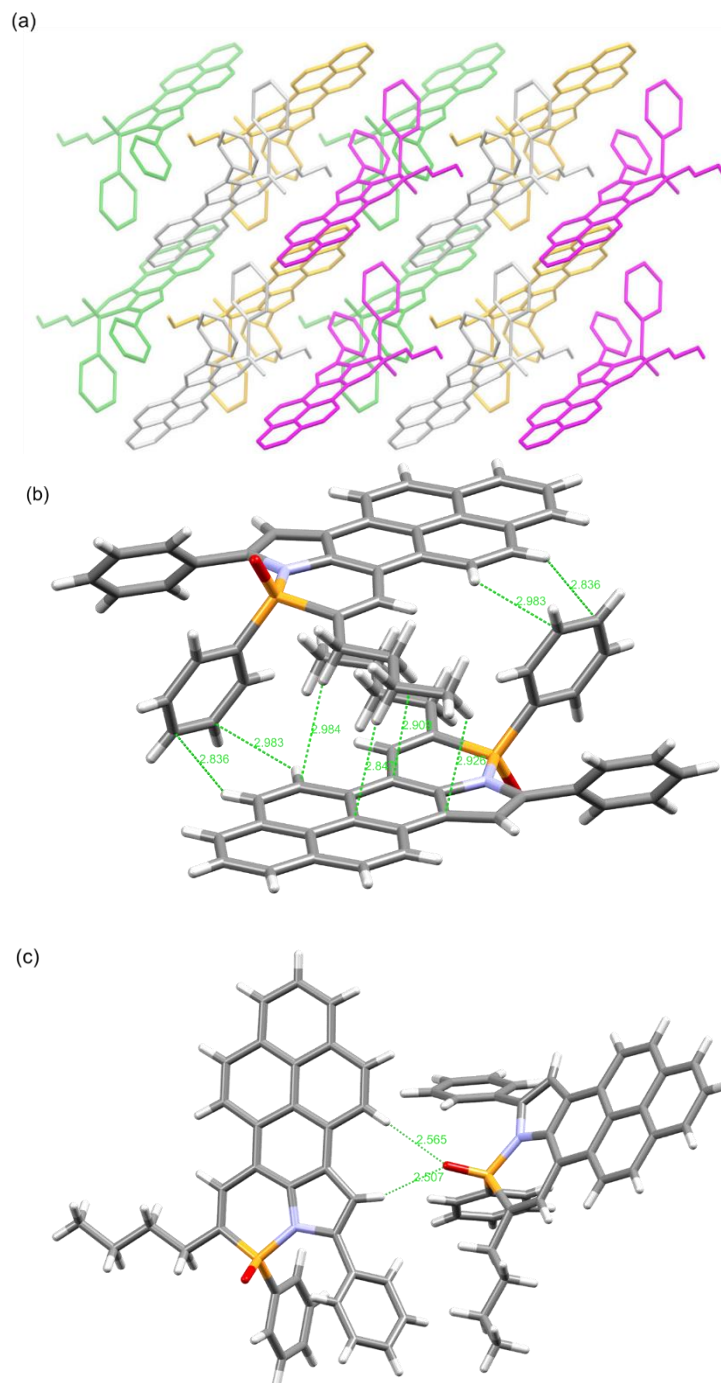


Figure I.5 (a) Packing diagram of **1a** as viewed along the *b* axis. (b) The multiple C–H··· π and (c) C–H···O=P intermolecular interactions in the unit cell. Distances in Å.

3. Photophysical Properties

UV/Vis data were obtained on an HP 8453 UV/Vis spectrometer. Fluorescence data were acquired with a Horiba Jobin-Yvon FluoroMax-4 fluorescence spectrophotometer. Dilute solutions in degassed spectral grade CHCl_3 in a 1 cm quartz cell were used for measurements. Absorption coefficients taken from the slope of the Beer's Law plot. Photoluminescence quantum yields were calculated by comparison with freshly prepared quinine sulfate in 0.5 M H_2SO_4 ($\Phi_F = 0.55$, $\lambda_{\text{ex}} = 366$ nm, for emission maxima ~ 450 nm), fluorescein in 0.1 M NaOH (aq.) ($\Phi_F = 0.91$, $\lambda_{\text{ex}} = 470$ nm, for emission maxima ~ 530 nm), Rhodamine 6G in EtOH ($\Phi_F = 0.95$, $\lambda_{\text{ex}} = 480$ nm, for emission maxima ~ 550 nm) and Nile Red in dioxane ($\Phi_F = 0.70$, $\lambda_{\text{ex}} = 460$ nm, for emission maxima ~ 600 nm) using an excitation slit width of 2 nm for all samples. To minimize the re-absorption effects, the absorbance in the 10 mm fluorescence cuvette was about 0.03~0.05 at their excitation wavelengths. The absolute photoluminescence quantum yield of colloidal sample of **2b** (in THF/water, 2/98, v/v) was measured using the Hamamatsu absolute PL quantum yield measurement system, the error is within $\pm 1\%$.

Fluorescence lifetimes were measured using time correlated single photon counting (TCSPC). Dilute solutions were prepared and placed in a 1 cm optical path quartz cuvette. A pulsed nanoLED was used to excite the samples at 344 nm at a 1 MHz repetition rate. The emission was detected *via* a longpass filter. For bi-exponential or tri-exponential decay histograms, the average fluorescence lifetime (τ_{avg}) is utilized and calculated based on the following equation:²⁵

$$\tau_{\text{avg}} = (\sum \alpha_i \tau_i^2 / \sum \alpha_i \tau_i)$$

in which α_i is the pre-exponential factor corresponding to the i^{th} decay time constant, τ_i . The radiative rate constant k_r and the non-radiative rate constant k_{nr} were estimated by using the equations $k_r = \Phi_F/\tau_F$ and $k_{nr} = (1-\Phi_F)/\tau_F$, where Φ_F is the photoluminescence quantum yield.

Solvent-dependent spectral shifts are interpreted in terms of the Lippert–Mataga plot,²⁶ which describes the Stokes shift $\Delta\nu$ (between the maxima of absorption and fluorescence emission, in cm^{-1}) as a function of the dipole moment change ($\Delta\mu = \mu_e - \mu_g$):^{25,26}

$$\Delta\nu = \frac{2\Delta f}{4\pi\epsilon_0 h c a^3} (\Delta\mu)^2 + \text{Constant}$$

(in SI units)

where ϵ_0 is the permittivity of vacuum, h is Planck's constant, c is the velocity of light, Δf is the solvent polarity function, and a is the Onsager cavity radius. The Onsager cavity radius ($a = 7.0 \text{ \AA}$) estimated from the quantum chemical calculation by using DFT method at the B3LYP/6-311G(d,p) level. Thus, the dipole moment change ($\Delta\mu = \mu_{\text{ex}} - \mu_g$) obtained from the solvatochromic shift is calculated to be 15.0 D (Figure I.15).

As the $S_0 \rightarrow S_1$ transitions in substituted pyrene derivatives are usually broad with an undefined vibrational pattern, the band maxima of the longest absorption and emission have been used to determine the apparent Stokes shift in this study. In the case of 1,4-dioxane, the “effective” dielectric constant ϵ is much higher as it adopts the boat conformation around dipolar species; while the protic solvent MeOH would interact with the strong hydrogen bond accepting P=O moiety in the molecule *via* hydrogen bonding, thus these two solvents were excluded in the plot.

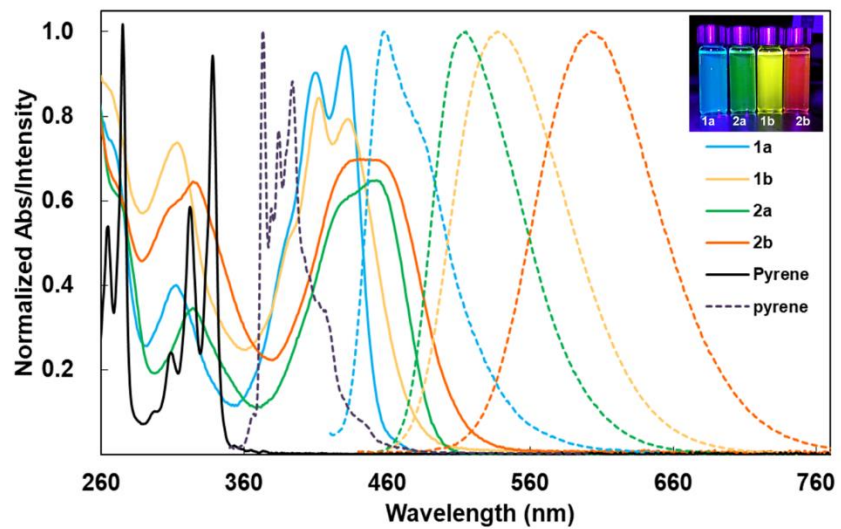


Figure I.6 Absorption (solid lines) and fluorescence (dotted lines) spectra of **1** and **2** as well as pyrene in CH_2Cl_2 at 298 K. Inset: emission color under 365 nm UV light.

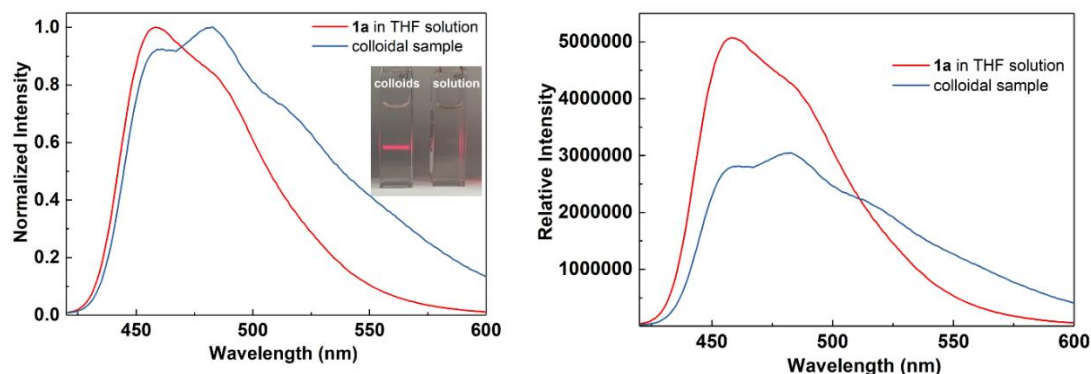


Figure I.7 Normalized fluorescence spectra (left) and relative fluorescence intensities (right) of **1a** (10 μM) in pure THF and the corresponding colloidal sample at 298 K. Inset: the Tyndall phenomenon observed for the colloids. The colloidal suspension was prepared by dispersing compound **1a** in THF/ H_2O mixture (2/98, v/v). The small red-shift and widening for the emission spectrum with diminished intensity were may be attributed to the increased solvent polarity enhanced by the water and the small tendency to form excitonic complexes.

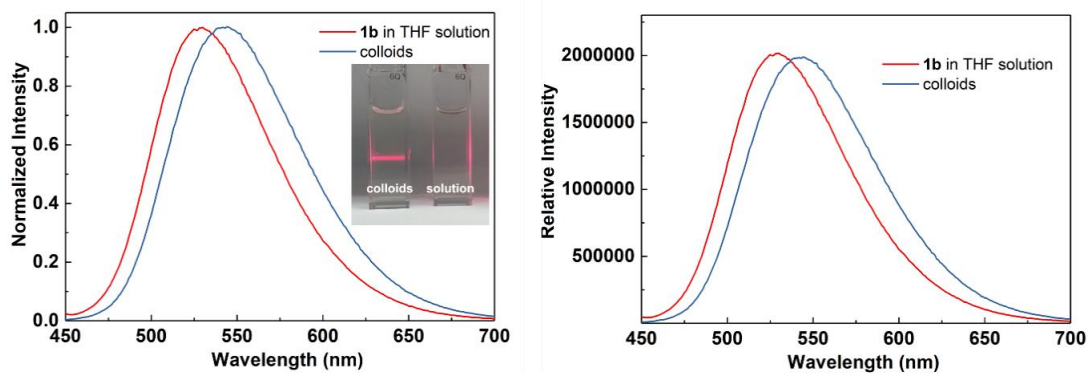


Figure I.8 Normalized fluorescence spectra (left) and relative fluorescence intensities (right) of **1b** (10 μM) in pure THF and the corresponding colloidal sample at 298 K. Inset: the Tyndall phenomenon observed for the colloids. The colloidal suspension was prepared by dispersing compound **1b** in THF/ H_2O mixture (2/98, v/v). The small red-shift for the emission maximum were found due to the increased solvent polarity, which is enhanced by the water.

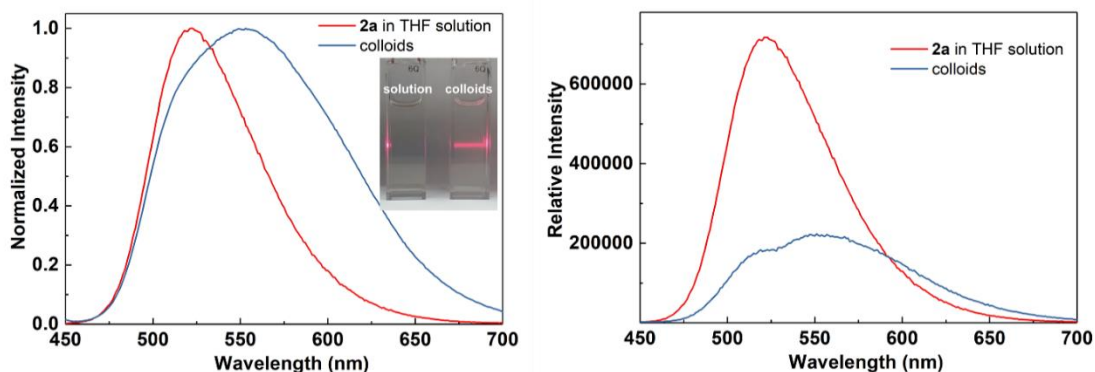


Figure I.9 Normalized fluorescence spectra (left) and relative fluorescence intensities (right) of **2a** ($10\ \mu\text{M}$) in pure THF and the corresponding colloidal sample at 298 K. Inset: the Tyndall phenomenon observed for the colloids. The colloidal suspension was prepared by dispersing compound **2a** in THF/ H_2O mixture (2/98, v/v). The small red-shift and widening for the emission spectrum accompanying diminished intensity may be attributed to the increased solvent polarity enhanced by water and the small tendency to form excitonic complexes.

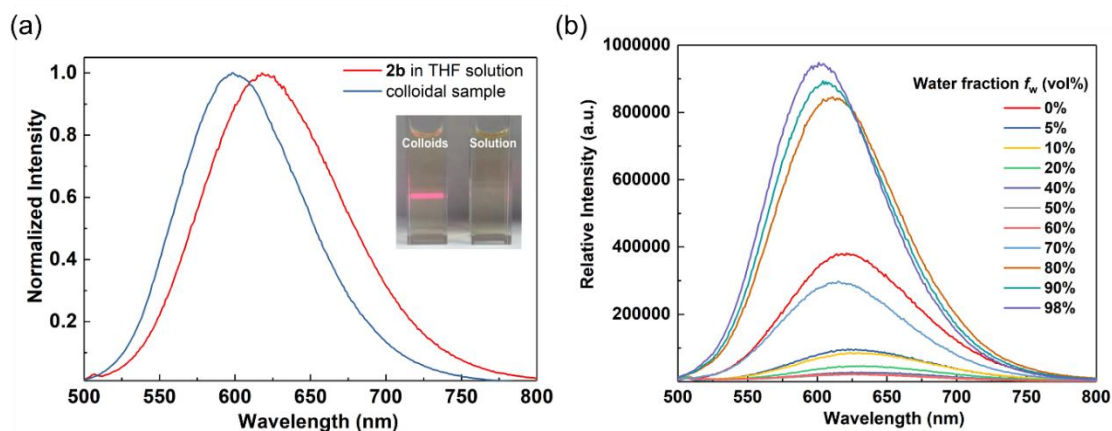


Figure I.10 (a) Fluorescence spectra of **2b** ($10\ \mu\text{M}$) in pure THF and the corresponding colloidal sample at 298 K. Inset: the Tyndall phenomenon observed for the colloids. The colloidal suspension was prepared by dispersing compound **2b** in THF/ H_2O mixture (2/98, v/v). (b) Relative fluorescence intensities of **2b** ($10\ \mu\text{M}$) in THF/water mixtures with varying water content. Excitation wavelength: 430 nm.

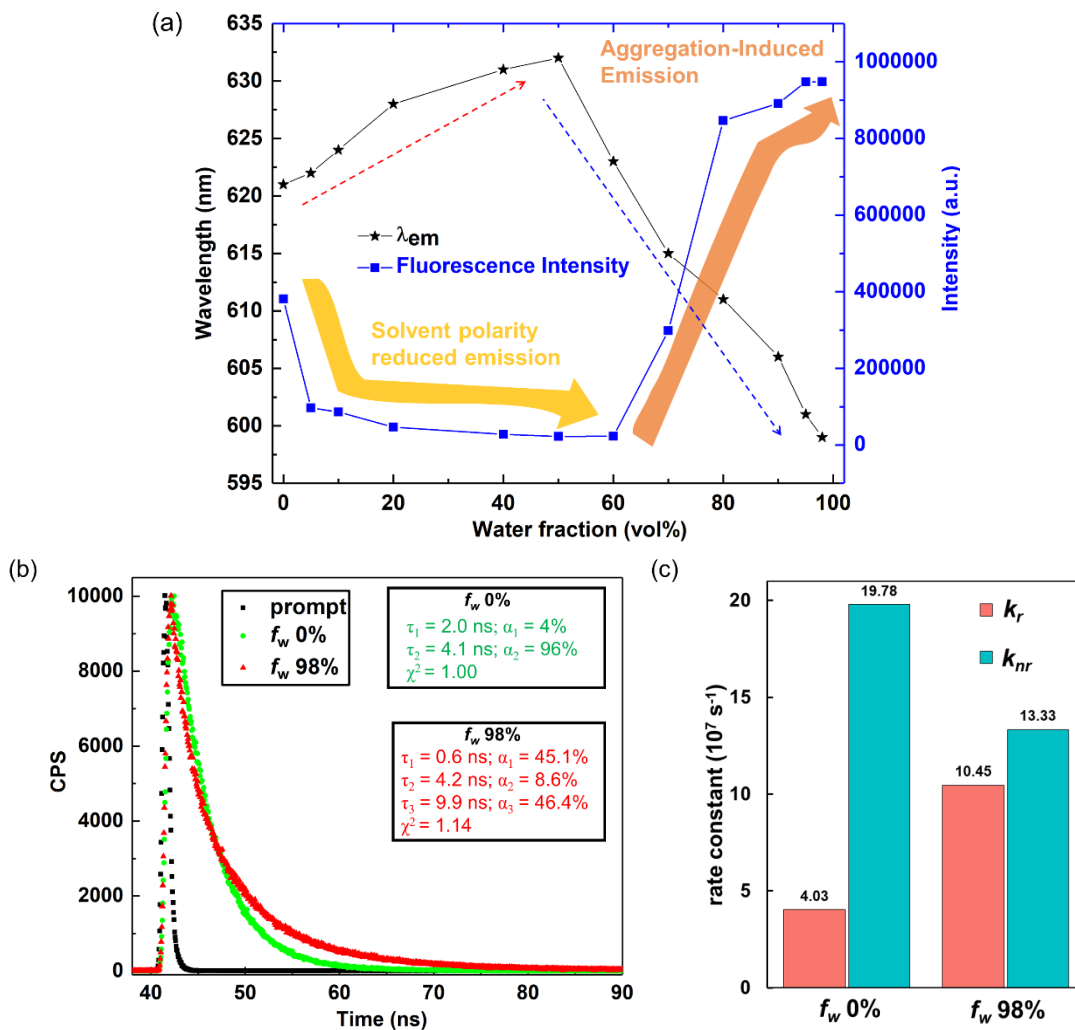


Figure I.11 (a) Plots of maximum emission intensity and wavelength (λ_{em}) of **2b** (10 μ M) versus varying water fraction (f_w) in the THF/water mixture. (b) Time-resolved fluorescence decay plots of **2b** in pure THF ($f_w = 0\%$) and 98% water in THF solution ($f_w = 98\%$), $\lambda_{ex} = 344$ nm. (c) Rate constants of radiative (k_r , red) and non-radiative decay (k_{nr} , green) of **2b** in pure THF ($f_w = 0\%$) and 98% water in THF solution ($f_w = 98\%$).

The small red-shift for the emission maximum and diminished intensity in the first stage were due to the increased solvent polarity, which is enhanced by the water. When the water fraction is up to 60%, the hypsochromic-shift in the emission maximum and enhanced fluorescence intensity were observed. The absolute photoluminescence quantum yield of colloidal sample of **2b** ($f_w = 98\%$) was determined to be 0.44.

The restricted intramolecular motion (RIR) of its substituents was realized upon aggregation due to the overcrowded environment within the non-K region of **2b**. The blue-shifted emission can be associated with considerable geometrical restrictions in the aggregated state, which lead to smaller distortion of the excited state and hence smaller Stokes shift.

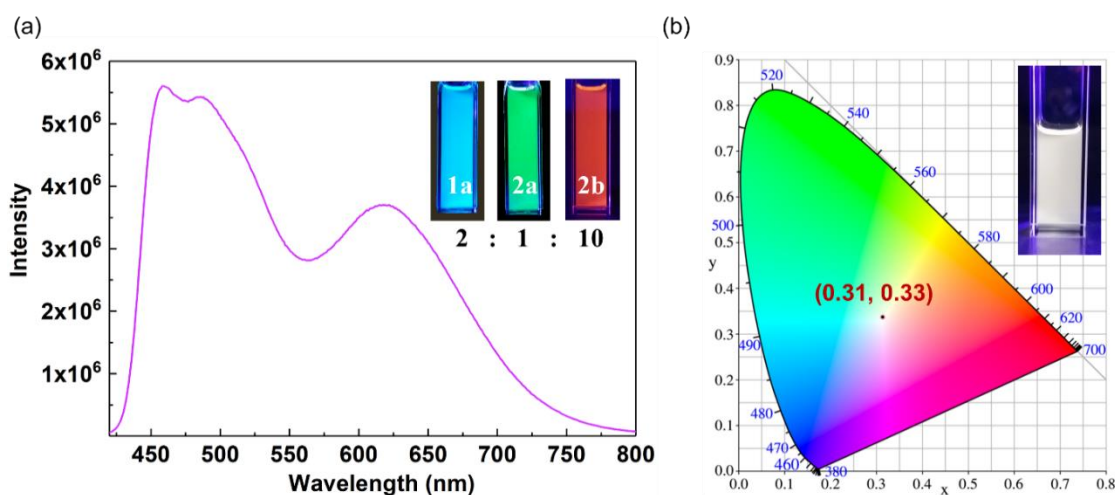


Figure I.12 Emission spectrum excited at 430 nm (a) and its emission color coordinates in the CIE 1931 chromaticity diagram (b) of the solution mixture (**1a/2a/2b**, ~2/1/10, in a screened molar ratio, total concentration: 10 μ M) in CH_2Cl_2 at 298 K. The pictures were taken under 365 nm UV light exposure.

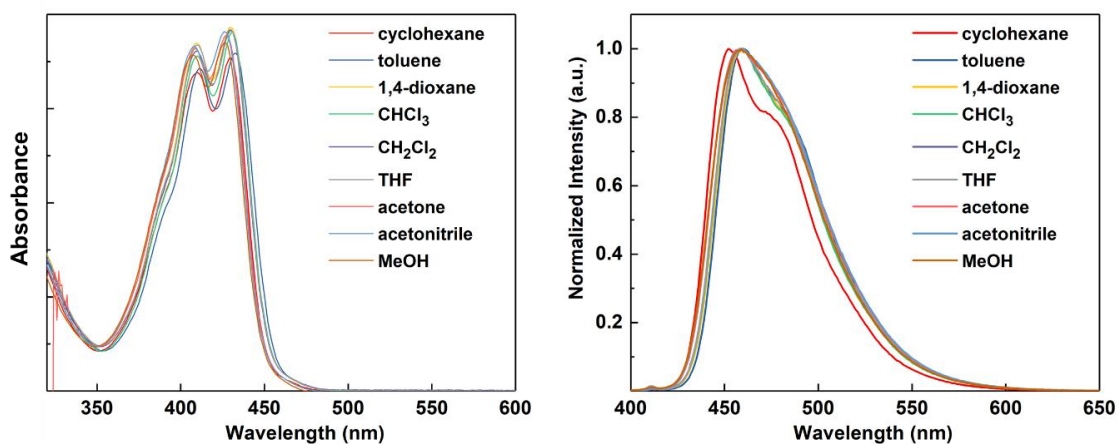


Figure I.13 Absorption (left) and fluorescence (right) spectra of **1a** in various solvents.

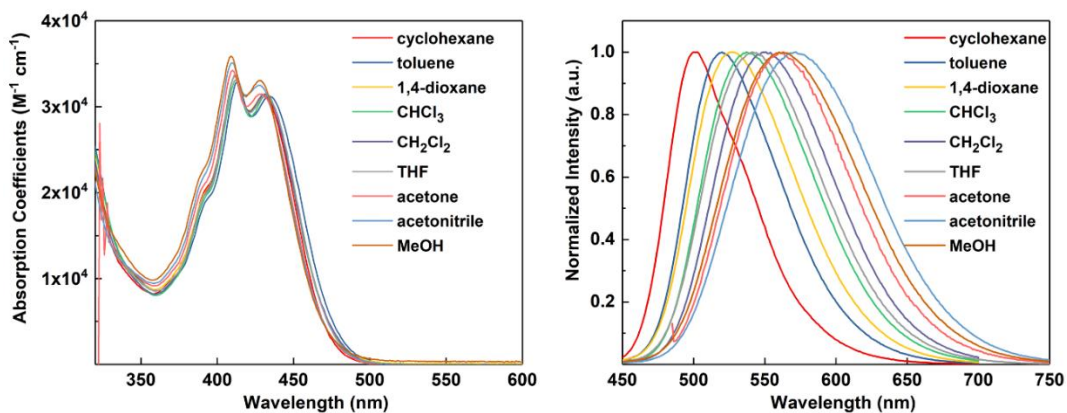


Figure I.14 Absorption (left) and fluorescence (right) spectra of **1b** in various solvents.

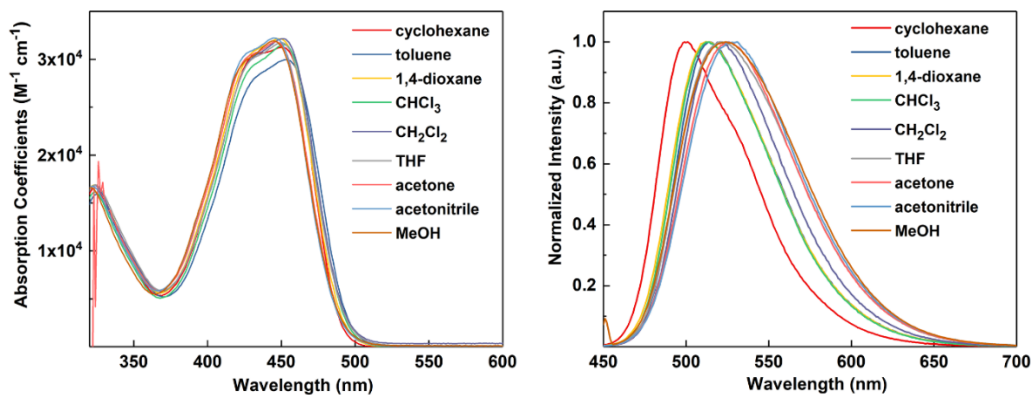


Figure I.15 Absorption (left) and fluorescence (right) spectra of **2a** in various solvents.

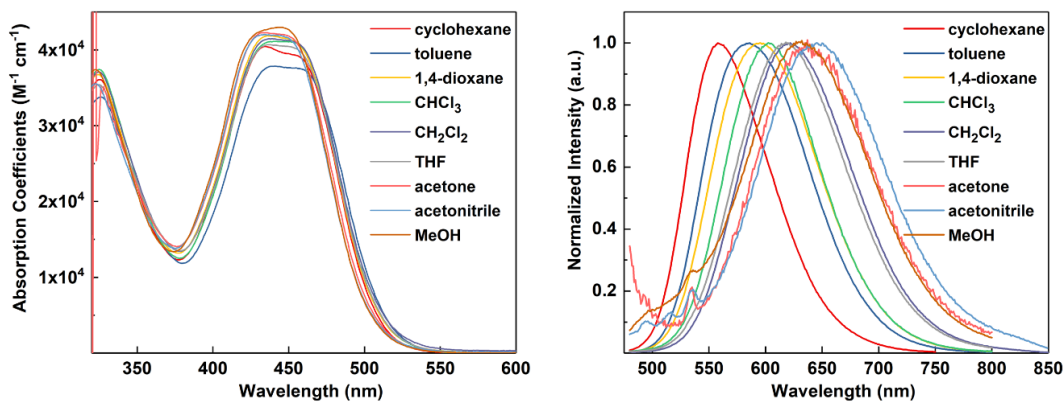


Figure I.16 Absorption (left) and fluorescence (right) spectra of **2b** in various solvents.

Table I.2 Photophysical data for compounds **1** and **2**

Compound	Solvent	$\lambda_{\text{abs}}(\text{nm})^a$	$\lambda_{\text{em}}(\text{nm})$	$\log \epsilon$ ($\text{M}^{-1} \text{cm}^{-1}$)	Stokes Shift (nm)	Stokes Shift (cm^{-1})	Φ_{F} (%) ^c	τ_{F} (ns) ^d
1a	cyclohexane	430	452	^b	22	1132	64	1.9
	toluene	433	460	^b	27	1356	60	1.7
	dioxane	430	460	4.59	30	1517	55	1.8
	CHCl ₃	431	458	4.58	27	1368	56	1.6
	CH ₂ Cl ₂	430	459	4.58	29	1469	57	1.6
	THF	430	459	4.58	29	1469	51	1.7
	acetone	427	459	4.58	32	1633	56	1.8
	MeCN	426	459	4.58	33	1688	54	1.8
	MeOH	426	459	4.57	33	1688	51	1.7

Compound	Solvent	$\lambda_{\text{abs}}(\text{nm})^a$	$\lambda_{\text{em}}(\text{nm})$	$\log \epsilon$ ($\text{M}^{-1} \text{cm}^{-1}$)	Stokes Shift (nm)	Stokes Shift (cm^{-1})	Φ_{F} (%) ^c	τ_{F} (ns) ^d
1b	cyclohexane	431	502	4.49	71	3281	56	1.8
	toluene	434	518	4.49	84	3736	61	2.0
	dioxane	432	526	4.50	94	4137	61	2.6
	CHCl ₃	433	537	4.50	104	4472	58	2.8
	CH ₂ Cl ₂	431	551	4.50	120	5053	62	3.8
	THF	432	541	4.50	109	4663	49	3.2
	acetone	429	560	4.50	131	5452	52	4.2
	MeCN	428	572	4.51	144	5882	39	4.8
	MeOH	428	563	4.52	135	5602	29	4.2

Compound	Solvent	$\lambda_{\text{abs}}(\text{nm})^a$	$\lambda_{\text{em}}(\text{nm})$	$\log \epsilon$ ($\text{M}^{-1} \text{cm}^{-1}$)	Stokes Shift (nm)	Stokes Shift (cm^{-1})	Φ_{F} (%) ^c	τ_{F} (ns) ^d
2a	cyclohexane	451	501	4.50	50	2213	54	1.9
	toluene	453	514	4.49	61	2620	66	2.5
	dioxane	448	514	4.51	66	2866	62	2.6
	CHCl ₃	452	514	4.50	62	2667	60	2.4
	CH ₂ Cl ₂	450	521	4.51	71	3028	61	2.9
	THF	451	521	4.50	70	2979	61	3.1
	acetone	446	526	4.50	80	3410	64	3.6
	MeCN	445	531	4.51	86	3639	63	3.7
	MeOH	444	524	4.50	80	3438	65	3.8

Compound	Solvent	$\lambda_{\text{abs}}(\text{nm})^a$	$\lambda_{\text{em}}(\text{nm})$	$\log \epsilon$ ($\text{M}^{-1} \text{cm}^{-1}$)	Stokes Shift (nm)	Stokes Shift (cm^{-1})	Φ_{F} (%) ^c	τ_{F} (ns) ^d
2b	cyclohexane	434	558	4.61	124	5120	44	4.3
	toluene	441	586	4.58	145	5611	49	6.2
	dioxane	436	595	4.62	159	6129	48	6.6
	CHCl ₃	441	603	4.61	162	6092	49	7.2
	CH ₂ Cl ₂	437	622	4.62	185	6806	23	5.8
	THF	437	620	4.61	183	6754	17	2.0(4)/4.1(96) ^e
	acetone	435	635	4.62	200	7188	11	1.8(78)/7.7(10) ^e
	MeCN	434	645	4.62	211	7240	0.4	0.5(78)/3.8(22) ^e
	MeOH	444	636	4.63	192	6799	0.4	0.3(85)/3.3(15) ^e

^aThe longest absorption maxima. ^b Not determined due to the limited solubility. ^c Relative quantum yields, errors within 5%. ^d Fitted with mono-exponential model. ^e Fitted with bi-exponential model and the amplitudes of two lifetimes given in parentheses.

Table I.3 Lippert-Mataga Plot data for **2b**

Solvent	$\lambda_{\text{abs}}(\text{nm})$	$\lambda_{\text{em}}(\text{nm})$	Δf	Stokes Shift (cm^{-1})
cyclohexane	434	558	0	5120
toluene	441	586	0.0131	5611
CHCl_3	441	603	0.01482	6092
CH_2Cl_2	437	622	0.2171	6806
THF	437	620	0.21	6754
acetone	435	635	0.2843	7188
MeCN	434	645	0.3086	7240

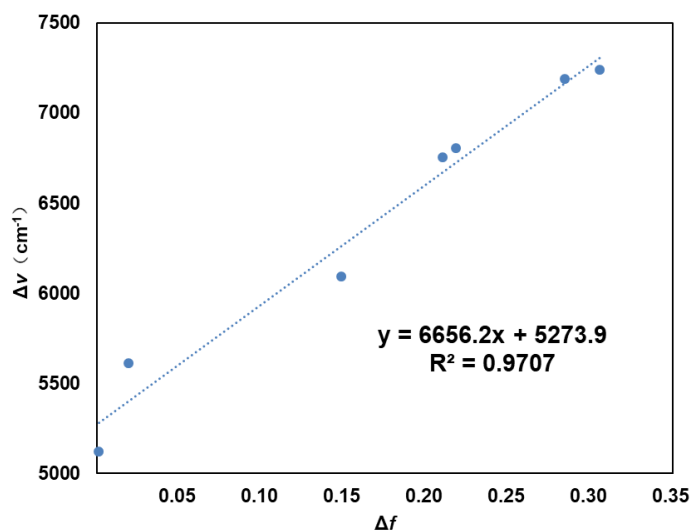


Figure I.17 Plot of the Stokes shift (cm^{-1} , $\Delta\nu$) versus the solvent polarity function (Δf) for **2b**.

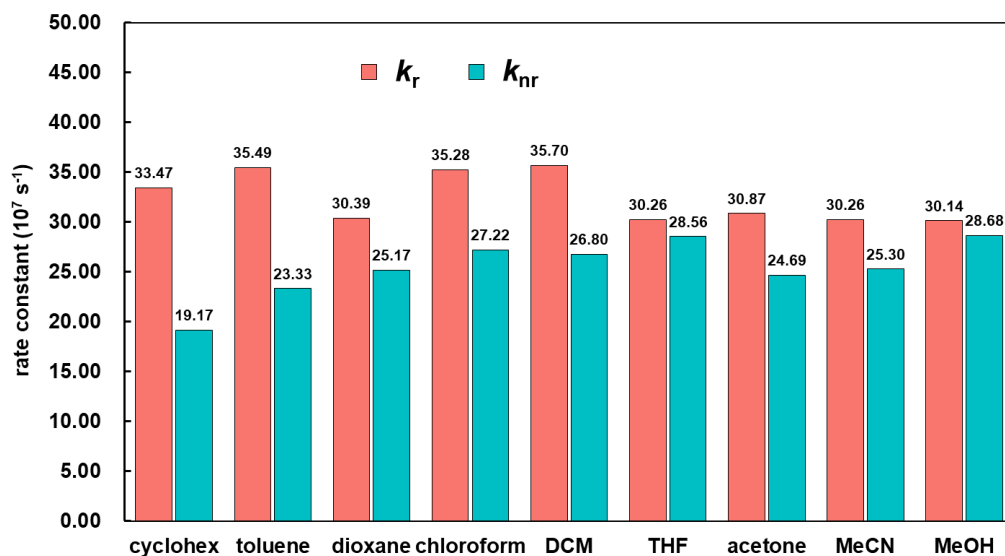


Figure I.18 Rate constants of radiative (k_r , red) and non-radiative decay (k_{nr} , green) of **1a** in various solvents.

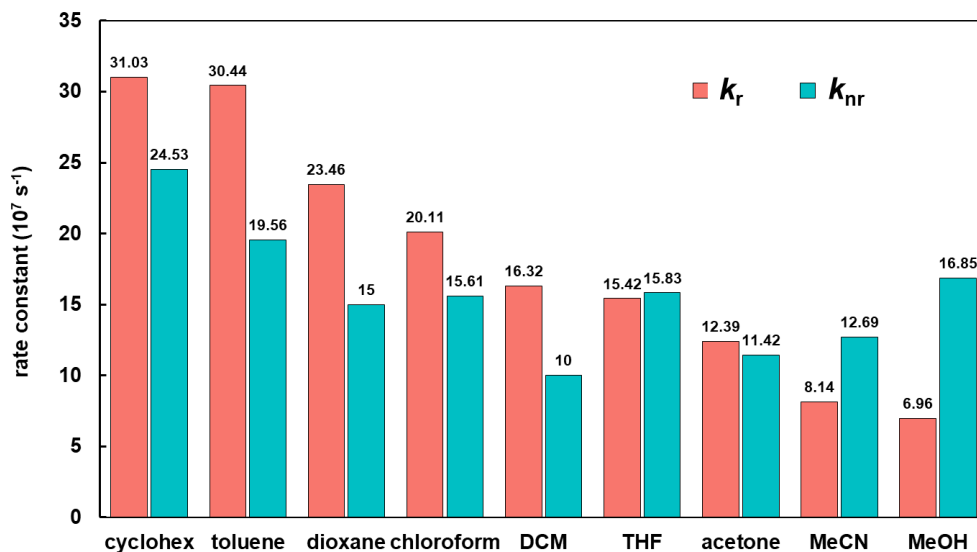


Figure I.19 Rate constants of radiative (k_r , red) and non-radiative decay (k_{nr} , green) of **1b** in various solvents.

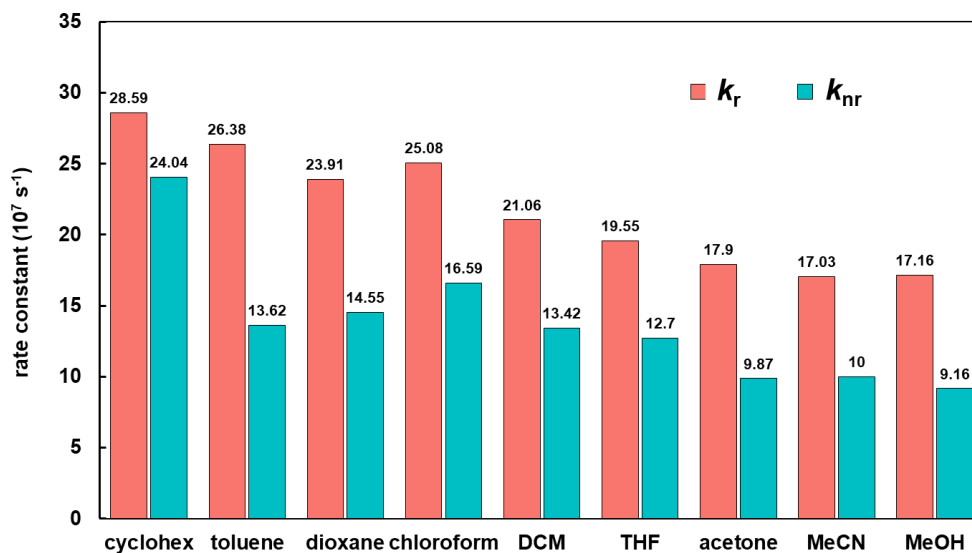


Figure I.20 Rate constants of radiative (k_r , red) and non-radiative decay (k_{nr} , green) of **2a** in various solvents.

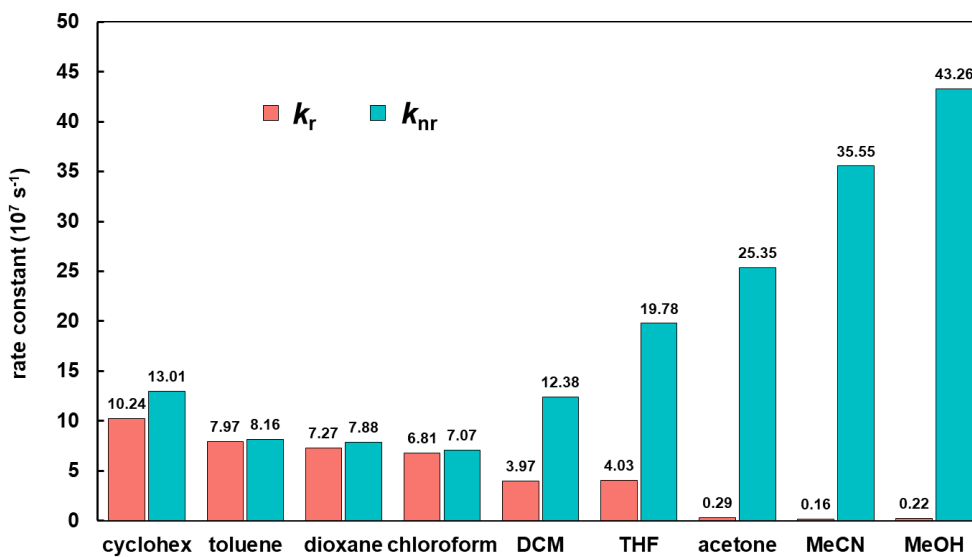


Figure I.21 Rate constants of radiative (k_r , red) and non-radiative decay (k_{nr} , green) of **2b** in various solvents. The abrupt decrease of the quantum yield of **2b** observed in highly polar solvents (MeCN, MeOH) could be related to the twisted intramolecular charge transfer (TICT)-like excited state, resulting in very small k_r .

4. Electrochemistry

All cyclic voltammetry (CV) experiments were conducted using a 3-electrode geometry using a Biologic SP-50 potentiostat. Electrolyte solutions (0.1 M) were prepared from anhydrous, deoxygenated CH_2Cl_2 and anhydrous Bu_4NPF_6 . The working electrode was a glassy carbon electrode (3-mm diameter), with a Pt-coil counter electrode and an Ag wire pseudo reference. Sample concentrations were ca. 1 mM. The ferrocene/ferrocenium (Fc/Fc^+) couple was used as an internal standard following each experiment. Potential values were re-referenced based on the redox potential of Fc/Fc^+ being -4.8 eV vs the vacuum level.²⁷ For reversible or quasi-reversible couples, $E_{\text{ox}(\text{red})} = 1/2(E_{\text{pc}} + E_{\text{pa}})$; for irreversible couples, value is estimated as the E_{pa} (E_{pc}) at peak current.

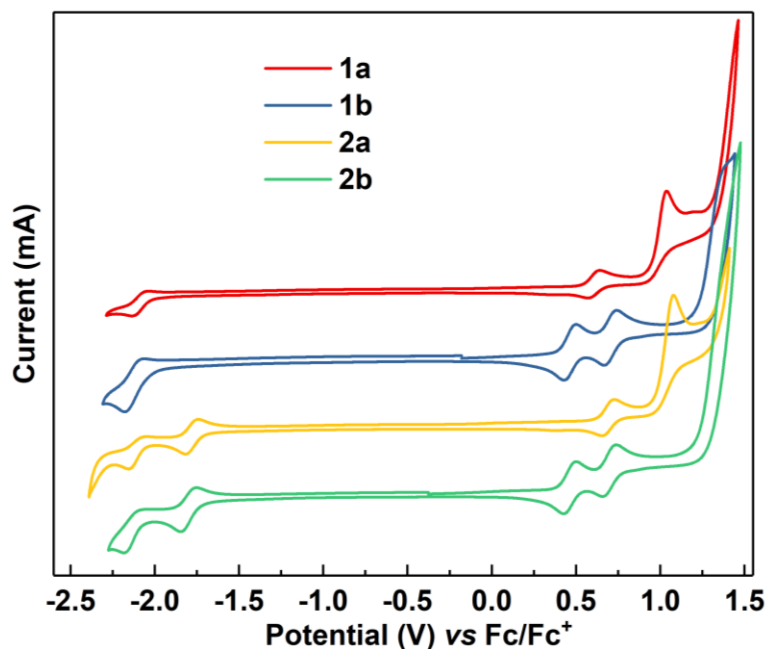


Figure I.22 Cyclic voltammograms of **1** and **2** (0.1 M Bu₄NPF₆ in CH₂Cl₂, potential vs Fc/Fc⁺, scanning rate $\nu = 50 \text{ mV s}^{-1}$).

Table I.4 Summary of electrochemical data of **1** and **2**

compd	E_{red}^1 (V) ^a	E_{red}^2 (V) ^a	E_{ox}^1 (V) ^a	E_{ox}^2 (V) ^a	E_{LUMO} (eV) ^b	E_{HOMO} (eV) ^b	E_g^{CV} (eV) ^c	E_g^{opt} (eV) ^d	E_g^{DFT} (eV) ^e
1a	-2.13	—	0.61	1.06	-2.67	-5.41	2.74	2.74	2.97
1b	-2.18	—	0.46	0.71	-2.62	-5.26	2.64	2.60	2.82
2a	-1.78	-2.16	0.69	1.08	-3.02	-5.49	2.47	2.52	2.79
2b	-1.79	-2.18	0.46	0.70	-3.01	-5.26	2.25	2.35	2.58

^a Potential vs Fc/Fc⁺. ^b $E_{\text{HOMO/LUMO}} = -(E_{\text{ox/red}} + 4.8 \text{ eV})$. ^c $E_g^{\text{CV}} = E_{\text{HOMO}} - E_{\text{LUMO}}$. ^d $E_g^{\text{opt}} = 1240/\lambda_{\text{onset}}$. ^e Determined by the DFT calculations (B3LYP/6-311G**).

5. Theoretical Calculations

The initial structures were generated from the X-ray crystallography data for **1a**. Other similar structures are adjusted according to the structures in the single crystal. These initial structures were optimized using the functional B3LYP and 6-311G(d,p) basis set as implemented in Gaussian 09.²⁸ In addition, all the optimized structures were confirmed by frequency analysis and the number of imaginary frequencies was zero. Initially, TD-DFT vertical excitation calculations were performed using the long-range-corrected CAM-B3LYP (which is reported are necessary to obtain a reliable energy ordering in the excited states of pyrene itself, it is composed of 19% HF exchange at short-range and 65% HF exchange at long-range)²⁹ and B3LYP (20% HF exchange) theory with the unified 6-311+G(d,p) basis set. We found that the former DFT method qualitatively reproduce the experimentally obtained absorption characteristics (possible vibrational progression on the PN-heterocyclic pyrene core may mix with the absorption band, like ca. 2320 cm⁻¹ in **1**, ca. 2220 cm⁻¹ in **2**, since the intensities for these two peaks are diminished as the ICT effect and structural/conformational flexibility increase), while the latter gave significantly red-shifted electronic transition energies with respect to the experimental values (Tables I.5-I.6). Nevertheless, all the methods assign the lowest energy absorption bands to the ground state (S₀) → the first excited state (S₁) electronic transitions with the largest oscillator strength, which are dominated by the transitions from HOMO to LUMO. The geometry optimization of S₁ for **2b** were carried out at TD-B3LYP/6-311G(d,p) level of theory. The PCM solvation model³⁰ was used to account for the solvent effects of the CH₂Cl₂. Orbital composition analysis with Ros-Schuit (C-squared Population Analysis, SCPA) method and Mayer bond order analysis using Multiwfn software.³¹

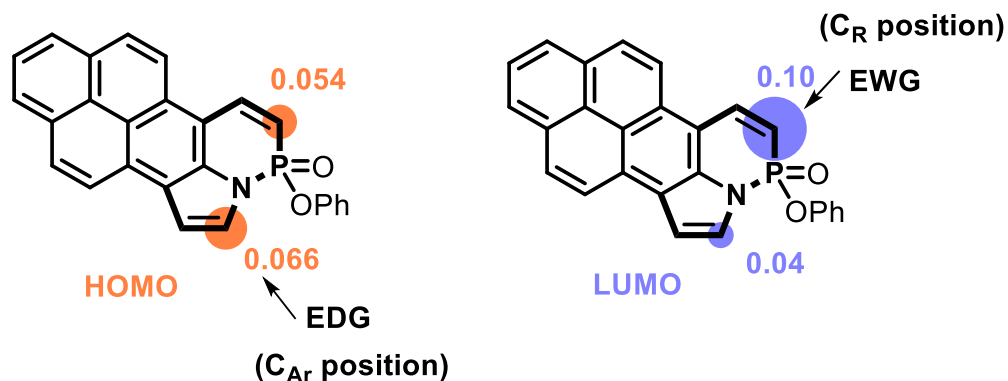


Figure I.23 Atomic contributions to HOMO (left) and LUMO (right) electron densities for the parent core. The orange/blue circle diameter represents the atomic contribution, calculated at the B3LYP/6-311G(d,p) level of theory. Only functionalizable positions are shown.

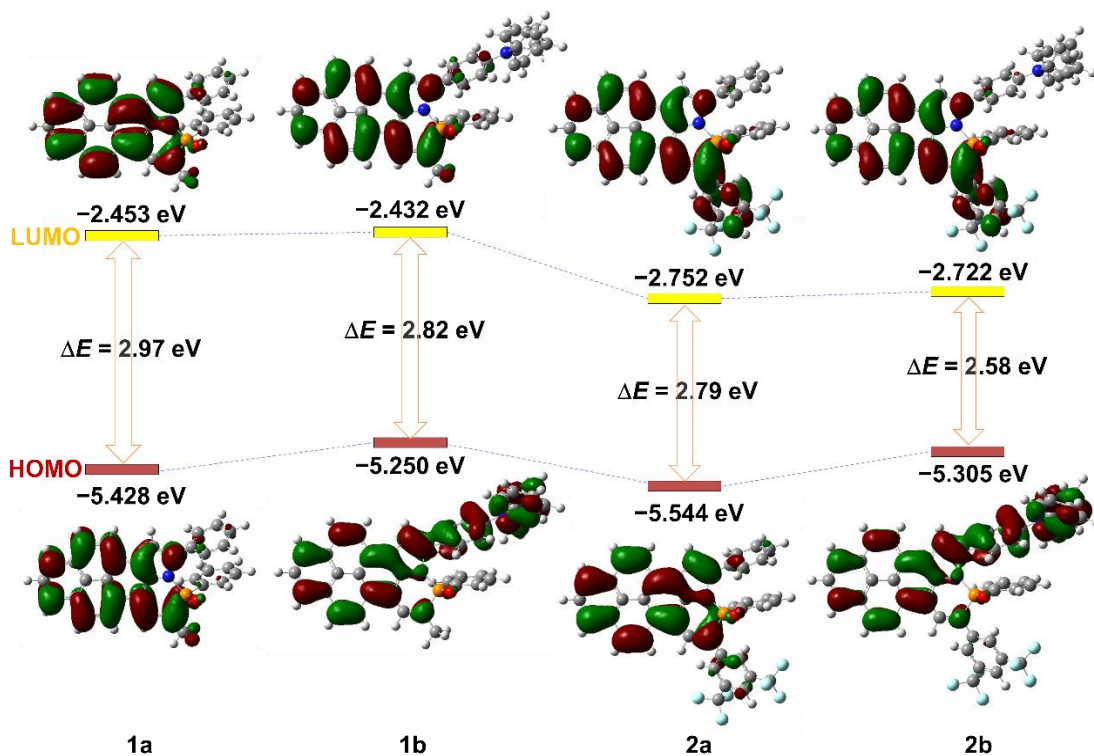


Figure I.24 Molecular orbital diagram for **1** and **2**, calculated at the B3LYP/6-311G(d,p) level of theory.

Table I.5 Selected wavelength, oscillator strength (*f*) and major configuration calculated at the PCM(CH₂Cl₂)-TD-CAM-B3LYP/6-311+G(d,p) level of theory

	λ_{cal} (nm)	electronic transitions	f	Major configurations
1a	404	$S_1 \leftarrow S_0$	1.2408	HOMO→LUMO (97%)
	348	$S_2 \leftarrow S_0$	0.083	HOMO-1→LUMO (76%), HOMO→LUMO+2 (8%), HOMO→LUMO+3 (6%)
	293	$S_3 \leftarrow S_0$	0.2946	HOMO-2→LUMO (10%), HOMO→LUMO+1 (23%), HOMO→LUMO+3 (41%)
	267	$S_6 \leftarrow S_0$	0.2078	HOMO-2→LUMO (31%), HOMO→LUMO+1 (12%), HOMO→LUMO+3 (25%), HOMO→LUMO+4 (13%)
...				
1b	409	$S_1 \leftarrow S_0$	1.4206	HOMO-1→LUMO (10%), HOMO→LUMO (86%)
	353	$S_2 \leftarrow S_0$	0.1745	HOMO-2→LUMO (55%), HOMO-1→LUMO (24%)
	322	$S_3 \leftarrow S_0$	0.2814	HOMO-2→LUMO (11%), HOMO-1→LUMO (31%), HOMO-1→LUMO+2 (10%), HOMO→LUMO+2 (12%), HOMO→LUMO+3 (12%)
...				
2a	428	$S_1 \leftarrow S_0$	1.2669	HOMO→LUMO (96%)
	359	$S_2 \leftarrow S_0$	0.1585	HOMO-1→LUMO (82%)
	307	$S_3 \leftarrow S_0$	0.3472	HOMO-2→LUMO (10%), HOMO→LUMO+2 (52%)
...				
2b	433	$S_1 \leftarrow S_0$	1.3541	HOMO-1→LUMO (18%), HOMO→LUMO (78%)
	367	$S_2 \leftarrow S_0$	0.3022	HOMO-2→LUMO (54%), HOMO-1→LUMO (27%)
	331	$S_3 \leftarrow S_0$	0.1888	HOMO-2→LUMO (19%), HOMO-1→LUMO (28%), HOMO→LUMO+5 (13%)
	307	$S_4 \leftarrow S_0$	0.3803	HOMO-1→LUMO (11%), HOMO→LUMO+2 (41%)
...				

Table I.6 Selected wavelength, oscillator strength (f) and major configuration calculated at the PCM(CH₂Cl₂)-TD-B3LYP/6-311+G(d,p) level of theory

	λ_{cal} (nm)	electronic transitions	f	Major configurations
1a	452	$S_1 \leftarrow S_0$	0.9763	HOMO→LUMO (97%)
	381	$S_2 \leftarrow S_0$	0.0913	HOMO-1→LUMO (84%), HOMO→LUMO+3 (7%)
	351	$S_3 \leftarrow S_0$	0.0574	HOMO→LUMO+1 (93%)
	311	$S_7 \leftarrow S_0$	0.1868	HOMO-2→LUMO (18%), HOMO→LUMO+3 (55%)
		...		
1b	495	$S_1 \leftarrow S_0$	0.6918	HOMO→LUMO (96%)
	429	$S_2 \leftarrow S_0$	0.4885	HOMO-1→LUMO (95%)
	368	$S_3 \leftarrow S_0$	0.035	HOMO-2→LUMO (70%), HOMO→LUMO+1 (13%)
	350	$S_3 \leftarrow S_0$	0.4576	HOMO→LUMO+2 (79%), HOMO→LUMO+3 (10%)
		...		
2a	489	$S_1 \leftarrow S_0$	0.9142	HOMO→LUMO (98%)
	401	$S_2 \leftarrow S_0$	0.1981	HOMO-1→LUMO (92%)
	375	$S_3 \leftarrow S_0$	0.0157	HOMO→LUMO+1 (98%)
	363	$S_4 \leftarrow S_0$	0.2122	HOMO-2→LUMO (12%), HOMO→LUMO+2 (83%)
	351	$S_5 \leftarrow S_0$	0.1329	HOMO-2→LUMO (76%), HOMO→LUMO+2 (11%)
		...		
2b	546	$S_1 \leftarrow S_0$	0.4590	HOMO→LUMO (98%)
	464	$S_2 \leftarrow S_0$	0.6173	HOMO-1→LUMO (97%)
	397	$S_3 \leftarrow S_0$	0.0401	HOMO→LUMO+1 (87%)
	393	$S_4 \leftarrow S_0$	0.089	HOMO-2→LUMO (81%)
	381	$S_5 \leftarrow S_0$	0.4755	HOMO→LUMO+2 (87%)
		...		

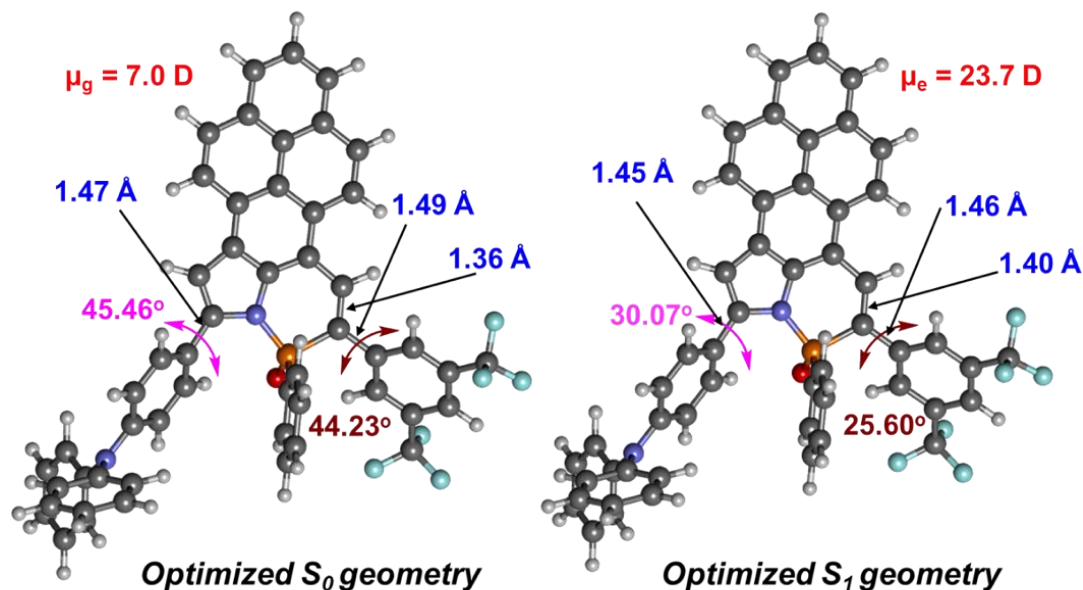


Figure I.25 Selected bond lengths (Å) and dihedral angles (°) in the optimized S_0 and S_1 structures of **2b** calculated by the DFT and TD-DFT methods at the PCM(DCM)-B3LYP/6-311G(d,p) levels of theory, respectively.

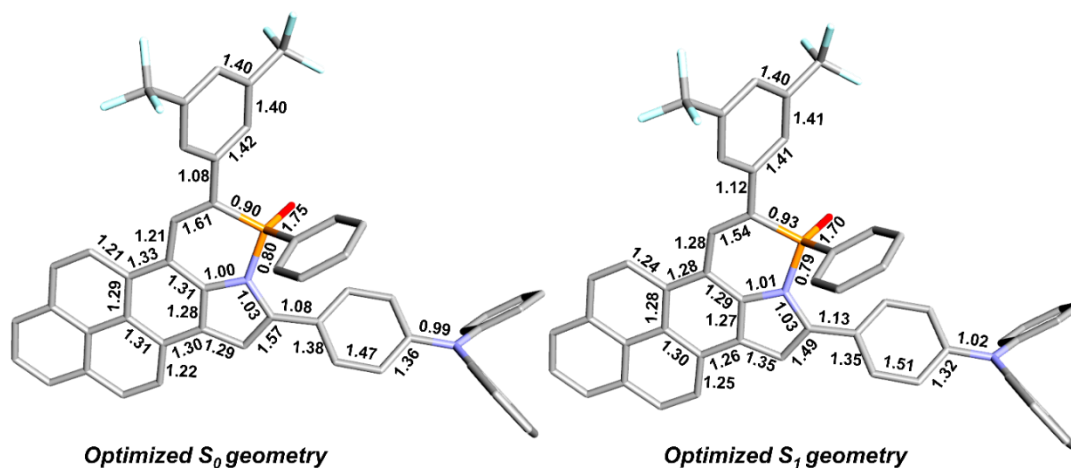


Figure I.26 Selected Mayer bond indices in the optimized S_0 and S_1 structures of **2b** calculated by the DFT and TD-DFT methods at the PCM(DCM)-B3LYP/6-311G(d,p) levels of theory, respectively.

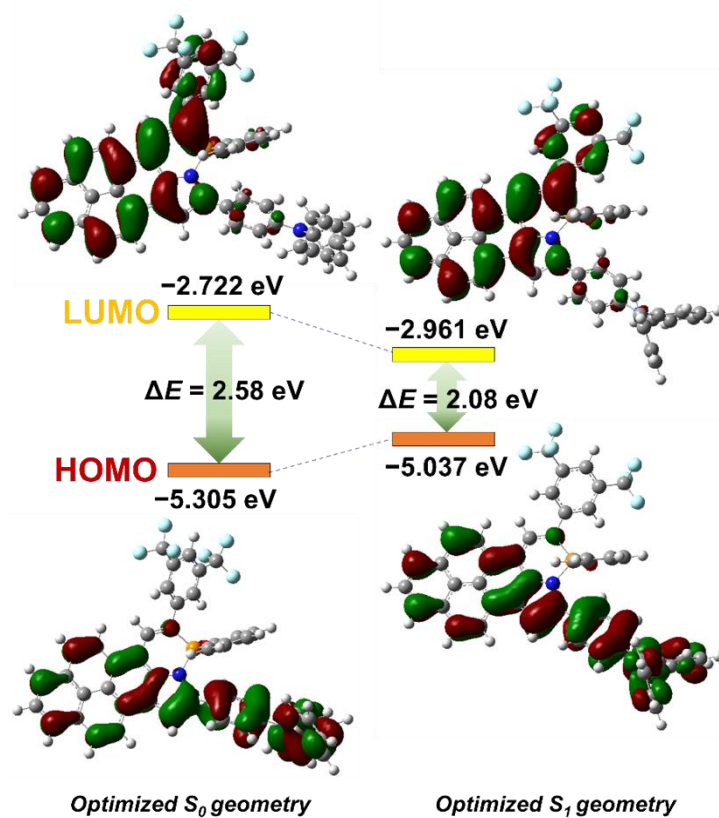


Figure I.27 HOMO-LUMO energies and their differences (ΔE) in the optimized S_0 and S_1 structures of **2b** calculated by the DFT and TD-DFT methods at the PCM(DCM)-B3LYP/6-311G(d,p) levels of theory, respectively.

Table I.7 Cartesian coordinates for compound **1a**

	X	Y	Z
P	1.07271	1.85190	-0.84132
O	1.75912	1.86337	-2.17463
N	0.29059	0.36049	-0.43130
C	-0.30069	3.01724	-0.72302
C	-1.58764	2.62532	-0.59726
C	-2.04300	1.26294	-0.42146
C	-1.09627	0.23466	-0.33634
C	-1.41167	-1.10931	-0.07226
C	-0.17112	-1.81462	0.00260
C	0.85022	-0.92824	-0.22115
C	-2.76335	-1.49432	0.07082
C	-3.76302	-0.48264	-0.04944
C	-3.40905	0.89212	-0.29020
C	-4.47584	1.84858	-0.39276
C	-5.78125	1.49078	-0.26972
C	-6.16574	0.13237	-0.02543
C	-5.13875	-0.85136	0.08512
C	-5.50169	-2.21016	0.33392
C	-4.46487	-3.19010	0.45081
C	-3.15396	-2.84482	0.32693
C	-6.85992	-2.54893	0.45984
C	-7.84953	-1.57994	0.34667
C	-7.50791	-0.25136	0.10682
C	2.28843	-1.25341	-0.23423
C	3.15508	-0.84532	-1.26019
C	4.48665	-1.25318	-1.26134
C	4.97727	-2.07503	-0.24841
C	4.12459	-2.48812	0.77453
C	2.79445	-2.08078	0.78296
C	2.21831	2.18282	0.52987
C	3.51496	2.62105	0.24142
C	4.39171	2.93053	1.27905
C	3.97703	2.80604	2.60377
C	2.68327	2.37208	2.89511
C	1.80337	2.06258	1.86235
H	-2.33609	3.40989	-0.60746
H	-0.03005	-2.87038	0.17142
H	-4.24196	2.88730	-0.58311
H	-6.55961	2.24112	-0.35793
H	-4.74443	-4.22075	0.64090
H	-2.38378	-3.60172	0.41801

H	-7.12812	-3.58283	0.64830
H	-8.89227	-1.85896	0.44613
H	-8.28255	0.50294	0.02015
H	2.78746	-0.21055	-2.05533
H	5.14078	-0.93120	-2.06379
H	4.49635	-3.12198	1.57161
H	2.14044	-2.39101	1.58924
H	3.83050	2.71005	-0.79073
H	5.39711	3.26605	1.05277
H	4.66070	3.04621	3.41000
H	2.36130	2.27359	3.92521
H	0.79965	1.72601	2.09595
C	0.09133	4.46599	-0.88476
H	-0.78829	5.10750	-0.80849
H	0.80702	4.77492	-0.11639
H	0.56350	4.64550	-1.85531
H	6.01453	-2.38997	-0.25484

Table I.8 Cartesian coordinates for compound **1b**

	X	Y	Z
P	1.13732	1.90003	-0.45490
O	1.89705	2.13900	-1.72543
N	0.30622	0.38378	-0.36152
C	-0.21800	3.06439	-0.19652
C	-1.51655	2.69127	-0.17785
C	-2.00654	1.33108	-0.24554
C	-1.08499	0.27979	-0.31698
C	-1.43536	-1.08146	-0.29555
C	-0.21287	-1.82075	-0.32063
C	0.83343	-0.93595	-0.36839
C	-2.79834	-1.44963	-0.25198
C	-3.77288	-0.40715	-0.21913
C	-3.38376	0.97900	-0.21055
C	-4.42682	1.96566	-0.17102
C	-5.74261	1.62560	-0.14355
C	-6.16204	0.25578	-0.14793
C	-5.15937	-0.75818	-0.18388
C	-5.55750	-2.12994	-0.18348
C	-4.54513	-3.14161	-0.21250
C	-3.22432	-2.81367	-0.24296
C	-6.92559	-2.45025	-0.15239
C	-7.89117	-1.45124	-0.12087

C	-7.51534	-0.11039	-0.11787
C	2.26314	-1.28399	-0.40810
C	3.16234	-0.74971	-1.34454
C	4.48426	-1.17155	-1.38822
C	4.95819	-2.15611	-0.50786
C	4.06113	-2.70122	0.42363
C	2.74451	-2.26731	0.47263
C	2.21309	1.94081	1.00945
C	3.51110	2.44692	0.88379
C	4.33409	2.53723	2.00469
C	3.86460	2.12392	3.25042
C	2.57018	1.61867	3.37910
C	1.74358	1.52913	2.26328
H	-2.24750	3.48669	-0.08358
H	-0.09961	-2.89312	-0.33686
H	-4.16606	3.01543	-0.17230
H	-6.50235	2.39939	-0.11955
H	-4.85161	-4.18212	-0.21046
H	-2.47324	-3.59458	-0.26591
H	-7.22107	-3.49388	-0.15294
H	-8.94192	-1.71675	-0.09760
H	-8.27118	0.66714	-0.09176
H	2.83052	0.01205	-2.03753
H	5.15733	-0.73612	-2.11621
H	4.40031	-3.46336	1.11389
H	2.07422	-2.69703	1.20778
H	3.87033	2.75750	-0.08952
H	5.34006	2.92785	1.90437
H	4.50620	2.19436	4.12134
H	2.20648	1.29379	4.34692
H	0.73970	1.13375	2.36911
C	0.20888	4.50942	-0.10625
H	-0.65961	5.15288	0.04484
H	0.90246	4.67091	0.72510
H	0.72001	4.83162	-1.01834
N	6.30406	-2.58818	-0.55843
C	6.96612	-2.72347	-1.81232
C	6.32670	-3.34993	-2.89054
C	8.26996	-2.23897	-1.98181
C	6.97692	-3.47747	-4.11449
H	5.32198	-3.73502	-2.76524
C	8.91959	-2.38576	-3.20408
H	8.76970	-1.74986	-1.15448
C	8.27717	-3.00058	-4.27839
H	6.46824	-3.96448	-4.93893

H	9.92836	-2.00530	-3.31953
H	8.78342	-3.10711	-5.23062
C	7.00755	-2.89381	0.64049
C	6.90728	-2.05549	1.75951
C	7.81823	-4.03475	0.71591
C	7.59636	-2.36115	2.92950
H	6.28944	-1.16733	1.70768
C	8.51752	-4.32352	1.88426
H	7.89856	-4.69062	-0.14240
C	8.40831	-3.49303	2.99913
H	7.50812	-1.70191	3.78586
H	9.14046	-5.21007	1.92569
H	8.94903	-3.72411	3.90941

Table I.9 Cartesian coordinates for compound **2a**

	X	Y	Z
P	1.08073	1.82858	-0.98826
O	1.68776	1.79759	-2.35873
N	0.30246	0.36193	-0.49900
C	-0.28109	3.01164	-0.81857
C	-1.57110	2.62595	-0.63430
C	-2.02378	1.27660	-0.42288
C	-1.07851	0.24491	-0.34939
C	-1.38981	-1.08915	-0.03903
C	-0.15048	-1.79966	0.00598
C	0.86569	-0.92612	-0.27880
C	-2.73656	-1.46022	0.17098
C	-3.73725	-0.44657	0.06143
C	-3.38936	0.91726	-0.23495
C	-4.45388	1.87479	-0.32930
C	-5.75510	1.52755	-0.14142
C	-6.13340	0.18152	0.16657
C	-5.10714	-0.80321	0.26621
C	-5.46431	-2.15029	0.57664
C	-4.42771	-3.13180	0.67944
C	-3.12176	-2.79941	0.48619
C	-6.81641	-2.47670	0.77529
C	-7.80657	-1.50646	0.67312
C	-7.47054	-0.18966	0.37157
C	2.29725	2.18799	0.30888
C	3.57367	2.62497	-0.06057
C	4.50309	2.96126	0.92118

C	4.16142	2.86386	2.26871
C	2.88779	2.43116	2.64000
C	1.95459	2.09608	1.66397
H	-2.31777	3.41114	-0.63516
H	-0.00800	-2.85138	0.19693
H	-4.22528	2.90496	-0.56681
H	-6.53345	2.27814	-0.22586
H	-4.70316	-4.15404	0.91518
H	-2.35233	-3.55790	0.56747
H	-7.08028	-3.50184	1.01131
H	-8.84470	-1.77605	0.82922
H	-8.24484	0.56575	0.29310
H	3.83279	2.69407	-1.10968
H	5.49231	3.29734	0.63334
H	4.88645	3.12503	3.03099
H	2.62290	2.35440	3.68796
H	0.96649	1.76119	1.95840
C	0.07467	4.44768	-0.94347
C	0.98778	4.90097	-1.90458
C	-0.51184	5.39249	-0.08604
C	1.28695	6.25825	-2.01146
H	1.44201	4.19282	-2.58554
C	-0.21108	6.74397	-0.20699
H	-1.19675	5.06544	0.68492
C	0.69266	7.19117	-1.17019
H	0.92173	8.24347	-1.26544
C	-0.81128	7.73880	0.74931
C	2.29295	6.69709	-3.04126
F	0.04039	8.03808	1.75994
F	-1.10964	8.90766	0.14022
F	-1.94650	7.28430	1.32025
F	2.24625	8.02509	-3.27401
F	3.55988	6.41110	-2.65453
F	2.10529	6.07640	-4.22701
C	2.30119	-1.25744	-0.33772
C	3.12835	-0.88549	-1.40889
C	2.84324	-2.05382	0.68548
C	4.45801	-1.29749	-1.44757
H	2.73175	-0.27804	-2.21143
C	4.17118	-2.46565	0.63933
H	2.21973	-2.33596	1.52555
C	4.98498	-2.08795	-0.42794
H	5.08167	-1.00372	-2.28428
H	4.57180	-3.07501	1.44146
H	6.02064	-2.40604	-0.46354

Table I.10 Cartesian coordinates for compound **2b**

	X	Y	Z
P	1.09355	1.82685	-0.83772
O	1.72796	1.90910	-2.19387
N	0.27307	0.34193	-0.50352
C	-0.24458	3.02140	-0.58302
C	-1.54667	2.65179	-0.46081
C	-2.03421	1.29919	-0.39657
C	-1.11392	0.24326	-0.40611
C	-1.46244	-1.10945	-0.25623
C	-0.24038	-1.85054	-0.25543
C	0.80335	-0.97646	-0.41360
C	-2.82381	-1.46874	-0.14452
C	-3.79936	-0.42523	-0.17553
C	-3.41306	0.95516	-0.29390
C	-4.45341	1.94310	-0.30900
C	-5.76830	1.60745	-0.22054
C	-6.18591	0.24309	-0.10381
C	-5.18389	-0.77100	-0.07914
C	-5.58067	-2.13731	0.04238
C	-4.56824	-3.14865	0.07555
C	-3.24845	-2.82640	-0.01076
C	-6.94696	-2.45324	0.12822
C	-7.91316	-1.45417	0.09859
C	-7.53845	-0.11839	-0.01483
C	2.23175	-1.32739	-0.46238
C	3.10572	-0.87953	-1.46576
C	4.42728	-1.30210	-1.50523
C	4.92723	-2.20364	-0.55258
C	4.05407	-2.66411	0.44585
C	2.73831	-2.22805	0.48964
C	2.29439	2.03600	0.50637
C	3.58898	2.46598	0.19670
C	4.51073	2.68574	1.21805
C	4.14343	2.47824	2.54651
C	2.85202	2.05091	2.85833
C	1.92672	1.83218	1.84259
H	-2.27562	3.45153	-0.40260
H	-0.12652	-2.92028	-0.18005
H	-4.19506	2.98917	-0.40388
H	-6.52757	2.38168	-0.24093

H	-4.87361	-4.18505	0.17076
H	-2.49759	-3.60716	0.01508
H	-7.24109	-3.49316	0.21909
H	-8.96278	-1.71614	0.16543
H	-8.29391	0.65954	-0.03556
H	2.75455	-0.18523	-2.21784
H	5.07942	-0.93272	-2.28657
H	4.41130	-3.36225	1.19214
H	2.08849	-2.59093	1.27732
H	3.86810	2.62073	-0.83808
H	5.51339	3.01792	0.97572
H	4.86173	2.65032	3.33988
H	2.56703	1.88844	3.89114
H	0.92523	1.50021	2.09145
N	6.27132	-2.63668	-0.59510
C	6.92331	-2.84707	-1.84406
C	6.27697	-3.53598	-2.87924
C	8.22641	-2.37511	-2.04978
C	6.91984	-3.73623	-4.09735
H	5.27273	-3.91204	-2.72572
C	8.86863	-2.59446	-3.26514
H	8.73150	-1.83794	-1.25621
C	8.21927	-3.27092	-4.29726
H	6.40594	-4.27092	-4.88832
H	9.87696	-2.22259	-3.40881
H	8.71945	-3.43418	-5.24464
C	6.99079	-2.87012	0.61253
C	6.93911	-1.94419	1.66312
C	7.76775	-4.02660	0.76044
C	7.64266	-2.18007	2.84073
H	6.34750	-1.04356	1.55264
C	8.48149	-4.24696	1.93508
H	7.80972	-4.74799	-0.04655
C	8.42018	-3.32920	2.98321
H	7.59323	-1.45410	3.64458
H	9.07817	-5.14679	2.03457
H	8.97235	-3.50627	3.89872
C	0.14546	4.45432	-0.57429
C	1.07345	4.97068	-1.49169
C	-0.41659	5.32979	0.36499
C	1.40963	6.32107	-1.47147
H	1.52084	4.31364	-2.22608
C	-0.07750	6.68050	0.37054
H	-1.11049	4.94963	1.10392
C	0.83808	7.18944	-0.54544

H	1.10515	8.23658	-0.53350
C	-0.66551	7.57543	1.42762
C	2.36117	6.85438	-2.50832
F	-0.05528	7.40395	2.62525
F	-0.55217	8.88285	1.11623
F	-1.97891	7.32389	1.62840
F	2.97611	7.98634	-2.10358
F	3.32734	5.96264	-2.81731
F	1.72442	7.15128	-3.66702

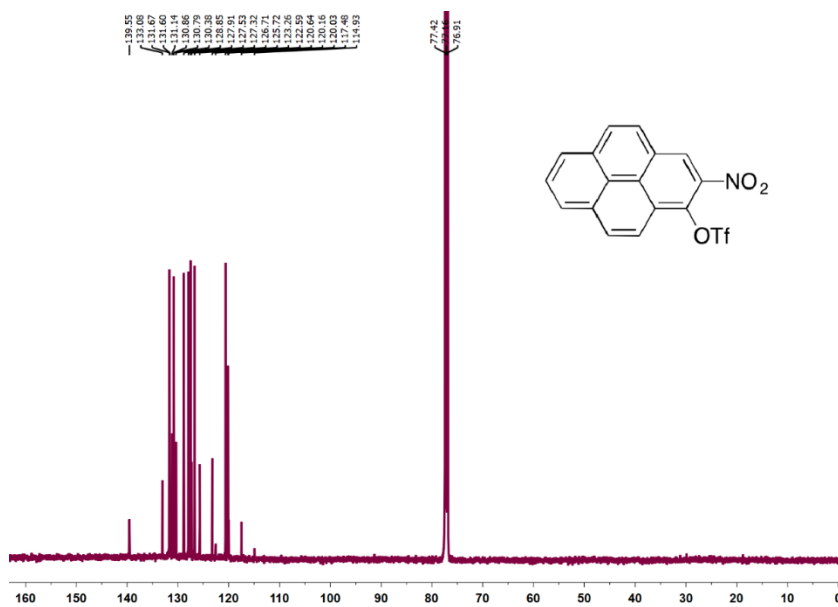
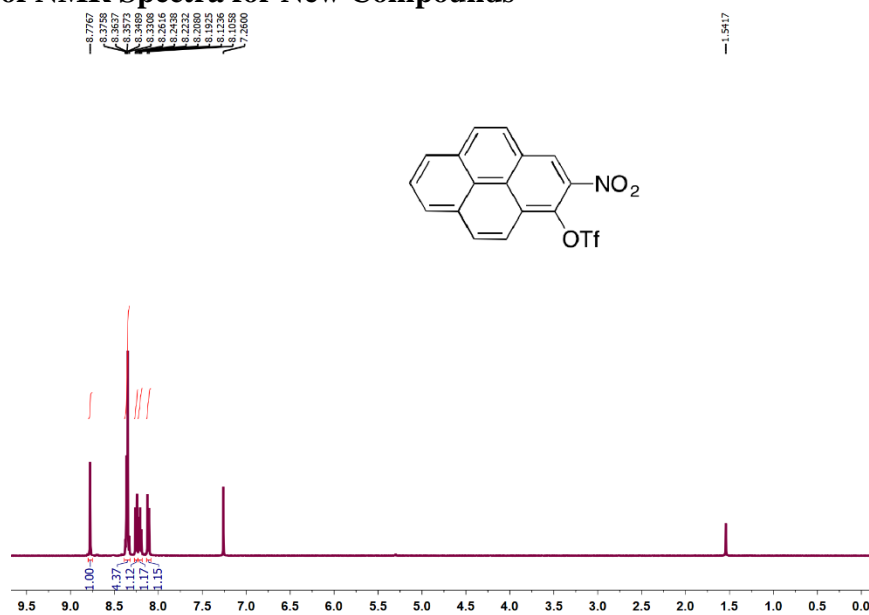
Table I.11 Cartesian coordinates for the first excited state (S_1) of compound **2b**

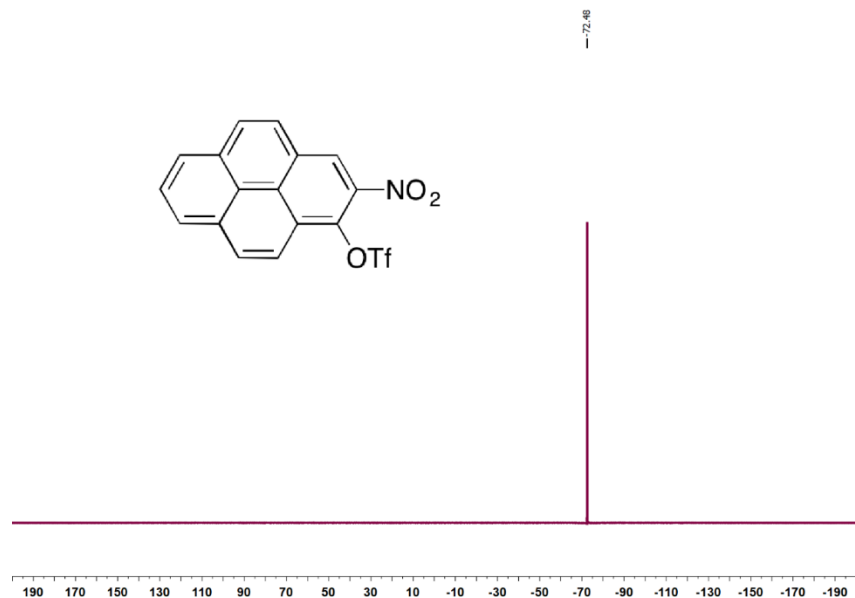
	X	Y	Z
P	0.60093	-0.68070	-0.52163
O	-0.08151	-1.21096	-1.75320
N	0.48327	1.05772	-0.36509
C	2.36036	-0.94440	-0.40561
C	3.26878	0.11631	-0.42278
C	2.95183	1.48994	-0.41723
C	1.60297	1.89665	-0.36922
C	1.18059	3.22863	-0.24093
C	-0.22076	3.19908	-0.11604
C	-0.65760	1.87444	-0.20648
C	2.13341	4.30038	-0.24171
C	3.51152	3.94039	-0.34280
C	3.92607	2.56483	-0.43026
C	5.31915	2.30143	-0.52586
C	6.25755	3.29952	-0.53038
C	5.88237	4.67105	-0.44067
C	4.49174	4.98402	-0.34823
C	4.08964	6.35557	-0.25899
C	2.70381	6.66046	-0.16245
C	1.76213	5.65836	-0.15339
C	5.07997	7.36428	-0.26739
C	6.42728	7.04141	-0.35850
C	6.83159	5.71168	-0.44397
C	-2.05189	1.48155	-0.18896
C	-2.59029	0.38116	-0.89789
C	-3.94220	0.11377	-0.88551
C	-4.83806	0.91862	-0.14589
C	-4.31099	2.01854	0.57233
C	-2.96430	2.29137	0.53837
C	-0.19792	-1.31093	0.99152

C	-1.12138	-2.35756	0.89831
C	-1.69584	-2.88772	2.05286
C	-1.35418	-2.37409	3.30180
C	-0.43304	-1.32915	3.39992
C	0.14767	-0.80260	2.25087
H	4.31616	-0.15511	-0.44323
H	-0.87850	4.04823	-0.02250
H	5.66269	1.27821	-0.60443
H	7.31065	3.05066	-0.60687
H	2.39865	7.69896	-0.09653
H	0.71076	5.91352	-0.08068
H	4.77033	8.40169	-0.19984
H	7.17080	7.83089	-0.36287
H	7.88497	5.46347	-0.51558
H	-1.93673	-0.25911	-1.47511
H	-4.31912	-0.73725	-1.43648
H	-4.97412	2.66015	1.13632
H	-2.59356	3.13876	1.09993
H	-1.38676	-2.75049	-0.07519
H	-2.40710	-3.70191	1.97485
H	-1.80102	-2.78726	4.19894
H	-0.16564	-0.92888	4.37100
H	0.86896	0.00241	2.33575
N	-6.19985	0.64166	-0.12473
C	-6.83732	0.00557	-1.23232
C	-6.59466	0.45446	-2.53696
C	-7.72232	-1.05694	-1.01012
C	-7.22562	-0.16706	-3.60873
H	-5.92804	1.29142	-2.70316
C	-8.35059	-1.66783	-2.08917
H	-7.90303	-1.40409	-0.00057
C	-8.10382	-1.22855	-3.39035
H	-7.03959	0.18766	-4.61540
H	-9.02727	-2.49557	-1.91352
H	-8.59497	-1.70853	-4.22823
C	-6.99765	0.98737	1.00813
C	-6.56688	0.65221	2.29808
C	-8.21984	1.64564	0.82554
C	-7.35308	0.98534	3.39557
H	-5.63189	0.12246	2.43186
C	-8.99894	1.97107	1.93001
H	-8.54531	1.90711	-0.17355
C	-8.56926	1.64471	3.21685
H	-7.01998	0.71733	4.39114
H	-9.93991	2.48833	1.78537

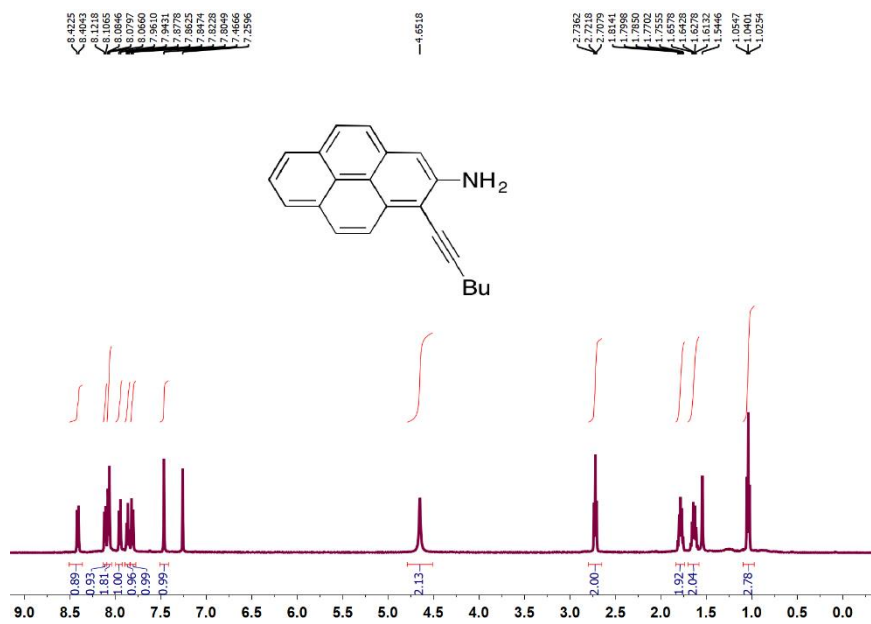
H	-9.18003	1.89977	4.07454
C	2.81072	-2.33314	-0.28620
C	2.05492	-3.42262	-0.77400
C	4.04310	-2.64576	0.33452
C	2.50277	-4.73114	-0.63941
H	1.12206	-3.23832	-1.28940
C	4.48640	-3.95643	0.44277
H	4.64766	-1.85483	0.75659
C	3.72532	-5.02371	-0.03706
H	4.07225	-6.04264	0.05629
C	5.77067	-4.24467	1.16847
C	1.68307	-5.84319	-1.23047
F	5.56351	-4.48383	2.48883
F	6.40105	-5.33684	0.67935
F	6.64776	-3.21827	1.10039
F	1.90363	-7.02795	-0.61707
F	0.35423	-5.60034	-1.15401
F	1.95969	-6.03592	-2.54533

6. Copies of NMR Spectra for New Compounds

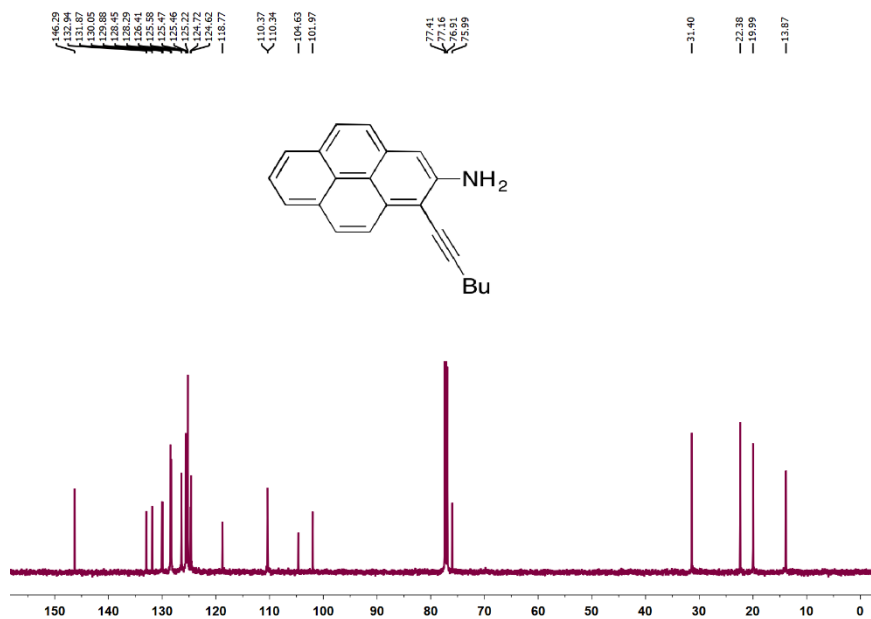




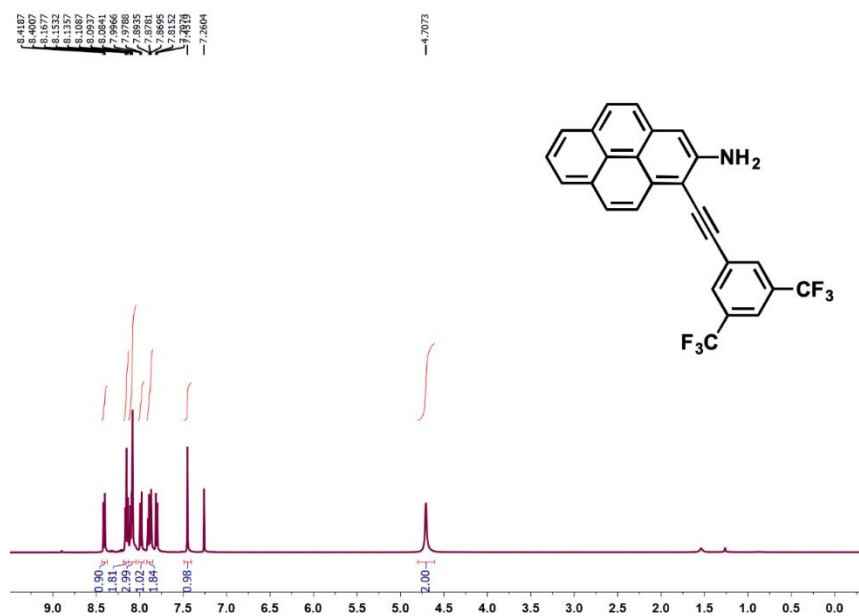
^{19}F NMR spectrum of **4** in CDCl_3 .



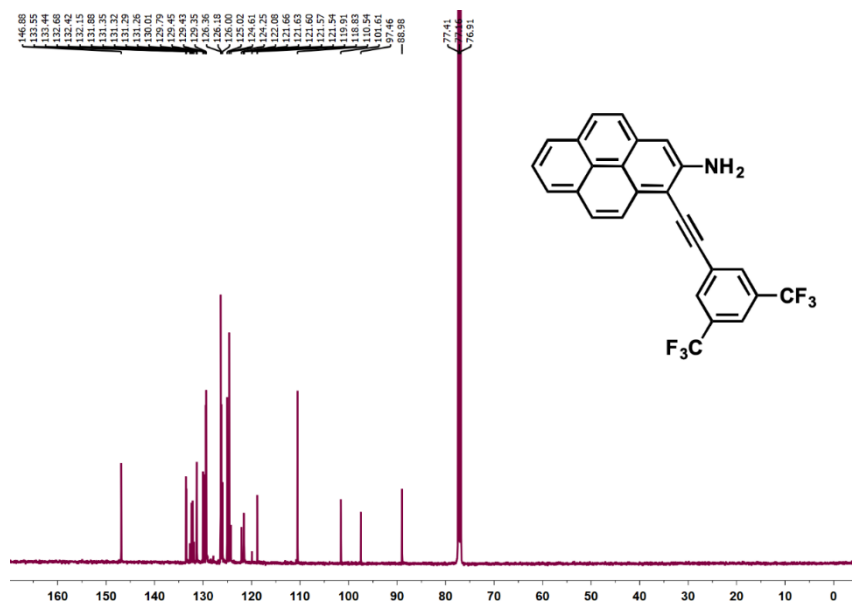
^1H NMR spectrum of **5a** in CDCl_3 .



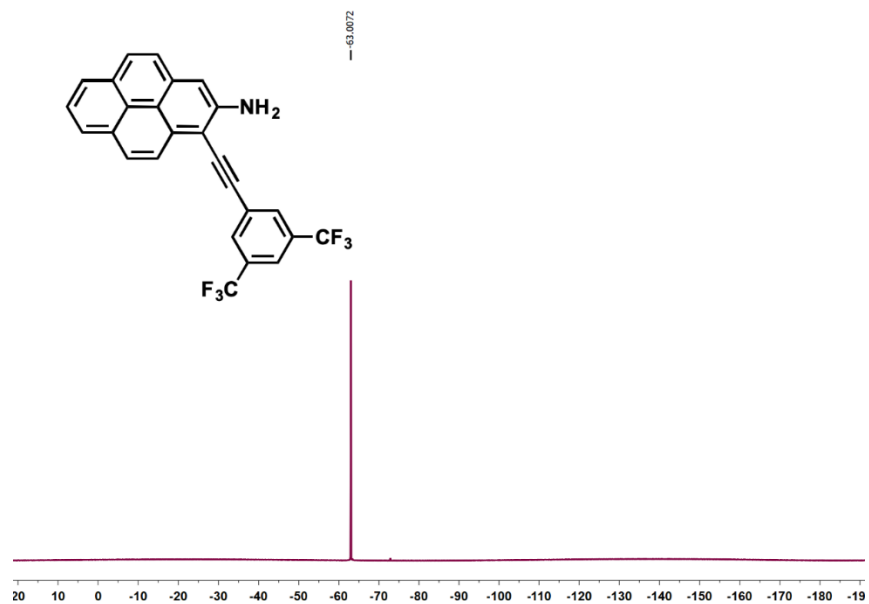
^{13}C NMR spectrum of **5a** in CDCl_3 .



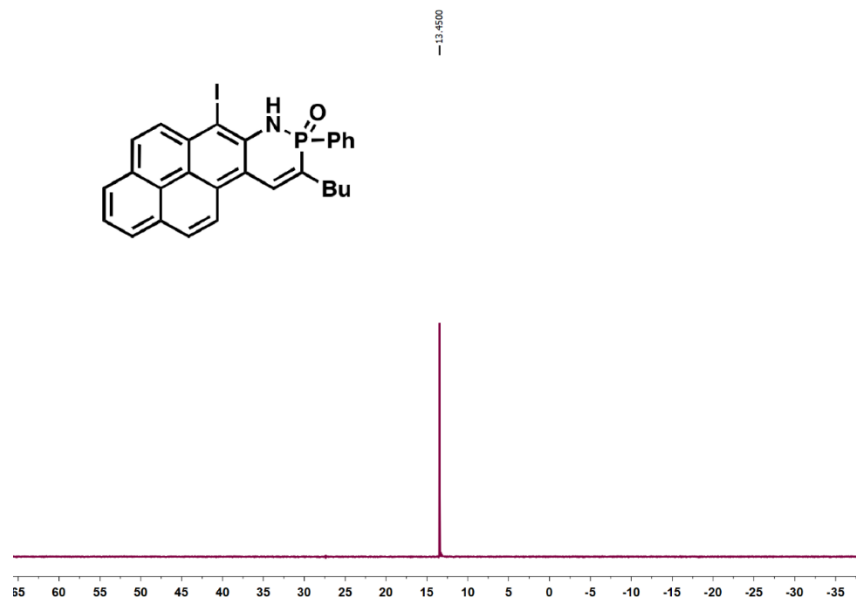
^1H NMR spectrum of **5b** in CDCl_3 .



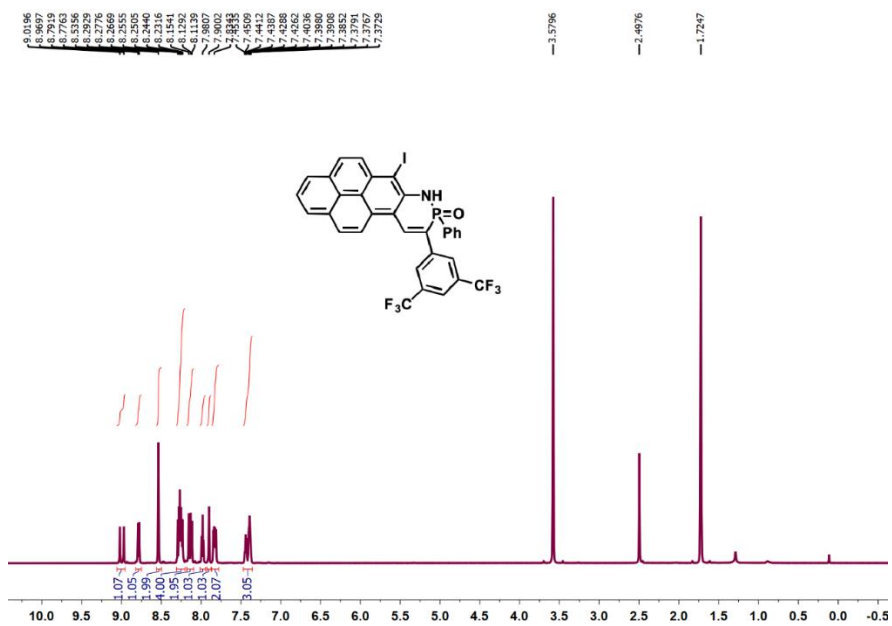
^{13}C NMR spectrum of **5b** in CDCl_3 .



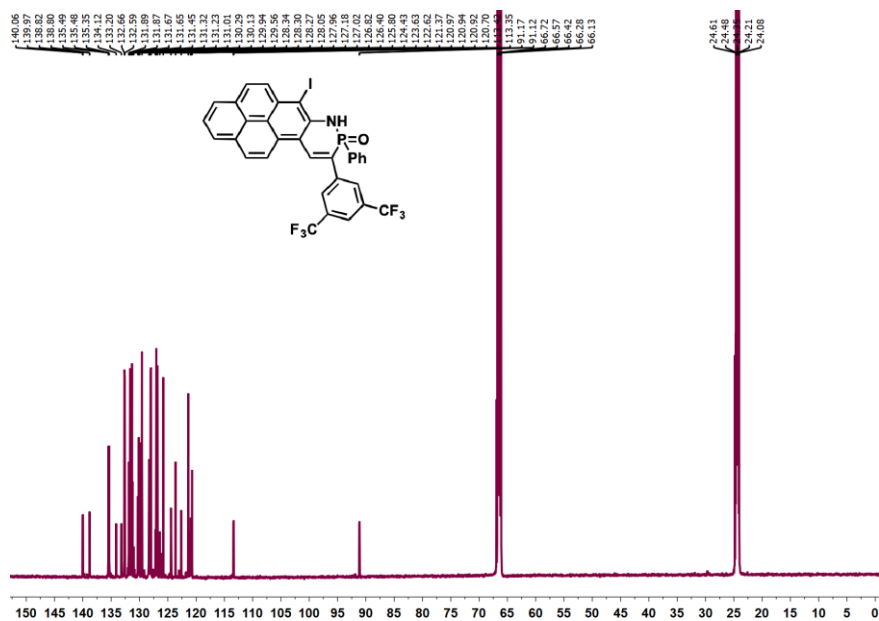
$^{19}\text{F}\{^1\text{H}\}$ NMR spectrum of **5b** in CDCl_3 .



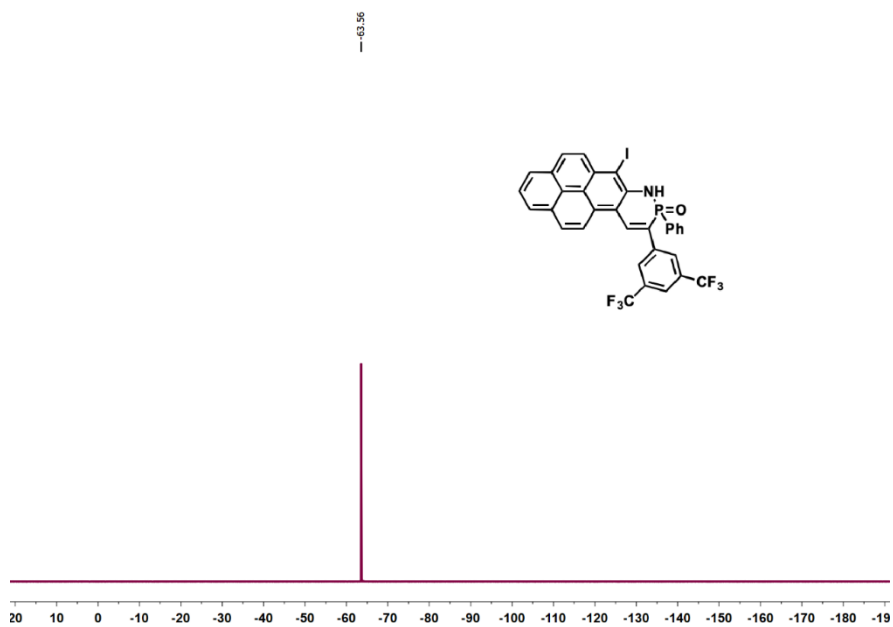
$^{31}\text{P}\{^1\text{H}\}$ NMR spectrum of **6a** in CDCl_3 .



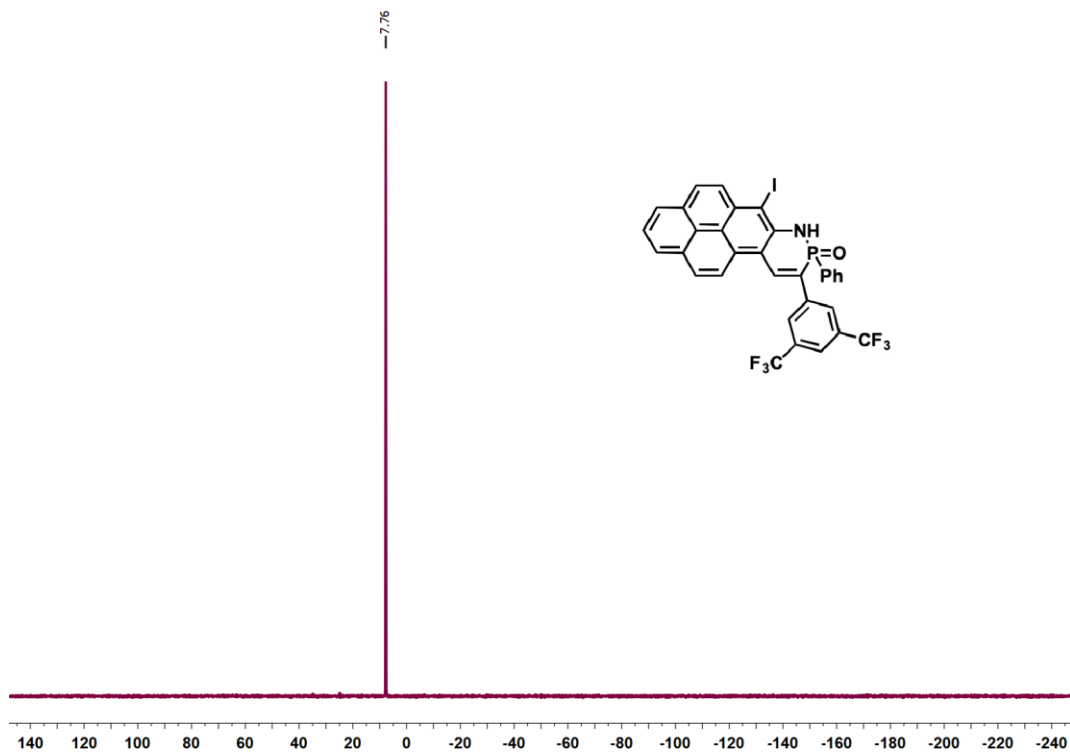
^1H NMR spectrum of **6b** in $\text{THF-}d_8$.



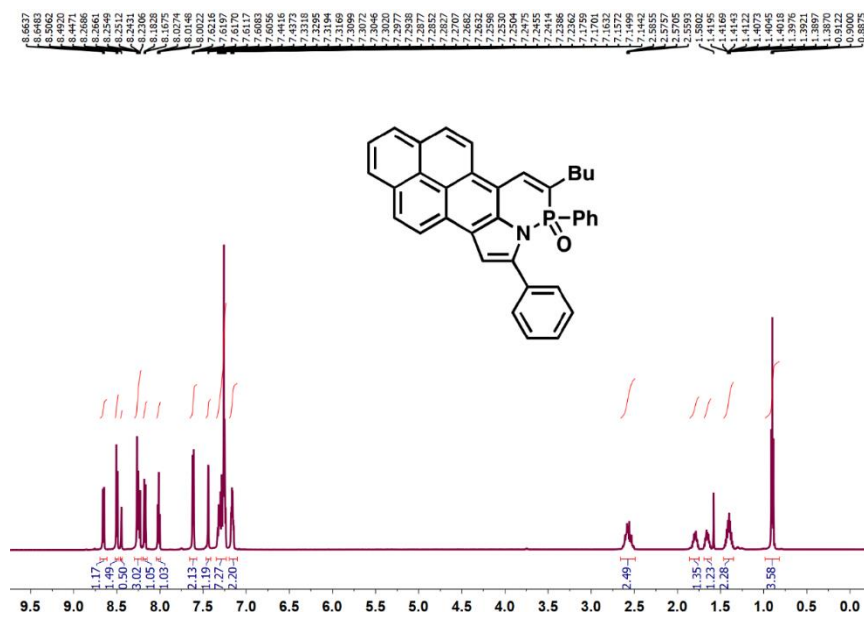
^{13}C NMR spectrum of **6b** in $\text{THF-}d_8$.



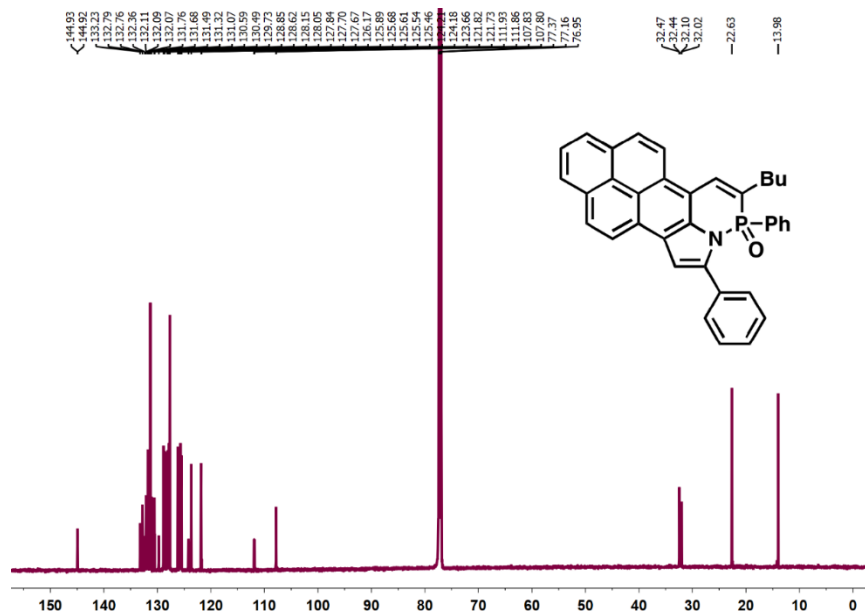
$^{19}\text{F}\{^1\text{H}\}$ NMR spectrum of **6b** in $\text{THF-}d_8$.

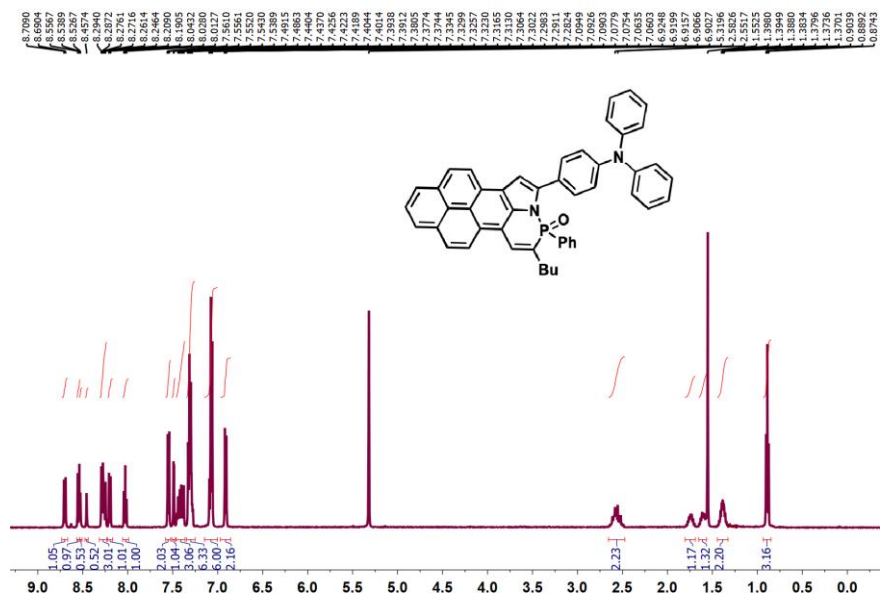


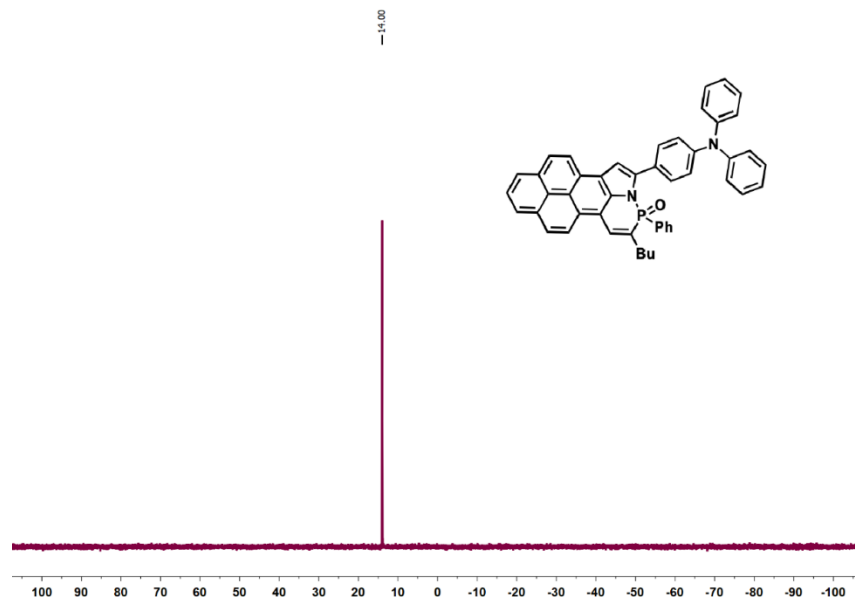
$^{31}\text{P}\{^1\text{H}\}$ NMR spectrum of **6b** in $\text{THF-}d_8$.



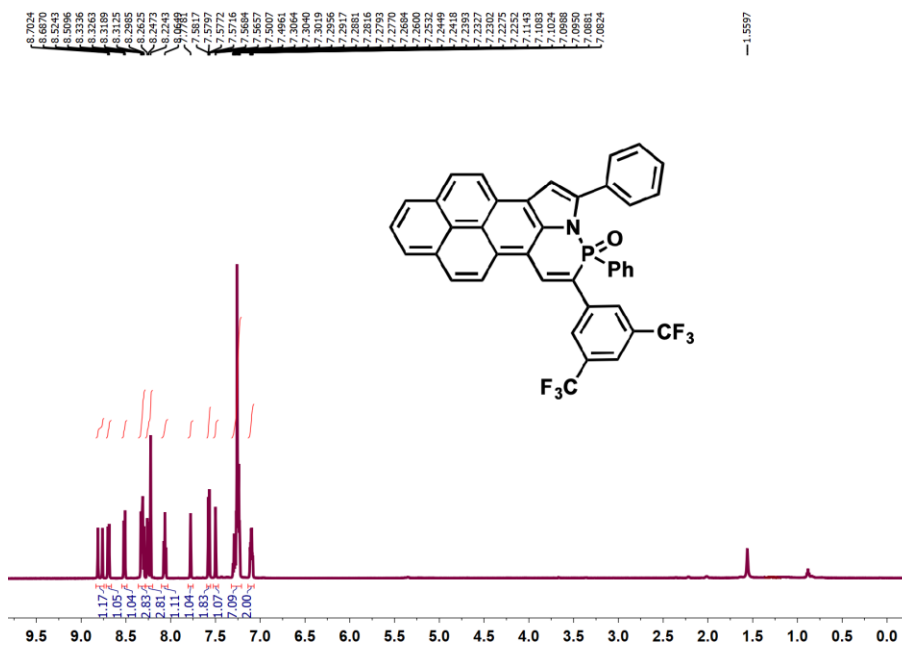
^1H NMR spectrum of **1a** in CDCl_3 .



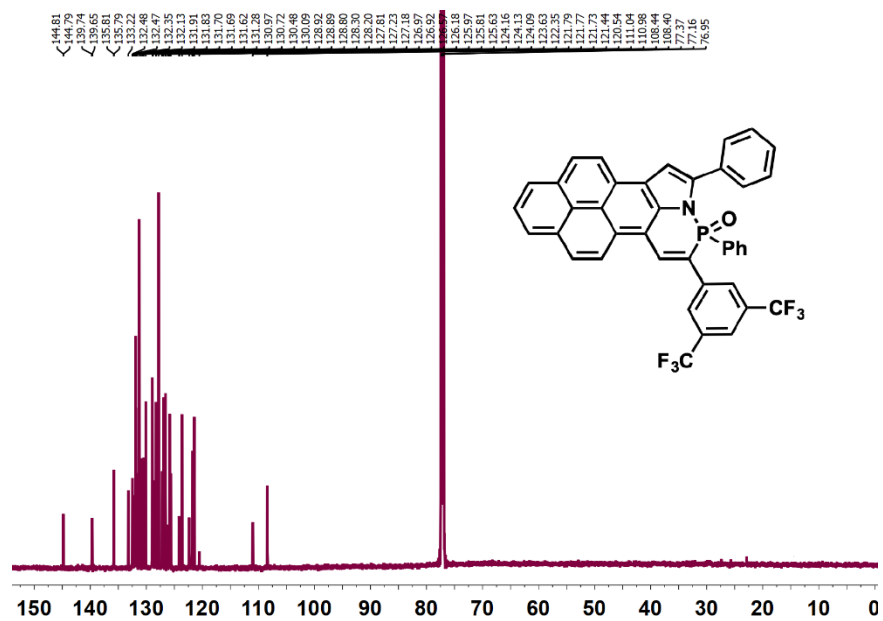




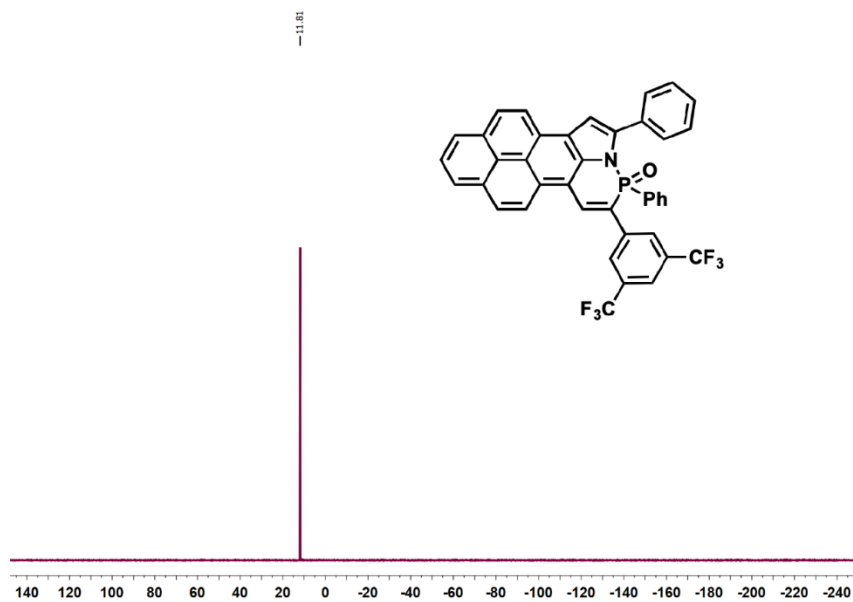
$^{31}\text{P}\{^1\text{H}\}$ NMR spectrum of **1b** in CDCl_3 .



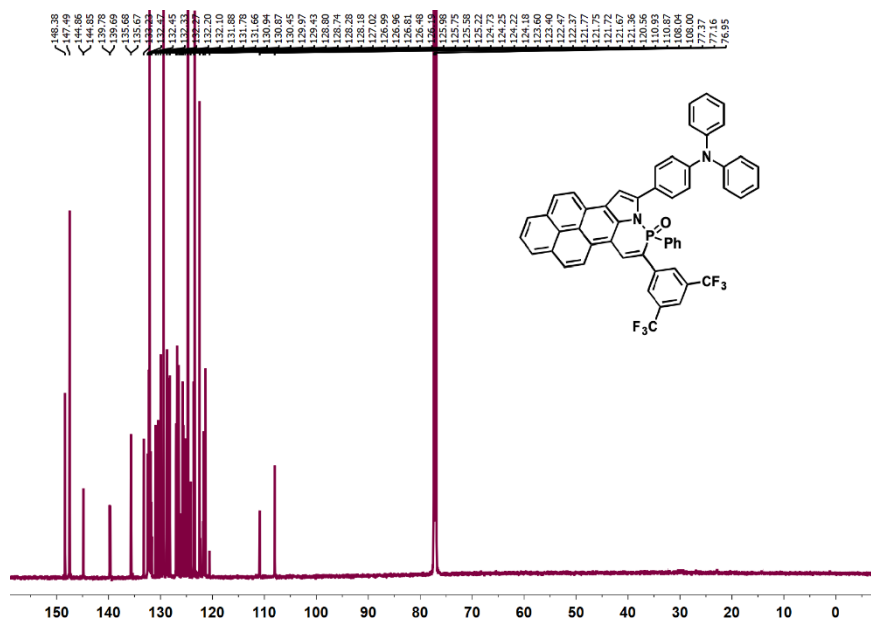
^1H NMR spectrum of **2a** in CDCl_3 .



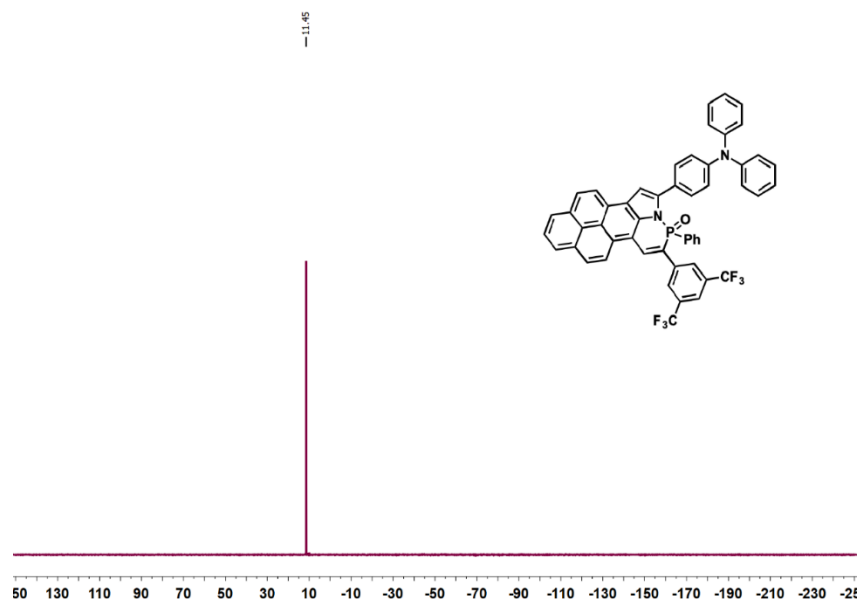
$^{13}\text{C}\{^1\text{H}\}$ NMR spectrum of **2a** in CDCl_3 .



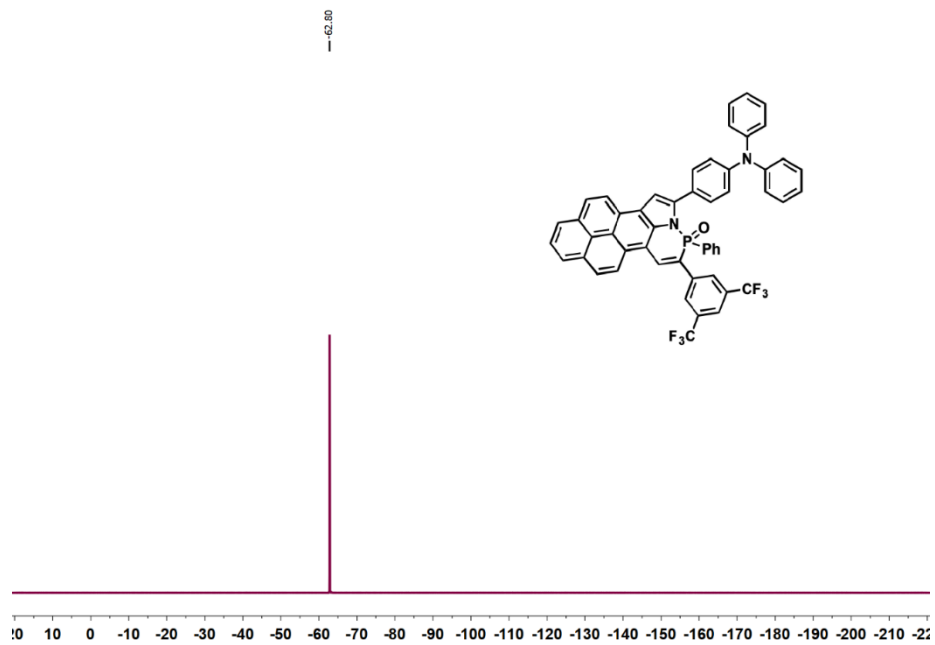
$^{31}\text{P}\{^1\text{H}\}$ NMR spectrum of **2a** in CDCl_3 .



$^{13}\text{C}\{^1\text{H}\}$ NMR spectrum of **2b** in CDCl_3 .



$^{31}\text{P}\{^1\text{H}\}$ NMR spectrum of **2b** in CDCl_3 .



$^{19}\text{F}\{^1\text{H}\}$ NMR spectrum of **2b** in CDCl_3 .

REFERENCES CITED

Chapter 1

- (1) Webber, M. J.; Langer, R. Drug Delivery by Supramolecular Design. *Chemical Society Reviews*. Royal Society of Chemistry November 7, 2017, pp 6600–6620.
- (2) Lancia, F.; Ryabchun, A.; Katsonis, N. Life-like Motion Driven by Artificial Molecular Machines. *Nature Reviews Chemistry*. Nature Publishing Group September 1, 2019, pp 536–551.
- (3) Webber, M. J.; Appel, E. A.; Meijer, E. W.; Langer, R. Supramolecular Biomaterials. *Nature Materials*. Nature Publishing Group December 18, 2015, pp 13–26.
- (4) Geng, W.-C.; Sessler, J. L.; Guo, D.-S. Supramolecular Prodrugs Based on Host–Guest Interactions. *Chem. Soc. Rev.* **2020**.
- (5) Sanabria Español, E.; Maldonado, M. Host–Guest Recognition of Pesticides by Calixarenes. *Crit. Rev. Anal. Chem.* **2019**, *49*, 383–394.
- (6) Moyer, B. A.; Delmau, L. H.; Fowler, C. J.; Ruas, A.; Bostick, D. A.; Sessler, J. L.; Katayev, E.; Dan Pantos, G.; Llinares, J. M.; Hossain, M. A.; Kang, S. O.; Bowman-James, K. Supramolecular Chemistry of Environmentally Relevant Anions. *Advances in Inorganic Chemistry*. Academic Press January 1, 2006, pp 175–204.
- (7) Katayev, E. A.; Pantos, G. D.; Reshetova, M. D.; Khrustalev, V. N.; Lynch, V. M.; Ustynyuk, Y. A.; Sessler, J. L. Anion-Induced Synthesis and Combinatorial Selection of Polypyrrolic Macrocycles. *Angew. Chemie Int. Ed.* **2005**, *44*, 7386–7390.
- (8) Sessler, J. L.; Katayev, E.; Dan Pantos, G.; Scherbakov, P.; Reshetova, M. D.; Khrustalev, V. N.; Lynch, V. M.; Ustynyuk, Y. A. Fine Tuning the Anion Binding Properties of 2,6-Diamidopyridine Dipyrromethane Hybrid Macrocycles. *J. Am. Chem. Soc.* **2005**, *127*, 11442–11446.
- (9) Huggins, M. T.; Butler, T.; Barber, P.; Hunt, J. Synthesis and Molecular Recognition Studies of Pyrrole Sulfonamides. *Chem. Commun.* **2009**, No. 35, 5254–5256.

- (10) Saha, S.; Akhuli, B.; Chakraborty, S.; Ghosh, P. Synthesis of a Preorganized Hybrid Macrobicycle with Distinct Amide and Amine Clefs: Tetrahedral versus Spherical Anions Binding Studies. *J. Org. Chem.* **2013**, *78*, 8759–8765.
- (11) Du, J.; Hu, M.; Fan, J.; Peng, X. Fluorescent Chemodosimeters Using “Mild” Chemical Events for the Detection of Small Anions and Cations in Biological and Environmental Media. *Chem. Soc. Rev* **2012**, *41*, 4511–4535.
- (12) Sessler, J. L.; Katayev, E.; Pantos, G. D.; Ustynyuk, Y. A. Synthesis and Study of a New Diamidodipyrromethane Macrocyclic Anion Receptor with a High Sulfate-to-Nitrate Binding Selectivity. Electronic Supplementary Information (ESI) Available: Detailed Experimental Data and UV-Vis Spectrophotometric Titration Data. See <http://www.rsc.org/suppdata/cc/B4/B403665d/>. *Chem. Commun.* **2004**, No. 11, 1276.
- (13) Liu, Y.; Sengupta, A.; Raghavachari, K.; Flood, A. H. Anion Binding in Solution: Beyond the Electrostatic Regime. *Chem* **2017**, *3*, 411–427.
- (14) Carroll, C. N.; Berryman, O. B.; Johnson, C. A.; Zakharov, L. N.; Haley, M. M.; Johnson, D. W. Protonation Activates Anion Binding and Alters Binding Selectivity in New Inherently Fluorescent 2,6-Bis(2-Anilinoethynyl)Pyridine Bisureas. *Chem. Commun.* **2009**, 2520.
- (15) Tresca, B. W.; Zakharov, L. N.; Carroll, C. N.; Johnson, D. W.; Haley, M. M. Aryl C-H···Cl- Hydrogen Bonding in a Fluorescent Anion Sensor. *Chem. Commun.* **2013**, *49*, 7240–7242.
- (16) Tresca, B. W.; Brueckner, A. C.; Haley, M. M.; Cheong, P. H. Y.; Johnson, D. W. Computational and Experimental Evidence of Emergent Equilibrium Isotope Effects in Anion Receptor Complexes. *J. Am. Chem. Soc.* **2017**, *139*, 3962–3965.
- (17) Vonnegut, C. L.; Shonkwiler, A. M.; Zakharov, L. N.; Haley, M. M.; Johnson, D. W. Harnessing Solid-State Packing for Selective Detection of Chloride in a Macrocyclic Anionophore. *Chem. Commun.* **2016**, *52*, 9506–9509.
- (18) Lohrman, J. A.; Deng, C. L.; Shear, T. A.; Zakharov, L. N.; Haley, M. M.; Johnson, D. W. Methanesulfonyl-Polarized Halogen Bonding Enables Strong Halide Recognition in an Arylethynyl Anion Receptor. *Chem. Commun.* **2019**, *55*, 1919–1922.

- (19) Gavette, J. V.; Mills, N. S.; Zakharov, L. N.; Johnson, C. A.; Johnson, D. W.; Haley, M. M. An Anion-Modulated Three-Way Supramolecular Switch That Selectively Binds Dihydrogen Phosphate, H_2PO_4^- . *Angew. Chemie Int. Ed.* **2013**, *52*, 10270–10274.
- (20) Watt, M. M.; Zakharov, L. N.; Haley, M. M.; Johnson, D. W. Selective Nitrate Binding in Competitive Hydrogen Bonding Solvents: Do Anion- π Interactions Facilitate Nitrate Selectivity? *Angew. Chemie Int. Ed.* **2013**, *52*, 10275–10280.
- (21) Eytel, L. M.; Brueckner, A. C.; Lohrman, J. A.; Haley, M. M.; Cheong, P. H. Y.; Johnson, D. W. Conformationally Flexible Arylethynyl Bis-Urea Receptors Bind Disparate Oxoanions with Similar, High Affinities. *Chem. Commun.* **2018**, *54*, 13208–13211.
- (22) Hartle, M. D.; Hansen, R. J.; Tresca, B. W.; Praker, S. S.; Zakharov, L. N.; Haley, M. M.; Pluth, M. D.; Johnson, D. W. A Synthetic Supramolecular Receptor for the Hydrosulfide Anion. *Angew. Chemie Int. Ed.* **2016**, *55*, 11480–11484.
- (23) Fargher, H. A.; Lau, N.; Zakharov, L. N.; Haley, M. M.; Johnson, D. W.; Pluth, M. D. Expanding Reversible Chalcogenide Binding: Supramolecular Receptors for the Hydroselenide (HSe^-) Anion. *Chem. Sci.* **2019**, *10*, 67–72.
- (24) Fargher, H. A.; Lau, N.; Richardson, H. C.; Cheong, P. H.-Y.; Haley, M. M.; Pluth, M. D.; Johnson, D. W. Tuning Supramolecular Selectivity for Hydrosulfide: Linear Free Energy Relationships Reveal Preferential C–H Hydrogen Bond Interactions. *J. Am. Chem. Soc.* **2020**, *142*, 8243–8251.
- (25) Berryman, O. B.; Johnson, C. A.; Zakharov, L. N.; Haley, M. M.; Johnson, D. W. Water and Hydrogen Halides Serve the Same Structural Role in a Series of 2+2 Hydrogen-Bonded Dimers Based on 2,6-Bis(2-Anilinoethynyl)Pyridine Sulfonamide Receptors. *Angew. Chemie Int. Ed.* **2008**, *47*, 117–120.
- (26) Tresca, B. W.; Hansen, R. J.; Chau, C. V.; Hay, B. P.; Zakharov, L. N.; Haley, M. M.; Johnson, D. W. Substituent Effects in CH Hydrogen Bond Interactions: Linear Free Energy Relationships and Influence of Anions. *J. Am. Chem. Soc.* **2015**, *137*, 14959–14967.
- (27) Johnson, C. A.; Berryman, O. B.; Sather, A. C.; Zakharov, L. N.; Haley, M. M.; Johnson, D. W. Anion Binding Induces Helicity in a Hydrogen-Bonding Receptor: Crystal Structure of a 2,6-Bis(Anilinoethynyl)Pyridinium Chloride. *Cryst. Growth Des.* **2009**, *9*, 4247–4249.
- (28) C. L. Vonnegut Ph.D. Thesis, University of Oregon, 2016.
- (29) C. N. Carroll Ph.D. Thesis, University of Oregon, 2011.

- (30) Adolfsson, H.; Moberg, C. Chiral Lewis Acid Catalysed Asymmetric Nucleophilic Ring Opening of Cyclohexene Oxide. *Tetrahedron: Asymmetry* **1995**, *6*, 2023–2031.
- (31) Schaub, T. A.; Brülls, S. M.; Dral, P. O.; Hampel, F.; Maid, H.; Kivala, M. Organic Electron Acceptors Comprising a Dicyanomethylene-Bridged Acridophosphine Scaffold: The Impact of the Heteroatom. *Chem. - A Eur. J.* **2017**, *23*, 6988–6992.
- (32) Regulska, E.; Romero-Nieto, C. Highlights on π -Systems Based on Six-Membered Phosphorus Heterocycles. *Dalt. Trans.* **2018**, *47*, 10344–10359.
- (33) Jiang, X. D.; Zhao, J.; Xi, D.; Yu, H.; Guan, J.; Li, S.; Sun, C. L.; Xiao, L. J. A New Water-Soluble Phosphorus-Dipyrromethene and Phosphorus-Azadipyrromethene Dye: PODIPY/Aza-PODIPY. *Chem. - A Eur. J.* **2015**, *21*, 6079–6082.
- (34) Grenon, N.; Baumgartner, T. Exploration of Hypervalent Lewis Acid/Base Interactions in 2-(2'-Thiazolyl)-3-Thienylphosphanes. *Inorg. Chem.* **2018**, *57*, 1630–1644.
- (35) Mathey, F. The Organic Chemistry of Phospholes. *Chem. Rev.* **1988**, *88*, 429–453.
- (36) Gong, P.; Ye, K.; Sun, J.; Chen, P.; Xue, P.; Yang, H.; Lu, R. Electroluminescence and Fluorescence Response towards Acid Vapors Depending on the Structures of Indole-Fused Phospholes. *RSC Adv.* **2015**, *5*, 94990–94996.
- (37) Romero-Nieto, C.; López-Andarias, A.; Egler-Lucas, C.; Gebert, F.; Neus, J. P.; Pilgram, O. Paving the Way to Novel Phosphorus-Based Architectures: A Noncatalyzed Protocol to Access Six-Membered Heterocycles. *Angew. Chemie - Int. Ed.* **2015**, *54*, 15872–15875.
- (38) Fukazawa, A.; Osaki, H.; Yamaguchi, S. Hydroxyphenyl-Substituted Benzophosphole Oxides: Impact of the Intramolecular Hydrogen Bond on the Fluorescence Properties. *Asian J. Org. Chem.* **2014**, *3*, 122–127.
- (39) Avarvari, N.; Le Floch, P.; Mathey, F. 1,3,2-Diazaphosphinines: New Versatile Precursors of 1,2-Azaphosphinines and Polyfunctional Phosphinines. *J. Am. Chem. Soc.* **1996**, *118*, 11978–11979.
- (40) Baumgartner, T. Insights on the Design and Electron-Acceptor Properties of Conjugated Organophosphorus Materials. *Acc. Chem. Res.* **2014**, *47*, 1613–1622.
- (41) Baumgartner, T.; Réau, R. Organophosphorus π -Conjugated Materials. *Chemical Reviews*. American Chemical Society November 2006, pp 4681–4727.

- (42) Wang, Z.; Gelfand, B. S.; Baumgartner, T. Dithienophosphole-Based Phosphinamides with Intriguing Self-Assembly Behavior. *Angew. Chemie Int. Ed.* **2016**, *55*, 3481–3485.
- (43) Ma, Y.-N.; Zhang, X.; Yang, S. Tandem Oxidative C–H Amination and Iodization to Synthesize Difunctional Atropoisomeric P-Stereogenic Phosphinamides. *Chem. - A Eur. J.* **2017**, *23*, 3007–3011.
- (44) Lin, Z.-Q.; Wang, W.-Z.; Yan, S.-B.; Duan, W.-L. Palladium-Catalyzed Enantioselective C–H Arylation for the Synthesis of P-Stereogenic Compounds. *Angew. Chemie Int. Ed.* **2015**, *54*, 6265–6269.
- (45) Tang, W.; Ding, Y. X. Synthesis of Phosphaisoquinolin-1-Ones by Pd(II)-Catalyzed Cyclization of o-(1-Alkynyl)Phenylphosphonamide Monoesters. *J. Org. Chem.* **2006**, *71*, 8489–8492.
- (46) Park, S.; Seo, B.; Shin, S.; Son, J.-Y.; Lee, P. H. Rhodium-Catalyzed Oxidative Coupling through C–H Activation and Annulation Directed by Phosphonamide and Phosphinamide Groups. *Chem. Commun.* **2013**, *49*, 8671.
- (47) Liu, L.; Zhang, A.-A.; Wang, Y.; Zhang, F.; Zuo, Z.; Zhao, W.-X.; Feng, C.-L.; Ma, W. Asymmetric Synthesis of P-Stereogenic Phosphinic Amides via Pd(0)-Catalyzed Enantioselective Intramolecular C–H Arylation. *Org. Lett.* **2015**, *17*, 2046–2049.
- (48) Campbell, I. G. M.; Way, J. K. 975. Synthesis and Stereochemistry of Heterocyclic Phosphorus Compounds. Part I. Preparation of (+)- and (–)-10-p-Dimethylaminophenyl-9,10-Dihydro-9-Aza-10-Phosphaphenanthrene. *J. Chem. Soc.* **1960**, *0*, 5034–5041.
- (49) Dewar, M. J. S.; Kubba, V. P. New Heteroaromatic Compounds. Part VI. Novel Heterocyclic Compounds of Phosphorus. *J. Am. Chem. Soc.* **1960**, *82*, 5685–5688.
- (50) Yan, J.; Li, Q.; Boutin, J. A.; Renard, M. P.; Ding, Y.; Hao, X.; ZHao, W.; Wang, M. High-Throughput Screening of Novel Antagonists on Melanin-Concentrating Hormone Receptor-1. *Acta Pharmacol. Sin.* **2008**, *29*, 752–758.
- (51) Sun, Y.; Cramer, N. Rhodium(III)-Catalyzed Enantiotopic C–H Activation Enables Access to P-Chiral Cyclic Phosphinamides. *Angew. Chemie Int. Ed.* **2017**, *56*, 364–367.
- (52) Zhao, D.; Nimphius, C.; Lindale, M.; Glorius, F. Phosphoryl-Related Directing Groups in Rhodium(III) Catalysis: A General Strategy to Diverse P-Containing Frameworks. *Org. Lett.* **2013**, *15*, 4504–4507.

- (53) Vonnegut, C. L.; Shonkwiler, A. M.; Khalifa, M. M.; Zakharov, L. N.; Johnson, D. W.; Haley, M. M. Facile Synthesis and Properties of 2- λ^5 -Phosphaquinolines and 2- λ^5 -Phosphaquinolin-2-Ones. *Angew. Chemie Int. Ed.* **2015**, *54*, 13318–13322.
- (54) Reynolds, G. A.; Drexhage, K. H. New Coumarin Dyes with Rigidized Structure for Flashlamp-Pumped Dye Lasers. *Opt. Commun.* **1975**, *13*, 222–225.
- (55) Becker, R. S.; Chakravorti, S.; Gartner, C. A.; de Graca Miguel, M. Photosensitizers: Comprehensive Photophysics/Photochemistry and Theory of Coumarins, Chromones, Their Homologues and Thione Analogues. *J. Chem. Soc. Faraday Trans.* **1993**, *89*, 1007–1019.
- (56) Cao, D.; Liu, Z.; Verwilt, P.; Koo, S.; Jangjili, P.; Kim, J. S.; Lin, W. Coumarin-Based Small-Molecule Fluorescent Chemosensors. *Chem. Rev.* **2019**, *acs.chemrev.9b00145*.
- (57) Traven, V. F.; Bochkov, A. Y. Synthesis and Photochromism of Aryl(Heteroaryl)- and Diheteroarylethenes – Coumarin Derivatives. *Heterocycl. Commun.* **2013**, *19*, 219–238.
- (58) Traven, V. F.; Manaev, A. V.; Bochkov, A. Y.; Chibisova, T. A.; Ivanov, I. V. *New Reactions, Functional Compounds, and Materials in the Series of Coumarin and Its Analogs**; 2012; Vol. 61.
- (59) Medina, F. G.; Marrero, J. G.; Macías-Alonso, M.; González, M. C.; Córdova-Guerrero, I.; Teissier García, A. G.; Osegueda-Robles, S. Coumarin Heterocyclic Derivatives: Chemical Synthesis and Biological Activity. *Nat. Prod. Rep.* **2015**, *32*, 1472–1507.
- (60) Pan, S.-L.; Li, K.; Li, L.-L.; Li, M.-Y.; Shi, L.; Liu, Y.-H.; Yu, X.-Q. A Reaction-Based Ratiometric Fluorescent Sensor for the Detection of Hg(II) Ions in Both Cells and Bacteria. *Chem. Commun.* **2018**, *54*, 4955–4958.
- (61) Salem, M. A.; Helal, M. H.; Gouda, M. A.; Ammar, Y. A.; A El-Gaby, M. S.; Abbas, S. Y. An Overview on Synthetic Strategies to Coumarins. *Synth. Commun.* **2018**, *48*, 1534–1550.
- (62) Uray, G.; Niederreiter, K. S.; Belaj, F.; Fabian, W. M. F. Long-Wavelength-Absorbing and -Emitting Carbostyrils with High Fluorescence Quantum Yields. *Helv. Chim. Acta* **1999**, *82*, 1408–1417.
- (63) Strohmeier, G. A.; Fabian, W. M. F.; Uray, G. A Combined Experimental and Theoretical Approach toward the Development of Optimized Luminescent Carbostyrils. *Helv. Chim. Acta* **2004**, *87*, 215–226.

- (64) Fabian, W. M. F.; Niederreiter, K. S.; Uray, G.; Stadlbauer, W. Substituent Effects on Absorption and Fluorescence Spectra of Carbostyrils. *J. Mol. Struct.* **1999**, *477*, 209–220.
- (65) Enoua, G. C.; Lahm, G.; Uray, G.; Stadlbauer, W. Syntheses and Fluorescent Properties of 6-Methoxy-2-Oxoquinoline-3,4-Dicarbonitriles and 6,7-Dimethoxy-2-Oxoquinoline-3,4-Dicarbonitriles. *J. Heterocycl. Chem.* **2014**, *51*, E263–E275.
- (66) de Macedo, M. B.; Kimmel, R.; Urankar, D.; Gazvoda, M.; Peixoto, A.; Cools, F.; Torfs, E.; Verschaeve, L.; Lima, E. S.; Lyčka, A.; Milićević, D.; Klásek, A.; Cos, P.; Kafka, S.; Košmrlj, J.; Cappoen, D. Design, Synthesis and Antitubercular Potency of 4-Hydroxyquinolin-2(1H)-Ones. *Eur. J. Med. Chem.* **2017**, *138*, 491–500.
- (67) Ahvale, A. B.; Prokopcová, H.; Šefčovičová, J.; Steinschifter, W.; Täubl, A. E.; Uray, G.; Stadlbauer, W. 4-Cyano-6,7-Dimethoxycarbostyrils with Solvent- and PH-Independent High Fluorescence Quantum Yields and Emission Maxima. *European J. Org. Chem.* **2008**, *2008*, 563–571.
- (68) Tashima, T. The Structural Use of Carbostyryl in Physiologically Active Substances. *Bioorg. Med. Chem. Lett.* **2015**, *25*, 3415–3419.
- (69) Vekariya, R. H.; Patel, H. D. Synthetic Communications Reviews Recent Advances in the Synthesis of Coumarin Derivative Via Knoevenagel Condensation: A Review *Synth. Commun.* **2014**, *1*, 2756–2788.
- (70) Wagner, B.; Wagner, D., B. The Use of Coumarins as Environmentally-Sensitive Fluorescent Probes of Heterogeneous Inclusion Systems. *Molecules* **2009**, *14*, 210–237.
- (71) Casley-Smith, J. R.; Morgan, R. G.; Piller, N. B. Treatment of Lymphedema of the Arms and Legs with 5,6-Benzo-[Alpha]-Pyrone. *N. Engl. J. Med.* **1993**, *329*, 1158–1163.
- (72) Jiao, C.-X.; Niu, C.-G.; Chen, L.-X.; Shen, G.-L.; Yu, R.-Q. A Coumarin Derivative Covalently Immobilized on Sensing Membrane as a Fluorescent Carrier for Nitrofurazone. *Anal. Bioanal. Chem.* **2003**, *376*, 392–398.
- (73) Liu, X.; Qiao, Q.; Tian, W.; Liu, W.; Chen, J.; Lang, M. J.; Xu, Z. Aziridinyl Fluorophores Demonstrate Bright Fluorescence and Superior Photostability by Effectively Inhibiting Twisted Intramolecular Charge Transfer. *J. Am. Chem. Soc.* **2016**, *138*, 6960–6963.

- (74) Liu, X.; Xu, Z.; Cole, J. M. Molecular Design of UV–Vis Absorption and Emission Properties in Organic Fluorophores: Toward Larger Bathochromic Shifts, Enhanced Molar Extinction Coefficients, and Greater Stokes Shifts. *J. Phys. Chem. C* **2013**, *117*, 16584–16595.
- (75) Kim, E.; Koh, M.; Lim, B. J.; Park, S. B. Emission Wavelength Prediction of a Full-Color-Tunable Fluorescent Core Skeleton, 9-Aryl-1,2-Dihydropyrrolo[3,4- *b*]Indolizin-3-One. *J. Am. Chem. Soc.* **2011**, *133*, 6642–6649.
- (76) Liu, X.; Cole, J. M.; Waddell, P. G.; Lin, T. C.; Radia, J.; Zeidler, A. Molecular Origins of Optoelectronic Properties in Coumarin Dyes: Toward Designer Solar Cell and Laser Applications. *J. Phys. Chem. A* **2012**, *116*, 727–737.
- (77) Duarte, F. J. (Frank J. .; Hillman, L. W.; Liao, P. F.; Kelley, P. *Dye Laser Principles : With Applications.*; Elsevier Science, 1990.
- (78) Takaesu, N. A.; Ohta, E.; Zakharov, L. N.; Johnson, D. W.; Haley, M. M. Synthesis and Properties of Naphtho[2,3- *e*]-1,2-Azaphosphorine 2-Oxides: PN-Anthracene Analogues. *Organometallics* **2017**, *36*, 2491–2493.
- (79) Deng, C.-L.; Bard, J. P.; Zakharov, L. N.; Johnson, D. W.; Haley, M. M. Naphtho[2,1- *e*]-1,2-Azaphosphorine 2-Oxide Derivatives: Synthesis, Optoelectronic Properties, and Self-Dimerization Phenomena. *J. Org. Chem.* **2019**, *84*, 8131–8139.
- (80) Bard, J. P.; Mancuso, J. L.; Deng, C. L.; Zakharov, L. N.; Johnson, D. W.; Haley, M. M. A Highly Fluorescent PN-Heterocycle-Fused Pyrene Derivative with Strong Self-Dimerisation through Hydrogen Bonding. *Supramol. Chem.* **2020**, *32*, 49–55.
- (81) Bard, J. P.; Bates, H. J.; Deng, C. L.; Zakharov, L. N.; Johnson, D. W.; Haley, M. M. Amplification of the Quantum Yields of 2- Λ 5-Phosphaquinolin-2-Ones through Phosphorus Center Modification. *J. Org. Chem.* **2020**, *85*, 85–91.
- (82) Winnik, F. Photophysics of Preassociated Pyrenes in Aqueous Polymer Solutions and in Other Organized Media. *Chem. Rev.* **1993**, *93*, 587–614.
- (83) Birks, J. B.; Christophorou, L. G. Excimer Fluorescence Spectra of Pyrene Derivatives. *Spectrochim. Acta* **1963**, *19*, 401–410.
- (84) Birks, J. B. Excimers. *Reports Prog. Phys.* **1975**, *38*, 903–974.
- (85) Haugland, R. P. Chapter 8 — Nucleic Acid Detection and Analysis. In *The handbook: a guide to fluorescent probes and labeling technologies*; Molecular probes, 2005.

- (86) Galla, H. J.; Hartmann, W. Excimer-Forming Lipids in Membrane Research. *Chem. Phys. Lipids* **1980**, *27*, 199–219.
- (87) Bains, G. K.; Kim, S. H.; Sorin, E. J.; Narayanaswami, V. The Extent of Pyrene Excimer Fluorescence Emission Is a Reflector of Distance and Flexibility: Analysis of the Segment Linking the LDL Receptor-Binding and Tetramerization Domains of Apolipoprotein E3. *Biochemistry* **2012**, *51*, 6207–6219.
- (88) Thordarson, P. Determining Association Constants from Titration Experiments in Supramolecular Chemistry. *Chem. Soc. Rev.* **2011**, *40*, 1305–1323.
- (89) Quinn, J. R.; Zimmerman, S. C.; Del Bene, J. E.; Shavitt, I. Does the A·T or G·C Base-Pair Possess Enhanced Stability? Quantifying the Effects of CH···O Interactions and Secondary Interactions on Base-Pair Stability Using a Phenomenological Analysis and Ab Initio Calculations. *J. Am. Chem. Soc.* **2007**, *129*, 934–941.
- 90 Deng, C.-L.; Bard, J. P.; Lohrman, J. A.; Barker, J. E.; Zakharov, L. N.; Johnson, D. W.; Haley, M. M. Exploiting the Hydrogen Bond Donor/Acceptor Properties of PN-Heterocycles: Selective Anion Receptors for Hydrogen Sulfate. *Angew. Chemie Int. Ed.* **2019**, *58*, 3934–3938.
- 91 Deng, C. L.; Bard, J. P.; Zakharov, L. N.; Johnson, D. W.; Haley, M. M. PN-Containing Pyrene Derivatives: Synthesis, Structure, and Photophysical Properties. *Org. Lett.* **2019**, *21*, 6427–6431.

Chapter 2

1. R. S. Becker, S. Chakravorti, C. A. Gartner and M. de Graca Miguel, *J. Chem. Soc., Faraday Trans.*, 1993, **89**, 1007.
2. G. A. Reynolds and K. H. Drexhage, *Opt. Commun.*, 1975, **13**, 222.
3. V. F. Traven, A. V. Manaev, A. Y. Bochkov, T. A. Chibisova and I. V. Ivanov, *Russ. Chem. Bull.*, 2012, **61**, 1342.
4. F. G. Medina, J. G. Marrero, M. Macías-Alonso, M. C. González, I. Córdova-Guerrero, A. G. Teissier García and S. Osegueda-Robles, *Nat. Prod. Rep.*, 2015, **32**, 1472.
5. V. F. Traven and A. Y. Bochkov, *Heterocycl. Commun.*, 2013, **19**, 219.
6. S.-L. Pan, K. Li, L.-L. Li, M.-Y. Li, L. Shi, Y.-H. Liu and X.-Q. Yu, *Chem. Commun.*, 2018, **54**, 4955.

7. M. A. Salem , M. H. Helal , M. A. Gouda , Y. A. Ammar , M. S. A. El-Gaby and S. Y. Abbas , *Synth. Commun.*, 2018, **48**, 1534.
8. M. B. de Macedo , R. Kimmel , D. Urankar , M. Gazvoda , A. Peixoto , F. Cools , E. Torfs , L. Verschaeve , E. S. Lima , A. Lyčka , D. Milićević , A. Klásek , P. Cos , S. Kafka , J. Košmrlj and D. Cappoen , *Eur. J. Med. Chem.*, 2017, **138** , 491.
9. A. B. Ahvale , H. Prokopcová , J. Šefčovičová , W. Steinschifter , A. E. Täubl , G. Uray and W. Stadlbauer , *Eur. J. Org. Chem.*, 2008, 563.
10. G. Uray , K. S. Niederreiter , F. Belaj and W. M. F. Fabian , *Helv. Chim. Acta*, 1999, **82**, 1408.
11. G. A. Strohmeier , W. M. F. Fabian and G. Uray , *Helv. Chim. Acta*, 2004, **87** , 215.
12. G. C. Enoua , G. Lahm , G. Uray and W. Stadlbauer , *J. Heterocycl. Chem.*, 2014, **51** , E263.
13. W. M. F. Fabian , K. S. Niederreiter , G. Uray and W. Stadlbauer , *J. Mol. Struct.*, 1999, **477** , 209.
14. T. Tashima *Bioorg. Med. Chem. Lett.*, 2015, **25** , 3415.
15. J. R. Casley-Smith , R. G. Morgan and N. B. Piller , *N. Engl. J. Med.*, 1993, **329** , 1158.
16. C. X. Jiao , C. G. Niu , L. X. Chen , G. L. Shen and R. Q. Yu , *Anal. Bioanal. Chem.*, 2003, **376** , 392.
17. R. Vekariya and H. Patel , *Synth. Commun.*, 2014, **44** , 2756.
18. B. D. Wagner *Molecules*, 2009, **14** , 210.
19. M. J. S. Dewar and V. P. Kubba , *J. Am. Chem. Soc.*, 1960, **82** , 5685.
20. I. G. M. Campbell and J. K. Way , *J. Chem. Soc.*, 1960, 5034.
21. W. Tang and Y.-X. Ding , *J. Org. Chem.*, 2006, **71** , 8489.
22. W. Tang , Y. Ding and Y.-X. Ding , *Tetrahedron*, 2008, **64** , 10507.
23. J. Yan , Q. Li , J. A. Boutin , M. P. Renard , Y. Ding , X. Hao , W. Zhao and M. Wang , *Acta Pharmacol. Sin.*, 2008, **29** , 752.

24. S. Park , B. Seo , S. Shin , J.-Y. Son and P. H. Lee , *Chem. Commun.*, 2013, **49** , 8671.
25. D. Zhao , C. Nimphius , M. Lindale and F. Glorius , *Org. Lett.*, 2013, **15** , 4504.
26. Z.-Q. Lin , W.-Z. Wang , S.-B. Yan and W.-L. Duan , *Angew. Chem., Int. Ed.*, 2015, **54** , 6265.
27. L. Liu , A.-A. Zhang , Y. Wang , F. Zhang , Z. Zuo , W.-X. Zhao , C.-L. Feng and W. Ma , *Org. Lett.*, 2015, **17** , 2046.
28. Y. Sun and N. Cramer , *Angew. Chem., Int. Ed.*, 2017, **56** , 364.
29. Y.-N. Ma , X. Zhang and S.-D. Yang , *Chem. – Eur. J.*, 2017, **23** , 3007.
30. Z. Wang , B. S. Gelfand and T. Baumgartner , *Angew. Chem., Int. Ed.*, 2016, **55** , 3481.
31. C. L. Vonnegut , A. M. Shonkwiler , M. M. Khalifa , L. N. Zakharov , D. W. Johnson and M. M. Haley , *Angew. Chem., Int. Ed.*, 2015, **54** , 13318.
32. N. A. Takaesu , E. Ohta , L. N. Zakharov , D. W. Johnson and M. M. Haley , *Organometallics*, 2017, **36** , 2491.
33. T. Martín , U. Obst and J. Rebek Jr. , *Science*, 1998, **281** , 1842.
34. F. Hof, Self-Assembled Tetrameric Capsules, PhD Thesis, The Scripps Research Institute, 2003.
35. See the detailed ESI in: J. R. Quinn , S. C. Zimmerman , J. E. Del Bene and I. Shavitt , *J. Am. Chem. Soc.*, 2007, **129** , 934.
36. E. Kim , M. Koh , B. J. Lim and S. B. Park , *J. Am. Chem. Soc.*, 2011, **133** , 6642.
37. X. Liu , Q. Qiao , W. Tian , W. Liu , J. Chen , M. J. Lang and Z. Xu , *J. Am. Chem. Soc.*, 2016, **138** , 6960.
38. X. Liu , Z. Xu and J. M. Cole , *J. Phys. Chem. C*, 2013, **117** , 16584.
39. D. B. Kimball , T. J. R. Weakley and M. M. Haley , *J. Org. Chem.*, 2002, **67** , 6395.
40. C. N. Carroll , O. B. Berryman , C. A. Johnson , L. N. Zakharov , M. M. Haley and D. W. Johnson , *Chem. Commun.*, 2009, 2520.
41. C. Hansch , A. Leo and R. W. Taft , *Chem. Rev.*, 1991, **91** , 165.

42. R Core Team (2017). R: A language and environment for statistical computing. R Foundation for Statistical Computing, Vienna, Austria. URL <https://www.R-project.org/>.
43. H. Wickham, *ggplot2: Elegant Graphics for Data Analysis*, Springer-Verlag, New York, 2009.
44. K. Slowikowski, *ggrepel: Repulsive Text and Label Geoms for 'ggplot2'*. R package version 0.7.0, 2017, <https://CRAN.R-project.org/package=ggrepel>.
45. C.-L. Deng, J. P. Bard, J. A. Lohrman, J. E. Barker, L. N. Zakharov, D. W. Johnson and M. M. Haley, *Angew. Chem., Int. Ed.*, 2019, **58**, 3934.
46. A. M. Brouwer, *Pure Appl. Chem.*, 2011, **83**, 2213.
47. P. Thordarson, *Chem. Soc. Rev.*, 2011, **40**, 1305.
48. D. E. Kvalnes, *J. Am. Chem. Soc.*, 1934, **56**, 667.
49. T. Lanza, M. Minozzi, A. Monesi, D. Nanni, P. Spagnolo and G. Zanardi, *Adv. Synth. Catal.*, 2010, **352**, 2275

Chapter 3

1. a) J. L. Sessler, P. A. Gale, W.-S. Cho, *Anion Receptor Chemistry*, RSC, Cambridge, 2006; b) K. Bowman-James, A. Bianchi, E. García-España, *Anion Coordination Chemistry*, Wiley-VCH, Weinheim, 2011.
2. a) P. Ebbesen, *J. Immunol.* 1972, **109**, 1296–1299; b) P. I. Jalava, R. O. Salonen, A. S. Pennanen, M. S. Happonen, P. Penttinen, A. I. Halinen, M. Sillanpää, R. Hillamo, M. R. Hirvonen, *Toxicol. Appl. Pharmacol.* 2008, **229**, 146–160; c) T. J. Grahame, R. B. Schlesinger, *Inhalation Toxicol.* 2005, **17**, 15–27.
3. D. D. Perrin, *Ionization Constants of Inorganic Acids and Bases in Aqueous Solution*, 2nd ed., Pergamon, New York, 1983.
4. a) J. H. Seinfeld, S. N. Pandis, *Atmospheric Chemistry and Physics: From Air Pollution to Climate Change*, Wiley, Hoboken, 2006; b) S. H. Lee, J. M. Reeves, J. C. Wilson, D. E. Hunton, A. A. Viggiano, T. M. Miller, J. O. Ballenthin, L. R. Lait, *Science* 2003, **301**, 1886–1888.
5. A. Bhattacharyya, *Synlett* 2012, **23**, 2142–2143.

6. a) E. A. Katayev, Y. A. Ustynyuk, J. L. Sessler, *Coord. Chem. Rev.* 2006, **250**, 3004–3037; b) S. O. Kang, M. A. Hossain, K. Bowman-James, *Coord. Chem. Rev.* 2006, **250**, 3038–3052.
7. a) J. L. Sessler, E. Katayev, G. D. Pantos, Y. A. Ustynyuk, *Chem. Commun.* 2004, 1276–1277; b) E. A. Katayev, N. V. Boev, V. N. Khrustalev, Y. A. Ustynyuk, I. G. Tananaev, J. L. Sessler, *J. Org. Chem.* 2007, **72**, 2886–2896; c) E. A. Katayev, C. D. Pantos, M. D. Reshetova, V. N. Khrustalev, V. M. Lynch, Y. A. Ustynyuk, J. L. Sessler, *Angew. Chem. Int. Ed.* 2005, **44**, 7386–7390; d) J. L. Sessler, E. Katayev, G. D. Pantos, P. Scherbakov, M. D. Reshetova, V. N. Khrustalev, V. M. Lynch, Y. A. Ustynyuk, *J. Am. Chem. Soc.* 2005, **127**, 11442–11446; e) E. A. Katayev, J. L. Sessler, V. N. Khrustalev, Y. A. Ustynyuk, *J. Org. Chem.* 2007, **72**, 7244–7252; f) S. Saha, B. Akhuli, S. Chakraborty, P. Ghosh, *J. Org. Chem.* 2013, **78**, 8759–8765; g) N. R. Song, J. H. Moon, J. Choi, E. J. Jun, Y. Kim, S.-J. Kim, J. Y. Lee, J. Yoon, *Chem. Sci.* 2013, **4**, 1765–1771.
8. a) K. C. Nam, S. O. Kang, H. S. Jeong, S. Jeon, *Tetrahedron Lett.* 1999, **40**, 7343–7346; b) M. T. Huggins, T. Butler, P. Barber, J. Hunt, *Chem. Commun.* 2009, 5254–5256.
9. E. M. Fatila, E. B. Twum, A. Sengupta, M. Pink, J. A. Karty, K. Raghava-chari, A. H. Flood, *Angew. Chem. Int. Ed.* 2016, **55**, 14057–14062 and references therein.
10. Q. He, P. Tu, J. L. Sessler, *Chem* 2018, **4**, 46–93.
11. G. A. Jeffrey, *An Introduction to Hydrogen Bonding*, Oxford University Press, Oxford, 1997.
12. a) C. N. Carroll, B. A. Coombs, S. P. McClintock, C. A. Johnson II, O. B. Berryman, D. W. Johnson, M. M. Haley, *Chem. Commun.* 2011, **47**, 5539–5541; b) B. W. Tresca, L. N. Zakharov, C. N. Carroll, D. W. Johnson, M. M. Haley, *Chem. Commun.* 2013, **49**, 7240–7242; c) C. N. Carroll, J. J. Naleway, M. M. Haley, D. W. Johnson, *Chem. Soc. Rev.* 2010, **39**, 3875–3888; d) C. L. Vonnegut, B. W. Tresca, D. W. Johnson, M. M. Haley, *Chem. Asian J.* 2015, **10**, 522–535; e) M. D. Hartle, R. J. Hansen, B. W. Tresca, S. S. Prakesel, L. N. Zakharov, M. M. Haley, M. D. Pluth, D. W. Johnson, *Angew. Chem. Int. Ed.* 2016, **55**, 11480–11484.
13. M. M. Watt, L. N. Zakharov, M. M. Haley, D. W. Johnson, *Angew. Chem. Int. Ed.* 2013, **52**, 10275–10280.
14. a) J. V. Gavette, N. S. Mills, L. N. Zakharov, C. A. Johnson II, D. W. Johnson, M. M. Haley, *Angew. Chem. Int. Ed.* 2013, **52**, 10270–10274; b) J. V. Gavette, C. J. Evoniuk, L. N. Zakharov, M. E. Carnes, M. M. Haley, D. W. Johnson, *Chem. Sci.* 2014, **5**, 2899–2905.

15. a) C. L. Vonnegut, A. M. Shonkwiler, M. K. Khalifa, L. N. Zakharov, D. W. Johnson, M. M. Haley, *Angew. Chem. Int. Ed.* 2015, **54**, 13318–13322; b) N. A. Takaesu, E. Ohta, L. N. Zakharov, D. W. Johnson, M. M. Haley, *Organometallics* 2017, **36**, 2491–2493.
16. J. R. Quinn, S. C. Zimmerman, J. E. Del Bene, I. Shavitt, *J. Am. Chem. Soc.* 2007, **129**, 934–941. A list of self-dimerization constants (K_{dim}) for related structures can be found in the Supporting Information.
17. a) I. Alkorta, J. Elguero, *J. Phys. Chem.* 1999, **103**, 272–279; b) C. A. Hunter, *Angew. Chem. Int. Ed.* 2004, **43**, 5310–5324.
18. *Inter alia*: a) R. Ahmed, A. Altieri, D. M. D. Souza, D. A. Leigh, K. M. Mullen, M. Pampmeyer, A. M. Z. Slawin, J. K. Y. Wong, J. D. Woollins, *J. Am. Chem. Soc.* 2011, **133**, 12304–12310; b) A. Theil, C. Mauve, M.-T. Adeline, A. Marinetti, J.-P. Sauvage, *Angew. Chem. Int. Ed.* 2006, **45**, 2104–2107; c) L. Liu, Y. Liu, P. Liu, J. Wu, Y. Guan, X. Hu, C. Lin, Y. Yang, X. Sun, J. Ma, L. Wang, *Chem. Sci.* 2013, **4**, 1701–1706; d) A. E. Stross, G. Iadevaia, C. A. Hunter, *Chem. Sci.* 2016, **7**, 94–101.
19. CCDC [1884079](#), [1884080](#), and [1884081](#) (**1 a**, **1 b**, **1 b**·TBAHSO₄) contain the supplementary crystallographic data for this paper. These data can be obtained free of charge from [The Cambridge Crystallographic Data Centre](#).
20. The 2D NMR experiments were carried out at much higher concentration range (23–30 mM) in this titration solvent. The NMR signals in host **1 a** proved to be concentration-independent, while only a very small shift (≈ 0.2 ppm) was observed for the phosphoramidate N–H^a in **1 b**, suggesting that possible aggregation of the receptors can be ruled out.
21. R. F. W. Bader, *Atoms in Molecules: A Quantum Theory*, Clarendon, Oxford, 1990.
22. a) U. Koch, P. L. A. Popelier, *J. Phys. Chem.* 1995, **99**, 9747–9754; b) K. Ponmalai, V. Nirmala, *J. Mol. Struct.* 2004, **694**, 33–38.
23. K. B. Wiberg, *Tetrahedron* 1968, **24**, 1083–1096.
24. a) B. A. Moyer, R. Custelcean, B. P. Hay, J. L. Sessler, K. Bowman-James, V. W. Day, S. O. Kang, *Inorg. Chem.* 2013, **52**, 3473–3490; b) I. Ravikumar, P. Ghosh, *Chem. Soc. Rev.* 2012, **41**, 3077–3098.

Chapter 4

1. Lavis, L. D.; Raines, R. T. Bright Ideas for Chemical Biology. *ACS Chem. Biol.* **2008**, **3**, 142–155.

2. Basabe-Desmonts, L.; Reinhoudt, D. N.; Crego-Calama, M. Design of Fluorescent Materials for Chemical Sensing. *Chem. Soc. Rev.* **2007**, *36*, 993– 1017.
3. Vendrell, M.; Zhai, D.; Er, J. C.; Chang, Y.-T. Combinatorial Strategies in Fluorescent Probe Development. *Chem. Rev.* **2012**, *112*, 4391– 4420.
4. Du, J.; Hu, M.; Fan, J.; Peng, X. Fluorescent Chemodosimeters Using “Mild” Chemical Events for the Detection of Small Anions and Cations in Biological and Environmental Media. *Chem. Soc. Rev.* **2012**, *41*, 4511– 4535.
5. Tabaković, I.; Tabaković, K.; Trkovnik, M.; Stunic, Z. Chemistry of Coumarins. Annelation of Coumarin Ring via Reaction of 3-Amino-4-hydroxycoumarin. *Org. Prep. Proced. Int.* **1985**, *17*, 133– 137.
6. Song, Y.; Chen, Z.; Li, H. Advances in Coumarin-Derived Fluorescent Chemosensors for Metal Ions. *Curr. Org. Chem.* **2012**, *16*, 2690– 2707.
7. Stefanachi, A.; Leonetti, F.; Pisani, L.; Catto, M.; Carotti, A. Coumarin: A Natural, Privileged and Versatile Scaffold for Bioactive Compounds. *Molecules* **2018**, *23*, 250– 284.
8. Becker, R. S.; Chakravorti, S.; Gartner, C. A.; de Graca Miguel, M. Photosensitizers: Comprehensive Photophysics/Photochemistry and Theory of Coumarins, Chromones, Their Homologues and Thione Analogues. *J. Chem. Soc., Faraday Trans.* **1993**, *89*, 1007– 1019.
9. Sethna, S. M.; Shah, N. M. The Chemistry of Coumarins. *Chem. Rev.* **1945**, *36*, 1– 62.
10. Tabaković, K.; Tabaković, I. Chemistry of Coumarins. Thermal Reactions of 4-Chloro-3-coumarinyl *N,N*-Dialkyldithiocarbamates and 3-Nitro-4-coumarinyl *N*-Phenyldithiocarbamate. *J. Heterocycl. Chem.* **1992**, *29*, 383– 385.
11. Pereira, T. M.; Franco, D. P.; Vitorio, F.; Kummerle, A. E. Coumarin Compounds in Medicinal Chemistry: Some Important Examples from the Last Years. *Curr. Top. Med. Chem.* **2018**, *18*, 124– 148.
12. Riveiro, M. E.; De Kimpe, N.; Moglioni, A.; Vázquez, R.; Monczor, F.; Shayo, C.; Davio, C. Coumarins: Old Compounds with Novel Promising Therapeutic Perspectives. *Curr. Med. Chem.* **2010**, *17*, 1325– 1338.
13. Cao, D.; Liu, Z.; Verwilt, P.; Koo, S.; Jangjili, P.; Kim, J. S.; Lin, W. Coumarin-Based Small-Molecule Fluorescent Chemosensors. *Chem. Rev.* **2019**, *119*, 10403– 10519.

14. Abernethy, J. L. The Historical and Current Interest in Coumarin. *J. Chem. Educ.* **1969**, *46*, 561– 568.
15. Harborne, J. B. The Natural Coumarins: Occurrence, Chemistry and Biochemistry. *Plant, Cell Environ.* **1982**, *5*, 435– 436.
16. Anamika; Utreja, D.; Ekta; Jain, N.; Sharma, S. Advances in Synthesis and Potentially Bioactive of Coumarin Derivatives. *Curr. Org. Chem.* **2019**, *22*, 2509– 2536.
17. Govori, S. Convenient Methods for the Synthesis of Pentacyclic Fused Heterocycles with Coumarin Moiety. *Synth. Commun.* **2016**, *46*, 569– 580.
18. Medina, F. G.; Marrero, J. G.; Macías-Alonso, M.; González, M. C.; Córdova-Guerrero, I.; Teissier García, A. G.; Osegueda-Robles, S. Coumarin Heterocyclic Derivatives: Chemical Synthesis and Biological Activity. *Nat. Prod. Rep.* **2015**, *32*, 1472– 1507.
19. Tasiór, M.; Kim, D.; Singha, S.; Krzeszewski, M.; Ahn, K. H.; Gryko, D. T. π -Expanded Coumarins: Synthesis, Optical Properties and Applications. *J. Mater. Chem. C* **2015**, *3*, 1421– 1446.
20. Liu, X.; Xu, Z.; Cole, J. M. Molecular Design of UV–Vis Absorption and Emission Properties in Organic Fluorophores: Toward Larger Bathochromic Shifts, Enhanced Molar Extinction Coefficients, and Greater Stokes Shifts. *J. Phys. Chem. C* **2013**, *117*, 16584– 16595.
21. Nad, S.; Kumbhakar, M.; Pal, H. Photophysical Properties of Coumarin-152 and Coumarin-481 Dyes: Unusual Behavior in Nonpolar and in Higher Polarity Solvents. *J. Phys. Chem. A* **2003**, *107*, 4808– 4816.
22. Jones, G.; Rahman, M. A. Fluorescence Properties of Coumarin Laser Dyes in Aqueous Polymer Media. Chromophore Isolation in Poly(methacrylic acid) Hypercoils. *J. Phys. Chem.* **1994**, *98*, 13028– 13037.
23. Cisse, L.; Djande, A.; Capo-Chichi, M.; Delatre, F.; Saba, A.; Tine, A.; Aaron, J.-J. Revisiting the Photophysical Properties and Excited Singlet-State Dipole Moments of Several Coumarin Derivatives. *Spectrochim. Acta, Part A* **2011**, *79*, 428– 436.
24. Cigán, M.; Donovalová, J.; Szöcs, V.; Gašpar, J.; Jakusová, K.; Gáplovský, A. 7-(Dimethylamino)coumarin-3-carbaldehyde and Its Phenylsemicarbazone: TICT Excited State Modulation, Fluorescent H-Aggregates, and Preferential Solvation. *J. Phys. Chem. A* **2013**, *117*, 4870– 4883.

25. Gandioso, A.; Bresolí-Obach, R.; Nin-Hill, A.; Bosch, M.; Palau, M.; Galindo, A.; Contreras, S.; Rovira, A.; Rovira, C.; Nonell, S.; Marchán, V. Redesigning the Coumarin Scaffold into Small Bright Fluorophores with Far-Red to Near-Infrared Emission and Large Stokes Shifts Useful for Cell Imaging. *J. Org. Chem.* **2018**, *83*, 1185– 1195.
26. Wang, Z.-S.; Cui, Y.; Hara, K.; Dan-Oh, Y.; Kasada, C.; Shinpo, A. A High-Light-Harvesting-Efficiency Coumarin Dye for Stable Dye-Sensitized Solar Cells. *Adv. Mater.* **2007**, *19*, 1138– 1141.
27. Bu, F.; Duan, R.; Xie, Y.; Yi, Y.; Peng, Q.; Hu, R.; Qin, A.; Zhao, Z.; Tang, B. Z. Unusual Aggregation-Induced Emission of a Coumarin Derivative as a Result of the Restriction of an Intramolecular Twisting Motion. *Angew. Chem., Int. Ed.* **2015**, *54*, 14492– 14497.
28. Chen, J.-X.; Liu, W.; Zheng, C.-J.; Wang, K.; Liang, K.; Shi, Y.-Z.; Ou, X.-M.; Zhang, X.-H. Coumarin-Based Thermally Activated Delayed Fluorescence Emitters with High External Quantum Efficiency and Low Efficiency Roll-off in the Devices. *ACS Appl. Mater. Interfaces* **2017**, *9*, 8848– 8854.
29. Hara, K.; Sato, T.; Katoh, R.; Furube, A.; Ohga, Y.; Shinpo, A.; Suga, S.; Sayama, K.; Sugihara, H.; Arakawa, H. Molecular Design of Coumarin Dyes for Efficient Dye-Sensitized Solar Cells. *J. Phys. Chem. B* **2003**, *107*, 597– 606.
30. Swanson, S. A.; Wallraff, G. M.; Chen, J. P.; Zhang, W.; Bozano, L. D.; Carter, K. R.; Salem, J. R.; Villa, R.; Scott, J. C. Stable and Efficient Fluorescent Red and Green Dyes for External and Internal Conversion of Blue OLED Emission. *Chem. Mater.* **2003**, *15*, 2305– 2312.
31. Jung, Y.; Jung, J.; Huh, Y.; Kim, D. Benzo[g]Coumarin-Based Fluorescent Probes for Bioimaging Applications. *J. Anal. Methods Chem.* **2018**, *2018*, 1– 11.
32. Ahvale, A. B.; Prokopcová, H.; Šefčovičová, J.; Steinschifter, W.; Täubl, A. E.; Uray, G.; Stadlbauer, W. 4-Cyano-6,7-dimethoxycarbostyrils with Solvent- and PH-Independent High Fluorescence Quantum Yields and Emission Maxima. *Eur. J. Org. Chem.* **2008**, *2008*, 563– 571.
33. de Macedo, M. B.; Kimmel, R.; Urankar, D.; Gazvoda, M.; Peixoto, A.; Cools, F.; Torfs, E.; Verschaeve, L.; Lima, E. S.; Lyčka, A.; Milićević, D.; Klásek, A.; Cos, P.; Kafka, S.; Košmrlj, J.; Cappoen, D. Design, Synthesis and Antitubercular Potency of 4-Hydroxyquinolin-2(1H)-ones. *Eur. J. Med. Chem.* **2017**, *138*, 491– 500.

34. Enoua, G. C.; Lahm, G.; Uray, G.; Stadlbauer, W. Syntheses and Fluorescent Properties of 6-Methoxy-2-oxoquinoline-3,4-dicarbonitriles and 6,7-Dimethoxy-2-oxoquinoline-3,4-dicarbonitriles. *J. Heterocycl. Chem.* **2014**, *51*, E263– E275.
35. Strohmeier, G. A.; Fabian, W. M. F.; Uray, G. A Combined Experimental and Theoretical Approach Toward the Development of Optimized Luminescent Carbostyrils. *Helv. Chim. Acta* **2004**, *87*, 215– 226.
36. Uray, G.; Niederreiter, K. S.; Belaj, F.; Fabian, W. M. F. Long-Wavelength-Absorbing and -Emitting Carbostyrils with High Fluorescence Quantum Yields. *Helv. Chim. Acta* **1999**, *82*, 1408– 1417.
37. Fabian, W. M. F.; Niederreiter, K. S.; Uray, G.; Stadlbauer, W. Substituent Effects on Absorption and Fluorescence Spectra of Carbostyrils. *J. Mol. Struct.* **1999**, *477*, 209– 220.
38. Tashima, T. The Structural Use of Carbostyryl in Physiologically Active Substances. *Bioorg. Med. Chem. Lett.* **2015**, *25*, 3415– 3419.
39. Casley-Smith, J. R.; Morgan, R. G.; Piller, N. B. Treatment of Lymphedema of the Arms and Legs with 5,6-Benzo- $[\alpha]$ -pyrone. *N. Engl. J. Med.* **1993**, *329*, 1158– 1163.
40. Bard, J. P.; Deng, C.-L.; Richardson, H. C.; Odulio, J. M.; Barker, J. E.; Zakharov, L. N.; Cheong, P. H.-Y.; Johnson, D. W.; Haley, M. M. Synthesis, Photophysical Properties, and Self-Dimerization Studies of 2- λ^5 -Phosphaquinolin-2-ones. *Org. Chem. Front.* **2019**, *6*, 1257– 1265.
41. Vonnegut, C. L.; Shonkwiler, A. M.; Khalifa, M. M.; Zakharov, L. N.; Johnson, D. W.; Haley, M. M. Facile Synthesis and Properties of 2- λ^5 -Phosphaquinolines and 2- λ^5 -Phosphaquinolin-2-ones. *Angew. Chem., Int. Ed.* **2015**, *54*, 13318– 13322.
42. Dewar, M. J. S.; Kubba, V. P. New Heteroaromatic Compounds. Part VI. Novel Heterocyclic Compounds of Phosphorus. *J. Am. Chem. Soc.* **1960**, *82*, 5685– 5688.
43. Campbell, I. G. M.; Way, J. K. Synthesis and Stereochemistry of Heterocyclic Phosphorus Compounds. Part I. Preparation of (+)- and (-)-10-p-Dimethylaminophenyl-9,10-Dihydro-9-Aza-10-Phosphaphenanthrene. *J. Chem. Soc.* **1960**, *0*, 5034– 5041.
44. Sun, Y.; Cramer, N. Rhodium(III)-Catalyzed Enantiotopic C-H Activation Enables Access to *P*-Chiral Cyclic Phosphinamides. *Angew. Chem., Int. Ed.* **2017**, *56*, 364– 367.

45. Tang, W.; Ding, Y. X. Synthesis of Phosphaisoquinolin-1-Ones by Pd(II)-Catalyzed Cyclization of *o*-(1-Alkynyl)Phenylphosphonamide Monoesters. *J. Org. Chem.* **2006**, *71*, 8489– 8492.
46. Yan, J. H.; Li, Q. Y.; Boutin, J. A.; Renard, M. P.; Ding, Y. X.; Hao, X. J.; Zhao, W. M.; Wang, M. W. High-Throughput Screening of Novel Antagonists on Melanin-Concentrating Hormone Receptor-1. *Acta Pharmacol. Sin.* **2008**, *29*, 752– 758.
47. Zhao, D.; Nimphius, C.; Lindale, M.; Glorius, F. Phosphoryl-Related Directing Groups in Rhodium(III) Catalysis: A General Strategy to Diverse P-Containing Frameworks. *Org. Lett.* **2013**, *15*, 4504– 4507.
48. Park, S.; Seo, B.; Shin, S.; Son, J.-Y.; Lee, P. H. Rhodium-Catalyzed Oxidative Coupling through C–H Activation and Annulation Directed by Phosphonamide and Phosphinamide Groups. *Chem. Commun.* **2013**, *49*, 8671– 8673.
49. Liu, L.; Zhang, A.-A.; Wang, Y.; Zhang, F.; Zuo, Z.; Zhao, W.-X.; Feng, C.-L.; Ma, W. Asymmetric Synthesis of P-Stereogenic Phosphinic Amides via Pd(0)-Catalyzed Enantioselective Intramolecular C–H Arylation. *Org. Lett.* **2015**, *17*, 2046– 2049.
50. Lin, Z.-Q.; Wang, W.-Z.; Yan, S.-B.; Duan, W.-L. Palladium-Catalyzed Enantioselective C–H Arylation for the Synthesis of P-Stereogenic Compounds. *Angew. Chem., Int. Ed.* **2015**, *54*, 6265– 6269.
51. Wang, Z.; Gelfand, B. S.; Baumgartner, T. Hydrogen Bonding Dithienophosphole-Based Phosphinamides with Intriguing Self-Assembly Behavior. *Angew. Chem., Int. Ed.* **2016**, *55*, 3481– 3485.
52. Ma, Y.-N.; Zhang, X.; Yang, S. Tandem Oxidative C-H Amination and Iodization to Synthesize Difunctional Atropisomeric P-Stereogenic Phosphinamides. *Chem. - Eur. J.* **2017**, *23*, 3007– 3011.
53. Takaesu, N. A.; Ohta, E.; Zakharov, L. N.; Johnson, D. W.; Haley, M. M. Synthesis and Properties of Naphtho[2,3-*e*]-1,2-azaphosphorine-2-oxides: PN-Anthracene Analogues. *Organometallics* **2017**, *36*, 2491– 2493.
54. Deng, C.-L.; Bard, J. P.; Lohrman, J. A.; Barker, J. E.; Zakharov, L. N.; Johnson, D. W.; Haley, M. M. Exploiting the Hydrogen Bond Donor/Acceptor Properties of PN-Heterocycles: Selective Anion Receptors for Hydrogen Sulfate. *Angew. Chem., Int. Ed.* **2019**, *58*, 3934– 3938.

55. Deng, C.-L.; Bard, J. P.; Zakharov, L. N.; Johnson, D. W.; Haley, M. M. Naphtho[2,1-*e*]-1,2-azaphosphorine 2-oxide Derivatives: Synthesis, Optoelectronic Properties, and Self-Dimerization Phenomena. *J. Org. Chem.* **2019**, *84*, 8131– 8139.
56. Deng, C.-L.; Bard, J. P.; Zakharov, L. N.; Johnson, D. W.; Haley, M. M. PN-Containing Pyrene Derivatives: Synthesis, Structure, and Photophysical Properties. *Org. Lett.* **2019**, *21*, 6427– 6431.
57. Schaub, T. A.; Brülls, S. M.; Dral, P. O.; Hampel, F.; Maid, H.; Kivala, M. Organic Electron Acceptors Comprising a Dicyanomethylene-Bridged Acridophosphine Scaffold: The Impact of the Heteroatom. *Chem. - Eur. J.* **2017**, *23*, 6988– 6992.
58. Romero-Nieto, C.; López-Andarias, A.; Egler-Lucas, C.; Gebert, F.; Neus, J. P.; Pilgram, O. Paving the Way to Novel Phosphorus-Based Architectures: A Noncatalyzed Protocol to Access Six-Membered Heterocycles. *Angew. Chem., Int. Ed.* **2015**, *54*, 15872– 15875.
59. Fukazawa, A.; Osaki, H.; Yamaguchi, S. Hydroxyphenyl-Substituted Benzophosphole Oxides: Impact of the Intramolecular Hydrogen Bond on the Fluorescence Properties. *Asian J. Org. Chem.* **2014**, *3*, 122– 127.
60. Regulska, E.; Romero-Nieto, C. Highlights on π -Systems Based on Six-Membered Phosphorus Heterocycles. *Dalt. Trans.* **2018**, *47*, 10344– 10359.
61. Grenon, N.; Baumgartner, T. Exploration of Hypervalent Lewis Acid/Base Interactions in 2-(2'-Thiazolyl)-3-Thienylphosphanes. *Inorg. Chem.* **2018**, *57*, 1630– 1644.
62. Gong, P.; Ye, K.; Sun, J.; Chen, P.; Xue, P.; Yang, H.; Lu, R. Electroluminescence and Fluorescence Response towards Acid Vapors Depending on the Structures of Indole-Fused Phospholes. *RSC Adv.* **2015**, *5*, 94990– 94996.
63. Jiang, X. D.; Zhao, J.; Xi, D.; Yu, H.; Guan, J.; Li, S.; Sun, C. L.; Xiao, L. J. A New Water-Soluble Phosphorus-Dipyrrromethene and Phosphorus-Azadipyrrromethene Dye: PODIPY/Aza-PODIPY. *Chem. - Eur. J.* **2015**, *21*, 6079– 6082.
64. Mathey, F. The Organic Chemistry of Phospholes. *Chem. Rev.* **1988**, *88*, 429– 453.
65. Avarvari, N.; Le Floch, P.; Mathey, F. 1,3,2-Diazaphosphinines: New Versatile Precursors of 1,2-Azaphosphinines and Polyfunctional Phosphinines. *J. Am. Chem. Soc.* **1996**, *118*, 11978– 11979.

66. Sun, W.-C.; Gee, K. R.; Haugland, R. P. Synthesis of Novel Fluorinated Coumarins: Excellent UV-Light Excitable Fluorescent Dyes. *Bioorg. Med. Chem. Lett.* **1998**, *8*, 3107–3110.
67. See the detailed list of similar dimers in the SI of: Quinn, J. R.; Zimmerman, S. C.; Del Bene, J. E.; Shavitt, I. Does the A.T or G.C Base-Pair Possess Enhanced Stability? Quantifying the Effects of CH \cdots O Interactions and Secondary Interactions on Base-Pair Stability Using a Phenomenological Analysis and ab initio Calculations. *J. Am. Chem. Soc.* **2007**, *129*, 934–941.
68. Brouwer, A. M. Standards for Photoluminescence Quantum Yield Measurements in Solution. *Pure Appl. Chem.* **2011**, *83*, 2213–2228.
69. Kuroda, K.; Maruyama, Y.; Hayashi, Y.; Mukaiyama, T. Conversion of Alcohols to Alkyl Aryl Sulfides by a New Type of Oxidation–Reduction Condensation Using Phenyl Diphenylphosphinite. *Bull. Chem. Soc. Jpn.* **2009**, *82*, 381–392.

Chapter 5

1. Anthony, J.E. *Angew. Chem. Int. Ed.* 2008, *47*, 452–483.
2. Wu, J.; Pisula, W.; Müllen, K. *Chem. Rev.* 2007, *107*, 718–747.
3. Figueira-Duarte, T.M.; Müllen, K. *Chem. Rev.* 2011, *111*, 7260–7314.
4. Haugland, R.P.; Spence, M.T.Z.; Johnson, I.D.; Basey, A. *The Handbook: A Guide to Fluorescent Probes and Labeling Technologies*, 10th; Molecular Probes: Eugene, OR, 2005.
5. Birks, J.B.; Christophorou, L.G. *Spectrochim. Acta.* 1963, *19*, 401–410.
6. Birks, J.B. *Rep. Prog. Phys.* 1975, *38*, 903–974.
7. Bains, G.K.; Kim, S.H.; Sorin, E.J.; Narayanaswami, V. *Biochemistry.* 2012, *51*, 6207–6219.
8. Galla, H.J.; Hartmann, W. *Chem. Phys. Lipids.* 1980, *27*, 199–219.
9. Winnik, F. *Chem. Rev.* 1993, *93*, 587–614.
10. Manandhar, E.; Wallace, K.J. *Inorg. Chim. Acta.* 2012, *381*, 15–43.
11. Lee, H.N.; Singh, N.J.; Kim, S.K.; Kwon, J.Y.; Kim, Y.Y.; Kim, K.S.; Yoon, J. *Tetrahedron Lett.* 2007, *48*, 169–172.

12. Shiraishi, Y.; Ishizumi, K.; Nishimura, G.; Hirai, T. *J. Phys. Chem. B.* 2007, 111, 8812–8822.
13. Templer, R.H.; Castle, S.J.; Curran, A.R.; Rumbles, G.; Klug, D.R. *Faraday Discuss.* 1998, 111, 41–53.
14. Pokhrel, M.R.; Bossmann, S.H. *J. Phys. Chem. B.* 2000, 104, 2215–2223.
15. Birks, J.B.; Lumb, M.D.; Munro, I.H.; Flowers, B.H. *Proc. R. Soc. Lon. Ser. A. Math. Phys. Sci.* 1964, 280, 289–297.
16. Vonnegut, C.L.; Shonkwiler, A.M.; Khalifa, M.M.; Zakharov, L.N.; Johnson, D.W.; Haley, M.M. *Angew. Chem. Int. Ed.* 2015, 54, 13318–13322.
17. Bard, J.P.; Deng, C.-L.; Richardson, H.C.; Odulio, J.M.; Barker, J.E.; Zakharov, L.N.; Cheong, P.H.-Y.; Johnson, D.W.; Haley, M.M. *Org. Chem. Front.* 2019, 6, 1257–1265.
18. Deng, C.-L.; Bard, J.P.; Zakharov, L.N.; Johnson, D.W.; Haley, M.M. *J. Org. Chem.* 2019, 84, 8131–8139.
19. Deng, C.-L.; Bard, J.P.; Zakharov, L.N.; Johnson, D.W.; Haley, M.M. *Org. Lett.* 2019, 21, 6427–6431.
20. Wang, Z.; Gelfand, B.S.; Baumgartner, T. *Angew. Chem. Int. Ed.* 2016, 55, 3481–3485.
21. Avarvari, N.; Le Floch, P.; Mathey, F. *J. Am. Chem. Soc.* 1996, 118, 11978–11979.
22. Tang, W.; Ding, Y.X. *J. Org. Chem.* 2006, 71, 8489–8492.
23. Yan, J.H.; Li, Q.Y.; Boutin, J.A.; Renard, M.P.; Ding, Y.X.; Hao, X.J.; Zhao, W.M.; Wang, M.W. *Acta Pharmacol. Sin.* 2008, 29, 752–758.
24. Park, S.; Seo, B.; Shin, S.; Son, J.-Y.; Lee, P.H. *Chem. Commun.* 2013, 49, 8671–8673.
25. Zhao, D.; Nimphius, C.; Lindale, M.; Glorius, F. *Org. Lett.* 2013, 15, 4504–4507.
26. Lin, Z.-Q.; Wang, W.-Z.; Yan, S.-B.; Duan, W.-L. *Angew. Chem. Int. Ed.* 2015, 54, 6265–6269.
27. Liu, L.; Zhang, A.-A.; Wang, Y.; Zhang, F.; Zuo, Z.; Zhao, W.-X.; Feng, C.-L.; Ma, W. *Org. Lett.* 2015, 17, 2046–2049.

28. Sun, Y.; Cramer, N. *Angew. Chem. Int. Ed.* 2017, 56, 364–367.
29. Ma, Y.-N.; Zhang, X.; Yang, S. *Chem. Eur. J.* 2017, 23, 3007–3011.
30. Dewar, M.J.S.; Kubba, V.P. *J. Am. Chem. Soc.* 1960, 82, 5685–5688.
31. Campbell, I.G.M.; Way, J.K. *J. Chem. Soc.* 1960, 5034–5041.
32. Deng, C.-L.; Bard, J.P.; Lohrman, J.A.; Barker, J.E.; Zakharov, L.N.; Johnson, D.W.; Haley, M.M. *Angew. Chem. Int. Ed.* 2019, 58, 3934–3938.
33. Takaesu, N.A.; Ohta, E.; Zakharov, L.N.; Johnson, D.W.; Haley, M.M. *Organometallics*. 2017, 36, 2491–2493.
34. Thordarson, P. *Chem. Soc. Rev.* 2011, 40, 1305–1323.
35. See the Supporting Information of the following for an extensive listing of similar hydrogen-bonded dimers: Quinn, J.R.; Zimmerman, S.C.; Del Bene, J.E.; Shavitt, I. *J. Am. Chem. Soc.* 2007, 129, 934–941.
36. Brouwer, A.M. *Pure Appl. Chem.* 2011, 83, 2213–2228.
37. Sheldrick, G.M. *Bruker/Siemens Area Detector Absorption Correction Program*; Bruker AXS: Madison, WI, 1998.
38. Sheldrick, G.M. *Acta Cryst.* 2015, C71, 3–8.

Chapter 6

1. K. S. Gayen, N. Chatterjee, *Asian J. Org. Chem.* **2020**, 9, 508–528.
2. T. Ozturk, E. Ertas, O. Mert, *Chem. Rev.* **2007**, 107, 5210–5278.
3. J. O. Moon, J. W. Lee, M. G. Choi, S. Ahn, S. K. Chang, *Tetrahedron Lett.* **2012**, 53, 6594–6597.
4. M. G. Choi, Y. H. Kim, J. E. Namgoong, S. K. Chang, *Chem. Commun.* **2009**, 3560–3562.
5. J. E. Park, M. G. Choi, S. K. Chang, *Inorg. Chem.* **2012**, 51, 2880–2884.
6. F. Carta, A. Maresca, A. Scozzafava, C. T. Supuran, *Bioorgan. Med. Chem.* **2012**, 20, 2266–2273.
7. S. Eor, J. Hwang, M. G. Choi, S. K. Chang, *Org. Lett.* **2011**, 13, 370–373.

8. Q. Q. Zhang, J. F. Ge, Q. F. Xu, X. B. Yang, X. Q. Cao, N. J. Li, J. M. Lu, *Tetrahedron Lett.* **2011**, *52*, 595–597.
9. S. Cha, J. Hwang, M. G. Choi, S. K. Chang, *Tetrahedron Lett.* **2010**, *51*, 6663–6665.
10. T. E. Ali, *Arkivoc* **2013**, *2014*, 21–91.
11. M. Yamashita, Preparation, Structure, and Biological Properties of Phosphorus Heterocycles with a C–P Ring System. In *Bioactive Heterocycles II*; Springer: Berlin, Germany, **2007**, *8*, pp. 173–222.
12. L. D. Quin, F. H. Osman, R. O. Day, A. N. Hughes, X.-P. Wu, L. Q. Wang, *New J. Chem.* **1989**, *13*, 375–381.
13. J. P. Bard, D. W. Johnson, M. M. Haley, *Synlett* **2020**, *31*, 1862–1877.
14. J. P. Bard, H. J. Bates, C.-L. Deng, L. N. Zakharov, D. W. Johnson, M. M. Haley, *J. Org. Chem.* **2020**, *85*, 85–91.
15. J. P. Bard, C.-L. Deng, H. C. Richardson, J. M. Odulio, J. E. Barker, L. N. Zakharov, P. H.-Y. Cheong, D. W. Johnson, M. M. Haley, *Org. Chem. Front.* **2019**, *6*, 1257–1265.
16. H. Teichmann, G. Hilgetag, *Angew. Chem., Int. Ed. Engl.* **1967**, *6*, 1013–1023.
17. L. M. Gregoret, S. D. Rader, R. J. Fletterick, F. E. Cohen, *Proteins Struct. Dyn. Bioinf.* **1991**, *9*, 99–107.
18. P. Zhou, F. Tian, F. Lv, Z. Shang, *Proteins Struct. Dyn. Bioinf.* **2009**, *76*, 151–163.
19. A. Maciejewski, R. P. Steer, *Chem. Rev.* **1993**, *93*, 67–98.
20. K. J. Falk, R. P. Steer, *J. Am. Chem. Soc.* **1989**, *111*, 6518–6524.
21. R. P. Steer, V. Ramamurthy, *Acc. Chem. Res.* **1988**, *21*, 380–386.
22. H. Saadeh, T. Goodson, L. Yu, *Macromolecules* **1997**, *30*, 4608–4612.
23. A. M. Brouwer, *Pure Appl. Chem.* **2011**, *83*, 2213–2228.
24. S. R. Meech, D. J. Phillips, *Photochem.* **1983**, *23*, 193–217.
25. M. D. Ediger, R. S. Moog, S. G. Boxer, M. D. Fayer, *P. Chem. Phys. Lett.* **1982**, *88*, 123–127.

Chapter 7

1. Lakowicz, J. R. (2006) Principles of Fluorescence Spectroscopy, 3rd ed., Springer, New York.
2. Waggoner, A., and Kenneth, S. *Enzymol.* **1995**, *246*, 362–373.
3. Johnson, I. *Histochem. J.* **1998**, *30*, 123–140.
4. Petit, J.-M., Denis-Gay, M., and Ratinaud, M.-H. *Biol. Cell* **1993** *78*, 1–13.
5. Johnsson, N., and Johnsson, K. *ACS Chem. Biol.* **2007**, 31–38.
6. Goddard, J.-P., and Reymond, J.-L. *Curr. Opin. Biotechnol.* **2004**, *15*, 314.
7. Giepmans, B. N. G., Adams, S. R., Ellisman, M. H., and Tsien, R. Y. *Science* **2006**, *312*, 217–224.
8. Zhang, J., Campbell, R. E., Ting, A. Y., and Tsien, R. Y. *Nat. Rev. Mol. Cell Biol.* **2002**, *3* 906–918.
9. Valeur, B. (2002) Molecular Fluorescence: Principles and Applications, Wiley-VCH, Weinheim.
10. Frangioni, J. V. In vivo near-infrared fluorescence imaging *Curr. Opin. Chem. Biol.* **2003**, *7*, 626–634.
11. Wolfbeis, O. S. (1985) The fluorescence of organic natural products. In *Molecular Luminescence Spectroscopy: Methods and Applications—Part 1* (Schulman, S. G., Ed.), pp 167–317, Wiley, New York.
12. Sun, W.-C., Gee, K. R., and Haugland, R. P. (1998) Synthesis of novel fluorinated coumarins: Excellent UV-light excitable fluorescent dyes *Bioorg. Med. Chem. Lett.* **1998** *8*, 3107–3110.
13. Hinkeldey, B., Schmitt, A., and Jung, G. *ChemPhysChem* **2008**, *9*, 2019–2027.
14. Song, L.; Hennink, E. J.; Young, T.; Tanke, H. J. *Biophys. J.* **1995**, *68*, 2588.
15. Sjoback, R.; Nygern, J.; Kubista, M. *Spectrochim. Acta Part A* **1995**, *51*, L7.
16. Song, L.; Varma, C. A. G. O.; Verhoeven, J. W.; Tanke, H. *Biophys. J.* **1996**, *70*, 2959.
17. Lavis, L.D. and Raines, R.T. *ACS Chem. Biol.* **2014**, *9*, 855–866.

18. Lavis, L.D. and Raines, R.T. *ACS Chem. Biol.* **2008**, *3*, 142–155.
19. Bard, J.P., Johnson, D.W., Haley, M.M. *Synlett* **2020**, *31*, 1862–1877.
20. Vonnegut, C.L.; Shonkwiler, A.M.; Khalifa, M.M.; Zakharov, L.N.; Johnson, D.W.; Haley, M.M. *Angew. Chem. Int. Ed.* **2015**, *54*, 13318–13322.
21. Bard, J.P.; Deng, C.-L.; Richardson, H.C.; Odulio, J.M.; Barker, J.E.; Zakharov, L.N.; Cheong, P.H.-Y.; Johnson, D.W.; Haley, M.M. *Org. Chem. Front.* **2019**, *6*, 1257–1265.
22. Bard, J.P., Bates, H.J., Deng, C.-L., Zakharov, L.N., Johnson, D.W., Haley, M.M. *J. Org. Chem.* **2020**, *85*, 85–91
23. Lipinski, C. A.; Lombardo, F.; Dominy, B. W.; Feeney, P. J. *Adv. Drug Deliv. Rev.* **1997**, *23*, 3–25.
24. Kourounakis, A. P., Xanthopoulos, D., & Tzara, A. *Med. Res. Rev.* **2019**, 1–44.
25. Brouwer, A.M. *Pure Appl. Chem.* **2011**, *83*, 2213–2228.

Chapter 8

1. P. Ebbersen *J. Immunol.* **1972**, *109*, 1296–1299.
2. S.H. Lee, J.M. Reeves, J.C. Wilson, D.E. Hunton, A.A. Viggiano, T.M. Miller, J.O. Ballenthin, L.R. *Lait Science* **2003**, *301*, 1886–1888.
3. T.J. Grahame, R.B. Schlesinger *Inhalation Toxicol.* **2005**, *17*, 15–27.
4. (a) P.I. Jalava, R.O. Salonen, A.S. Pennanen, M.S. Happonen, P. Penttinen, A.I. Halinen, M.Sillanpaa, R. Hillamo, M.R. Hirvonen *Toxicol. Appl. Pharmacol.* **2008**, *229*, 146–160. (b) J.L. Sessler, P.A. Gale, W.-S. Cho, *Anion Receptor Chemistry*, RSC, Cambridge, UK, **2006**.
5. M.I. Ojovan, W.E. Lee, *An Introduction to Nuclear Waste Immobilisation*; Elsevier: Amsterdam, The Netherlands, **2005**; Chapter 17.
6. X. Feng, P.R. Hrma, J.H. Westsik, Jr., N.R. Brown, M.J. Schweiger, H. Li, J.D. Vienna, G. Chen, G.F. Piepel, D.E. Smith, B.P. McGrail, S.E. Palmer, D. Kim, Y. Peng, W.K. Hahn, A.J. Bakel, W.L. Ebert, D.K. Peeler, C. Chang, *Glass Optimization for Vitrification of Hanford Site Low-Level Tank Waste*; Report PNNL10918; Pacific Northwest National Laboratory: Richland, WA, March **1996**.
7. H. Li, *Letter Report-Minor Component Study for Low-Level Radioactive Waste Glasses*; Report PNNL-11053; Pacific Northwest National Laboratory: Richland, WA, March **1996**.

8. D.S. Kim, W.C. Buchmiller, M.J. Schweiger, J.D. Vienna, D.E. Day, C.W. Kim, D. Zhu, T.E. Day, T. Neidt, D.K. Peeler, T.B. Edwards, I.A. Reamer, R.J. Workman, Iron Phosphate as an Alternative Waste-Form for Hanford LAW; Report PNNL-14251; Pacific Northwest National Laboratory: Richland, WA, February **2003**.
9. J.L. Sessler, E. Katayev, G.D. Pantos, Y.A. Ustynyuk, Synthesis and Study of a New Diamidodipyrromethane Macrocycle. An Anion Receptor with a High Sulfate-to-Nitrate Binding Selectivity. *Chem. Commun.* **2004**, 1276–1277.
10. J.L. Sessler, E. Katayev, G.D. Pantos, P. Scherbakov, M.D. Reshetova, V.N. Khrustalev, V.M. Lynch, Y.A. Ustynyuk, Fine Tuning the Anion Binding Properties of 2,6-Diamidopyridine Dipyrromethane Hybrid Macrocycles. *J. Am. Chem. Soc.* **2005**, *127*, 11442–11446.
11. E.A. Katayev, C.D. Pantos, M.D. Reshetova, V.N. Khrustalev, V.M. Lynch, Y.A. Ustynyuk, J.L. Sessler, Anion-Induced Synthesis and Combinatorial Selection of Polypyrrolic Macrocycles. *Angew. Chem. Int. Ed.* **2005**, *44*, 7386–7390.
12. E.A. Katayev, J.L. Sessler, V.N. Khrustalev, Y.A. Ustynyuk, Synthetic Model of the Phosphate Binding Protein: Solid-State Structure and Solution-Phase Anion Binding Properties of a Large Oligopyrrolic Macrocycle. *J. Org. Chem.* **2007**, *72*, 7244–7252.
13. M. T. Huggins, T. Butler, P. Barber, J. Hunt, Synthesis and Molecular Recognition Studies of Pyrrole Sulfonamides. *Chem. Commun.* **2009**, 5254–5256.
14. S. Saha, B. Akhuli, S. Chakraborty, P. Ghosh, Synthesis of a Preorganized Hybrid Macrobicycle with Distinct Amide and Amine Clefts: Tetrahedral versus Spherical Anions Binding Studies. *J. Org. Chem.* **2013**, *78*, 8759–8765.
15. C.N. Carroll, B.A. Coombs, S.P. McClintock, C.A. Johnson II, O.B. Berryman, D.W. Johnson, M.M. Haley, Anion-Dependent Fluorescence in Bis(anilinoethynyl)pyridine Derivatives: Switchable ON–OFF and OFF–ON Responses. *Chem. Commun.* **2011**, *47*, 5539–5541.
16. B.W. Tresca, L.N. Zakharov, C.N. Carroll, D.W. Johnson, M.M. Haley, Aryl C–H···Cl[−] Hydrogen Bonding in a Fluorescent Anion Sensor. *Chem. Commun.* **2013**, *49*, 7240–7242.
17. M.D. Hartle, R.J. Hansen, B.W. Tresca, S.S. Praker, L.N. Zakharov, M.M. Haley, M.D. Pluth, D.W. Johnson, A Synthetic Supramolecular Receptor for the Hydrosulfide Anion. *Angew. Chem. Int. Ed.* **2016**, *55*, 11480–11484.

18. C.-L. Deng, J.P. Bard, J.A. Lohrman, J.E. Barker, L.N. Zakharov, D.W. Johnson, M.M. Haley, Exploiting the Hydrogen Bond Donor/Acceptor Properties of PN-Heterocycles: Selective Anion Receptors for Hydrogen Sulfate. *Angew. Chem. Int. Ed.* **2019**, *58*, 3934–3938.
19. P. Thordarson *Chem. Soc. Rev.* 2011, *40*, 1305–1323.

Appendix A

1. G. M. Sheldrick, *Bruker/Siemens Area Detector Absorption Correction Program*, Bruker AXS, Madison, WI, 1998.
2. G. M. Sheldrick, *Acta Cryst.* 2015, **C71**, 3.
3. Gaussian 09, Revision D.01, M. J. Frisch, G. W. Trucks, H. B. Schlegel, G. E. Scuseria, M. A. Robb, J. R. Cheeseman, G. Scalmani, V. Barone, G. A. Petersson, H. Nakatsuji, X. Li, M. Caricato, A. Marenich, J. Bloino, B. G. Janesko, R. Gomperts, B. Mennucci, H. P. Hratchian, J. V. Ortiz, A. F. Izmaylov, J. L. Sonnenberg, D. Williams-Young, F. Ding, F. Lipparini, F. Egidi, J. Goings, B. Peng, A. Petrone, T. Henderson, D. Ranasinghe, V. G. Zakrzewski, J. Gao, N. Rega, G. Zheng, W. Liang, M. Hada, M. Ehara, K. Toyota, R. Fukuda, J. Hasegawa, M. Ishida, T. Nakajima, Y. Honda, O. Kitao, H. Nakai, T. Vreven, K. Throssell, J. A. Montgomery, Jr., J. E. Peralta, F. Ogliaro, M. Bearpark, J. J. Heyd, E. Brothers, K. N. Kudin, V. N. Staroverov, T. Keith, R. Kobayashi, J. Normand, K. Raghavachari, A. Rendell, J. C. Burant, S. S. Iyengar, J. Tomasi, M. Cossi, J. M. Millam, M. Klene, C. Adamo, R. Cammi, J. W. Ochterski, R. L. Martin, K. Morokuma, O. Farkas, J. B. Foresman and D. J. Fox, Gaussian, Inc., Wallingford CT, 2016.

Appendix B

1. E. M. Fatila, E. B. Twum, A. Sengupta, M. Pink, J. A. Karty, K. Raghava-chari, A. H. Flood, *Angew. Chem. Int. Ed.* **2016**, *55*, 14057–14062.
2. G. M. Sheldrick, *Bruker/Siemens Area Detector Absorption Correction Program*, Bruker AXS, Madison, WI, **1998**.
3. P. van der Sluis and A. L. Spek, *Acta Cryst., Sect. A* **1990**, *A46*, 194–201.
4. G. M. Sheldrick, *Acta Cryst. C* **2015**, *71*, 3–8.
5. (a) P. Thordarson, *Chem. Soc. Rev.* **2011**, *40*, 1305–1323; (b) K. A. Connors, *Binding Constants*; John Wiley & Sons: New York, **1987**.

6. (a) R. Sure and S. Grimme, *J. Chem. Theory Comput.* **2015**, *11*, 3785–3801; (b) J. Řezáč and P. Hobza, *J. Chem. Theory Comput.* **2012**, *8*, 141–151.
7. Y. Zhao and D. G. Truhlar, *Theor. Chem. Acc.* **2008**, *120*, 215–241.
8. J. Tomasi, B. Mennucci and E. Cances, *J. Mol. Struct.: THEOCHEM* **1999**, *464*, 211–226.
9. A. Schäfer, C. Huber and R. Ahlrichs, *J. Chem. Phys.* **1994**, *100*, 5829–5835.
10. R. F. W. Bader, *Atoms in Molecules, A Quantum Theory*; Oxford University Press: Oxford, **1990**.
11. P. L. A. Popelier, *Atoms in molecules. An introduction*. Prentice Hall, Harlow, **2000**.
12. E. R. Johnson, S. Keinan, P. Mori-Sánchez, A. Contreras-García, A. J. Cohen and W. Yang, *J. Am. Chem. Soc.* **2010**, *132*, 6498–6506.
13. MOPAC2016, J. J. P. Stewart, Stewart Computational Chemistry, Colorado Springs, CO, USA, [HTTP://OpenMOPAC.net](http://OpenMOPAC.net), **2016**.
14. Gaussian 09, Revision E.01, M. J. Frisch, G. W. Trucks, H. B. Schlegel, G. E. Scuseria, M. A. Robb, J. R. Cheeseman, G. Scalmani, V. Barone, B. Mennucci, G. A. Petersson, H. Nakatsuji, M. Caricato, X. Li, H. P. Hratchian, A. F. Izmaylov, J. Bloino, G. Zheng, J. L. Sonnenberg, M. Hada, M. Ehara, K. Toyota, R. Fukuda, J. Hasegawa, M. Ishida, T. Nakajima, Y. Honda, O. Kitao, H. Nakai, T. Vreven, J. A. Montgomery, Jr., J. E. Peralta, F. Ogliaro, M. Bearpark, J. J. Heyd, E. Brothers, K. N. Kudin, V. N. Staroverov, T. Keith, R. Kobayashi, J. Normand, K. Raghavachari, A. Rendell, J. C. Burant, S. S. Iyengar, J. Tomasi, M. Cossi, N. Rega, J. M. Millam, M. Klene, J. E. Knox, J. B. Cross, V. Bakken, C. Adamo, J. Jaramillo, R. Gomperts, R. E. Stratmann, O. Yazyev, A. J. Austin, R. Cammi, C. Pomelli, J. W. Ochterski, R. L. Martin, K. Morokuma, V. G. Zakrzewski, G. A. Voth, P. Salvador, J. J. Dannenberg, S. Dapprich, A. D. Daniels, O. Farkas, J. B. Foresman, J. V. Ortiz, J. Cioslowski and D. J. Fox, Gaussian, Inc., Wallingford CT, **2013**.
15. K. B. Wiberg, *Tetrahedron* **1968**, *24*, 1083–1096.
16. (a) T. Lu and F. Chen, *J. Comput. Chem.* **2012**, *33*, 580–592; (b) T. Lu and F. Chen, *J. Mol. Graphics Modell.* **2012**, *38*, 314–323.

Appendix C

1. Sheldrick, G. M. Bruker/Siemens Area Detector Absorption Correction Program, Bruker AXS, Madison, WI, 1998.

2. Van der Sluis, P.; Spek, A. L. BYPASS: an effective method for the refinement of crystal structures containing disordered solvent regions. *Acta Cryst., Sect. A* **1990**, *A46*, 194–201.
3. Sheldrick, G. M. Crystal structure refinement with SHELXL. *Acta Cryst.* **2015**, *C71*, 3–8.
4. Adamo, C.; Barone, V. Toward reliable density functional methods without adjustable parameters: The PBE0 model *J. Chem. Phys.* **1999**, *110*, 6158–6169.
5. Bremond, E.; Savarese, M.; Su, N. Q.; Perez-Jimenez, A. J.; Xu, X.; Sancho-Garcia, J. C.; Adamo, C. Benchmarking density functionals on structural parameters of small-/medium-sized organic molecules *J. Chem. Theory Comput.* **2016**, *12*, 459–465.
6. Schuafers, A.; Huber, C.; Ahlrichs, R. Fully optimized contracted Gaussian basis sets of triple zeta valence quality for atoms Li to Kr *J. Chem. Phys.* **1994**, *100*, 5829–5835.
7. Gaussian 09, Revision E.01, Frisch, M. J.; Trucks, G. W.; Schlegel, H. B.; Scuseria, G. E.; Robb, M. A.; Cheeseman, J. R.; Scalmani, G.; Barone, V.; Mennucci, B.; Petersson, G. A.; Nakatsuji, H.; Caricato, M.; Li, X.; Hratchian, H. P.; Izmaylov, A. F.; Bloino, J.; Zheng, G.; Sonnenberg, J. L.; Hada, M.; Ehara, M.; Toyota, K.; Fukuda, R.; Hasegawa, J.; Ishida, M.; Nakajima, T.; Honda, Y.; Kitao, O.; Nakai, H.; Vreven, T.; Montgomery, J. A., Jr.; Peralta, J. E.; Ogliaro, F.; Bearpark, M.; Heyd, J. J.; Brothers, E.; Kudin, K. N.; Staroverov, V. N.; Kobayashi, R.; Normand, J.; Raghavachari, K.; Rendell, A.; Burant, J. C.; Iyengar, S. S.; Tomasi, J.; Cossi, M.; Rega, N.; Millam, J. M.; Klene, M.; Knox, J. E.; Cross, J. B.; Bakken, V.; Adamo, C.; Jaramillo, J.; Gomperts, R.; Stratmann, R. E.; Yazyev, O.; Austin, A. J.; Cammi, R.; Pomelli, C.; Ochterski, J. W.; Martin, R. L.; Morokuma, K.; Zakrzewski, V. G.; Voth, G. A.; Salvador, P.; Dannenberg, J. J.; Dapprich, S.; Daniels, A. D.; Farkas, O.; Foresman, J. B.; Ortiz, J. V.; Cioslowski, J.; Fox, D. J. Gaussian, Inc., Wallingford CT, **2013**.
8. Miertus, S.; Scrocco, E.; Tomasi, J. Electrostatic interaction of a solute with a continuum. A direct utilization of AB initio molecular potentials for the prevision of solvent effects *J. Chem. Phys.* **1981**, *55*, 117–129.
9. Barone, V.; Cossi, M.; Tomasi, J. Geometry optimization of molecular structures in solution by the polarizable continuum model *J. Comput. Chem.* **1998**, *19*, 404–417.
10. Thordarson, P. Determining association constants from titration experiments in supramolecular chemistry. *Chem. Soc. Rev.* **2011**, *40*, 1305–1323.

11. Zhao, Y.; Truhlar, D. G. The M06 suite of density functionals for main group thermochemistry, thermochemical kinetics, noncovalent interactions, excited states, and transition elements: two new functionals and systematic testing of four M06-class functionals and 12 other functionals *Theor. Chem. Acc.* **2008**, *120*, 215–241.
12. Lu, T.; Chen, F. Multiwfn: A multifunctional wavefunction analyzer *J. Comput. Chem.* **2012**, *33*, 580–592.

Appendix E

1. A. M. Brouwer, *Pure Appl. Chem.* **2011**, *83*, 2213–2228.
2. S. R. Meech, D. J. Phillips, *Photochem.* **1983**, *23*, 193–217.
3. M. D. Ediger, R. S. Moog, S. G. Boxer, M. D. Fayer, *P. Chem. Phys. Lett.* **1982**, *88*, 123–127.
4. J. P. Bard, C.-L. Deng, H. C. Richardson, J. M. Odulio, J. E. Barker, L. N. Zakharov, P. H.-Y. Cheong, D. W. Johnson, M. M. Haley, *Org. Chem. Front.* **2019**, *6*, 1257–1265.
5. J. P. Bard, H. J. Bates, C.-L. Deng, L. N. Zakharov, D. W. Johnson, M. M. Haley, *J. Org. Chem.* **2020**, *85*, 85–91.
6. G. M. Sheldrick, *Bruker/Siemens Area Detector Absorption Correction Program*, Bruker AXS, Madison, WI, 1998.
7. G. M. Sheldrick, *Acta Cryst. C* **2015**, *71*, 3–8.

Appendix I

1. Figueira-Duarte, K.; Mullen, K. *Chem. Rev.* **2011**, *111*, 7260–7314.
2. (a) Manandhar, E.; Wallace, K. J. *Inorg. Chim. Acta* **2012**, *381*, 15–43. (b) Karuppannan, S.; Chambron, J.-C. *Chem. - Asian J.* **2011**, *6*, 964–984.
3. (a) Winnik, F. M. *Chem. Rev.* **1993**, *93*, 587–614. (b) Birks, J. B.; Christophorou, L. G. *Spectrochim. Acta* **1963**, *19*, 401–410. (c) Birks, J. B. *Photophysics of Aromatic Molecules*; Wiley: London, 1970.
4. (a) Feng, X.; Hu, J.-Y.; Redshaw, C.; Yamato, T. *Chem. - Eur. J.* **2016**, *22*, 11898–11916. (b) Casas-Solvas, J. M.; Howgego, J. D.; Davis, A. P. *Org. Biomol. Chem.* **2014**, *12*, 212–232.

5. (a) Regulska, E.; Romero-Nieto, C. *Dalton Trans.* **2018**, 47, 10344–10359. (b) Hindenberg, P.; Romero-Nieto, C. *Synlett* **2016**, 27, 2293–2300. (c) Hindenberg, P.; Busch, M.; Paul, A.; Bernhardt, M.; Gemessy, P.; Rominger, F.; Romero-Nieto, *Angew. Chem., Int. Ed.* **2018**, 57, 15157–15161.
6. (a) Baumgartner, T.; Jakle, F. *Main Group Strategies Towards Functional Hybrid Materials*; Wiley-VCH: Weinheim, 2018. (b) Parke, S. M.; Boone, M. P.; Rivard, E. *Chem. Commun.* **2016**, 52, 9485–9505.
7. (a) Mateo-Alonso, *Chem. Soc. Rev.* **2014**, 43, 6311–6324. (b) Li, J.; Chen, S.; Wang, Z.; Zhang, Q. *Chem. Rec.* **2016**, 16, 1518–1530.
8. (a) Lee, J.; Park, J. *Org. Lett.* **2015**, 17, 3960–3963. (b) Chua, C. J.; Ren, Y.; Baumgartner, T. *Organometallics* **2012**, 31, 2425–2436. (c) Mallesham, G.; Swetha, C.; Niveditha, S.; Mohanty, M. E.; Babu, N. J.; Kumar, A.; Bhanuprakash, K.; Rao, V. J. *J. Mater. Chem. C* **2015**, 3, 1208–1224. (d) Baumgartner, K.; Kirschbaum, T.; Krutzek, F.; Dreuw, A.; Rominger, F.; Mastalerz, M. *Chem. - Eur. J.* **2017**, 23, 17817–17822. (e) Merz, J.; Fink, J.; Friedrich, A.; Krummenacher, I.; Al Mamari, H.; Lorenzen, S.; Hahnel, M.; Eichhorn, A.; Moos, M.; Holzapfel, M. *Chem. - Eur. J.* **2017**, 23, 13164–13180.
9. Zhang, S.; Qiao, X.; Chen, Y.; Wang, Y.; Edkins, R. M.; Liu, Z.; Li, H.; Fang, Q. *Org. Lett.* **2014**, 16, 342–345.
10. Mocanu, A.; Szucs, R.; Caytan, E.; Roisnel, T.; Dorcet, V.; Bouit, P.-A.; Nyulaszi, L.; Hissler, M. *J. Org. Chem.* **2019**, 84, 957–962.
11. Yao, X. L.; Zhang, K.; Müllen, K.; Wang, X. Y. *Asian J. Org. Chem.* **2018**, 7, 2233–2238.
12. Vanga, M.; Lalancette, R. A.; Jakle, F. *Chem. - Eur. J.* **2019**, 25, 101–140.
13. (a) Vonnegut, C. L.; Shonkwiler, A. M.; Khalifa, M. K.; Zakharov, L. N.; Johnson, D. W.; Haley, M. M. *Angew. Chem., Int. Ed.* **2015**, 54, 13318–13322. (b) Takaesu, N. A.; Ohta, E.; Zakharov, L. N.; Johnson, D. W.; Haley, M. M. **2017**, 36, 2491–2493. (c) Bard, J. P.; Deng, C.-L.; Richardson, H. C.; Odulio, J. M.; Barker, J. E.; Zakharov, L. N.; Cheong, P. H.-Y.; Johnson, D. W.; Haley, M. M. *Org. Chem. Front.* **2019**, 6, 1257–1265. (d) Deng, C.-L.; Bard, J. P.; Zakharov, L. N.; Johnson, D. W.; Haley, M. M. *J. Org. Chem.* **2019**, 84, 8131–8139.
14. (a) Liu, X.; Xu, Z.; Cole, J. M. *J. Phys. Chem. C* **2013**, 117, 16584–16595. (b) Liu, X.; Qiao, Q.; Tian, W.; Liu, W.; Chen, J.; Lang, M. J.; Xu, Z. *J. Am. Chem. Soc.* **2016**, 138, 6960–6963.
15. Kwon, J. E.; Park, S.; Park, S. Y. *J. Am. Chem. Soc.* **2013**, 135, 11239–11246.

16. (a) Englman, R.; Jortner, J. *Mol. Phys.* **1970**, *18*, 145–164. (b) Siebrand, W. *J. Chem. Phys.* **1971**, *55*, 5843.
17. Islam, M. M.; Hu, Z.; Wang, Q.; Redshaw, C.; Feng, X. *Mater. Chem. Front.* **2019**, *3*, 762–781.
18. Chen, L.; Peng, S.; Chen, Y. *ACS Appl. Mater. Interfaces* **2014**, *6*, 8115–8123.
19. Lemaire, M.; Guy, A.; Roussel, J.; Guette, N. *Tetrahedron* **1987**, *43*, 835–844.
20. Mujkic, M.; Lentz, D. *Dalton Trans.* **2012**, *41*, 839–849.
21. Lin, C.-H.; Chang, Y.-Y.; Hung, J.-Y.; Lin, C.-Y.; Chi, Y.; Chung, M.-W.; Lin, C.-L.; Chou, P.-T.; Lee, G.-H.; Chang, C.-H.; Lin, W. C. *Angew. Chem., Int. Ed.* **2011**, *50*, 3182–3186.
22. Zielinska, B. *Polycyclic Aromat. Compd.* **1990**, *1*, 207–211.
23. Sheldrick, G. M.; Bruker/Siemens Area Detector Absorption Correction Program, Bruker AXS, Madison, WI, **1998**.
24. Sheldrick, G. M. *Acta Cryst. C* **2015**, *71*, 3–8.
25. Lakowicz, J. R. *Principles of Fluorescence Spectroscopy*, 3rd ed.; Springer: New York, 1999.
26. (a) Lippert, V. E. *Z. Naturforsch., A: Phys. Sci.* **1955**, *10*, 541–545. (b) Mataga, N.; Kaifu, Y.; Koizumi, M. *Bull. Chem. Soc. Jpn.* **1956**, *29*, 465–470.
27. Pommerehne, J.; Vestweber, H.; Guss, W.; Mahrt, R. F.; Bassler, H.; Porsch, M.; Daub, J. *Adv. Mater.* **1995**, *7*, 551–554.

28. Gaussian 09, Revision E.01, Frisch, M. J.; Trucks, G. W.; Schlegel, H. B.; Scuseria, G. E.; Robb, M. A.; Cheeseman, J. R.; Scalmani, G.; Barone, V.; Mennucci, B.; Petersson, G. A.; Nakatsuji, H.; Caricato, M.; Li, X.; Hratchian, H. P.; Izmaylov, A. F.; Bloino, J.; Zheng, G.; Sonnenberg, J. L.; Hada, M.; Ehara, M.; Toyota, K.; Fukuda, R.; Hasegawa, J.; Ishida, M.; Nakajima, T.; Honda, Y.; Kitao, O.; Nakai, H.; Vreven, T.; Montgomery, J. A., Jr.; Peralta, J. E.; Ogliaro, F.; Bearpark, M.; Heyd, J. J.; Brothers, E.; Kudin, K. N.; Staroverov, V. N.; Kobayashi, R.; Normand, J.; Raghavachari, K.; Rendell, A.; Burant, J. C.; Iyengar, S. S.; Tomasi, J.; Cossi, M.; Rega, N.; Millam, J. M.; Klene, M.; Knox, J. E.; Cross, J. B.; Bakken, V.; Adamo, C.; Jaramillo, J.; Gomperts, R.; Stratmann, R. E.; Yazyev, O.; Austin, A. J.; Cammi, R.; Pomelli, C.; Ochterski, J. W.; Martin, R. L.; Morokuma, K.; Zakrzewski, V. G.; Voth, G. A.; Salvador, P.; Dannenberg, J. J.; Dapprich, S.; Daniels, A. D.; Farkas, O.; Foresman, J. B.; Ortiz, J. V.; Cioslowski, J.; Fox, D. J. Gaussian, Inc., Wallingford CT, **2013**.
29. Yanai, T.; Tew, D. P.; Handy, N. C. *Chem. Phys. Lett.* **2004**, *393*, 51–57.
30. Scalmani, G.; Frisch, M. J. *J. Chem. Phys.* **2010**, *132*, 114110.
31. Lu, T.; Chen, F. *J. Comput. Chem.* **2012**, *33*, 580–592.